ADVANCES IN INTELLIGENT SYSTEMS AND COMPUTING 195

Valentina Emilia Balas
János Fodor
Annamária R. Várkonyi-Kóczy
József Dombi
Lakhmi C. Jain (Eds.)

Soft Computing Applications

Springer

Advances in Intelligent Systems and Computing 195

Editor-in-Chief

Prof. Janusz Kacprzyk
Systems Research Institute
Polish Academy of Sciences
ul. Newelska 6
01-447 Warsaw
Poland
E-mail: kacprzyk@ibspan.waw.pl

For further volumes:
http://www.springer.com/series/11156

Valentina Emilia Balas, János Fodor,
Annamária R. Várkonyi-Kóczy, József Dombi,
and Lakhmi C. Jain (Eds.)

Soft Computing Applications

Proceedings of the 5th International Workshop Soft Computing Applications (SOFA)

Springer

Editors
Prof. Valentina Emilia Balas
Associate Professor
Aurel Vlaicu University from Arad
Arad
Romania

Prof. József Dombi
Department of Informatics
University of Szeged
Szeged
Hungary

Prof. János Fodor
Professor
Institute of Applied Mathematics
Óbuda University
Budapest
Hungary

Prof. Lakhmi C. Jain
School of Electrical and Information
Engineering
University of South Australia
Adelaide
South Australia SA
Australia

Prof. Annamária R. Várkonyi-Kóczy
Professor
Institute of Mechatronics and Vehicle
Engineering
Obuda University
Budapest
Hungary

ISSN 2194-5357
e-ISSN 2194-5365
ISBN 978-3-642-33940-0
e-ISBN 978-3-642-33941-7
DOI 10.1007/978-3-642-33941-7
Springer Heidelberg New York Dordrecht London

Library of Congress Control Number: 2012949235

Preface

This volume contains the Proceedings of the 5$^{\text{th}}$ International Workshop on Soft Computing Applications (SOFA 2012). The main goal of the Workshop is to communicate and publish new theoretical and applicative research results, in the areas of Fuzzy Logic, Neural Networks, Evolutionary Computing, and other methods belonging or connected to Soft Computing (SC). A second and just as important goal is to encourage new reflections on SC issues and new links between interested researchers, R&D engineers, managers and so on.

The concept of Soft Computing - which was introduced by Lotfi Zadeh in 1991 - serves to highlight the emergence of computing methodologies in which the accent is on exploiting the tolerance for imprecision and uncertainty to achieve tractability, robustness and low solution cost. The principal constituents of soft computing are fuzzy logic, neurocomputing, evolutionary computing and probabilistic computing, with the later subsuming belief networks, chaotic systems and parts of learning theory. Soft computing facilitates the use of fuzzy logic, neurocomputing, evolutionary computing and probabilistic computing in combination, leading to the concept of hybrid intelligent systems. Such systems are rapidly growing in importance and visibility.

Nowadays in our complex world all problems cannot be dealt with conventional mathematical methods. With the help of soft computing techniques, that offer complementary methods allowing flexible computing tools, it is possible to find good solutions.

The book covers a broad spectrum of soft computing techniques, theoretical and practical applications employing knowledge and intelligence to find solutions for world industrial, economic and medical problems. The combination of such intelligent systems tools and a large number of applications introduce a need for a synergy of scientific and technological disciplines in order to show the great potential of Soft Computing in all domains.

The conference papers included in these proceedings, published post conference, were grouped into the following area of research:

- Soft Computing and Fusion Algorithms in Biometrics,
- Fuzzy Theory, Control andApplications,
- Modelling and Control Applications,
- Steps towards Intelligent Circuits,

- Knowledge-Based Technologies for Web Applications, Cloud Computing and Security Algorithms,
- Computational Intelligence for Biomedical Applications,
- Neural Networks and Applications,
- Intelligent Systems for Image Processing,
- Knowledge Management for Business Process and Enterprise Modelling.

In SOFA 2012 we had five eminent Keynote Speakers: Professor Lotfi A. Zadeh (USA), Professor Michio Sugeno (JAPAN), Professor Kay Chen Tan (Singapore), Professor Michal Baczynski (Poland) and Professor Laszlo B. Kish (USA). Their summaries or extended talks are included in this book.

The book is directed to all interested readers to evaluate to potential of Soft Computing: researchers in laboratories and universities interested to solve real problems, managers looking for tools and new views to improve their business.

We especially thank the honorary chair of SOFA 2012 Prof. Lotfi A. Zadeh who encouraged and motivated us. He participated actively in our workshop of this edition by sending us an interesting video tape lecture.

Special thanks to Professor Michio Sugeno who showed a constant support during all these years by participating to the last four SOFA editions.

We would like to thank the authors of the submitted papers for keeping the quality of the SOFA 2012 conference at high levels. The editors of this book would like to acknowledge all the authors for their contributions and also the reviewers.

For their help with organizational issues of all SOFA editions we express our thanks to TRIVENT Conference Office, Mónika Jetzin and Teodora Artimon for having customized the software Conference Manager, registration of conference participants and all local arrangements.

Special thanks go to Janusz Kacprzyk (Editor in Chief, Springer, Advances in Intelligent and Soft ComputingSeries) for the opportunity to organize this guest edited volume.

We are grateful to Springer, especially to Dr. Thomas Ditzinger (Senior Editor, Applied Sciences & Engineering Springer-Verlag) for the excellent collaboration and patience during the evolvement of this volume.

We hope that the readers will find this collection of papers inspiring, informative and useful. We also hope to see you at a future SOFA event.

Valentina Emilia Balas, Romania
János C. Fodor, Hungary
Annamaria R. Várkonyi-Kóczy, Hungary
József Dombi, Hungary
Lakhmi C. Jain, Australia

Contents

Keynote Invited Talks

Soft Computing and Fusion Algorithms in Biometrics

Fuzzy Theory, Control and Applications

Modelling and Control Applications

Steps towards Intelligent Circuits

Knowledge-Based Technologies for Web Applications, Cloud Computing and Security Algorithms

Computational Intelligence for Biomedical Applications

Neural Networks and Applications

Intelligent Systems for Image Processing

Knowledge Management for Business Process and Enterprise Modeling

List of Contributors

Lotfi A. Zadeh
Department of EECS, University of California, Berkeley, USA

Michio Sugeno
European Centre for Soft Computing Mieres-Asturias, Spain

Kay Chen Tan
Department of Electrical and Computer Engineering, National University of Singapore, Singapore

Michał Baczyński
University of Silesia, Institute of Mathematics, Katowice, Poland

R. Mingesz
Department of Technical Informatics, University of Szeged, Hungary

Laszlo B. Kish
Texas A&M University, Department of Electrical and Computer Engineering, USA

Z. Gingl
Department of Technical Informatics, University of Szeged, Hungary

C.G. Granqvist
Department of Engineering Sciences, The Ångström Laboratory, Uppsala University, Uppsala, Sweden

H. Wen
Texas A&M University, Department of Electrical and Computer Engineering, USA and Hunan University, College of Electrical and Information Engineering, China

F. Peper
National Institute of Information and Communication Technology, Kobe, Japan

T. Eubanks
Sandia National Laboratories, Albuquerque, USA

G. Schmera
Space and Naval Warfare Systems Center, San Diego, CA 92152, USA

Bojan Jovanović
University of Niš, Faculty of Electronic Engineering, Dept. of Electronics, Niš, Serbia

Milun Jevtić
University of Niš, Faculty of Electronic Engineering, Dept. of Electronics, Niš, Serbia

Tsung-Chih Lin
Department of Electronic Engineering, Feng-Chia University, Taichung, Taiwan

Wei-Nan Liao
Department of Electronic Engineering, Feng-Chia University, Taichung, Taiwan

Valentina Emilia Balas
Department of Automation and Applied Informatics, Aurel Vlaicu University of Arad, Arad, Romania

Mircea A. Ciugudean
Politechnica University of Timisoara

Marius M. Balas
Department of Automation and Applied Informatics, Aurel Vlaicu University of Arad, Arad, Romania

Marius Socaci
Department of Automation and Applied Informatics, Aurel Vlaicu University of Arad, Arad, Romania

Onisifor Olaru
"Constantin Brancusi" University of Targu Jiu, Romania

Elisa Valentina Moisi
Department of Computer Science and Information Technology, Faculty of Electrical Engineering and Information Technology, University of Oradea, Oradea, Romania

Vladimir Ioan Cretu
Department of Computer and Software Engineering, "Politehnica" University of Timisoara, Timisoara, Romania

Benedek Nagy
Department of Computer Science, Faculty of Informatics, University of Debrecen, Debrecen, Hungary

Silviu Ioan Bejinariu
Institute of Computer Science, Romanian Academy, Iasi Branch

Florin Rotaru
Institute of Computer Science, Romanian Academy, Iasi Branch

Cristina Diana Niţă
Institute of Computer Science, Romanian Academy, Iasi Branch

Adrian Ciobanu
Institute of Computer Science, Romanian Academy, Iasi Branch

Mihaela Costin
Institute of Computer Science, Romanian Academy, Iasi Branch

Tudor Barbu
Institute of Computer Science, Romanian Academy, Iasi Branch

Dorel Aiordachioaie
Electronics and Telecommunications Department, "Dunarea de Jos" University of Galati, Galati, Romania

Laurentiu Frangu
Electronics and Telecommunications Department, "Dunarea de Jos" University of Galati, Galati, Romania

N.A. Chira
Department of Automation and Applied Informatics, Aurel Vlaicu University of Arad, Arad, Romania

S.A. Matisan
Department of Automation and Applied Informatics, Aurel Vlaicu University of Arad, Arad, Romania

F.M. Suciu
Department of Automation and Applied Informatics, Aurel Vlaicu University of Arad, Arad, Romania

Dragan G. Radojević
University of Belgrade, Mihajlo Pupin Institute, Belgrade, Serbia

Pavle Milošević
Faculty of Organizational Sciences, University of Belgrade, Belgrade

Ivan Nešić
Faculty of Organizational Sciences, University of Belgrade, Belgrade

Ana Poledica
Faculty of Organizational Sciences, University of Belgrade, Belgrade

Bratislav Petrović
Faculty of Organizational Sciences, University of Belgrade, Belgrade

Aleksandar Rakicevic
Faculty of Organizational Sciences, University of Belgrade, Belgrade

Emanuel Ciprian Sasu
Department of Automation and Applied Informatics, "Politehnica" University, Timisoara, Romania

Octavian Prostean
Department of Automation and Applied Informatics, "Politehnica" University, Timisoara, Romania

Radu Boraci
Department of Automation and Applied Informatics, "Politehnica" University, Timisoara, Romania

Cristian Vasar
Department of Automation and Applied Informatics, "Politehnica" University, Timisoara, Romania

Maria Graça Ruano
CISUC, University of Coimbra and University of Algarve, Portugal

César A. Teixeira
CISUC, University of Coimbra, Portugal

Javid J. Rahmati
University of Algarve, Portugal

António E. Ruano
Centre for Intelligent Systems, IDMEC, IST and the University of Algarve, Portugal

S.H. Karamchandani
Indian Institute of Technology – Bombay, Mumbai, India

V.K. Madan
Kalasalingam University, Krishnankoil, Virudhunagar, India

P.M. Kelkar
Sneha Health Care Centre, Mumbai, India

S.N. Merchant
Indian Institute of Technology – Bombay, Mumbai, India

U.B. Desai
Indian Institute of Technology – Hyderabad, India

Daniel Dragu
Department of Automation and Applied Informatics, "Politehnica" University, Timisoara, Romania

Valentin Gomoi
Department of Automation and Applied Informatics, "Politehnica" University, Timisoara, Romania

Vasile Stoicu-Tivadar
Department of Automation and Applied Informatics, "Politehnica" University, Timisoara, Romania

Doru Anastasiu Popescu
Faculty of Mathematics and Computer Science, University of Pitesti, Romania and National College "Radu Greceanu" Slatina, Romania

Dragos Nicolae
National College "Radu Greceanu" Slatina, Romania

Ioan Virag
Department of Computer Science, "Vasile Goldis" Western University of Arad, Romania

Antoanela Naaji
Department of Computer Science, "Vasile Goldis" Western University of Arad, Romania

Marius Popescu
Department of Computer Science, "Vasile Goldis" Western University of Arad, Romania

Alina Mădălina Lonea
Department of Automation and Applied Informatics, "Politehnica" University, Timisoara, Romania

Daniela Elena Popescu
Computer Engineering Department, University of Oradea, Faculty of Electrical Engineering and Information Technology, Oradea, Romania

Octavian Prostean
Department of Automation and Applied Informatics, "Politehnica" University, Timisoara, Romania

Huaglory Tianfield
School of Engineering and Built Environment, Glasgow Caledonian University, Glasgow, United Kingdom

Cosmin Koch-Ciobotaru
Department of Automation and Applied Informatics, "Politehnica" University, Timisoara, Romania

Ildiko Tatai
"Politehnica" University, Timisoara, Romania

Marian Greconici
"Politehnica" University, Timisoara, Romania

Ovidiu Gana
"Politehnica" University, Timisoara, Romania

Marius Babescu
"Politehnica" University, Timisoara, Romania

Gabriel Gîrban
"Politehnica" University, Timisoara, Romania

Mircea Popa
"Politehnica" University, Timisoara, Romania

Gheorghe Sima
Aurel Vlaicu University of Arad, Arad, Romania

Iñigo Monedero
School of Computer Science and Engineering, Electronic Technology Department, Seville, Spain

Félix Biscarri
School of Computer Science and Engineering, Electronic Technology Department, Seville, Spain

Carlos León
School of Computer Science and Engineering, Electronic Technology Department, Seville, Spain

Juan Ignacio Guerrero
School of Computer Science and Engineering, Electronic Technology Department, Seville, Spain

Viorel Nicolau
Department of Electronics and Telecommunications, "Dunarea de Jos" University of Galati, Romania

Mihaela Andrei
Department of Electronics and Telecommunications, "Dunarea de Jos" University of Galati, Romania

Guilherme Madureira
Institute of Meteorology, Geophysical Center of S. Teotónio, Portugal

Cristiano L. Cabrita
University of Algarve, Portugal

Pedro M. Ferreira
Algarve STP – Algarve Science & Technology Park, Portugal

László T. Kóczy
Faculty of Engineering Sciences, Széchenyi István University, Gyõr, Hungary

Petru Radu
School of Engineering and Digital Arts, University of Kent, Canterbury, U.K.

Konstantinos Sirlantzis
School of Engineering and Digital Arts, University of Kent, Canterbury, U.K.

Gareth Howells
School of Engineering and Digital Arts, University of Kent, Canterbury, U.K.

Sanaul Hoque
School of Engineering and Digital Arts, University of Kent, Canterbury, U.K.

Farzin Deravi
School of Engineering and Digital Arts, University of Kent, Canterbury, U.K.

Cristina Madalina Noaica
Artificial Intelligence & Computational Logic Laboratory, Mathematics & Computer Science Dept., Spiru Haret University, Bucharest, Romania

Robert Badea
Artificial Intelligence & Computational Logic Laboratory, Mathematics & Computer Science Dept., Spiru Haret University, Bucharest, Romania

Iulia Maria Motoc
Artificial Intelligence & Computational Logic Laboratory, Mathematics & Computer Science Dept., Spiru Haret University, Bucharest, Romania

Claudiu Gheorghe Ghica
Artificial Intelligence & Computational Logic Lab., Mathematics & Computer Science Dept., Spiru Haret University, Bucharest, Romania, Programmer at Clintelica AB

Alin Cristian Rosoiu
Game Tester at *UbiSoft* Romania

Nicolaie Popescu-Bodorin
Artificial Intelligence & Computational Logic Laboratory, Mathematics & Computer Science Dept., Spiru Haret University, Bucharest, Romania

Crina Raţiu
Daramec SRL, Arad, România

Dominic Bucerzan
Department of Mathematics-Informatics, Faculty of Exact Sciences, "Aurel Vlaicu" University of Arad, România

Mihaela Crăciun
Department of Mathematics-Informatics, Faculty of Exact Sciences, "Aurel Vlaicu" University of Arad, România

Diana Betina Mirsu
Faculty of Management in Production and Transportation "Politehnica" University of Timisoara, Romania

Irina-Steliana Stan
Department of Economic Informatics, Faculty of Cybernetics, Statisics and Economic Informatics, Academy of Economic Studies, Bucharest, Romania

Ion-Sorin Stroe
Department of Economic Informatics, Faculty of Cybernetics, Statisics and Economic Informatics, Academy of Economic Studies, Bucharest, Romania

Serban Popa
Faculty of Management in Production and Transportation, "Politehnica" University of Timisoara, Romania

Cristian Olariu
"Politehnica" University of Timisoara, Romania

Alexandru Canda
"Politehnica" University of Timisoara, Romania

Anca Draghici
Faculty of Management in Production and Transportation, "Politehnica" University of Timisoara, Romania

Tomislav Rozman
BICERO, Business Informatics Center Rozman Ltd., Maribor, Slovenia

Ahmad Taher Azar
Misr University for Science & Technology (MUST), 6th of October City, Egypt

Shaimaa A. El-Said
Faculty of Engineering - Zagazig University, Zagazig, Sharkia, Egypt

Teodora Olariu
Vasile Goldis Western University of Arad, Romania

Behnam Yavari
School of Electrical and Computer Engineering Shiraz University, Shiraz, Iran

Seyed Hamidreza Abbasi
School of Electrical and Computer Engineering Shiraz University, Shiraz, Iran

Faridoon Shabaninia
School of Electrical and Computer Engineering Shiraz University, Shiraz, Iran

F. Khan
Department of Software Engineering University of Engineering and Technology Taxila, Pakistan

Amna Altaf
Department of Software Engineering University of Engineering and Technology Taxila, Pakistan

Amr F. Farag
Department of Systems and Biomedical Engineering, Cairo University, Giza, Egypt and Department of Biomedical Engineering, Shorouk Higher institute of Engineering, EL-Shorouk, Egypt

Shereen M. El-Metwally
Department of Systems and Biomedical Engineering, Cairo University, Giza, Egypt

Ahmed Abdel Aal Morsy
Department of Systems and Biomedical Engineering, Cairo University, Giza, Egypt

Rim Boughdiri
REGIM: REsearch Group on Intelligent Machines, University of Sfax, National Engineering School of Sfax (ENIS), Tunisia and LSIS, CNRS UMR 7296. Dom. Universitaire St Jérôme, Marseille, France

Hala Bezine
REGIM: REsearch Group on Intelligent Machines, University of Sfax, National Engineering School of Sfax (ENIS), Tunisia

Nacer K. M'Sirdi
LSIS, CNRS UMR 7296. Dom. Universitaire St Jérôme, Marseille, France

Aziz Naamane
LSIS, CNRS UMR 7296. Dom. Universitaire St Jérôme, Marseille, France

Adel M. Alimi
REGIM: REsearch Group on Intelligent Machines, University of Sfax, National Engineering School of Sfax (ENIS), Tunisia

Raghesh Krishnan K.
Department of Information Technology, Amrita Vishwa Vidyapeetham, Amrita Nagar, Coimbatore Tamilnadu, India

R. Sudhakar
Department of Electronics and Communication Engineering, Dr. Mahalingam College of Engineering and Technology, Pollachi Tamilnadu, India

Davood Mohammadi Souran
School of Electrical and Computer Engineering Shiraz University, Shiraz, Iran

Nasim Paykari
School of Electrical and Computer Engineering Shiraz University, Shiraz, Iran

Gabriela Prostean
Faculty of Management in Production and Transportation, "Politehnica" University of Timisoara, Romania

Adrian Adam
Faculty of Management in Production and Transportation, "Politehnica" University of Timisoara, Romania

Adela D. Berdie
Department of Electrical Engineering and Industrial Informatics, Faculty of Engineering Hunedoara, "Politehnica" University of Timisoara, Hunedoara, Romania

Mihaela Osaci
Department of Electrical Engineering and Industrial Informatics, Faculty of Engineering Hunedoara, "Politehnica" University of Timisoara, Hunedoara, Romania

Nicolae Budişan
Department of Automation and Applied Informatics, "Politehnica" University, Timisoara, Romania

Ana Daniela Hammes
Cellent AG Stuttgart, Germany

Manuela Panoiu
Department of Electrical Engineering and Industrial Informatics, Faculty of Engineering Hunedoara, "Politehnica" University of Timisoara, Hunedoara, Romania

Caius Panoiu
Department of Electrical Engineering and Industrial Informatics, Faculty of Engineering Hunedoara, "Politehnica" University of Timisoara, Hunedoara, Romania

Loredana Ghiormez
Faculty of Automation and Computers, "Politehnica University", Timişoara, Romania

Matei Tămăşilă
"Politehnica" University, Timisoara, Romania

Ilie Mihai Tăucean
"Politehnica" University, Timisoara, Romania

Marius Bîzgă
Automation Department, Rovinari Power Plant, Romania

Soheil Davari
Department of Industrial Engineering, Amirkabir University of Technology, Tehran, Iran

Mohammad Hossein Fazel Zarandi
Department of Industrial Engineering, Amirkabir University of Technology, Tehran, Iran

Outline of a Restriction-Centered Theory of Reasoning and Computation in an Environment of Uncertainty, Imprecision and Partiality of Truth*

(Video Tape Lecture)

Lotfi A. Zadeh

Department of EECS,
University of California,
Berkeley, CA 94720-1776
zadeh@eecs.berkeley.edu

Abstract. The theory which is outlined in this lecture, call it RRC for short, is a departure from traditional approaches to reasoning and computation. A principal advance is an enhanced capability for reasoning and computation in an environment of uncertainty, imprecision and partiality of truth. The point of departure in RRC is a basic premise—in the real world such environment is the norm rather than exception.

A concept which has a position of centrality in RRC is that of a restriction. Informally, a restriction is an answer to the question: What is the value of a variable X? More concretely, a restriction, R(X), on a variable, X, is a limitation on the values which X can take—a limitation which is induced by what is known or perceived about X. A restriction is singular if the answer to the question is a singleton; otherwise it is nonsingular. Generally, nonsingularity implies uncertainty. A restriction is precisiated if the limitation is mathematically well defined; otherwise it is unprecisiated. Generally, restrictions which are described in a natural language are unprecisiated.

There are many kinds of restrictions ranging from very simple to very complex. Examples. $3 \leq X \leq 6$; X is normally distributed with mean m and variance σ^2; X is small; it is very likely that X is small; it is very unlikely that there will be a significant increase in the price of oil in the near future.

The canonical form of a restriction is an expression of the form X isr R, where X is the restricted variable, R is the restricting relation and r is an indexical variable which defines the way in which R restricts X.

In RRC there are two principal issues—representation and computation. Representation involves representing a semantic entity, e.g., a proposition, as a restriction. For

* Research supported in part by ONR N00014-02-1-0294, Omron Grant, Tekes Grant, Azerbaijan Ministry of Communications and Information Technology Grant, Azerbaijan University Grant and the BISC Program of UC Berkeley.

V.E. Balas et al. (Eds.): Soft Computing Applications, AISC 195, pp. 1–3.
springerlink.com

computation with restrictions what is employed is the extension principle. The extension principle is a collection of computational rules which address the following problem. Assume that Y=f(X). Given a restriction on X and/or a restriction on f, what is the restriction on Y, R(Y), which is induced by R(X) and R(f)? Basically, the extension principle involves propagation of restrictions. Representation and computation with restrictions is illustrated with examples.

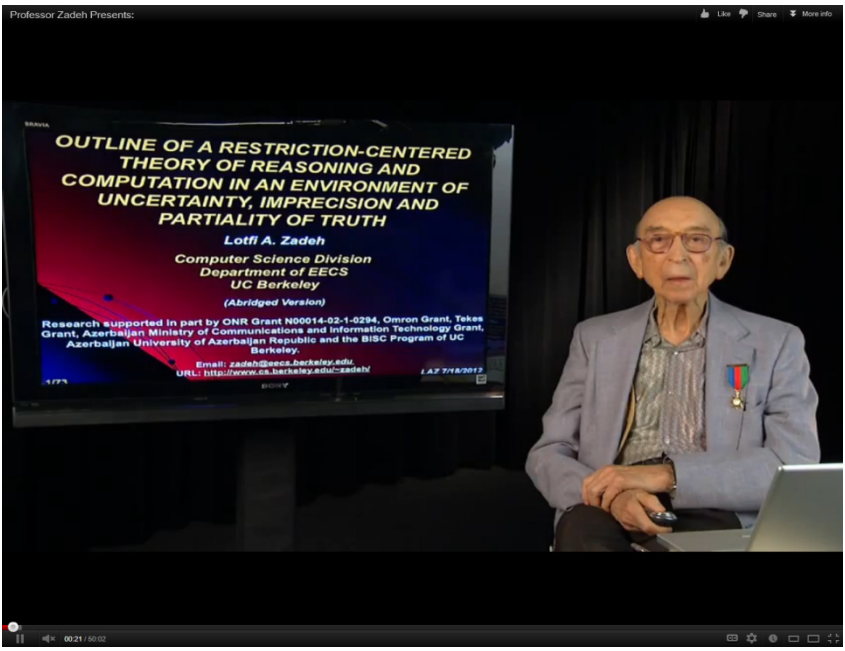

Biographical Note

LOTFI A. ZADEH is Professor Emeritus, Computer Science Division, Department of EECS, University of California, Berkeley. In addition, he is serving as the Director of BISC (Berkeley Initiative in Soft Computing). Since the publication of his first paper on fuzzy sets in 1965, his research has been focused on fuzzy logic and its applications.

Lotfi Zadeh has received many awards, among them the IEEE Medal of Honor, IEEE Education Medal, IEEE Richard W. Hamming Medal, the ACM Allen Newell Award, the Honda Prize, the Okawa Prize, the Kaufmann Prize and Gold Medal, Grigore Moisil Prize, the Kampe de Feriet Award, Bolzano Medal, the Nicolaus Copernicus Medal, Norbert Wiener Award, the Benjamin Franklin Medal and the Friendship Order from the President of the Republic of Azerbaijan. He was inducted into the Silicon Valley Engineering Hall of Fame, the AI Hall of Fame and the Nixdorf Museum Wall of Fame. He is a recipient of twenty-five honorary doctorates, and is a member of the National Academy of Engineering. In addition, he is a foreign member of the Finnish Academy of Sciences, the Polish Academy of Sciences, the Korean Academy of Science & Technology, the Bulgarian Academy of Sciences, the Azerbaijan Academy of Sciences, Hungarian Academy of Engineering and Romanian Academy of Technical Sciences. His work is associated with 100,584 Google Scholar citations.

http://www.cs.berkeley.edu/~zadeh/

On Structure of Uncertainties

Michio Sugeno

European Centre for Soft Computing Mieres-Asturias, Spain
michio.sugeno@gmail.com

Abstract. As a conventional concept of uncertainty, we are familiar with the 'probability' of a phenomenon. Also we often discuss the 'uncertainty' of knowledge. Recently, Fuzzy Theory has brought a hidden uncertainty, 'fuzziness', to light. Reflections on these ideas lead to a fundamental question: What kinds of uncertainty are we aware of? Motivated by this question, this study aims to explore categories and modalities of uncertainty. For instance, we have found that:

(i) 'form' is a category of uncertainty;
(ii) 'inconsistency' is a modality of uncertainty;
(iii) the inconsistency of form is one of the major uncertainties.

Through the classification of adjectives implying various uncertainties, we elucidate seven uncertainties (or nine if subcategories are counted) and identify three essential ones among them, such as the fuzziness of wording. Finally the structure of uncertainty will be shown. The obtained structure is verified by psychological experiments, while the validity of three essential uncertainties is examined by linguistic analysis.

Michio Sugeno

Short biography

After graduating from the Department of Physics, The University of Tokyo, Michio Sugeno worked at Mitsubishi Atomic Power Industry. Then, he served the Tokyo Institute of Technology as Research Associate, Associate Professor and Professor

V.E. Balas et al. (Eds.): Soft Computing Applications, AISC 195, pp. 5–6.
springerlink.com

from 1965 to 2000. After retiring from the Tokyo Institute of Technology, he worked as Laboratory Head at the Brain Science Institute, RIKEN from 2000 to 2005, and then, as Distinguished Visiting Professor at Doshisha University from 2005 to 2010. He is currently Emeritus Professor at the Tokyo Institute of Technology, Japan, and Emeritus Researcher at the European Centre for Soft Computing, Spain.

He was President of the Japan Society for Fuzzy Theory and Systems from 1991 to 1993, and also President of the International Fuzzy Systems Association from 1997 to 1999. He is the first recipient of the IEEE Pioneer Award in Fuzzy Systems with Zadeh in 2000. He also received the 2010 IEEE Frank Rosenblatt Award.

Advances in Evolutionary Multi-objective Optimization

Kay Chen Tan

Department of Electrical and Computer Engineering
National University of Singapore
4 Engineering Drive 3, Singapore 117576
eletankc@nus.edu.sg

Abstract. Multi-objective evolutionary algorithms are a class of stochastic optimization Techniques that simulate biological evolution to solve problems with multiple (and often conflicting) objectives.

Advances made in the field of evolutionary multi-objective optimization (EMO) are the results of more than two decades of research, studying various topics that are unique to MO problems, such as fitness assignment, diversity preservation, balance between exploration and exploitation, elitism and archiving. However many of these studies assume that the problem is deterministic, while the EMO performance generally deteriorates in the presence of uncertainties. In certain situations, the solutions found may not even be implementable in practice. The lecture will first provide an overview of evolutionary computation and its application to multi-objective optimization. It will then discuss challenges faced in EMO research and present various EMO features and algorithms for good optimization performance. Specifically, the impact of noise uncertainties will be described and enhancements to basic EMO algorithmic design for robust optimization will be presented. The lecture will also discuss the applications of EMO techniques for solving engineering problems, such as control system design and scheduling, which often involve different competing specifications in a large and constrained search space.

Kay Chen TAN is currently an Associate Professor in the Department of Electrical and Computer Engineering, National University of Singapore. He is actively pursuing
Research in computational and artificial intelligence, with applications to multi---objective optimization, scheduling, automation, data mining, and games.

Dr Tan has Published over 100 journal papers, over 100 papers in conference proceedings, co--authored 5 books including Multiobjective Evolutionary Algorithms and Applications (Springer-Verlag, 2005), Modern Industrial Automation Software Design (John Wiley, 2006; Chinese Edition, 2008), Evolutionary Robotics: From Algorithms to Implementations (World Scientific, 2006; Review), Neural Networks: Computational Models and Applications (Springer-Verlag, 2007), and Evolutionary Multi-objective Optimization in Uncertain Environments: Issues and Algorithms (Springer-Verlag, 2009), co-edited 4 books including Recent Advances in

V.E. Balas et al. (Eds.): Soft Computing Applications, AISC 195, pp. 7–8.
springerlink.com

Simulated Evolution and Learning (World Scientific, 2004), Evolutionary Scheduling (Springer-Verlag, 2007), Multiobjective Memetic Algorithms (Springer-Verlag, 2009), and Design and Control Of Intelligent Robotic Systems (Springer-Verlag, 2009).

Dr Tan is currently a Distinguished Lecturer of IEEE Computational Intelligence Society. He has been invited to be a keynote/invited speaker for over 25 international conferences. He served in the international program committee for over 100 conferences and involved in the organizing committee for over 30 international conferences, including the General Co-Chair for IEEE Congress on Evolutionary Computation 2007 in Singapore and the General Co-Chair for IEEE Symposium on Computational Intelligence in Scheduling in Tennessee, USA.

Dr Tan is currently the Editor-in-Chief of IEEE Computational Intelligence Magazine (5-Year IF: 4.094; IF: 2.833 –Rank 13 out of all 127 IEEE journals). He also serves as an Associate Editor / Editorial Board member of over 15 international journals, such as IEEE Transactions on Evolutionary Computation, IEEE Transactions on Computational Intelligence and AI in Games, Evolutionary Computation (MIT Press), European Journal of Operational Research, Journal of Scheduling, and International Journal of Systems Science.

Dr Tan is the awardee of the 2012 IEEE Computational Intelligence Society (CIS) Outstanding Early Career Award for his contributions to evolutionary computation in multi-objective optimization. He also received the Recognition Award (2008) from the International Network for Engineering Education & Research (iNEER) for his outstanding contributions to engineering education and research. He was also a winner of the NUS Outstanding Educator Awards (2004), the Engineering Educator Awards (2002, 2003, 2005), the Annual Teaching Excellence Awards (2002, 2003, 2004, 2005, 2006), and the Honour Roll Awards (2007). Dr Tan is currently a Fellow of the NUS Teaching Academic.

On the Applications of Fuzzy Implication Functions

Michał Baczyński

University of Silesia
Institute of Mathematics
Katowice, Poland
michal.baczynski@us.edu.pl

Abstract. Fuzzy implication functions are one of the main operations in fuzzy logic. They generalize the classical implication, which takes values in the set {0,1}, to fuzzy logic, where the truth values belong to the unit interval [0,1]. The study of this class of operations has been extensively developed in the literature in the last 30 years from both theoretical and applicational points of view.

In our talk we will concentrate on many different applications of this class of functions. Firstly we will discuss some aspects of mathematical fuzzy logic. Next we will show they role in finding solutions of different fuzzy relational equations. In the next part we present their relevance in approximate reasoning and fuzzy control. In this section we will discuss various inference schemas and we will also show some results connected with fuzzy implications, which are related with reducing the complexity of inference algorithms. In the final part of our talk we will show the importance of fuzzy implication functions in fuzzy mathematical morphology and image processing.

Michał Baczyński was born in Katowice, Poland. He received the M.Sc. and Ph.D. degrees in mathematics from the Department of Mathematics, Physics, and Chemistry, University of Silesia, Katowice, in 1995 and 2000, respectively. He received the "habilitation" degree in computer science from the Systems Research Institute, Polish Academy of Sciences, Warsaw, Poland, in 2010.

He is currently with the Institute of Mathematics, University of Silesia. He has co-authored a research monograph on Fuzzy Implications and is the author or co-author

V.E. Balas et al. (Eds.): Soft Computing Applications, AISC 195, pp. 9–10.
springerlink.com

of more than 40 published papers in refereed international journals and conferences. He has been invited to be an invited speaker for 2 international conferences, in particular at last EUSFLAT - LFA 2011 Conference in Aix-Les-Bains, France. He is also a regular reviewer for many respected international journals and a member of various committees in international conferences. His current research interests include fuzzy aggregation operations, chiefly fuzzy implications, approximate reasoning, fuzzy systems, and functional equations. Dr. Baczyński is a member of the European Society for Fuzzy Logic and Technology (EUSFLAT) and the Polish Mathematical Society (PTM).

Information Theoretic Security by the Laws of Classical Physics

(Plenary Paper)

R. Mingesz[1], L.B. Kish[2], Z. Gingl[1], C.G. Granqvist[3], H. Wen[2,4], F. Peper[5], T. Eubanks[6], and G. Schmera[7]

[1] Department of Technical Informatics, University of Szeged, Árpád tér 2, Szeged, H-6701, Hungary
{mingesz,gingl}@inf.u-szeged.hu
[2] Texas A&M University, Department of Electrical and Computer Engineering, College Station, TX 77843-3128, USA
Laszlo.Kish@ece.tamu.edu
[3] Department of Engineering Sciences, The Ångström Laboratory, Uppsala University, P.O. Box 534, SE-75121 Uppsala, Sweden
Claes-Goran.Granqvist@Angstrom.uu.se
[4] Hunan University, College of Electrical and Information Engineering, Changsha 410082, China
he_wen82@126.com
[5] National Institute of Information and Communication Technology, Kobe, Hyogo 651-2492, Japan
peper@nict.go.jp
[6] Sandia National Laboratories, P.O. Box 5800, Albuquerque, NM 87185-1033, USA
tweuban@sandia.gov
[7] Space and Naval Warfare Systems Center, San Diego, CA 92152, USA
gabe.schmera@navy.mil

Abstract. It has been shown recently that the use of two pairs of resistors with enhanced Johnson-noise and a Kirchhoff-loop—*i.e*., a Kirchhoff-Law-Johnson-Noise (KLJN) protocol—for secure key distribution leads to information theoretic security levels superior to those of a quantum key distribution, including a natural immunity against a man-in-the-middle attack. This issue is becoming particularly timely because of the recent full cracks of practical quantum communicators, as shown in numerous peer-reviewed publications. This presentation first briefly surveys the KLJN system and then discusses related, essential questions such as: what are perfect and imperfect security characteristics of key distribution, and how can these two types of securities be unconditional (or information theoretical)? Finally the presentation contains a live demonstration.

Keywords: information theoretic security, unconditional security, secure key exchange, secure key distribution, quantum encryption.

V.E. Balas et al. (Eds.): Soft Computing Applications, AISC 195, pp. 11–25.
springerlink.com

1 Introduction: Quantum Security Hacked

Practical quantum communicators—including several commercial ones—have been fully cracked, as shown in numerous recent papers [1-15], and Vadim Makarov, who is one of the leading quantum crypto crackers, says in *Nature News* that "Our hack gave 100% knowledge of the key, with zero disturbance to the system" [1]. This claim hits at the foundations of quantum encryption schemes because the basis of the security of quantum key distribution (QKD) protocols is the assumption that any eavesdropper (Eve) will disturb the system enough to be detected by the communicator parties (Alice and Bob). Furthermore this proves that we were right in 2007 when claiming in our *SPIE Newsroom* article [16] that quantum security is mainly theoretical because, at that time, no effort had been made to experimentally crack the communicators; instead research grants supported the development of new QKD schemes but not the "politically incorrect" challenge to crack them.

However, the last few years have seen a radically changed picture [1-15] on the security of practical quantum communicators, and even a full-field implementation of a perfect eavesdropper on a quantum cryptography system has been carried out [2], which is a most difficult task and is an attack on an already established "secure" QKD connection. These cracking schemes are referred to as "hacking" because they utilize physical non-idealities in the building elements of QKD devices. The number of these non-idealities is large, and so is the number of hacking types. The key lessons that has been learned here are that

(*i*) Quantum security at the moment is theoretical, and the applied theory is incorrect for practical devices; a new defense mechanism must be developed for each type of hacking attack, and the potential for yet unexplored non-idealities/ attacks is huge, and

(*ii*) Security analysis, taking into the account of the real physics of the devices, is essential when security matters.

An important aspects all these quantum attacks is the extraordinary (100%) success ratio (*i.e*., information leak) of extracting the "secure" key bits by Eve, while Alice and Bob do not have a clue that efficient eavesdropping is going on. At this point we note that this information leak was only 0.19% for the *classical* secure communication scheme we are discussing in this paper in the case of a similar situation wherein the strongest vulnerability based on physical non-idealities was used; this is discussed further below.

Inspired by these interesting developments we discuss related issues in the key exchange system of the classical physical Kirchhoff-Law-Johnson-Noise (KLJN) protocol [16]. It should be noted here that there is a general misunderstanding of the KLJN scheme among people lacking the relevant expertise in statistical physics and noise-in-circuitry, as evidenced for example in the Wikipedia entry "Kish cypher" and its "talk page" where, most of the time, both the supporters and the opponents are wrong and the debate falls very short of an objective scientific discussion (amusingly, even the name "cypher" is incorrect). Therefore, after briefly surveying the KLJN system and its properties, we clarify the meaning of *perfect security* and *imperfect*

security levels and also define the conditions of these measures: *information theoretic security* (or *unconditional security*) and its limited version *computationally unconditional security*. Furthermore we mention existing integer-number-based key exchange protocols that have (computationally) *conditional security*. It will be seen that theoretical/ideal QKD and KLJN protocols have perfect information theoretic (unconditional) security. However these schemes, when realized with practical/realistic (physical/non-ideal) building elements have imperfect security that is still information theoretic (unconditional), even though current QKD cracks [1-15] indicate that KLJN performs better.

2 The KLJN Secure Key Exchange Protocol

It is often believed that quantum physics represents modern science and that classical physics is old and outdated. Of course this is not true because the two fields rather pertain to different physical size regimes—the "small" versus the "large" where the appropriate rules of physics are different—not different periods of science history. The above claim regarding "modern" and "old" cannot be maintained even for the history of physics, though, when the point at issue concerns spontaneous random fluctuation phenomena, that are simply referred to as "noise", and it is true for even the most general and omnipresent type of classical physical noise, *viz*., thermal noise (voltage or current fluctuations in thermal equilibrium) which is a younger field of physics than quantum mechanics. Indeed two Swedish scientists, John Johnson and Harry Nyquist both working at Bell Labs, discovered/explained the thermal noise voltage of resistors [17,18] several years after the completion of the foundations of quantum physics [19].

Similarly, quantum heat engines [20] with optional internal coherence effects [21] were proposed several years earlier than the application [22] of the thermal noise of resistors for a heat engine scheme with similar coherence effects.

Finally, the application of thermal noise for unconventional informatics, namely for noise-based logic and computing [23-30] and the KJLN secure key exchange [31-46], emerged decades later than the corresponding quantum informatics schemes such as quantum computing [47] and quantum encryption [48-50].

It is interesting to not that some "exotic" phenomena previously thought to belong to the class of "quantum-weirdness" occur and can be utilized also in the noise schemes, for example: teleportation/telecloning in KLJN networks [45] and entanglement in noise-based logic [23-30].

2.1 The Kirchhoff-Law-Johnson-Noise Key Distribution[1]

The KLJN secure key exchange scheme was introduced in 2005 [31-33] and was built and demonstrated in 2007 [34]; it is founded on the robustness of classical information as well as stochasticity and the laws of classical physics. It was named by

[1] This section is a modified version of related expositions elsewhere [36,46].

its creators the "Kirchhoff-loop-Johnson(-like)-Noise" scheme, while on the internet—in blogs and similar sites, including Wikipedia—it has widely been nicknamed "Kish cypher" or "Kish cipher" (where both designations are wrong). The concept has often been misinterpreted and misjudged.

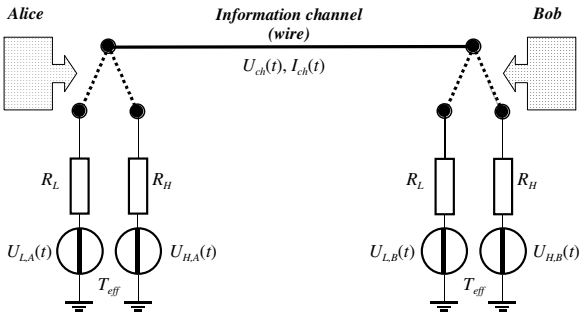

Fig. 1. Core of the KJLN secure key exchange system [31]. In the text below, the mathematical treatment is based on the power density spectra of the voltages and currents shown in the figure.

The KLJN scheme is a statistical-physical competitor to quantum communicators whose security is based on Kirchhoff's Loop Law and the Fluctuation-Dissipation Theorem. More generally, it is founded on the Second Law of Thermodynamics, which indicates that the security of the ideal scheme is as strong as the impossibility to build a perpetual motion machine of the second kind.

We first briefly survey the foundations of the KLJN system [31,33,36]. Figure 1 shows a model of the idealized KLJN scheme designed for secure key exchange [31]. The resistors R_L and R_H represent the low, *L* (0), and high, *H* (1), bits, respectively. At each clock period, Alice and Bob randomly choose one of the resistors and connect it to the wire line. The situation *LH* or *HL* represents secure bit exchange [31], because Eve cannot distinguish between them through measurements, while *LL* and *HH* are insecure. The Gaussian voltage noise generators (white noise with publicly agreed bandwidth) represent a corresponding thermal noise at a publicly agreed effective temperature T_{eff} (typically $T_{eff} > 10^9$ K [34]). According to the Fluctuation-Dissipation Theorem, the power density spectra $S_{u,L}(f)$ and $S_{u,H}(f)$ of the voltages $U_{L,A}(t)$ and $U_{L,B}(t)$ supplied by the voltage generators in R_L and R_H are given by

$$S_{u,L}(f) = 4kT_{eff}R_L \quad \text{and} \quad S_{u,H}(f) = 4kT_{eff}R_H\,, \tag{1}$$

respectively.

In the case of secure bit exchange (*i.e.*, the *LH* or *HL* situation), the power density spectrum of channel voltage $U_{ch}(t)$ and channel current $I_{ch}(t)$ are given as

$$S_{u,ch}(f) = 4kT_{eff}\,\frac{R_L R_H}{R_L + R_H}\,, \tag{2}$$

and

$$S_{i,ch}(t) = \frac{4kT_{eff}}{R_L + R_H}; \tag{3}$$

further details are given elsewhere [31,36]. It should be observed that during the *LH* or *HL* case, linear superposition turns Equation (2) into the sum of the spectra of two situations, *i.e*., when only the generator in R_L is running one gets

$$S_{L,u,ch}(f) = 4kT_{eff}R_L\left(\frac{R_H}{R_L + R_H}\right)^2 , \tag{4}$$

and when the generator in R_H is running one has

$$S_{H,u,ch}(f) = 4kT_{eff}R_H\left(\frac{R_L}{R_L + R_H}\right)^2 . \tag{5}$$

The ultimate security of the system against passive attacks is provided by the fact that the power $P_{H\to L}$, by which the Johnson noise generator of resistor R_H is heating resistor R_L, is equal to the power $P_{L\to H}$ by which the Johnson noise generator of resistor R_L is heating resistor R_H [31,36]. A proof of this can also be derived from Equation (3) for a frequency bandwidth of Δf by

$$P_{L\to H} = \frac{S_{L,u,ch}(f)\Delta f}{R_H} = 4kT_{eff}\frac{R_L R_H}{(R_L + R_H)^2} , \tag{6a}$$

and

$$P_{H\to L} = \frac{S_{H,u,ch}(f)\Delta f}{R_L} = 4kT_{eff}\frac{R_L R_H}{(R_L + R_H)^2} . \tag{6b}$$

The equality $P_{H\to L} = P_{L\to H}$ (*cf*. Equations 6) is in accordance with the Second Law of Thermodynamics; violating this equality would mean not only going against basic laws of physics and the inability to build a perpetual motion machine (of the second kind) but also allow Eve to use the voltage-current cross-correlation $\langle U_{ch}(t)I_{ch}(t)\rangle$ to extract the bit [31]. However $\langle U_{ch}(t)I_{ch}(t)\rangle = 0$, and hence Eve has an insufficient number of independent equations to determine the bit location during the *LH* or *HL* situation. The above security proof against passive (listening) attacks holds only for Gaussian noise, which has the well-known property that its power density spectrum or autocorrelation function provides the maximum information about the noise and no higher order distribution functions or other tools are able to contribute additional information.

It should be observed [31,33,34,36] that deviations from the shown circuitry—including parasitic elements, inaccuracies, non-Gaussianity of the noise, *etc*.—will cause a potential information leak toward Eve. One should note that the circuit symbol "line" in the circuitry represents an ideal wire with uniform instantaneous

voltage and current along it. Thus if the wire is so long and the frequencies are so high that waves appear in it, this situation naturally means that the actual circuitry deviates from the ideal one because neither the voltage nor the current is uniform along the line [31].

To provide unconditional security against invasive attacks, including the man-in-the-middle attack, the fully armed KLJN system shown in Figure 2 monitors the instantaneous current and voltage values at both ends (*i.e.*, for Alice as well as Bob) [33,34,36], and these values are compared either via broadcasting them or via an authenticated public channel. An alarm goes off whenever the circuitry is changed or tampered with or energy is injected into the channel. It is important to note that these current and voltage data contain all of the information Eve can possess. This implies that Alice and Bob have full knowledge about the information Eve may have; this is a particularly important property of the KLJN system, which can be utilized in secure key exchange.

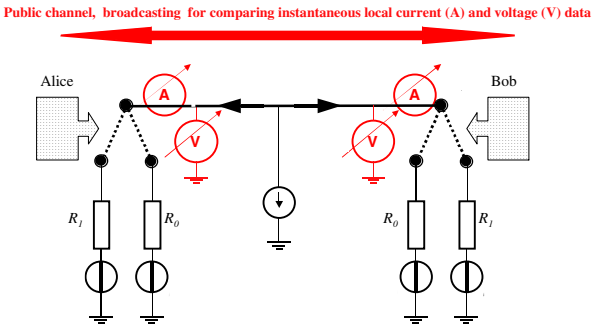

Fig. 2. Sketch of the KLJN wire communication arrangement [33,36]. To detect the invasive eavesdropper (represented, for example, by the current generator at the middle), the instantaneous current and voltage data measured at the two ends are broadcasted and compared. The eavesdropping is detected immediately, within a small fraction of the time needed to transfer a single bit. Thus statistics of bit errors is not needed, so the exchange of even a single key bit is secure.

The situation discussed above implies the following important features of the KLJN system [31,33,34,36]:

(1) In a practical (non-idealized) KLJN system, Eve can utilize device non-idealities to extract some of the information by proper measurements. This is measurement information and does not depend on Eve's computational and algorithmic ability, *i.e.*, the level of security is computationally unconditional. The maximum leak toward Eve can be designed by Alice and Bob by supposing the physically allowed best/ultimate measurement system for Eve. This designed level of security is unconditional in every sense.

(2) Even when the communication is disturbed by invasive attacks or inherent non-idealities in the KLJN arrangement, the system remains secure because no information can be eavesdropped by Eve without the full knowledge of Alice and Bob

about this potential incidence, and without the knowledge of the full information that Eve might have extracted (a full analysis of this aspect is provided elsewhere [36]).

(3) In other words, the KLJN system is always secure, even when it is built with non-ideal elements or designed for a non-zero information leak, in the following sense: The current and voltage data inform Alice and Bob about the exact information leak and hence, for each compromised key bit, they can decide to discard it or even to use it to mislead/manipulate Eve [36].

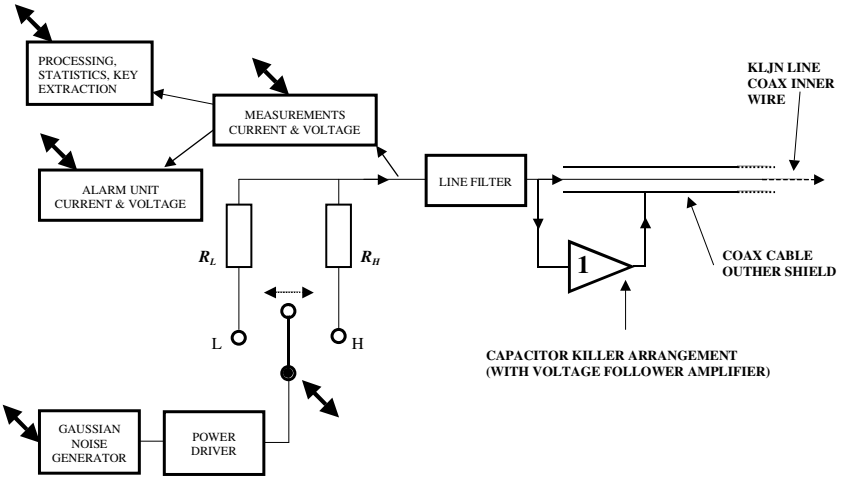

Fig. 3. A practical KLJN device set-up [34]. Double-ended arrows symbolize computer control.

(4) The KLJN arrangement is naturally and fully protected against the man-in-the-middle attack [33] even during the very first run of the operation when no hidden signatures can be applied. This feature is provided by the unique property of the KLJN system that zero bit information can only be extracted during a man-in-the-middle attack because the alarm goes off before the exchange of a single key bit has taken place [33].

(5) The security of the KLJN system is not based on the error statistics of key bits, and even the exchange of single key bits is secure.

Figure 3 outlines a prototype of the KLJN device [34]. The various non-idealities have been addressed by different tools with the aim that the information leak toward Eve due to non-idealities should stay below 1% of the exchanged raw key bits. For the KLJN device it was 0.19% for the most efficient attack [18]. Here we briefly address two aspects of non-idealities:

(*i*) The role of the line filter (and of the band limitation of the noise generator) is to provide the no-wave limit in the cable, *i.e*., to preserve the core circuitry (*cf*. Figure 1) in the whole frequency band. This implies that the shortest wavelength component in the driving noise should be much longer than twice the cable length in order to guarantee that no active wave modes and related effects (*e.g*., reflection, invasive attacks at high frequencies, *etc*.) take place in the cable.

(*ii*) Another tool to fight non-idealities is the cable capacitance compensation ("capacitor killer") arrangement (*cf.* Figure 3). With practical cable parameters and their limits, there is a more serious threat of the security: the cable capacitance shortcuts part of the noise current which results in a greater current at the side of the lower resistance end thus yields an information leak. This effect can be avoided by a cable-capacitor-killer [34] using the inner wire of a coax cable as KLJN line while the outer shield of the cable is driven by the same voltage as the inner wire. However, this is done via a follower voltage amplifier with zero output impedance. The outer shield will then provide all the capacitive currents toward the ground, and the inner wire will experience zero parasitic capacitance. Without "capacitor killer" arrangement and practical bare-wire line parameters, the recommended upper limit of cable length is much shorter and depends on the driving resistor values R_L and R_H .

2.2 Security Proofs and Attacks

The ideal system is absolutely secure, but real systems are rarely ideal and thus hacking attacks are possible by using non-idealities. Fortunately the KLJN system is very simple, implying that the number of such attacks is limited. Several hacking attack types based on the non-ideality of circuit elements causing deviations from the ideal circuitry have been published [36-42]. Each of these attacks triggered a relevant security proof that showed the efficiency of the defense mechanism (*cf.* Figure 2). Furthermore, all known attack types were experimentally tested [34], and the theoretical security proofs were experimentally confirmed.

For practical conditions, the most effective attack employed voltage-drop-related effects on non-zero wire resistance [32,37,38]. It should be noted that serious calculation errors were made by Scheuer and Yariv [37] resulting in a thousand times stronger predicted value of the effect than its real magnitude. The errors were pointed out and the calculations were corrected by Kish and Scheuer [38]. In an experimental demonstration [34], the strongest leak was indeed due to wire resistance, and 0.19% of the bits leaked out ($1.9*10^{-3}$ relative information leak) to Eve, while the fidelity of the key exchange was 99.98% (which means 0.02% bit error rate). This is a very good raw bit leak, and it can easily be made infinitesimally small by simple two-step privacy amplification, as further discussed in Section 2.3.

A general response to the mentioned and other types of small-non-ideality attacks was also presented [39], and the related information leak was shown to be miniscule due to the very poor statistics that Eve could obtain.

Other attack types of less practical significance were based on differences in noise temperatures by Hao [40], which were proven theoretically [41] and experimentally [34] insignificant. The very high accuracy of digital simulations and digital-analog converters (at least 12-bit resolution) allows setting the effective temperature so accurately (0.01% or less error) that this type of inaccuracy-based information leak is not observable. In the case of 12-bit resolution, the theoretical value of the relative information leak is $6*10^{-11}$, *i.e.*, to leak out one effective bit would require a

600 Megabit long key. Therefore this effect was not visible in the experiments even though extraordinarily long (74497) key bits were generated/exchanged in each run [34].

The practical inaccuracy of commercial low-cost resistors (1%) at the two ends [34,41] is a much more serious issue; the theoretical value is $<10^{-4}$ relative information leak (about 7 bits leak from the 74497 bit long key) for a resistance inaccuracy of 1% [34]. However, its impact was still not measurable because of the statistical inaccuracies, $\sqrt{74497} \approx 270$ bits, at this key length. These inaccuracies were about forty times greater than the theoretical information leak of 7 [34].

Wire capacitance would be the most serious source of information leak without the cable-capacitance-killer arrangement, but cable inductance effects are negligible [36].

Another attack [42] focusing on delay effects obtained 70% information leak with a wire simulation software by using physically invalid parameters, such as cable diameters being 28,000 greater than the diameter of the known universe at two km cable length (the error in this attack [42] was pointed out in a subsequent paper [36]). Although this attack was flawed, it is remarkable that even this non-existent, high information leak can be removed by a three-step privacy amplification as discussed in Section 2.3.

It is important to note that the level of allowed information leak is the choice of Alice and Bob, and its actual value is determined only by the invested resources and also typically depends on how much speed is given up. For example, the information leak due to the wire resistance scales inversely with the 4^{th} power of wire diameter, which means that employing a ten times thicker cable would reduce the relative information leak of 0.19% to $1.9*10^{-7}$.

For Eve the best attack strategy is to observe the public data exchange about the instantaneous current and voltage amplitudes between Alice and Bob. Those data contain the highest amount of eavesdropping information because they are measured in the most ideal way, and Alice and Bob also base their decision about the bit values on those. Enhancing Eve's infrastructure beyond that ability does not improve her situation, and thus the security is information theoretic/ unconditional.

2.3 Privacy Amplification in Non-ideal Systems

Privacy amplification is a classical software-based technique, which was originally developed for QKD to ensure the security of an encryption scheme with partially exposed key bits. Horvath *et al.* [43] realized simple privacy amplification by executing XOR logic operation on the subsequent pairs of the key bits, thereby halving the key length while progressively reducing the information leak. If the reduction of the information leak is not enough, the same procedure can be repeated on the new key. The resulting key length scales with 0.5^N, where N is the number of these privacy amplification steps. It was found that, in contrast to quantum key distribution schemes, the high fidelity of the raw key generated in the KLJN system allows the users to always extract a secure shorter key. The necessary conditions are sufficiently high fidelity (small bit error rate), which the KLJN provides, and an upper

limit less than one on the eavesdropper probability to correctly guess the exchanged key bits, which means the key exchange is not fully cracked (less than 100% relative information leak is present). The number of privacy amplification steps needed to achieve an information leak of less than 10^{-8} in the case of the 0.19% raw bit information leak is two, thus resulting in a corresponding slowdown by a factor of four [43]. In the case of the 70% information leak obtained by the flawed simulations in earlier work [42], the necessary number of privacy amplification steps is three thus resulting in a slowdown of a factor of eight [43].

3 Security Measures and Their Conditions

In this section we discuss security measures [52,53] and apply them to compare QKD, KLJN and software security schemes.

A *perfect security* level means that the information channel capacity of the eavesdropping-channel from Alice/Bob toward Eve is zero. *Imperfect security* level means that the information channel capacity of the eavesdropping-channel from Alice/Bob toward Eve is non-zero. We call the encryption "cracked" if Eve can extract all of the information communicated between Alice and Bob. Thus an imperfect security level does not necessarily mean that the encryption is cracked. If the bit-error-rate (BER) is negligible then, by using privacy amplification, the effective level of imperfect security can be enhanced so that it can arbitrarily approach the perfect security level.

To characterize the situations of perfect and imperfect security levels, we must address the conditions where these levels hold. Conditions that both QKD and the KLJN protocols represent are called *information theoretic security*, or *unconditional security*. We note, in passing, that these terms are often completely misunderstood by people who write into Wikipedia and to blog sites about the KLJN system, and these mistakes lead to incorrect conclusions and self-contradicting arguments.

The most rigorous security condition is *information theoretic security*, which means that the information content of the data Eve can extract is limited by information theory even if Eve is using the hypothetical most powerful processing of the extracted data. *Unconditional security* is a similar term indicating security when Eve has unlimited resources. It often means a computationally unconditional security measure, which limits the infrastructure to computers and algorithms, so it has limited validity compared to information theoretic security. Computationally unconditional security simply means that the information content of the data that Eve is able to extract is limited even if she has infinite computing power.

For example, today's generally used software algorithms utilizing prime numbers for key generation and distribution have neither information-theoretic nor computationally unconditional security. All of the information about the key exists in the data observed in the line by Eve, in a decodable form, thus it cannot be information theoretically secure. This information can be fully decoded with a sufficiently fast computer or integer-factoring algorithm, or with a normal computer running for long-enough but finite time. The security is (computationally) conditional:

it is based on the assumption that Eve does not have an efficient algorithm or a fast-enough computer to decode the key within the practically relevant time frame.

It is important to note that even imperfect security can be information theoretical or (computationally) unconditional [53]. Such a situation occurs with a physically secure key distribution only, such as QKD or KLJN, because the information leak will be determined by measurement information and not by computation or algorithmic decoding.

The way in which ideal/theoretical QKD makes the key exchange secure is based on the no-cloning theorem of quantum physics: photon states cannot be cloned without introducing errors. Because information bits are carried by (theoretically) single photons, Eve must clone the photon if she wants to measure one; otherwise the information is destroyed before reaching the receiving party. Thus Eve must clone the photon, which introduces extra errors into the line. When Alice and Bob recognize the increased bit-error-rate, they conclude that eavesdropping has happened and they discard the bit-package exhibiting the increased error rate.

The ideal QKD protects the system against eavesdropping, but this is strictly true only for an infinitely long key because Alice and Bob must prepare error statistics, and exact statistics requires infinite time. Otherwise, due to statistical fluctuations in the BER, Alice and Bob can never be absolutely sure that the key was not eavesdropped. To illustrate this problem, we can go to the simplest type of attacks: the intercept-resend attack for the BB84 QKD protocol (see, for example, [51]). The probability $P(N)$ that the eavesdropping will be discovered while Eve extracts N key bits is not 1 but

$$P_h = 1 - \left(\frac{3}{4}\right)^N \quad . \tag{7}$$

Equation (7) shows that, even though a reasonably long key will be very secure and that security can further be enhanced by privacy amplification (see above), the security is not perfect although it can arbitrarily approach the perfect security level. However, if we want to extract only a single key bit, the security is extremely poor because Eve has 25% chance to succeed.

The way by which the ideal/theoretical KLJN scheme makes the key exchange secure depends on the type of the attack: whether it is passive (listening) or invasive (introducing energy in the channel and/or modifying the channel circuitry). In the case of passive listening, information theoretic security due to zero information in the extracted data is guaranteed by the Second Law of Thermodynamics, and this is true even for single-bit attacks where QKD fails. In the case of invasive attacks, the defense mechanics is similar to that of QKD; Alice and Bob will observe deviations between instantaneous signals and they detect the presence of eavesdropping virtually immediately so that, again, even a single bit attack has no chance. Table 1 shows the summary/conclusion about the security level of various key exchange protocols.

In conclusion, the ideal KLJN protocol protects a system against invasive eavesdropping and provides zero information to passive eavesdroppers.

Table 1. Comparison of relevant security levels for existing key exchange systems. Practical physically secure key distributions can never have perfect security, they can only approach it.

	Perfect	**Imperfect**	**Information theoretic or unconditional**	**Conditional**
QKD theoretical	**Yes** for the whole key **No** for a single bit	**No** for the whole key **Yes** for a single bit	**Yes**	**No**
KLJN theoretical	**Yes** for both the whole key and a single bit	**No**	**Yes**	**No**
QKD practical	**No**	**Yes**	**Yes**	**No**
KLJN practical	**No**	**Yes**	**Yes**	**No**
Software and prime number based	**Yes**	**No**	**No**	**Yes**

Acknowledgement. LBK is grateful to Vincent Poor for a discussion about unconditional (information theoretic) security of practical secure physical systems with imperfect security. This work was partially supported by grant TAMOP-4.2.1/B-09/1/KONV-2010-0005. HW's work was partially supported by the National Natural Science Foundation of China under grant 61002035.

References

[1] Merali, Z.: Hackers blind quantum cryptographers. Nature News (August 29, 2009), doi:10.1038/news.2010.436

[2] Gerhardt, I., Liu, Q., Lamas-Linares, A., Skaar, J., Kurtsiefer, C., Makarov, V.: Full-field implementation of a perfect eavesdropper on a quantum cryptography system. Nature Communications 2 (article number 349) (2011), doi:10.1038/ncomms1348.

[3] Lydersen, L., Wiechers, C., Wittmann, C., Elser, D., Skaar, J., Makarov, V.: Hacking commercial quantum cryptography systems by tailored bright illumination. Nature Photonics 4, 686–689 (2010), doi:10.1038/NPHOTON.2010.214

[4] Gerhardt, I., Liu, Q., Lamas-Linares, A., Skaar, J., Scarani, V., Makarov, V., Kurtsiefer, C.: Experimentally faking the violation of Bell's inequalities. Phys. Rev. Lett. 107, 170404 (2011), doi:10.1103/PhysRevLett.107.170404

[5] Makarov, V., Skaar, J.: Faked states attack using detector efficiency mismatch on SARG04, phase-time, DPSK, and Ekert protocols. Quantum Information and Computation 8, 622–635 (2008)
[6] Wiechers, C., Lydersen, L., Wittmann, C., Elser, D., Skaar, J., Marquardt, C., Makarov, V., Leuchs, G.: After-gate attack on a quantum cryptosystem. New J. Phys. 13, 013043 (2011), doi:10.1088/1367-2630/13/1/013043
[7] Lydersen, L., Wiechers, C., Wittmann, C., Elser, D., Skaar, J., Makarov, V.: Thermal blinding of gated detectors in quantum cryptography. Optics Express 18, 27938–27954 (2010), doi:10.1364/OE.18.027938
[8] Jain, N., Wittmann, C., Lydersen, L., Wiechers, C., Elser, D., Marquardt, C., Makarov, V., Leuchs, G.: Device calibration impacts security of quantum key distribution. Phys. Rev. Lett. 107, 110501 (2011), doi:10.1103/PhysRevLett.107.110501
[9] Lydersen, L., Skaar, J., Makarov, V.: Tailored bright illumination attack on distributed-phase-reference protocols. J. Mod. Opt. 58, 680–685 (2011), doi:10.1080/09500340.2011.565889
[10] Lydersen, L., Akhlaghi, M.K., Majedi, A.H., Skaar, J., Makarov, V.: Controlling a superconducting nanowire single-photon detector using tailored bright illumination. New J. Phys. 13, 113042 (2011), doi:10.1088/1367-2630/13/11/113042
[11] Lydersen, L., Makarov, V., Skaar, J.: Comment on Resilience of gated avalanche photodiodes against bright illumination attacks in quantum cryptography. Appl. Phys. Lett. 99, 196101 (2011), doi:10.1063/1.3658806
[12] Sauge, S., Lydersen, L., Anisimov, A., Skaar, J., Makarov, V.: Controlling an actively-quenched single photon detector with bright light. Opt. Express 19, 23590–23600 (2011)
[13] Lydersen, L., Jain, N., Wittmann, C., Maroy, O., Skaar, J., Marquardt, C., Makarov, V., Leuchs, G.: Superlinear threshold detectors in quantum cryptography. Phys. Rev. Lett. 84, 032320 (2011), doi:10.1103/PhysRevA.84.032320
[14] Lydersen, L., Wiechers, C., Wittmann, C., Elser, D., Skaar, J., Makarov, V.: Avoiding the blinding attack in QKD; REPLY (COMMENT). Nature Photonics 4, 801 (2010), doi:10.1038/nphoton.2010.278
[15] Makarov, V.: Controlling passively quenched single photon detectors by bright light. New J. Phys. 11, 065003 (2009), doi:10.1088/1367-2630/11/6/065003
[16] Kish, L.B., Mingesz, R., Gingl, Z.: Unconditionally secure communication via wire. SPIE Newsroom (2007), doi:10.1117/2.1200709.0863
[17] Johnson, J.B.: Thermal agitation of electricity in conductors. Nature 119, 50–51 (1927)
[18] Nyquist, H.: Thermal agitation of electric charge in conductors. Phys. Rev. 32, 110–113 (1928)
[19] Born, M., Heisenberg, W., Jordan, P.: Quantum mechanics II. Z. Phys. 35, 557–615 (1926)
[20] Allahverdyan, A.E., Nieuwenhuizen, T.M.: Extraction of work from a single thermal bath in the quantum regime. Phys. Rev. Lett. 85, 1799–1802 (2000)
[21] Scully, M.O., Zubairy, M.S., Agarwal, G.S., Walther, H.: Extracting work from a single heat bath via vanishing quantum coherence. Science 299, 862–864 (2003)
[22] Kish, L.B.: Thermal noise engines. Chaos Solit. Fract. 44, 114–121 (2011), http://arxiv.org/abs/1009.5942
[23] Kish, L.B.: Noise-based logic: Binary, multi-valued, or fuzzy, with optional superposition of logic states. Phys. Lett. A 373, 911–918 (2009)
[24] Kish, L.B., Khatri, S., Sethuraman, S.: Noise-based logic hyperspace with the superposition of 2^N states in a single wire. Phys. Lett. A 373, 1928–1934 (2009)

[25] Bezrukov, S.M., Kish, L.B.: Deterministic multivalued logic scheme for information processing and routing in the brain. Phys. Lett. A 373, 2338–2342 (2009)
[26] Gingl, Z., Khatri, S., Kish, L.B.: Towards brain-inspired computing. Fluct. Noise Lett. 9, 403–412 (2010)
[27] Kish, L.B., Khatri, S., Horvath, T.: Computation using noise-based logic: Efficient string verification over a slow communication channel. Eur. J. Phys. B 79, 85–90 (2011), http://arxiv.org/abs/1005.1560
[28] Peper, F., Kish, L.B.: Instantaneous, non-squeezed, noise-based logic. Fluct. Noise Lett. 10, 231–237 (2011), http://www.worldscinet.com/fnl/10/1002/open-access/S0219477511000521.pdf
[29] Wen, H., Kish, L.B., Klappenecker, A., Peper, F.: New noise-based logic representations to avoid some problems with time complexity. Fluct. Noise Lett. (June, in press, 2012 issue), http://arxiv.org/abs/1111.3859
[30] Mullins, J.: Breaking the noise barrier. New Scientist (2780) (September 29, 2010), http://www.newscientist.com/article/mg20827801.500-breaking-the-noise-barrier.html?full=true
[31] Kish, L.B.: Totally secure classical communication utilizing Johnson(-like) noise and Kirchhoff's law. Phys. Lett. A 352, 178–182 (2006)
[32] Cho, A.: Simple noise stymie spies without quantum weirdness. Science 309, 2148 (2005), http://www.ece.tamu.edu/~noise/news_files/science_secure.pdf
[33] Kish, L.B.: Protection against the man-in-the-middle-attack for the Kirchhoff-loop-Johnson(-like)-noise cipher and expansion by voltage-based security. Fluct. Noise Lett. 6, L57–L63 (2006), http://arxiv.org/abs/physics/0512177
[34] Mingesz, R., Gingl, Z., Kish, L.B.: Johnson(-like)-noise-Kirchhoff-loop based secure classical communicator characteristics, for ranges of two to two thousand kilometers, via model-line. Phys. Lett. A 372, 978–984 (2008)
[35] Palmer, D.J.: Noise encryption keeps spooks out of the loop. New Scientist (2605), 32 (2007), http://www.newscientist.com/article/mg19426055.300-noise-keeps-spooks-out-of-the-loop.html
[36] Kish, L.B., Horvath, T.: Notes on recent approaches concerning the Kirchhoff-law-Johnson-noise-based secure key exchange. Phys. Lett. A 373, 901–904 (2009)
[37] Scheuer, J., Yariv, A.: A classical key-distribution system based on Johnson (like) noise – How secure? Phys. Lett. A 359, 737–740 (2006)
[38] Kish, L.B., Scheuer, J.: Noise in the wire: The real impact of wire resistance for the Johnson(-like) noise based secure communicator. Phys. Lett. A 374, 2140–2142 (2010)
[39] Kish, L.B.: Response to Scheuer-Yariv: A classical key-distribution system based on Johnson (like) noise – How secure? Phys. Lett. A 359, 741–744 (2006)
[40] Hao, F.: Kish's key exchange scheme is insecure. IEE Proc. Inform. Sec. 153, 141–142 (2006)
[41] Kish, L.B.: Response to Feng Hao's paper Kish's key exchange scheme is insecure. Fluct. Noise Lett. 6, C37–C41 (2006)
[42] Liu, P.L.: A new look at the classical key exchange system based on amplified Johnson noise. Phys. Lett. A 373, 901–904 (2009)
[43] Horvath, T., Kish, L.B., Scheuer, J.: Effective privacy amplification for secure classical communications. Europhys. Lett. 94, 28002 (2011), http://arxiv.org/abs/1101.4264

[44] Kish, L.B., Saidi, O.: Unconditionally secure computers, algorithms and hardware. Fluct. Noise Lett. 8, L95–L98 (2008)
[45] Kish, L.B., Mingesz, R.: Totally secure classical networks with multipoint telecloning (teleportation) of classical bits through loops with Johnson-like noise. Fluct. Noise Lett. 21, C9-C21 (2006)
[46] Kish, L.B., Peper, F.: Information networks secured by the laws of physics. IEICE Trans. Commun. E95-B, 1501–1507 (2012)
[47] http://en.wikipedia.org/wiki/Quantumcomputer
[48] Wiesner, S.: Conjugate coding. SIGACT News 15, 78–88 (1983)
[49] Bennett, C.H., Brassard, G.: Quantum cryptography and its application to provably secure key expansion, public-key distribution, and coin-tossing. In: Proc. IEEE Internat. Symp. Inform. Theor., St-Jovite, Canada, p. 91 (1983)
[50] Brassard, G.: Brief history of quantum cryptography: A personal perspective. In: Proc. IEEE Information Theory Workshop on Theory and Practice in Information Theoretic Security, Awaji Island, Japan, pp. 19–23 (2005), http://arxiv.org/abs/quant-ph/0604072
[51] Xu, F., Qi, B., Lo, H.K.: Experimental demonstration of phase-remapping attack in a practical quantum key distribution system. New J. Phys. 12, 113026 (2010), http://arxiv.org/abs/1005.2376
[52] Liang, Y., Poor, H.V., Shamai, S.: Information Theoretic Security. Foundations and Trends in Communications and Information Theory 5, 355–580 (2008), doi:10.1561/0100000036
[53] Vincent Poor, private communications

The Biometric Menagerie – A Fuzzy and Inconsistent Concept

Nicolaie Popescu-Bodorin[1], Valentina Emilia Balas[2], and Iulia Maria Motoc[1]

[1] Artificial Intelligence & Computational Logic Lab.,
Mathematics & Computer Science Department,
Spiru Haret University, Bucharest Romania
{bodorin,motoc}@irisbiometrics.org
[2] Automatics and Applied Software Department,
Faculty of Engineering, Aurel Vlaicu University,
Arad, Romania
balas@drbalas.ro

Abstract. This paper proves that in iris recognition, the concepts of *sheep*, *goats*, *lambs* and *wolves* - as proposed by Doddington and Yager in the so-called Biometric Menagerie, are at most fuzzy and at least not quite well defined. They depend not only on the users or on their biometric templates, but also on the parameters that calibrate the iris recognition system. This paper shows that, in the case of iris recognition, the extensions of these concepts have very unsharp and unstable (non-stationary) boundaries. The membership of a user to these categories is more often expressed as a degree (as a fuzzy value) rather than as a crisp value. Moreover, they are defined by fuzzy Sugeno rules instead of classical (crisp) definitions. For these reasons, we said that the Biometric Menagerie proposed by Doddington and Yager could be at most a fuzzy concept of biometry, but even this status is conditioned by improving its definition. All of these facts are confirmed experimentally in a series of 12 exhaustive iris recognition tests undertaken for University of Bath Iris Image Database while using three different iris code dimensions (256x16, 128x8 and 64x4), two different iris texture encoders (Log-Gabor and Haar-Hilbert) and two different types of safety models.

Keywords: iris recognition, fuzzy, inconsistent, biometric menagerie.

1 Introduction

While working around speech recognition, Doddington et al. introduced in [2] four concepts reflecting four types of users: *sheep*, *goats*, *lambs* and *wolves* – which together form the so-called Biometric Menagerie. The second section of this paper presents an objective critique of this concept.

As far as we know, in 2010, N. Yager et al. [12] generalized Doddington's classification (also known as Doddington's zoo) for all fields of biometrics. Since then, just two papers investigating the presence of sheep, goats, lambs and wolves in certain benchmark databases have been published.

V.E. Balas et al. (Eds.): Soft Computing Applications, AISC 195, pp. 27–43.
springerlink.com

After [7] and [4], this is the third paper that analyses the partitioning of the iris code space extracted for a certain database (University of Bath Iris Image Database, UBIID, [10] – in our case) as a Fuzzy Biometric Menagerie showing that the extensions of the concepts *wolf*, *lambs*, *sheep* and *goats* have very unsharp and unstable (non stationary) boundaries. Moreover, the membership of a user to these categories can be more often expressed as a degree (as a fuzzy value) rather than as a crisp value. The fact that the Biometric Menagerie could be a fuzzy concept is confirmed experimentally here in a series of 12 exhaustive iris recognition tests undertaken for UBIID [10] by using three different iris code dimensions (256x16, 128x8 and 64x4), two different iris texture encoders (Log-Gabor and Haar-Hilbert [6]) and two different types of safety models [8]. All of these tests illustrate that the partitioning of template-space accordingly to the fuzzy concepts *wolves*, *lambs*, *sheep*, and *goats* depends not only on the users or on their biometric templates, but also on the parameters that calibrate the iris recognition system – fact which is also confirmed in [3] for a different iris image database (Iris Challenge Evaluation, [3]).

2 'Biometric Menagerie' in Iris Recognition. Open Problems and Contradictory Issues

Doddington et al. [2] and Yager et al. [12] defined the concepts of *sheep-user*, *goat-user*, *lamb-user* and *wolf-user* as follows:

Definition 1 (Yager, [12]):

- The *sheep* are those users for which the similarity score is high for genuine comparisons and low for imposter comparisons;
- The *goats* are those users which, most of the time, obtain low similarity scores for genuine comparisons;
- The *lambs* are those users easy to imitate (by *wolves*) and for which the similarity score for imposter comparison can be relatively high.
- The *wolves* are those users particularly good at impersonating other users (or in other words, as Yager said, the *wolves* "prey upon *lambs*" [12]) obtaining relatively high similarity scores for imposter comparison between them and the lambs.

2.1 Classifying Users vs Classifying Templates

Firstly, anyone should remark (we certainly did it) that classifying users in the first place is not necessarily a very good idea, simply because, any claimed relation that possibly hold two users or more is caused by something that happens with certain binary biometric templates stored in the system on their name. What happens with the templates determines what happens with the users, not vice versa. Hence, in any biometric system (including those based on iris recognition), the natural approach to classifying users goes through classifying biometric templates (through classifying iris codes - in our particular case). Therefore, a correct foundation for a hypothetically objective model called Biometric Menagerie should start with defining the *'animals'* [12] by analyzing their hypostases, i.e. in terms of biometric templates:

Definition 2:

- The *sheep-templates* are those for which the similarity scores associated to their genuine comparisons are *high enough* and the similarity scores associated to their imposter comparisons are *low enough* such that a safety threshold or a safety interval to separate the two distributions of genuine and imposter scores computed for them;
- The *goat-templates* are those that, *most of the time* or *too often*, obtain low similarity scores for their genuine comparisons;
- The *lamb-templates* are those *easy to imitate* (by wolves) and for which the similarity scores associated to their imposter comparisons can be relatively high;
- The *wolf-templates* are those particularly good at matching lamb-templates, obtaining *relatively high* similarity scores for imposter comparison between them and their pray (lamb-templates);
- *Biometric Menagerie* is a partitioning of biometric template space into the four classes defined above.

2.2 Fuzzy Biometric Menagerie vs System Calibration

Secondly, even admitting the fact that Biometric Menagerie is a well-defined concept, all conditions expressed in the above two definitions are rather fuzzy if-then Sugeno rules [11] than regular conditions of a classical definition – i.e. conditions on *genus and differentia* that do not contain fuzzy elements. More precisely, both definitions are intensional, the genus being the space of biometric templates, whereas a fuzzy rule declares the differentia. Therefore, there is no doubt that Biometric Menagerie is a fuzzy partitioning of the biometric templates space in sub-classes defined as extensions of the fuzzy concepts (pre-images of the fuzzy labels) sheep, goats, lambs and wolves, regardless the fact that it could refer to users or to biometric templates. As an example, let us formalize one condition of the second definition as a fuzzy if-then Sugeno rule:

IF: [T is a biometric template associated to *high* genuine scores and *low* imposter scores] THEN: [T is a sheep-template]

whose structure is similar to that of a linguistic control rule [11] describing a multi-input & single-output system:

IF: [X is *f-label-1* and Y is *f-label-2*] THEN: [Z is *f-label-3*.]

As seen above, the concept of sheep-template is fuzzy and so it is the entire Biometric Menagerie. Despite the fact that the genus of sheep-template is a crisp set, is the fuzzy rule from above that declares the differentia using the fuzzy linguistic labels *'high'* and *'low'* whose possible quantitative semantics correspond to a choice of some underlying fuzzy sets associated with some membership functions. Someone must

choose a numerical interpretation of what it means to be *high* as a genuine score and *low* as an imposter score, operation usually referred to as a part of calibrating the biometric system. Therefore, our first hunch (now partially validated through experimental work) was that the Biometric Menagerie is rather depending on the calibration of biometric system than being an objective concept, well defined and applicable in general for the users that pass through different single-biometric systems that use the same biometric trait (iris, face, fingerprint, palm-vein, etc.).

2.3 From Partitioning Templates to Partitioning Users

Let us assume that in an iris recognition system we need to define a partitioning of the users according to what happens with their biometric templates. For example, we could consider the case in which a user U_1 posses a template T_1 that candidates for the role of being a wolf-template by obtaining six imposter similarity scores high enough to generate six false accepts with six different users. In the same system, a user U_2 posses the templates T_2^1, T_2^2, T_2^3, each of them obtaining two imposter similarity scores high enough such that together they generate the same number of six false accepts with six different users. As seen in our example, detecting a wolf-user could be a problem of finding a group of template-wolves that together satisfy some conditions. The question is which one of those two users is a wolf-user. The answer hardly depends on a convention that the system use for qualifying users as wolves based on what happens with their templates (taken individually or as a group). At least because it relies on the detection of some wolf-templates - detection done by following a fuzzy rule (as described above), such a convention is a fuzzy if-then rule also:

IF:	for the user U there is a group G of its templates satisfying a *well chosen* f-convention *FC*	THEN:	U is a *wolf-user*

Hence, in the rule described above, besides the fact that the detection of the individual wolf-templates is fuzzy, there are two additional degrees of freedom for interpreting the fuzzy labels *"well chosen"* and *"FC"*. This fact makes the process of identifying the wolf-users even fuzzier and more subjective than the process of finding wolf-templates. Consequently, the concept of Biometric Menagerie as introduced by Doddington et al. in [2] and Yager et al. in [12] and even the concept of Biometric Menagerie discussed here in definition 2 are all fuzzy and subjective concepts, regardless if they consist in partitioning users or templates.

The fact itself that the process of partitioning the users or the templates in a Biometric Menagerie is a fuzzy one cannot be negatively connotated by default, excepting, of course, the cases in which there is not enough cointension between this artificial partitioning and the natural tendency of grouping that users actually have in reality. Unfortunately, this is exactly the case here, as shown below.

Biometric recognition is a diachronic process and therefore the basic vocabulary of any recognition theory should refer user instances, i.e. pairs (U, t) where U is a user and t is a time.

A recognition theory is logically consistent if and only if, regardless the time values t_1 and t_2, the similarity $(U_1, t_1) \equiv (U_2, t_2)$ certainly take place only for the same user $U_1 = U_2$. In other words, all users enrolled in the system diachronically generate a

set of genuine comparisons that posses the pattern (U, t_1)-to-(U, t_2) and a set of imposter comparisons that also share a common pattern (U_1, t)-to-(U_2, τ) with $U_1 \neq U_2$ (the relation between t and τ having no importance in this case). Hence, the natural tendency of grouping that user instances actually have points out to only two classes, not to four classes – as the Biometric Menagerie has.

The situation described above is an important example illustrating that *fuzzy* could sometimes mean *logically inconsistent*, such is the case of artificial partitioning of the users in a Biometric Menagerie with four fuzzy classes, while the natural tendency of grouping that the users actually have in a consistent theory of recognition point out to a binary classification.

2.4 FBM vs. Iris Codes Space Homogeneity

According to the above definitions, the wolves are those users (proved or suspected – depending on how accurate the wolf definition actually is) responsible for much of the False Accept Rate (FAR), whereas the goats are the users responsible for much of the False Reject Rate (FRR). This is why the current paper gives a special attention to these two categories of users.

However, right from this moment it is very clear that accepting the above definitions would mean to accept that some users would be somehow special (more special than others) and therefore, some elements of the iris code space would be somehow more special than others, hence, the question if the iris code space is homogeneous or heterogeneous would certainly appear.

A thing to know for sure is if the iris code space actually is homogeneous or not. We believe it is. The situation described above is a classical kind of example illustrating that when adding something that initially appears inoffensive to a model (like a classification of users – in the current case) actually blows up the foundations of the model by introducing the contradiction in its logic. Let us assume that the iris code space is heterogeneous (i.e. it supports the definition 2) and that the partitioning of iris codes space is cointensive with a corresponding partitioning of user space, which consequently is heterogeneous on its turn. Can anybody tell us what makes the user space heterogeneous in the first place?

In a lottery, many players can win the minor prizes by partially matching the official extracted variant. Hence, we could say that the extracted variant is a wolf hunting on lambs (the winners of the minor prizes). We could say, but we do not say that. Nothing aggregates the group of these winners together, except the pure chance. In the same manner, the odds produce the matching between one specific iris code and many others purely by chance, meaning that the iris code space is locally too agglomerated and this agglomeration could become homogeneously present in the iris code space. The solution is not to invent wolves and lambs, but to recalibrate the system by increasing the power of discrimination between the future biometric templates.

2.5 FBM vs. Similarity Score Symmetry

The fact that Biometric Menagerie is fuzzy (regardless it refers to users or templates) is not the worst thing in the world. The real problem is that it is not objective. In order to prove that, let us comment the wolf-lamb relation.

According to Yager et al. [12], wolf-lambs relation is one-to-many, one wolf taking many lambs. However, in a biometric system in which the relation between users (between templates) is symmetric (why should not be?), if the user U_1 (the template T_1) impersonates the user U_2 (the template T_2), it is equally true that the user U_2 (the template T_2) impersonates the user U_1 (the template T_1), also. Therefore, it is not clear at all who is the hunter and who is hunted. Someone has chosen to say that, most probably (according to some experiences), the wolves take many lambs. Our question is: what if, actually, *many wolves target the same lamb*.

The situation described above allows us to say that denoting some users (templates) as wolves and others as lambs is a pure subjective convention which really affects the objectivity of Biometric Menagerie as a concept.

3 Experimental Results

This section presents the results of 12 exhaustive iris recognition tests, undertaken on the database [10], using iris codes of dimensions 256x16, 128x8 and 64x4.

All tests use the second version of Circular Fuzzy Iris Segmentation procedure (CFIS2, proposed in [5], available for download in [7]), the iris segments being further normalized to the appropriate dimension and encoded as binary iris codes by using Haar-Hilbert [6] and Log-Gabor [6] texture encoders. Each comparison between iris codes results in a matching score computed as Hamming similarity (unitary complement of Hamming distance). For each test, all-to-all comparisons result in similarity scores further interpreted as being *low* or *high* enough to motivate a biometric decision accordingly to the following two fuzzy if-then Sugeno [11] rules:

IF:	MS(C) is *low*	THEN:	C is (an) *imposter comparison*
IF:	MS(C) is *high*	THEN:	C is (a) *genuine comparison*

where MS is the matching score and C is a comparison.

3.1 Two Paradigms of Test Scenarios

For each test, the precisiation of the security model assumes the deffuzification of the fuzzy labels *'low'* and *'high'* as intervals situated on the left and right sides relative to a threshold value identified as the abscise of the EER point:

$$t_{EER} = (FAR^{-1}(EER) = FRR^{-1}(EER)),$$

or either relative to a safety interval initialized and determined maximally by the minimum Genuine Score (mGS) and the Maximum Imposter Score (MIS), and further decreased iteratively until the extensions of the f-concepts *'wolf'* and *'lamb'* become populated with some examples of wolf- and lamb-templates, respectively. For a given calibration of the recognition system established in terms of segmentation, normalization and encoding procedures, the safety model corresponding to the second case described above (that using a safety interval) is described by the following fuzzy 3-valent disambiguated model:

IF:	MS(C) is *under* the safety band	THEN:	C is an *imposter comparison*
IF:	MS(C) is *within* the safety band	THEN:	C is *undecidable*
IF:	MS(C) is *above* the safety band	THEN:	C is a *genuine comparison*

3.2 The Dynamics of FBM. The First and the Last Wolves and Goats

If the safety band is maximal - i.e. the safety band is the interval [mGS, MIS], all the comparisons within MS^{-1}([mGS, MIS]) are undecidable and therefore there are no wolfs, no lambs and no goats in the system, all users and templates qualifying as sheep. When the safety band narrows from both sides toward the threshold corresponding to the experimentally determined EER point, the examples of wolf-, lamb- and goat-templates slightly came into view. For this reason, we called these kind of templates *marginal wolf-*, *lamb-* and *goat-templates*. They are the first wolves, lambs and goats that appear in the system when the level of security decreases from the maximal safety band toward the threshold t_{EER}. The idea of searching for wolves and goats while the safety band narrows toward t_{EER} allow us to analyze the dynamics of Biometric Menagerie along the process of decreasing the safety level in a balanced manner that negotiates between false accepts and false rejects. Besides, in order to compare the partitioning of the users/templates in two different iris recognition systems, it was necessary to identify functioning regimes in which the two systems are objectively comparable. We found two functioning regimes of this kind: one identified through the maximal safety band [mGS, MIS] and other identified through t_{EER}. These two functioning regimes are the extreme cases between which anyone can study the variability of Biometric Menagerie while the safety band converges to t_{EER} through hypostases that balance the FAR-FRR risks. Safety band hypostases together simulate a family of decreasing nested Cantor intervals allowing us to see the stabilization of the Biometric Menagerie as a process of convergence, along which different iris recognition system are comparable. The last interval of this family is the smallest (first) in the order of inclusion and the last in the order given by the balanced risks assumed in the system. For this reason, we called the members of Biometric Menagerie detected when the system runs at EER, as being the last ones (*last wolf-, lamb- and goat-templates*). They are the last detected of their kind when system security falls in a balanced manner to the EER. All of these things allow us to state the following definition:

Definition 3: Let us consider an iris recognition system in which the score distributions overlap each other. Then:

- the *first wolf-, lamb- and goat-templates* are those detected when the system is running at the security level given by the first fuzzy 3-valent disambiguated model [8] in which they appear when the maximal safety band [mGS, MIS] narrows to t_{EER} such that to keep FAR-FRR risks balanced.
- the *last wolf-, lamb- and goat-templates* are those detected when the system is running at EER (i.e. the system is running on that safety threshold which balances the FAR-FRR risks).

3.3 Two Series of Tests

The first series of six tests aims to identify the indices of the *first wolf* and *goat-templates* detected when running the system with different encoders (Haar-Hilbert and Log-Gabor), with different iris code dimensions (256x16, 128x8, 64x4), at a high security level given by that safety band who allows the wolves and the goats to appear in the system. Table 1 shows the values determining the safety bands detected for each of these tests.

Table 1. The safety bands and their width for the first series of six all-to-all iris recognition tests

	Iris code dimension	64x4	128x8	256x16
Log-Gabor encoder	Safety band	[0.6003, 0.9075]	[0.6277, 0.6555]	[0.5566, 0.5757]
	Width	0.3072	0.0278	0.0191
Haar-Hilbert encoder	Safety Band	[0.6091, 0.6722]	[0.5456, 0.6823]	[0.5224, 0.5467]
	Width	0.0631	0.1367	0.0243

The second series of six tests has the same purposes as the first one, but each time the system is running at a maximally acceptable balanced degradation of the security level given by functioning at EER threshold (t_{EER}). Table 2 shows the values determining the safety bands detected for each of these tests.

Table 2. The EER and t_{EER} for the second series of six all-to-all iris recognition tests

	Iris code dimension	64x4	128x8	256x16
Log-Gabor encoder	EER	4.08E-2	9.37E-4	6.03E-4
	t_{EER}	0.7529	0.6392	0.5686
Haar-Hilbert encoder	EER	8.60E-3	1.70E-3	2.30E-3
	t_{EER}	0.6471	0.5765	0.5490

As seen in Table 2, accordingly to the EER criterion, the best calibration of the iris recognition system is that one using iris segments of dimension 256x16 and based on Log-Gabor encoder (EER = 6.0265E-4).

Also, the best calibration presented in Table 1 is that one having the smallest overlapping between the two score distributions, namely that one using iris segments of dimension 256x16 and based on Log-Gabor encoder (for which the amplitude of the overlapping is 0.0191).

3.4 Detecting the Marginal Wolf and Goat Templates

We recall that the safety bands used in the first series of six iris recognition tests are adaptively determined by narrowing the maximal safety band [mGS, MIS] toward t_{EER} while keeping the FAR-FRR risks balanced, until some examples of wolf and goat templates appear in the system (ensuring that the extensions of the corresponding concepts are not empty). Hence, each test results in a set containing the *first* (the *marginal*) *goat-* and *wolf-templates* corresponding to a given calibration of the biometric system in terms of encoder and iris code size.

Fig. 1 illustrates the fact that although the iris code dimension increases, the number of impersonations oscillates when using Log-Gabor encoder, and increases when using Haar-Hilbert encoder. As seen by comparing Fig. 1.a and Fig. 1.b (both of them obtained for the iris codes of dimension 64x4), the number of cases of impersonation was higher for the wolf-template obtained for Haar-Hilbert encoder than the one obtained for Log-Gabor encoder.

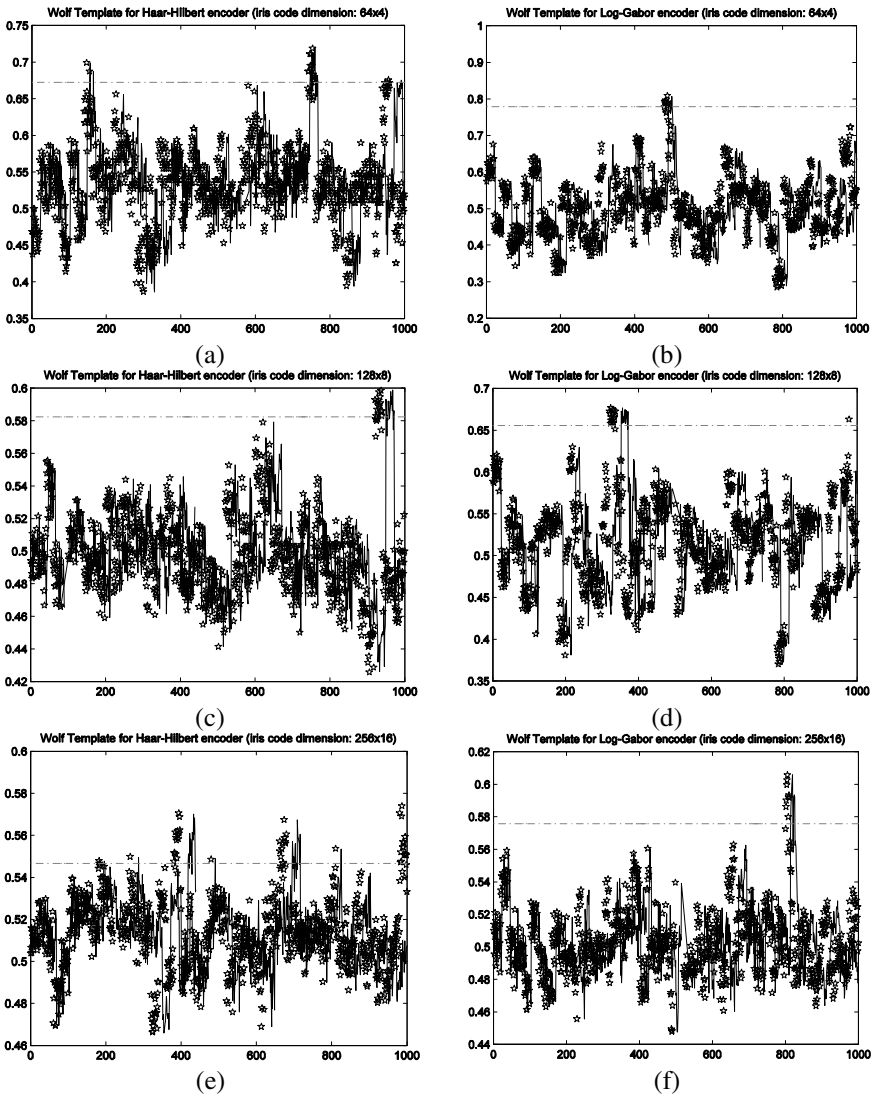

Fig. 1. The *marginal wolf-templates* obtained for Haar-Hilbert (64x4 – a, 128x8 – c, 256x16 – e) and Log-Gabor (64x4 – b, 128x8 – d, 256x16 – f) encoders

Table 3. The *marginal wolf-/goat-templates* obtained by finding the corresponding safety band

	Iris code dimension Template type	64x4 Wolf | Goat	128x8 Wolf | Goat	256x16 Wolf | Goat
Log-Gabor encoder	Number of comparisons	7 | 4	17 | 3	9 | 3
	Template's index	**334 | 496**	**484 | 475**	**505 | 565**
Haar-Hilbert encoder	Number of comparisons	15 | 3	15 | 3	46 | 4
	Template's index	**549 | 565**	**88 | 565**	**236 | 565**

For iris codes of dimension 128x8 (Fig. 1.c and Fig. 1.d), the number of impersonations obtained when using Haar-Hilbert encoder is smaller that when using Log-Gabor encoder. For iris code of dimension 256x16, the Haar-Hilbert encoder obtained the greatest number of impersonations, as we can observe also by comparing the behavior of the wolf templates represented in Fig. 1.e and Fig. 1.f.

Table 3 presents the results obtained in these six tests performed to find the *marginal wolf-templates*. As seen in Table 3, each test points out to a different *marginal wolf-template* (which is an experimental result that agrees to those presented in [4] for the wolves detected in ICE database [3]).

The number of (qualifying) comparisons recorded in Table 3 must be interpreted differently according to the type of determination that it is linked to: for a wolf it represents the number of false accepts, whereas for a goat it represents the number of false rejects. For example: when using Log-Gabor encoder to generate iris codes of dimension 64x4, the detected *marginal wolf-template* is 334 and it generates 7 cases of impersonation, whereas in the same conditions the *marginal goat-template* is 496 and it generates 4 cases of false reject. What is spectacular in the Table 3 in the first place is that the *marginal goat-template* 496 (Log-Gabor, 64x4) and the *marginal wolf-template* 484 (Log-Gabor, 128x8) point out to the same eye, namely the 25th eye, i.e. the left eye of the 13th user from the database UBIID, [10]. Section 2.3 illustrated the fact that trying to qualify users as wolves or goats based on what happens with their template is not quite a simple and evident task. The situation described here reveals an additional degree of difficulty to the same problem, also. Based on the data reported in Table 3, is the left eye of 13th user a wolf, a goat or both? This aspect is also a facet of the inconsistency of Biometric Menagerie as a concept.

Fig. 2 illustrates that along with the increasing of the iris code dimension the number of rejections decreases for Log-Gabor encoder and increases for Haar-Hilbert encoder. In each graphic, we drawn the left limit of the safety band (dotted line) and the minimum genuine score (dashed line) obtained for the corresponding *marginal goat template*. Fig. 2.a and Fig. 2.b present the behavior of the *marginal goat-templates* obtained for iris codes of dimension 64x4. The template obtained for Log-Gabor encoder has a bigger number of rejections than the one resulted for Haar-Hilbert encoder. On the contrary, the numbers of rejections for the templates represented in Fig. 2.c and Fig. 2.d are the same for both encoders.

As seen in Fig. 2.e and Fig. 2.f, there are more cases of false reject for the *marginal goat-template* obtained with Haar-Hilbert encoder than for the one obtained with Log-Gabor encoder.

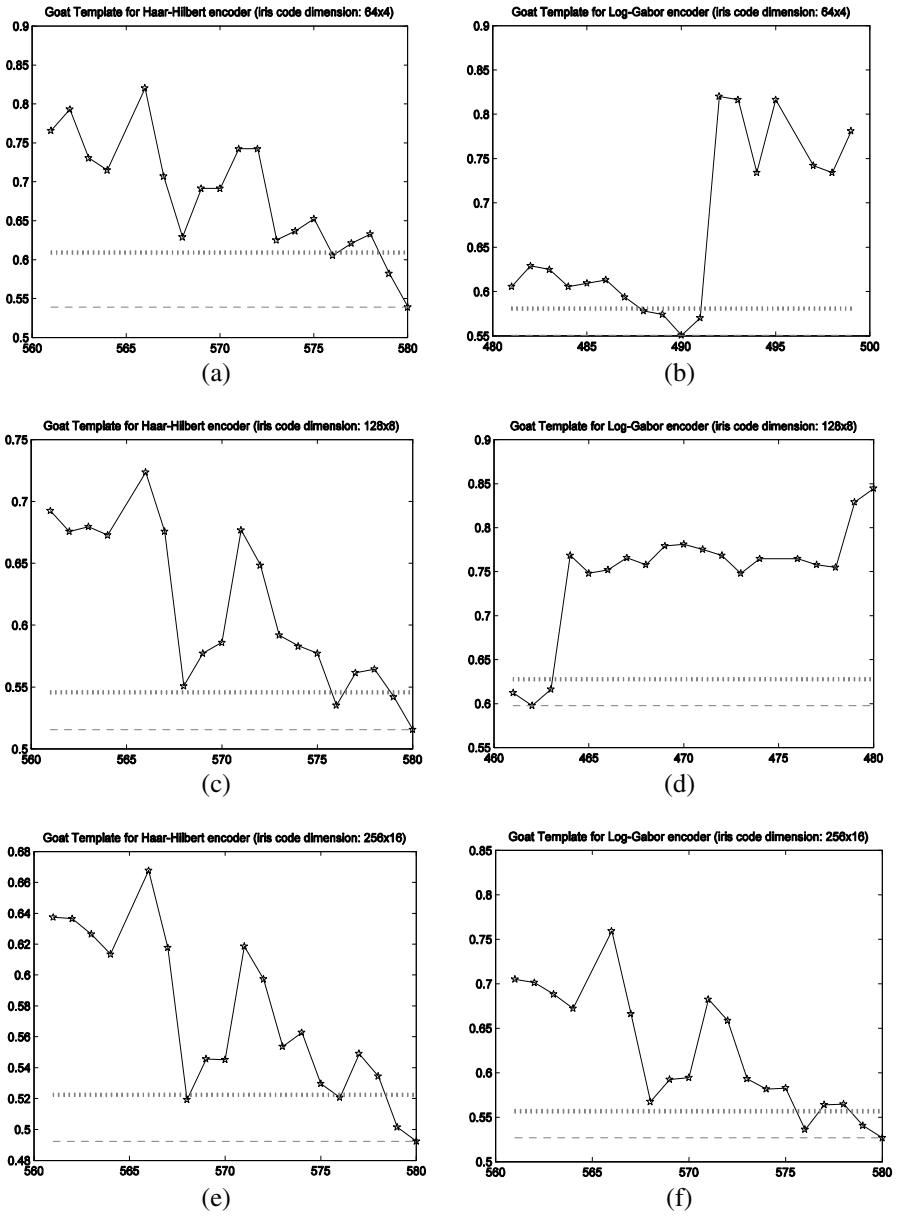

Fig. 2. The *marginal goat-templates* obtained for Haar-Hilbert (64x4 – a, 128x8 – c, 256x16 – e) and Log-Gabor (64x4 – b, 128x8 – d, 256x16 – f) encoders

Let us comment another remarkable thing seen in the same Table 3: the *marginal goat-template* obtained for Haar-Hilbert encoder was the same in all three tests. Moreover, it is the *last goat-template* obtained for the same encoder (see Table 4, from below). This situation suggests that the concept of *'goat-template' could* be an objective concept (in certain conditions) unifying the concepts of *first* (*marginal*) and *last goat-templates* by actually depending much on the encoded iris segment and less on the size of the template. The third notable thing visible in Table 3 is that the *marginal wolf-templates* obtained for the six tests were not only different, but also came from different eyes (users). Different iris recognition systems can perceive differently the *marginal wolf-templates*, and consequently, the concept of *marginal wolf-template* is certainly far from being objective.

3.5 Detecting the Last Wolf and Goat Templates at t_{EER}

We recall that the safety levels corresponding to the second series of six exhaustive all-to-all iris recognition tests (further presented here) are those given by running the recognition system at EER threshold t_{EER}. Hence, according to the definition 2, each of these tests results in a set containing the *last goat-* and *wolf-templates* corresponding to a given calibration of the biometric system in terms of encoder and iris code size.

Fig. 3 presents the similarity scores obtained by the *last wolf-templates* mentioned in Table 4 and detected in this second series of tests.

Table 4. The *last wolf-/goat-templates* obtained by running the system at t_{EER}

	Iris code dimension Template type	64x4 Wolf | Goat	128x8 Wolf | Goat	256x16 Wolf | Goat
Log-Gabor encoder	Number of comparisons	63 | 11	22 | 4	14 | 5
	Template's index	**236 | 493**	**392 | 462**	**236 | 565**
Haar-Hilbert encoder	Number of comparisons	43 | 8	19 | 6	40 | 9
	Template's index	**549 | 565**	**88 | 565**	**236 | 565**

Table 5. The cumulative results of the two series of all-to-all exhaustive iris recognition tests (on UBIID, [10]) expressed in terms of *first* and *last goat- and wolf-templates*

Calibration	Goats		Wolves	
	First (Marginal)	Last	First	Last
LG, 64x4	496	493	334	236
LG, 128x8	475	462	484	392
LG, 256x16	565	565	505	236
HH, 64x4	565	565	549	549
HH, 128x8	565	565	88	88
HH, 256x16	565	565	236	236

Table 6. The cumulative results of the two series of all-to-all exhaustive iris recognition tests (on UBIID, [10]) expressed in terms of *possible first* and *last goat- and wolf-users*

Calibration	Goats		Wolves	
	First (Marginal)	Last	First	Last
LG, 64x4	25	25	17	12
LG, 128x8	24	24	25	20
LG, 256x16	28	28	26	12
HH, 64x4	29	29	23	23
HH, 128x8	29	29	5	5
HH, 256x16	29	29	12	12

As in the previously discussed case of *marginal wolf-templates*, it is visible in Table 4 that the *last wolf-templates* obtained for the six tests were not only different, but also came from different eyes (users). Different iris recognition systems can perceive differently the *last wolf-templates*, and consequently, the concept of *last wolf-template* is far from being objective.

However, there are three different tests pointing out to the template no. 236 (see Table 4) as a *last wolf-template*. Still, this fact alone is not enough for qualifying the concept as being objective. Its extension is strongly dependent on system calibration variables such as the iris code dimension and the texture encoder.

Fig. 4 represents the similarity scores corresponding to the genuine comparisons generated by the *last goat-templates* obtained from the tests that use Haar-Hilbert and Log-Gabor encoders. It illustrates the fact that along with the increasing size of the iris code, the number of false rejects could decrease sometimes.

Table 5 and Table 6 illustrate the cumulative results of the two series of all-to-all exhaustive iris recognition tests (on UBIID, [10]) expressed in terms of *first* and *last goat-* and *wolf-templates* (Table 5), and in terms of *possible first* and *last goat-* and *wolf-users* (Table 6). We said "possible first and last goat- and wolf-users" because, as seen in Section 2.3, the process of identifying the wolf-users is even fuzzier and more subjective than the process of finding wolf-templates (there is not an unique rule that could qualify users as wolves based on what is happening with their templates). Specifically, the if-then fuzzy rule used here for this purpose is simple as follows:

IF: U *posses a wolf-/goat-template* THEN: U is a *wolf-/goat-user.*

The data within Table 5 generate the data within Table 6 by applying the above if-then fuzzy rule. The data within both tables allow us to conclude that the goat is the most objective concept of the Fuzzy Biometric Menagerie and Haar-Hilbert encoder is more objective than Log-Gabor encoder.

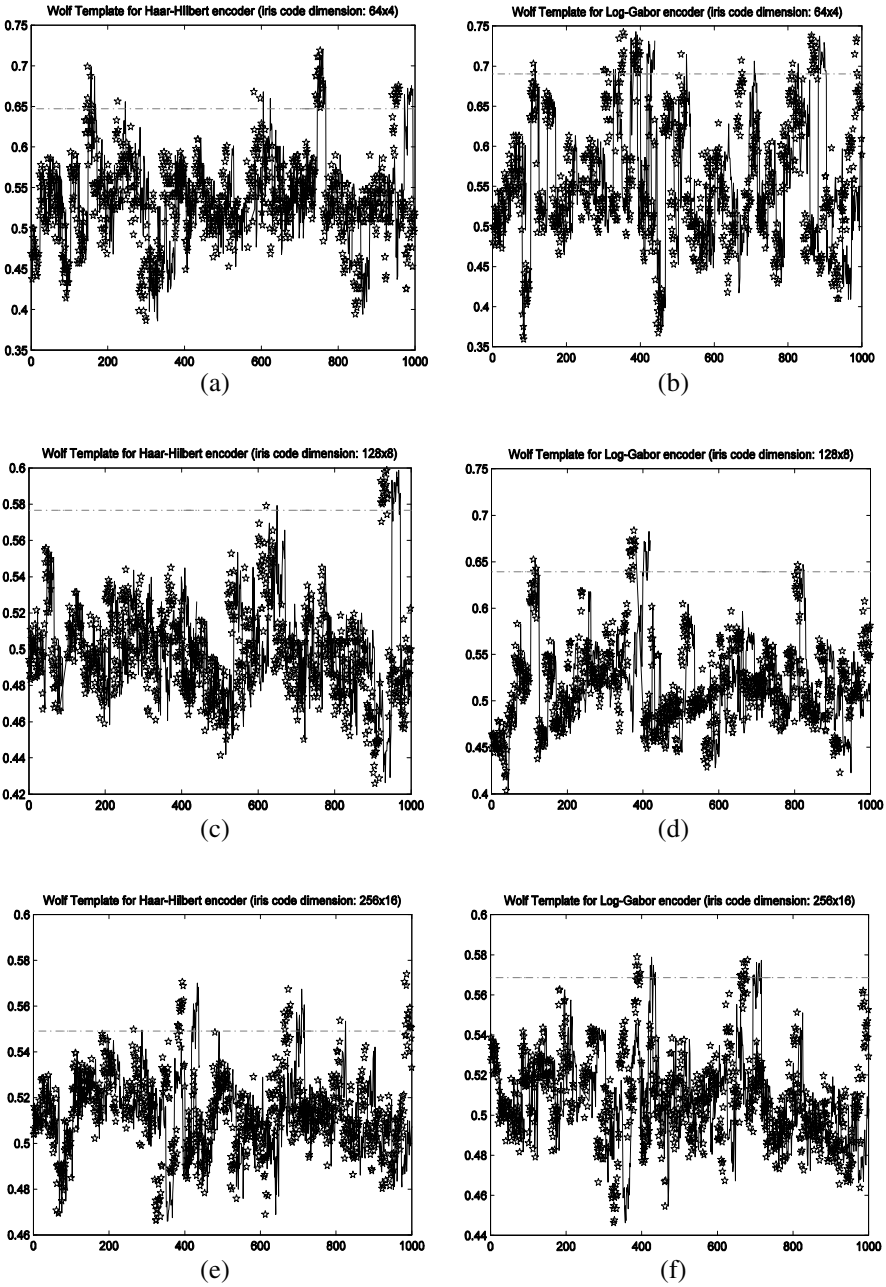

Fig. 3. The similarity scores corresponding to the imposter comparisons generated by the *last wolf-templates* obtained for Haar-Hilbert (64x4 – a, 128x8 – c, 256x16 – e) and Log-Gabor (64x4 – b, 128x8 – d, 256x16 – f) encoders

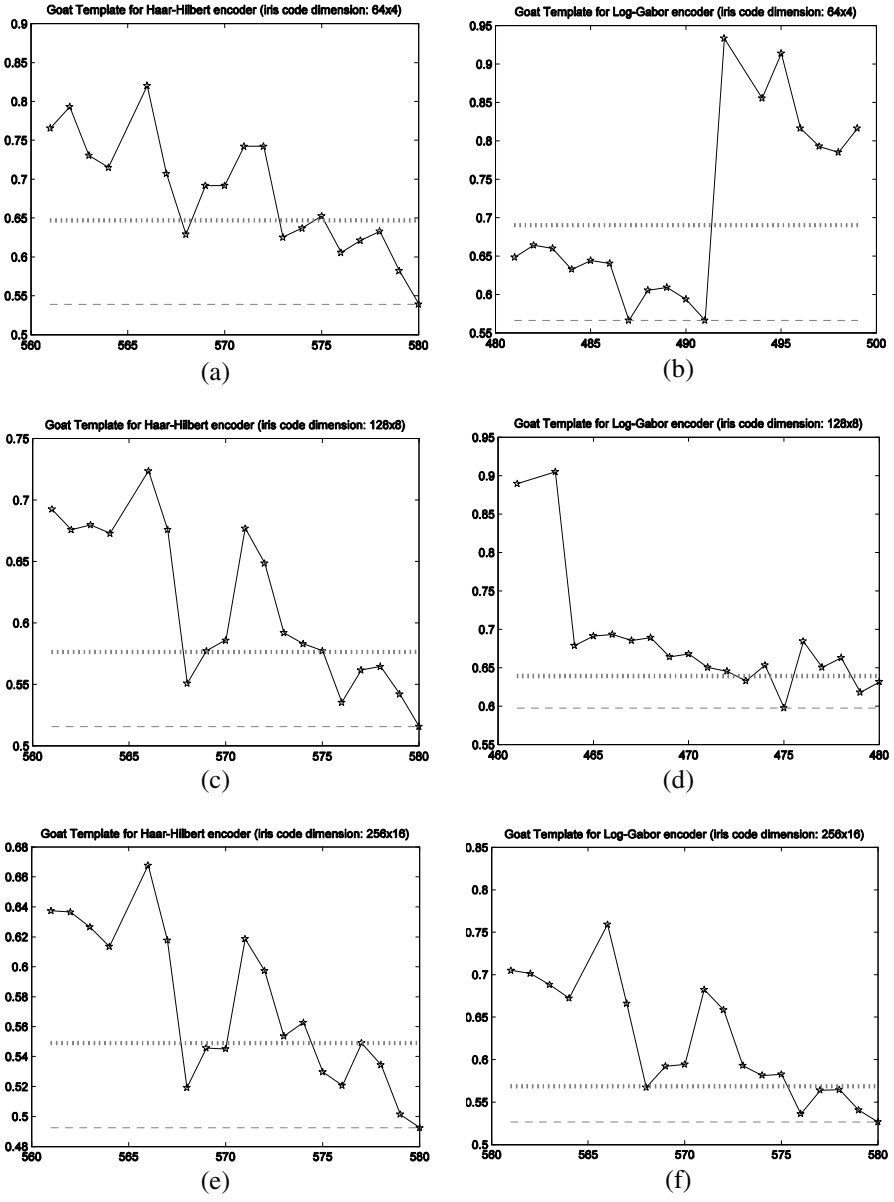

Fig. 4. The similarity scores corresponding to the genuine comparisons generated by the *last goat-templates* obtained from the tests that use Haar-Hilbert (iris code dimension: 64x4 – a, 128x8 – c, 256x16 – e) and Log-Gabor (iris code dimension: 64x4 – b, 128x8 – d, 256x16 – e) encoders

4 Conclusions

This paper shown that, at least in iris recognition, the Biometric Menagerie is a fuzzy and inconsistent concept, regardless if it refers to the users or to their biometric templates. Twelve exhaustive all-to-all iris recognition tests proved this point by conter-example. They also suggest that the goat is the most objective concept of the Fuzzy Biometric Menagerie and that Haar-Hilbert encoder is more objective than Log-Gabor encoder is.

The experimental results presented in this paper shown that the fuzzy-linguistic labels defining the Biometric Menagerie in terms of *wolf-*, *sheep-*, *lamb-*, *goat-users* and those defining the Fuzzy Biometric Menagerie in terms of *first/last wolf-*, *sheep-*, *lamb-*, *goat-templates* or in terms of *possible wolf-*, *sheep-*, *lamb-*, *goat-users*, all of them depend on the calibration of the iris recognition system.

Paradoxically, this paper gave a new perspective on the fuzzy concepts sheep, goats, lambs and wolves, but a very critical one. By illustrating the fact that, different iris recognition systems actually perceive differently the wolf- and goat-templates, the current paper qualifies the concept of Biometric Menagerie as not heaving one of the most important and most needed attribute of a concept, namely the *universality* with respect to a *genus*.

We wonder if anybody could indicate us a sufficiently large class of iris recognition systems for which the partitioning of the users/templates as a Biometric Menagerie (fuzzy or not) is at least *almost* the same.

Until then, we will remember one of Newton's mottos: *hypotheses non fingo*.

Acknowledgments. The authors would like to thank Professor *Donald Monro* (Dept. of Electronic and Electrical Engineering, University of Bath, UK) for granting the access to the Bath University Iris Image Database.

References

[1] Balas, V.E., Motoc, I.M., Barbulescu, A.: Combined Haar-Hilbert and Log-Gabor Based Iris Encoders. In: Balas, V.E., Fodor, J., Varkonyi-Koczy, A. (eds.) New Concepts and Applications in Soft Computing. SCI, vol. 417, pp. 1–26. Springer, Heidelberg (2012)

[2] Doddington, G., Liggett, W., Martin, A., Przybocki, M., Reynolds, D.: Sheep, Goats, Lambs and Wolves. In: A Statistical Analysis of Speaker Performance in the NIST 1998 Speaker Recognition Evaluation. In: Int'l Conf. Spoken Language Processing (ICSLP), Sydney, vol. 4, pp. 1351–1354 (1998)

[3] Iris Challenge Evaluation, N.I.S.T. retired Mars (2011), `http://iris.nist.gov/ice/`

[4] Paone, J., Flynn, P.: On the consistency of the biometric menagerie for irises and iris matchers. In: Proc. IEEE Int. Workshop on Information Forensics and Security (WIFS), pp. 1–6 (2011)

[5] Popescu-Bodorin, N.: Exploring New Directions in Iris Recognition. In: 11th International Symposium on Symbolic and Numeric Algorithms for Scientific Computing. Conference Publishing Services – IEEE Computer Society, pp. 384–391 (2009)

[6] Popescu-Bodorin, N., Balas, V.E.: Comparing Haar-Hilbert and Log-Gabor based iris encoders on Bath Iris Image Database. In: Proc. 4th Int. Work. on Soft Computing Apps., pp. 191–196. IEEE Press (2010)
[7] Popescu-Bodorin, N.: Processing Toolbox for the University of Bath Iris Image Database, PT-UBIID-v.02 (2010), http://fmi.spiruharet.ro/bodorin/pt-ubiid/
[8] Popescu-Bodorin, N., Balas, V.E., Motoc, I.M.: 8-Valent Fuzzy Logic for Iris Recognition and Biometry. In: Proc. 5th IEEE Int. Symp. on Computational Intelligence and Intelligent Informatics, Floriana, Malta, September 15-17, pp. 149–154. IEEE Press (2011)
[9] Popescu-Bodorin, N., Balas, V.E., Motoc, I.M.: Iris Codes Classification Using Discriminant and Witness Directions. In: Proc. 5th IEEE Int. Symp. on Computational Intelligence and Intelligent Informatics, Floriana, Malta, September 15-17, pp. 143–148. IEEE Press (2011)
[10] Bath University Iris Image Database, http://www.smartsensors.co.uk/informations/bath-iris-image-database/
[11] Sugeno, M., Yasukawa, T.: A Fuzzy-Logic-Based Approach to Qualitative Modeling. IEEE Trans. on Fuzzy Systems 1(1), 7–31 (1993)
[12] Yager, N., Dunstone, T.: The biometric menagerie. IEEE Transactions on Pattern Analysis and Machine Intelligence 32(2), 220–230 (2010)
[13] Zadeh, L.A.: A New Direction in AI - Toward a Computational Theory of Perceptions. AI Magazine 22(1), 73–84 (2001)
[14] Zadeh, L.A.: Toward extended fuzzy logic A first step. Fuzzy Sets and Systems 160, 3175–3181 (2009)

A Multi-algorithmic Colour Iris Recognition System

Petru Radu, Konstantinos Sirlantzis, Gareth Howells,
Sanaul Hoque, and Farzin Deravi

School of Engineering and Digital Arts,
University of Kent, Canterbury, U.K
{pr95,k.sirlantzis,w.g.j.howells,s.hoque,f.deravi}@kent.ac.uk

Abstract. The reported accuracies of iris recognition systems are generally higher on near infrared images than on colour RGB images. To increase a colour iris recognition system's performance, a possible solution is a multi-algorithmic approach with an appropriate fusion mechanism. In the present work, this approach is investigated by fusing three algorithms at the score level to enhance the performance of a colour iris recognition system. The contribution of this paper consists of proposing 2 novel feature extraction methods for colour iris images, one based on a 3-bit encoder of the 8 neighborhood and the other one based on gray level co-occurrence matrix. The third algorithm employed uses the classical Gabor filters and phase encoding for feature extraction. A weighted average is used as a matching score fusion. The efficiency of the proposed iris recognition system is demonstrated on UBIRISv1 dataset.

1 Introduction

Iris recognition has become an emerging research topic due to its rich texture with a high number of degrees of freedom [1], which has allowed researchers to develop a large variety of iris authentication algorithms. Although the performance of the iris recognition algorithms is high [2, 3], they require a large amount of constraints on the user due to the fact that near infrared illumination is necessary for good quality images and a reliable operation.

The majority of iris recognition systems published in the literature have only been benchmarked on near infrared images, leaving a question mark on whether these algorithms can perform on colour iris images with a comparable accuracy. The pioneering iris recognition system proposed in [1], which uses phase based coding and binary features extracted from near infrared images is deployed in most of the commercial and military iris recognition devices currently available. This fact led to the formation of large iris databases which contain images acquired under near infrared illumination.

The United States National Institute of Standards and Technology (NIST) [4] conducted a series of iris recognition competitions [5], where the submitted algorithms were tested on large scale databases containing near infrared iris images. These competitions allowed the creation of an ISO standard for near infrared iris images [6], which will promote the interoperability between various iris recognition acquisition devices and authentication algorithms. Generally the near infrared iris image data

V.E. Balas et al. (Eds.): Soft Computing Applications, AISC 195, pp. 45–56.
springerlink.com

standard specifies the thresholds for different iris image quality measures, which from a practical point of view are translated into how large the constraints on the user have to be.

For iris images acquired in visible spectrum there hasn't been created a standard yet, but over the past several years advances have been made in colour iris recognition. However, the accuracies obtained in visible spectrum are not yet comparable to those obtained under near infrared illumination [7]. The practicability of a colour iris recognition system is considerably increased when compared to a near infrared iris recognition system because the constraints on the user are significantly relaxed. One of the pioneers of iris recognition in visible spectrum is Hugo Proenca, who organized a colour iris recognition competition called Noisy Iris Challenge Evaluation (NICE). It took place in 2 parts: part1 assessed only the segmentation of a subset of UBIRISv2 [8] dataset and in part 2 the classification algorithms were assessed on the same images. Proenca et al analyzed the results of the second part of NICE competition in [7], where they reported that by employing a multi-algorithmic approach between the top 5 ranked algorithms, the accuracy of the system increases significantly.

In this paper we employ a multi-algorithmic approach to enhance a colour iris recognition systems' accuracy, motivated by the results reported in [7]. We use three iris recognition algorithms, two proposed by us in the present paper and one is the classical method proposed in [1].

The main novelty of the present work consists of 2 iris feature extraction methods. The first one uses the gray levels of the 8 neighborhood of a pixel from the iris texture and the second one uses the gray level co-occurrence matrices (GLCM) of the iris texture, calculated for 8 directions. Also, we propose a transformation of the match scores of the iris recognition systems which enhances the separation between authentic and impostor score distributions. Further, we analyze how the system performs when only a small number of pixels around the pupil are unwrapped compared to the case when a large number of pixels around the pupil are used to form the unwrapped image.

The remainder of the paper is organized as follows: in Section 2, the component algorithms of the multi-algorithm iris recognition systems are detailed. In Section 3 the separation enhancement method between authentic and impostor score distributions is presented. The experimental results are reported in Section 4 and conclusions are given in Section 5.

2 Proposed Multi-algorithmic Iris Recognition System

In Fig. 1 the block diagram of the proposed multi-algorithmic iris recognition system is presented. As may be observed, the system only uses the red channel to extract the information from the iris texture. The red channel has the closest wavelength to the near infrared domain and yields the best accuracy from the RGB colour space, as reported in [9].

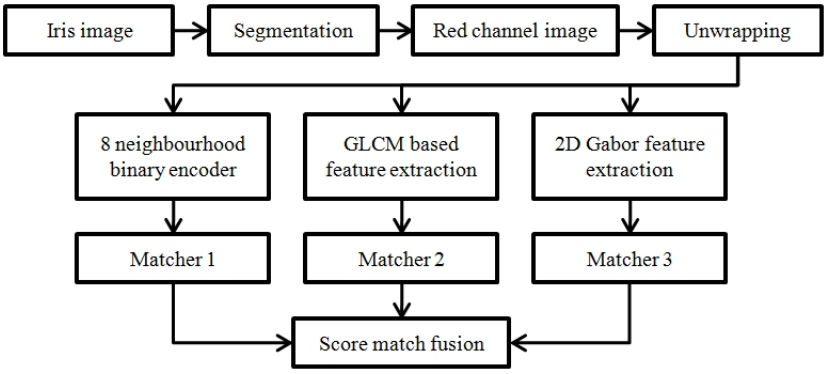

Fig. 1. Multi-algorithmic iris recognition system architecture

2.1 Preprocessing

An iris recognition system consists of five main stages: acquisition, segmentation, normalization, feature extraction and matching. For segmentation, the algorithm proposed in [10] was employed. In this work, we benchmarked the multi-algorithmic system on images from UBIRISv1 [11], Session 1 dataset. The segmentation accuracy on these images was approximately 95%. The remaining 5% were manually segmented, as they contain strong occlusions or other noise factors which make the segmentation difficult.

The unwrapping was done using the rubber sheet model proposed in [1]. To avoid including the eyelashes in the unwrapped image, the circle sector defined between -45^o and +45^o of vertical axis was not considered. The unwrapped image dimension initially is 120 by 50 pixels for the 8 neighborhood binary encoder and the classical phase based feature extraction and 360 by pixels 50 for the GLCM based system. Then, 100 pixels are considered around the pupil and the resulting unwrapped image dimension is 120 by 100 pixels and 360 by 100 pixels respectively.

As an efficient image enhancement was reported in [12] to be the second time consuming task from an iris recognition system after segmentation, our system does not employ any image enhancement techniques.

2.2 8-Neighborhood Binary Encoder

The pixel relationships are the basis of the least computationally demanding texture analysis techniques, as there is no filtering operation necessary. By using the 8 neighborhood of a pixel, we propose an iris feature extraction method which is computationally efficient and is therefore suitable to be implemented on mobile or embedded devices.

The working principle of the proposed feature extraction method is a simple, yet effective one: the 8 positions of the 8-neighborhood of a pixel may be encoded on 3 bits, as shown in Fig. 2. When the center pixel is immediately near its neighbors, we

have an offset of 1, but the offset may be higher. Considering the values of the 8 neighbors of a pixel, the 3 bits corresponding to that pixel are the binary code corresponding to the position of the highest intensity value of the 8 neighbor pixels.

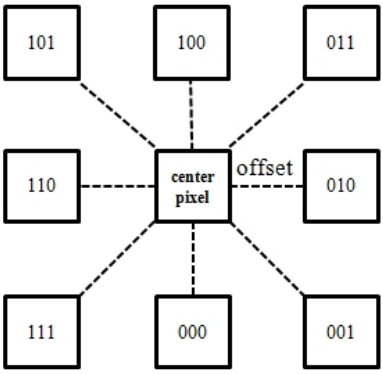

Fig. 2. Binary encoding of 8 neighborhood of a pixel

Additionally to encoding the position of the maximum pixel value of the 8-neighborhood, the value of the center pixel is compared to the mean of the 8-neighborhood. If the center pixel has a value smaller than the average, a logical 0 is concatenated to the 3 bits corresponding to the position of the maximum neighbor, otherwise a logical 1 is concatenated.

The 8-neighborhood does not have necessarily to be considered for every other pixel, it may be considered with a step for the horizontal scan and one for the vertical scan. In this way this feature extraction method becomes even more computationally efficient. We investigated how the performance varies with the step size via a direct search. As a matching algorithm, the Hamming distance is used [1].

The three parameters of this feature extraction method are the offset, the horizontal scanning step and the vertical scanning step. We found these parameters empirically, by taking the first 40 classes from UBIRISv1 [11] Session 1 dataset and computing the decidability index [1], which is a measure of the separation between the authentic and impostor score distributions. We found that the maximum decidability index was obtained for an offset of 7 pixels, a horizontal step of 1 pixel and a vertical step of 5 pixels. The resulting feature size is 3392 bits for the 120 by 50 pixels unwrapped image and 7632 bits for the 120 by 100 pixels image.

2.3 Co-occurrence Matrix Based Features

The co-occurrence matrix C for a 8-bit gray level image *I* is a 256 by 256 matrix which contains on row i and column j the counts of the number of pixels pairs with the intensity values i and j, which are separated by an offset and are at a relative inclination [13]:

$$C_{i,j=}\sum_{x=1}^{256}\sum_{y=1}^{256}\left(I_{x,y}=i\right)\wedge\left(I_{x',y'}=j\right) \tag{1}$$

where x' and y' are the offsets given by the distance d and inclination θ:

$$\begin{cases}x'=x+d\cos\theta\\y'=y+d\sin\theta\end{cases} \tag{2}$$

The GLCM is symmetrical and if it has higher values around the main diagonal, it means that the image contrast is low. In the proposed feature extraction method, 8 co-occurrence non-symmetrical matrices were computed for an unwrapped iris image, corresponding to the directions given by the 8-neighborhood. A fused GLCM was obtained by averaging the 8 initial GLCM.

As the iris texture generally does not have high contrast, the higher values of the fused GLCM were concentrated around the main diagonal. The presence of noises such as eyelashes or reflections in the unwrapped iris image will be observed in high values in corner regions of the GLCM. From the original fused GLCM we only keep the part of the matrix with rows and columns indexes between 75 and 135. Therefore, the feature size will be $(135\text{-}75+1)^2 = 3721$ integer positive values. The indexes 75 and 135 were determined empirically with the criterion of maximizing the decidability index for 40 classes from UBIRISv1 dataset, Session 1, while keeping a manageable feature size of 3621 bytes. The larger the amount of data from the original GLCM is used, the higher the accuracy of the system will be, but the tradeoff is a higher computational demand and a larger template size.

From the selected 61 by 61 pixels matrix, we consider 20 vectors parallel and above the main diagonal and 20 vectors parallel and below the main diagonal. The main diagonal was not considered because it provides information about the pixels with the same intensity level. Let us denote the 20 vectors above the diagonal with v_1, …, v_{20} and the 20 vectors below the main diagonal v_{-1}, …, v_{-20}. In the matching phase, initially the Euclidian distances are computed between the corresponding vectors extracted from the probe and gallery images. As two initial scores, the means of the square roots of the Euclidean distances of the vectors above and below the main diagonal are computed using equations (3). The square root was used as a non-linear transformation to make the authentic and impostor score distributions narrower.

$$\begin{cases}\mathrm{M1}=\dfrac{1}{20}\displaystyle\sum_{i=1}^{20}\sqrt{\left\|v_i^{gallery},v_i^{probe}\right\|}\\[2ex]\mathrm{m2}=\dfrac{1}{20}\displaystyle\sum_{i=-20}^{-1}\sqrt{\left\|v_i^{gallery},v_i^{probe}\right\|}\end{cases} \tag{3}$$

The two means from equations (3) are used to compute the intermediate scores from equations (4). The hyperbolic tangent function is used to normalize the scores between 0 and 1. Hyperbolic tangent function takes values between 0 and 1 for positive

arguments and maps all its arguments which are above 2.5 very close or equal to 1. The argument of hyperbolic tangent was used to bring the impostors scores above the value of 2.5 and the authentic scores as small as possible.

$$\begin{cases} \text{dist1} = \tanh\left(\log\dfrac{20}{1+e^{m1}}\right)^6 \\ \text{dist2} = \tanh\left(\log\dfrac{20}{1+e^{m2}}\right)^6 \end{cases} \tag{4}$$

The final co-occurrence matrix score (CMS) is obtained using equation (5) to fuse dist1 and dist2. dist1 and dist2 are below 1, and the product dist1*dist2 will be close to 0 for authentics and much larger for impostors. The absolute value of the base 2 logarithm of a number which is below 0.15 for example is above 2.5, while the absolute value of the base 2 logarithm of a number which is above 0.6 is below 0.6.

$$CMS = 1 - \tanh|\log_2(\text{dist1} * \text{dist2})| \tag{5}$$

2.4 Classical Phase-Based Feature Extraction

This method employs the classical 2D Gabor filters [1] to extract the information from the iris texture. The features are binary strings extracted using one set of parameters of the 2D Gabor filters. For each pixel of the unwrapped image, 2 bits of information are stored. We observed that if the 2 bits are extracted from every other pixel, the drop in performance is negligible.

The feature size is 3000 bits for the 120 by 50 pixels unwrapped iris image and 6000 bits for the 120 by 100 pixels image. For matching, the classical Hamming distance was used.

The issue of rotation is addressed by shifting one binary string 4 bits to the left and 4 bits to the right and the minimum Hamming distance out of the 9 computations is stored. The same method was applied to compensate for rotation of the features extracted using the 8-neighborhood binary encoder. The features extracted using GLCM are rotational invariant.

3 Enhancing the Authentic and Impostor Distributions

In any iris recognition system it is desirable to have a decidability index [1] between impostor and authentic score distributions as large as possible. A classical iris recognition system has most of the authentic scores concentrated in the range [0;0.2], while most of the impostor scores are above 0.4 [14-16].

In this paper we propose a transformation of the scores of an iris recognition system with the properties mentioned above by using equation (6). We will call the transformation (6) Kent Transform (KT). The reasoning of such a transform is the following: a non linear transformation that enhances the separation between 2 distributions which contain values between 0 and 1 is represented by $|\log_{10}(\text{value}^2)|$. This

expression will map values close to 0 above 1 and values above 0.32 below 1. When computing 1 – hyperbolic tangent of this expression, the values from the two original distributions will be more separated than they were initially.

$$\mathrm{KT}(\mathrm{score}) = 1 - \tanh|\log_{10}(\mathrm{score}^2)| \quad (6)$$

We will demonstrate the efficiency of the KT in the experimental results section, but let us first replace the scores of 0.2 and 0.4 in the above formula. Initially, the difference between the impostor score of 0.4 and authentic score of 0.2 is 0.2. After applying the KT we obtain KT(0.4) = 0.33 and KT(0.2) = 0.11 and the difference between the scores is now 0.22, larger by 10%.

When the impostor and authentic scores have values very close to the decision boundary, for example the impostor score is 0.35 and the authentic score is 0.3, then the difference of 0.05 between the 2 scores is increased by 18% to 0.059 when KT is applied. Therefore, the KT is a non-linear transformation which reduces the overlap between the authentic and impostor score distributions of an iris recognition system. KT may as well be applied to any type of biometric system which has the matching scores for authentics and impostors similar to those of a classical iris recognition system.

4 Experimental Results

The database used in our experiments was UBIRISv1 [11] Session 1. This session has 241 users enrolled with one eye. There are 5 colour RGB images for each user. The images were acquired in a semi-controlled environment, by reducing the noise factors, such as reflections, poor illumination or poor focus. The users were at a distance of 20 cm from the acquisition device. However, 10 images out of the total of 1205 are strongly or totally occluded and therefore no useful information can be extracted from them. We ran the experiments on all the images from the dataset, including the occluded ones.

The experimental setup consists of the classical one vs one score generation for all possible combinations between same class images and different class images. The fusion between the scores produced by the 3 algorithms was done by using weighted average. The weights for the 3 algorithms were determined using the first 40 classes via a direct search.

4.1 Using 50 Pixels around the Pupil

In Table 1, the decidability index is reported for all the images of UBIRISv1 Session 1 dataset and the 3 algorithms together with the means and standard deviations (in brackets) of the authentic and impostor distributions. There are 723000 impostor scores and 2410 authentic scores.

The KT is applied to the 8-neighborhood based algorithm and to the 2D Gabor filter based algorithm. The KT is not applied to the GLCM based algorithm because equation (5) which produces the matching scores of this algorithm is similar to KT.

Table 1. Decidability index and distribution means and standard deviations (in brackets) for the 3 algorithms

Algorithm	Authentic mean and std. deviation	Impostor mean and std. deviation	Decidability index
8-neighborhood	0.30 (0.038)	0.39 (0.017)	3.22
8-neighborhood with KT	0.22 (0.043)	0.33 (0.021)	3.31
GLCM	0.10 (0.227)	0.76 (0.336)	2.31
2D Gabor	0.20 (0.064)	0.40 (0.034)	3.92
2D Gabor with KT	0.12 (0.066)	0.34 (0.042)	4.03

In Table 2, the decidability index together with False Reject Rate (FRR) for 2 values of the False Acceptance Rate (FAR) and Equal Error Rate (EER) are reported for the last 201 classes left after the weights were determined using the first 40 classes. The weights obtained for the 2D Gabor with KT, 8-neighborhood with KT and GLCM algorithms are 0.61, 0.31 and 0.08 respectively.

Table 2. Performance measures for the 3 algorithms and fusion approach when 50 pixels around the pupil are used

Algorithm	Decidability index	FRR for FAR=0.01%	FRR for FAR=0.1%	EER
2D Gabor with KT	4.09	10.70 %	7.41 %	3.63 %
8-neighborhood with KT	3.33	22.34 %	11.74 %	3.51 %
GLCM	2.27	99.62 %	97.82 %	15.47 %
Fusion	4.38	11.39 %	7.91 %	3.33 %

From Table 2 may be observed that the GLCM based system performs poor compared to the other 2 algorithms, but when the scores of the 3 algorithms are fused, the decidability index of the best algorithm is increased by approximately 7% and the EER is decreased by approximately 8.2%. We have eliminated the GLCM based algorithm and implemented a weighted average between the other 2 systems, but the decidability index and the EER could only be improved by less than 1%.

4.2 Using 100 Pixels around the Pupil

In Table 3, the decidability index is reported for all the images of the 201 classes used for testing, together with the FRR for given thresholds of the FAR. In this case the optimum weights for 2D Gabor with KT, 8-neighborhood with KT and GLCM algorithms are 0.55, 0.34 and 0.11 respectively.

Table 3. Performance measures for the 3 algorithms and fusion approach when 100 pixels around the pupil are used

Algorithm	Decidability index	FRR for FAR=0.01%	FRR for FAR=0.1%	EER
2D Gabor with KT	4.93	4.42 %	3.38 %	2.45 %
8-neighborhood with KT	3.92	7.51 %	4.12 %	2.45 %
GLCM	3.19	99.58%	98.09 %	8.05 %
Fusion	5.17	10.7 %	4.67 %	2.25 %

The fusion of the 3 algorithms improves the decidability index by approximately 5% and the EER by approximately 8%. However, fusing of the 3 algorithms is not suitable if a low FAR is required for the operation of the iris recognition system.

In Fig. 3, the Receiving Operational Characteristic (ROC) curve is plotted for the 8-neighborhood and 2D Gabor algorithms, together with the ROC curve for the fusion of the 3 algorithms.

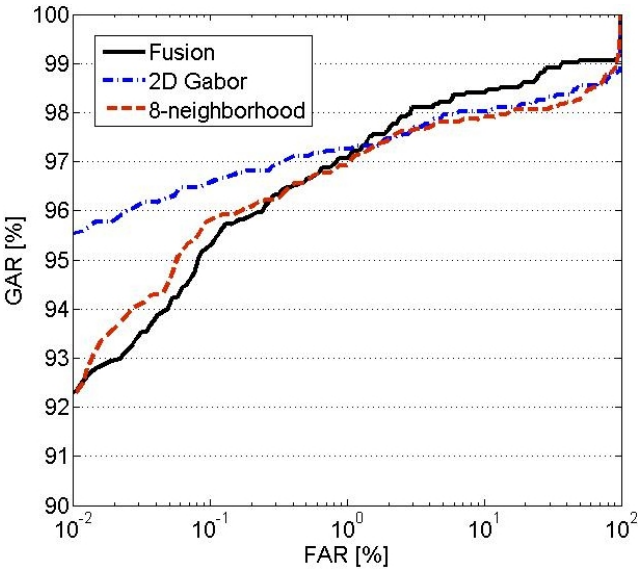

Fig. 3. ROC curve for 8-neighborhood, 2D Gabor and fusion of the 3 algorithms

To observe the improvement brought by using 100 pixels around the pupil over the case when only 50 pixels are used, we plotted in Fig. 4 the authentic and impostor distributions of the fused scores for the 3 algorithms produced on the 201 test classes. The EER when using 100 pixels around the pupil is improved by 32.42% compared to the case when only 50 pixels are used.

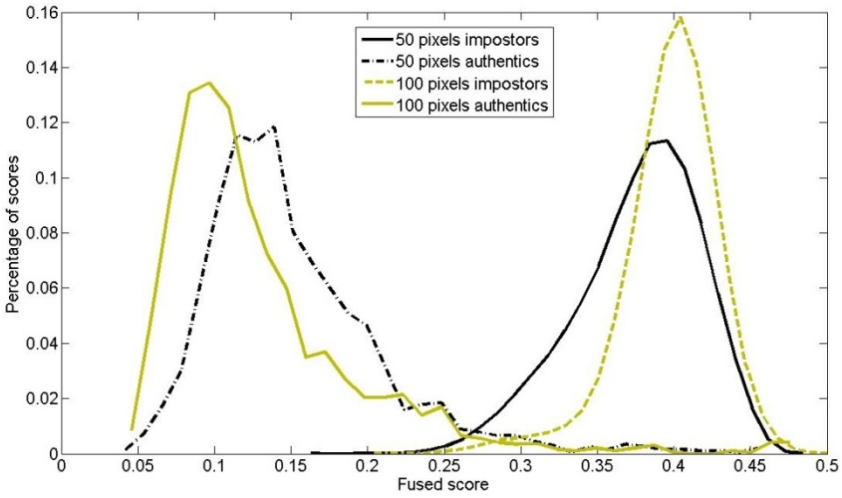

Fig. 4. Authentic and impostor fused score distributions when using 50 pixels and 100 pixels around the pupil

In Table 4. we compare the performance of the proposed fusion approach with that reported in [17] on UBIRISv1 Session 1. As may be observed, our system performs significantly better than the approach proposed in [17].

Table 4. Performance comparison of proposed approach with published works

Method	GAR for FAR = 1%
Hosseini et al [17]	81.70 %
Proposed 2D Gabor algorithm	97.19 %
Proposed 8-neighborhood algorithm	96.98 %
Proposed fusion approach	97.16 %

5 Conclusions

Iris recognition on colour images is a challenging task, becoming an emergent research topic. In this work we propose two iris recognition algorithms, one based on the 8-neighborhood of the iris texture and one based on the GLCM. By fusing the two proposed iris recognition algorithms at the score level with the classical 2D Gabor filter algorithm introduced by Daugman, the EER of the system is improved by approximately 8%.

We introduced a non-linear transformation called Kent Transform, which applied to the matching score of an iris recognition system is increasing the decidability index of the system. We also investigated how the performance of a colour iris recognition

system is affected when using only 50 pixels around the pupil compared to the case when 100 pixels around the pupil are used.

The experimental results show that a multi-algorithmic approach for colour iris recognition is beneficial, even when the accuracy of some component algorithms is significantly poorer compared to the best performing algorithm.

References

1. Daugman, J.G.: High confidence visual recognition of persons by a test of statistical independence. IEEE Transactions on Pattern Analysis and Machine Intelligence 15(11), 1148–1161 (1993)
2. Ma, L., Wang, Y.H., Tan, T.N.: Iris recognition using circular symmetric filters. In: Kasturi, R., Laurendeau, D., Suen, C. (eds.) Proceedings of 16th International Conference on Pattern Recognition, vol. II, pp. 414–417. IEEE Computer Soc., Los Alamitos (2002)
3. Ma, L., Tan, T.N., Wang, Y.H., Zhang, D.X.: Efficient iris recognition by characterizing key local variations. IEEE Transactions on Image Processing 13(6), 739–750 (2004)
4. NIST. National Institute of Standards and Technology (2010), http://www.nist.gov (cited June 30, 2012)
5. Grother, P., Tabassi, E., Quinn, G.W., Salamon, W.: IREX 1 Report - Performance of Iris Recognition Algorithms on Standard Images (2009)
6. Standardization, I.O. f. ISO/IEC 19794-6:2011 (2011), http://www.iso.org/iso/iso_catalogue/catalogue_tc/catalogue_detail.htm?csnumber=50868 (cited May 30, 2012)
7. Proenca, H., Alexandre, L.A.: Toward Covert Iris Biometric Recognition: Experimental Results From the NICE Contests. IEEE Transactions on Information Forensics and Security 7(2), 798–808 (2012)
8. Proenca, H., et al.: The UBIRIS.v2: A Database of Visible Wavelength Iris Images Captured On-the-Move and At-a-Distance. IEEE Transactions on Pattern Analysis and Machine Intelligence 32(8), 1529–1535 (2010)
9. Radu, P., Sirlantzis, K., Howells, W.G.J., Deravi, F., Hoque, S.: Information Fusion for Unconstrained Iris Recognition. International Journal of Hybrid Information Technology 4(4), 1–12 (2011)
10. Radu, P., Sirlantzis, K., Howells, W.G.J., Hoque, S., Deravi, F.: A Versatile Iris Segmentation Algorithm. In: Arslan Bromme, C.B. (ed.) BIOSIG 2011. Kollen Druck+Vwrlag, Darmstadt, pp. 137–151 (2011)
11. Proença, H., Alexandre, L.A.: UBIRIS: A Noisy Iris Image Database. In: Roli, F., Vitulano, S. (eds.) ICIAP 2005. LNCS, vol. 3617, pp. 970–977. Springer, Heidelberg (2005)
12. Vatsa, M., Singh, R., Noore, A.: Improving iris recognition performance using segmentation, quality enhancement, match score fusion, and indexing. IEEE Transactions on Systems Man and Cybernetics Part B-Cybernetics 38(4), 1021–1035 (2008)
13. Nixon, M.S., Aguado, A.S.: Feature Extraction and Image Processing, ed. Newnes 2002: Newness
14. Daugman, J.: How iris recognition works. IEEE Transactions on Circuits and Systems for Video Technology 14(1), 21–30 (2004)

15. Balas, V.E., Motoc, I.M., Barbulescu, A.: Combined Haar-Hilbert and Log-Gabor Based Iris Encoders. In: Balas, V.E., Fodor, J., Varkonyi-Koczy, A. (eds.) New Concepts and Applications in Soft Computing. Studies in Computational Intelligence, vol. 417, pp. 1–26. Springer, Heidelberg (2012)
16. Popescu-Bodorin, N., Balas, V.E.: Comparing Haar-Hilbert and Log-Gabor based iris encoders on Bath Iris Image Database. In: 2010 4th International Workshop on Soft Computing Applications, SOFA (2010)
17. Hosseini, M.S., Araabi, B.N., Soltanian-Zadeh, H.: Pigment Melanin: Pattern for Iris Recognition. IEEE Transactions on Instrumentation and Measurement 59(4), 792–804 (2010)

Examples of Artificial Perceptions in Optical Character Recognition and Iris Recognition

Cristina Madalina Noaica[1], Robert Badea[1], Iulia Maria Motoc[1], Claudiu Gheorghe Ghica[1,2], Alin Cristian Rosoiu[3], and Nicolaie Popescu-Bodorin[1]

[1] Artificial Intelligence & Computational Logic Laboratory,
Mathematics & Computer Science Dept.,
Spiru Haret University, Bucharest, Romania
{noaica,badea,motoc}@irisbiometrics.org.
bodorin@ieee.org
[2] Programmer at Clintelica AB
claudiu.ghica@clintelica.com
[3] Game Tester at *UbiSoft* Romania
alin-cristian.rosoiu@ubisoft.com.

Abstract. This paper assumes the hypothesis that *human learning* is *perception based*, and consequently, the learning process and perceptions should not be represented and investigated independently or modeled in different simulation spaces. In order to keep the analogy between the *artificial* and *human learning*, the former is assumed here as being based on the *artificial perception*. Hence, instead of choosing to apply or develop a Computational Theory of (human) Perceptions, we choose to mirror the *human perceptions* in a numeric (computational) space as *artificial perceptions* and to analyze the interdependence between *artificial learning* and *artificial perception* in the same numeric space, using one of the simplest tools of Artificial Intelligence and Soft Computing, namely the perceptrons. As practical applications, we choose to work around two examples: Optical Character Recognition and Iris Recognition. In both cases a simple Turing test shows that *artificial perceptions* of the difference between two characters and between two irides are fuzzy, whereas the corresponding *human perceptions* are, in fact, crisp.

Keywords: crisp human perception, fuzzy artificial perception, perceptron.

1 Introduction

In the last decade, Zadeh pointed out the necessity of introducing a Computational Theory of Perceptions (CTP). More precisely, Zadeh outlined in [21] a computational theory of human perceptions, i.e. a formal theory which should enable software agents to compute (and hopefully, to reason) with human perceptions "*described by propositions drawn from a natural language*" [21] as answers to some questions. The process of describing human perceptions in a natural language sets out a correspondence perceptions-propositions and results in what Zadeh called "*perception-based information*" (PBI). Here in this paper PBI is viewed as a special syntactic-semantic

V.E. Balas et al. (Eds.): Soft Computing Applications, AISC 195, pp. 57–69.
springerlink.com

representation space, as a subset of legal syntaxes within a given natural language, which are charged with fuzzy meanings. As an example, from a syntactic point of view, there is nothing fuzzy about the string "young person", whereas the fuzzy meaning that humans usually associate to this string makes it f-granular. By paraphrasing Zadeh, this means that the boundaries of perceived "young person" class are unsharp and the values of age ranges are represented in natural language as fuzzy linguistic labels (for example: "young", "middle aged", "old" etc.), as f-granules of (perceived) age, where, as Zadeh said, "*a granule being a clump of values (points, objects) drawn together by indistinguishability, similarity, proximity, and function*" [21].

Zadeh illustrated the fact that perceptions are represented in natural language as propositions by giving the following example [21]: "*it is unlikely that there will be a significant increase in the price of oil in the near future*" (which is further denoted here as $\mathcal{A}$) – an assertion that aggregates together fuzzy linguistic labels (words – from the syntactic point of view, perceptions – from the semantic point of view) as aliases of some *f-granules* of *perceived likelihood* ('is unlikely'), *amplitude of variation* ('significant increase') and *time* ('near future').

However, here we assume that instead of representing a human perception, the assertion $\mathcal{A}$ is a piece of knowledge belonging in an economical theory of oil market. How meaningful is $\mathcal{A}$ (the message) depends at least on the writer (the source of the message), reader (the destination of the message) and on the context in which they communicate (the environment). For example, the credibility and the meaning that the reader could assign to the enounce $\mathcal{A}$ vary dramatically when instead of being asserted by a six years old kid it is announced by a spokesman of British Petroleum. Conversely, even if the most qualified economist of the oil market makes the assertion $\mathcal{A}$, there will be dramatic differences between the ways in which different people of different ages and qualifications would assign a meaning to it. Moreover, the assertion $\mathcal{A}$ could be just a part of a communication strategy whose goal is to manipulate the market players.

Since the meanings given by different people to the assertion $\mathcal{A}$ are far enough from being "*drawn together by indistinguishability, similarity, proximity, and function*" [21], the example given by Zadeh actually illustrates that assigning certain meanings to a human perception represented as a proposition in a natural language could result in very volatile / unstable results. On the other hand, such an operation is very similar with trying to decode a message without knowing how exactly the message was encoded in the first place.

This paper assumes the hypothesis that *human learning* is *perception based*, and consequently, the learning process and perceptions should not be represented and investigated independently or modeled in different simulation spaces. On the other hand, in order to keep the analogy between the *artificial* and *human learning*, the former is assumed here as being based on the *artificial perception*. Hence, instead of choosing to apply or develop a Computational Theory of (human) Perceptions [21], we choose to mirror the *human perceptions* in a numeric (computational) space - as *artificial perceptions,* and to analyze the interdependence between *artificial learning* and *artificial perception* in the same numeric space. An alternative that we do not follow here would be to consider learning process as a topic of Artificial Intelligence and perceptions as a topic of a Computational Theory of Perceptions. This paper

analyzes the interdependence between learning and perceptions using one of the simplest tools of Artificial Intelligence and Soft Computing, namely the perceptrons [15]. As practical applications, we choose to work around two examples: Optical Character Recognition (OCR) and Iris Recognition (IR).

1.1 Outline

The first question that must be answered here is what exactly do we understand here by "*artificial perception*". The second section of this work discusses this topic.

As it can be seen in [21], Zadeh insists on the ideas that (human) "*perceptions, in general, are both fuzzy and granular or, for short, f-granular*" and that "*in much, perhaps most, of human reasoning and concept formation, the granules are fuzzy*" - i.e. human reasoning and the concepts are f-granular.

However, in the two examples that follow to be presented here, the situation is a little bit different: in both cases a simple Turing test [18] shows that *artificial perceptions* of the difference between two different characters and between two different irides are fuzzy, whereas the corresponding *human perceptions* are, in fact, crisp. Despite being contradictory to Zadeh's beliefs expressed above, this situation comes very naturally, because ultimately, a perceptron emulates the human intelligent behavior through an artificial one, which compared to the original is weakened and imprecise enough. The third and the fourth sections from here aim to illustrate this situation in detail using the practical examples of OCR and IR, respectively. Concluding remarks of this study are presented in the fifth section.

2 The Artificial Perception

In their seminal work, McCulloch and Pitts [10] formalized the neural networks as a recursively constructed language of *temporal propositional expressions* [10] (build by complexification rules with elementary proposition such as $N_i(t)$ – i.e. the unit i fires at time t). This means that, naturally, a neural network is fully described if we know its structure and if we know why, when and how its neurons fire. Later, Rosenblatt [15], [16] took two important steps further in Artificial Intelligence (AI). Firstly, he defined the Perceptron as an elementary virtual (simulated / artificial) unit able to encode artificial perceptions in a manner similar to that in which is assumed that the human brain supports visual perception [15]. Secondly, he advanced the field of neural networks from a theoretical study to practical implementations on circuits [16].

2.1 Artificial Intelligence vs. Human Intelligence

Somehow paradoxically, the two works of McCulloch, Pitts [10] and Rosenblatt [15], [16], taken together, still drawn the limits in which the neural networks have been modeled and used up to this date. Of course, some improvements and some diversification are visible with respect to the structure (recurrent networks, for example), dynamic (self-organizing maps [9], for example), neuron design (fuzzy [19] and neo-fuzzy neurons [20]) and to the area of application [1], [2], [4], [5], [7], [8]. However,

all of these newer developments and variations are much too close, and too tributary to the initial design specified by McCulloch, Pitts and Rosenblatt. Maybe this is the reason why, as J. Copeland said in [6], "*five decades since the inception of AI have brought only very slow progress, and early optimism concerning the attainment of human-level intelligence has given way to an appreciation of the profound difficulty of the problem*". Still, it should be very clear for anybody that there is no such logical thing as criticizing AI in itself. All AI tools are our creations and they have only those limitations that we cannot overcome when we design them. Hence, the problem of programming artificial intelligent agents is recursively depending on itself: the AI tools would not have unwanted/unexpected limitations if someone (or something) could be able to design them intelligently. The lower our level of understanding (our own) intelligence, the greater the limitations of the AI tools that we design. The vicious circle does not break here because, in order to find what intelligence is, we should start knowing/acquiring this concept through as many of its hypostases as possible, but on the other hand, the task of recognizing the hypostases of intelligence is not always simple and successful. Moreover, even that we may recognize a hypostasis of intelligence, there is no guarantee that we could understand how it is produced. Hence ultimately, if we accept that AI is "*the science of making computers do things that require intelligence when done by humans*" [6], we should also accept that the limitations of our AI tools originate in our limited knowledge of ourselves and, by consequence, in our limited capacity of designing them intelligently.

Another problematic issue in the present state of AI is a very well established tendency for overvaluation, whose roots grown right from the beginnings. For example, despite the fact that Rosenblatt introduced the perceptrons as elementary units designed to encode artificial perceptions (as their name suggests), when he approached the "*mathematical analysis of learning in the perceptron*" [15], he involuntarily made an association between *learning* and *perceptrons*. Over time, this association somehow has come to be treated, seen and claimed as it would be a strong bound between learning and perceptrons, a bound whose strength increased in time for no plausible logical reasons, only by frequent use, overvaluation and mistake.

2.2 Overvaluation

The belief that *perceptrons learn* is widely spread today in AI community and often treated as an objective fact. The truth is that *human learning* is something much more complex than the process of "*learning in the perceptron*" [15]. The latter is nothing more than an expression denoting a very basic piece of learning, namely a process that encodes (memorizes) experiences in a numeric space. This process results in a collection of numbers called trained memory. However, the process of *human learning* results (among many other things) in texts like this one that we write here, i.e. in well-articulated logical discourses about a certain part of reality perceived by us. Our discourses are pieces of complex knowledge expressed with formal correctness and produced by our brain – a complex system of neural networks able to play cooperative games, able to make massively distributed and massively parallel computations, but unfortunately unable to describe itself. This is why reverse engineering the human brain is one of the most relevant tasks for all AI sub-disciplines of our days and is the

only task that could make us hope we will ever succeed to endow a machine with *artificial learning* capabilities.

The discrepancy between expectations and achievements in AI is fueled by overvaluation in the first place. Any objective and well-educated mind knows that what a system could achieve depends on how controllable it is and on what states are observable. In other words, from a formal standpoint, what is achievable on a given system is syntactically correct and semantically relevant (all in all, is formally demonstrable) in the formal language and theory that describe the system. Hence, full understanding of a given system means that our expectations and system behavior perfectly match each other.

The overvaluation occurs especially in the cases in which an observable state is treated as being something that it is not and/or as having properties that it does not have. A special paradigm of *learning* treated in AI is that of supervised learning by exposure to examples. The simplest case assumes that a *perceptron learns* to differentiate between two classes of examples (learns a binary classification). We marked the sequence "*perceptron learns*" because, as this paper follows to show, it is more appropriate to say that the (memory of a) *perceptron encodes* the separation between two linearly separable classes of examples. The process of *learning* is far much complicated (as a routine) and far more spectacular as results than the simple mechanical encoding procedure through which a perceptron memorizes the separation between two classes of examples. Human learning, artificial learning, artificial perception and mechanical encoding actually are four different things in AI: *human learning* is a target behavior, *artificial learning* is a computational simulation of human learning, *artificial perception* is an analogy of *human perception*, learning is perception based and *mechanical encoding* is a procedure that may allow artificial perception. Saying that *mechanical encoding* is the same thing with *artificial perception* or with *artificial learning* is nothing else than overvaluation. Talking about learning without making the differences between *human* and *artificial learning* is also an overvaluation of the latter.

2.3 What Is the Artificial Perception?

Firstly, let us discuss about the *artificial representation of human perception* and to illustrate them on the simple case of a binary classification encoded as a trained memory. Let us consider two classes C^+ and C^- of linearly separable n-dimensional

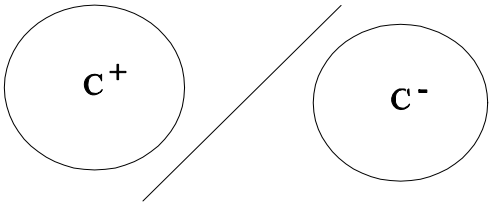

Fig. 1. Graphical representation of two linearly separable classes

positive and negative examples, respectively (as those represented in Fig. 1), used as training examples for the artificial neuron (perceptron) described in Fig. 2, where:

$$X=[x_1, x_2, \dots, x_n]$$

is the current example applied to the neuron,

$$W=[w_1, w_2, \dots, w_n]$$

is the synaptic memory, θ is the threshold and the fire function

$$Y^{\pm}(X) = f^{\pm}(X, W, \theta)$$

establishes the instant input-output relation of the neuron:

$$f^{\pm}(X, W, \theta) = \text{sign}(W.X - \theta), \quad (1)$$

as a function depending on the instant internal activation of the neuron:

$$h(X, W) = W.X, \quad (2)$$

and on the threshold θ, where the dot operation in formula (2) signifies the scalar product.

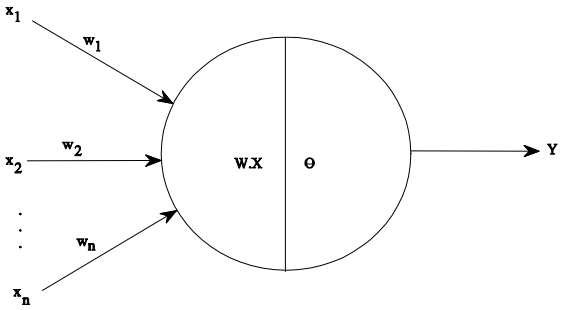

Fig. 2. Graphical representation of a perceptron

With these notations, the (memory of the) neuron is said to be trained if and only if:

$$\forall X \in C^+ \cup C^-,\ Y^{\pm}(X) = IC^+(X) - IC^-(X), \quad (3)$$

where IC^+ and IC^- are the regular indicator functions (binary membership functions / characteristic functions) of classes C^+ and C^-, hence:

$$Y^{\pm}(X) = 1 \text{ iff } X \in C^+ \text{ and } Y^{\pm}(X) = -1 \text{ iff } X \in C^- . \quad (4)$$

Hence, if the (memory of the) neuron is trained, then:

$$Y^{\pm}(C^+) = \{+1\} \text{ and } Y^{\pm}(C^-) = \{-1\}. \quad (5)$$

The case from above describes an artificial neuron with bipolar output (±1). When the output is binary, the classes may be denoted as C^1 and C^0, whereas the (memory of the) neuron is said to be trained if and only if:

$$\forall X \in C^0 \cup C^1,\ Y^{01}(X) = IC^1(X), \tag{6}$$

where IC^1 is the indicator function of class C^1 and the new instant input-output relation is as follows:

$$f^{01}(X, W, \theta) = \text{logical}(\ f^{\pm}(X, W, \theta) + 1\ ) \in \{0,1\}. \tag{7}$$

With these notations, if the (memory of the) neuron is trained, then:

$$Y^{01}(C^1) = \{1\} \text{ and } Y^{01}(C^0) = \{0\}. \tag{8}$$

In the two cases described above, each of the formulae (5) and (8) is an *artificial representation of the human perception* illustrated in Fig. 1, representation written in a first order logico-arithmetic formal language that aggregates constants (±1 or 0,1), inputs (X), states / memory instances (W, θ) and outputs (Y) accordingly to the production rules (1)-(8), as appropriate. If we do not wish to know such an artificial representation as a predicate, we still have the possibility to know it as an internal state (as a numeric constant), namely as the trained memory (W_t, θ_t). However, interpreting the assertion (W_t, θ_t) means to assign certain meanings to (a human perception represented as) a proposition (W_t, θ_t) written in a numerical language, a process that could result in very volatile / unstable results if the encoding-decoding rules (1)-(8) are not known, just like in the case of assertion $\mathcal{A}$ discussed in the introduction. On the contrary, knowing the production rules (1)-(8) may allow one to produce a different trained memory $(\widehat{W}_t, \widehat{\theta}_t)$, which still has the same meaning as (W_t, θ_t).

Consequently, the above examples and comments illustrate that human perceptions are encodable (human perceptions can be artificially represented) as trained memory sequences (numeric constants) even by using simplified models of the perceptron initially proposed by Rosenblatt [15], [16]. What is new here is the fact that we point out to a second form of artificial representation for the human perceptions, which consists in pieces of formal knowledge (not just in numeric constants), in demonstrable formulae within specific logico-arithmetic formal theories associated to a certain perceptron design.

Regardless their particular type, for the *artificial representations of the human perceptions* to become *artificial perceptions*, it is necessary that the artificial agent who finds and stores them to be self-aware and aware of the meanings that these artificial representations have. Hypothetically, an artificial agent that would actually have *artificial perceptions* should be able to produce propositions like "*I perceive that …*" and should to be aware of their meanings. Nevertheless, self-awareness and understanding meanings are open problems in AI today. Until the moment when significant progress will have been made on these two directions, the *artificial perception* is just a meaning (and a name) assigned in and by our mind for an *artificial representation of some human perception*. However, we analyze the possibility of developing self-aware software agents based on the basic design of a Cognitive Intelligent Agent given in [14].

3 Human vs. Artificial Perception of Similarity in OCR

In the particular case analyzed here, the dissimilarity between two hypostases of two different characters is artificially represented as linear separation. For example, when a perceptron instructed to recognize the character 'A' against all the other characters is fully trained, all instances of 'A' from the training set are linearly separated from all instances of all the other characters by a hyperplane whose parameters form the trained memory W. Hence, the difference D between the minimum activation computed for the positive examples and the maximum activation obtained for the negative examples is an artificial perception of the dissimilarity (separation) between the two classes. Let X^+_{min} be the positive example that realizes the minimum activation and let X^-_{max} be the negative example that realizes the maximum activation. With this notations, the number D/||W|| is the distance between two hyperplanes orthogonal to W, one containing X^+_{min} and the other containing X^-_{max}. Hence, the number d'=D/||W|| is also an artificial perception of the dissimilarity between the two classes (namely: C^+ containing 'A' instances, and C^- containing instances of other characters).

On the other hand, the distance between the two sets C^+ and C^-,

$$d\left(C^+,C^-\right)=\min(\{d(X, Y)|\ X\in C^+, Y\in C^-\}), \tag{9}$$

is the most objective expression of the dissimilarity between the two classes C^+ and C^-. The question is how accurate is the artificial perception d' compared to actual distance d.

Let X^+_{max} be the positive example that realizes the maximum activation and let X^-_{min} be the negative example that realizes the minimum activation. Then the number $\left|W.X^+_{max} - W.X^+_{min}\right| / \|W\|$ is an artificial perception for the diameter of the class C^+, whereas the number $\left|W.X^-_{max} - W.X^-_{min}\right| / \|W\|$ is an artificial perception for the diameter of C^-.

All in all, the trained memory W sets up an artificial perception (a geometrical view/perspective) that imprecisely encodes the diameter of C^-, the distance from C^- to C^+ and the diameter of C^+ as the numbers $\left|W.X^-_{max} - W.X^-_{min}\right| / \|W\|$, $d(C^+, C^-)$ and $\left|W.X^+_{max} - W.X^+_{min}\right| / \|W\|$. This situation allows us to establish an artificial 3D geometrical conventional representation of the two classes and of the perceived separation between them. The comparison between the ratio d'/d and the real unit tells us when the artificial perception of the separation between the two classes of characters is objective or maximally cointensive with the reality (d'/d=1), fuzzy undervaluated (d'/d<1), or fuzzy overvaluated (d/d'<1). This is why we sustain that even in the classic perceptron the artificial perception / learning is fuzzy (in terms of results). Besides, the update procedure through which the memory of the perceptron changes can be a part of a fuzzy if-then Sugeno rule [17] also. For example, let us consider the following class of if-then linguistic control rules:

IF:

C^- and C^+ are two separable classes of examples
And
W is a memory that must be trained
And
N is an *well-chosen* maximal number of epochs
And
R is a *well-chosen* real function having the abscise as asymptote at $+\infty$
And
SP is an *well-chosen* procedure of selecting four examples on which the memory W is trained during an epoch

THEN:

the update rule $(W_{n+1},t_{n+1}) = (W_n, t_n) + U(SP(n), n)$ converges *rapidly enough* to a *sufficiently well-trained* memory W .

instantiated as follows:

- C^+ contains 34 'A' instances, each of them memorized as 8-bit unsigned integer matrices of dimension 16x16, and C^-contains 34 instances for each of the other characters, memorized in the same manner;
- W is a memory randomly initialized;
- N is 1000;
- $R(n)= n*(\log_2(n))/2^n$;
- the selection procedure SP return the first two positive examples currently producing the smallest activations $(X^{1+}_{min}, X^{2+}_{min})$ and the first two negative examples currently producing the greatest activations $(X^{1-}_{max}, X^{2-}_{max})$;
- the update rule assumes that:

$$W_{n+1} = W_n + (X^{1+}_{min} + X^{2+}_{min}) *R(n),\ t_{n+1} = t_n - sqrt(\|W_n\|)$$
$$W_{n+1} = W_n - (X^{1-}_{max} + X^{2-}_{max})*R(n),\ t_{n+1} = t_n + sqrt(\|W_n\|)$$

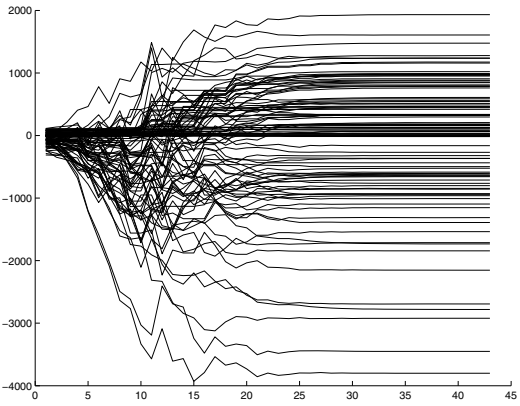

Fig. 3. Convergence of all synaptic memory components along the increasing number of epochs

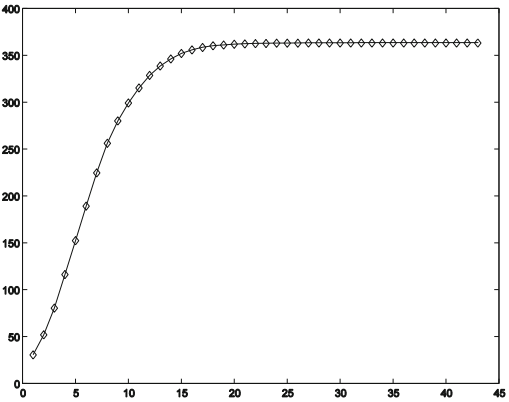

Fig. 4. Convergence of the neuronal threshold along the increasing number of epochs

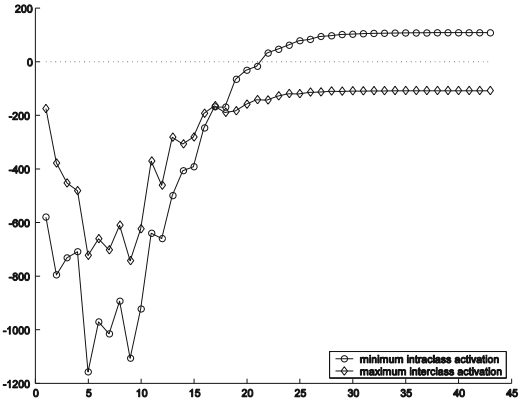

Fig. 5. Convergence of the minimum intraclass activation and maximum interclass activation, along the increasing number of epochs

An implementation of the above fuzzy training rule produced the results presented in figures 3-5 after 43 epochs. The only problem is that the distance between the classes C^- and C^+ as it is artificially perceived by the neuron is approximately d'=216, whereas the actual distance between the two classes is approximately d=730, hence the artificial perception of the separation between the two classes of characters is undervaluated (i.e. d'/d<1). The perceived diameters of the classes C^+ and C^- are 758 and 380, whereas the actual diameters of the two classes are 2019 and 3060, respectively.

However, accordingly to a very simple Turing test [18], the human decisions on recognizing characters are binary and have nothing to do with the numerical representations mentioned above. This is an example in which the human perception is actually crisp, whereas the artificial perception is actually fuzzy (partial, imprecise).

4 Human vs. Artificial Perception of Similarity in Iris Recognition

The most popular way of comparing two binary iris codes is to compute the Hamming distance or the Hamming similarity for the two codes. In this case, the similarity score is a fuzzy value within [0, 1]. However, as seen in [13], Hamming distance corresponds to an artificial perception encoded as a synaptic memory referred to as an untrained discriminant direction (see the formulae 1-4 in [13]).

In iris recognition, the training of the discriminant directions aims to diminish the confusion between the fuzzy intervals that underlay the biometric decisions (see Fig.1 from [11], and Fig. 4-5 from [3], for example).

An incipient stage of training the discriminant directions would mean that a narrow safety band (Fig. 2-3 from [13]) separates the two classes of imposter and genuine scores. An advanced stage of training the discriminant directions means that a comfortably wide safety band (Fig. 4-5 from [13]) separates the two classes of genuine and imposter scores. Nevertheless, as seen in Fig. 2-5 from [13], the biometric decisions corresponds to a fuzzy partitioning of the [0,1] interval, regardless the fact that the discriminant directions are trained (sufficiently) or not, i.e. in iris recognition, the artificial perception of the similarity between individuals is fuzzy.

On the contrary, accordingly to a very simple Turing test, the human decisions on recognizing irides are binary (as seen in Fig. 1.a [12]). This is another example in which the human perception is actually crisp, whereas the artificial perception is actually fuzzy (partial, imprecise).

5 Conclusion

Zadeh insisted on the ideas that (human) "*perceptions, in general, are both fuzzy and granular or, for short, f-granular*" and that "*in much, perhaps most, of human reasoning and concept formation, the granules are fuzzy*". According to this point of view, human reasoning, human concepts and human perceptions are f-granular.

On the contrary, in the two practical examples given here (Optical Character Recognition and Iris Recognition) in order to illustrate the concept of artificial perception, the situation is a little bit different. In both cases a simple Turing test shows that *artificial perceptions* of the dissimilarity between two different characters and between two different irides are fuzzy, whereas the corresponding *human perceptions* are, in fact, crisp. Despite being contradictory to Zadeh's belief expressed above, this fact comes very naturally, because ultimately, a perceptron emulates the human intelligent behavior through an artificial one, which compared to the original is weakened and imprecise enough.

Acknowledgments. We would like to thank *UbiSoft Romania* and *Spiru Haret University, Romania* for sponsoring this paper and for supporting the research efforts assumed by the team of *IEEE Student Members* working in the Artificial Intelligence & Computational Logic Laboratory - http://fmi.spiruharet.ro/bodorin/aicl/ .

References

[1] Ahangar, R.G., Ahangar, M.F.: Handwritten Farsi Character Recognition using Artificial Neural Network. International Journal of Computer Science and Information Security 4(1 & 2) (2009)
[2] Azoff, E.M.: Neural Network Time Series Forecasting of Financial Markets. John Wiley & Sons Inc. (1994)
[3] Balas, V.E., Motoc, I.M., Barbulescu, A.: Combined Haar-Hilbert and Log-Gabor Based Iris Encoders. In: Balas, V.E., Fodor, J., Varkonyi-Koczy, A. (eds.) New Concepts and Applications in Soft Computing. Studies in Computational Intelligence, vol. 417, pp. 1–26. Springer, Heidelberg (2012)
[4] Bhattacharjee, D., Basu, D.K., Nasipuri, M., Kundu, M.: Human Face Recognition Using Fuzzy Multilayer Perceptron. Journal of Soft Computing - A Fusion of Foundations, Methodologies and Applications Achive 14, 559–570 (2010)
[5] Coates, A., Carpenter, B., Case, C., Satheesh, S., Suresh, B., Wang, T., Ng, A.Y.: Text Detection and Character Recognition in Scene Images with Unsupervised Feature Learning. In: Proc. 11th Int. Conf. on Document Analysis and Recognition, ICDAR (2011)
[6] Copeland, B.J.: What is Artificial Intelligence? In: The Turing Archive for the History of Computing, http://www.alanturing.net/ (retrieved on May 29, 2012)
[7] Jain, L.C., Martin, N.M.: Fusion of Neural Networks, Fuzzy Systems and Genetic Algorithms: Industrial Applications. CRC Press (1998)
[8] Kasabov, N.K.: Foundations of Neural Networks, Fuzzy Systems, and Knowledge Engineering. MIT Press (1998)
[9] Kohonen, T.: The Self-Organizing Map. Proc. of the IEEE 78(9), 1464–1480 (1990)
[10] McCullock, W., Pitts, W.: A Logical Calculus of Ideas Immanent in Nervous Activity. Bulletin of Mathematical Biophysics 5, 115–133 (1943)
[11] Motoc, I.M., Noaica, C.M., Badea, R., Ghica, C.G.: Noise Influence on the Fuzzy-Linguistic Partitioning of Iris Code Space. In: 5th International Workshop on Soft Computing Applications, Szeged, Hungary, August 22-24 (2012)
[12] Popescu-Bodorin, N., Balas, V.E., Motoc, I.M.: 8-Valent Fuzzy Logic for Iris Recognition and Biometry. In: Proc. 5th IEEE Int. Symp. on Computational Intelligence and Intelligent Informatics, pp. 149–154. IEEE Press (2011)
[13] Popescu-Bodorin, N., Balas, V.E., Motoc, I.M.: Iris Codes Classification Using Discriminant and Witness Directions. In: Proc. 5th IEEE Int. Symp. on Computational Intelligence and Intelligent Informatics, pp. 143–148. IEEE Press (2011)
[14] Popescu-Bodorin, N., Balas, V.E.: From Cognitive Binary Logic to Cognitive Intelligent Agents. In: Proc. 14th Int. Conf. on Intelligent Engineering Systems, pp. 337–340. Conference Publishing Services - IEEE Computer Society (May 2010)
[15] Rosenblatt, F.: The Perceptron, A Perceiving and Recognizing Automaton. Report No. 85-460-1, Cornell Aeronautical Laboratory (January 1957)

[16] Rosenblatt, F.: Pattern Recognizing Apparatus. U.S. Patent No. 3192505 (July 14, 1961/June 29, 1965)
[17] Sugeno, M., Yasukawa, T.: A Fuzzy-Logic-Based Approach to Qualitative Modeling. IEEE Trans. on Fuzzy Systems 1(1), 7–31 (1993)
[18] Turing, A.M.: Computing machinery and intelligence. Mind 59, 433–460 (1950)
[19] Yamakawa, T.: Pattern recognition hardware system employing a fuzzy neuron. In: Proc. Int. Conf. on Fuzzy Logic and Neural Networks, Iizuka, Japan, pp. 943–948 (July 1990)
[20] Yamakawa, T., Uchino, E., Miki, T., Kusanagi, H.: A neo fuzzy neuron and its applications to system identification and prediction of the system behavior. In: Proc. 2nd Int. Conf. on Fuzzy Logic and Neural Networks, Iizuka, Japan, pp. 477–483 (1992)
[21] Zadeh, L.A.: A New Direction in AI - Toward a Computational Theory of Perceptions. AI Magazine 22(1), 73–84 (2001)

Noise Influence on the Fuzzy-Linguistic Partitioning of Iris Code Space

Iulia Maria Motoc[1], Cristina Madalina Noaica[1], Robert Badea[1], and Claudiu Gheorghe Ghica[1,2]

[1] Artificial Intelligence & Computational Logic Lab.,
Mathematics & Computer Science Department,
Spiru Haret University, Bucharest, Romania
{motoc,noaica,badea}@ irisbiometrics.org
[2] Clintelica AB
claudiu.ghica@clintelica.com

Abstract. This paper analyses the set of iris codes stored or used in an iris recognition system as an f-granular space. The f-granulation is given by identifying in the iris code space the extensions of the fuzzy concepts *wolves*, *goats*, *lambs* and *sheep* (previously introduced by Doddington as *'animals'* of the biometric menagerie) – which together form a partitioning of the iris code space. The main question here is how objective (stable / stationary) this partitioning is when the iris segments are subject to noisy acquisition. In order to prove that the f-granulation of iris code space with respect to the fuzzy concepts that define the biometric menagerie is unstable in noisy conditions (is sensitive to noise), three types of noise (*localvar*, *motion blur*, *salt and pepper*) have been alternatively added to the iris segments extracted from University of Bath Iris Image Database. The results of 180 exhaustive (all-to-all) iris recognition tests are presented and commented here.

Keywords: fuzzy biometric menagerie, salt and pepper noise, motion blur, localvar noise.

1 Introduction

This paper assumes that the set of iris codes stored or used in an iris recognition system is an f-granular [12] space. The f-granules of this space are collections of iris codes identified as extensions of the fuzzy concepts *wolves*, *goats*, *lambs* and *sheep* introduced by Doddington (in speech recognition, [3]) and Yager (in iris recognition, [11]) as *'animals'* of the biometric menagerie, which together form a partitioning of the iris code space (further denoted as ICS). Let us denote this partitioning as Fuzzy Biometric Menagerie (FBM, [9]). Is FBM an objective (stable / stationary) attribute of the group of persons that pass through different iris recognition systems functioning in different calibration regimes? Different iris recognition system may have different security levels (is not the same thing to use a safety threshold and to use a safety band for separating genuine and imposter comparisons, for example), different procedures for encoding the iris texture, may use iris codes of different size and iris images

V.E. Balas et al. (Eds.): Soft Computing Applications, AISC 195, pp. 71–82.
springerlink.com

acquired in noisy conditions. Is FBM invariable when any of these calibration parameters change? This question partially got its answer in [9] where Popescu-Bodorin et al. have shown that a change of the iris texture encoder, of the iris code size, or of the security settings determines a change of the FBM partitioning.

As a continuation of the research undertaken in [9], this paper demonstrates that noisy acquisition procedures also change the FBM partitioning of ICS.

In order to prove that a noisy acquisition change the FBM partitioning of ICS, 180 exhaustive iris recognition tests were performed using iris codes of dimensions 64x4, 128x8 and 256x16, obtained from the unwrapped iris segments that were randomly artificially noised with *localvar*, *salt and pepper* and *motion blur*. The tests were performed using two security settings (EER threshold and a safety band) that allow us to identify the *extensions of the f-concepts wolf / goat*. In order to highlight that the FBM partitioning of the ICS is unstable, the experimental results of our tests were compared with those obtained in [9], also.

2 FBM vs. System Logic and Safety Models

All templates stored in an iris recognition system are *sheep-templates* if and only if, there is a clear gap between the maximum imposter similarity score and the minimum genuine similarity score. In other words, the *sheep-templates* are those validating a *consistent theory* of iris recognition like the ones formalized in [8] as:

$$\mathcal{P}_C \rightarrow [max\{S(C)|C \in \mathcal{I}\} \lneqq min\{S(C)\}|C \in \mathcal{G}],$$

$$\mathcal{P}_C \rightarrow [max\{S(C)|C \in \mathcal{I}\} \ll min\{S(C)|C \in \mathcal{G}\}],$$

where P_C denotes "*a conjunction of prerequisite conditions (relative to the image acquisition and processing at all levels from eye image to the iris code) expressed in binary logic*" (as said in [8]), $C = \mathcal{I} \cup \mathcal{G}$ is the natural disjoint partitioning of comparison space in imposter and genuine pairs, S is the similarity score and C denotes a comparison.

The fact that experimental genuine and imposter score distributions do not overlap each other certifies that no impersonation occurred in the system (there is no support for a false accept) and no user matches himself so bad such that to generate a false reject. Therefore, in such a case the extensions (the referents) of the concepts '*wolves'*, '*goats'* and '*lambs'* are empty, whereas the extension of the concept '*sheep'* is the entire set of iris codes recorded / tested in the biometric system. Fig. 7.c from [2] illustrates such an example. As seen there, in an example like that, the pessimistic envelopes of the imposter and genuine score distributions may help one identifying templates (or users) that are good candidates for the roles of lamb, wolf or goat, in a future in which the number of users or at least the number of templates stored in the database grows. This perspective is very well described by a Fuzzy 3-Valent Disambiguated Model (F3VDM, [7]) of biometric security. The following figure illustrates the correspondence between the FBM and the F3VDM associated to the iris recognition tests undertaken in [2] for the dual iris combined HH&LG Encoder (see also Fig. 7.c, Fig. 7.d, Fig. 8, Table 2 in [2]) approach:

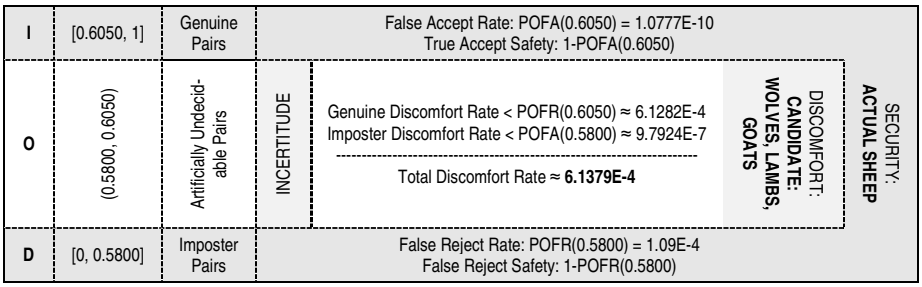

Fig. 1. An illustration of the relation between the Fuzzy Biometric Menagerie and the Fuzzy 3-Valent Disambiguated Model of biometric security

On the contrary, an overlapping between the genuine and imposter distributions certifies that there are indeed ambiguous scores obtained in the system, scores for which an imposter pair (comparison) could be labeled as being a genuine pair (comparison) or vice versa, depending on what threshold the system would use for giving the biometric decision. For example, if the score distributions overlap each other and the threshold is under the minimum genuine score, we could talk about goats in terms of candidates and about wolves and lambs as exemplified certitudes. If the score distributions overlap each other and the threshold is above the maximum imposter score, we could talk about wolves and lambs in terms of candidates and about goats as exemplified certitudes. When the distributions overlap each other and the security threshold is strictly between the minimum genuine and the maximum imposter score, all the concepts wolves, lambs and goats are exemplified.

3 Experimental Results

All the tests undertaken in this paper relay on the University of Bath Iris Image Database (UBIID, [10]). Circular Fuzzy Iris Segmentation procedure (proposed in [4], [5], available for download in [6]) facilitates the extraction of the unwrapped iris segments for the iris image available in the database. In order to extract the iris segments characteristics we used two encoders: Log-Gabor and a modified version of Haar-Hilbert [5] (the version from [6] has a limitation with respect to iris code size).

As seen in [9], the partitioning of the iris code space as a Biometric Menagerie is fuzzy and not quite objective. In other words, Fuzzy Biometric Menagerie is sensitive to system calibration variables. This article analyzes if the Fuzzy Biometric Menagerie is sensitive also to noise, or not. We consider here the cases in which artificial noise (localvar, motion blur and salt and pepper) is added to the initial iris segments.

The purpose of the tests was to realize a FBM partitioning of ICS while using a threshold and a safety band for each of the iris segment dimensions and for each type of artificial noise added (using the same noise intensity for the iris segments of the same dimension). Noise parameters were set such that the EER values of our tests to be double (at most) than those obtained in [9] for iris recognition tests that did not use

noise. The *marginal* and the *last wolf-* and *goat-templates* (introduced in [9]) identified in our tests were also compared with the ones obtained in [9] to show that the FBM partitioning is unstable and its instability is influenced by noise (artificial noise in this case). The total number of exhaustive iris recognition tests undertaken here is 180. A series of five tests has been done for each type of noise, iris code dimension, encoder used and security setting.

Because of the space restrictions that we must respect here, this paper presents only a selection of experimental results corresponding to 180 exhaustive all-to-all iris recognition tests described in the technical report [1].

The first half of this section presents results obtained after using a safety band that was narrowed until *marginal/first wolf-* and *goat-templates* [9] were found, while the second half presents *last wolf-* and *goat-templates*, i.e. results obtained after using the EER threshold (t_{EER}).

3.1 Experimental Results Obtained for Safety Bands

As in [9], the safety bands used here are determined by narrowing the maximal safety band [mGS, MIS] until goat and wolf-templates appear in the system, meaning that the concepts of *wolf-* and *goat-templates* refer non-empty sets of iris codes. More exactly, the templates determined in this section are the *first wolf* and *goat-templates* obtained for the first safety band that allow them to exist.

Fig. 2 presents the behavior of four *marginal wolf-templates* obtained for Haar-Hilbert and Log-Gabor encoders, and illustrates the fact that the number of impersonations could increase along with the increase of the iris code dimension.

Fig. 2.a and Fig. 2.b present the similarity scores obtained for the *first wolf-templates* (determined as iris codes of dimension 64x4). By comparing them, we can notice that the number of impersonations associated to *first wolf-templates* could differ from one encoder to another.

For iris codes of dimension 128x8, the *first wolf-template* with the highest number of impersonation was the one obtained for Haar-Hilbert encoder, as seen in Fig. 2.c and Fig. 2.d.

Table 1 presents the *marginal wolf-templates* obtained for Haar-Hilbert encoder when using iris codes of dimension 64x4 after performing 15 tests (3 series of 5 tests, each series with a different type of noise). The noise introduced in the unwrapped iris segments clearly influences the FBM partitioning of ICS. Consequently, almost all marginal wolf-templates detected in our tests differ from that obtained and presented in [9]. More than that, the templates obtained here for the same noise and same intensity are different, which means that the marginal wolf-templates depend also on the randomness of the noise.

Table 2 presents the *marginal wolf-templates* as iris codes of dimension 128x8 obtained using Log-Gabor encoder. The templates identified here as *marginal wolf-templates* are different from that obtained in [9] for the same encoder (see Table 3 from [9]). This fact supports the idea that the *marginal wolf-template* depends on the noise. Table 2 illustrates that, for *localvar* noise, the *marginal wolf-templates*

are identical to each other, which leads to the idea that the randomness of this type of noise do not affect any of the results (template, number of impersonations, safety band and its width). For *salt and pepper* and *motion blur*, the templates differ in three out of ten cases, which mean that the result could depend on the type of noise.

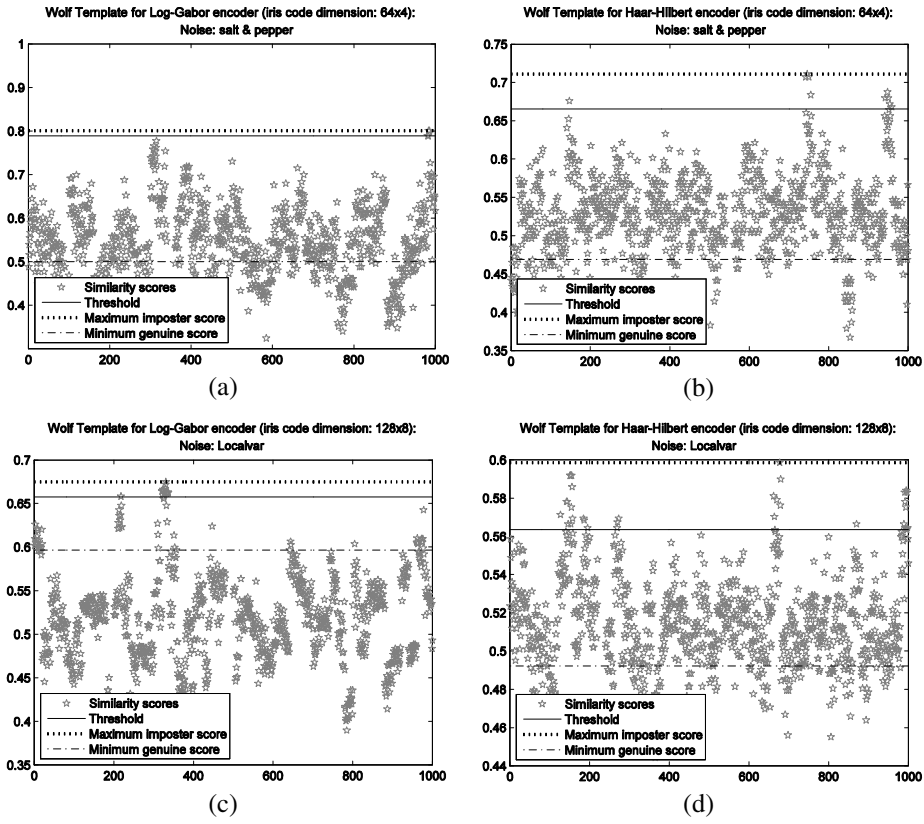

Fig. 2. The similarity scores associated to the imposter comparisons generated by the *marginal wolf-templates* along four tests: Log-Gabor (64x4, salt and pepper, 357 - a; 128x8, localvar, 482 - c) and Haar-Hilbert (64x4, salt and pepper, 546 - b, 128x8, localvar, 227- d) encoders

Table 1. Marginal *wolf-templates* obtained for Haar-Hilbert encoder (64x4)

	Impersonations	Template	Safety band	Width
Images without noise [9]	15	549	[0.6091, 0.6722]	0.0631
Salt and pepper	4, 8, 3, 3, 10	503, 165, 88, 230, 546	[0.5044, 0.6987], [0.5656, 0.6648], [0.5127, 0.6944], [0.5317, 0.7066], [0.5338, 0.6655]	0.1943, 0.0992, 0.1817, 0.1749, 0.1317
Motion Blur	3, 4, 3, 4, 3	239, 387, 959, 807, 505	[0.5630, 0.6987], [0.5595, 0.6905], [0.5741,0.6994], [0.5523, 0.7016], [0.5534, 0.7044]	0.1357, 0.1310, 0.1253, 0.1493, 0.1510
Localvar	3, 3, 3, 3, 4	541, 501, 510, 926, 755	[0.5791, 0.7139], [0.5864, 0.7183], [0.5708, 0.7144], [0.5117, 0.7061], [0.5584, 0.7072]	0.1348, 0.1319, 0.1436, 0.1944, 0.1488

Table 2. Marginal *wolf-templates* obtained for Log-Gabor encoder (128x8)

	Impersonations	Template	Safety band	Width
Images without noise [9]	17	484	[0.6277, 0.6555]	0.0278
Salt and pepper	9, 7, 14, 12, 8	**481**, **481**, 482, **481**, **481**	[0.6206, 0.6695], [0.6197, 0.6645], [0.6197, 0.6527], [0.6227, 0.6596], [0.6216, 0.6714]	0.0489, 0.0448, 0.0330, 0.0369, 0.0498
Motion Blur	11, 10, 9, 19, 17	**481**, **481**, **481**, 485, 484	[0.6158, 0.6654], [0.6258, 0.6671], [0.6039, 0.6735], [0.6163, 0.6415], [0.6114, 0.6484]	0.0496, 0.0413, 0.0696, 0.0252, 0.0370
Localvar	14, 14, 14, 14, 14	**482**, **482**, **482**, **482**, **482**	[0.6267, 0.6575], [0.6267, 0.6575], [0.6267, 0.6575], [0.6267, 0.6575], [0.6267, 0.6575]	0.0308, 0.0308, 0.0308, 0.0308, 0.0308

The comparison between Fig. 3.a – Fig. 3.b and Fig. 3.c – Fig. 3.d illustrates that, along with the increasing dimension of the iris code, the number of mismatches corresponding to the *marginal goat-templates* can decrease considerably when the iris codes are generated using Log-Gabor encoder.

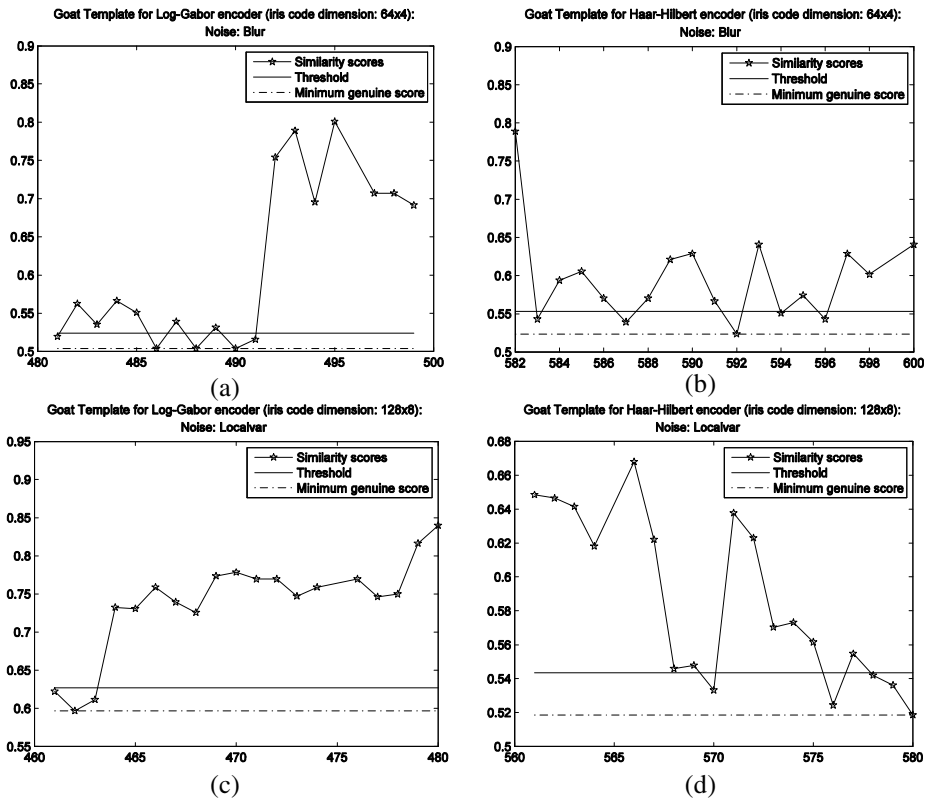

Fig. 3. The similarity scores associated to the genuine comparisons generated by the *first goat-templates* along four tests: Log-Gabor (64x4, blur, 496 - a; 128x8, localvar, 475 - c) and Haar-Hilbert (64x4, blur, 581 - b, 128x8, localvar, 565 - d) encoders

The discomfort rate could decrease along with the increase of the iris code dimension, as seen in Fig. 3.c and Fig. 3.d.

As seen in Table 3, for each noise, in one out of five tests, the *marginal goat-template* was the same with that presented in Table 3 from [9]. This can happen from two reasons: (1) the Haar wavelet transform was able to remove a significant part of the noise, and (2) the noise influence can be insignificant enough to have the same goat-template. For each noise, the templates were different in 3 out of 5 successive tests, performed at the same noise intensity, which means that the randomness of the noise could change the *marginal goat-template*.

Table 4 illustrates that 5 out of 15 *marginal goat-templates* obtained in our tests are identical with that presented in [9], the reasons being the same as the ones presented above. Even if in the majority of our tests the *marginal goat-templates* were different from the one presented in [9], the templates were identical for all three noises.

Table 3. Marginal *goat-templates* obtained for Haar-Hilbert encoder (64x4)

	Rejections	Template	Safety band	Width
Images without noise [9]	3	**565**	[0.6091, 0.6722]	0.0631
	2, 2,	**580**, 566,	[0.5044, 0.6987], [0.5656, 0.6648],	0.1943,0.0992,
Salt and pepper	2 ,2 ,	581, **565**,	[0.5127, 0.6944], [0.5317, 0.7066],	0.1817,0.1749,
	2	**580**	[0.5338, 0.6655]	0.1317
	2, 2,	566, **581**,	[0.5630, 0.6987], [0.5595, 0.6905],	0.1357, 0.1310,
Motion Blur	2, 3,	597, **565**,	[0.5741, 0.6994], [0.5523, 0.7016],	0.1253, 0.1493,
	5	**581**	[0.5534, 0.7044]	0.1510
	2, 2,	582, 566,	[0.5791, 0.7139], [0.5864, 0.7183],	0.1348, 0.1319,
Localvar	2, 2,	**581**, **565**,	[0.5708, 0.7144], [0.5517, 0.7061],	0.1436, 0.1544,
	2	**581**	[0.5584, 0.7072]	0.1488

Table 4. Marginal *goat-templates* obtained for Haar-Hilbert encoder (128x8)

	Rejections	Template	Safety band	Width
Images without noise [9]	3	**565**	[0.5456, 0.6823]	0.1367
	2, 2,	580, **565**,	[0.5198, 0.5925], [0.5256, 0.5955],	0.0727, 0.0699,
Salt and pepper	2, 2,	580, 580,	[0.5336, 0.5963], [0.5278, 0.5864],	0.0627, 0.0586,
	2	580	[0.5307, 0.5884]	0.0577
	2, 2,	580, 580,	[0.5287, 0.5983], [0.5365, 0.5944],	0.0767, 0.0579.
Motion Blur	2, 2,	580, 580,	[0.5237, 0.6004], [0.5256, 0.5945],	0.0767, 0.0689,
	2	580	[0.5178, 0.6013]	0.0835
	5, 2,	**565**, **565**,	[0.5436, 0.5863], [0.5228, 0.5885],	0.0427, 0.0657,
Localvar	2, 2,	**565**, 580,	[0.5322, 0.5635], [0.5162, 0.5766],	0.0313, 0.0604,
	2	**565**	[0.5188, 0.5935]	0.0747

3.2 Experimental Results Obtained for t_{EER} Thresholds

This subsection presents the results obtained in 60 selected exhaustive iris recognition tests performed by running the biometric system at EER threshold t_{EER}. The intensity of the noise in all of these tests was limited by the condition that for a given encoder and for a given code dimension, the EER values obtained in our test to be at most double than the values obtained in [9].

Fig. 4.a and Fig. 4.b represent the behavior of the *last wolf-templates* under the influence of *localvar*, showing that the number of impersonations is higher for the template obtained for Log-Gabor than the one obtained for Haar-Hilbert. On the contrary, for the *last wolf-templates* represented in Fig. 4.c and Fig. 4.d, the number of impersonations is higher for the one obtained for Haar-Hilbert encoder.

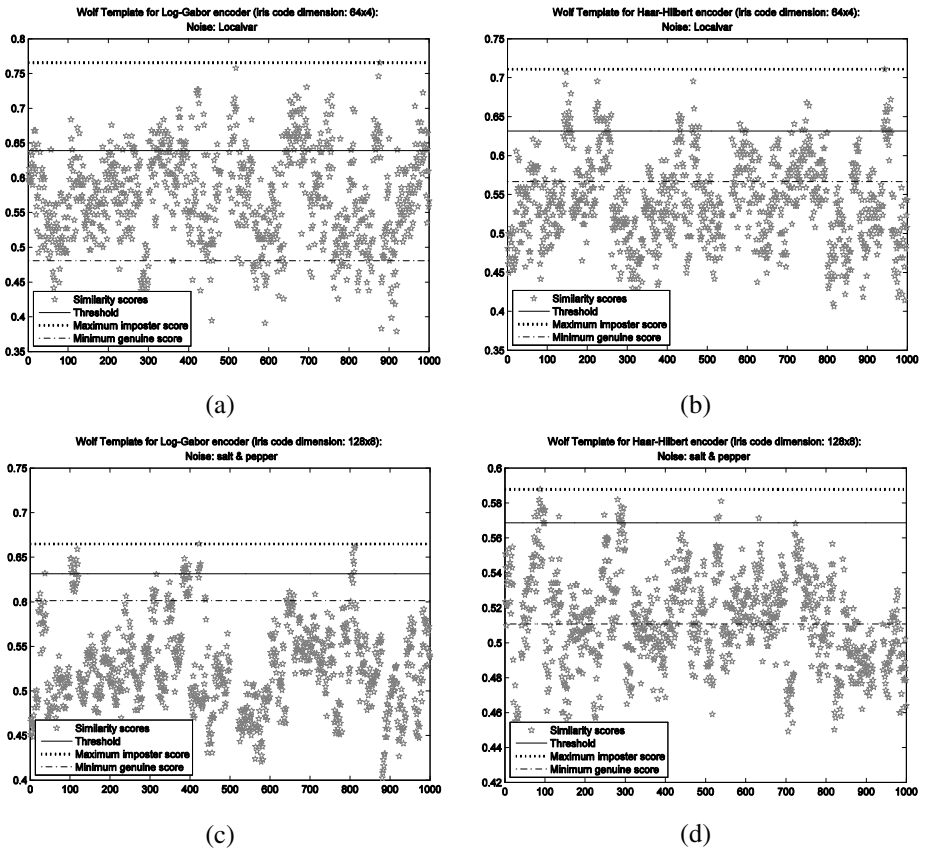

Fig. 4. The similarity scores associated to the imposter comparisons generated by the *last wolf-templates* along four tests: Log-Gabor (64x4, localvar, 495 - a; 128x8, salt and pepper, 505 - c) and Haar-Hilbert (64x4, localvar, 548 - b, 128x8, salt and pepper, 924 - d) encoders

Table 5 presents the experimental results obtained in [9] and in our iris recognition tests when searching for *last wolf-templates*. All tests use iris codes of dimension 64x4 generated with Log-Gabor iris texture encoder. For each artificial noise, the *last wolf-templates* detected in our tests are different from the one mentioned in Table 3 from [9] and, most of them, are even different from each other. By comparing our results with those obtained in [9], for the same experimental setup (except the presence of the noise), it can be observed that the number of impersonations obtained in [9] is significantly smaller than the ones obtained in our tests (the presence of noise stimulates impersonation). The EER points from our tests are different from each other (with one exception, when the EER value is 4.37E-2 for the fourth test in both *salt and pepper* and *motion blur*) and different from those presented in [9]. These results advocate for the subjectivity of "*last wolf-template*" concept.

Table 6 stores the experimental results obtained in those tests in which the Log-Gabor iris texture encoder generates iris codes of dimension 128x8. By

comparison, the *last wolf-templates* identified in our tests are all different from the one presented in [9], and in general different from each other, also. This highlights the fact that the noise is a very important factor that affects the FBM partitioning of ICS. By analyzing the *last wolf-templates* resulted from our tests for each noise, we found noticeable that the extension of the *f-concept wolf* changes from one test to another. The tests using the *localvar* noise are the only ones that provide identical *last wolf-templates*. However, this is an isolated case that could not advocate for the objectivity of the '*wolf*' concept.

Table 5. *Last wolf-templates* obtained for Log-Gabor encoder (64x4)

	Impersonation	Template	EER	t_{EER}
Images without noise [9]	63	236	4.08E-2	0.7529
Salt and pepper	134, 156, 147, 137, 135	679, 250, 382, 240, 250	4.27E-2, 4.55E-2, 4.82E-2, 4.37E-2, 4.28E-2	0.6471, 0.6431, 0.6431, 0.6431, 0.6471
Motion blur	147, 147, 147, 171, 139	679, 669, 389, 389, 240	4.29E-2, 4.32E-2, 4.16E-2, 4.37E-2, 4.11E-2	0.6431, 0.6431, 0.6431, 0.6431, 0.6431
Localvar	134, 183, 163, 148, 169	238, 495, 387, 117, 492	4.18E-2, 4.51E-2, 4.56E-2, 4.54E-2, 4.57E-2	0.6431, 0.6392, 0.6392, 0.6392,0.6392

Table 6. Last *wolf-templates* obtained for Log-Gabor encoder (128x8)

	Impersonations	Template	EER	t_{EER}
Images without noise [9]	22	392	9.37E-4	0.6392
Salt and pepper	25, 24, 29, 22, 29	**387**, 395, **387**, 484, **505**	1.70E-3, 1.30E-3, 1.80E-3, 1.80E-3,1.70E-3	0.6314, 0.6353, 0.6275, 0.6314, 0.6314
Motion blur	23, 24, 27, 21, 28	**387**, 485, **505**, 481, 118	1.40E-3, 1.70E-3, 1.30E-3, 1.40E-3, 1.80E-3	0.6353, 0.6353, 0.6353, 0.6353,0.6314
Localvar	20, 20, 20, 20, 20	**482**, **482**, **482**, **482**, **482**	1.10E-3, 1.10E-3, 1.10E-3, 1.10E-3, 1.10E-3	0.6392, 0.6392, 0.6392, 0.6392, 0.6392

Fig. 5.a and Fig. 5.b represent the behavior of the *last goat-templates* resulted for iris codes of dimension 64x4 generated under the influence of *salt and pepper* noise. Between the two presented templates, the one encoded with Haar-Hilbert has the highest number of rejections (17) which means that the noise distribution affected this template more than the one obtained for Log-Gabor. The similarity scores oscillate more in Fig. 5.a than in Fig. 5.b. The same thing happens in Fig. 5.c and Fig. 5.d. This shows that Haar-Hilbert encoder is much more sensitive to noise influence.

Table 7 presents the case when one of the *last goat-templates* obtained in our tests is identical with the one presented in [9]. However, this is an isolated case, also. Table 8 stores the experimental results obtained using iris codes of dimension 128x8. All our tests in this series indicate the same *last goat-template*, which is the same template obtained in [9], as well. After a visual examination of the eye image that corresponds to the *last goat-template detected* (565), and after a visual comparison of the pairs of images associated to the genuine goat scores, we found that: firstly, the subject wear contact lens (the contact lenses can damage the segmentation process

performance), and secondly, the limbic boundary detected for the image 565 was misplaced accidentally, and therefore the physical support indicated by it is not the actual limbic boundary. This situation highlights the fact that the FBM partitioning of ICS is depending on the segmentation process, also.

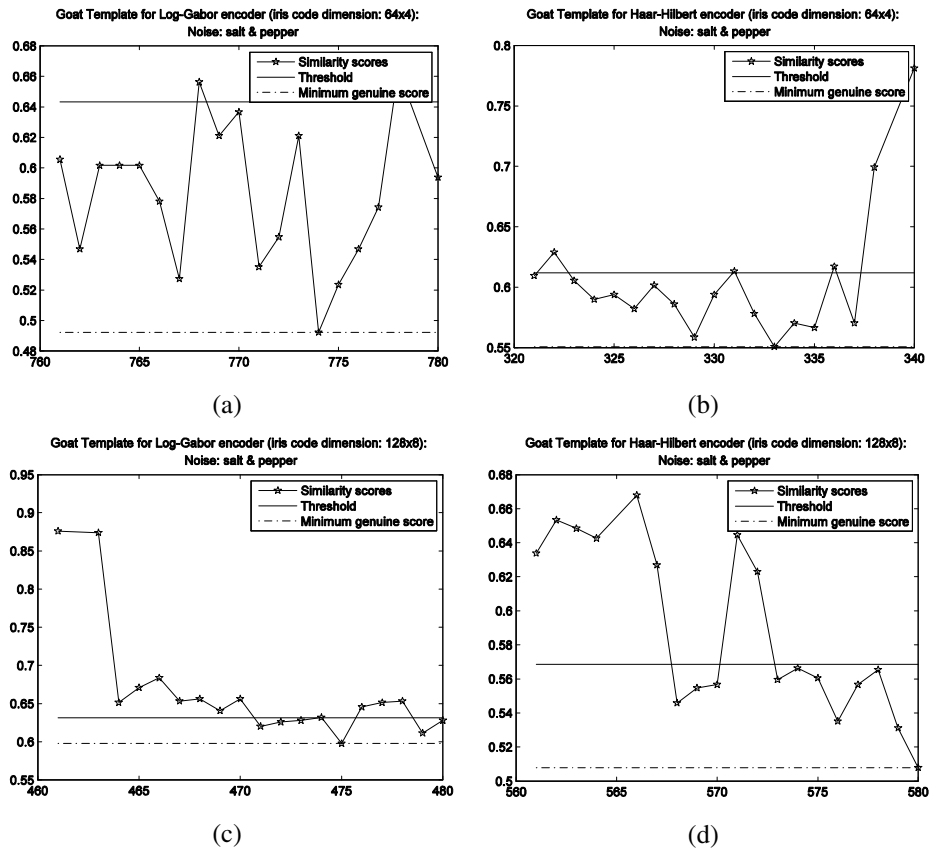

Fig. 5. The similarity scores associated to the genuine comparisons generated by the *last goat-templates* along four tests: Log-Gabor (64x4, salt and pepper, 779 - a; 128x8, salt and pepper, 462 - c) and Haar-Hilbert (64x4, salt and pepper, 339 - b, 128x8, salt and pepper, 565 - d) encoders

Table 7. *Last goat-templates* obtained for Log-Gabor encoder (64x4)

	Rejections	Template	EER	t_{EER}
Images without noise [9]	11	**493**	4.08E-2	0.7529
Salt and pepper	12, 18, 15, 17, 18	**493**, 993, **359**, **779**, 443	4.27E-2, 4.55E-2, 4.82E-2, 4.37E-2, 4.28E-2	0.6471, 0.6431, 0.6431, 0.6431, 0.6471
Motion blur	14, 15, 17, 12, 15	**360**, **359**, **779**, 817, **360**	4.29E-2, 4.32E-2, 4.16E-2, 4.37E-2, 4.11E-2	0.6431, 0.6431, 0.6431, 0.6431, 0.6431
Localvar	13, 15, 14, 16, 16	**359**, 429, **359**, **359**, 119	4.18E-2, 4.51E-2, 4.56E-2, 4.54E-2, 4.57E-2	0.6431, 0.6392, 0.6392, 0.6392, 0.6392

Table 8. *Last goat-templates* obtained for Haar-Hilbert encoder (128x8)

	Rejections	Template	EER	t_{EER}
Images without noise [9]	6	565	1.70E-3	0.5765
Salt and pepper	9, 8, 8, 11, 11	565, 565, 565, 565, 565	2.70E-3, 2.60E-3, 2.70E-3, 2.80E-3, 2.60E-3	0.5686, 0.5686, 0.5686, 0.5686, 0.5686
Motion blur	8, 8, 9, 8, 10	565, 565, 565, 565, 565	2.20E-3, 2.00E-3, 2.10E-3, 2.10E-3, 2.30E-3	0.5765, 0.5765, 0.5765, 0.5765, 0.5765
Localvar	9, 10, 9, 8, 8	565, 565, 565, 565, 565	3.40E-3, 3.10E-3, 3.10E-3, 2.60E-3, 3.40E-3	0.5647, 0.5647, 0.5647, 0.5686, 0.5647

All the 120 experimental results presented in this section show that the noise is an important factor that influences the FBM partitioning of ICS. There have been a few cases when the template was candidate to be a *last wolf-/goat-template* several consecutive times but these cases are isolated, or there is a strong and objective reason for them to happen (as the one presented in Table 8). In conclusion, the instability of the identified wolf / goats templates indicates that a noisy acquisition process is an important factor that could influence the performances of an iris recognition system.

4 Conclusions

This paper shown that the FBM partitioning of iris code space, the consistency and fuzziness of FBM and of its underlying concepts all depend not only on the system calibration (in terms of iris texture encoder and iris code dimension), but also on the noise that could affect iris image acquisition process. The experimental results from a total of 36 series of iris recognition tests (5 test in each series) undertaken for Bath Database shown that, in iris recognition, the so-called Biometric Menagerie definitely is a fuzzy and inconsistent concept. The extensions of the fuzzy concepts *'wolf'* and *'goat'* vary under the influence of noisy acquisition and system calibration.

References

[1] Badea, R., Noaica, C.M, Motoc, I.M.: Technical Report - Biometric Menagerie is sensitive to noise. Artificial Intelligence & Computational Logic Laboratory, Mathematics and Computer Science Department, Spiru Haret University (June 2012).

[2] Balas, V.E., Motoc, I.M., Barbulescu, A.: Combined Haar-Hilbert and Log-Gabor Based Iris Encoders. In: Balas, V.E., Fodor, J., Varkonyi-Koczy, A. (eds.) New Concepts and Applications in Soft Computing. Studies in Computational Intelligence, vol. 417, pp. 1–26. Springer, Heidelberg (2012)

[3] Doddington, G., Liggett, W., Martin, A., Przybocki, M., Reynolds, D.: Sheep, Goats, Lambs and Wolves: A Statistical Analysis of Speaker Performance in the NIST 1998 Speaker Recognition Evaluation. In: Int'l Conf. Spoken Language Processing (ICSLP), Sydney, vol. 4, pp. 1351–1354 (1998)

[4] Popescu-Bodorin, N.: Exploring New Directions in Iris Recognition. In: 11th International Symposium on Symbolic and Numeric Algorithms for Scientific Computing. pp. 384–391. Conference Publishing Services – IEEE Computer Society (September 2009)

[5] Popescu-Bodorin, N., Balas, V.E.: Comparing Haar-Hilbert and Log-Gabor based iris encoders on Bath Iris Image Database. In: Proc. 4th Int. Work. on Soft Computing Apps., pp. 191–196. IEEE Press (July 2010)
[6] Popescu-Bodorin, N.: Processing Toolbox for the University of Bath Iris Image Database (PT-UBIID-v.02) (2010), http://fmi.spiruharet.ro/bodorin/pt-ubiid/
[7] Popescu-Bodorin, N., Balas, V.E., Motoc, I.M.: 8-Valent Fuzzy Logic for Iris Recognition and Biometry. In: Proc. 5th IEEE Int. Symp. on Computational Intelligence and Intelligent Informatics, Floriana, Malta, September 15-17, pp. 149–154. IEEE Press (2011)
[8] Popescu-Bodorin, N., Balas, V.E., Motoc, I.M.: Iris Codes Classification Using Discriminant and Witness Directions. In: Proc. 5th IEEE Int. Symp. on Computational Intelligence and Intelligent Informatics, Floriana, Malta, September 15-17, pp. 143–148. IEEE Press (2011)
[9] Popescu-Bodorin, N., Balas, V.E., Motoc, I.M.: Biometric Menagerie - Fuzzy and Inconsistent. In: 5th International Workshop on Soft Computing Applications, Szeged, Hungary, August 22-24 (2012)
[10] Smart Sensors Limited, IRIS DB 50 (the former University of Bath Iris Image Database), http://www.smartsensors.co.uk/informations/bath-iris-image-database/ (retrieved on November 19, 2011)
[11] Yager, N., Dunstone, T.: The biometric menagerie. IEEE Transactions on Pattern Analysis and Machine Intelligence 32(2), 220–230 (2010)
[12] Zadeh, L.A.: A New Direction in AI - Toward a Computational Theory of Perceptions. AI Magazine 22(1), 73–84 (2001)

Excluded Middle and Graduation

Dragan G. Radojević

University of Belgrade, Mihajlo Pupin Institute,
Volgina 15, 11000 Belgrade, Serbia
dragan.radojevic@pupin.rs

Abstract. Excluded middle is one of the fundamental laws of the thought according to Aristotle and Boolean algebra. The valued interpretation of this law in the classical (two-valued) case is: an object has or does not have the analyzed property (for example, in the propositional logic: a proposition is either truth or untruth). It is known that the excluded middle is not valid in the frame of the conventional fuzzy logic in a wider sense (fuzzy sets theory, fuzzy logic in narrow sense, fuzzy relations) and, as a consequence, the conventional approaches are not in the Boolean frame (They are not Boolean consistent generalization of the classical case). In this paper, the algebraic explanation of the excluded middle is presented. To each property uniquely corresponds its complementary property (For example: in logic the complement of truth is untruth). Complementary property is determined by (a) *excluded middle*: it contains everything which analyzed property doesn't contain (there is nothing between)**;** and by (b) *non-contradiction*: there is nothing common with the analyzed property. Excluded middle and non-contradiction are the fundamental algebraic principles (value indifferent: valid in all valued realizations)!

Keywords: Excluded middle, Classical logic, Conventional fuzzy logic, Consistent real-valued realization of Boolean algebra.

1 Introduction

According to Aristotle, the excluded middle, non-contradiction and equivalence are the laws of thought. In the famous George Boole's book "The Laws of Thought" the excluded middle is also the fundamental law. A classical realization of the Boolean algebra is two-valued. The excluded middle in the classical logic is defined in the following way: "*Proposition is truth or untruth*" (complementary law is no contradiction: "*Proposition can't be truth and untruth*"). The conceptual problem arises by introducing the third value or more values (multi-valued logics) until real-valued and/or fuzzy logics. In the fuzzy logic, a fuzzy proposition can simultaneously possess both the truth property and the untruth property and in the fuzzy set theory one element has the analyzed property and, at the same time, it does not have this property and/or it has a complementary property. So, the classical definition of the excluded middle is correct only in two-valued realization.

V.E. Balas et al. (Eds.): Soft Computing Applications, AISC 195, pp. 83–91.
springerlink.com

The conventional fuzzy logics based on the truth functional principle are not in the Boolean frame. The truth functional principle is valid and/or it keeps the Boolean properties only in the classical two-valued case and/or it is not the fundamental principle and as a consequence it can't be the base of the Boolean consistent generalization of the valued realization. Actually, the truth functional principle is only a figure at the value level of the algebraic fundamental principle – structural functionality. The structure of the analyzed Boolean function (the element of the analyzed Boolean algebra) defines which atoms are included in it and/or which are not. This algebraic (value indifferent) characteristic is 0-1 vector of the length equal to the number of the atomic elements of the analyzed Boolean algebra, where 1 is the indicator that the corresponding atom is included in the analyzed element of the Boolean algebra and 0 means that this atom is not included. A structure of the combined element of the analyzed Boolean algebra is uniquely defined by the structures of its components – a structural functional principle. All Boolean axioms and theorems are valid for the structures of the elements of the Boolean algebra. As a consequence, all Boolean axioms and theorems are valid at the valued level independently of the realization type: two-valued, three-valued, many valued until real-valued.

2 Computing by Properties

In the theory of sets, the analyzed property generates corresponding set in the analyzed domain. The fundament of the computational cognition is computing with properties. In the new approach [2] a frame for computing with properties is the Boolean algebra. It is supposed in this paper that theorems and axioms of the Boolean algebra are the laws of the cognition generally, whereby the cognition is a fundament of the thought. This assumption implicates that the laws of cognition are irrelevant of the cognition domain, as well as of the valued type of the cognition - two-valued "black-white" approach characteristic for the classical cases or the generalized approaches until real-valued approach applied to fuzzy approaches. An algebraic interpretation is value indifferent. Real-valued realization of the Boolean algebra is a base for the consistent realization of the fuzzy logic in wider sense [3] as a real base for generalization of the classical theories based on the classical two-valued realization of the Boolean algebra [4]. All axioms and theorems of Boolean algebra, including the excluded middle, are valid in the Boolean consistent fuzzy logic in wider sense.

Fundamental task of the cognition is to distinguish the objects which are based on the relevant properties (characteristics, attributes ...). In the classical case one object has or doesn't have the analyzed property. Two objects can be distinguished, according to the analyzed property, if one has and the other one doesn't have this property. Two objects are identical according to the analyzed property, if both have or don't have this property. If one wants to distinguish a large number of objects in the classical way, then the complexity of the problem arises. This problem can elegantly be resolved by introducing the intensity (graduation) of properties; since one can differentiate two objects according to the same property if it is realized with different intensity (one object has the same property as the other one but with different intensity).

So, from the cognition point of view, the main advantage of graduation or intensity of the property is the reduction of the complexity, so that much more can be done with less in the process of the cognition.

Shortness or absence of the analyzed property is also a property – complementary property, which is uniquely determined with the analyzed property:

- Property and its complementary property don't have anything in common (law of non-contradiction).
- Anything which is not contained in the analyzed property is contained in its complementary property (law of excluded middle).

In general case, unlike the classical two-valued case, the analyzed object simultaneously possesses the analyzed property with some intensity and possesses the complementary property with the complementary intensity, so the sum of these two intensities is identically equal to one.

On the base of intensity of possessing independent properties of the analyzed element, one can calculate intensity of the combined properties using a real-valued realization of the Boolean algebra.

2.1 Context of Properties

A finite set of the independent (primary) properties

$$\Omega = \{p_1, ..., p_n\} \tag{1}$$

is the *context of properties*. The Boolean algebra uniquely corresponds to any context of properties. The Boolean algebra of properties has the following mathematical structure $\langle \mathrm{BA}(\Omega), \wedge, \vee, \bar{} \rangle$.

The set of properties $\mathrm{BA}(\Omega)$ is defined as follows:

$$\mathrm{BA}(\Omega) = \mathrm{P}(\mathrm{P}(\Omega)). \tag{2}$$

In the case when the context of properties is extended with the new independent properties which contains the corresponding new Boolean algebra, the old Boolean algebra is generated with the previous context of property. It is well know that if the number of the context elements is $n = |\Omega|$ then the number of all properties generated by corresponding Boolean algebra is $|\mathrm{BA}(\Omega)| = 2^{2^n}$.

In the case when $n = 0$ (context of property is empty $(\Omega = \varnothing)$), the Boolean algebra of property has two elements – two constants: **1 –** obligatory property and **0** – impossible property (complementary to obligatory property). Intensity of obligatory property **1** of any element of analyzed universe is identical to 1, and intensity of the impossible property **0** of any element of the analyzed universe is identical to **0**. As a consequence, these two properties cannot discern elements of the analyzed universe since all elements have them in the identical way.

In the case of the only one primary property (assign it by P), a corresponding Boolean algebra has four elements: besides **1** and **0,** it also has the analyzed property P and its complementary property $\overline{P}$. The complementary property $\overline{P}$ is uniquely defined by the primary property P applying laws of the excluded middle and contradiction.

$$P \vee \overline{P} = \mathbf{1}, \qquad P \wedge \overline{P} = \mathbf{0}. \tag{3}$$

In the case of property: (a) excluded middle: the *analyzed property includes everything that does not contain its complementary property (there is nothing between);* and (b) contradiction: the *analyzed property and its complementary property don't have anything in common*, Fig 1.

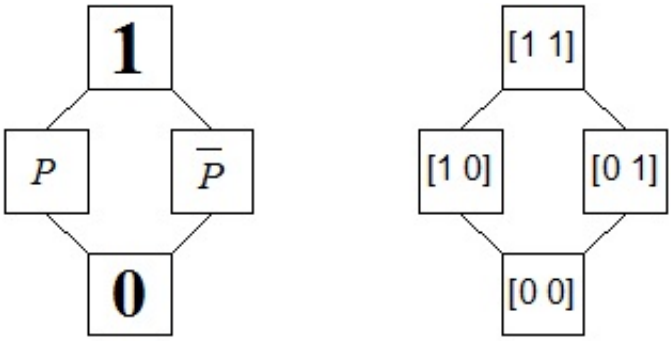

Fig. 1. Hasse diagram of Boolean algebra and corresponding structures generated by one property

In the classical case one object possesses or doesn't possess the analyzed property (possesses its complementary property), and at the same time it cannot possess and don't possess. That means that in the classical case the possessing of the properties preserves the Boolean characteristics of properties. But it is true only in the classical two-valued case. In general case, the information of intensity of possessing the analyzed property cannot preserve Boolean characteristics. For example, if a property is realized with intensity equal 0.5 (the analyzed object possesses property with the intensity 0.5) then, simultaneously, the complementary property has the intensity 0.5, but although they have the same values of the intensity they don't have anything in common.

2.2 Atomic Properties

The simplest elements of the Boolean algebra of the properties are the atomic properties [3]. In the given context of the properties, the atomic properties are uniquely defined.

***Example*:** *In the case of the following contexts* $\Omega = \{p_1, p_2\}$, *the corresponding atomic properties are:* $p_1 \cap p_2$, $p_1 \cap \overline{p}_2$, $\overline{p}_1 \cap p_2$, $\overline{p}_1 \cap \overline{p}_2$.

Any property (element of the Boolean algebra of properties) generated by the given context of properties, is uniquely defined by the structures – a set of the atomic properties (atoms) which are included in it. The complementary property of the analyzed property contains all other atoms which are not included in the analyzed property (excluded middle: there is not any atom which is not included in the analyzed property or its complementary property) and there isn't any atom which is simultaneously in the analyzed property and in its complement (non contradiction).

So, the union of any property and its complement contains all atoms of the corresponding Boolean algebra (it is equal to constant **1**) and their intersection is an empty set (it is equal to the constant **0**). As a consequence, the laws of cognition and/or thought: non contradiction and excluded middle have to be valid independently of their valued realization (as in the classical case and thus in the multi-valued until the real-valued case).

The number of the atomic properties (atomic elements) of the finite or atomic Boolean algebra of properties, generated by n primary (independent) properties, is equal 2^n.

The atomic properties of the analyzed Boolean algebra defined by the given context of properties $\Omega = \{p_1, ..., p_n\}$ are:

$$\alpha(S)(p_1, ..., p_n) = \bigwedge_{a_i \in S} p_i \bigwedge_{a_j \in \Omega \setminus S} \overline{p}_j, \qquad S \in \mathrm{P}(\Omega) \tag{4}$$

The corresponding polynomial representation of the atomic element of the Boolean algebra of the property is [3]:

$$\alpha^{\otimes}(S)\left(a_1^v, ..., a_n^v\right) = \bigotimes_{a_i \in S} a_i^v \bigotimes_{a_j \in \Omega \setminus S} \left(1 - a_i^v\right), \quad a_i^v, a_j^v \in [0,1]. \tag{5}$$

The values of atoms in general case are from the real interval [0, 1], but the sum of atom values is identically equal to one [3]:

$$\sum_{S \in \mathrm{P}(\Omega)} \alpha^{\otimes}(S)\left(a_1^v, ..., a_n^v\right) \equiv 1. \tag{6}$$

It is clear that classical (two-valued) case, as a special case, satisfies this identity since only one atom is equal to one and all the others are equal to 0. The atomic properties are the simplest in the sense that they don't have anything in common and they build any other property (the element of the Boolean algebra of property). The atomic properties which are included in the analyzed property are defined by their logical structures.

2.3 Structure of Property and Excluded Middle

Structure $\sigma_\varphi : \mathrm{P}(\Omega) \to \{0,1\}$ of the analyzed property $\varphi \in \mathrm{BA}(\Omega)$ is vector which elements are relations of the inclusion of the atomic properties in it.

$$\sigma_\varphi(S) = \begin{cases} 1, & \alpha(S)(p_1,...,p_n) \subset \varphi(p_1,...,p_n) \\ 0, & \alpha(S)(p_1,...,p_n) \not\subset \varphi(p_1,...,p_n) \end{cases}; \quad S \in \mathrm{P}(\Omega). \tag{7}$$

A structure of the analyzed element gives information which atomic elements of the Boolean algebra, are included in it and/or which are not. The fundamental or algebraic principle is a structural functionality: a *structure of any combined element of the Boolean algebra can be directly calculated by the structures of its component.* Any Boolean function (element of the analyzed finite Boolean algebra) can be represented as a polynomial expression [3]:

$$\varphi^{\otimes}(p_1,...,p_n) = \sum_{S \in \mathrm{P}(\Omega)} \sigma_\varphi(S)\alpha^{\otimes}(p_1,...,p_n) \tag{8}$$

The Boolean algebraic properties keep the structures of the Boolean elements. Since the element structures of the analyzed Boolean algebra are valued indifferently, then all the Boolean laws have to be preserved in any valued realization. A structural functionality principle has its consistent value representation ***only in two-valued realization***, known as a *truth functionality principle*. The usage of the truth functionality principle in multi-valued and/or real-valued or fuzzy cases is the main reason why these generalizations cannot be Boolean consistent.

The excluded middle in the consistent realization [3] is valid as all other Boolean laws. The elements of the analyzed property structure and its complementary properties are in the following relations:

$$\begin{aligned} &\varphi \in \mathrm{BA}(\Omega) \\ &\sigma_\varphi(S) = 1 \quad \leftrightarrow \quad \sigma_{\overline{\varphi}}(S) = 0 \\ &\sigma_\varphi(S) = 0 \quad \leftrightarrow \quad \sigma_{\overline{\varphi}}(S) = 1, \quad \forall S \in \mathrm{P}(\Omega). \end{aligned}$$

From which follows:

$$\sigma_{\varphi \vee \overline{\varphi}}(S) \equiv 1, \quad \forall S \in \mathrm{P}(\Omega). \tag{9}$$

Since the sum of values of all atomic elements is identically equal to 1, follows:

$$\varphi \vee \overline{\varphi} = 1. \tag{10}$$

The excluded middle is valid in all valued realizations.

Example: *In conventionally fuzzy set theory for fuzzy set A and its complement we have the following situation, fig 2.*

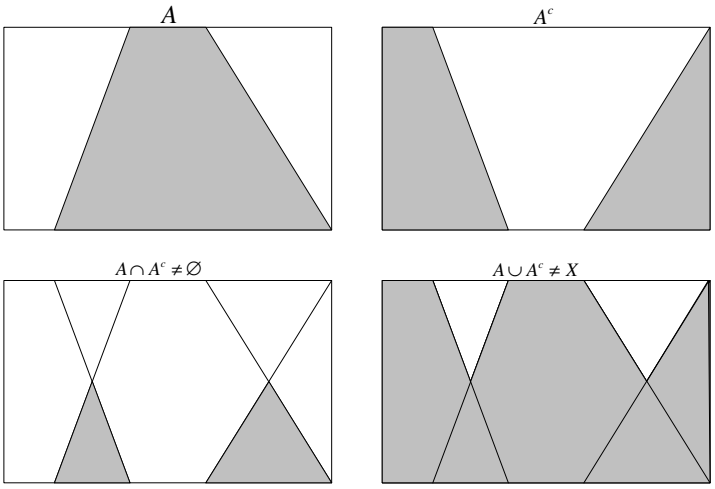

Fig. 2. Conventional fuzzy sets its complement and their intersection and union (contradiction and excluded middle are nog satisfied)

When we applied new appraoch we have Boolean consistent realizations, ilustrated on the figure3.

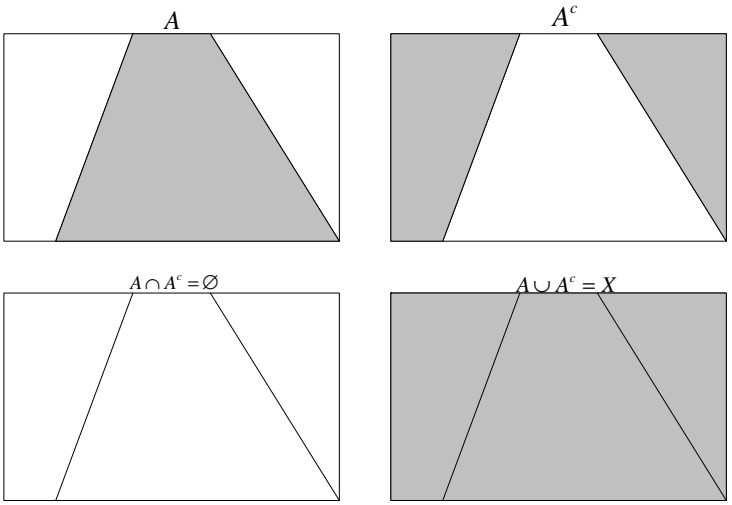

Fig. 3. For Boolean consistent fuzzy complement: laws of contradiction and excluded middle are satisfied contrary to fuzzy conventionally approaches

3 Conclusion

The excluded middle - the laws of thought, defined in antic time, is undoubtedly valid in the classical two-valued logic. However, it is questionable in the conventional multi-valued logics and the real-valued or the fuzzy logics which are based on the truth functional principle. The principle of the structural functionality [3] is fundamental and/or algebraic - valued indifferent principle. The structural principle says that the structure of the combined expression or property (in which atomic properties or atomic expressions are included and/or not) can be defined directly on the basis of the structures of its components. So, the structure is value indifferent or real algebraic property. The famous and favoured truth functional principle is only a figure of the structural functional principle at the value level for the classical two-valued case. In general multi-valued or real-valued case, the truth functionality is not able to preserve all laws of the Boolean algebra simultaneously. As a consequence, only generalization based on the structural functional principle is the Boolean consistent generalization. All the laws of the Boolean algebra are preserved in the consistent value generalization. Known definition of the excluded middle and non-contradiction are relevant only for the two-valued case. In general case, these two laws can be interpreted in the theory of the Boolean consistent fuzzy sets in the following way: any property uniquely defines its complementary properties so that they don't have anything in common (non-contradiction) and everything, which the analyzed property doesn't have, has its complementary property (excluded middle). It means that one object has the analyzed property with some intensity and its complementary property with complementary intensity so that the sum of the intensity of the complementary properties has to be identical to one (in the classical case if an object has the analyzed property with intensity equal to one then the intensity of the complementary property has to be zero and vice versa). Every finite Boolean algebra has atoms as the simplest elements. Any combined element of the Boolean algebra contains some atoms. A complementary element of the Boolean algebra contains all atoms which are not contained in the analyzed element. As a consequence, there are not any atoms which are in the analyzed element and in its complement (non-contradiction) and all atoms which are not in the analyzed element are in its complement element (excluded middle). In the classical case only one atom is realized with the intensity equal to one and all others have the intensity equal to zero. In general case more than one atom can have values larger than zero but so that its sum must be equal to one. So the sum of the intensity of the analyzed property and its complementary property of any object of the universe is equal to one.

References

Zadeh, L.: Fuzzy Sets. Information And Control 8, 338–353 (1965)

Radojević, D.: [0,1]-Valued logic: A natural generalization of Boolean logic. YUJOR 10(2), 185–216 (2000)

Radojević, D.: Interpolative Realization of Boolean algebra as a Consistent Frame for Gradation and/or Fuzziness. In: Nikravesh, M., Kacprzyk, J., Zadeh, L.A. (eds.) Forging New Frontiers: Fuzzy Pioneers II. STUDFUZZ, pp. 295–318. Springer, Heidelberg (2007)

Radojević, D.: Real sets as consistent Boolean generalization of classical sets. In: Zadeh, L.A., Tufis, D., Filip, F.G., Dzitac, I. (eds.) From Natural Language to Soft Computing: New Paradigms in Artificial Intelligence, pp. 150–171. House of Romanian Academy (2009) ISBN 978-973-27-1678-6

Models for Ranking Students: Selecting Applicants for a Master of Science Studies

Pavle Milošević[1], Ivan Nešić[1], Ana Poledica[1],
Dragan G. Radojević[2], and Bratislav Petrović[1]

[1] Faculty of Organizational Sciences, University of Belgrade,
Jove Ilića 154, Belgrade, 11000, Serbia
pasha.47@gmail.com
ivan.nesic@ewcom.ch
{ana.poledica,bratislav.petrovic}@fon.bg.ac.rs
[2] Mihajlo Pupin Institute, Volgina 154,Belgrade, 11000, Serbia
dragan.radojevic@automatika.imp.bg.ac.rs

Abstract. In this paper, we present a problem of candidates ranking for Master of Science studies at Faculty of Organizational Sciences, Belgrade (FOS). Current ranking model is based on weighted sum of two factors: average grade gained at undergraduate studies and number of points scored at the entrance exam for master studies. This universal model, although widespread and frequently used, is not entirely appropriate for a number of different Master of Science programs at FOS. Major problems of current model are that the model does not emphasize essential knowledge in accordance to wanted program and that the weighted sum is unable to model connection between variables. This paper presents a series of models, each more complex than the previous one, which are aggregating more relevant factor for ranking. Logical Aggregation (LA) is used as a method for the aggregation of certain variables in the last few models. LA is based on Interpolative Boolean algebra (IBA), a consistent multi-valued realization of Boolean algebra. This paper may be particularly interesting to all of those dealing with any form of students ranking, especially to university departments involved in enrolling students and selection for scholarships.

Keywords: weighted sum, fuzzy logic, Interpolative Boolean algebra, Logical aggregation, ranking students.

1 Introduction

Since 2007 Faculty of Organizational Sciences (FOS) has been enrolling students to Master of Science studies. The criterions of enrollment are entrance exam output and average grade at undergraduate level. Considering the differences between the courses existing at Master of Science studies at FOS, this universal ranking model may not be completely appropriate. The student's average grade is taken as indicator of previously acquired knowledge. That grade, as it is, does not show candidate's specific knowledge. For example, knowledge and grades gained at management domain should be additionally scored for enrolling in management departments. In this way

V.E. Balas et al. (Eds.): Soft Computing Applications, AISC 195, pp. 93–103.
springerlink.com

the advantage at the enrollment would be given to the candidates who showed special interests in certain domain.

The propositions of enrollment and description of the module that will be used as an example are given at Section 2. The current ranking model based on weighted sum and its deficiencies are explained at Section 3. The details are underlined by description of necessary criterions considering the specific module. In Section 4 there is the proposition considering the usage of changed weighted sum, which includes several factors. One of them, the one which underlines required specific knowledge, is aggregated by fuzzy logic. There is also a theoretical introduction to fuzzy logic. The subject of Section 5 is Interpolative Boolean algebra (IBA) and Logical aggregation (LA). IBA threats negation differently from fuzzy logic. There is also a suggestion of pseudo-logical function as criterion function. One of the criterions is aggregated using logical aggregation, which is based on IBA. In Section 6 there is an example of classical student ranking and the ranking using models suggested at previous sections and these results are analyzed and compared. In final section we give our conclusions and guidelines for the future work.

2 Proposition for Enrollment to a Master of Science Program at FOS

Eight different study programs are offered for enrollment at FOS, considering the proposition for student's enrollment to Master of Science studies 2011/2012. Every single program is divided into modules or study groups that candidate enrolls. There are thirty six modules, which are the forms of additional guidance. Study groups are highly specialized in very different areas. Some of fields that are modules focused on are Software engineering, E-business, Ecological Management, Business Intelligence and Decision Making, etc. Students are ranked in one of six rang lists depending on chosen Master of Science program. The criterions of enrollment for all study departments are the entrance exam output and the average grade at undergraduate level. The number of points at the entrance exam is more important than the average grade in 3/2 ratio.

Ranking models presented and analyzed in this paper will be focused on module Operational Researches. This module is analyzed because certain similarities with module Computer Statistics, the other module on the same program, and universal qualification exam, that is used for two more study departments. Module Operational Researches is a part of study department Operational Researches and Computer Statistics. Thirty five students can be enrolled to this module, and twelve of them have full scholarship. The qualification exam itself consists of thirty test questions with five offered answers each, but only one correct. The questions consider operational researches, statistics, software design, database and informational systems. This kind of qualification exam (the same test and the same literature) is used for Informational Systems and Technologies study department, as well as Software Engineering and Computer Sciences study departments. Candidates who enroll this module are ranked on a ranking list for the particular study department.

3 Current Ranking Model Based on Weighted Sum

The weighted sum model is probably the most commonly used approach for modeling this kind of problems. It ranks candidates based on weighted sum of normalized attributes. Weights in the model can be static or moving. The normalizing of the attributes ensures their comparability, as otherwise high numbered attributes would make disproportionate contributions to the overall score [9]. Weighted sum general form for one dimensional problem is following:

$$\sum_{i=1}^{n} w_i * u_i = p \tag{1}$$

According to previous, the conclusion is that weighted sum of criterion is used as a student ranking criterion and have this form:

$$w_1 * u + w_2 * k = p \tag{2}$$

It contains the following variables:

- u – average grade gained at undergraduate level in the interval [0, 100];
- k – number of points on the entrance exam for Master of Science studies in the interval [0, 100];
- p – candidate's total points in the interval [0, 100].

Values w_1 and w_2 are weights in this model, whose values are predefined at the enrolment proposition, so the criterion function has the following form:

$$0.4 * u + 0.6 * k = p \tag{3}$$

This function is modeled by weighted sum considering only the values of variables. This way, it is not possible to model their conditionality or connection between the variables using the logical operators.

The qualification exam to module Operational Researches consists of questions considering different domains: informational systems, computer sciences, operational researches, and statistics. All the questions are scored the same way. This is illogical – it is wanted to have knowledge considering all of these domains, but knowledge considering operational researches should be the most important.

Average grade shows the general picture about candidate's success at undergraduate level. However, the grades in subjects which are focused to operational researches, statistics, mathematics, and system theory should be more important if enrolling this module. Analogous to that, subjects focused on informational systems, programming, database and data structures etc. should be underlined if enrolling the study program Informational Systems and Technologies.

The flaw is also restriction of weighted sum itself – it cannot be used to model logical expressions. This restriction has a certain number of models for multi-criteria decision making, like the weighted product model, AHP, etc.

3.1 New Model Based on Weighted Sum

The first two comments, that the data aggregated using arithmetic mean and that total score at qualification exam does not underline characteristic data important for the program of Master of Science studies, can be solved by modeling new weighted sum:

$$w_1 * u + w_2 * u_2 + w_3 * k + w_4 * k_2 = p \tag{4}$$

Two new components figure in this expression, and they are:

- u_2 – average grade at undergraduate level at subjects which are focused on operational researches, statistics, mathematics, and system theory in the interval [0, 100];
- k_2 – points gained at qualification exam to Master of Science studies, but specifically in questions considering operational researches and statistics, in the interval [0, 100].

Values w_1, w_2, w_3 and w_4 are weights in this model. Values of this factors are 0.3, 0.1, 0.5 and 0,1, respectively, so the criterion function has the following form:

$$0.3 * u + 0.1 * u_2 + 0.5 * k + 0.1 * k_2 = p \tag{5}$$

The significance of specific knowledge, important for the enrolling Master of Science studies, is underlined by new variables. Other requirements can be emphasized by introducing new variables and setting the corresponding weights. However, the criterion function defined this way does not solve the problem, because the subject of interests is qualification exam achievement and appropriate subjects accomplishment, and not these two variables separately.

4 Ranking Using Fuzzy Logic

The reason for introducing logic into consideration is the need of modeling conditions like following: “Candidate’s ranking on the list should depend on number of points on the entrance exam for Master of Science studies obtained on matters related to operational researches and statistics and the average grade at undergraduate level at subjects that are focused on operational researches, statistics, mathematics, and systems theory“. This condition implies that predefined variables u_2 and k_2 should be connected by conjunction. Weighted sum considers variables separately and can’t model interaction between them, so it is not sufficient to model this problem. It is necessary to introduce logic and logical operators, which can provide more options for aggregation.

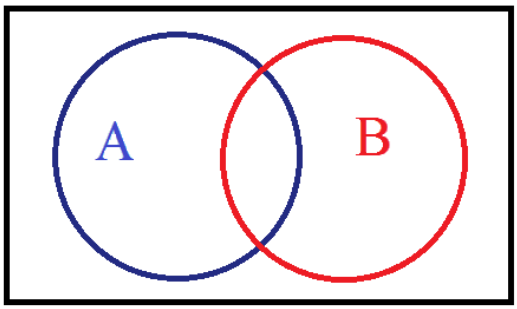

Fig. 1. What can be modeled using weighted sum, representation using sets

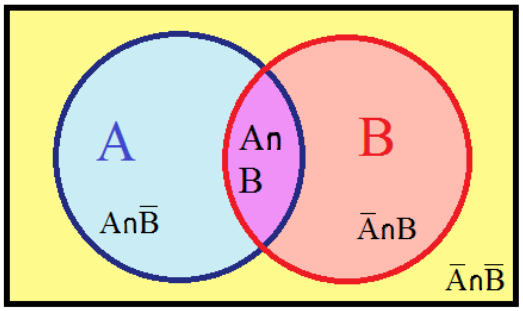

Fig. 2. What can be modeled using fuzzy logic, representation using sets

Classical logic deals with variables that are either true or false, that are either 0 or 1. Values in described problem are decimal, so it is not appropriate. That is the reason for interduction and usage of fuzzy logic.

4.1 Fuzzy Logic

Fuzzy logic is generalization of classical logic – it can process all values in interval from 0 to 1. Fuzzy logic is not fuzzy. Basically, fuzzy logic is a precise logic of imprecision and approximate reasoning [11]. Fuzzy logic is developed on fuzzy sets theory. It is particularly suitable for working with linguistic variables like *hot*, *very good*, *around twenty*, *not that busy*. Compared with conventional approaches, fuzzy control utilizes more information from domain experts and relies less on mathematical modeling about a physical system.

Functions that qualify as fuzzy intersections and fuzzy unions are usually referred as t-norms and t-conorms (or s-norms), respectively. The standard fuzzy intersection is min operator, and it produces the smallest membership value of all the t-norms [8]. On top of that, algebraic product is used often as fuzzy intersection. The standard fuzzy union is max operator, and it produces the smallest membership value of all the t-conorms. Probabilistic sum is another operator often used as s-norm.

Conventional fuzzy logic is based on principle of truth functionality - the truth valued of a complex formula is uniquely determined by the truth values of its subformulas. In the general, it doesn't follow the law of excluded middle, one of the Boolean laws. Some authors say that fuzzy set theory simply does not happen to have an axiom of the excluded middle – it does not need, constrained by, such an axiom [8]. Others see this as inconsistency and problem.

4.2 New Model Based on Fuzzy Logic

The modified weighted sum is used to rank students. The third element of weighted sum is changed, and it is defined as: "Conjunction of average grade at undergraduate level at subjects that are focused on operational researches, statistics, mathematics, and systems theory and number of points on the entrance exam for Master of Science studies obtained on matters related to operational researches and statistics". In accordance to that, weighted sum is:

$$w_1 * u + w_2 * k + w_3 * 100 * (u_2 \wedge k_2) = p \tag{6}$$

Variable u_2 are normalized in the interval [0, 1]. Variable k_2 is linguistic variable, with suggested values: *very low, low, medium, high, and very high*. These linguistic terms first can be converted to fuzzy numbers using a conversion scale. Then a fuzzy scoring method is used to convert each fuzzy number to a corresponding crisp value. According to Chen and Hwang's five-scale fuzzy linguistic scaling [1], listed variables are converted to crisp values - 0.091, 0.283, 0.5, 0.717, 0.909 respectively. Weights w_1, w_2 and w_3 have following values - 0.3, 0.5 and 0,2. Product is used as t-norm. The third element in weighted sum is multiplied by 100, so all elements would have the same order of magnitude. In accordance to that, weighted sum has the following form:

$$0.3 * u + 0.5 * k + 0.2 * 100 * u_2 * k_2 = p \tag{7}$$

5 Ranking Using Pseudo-logical Aggregation

5.1 Interpolative Boolean Algebra and Logical Aggregation

Interpolative Boolean algebra is a consistent multi-valued realization of Boolean algebra in the sense that it preserves all the laws which Boolean algebra relies on. It has two levels – symbolic and valued. On symbolic level all laws of Boolean algebra are valued indifferent. IBA element represents the analyzed object. IBA element on symbolic level is treated independently of its realization. All elements consist of one or more atomic element. Expressions are calculated based on the principle of structural functionality: Structure of any IBA element can be directly calculated on the basis of structures of its components [4, 5]. This principle treats negation differently and that allows preservation of the law of excluded middle.

IBA is technically based on generalized Boolean polynomials (GBP). GBP uniquely corresponds to any element of Boolean algebra and any Boolean function can be transformed into corresponding GBP. Operators allowed in GBP are plus, minus and

generalized product. Generalized product (GP) is any function ⊗: [0,1]⊗[0,1]→[0,1] that satisfied all four conditions of t-norms: Commutativity, Associativity, Monotonicity, Boundary condition and Non-negativity condition [6]:

$$\sum_{K\in P(\Omega/S)} (-1)^{|K|} \otimes A_i(x) \geq 0, S \in P(\Omega), A_i(x) \in [0,1], A_i \in \Omega \tag{8}$$

On a valued level the IBA is value realized – elements take values from an interval [0, 1] and suitable operator for GP is chosen.

Consistent and transparent procedure based on IBA for aggregating factors is called Logical aggregation. Logical aggregation is the fusion of the primary attributes of quality in a crisp value. The task of LA is the fusion of primary attributes' values into one resulting globally representative value using logical tools [3]. It has two steps:

- Normalization of attributes' values

$$\|\bullet\|: \Omega \rightarrow [0,1] \tag{9}$$

- Aggregation of normalized values of features into one resulting value by logical or pseudo-logical function as a LA operator [7]

$$Aggr[0,1]^n \rightarrow [0,1] \tag{10}$$

Pseudo-logical function, called pseudo GBP, is a linear convex combination of generalized Boolean polynomials. In this paper it is the proposed approach for aggregation.

A logical aggregation depends on the measure of an aggregation operator as well as of generalized product. Aggregation measure is a structural function of pseudo-logical function.

5.2 New Model Based on Pseudo Logical Aggregation

Two different functions are proposed as pseudo-logical function for ranking. Both are similar to the weighted sum presented in Section 4.2: first two elements and weights in sum are the same (0.3, 0.5 and 0,2 respectively). The third element in sum is the difference.

Case 1: In this model, candidates who have successfully mastered the material on operational research have the advantage. If they haven't, the important thing is that they learned operational researches and statistics for entrance exam, as well as they have good prior knowledge in mathematics.

The third element of weighted sum is defined this way: "If candidate's average grade at undergraduate level at subjects that are focused on operational researches and statistics is well, we are interested only in it. If it is not well, we are interested in the average grade at undergraduate level at subjects that are focused on mathematics and

systems theory and number of points at the entrance exam for Master of Science studies obtained on matters related to operational researches and statistics."

Pseudo-logical function for ranking with this condition has the following form:

$$w_1 * u + w_2 * k + w_3 * 100 * (a \vee (\neg a \wedge d \wedge x)) = p \tag{11}$$

The third element is transformed on symbolic level:

$$a \vee (\neg a \wedge d \wedge x) = a + d \otimes x - a \otimes d \otimes x \tag{12}$$

After that, expression can be calculated. The operator of generalized product $\otimes$ is product ($\otimes$:=*):

$$w_1 * u + w_2 * k + w_3 * 100 * (a + d * x - a * d * x) = p \tag{13}$$

Case 2: In this model, candidates who have successfully mastered the material on operational research and statistics at undergraduate studies have the advantage. If they haven't mastered operational researches, the important thing is that they learned operational researches and statistics for entrance exam, as well as they have good prior knowledge in mathematics. This model is interesting because results considering operational researches and statistics are separated and interpreted it in different ways.

The third variable of weighted sum is defined like this: "If candidate's average grade at undergraduate level at subjects that are focused on operational researches is well, we are interested in the average grade at undergraduate level at subjects that are focused on statistics, too. If it is not well, we are interested in the average grade at undergraduate level at subjects that are focused on mathematics and systems theory and number of points at the entrance exam for Master of Science studies obtained on matters related to operational researches and statistics."

Pseudo-logical function for ranking with this condition has the following form:

$$w_1 * u + w_2 * k + w_3 * 100 * ((b \wedge c) \vee (\neg b \wedge d \wedge x)) = p \tag{14}$$

The third element is transformed on symbolic level:

$$(b \wedge c) \vee (\neg b \wedge d \wedge x) = b \otimes c + d \otimes x - b \otimes d \otimes x \tag{15}$$

After that, expression can be calculated. The operator of generalized products $\otimes$ is product ($\otimes$:=*):

$$w_1 * u + w_2 * k + w_3 * 100 * (b * c + d * x - b * d * x) = p \tag{16}$$

Variables in presented expressions are:

- u – average grade gained at undergraduate level in the interval [0, 100];
- k – number of points at the entrance exam for Master of Science studies in the interval [0, 100];

- *a* – average grade gained at undergraduate level at subjects that are focused on operational researches and statistics, normalized in the interval [0, 1];
- *b* – average grade gained at undergraduate level at subjects that are focused on operational researches, normalized in the interval [0, 1];
- *c* – average grade gained at undergraduate level at subjects that are focused on statistics, normalized in the interval [0, 1];
- *d* – average grade gained at undergraduate level at subjects that are focused on mathematics and systems theory, normalized in the interval [0, 1];
- *x* – number of points at the entrance exam for Master of Science studies obtained on matters related to operational researches and statistics, normalized in the interval [0, 1];
- *p* – candidate's total points in the interval [0, 100].

The third element in weighted sum is multiplied by 100, so all elements would have the same order of magnitude.

6 Analysis and Comparison of Proposed Models

In this section suggested models are simulated and compared. Thirty students' data are used for simulation. Data were collected via internet survey. Twenty four students have scored maximum on theirs qualification exam. Data on the exact number of points at the entrance exam for Master of Science studies obtained on matters related to operational researches and statistics do not exist, because it is not important for current ranking model. Students were asked to write their hypothesis about scored points at that study fields (fuzzy number) which is converted in according to Chen and Hwang's conversion scales with five different linguistic terms. Data on the eight students is shown in following table. These students are chosen because their characteristics are suitable to present differences in the rankings using different models.

Table 1. Input data

Student	u	k	a	b	c	d	x
A	100	100	1.00	1.00	1.00	1.00	1.00
B	99.0	100	0.94	0.90	1.00	0.92	1.00
C	98.6	100	1.00	1.00	1.00	1.00	1.00
D	90.7	100	0.88	1.00	0.70	0.70	1.00
E	89.0	100	0.90	0.90	0.90	0.83	1.00
F	77.0	98.0	0.62	0.60	0.65	0.68	1.00
G	88.0	85.0	0.90	0.90	0.90	0.90	0.95
H	77.0	80.0	0.72	0.70	0.75	0.80	0.90

Table 2. Output data

Student	Current model	Model based on weighted sum	Model based on fuzzy logic	Model 1 based on pseudo LA	Model 2 based on pseudo LA
A	100.00	100.00	100.00	100.00	100.00
B	99.60	99.10	98.50	99.60	99.54
C	99.44	99.58	99.58	99.58	99.58
D	96.28	95.21	93.21	96.49	91.21
E	95.60	95.47	94.23	96.36	94.56
F	89.60	88.53	84.97	89.67	85.34
G	86.20	87.40	86.00	88.61	86.81
H	78.80	79.60	76.60	81.53	77.92

Table 3. Students‘ rankings

Student	Current model	Model based on weighted sum	Model based on fuzzy logic	Model 1 based on pseudo LA	Model 2 based on pseudo LA
A	1	1	1	1	1
B	2	3	3	2	3
C	3	2	2	3	2
D	4	5	5	4	5
E	5	4	4	5	4
F	6	6	7	6	7
G	7	7	6	7	6
H	8	8	8	8	8

Rankings given by different models differ. The first model is an initial model, which is applying in practice. The second and the third model are transitional. Last two models are the final proposed models. Differences in students' ranking are caused by emphasizing specific factors and different method of aggregation. Users can model their own pseudo-logical function according to their needs.

Student A and student H are the first and the last at every ranking list. It is noticeable that students B and C, students D and E, and students F and G have different rankings when different model is in use. Student B has higher average grade than student C, so he is better than student C in accordance to initial model. Student B has much lower grade at subjects that are focused on operational researches than student C, so other models favour student C. In first model based on pseudo LA that variable doesn't figure (that model has arithmetic mean of grades at subjects that are focused on operational researches and also statistics, as one variable). It is similar for students G and F. The main difference between students D and E is that student E's grades are balanced, opposite of student D's. This explains the large difference between these students when the last model is in use (it has conjunction of attributes that have the most different values).

7 Conclusion

The Master of Science programs at Faculty of Organizational Sciences specialize students for different occupations – managers, programmers, analytics, database specialists, etc. The advantage at ranking should be given to students who showed great results at subjects which are related to chosen domains. The ranking model must acknowledge the requirements that are expressed using the logical connective and should process fuzzy values, so the usage of fuzzy logic is necessary. It is important to find and point out small differences between inputs and to treat negation in a proper way. That can be achieved by using the suggested models based on LA. LA is a technique which gives the user the most options in modeling. Ranking students with pseudo-logical function gives results similar to current, but different enough to introduce these proposals and test it practically. Users can model their own pseudo-logical function in accordance to their requests and needs.

References

1. Chen, S.J., Hwang, C.L., Hwang, F.P.: Fuzzy Multiple Attribute Decision Making. Methods and Applications. Springer, New York (1992)
2. Hsieh, C.S., Wu, C.H., Huang, T., Chen, Y.W.: Analyzing the Characteristics of Fuzzy Synthetic Decision Methods on Evaluating Student's Academic Achievement. In: International Conference on Artificial Intelligence and Computational Intelligence, pp. 491–495. Conference Publications (2009)
3. Mirković, M., Hodolič, J., Radojević, D.: Aggregation for Quality Management. Yugoslav Journal for Operational Research 16(2), 177–188 (2006), doi:10.2298/YJOR0602177M
4. Radojević, D.: Interpolative Realization of Boolean Algebra. In: The 8th Symposium on Neural Network Application in Electrical Engineering, pp. 201–206. Conference Publications (2006), doi:10.1109/NEUREL.2006.341214
5. Radojević, D.: Interpolative realization of Boolean algebra as a consistent frame for gradation and/or fuzziness. In: Nikravesh, M., Kacprzyk, J., Zadeh, L.A. (eds.) Forging New Frontiers: Fuzzy Pioneers II. STUDFUZZ, vol. 218, pp. 326–351. Springer, Heidelberg (2007)
6. Radojević, D.: Fuzzy Set Theory in Boolean Frame. International Journal of Computers Communications and Control 3(S), 121–131 (2008)
7. Radojević, D.: Logical Aggregation Based on Interpolative Boolean Algebra. Mathware & Soft Computing 15, 125–141 (2008)
8. Ross, T.: Fuzzy Logic With Engineering Application, 3rd edn. John Wiley & Sons, Ltd., Chichester (2010)
9. Triantaphyllou, E.: Multi-Criteria Decision Making Methods: A Comparative Study. Kluwer Acad. Publ., Dordrecht (2000)
10. Yeh, C.: The Selection of Multiattribute Decision Making Methods for Scholarship Student Selection. International Journal of Selection and Assessment 11(4), 289–296 (2003), doi:10.1111/j.0965-075X.2003.00252.x
11. Zadeh, A.L.: Is there a need for fuzzy logic? Information Sciences: an International Journal 178(13), 2751–2779 (2008), doi:10.1016/j.ins.2008.02.012

Modeling Candlestick Patterns with Interpolative Boolean Algebra for Investment Decision Making

Ivan Nešić, Pavle Milošević, Aleksandar Rakicevic,
Bratislav Petrović, and Dragan G. Radojević

Faculty of Organizational Sciences,
University of Belgrade, Jove Ilica 154, Belgrade, Serbia
ivan.nesic@ewcom.ch, pasha.47@gmail.com,
{aleksandar.rakicevic,bratislav.petrovic}@fon.bg.ac.rs,
dragan.radojevic@pupin.rs

Abstract. In this paper we present one way of modeling candlestick patterns using interpolative Boolean algebra (IBA). This method shows a degree of fulfillment for observed patterns, thus giving traders easy interpretation of by how much candlesticks fit into different patterns. Candlestick patterns have been used for financial forecasting for a couple of decades on Western markets and they have become a mainstream trader's tool. Since the need for automated candlestick patterns discovery arose, some papers proposed fuzzy approach as a solution. Our decision to use IBA for modeling candlestick patterns comes from the fact that fuzzy logic has it limits and cannot be applied to these models. Proposed method is another approach to the same problem, but it could not be modeled using conventional fuzzy logic, because it is necessary for it to be in the Boolean frame. Results obtained from our tests are satisfactory and also open the opportunity for combining this technique with existing ones.

Keywords: interpolative Boolean algebra, real valued logic, candlestick patterns, financial forecasting.

1 Introduction

Usage of candlestick patterns as financial indicators has been defended and disputed in literature during the last decade. They prove to be useful on some markets and shown unprofitable on others. The fact is that candlestick patterns were invented for rise markets during the second half of the 1700s and some conclude that they are not suitable for today markets [9]. Anyhow, fact is that traders use this kind of technical analysis on an everyday basis. It is supposed to reveal emotional beliefs of traders on the market, since they too affect the price [10]. This kind of behaviour is not completely rational, and technical analysis transforms thought process of investors into charts in an effort to forecast the price change.

Models are individual for each trader, so there is no optimal solution to this problem. Instead, methodology that can help traders to express their personal preferences is needed. Emerging papers in scope of candlestick patterns show an uprising interest

V.E. Balas et al. (Eds.): Soft Computing Applications, AISC 195, pp. 105–115.
springerlink.com

in imprecise modelling. Many of these papers show respectful results. Since conventional fuzzy logic does not treat consistently all logical relations, using it for proposed models is not satisfactory. To address this problem, interpolative Boolean algebra is introduced to candlestick modelling.

For defining candlestick patterns, method proposed in this paper uses interpolative Boolean algebra as a consistent fuzzy technique [11]. Conventional fuzzy approach is hindered by the fact that it cannot consistently describe elements of Boolean algebra and stay in a Boolean frame [14]. One occurrence is for instance the law of contradiction ($A \cap \overline{A}$). Therefore, proposed models cannot be implemented with traditional fuzzy approach. IBA or consistent fuzzy technique, as it is sometimes referred in literature, must be applied to improve upon strongly set conventional fuzzy logic.

For test purposes we used random data interval from a stock market. Our results reveal that transforming candlestick parameters, by using proposed methodology, into intensity of a candlestick pattern, truly mimics human perception.

The rest of the paper is organized into four sections. Section 2 analyses contemporary literature, in section 3 data and methodology are described, results are explained in section 4 and the last section concludes the paper.

2 Literature Review

Effectiveness of Japanese candlestick patterns on stock and similar markets is perpetually re-examined. There are papers which suggest that usage of such patterns for forecasting on stock markets is unjustified. For instance, studies conducted in [1] and [9] show that candlestick patterns as a type technical analysis do not produce profit. In [9] authors used thirty-five individual stock indexes with carefully chosen sample period of ten years. Robustness of the system was tested using the bootstrap methodology. One of the criticisms was addressed to the fact that candlestick patterns were originally devised for rice markets.

In contrast, recent study conducted in [8] shows that some types of candlestick technical analysis patterns are indeed profitable when applied to Taiwan stock market. Data used for testing this method comprised of individual stocks found in Taiwan 50. To check the robustness of results, again, bootstrap methodology was used. Despite the fact that some of these results put shadow onto candlestick patterns effectiveness, many papers have been written regarding their usage in forecasting.

Research presented in [7] created an expert system based on candlestick chart analysis. Their system looks up in a database for signals and interprets them as candlestick patterns. They get 72% accurate results on the Korean stock market. The model is rule-based.

Tool which uses fuzzy candlestick patterns to describe investment knowledge on the Taiwan stock market was presented in [5]. By using fuzzy technique, they are addressing the problem of candlestick pattern definition vagueness which arises from different authors' comprehensions of the same pattern. In another paper, group of same authors compare their method with previously presented ones, acquiring better results [6]. Finally, in [4] Lee constructs personal ontology to describe candlestick patterns.

Approaches presented in [2] use candlestick method in gating network, by using rules for describing the market and also by fuzzy logic-based weight generator, as part of their hybrid system. As they have shown, fuzzy logic based systems deliver smoother and more accurate forecasting results. Another fuzzy-candlestick model for reversal point prediction was presented in [3]. It tries to set a warning before a reversal of a stock price occurs. Reported results show precision far greater than 50%.

3 Data and Methodology

The origin of candlesticks dates from the mid-18th century, and was firstly introduced by a youngest child of Munehisa family named Homma [10]. From his excellence in the field of trading, people started calling him "god of the markets". After Nison introduced Japanese candlestick trading techniques to western markets, they rapidly gained popularity. Today, candlesticks chart analysis is widely used type of technical analysis. Candlestick patterns should reflect psychological state of the market and traders should be able to base their decisions upon recognized patterns.

Candlesticks are formed out of the open, high, low and close price for a predefined time period Fig. 1. Body color of a candlestick depends on whether the close price is higher or lower than the open price. If it is higher, body usually has a white or an empty filling and oppositely, if it is lower, body is black or filled. Lines called shadows above and under body represent highest and lowest price of the time interval, respectively. Body size indicates the market momentum and the shadows show extremes of the price movement. Body and shadows are usually described as long or short.

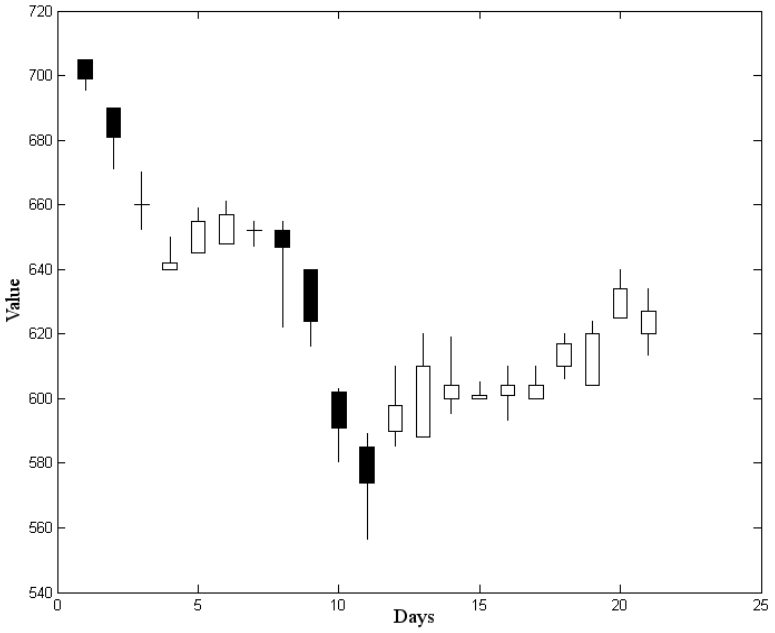

Fig. 1. Candlestick examples

The way a candlestick can reflect the market state can be given with the following example. Candle with white body without shadows is called the White Marubozu pattern. Open price equals lowest price, and close price equals the highest. That means buyers are very bullish, since market opened at one price and closed at another, and the price never dropped below initial price, and it closed well above it. The opposite rule applies for black body, Black Marubozu.

Interpretation of candlestick patterns is individual. Investors can obtain different pieces of information from the same pattern and apply custom set of rules. To make the modeling possible, we use interpolative Boolean algebra. With this consistent fuzzy technique we are able of modeling vagueness of candlestick patterns recognition. This new approach simplifies pattern definition, making it easier for investors to use. Usage is straightforward and only basic mathematical skills are required. Need for gradation is also satisfied, for instance we can calculate how intensive White Marubozu is. This provides information about certainty that the pattern emergence will reflect the future market movement.

3.1 Candlestick Fuzzy Modeling

Since idea behind imprecise or fuzzy modeling of candlesticks is already being explored in literature, we will first shortly explain approach presented in [4, 5, and 6]. To describe a candlestick line in an imprecise manner as long, middle or short, four linguistic variables are defined: EQUAL, SHORT, MIDDLE and LONG. They indicate fuzzy sets of shadows and body length. Membership function μ(x) of linguistic variables is described on Fig. 2.

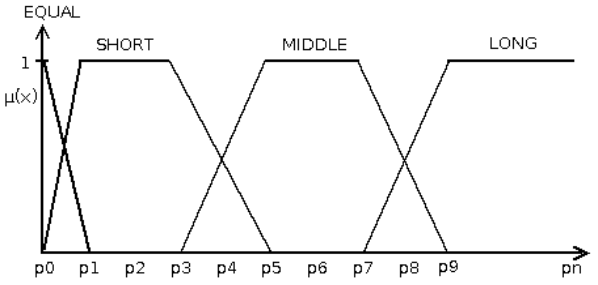

Fig. 2. Fuzzy sets of shadows and body length

Values are set from p_0 to p_n, depending on the maximum percentage change of observed time series per interval. For example, on TAIEX values should range from 0 to 14 since they can only change so much per day interval. X-axis is a real value of body or shadow. Input values for membership functions can be calculated with following equations:

$$L_{upper\_shadow} = \frac{high - \max(open, close)}{open} \times 100$$
$$L_{lower\_shadow} = \frac{\min(open, close) - low}{open} \times 100 \quad (1)$$
$$L_{body} = \frac{high - \max(open, close)}{open} \times 100.$$

Those input values are comparable to the values later presented as the percentage limits normalization explained later. Also, additional calculations should be made for the determination of body type. There are three states of the body: BLACK, WHITE and CROSS. The last-mentioned is the situation where body has the 0 size or in another words open equals close price. Additional set of rules is defined as follows:

$$IF\ open - close > 0\ THEN\ \text{body is BLACK}$$
$$IF\ open - close < 0\ THEN\ \text{body is WHITE} \quad (2)$$
$$IF\ open - close = 0\ THEN\ \text{body is CROSS}.$$

Multiple candlestick relations are modeled in the same sense, by defining five linguistic variables to represent open style relations and five for close style. Fuzzy modifiers and trend modeling is also introduced. Complete procedure is described in [6].

3.2 Candlestick Modeling with Interpolative Boolean Algebra

IBA requires for all values to be on the [0,1] interval. Candlestick values must be normalized taking those rules into consideration. If we know maximal possible price change, it could be better to treat extreme movements with higher degree. For instance on TAIEX, the upward movement of 7% can be considered as 1 and downward movement of 7% as 0. The problem is that near border movements are really scarce and with this kind of normalization normalized candlesticks would be too small for IBA to properly treat them. Also, with this kind of normalization, all open prices are set to a fixed value. In case where symmetrical maximal and minimal price changes are to be expected, that is the 0.5 value, otherwise it is some other. That means that data of relative position between candlesticks is lost. One solution for this problem is min-max normalization performed on the whole data set. However, this will not address the first problem. Another option is to normalize groups of elements that create a single pattern. This way, relevant bars will maintain their relations. It is clear that there is no single solution for every problem, so type of normalization should be chosen according to specific needs. Aggregation of two or more differently normalized data sets should also be considered. For example purposes in this paper, we used min-max normalization on pattern groups since there are no disadvantages of using it on selected cases.

In [11] is presented [0,1]-valued logic that is in the Boolean frame. This gives us the opportunity to use consistent fuzzy relations or interpolative relations [12], to measure logical similarity and dissimilarity between individuals. Interpolative Boolean algebra provides a frame for consistent realization of all possible elements of finite Boolean algebra. It is consistent in a sense that it preserves all the laws on which Boolean algebra relies.

In this paper classical Boolean expressions are used for modeling candlestick patterns. As an example, a few expressions have been described. Equivalence is used when we want to state that parameters are equal. Relation of equivalence ($\Leftrightarrow$) is well-known expression of logical similarity between objects. Equivalence of two objects A and B is noted as:

$$A \Leftrightarrow B = (A \cap B) \cup (\overline{A} \cap \overline{B}). \tag{3}$$

For Doji pattern open equals close price so it can be defined with ease by stating open$\Leftrightarrow$close.

If we do not want attributes to be the same, logical choice of an operator is exclusive disjunction ($\veebar$). Relation of exclusive disjunction is complementary relation to the equivalence relation:

$$A \veebar B = 1 - \left(A \Leftrightarrow B\right) = (A \cap \overline{B}) \cup (\overline{A} \cap B). \tag{4}$$

Long day pattern can be modeled as an exclusive disjunction between open and close price. It can be expressed as close and open prices as far apart as possible.

Maximal value for relation of exclusive disjunction between open and close price is obtained when open and close prices have extreme but different values. For instance open price has a value of 1 and close price has a value of 0.

Very useful expression is implication ($\rightarrow$). It can be viewed as a non-strict inequality relation, or simplified less or equals $\leq$.

$$A \rightarrow B = (\overline{A} \cup B). \tag{5}$$

For instance, this expression can be used for defining the Engulfing pattern which is described as a candlestick with a small body which is engulfed by a bigger body of the next bar.

Because there relations are based on interpolative Boolean algebra (IBA), which is real-valued [0,1]-valued realization of finite Boolean algebra [13] we need to find their generalized Boolean polynomial. Any element from the IBA has its corresponding generalized Boolean polynomial (GBP) [14].

Transformation from Boolean expressions to GBP is described and the example of the process for exclusive disjunction is given by the following expression:

$$\begin{aligned}(A\underline{\vee}B)^{\otimes} &= [(A\cap\overline{B})\cup(\overline{A}\cap B)]^{\otimes}\\ &= (A\cap\overline{B})^{\otimes}+(\overline{A}\cap B)^{\otimes}-(A\cap\overline{B})^{\otimes}\otimes(\overline{A}\cap B)^{\otimes}\\ &= A\otimes(1-B)+(1-A)\otimes B-[A\otimes(1-B)]\otimes[(1-A)\otimes B]\\ &= A+B-2(A\otimes B).\end{aligned} \tag{6}$$

Generalized product ($\otimes$) is any function that satisfies conditions of commutativety, associativity, monotonicity, 1 as identity and non-negativity condition:

$$\otimes:[0,1]\times[0,1]\to[0,1]. \tag{7}$$

If both attributes have the same type, we can use minimum t-norm as a generalized product. That would mean they are correlated. For instance, if we compare two persons by their height, intersection of their heights is smaller person's height. If attributes are non-correlated, product t-norm should be used instead. An example of this is if compare two persons by their height and their wealth. At last, if they are negatively correlated Łukasiewicz t-norm should be used.

Example above (6) can now be transformed to:

$$(A\,\underline{\vee}\,B)^{\otimes} = A+B-2(A\otimes B) = A+B-2\min(A,B). \tag{8}$$

Next, example models for candlestick patterns are given. This should illustrate how fuzziness can help in determining the intensity and avoid completely discarding candlestick patterns that only on small part do not satisfy conditions.

White Marubozu:

$$open \Leftrightarrow low \quad\wedge\quad close \Leftrightarrow high\,. \tag{9}$$

Doji:

$$open \Leftrightarrow close\,. \tag{10}$$

Hammer:

$$close \Leftrightarrow high \quad\wedge\quad open\ \underline{\vee}\ low\,. \tag{11}$$

Bullish Engulfing:

$$high1 \to close2 \wedge open2 \to low1 \wedge close2 \to open2. \tag{12}$$

Variables high1 and low1 represent high and low prices of preceding candlestick and open2 and close2 open and close prices about the latter. Last part says that close price should be smaller than the open price of the second candlestick.

4 Results

Tests show that candlestick patterns modelled using IBA can provide good representation of how human traders percept market movements. For traders this means a significant help since they do not have to monitor changes personally, but instead just wait for signals when a pattern is formed. This can further automate the process, since traders can create rules on which when event is triggered actions could be taken automatically. IBA can also be used for automation as a logical aggregation tool.

In this section, we will compare how models are defined using IBA and fuzzy approach. For instance, we will compare Bullish Engulfing model presented in [4] with ours (12). For the sake of simplicity, previous trend information is omitted.

One needs to define all attributes using linguistic variables in fuzzy approach. Since we have two candlesticks composing this pattern we need information about open style, close style, upper shadow, body size, body colour and lower shadow for both candlesticks. This gives great flexibility in defining patterns and is further supported by possibility to custom-tailor membership function. Rules can be expressed as (13).

$$\begin{aligned} &IF\ line1\_open\_style = OPEN\_LOW \\ &AND\ line1\_close\_style = CLOSE\_HIGH \\ &AND\ line1\_body\_size = LONG \\ &AND\ line1\_body\_color = WHITE \\ &AND\ line2\_open\_style = OPEN\_HIGH \\ &AND\ line2\_close\_style = CLOSE\_LOW \\ &AND\ line2\_body\_size = SHORT \\ &AND\ line2\_body\_color = BLACK. \end{aligned} \tag{13}$$

Our approach was already described with (3.12). It is straightforward and all tweaking has to be done using logical expressions. With (3.12) it is described that high price of previous candlestick is smaller than the close price of the following one and that low price of the first one is above the value of the second candlestick open price. Last part of the expression shows that body of the first candlestick should be black. In other words, first candlestick is completely engulfed by the body of a following candlestick and is bearish.

Next part presents some usage cases. Only one bar candlestick patterns are used in the example Fig. 3. Table 1 contains data on which Fig.4.1 charts are made.

Some described models (9-12) are very rough and could use some improvement. Obviously, Marubozu pattern is not complete, since by this definition candlestick is recognized as Marubozu even when Doji without shadows occurs. One way of improving Marubozu model is to compare it with Doji. Since there is no ambiguity in definition of the Doji pattern, we can use it to improve upon other models. For instance, Marubozu is Marubozu, only when it is not a Doji. Marubozu model described by (9) can have high intensity even when Doji appears. Maybe it is correct to treat it

in such a way in some cases, but traders would probably dismiss Marubozu if it does not have larger body. That leaves us with at least two options. One is to look for Marubozu when Doji does not occur and the other is to look for Marubozu when Doji is described as less intensive.

The first scenario, White Marubozu and not Doji, depicts traders who consider that Marubozu patterns cannot occur unless body has the opposite size of an ideal Doji body size. Second scenario, White Marubozu larger than Doji, is less harsh and the condition is met when Doji's intensity is smaller than the one of Marubozu. It is interesting to note that both scenarios give very similar results, but the latter one, case with the converse implication between indicators, is more tolerant. It also appears shifted up compared to the first scenario.

Results depend on type of normalization chosen. For Hammer, if data are normalized using min-max for each bar, we get redundant calculations left and right from $\wedge$. But, if we choose some other type of normalization, results will change accordingly.

For data presented in Table 1 and Fig. 3 we used min-max normalization on each candlestick. If min-max normalization on the whole interval was used, results would be different. In this example, most notable difference is how logical relations influence changes. Sheffer stroke between White Marubozu and Doji will almost never produce maximal intensity. If converse implication is used, Doji has very little influence on White Marubozu.

Table 1. Original data and IBA modelling results

Open	High	Low	Close	White Marubozu	Dodji	Marubozu $\wedge \neg$ Dodji	Marubozu $\leftarrow$ Dodji
515	519	510	515	0,4444	1,0000	0,0000	0,4444
510	515	510	513	0,6000	0,4000	0,3600	0,8400
519	534	517	522	0,2941	0,8235	0,0519	0,4187
524	549	524	538	0,5600	0,4400	0,3136	0,8064
550	592	550	590	0,9524	0,0476	0,9070	0,9977
584	590	570	580	0,3000	0,8000	0,0600	0,4400
590	638	590	621	0,6458	0,3542	0,4171	0,8746
630	683	630	675	0,8491	0,1509	0,7209	0,9772
743	743	720	740	0,0000	0,8696	0,0000	0,1304
777	788	730	771	0,1897	0,8966	0,0196	0,2735
731	735	709	722	0,1538	0,6538	0,0533	0,4467
672	740	672	711	0,5735	0,4265	0,3289	0,8181
722	759	722	750	0,7568	0,2432	0,5727	0,9408
515	519	510	515	0,4444	1,0000	0,0000	0,4444

As generalized product in GBP for Doji and Marubozu we use minimum t-norm, since all inputs have the same nature. But, for relations between candlesticks, we use product t-norm. In situations where the proposed method needs more tuning, pseudo-logical polynomial can be used to introduce weights [15].

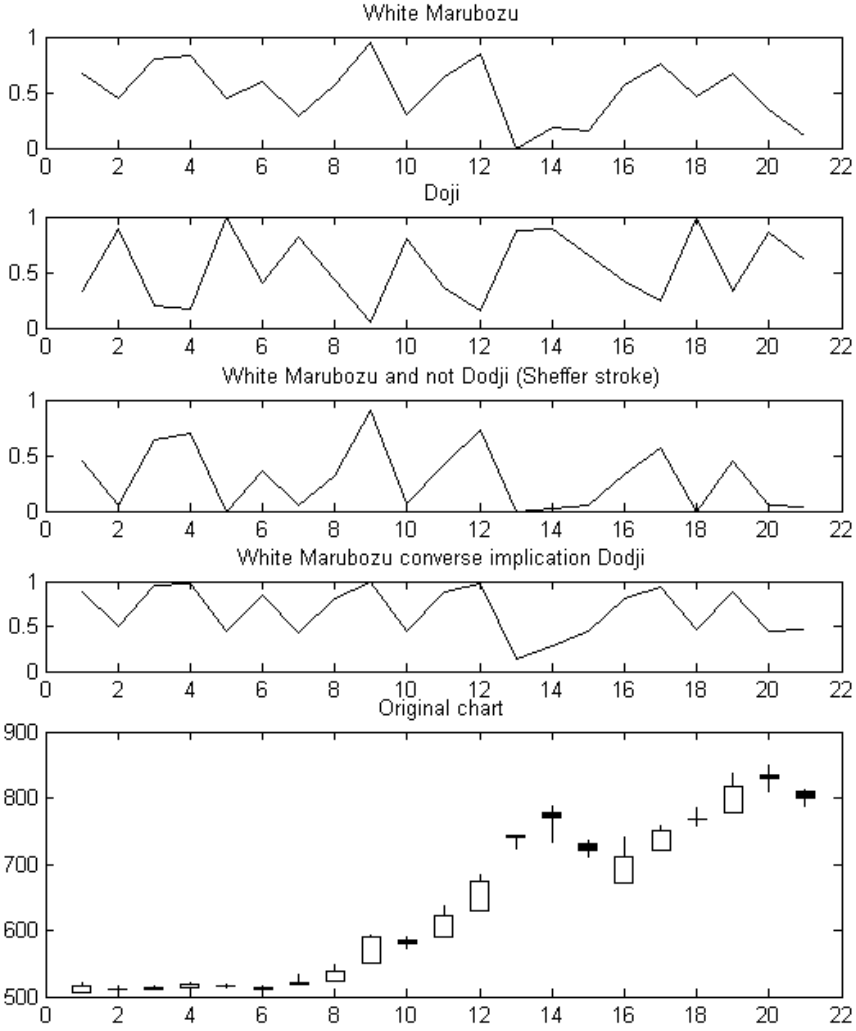

Fig. 3. IBA White Marubozu and Doji results

5 Conclusion

In this paper we wanted to introduce IBA to candlestick patterns modelling. By using proposed method it should be easy for traders to model their ideas of candlestick patterns, whether simple or complex. In the results section we have shown that our approach is indeed successful. By using this technique it is also possible to incorporate other methods of candlestick patterns modelling. To our best knowledge this is the first paper to address candlestick patterns modelling using IBA.

Previous studies used conventional fuzzy logic to model candlestick patterns, and have shown very good results. The most notable void in this approach is arising

model complexity, when more patterns should be aggregated in one new pattern. The approach in this paper on the other hand, lacks the ability to directly describe attributes with linguistic variables, but rather it uses relations between them. Once modeled, candlestick patterns can be simply put in any relation.Our methodology uses basic logic expressions to model everything from candlestick patterns to custom candlestick related indicators and then uses IBA to translate these expressions into values.

We believe that this new approach will give more flexibility in candlestick pattern modelling, which would in return give better support in investment decision making.

References

1. Horton, M.J.: Stars, crows, and doji: The use of candlesticks in stock selection. The Quarterly Review of Economics and Finance (2009), doi:10.1016/j.qref.2007.10.005
2. Kamo, T., Dagli, C.: Hybrid approach to the Japanese candlestick method for financial forecasting. Expert Systems with Applications (2009), doi:10.1016/j.eswa.2008.06.050
3. Lan, Q., Zhang, D., Xiong, L.: Reversal Pattern Discovery in Financial Time Series Based on Fuzzy Candlestick Lines. Systems Engineering Procedia (2011), doi:10.1016/j.sepro.2011.10.021
4. Lee, C.-H.L.: Modeling Personalized Fuzzy Candlestick Patterns for Investment Decision Making. IEEE Computer Society (2009), doi:10.1109/APCIP.2009.207
5. Lee, C.-H.L., Chen, W., Liu, A.: Candlestick Tutor: An Intelligent Tool for Investment Knowledge Learning and Sharing. IEEE Computer Society (2005), doi:10.1109/ICALT.2005.82
6. Lee, C.-H.L., Liu, A., Chen, W.-S.: Pattern Discovery of Fuzzy Time Series for Financial Prediction. IEEE Transactions on Knowledge and Data Engineering (2006), doi:10.1109/TKDE.2006.80
7. Lee, K.H., Jo, G.S.: Expert system for predicting stock market timing using a candlestick chart. Expert Systems with Applications (1999), doi:10.1016/S0957-4174(99)00011-1
8. Lu, T.-H., Shiu, Y.-M., Liu, T.-C.: Profitable candlestick trading strategies—The evidence from a new perspective. Review of Financial Economics (2012), doi:10.1016/j.rfe.2012.02.001
9. Marshall, B.R., Young, M.R., Rose, L.C.: Candlestick technical trading strategies: Can they create value for investors? Journal of Banking & Finance (2006), doi:10.1016/j.jbankfin.2005.08.001
10. Nison S.: Japanese Candlestick Charting Techniques: A Contemporary Guide to the Ancient Investment Techniques of the Far East. New York Institute of Finance, USA (1991)
11. Radojevic, D.: New [0,1]-valued logic: A natural generalization of Boolean logic. Yugoslav Journal of Operational Research - YUJOR 10(2), 185–216 (2000)
12. Radojevic, D.: Interpolative Relations and Interpolative Preference Structures. Yugoslav Journal of Operational Research - YUJOR 15(2), 171–189 (2005)
13. Radojevic, D.: Interpolative Realization of Boolean Algebra as a Consistent Frame for Gradation and/or Fuzziness. Forging New Frontiers: Fuzzy Pioneers (2008), doi:10.1007/978-3-540-73185-6_13
14. Radojevic, D.: Fuzzy Set Theory in Boolean Frame, Workshop invited key lecture. International Journal of Computers, Communications & Control 3, 121–131 (2008)
15. Radojevic, D.: Logical Aggregation Based on Interpolative Boolean Algebra. Mathware & Soft Computing 15(1), 125–141 (2008)

Using Fuzzy Logic to Determine If the Traffic Is Constant or Not in DTF Method

Emanuel Ciprian Sasu and Octavian Prostean

"Politehnica" University, Timisoara, Romania
cipisasu@ee-software.com,
octavian.prostean@aut.upt.ro

Abstract. This paper applies Fuzzy Logic in Destination Traffic Fingerprint Method, to the process of establishing if the traffic to a specific IP destination is constant. In order to obtain strong fingerprints, it is absolutely necessary to distinguish between constant traffic and non-constant traffic.

Keywords: DTF Method, MAC Spoofing, Intrusion Detection, Fuzzy Control.

1 Introduction

Destination Traffic Fingerprint Method (DTF) is described in detail in previous works and therefore we will not focus on this here. In [1] we describe in detail the method, which applies to network intrusion detection issue, when an intruder seeks to enter a network by spoofing the MAC address of an authorized network station.

This security issue of MAC spoofing is addressed in the literature in many articles, like those in [3-10]. All of them are trying to improve network security by quickly identify all the situations when the MAC address found in the packets that transit the network is spoofed.

DTF Method identifies each authorized network station by a fingerprint, made of a set of IP destinations that are constantly found in the traffic. Each IP destination is accompanied by a percentage value which represents the presence of that IP in the traffic, considering the time at a minute level. After the generation of the reference fingerprint, the actual fingerprint taken in real time traffic, is compared with the reference fingerprint and the Overall Degree of Recognition is computed. This percentage value tells how much can be trusted that a MAC address is what it claims to be.

The most important part in the process is the generation of the reference fingerprint. This is because a strong fingerprint will bring to a fast and accurate recognition, while a poor fingerprint will generate false alarms or will obtain the result in a long time. As it was said before, the fingerprint is composed by a set of pairs, each pair binding a specific IP address with its percentage of presence.

Keeping in mind that the calculations are updated at a minute level, the most simple method to determine the percentage of presence of a certain IP destination, is to divide the total number of minutes when it was traffic to the IP destination, to the

V.E. Balas et al. (Eds.): Soft Computing Applications, AISC 195, pp. 117–128.
springerlink.com

total number of minutes of the recorded time interval. But, as it was proved in [1] and [2], this way is not applicable by itself, because there are certain number of cases when the presence is not constant all over the time interval, but shows only high values on some divisions of the interval.

2 Applying Fuzzy Logic for the Determination of Constant Traffic

2.1 Describing the Applicability of Fuzzy Logic in DTF Method

The algorithm that is implemented in DTF method can be divided in four distinct modules, as shown in Fig. 1. The first module, „Network Monitoring with Packet Analysis" deals with network packets which are captured at a certain point in the network. All the packets are analyzed and recorded in a database using a specific format because it is important in the following sections of the algorithm to have statistics at a minute level for each IP destination that is found in the traffic. Network Monitor with Packet Analyzer.

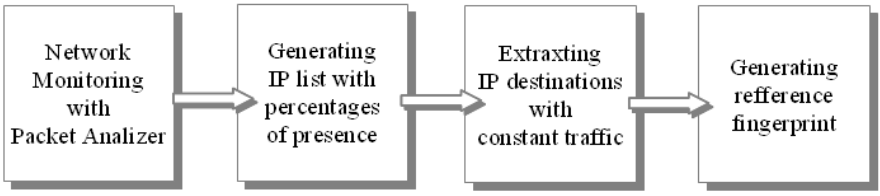

Fig. 1. The Generation of the reference fingerprint in DTF Method

The second module will generate a list of the IP destinations, together with the percentages of presence. Each percentage of presence for a specific IP address is calculated as the ratio between the number of minutes when we found traffic to the IP, and the total number of minutes in the evaluated time interval.

The third module is the most important because it filters the list of IP destinations and outputs only those that have a constant traffic. The main problem is to define „constant traffic" and extract the IP destinations that fit in this category. This part is the most important because the real time identification process is totally based on the constant nature of the traffic. If the IP destinations do not have a constant traffic, then the entire process will fail and the signals that are generated will be useless.

The last module will gather the results received from the previous module and compose the reference fingerprint of the MAC address. This reference fingerprint will be used later to distinguish between real and spoofed MAC addresses.

In this environment, the fuzzy logic applies very well in the third part, when we need to determine if the traffic is constant or not. Fuzzy logic is a very good and powerful tool, as it is prooved in [11] and [12], that fits very well on the topic of DTF method, for the determination of the constant nature of the traffic. Fig. 2 shows the implementation as a mandami system with four inputs and one output.

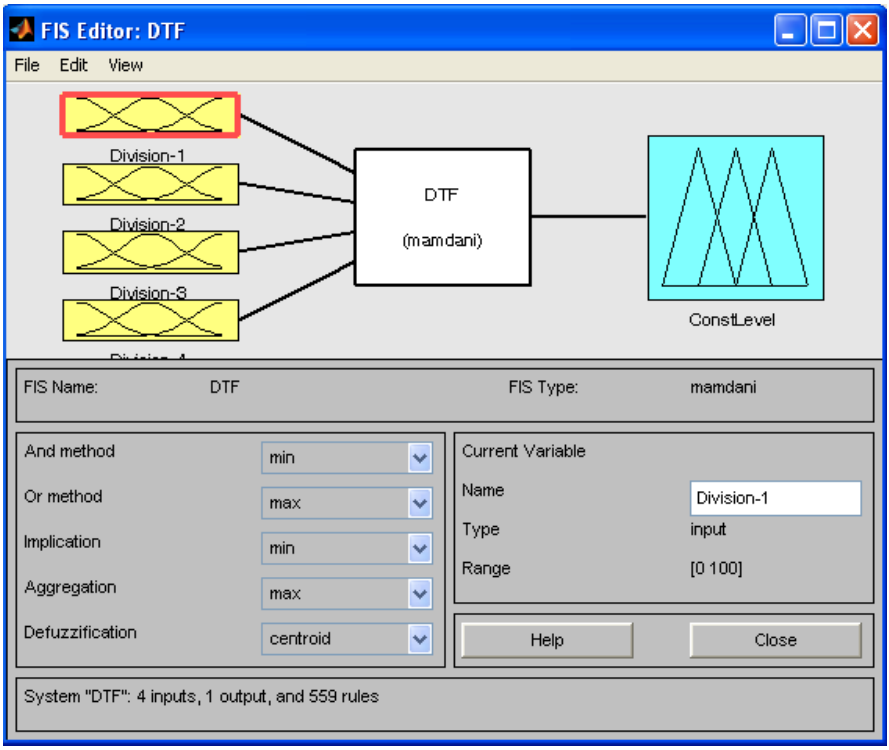

Fig. 2. Fuzzy system for the determination of constant traffic

The system will evaluate the traffic to a specific IP destination, on a time interval *T*. The input variables are in fact four equal divisions of the time interval *T*. For each division the percentage of presence is calculated and sent to the entrance of the mandami system, which will generate at the output an answer regarding the level of constancy for the traffic. The fact that each input is a division of the original interval, means that all will have the same functionality. The difference is only the sequence of minutes that are evaluated in each division.

For DTF Method is very important to carefully distinguish the IP destinations that have a constant traffic, from those that do not. The main idea is that the evaluated time interval is divided in four equal divisions and for each division DTF calculates the percentage of presence. Then, by comparing the four separate percentages, it is more clear if the traffic is constant or not.

2.2 Input Structure

The domain range of the variable is considered [0..100], because each of the four input variables represents the percentage of presence in the traffic, for the evaluated IP destination.

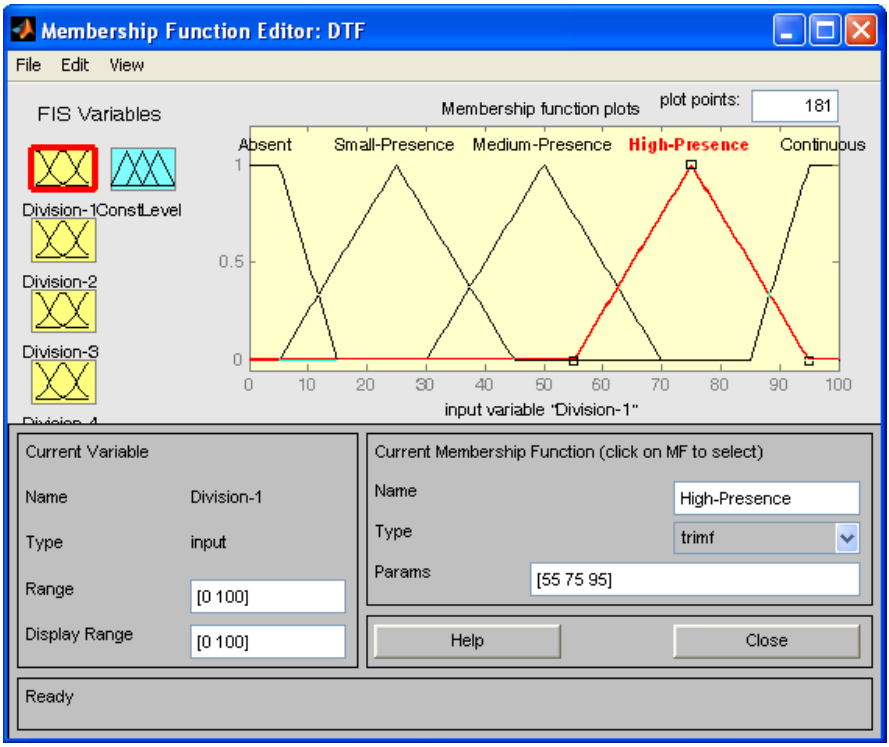

Fig. 3. The structure for each input variable

For the possible values of percentage of presence, were defined five membership functions as follows:

- "Continuous" - a trapmf function characterized by the parameters [85 95 100 100], representing a traffic with a presence rate so high, that it can be considered continuous.
- "High-Presence" - a trimf function characterized by the parameters [55 75 95], representing a traffic with high rates of presence
- "Medium-Presence" - a trimf function characterized by the parameters [30 50 70], representing a traffic with medium rates of presence
- "Small-Presence" - a trimf function characterized by the parameters [5 25 45], representing a traffic with low rates of presence
- "Absent" - a trapmf function characterized by the parameters [0 0 5 15], representing a traffic with a presence rate so low that it can be considered as absent.

In other words, in order to say that a traffic is continuous, it needs to have very high rates for the percentage of presence, almost 100%. Then by high presence we understand the situations when the percentage of presence is around 75%. Medium

presence is defined around 50% and small presence is around 25%. If the presence is very very small, the fuzzy model will consider it as absent.

In practice, the percentage of presence is not limited to some individual values like 25% / 50% / 75% / 100%. Instead, the values are spread in all of the interval between 0% and 100%. That is why the fuzzy model uses trimf functions and trapmf functions, to fully characterize the real traffic.

It is very important to notice at this point, that DTF Method is not interested absolutely to find IP destinations with high or continuous presence . It is desirable to create reference fingerprints with IP destinations that have this kind of traffic, but is not absolutely necessary. What is more important is to have a constant traffic. This means that even if we have small presence, but constant in time, we can use this to create reference fingerprints.

So, the level of the percentage of presence does not need to be very high. But, the level will determine the "strength" of the reference fingerprints. By "strength" we understand how fast and how certain is the identification process in real time. Having high rates of presence in a reference fingerprint, will determine a fast and accurate recognition. Lower rates could also bring to the recognition of the MAC address, but may be it needs a longer time.

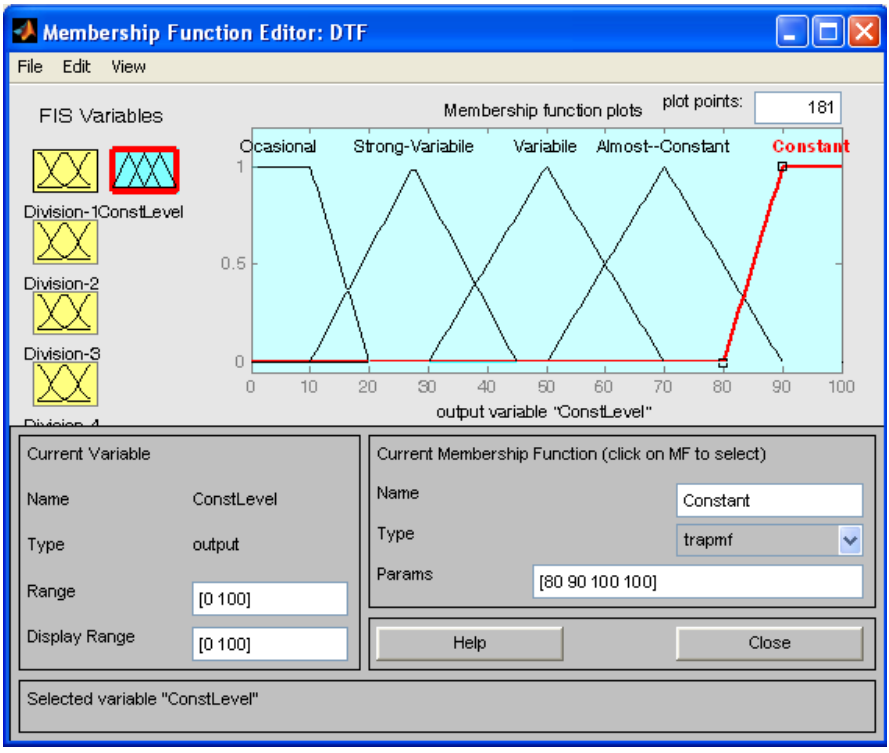

Fig. 4. The structure for output variable

2.3 Output Structure

The output has to reflect the constant or non-constant nature of the traffic to a specific IP destination. That is why, five membership functions were defined, according to the following specifications.

- "Constant" - a trapmf function characterized by the parameters [80 90 100 100], representing a traffic which is constant over the four time divisions.
- "Almost Constant" - a trimf function characterized by the parameters [50 70 90], representing a traffic which shows some variations over the four time divisions, but still can be considered almost constant.
- "Variable" - a trimf function characterized by the parameters [30 50 70], representing a traffic which is found in all four divisions, but the percentage of presence is variable and thus, the traffic can not be used as a part of a reference fingerprint in DTF Method.
- "Strong Variable" - a trimf function characterized by the parameters [10 27.5 45], representing a traffic which shows very big variations in time for the percentage of presence.
- "Occasionally" - a trimf function characterized by the parameters [0 0 10 20], representing a traffic which is found only sometimes.

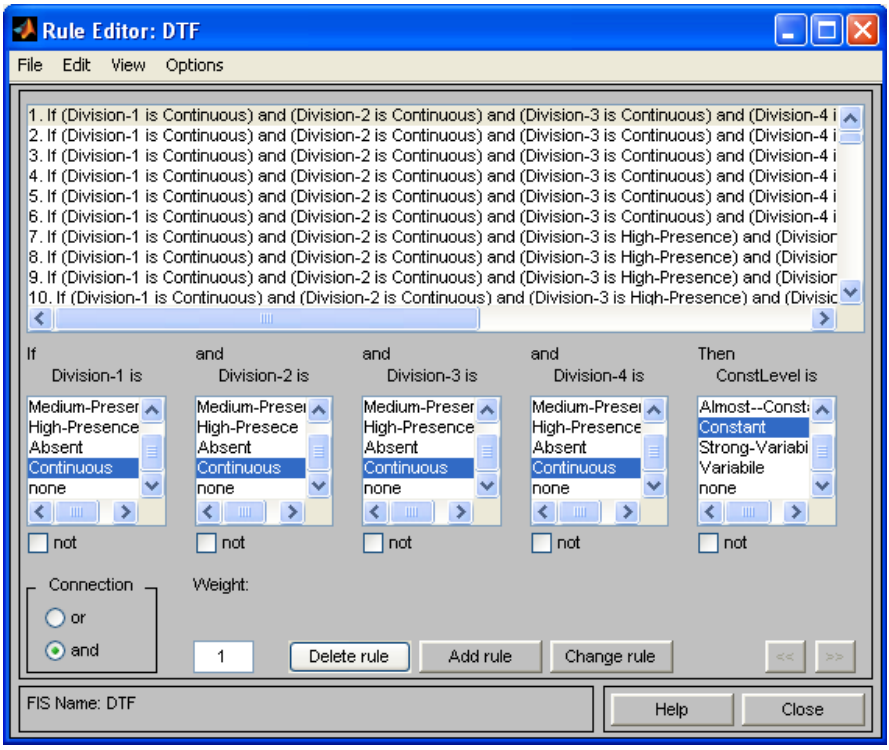

Fig. 5. The rules

2.4 The Rules Defined to Generate the Output

The rules have to generate the output from the received inputs. Each input represents the percentage of presence in the traffic, of a certain IP destination. We have four inputs because the time interval was split in four equal divisions.

We keep in mind that the "constant" state of the traffic does not really refers to high rates of presence, but instead it refers to the differences between the values that are extracted in the four equal time divisions. In this circumstances, the rules were generated using the following conventions.

The system will output "Constant" when:

- all four inputs are the same
- 3 inputs are level "*L"* and one is level "*L-1"* or "*L+1"*
- 2 inputs are level "*L"* and 2 are level "*L-1"* or "*L+1"*
- other situations, depending also on the order of input values

The system will output "Almost-Constant" when the above conditions are not met, but are close to them. For example, 3 inputs are level *L* and and one is level "*L-2" or "L+2"*. But also, other entries could bring to the same output.

For "Variable", the differences are big between the levels in different divisions. Or, even if we have high rates in two or three divisions, if the traffic is missing in one division, the fuzzy rule will consider it variable.

To output a "Strong Variable" value, it is necessary to have very big variations. For "Occasionally", two or three "Absent" inputs have to be present.

All the above examples of rules were given in order to obtain a brief description of the model itself. All the rules operate together to process the four inputs and generate the output as much close as possible to obtain the best results. Each individual case was carefully considered and the appropriate rules were created.

3 Using the Fuzzy Model in the Reference Fingerprint Generation Process

The reference fingerprint generation will strongly affect the performances of the real time recognition process. That is why it is very important to isolate all the IP addresses that really prove to have a constant traffic.

Through regular calculations, the percentage of presence of a certain IP address is calculated by dividing the total number of minutes when we had traffic to that IP, by the total number of the minutes from the evaluated time interval. Even though it is a simple formula, the result does not necessary reflect the constant nature of the traffic during the entire process.

Applying fuzzy logic to the process of reference fingerprint generation will improve the performances and will bring to clear differentiation between constant and non-constant traffic. For a better understanding, we will focus on a few study cases, where fuzzification brings a fast and accurate generation of the result.

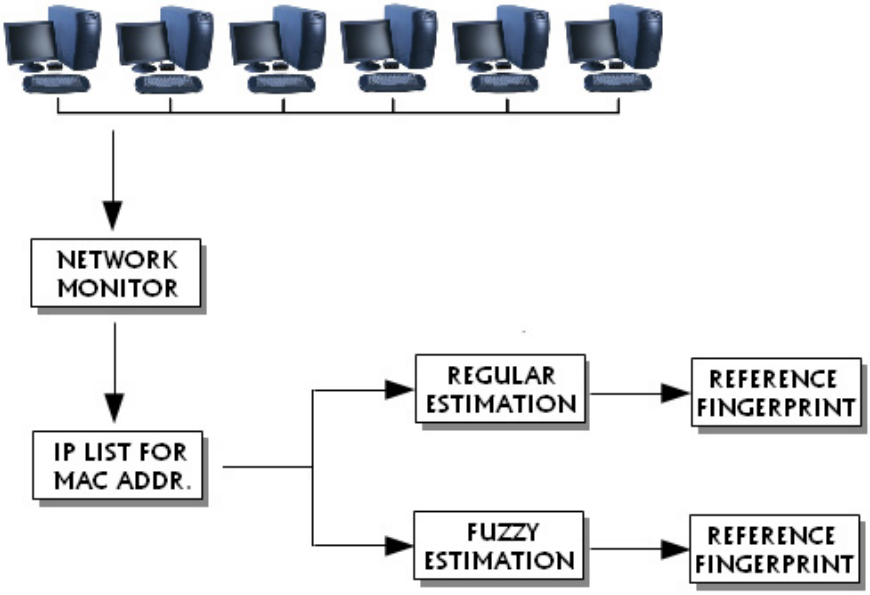

Fig. 6. Reference Fingerprint generation using two different alternatives

The comparison between a regular determination of the constant traffic and a fuzzy determination, can be represented as in Fig. 6. The network is monitored at a certain point and the list of IP destination is extracted. This list contains not only the IP addresses, but also the set of minutes when there was traffic to each of them.

This resulting list is passed to the entries of two different modules, in order to estimate if the traffic is constant or not. Each estimation module will generate the result by a different calculation process. The Regular Estimation module will apply the ratio mentioned above, while the Fuzzy Estimation module will apply the rules described in the previous chapter. As a result, two different reference fingerprints will be obtain.

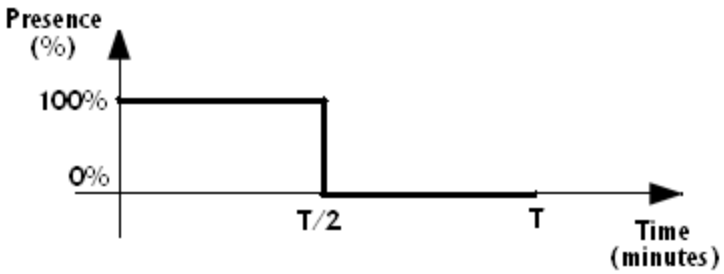

Fig. 7. Presence of 100% in first half of the interval and 0% in the second half

The example shown in Fig 7 can be considered as a „tricky case". The traffic to one IP destination is present in all the minutes from the first half of the evaluated time and then it was completely absent in the second half. If we apply the regular formula to calculate the percentage of presence, we obtain a value of 50% and this could be wrong interpreted as a constant traffic, with a high rate of presence. Instead, the fuzzy model will identify correctly the absence and will output a „Variable" result.

An isolated traffic can also be distinguished from a constant traffic with low rates for the percentage of presence. Dividing the time interval for the evaluated period in four equal divisions will determine four different percentages of presence. The fuzzy model will correctly locate the isolated traffic in one or two divisions and will output „Variable", „Strong-Variable" or „Occasionally".

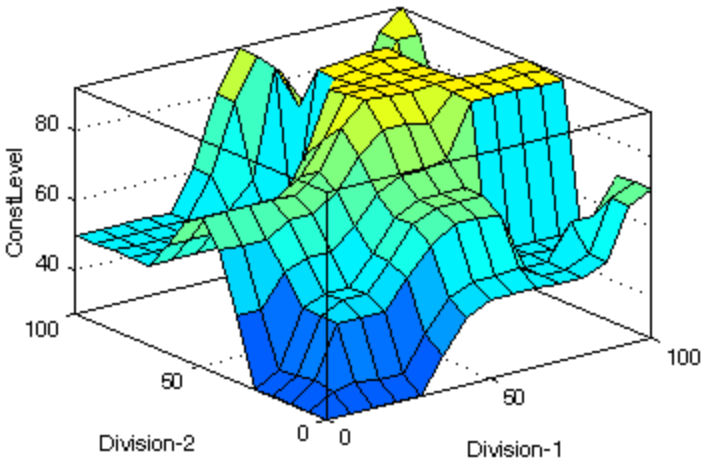

Fig. 8. Surface view of the fuzzy model

The rules work together in the fuzzy model to generate the proper output. Fig. 8 shows the surface view of the representation using Fuzzy Logic Toolbox [13]. The results are much better than the regular determination because it considers the differences between time divisions and not the level of the percentage of presence in the entire interval.

The reference fingerprints generated by regular estimations will easily accept IP destinations that do not have a real traffic. This means that in the process of MAC validation, the system will search for IP addresses that are missing from the actual fingerprints and wrong interpreting the MAC address as spoofed. Even if all the components of the reference fingerprint are found in the traffic, the stability of the system is weak, and can be broke very fast, raising false alarms that could also bring to wrong decisions in the administration levels.

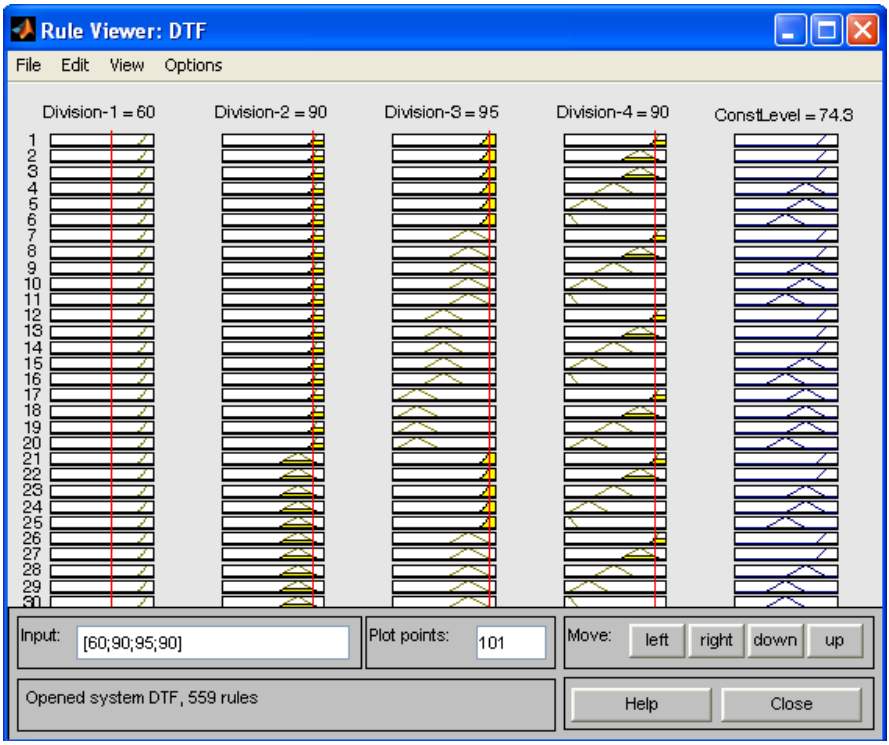

Fig. 9. The rule viewer of the fuzzy model

The Rule Viewer shown in Fig. 9 is also a good tool in the study because we can visualize the specific rules that are used in each case. The Rule Viewer can be used to manually change the input values, by simply clicking on the desired position, for every input. The output will change according to the modifications enabling the user to see the impact of the change.

4 Conclusions

The use of fuzzy logic is a very good approach in DTF Method, when we want to establish if the traffic is constant or not. The result is given as a percentage value and also as a set composed by: „Constant", „Almost-Constant", „Variable", „Strong-Variable", „Occasionally".

The most important segment in DTF Method is the generation of the reference fingerprints. If a fingerprint contains IP addresses that do not form a constant traffic, then the recognition process will be altered and false alarms will be raised. That is why is so important to be sure that in a reference fingerprint we have only addresses with true constant traffic.

As discussed in previous works, one method that can be used to distinguish between constant traffic and non-constant traffic, is to divide the time interval in four divisions and calculate the percentage of presence in each. Fuzzy logic helps in this process, by evaluating the four entries and generating the right output.

Matlab simulation provides a better understanding of the rules and the way they are used to provide the result. Many tools are available to monitor and visualize the system, Each block in the diagram can be easily installed and configured.

As a final conclusion, applying fuzzy logic in DTF method enhances the power of the method by providing a fast and accurate determination of the constant or non constant traffic, which is the most important issue. Stronger fingerprints lead to better results and what makes a fingerprint to be strong is components that really have a constant traffic. Fuzzy logic proved to be a powerful tool in this process.

References

1. Sasu, E.C., Prostean, O.: Using Constant Traffic to Specific IP Destinations for Detecting Spoofed MAC Addresses in Local Area Networks. In: IEEE International Joint Conferences on Computational Cybernetics and Technical Informatics, Timisoara, Romania, pp. 677–681 (2010)
2. Sasu, E.C., Prostean, O.: Testing DTF Method for Applicability in a Real Environment. In: 7th IEEE International Symposium on Applied Computational Intelligence and Informatics, Timisoara, Romania, pp. 285–289 (2012)
3. Wang, H., Jin, C., Shin, K.G.: Defense Against Spoofed IP Traffic Using Hop-Count Filtering. IEEE/ACM Transactions on Networking 15(1), 40–53 (2006)
4. Sheng, Y., Tan, K., Chen, G., Kotz, D., Campbell, A.: Detecting 802.11 MAC Layer Spoofing Using Received Signal Strength. In: IEEE INFOCOM 2008 Proceedings, Phoenix, USA, pp. 2441–2449 (2008)
5. Chandrasekaran, G., Francisco, J., Ganapathy, V., Gruteser, M., Trappe, W.: Detecting Identity Spoofs in IEEE 802.11e Wireless Networks. In: IEEE GLOBECOM 2009 Proceedings, Honolulu, Hawaii, USA (2009)
6. Goel, S., Kumar, S.: An Improved Method of Detecting Spoofed Attack in Wireless LAN. In: First International Conference on Networks & Communications, Chennai, India, pp. 104–108 (2009)
7. Martinez, A., Zurutuza, U., Uribeetxeberria, R., Fernandez, M., Iizarraga, J., Serna, A., Velez, I.: Beacon Frame Spoofing Attack Detection in IEEE 802.11 Networks. In: The Third International Conference on Availability, Reliability and Security, Barcelona, Spain, pp. 520–525 (2008)
8. Huang, H., Chang, K., Lu, Y., Yang, C.: Countermeasures against MAC Address Spoofing in Public Wireless Networks using Lightweight Agents. In: 5th International ICST Conference on Wireless Internet, Singapore, China (2010)
9. Bansal, R., Tiwari, S., Bansal, D.: Non-Cryptographic Methods of MAC Spoof Detection in Wireless LAN. In: 6th International Conference on Natural Language Processing, Pune, India (2008)

10. Chumchu, P., Saelim, T.: A New MAC Address Spoofing Detection Algorithm using PLCP Header. In: The International Conference on Information Networking 2011, Kuala Lumpur, Malaysia, pp. 48–53 (2010)
11. Zadeh, L.A.: Fuzzy Sets. Information and Control 8(3), 338–353 (1965)
12. Zadeh, L.A.: The role of Fuzzylogic in modeling, identification and control. Modeling, Identification and Control 15(3), 191–203 (1994)
13. MathWorks, Fuzzy Logic Toolbox, http://www.mathworks.com/products/fuzzy-logic/

Design an Optimal Fuzzy PID Controller for Herbal Machine Harvester with Gripping-Belt Speed

Behnam Yavari, Seyed Hamidreza Abbasi, and Faridoon Shabaninia

School of Electrical and Computer Engineering
Shiraz University, Shiraz, Iran
Behnamyavari64@gmail.com, Hamid_abs62@yahoo.com,
Shabani@shirazu.ac.ir

Abstract. Today fuzzy logic is used to solve various engineering issues. In this paper a novel approach for tuning the PID controller for Gripping-Belt of Herbal machine Harvester speed control is proposed. Designing the values of proportional, integral and derivative constants are divided into three stages one for each constant. The Optimal Fuzzy system identifies the constants at each stage. The *Kp*, *Ki* and *Kd* are set by the optimized fuzzy logic controller to improve the performance of rise time, peak overshoot, oscillation and the settling time. Gripping-belt for herbal machine harvester with the control issues were discussed, given the gripping-belt approximation model with a control system using Matlab/Simulink and Fuzzy Logic Toolbox software kit built with herbal medicine harvester holding a simulation model and controller. The control system of the conventional fuzzy control, PID control and optimal fuzzy self-tuning PID control simulation results show that the optimal fuzzy self-tuning PID control for better dynamic response to achieve the desired control effect.

Keywords: Herbal machine harvester, Optimal fuzzy PID controller, Simulation, Speed control, SQP algorithm.

1 Introduction

With the continuous improvement of quality requirements harvest and rapid development of control theory, the new control technology applied to agricultural harvesting machine automation has become an inevitable trend. The gripping-belt should always track with the speed of the machine operating. However, Gripping-belt of herbal machine harvester with the existence of delay and inertia, due to harsh operating environment of agricultural machinery, and herbs grown by the low-lying density of the system parameters are also some uncertainty, so the system is uncertain nonlinear stochastic systems [1]. Traditional PID controller is linear, fuzzy control is not enough fast, the system is time-varying and nonlinear, so it is not easy to obtain satisfactory control quality.

Optimal fuzzy PID control can deal with uncertainties, time-varying, nonlinearity and sudden changes [2]. Studies have shown that fuzzy control because of its ambiguity, making it difficult to achieve high steady-state accuracy [3].In this paper, fuzzy

V.E. Balas et al. (Eds.): Soft Computing Applications, AISC 195, pp. 129–140.
springerlink.com

control, conventional PID and optimal control combined to a form, optimal fuzzy PID control method. Fuzzy control has both the flexibility and adaptability advantages, but also PID control has stability and high accuracy. Trough optimization all these advantages will improve. Moreover, in a study of optimal design for fuzzy controllers, two relationships must be established: 1) design parameters and control nonlinearity, and 2) control nonlinearity and process performance.

This work is an attempt to undertake the development of a new analytical approach to the optimal design of fuzzy controllers. For an optimal system design using genetic algorithms, an overall performance index is proposed including several individual performance indexes. Finally, numerical studies are performed on several processes including nonlinearities due to time delay and saturation [6].

2 Methodology of Control System

Automatic control system without optimization of gripping-belt of herbal machine harvester is shown in Fig.1. The system consists of controller, stepper motor, hydraulic valves, hydraulic motors and speed sensors and other components [1]. System works by the controller and stepper motor direction of rotation of the corner; stepper motor and hydraulic valve rigid link directly to drive spool rotation, then driven by a hydraulic motor hydraulic valve work, the hydraulic motor speed sensors on the hydraulic motor speed feedback to the controller, so the controller can control the whole system.

The whole system formed a closed loop system. Fig. 2 shows the proposed methodology with respect to the data or parameter flow in off-line design [2].

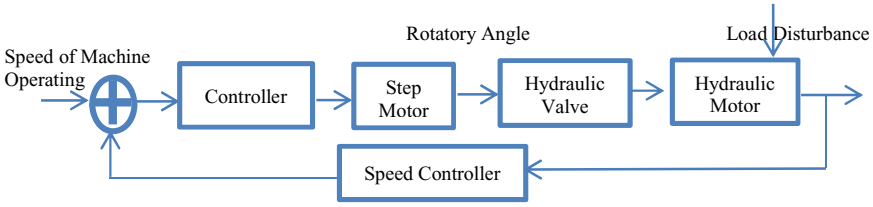

Fig. 1. Working principle of system

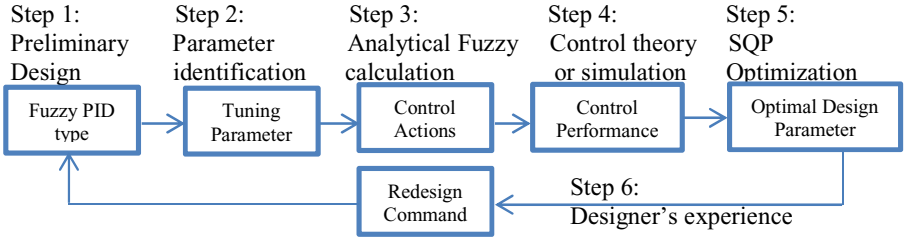

Fig. 2. Proposed methodology with respect to the data or parameter flows for optimal design of fuzzy PID controllers

In Step 1, the structure of a fuzzy PID controller is designed and the structural parameters are set for the preliminary design. The tuning parameters are identified in Step 2, while in Step 3 an analytical fuzzy calculation is performed, which produces a closed-form relationship between the design parameters and control action for the fuzzy inference. In Step 4, numerical simulation (or control theory) is used to obtain the control performance data. In Step 5, genetic-based optimizations are carried out to produce optimal design parameters. This also provides useful information for the redesign of the original system. Finally, if necessary, redesign is undertaken using the designer's expertise for further improvement to the control system. Note that the theoretical study in Step 3 makes the fuzzy controller transparent. This step is important since it will establish a close link between fuzzy control design technique and classical/modern control theory.

3 Design of Optimal Fuzzy PID Controller

Optimal control theory is one of the most important subsets of automatic control theory. The goal of optimal control is to find an ideal control input $u(t)$ in a specific time interval that can derive the plant along a trajectory so that the cost function is minimized [3].

$$\dot{X}(t) = f(X, u, t),$$

Where X represents the state of the system, u is the input, and t is the time. For a fixed final state control problem, the cost is:

$$J = \phi(x(T), T) + \int_{t_0}^{T} L(X, u, t)\,\mathrm{d}t \ ,$$

Where $\phi(x(T), T)$ is the final weighting function, which depends on the final state $x(T)$ and the final time T, and the weighting function $L(X, u, t)$ depends on the state and input at intermediate times in $[t_0, T]$. The goal of optimal control $u^*(t)$, on the time interval $[t_0, T]$ that derives the main system such that the cost function is minimized.

In this paper we use a fuzzy PID control method which employs a SQP optimization algorithm [5] to find the optimal solution by minimizing a well-defined cost function. As the result, the optimal fuzzy PID parameter tuner provides an online PID parameter tuning strategy for a standard PID controller as shown in Fig.3.

Our method in this article is based on optimal control theory and employs an optimization algorithm to find the optimal fuzzy PID parameter tuner that minimizes the cost function by combining fuzzy logic knowledge. The structure of the control system with a fuzzy PID parameter tuner is shown in Fig.3.

The objective of the system is to find the optimal control solution by evaluating the well-defined cost function and adjusting the parameters of three fuzzy PID parameters can be established. Three fuzzy parameter tuners are designed based on the mapping from error and derivative of error to PID controller parameters; $k_P(t)$, $k_i(t)$ and $k_d(t)$ as shown in Fig.4.

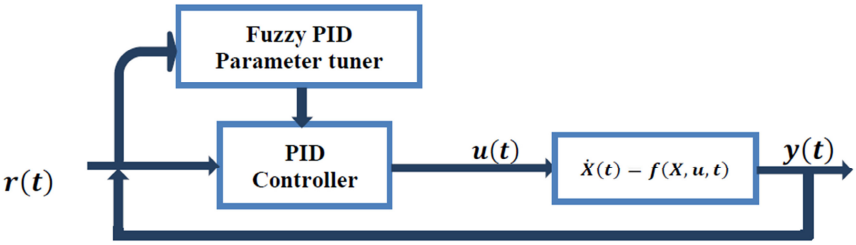

Fig. 3. General control system with a fuzzy PID parameter tuner and a PID controller

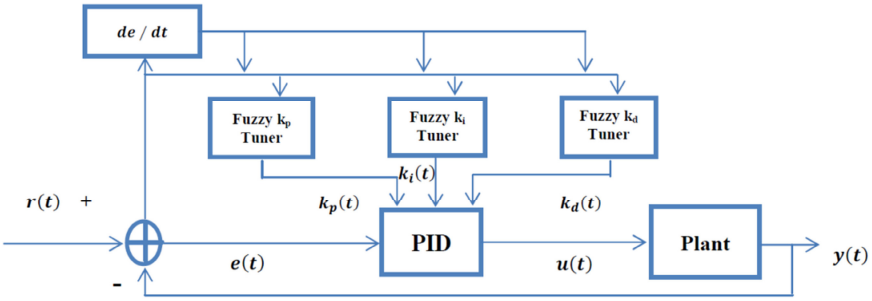

Fig. 4. Self-tuning fuzzy PID control structure

One major part of the proposed method is employ SQP (sequential quadratic programming) optimization algorithm to find the optimal fuzzy PID parameter tuners based on the cost function. The proposed method includes six steps:

1. Design the cost function,
2. Initial fizzy parameter tuner structure design,
3. Parameterization design from the initial tuner,
4. Establishment of constraints,
5. Optimization of the fuzzy PID parameter tuners,
6. Assessment of the rules.

A flow chart of the proposed method is shown in Fig.5.

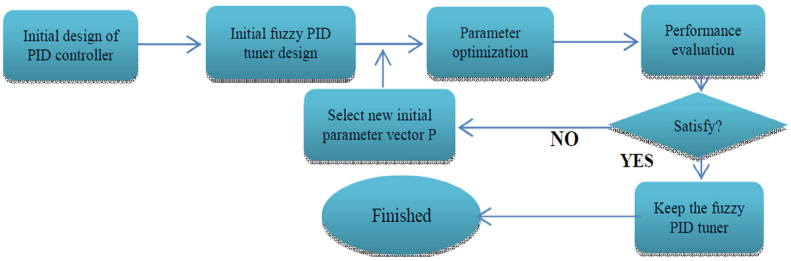

Fig. 5. Illustration of the proposed fuzzy tuner optimization method

Sequential quadratic programming (SQP) [6] which represent the state of the art in nonlinear programming methods can handle both equality and inequality constraints. This method is similar to Newton's method for constraint optimization. SQP algorithm is applied to search the space of the parameter vector until the minimal cost is reached. Although the Mathlab Optimization Toolbox provides 4 SQP algorithms, in this paper we use fmincon (Find minimum of constrained nonlinear multivariable function) because it is one kind of nonlinear programming optimization algorithms suitable for complex system optimization.

As shown in Fig.5 an optimization procedure will iterate many times to reach the final solution satisfying the design criteria. At each iteration, it is necessary to adjust the parameter vector such the sufficient improvement can be achieved. In the application of this paper, at each optimization iteration, in ninety-five percent of the cost could be achieved compared with the previous iteration cost, we consider improvement sufficient. It may be reasonable to change ninety-five percent to other to other values for a different application.

4 Principle of Fuzzy PID Controller

In this section we propose the fuzzy PID controller and show the results. In the next section we optimize the controller parameters and compare between the results of these two methods.

Fuzzy PID controller controls the PID parameters, online by using the fuzzy controller. In the first step it finds PID regulator 3 parameters (k_P, k_I and k_D) with tuning the error (e) and the rate change of error (ec) between the fuzzy relations. The controller adjust the k_P, k_I and k_D online according the control law, and then substitute the adjusted parameters into the PID equation to compare the results which be the output for the controller.

R_{ij} : if x is A_i and y is B_j Then: $u^{ij}(t) = K_P^{ij}\mathrm{e}(t) + K_I^{ij}\int e(t)dt + K_D^{ij}\dot{e}_{(t)}$;

$$K_I = K_P\frac{T}{T_I}\ ; \qquad K_B = K_P\frac{T_D}{T}$$

Where x denotes $e(t)$ and $x \in X$, y denotes $\dot{e}(t)$ and $y \in Y$, i=1,2,…,n and g=1,2,…,m.

T_I and T_D are regulator proportional, integral and differential time, and T is sampling period.

$u(t)$ denotes output variable.

Employing singleton fuzzifier, sum-product interface and center-average defuzzifier, the output of the fuzzy PID controller is expressed as:

$$u(t) = \frac{\sum_{i=1}^{n}\sum_{j=1}^{m} A_i(x)B_j(y)u^{ij}}{\sum_{i=1}^{n}\sum_{j=1}^{m} A_i(x)B_j(y)}$$

In this paper a fuzzy PID controller for the sample input speed deviation "e" $(v_0 - v)$ and the change rate of velocity deviation "ec" $[\frac{\mathrm{d}}{dt}(v_0 - v)]$, motor control pulse output. PID controller, ΔK_P, ΔK_I and ΔK_D, the change of the K_P, K_I and K_D are used as the output of fuzzy controller.

The speed deviation change and speed deviation change rate of the domain location (-3,3), the output universe of ΔK_P, ΔK_I and ΔK_D is set at (-0.5,0.5), (-0.1,0.1), (-0.05,0.05). The fuzzy sets are divided into seven levels: {negative large, negative middle, negative small, zero, positive small, positive middle, positive large}, usually denoted as {NB, NM, NS, ZO, PS, PM, PB} [1].

The system uses triangular membership functions, and in the range of the two endpoints of the domain, in order to achieve a smooth curve membership function, respectively S-type and Z-type membership function. Membership functions curve corresponding to each variable shown in Fig.6 for inputs and Fig.7 for outputs.

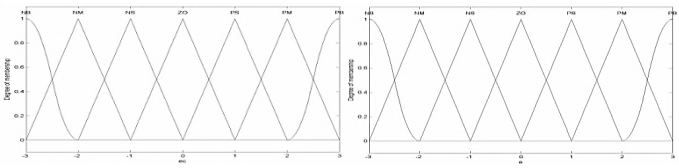

Fig. 6. The membership function curve of inputs; e & ec

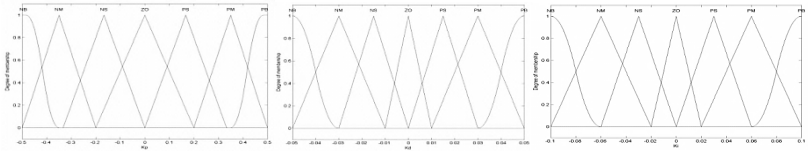

Fig. 7. The membership function curve of output; K_P, K_i, K_d

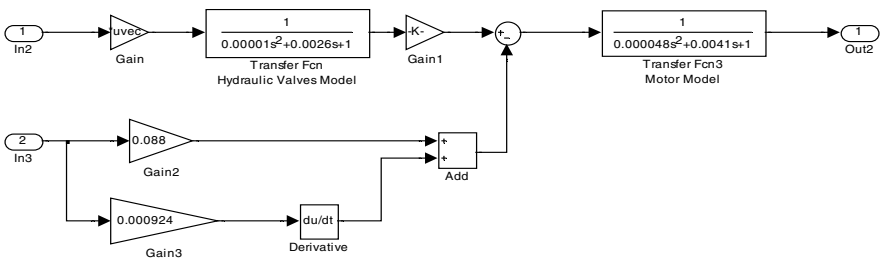

Fig. 8. Speed control subsystem block diagram

Based on the principle of fuzzy self-tuning PID, the use of "IF A and B THEN C and D and E" form of trial by repeatedly comparing the final set, and control rules, as shown in Table.1.

Table 1. Fuzzy rule table

EC/E	NB	NM	NS	ZO	PS	PM	PB
NB	PB/NB/PS	PB/NB/NS	PB/NM/NB	PM/NM/NB	PS/NS/NB	ZO/ZO/NM	ZO/ZO/PS
NM	PB/NB/PS	PB/NM/NB	PB/NM/NB	PM/NS/NM	PS/NS/NM	ZO/ZO/NS	NS/PS/ZO
NS	PM/NB/ZO	PM/NM/NS	PB/NS/NM	PS/ZO/NM	PS/ZO/NS	ZO/PS/NS	NS/PS/ZO
ZO	PM/NM/ZO	PM/NM/NS	PS/NS/NS	ZO/ZO/NS	NS/PS/NS	NS/PM/NS	NM/PM/ZO
PS	PS/NM/ZO	PS/NS/PM	ZO/ZO/PS	NS/PS/ZO	NM/PS/ZO	NM/PM/PS	NB/PB/ZO
PM	PS/ZO/PS	ZO/ZO/PB	NS/ZO/PS	NM/PS/PS	NM/PM/PB	NB/PM/PB	NB/PB/PS
PB	ZO/ZO/PB	ZO/ZO/PM	NM/PS/PM	NM/PM/PS	NB/PM/PB	NB/PB/PS	NB/PB/PB

Application of the PID parameter of fuzzy reasoning, found under the modified parameters into the calculated as follows [1]:

$$K_P = K_P' + \Delta K_P$$

$$K_I = K_I' + \Delta K_I$$

$$K_D = K_D' + \Delta K_D$$

Here: K_P', K_I' and K_D' are used for the previous setting good parameters.

Approximately the transfer function of the controlled object is: [7, 8].

$$G(s) = \frac{k_f \dfrac{k_q}{D_m}}{\left(\dfrac{s^2}{\omega_v^2} + \dfrac{2\xi_v}{\omega_v}s + 1\right)\left(\dfrac{s^2}{\omega_h^2} + \dfrac{2\xi_h}{\omega_h}s + 1\right)}$$

External load torque hydraulic motor angular velocity transfer function can be expressed as: [7, 8].

$$\frac{\omega_m}{T_L(s)} = \frac{-\dfrac{k_{ce}}{D_m^2}\left(1 + \dfrac{V_t}{4\beta_e K_{ce}}s\right)}{\dfrac{s^2}{\omega_4^2} + \dfrac{2\xi_h}{\omega_n}s + 1}$$

Simulation of the fuzzy PID control system using Simulink/Matlab R2011a version of 7.12.0 is shown in Fig.9 and the speed control subsystem block diagram is shown in Fig.10.

Simulation parameters were shown in Table.2.

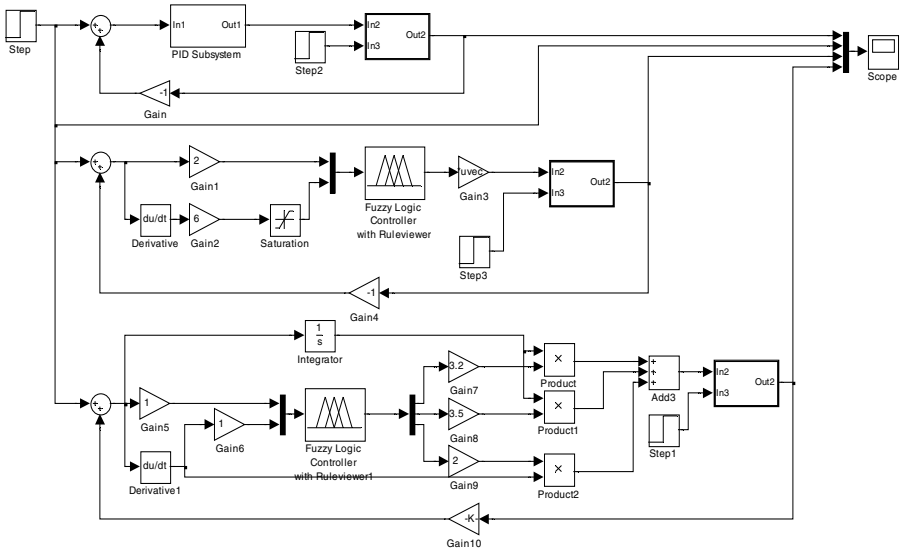

Fig. 9. Simulink simulation block diagram of PID control, fuzzy control and fuzzy PID control

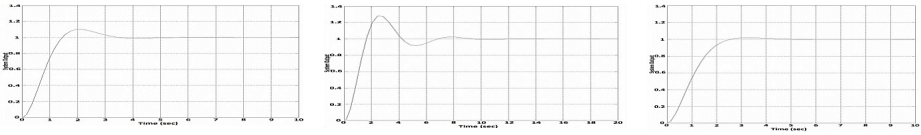

Fig. 10. PID, Fuzzy and Fuzzy PID control dynamic curve

Table 2. Simulation parameters

Symbol	Value	Symbol	Value
D_m (m^3/rad)	3.2×10^{-6}	V_t (m^3)	6.4×10^{-5}
β_e (pa)	1.7×10^{9}	ξ_v	0.41
k_{ce} (m^5/N.S)	9×10^{-13}	k_f	0.12
ω_v (rad/s)	314	ξ_h	0.3
ω_h (rad/s)	145	k_q	3.2×10^{-6}

5 Simulation and Results without Optimization

Simulation curve of PID, Fuzzy and Fuzzy PID controllers shown in Fig.10.

By comparing these three curves the following conclusion can be drawn, as shown in Table.3.

Table 3. Comparison of simulation results

Indicators Type	Peak Time s)	Adjustment Time (s)	Overshoot (%)	Steady state error (%)
PID	2.5	14	30	0
Fuzzy	2	7	10	4
Fuzzy-PID	3	5	0	0

6 Optimization Algorithm and Results

6.1 Algorithm

We chose to employ Sequential Quadratic Programming (SQP) [6], one of the gradient-based nonlinear programming optimization algorithms, to search the optimal parameter vector *p* for the given format of *J*. The reason for choosing SQP was for its effectiveness and capability of handling both equality and inequality constraints. It is provided by the Matlab Optimization toolbox.

$$J = \phi(t, t_0) + \int_{t_0}^{T} e^2(t)\,\mathrm{d}t$$

where $\phi(t, t_0)$ represents the level of overshoot and the integral term represents the overall performance. The optimization objective is to find the parameter vector *p* satisfying the design criteria. The determination of parameter vector *p* is important for the optimization process. The parameter vector should be chosen as the set of independent variables of the fuzzy tuner. It will include the membership function shape, position and scaling factors. The sample parameter vector *p* is represented as follows:

$$p = [p_1\ p_2\ \ldots p_k\ \ s_1\ s_2 \ldots s_m]$$

where $p_1\ p_2\ \ldots p_k$ are parameters determining the position and shape of the membership functions, $s_1\ s_2 \ldots s_m$ are scaling factors, k is the number of variables representing membership functions, and m is the number of scaling factors. The dimension of *p* for the optimization process needs to be decided carefully. It would be ideal to allow all parameters of the fuzzy tuners to be tuned. However, the computational complexity will become critical if *p* becomes too large.

Once the optimization procedure is completed, we will evaluate the results according to the cost function *J*, and decide if the optimization process should be repeated to discover whether any further performance improvements may be possible.

6.2 Result

The optimization algorithm will optimize the control performance by finding the optimal parameters of the controller. Fig.11 shows the progress of the cost function *J* during the optimization procedure.

Based on the predefined performance index, when the optimization process is finished, the parameter vector is:

$$p = [-1.35 \;\; 2.24 \;\; 0.73 \;\; 11.2 \;\; 0.62 \;\; 5.41 \;\; -2.13 \;\; 2.81 \;\; 2.32 \;\; -0.37 \;\; -1.39 \;\; 2.68 \;\; 0.49 \;\; 0.098 \;\; 4.52 \;\; 0.24 \;\; 1.58]$$

Optimization procedure makes optimized changes on the membership function curve of outputs.

Reducing the number of linguistic variables is another benefit of optimization of fuzzy controller. Here we had seven linguistic variables, and after optimization we have just five. The new membership functions are shown in Fig.12.

The dynamic curve (step response) also improves as shown in Fig.13.

In Table.4 comparison between the simulation results of fuzzy PID and optimal fuzzy PID controllers shows the benefits of our design method.

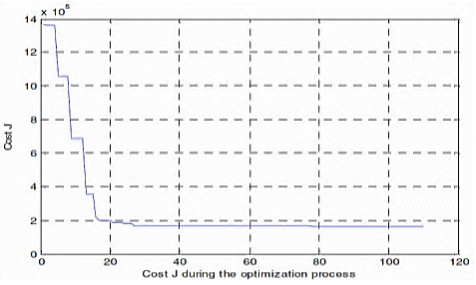

Fig. 11. Improvement of *J* during the optimization procedure

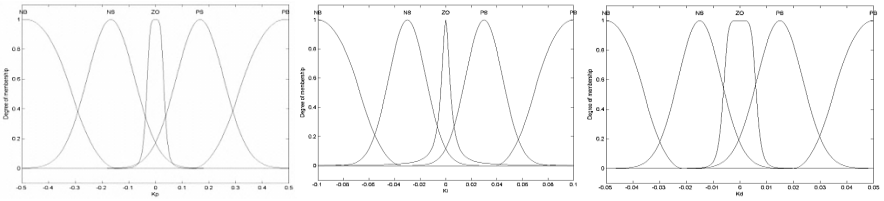

Fig. 12. The membership function curve of outputs after optimization; K_P, K_i and K_d

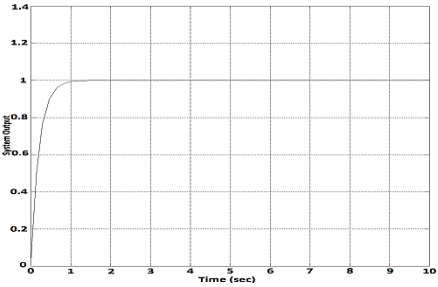

Fig. 13. The optimal fuzzy PID control dynamic curve

Table 4. Comparison of simulation results between fuzzy PID and optimal fuzzy PID controller

Indicators Type	Peak Time (s)	Adjustment Time (s)	Overshoot (%)	Steady state error (%)
Fuzzy PID	3	5	0	0
Optimal Fuzzy PID	1	2	0	0

7 Conclusion

In this paper, a new optimal fuzzy PID design method is proposed by utilizing the SQP nonlinear programming optimization algorithm. The simulation results of herbal machine harvester motor application are presented. It has turned out that with the optimization algorithms, the fuzzy PID optimal controller design and the desired overall control performance can be achieved by selecting a proper cost function. Also the parameter vector and optimization algorithm play key roles in this approach.

References

1. Huang, J., Wang, J.: The research of fuzzy self-tuning PID in chinese traditional herbal harvester with gripping belt speed. In: Proc. of Int. Conf. on Electronic & Mechanical Engineering and Information Technology, Jiamusi, China, August 12-14, pp. 2019–2024 (2011)
2. Kennedy, J.: Force Control of Hydraulic Servo System Master of Science Dissertation, Faculty of the Graduate School University of Missouri (May 2009)
3. Lewis, F.L., Syrmos, V.L.: Optimal Control, 3rd edn. J. Wiely, New Jersey (2012)
4. Nocedal, J., Wright, S.J.: Numerical Optimization. Springer, New York (1999)

5. Rustem, B.: Algorithms for Nonlinear Programming and Multi-Objective Decisions. Princeton University Press, New Jersey (2002)
6. Tang, K.S., Man, K.F., Chen, G., Kwong, S.: An Optimal Fuzzy PID Controller. IEEE Transactions on Industrial Electronics, Journals & Magazines, 757–765 (August 2001)
7. Xing, W.C.: Hydraulic Control System, pp. 67–100. Machine Press, Beijing (2009)
8. Yu, C.C.: Autotuning of PID Controllers. Springer (2006)

Comparative Study between Tank's Water Level Control Using PID and Fuzzy Logic Controller

Davood Mohammadi Souran, Seyed Hamidreza Abbasi, and Faridoon Shabaninia

School of Electrical and Computer Engineering
Shiraz University, Iran
{davood_souran,Hamid_abs62}@yahoo.com,
Shabani@shirazu.ac.ir

Abstract. Conventional Proportional Integral Controllers are used in many industrial applications due to their simplicity and robustness. The parameters of the various industrial processes are subjected to change due to change in the environment. These parameters may be categorized as input flow, output flow, water level of the industrial machinery in use. Various process control techniques are being developed to control these variables. In this paper, the Water Level parameters of a Tank are controlled using conventional PID controller and then optimized using fuzzy logic controller. Considering final results, the comparison between literature and the results of this paper`s method illustrates that fuzzy logic controller results are considerably striking rather than others. The measured maximum overshoot for fuzzy logic controller in comparison with the measured value for the conventional PID controller reduced effectively. Besides, the settling times for both fuzzy logic and PID controllers are measured and it shows that the efficiency of fuzzy logic controller is completely reliable than the others which shows the superiority of fuzzy logic controller.

Keywords: Fuzzy Logic Controller, PID controller , Water Level.

1 Introduction

PID control is widely used in industrial applications although it is a simple control method. Stability of PID controller can be guaranteed theoretically, and zero steady-state tracking error can be achieved for linear plant in steady-state phase. Computer simulations of PID control algorithm have revealed that the tracking error is quite often oscillatory, however, with large amplitudes during the transient phase. To improve the performance of the PID controllers, several strategies have been proposed, such as adaptive and supervising techniques.

Fuzzy control methodology is considered as an effective method to deal with disturbances and uncertainties in terms of ambiguity. Fuzzy PID controller combining fuzzy technology with traditional PID control algorithm to become more effective in artificial intelligence control [1],[2]. The most common problem resulted early depending on the complexity of Fuzzy Logic Control (FLC) is the tuning problem. It is hard to design and tune FLCs manually for the most machine problems especially

V.E. Balas et al. (Eds.): Soft Computing Applications, AISC 195, pp. 141–153.
springerlink.com

used in industries like nonlinear systems. For alleviation of difficulties in constructing the fuzzy rule base, there is the conventional nonlinear design method [3] which was inherited in the fuzzy control area, such as fuzzy sliding control, fuzzy scheduling [4],[5], and adaptive fuzzy control [6],[7]. The error signal for most control systems is available to the controller if the reference input is continuous. The analytical calculations present two inputs FLC employing proportional error signal and velocity error signal. PID controller is the most common controller used in industries, most of development of fuzzy controllers revolve around fuzzy PID controllers to insure the existence of conventional controllers in the overall control structure, simply called Hybrid Fuzzy Controllers [8],[9].

2 Proportional_Integral_Derivative Controller

A proportional–integral–derivative controller (PID controller) is a generic control loop feedback mechanism (controller) widely used in industrial control systems – a PID is the most commonly used feedback controller. A PID controller calculates an "error" value as the difference between a measured process variable and a desired set point. The controller attempts to minimize the error by adjusting the process control inputs. In the absence of knowledge of the underlying process, PID controllers are the best controllers. However, for best performance, the PID parameters used in the calculation must be tuned according to the nature of the system – while the design is generic, the parameters depend on the specific system. The PID controller calculation (algorithm) involves three separate parameters ,and is accordingly sometimes called three-term control: the proportional, the integral and derivative values, denoted P, I, and D. The proportional value determines the reaction to the current error, the integral value determines the reaction based on the sum of recent errors, and the derivative value determines the reaction based on the rate at which the error has been changing. The weighted sum of these three actions is used to adjust the process via a control element such as the position of a control valve or the power supply of a heating element. Heuristically, these values can be interpreted in terms of time: P depends on the present error, I on the accumulation of past errors, and D is a prediction of future errors, based on current rate of change. By tuning the three constants in the PID controller algorithm, the controller can provide control action designed for specific process requirements. The response of the controller can be described in terms of the responsiveness of the controller to an error, the degree to which the controller overshoots the set point and the degree of system oscillation. Note that the use of the PID algorithm for control does not guarantee optimal control of the system or system stability. Some applications may require using only one or two modes to provide the appropriate system control. This is achieved by setting the gain of undesired control outputs to zero. A PID controller will be called a PI, PD, P or I controller in the absence of the respective control actions .PI controllers are fairly common, since derivative action is sensitive to measurement noise, whereas the absence of an integral value may prevent the system from reaching its target value due to the control action .

3 Fuzzy Logic Based Controller

Fuzzy controllers are very simple conceptually. They consist of an input stage, a processing stage, and an output stage. The input stage maps sensor or other inputs, such as switches, thumbwheels, and so on, to the appropriate membership functions and truth values. The processing stage invokes each appropriate rule and generates a result for each, then combines the results of the rules. Finally, the output stage converts the combined result back into a specific control output value. The most common shape of membership functions is triangular, although trapezoidal and bell curves are also used, but the shape is generally less important than the number of curves and their placement. As discussed earlier, the processing stage is based on a collection of logic rules in the form of IF-THEN statements, where the IF part is called the "antecedent" and the THEN part is called the "consequent". Typical fuzzy control systems have dozens of rules. Consider a rule for a tank: IF (tank Water level is "high") THEN (input flow is "low").

4 Problem Formulation

A Tank of a plant is taken as a case study and the Water Level control of the Tank is achieved using conventional PID controller and intelligent fuzzy logic based controller. The comparison of both the controller performance is analyzed in this chapter.

Set point of Tank Water Level = 1.

5 Mathematical Modelling & Controller Design

The basic conventional feedback controller is shown in figure 1. In conventional PID controller the controller and the process are in series where as a feedback from the output is given to the input. The tank of plant is mathematically modeled using experimental data available and the transfer function of the above system is achieved as

$$G(s) = \frac{5(S+1)}{S(S+1)(S+6)}$$

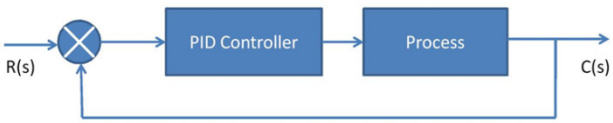

Fig. 1. Block diagram of classical control architectur

The stability analysis of the system is done and the bode plot of the system is plotted which is shown in figures 2 .

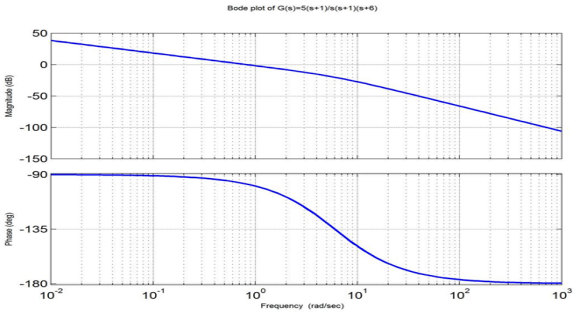

Fig. 2. Frequency domain analysis of the system

6 PID Controller Design and Tuning

A feedback control system measures the output variable and sends the control signal to the controller. The controller compares the value of the output signal with a reference value and gives the control signal to the final control element via the actuator.

The characteristic equation obtained as below

$$S^3 + 6S^2 + 5S + K_{cu} = 0 \tag{1}$$

Applying Routh criteria in eq (1) we get K_{cu}=30

From auxiliary equation in routh criteria we get ω=2.03 and T=2.69.

The equation of ideal PID controller is

$$u(t) = K_c\left(e(t) + \frac{1}{\tau_i}\int_0^t e(t)\,dt + \tau_d\frac{de(t)}{dt}\right)$$

$$u(t) = K_c\left(1 + \frac{1}{\tau_i s} + \tau_d s\right)e(s)$$

$$u(t) = K_c\left(\frac{1 + \tau_i s + \tau_i\tau_d s^2}{\tau_i s}\right)e(s)$$

The real PID controller is

$$u(t) = K_c\left(\frac{1 + \tau_i s}{\tau_i s}\right)\left(\frac{1 + \tau_d s}{1 + \alpha\tau_d s}\right)e(s)$$

The PID controller is traditionally suitable for second and lower order systems. It can also be used for higher order plants with dominant second order behavior. The Ziegler- Nichols (Z-N) methods rely on open-loop step response or closed-loop frequency response tests. A PID controller is tuned according to a table based on the process

response test. According to Zeigler-Nichols frequency response tuning criteria $K_p=0.6K_{cu}$, $\tau_i=0.5T$ and $\tau_d=0.125T$.

For the PID controller in the heat exchanger, the values of tuning parameters obtained are $K_p=32$, $\tau_i=1.5$, $\tau_d=0.29$ and P=30 , I=21.2, D=9 .

Usually, initial design values of PID controller obtained by all means needs to be adjusted repeatedly through computer simulations until the closed loop system performs or compromises as desired. This stimulates the development of "intelligent" tools that can assist the engineers to achieve the best overall PID control for entire operating envelops.

7 Water Level Control Using Fuzzy Logic Controller

PID controller is a standard control structure for classical control theory. But the performance is greatly distorted and the efficiency is reduced due to non-linearity in the process plant. The fuzzy PID controllers are the natural extension of their conventional version, which preserve their linear structure of PID controller. The fuzzy PID controllers are designed using fuzzy logic control principle in order to obtain a new controller that possesses analytical formulas very similar to digital PID controllers. Fuzzy PID controllers have variable control gains in their linear structure. These variable gains are nonlinear function of the errors and changing rates of error signals. The main contribution of these variable gains in improving the control performance is that they are self- tuned gains and can adapt to rapid changes of the errors and rate of change of error caused by time delay effects, nonlinearities and uncertainties of the underlying process.

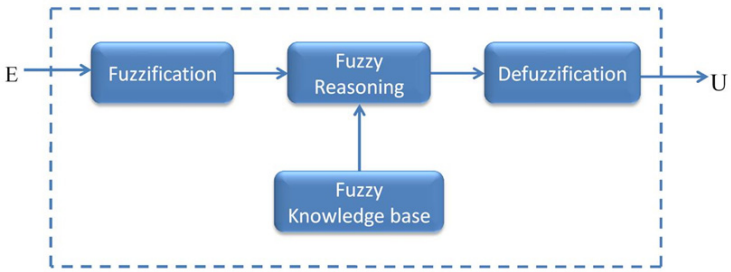

Fig. 3. Architecture of fuzzy control

In this paper we have considered different linguistic variables and details of these variables are shown in table1.

Table 1. Linguistic Variable Of Fuzzy Logic Control

Error e(t)		**change in error de/dt**		**Controller output U(t)**	
NB	Negative Big	***NB***	Negative Big	***NB***	Negative Big
NM	Negative Medium	***NM***	Negative Medium	***NM***	Negative Medium
NS	Negative Small	***NS***	Negative Small	***NS***	Negative Small
ZE	Zero	***ZE***	Zero	***ZE***	Zero
PS	Positive Small	***PS***	Positive Small	***PS***	Positive Small
PM	Positive Medium	***PM***	Positive Medium	***PM***	Positive Medium
PB	Positive Big	***PB***	Positive Big	***PB***	Positive Big

Designing a good fuzzy rule base is the key to obtain satisfactory control performance for a particular operation. Classical analysis and control strategy are incorporated in the rule base. The rule base used in simulation is summarized in table II. Each rule has the form IF e(t) is NB AND Δe(t) is NB THEN u(t) is NB. The control literature has worked towards reducing the size of the rule base and optimizing the rule base using different optimization technique like PSO for intelligent controller. At last defuzzified output is obtained from the fuzzy inputs. In this research work centroid method of de fuzzification is used. It is given as below.

$$u^* = \frac{\int \mu_c(u) * u du}{\int \mu_c(u) du}$$

Table 2. IF-THEN Rule Base For Fuzzy Logic Control

U(t)		**Error change de/dt**						
		NB	***NM***	***NS***	***ZO***	***PS***	***PM***	***PB***
error	***NB***	NB	NB	NB	NB	NB	NM	ZE
	NM	NB	NB	NB	NB	NM	ZE	PM
	NS	NB	NB	NB	NM	ZE	PM	PB
	ZE	NB	NB	NM	ZE	PM	PB	PB
	PS	NB	NM	ZE	PM	PB	PB	PB
	PM	NM	ZE	PM	PB	PB	PB	PB
	PB	ZE	PM	PB	PB	PB	PB	PB

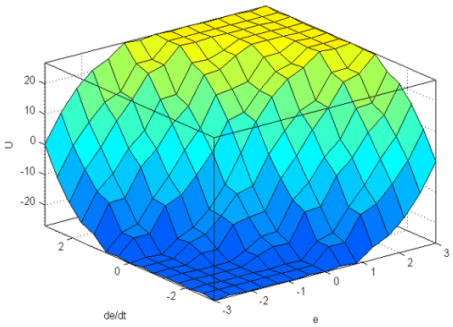

Fig. 4. Surface view of FIS

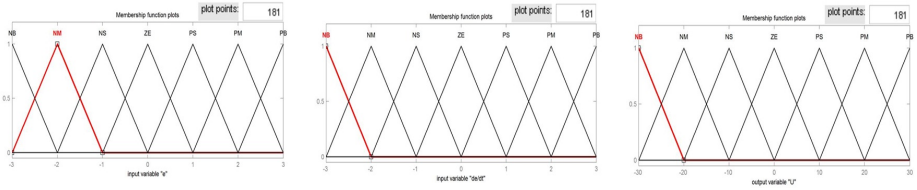

Fig. 5. Triangular Membership Function for e , de/dt and u

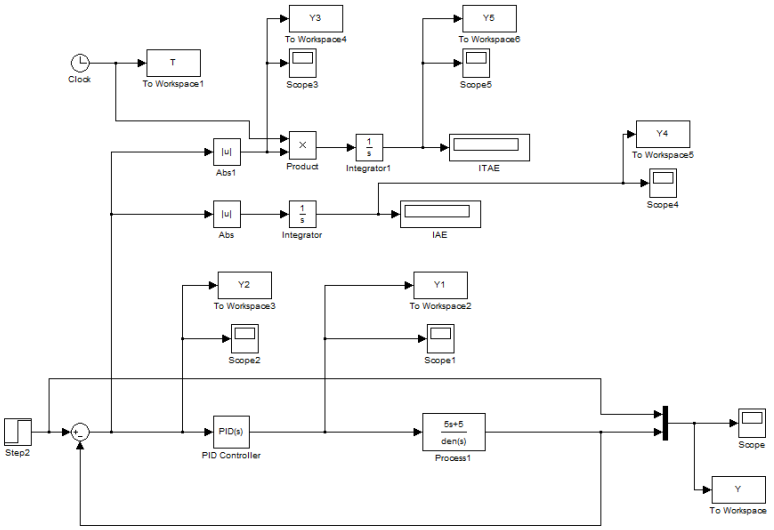

Fig. 6. Simulink representation of feedback control with PID controller of fuzzy control

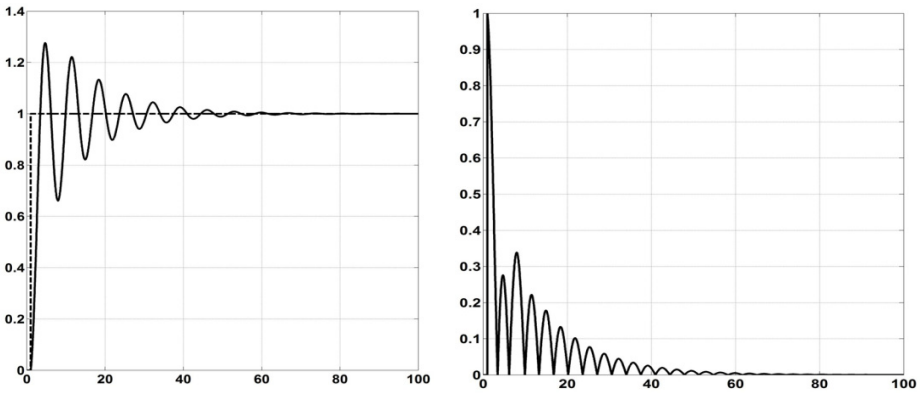

Fig. 7. Step response of the system with input and output and error signal after passing through the absolute value function

8 Simulink Representation Of Level Control Using Fuzzy Logic Controller

Simulink is a software package for modeling, simulating, and analyzing dynamical systems. It supports linear and nonlinear systems, modeled in continuous time, sampled time, or a hybrid of the two. Water level control using simulink is modeled as given below: Figure 8 shows the simulink model of fuzzy PD controller in plant. It gives the better performance in comparison to conventional PID controller which simulink model shown in figure 6.

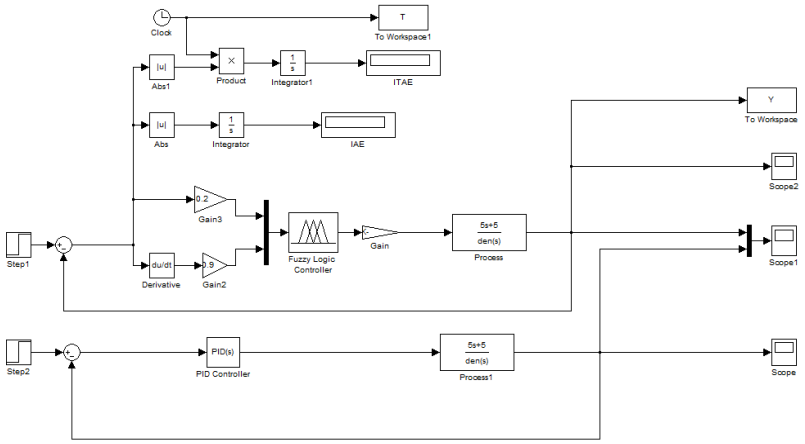

Fig. 8. Simulink representation of system with Fuzzy PD controller

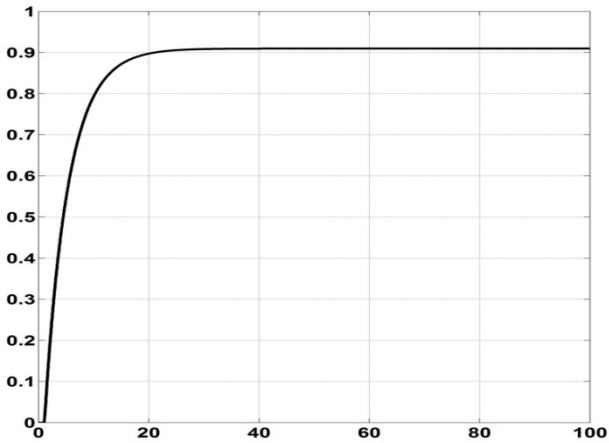

Fig. 9. Step response of system with fuzzy PD controller

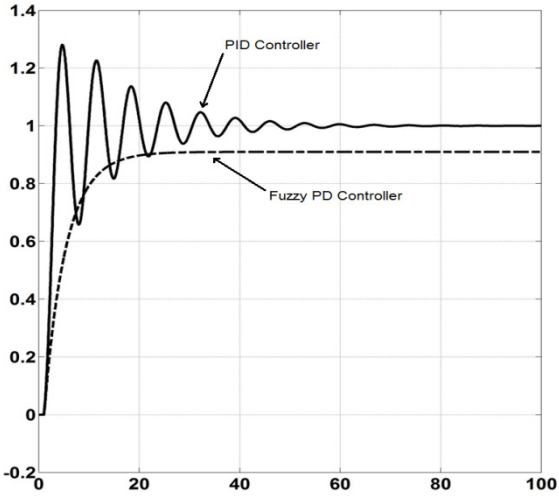

Fig. 10. Comparison between PID controller and Fuzzy PD controller

Figure 11 shows the simulink model of fuzzy PD+fuzzy_ PI controller In plant. It improves the performance index in comparison to Fuzzy PD controller which simulink mode l is shown in figure 8.

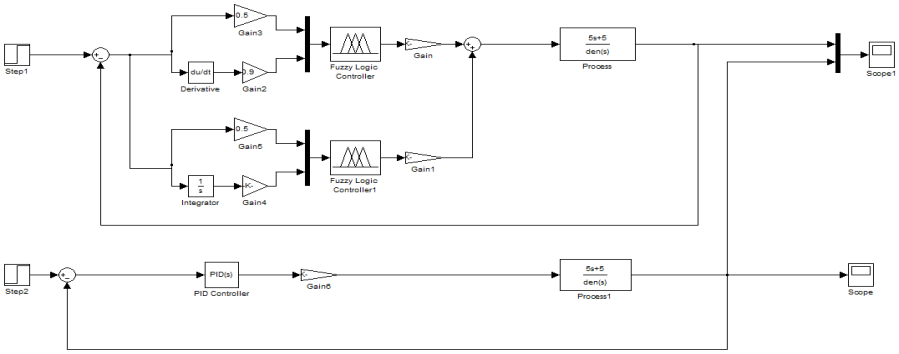

Fig. 11. Simulink representation of system with Fuzzy PD+Fuzzy PI controller

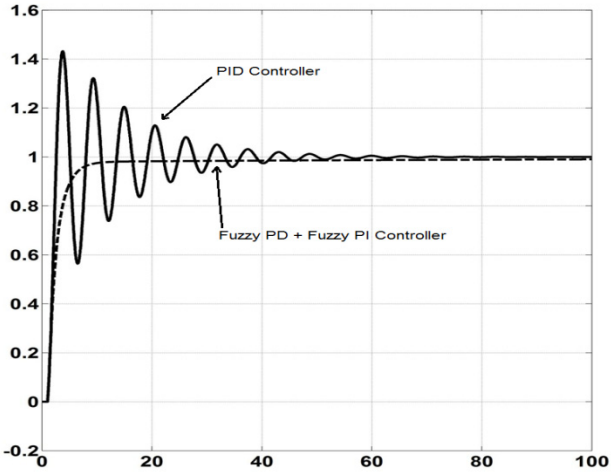

Fig. 12. Comparison between PID controller and Fuzzy PD+Fuzzy PI controller

Figure 13 shows the simulink model of fuzzy PD+PID_ controller that improves the performance index such as maximum overshoot and settling time in comparison to simulink model of fuzzy PD+fuzzy PI controller and fuzzy PD controller in plant which is shown in figure 11 and figure 8.

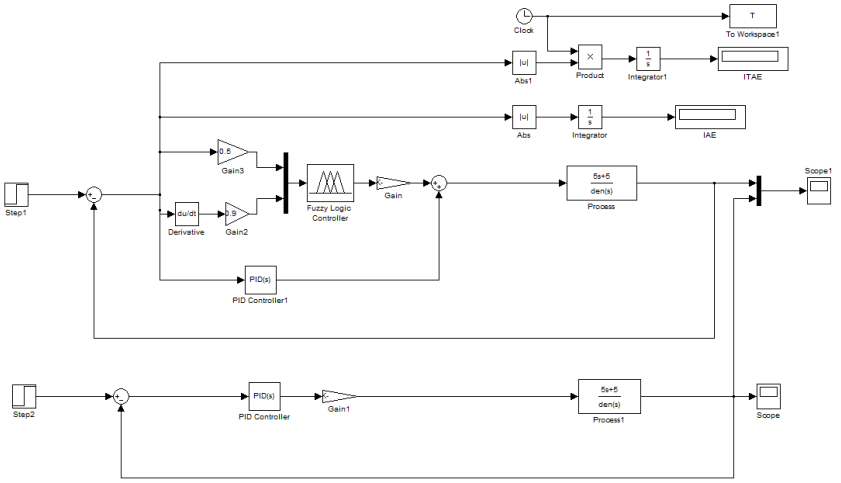

Fig. 13. Simulink representation of system with Fuzzy PD+PID controller

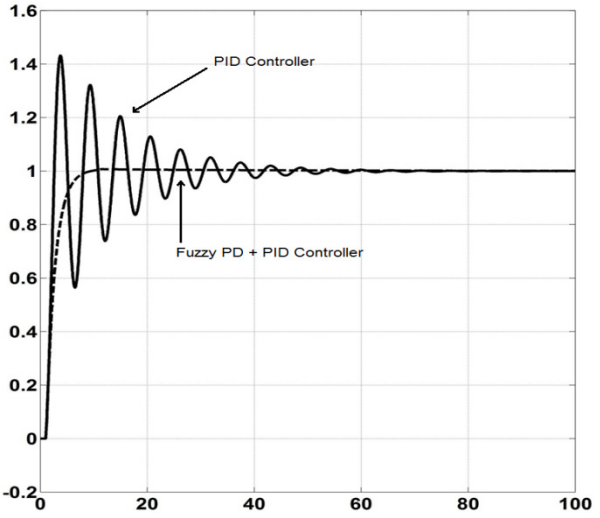

Fig. 14. Comparison between PID controller and Fuzzy PD+PID controller

This section shows a comparative study between different controllers. In this paper we have considered the steady state and transient state parameters. These parameters are maximum overshoot, settling time.All comparisons done between the PID controller and top fuzzy controller (fuzzy PD+PID controller).

Table 3. Comparison of Maximum overshoot and settling time for conventional PID controller and fuzzy PD+PID control

S. NO	Controller	Maximum Over-shot	Settling Time
1	PID Controller	43.40%	67 sec
2	Fuzzy PD+PID Controller	0.72%	23 sec

Table 4. Comparison of Integral Of Absolute Error (IAE) And Integral Of Time And Absolute Error (ITAE) For PID Controller And Fuzzy PD+PID Controller

S. NO	Controller	IAE	ITAE
1	PID Controller	4.746	58.52
2	Fuzzy PD+PID Controller	1.922	13.57

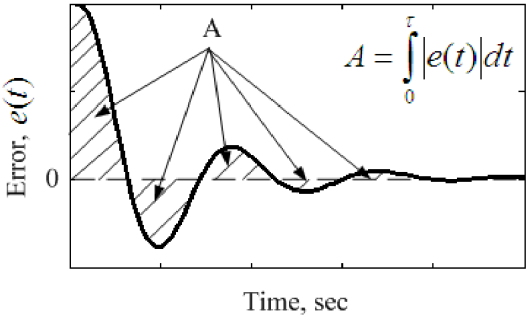

Fig. 15. A typical closed_loop error time history

9 Conclusion

In this paper a process control case study taking tank has been implemented. Tank water level is controlled by sensors monitor level. First of all a mathematical model of the system is developed and a conventional PID controller is implemented in it. The PID controller gives a very high overshoot and high settling time .So we proposed and implemented artificial intelligence principles in the controller architecture. Then we implemented some fuzzy logic control. The fuzzy logic control gives a much better response then the conventional PID controller. In future scope we can implement neural network based feedforward controller and genetic algorithm based online optimization techniques to improve the control performance.

References

[1] Mamdani, E.H.: Application of Fuzzy Algorithms for the Control of a Dynamic Plant. Proc. IEEE (December 1974)
[2] Zadeh, L.A.: Fuzzy logic = computing with words. IEEE Trans. Fuzzy Syst. 4, 103–111 (1996)
[3] Khallil, H.K.: Nonlinear Systems. Macmilan, New York (1992)
[4] Chen, G., Pham, T.: Introduction to fuzzy sets, fuzzy logic, and fuzzy control systems. CRC, New York (2001)
[5] Zhao, Z.Y., Tomizuka, M., Isaka, S.: Fuzzy gain scheduling of PID controllers. IEEE Trans. Syst. Man Cybern. 23, 1392–1398 (1993)
[6] Wang, L.X.: A course in Fuzzy systems and controls. Prentice-Hall, Upper Saddle River (1997)
[7] Wang, L.X.: Adaptive Fuzzy Systems and Control: Design and Stability Analysis. Prentice-Hall, Upper Saddle River (1994)
[8] Li, W.: Design of a hybrid fuzzy logic proportional plus conventional integral-derivative controller. IEEE Trans. Fuzzy Syst. 6, 449–463 (1998)
[9] Er, M.J., Sun, Y.L.: Hybrid fuzzy proportional-integral plus conventional derivative control of linear and nonlinear systems. IEEE Trans. Ind. Electron. 48, 1109–1117 (2001)

Design of MIMO Mamdani Fuzzy Logic Controllers for Wall Following Mobile Robot

Nasim Paykari, Seyed Hamidreza Abbasi, and Faridoon Shabaninia

School of Electrical and Computer Engineering
Shiraz University, Iran
Nasim.paykari@gmail.com, Hamid_abs62@yahoo.com
Shabani@shirazu.ac.ir

Abstract. This paper describes the design of wall tracking robot mobile based on intelligent controller, Fuzzy Logic controller, that it's equipped with three ultrasonic sensors. The distance of robot from the wall read by two ultrasonic sensors placed on left side and another in head of robot. The measured values of sensors are inputs for fuzzy logic controller that generates motor commands, directly for right motor and indirect for left motor. The range of fuzzy controller output set to be used in duty cycle of PWM signal. For design the rules, we have an algorithm to determine of best rule for each position. In addition it has been tried within increase accuracy also the speed factor improves. The controllers are design in MATLAB® Fuzzy Logic Toolbox.

Keywords: Wall following, Fuzzy logic controller, Fuzzy set, Ultrasonic sensor.

1 Introduction

Since Lotfi Zadeh development fuzzy logic in 1965, it has been applied in many number of real life applications. One of these applications is: control of mobile robots.

In order to design a map for indoor navigation, mobile robot must be endowed with wall tracking behavior. The controller for this aim can be designed either using intelligent algorithms, fuzzy logic. Fuzzy logic offers an uncertainty in solution to handle real world by using human experience in the base of design. Many papers and researches have utilized fuzzy logic in controllers of wall following mobile robot. In [1] a wall following controller is designed using fuzzy logic and is sets with the help of genetic algorithm to optimize the membership functions so that the robot moves fast and as smoothly as possible. The designed controller is tested on a mobile robot that is has 12 ultrasonic sensors and maximum speed of 0.25m/s. In [2], fuzzy logic controller is designed for wall tracking task and is implemented. The designed controller equipped with five infrared sensors. Experimental results describe the advantages of fuzzy logic to control wall tracking of car. In [3], a fuzzy logic controller design for an autonomous robot equipped with three ultrasonic sensors, designed to take part in an IEEE competition, held at Cleveland State University in 2004. The robot is modeled in MATLAB Simulink and fuzzy rules are design for best results. The controller is implemented also, using two microcontrollers. One of them for calculates the

V.E. Balas et al. (Eds.): Soft Computing Applications, AISC 195, pp. 155–164.
springerlink.com

present error in distance and angle and sends the best control signals to the next microcontroller which generates PWM signals that they are provide servo motors commend. In [4], a compare performed between fuzzy controller and neuro-fuzzy controller for wall tracking mobile robot is down. Both these controllers are implemented. The results have shown that neuro-fuzzy controller is better choice than fuzzy controller. In [5], a neural integrated fuzzy controller (NiF-T) is developed for nonlinear dynamic control problems and is applied to control three mobile robot including wall tracking, hall centering and convoying that its consist of three parts including membership function for fuzzy logic, a neural network rule and output refinement neural network. One of the controller properties is that it handles with a small number of rules. In [6], a reinforcement ant optimized fuzzy controller (RAOFC) is used. The antecedent in each fuzzy rule uses type-2 fuzzy set and its increase fuzzy controller robustness while consequent is drawing by Q-value aided ant colony optimization. By using online aligned interval type-2 fuzzy clustering method (AIT2FC) each rule is automatically generated. The designed controller is equipped with four range finding sonar sensors. These approaches to wall tracking mobile robot control have many good properties. In [7], used a controller based intelligent, fuzzy logic to follow the wall used three ultrasonic sensors in back, forward and head of robot, but one of them not used in fuzzy logic design. The result shows that robot can follow a rectangular wall. In [8], designer used error and error derivative in design of fuzzy controller. The gain scheduling controller will be used before the FLC to control the error. The error value determined the value gain. For optimize the method test three gain parameter, 1, 2 and 6. The robot took the regular KBFLC system more than 4 s to get the robot back from 10 cm error. It needed about 2.5 s for optimized KBFLC to retrieve the robot from the same amount of error.

In this paper, design of fuzzy logic controller for wall following behavior of mobile robot is presented. System has two fuzzy controllers that each of them has three inputs and one output. The range information from ultrasonic sensors forms input to the controller while outputs controlling the speed of motors. The fuzzy controller is designed using MATLAB® Simulink and Fuzzy Toolbox. More details could be found in following section. In the sections that follow, mobile robot architecture, fuzzy controller development and finally simulation results are presented.

2 Preliminaries of Robot

2.1 Mobile Robot Architecture

The simulation based on two motors works dependently to control two wheels. A third wheel (caster) is provided for support. Three ultrasonic sensors named as front sensor (Fs), back sensor (BS) and one sensor in head named heading sensor (HS) comprise the sensory system of the robot, ultrasonic sensors are mounted on the left side of the robot to track wall at the set point distance and head sensor mounted on head of robot to report rectangular and triangular walls in front of robot, to the controllers. The range information from three sensors is merged to generate three inputs for fuzzy logic controllers. The robot length is 20cm and the width is 10cm. Some of

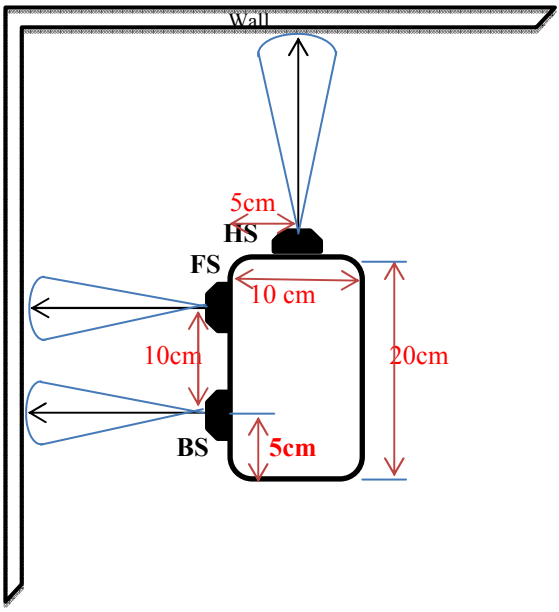

Fig. 1. Robot dimensions and placement of sensors

detail has been shown in Fig. 1. Assume the radius for wheels are 2.5cm and Maximum speed of motors is 1 m/s.

2.2 Robot Kinematics Analysis

As shown in Fig. 2(a), there are three situations while robot following the wall. Each of these situations should corrected by the controllers. This correction is done by reducing the speed of the wheels (one of them), change the angle of the robot axis relative to the wall.

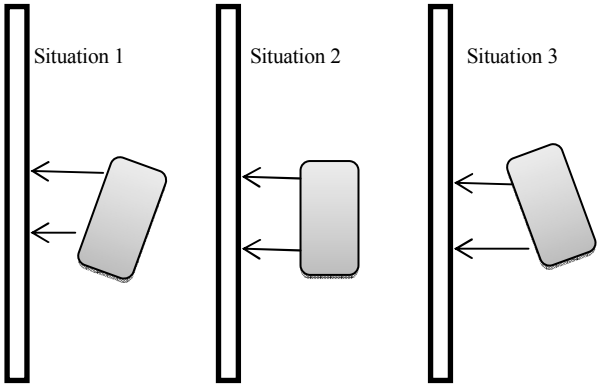

Fig. 2. (a): Modes of the robot position relative to the wall

Movement can be done on the ellipse environmental. If the sensor and control update time is short, we can consider this movement on a linear and vector of the ellipse sector and decompose into constituent components.

According to Fig. 2(b):

$$M=(x_2-x_1)\ X + (y_2-y_1)\ Y \tag{1}$$

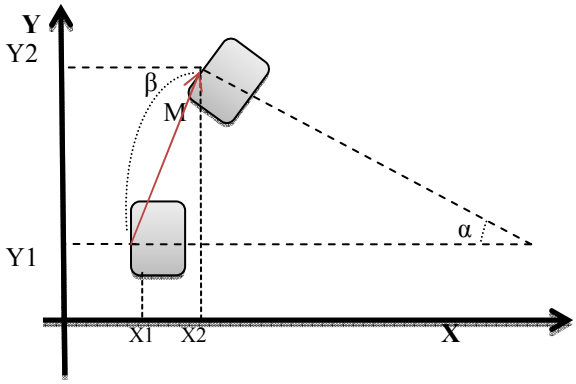

Fig. 2. (b): Analysis the robot motion

The wheel speed difference is motion along X axis, rotation factor, and equal part of speed two wheels operate as the forward driving factor. We take α small enough (with little time to update sensor and controller, this assumption is practical) so $\beta = \vec{M}$. Similar equations on the right wheel and the sensors are established.

3 Fuzzy Logic Development

MATLAB® Fuzzy Logic Toolbox is used to design of fuzzy logic controller (FLC). The toolbox contains functions, graphical user interfaces and data structures that allow the user to quickly design, test, simulate and modify a fuzzy inference system. The steps in FLC design are described in this section.

To follow the left wall at a set distance, two fuzzy controllers are designed. These controllers are same in the membership function input and different in rule base and output. This model design helps to understand the concept of design fuzzy logic and relationships between inputs and outputs (rule base).

In this paper there are two controller FLC 1 and FLC 2 with three outputs and one output.

3.1 Fuzzification

Two fuzzy controllers using three inputs For FLC1,same FLC2, one of inputs are 'BS', the distance between back of robot and left wall, next input is difference between 'FS' and 'BS', instead of using the sensor input 'FS', to detect one of three situations listed in section II.b, we named this input 'DS'. If the angle faced wall with left wall is less than 139.87 degree and greater than 90 degrees, 'FS' and 'BS' with an irreversible delay detect it and robot will crash. If the angle less than 90 degree two sensors will not able to detect the wall and crash would be inevitable. For these reasons and to compensate for this defect used 'HS' input as distance between robot head and faced wall.

The 'DS' input to FLC1 and FLC2 is described by 5 fuzzy sets: VN, N, Z, P, VP. The information from BS is described by 5 fuzzy set: Vclose, Close, Med, Far, VFar and The information from BS is described by 2 linguistic variables: Close and far that it acts as a limit on both sensor values.

The membership function for 'DS' as shown in Fig. 3(a), are described by the equations:

$$\mu_{DS,VN}=\begin{cases} -\frac{1}{22.5}(ds+7.5) & -30 \le ds \le -7.5 \\ 0 & ds \ge -7.5 \end{cases} \tag{2}$$

$$\mu_{DS,N}=\begin{cases} 0 & ds \le -20 \\ \frac{1}{9}(ds+20) & -20 \le ds \le -11 \\ -\frac{1}{9}(ds+2) & -11 \le ds \le -2 \\ 0 & ds \ge -2 \end{cases} \tag{3}$$

$$\mu_{DS,Z}=\begin{cases} 0 & ds \le -7.5 \\ \frac{2}{13}(ds+7.5) & -7.5 \le ds \le -1 \\ 1 & -1 \le ds \le 1 \\ -\frac{2}{13}(ds-7.5) & 1 \le ds \le 7.5 \\ 0 & ds \ge 7.5 \end{cases} \tag{4}$$

$$\mu_{DS,P}=\begin{cases} 0 & ds \le 2 \\ \frac{1}{9}(ds-2) & 2 \le ds \le 11 \\ -\frac{1}{9}(ds-20) & 11 \le ds \le 20 \\ 0 & ds \ge 20 \end{cases} \tag{5}$$

$$\mu_{DS,VP}=\begin{cases} 0 & ds \le 7.5 \\ \frac{1}{22.5}(ds-7.5) & 7.5 \le ds \le 30 \end{cases} \tag{6}$$

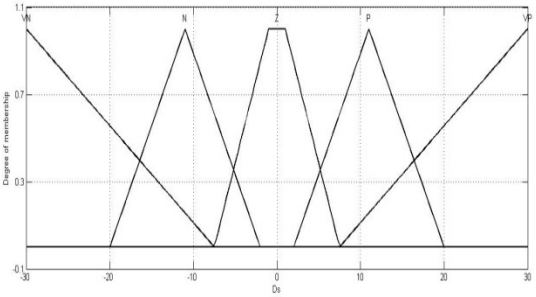

Fig. 3. (a): Fuzzy sets for DS

Using the DS, position of the robot towards the wall can be detected. In the next section, this detection algorithm will help to determine and refine the rules.

The next input is BS is measured distance from the back sensor robot, this input is represented by five fuzzy set: Vclose, Close, Med, Far, VFar. FS can also be used instead of BS, but, in set of rules there are certain states that are allowed to FS set out and continue the incorrect move to adjust the BS in first, then FS regulated by other rules. Last input, HS, can be used for rotation in the angles that can't be detected by other inputs, Fs and BS. This sensor can detect the rectangular angle or triangular corner and with measuring the distance between the head sensor and wall, act as limiting. HS is shown by two fuzzy set: Close and Far. As long as HS to less than 300 mm, 3 times as long as the length of robot, does not affect output. Until the robot reaches a distance equal to 1.5 times the reaction is very mild but when Hs is less than this value, 1.5 times, the reaction will be very sever, as shown in result Simulink.

In this design the outputs are DM and Rm. The right motor speed of robot, RM, used in order to wall tracking by decrease or increase the velocity relative. It is also possible to use the left motor adjust. Hereby the reaction rate increase and robot design with high-speed motor is also possible. In this paper, instead of using Lm, the difference between motors speed, Lm and RM, as the other output is used that, in addition to examining and understanding the rules are easy, helps to design a simple algorithm using triple mode. For DM, the fuzzy sets are: VN, N, Z, P, and VP. The discourse rang being from zero to hundred which describes the duty cycle of PWM signal. And for RM we have four fuzzy sets include: Stop, Slow, Med, and Fast. As shown in Fig. 3(b) for these fuzzy sets the equations are:

$$\mu_{\text{RM, Stop}}=\begin{cases} -\frac{1}{33}(dm+33) & 0 \le dm \le 33 \\ 0 & dm \ge 33 \end{cases} \tag{7}$$

$$\mu_{\text{RM, Slow}}=\begin{cases} 0 & dm \le 16 \\ \frac{1}{17}(dm-16) & 16 \le dm \le 33 \\ -\frac{1}{17}(dm-50) & 33 \le dm \le 50 \\ 0 & dm \ge 50 \end{cases} \tag{8}$$

$$\mu_{RM,\,Med}=\begin{cases}0 & dm \le 33\\ \frac{1}{17}(dm-33) & 33 \le dm \le 50\\ -\frac{1}{17}(dm-67) & 50 \le dm \le 67\\ 0 & dm \ge 67\end{cases} \quad (9)$$

$$\mu_{RM,\,Fast}=\begin{cases}0 & dm \le 50\\ \frac{1}{34}(dm-50) & 50 \le dm \le 84\\ 1 & 84 \le dm \le 100\end{cases} \quad (10)$$

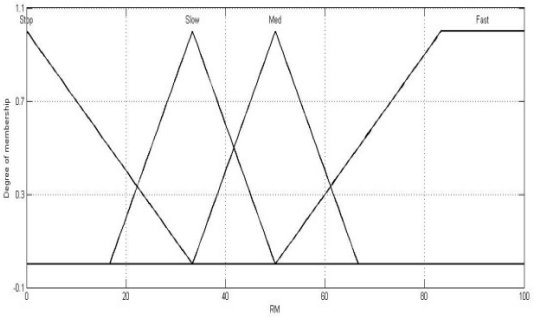

Fig. 3. (b): Fuzzy sets for RM

3.2 Fuzzy Rule Base

This section is a relation between inputs and outputs to have best response. To follow wall at set distance, each controllers have 30 rules that design by Mamdani method. When the wall is convex or slope toward the outside, speed of right motor should greater than speed of left motor. Now the situation and severity of the curvature and slope reaction of controller is deferent. These principles should respect for all rules. One part of the rules design algorithm is shows in fig. 3(c), when HS is far. Red arrows show that what situation comes up if wall direction continues without any change. HS is an important agent when the robot is near of forward wall and it can affect the performance of other input, DS and BS, in output.

For example one of Rules is shown:

Rule 1: If DS is VN and BS is Vclose and HS is Far then RM is Stop (FLC1) and DM is VP (FLC2).

When speed of left motor should greater than speed of right motor we have to start and continue the speed of right motor in Stop or Slow.

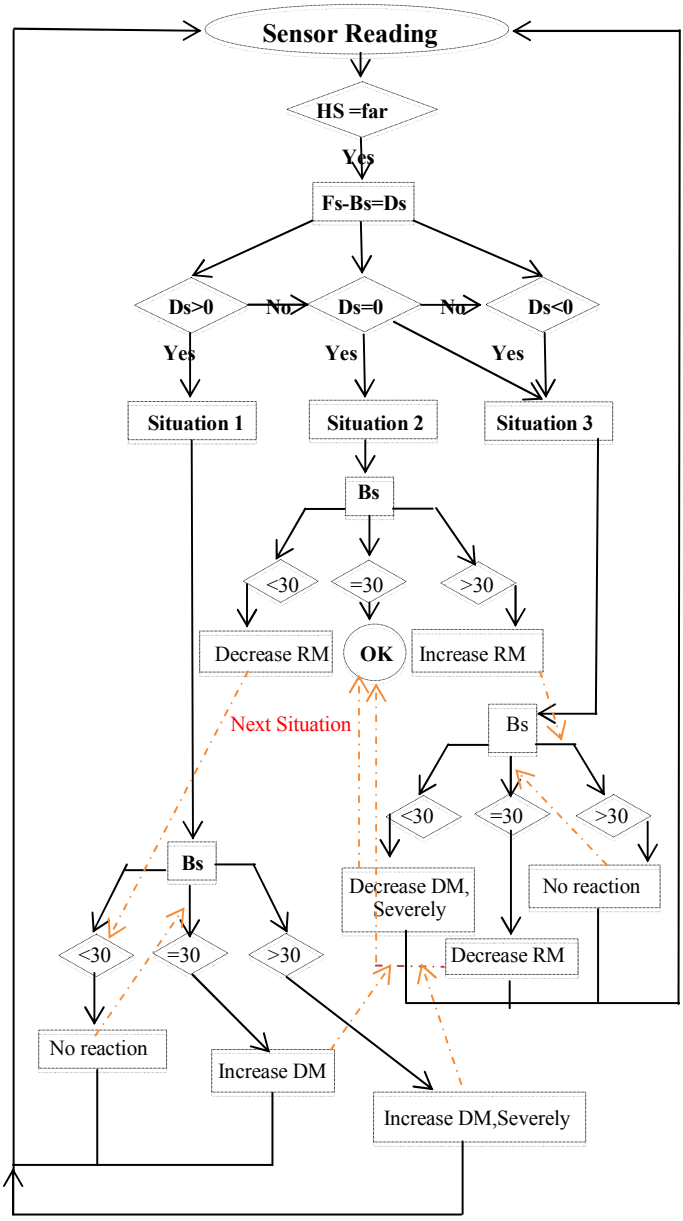

Fig. 3. (c): Algorithm of rules design

One of the worst obstacles occurs, when the robot to be trapped in a corner that next corner immediate appears. This condition occurs when there is a wall on the right side of the robot; the sensors are not able to detect it. In this case robot right wheel 50 in and DM is 49.8, means the LM is 0.2 and robot can 180 degree rotation in a space slightly larger than the robot, and be able to escape from this trap also.

3.3 Defuzzification

The result of fuzzy controller should convert to a crisp output to be understanding by other systems, defuzzification. This is done in many ways that common and useful method is Center of Area, COA, method. The COA described by:

$$COA = (\int_{x=min}^{max} F(x) * x * dx)/(\int_{x=min}^{max} F(x) * dx) \quad (11)$$

In this equation COA is crisp value, speed of right and left motor robot and F(x) are sampled value of total output membership function.

4 Results

To test the model and for comparison, Fig. 4 shows the change in one input whereas two other inputs are fixed:

As shown in Fig. 4 (a) & (b) & (c): if BS changed in 0 up to 60, RM beginning at its maximum value and then decreases, but when the BS reaches 30 and up to 40, RM increases, as in the previous section described, at first appears BS in desire range then FS is adjusted. For changed in DS first RM increase because LM should be less than RM and then RM reduced until LM can be greater than RM. This design will cause the robot to be at maximum possible speed designed. Change in HS does not affect at first but when it's close to the wall, filter the other parameter and change the situation.

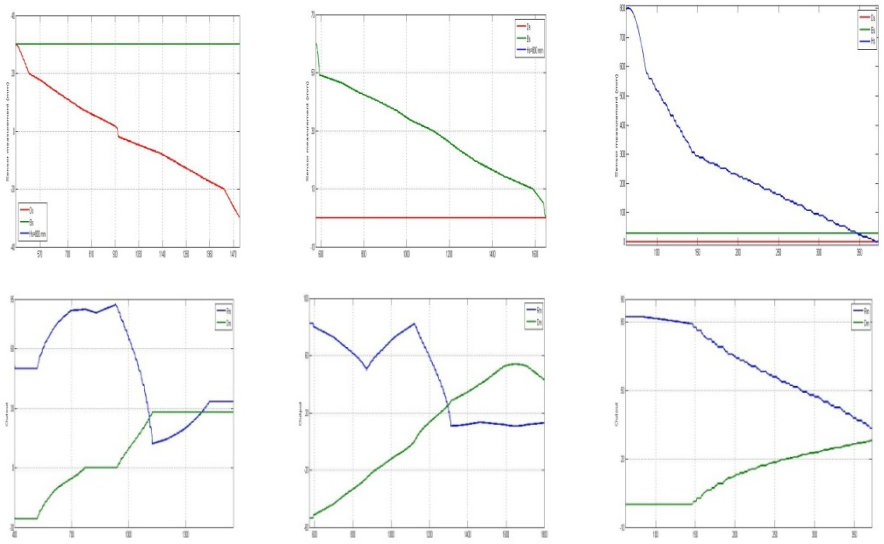

a) Response for chang in DS b) Response for chang in BS c) Response for chang in HS

Fig. 4. Range of change output (one of input changed and other two inputs fixed at the desire distance)

5 Conclusion

This paper developed the old technique of fuzzy controllers for a mobile robot. Three ultrasonic sensors are mounted on the left and head of robot. The controller accepts inputs from these sensors and generates motor commands to remain the robot in desired distance. The controllers tested in a Simulink and the results of simulation have shown the validity of controller to follow walls of various shapes including straight, curved, rectangular, triangular trajectories. The prominence of this design is that in a very steep slope have right reactions and can be used in the high-speed motor with change in range of output.

References

1. Holder, M.B., Trivedi, M.M., Marapane, S.B.: Mobile robot navigation by wall following using a rotating ultrasonic scanner. In: Proc. ICPR, vol. 3, pp. 298–302 (1996)
2. Masmoudi, M.S., Song, I., Karray, F., Masmoudi, M., Derbel, N.: FPGA implementation of fuzzy wall following control. In: Proc. 16th International Conference on Microelectronics, pp. 133–139 (2004)
3. Peri, V.M., Simon, D.: Fuzzy logic control for an autonomous robot. In: Proc. Annual Meeting of North American Fuzzy Information Society, pp. 337–342 (2005)
4. Saleh, J.A., Karray, F., Masmoudi, M.S., Masmoudi, M.: Soft computing techniques in intelligent wall following control for a car-like mobile robot. In: International Conference on Signals, Circuits and Systems, pp. 1–6 (2009)
5. Ng, K.C., Trivedi, M.M.: A neuro-fuzzy controller for mobile robot navigation and multirobot convoying. IEEE Transactions on Systems, Man and Cybernatics 28(6), 829–840 (1998)
6. Juang, C.-F., Hsu, C.-H.: Reinforcement ant optimized fuzzy controller for mobile robot wall following control. IEEE Transactions on Industrial Electronics 56(10), 3931–3940 (2009)
7. Farooq, U., Khalid, A., Amar, M., Habiba, A., Shafique, S., Noor, R.: Design and low cost Implementation of fuzzy logic controller for following behavior of a mobile robot. In: 2010 2nd International Conference on Signal Processing Systems (ICSPS), V2-740 – V2-746
8. Aljanaideh, K., Demirili, K.: Gain Scheduling Fuzzy Logic Controller For a Wall-Following Mobile Robot, pp. 1–6, 978-1-4244-758-3/10/$26.00©2010IEEE

The Single-Allocation Hierarchical Hub-Median Problem with Fuzzy Flows

Soheil Davari and Mohammad Hossein Fazel Zarandi

Department of Industrial Engineering,
Amirkabir University of Technology,
424 Hafez Avenue, Tehran, Iran
soheildavari@ieee.org, zarandi@aut.ac.ir

Abstract. This paper addresses the problem of designing a hierarchical single-allocation hub-median (SA-H-HM) network considering fuzzy flows between nodes. The problem is modeled as a fuzzy mathematical programming model and a hybrid algorithm of population-based iterated local search (PILS) and fuzzy simulation is employed. Results clearly show that PILS is efficient in reaching solutions with virtually all the errors less than one percent to the optimal solutions. Moreover, the proposed PILS is capable to escape local optima. Finally, the results of the hybrid algorithm give insights about the problem under uncertainty.

Keywords: Iterated local search, Facility location, Hub-and-spoke, Optimization, Simulation.

1 Introduction

Facility location (FL) has been a noteworthy problem in supply chain management around the world. Normally, FL is affected by numerous factors, such as environmental, political, financial, and even sociological issues. Hub location problem has been one of the main variants of FL which has attracted the attention of both academicians and practitioners around the world.

A hub-and-spoke network is designed in order to route the traffic in a network of nodes through hub nodes. The main feature of such a network is the restriction applied to direct flows between demand nodes. Each hub network is composed of two layers as hub-level network which connects the hubs, and the spoke level which is the network of demand allocation to hub nodes. HLP arises in many different contexts such as telecommunications, supply chain management, airline industry, computer networks, etc. Design of hierarchical hub networks is a variant of traditional HLP which is applicable in many kinds of networks (A sample hierarchical hub network is depicted in figure 1). In this hierarchical hub network, the first layer of hubs (nodes 12, 13, and 14) are connected and each node in the second layer of hubs is allocated to one of the hubs in the first layer. Prominent applications of the problem are in cross-docking and distribution network design.

V.E. Balas et al. (Eds.): Soft Computing Applications, AISC 195, pp. 165–181.
springerlink.com

One of the fundamental issues to deal with in most of the real-world applications is the imprecision in data and HLP is no exception. Based on the semantic of the problem, random variables or fuzzy variables are used in order to model the problem in an uncertain environment. However, in many contexts where there is not enough historical data, or when data are unreliable, using fuzzy variables is regarded as an alternative which can be used to define demands in a network, travel times, or any other unknown parameter in the problem.

In this paper, a hierarchical hub-and-spoke network is to be designed in which demands are not known precisely. These demands are estimated as fuzzy variables and a hybrid algorithm is proposed to solve it. This hybrid algorithm is comprised of an efficient population-based iterated local search and a fuzzy simulation.

The outline of this paper is as follows: The paper proceeds giving a concise review over the literature of hub location problem. Then, section 3 will be dedicated to problem definition. The proposed solution approach will be detailed in section 4. Section 5 deals with numerical experiments and some analysis on results. Finally, the paper will be summarized in section 6 and some future research areas will be proposed.

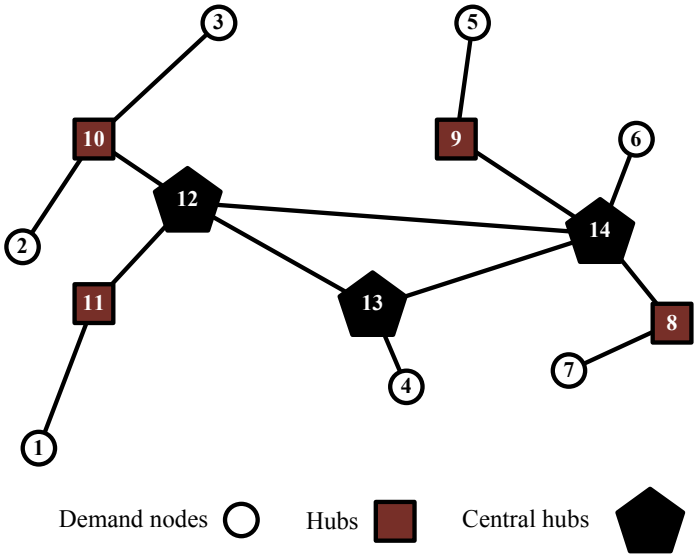

Fig. 1. A sample hierarchical hub network

2 Literature Review

From the beginning of the 21st century, an increase in the number of publications regarding hub location problem has been witnessed. The concept of HLP dates back to 1960s when Goldman [1] defined the network hub location problem for the first time. Later, the study of HLP received much attention from scientists after the influential paper of O'Kelly [2] presenting the first mathematical formulation for a hub location problem. Since the introduction of HLP, an extensive body of literature has been dedicated to the median problems. Campbell [3] is considered as the first to

propose a mathematical formulation for the single-allocation hub median problem. In this paper, we do not aim to review all the pertinent work to hub-median location problems (interested readers are referred to valuable reviews such as Alumur and Kara [4]). However, table 1 highlights the most notable publications in the hub location literature in the recent decade.

Using non-exact methods to solve HLP has not still gained much attention among researchers. As an example of using non-exact solution methods, Calik et al. [5] proposed a tabu-search based heuristic to solve the incomplete hub-covering location problem. Some other attempts of using heuristics and metaheuristics for HLP are as follows: genetic algorithm by Cunha and Silva [6], ant colony by Meyer et al. [7], and variable neighborhood search by Ilic et al. [8].

Table 1. Some recent contributions to hub location problem

Subject	Author(s)
Hub arc location problem	Campbell et al. ([9], [10])
HLP considering congestion at hubs	Elhedhli and Hu [11]
Latest arrival HLP with stopovers	Yaman et al. [12]
HLP as a set of *M*/*M*/1 queuing hubs nodes	Rodriguez et al. [13]
Conditional *p*-hub median location problem	Eiselt and Marianov [14]
Stochastic *p*-hub center with service level constraints	Sim et al. [15]
Reliable hub location problem	Kim and O'Kelly [16]
HLP for time definite transportation	Campbell [17]
Efficient formulations of incomplete HLP	Alumur and Kara [18]
HLP with multiple capacity levels	Correia et al. [19]
Competitive HLP in liner service providers	Gelareh et al. [20]
Game theoretical model in HLP	Lin and Lee [21]
Design of an intermodal hub-and-spoke network	Ishfaq and Sox [22]
A real-world case study of HLP in Morocco	Menou et al. [23]
Stochastic uncapacitated HLP	Contreras et al. [24]
HLP with capacity decision and balancing requirements	Correia et al. [25]
Partitioning-hub-location-routing problem	Catanzaro et al. [26]
Allocation strategies in HLP	Yaman [27]
Ordered median hub location problem	Puerto et al. [28]
HLP with decentralized management	Vasconcelos et al. [29]
Evolutionary algorithm for capacitated HLP	Kratica et al. [30]

Table 1. (*continued*)

M/M/c queuing model for hub covering problem	Mohammadi et al. [31]
Hub network design of wagonload traffic	Sender and Clausen [32]
Using fuzzy goal programming in reliable HLP	Hansen and Mladenovic [33]
HLP in transportation networks	Gelareh and Nickel [34]
Fuzzy dynamic virtual HLP	Taghipourian et al. [35]
Hub covering location with different coverage types	Karimi and Bashiri [36]
Single allocation hub location problem under congestion	De Camargo and Miranda [37]
The *Q*-coverage hub covering problem with dispersion	Fazel Zarandi et al. [38]
Multimodal hub location and hub network design	Alumur et al. [39]
HLP with uncertainty	Alumur et al. [40]
Uncapacitated single allocation *p*-hub maximal covering problem.	Hwang and Lee [41]
Applying minimum-risk criterion to stochastic hub location problems	Zhai et al. [42]

Table 2. Some problems solved in fuzzy environment using credibility theory

Author	**Problem**
Peng and Liu [43]	Parallel machine scheduling
Zhao and Liu [44]	Standby redundancy optimization
Zheng and Liu [45]	Vehicle routing problem
Liu and Li [46]	Quadratic assignment problem
Huang [47]	Portfolio selection
Yang and Liu [48]	Fixed charge solid transportation
Zhou and Liu [49]	Location-allocation problem
Erbao and Mingyong [50]	Vehicle routing problem
Lan et al. [51]	Multi-period production planning
Liu and Gao [52]	Multi-job assignment problem
Davari et al. [53]	Maximal covering location problem
Li et al. [54]	Portfolio selection
Ke and Liu [55]	Project scheduling
Wen and Kang [56]	Location-allocation problem
Fazel Zarandi et al. [57]	Location-routing problem
Davari and Fazel Zarandi [58]	Hub location problem
Lau et al. [59]	Design of distribution system

Fuzzy logic has been a popular tool to deal with problems under uncertainty. The need to use fuzzy logic in problems arises whenever there are some vague or uncertain parameters. Wherever there is an uncertainty of the fuzzy type, credibility theory has been a popular approach. Some instances of using credibility theory in various problems are presented in table 2.

Considering the review paper by Alumur and Kara [4] and our extensive review of the publications from 2008 to date, it becomes clear that non-exact methods has not attracted the attention of scientists much to date. Moreover, using fuzzy variables in HLP is still a relatively untouched research area. Hence, this paper contributes to the literature addressing SA-H-MP with fuzzy flows between nodes.

3 Problem Definition

The hierarchical hub median problem is addressed in Yaman et al. [60] presenting a mixed integer mathematical model. The assumptions in their paper are as follows:

- The triangle inequality holds for the distances (costs) in the network.
- Each demand node can be assigned to a non-central hub or a central hub.
- The network between central hubs is complete.
- The economies of scale for the flow between central hubs are not higher than the economies of scale for flows between non-central hubs and central hubs.
- The matrix of costs to travel in the network is symmetric.

They represented the set of nodes, possible nodes for non-central hubs, and candidate nodes for central hubs as I, H, and C respectively. It should be noted that $H \subseteq I$ and $C \subseteq H$. In their formulation, Z_{ijl} is a binary variable taking a one value if node $i \in I$ is assigned to hub $j \in H$ and hub j is allocated to central hub $l \in C$. Like that, if $j \in H$ becomes a hub node and allocated to the central hub $l \in C$, then the value of Z_{jjl} equals 1. Moreover, if node $l \in C$ is a hub, then Z_{lll} takes a value of 1. g^i_{jl} is the amount of flow for $i \in I$ as origin or destination between hub $j \in H$ and central hub $l \in C$. f^i_{kl} denotes the amount of traffic of node $i \in I$ as origin travelling from central hub $k \in C$ to central hub $l \in C \backslash \{k\}$. Moreover, p and p_0 are the number of non-central hubs and central hubs to be located. The amount of flow to be routed from node $i \in I$ to node $m \in I$ is shown as t_{im}. The cost of routing a unit of flow from node $i \in I$ to node $j \in I$ is shown as d_{ij}. The discount factor of routing between hubs and central hubs is shown as α_H and the discount factor of routing between central hubs as α_C. Now, the mathematical formulation of Yaman et al. [60] is as below:

$$\min \sum_{i \in I} \sum_{m \in I} (t_{im} + t_{mi}) \sum_{j \in H} d_{ij} \sum_{l \in C} z_{ijl} + \sum_{i \in I} \sum_{j \in H} \sum_{l \in C \backslash \{j\}} \alpha_H d_{jl} g^i_{jl} + \sum_{i \in I} \sum_{j \in H} \sum_{l \in C \backslash \{j\}} \alpha_C d_{jl} f^i_{jl} \tag{1}$$

$$\sum_{j\in H}\sum_{l\in C} z_{ijl} = 1 \quad \forall i \in I \tag{2}$$

$$z_{ijl} \le z_{jjl} \quad \forall i \in I, j \in H \setminus \{i\}, l \in C \tag{3}$$

$$\sum_{m\in H} z_{jml} \le z_{lll} \quad \forall j \in H, l \in C \setminus \{j\} \tag{4}$$

$$\sum_{j\in H}\sum_{l\in C} z_{jjl} = p \tag{5}$$

$$\sum_{l\in C} z_{lll} = p_0 \tag{6}$$

$$\sum_{k\in C\setminus\{l\}} f_{lk}^{i} - \sum_{k\in C\setminus\{l\}} f_{kl}^{i} = \sum_{m\in I} t_{im} \sum_{j\in H} (z_{ijl} - z_{mjl}) \quad \forall i \in I, l \in C \tag{7}$$

$$g_{jl}^{i} \ge \sum_{m\in I\setminus\{j\}} (t_{im} + t_{mi})(z_{ijl} - z_{mjl}) \quad \forall i \in I, j \in H, l \in C \setminus \{j\} \tag{8}$$

$$z_{ljl} = 0 \quad \forall j \in H, l \in C \setminus \{j\} \tag{9}$$

$$g_{jl}^{i} \ge 0 \quad \forall i \in I, j \in H, l \in C \tag{10}$$

$$f_{kl}^{i} \ge 0 \quad \forall i \in I, k \in C, l \in C \setminus \{k\} \tag{11}$$

$$z_{ijl} \in \{0,1\} \quad \forall i \in I, j \in H, l \in C \tag{12}$$

Equation (1) is the objective function which is found adding the cost of routing between demand nodes and allocated hubs/central hubs, between the hub nodes and central hubs, and also among the central hubs. Constraint (2) states that each demand node must be assigned to one and only one hub and a central hub. This constraint governs that the problem is a single-allocation hub location problem. Constraint (3) is used to guarantee that if node *i* is assigned to hub *j* and central hub *l*, the j^{th} node will be a hub and is allocated to a central hub at node *l*. Constraint (4) governs that if node *j* is assigned to the central hub *l*, then, node *l* must be a central hub. Constraints (5) and (6) determine the number of hubs and central hubs to be established. Constraint (7) is the traditional flow balance constraints which are customized to be used in SA-H-MP. Constraints (8) and (10) are used in order to compute the values of g_{jl}^{i} using assignment variables. Equation (9) strengthens the LP relaxation of the problem. Constraints (11) and (12) are ordinary constraints to limit *z* values to take binary values and *f* values to be positive.

Knowing that considering $p=p_0$, relaxes the problem into the traditional *p*-hub median problem, Yaman et al. [60] proved that the SA-H-MP is NP-hard (the classical *p*-hub median problem is NP-hard (as shown in [61]). This means that for comparatively larger datasets, exact solution approaches are handicapped to reach optimal solutions in a reasonable amount of time. This paper puts forward an efficient PILS algorithm to solve SA-H-MP. The proposed PILS will be detailed in the next section.

4 Solution Procedure

Research in metaheuristics for combinatorial optimization problems has lately experienced a noteworthy shift towards the hybridization of metaheuristics with other techniques for optimization [62]. This paper contributes to the literature by proposal of an efficient PILS to solve SA-H-MP which is presented and its components are elaborated.

4.1 Population-Based Iterated Local Search

ILS has been applied to a wide range of applications, including quadratic assignment problem [63], vehicle routing problem ([64], [65]), and flowshop scheduling problem [66], and location-routing problem [67]..

An efficient hybrid metaheuristic to be employed in combinatorial optimization problems is combination of population-based algorithms and local search. Population-based methods are good in identifying promising areas of the search space in which local search methods can then quickly determine the best solutions [62]. Therefore, high-quality results can be obtained by integration of population-based procedures and local search methods. Population-based ILS is an extension to ILS which holds a population of solutions instead of a single solution. The pseudo-code of PILS is given in figure 2. In this paper, PILS is employed to solve SA-H-HM and then it will be integrated with a fuzzy simulation to solve SA-H-HM with uncertain flows in the network.

PILS procedure
P←Generate initial population of size n
Apply a local search procedure for all solutions in the population
While (termination criteria are not met)
  P'←P
For all $s \in P$
  s'←Perturb(s)
  s''←Localsearch(s')
  P'←P'$\cup\{s''\}$
End for
Update P as the best n solution of P'
End while

Fig. 2. The pseudo-code of PILS

Encoding Scheme

It is well-known that an efficient representation scheme plays a pivotal role in the performance of any metaheuristic. The approach which is used in this paper comprises two segments in which the first segment represents the allocation of nodes and the

second segment includes the indices for non-central hubs. In the first segment, the element in i^{th} position shows the index of the hub to which node i is allocated. Needless to say, the values of the elements in the first segment can be selected among the values in H. Besides, the second segment includes the indices of hub nodes $i \in H \backslash C$. Using this procedure, the set of central hubs can be easily determined. Assuming the cardinality of nodes, hub nodes, and central hubs to be n, h, and c respectively, while the length of the first segment equals n, the second segment contains h bits. Therefore, the length of the solution string is always fixed and equals $n+h$. Figure 3 shows a sample for the proposed representation scheme.

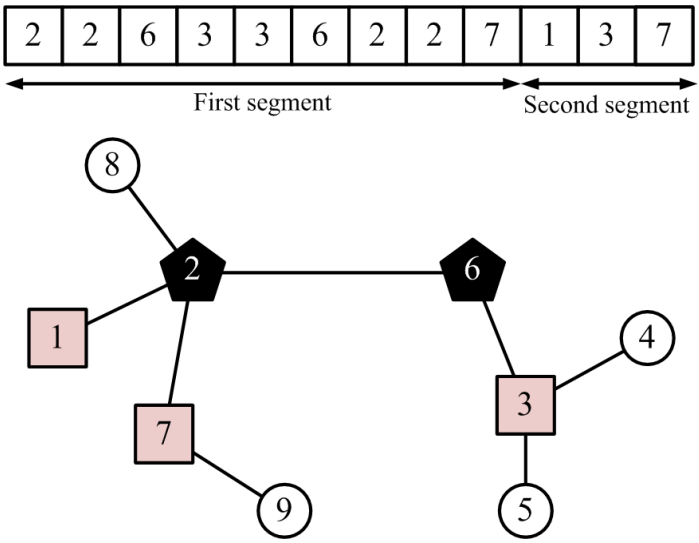

Fig. 3. Solution representation in the proposed PILS

Perturbation

Selection of a proper set of perturbation moves is of utmost importance in ILS. An improper selection of perturbation moves may lead to incapability of the algorithm to escape local optima or may make the procedure similar to a random restart search procedure. In the proposed PILS procedure, two neighborhood search procedures were employed as perturbation moves which are called $N_1(x)$ and $N_2(x)$ in which x represents the current solution. While $N_1(x)$ swaps the role of a central hub and a non-central hub, $N_2(x)$ swaps the role of a spoke and a non-central hub node. A sample of these structures is shown in figure 4. It is worth to note that throughout the proposed algorithm, if no improvement is attained using $N_1(x)$ and its subsequent local search procedure, $N_2(x)$ is applied.

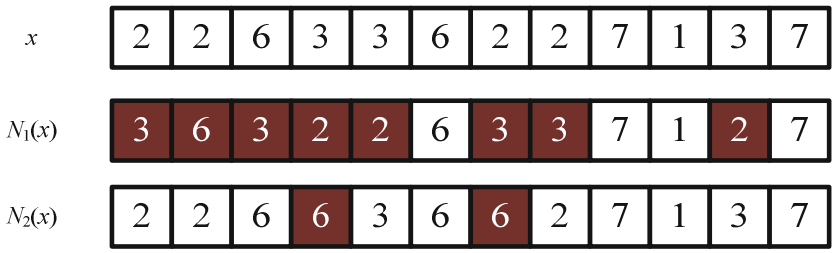

Fig. 4. Samples of perturbation in the proposed PILS

Local Search

A local search procedure is applied in order to find a local optimum within a neighborhood of the current solution. There are two distinct policies to employ a local search procedure. While it is possible to terminate the local search procedure whenever a better solution is found, another procedure is to select the best solution found using the local search procedure in a number of runs. Our preliminary experiments showed that using a combination of these two procedures increases the chance to reach a better solution. Hence, using a roulette-wheel procedure, one of these two procedures was employed whenever the local search procedure is called. Figure 5 shows a sample of employing the local search procedure on a solution.

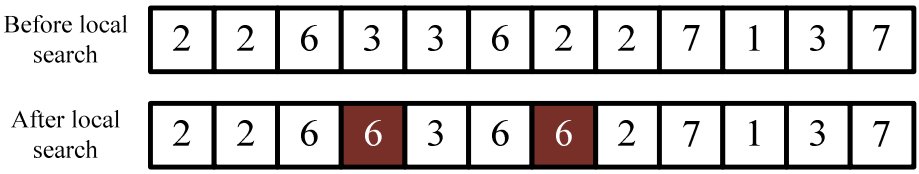

Fig. 5. Sample of the local search procedure in the proposed PILS

4.2 Fuzzy Simulation

Assuming the flows in the network to be fuzzy variables, the problem becomes to optimize the following mathematical problem:

$$\min E[\sum_{i\in I}\sum_{m\in I}(t_{im}+t_{mi})\sum_{j\in H}d_{ij}\sum_{l\in C}z_{ijl}+\sum_{i\in I}\sum_{j\in H}\sum_{l\in C\setminus\{j\}}\alpha_H d_{jl}g^{i}_{jl}+$$
$$\sum_{i\in I}\sum_{j\in H}\sum_{l\in C\setminus\{j\}}\alpha_C d_{jl}f^{i}_{jl}] \qquad (13)$$
$$\text{constraints } 2\text{-}12$$

Since values of t_{ij} are not deterministic, in order to solve (13), there is a need to use a fuzzy simulation. Liu [68] presented a simulation algorithm for problems of type $x\rightarrow E[f(x,\xi)]$ which is shown in figure 6.

Step 1. Set e=0.
Step 2. Randomly generate θ_k from the credibility space (Θ, P, Cr), write $\upsilon_k=(2Cr\{\theta_k\})\wedge 1$ and produce $\xi_k=\xi(\theta_k)$,k=1,2,…,N respectively. Equivalently, randomly generate ξ_k and write $\upsilon_k=\mu(\xi_k)$ for k = 1, 2, …, N, where μ is the membership function of ξ.
Step 3. Set two numbers $a=f(x,\xi_1)\wedge f(x,\xi_2)\wedge\ldots\wedge f(x,\xi_N)$ and $b=f(x,\xi_1)\vee f(x,\xi_2)\vee\ldots\vee f(x,\xi_N)$.
Step 4. Randomly generate r from $[a,b]$.
Step 5. If $r\geq 0$, then $e\leftarrow e+Cr\{f(x,\xi)\geq r\}$
Step 6. If $r<0$, then $e\leftarrow e-Cr\{f(x,\xi)\leq r\}$
Step 7. Repeat the fourth to sixth steps for N times.
Step 8. $U(x)=a\vee 0+b\wedge 0+e*(b-a)/N$.

Fig. 6. The simulation algorithm for $E[f(x,\xi)]$ proposed by Liu [68]

For the sake of brevity, we have not included basics of credibility theory in this paper. For a thorough introduction to credibility theory and measures, interested readers may consult Liu [68] and references therein.

5 Numerical Examples

In this section, the procedure to generate test problems is elaborated. In addition, the performance of the proposed algorithms on these test problems is examined.

5.1 Test Problems

In order to validate the proposed algorithm, the CAB dataset was used, as is customarily done in the literature. It has been assumed that all the nodes in the CAB can host a facility. Moreover, test problems were generated changing the values of α_C, α_H, p, and p_0.

5.2 Computer Specifications

All the test problems were run on a 2.53 GHz CPU equipped with 4 Gigabytes of RAM, using the CPLEX 12.2 solver. Moreover, the proposed PILS and fuzzy simulation were coded using C++.

5.3 Results, Validation, and Discussions

In order to examine the performance of the proposed solution procedure, a set of experiments were carried out on the aforementioned test problems. First, in order to analyze how optimal are the results of the proposed PILS, its results were compared with optimal solutions of CPLEX. A possible performance measure for the proposed PILS is its relative percentage deviation (RPD) which is defined as:

$$\text{RPD} = \frac{Z_{\text{PILS}} - Z^*}{Z^*} * 100 \tag{14}$$

where Z_{PILS} and Z^* are the best result of the proposed PILS and the optimal results of CPLEX, respectively. Each test problem was solved ten times and worst, median, and best results are reported in tables 3 and 4. For the sake of brevity, only cases with (α_C, α_H)=(0.8,0.8) and (α_C, α_H)=(0.6,0.9) are reported using various numbers for (p,p_0). In these tables, for the instances for which PILS was able to reach optimal solutions in all the ten runs, the corresponding row is highlighted as grey. Results bear out that while the proposed PILS leads to solutions no worse than one percent upper than the optimal results, its runtimes are considerably lower. It is worth to note that CPLEX was unable to reach optimal solutions in more than two hours. Since a fuzzy simulation is to be embedded within the proposed solution algorithm, it is clear that using CPLEX to solve the uncertain version of the problem is virtually impossible. Moreover, the proposed solution algorithm is able to reach optimal solutions in many cases. Figure 7 depicts a histogram for the gaps of the solutions found using PILS. It is clear that in more than seventy percent of experiments, PILS was able to reach optimal solutions. Besides, in only 4.7% of instances, the error is more than 0.5%. Considering the findings of the experiments, it is clear that the proposed PILS performs well on test problems. Hence, a fuzzy simulation can be embedded in the proposed PILS to solve the problem with fuzzy flows.

Table 3. Results of running the proposed PILS for (α_C,α_H)=(0.6,0.9)

p	p_0	CPLEX		PILS						
		Time	**Fitness**	**Time**	**Best**	**Gap%**	**Median**	**Gap%**	**Worst**	**Gap%**
3	1	136	9923897797	300	9923897797	0.00%	9923897797	0.00%	9923897797	0.00%
3	2	2133	9923897797	300	9923897797	0.00%	9923897797	0.00%	9923897797	0.00%
3	3	25	9896424156	300	9896424156	0.00%	9896424156	0.00%	9896424156	0.00%
4	2	3115	9528786908	300	9528786908	0.00%	9528786908	0.00%	9568457101	0.42%
4	3	9416	9406173571	300	9406173571	0.00%	9406173571	0.00%	9474656081	0.73%
4	4	44	9288636845	300	9288636845	0.00%	9288636845	0.00%	9288636845	0.00%
5	3	7571	9098003487	300	9098003487	0.00%	9098003487	0.00%	9146852572	0.54%
5	4	10431	8962997030	300	8962997030	0.00%	8962997030	0.00%	8993398947	0.34%
5	5	122	8831244506	300	8831244506	0.00%	8831244506	0.00%	8831244506	0.00%
6	4	7865	8689594212	300	8689594212	0.00%	8780392471	1.04%	8780392471	1.04%
6	5	9567	8562974155	300	8562974155	0.00%	8584361231	0.25%	8584361231	0.25%
6	6	130	8463112374	300	8463112374	0.00%	8463112374	0.00%	8463112374	0.00%

Table 4. Results of running the proposed PILS for (α_C,α_H)=(0.8,0.8)

p	p_0	CPLEX		PILS						
		Time	Fitness	Time	Best	Gap%	Median	Gap%	Worst	Gap%
3	1	300	10426074560	300	10426074560	0.00%	10426074560	0.00%	10426074560	0.00%
3	2	664	9464597766	300	9464597766	0.00%	9464597766	0.00%	9464597766	0.00%
3	3	10	8826647392	300	8826647392	0.00%	8826647392	0.00%	8826647392	0.00%
4	2	1470	9311789331	300	9311789331	0.00%	9333360883	0.23%	9333360883	0.23%
4	3	2379	8606860144	300	8606860144	0.00%	8606860144	0.00%	8606860144	0.00%
4	4	13	8020821500	300	8020821500	0.00%	8020821500	0.00%	8020821500	0.00%
5	3	3447	8454051709	300	8454051709	0.00%	8477251006	0.27%	8477251006	0.27%
5	4	2184	7931288504	300	7931288504	0.00%	7931288504	0.00%	7951632063	0.26%
5	5	19	7486046509	300	7486046509	0.00%	7486046509	0.00%	7486046509	0.00%
6	4	3870	7862099067	300	7872289169	0.13%	7872289169	0.13%	7907205858	0.57%
6	5	2060	7399297863	300	7399297863	0.00%	7399297863	0.00%	7399297863	0.00%
6	6	23	7071536179	300	7071536179	0.00%	7071536179	0.00%	7071536179	0.00%

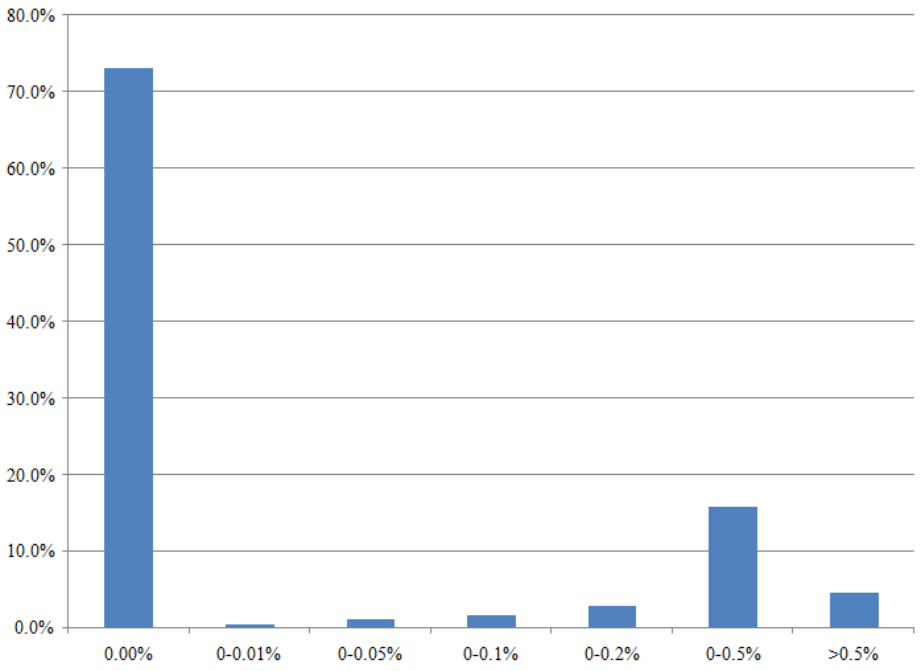

Fig. 7. The overall performance of the proposed PILS as a histogram

In order to assess the performance of the simulation-embedded PILS, test problems with flows as triangular fuzzy variables were generated. The triangular fuzzy variables were generated randomly as (r_1, r_2, r_3) in which r_2 is identical to the flows in the standard CAB dataset. Besides, values of r_1 and r_3 were generated to be within 10 percent lower and upper than the value of r_2 for each flow. Each problem was solved using 1000 iterations in the fuzzy simulation step. Figure 8 depicts one sample output of the problem for the case with (α_C, α_H, p, p_0)=(0.6, 0.9, 5, 3). Clearly, the outputs of the crisp and fuzzy versions differ to some extent. For instance, while in the crisp version, Los Angeles and Washington DC are selected to host central hubs, these two are substituted by Philadelphia and Phoenix in the fuzzy version. Needless to say, the uncertainty in the flows is the reason for such a discrepancy between the solutions. It is easy to deduce that solutions are directly related to the amount of uncertainty in the flows.

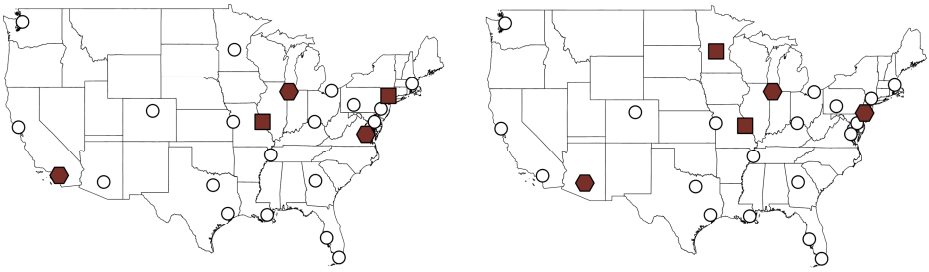

Fig. 8. Comparing the outputs for the problem with (α_C,α_H,p,p_0)=(0.6,0.9,5,3)

6 Conclusion and Future Research Areas

To sum up, the current paper addresses the problem of designing a hierarchical hub-and-spoke network where flows between nodes are uncertain. It was assumed that owing to unavailability of data, these flows were estimated as fuzzy variables. In order to solve the problem, an efficient population-based iterated local search was designed which is capable of reaching solutions with errors less than one percent. Afterwards, a fuzzy simulation was embedded in the proposed solution approach to find solutions of the fuzzy version. Our results showed that the proposed simulation-embedded PILS is quite efficient in finding solutions. This paper can be extended in various directions, such as proposal of some other algorithms, using fuzzy goal programming to solve the problem, considering a case where stochastic variables are present in the problem, and addressing other variants of designing a hierarchical hub-and-spoke network such as inclusion of capacities in the network.

References

1. Goldman, A.J.: Optimal location for centers in a network. Transportation Science 3, 352–360 (1969)
2. O'Kelly, M.E.: A quadratic integer program for the location of interacting hub facilities. European Journal of Operational Research 32(3), 393–404 (1987)
3. Campbell, J.F.: Integer programming formulations of discrete hub location problems. European Journal of Operational Research 72(2), 387–405 (1994)
4. Alumur, S., Kara, B.Y.: Network hub location problems: The state of the art. European Journal of Operational Research 190(1), 1–21 (2008)
5. CalIk, H., et al.: A tabu-search based heuristic for the hub covering problem over incomplete hub networks. Computers & Operations Research 36(12), 3088–3096 (2009)
6. Cunha, C.B., Silva, M.R.: A genetic algorithm for the problem of configuring a hub-and-spoke network for a LTL trucking company in Brazil. European Journal of Operational Research 179(3), 747–758 (2007)
7. Meyer, T., Ernst, A.T., Krishnamoorthy, M.: A 2-phase algorithm for solving the single allocation p-hub center problem. Computers & Operations Research 36(12), 3143–3151 (2009)
8. Ilic, A., et al.: A general variable neighborhood search for solving the uncapacitated single allocation p-hub median problem. European Journal of Operational Research 206(2), 289–300 (2010)
9. Campbell, J.F., Ernst, A.T., Krishnamoorthy, M.: Hub arc location problems: Part I – Introduction and results. Management Science 51(10), 1540–1555 (2005)
10. Campbell, J.F., Ernst, A.T., Krishnamoorthy, M.: Hub arc location problems: Part II – Formulations and optimal algorithms. Management Science 51(10), 1556–1571 (2005)
11. Elhedhli, S., Hu, F.X.: Hub-and-spoke network design with congestion. Computers & Operations Research 32(6), 1615–1632 (2005)
12. Yaman, H., Kara, B.Y., Tansel, B.Ç.: The latest arrival hub location problem for cargo delivery systems with stopovers. Transportation Research Part B: Methodological 41(8), 906–919 (2007)
13. Rodríguez, V., Alvarez, M.J., Barcos, L.: Hub location under capacity constraints. Transportation Research Part E: Logistics and Transportation Review 43(5), 495–505 (2007)
14. Eiselt, H.A., Marianov, V.: A conditional p-hub location problem with attraction functions. Computers & Operations Research 36(12), 3128–3135 (2009)
15. Sim, T., Lowe, T.J., Thomas, B.W.: The stochastic p-hub center problem with service-level constraints. Computers & Operations Research 36(12), 3166–3177 (2009)
16. Kim, H., O'Kelly, M.E.: Reliable p-Hub Location Problems in Telecommunication Networks. Geographical Analysis 41, 283–306 (2009)
17. Campbell, J.F.: Hub location for time definite transportation. Computers & Operations Research 36(12), 3107–3116 (2009)
18. Alumur, S.A., Kara, B.Y., Karasan, O.E.: The design of single allocation incomplete hub networks. Transportation Research Part B: Methodological 43(10), 936–951 (2009)
19. Correia, I., Nickel, S., Saldanha-da-Gama, F.: Single-assignment hub location problems with multiple capacity levels. Transportation Research Part B: Methodological 44(8-9), 1047–1066
20. Gelareh, S., Nickel, S., Pisinger, D.: Liner shipping hub network design in a competitive environment. Transportation Research Part E: Logistics and Transportation Review 46(6), 991–1004 (2010)

21. Lin, C.-C., Lee, S.-C.: The competition game on hub network design. Transportation Research Part B: Methodological 44(4), 618–629 (2010)
22. Ishfaq, R., Sox, C.R.: Hub location-allocation in intermodal logistic networks. European Journal of Operational Research 210(2), 213–230 (2011)
23. Menou, A., et al.: Decision support for centralizing cargo at a Moroccan airport hub using stochastic multicriteria acceptability analysis. European Journal of Operational Research 204(3), 621–629 (2010)
24. Contreras, I., Cordeau, J.-F., Laporte, G.: Stochastic uncapacitated hub location. European Journal of Operational Research 212(3), 518–528 (2011)
25. Correia, I., Nickel, S., Saldanha-da-Gama, F.: Hub and spoke network design with single-assignment, capacity decisions and balancing requirements. Applied Mathematical Modelling 35(10), 4841–4851 (2011)
26. Catanzaro, D., et al.: A branch-and-cut algorithm for the partitioning-hub location-routing problem. Computers & Operations Research 38(2), 539–549 (2011)
27. Yaman, H.: Allocation strategies in hub networks. European Journal of Operational Research 211(3), 442–451 (2011)
28. Puerto, J., Ramos, A.B., Rodríguez-Chía, A.M.: Single-allocation ordered median hub location problems. Computers & Operations Research 38(2), 559–570 (2011)
29. Vasconcelos, A.D., Nassi, C.D., Lopes, L.A.S.: The uncapacitated hub location problem in networks under decentralized management. Computers & Operations Research 38(12), 1656–1666 (2011)
30. Kratica, J., et al.: An evolutionary-based approach for solving a capacitated hub location problem. Applied Soft Computing 11(2), 1858–1866 (2011)
31. Mohammadi, M., Jolai, F., Rostami, H.: An M/M/c queue model for hub covering location problem. Mathematical and Computer Modelling 54(11-12), 2623–2638 (2011)
32. Sender, J., Clausen, U.: A new hub location model for network design of wagonload traffic. Procedia - Social and Behavioral Sciences 20(0), 90–99 (2011)
33. Hansen, P., Mladenovic, N.: Design of a reliable hub-and-spoke network using an interactive fuzzy goal programming. European Journal of Operational Research 130, 449–467 (2011)
34. Gelareh, S., Nickel, S.: Hub location problems in transportation networks. Transportation Research Part E: Logistics and Transportation Review 47(6), 1092–1111 (2011)
35. Taghipourian, F., et al.: A fuzzy programming approach for dynamic virtual hub location problem. Applied Mathematical Modelling
36. Karimi, H., Bashiri, M.: Hub covering location problems with different coverage types. Scientia Iranica 18(6), 1571–1578 (2011)
37. de Camargo, R.S., Miranda, G.: Single allocation hub location problem under congestion: Network owner and user perspectives. Expert Systems with Applications 39(3), 3385–3391 (2012)
38. Fazel Zarandi, M.H., Davari, S., Haddad Sisakht, S.A.: The Q-coverage multiple allocation hub covering problem with mandatory dispersion. Scientia Iranica (2012)
39. Alumur, S.A., Kara, B.Y., Karasan, O.E.: Multimodal hub location and hub network design. Omega 40(6), 927–939 (2012)
40. Alumur, S.A., Nickel, S., Saldanha-da-Gama, F.: Hub location under uncertainty. Transportation Research Part B: Methodological 46(4), 529–543 (2012)
41. Hwang, Y.H., Lee, Y.H.: Uncapacitated single allocation p-hub maximal covering problem. Computers & Industrial Engineering 63(2), 382–389 (2012)
42. Zhai, H., Liu, Y., Chen, W.: Applying Minimum-Risk Criterion to Stochastic Hub Location Problems. Procedia Engineering 29(0), 2313–2321 (2012)

43. Peng, J., Liu, B.: Parallel machine scheduling models with fuzzy processing times. Information Sciences 166(1-4), 49–66 (2004)
44. Zhao, R., Liu, B.: Standby redundancy optimization problems with fuzzy lifetimes. Computers & Industrial Engineering 49(2), 318–338 (2005)
45. Zheng, Y., Liu, B.: Fuzzy vehicle routing model with credibility measure and its hybrid intelligent algorithm. Applied Mathematics and Computation 176(2), 673–683 (2006)
46. Liu, L., Li, Y.: The fuzzy quadratic assignment problem with penalty: New models and genetic algorithm. Applied Mathematics and Computation 174(2), 1229–1244 (2006)
47. Huang, X.: Fuzzy chance-constrained portfolio selection. Applied Mathematics and Computation 177(2), 500–507 (2006)
48. Yang, L., Liu, L.: Fuzzy fixed charge solid transportation problem and algorithm. Applied Soft Computing 7(3), 879–889 (2007)
49. Zhou, J., Liu, B.: Modeling capacitated location-allocation problem with fuzzy demands. Computers & Industrial Engineering 53(3), 454–468 (2007)
50. Erbao, C., Mingyong, L.: A hybrid differential evolution algorithm to vehicle routing problem with fuzzy demands. Journal of Computational and Applied Mathematics 231(1), 302–310 (2009)
51. Lan, Y.-F., Liu, Y.-K., Sun, G.-J.: Modeling fuzzy multi-period production planning and sourcing problem with credibility service levels. Journal of Computational and Applied Mathematics 231(1), 208–221 (2009)
52. Liu, L., Gao, X.: Fuzzy weighted equilibrium multi-job assignment problem and genetic algorithm. Applied Mathematical Modelling 33(10), 3926–3935 (2009)
53. Davari, S., Fazel Zarandi, M.H., Hemmati, A.: Maximal Covering Location Problem (MCLP) with fuzzy travel times. Expert Systems with Applications 38(12), 14535–14541 (2011)
54. Li, X., et al.: A hybrid intelligent algorithm for portfolio selection problem with fuzzy returns. Journal of Computational and Applied Mathematics 233(2), 264–278 (2009)
55. Ke, H., Liu, B.: Fuzzy project scheduling problem and its hybrid intelligent algorithm. Applied Mathematical Modelling 34(2), 301–308 (2010)
56. Wen, M., Kang, R.: Some optimal models for facility location-allocation problem with random fuzzy demands. Applied Soft Computing 11(1), 1202–1207 (2011)
57. Fazel Zarandi, M.H., Hemmati, A., Davari, S.: The multi-depot capacitated location-routing problem with fuzzy travel times. Expert Systems with Applications 38(8), 10075–10084 (2011)
58. Davari, S., Fazel Zarandi, M.H.: The single-allocation hierarchical hub median location problem with fuzzy demands. African Journal of Business Manegement 6(1), 347–360 (2012)
59. Lau, H.C.W., et al.: A credibility-based fuzzy location model with Hurwicz criteria for the design of distribution systems in B2C e-commerce. Computers & Amp; Industrial Engineering 59(4), 873–886 (2010)
60. Yaman, H.: The hierarchical hub median problem with single assignment. Transportation Research Part B: Methodological 43(6), 643–658 (2009)
61. Kara, B.Y.: Modeling and analysis of issues in hub location problems. Ph.D. Thesis, in Industrial Engineering Department, Bilkent University (1999)
62. Blum, C., et al.: Hybrid metaheuristics in combinatorial optimization: A survey. Applied Soft Computing 11(6), 4135–4151 (2011)
63. Stützle, T.: Iterated local search for the quadratic assignment problem. European Journal of Operational Research 174(3), 1519–1539 (2006)

64. Hashimoto, H., Yagiura, M., Ibaraki, T.: An iterated local search algorithm for the time-dependent vehicle routing problem with time windows. Discrete Optimization 5(2), 434–456 (2008)
65. Laurent, B., Hao, J.-K.: Iterated local search for the multiple depot vehicle scheduling problem. Computers & Industrial Engineering 57(1), 277–286 (2009)
66. Josef Geiger, M.: Decision support for multi-objective flow shop scheduling by the Pareto Iterated Local Search methodology. Computers & Industrial Engineering. Corrected Proof (in press)
67. Derbel, H., et al.: An Iterated Local Search for Solving A Location-Routing Problem. Electronic Notes in Discrete Mathematics 36, 875–882 (2010)
68. Liu, B.: Uncertainty Theory, 3rd edn., http://orsc.edu.cn/liu/up.pdf

Experimental Application of a Pragmatic Method to Design Control Strategy for Low Power Wind Energy Conversion System

Radu Boraci and Cristian Vasar

"Politehnica" University of Timisoara/
Department of Automation and Applied Informatics, Romania
{radu.boraci,cristian.vasar}@aut.upt.ro

Abstract. This paper proposes a method for designing, implementation and experimental validation of a control strategy dedicated to a low power wind generator. It was developed theoretically then applied to a low speed wind generator prototype. The proposed wind energy conversion system control structure is briefly described, including its subsystems and components, respectively the wind turbine, permanent magnets synchronous generator, electronic converters and brake system. There were taken into consideration the components characteristics determined theoretically and experimentally obtained from components manufacturers or a dedicated laboratory model. The control law for the optimal operation regime of the wind turbine was designed considering the wind speed and the individual characteristics of the wind energy conversion system components and their operating restrictions. Also, there were determined the start and stop conditions, the allowed turbine speed ranges and the consequent braking regimes. Simulation and experimental results demonstrate the effectiveness of the proposed approach.

Keywords: small windmills, wind turbines, magnet poles synchronous generators, windgenerator electronics, braking systems, control methods and algorithms.

1 Introduction

During last decades, the interest for renewable energy technologies increased both for scientists and the industrial environment. In this field, a special place is taken by the wind energy conversion systems (WECSs). The control strategies used to convert wind into electricity covers a broad range, from those based on constant speed to the advanced ones for variable speed supported by electronic converters, for on-grid or off-grid WECSs [1,2] .

An important demand can be noticed on the market for low speed wind generators (1 to 10 KW), operating in locations with various wind profiles. Most of these WECSs are based on wind turbines with non-regulated blades and permanent magnet synchronous generators functioning at variable speed to optimize the power extracted

V.E. Balas et al. (Eds.): Soft Computing Applications, AISC 195, pp. 183–195.
springerlink.com

from wind. They are interfaced with consumers or grid using static electronic converters with variable frequency and voltage for input and constant frequency and voltage for output.

One experimental setup for a low power WECS (presented in figure 1) was developed by Politehnica University of Timisoara, in the frame of the European Economic Area Grant "Improvement of the structure and efficiency of small horizontal axis wind generators with non-regulated blades.

Fig. 1. Experimental windgenerator

The WECS components were developed, implemented, studied and optimized considering the actual trends in this field.

2 WECS Components

2.1 Wind Turbine

One important component of the presented system is the wind turbine. The blades are twisted in space, with metal insertion and variable geometry. They are equipped with

flaps for noise reduction and finite span effect that requires a special study to find the optimal control solution.

A special requirement for the wind turbine was to be able to provide energy even at low wind speed. This condition lead to the necessity to limit the rotation speed at higher wind speeds. Thus it was developed a protection mechanism to adapt the blade stall in order to adjust the turbine aerodynamic characteristics, limiting the power extracted from wind and the rotation speed.

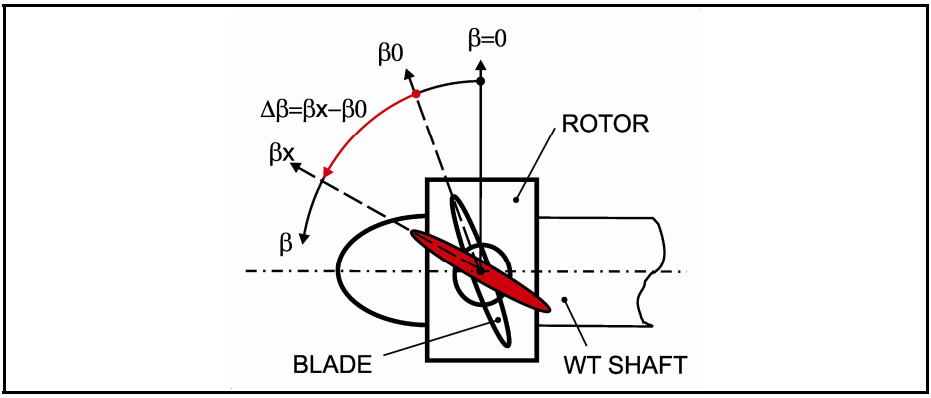

Fig. 2. The rotor of wind turbine

The rotor of wind turbine is presented in Figure 2.The blade absolute position is defined by the β_x angle. In normal operation, when the limitation system is not active, the blades angle is β_0.

The relative position of the blade is

$$\Delta\beta = \beta_x - \beta_0 \, , \, \Delta\beta = 0 \ldots 45 \text{ dgr.} \tag{1}$$

The manufacturing procedure was based on fiberglass reinforced polyester for obtaining products with a complex structure [3] .

2.2 Permanent Magnet Synchronous Generator

Based on the wind turbine estimated characteristics and existing statistical data, there resulted the following rated values for designing the permanent magnet synchronous generator (PMSG): $(P_{PMSG})_{rated}$ = 5400W, $(n_{PMSG})_{rated}$ = 122 rpm.

The PMS generator integrates a electromechanical brake and was manufactured by S.C. BEGAELECTROMOTOR S.A. Timişoara, România. The actual physical parameters were determined through experimental tests in the laboratory as follows for cosφ = 1:

P_{rated} = 6075 W - rated power;
U_{rated} = 162 V - rated phase voltage;
I_{rated} = 12.5 A - rated phase current;
M_{rated} = 484 N m - rated torque;
η_{rated} = 0,91 - rated efficiency;
Φ_{f0} = 1,42 Wb - excitation magnetic flux;
$L_d = L_q$ = 0.03 H - phases inductances;
$X_d = X_q$ = 6.15 Ω - phases reactances;
J = 40 kg m2 - inertia torque
p = 16 - number of poles pair,
R = 1.5 Ω - stator resistance.

2.3 Interfacing Power Converters

The considered structure for the electronic conversion system is depicted in figure 3, where the following components can be noticed: wind turbine (WT), permanent magnet synchronous generator (PMSG), diode bridge (DB), hybrid dc-dc converter (HDC), boost voltage inverter (BVI), safety electromechanical brake, Brake load (electrodynamic brake resistor), Supper capacitor and Dump load.

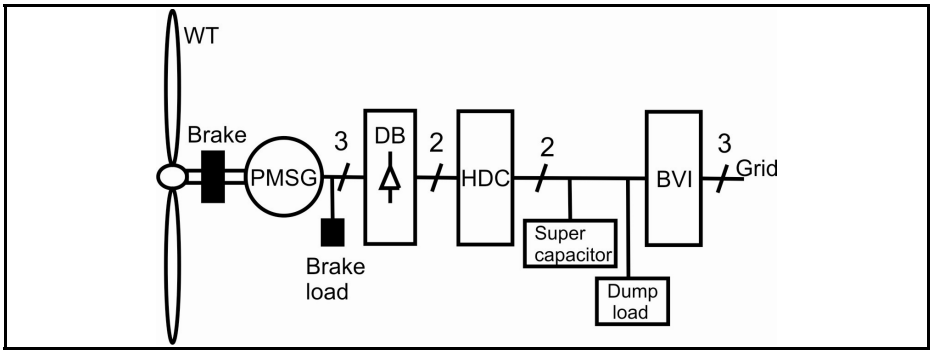

Fig. 3. WECS structure

For similar wind generators, many authors proposed new hybrid and Z configurations for dc-dc and dc-ac converters structures, with high voltage gain [4, 5] .

In the considered case, as common solution for low power WECS, the three phase voltage provided by PMSG is rectified by a 6 diodes bridge. The electronic conversion system is based on an intermediary DC circuit with variable voltage, connected between HDC and BVI.

The nominal voltage for super capacitor has to be between 100 and 150 V to assure a low current in the PMSG windings, and increase overall efficiency.

The HDC ratio for input/output voltage is given by (2), considering both economical and technical issues [5,6]:

$$V_{SC} = \frac{D}{2-D} V_{DB} \tag{2}$$

where

V_{SC} - Super Capacitor voltage,
V_{DB} - output voltage of diode bridge,
D - duty cycle.

2.4 WECS Braking Systems

For safety reasons, the developed WECS was equipped with three independent braking systems [7] .

The electro-dynamical brake consists of power resistors continuous controlled connected directly to PMSG terminals.

The aero-dynamical brake is integrated in the wind turbine structure, consisting of a centrifugal mechanism able to limit the rotation speed (reducing also the provided power) by modifying the rotor geometry [8] .

The electro-mechanical brake is integrated in the PMSG, consisting of a pair of friction discs electromagnetically actuated provided a braking torque of 450 Nm. This brake is used especially in emergency situations.

3 Mathematical Models

3.1 Wind Turbine Model

The mathematical model complexity for the considered wind turbine is higher due to the centrifugal protection autonomous system. At various over-speed values the blades adapt their angle in order to change the aerodynamic behavior, decreasing the rotor speed

The estimates based on the mathematical model developed by designers [3,4,9], that take into consideration the blade shape, and turbine architecture, for $\Delta\beta = 0 \ldots 45$ dgr , for the torque coefficient $C_M(v, n, \Delta\beta)$are the following:

$$C_M(v, n, \Delta\beta) = C_{M0\beta}(\Delta\beta) + a_\beta(\Delta\beta)\, \lambda^{\alpha-1}(v, n) - b_\beta(\Delta\beta)\, \lambda^{\beta-1}(v, n) \tag{3}$$

where:

$C_{M0\beta}(\Delta\beta)$, $a_\beta(\Delta\beta)$, $b_\beta(\Delta\beta)$ expressed as function of angular position of the blades relative to installation position, $\Delta\beta$, are:

$$\begin{aligned} C_{M0\beta}(\Delta\beta) &= (c_{\beta 1} + c_{\beta 2}\, \Delta\beta)/(1 + c_{\beta 3}\, \Delta\beta + c_{\beta 4}\, \Delta\beta^2) \\ a_\beta(\Delta\beta) &= (a_{\beta 1} + a_{\beta 2}\, \Delta\beta^1)/(1 + a_{\beta 3}\, \Delta\beta^1 + a_{\beta 4}\, \Delta\beta^2) \\ b_\beta(\Delta\beta) &= (b_{\beta 1} + b_{\beta 2}\, x)/(1 + b_{\beta 3}\, x + b_{\beta 4}\, x\text{^}2) \end{aligned} \tag{4}$$

The coefficients obtained through linear regression are given in Table 1.

Table 1. Linear regression coefficients

$c_{\beta 1}$ = 0.012512548 ;	$c_{\beta 2}$ = 0.010797253 ;
$c_{\beta 3}$ = 0.04617332 ;	$c_{\beta 4}$ = 9.6420381e-007 .
$a_{\beta 1}$ = 0.061078896 ;	$a_{\beta 2}$ = -0.0047310111 ;
$a_{\beta 3}$ = -0.0075548307 ;	$a_{\beta 4}$ = -0.00010627525 .
$b_{\beta 1}$ = 0.0042482559 ;	$b_{\beta 2}$ = -0.00013577705 ;
$b_{\beta 3}$ = -0.09017725 ;	$b_{\beta 4}$ = 0.0038774948 .

The resulting shaft torque of wind turbine:

$$M_{arb\beta}(v,n,\Delta\beta) = C_{M\beta}(v,n,\Delta\beta)\,\rho\, v^2\, A_v\, R/2 \tag{5}$$

Shaft power coefficient:

$$C_{P\beta}(v,n,\Delta\beta) = C_{M\beta}(v,n,\Delta\beta)\,\lambda(v,n) \tag{6}$$

$$C_{P\beta}(v,n,\Delta\beta) = C_{M0\beta}(\Delta\beta)\;\lambda(v,n) + a_\beta(\Delta\beta)\,\lambda^\alpha(v,n) - b_\beta(\Delta\beta)\,\lambda^\beta(v,n)$$

Shaft power:

$$P_{arb\beta}(v,n,\Delta\beta) = M_{arb\beta}(v,n,\Delta\beta)\,\omega(n)$$

$$P_{arb\beta}(v,n,\Delta\beta) = C_{M\beta}(v,n,\Delta\beta)\,\rho\, v^2\, A_v\, R\,\omega(n)/2 \tag{7}$$

In normal operation the blades angular variation is $\Delta\beta = 0$.

If the rotor speed increases above rated values, the autonomous centrifugal braking system determines a variation of blades angle $0 < \Delta\beta \le 45$.

3.2 PMSG Model

The considered PMSG has the following model [10]:

$$\begin{cases} \dfrac{di_d}{dt} = \dfrac{1}{L_d}\left(u_d - Ri_d + p\,\omega_r L_q\, i_q\right) \\ \dfrac{di_q}{dt} = \dfrac{1}{L_q}\left(u_q - Ri_q + p\,\omega_r L_d\, i_d - p\,\omega_r \Phi_f\right) \\ J\dfrac{d}{dt}\omega_r = p\dfrac{1}{J}\left[\dfrac{3}{2}p\left[i_q\Phi_f + \left(L_d - L_q\right)i_d\, i_q\right] + M_m\right] - \dfrac{F}{J}\omega_r \\ \dfrac{d\theta}{dt} = \omega_r \end{cases} \tag{8}$$

Where:

i_q, i_d - q and d axes currents,
v_q, v_d - q and d axes voltages,
ω_r - rotor angular speed,
Φ_f – permanent magnets' flux amplitude,
F = 0.004924 Nm s - total friction coefficient,
$J = J_{WT} + J_{PMSG} = 445 + 40 = 485$ kg m^2 – total moment of inertia.

The shaft power P_m corresponding to a given value of generator electric power, can be calculated based on the generator efficiency $\eta_G(n, I_G)$:

$$P_m = P_G / \eta_G \tag{9}$$

In the considered case the efficiency resulted from generator design is:

$$\eta_G(n, I_G) = 4.25\ n\ I_G / (0.09\ I_G^3 + 2.9\ I_G^2 + 4.25\ n\ I_G + 0.075\ n^{1.5}) \tag{10}$$

resulting

$$P_m = F_{pm}(n, I_G) = P_G(n, I_G) / \eta_G(n, I_G) \tag{11}$$

The equation for the wind turbine-generator subsystem, in stationary regime, can be obtained considering the wind turbine power $P_{wt}(n,v)$ and the generator shaft power $P_m(n, I_G)$:

$$P_{wt}(n,v)\ \eta_G(n, I_G) = P_G(n, I_G) \tag{12}$$

4 Control of the Wind Energy Conversion System

In order to achieve an efficient control of a WECS, there are necessary good models and characteristics for system components, provided usually by their manufacturer. In our situation, they were not available, and one task prior to develop the control algorithm was to obtain proper models and characteristics, using the developed WECS experimental model. This approach, starting from real data and experimental models was the motivation to refer it as a pragmatic method to design the control strategy.

In normal operating regime (wind power conversion regime), the start-up is validated if the HDC input voltage exceeds a minimum threshold $(U_{HDC})_{input} > (U_{HDC})_{START\ min}$= 190 V assuring the conduction state for the hybrid converter. The no-load phase voltage of PMSG to this threshold is $(U_{PMSG})_{START\ min}$ = 77.86 V, respectively a rotation speed $n_{START\ min}$ = 52 rpm and a wind speed $v_{START\ min}$ = 4.76 m/s. The considered start-up values $(U_{HDC})_{START\ min}$, $n_{START\ min}$, $v_{START\ min}$, were determined experimentally using the ;laboratory modelof WECS .

In diagrams $P_{WT}(v,n)$ and $M_{WT}(v,n)$ presented in Figure 4 – the start-up point is denoted with "a".

The automatic cut-off values $(U_{HDC})_{STOP}$, $(U_{PMSG})_{STOP}$, n_{STOP} , v_{STOP} , at small wind speeds, also have been determined on the laboratory model, and are nenoted with “d” in Figure 4.

The WECS nominal regime is determined considering the following physical constraints: the maximal input voltage of HDC, U_{HDCmax} = 380 V and the maximal current for WECS component, in our case I_{HDCmax} = 12.5A.

The experimental tests reveal that above mentioned constraints are accomplished at the rotation speed n = 112 rpm, generator phase voltage U_{PMSG} = 155 V, generator current I_{PMSG} = 12.5A, generator electric power P_{PMSG} = 5400 W, wind speed v = 8.5 m/s (see point “c” in Figure 4). The mentioned operation values will be considered as rated values of WECS [11].

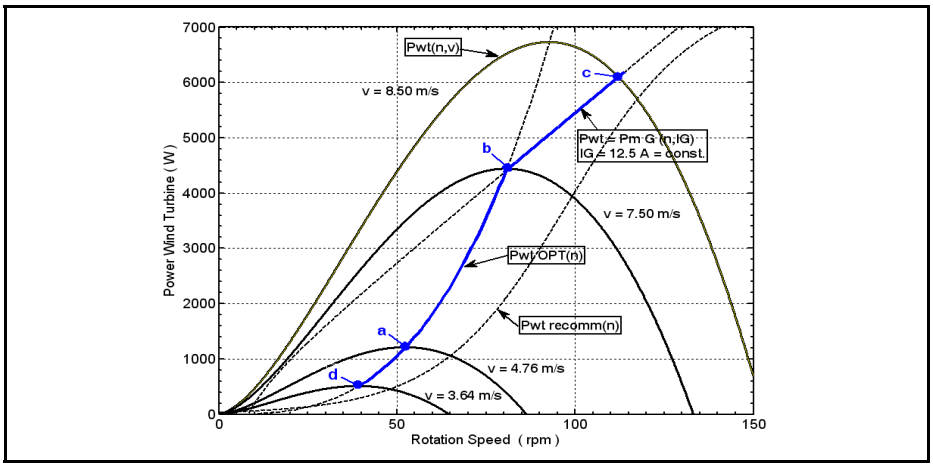

Fig. 4. The P_{WT} (v, n), $P_{WT\ opt}$(n) characteristics and the start-up ***a*** and cut-off ***d*** points in energy generating regime

Based on the above considerations it was developed the control strategy for WECS presented in Figure 5.

S00 represents the state when WT is stopped, and the brake is activated, wind speed being insufficient.

After Δt_1 (experimental established $\Delta t_1 = 10[\min]$), the system state changes to a waiting state **S10**, releasing the electro-mechanic brake and wait for rotation speed increase.

If after a predefined time, the rotation speed is below the rated value, Δt_2, $0 < n < n_{START}$, the system returns to **S00**.

If the rotation speed $n > n_{START}$, the system moves to **S20** which represent optimal point functioning.

If the rotation speed decrease below a threshold value n_{min}, the system returns to **S10** state.

If the rotation speed exceeds a nominal value n_{NOM}, the system enter in the limitation state **S30**, providing the constant current I_G. In this case, if the rotation decreases($n < n_{NOM}$) the system returns to S20 state.

If the speed exceeds the maximal value n_{MAX}, the system enters the state **S40** corresponding to an extreme operation at high wind speed, when all the braking systems are activated successively: aerodynamically braking through blade rotation angle $0 < \Delta\beta \le \Delta\beta_{MAX}$, electromagnetic braking through current $I_G = I_{G\_ELBRAKE}$, and electro-mechanical braking activation, in order to limit the wind turbine speed in the range $n_{MAX} \le n < n_{EXTREM}$.

The system returns to state S30 if the speed decreases $n < n_{MAX}$.

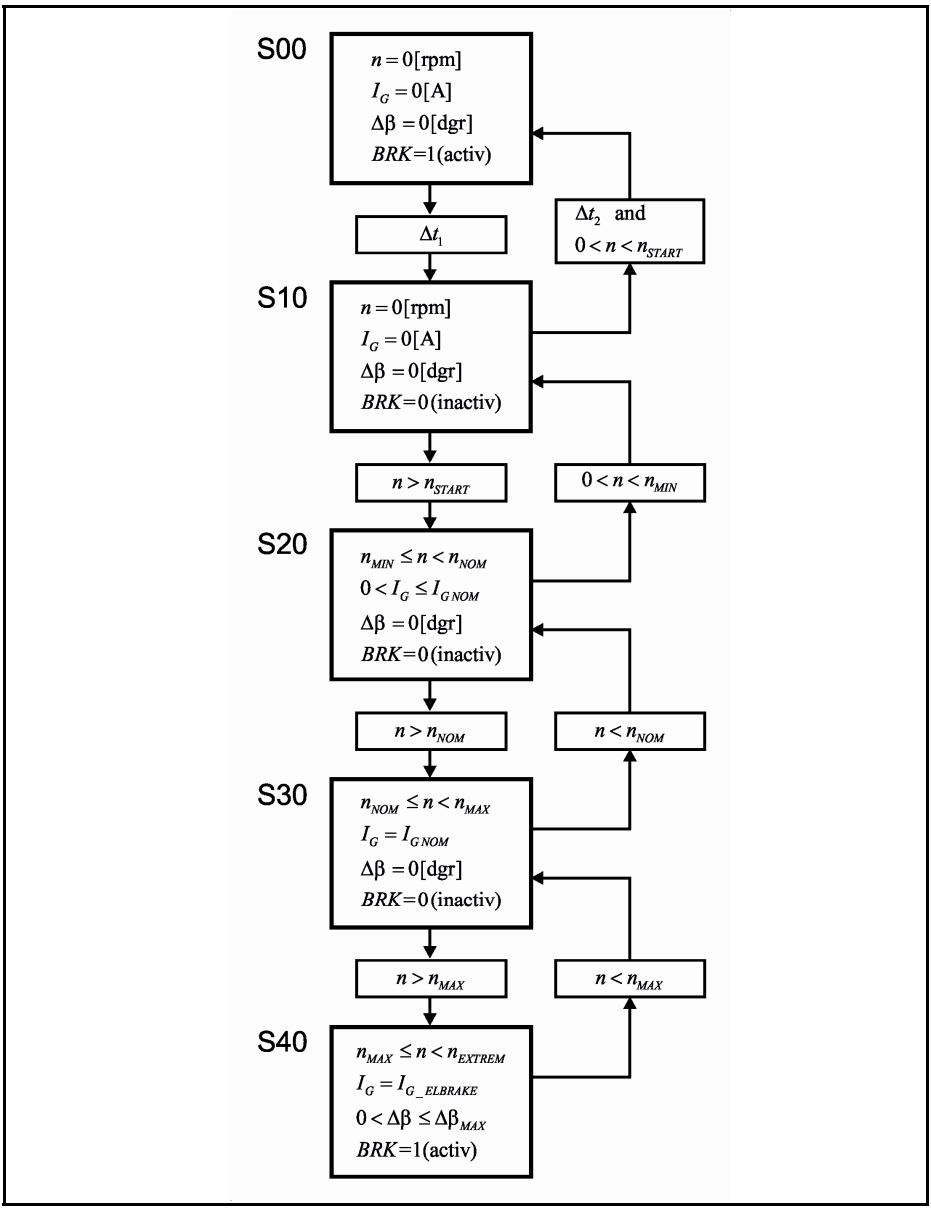

Fig. 5. The WECS control algorithm

The aero-dynamical braking system is able to limit the speed $n < n_{EXTREM}$, statement verified at wind speed v = 70 m/s as presented in Figure6.

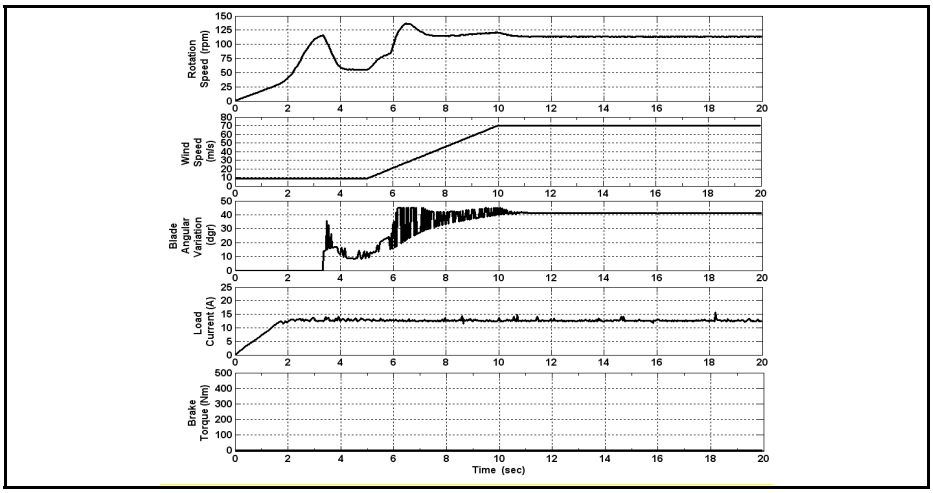

Fig. 6. WECS at extreme values of the wind speeds, v = 70 m/s

5 Simulation/Experimental Results

The wind turbine characteristic is presented in figure 7, with blades in initial position $\Delta\beta = 0 = \text{const}$. The turbine was designed to provide $P_{WT}(n_{wt}, v)$, even for low wind speed.

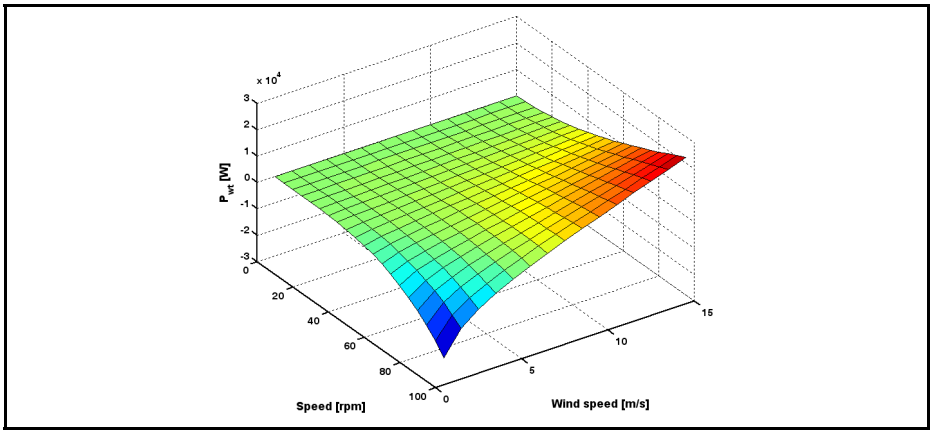

Fig. 7. Turbine characteristics $P_{WT}(n_{wt}, v)$ for $\Delta\beta = 0$.

At high rotation speed, and blade position $\Delta\beta = \Delta\beta_{MAX} = 45$ dgr, the turbine presents high aero-dynamical braking torque, as depicted in figure 8.

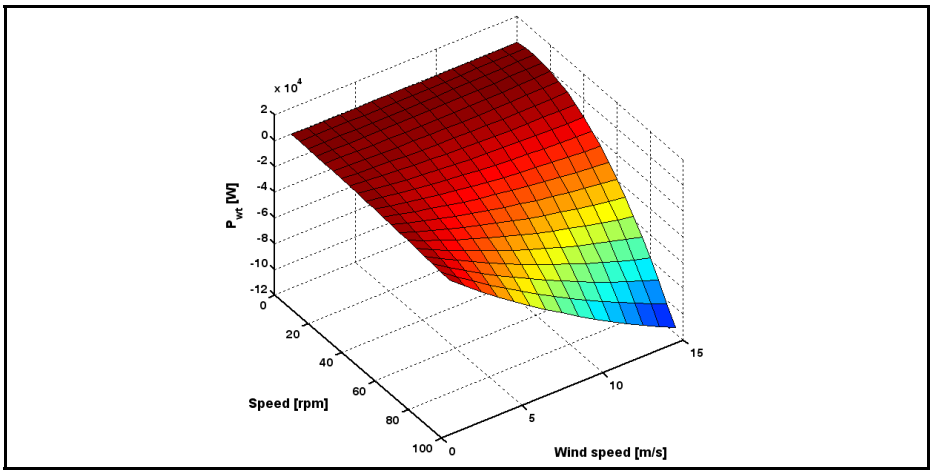

Fig. 8. Turbine characteristics $P_{WT}(n_{wt}, v)$ for $\Delta\beta = 45$

The power provided by wind turbine, at constant wind speed v = 8 m/s, in function of rotation speed and angle $\Delta\beta$ is presented in Figure 9.

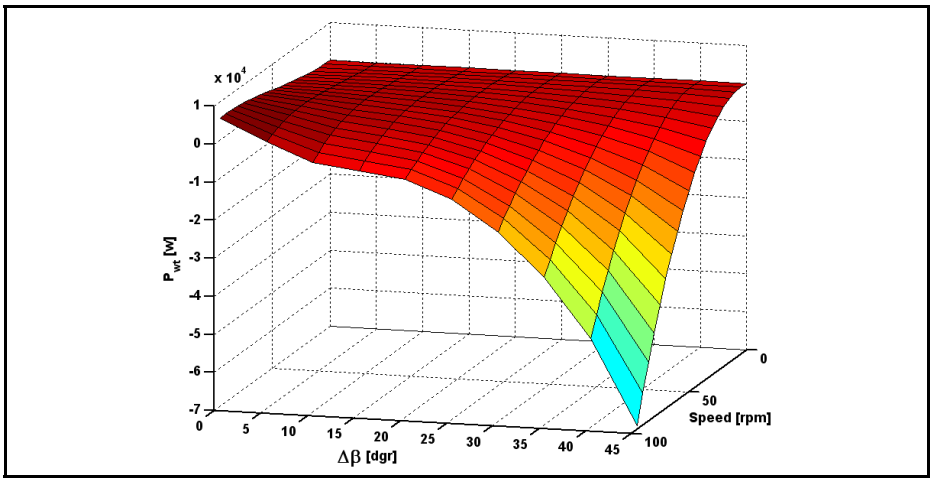

Fig. 9. Turbine characteristics $P_{WT}(n_{wt}, v)$ for $\Delta\beta = 0 \ldots 45$.

The wind turbine power curve for the optimal regime $P_{WT\_Opt}(n)$ and respectivelly the equivalent shaft power $P_{WT}(n)$, for a number of $N_{point} = 10279$ measurements during the operating regime is depicted in Figure 10. The considered efficiency of the PMSG is $\eta_{PMSG} = 91\%$.

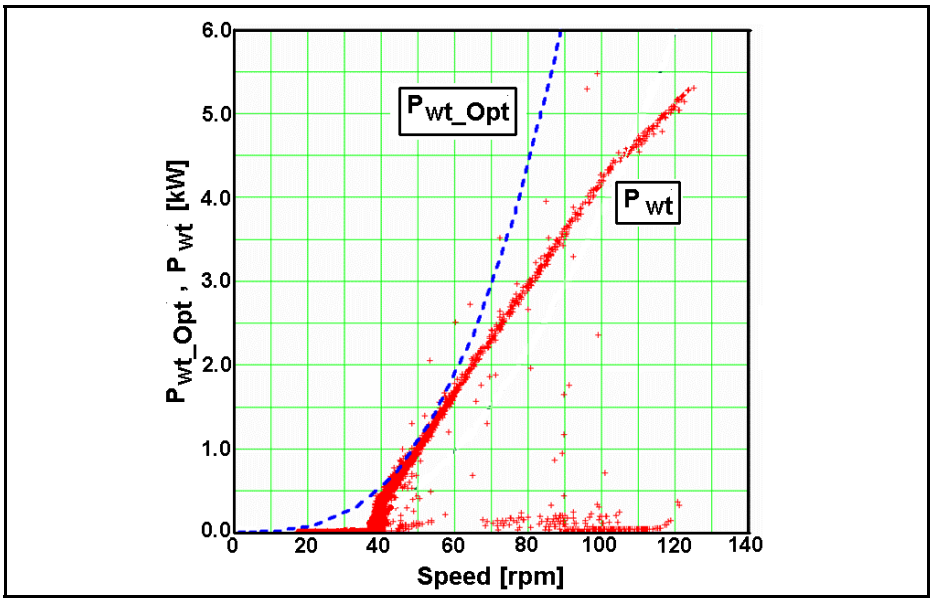

Fig. 10. Optimal regime power $P_{WT\_Opt}(n)$ and equivalent shaft power $P_{WT}(n)$

There can be noticed that shaft power distribution corresponds to reference curve of WECS. The power conversion is started at a rotation speed of 40 rpm and the functioning in optimal regime along $P_{WT\_Opt}(n)$ curve (with an insignificant deviation) is until 80 rpm, followed by a constant current regime limited at I_G = 12.5 A for speeds above 80 rpm.

6 Conclusions

The studies performed on the laboratory models confirmed the hypothesis adopted in designing the WECS and its elements.

The control algorithm in different operation regimes (nominal or faulty) has been also confirmed, through the experimental tests on the developed laboratory model, complying all conditions imposed by the present-day standards in the domain of WECS [12].

References

1. Chen, Z., Guerrero, J.M., Blaabjerg, F.: A review of the state of the art of power electronics for wind turbines. IEEE Trans. Power Electr. 24(8), 1859–1875 (2009)
2. Muntean, N., Cornea, O., Petrila, D.: A New Conversion and Control System for a Small Off – Grid Wind Turbine. In: 12th International Conference on Optimization of Electrical and Electronic Equipment, OPTIM 2010, pp. 1167–1173. IEEE (2010); 978-1-4244-7020

3. Milos, T., Gyulai, F.: CAD technique for blade design of small power wind turbine. In: Proceedings of the International Conference on Hydraulic Machinery and Equipments, HME 2008, Timisoara, Romania (2008)
4. Peng, F.Z.: Z-source inverter. IEEE Trans. Ind. Applic. 39, 504–510 (2003)
5. Axelrod, B., Berkovich, Y., Ioinovici, A.: Switched-capacitor/ switched inductor structures for getting transformer less hybrid dc-dc PWM converters. IEEE Trans. Circ. and Syst. 55(2), 687–696 (2008)
6. Gao, F., Loh, P.C., Teodorescu, R., Blaabjerg, F.: Diode assisted buck boost voltage source inverters. IEEE Trans. Power Electr. 24(9), 2057–2064 (2009)
7. Koch-Ciobotaru, C., Boraci, R., Filip, I., Vasar, C.: Study of brake transient regimes for a small wind generator. In: IEEE 3rd International Symposium on Exploitation of Renewable Energy Sources (EXPRES), March 11-12, pp. 85–89 (2011)
8. Milos, T., Bej, A., Dobanda, E., Manea, A., Badarau, R., Stroita, D.: Blade design using CAD technique for small power wind turbine. In: International Joint Conference on Computational Cybernetics and Technical Informatics (ICCC-CONTI), Timisoara, Romania, May 27-29, pp. 571–575 (2010)
9. Babescu M.: Electrical machines. The ortogonal model. Publishing House Politehnica, Timisoara (2000)
10. Koch-Ciobotaru, C., Boraci, R., Prostean, O., Budisan, N.: Optimal control for a variable-speed wind turbine. In: 6th IEEE International Symposium on Applied Computational Intelligence and Informatics (SACI), May 19-21, pp. 541–544 (2011)
11. Boraci, R., Koch-Ciobotaru, C., Protean, O., Budisan, N.: Experimental determination of an optimal control law of a small windgenerator. In: IEEE 6th IEEE International Symposium on Applied Computational Intelligence and Informatics (SACI), May 19-21, pp. 545–548 (2011)
12. International Standard IEC 614000-2, Part.2: Design requirements for small wind turbines

Model Predictive Control for Inside Temperature of an Energy Efficient Building

Cosmin Koch-Ciobotaru

"Politehnica"University of Timisoara,
Department of Automation and Applied Informatics,
Bd. V. Parvan 2, 300223 Timisoara, Romania
cosmin.koch@aut.upt.ro

Abstract. The paper presents the development and implementation of a model predictive control (MPC) used for inside temperature control of a building. The inside temperature is tracking a prescribed reference inside a comfort zone define by the optimization problem implementing offset free control through a Kalman filter state estimator. The MPC is validated by simulation and experiment using a building thermal model, a 24 hour ahead predicted solar irradiance and ambient temperature and measured actual weather data and inside temperature for the closed loop simulation operation.

Keywords: Model predictive control, energy efficient building, Kalman filter, offset free control, quadratic program.

1 Introduction

As the building sector represents a major consumer in the world, with an estimated 26.5% of the total global consumption in 2009 according to [1], research on developing energy efficient buildings represents a large energy savings potential.

The model predictive control algorithm is well suited for energy efficient buildings and systems where both the control variables and state variables have physical constraints. The MPC is able to take action before a predicted event actually takes place; in this case, the system having large time constants, the electrical heaters are turned off prior to mid day, where the solar irradiance has a powerful effect on increasing the inside temperature.

In building temperature control there are two large approaches on MPC algorithms: the first are tracking a prescribed reference, minimizing the difference between the controlled variable and the reference inside temperature as in [2] and [3] and the economic MPC which minimizes the cost of energy in keeping the inside temperature inside the comfort zone [4].

In [5] is studied the impact of modeling accuracy on the MPC of the passive building thermal capacitance to minimize an objective function.

MPC algorithms for controlling the inside temperature were developed considering weather predictions as in [6] and stochastic disturbances in [2] or human presence [7].

The objective function of the PMC can be stated as a linear programming LP problem as [8] or as a quadratic problem QP as in [2].

V.E. Balas et al. (Eds.): Soft Computing Applications, AISC 195, pp. 197–208.
springerlink.com

This paper presents a MPC for controlling the inside temperature of a building to track the prescribed reference formulated as a quadratic problem, with prediction on the two disturbances, the solar radiation and ambient temperature.

2 Model of the System

The temperature dynamics of a given space can be modeled with the help of an equivalent electric circuit. This paper considers the simplified thermal model of an eight room building from SYSLAB facility from DTU Elektro at RISO campus. The building has 125 squared meters and one electrical heater in each room, except two rooms which are equipped with two electrical heaters each. The parameter identification and validation tests of the mathematical model are presented in the work of Bacher and Thavlov[9].

The objective of this paper is to develop, implement, and test through simulations and experiment, a model predictive controller which considers the inside temperature of the building as the controlled variable. The objective is for the controlled variable to track the prescribed reference, minimizing the peak consumption and maintain the inside temperature inside the comfort zone considering the difference between the predicted and measured perturbation: the solar irradiance and ambient temperature. This paper uses offline 24 hours ahead prediction data for the ambient temperature and solar irradiance and online measured values of weather data taken from the local weather station.

The building can be estimated as having a single room, with an additional assumption that each electrical heater has the same power (1kW) and the same effect on the inside temperature on this one room model. The equivalent (RC) electric circuit of the building is shown in Fig.1.

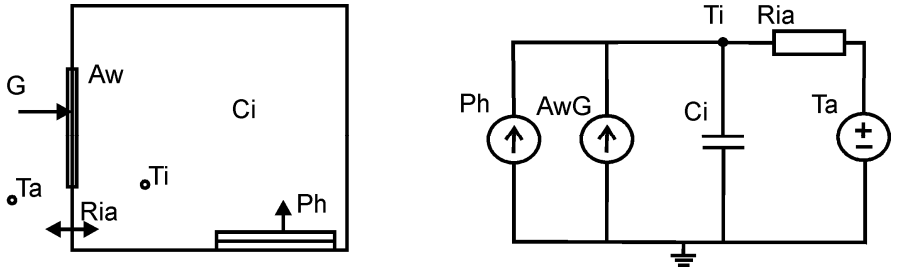

Fig. 1. Equivalent thermal model of the building

The mathematical thermal model of the one room equivalent building is shown in (1):

$$C_i \frac{dT_i}{dt} = \frac{1}{R_{ia}}\left(T_a - T_i\right) + A_w G + P_h \tag{1}$$

Where

C_i – thermal capacitance of the house

R_{ia} – thermal resistance of walls and windows isolating the house from the outside environment

A_w – window effective area
T_i – inside temperature
T_a – ambient temperature
G – solar irradiance on the house

For developing the MPC, the state-space model from (2) is needed. The parameters of the model are presented in Table 1.

$$\begin{cases} x_{k+1} = Ax_k + Bu_k + Ed_k \\ z_k = Cx_k \end{cases} \tag{2}$$

Table 1. Model parameters

C_i [kW/°C]	R_{ia} [°C/ kW]	A_W [m^2]	A	B	E	C
3.42	4,87	5,53	[0.99]	[0.0487]	[0.01, 0.2695]	[1]

3 MPC Algorithm

Model predictive control uses a mathematical model of the system, a discrete state space system in this paper, to estimate the process output for a fixed number of steps N into the future predicted horizon, according to the current internal state values, the predictions, and the reference trajectory. The MPC calculates the control sequence of the future N steps by minimizing an objective function. From this sequence only the first control output is considered and at the next time step the optimization is recalculated according to the new values available.

The MPC starts from a model, in this paper a state-space model, presented in (2), and an optimization function as seen in (3).

$$\min_{u \in R^n} f(u) = \frac{1}{2}\sum_{k=0}^{N} \left\| z_k - r_k \right\|_Q^2 + \frac{1}{2}\sum_{k=0}^{N-1} \left\| \Delta u_k \right\|_S^2 \tag{3}$$

This is a weighted quadratic optimization function with two objectives:

- The output variable (z_k) to track the reference (r_k), and
- doing so with small variations (Δu_k)

This optimization is realized for the next N steps interval, from which only the first term is considered for the controller output. At the next step, the optimization problem is recalculated, with the new values for the inputs, predictions, and measurements specific to that step.

Another important aspect of this control is the ability to alter the importance of the optimization terms in the optimization function by using weight coefficients, in this case Q for minimizing the trajectory difference and S for minimizing the variations of the manipulated variables.

The controller was developed in Matlab, using the *quadprog* solver, from the optimization toolbox. The optimization problem from (3) had to be rewritten in the form of (4), specific to this Matlab solver.

$$\min_{U} f = \frac{1}{2} U^{'} H U + g^{'} U \tag{4}$$

Subject to

$$A_q U \le b_q \tag{5}$$

From (2), the output values of the system can be estimated for the next prediction horizon, z_i , (i=1...N) considering the following values: x_0 - as the initial value for the state variable at each time step interval, D- the predicted disturbance vector over the predicted horizon and U - the system input, the command variable for the control algorithm, in this case the output power of the heaters. The predicted output values for the next N steps are:

$$\underbrace{\begin{bmatrix} z_1 \\ z_2 \\ z_3 \\ \vdots \\ z_N \end{bmatrix}}_{=Z} = \underbrace{\begin{bmatrix} CA \\ CA^2 \\ CA^3 \\ \vdots \\ CA^N \end{bmatrix}}_{=\Phi} x_0 + \underbrace{\begin{bmatrix} H_1 & 0 & 0 & \cdots & 0 \\ H_2 & H_1 & 0 & \cdots & 0 \\ H_3 & H_2 & H_1 & \cdots & 0 \\ \vdots & \vdots & \vdots & \ddots & 0 \\ H_N & H_{N-1} & H_{N-2} & \cdots & H_1 \end{bmatrix}}_{=\Gamma} \begin{bmatrix} u_0 \\ u_1 \\ u_2 \\ \vdots \\ u_{N-1} \end{bmatrix} + \underbrace{\begin{bmatrix} H_{1,d} & 0 & 0 & \cdots & 0 \\ H_{2,d} & H_{1,d} & 0 & \cdots & 0 \\ H_{3,d} & H_{2,d} & H_{1,d} & \cdots & 0 \\ \vdots & \vdots & \vdots & \ddots & 0 \\ H_{N,d} & H_{N-1,d} & H_{N-2,d} & \cdots & H_{1,d} \end{bmatrix}}_{=\Gamma_d} \begin{bmatrix} d_0 \\ d_1 \\ d_2 \\ \vdots \\ d_{N-1} \end{bmatrix} \tag{6}$$

where:

$$H_k = CA^{k-1}B \tag{7}$$

$$H_{k,d} = CA^{k-1}E \tag{8}$$

Equation (6) can be rewritten in a simpler way to handle, as shown in (9)

$$Z = \Phi x_0 + \Gamma U + \Gamma_d D \tag{9}$$

By developing the first term of (3) and using (9) , it is obtained:

$$f_z = \frac{1}{2}\sum_{k=0}^{N}\left\|z_k - r_k\right\|_Q^2 = \frac{1}{2}\sum_{k=0}^{N}\left\|Z - R\right\|_Q^2 = \frac{1}{2}\sum_{k=0}^{N}\left\|\Gamma U - b\right\|_Q^2 \tag{10}$$

Where

$$b = R - \Phi x_0 - \Gamma_d D \tag{11}$$

By considering the form of (4), (10) is written as (12):

$$\begin{aligned} f_z &= \frac{1}{2}\sum_{k=0}^{N}\left\|\Gamma U - b\right\|_Q^2 = \frac{1}{2}\left(\Gamma U - b\right)^{'} Q\left(\Gamma U - b\right) = \\ &= \frac{1}{2}U^{'}\Gamma^{'}Q\Gamma U - \left(\Gamma^{'}Qb\right)^{'}U + \frac{1}{2}b^{'}Qb \end{aligned} \tag{12}$$

For the second term of (3), the following form is obtained:

$$f_\Delta = \frac{1}{2}\sum_{k=0}^{N-1}\left\|\Delta u_k\right\|_S^2 = \frac{1}{2}\left\|\begin{bmatrix} u_0 \\ u_1 \\ \vdots \\ u_{N-1} \end{bmatrix} - \begin{bmatrix} u_{-1} \\ u_0 \\ \vdots \\ u_{N-2} \end{bmatrix}\right\|_S^2 \tag{13}$$

Which develops into (14):

$$f_\Delta = \frac{1}{2}\begin{bmatrix} u_0 \\ u_1 \\ u_2 \\ \vdots \\ u_{N-1} \end{bmatrix}^{'}\underbrace{\begin{bmatrix} 2S & -S & 0 & \cdots & 0 \\ -S & 2S & -S & \cdots & 0 \\ 0 & -S & 2S & \cdots & 0 \\ \vdots & \vdots & \vdots & \ddots & -S \\ 0 & 0 & 0 & -S & S \end{bmatrix}}_{=H_S}\begin{bmatrix} u_0 \\ u_1 \\ u_2 \\ \vdots \\ u_{N-1} \end{bmatrix} + \underbrace{\left(-\begin{bmatrix} S \\ 0 \\ 0 \\ \vdots \\ 0 \end{bmatrix}u_{-1}\right)}_{=M_{u-1}}\begin{bmatrix} u_0 \\ u_1 \\ u_2 \\ \vdots \\ u_{N-1} \end{bmatrix} \tag{14}$$

And for the required form of (4), the second term of (3) is:

$$f_\Delta = \frac{1}{2}U^{'}H_S U + M_{u_{-1}}u_{-1}U \tag{15}$$

From (12) and (15), the parameters H and g of (4) can be identified from the initial objective function of (3), in order to use the Matlab toolbox:

$$H = \Gamma^{'} Q \Gamma + H_S \tag{16}$$

$$g = -\Gamma^{'} Q\left(R - \Phi x_0 - \Gamma_d D\right) + M_{u_{-1}} u_{-1} \tag{17}$$

An advantage of the MPC is the ability to deal with constraints, both on the manipulated and controlled variables. The constraints on the two types of variables defined in (18) and (19) have to be written as a function of the manipulated variable and written in the form of variables A_q and b_q from (3).

$$U_{\min} \le U \le U_{\max}, k = 0...N-1 \tag{18}$$

$$Z_{\min} \le Z \le Z_{\max}, k = 0...N \tag{19}$$

As (19) have to be a function of manipulated variable U, the equation is rewritten as (20) and (21) as only the "smaller than" relation can be used for both the ends of the interval.

$$Z_{\min} - \Phi x_0 - \Gamma_d D \le \Gamma U \tag{20}$$

$$-Z_{\max} + \Phi x_0 + \Gamma_d D \le -\Gamma U \tag{21}$$

The parameters A_q and b_q from (4), for the considered model have the following relation:

$$A_q = \begin{bmatrix} I_N \\ -I_N \\ \Gamma \\ -\Gamma \end{bmatrix} \quad b_q = \begin{bmatrix} U_{\min} \\ -U_{\max} \\ Z_{\min} - \Phi x_0 - \Gamma_d D \\ -Z_{\max} + \Phi x_0 + \Gamma_d D \end{bmatrix} \tag{22}$$

Parameters H, g, A_q, and b_q from (16), (17), and (22) will be computed and used as call parameters for the *quadprog* solver:

$$U = \text{quadprog}(H, g, A_q, b_q) \tag{23}$$

The function returns the next N values of the manipulated variable U, which represents the output power of the electrical heaters for the N step prediction interval. From this, only the first value U_1 is used, and at the next step the optimization problem is recalculated.

4 Offset Free MPC

The system used in this paper and described in (3) uses two disturbance predictions which both have a large influence on the system output (inside temperature). These

are the solar irradiance and the outside ambient temperature. These data are provided by the local weather station with 24 hours-ahead prediction. However, like in the general case, these predictions are not perfect as it is shown in the figures of the next section.

These differences between the actual and the predicted values have to be considered in the model, otherwise they will introduce an offset in the controlled variable.

One of the possibilities to incorporate an integrator in the system model is to extend the state-space model with a number of additional states equal to the disturbances, and using a Kalman filter for their estimation. The offset free control has been discussed in [10] and [11].

If stochastic perturbation on the state variables (ω_k), on the system output (v_k) and errors in prediction (ξ_k) are considered, the augmented system (3) becomes:

$$\begin{cases} x_{k+1} = Ax_k + Bu_k + E\left(d_k + \eta_k\right) + \omega_k \\ \eta_{k+1} = \eta_k + \xi_k \\ z_k = Cx_k + v_k \end{cases} \tag{24}$$

And in the state-space form of:

$$\begin{cases} \begin{bmatrix} x_{k+1} \\ \eta_{k+1} \end{bmatrix} = \underbrace{\begin{bmatrix} A & E \\ 0 & I \end{bmatrix}}_{=\tilde{A}} \begin{bmatrix} x_k \\ \eta_k \end{bmatrix} + \begin{bmatrix} B \\ 0 \end{bmatrix} u_k + \begin{bmatrix} E \\ 0 \end{bmatrix} d_k + \begin{bmatrix} \omega_k \\ \xi_k \end{bmatrix} \\ z_k = \underbrace{\begin{bmatrix} C & 0 \end{bmatrix}}_{=\tilde{C}} \begin{bmatrix} x_k \\ \eta_k \end{bmatrix} + v_k \end{cases} \tag{25}$$

where $\omega_k \approx N(0,Q_w)$; $\xi_k \approx N(0,Q_{xi})$; $v_k \approx N(0,R_v)$ are zero-mean white-noise

The system from (25) is used to resolve the MPC problem according to the equations presented in section 3.

For the off-set free control, the states are estimated as follows:

$$\begin{bmatrix} \hat{x}_{k|k} \\ \hat{\eta}_{k|k} \end{bmatrix} = \begin{bmatrix} \hat{x}_{k|k-1} \\ \hat{\eta}_{k|k-1} \end{bmatrix} + K\left(z_k - C\hat{x}_{k|k-1}\right) \tag{26}$$

And the prediction of future augmented states is obtained by:

$$\begin{bmatrix} \hat{x}_{k+1|k} \\ \hat{\eta}_{k+1|k} \end{bmatrix} = \begin{bmatrix} A & E \\ 0 & I \end{bmatrix} \begin{bmatrix} \hat{x}_{k|k} \\ \hat{\eta}_{k|k} \end{bmatrix} + \begin{bmatrix} B \\ 0 \end{bmatrix} u_k + \begin{bmatrix} E \\ 0 \end{bmatrix} d_k \tag{27}$$

Equations (26) and (27) are the measurement update and time update state of a Kalman filter used to introduce an integrator element into the control. The two equations can be written in a condensed form:

$$\begin{bmatrix} \hat{x}_{k+1|k} \\ \hat{\eta}_{k+1|k} \end{bmatrix} = \tilde{A}\begin{bmatrix} \hat{x}_{k|k-1} \\ \hat{\eta}_{k|k-1} \end{bmatrix} + \begin{bmatrix} B \\ 0 \end{bmatrix} u_k + \begin{bmatrix} E \\ 0 \end{bmatrix} d_k + \tilde{A}K\left(z_k - C\hat{x}_{k|k-1}\right) \tag{28}$$

Where the Kalman filter gain is computed offline according to:

$$K = P\tilde{C}^{'}\left(\tilde{C}P\tilde{C}^{'} + R_v\right)^{-1} \tag{29}$$

And P is the unique symmetric positive semidefinite solution of the discrete algebraic Riccati equation:

$$P = \tilde{A}P\tilde{A}^T + Q - \tilde{A}P\tilde{C}^T\left(\tilde{C}P\tilde{C}^T + R_V\right)^{-1}CPA^T \tag{30}$$

5 Simulation and Experiment

For the simulation and experiment, the augmented model from (24) is used with a prediction horizon of 50 steps of 10 minutes and parameters from Table 1.

For the Kalman filter implementation the following values were chosen for the covariance matrices: R_v = [0.01], Q_w = [0.015], Q_{xi} = [1 0; 0 1].

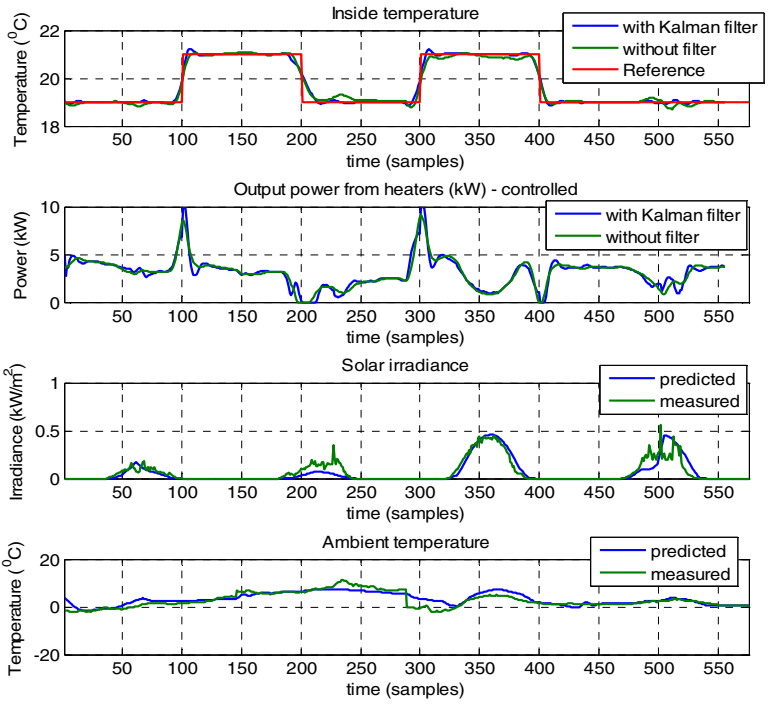

Fig. 2. Simulation results considering continuous consumption of the electrical heaters Φ_{normal}=0.0195 and $\Phi_{observer}$=0.0165

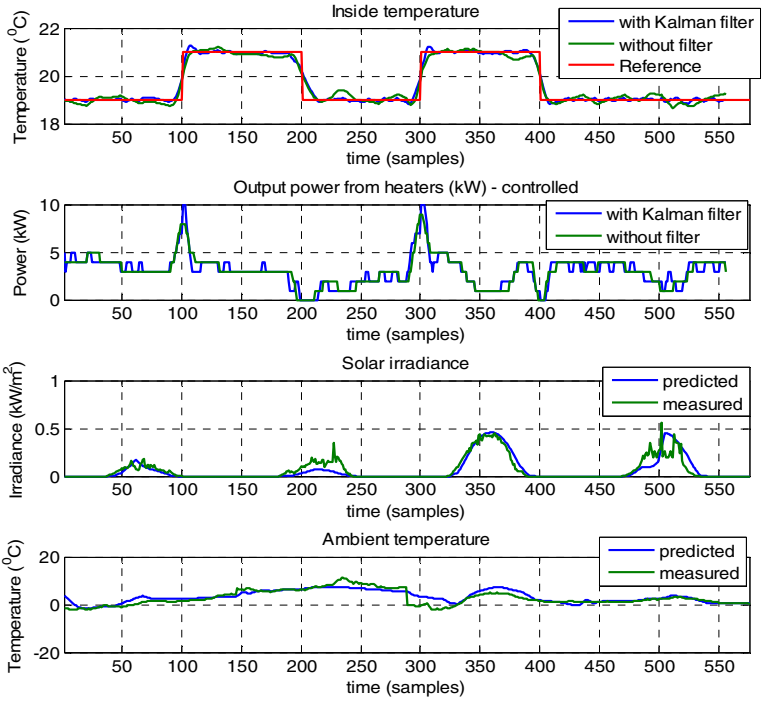

Fig. 3. Simulation results considering 1kW steps consumption of the electrical heaters; Φ_{normal}=0.0252 and $\Phi_{observer}$=0.0174

The simulation presented in Fig. 2 was performed by considering real weather data taken from the SYSLAB facility: historical 24 hour prediction data set for four days in May and the historical measured data for the same period of time.

The constraints on the manipulated variable, inside temperature are set to be 20° and 25° C. The limits on the manipulated variable, the electrical heaters output power, is set to U_{min}=0 and U_{max}=10.

In both simulation, as seen in the "Inside temperature" plot, are represented three variables: the prescribed reference, the inside temperature when using for the optimization problem the system from (2), which presents offset and the augmented system (24) for offset free solution by using the Kalman filter to estimate the initial states x_0. For comparison reasons, a cost function was introduced:

$$\overline{\Phi} = \frac{1}{2(T_f - T_0)} \sum_{t=T_0}^{T_f} (z_k - r_k)^2 \tag{31}$$

The solution of the optimization problem is a real number. In order to operate the ten 1kW electrical heaters, this solution was rounded to the closest integer to the actual solution. The results by using a more realistic 1kW step power consumption of the electrical heaters are presented in Fig. 3.

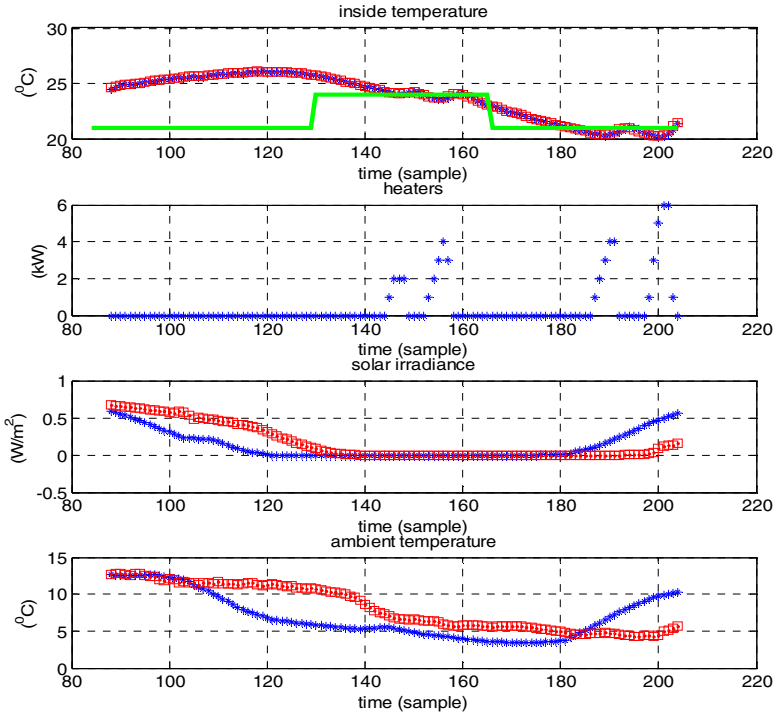

Fig. 4. Experimental results

Even if in the second simulation the performance is lower for both MPC solutions compared to the first simulation, the usage of the observer can be well justified as $\Delta\Phi_{normal}$= 0.0057 and $\Delta\Phi_{obsever}$= 0.0009 and will be more meaningful in the case additional unknown disturbances affect the system.

A validation experiment was conducted using the MPC developed in Matlab. Using the described MPC, and online measurements of the inside temperature, solar irradiance and ambient temperature the controlled variable (inside temperature) was tracking the prescribed trajectory, as seen in Fig. 4.

Some additional errors and perturbations were observed: the inside temperature was considered as the average of the temperature inside the eight rooms the electrical heaters had different output powers and the system had a very simplified model. Another issue was the relatively hot and sunny weather which interfered with the experiment, the amount of energy from the exterior being enough to heat the house to the desired temperature and even to exceed it.

The MPC developed in this paper can affect the controlled variable in a single way: it can only increase the inside temperature by increasing the output power of the heaters and not to cool down the temperature since it does not use any air conditioning unit. This phenomenon is clear in the first part of the experiment, when the inside of the building is overheated by the weather during the day.

As it can be seen from fig. 4, at the end of the first day (sample 126 is 9 PM), the temperature inside the house is 26 degrees and the MPC can operate only during the night to track the prescribed values.

The controller of this process can affect only one direction of the system, that is the MPC cab only increase the temperature by turning heaters on and cannot take any action in lowering it. The decrease in temperature must come naturally, and the MPC can only set all the heaters to off.

6 Conclusions

The controlled variable of the MPC presents offset free by using augmented state space model, considering an additional state for the two disturbances of the system, the solar irradiance and the ambient temperature.

The influence of using an observer to estimate the unmeasured disturbances that affect the process is reflected in the performance cost comparing the evolution of the system for the two cases: when using an observer and when the disturbance is not considered by the controller.

The simulated MPC algorithm was validated through experiments using a 125 square meter building and predicted and measured weather data.

The MPC presented in this paper it is a “one sided control” since it can influence only the increase of the inside temperature, by the use of the electric heaters and not the cooling of the building. The cooling of the building comes as a natural factor, influence only by the disturbances.

Acknowledgments. This work was partially supported by the strategic grant POSDRU/88/1.5/S/50783 (2009) of the Ministry of Labor, Family and Social Protection, Romania, co-financed by the European Social Fund – Investing in People.

References

1. European Commission eurostat - Energy Consumption Statistics, `http://epp.eurostat.ec.europa.eu/statistics_explained/index.php/Consumption_of_energy`
2. Oldewurtel, F., Parisio, A., Jones, C.N., Morari, M., Gyalistras, D., Gwerder, M., Stauch, V., Lehmann, B., Wirth, K.: Energy Efficient Building Climate Control using Stochastic Model Predictive Control and Weather Predictions. In: America Control Conference, pp. 5100–5105 (2010)
3. Balan, R., Stan, S.D., Lapusan, C.: A Model Based Predictive Control Algorithm for Building Temperature Control. In: 3rd IEEE International Conference on Digital Ecosystems and Technologies, pp. 540–545. IEEE Press (2009)
4. Halvgaard, R., Niels, K.P., Madsen, H., Jørgensen, J.B.: Economic Model Predictive Control for Building Climate Control in a Smart Grid. In: IEEE PES Innovative Smart Grid Technologies (ISGT). IEEE Press (2012)

5. Liu, S., Henze, G.P.: Impact of Modeling Accuracy on Predictive Optimal Control of Active and Passive Building Thermal Storage Inventory. ASHRAE Transactions, 151–163 (2004)
6. Prívara, S., Široký, J., Ferkl, L., Cigler, J.: Model predictive control of a building heating system: The first experience. Energy & Buildings 43(2-3), 564–572 (2011)
7. Erickson, V., Lin, Y., Kamthe, A., Rohini, B., Surana, A., Cerpa, A., Sohn, M., Narayanan, S.: Energy efficient building environment control strategies using real-time occupancy measurements. In: 1st ACM Workshop Embedded Sensing Systems for Energy Efficiency in Buildings, pp. 19–24 (2009)
8. Hazyuk, I., Ghiaus, C., Penhouet, D.: Optimal temperature control of intermittently heated buildings using Model Predictive Control: Part II Control Algorithm. Building and Environment Journal, 388–394 (2012)
9. Bacher, P., Thavlov, A., Madsen, H.: Models for Energy Performance Analysis. Technical report, Informatics and Mathematical Modeling Technical University of Denmark (2010)
10. Pannochia, G., Rawlings, J.: Disturbance Models for Offset-Free Model Predictive Control. AIChE Journal 49(2), 426–437 (2003)
11. Huusom, J.K., Poulsen, N.K., Jørgensen, S.B., Jørgensen, J.B.: Tuning of Methods for Offset Free MPC based on ARX Model Representations. In: Proceedings of the American Control Conference, pp. 2255–2360 (2010)

Optimization of the Power Transfer Control between the Ports of a Double Bridge DC – DC Power Converter Type Gyrator

Ildiko Tatai and Marian Greconici

Department of Physical Foundation of Engineering, Politehnica University of Timisoara, Timisoara, Romania
{ildiko.tatai,marian.greconici}@et.upt.ro

Abstract. The paper refers to a double - bridge dc - dc power converter which behaves as a gyrator. The paper points out a simple method to control the power transfer from one port to the other of this gyrator, by modifying the delay between the switching bridges. This power transfer control is analyzed.

Keywords: gyrator, dc-dc power converter, power transfer.

1 Introduction

The ideal gyrator was introduced in literature by B.D.H. Tellegen, to simplify the electrical circuits synthesis [1].

Although Tellegen considered the gyrator as a circuit element. Since the gyrator concept was introduced, a large development in the gyrator implementation direction has been produced, i.e. implementation of a circuit.

Two gyrator categories are distinguished: the first use electronic devices and the second type is based on physical effects.

The first built gyrator type was the Faraday effect based gyrator, used in microwaves applications [2]. The gyrator based on physical effects category includes the Hall effect based gyrator [3]. Because of his resistive character, this type of gyrators can work in a large frequency range, but their technical applications are limited, because of high losses and small values of current-tension conversion factor.

The gyrator implementation solutions using electronical components have evolved step by step with the development of active semiconductor device technology. The development of semiconductor devices, the integrated circuits, simplified the gyrators construction, improving their performances. Nowadays the gyrators can be viewed to another scale, as circuit elements, fulfilling the Tellegen wish [4].

In power electronics are recently mentioned applications of gyrators [5]. For a large category of dc-dc converters, the mean values of the currents and voltages on a work cycle regarding to the two gyrator ports satisfy the specific relations of a gyrator [6], [7], [8]. Such a gyrator is the double bridge dc-dc power converter. It consist of two switching bridges, linked by a reciprocal two-port network.

In this paper the two-port network parameter expressions are determined for this structure, according to delay between the switching bridges. The effect of the T_D time delay between the switching bridges over the power transfer from one port to the other of this gyrator is analyzed.

V.E. Balas et al. (Eds.): Soft Computing Applications, AISC 195, pp. 209–216.
springerlink.com

2 The Ideal Gyrator

The ideal gyrator as it was defined by Tellegen is an antireciprocal, resistive, linear and lossless two-port network, with the circuit symbol shown in Fig.1.

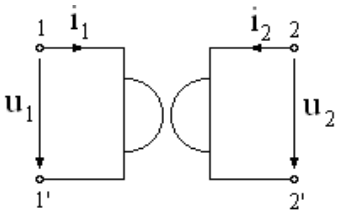

Fig. 1. Circuit symbol for a gyrator

The ideal gyrator converts the current at one port in to a voltage and reverse:

$$\begin{aligned} u_1 &= R_{12} i_2 \\ u_2 &= R_{21} i_1 \end{aligned} \tag{1}$$

$$\begin{aligned} i_1 &= G_{12} u_2 \\ i_2 &= G_{21} u_1 \end{aligned} \tag{1'}$$

Equations (1) and (1') are the constitutive equations of the ideal gyrator.

A property of the gyrator is that the sum of the powers at both ports is zero

$$u_1 i_1 + u_2 i_2 = 0\,, \tag{2}$$

the passive rule being assumed at both ports. That means the power supplied at one port will be fully recovered at the other port (the so - called POPI property – Power Output equals Power Input [9]).

From (1), (1') and (2) conditions result that the transfer resistances, respectively the transfer conductance of this circuit elements are equal and with opposite sign: $R_{12} = -R_{21}$ respectively $G_{12} = -G_{21}$.

3 Double Bridge DC-DC Power Converter

In some applications the energy transfer control between two physical subsystems is necessary (for example two dc energy subsystems). This is possible using a reciprocal two-port network structure inserted between two switching bridges [6], [10], [11], according to the Fig.2. The power transfer from one port to the other is controlled by modifying the delay between the switching bridges.

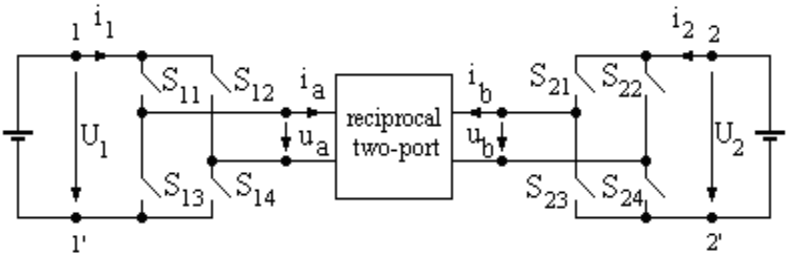

Fig. 2. Schematics of the double bridge dc-dc converter

Assuming that the switches (S_{11} – S_{14}, respectively S_{21} –S_{24}) are ideal, the both ports of the two-port network are fed with rectangular voltages with magnitude U_1, respectively U_2, delayed by T_D (Fig.3).

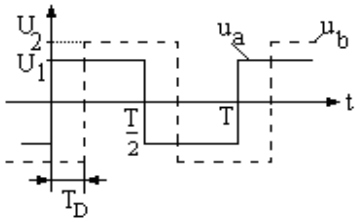

Fig. 3. The rectangular voltages to the ports of the reciprocal two-port network

The analysis of this type of converter behavior as a gyrator is presented in [12], [13] and is based on the Fourier spectral decomposition of the rectangular voltage waveform, determining the i_a a and i_b currents expression depending on the two-port parameters. The i_1 and i_2 currents at the converter ports can be expressed in term of i_a and i_b, resulting the mean currents I_1 and I_2 integrating over a period T:

$$\begin{aligned} I_1 &= G_{11}U_1 + G_{12}U_2 \\ I_2 &= G_{21}U_1 + G_{22}U_2, \end{aligned} \tag{3}$$

where

$$G_{11} = \frac{8}{\pi^2} \sum_{k=1,3,\ldots} \frac{1}{k^2} G_{11}^{(k)} \tag{4}$$

$$G_{12} = \frac{8}{\pi^2} \sum_{k=1,3,\ldots} \frac{1}{k^2} (G_{12}^{(k)} \cos k\omega T_D - B_{12}^{(k)} \sin k\omega T_D) \tag{5}$$

$$G_{21} = \frac{8}{\pi^2} \sum_{k=1,3,\ldots} \frac{1}{k^2} (G_{21}^{(k)} \cos k\omega T_D + B_{21}^{(k)} \sin k\omega T_D) \tag{6}$$

$$G_{22} = \frac{8}{\pi^2} \sum_{k=1,3,\ldots} \frac{1}{k^2} G_{22}^{(k)} \tag{7}$$

The parameters of the two-port network (terminals 11', 22') depend on the internal reciprocal two-port parameters, the switching frequency and the time delay between the switching bridges (T_D).

If the internal two-port is reciprocal ($G_{12}^{(k)} = G_{21}^{(k)}$, $B_{12}^{(k)} = B_{21}^{(k)}$) and lossless ($G_{11}^{(k)} = G_{22}^{(k)} = 0$), the converter parameter expressions are:

$$G_{11} = 0 \tag{8}$$

$$G_{12} = -\frac{8}{\pi} \sum_{k=1,3,\ldots}^{\infty} \frac{1}{k^2} B_{12}^{(k)} \sin k\omega T_D \tag{9}$$

$$G_{21} = \frac{8}{\pi} \sum_{k=1,3,\ldots}^{\infty} \frac{1}{k^2} B_{12}^{(k)} \sin k\omega T_D \tag{10}$$

$$G_{22} = 0\,, \tag{11}$$

which means the converter is a ideal gyrator, for any value of T_D, because $G_{12} = -G_{21}$. If the internal two-port is a RLC reciprocal two-port, for $T_D = T/4$, the (4)-(7) expressions becomes:

$$G_{11} = \frac{8}{\pi^2} \sum_{k=1,3,\ldots} \frac{1}{k^2} G_{11}^{(k)} \tag{12}$$

$$G_{12} = -\frac{8}{\pi} \sum_{k=1,3,\ldots}^{\infty} \frac{1}{k^2} B_{12}^{(k)} \sin k\omega \frac{\pi}{2} \tag{13}$$

$$G_{21} = \frac{8}{\pi} \sum_{k=1,3,\ldots}^{\infty} \frac{1}{k^2} B_{12}^{(k)} \sin k\omega \frac{\pi}{2} \tag{14}$$

$$G_{22} = \frac{8}{\pi^2} \sum_{k=1,3,\ldots} \frac{1}{k^2} G_{22}^{(k)}\,. \tag{15}$$

In this case the converter is a lossy gyrator.

4 The Power Transfer Analysis

Assuming that the internal two-port is reciprocal, symmetrical and lossless, the dc powers at the gyrator ports can be expressed as:

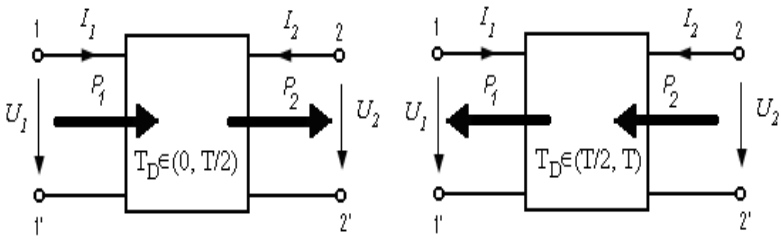

Fig. 4. The power transfer

$$P_1 = U_1 I_1 = G_{12} U_1 U_2 = U_1 U_2 \frac{8}{\pi} \sum_{k=1,3,\ldots}^{\infty} \frac{1}{k^2} \left(-B_{12}^{(k)} \sin k\omega T_D \right)$$
$$P_2 = U_2 I_2 = G_{21} U_1 U_2 = U_1 U_2 \frac{8}{\pi} \sum_{k=1,3,\ldots}^{\infty} \frac{1}{k^2} \left(B_{12}^{(k)} \sin k\omega T_D \right). \quad (16)$$

The sign of the two powers depend on the sign of the transfer conductances, that is on time delay T_D, that means the direction of power transfer can be easily controlled electronically by time delay T_D. If T_D (0, T/2) the power is transferred from the port 1 to the port 2, and if T_D (T/2, T) the power is transferred in the opposite direction. For $T_D = 0$, $T_D = T/2$ and $T_D = T$ the power at both ports are zero, is no power transfer between ports.

If $T_D = T/4$ then $G_{12} = -\frac{8}{\pi} \sum_{k=1,3,\ldots}^{\infty} \frac{1}{k^2} B_{12}^{(k)}$ and $G_{21} = -G_{12}$. Also for $T_D = 3T/4$ the G_{12} and G_{21} parameters changes its sign, so the power transfer direction is reversed. For this two cases the transferred power is maximum.

From (16) we see that not only the power direction can be modified but its size as well.

5 Simulation Results

Considering a reciprocal, symmetrical and lossless internal two-port network (Fig. 5), the simulation results for power transfer are presented below. At the both ports of the gyrator the voltages are $U_1 = U_2 = 4V$, and the period is T = 10ms.

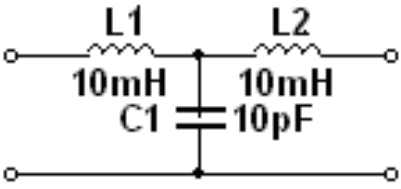

Fig. 5. The internal two-port network

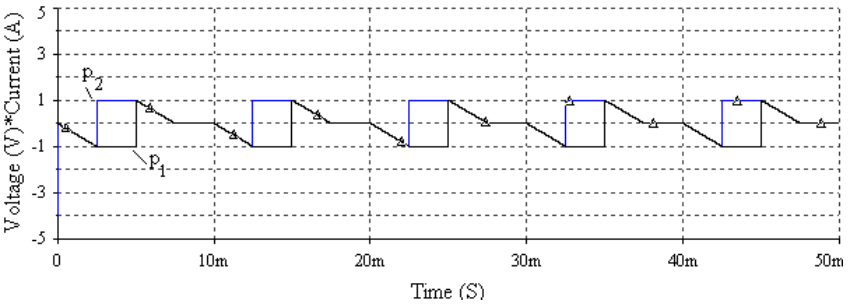

Fig. 6. The maximum power transfer from the port 1 to the port 2

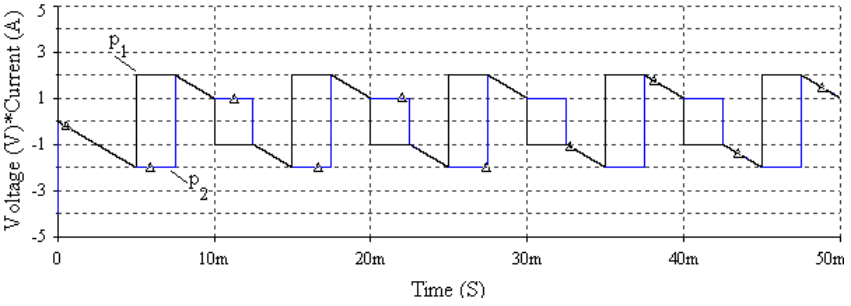

Fig. 7. The maximum power transfer from the port 2 to the port 1

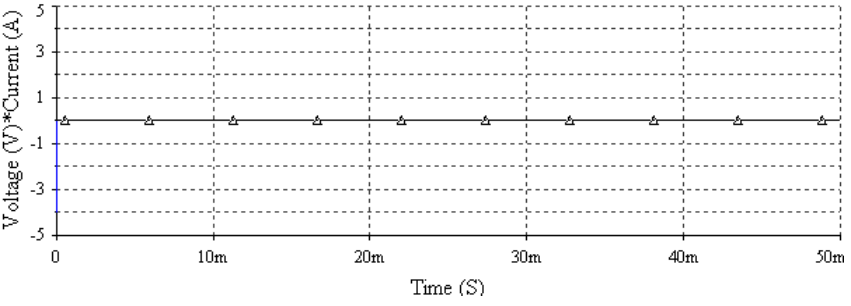

Fig. 8. No power transfer between ports for $T_D = 0$

If T_D (0, T/2) the power is transferred from the port 1 to the port 2. The maximum power transfer occurs when the time delay between the switching bridges is $T_D = T/4 = 2.5$ ms (Fig. 6).

If T_D (T/2, T) the power is transferred from the port 2 to the port 1. In this case the maximum power transfer occurs when $T_D = 3T/4 = 7.5$ ms (Fig. 7).

Is no power transfer between the ports if $T_D = 0$, $T_D = T/2$ and $T_D = T$, the power at both ports are zero (Fig.8, Fig.9, Fig. 10 respectively).

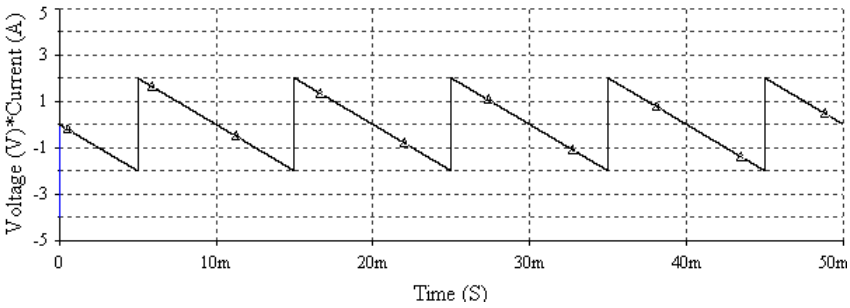

Fig. 9. No power transfer between ports for $T_D = T/2$

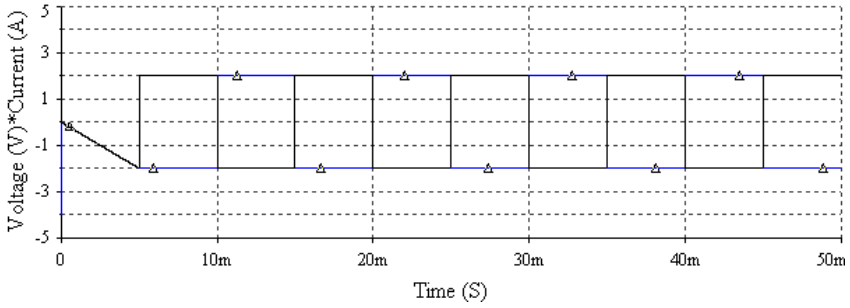

Fig. 10. No power transfer between ports for $T_D = T$

For the last two cases ($T_D = T/2$ and $T_D = T$) as we see in Fig. 9 and Fig.10 the powers at both ports of the gyrator are zero over a period T.

We can see that the optimization of the power transfer control between the ports is realized, by modifying the gyration conductance, through switching time delay T_D (properly chosen) between the bridges of a commutation–operated double–bridge DC-DC converter.

References

1. Tellegen, B.D.H.: The gyrator – a new electric network element. Phylips Res. Rep. 3, 81–101 (1948)
2. Hogan, C.L.: The Ferromagnetic Faraday Effect at Microwave Frequencies and its Applications-The Microwave Gyrators. The Bell Systems Technical Journal XXXI(1), 1–31 (1952)
3. Şora, C.: Introduction in the study of Hall generator. Ed. Academiei (1969) (in Romanian)
4. Voorman, J.O.: The gyrator as a monolithic circuit in electronic systems, Ph.D.Thesis, Univ. of Nijmen, Holland (1977)
5. Singer, S.: Gyrator application in power processing circuits. IEEE Trans. on Ind. Elec. IE(3), 313–318 (1987)
6. Ehsani, M., Husain, I., Bilgic, M.O.: Power converter as natural gyrators. IEEE Trans. on Circuits and Syst. 40(12), 946–949 (1993)

7. Shmilovitz, D., Yaron, I., Singer, S.: Transmission-Line-Based Gyrator. IEEE Trans. on Circuits and Syst. 45(4), 428–433 (1998)
8. Pastor, A.C., et al.: Analysis and design of power gyrators in sliding-mode operation. IEEE Proc. Electric Power Appl. 152(4), 821–826 (2005)
9. Singer, S., Erickson, R.W.: Canonical modeling of power processing circuits based on the POPI concept. IEEE Trans. on Power Electronics 7(1), 37–43 (1992)
10. Hărăguş, Ş.: Two-port dc parameters of a double bridge dc-dc power converter. Bul. Şt. al Univ. "Politehnica" Timişoara (Romania), Tom. 44(58), fasc. 2, 11–18 (1999)
11. Hărăguş, Ş., Toader, D., Tatai, I.: Gyrators in electrical power management systems. In: The 7th International Conference on Renewable Sources and Environmental Electro-Technologies, RSEE 2008, Oradea, Romania, pp. 64–69 (2008)
12. Hărăguş, Ş.: The analysis of gyrator – like behavior of a double bridge dc – dc power converter. Bul. Şt. al Univ. "Politehnica" Timişoara (Romania), Tom. 43(57), fasc. 2, 35–40 (1998)
13. Hărăguş, Ş.: Some aspects concerning the gyrator-like behavior of controlled double-bridge power converter. Analele Univ. Oradea, Fasc. Electrotehnica, 27 (1999)

Maximization of the Energy and Flattening of Fluctuations for the Power Generated into the Network at a Wind Driven Electro Energetic System

Ovidiu Gana, Octavian Prostean, and Marius Babescu

University Politehnica, Timişoara, Romania
gana_anaq2@yahoo.com, Octavian.prostean@aut.upt.ro,
marius.babescu@et.upt.ro

Abstract. This paper proposes for an optimal functioning of an electro energetically wind system an original method. A mathematical model is used for analyzing energy characteristics of the electric power generation system. The system is composed from a synchronous generator with permanent magnet excitation from the wind turbine, a synchronous generator with permanent magnets (WT+PMSG), an active rectifier and inverter with PΩM, an electric accumulator and a super capacitor.

This paper is trying to solve fundamental problems of the WT measuring the wind speed, on given time intervals. Problems are related to the determination of the generator speed in the way that the captivated energy to be maximal. To reach this, a correlation between the load of the generator and the variation of kinetic energy of the moving rotation masses need to be made; fluctuations of the power given in the standard national network need to be smoothed; algorithms are needed to control the active rectifier, inverter and DC+DC for a variable speed wind turbine; analytical relations are needed for a constant generation of voltage and power in the system; fluctuations need to be loaded in the electric accumulator (EA) and super capacitor (SC).

Recommendations are given for choosing control algorithms and structural circuits for a wind power system at a variable speed of the wind turbine (WT).

Keywords: wind turbine, mathematical model, variable power on the turbine, electric accumulators, constant power in the system, super capacitors, power control.

1 Introduction

Most of the papers [16-21] analyze the evaluation of the power variations in time. Developing an automatic controller for the wind system is a very complex job because the fluctuations of the wind speed are unpredictable in time [1, 4, 7], maximum and minimum values for the wind speed are significant and controller needs to be able to handle this variations [2, 3], to acquire maximum wind energy. A technical and economical effort is imposed [5, 6].

V.E. Balas et al. (Eds.): Soft Computing Applications, AISC 195, pp. 217–236.
springerlink.com

From the energy point of view it is impossible to function in the optimal zone because momentum of inertia is large [8, 9], and this makes the speed of the group WT+PMSG to be unable to follow the optimal prescribed values (maximum power points). To function at the maximum power points is necessary that the wind speed to have slow variations in time and the equivalent momentum of inertia to have a low value.

Wind installations with a power larger than 1 MW cannot realize the above conditions because the wind is varying significantly in time [10, 15].

When the generator PMSG is connected to the national energy network (with given frequency and voltage) power oscillations can cause instability for the electro energetic system [11, 13]. Tuning the regulators for this system is different than the classical industrial applications [12, 14] (control for movements, power, etc.), because the wind speed has an unpredictable variation in time and so the constants of the regulator must be adapted to the new meteorological conditions (variation of the wind speed in time).

Considering the above facts, appears the problem of finding the value for the wind speed to obtain a maximum electrical energy from the system (WT+PMSG) on a long time interval (days, hours) until the wind speed decreases under the functional working speed of 3m/s.

Acquiring the maximum wind energy makes the wind turbine to work optimal and to give maximum energy.

2 Mathematical Models for the Turbine and Generator

This chapter proposes mathematical models used later in calculations for the turbine and generator.

2.1 Mathematical Model for the Wind Turbine (WT)

An original model for the wind turbine that allows estimation for the reference speed ω_{ref} was considered. Components of the generator load are calculated with the value of ω_{ref} (one given by the wind, and one given by the kinetic energy variations).

Horizontal axis wind turbines (HAWT) are most popular and most preferred. The maximum power these turbines can develop depends of the cubed wind speed (V) (1)

$$P_{max} = \frac{1}{2}\rho A V^3 = \omega_{WT} \cdot \omega \tag{1}$$

Where ω is angular speed on the wind turbine axis, ρ is air density, A is circle surface described by the blades of the WT and Ω_{WT} is couple of WT.

Every wind system which produces electrical energy has the driving strategy to assume functioning in the points P_K, appropriate to the maximum power.

Maximum power P that a wind turbine can develop at the speed V depends approximately square of the rotor angular speed ω, like in the Fig. 1.

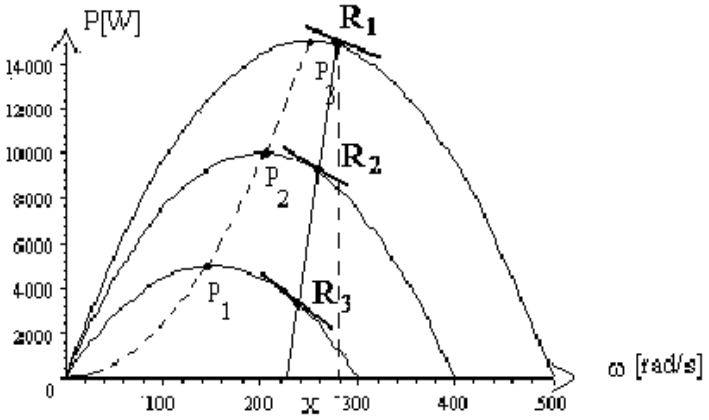

Fig. 1. Set of maximum turbine power curves related with generator speed for different wind velocities

Ideal maximum points P_1, P_2, P_3 are corresponding to the wind speeds V_1, V_2 and V_3, respectively rotor angular speeds ω_1^*, ω_2^* and ω_3^*. Real functioning points are in the stable zone R_1, R_2, R_3.

Keeping in mind a linear mechanical characteristic, in the zone where the wind turbine is functioning ,the dependence of the couple to the speed of wind can be written in the equation (2):

$$M_{WT} = aV^b\omega + cV^d \tag{2}$$

Coefficients that depends of the turbine geometry are extracted from the turbine datasheet and they are marked a, b, c, d (Fig. 2).

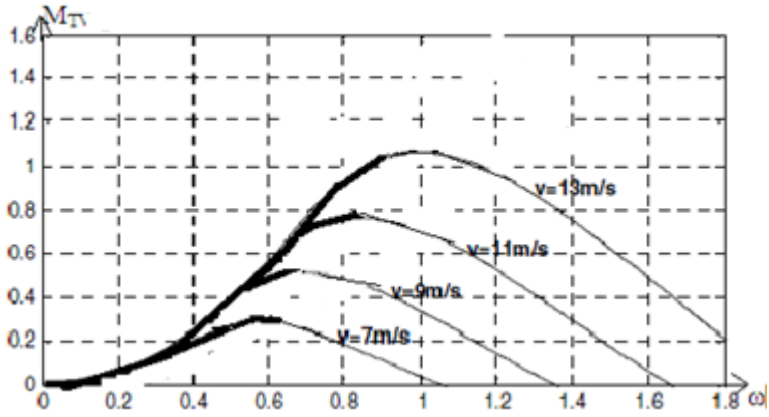

Fig. 2. Turbine characteristic given in the turbine datasheet

Experimentally obtained mechanical characteristics of the wind turbine WT [16-21] and determination of the wind turbine coefficients a, b, c, d can be seen in Fig. 3.

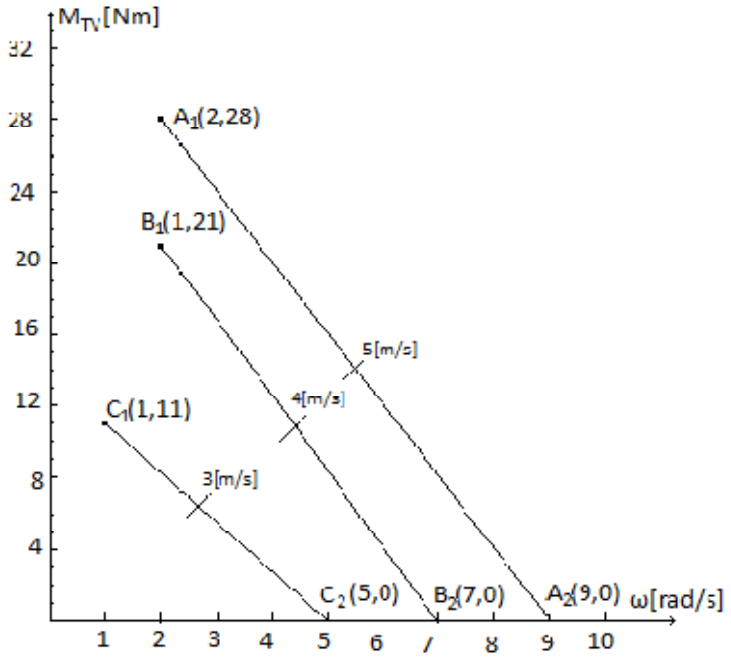

Fig. 3. Representation of the coefficients on the mechanical characteristic of the wind turbine

Writing the relation (2) for two wind speeds V_1= 5 m/s and V_2= 4 m/s in four functioning points $A_1(2,28)$, $A_2(9,0)$ for V_1 = 5 m/s and $B_1(1,21)$, $B_2(7,0)$ for V_1 = 4 m/s results the equation (3) and so results the wind turbine mechanical characteristic (4)

$$\begin{cases} 28 = a \cdot 5^b 2 + c5^d \\ 0 = a \cdot 5^b 9 + c5^d \\ 21 = a \cdot 45^b 1 + c4^d \\ 28 = a \cdot 4^b 7 + c4^d \end{cases} \begin{cases} a = -1.5268 \\ b = 0.59841 \\ c = 2.2430 \\ d = 1.7247 \end{cases} \tag{3}$$

$$\omega_{WT} = -1.5268V^{0.59841} \cdot \omega + 2.243V^{1.7247} \tag{4}$$

Verifying this characteristic for the wind speed V= 3 m/s in the points $C_1(1,11)$, $C_2(5,0)$ for point $C_1(1,11)$ is obtained (5) and for point $C_2(5,0)$ is obtained (6).

$$\begin{gathered} \omega_{WT} = -1.5268V^{0.59841} \cdot 3^{0.59841} \cdot 1 + 2.243 \cdot 3^{1.7247} \\ \omega_{WT} = 11.0972 \text{ (raported } to \text{ } 11\ Nm\text{)} \end{gathered} \tag{5}$$

$$\omega_{WT} = -1.5268V^{0.59841} \cdot 3^{0.59841} \cdot 5 + 2.243 \cdot 3^{1.7247}$$
$$\omega_{WT} = 0.18618 \text{ (raported } to\ 0\ Nm) \tag{6}$$

At large wind speeds only a small difference is observed and this guarantees the usage of the following base equation (4) for the mechanical characteristic.

Equation (8) presents a simplified form for the mechanical characteristic equation (4).

$$\omega_{WT} = -1.5V^{0.6} \cdot 3^{0.6} \cdot 1 + 2.25 \cdot 3^{1.8} \tag{7}$$

At a transmission ratio of 314/20 reduction of the couple ΩWT at the axis of the generator, is done by transformation $\omega_{WT} \rightarrow 20/314$. ΩWT at the axis of the generator must be multiplied by 20/314.Expression (8) gives the couple developed by WT at generator axis.

$$\omega_{WT} = (-9.5541 \cdot 10^{-2} \cdot V^{0.6} \cdot \omega + 2.25 \cdot V^{1.8}) \cdot \frac{20}{314} \tag{8}$$

Determination of maximum power point

Maximum power point (11) is obtained from the differentiate (9), (10). This confirms that the maximum power depends to the cube of speed.

$$\frac{dP}{d\omega} = \frac{d}{d\omega}(aV^b\omega^2 + cV^d\omega)$$
$$\frac{dP}{d\omega} = 2aV^b\omega + cV^d = 0 \tag{9}$$
$$\omega^* = \frac{-c}{2a} \cdot V^{d-b} = \frac{2.25}{3} \tag{10}$$
$$P_{max} = \omega_{WT}^* \cdot \omega^* = 0.84V^3 \tag{11}$$

The original mathematical model of the wind turbine (WT) [22] allows the determination of the optimal functioning speed to ensure a maximum acquired energy.

2.2 Mathematical Model of the Synchronous Generator (SG)

In dynamic regime SG with excitation in direct current (DC) is characterized in the orthogonal model by the equations (12):

$$\begin{cases} -U\sqrt{3}sinq = R_dI_d + L_d\frac{dI_d}{dt} - \omega L_qI_q + M_E\frac{dI_e}{dt} + M_D\frac{dI_D}{dt} - \omega M_QI_Q \\ -U\sqrt{3}cosq = \omega L_dI_d + R_qI_q + L_q\frac{dI_q}{dt} - \omega M_EI_E + \omega M_DI_D\ M_Q\frac{dI_Q}{dt} \\ U_E = M_E\frac{dI_d}{dt} + R_EI_E + L_E\frac{dI_E}{dt} + M_{ED}\frac{dI_D}{dt} \\ 0 = M_D\frac{dI_d}{dt} + M_{ED}\frac{dI_E}{dt} + R_DI_D + L_D\frac{dI_D}{dt} \\ 0 = M_Q\frac{dI_q}{dt} + R_QI_Q + L_Q\frac{dI_Q}{dt} \\ J\frac{d\omega}{dt} = p_1\left[\left(L_d - L_q\right) + M_EI_qI_E - M_QI_dI_Q + M_DI_qI_D\right] - M_{motor} \end{cases} \tag{12}$$

Parameters for the generator used in (12) are: R_E - resistance of the excitation coil; R_D - resistance of damping coil from d axis; R_Q - resistance of damping coil from q axis; L_D - inductance of damping coil from d axis ;M_{ED} - mutual inductance between excitation coil and D coil ;M_D - mutual inductance between d(stator) coil and D; L_Q - inductance of amortization coil on the q axis; M_Q - mutual inductance between stator inductance q and Q winding;R_1 - resistance of stator coil; L_d – inductance of stator coil on the d axis; L_q - inductance of stator coil on q axis; M_{ED} - mutual inductance between excitation coil and d coil; L_e - inductance of excitation coil.

Synchronous generator with permanent magnets (PMSG) is characterized in the orthogonal model [22] by the equations (13) where ψ_{MP} is permanent magnet flux.

$$\begin{cases} -U\sqrt{3}sinq = R_d I_d + L_d \dfrac{dI_d}{dt} - \omega L_q I_q + M_D \dfrac{dI_D}{dt} - \omega M_Q I_Q \\ -U\sqrt{3}cosq = \omega L_d I_d + R_q I_q + L_q \dfrac{dI_q}{dt} + \omega M_D I_D \; M_Q \dfrac{dI_Q}{dt} + \omega \psi_{MP} \\ 0 = M_D \dfrac{dI_d}{dt} + R_D I_D + L_D \dfrac{dI_D}{dt} \\ 0 = M_Q \dfrac{dI_q}{dt} + R_Q I_Q + L_Q \dfrac{dI_Q}{dt} \\ J\dfrac{d\omega}{dt} = p_1\left[\left(L_d - L_q\right) I_d I_q + I_q \psi_{MP} - M_Q I_d I_Q + M_D I_q I_D\right] - M_{motor} \end{cases} \tag{13}$$

Because of large inertia moments processes are slow. In the current applications of wind systems are used simplified orthogonal models (Fig. 4).

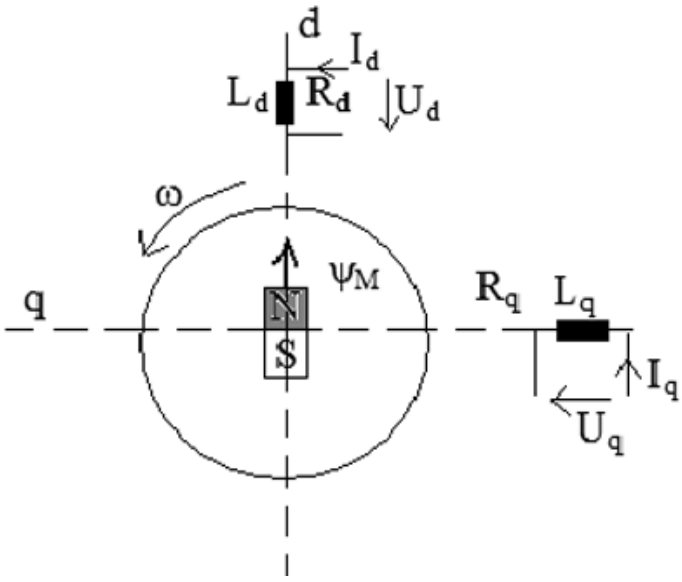

Fig. 4. Simplified orthogonal model of a synchronous generator with permanent magnets (PMSG)

PMSG is using in stationary regime an algebraic system defined by the couple M_{PMSG} (14):

$$\begin{cases} -U\sqrt{3}sinq = R_1 I_d + L_d \frac{dI_d}{dt} - \omega L_q I_q \\ U\sqrt{3}cosq = R_1 I_q + \omega L_d I_{d+} \omega \psi_{MP} \\ M_{PMSG} = J\frac{d\omega}{dt} = p_1(L_d - L_q) I_d I_q + I_q \psi_{MP} \end{cases} \quad (14)$$

3 Controlling the System (WT + PMSG)

Optimal control of a wind system assumes acquiring maximum wind energy even if the wind has large variations in time. This imposes control of the speed and couple at the turbine and adapting the generator load to the wind speed.

Electric generator must get maximum wind energy available in the sampled time interval Δt and energy difference for the kinetic rotation masses.

The connection between the wind turbine (WT), generator (PMSG), converter (R1), converter (I1) , controller (CONTROL) , anemometer (AN) and storage block (EA,SC) are presented in Fig. 5.

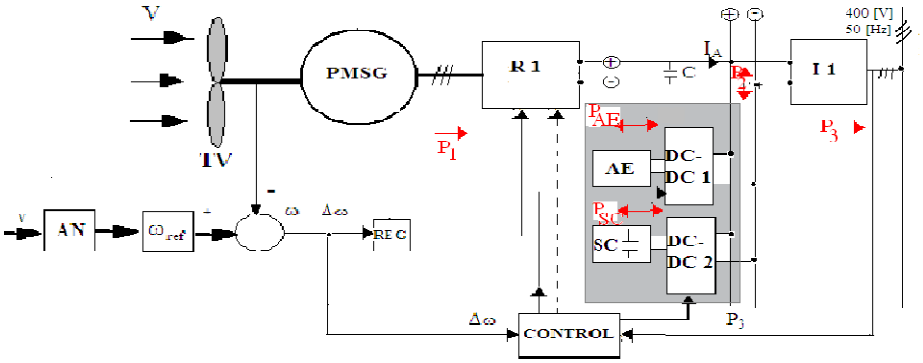

Fig. 5. Control block diagram for the system

Maximum wind energy available, at the wind speed V(t) on the time interval Δt is extracted from imposed speed Ω_{ref}, and variations of kinetic energy from the increasing (decreasing)of the additional load of the electric generator .

Wind system is functioning optimal at its energetically maximum, wind turbine WT is receiving a maximum possible energy on a given time interval, in terms of days.

Driving at maximum power without controlling the wind speed is useless because maximum energy cannot be obtained even if in short time intervals the electric power is maxim, because the supplementary energy is obtained from variation of kinetic energy from moving rotation masses.

Mechanical inertia moments' being high, specific angular speed does not follow the optimal value of the wind speed, which is modified often, and unpredictable.

To obtain a maximum power, large suddenly charging is disturbing significantly system stability by imposing power fluctuations between the turbine and the electric consumer system (electric accumulators (EA) or a standard power network).

The couple expression that the wind turbine (WT) develops reduced to the axis of the generator is introduced in (8):

3.1 Calculation of Speed / Reference Speed ω_{ref}

Reference speed ω_{ref} has a large importance because it allows an optimal driving of the system(WT+PMSG), although is extracting the maximum mechanical energy at a variable wind speed.

By maximizing the mechanical energy Ω_m on a period of time T, ω_{ref} is determinate and from the variation of the wind speed results (14). Considering that ω_{ref} on the time interval t= [0→T], at $d\Omega m / d\omega = 0$ results (18).

$$\Omega_m = \omega_{ref} \int_0^T M_{WT}\, dt \tag{15}$$

$$\Omega_m = \int_0^T M_{WT}\, dt = \int_0^T \left(9.5541 \cdot 10^{-2} \cdot (V)^{0.6} \omega_{ref} + 2.25 \cdot (V)^{1.8}\right) \cdot \frac{20}{314} dt \tag{16}$$

$$\Omega_m = -\omega_{ref}^2 \int_0^T 9.5541 \cdot 10^{-2} \cdot (V)^{0.6}\ \frac{20}{314} dt + \omega_{ref} + \int_0^T \cdot 2.25 \cdot (V)^{1.8} \frac{20}{314} dt \tag{17}$$

$$\omega_{ref} = \frac{\int_0^T 2.25(V)^{1.8} \frac{20}{314} dt}{2 \int_0^T 9.5541 \cdot 10^{-2} \cdot (V)^{0.6} \frac{20}{314} dt} \tag{18}$$

Functioning at optimal angular speed (ω) is realized by estimating the wind speed with an anemometer (AN) and calculating ω_{ref}.

The prescribed angular ω_{ref} is ensured with the controller, but tuning this regulator is a problem because the wind speed is unpredictable in time and for this reason the load estimation at PMSG is preferred for calculation of ω_{ref} and kinetic energy variations of rotation moving masses on the time interval T (example T=600 s), interval in which the load R1 is calculated as in (19).

$$\begin{cases} -RI_d = 1.6I_d - \omega \cdot 0.08 I_q \\ M_G = -0.01 I_d I_q + \psi_M I_q \\ RI_d^2 + RI_q^2 = 120 \cdot I_A \\ \omega = \omega_{ref} \\ \psi_M = 1.3 \\ M_G = -M_{WTequiv} \end{cases} \tag{19}$$

The system (WT+PMSG) is functioning optimally with this load resistance R, getting a maximum wind energy on a time interval T=600 s and gives the power in (20).

$$P_{WT} = \Omega_{WT} \cdot\ \omega_{ref} \tag{20}$$

Power P_{WT} is modifying after a time T in function of the evolution of the wind speed in time.

In the case where mean value of the wind speed is increasing on the time interval T, the power given into network P_3 (represented in Fig.5) is maintained to the initial value of the P_{WT}.

Until the wind speed decreases, until P_3 = ct the excess power (21) is sent to the storage block composed of electric accumulator (EA) and super capacitor (SC) (Fig. 6). After this WT will get energy from the storage block and will be send it into network for compensation.

$$\Delta P_{TV} = P_{TV}(t = T) - P_{TV}(t = 0) \tag{21}$$

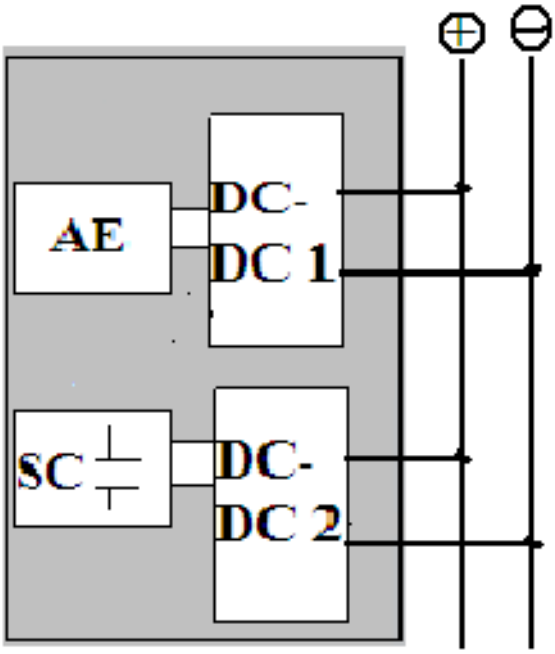

Fig. 6. Electric accumulator and super capacitor block

3.2 Deduction of Related Load from Difference of the Kinetic Energy

At the moment t, optimum function is reached at $\omega = \omega_{ref}$, but ω_{real} is different from ω_{ref} and so the generator should be charged/discharged with the difference of kinetic energy (22):

$$D\Omega = \frac{1}{2}J\left[\left(\Omega_{ref}\right)^2 - \Omega_{ref}^2\right] \tag{22}$$

Angular speed ω_{REAL} is known by direct measurement or by solving the equation of movement.

This difference of energy will be found in the supplementary energy stored in the electric accumulator EA. This is equivalent with increasing or decreasing mechanical power entered in PMSG with quantity $\Delta\Omega_G$ (23).

$$\Delta\Omega_G = \Delta M_G \cdot \omega_{real} \cdot 600 \tag{23}$$

The excess of couple $\Delta\Omega_G$ (24) results from the equality of both energy

$$\Delta\Omega_2 = \Delta\Omega_G. \\ 0.5J\left(\Omega_{ref}\ \right)^2 - \Omega_{real}^2\Big) = dM \cdot \Omega_{real} \cdot 600 \tag{24}$$

On the time interval **T**=600 the mean couple of the wind turbine $\Omega_{WT}$is (25).

$$\Omega_{WT} = \frac{1}{600}\int_t^{t+600}\Big[-9.5541 \cdot 10^{-2} \cdot (8.5 + 1.5sin(0.001t) - \frac{8}{7000}t \\ + sin(0.3t))^{0.6} \cdot \Omega_{ref} \\ + 2.25\left(8.5 + 1.5\sin(0.001t) - \frac{8}{7000}t \right. \\ \left. + sin(0.3t))^{1.8}\right)\frac{20}{314}dt\Big] \tag{25}$$

Equivalent couple of the turbine decreased with ΔM_G (24) is equal with the generator M_G and results the algebraic system (25) from witch the load of the generator PMSG R_{ref} and I_{ref} is obtained.

$$\Omega_{WT\ equiv} = \Omega_{WT} - \Delta\Omega_G \tag{26}$$

4 Simulations for Wind Speeds Variable in Time

The behavior of the system (WT+PMSG), at variable wind speeds is analyzed with mathematical models for the speed of the turbine generator and with an electronic power block .

From the energetic point of view, optimal functioning is ensured by estimating the load based on RPM/reference speed (ω_{ref}) and the variations of kinetic energy of moving rotation masses.

In the time interval T = 600s at load resistance calculated from ω_{ref} (which is based on the wind speed) at variations of kinetic energy the power variation in time is obtained like in the Fig. 7.

For the power P_3, given in the network is considering the smallest value P_3=603.5 W. Power that is grater that this value will be stored in the accumulator block, in the period in which the wind speed is high and will be given in the network in the period when the wind speed decreases.

Controlling the system (WT+PMSG) ensure functioning at a maximum received wind energy for wind speeds variable in time, although the turbine power is following wind speed variations, the given power in the network is constant because power fluctuations are directed to the storage block (EA+SC).

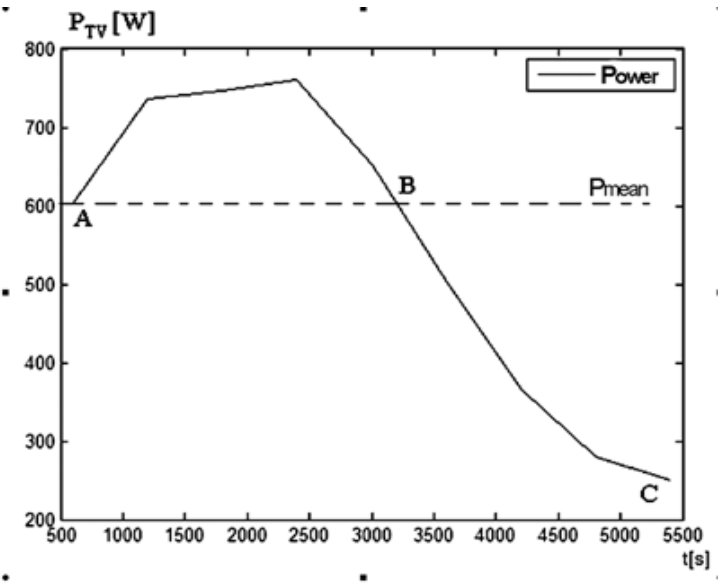

Fig. 7. Wind turbine power variation

Regulation method is based on continuous wind speed variation in time and establishing the load at generator in function at this value of the speed.

Power tops are sent in the battery (EA) and in the super capacitor (SC) by smoothing the available power curve at P_{WT}, so in the energetic system the given power is constant.

For a wind sped of the form (27) the mean value V_{mean} has the expression (28). Variations in time are presented in Fig. 8.

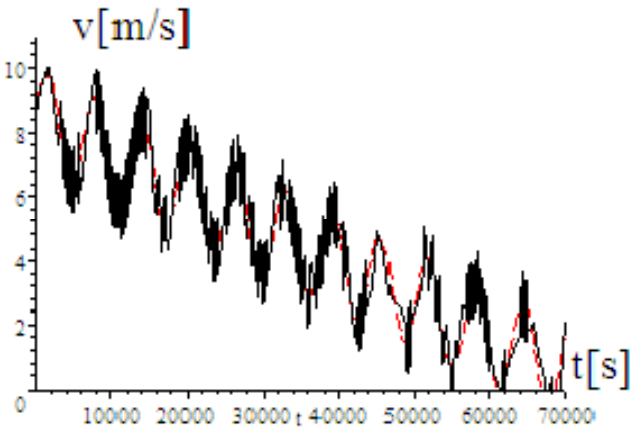

Fig. 8. Wind speed variation

$$V_{(t)} = 8.5 + 1.5\,sin(0.001t) - \frac{8}{70000t} + sin(6t) \tag{27}$$

$$V_{mean} = 8.5 + 1.5\sin(0.001t) - \frac{8}{70000t} \tag{28}$$

Received power from the WT depends of the wind speed cube. K is a constant specific to the used WT

$$P_{TV} = K \cdot V^3 = K(8.5 + 1.5\sin(0.001t) - \frac{8}{70000}t + \sin(6t))^3 \tag{29}$$

Mean power on a time interval t=7000 s (about 2 h), has the value(30).

$$P_{TVmean} = \frac{1}{70000}\int_0^{70000} K \cdot V^3 \cdot dt \tag{30}$$

$$P_{TVmean} = \frac{1}{70000}\int_0^{70000} K \cdot \left[8.5 + 1.5\sin(0.001t) - \frac{8}{70000}t + \sin(6t)\right]^3 \cdot dt = 587.46K \tag{31}$$

In the zone AB from Fig. 7, received turbine (WT) power is larger than the mean value and so it will be stored in the EA and SC, and in the zone of BC the process will be reversed.

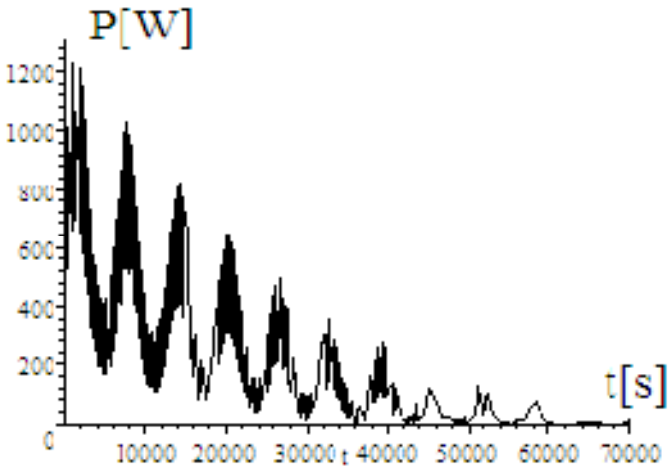

Fig. 9. Power received from the turbine

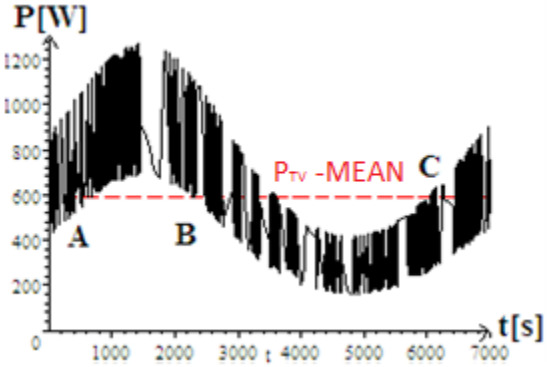

Fig. 10. Mean power value of TV

Statements from above are valid just on an ideal case (mechanical systems with small momentum of inertia). In reality at large inertia moments a functionality in the maximum power points [5,7,9] cannot be assured.

Wind system (WT+PMSG) control method presented below, original and efficient, solve in a realistic mode the optimal functioning at its energetically maximum.

Power received by the WT, at ω =162.41 rad/s = ct, on a time period T=600s, have the value from relation (32).

$$P_{WT} = \Omega_{WT} \cdot \omega = (-9.5541 \cdot 10^2 \cdot (V)^{0.6} \cdot \omega + 2.25(V)^{1.8}) \cdot \frac{20}{314} \cdot \omega$$

$$P_{WT} = -9.5541 \cdot 10^{-2} \left[8.5 + 1.5\sin(0.001t) - \frac{8}{70000}t + \sin(6t))^{0.6} \cdot 162.41 + 2.25(8.5 + 1.5\sin(0.001t) - \frac{8}{70000}t + \sin(6t))^{1.8}\right] \cdot \frac{20}{314} \cdot 162.41 \quad (32)$$

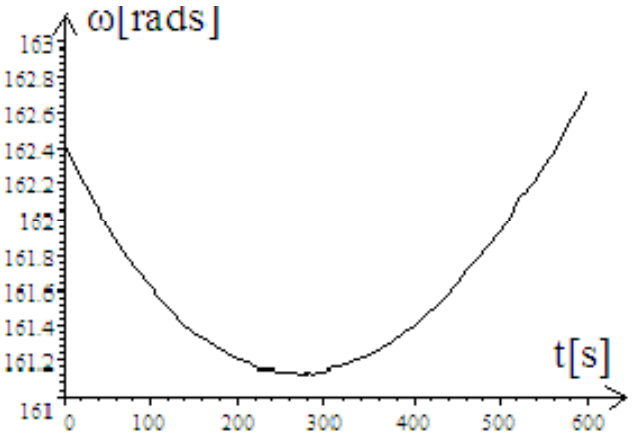

Fig. 11. Evolution of the angular wind speed ω

Generator (PSMG) at load resistance R=70.507 Ω is getting the power P_{PMSG} = 603.5W (33) and with the evolution in time of the angular wind speed ω the equation of movement is obtained (34).

$$P_{PMSG} = M_{PMSG} \cdot \omega = 845\omega[5(R_K) + 8$$
$$\frac{4.0\omega^2 + 625.0(R_K)^2 + 2000R_K + 1600}{(1250(R_K)^2 + 4000R_K + 3200 + 7\omega^2)^2} \cdot \omega = 845 \cdot 162.41(5 \cdot (70.507) + 8)$$

$$\frac{4.0(162.41)^2 + 625.0(70.507)^2 + 2000 \cdot 70.507 + 1600}{(1250(70.507)^2 + 4000 \cdot 70.507 + 3200 + 7 \cdot (162.41)^2)^2} \cdot 162.41 = 603.5\ W \tag{33}$$

$$\begin{cases} -845(5 \cdot R_K) + 8 = M_{PMSG} \cdot \omega \\ \frac{4.0\omega^2+625.0(R_K)^2+2000R_K+1600}{(1250(R_K)^2+4000R_K+3200+7\omega^2)^2} + (9.55 \cdot 10^{-2} \cdot (V_K)^{0.6} \cdot \omega + \\ 2.25\ \cdot (V_K)^{1.8}) \cdot \frac{20}{314} = 50\ \frac{d\omega}{dt} \\ \omega(0) = \omega_1 \end{cases} \tag{34}$$

Generator (PSMG) at load resistance R=70.507Ω and

$V_K = 8.5 + 1.5\sin(0.001t) - \frac{8}{70000t} + \sin(6t)$, results from (32), (33), (34)

$$\begin{cases} -845(70.507) + 8 = M_{PMSG} \cdot \omega \\ \frac{4.0\omega^2+625.0(70.507)^2+2000\cdot70.507+1600}{(1250(70.507)^2+4000\cdot70.507+3200+7\omega^2)^2} + 9.55 \cdot 10^{-2} \cdot \\ \left(8.5 + 1.5\sin(0.001t) - \frac{8}{70000}t + \sin(6t))^{0.6} \cdot \omega \right. \\ \left. +2.25(8.5 + 1.5\sin(0.001t) - \frac{8}{70000}t + \sin(6t))^{1.8} \right) \cdot \frac{20}{314} = 50\ \frac{d\omega}{dt} \\ \omega(0) = 162.41 \end{cases} \tag{35}$$

$$\begin{cases} -RI_d = 1.6I_d - \omega \cdot 0.08I_q \\ M_G = -0.01I_dI_q + \psi_M I_q \\ RI_q = 1.6I_q + \omega \cdot 0.07I_d + \omega\psi_M \\ \omega = 162.41 \\ \psi_M = 1.3 \\ M_G = 3.7159 \end{cases} \tag{36}$$

$$\begin{cases} load\ of\ GSMP: R_1 = 70.507w \\ \omega_1 = 162.41\ rad/s \end{cases} \tag{37}$$

Calculation of angular speed and load resistance was done with the algorithm from Fig. 12.

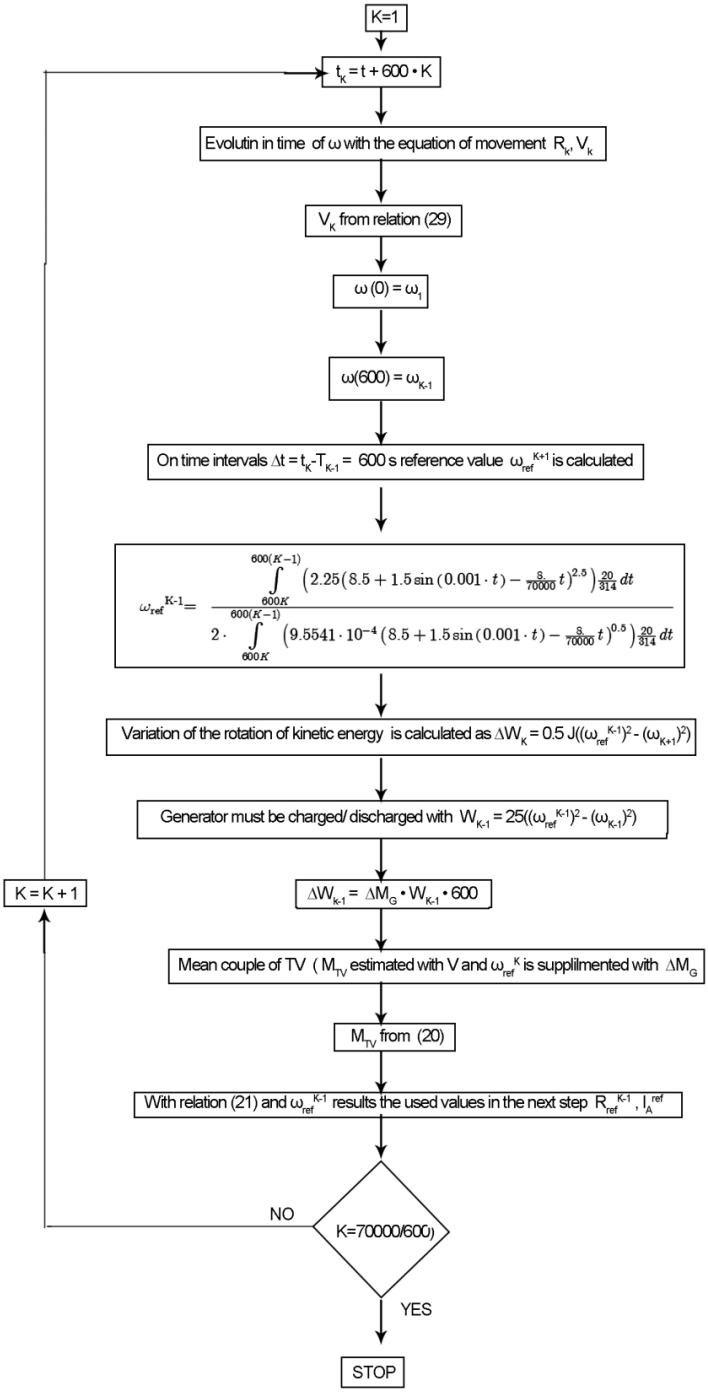

Fig. 12. Calculation algorithm for angular speed and load resistance

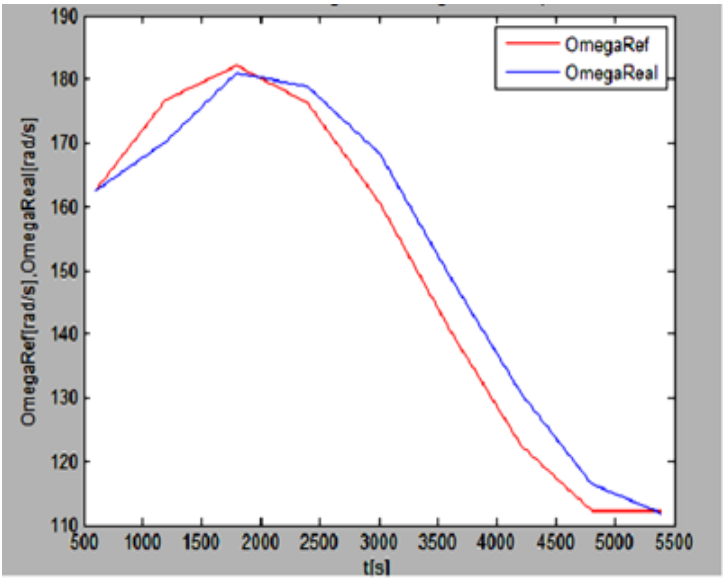

Fig. 13. Variation of ω and ω ref

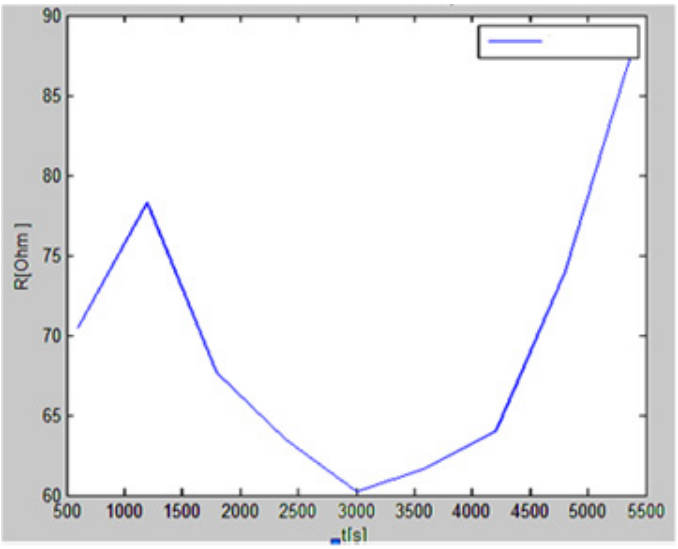

Fig. 14. Variation of resistance

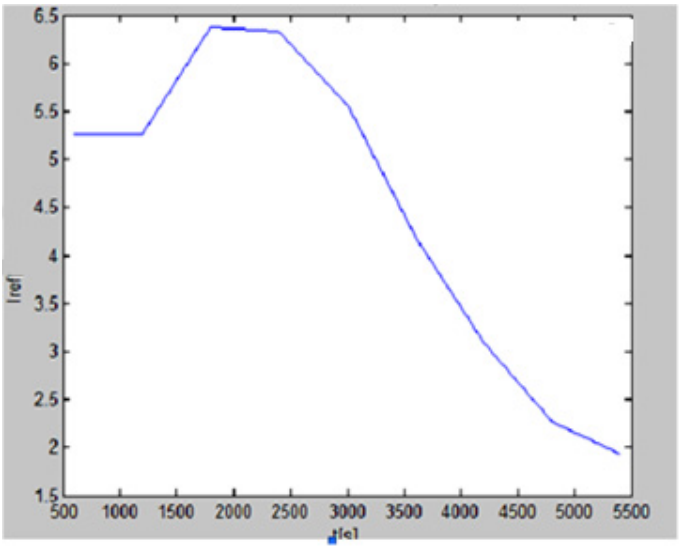

Fig. 15. Variation of current

In Fig. 13, Fig. 14 and Fig. 15 are presented representation for the variations of the angular speed ω in time, load resistance R and intermediary current circuit obtained by calculations .

The evolution in time of system (WT+PMSG) is done by solving the equation of movement.

Load resistance was calculated with consideration of reference elements ω_{ref} and kinetic energy variations in steps of 600s, values that are calculated by measuring wind speed in time with an anemometer (AN).

Driving the system (WT+PMSG) does not impose usage of regulators, just measuring the wind speed in time. As can be seen in the next given simulations functioning is stable, without overrides and electrical energy that is obtained on a long time interval (hours, days) is maximum.

From Fig. 16 results that angular speed ω_{real} of the generator is following the reference angular speed ω_{ref}, calculated from wind speed measured in time

On time interval where from kinetic energy calculations $\omega_{ref} > \omega_{real}$, variations are get to the equality on all speeds (RPM) from the calculated generator load, from the turbine power and from the kinetic energy variations.

By measuring the wind speed and bringing the generator speed in the optimal zone from energetically point of view, the stability in time of the driven system is ensured even in the conditions where wind speed variations are significant.

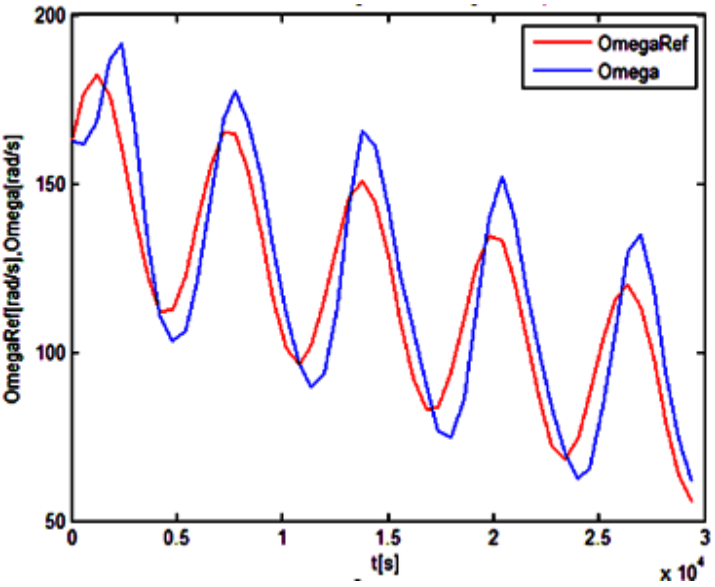

Fig. 16. Variation of ω and ω_{ref}

5 Conclusions

Driving the system (WT+PMSG) ensure functioning at maximum wind energy that is variable in time. Although the power of the turbine is following the variations of the wind speed, the power given in the network is constant because the power variations are taken by the storage block (EA+SC).

Regulation method is based on continuous measurement of wind speed in time and establishing the load at the generator in function of this speed. System stability was demonstrated by numerical simulations of fundamental elements: angular speed, load current and power.

In this paper fundamental problems of driving wind systems where improved. Optimal speed for generator was calculated to ensure maximum energy generation from the system. Stability of the generator load is based on driving the wind speed and variations of kinetic energy. Powering the network on long time intervals, at a constant power and the excess power variations into storage block (EA+SC) is possible.

References

1. Ahmed, A., ElshEAr, M., Mohammed, A.: Reactive Power Compensation Control for Stand-Alone Synchronous Generator-Based Wind Energy Conversion System. In: IECON 2010, pp. 3216–3221 (2010)

2. Alepuz, S., Calle, A., Busquets, M., Bordonau, J., Kouro, S., Wu, B.: Control Scheme for Low Voltage Ride-Through Compliance in Back-to-back NPC Converter Based Wind Power Systems. In: Industrial Electronics (ISIE), pp. 2357–2362 (2010)
3. Bobanac, V., Jelavić, M., Perić, N.: Linear Parameter Varying Approach to Wind Turbine Control. In: Power Electronics and Motion Control Conference, EPE/PEMC, pp. T12-60–T12-67 (2010)
4. Chih-Chiang Hua, A., Chien-Hung Cheng, B.: Design and Implementation of Power Converters for Wind Energy Conversion System. In: Power Electronics Conference (IPEC), pp. 323–328 (2010)
5. Drugă, M., Nichita, C., Barakat: Performances Study of Direct coupled PM Generator based Small Wind Converters. In: Electrical Machines, ICEM (2010)
6. Freire, N.M., Estima, J., Cardoso, M.: Converters Fault-Diagnosis in PMSG Drives for Wind Turbine Applications. In: IECON 2010, pp. 397–402 (2010)
7. Gamboa, G., Elmes, J., Hamilton, Baker, J., Pepper, M., Batarseh, I.: A Unity Power Factor: Maximum Power PointTracking Battery Charger for Low Power WindTurbines. In: Applied Power Electronics Conference and Exposition (APEC), pp. 143–148 (2010)
8. Grabic, S., Celanovic, N., Katic, V.: Fixed speed wind turbine topology based on actively damped PMSG. In: Power Electronics and Motion Control Conference (EPE/PEMC), pp. S14-1–S14-8 (2010)
9. Ivanović, Z., Dokić, B., Blanuša, B., Knežić, M.: Boost Converter Efficiency Optimization in Wind Turbine. In: Power Electronics and Motion Control Conference (EPE/PEMC), pp. T3-1–T3-5 (2010)
10. Jafar, M., Molinas, M.: A Series Injection Strategy for Reactive Power Compensation of Line Commutated HVDC for Offshore Wind Power. In: Industrial Electronics (ISIE), pp. 2339–2344 (2010)
11. Kawakami, N., Motohiro, I., Bando, M., Sakanaka, Y., Ogawa, K., Matsuda, K.: Development and Field Experiences of Stabilization System using 34MW NAS Batteries for a 51MW Wind Farm. In: Industrial Electronics (ISIE), pp. 2371–2376 (2010)
12. Kortabarria, I., Andreu, J., Martnez, I., Ibarra, E., Robles, E.: Maximum Power Extraction Algorithm for a Small Wind Turbine. In: Power Electronics and Motion Control Conference (EPE/PEMC), pp. T12-49–T12-54 (2010)
13. Klumpner, C., Al, B., Hann, D.: A Power Electronic Controlled Dump Load with Negligible Harmonics for Accurate Loading Used in Testing Small Wind Turbines. In: Industrial Electronics (ISIE), pp. 596–601 (2010)
14. Lee, H., Kharitonov, S., Brovanov, S., Zinoviev, V., Reznichenko, M.: An Analysis of a Wind Power System Including PMG, Active Rectifier and Voltage Source Inverter. In: Compatibility and Power Electronics (CPE), pp. 2569–2576 (2010)
15. Lee, S., Lee, K.: Performance Improvement of a DFIG in a Wind Turbine under an Unbalanced Grid-Voltage Condition. In: Industrial Electronics (ISIE), pp. 986–991 (2010)
16. Li, J., Li, D., Hong, L., Xie, C., Chen, G.: A Novel Power-flow Balance LVRT Control Strategy for Low-speed Direct-drive PMSG Wind Generation System. In: IECON, pp. 742–747 (2010)
17. Munteanu, I., Bratcu, A., Cutululis, N., Ceangă, E.: Optimal Control of Wind Energy Systems. Springer Verlag London Limited, Intelligent Environments (IE) (2008)
18. Okazaki, Y., Yoshida, M., Fujiwara, K.: Charging Method of EDLCs by Wind Power Generation in Stand Alone System. In: Power Electronics Conference (IPEC), pp. 2577–2584 (2010)

19. Van Dessel, M., Gay, M., Deconinck, G.: Simulation of grid connected PM generator for wind turbines. In: Industrial Electronics (ISIE), pp. 1479–1484 (2010)
20. Yuan, X., Li, Y., Chai, J.: A Transformerless Modular Permanent Magnet Wind Generator System with Minimum Generator Coils. In: Applied Power Electronics Conference and Exposition (APEC), pp. 2104–2110 (2010)
21. Yuan, X., Chai, J., Li, Y.: Control of Variable Pitch, Variable Speed Wind Turbine in Weak Grid Systems. In: Energy Conversion Congress and Exposition (ECCE), pp. 3778–3885 (2010)
22. Babescu, M.: Masini Electrice - Modelul Ortogonal. Politehnica (1992)

A Brief Outline of Computational Limitations on Actual Wireless Sensor Networks

Gabriel Gîrban and Mircea Popa

Politehnica University of Timisoara,
Pta. Victoriei 2, 300006 Timisoara, Romania
{gabriel.girban,mircea.popa}@cs.upt.ro

Abstract. This paper is related to the problem of low computational resources available on actual processing modules used in the nodes of wireless sensor networks, in the context of continuously increasing complexity of optimization algorithms, communication protocols and implemented services. The increase in complexity is driven by the efforts to conserve the energy and to enhance the network throughput but it is also caused by the evolution of these technologies toward the integration into the Internet of Things. The results obtained give an overview on the computational resources (computing time and memory size) necessary to perform the usual arithmetic operations using different representations of the operands on multiple platforms. These results are aimed to support the optimal selection of WSN platforms relatively to the computational effort required by specific application as well as the adaptation of the operations performed and of the related operands to a specified platform.

Keywords: WSN, computational effort, computational resources.

1 Introduction

The main characteristics of a node in wireless sensor networks (WSN) are data acquisition, its primary processing, storing and cooperatively sending the results through the network to a data collection center. The data acquisition is generally performed using sensors which will collect the information about a specific physical phenomena through digital or analog signals. These signals are used by the processing module (usually a low power, low cost microcontroller) to store the information in memory and to transmit it in a required format to be used by upper application layers. Communication is done via a transceiver circuit that can be independent or integrated with the processing module on the same system-on-chip (eg. ATmega128 RFAx [1] on WiSMote mini motes [2] and MC13224V [3] in case of Redbee nodes [4]). A brief description of hardware architectures and related software platforms for eight wireless sensors is performed in [5].

First applications based on wireless sensor networks were focused on monitoring of a specific natural or technological system, detecting certain events and reporting them to the upper application layers. There was a low computational effort required for adaptation of the data resolutions and creating the communication messages.

V.E. Balas et al. (Eds.): Soft Computing Applications, AISC 195, pp. 237–249.
springerlink.com

To overcome the limitations of this approach in terms of energy efficiency, intensive research has been performed in this area to conserve the energy through duty cycling algorithms for data acquisition, data aggregation, advanced network topologies and communication protocols. On the other hand, the development of Internet technologies and development of Internet enabled electronic devices (mobile phones, appliances, etc.), evolves toward a greater integration and accessibility of web applications and services through concepts like Web 2.0 and Internet of Things (IoT), trends in which an important role is played by WSN networks [6]. Thus, implementation of more complex algorithms and integration of advanced network protocols and services require additional memory resources and processing power, increasing the impact of limited computational resources in the area of wireless sensor networks. The case study presented in [7] can be taken as an example of the memory resources available in the nodes of these networks. The integration of a framework allowing simple request/response interactions of the WSN with other standard networks through Web services, requires more than 60 % from ROM memory for the operating system core, medium access protocols, data acquisition code, Web services and "6LoWPAN" protocol suite [8]. In this case, less than 40 % is available for energy optimization algorithms, application services and implementation of more complex interactions.

This paper is related to the problem of low computational resources available on actual processing modules used in the nodes of sensor networks. Its purpose is to determine the computational resources (computing time and memory size) necessary to perform the usual arithmetic operations using different representations of the operands on multiple platforms. The obtained results are aimed to support the optimal selection of WSN platforms relatively to a specific application and the adaptation to the used platform of the operations performed and of the related operands.

In the following section, an overview of the actual representative WSN motes is presented, highlighting the properties of their processing units in terms of processing power and memory capacity. The third section describes the methodology used for determination of the required resources for all the sensor families that were analyzed in this paper while the fourth sections provides the results obtained.The last section concludes this paper.

2 Processing Modules in Wireless Sensors

There are various technologies used for the processing module, with simple microcontrollers or systems-on-chip based on RISC or CISC architectures and even combinations of microcontrollers with FPGA modules like on the Cookies platforms [9]. An overview of the processing and communication modules used in the popular wireless sensors is given in Table 1.

The predominant use of microcontrollers belonging to the same families can be observed in Table 1, differences between the microcontrollers within a family being determined by the size of memory elements, the types of some peripherals, the frequency of synchronization signal and by the processing power (MIPS / MHz)

Table 1. Processing and communication modules on several wireless sensors (SoC is used for system-on-chip)

WSN mote	Microcontroller	Architecture	Radio
Iris mote	ATmega 1281	8 bits, Harvard, RISC	IEEE802.15.4
Wasp mote	ATmega 1281	8 bits, Harvard, RISC	IEEE802.15.4
BTnode	ATmega 128L	8 bits, Harvard, RISC	IEEE802.15.1 IEEE802.15.4
MICAz	ATmega 128L	8 bits, Harvard, RISC	IEEE802.15.4
WisMoteMini	ATmega128 RFAx	8 bits, Harvard, RISC, SoC	IEEE802.15.4
GWnode	PIC18LF8722	8 bits, Harvard, RISC	173 MHz
Rene	ATmega8535	8 bits, Harvard, RISC	916 MHz
AVRraven	ATmega1284p	8 bits, Harvard, RISC	IEEE802.15.4
Mulle	Renesas M16C 62P	16 bits, vonNeumann, CISC	IEEE802.15.1 IEEE802.15.4
EPIC mote	MSP430	16 bits, vonNeumann, RISC	IEEE802.15.4
Kmote	MSP430	16 bits, vonNeumann, RISC	IEEE802.15.4
TelosB	MSP430	16 bits, vonNeumann, RISC	IEEE802.15.4
Eyes IFXv2	MSP430F16x	16 bits, vonNeumann, RISC	868 MHz
shimmer	MSP430F1611	16 bits, vonNeumann, RISC	IEEE802.15.4
BEAN	MSP430F169	16 bits, vonNeumann, RISC	300-1000 MHz
WisMote	MSP430F5437	16 bits, vonNeumann, RISC	IEEE802.15.4
Redbee	MC13224V	32 bits, arm7 (Harvard), RISC, SoC	IEEE802.15.4
Egs	ARM Cortex M3	32 bits, arm7 (Harvard), RISC	IEEE802.15.1
Lotus	ARM Cortex M3	32 bits, arm7 (Harvard), RISC	IEEE802.15.4
IMote 2.0	Marvell PXA271	32 bits, arm5 (Harvard), RISC	IEEE802.15.4

The radio interfaces belong to IEEE 802.15 standards defined for wireless personal networks (WPANs), and are oriented to omni-directional communication using small circuits with low power consumption. These radio modules are considered to have the greatest impact on the energy consumption of wireless sensors. The IEEE 802.15.1 WPAN standard (Bluetooth) is designed for average transfer rates and allows transmission of the voice signal, while WPAN IEEE 802.15.4 (Zigbee) is focused on low power consumption but has lower transfer rates.

The processing power of the microcontrollers is determined by the number of operations executed in a time unit and a usual metric is MIPS (million instructions per second). A significant improvement of the processing performance can be obtain when using a higher frequency for the clock signal, but it has a negative impact on the

energy conservation as the CPU power consumption is directly proportional to this frequency ($P \approx C\ V^2\ f$).

For a better comparison of processing resources of wireless sensors, several elements should be considered. An overview of the data size (bits), clock frequency (MHz) and processing power (MIPS) for the microcontrollers enumerated in Table 1 is presented in Fig. 1.

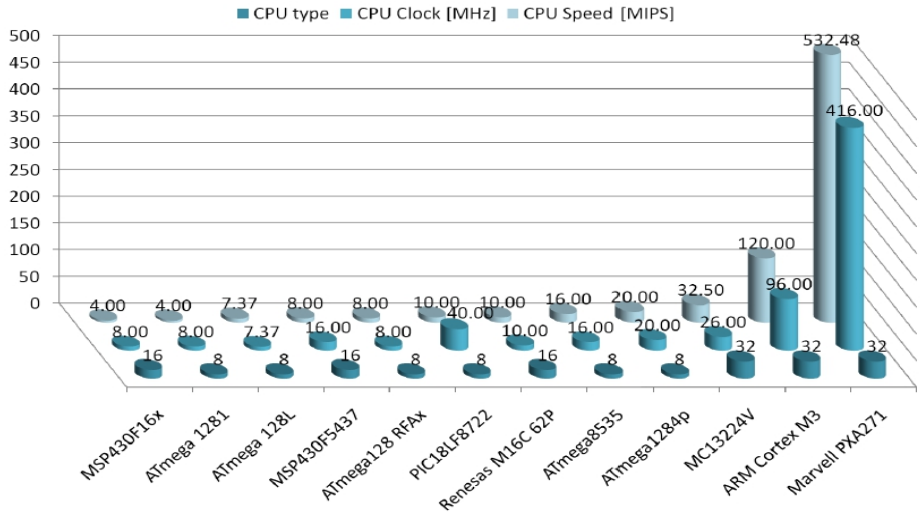

Fig. 1. Properties of the processing modules used in wireless sensors.

Although, according to the values in Fig. 1, the superiority of 32 bits architectures is evident, in terms of the compromise between price, power consumption and processing power, the analyzed 8 and 16 bits architectures offer a better approach.

The storage resources of the analyzed wireless nodes are depicted in Fig. 2, which provides a comparison of the used microcontrollers from the size of internal RAM and internal Flash memory point of view.

It can be observed that RAM memory, used in general for the storage of variables and stack, is much less than the code memory (from 3 to 20 %) but there are two exceptions related to Xscale (PXA271) and MC13224V platforms.

In case of the PXA271 microcontroller [10], a different scale of magnitude is used to represent the memory capacity, this microcontroller being designed for more complex applications which emphasis processing of large data flows. It is not equipped with a classic ADC module, but integrates a sound processing controller. It has a relatively high power consumption compared to the other microcontrollers used in wireless nodes.

The Freescale system-on-chip MC13224V [3] appears to contain a reasonable storage space, but there are some issues about the size of internal RAM and Flash memory type. Being equipped with a serial Flash memory, the code can not be executed directly from this memory and during the start-up phase it must be copied

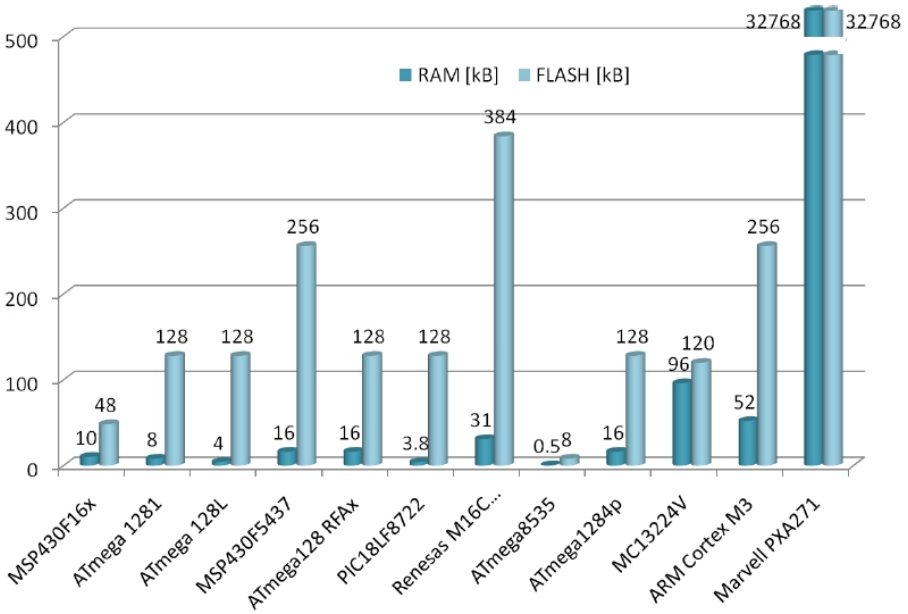

Fig. 2. Storage resources in wireless sensors.

into the RAM memory to be executed. By using a smaller RAM size than the Flash memory size, allocation problems may arise in the case of applications requiring a considerable program code. This shortcoming is partially substituted by the presence of another type of internal ROM memory, which is able to store executable code directly, but it was designed to contain the stack of communication protocols.

3 Methodology

In order to analyze the possibility of implementing application specific services and mathematical models, communication protocols and network monitoring strategies on WSN nodes, it is necessary to know the amount of resources (code and data) involved by the related operations. Thus, the following sections will present the resources required on four wireless sensor families for operations like comparison, addition, multiplication, division and exponentiation, using integer operands represented on 8, 16, 32 and 64-bits or simple precision, floating point operands.

For implementation we have used the Tiny OS environment [11] (GNU C cross compiler) with the default optimization. The code used to determine the necessary resources on four different platforms (see Table 2) is structured in three files, and can be summarized by the expression: $a = b$ *operator* c.

Table 2. Wireless sensors platforms

Atmega12xx	MSP430xx	PIC18LF8722	Renesas M16C62P	Marvell PXA271
MICA2	Epic	Gwnode	Mulle	Imote2
	Eyesifx			
MICA2dot	Eyesifxv1			
	Eyesifxv2			
	Shimmer			
	Shimmer2			
MICAz	Telos			
	Telosa			
Iris	Telosb			
	Tmote			

The goal is to identify the resources required by the compiler and related library functions to execute the operator and to store the results. For determination of the relative resources, we have duplicated the operations to be performed and compared the size of generated code with the one obtained for previous expressions *a = b operator c* and *a2 = b2 operator c2*. To implement the exponentiation operation, the *pow* function has been used for Atmega12x family and the *powf* function for the other families, both functions using floating point operands and therefore implicit conversions when passing the integer parameters or when assigning integer results.

Results were obtained by compiling the code described below, taking into account all the combinations *operation - operands* for the 16 nodes enumerated in Table 2. The data obtained relatively to the nodes that are based on microcontrollers from the same family are identical.

The content of the three files is specified below using nesC terminology [12]:

1. configs.h:

```
 1:#ifndef CONFIGS_H
 2:# define CONFIGS_H
 3:
 4:# ifdef T_U8
 5:# define DATA_T uint8_t
 6:# elif T_U16
 7:# define DATA_T uint16_t
 8:# elif T_u32
 9:# define DATA_T uint32_t
10:# elif T_64
11:# define DATA_T uint64_t
12:# else
13:# define DATA_T float
14:# endif
15:
16:# ifdef OP_ADD
17:#  define OP(a,b) a+b
18:# elif OP_MUL
19:#  define OP(a,b) a*b
20:# elif OP_DIV
21:#  define OP(a,b) a/b
22:# else
23:#  ifndef
      _H_atmega128hardware_H
24:# define OP(a,b) powf(a,b)
25:# else
26:# define OP(a,b) pow(a,b)
27:# endif
28:# endif
29:#endif //CONFIGS_H
```

2. AppC.nc:

```
1:configuration AppC{
2:
3:}
```

```
4:
5:implementation{
6: components
   ComponentC,MainC;
7: ComponentC.Boot-
   >MainC.Boot;
8:}
```

3. ComponentC.nc:

```
 1:#include <math.h>
 2:#include <configs.h>
 3:
 4:module ComponentC
 5: {uses interface Boot;}
 6:implementation{
 7:#ifndef REF_SW
 8: DATA_T a,b,c;
 9:#endif
10:#ifdef CMP_SW
11: DATA_T a2,b2,c2;
```

```
12:#endif
13:
14:event void Boot.booted()
15:{
16: //entry point
17:# ifndef REF_SW
18:   c=OP(a,b);
19:# endif
20:# ifdef CMP_SW
21:   c2=OP(a2,b2);
22:# endif
23: }
24:}
```

4 Obtained Results

4.1 The Atmega128x Platform

The microcontrollers from Atmega12x family have an 8 bits architecture characterized by a reduced set of instructions with no direct support for division operations and floating-point operands. This is reflected by the additional number of bytes required by the related operations (Fig. 3 and Fig. 4).

The size of the code that implements the 64 bits division operation is approximately 3 % of program memory and a percentage of approximately 1.5 to 2.3% of the resources is needed to implement the exponentiation operation. The size of generated code in Fig. 3 is indirectly providing information about the execution time, thus it can be observed that operations using floating point and 64 bits integer operands require more memory resources (from 10 to more than 100 times) and therefore more time to be executed. It can be concluded that these operands and the exponentiation function as well, must be avoided on wireless sensors based on microcontrollers from Atmega12x family.

4.2 The PIC18LF8722 Platform

This platform has many similarities with Atmega12x in terms of available resources, the RAM and ROM memories have a comparable size, the multiply instruction is available in the instructions set while there is a lack of division instructions. Therefore, the differences which may occur in the generated code are mainly caused by the used compilers.

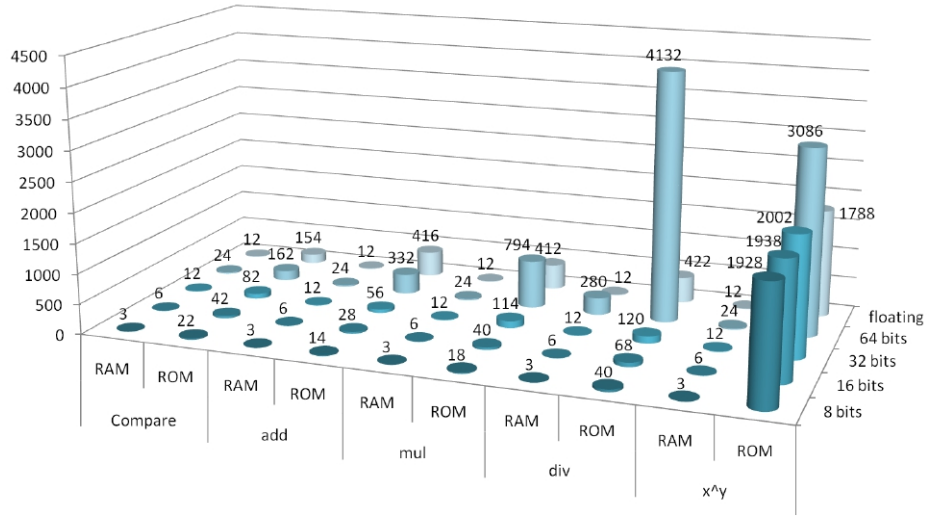

Fig. 3. Memory resources required by operations and related operands on Atmga12x based motes

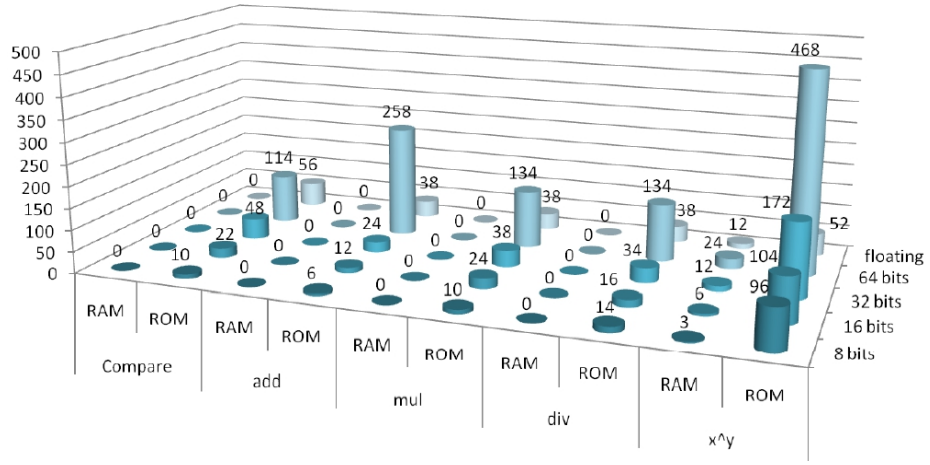

Fig. 4. Additional memory resources required by each new operation on Atmga12x based motes

4.3 The MSP430x Platform

MSP430x platform architecture is based on a 16 bits reduced instruction set and, unlike the Atmega12x microcontrollers, the multiply instructions is not available. The memory resources required to implement the usual arithmetic operations are described in Fig. 5 and Fig. 6.

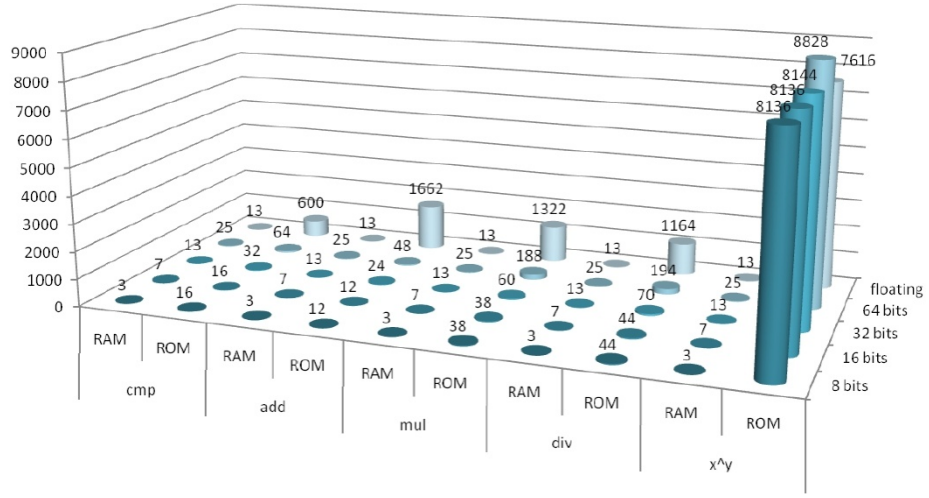

Fig. 5. Memory resources required by several operations and related operands on MSP430x based motes

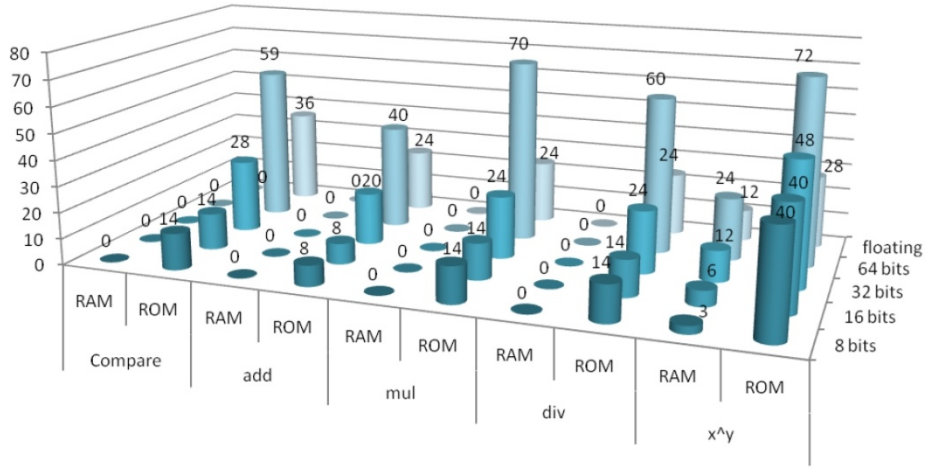

Fig. 6. Additional memory resources required by each new operation on MSP430x based motes

A significant impact on program memory is related to the exponentiation operation, as it is ranging from 3 % on MSP430F5437 to 16 % of the total memory resources for MSP430F16x variants. Also, the functions associated to the floating point operations induce a consumption of about 2 % of Flash memory for MSP430F16x.

Unlike the Atmega12x microcontrollers, the use of 64 bits operands on this platform requires less than 5 times the code size needed when the same operations are using operands represented on bytes. As a comparison, when dividing 64 bits

operands using Atmega12x microcontrollers, the generated code requires 20 times more ROM memory than on MSP430x microcontrollers.

The use of floating point operands and implicit of the exponentiation function must be also avoided.

4.4 The Renesas M16C62P Platform

Although this platform, unlike the afore mentioned, is based on a 16 bits complex instruction set architecture with multiple operations available at hardware level (as of addition, subtraction, multiplication and division), there are significantly more memory resources necessary to implement the expressions taken as reference in this section. The code generated for the division and exponentiation function using 32 or 64 bits operands involves approximately 1.5 % of the available RAM memory (equivalent with 13 % of available RAM on Atmega128x platform). In terms of the required ROM memory, the floating point operations need about 9 % of the internal Flash (which is more than 25 % of internal Flash available on Atmega128x platforms). Also the division operations using 64 bits operands involve approximately 2 % of internal ROM memory capacity. The complete data are provided in Fig. 7 and Fig. 8.

Additional restrictions, besides avoiding floating point and 64 bits operands, should be considered on this platform when dividing using 32 bits operands.

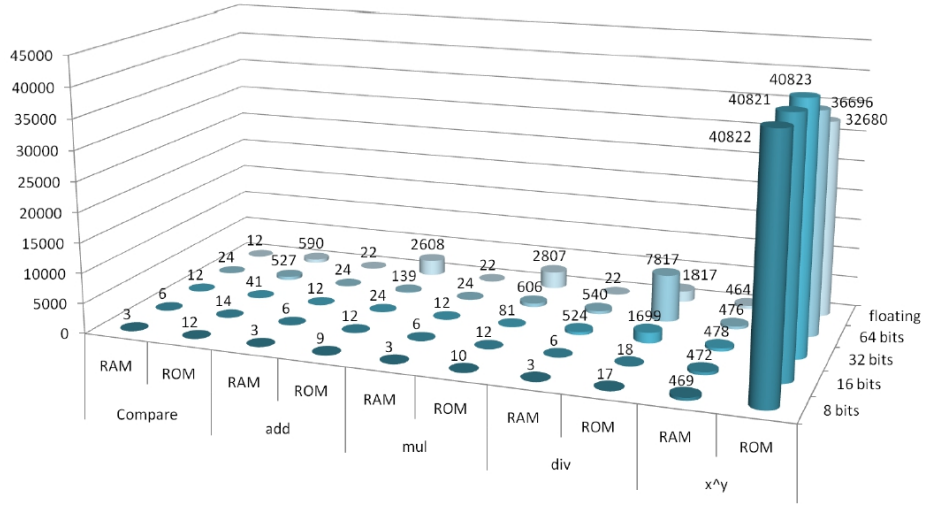

Fig. 7. Memory resources required by several operations and related operands on Renesas M16C62P based motes

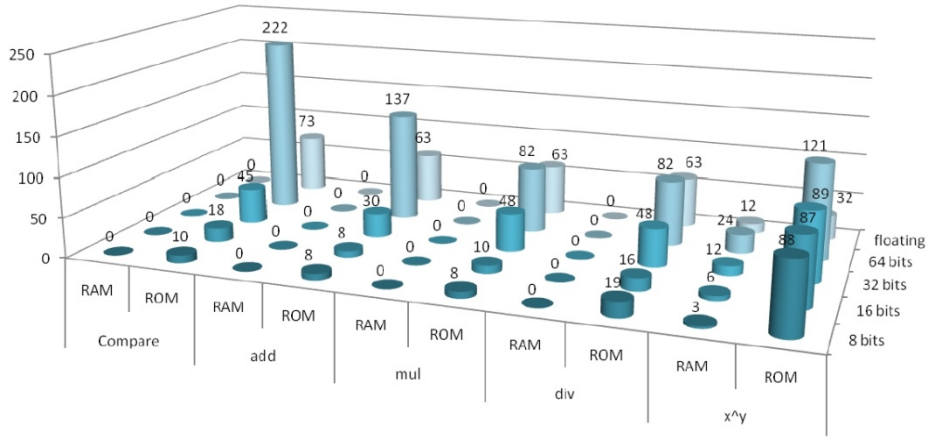

Fig. 8. Additional memory resources required by each new operation on M16C62P based motes

4.5 The PXA271 Platform

The instruction set of PXA271 microcontrollers is compatible with ARMv5 TE, but it lacks the floating point instructions. Thus, even if the resources available are incomparable with previous architectures, when considering the size of code generated for the proposed operations, it might be considered comparable.

The maximum resources in case of PXA271 platform, is required by the exponentiation operations (0.05 % of internal Flash), all the values obtained being described in Fig. 9.

The floating point operands and operations requiring them (exponentiation) must be avoided while some restrictions may be considered for dividing with 64 bits operands.

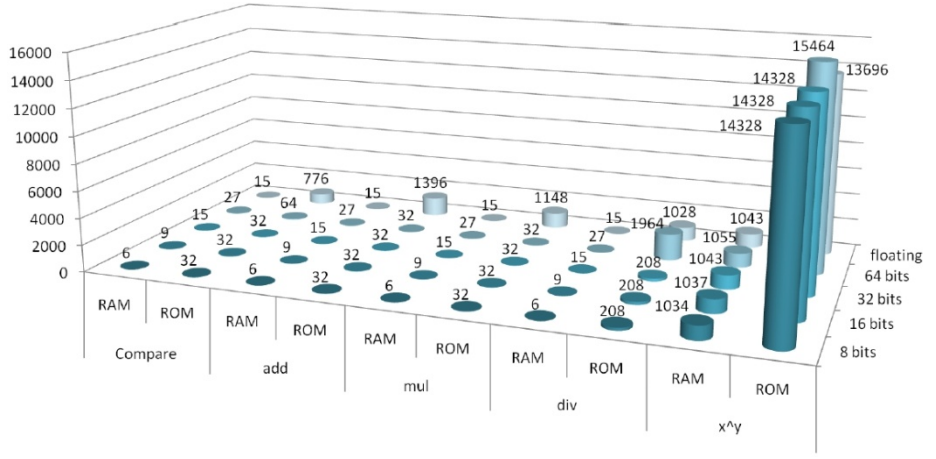

Fig. 9. Memory resources required by several operations and related operands on PXA271 based motes

5 Conclusions

Through this paper are presented the code and data resources required by the common operations (arithmetic, relational and storage) on actual wireless sensor nodes.

As expected, due the missing support for floating point operations on the hardware level, these type of operands and related operations must be avoided in sensor networks. Although WSN networks are generally designed to process information from natural and technological systems, information that is more accurately represented by floating point data, it is mapped on integers and all operations will be performed using integer operands but keeping the real significance of the results. The size of integer operands as well as the type of operations to be used must be chosen in a platform dependent manner, as it may be possible to handle data with higher resolution but not all the operations are efficient from computing time and related memory requirements. Also, the size of operands should be limited, where it is possible, in order to have a correspondence with the types of instructions available on the target processor. The exponentiation operation must be implemented to work with integer operands while the number of loops should be limited in the related algorithm.

The results of such analysis are necessary to optimize the size and resolution of the data in the wireless nodes with critical computational resources. An example of such applications is the integration, at a node level, of services that can be accessed from outside of the sensor network using Internet protocols (an Internet of Things).

Acknowledgments. This work was partially supported by the strategic grant POSDRU/88/1.5/S/50783, Project ID50783 (2009), co--financed by the European Social Fund - Investing in People, within the Sectoral Operational Programme Human Resources Development 2007 - 2013.

References

1. Atmel: 8-bit AVR Microcontroller with Low Power 2.4GHz Transceiver for ZigBee and IEEE 802.15.4 (2011), http://www.atmel.com/Images/8266S.pdf
2. Arago Systems: WiSMote mini (2012), http://www.aragosystems.com/images/stories/WiS-Mote/Doc/wismote_mini_en.pdf
3. Freescale Semiconductor: MC1322x - Advanced ZigBee™- Compliant Platform-in-Package, PiP (2010), http://www.freescale.com/files/rf_if/doc/data_sheet/MC1322x.pdf
4. Redwire: Redbee 802.15.4 Module, http://www.redwirellc.com/store/node/3
5. Bischoff, R., Meyer, J., Feltrin, G.: Wireless Sensor Network Platforms. In: Boller, C., et al. (eds.) Encyclopedia of Structural Health Monitoring, pp. 1229–1238. John Wiley & Sons, Chichester (2009)
6. European Future Internet Portal, http://www.future-internet.eu/

7. Castellani, A.P., Bui, N., Casari, P., et al.: Architecture and Protocols for the Internet of Things: A Case Study. In: 8th IEEE Intl. Conf. on Pervasive Computing and Communication (PerCom 2010), pp. 678–683. IEEE Press (2010)
8. Shelby, Z., Borman, C.: 6LoWPAN: The Wireless Embedded Internet. John Wiley & Sons, Chichester (2009)
9. Valverde, J., Otero, A., Lopez, M., et al.: Using SRAM Based FPGAs for Power-Aware High Performance Wireless Sensor Networks. Sensors 12(3), 2667–2692 (2012)
10. Marvell: PXA270M Processor (2010), http://www.marvell.com/application-processors/pxa-family/assets/pxa_27x_spec_update.pdf
11. TinyOS Documentation Wiki, http://docs.tinyos.net/tinywiki/
12. Gay, D., Levis, P., Culler, D., Brewer, E.: Nesc v1.1 Language Reference, http://nescc.sourceforge.net/papers/nesc-ref.pdf

The Quality of Following the Welding Path with Arc Sensors

Gheorghe Sima

"Aurel Vlaicu" University of Arad, 77 Revolutiei Ave., 310130 Arad, Romania
gheorghe.sima@klastorf.ro

Abstract. The paper presents the principle of following the welding path with the help of arc sensors. Both theoretical considerations and industrial applications are presented. A mathematic model of an arc sensing system is also shown. The minimum and maximum outline shapes that can be followed with path sensors have been established by trials. This is important for its design and further development.

Keywords: quality, welding, arc sensor, mathematic model, structures.

1 Introduction

Under current conditions the main characteristic of a product is its quality. For welded structures one of the most important steps in achieving the desired quality is the correct leading of the welding head along the welding path. Automated and robot systems use path sensors. Under the notion of "sensors for the electric arc welding", we understand the devices and apparatuses that, as a component of the welding system, observe a certain phenomenon or non-dimensional data regarding "status" or, considering circumstances, the geometry (configuration) of the pieces that are to be welded. The information is transmitted further under different means (signals) for the purpose of following and maintaining the phenomenon within the desired parameters, as in the case of a welding process, the regulation of the welding head along with the path, and the regulation of the welding process measures [1].

By sensor one can understand the part of a measuring device that is unconditionally exposed to the measuring phenomenon. In industrial robot construction sensors are used for measuring non-cinematic dimensions referring to the state of the environment, physical measures, stochastic influences of the environment, as well as the observance of shapes and positions of objects.

In the general case the sensor gives the coordinates of the path by means of the Jc vector components (figure 1).

The sensor provides the coordinates of the Jc path and the Jcx vector which is the intersection between the level tangent to the path and the sensor detection level.

To compute the path vector, each of its components has to be calculated using the following formula [2]:

V.E. Balas et al. (Eds.): Soft Computing Applications, AISC 195, pp. 251–260.
springerlink.com

$$J_C x = J_C x' - (J_C x' \cdot J_C y) \cdot J_C y$$

$$J_C z = J_C x \cdot J_C y$$

In order to calculate the component $J_C y$ in a point "k" several formulae can be used:

- the Stirling's formula

$$J_C y(k) = 1/2p[3J_C(k) - 4J_C(k-1) + J_C(k-2)]$$

where: p = the sampling pace of the path.

- the polynomial interpolation formula

$$J_C y(k) = 1/20p[21J_C(k) - 13J_C(k-1) - 17J_C(k-2) + 9J_C(k-3)]$$

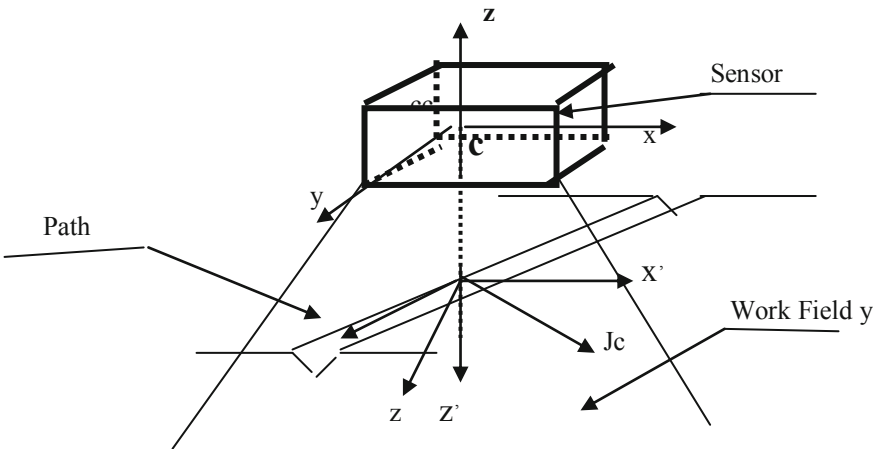

Fig. 1. Sketch of the sensor path following

Through analysis of the information transmitted by the sensor, the command system determines the position and the path route. Thus, the movement of the welding head along the path can be controlled, with the exception of certain deviations that depend on the type of sensor used and the complexity of the path route.

The detection systems (sensors) for the path of the pieces to be welded are necessary for their automated welding because their precise position cannot be known. This is due to the fact that the repetition of the piece positions in the welding process is not sufficient in order to guarantee the welding in good conditions [3].

This repetition lack can be due to:

- flaws in the welding device;
- reciprocal position of piece assembly;
- deformations during the welding.

At the moment, welding devices and robots lacking path sensors mainly weld pieces with small deformities and therefore small dimensions and few welded joinings. By using path sensors the application field for the automated welding will be enlarged. Additionally, using sensors has produced an important impact upon the extension of the welding proceedings, and a precise positioning of the electrode wire in relation to the path allows for a higher receptiveness of the application conditions and consequently a higher welding speed with beneficial endings on the termic effects [4].

A sensor is capable to determine the spatial and geometrical characteristics of the path and/or the welding pieces. The ideal sensor executes:

- determining the start and end spot of the welding path.
- following the path route for the welding.
- measuring the geometrical characteristics.
- it functions in the presence of the electric arc and during the oscillation movement of the welding head and it is viable in the welding environment (drops, fume, heat, the arc light, magnetic field, etc.)
- it does not increase the dimension of the welding head and, if possible, works without supplementary facilities.
- it is dependent from the used welding process.

2 A Mathematic Model of the Arc Sensor

A model of an arc sensing system is shown in figure 2.

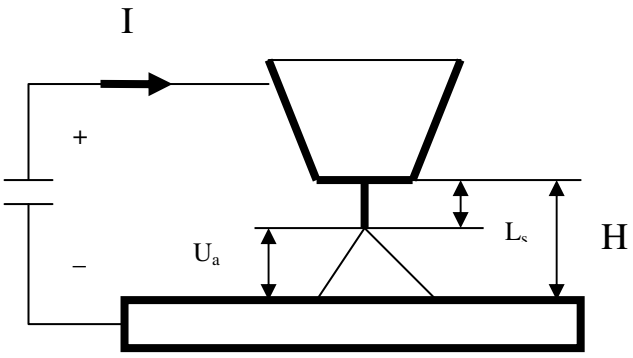

Fig. 2. A model of the arc welding

Obviously two equilibrium conditions must be satisfied by the system: one is of the electric circuit and the other is admission free length of the wire feeding system. According to the following equations it may be established:

$$U_a = K_s L_s (1 + I) + K_p I$$

where: U_a is the voltage arc, K_s coefficient of the potential gradient of the arc column, L_s admission free length of the wire and I welding current.

$$V_d = K_a I + K_b I^2 L_s + C_{ab}$$

where: V_d the wire feed rate, K_a coefficient of the melting rate contributed by the arc, K_b coefficient of the melting rate contributed by the resistance heat, C_{ab} general coefficient.

With the above equations, the following equation may be derived:

$$H = A + BI - K_a/K_b\, I^{-1} + K_s/K_bK_a\, V_d I^{-1} - C_{ab}/K_b\, I^{-2} + 1/K_bV_d\, I^{-2}$$

where: $A = f(K_x, U)$, $B = f(K_x)$

To simplify the expression, all the complex coefficients are replaced by single coefficients.

$$K_1 = - K_a/K_b\ ,\ K_2 = K_s/K_bK_a\ ,\ K_3 = - C_{ab}/K_b\ ,\ K_4 = 1/K_b$$

It may be rewritten:

$$H = A + BI + K_1V_dI^{-1} + K_2I^{-2} + K_3V_dI^{-2}$$

This expresses the desired static characteristics of the arc sensor. In the practical application of the equation the coefficients must be determined and the equation should be simplified.

3 The Path Following Fidelity

The detection systems (sensors) for the path of the pieces to be welded are necessary for their automated welding because their precise position cannot be known. This is due to the fact that the repetition of the piece positions in the welding process is not sufficient in order to guarantee the welding in good conditions [5].

The sensor has existed for a number of years but recently the performance and reliability has become far more dependable. The sensor approach works in a similar manner as the tactile sensing system, providing an interrupt for the robot controller to make decisions. The sensor, however, is non-contact and operates using an analogue inductive field. The advantage of this approach lies in the innovative skill of the robot programmer. A well conceived, strategic route of the robot traveling over the component will provide benefits of reduced sensing time and more reliable data received.

The Proximity Sensor is attached adjacent to the welding torch, while not compromising the desired welding torch approach angles when in operation. The robot travels over the parts and edges to be found, and any signal changes or interrupts are monitored and acted upon by the robot controller. The speed of travel and level of sensitivity are a derivative of the chosen sensor. Multiple readings from the sensor can be combined with logical instructions, providing simple X, Y and Z information, as well as angular and rotational data [6].

A sensor is capable to determine the spatial and geometrical characteristics of the path and/or the welding pieces. The ideal sensor executes:

- localizing the path for the welding.
- determining the start and end spot of the welding path.

- following the path route for the welding.
- measuring the geometrical characteristics.
- it functions in the presence of the electric arc and during the oscillation movement of the welding head and is viable in the welding environment (drops, fume, heat, the arc light, magnetic field, etc.)
- it does not increase the dimension of the welding head and, if possible, it works without supplementary facilities.
- it is independent from the used welding process.

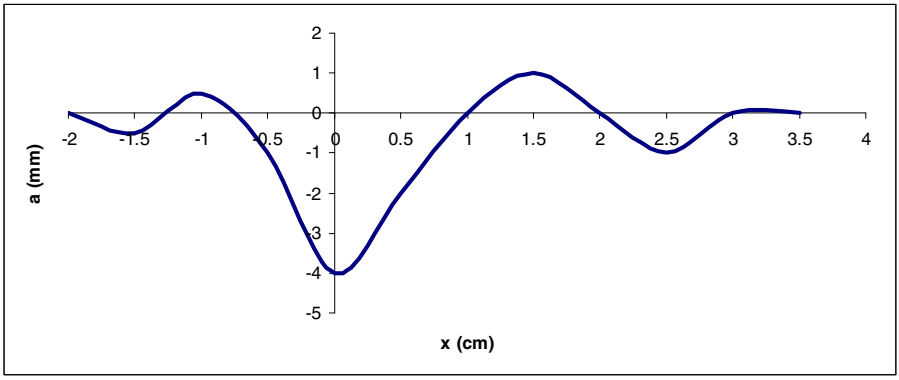

Fig. 3. Deviation from the path with exterior radii, 10 mm, for corner welding

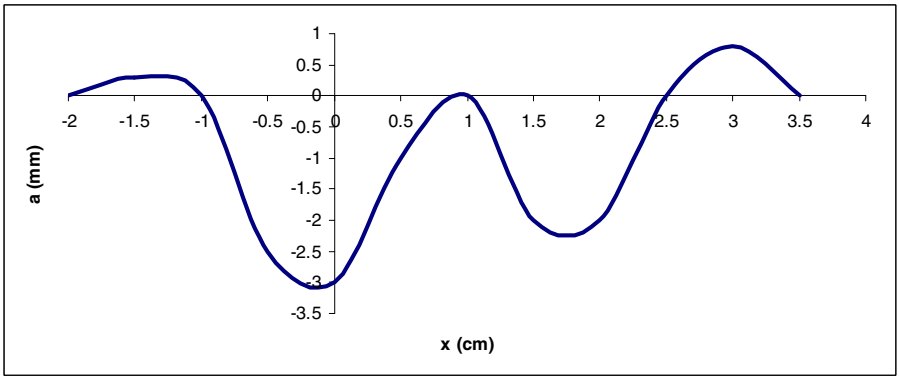

Fig. 4. Deviation from the path with exterior radii, 20 mm, for corner welding

During the welding process, as a consequence of the termic effect, there is a deformation of the pieces to be welded, which leads to the path trajectory to be modified during the welding operation. For a corner welding using tin plates 5mm thick and 1,000mm long, the momentary deformities are used for experiment.

The following precision depends on a series of factors such as the sensor performances and the welding path (route and section). For the arc sensors, upon interpreting the experimental results for different radii and paths, the deviation of the welding head from the best trajectory can be drawn (figures 3, 4, 5, 6, 7 and 8).

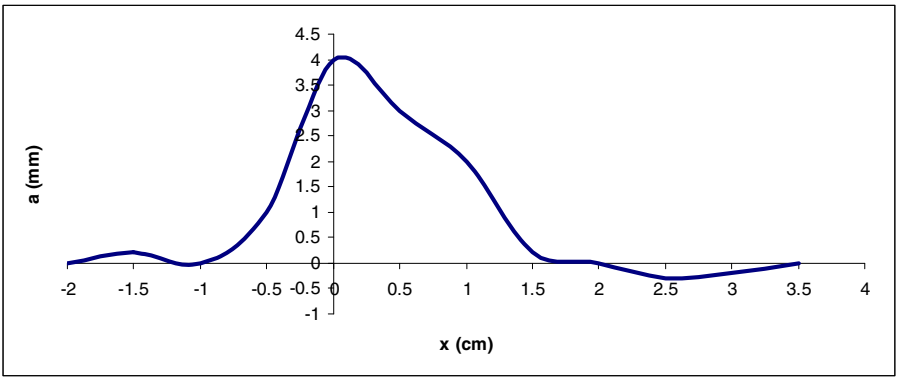

Fig. 5. Deviation from the path with interior radii, 10 mm, for corner welding

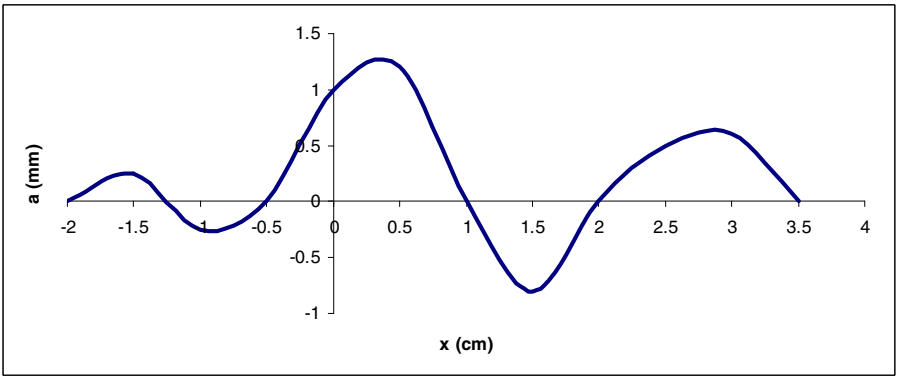

Fig. 6. Deviation from the path with interior radii, 30 mm, for corner welding

In welding applications recent and ongoing advances in sensor technology are enabling previously prohibited joint tolerances and configurations to be effectively produced with acceptable quality and weld integrity. Moreover, the technology has become performance and cost competitive for general industrial organizations, not just for the large dollar automotive and tier-one manufacturers.

There are three challenging phases of the welding process where the introduction of sensors has enabled the use of robotic automation in the welding of inconsistent joints:

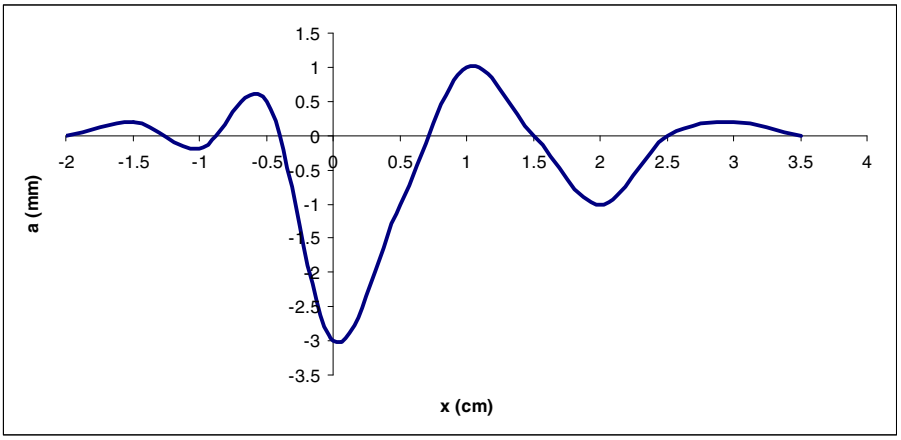

Fig. 7. Deviation for head to head V joining, with 10 mm radii

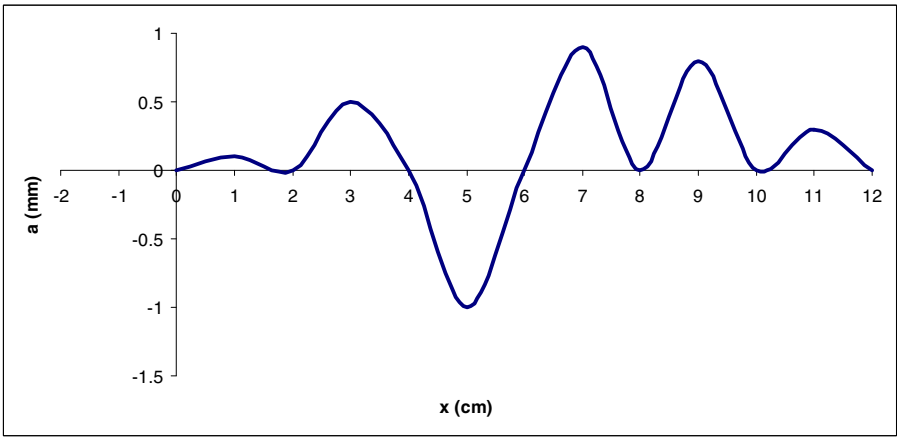

Fig. 8. Deviation for head to head V joining, with 30 mm radii

- detection, finding the edge or start of a weld seam. A number of media have been successfully developed that effectively resolve this process demand. They generally differ in accuracy, speed of acquisition, complexity and cost [7].
- tracking, maintaining the desired weld path. In some instances the start or edge of the joint may be relatively simple to control within the tooling or fixturing. The seam itself, however, may vary due to manufacturing methodology or thermal influences of the process. Tracking of the seam by various methods can overcome this shortcoming of manufactured parts. This offers another opportunity to automate the welding of previously prohibited joints and components.

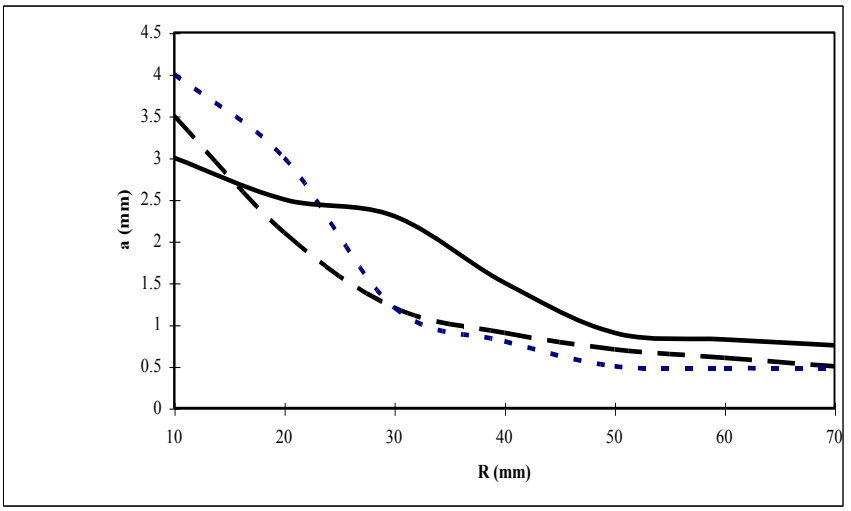

- - - exterior radii. ..... interior radii. —— alternatively radii.

Fig. 9. Deviation for corner welding when using arc sensors

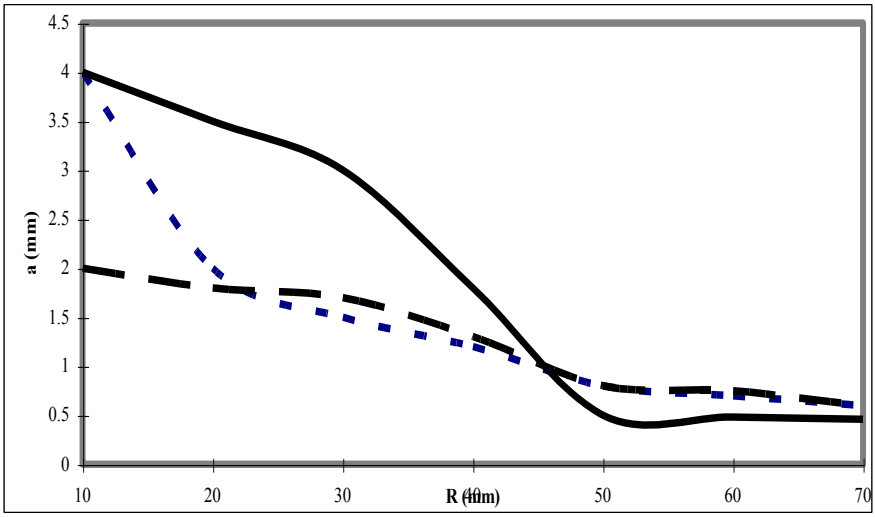

- - - exterior radii. ..... interior radii. ____ alternatively radii

Fig. 10. Deviation for head to head V joining when using arc sensors

After analyzing the tracking conditions with the help of the arc sensor, it has been noticed that the deviation from the optimal position of the welding head depends on the following:

- type of the welding system;
- precision degree of the tracking;
- shape of the joint;
- path of the welded joint;
- accuracy of processing the parts
- measuring, this helps in decisions that can be made to influence the robot path and speed within the joint; the process itself can be adapted to suit the local varying conditions [8], [10].

The synthesis of the precision degree of the path tracking in welding is presented in figure 9 and figure 10.

4 Conclusions

Sensors collect information from the robot, peripheral devices and process and transfer this information to a controller. In arc welding, it is critical to consider deformation from high heat input and, therefore, a closed loop control with a sensor is necessary. Also, in an automatic welding system the errors caused by manufacturing tolerances of manipulator and work pieces have to be considered. Various types of sensors for robot arc welding may be considered, depending on the application [9].

The following precision of approx. +/-0.5 mm on the horizontal and vertical directions of the welding head, and an orientation error of approx. +/-3 degrees for linear welding will not be respected in the case of circular outlines when there is a rising deviation of the above-mentioned values compares to the prescribed outline, together with the decrease of the radium. Hence the observation that in corner weldings the orientation error becomes higher, that is, the approximate value of the welding head is registered, which can lead to flatter sewings in the field of the smaller radii, as for radii under 10mm the melting of the vertical part of the path cannot be guaranteed. Trials for exterior radii have shown that a ceasing of the oscillation is not wanted and because of the edge denting, the lack of penetration and the arching of the sewing, it is recommended that the exterior radii do not exceed 45 mm.

For the interior corner weldings, satisfying results have been produced in the welding with radii higher than 20 mm. With smaller radii, the electric arc burns with the length of the wire reduced to the superior flank, which leads to an incomplete penetration in the area of the base plate and makes the orientation of the welding head more difficult with smaller radii. Upon analysis of the deviation from the trajectory with exterior radii smaller than 30 mm, sewings will be observed that do not fit into the class of admitted weldings for high quality welded structures.

For V-shaped weldings, with an arched route, a welding radium of minimum 30mm is indicated. Using welding routes with higher radii that those presented above lead us to obtain welded joinings of good shapes and measures, which approves the introduction of the leading system for the welding head by using arc and tactile sensors.

In the case of welding thinner plates, over placed through corner weldings in the arc sensor weldings, there may be deviations (movements) of the welding belt due to

the fact that during the welding, the sensor may mistake the axis of the path with the superior edge. This phenomenon is amplified in the case of radii weldings. In these cases the welding belt is not deposited in the joining, but on the edge, thus bringing about welding defects up to the control spot, when the welding gets back on the established track.

During the welding procedure, the way the welded joinings are made has an important role.

If the welded joinings are too large at the passage of the welding head over them, following flaws may occur, the welding head will take a wrong trajectory. If the welded joining spots are bigger than 3mm, deviations of the welding belt will happen after passing these joining spots.

The use of sensors leads to obtaining quality joinings. In special cases in designing welded structures, one has to take into account the conditions of stable following of the path.

References

1. Megahed, S., et al.: Principles of Robot Modeling and Simulation. Wiley Publishers (1993)
2. Sima, G., Hutiu, G., Carlan, D.: New Option for Quality-Sensors. In: The 13th Symposium on Analytical and Environmental Problems, Szeged, pp. 216–220 (September 25, 2006)
3. Sun, J., Olbrot, A.W., Polis, M.P.: Robust stabilization and robust performance using model reference control and modeling error compensation. IEEE Transactions on Automatic Control 39(3), 630–635 (1994)
4. Pan, J.: Modern Arc Welding Control, pp. 189–214. China Machine Press (2000)
5. *** Sensor Based Adaptive Arc Welding. Robotic Automation, 8–10
6. Sima, G.: Sisteme senzoriale utilizate la sudare. Editura Gutemberg Arad (2001)
7. Negrean, I.: Geometrical and kinematic modeling, Bucharest (1997)
8. *** Trends in welding. AGA AB, Sweden (1994)
9. Ryuh, B., Pennock, G.R.: Arc Welding Robot Automation Systems. In: KinHuat, L. (ed.) Industrial Robotics - Programming, Simulation and Applications, pp. 596–603. ARS, Germany (2006)
10. Kim, R.-H., Choi, G.-D., Kim, C.-H., Cho, D.-W., Na, S.-J.: Arc Characteristics in Pulse-GMA Welding with Acute Groove Angles. Supplement to the Welding Journal, 101s–105s (April 2012)

Modeling of the Electric Arc Behavior of the Electric Arc Furnace

Manuela Panoiu[1], Caius Panoiu[1], and Loredana Ghiormez[2]

[1] Department of Electrical Engineering and Industrial Informatics,
Faculty of Engineering Hunedoara,
Politehnica University of Timisoara,
Hunedoara, Romania
{manuela.panoiu,caius.panoiu}@fih.upt.ro
[2] Faculty of Automation and Computers,
Politehnica University of Timişoara, Romania
loredanag@fih.upt.ro

Abstract. During the electric arc furnace operation appear disturbances, which can affect the other equipments that are connected to the same power network. So it is necessary to develop models for the electric arc which characterizes the electric arc behavior in order to identify methods and solutions through which the disturbances that appear in the power network can be reduced.

This paper presents two proposed models used to simulate the electric arc behavior of a 3-phase electric arc furnace which were implemented using the Simulink toolbox of Matlab. In order to facilitate the analysis of the influence of the model parameters, graphical user interfaces were implemented. Then, the simulation results were compared with known results.

Keywords: electric arc furnace, voltage-current characteristic, electric arc model.

1 Introduction

Because of the electric arc dynamic behavior during melting process, the electric arc furnaces are an important source of disturbances of which can be mentioned: harmonic currents, reactive power circulation, unbalanced load, voltage flicker. Regardless of the furnace type (DC or AC), disturbances are of random nature and generate high-order harmonics.

Generally, most AC electric arc furnaces are of high and very high power (UHP EAF), disturbances produced by them being larger. Considerable attention for power quality, asked for some actions by which these disturbances should be eliminated or reduced. In these conditions it is important to study the electric arc behavior, because, this being a nonlinear circuit element, it is the main cause of the produced disturbances by electric arc furnaces.

V.E. Balas et al. (Eds.): Soft Computing Applications, AISC 195, pp. 261–271.
springerlink.com

2 The Electric Arc Behavior

As it was presented in [4] and [7] it can be considered that during electric arc functioning supplied by alternative voltage, the electric arc circuit can be represented as in figure 1 and figure 2 shows the waveforms of the electrical parameters [3] of the electric arc. Parameters R and L are the resistance and the equivalent inductivity of the power supply circuit, and R_{arc} and u_{arc}, the resistance, respectively the voltage of the electric arc.

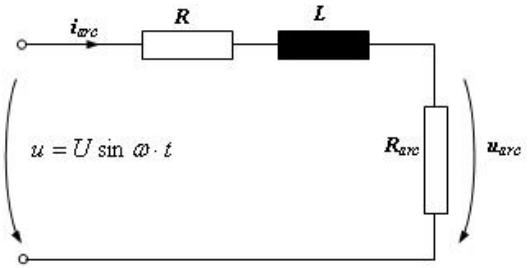

Fig. 1. The electric arc circuit supplied by alternative voltage

Figure 3 shows the typical voltage-current characteristic of the electric arc illustrated in [4], the continuous line illustrating the real characteristic and the dashed line representing the linear characteristic of the electric arc.

3 The Analysis of the Electric Arc Behavior

In order to implement the mathematical models of the electric arc the power supply diagram of the electric arc furnace for a single phase [5] was used because its behavior is almost the same for the other two phases. This diagram can be observed in figure 4, this including the electric arc circuit supplied by alternative voltage from figure 1.

In figure 4, the significance of the parameters is the following:

- *u(t)* – is the power supply voltage;
- Z_S – is the system impedance;
- *pcc* – is the point of common coupling;
- Z_T – is the transformer impedance, used to supply the furnace;
- *AF* – is the low voltage side of the transformer;
- *Furnace* represents the electric arc furnace which is powered by the transformer.

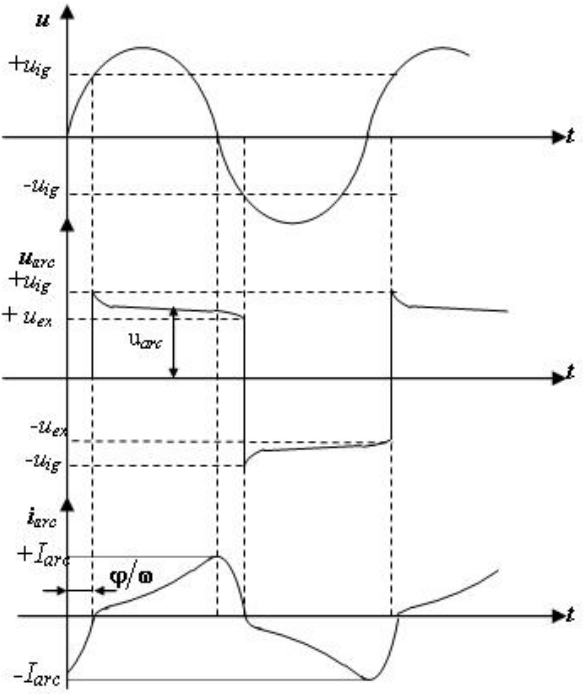

Fig. 2. The waveforms of the electric parameters in the electric arc circuit

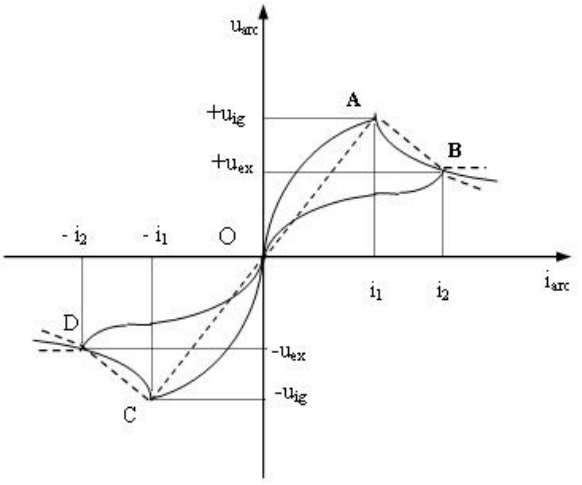

Fig. 3. The real and linear voltage-current characteristic of the electric arc

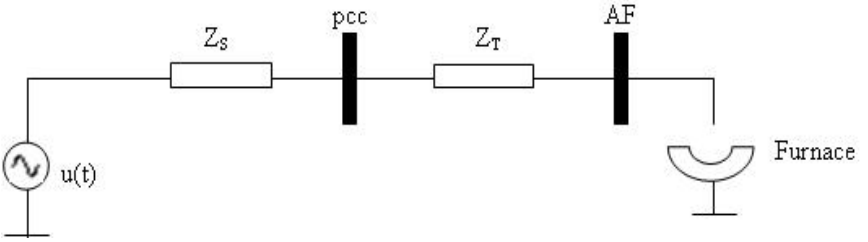

Fig. 4. The power supply diagram of the electric arc furnace for a single phase

4 Models of the Electric Arc

In the reference literature [1], [2], [3], [6], [9], [10] there are many models of the electric arc. Starting from a model which exists in the reference literature one model that extends the existing one will be proposed and the second model, suggested in this paper being a new one. The proposed models in this paper are focused on reproducing the voltage-current characteristic of the electric arc. Matlab environment was used to simulate models.

4.1 Models Based on the Linear Voltage-Current Characteristic of the Electric Arc

The model under analysis is described in [5] and [11] is based on the linear approximation of the typical voltage-current characteristic of the electric arc. This model is given in relation (1).

$$u = \begin{cases} R_1 \cdot i, & i \in [-i_1, i_1) \\ R_2 \cdot i + u_{ig} \cdot (1 - R_2 / R_1), & i \in [i_1, i_2] \\ R_2 \cdot i - u_{ig} \cdot (1 - R_2 / R_1), & i \in [-i_2, -i_1) \end{cases} \quad (1)$$

where,

$$i_1 = u_{ig} / R_1 \quad (2)$$

$$i_2 = u_{ex} / R_2 - u_{ig} \cdot (1/R_2 - 1/R_1) \quad (3)$$

In relations (2) and (3) the following parameters were used:

- R_1 – the line slope resulted when the voltage-current characteristic is approximated with a line ranging within $[-i_1, i_1)$;
- R_2 – the line slope resulted when the voltage-current characteristic is approximated with a line ranging within $[-i_2, -i_1)$ or $[i_1, i_2]$;
- i_1 – the value of the electric arc current reached at the ignition voltage of the electric arc (u_{ig});
- i_2 – the value of the electric arc current reached at the extinction voltage of the electric arc (u_{ex}).

Starting from the model presented in relation (1) an improved model has been implemented, which extends the existing one, this being presented in relation (4). The proposed model approximates more accurately the typical voltage-current characteristic of an electric arc. When the electric arc voltage reaches the extinction voltage value, u_{ex}, arc voltage continues its variation for a moment of time, and will not change it immediately.

$$u = \begin{cases} R_1 \cdot i, & i \in [-i_1, i_1] \\ R_2 \cdot i + u_{ig} \cdot (1 - R_2 / R_1), & i \in (i_1, i_2] \\ R_2 \cdot i_2 + u_{ig} \cdot (1 - R_2 / R_1), & i > i_2 \\ R_2 \cdot i - u_{ig} \cdot (1 - R_2 / R_1), & i \in [-i_2, -i_1) \\ R_2 \cdot (-i_2) - u_{ig} \cdot (1 - R_2 / R_1), & i < -i_2 \end{cases} \quad (4)$$

Within this model three functioning zones of the electric arc are distinguished, i.e.: the two presented before, and the third zone is the one corresponding to the current values below i_2, respectively above $-i_2$. In this zone one can notice that the electric arc voltage is maintained constant at the value calculated with (5).

$$u = R_2 \cdot i_2 + u_{ig} \cdot (1 - R_2 / R_1) \quad (5)$$

When current of the arc is below $-i_2$, the voltage is calculated with expression (6).

$$u = R_2 \cdot (-i_2) - u_{ig} \cdot (1 - R_2 / R_1) \quad (6)$$

Figure 5 shows a comparison between the two graphics, one being obtained with the existent model in the reference literature and the other with the first model proposed and illustrated in this paper.

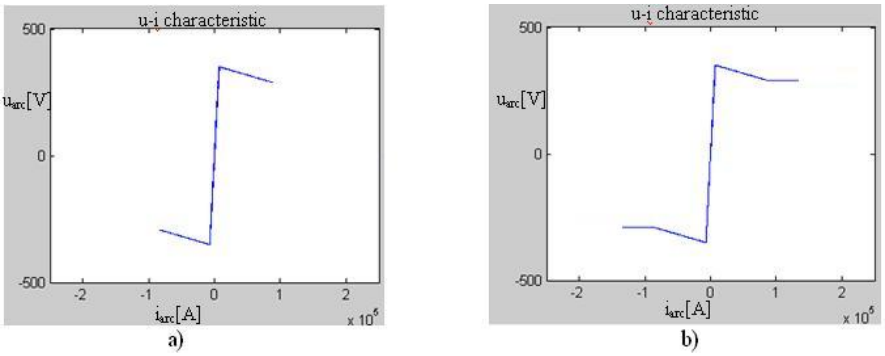

Fig. 5. The linear voltage-current characteristic obtained with the existent model (a) and with the first proposed model (b)

An interface in the environment Matlab version 2012, which is presented hereinafter, was implemented to see how the voltage-current characteristic of the electric arc is influenced by the model parameters.

Figure 6 shows the interface implemented in Matlab used to simulate the electric arc behavior. The components given by this interface are used to modify the model parameters, i.e. R_1, R_2, u_{ig}, u_{ex}.

A range of values for each parameter was selected, within which these can vary. Also, the interface has four buttons, each one having a different function.

The *Load model* button has the role to open the proposed model implemented in Simulink (Matlab), and then the parameter values are transmitted from the interface to the Matlab function implemented in Simulink.

The *Simulation* button can be pressed after the *Load model* button was pressed. The simulation button will draw the dynamic voltage-current characteristic of an electric arc, as model parameters can be varied in real time to see their impact upon the electric arc.

The *Stop Simulation* button has the role to stop the simulation and this can be started only if the *Simulation* button is pressed.

The *Exit* button has the role to close the interface, when it is pressed.

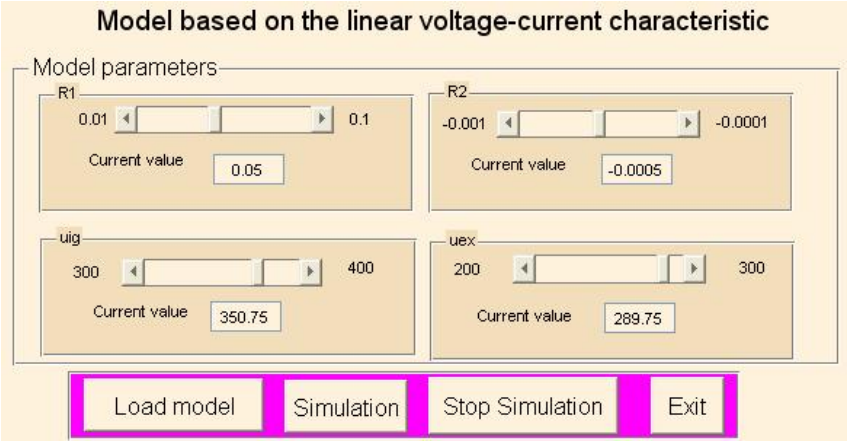

Fig. 6. The Matlab interface of the first proposed model

Using this interface one can obtain the dynamic voltage-current characteristic of the electric arc, which is presented in figure 7.

In the graph obtained from figure 7, it can be noticed that the interval in which the characteristic is defined is [-2x105, 2x105], and the dynamic voltage-current characteristic is linear.

As compared to the model presented in [5] the following differences arise:

- A different electric arc functioning zone is defined;
- In the case the value of the current is below $-i_2$ or above than i_2, one can notice that the voltage variation is constant, maintained at the extinction voltage value of the electric arc;
- The range within which the dynamic voltage-current characteristic can vary is larger than the one illustrated by the model presented in [5].

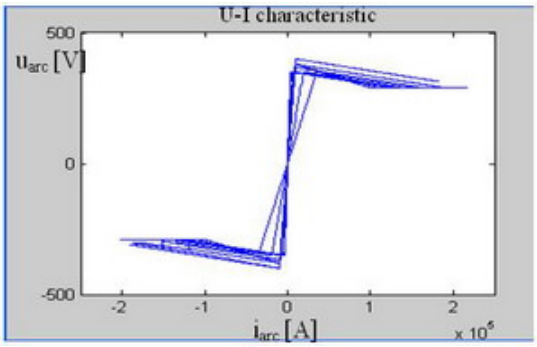

Fig. 7. The dynamic voltage-current characteristic obtained with the interface of the first proposed model

Figure 8 shows the current, respectively the voltage variations of the electric arc, obtained during the simulation of the electric arc behavior with the model previously proposed.

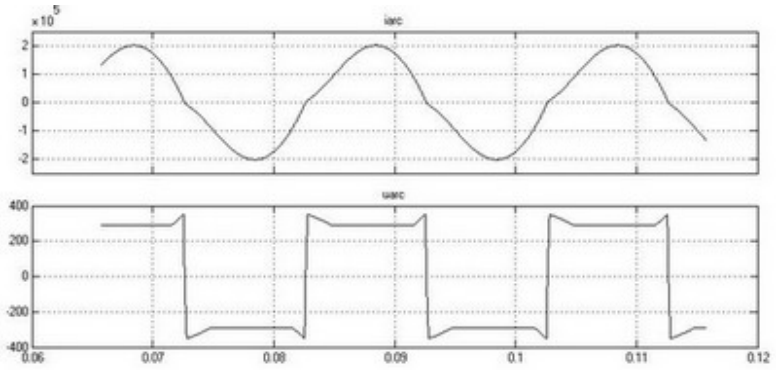

Fig. 8. The current and voltage waveforms of the electric arc

4.2 The Second Proposed Model, Based on the Voltage-Current Characteristic of the Electric Arc

The second model which is proposed in this paper being presented in relation (7) is a new model of the electric arc, which approximates more accurately the voltage-current characteristic of the electric arc. In its realization the characteristic can be divided in more sections in order to obtain a more accurate voltage-current characteristic of the electric arc. In this model, the arc melting process is divided into five sections; the values of the electric arc current correspond to:

- $\pm i_1$ corresponding to the ignition voltage of the electric arc on the two polarities;
- $\pm i_2$ corresponding to the medium value between the ignition and the extinction voltage of the electric arc;
- $\pm i_3$ corresponding to the extinction voltage of the electric arc.

In the first section, the value of the electric arc current is modified from $-i_3$ to i_1 or from $-i_1$ to i_3, in this section the voltage-current characteristic being approximated with a line and calculated with the first relation from (7). In this section the voltage magnitude increases from the extinction to the ignition voltage of the electric arc.

The second section corresponds to the value of the current ranging within $[i_1, i_2)$, or $[-i_1, -i_2)$, di/dt >0. In this section, the value of the electric arc voltage suddenly drops from the ignition voltage to the average value (u_m) of the electric arc, having an exponential variation.

The third zone corresponds to the value of the current ranging within $[i_2, i_m)$, di/dt>0 or $[-i_2, -i_m)$, di/dt<0, in this section being noticed that the voltage-current characteristic of the electric arc has a linear variation, the line slope being R_1.

In the fourth section it can be noticed that the voltage-current characteristic has a constant variation, and the value of the electric arc current is above i_m or below $-i_m$.

In the last section the value of the current can be above i_3 and di/dt <0 or below $-i_3$ and di/dt>0.

$$u=\begin{cases} -u_{ex}+(i_3-i_m)\cdot R_3 & i<-i_m \ \text{şi}\ \dfrac{di}{dt}\geq 0 \\ & \text{sau}\ i\in[-i_m,-i_3)\ \text{şi}\ \dfrac{di}{dt}\geq 0 \\ & \text{sau}\ i<-i_m\ \text{şi}\ \dfrac{di}{dt}<0 \\ R_1\cdot i & i\in[-i_3,i_1)\ \text{şi}\ \dfrac{di}{dt}\geq 0 \\ & \text{sau}\ i\in[-i_1,i_3)\ \text{şi}\ \dfrac{di}{dt}<0 \\ u_{ex}+(u_{ig}-u_{ex})\cdot e^{(i_1-i)/i_4} & i\in[i_1,i_2)\ \text{şi}\ \dfrac{di}{dt}\geq 0 \\ u_m+(i-i_2)\cdot R_2 & i\in[i_2,i_m]\ \text{şi}\ \dfrac{di}{dt}\geq 0 \\ u_{ex}+(i_m-i_3)\cdot R_3 & i>i_m\ \text{şi}\ \dfrac{di}{dt}\geq 0 \\ & \text{sau}\ i>i_m\ \text{şi}\ \dfrac{di}{dt}<0 \\ & \text{sau}\ i\in[i_3,i_m]\ \text{şi}\ \dfrac{di}{dt}<0 \\ -u_{ex}+(u_{ex}-u_{ig})\cdot e^{(i_1+i)/i_4} & i\in[-i_2,-i_1]\ \text{şi}\ \dfrac{di}{dt}\geq 0 \\ -u_m+(i+i_2)\cdot R_2 & i\in[-i_m,-i_2]\ \text{şi}\ \dfrac{di}{dt}<0 \end{cases} \tag{7}$$

In this model the values of the current were calculated with relation (8).

$$\begin{cases} i_1=u_{ig}/R_1 \\ i_2=2\cdot i_1 \\ i_3=u_{ex}/R_1 \\ i_4=1.5\cdot i_1 \end{cases} \tag{8}$$

Figure 9 shows the voltage-current characteristic of the electric arc obtained with the model presented before. It can be noticed that this characteristic approximates more accurately the typical voltage-current characteristic of the electric arc. In order to obtain the dynamic voltage-current characteristic of the electric arc with this model, a graphical user interface was implemented, similar to the first proposed model, figure 10 showing this dynamic characteristic.

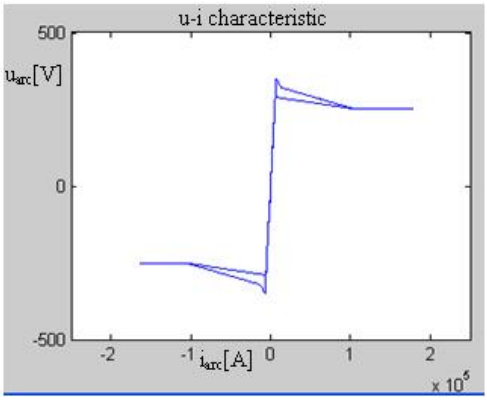

Fig. 9. The static voltage-current characteristic of the electric arc obtained with the second proposed model

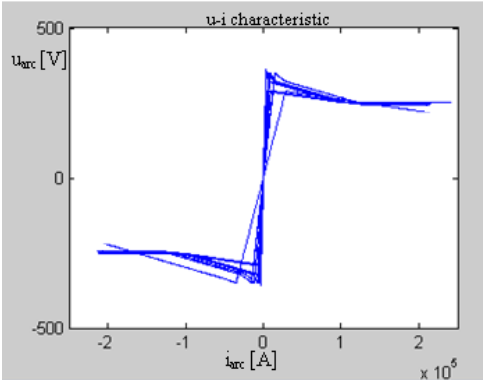

Fig. 10. The dynamic voltage-current characteristic obtained with the second proposed model.

Figure 11 illustrates the current, respectively the voltage variations of the electric arc obtained during the simulation of the electric arc behavior with the second model proposed before.

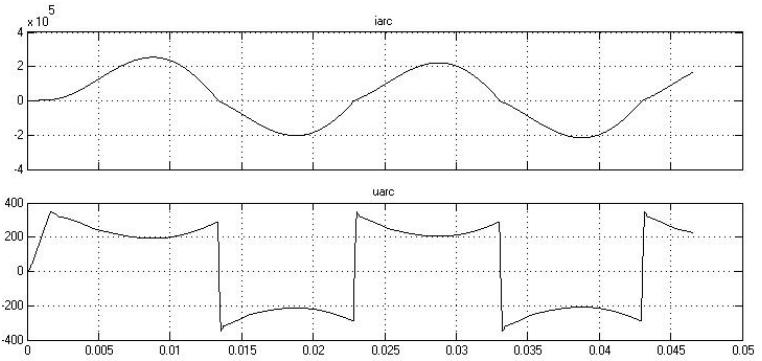

Fig. 11. The current and voltage waveforms of the electric arc for the second proposed model

5 Conclusions

Starting from the existing model in the reference literature, the authors of this paper proposed and implemented two models used to simulate the electric arc functioning. The improved models introduced by this paper help to obtain the dynamic or static voltage-current characteristics of the electric arc. It can be noticed that these characteristics obtained with the proposed models represent more accurately the real characteristic of the electric arc, as compared to the model presented in [5], because in reality, when the voltage of the arc reaches the extinction voltage value, u_{ex}, the arc voltage continues its variation for a moment of time, and will not change it immediately.

Using the proposed models by this paper, other models that accurately approximate this characteristic can be obtained.

References

1. Alonso, M.A.P.: An Improved Time Domain Arc Furnace Model for Harmonic Analysis. IEEE Transactions on Power Delivery 19(1), 367–373 (2004)
2. Collantes-Bellido, R., Gomez, T.: Identification and Modelling of a Three Phase Arc Furnace for Voltage Disturbance Simulation. IEEE Transactions on Power Delivery 12(4), 1812–1817 (1997)
3. Chang, G.W., Chen, C.-I., Liu, Y.-J.: A Neural-Network-Based Method of Modeling Electric Arc Furnace Load for Power Engineering Study. IEEE Transactions on Power Systems 25(1), 138–146 (2010)
4. Golovanov, N., Sora, I., Altii, S.: Electrothermics and electro-technologies, vol. I. Publishing house Tehnica, Bucuresti (1997)
5. Golkar, M.A., Tavakoli Bina, M., Meschi, S.: A Novel Method of Electrical Arc Furnace Modeling for Flicker Study. In: International Conference on Renewable Energies And Power Quality (ICREPQ 2007), Sevilla, March 28–30, pp. 620–626 (2007)

6. Wang, F., Jin, Z., Zhu, Z.: Modeling and Prediction of Electric Arc Furnace Based on Neural Network and Chaos Theory. In: Wang, J., Liao, X.-F., Yi, Z. (eds.) ISNN 2005. LNCS, vol. 3498, pp. 819–826. Springer, Heidelberg (2005)
7. Panoiu, M., Panoiu, C.: Nonlinear processes modeling and simulation in electrothermics. Publishing House Mirton, Timisoara (2008)
8. Panoiu, M., Panoiu, C., Sora, I., Osaci, M., Muscalagiu, I.: Modeling, Simulating and Experimental Validation of the AC Electric Arc in the Circuit of Three-Phase Electric Furnaces. In: EUROSIM 2007 Congress, Ljubljana, Slovenia, September 9-13, pp. 241–250 (2007)
9. Petersen, H.M., Koch, R.G., Swart, P.H.: Modelling Arc Furnace Flicker and Investigating Compensation Techniques. IEEE Trans. on Power Delivery, 1733–1740 (1995)
10. Hooshmand, R., Banejad, M., Esfahani, M.T.: A New Time Domain Model For Electric Arc Furnace. Journal of Electrical Engineering 59(4), 195–202 (2008)
11. Varadan, S., Makram, E.B., Girgis, A.A.: A New Time Domain Voltage Source Model for an Arc Furnace using EMPT. IEEE Transactions on Power Delivery 11(3), 1685–1691 (1996)

Live Steam Temperature Control Loop for 1035 t/h Benson Boiler

Onisifor Olaru[1] and Marius Bîzgă[2]

[1] "Constantin Brâncuşi"University of Târgu Jiu,
Faculty of Engineering
[2]Automation Department,
Rovinari Power Plant
onisifor.olaru@yahoo.com

Abstract. The paper presents the methods for process analyzing to determine optimal parameters of the control loops using the advantages of distributed control systems. The processes at the coal fired boilers are the most complex and very difficult to model by analytical methods. The paper reveals an example for using the step response method to determine the mathematical model of the live steam temperature control – 1035 t/h Benson boiler – Rovinari Power Plant.

Keywords: temperature control loop, transfer function, step response method, mathematical model.

1 Introduction

Rovinari Power Plant is located at 25 km S-W from Târgu Jiu and next to the town Rovinari, very close to the coal pits: Rovinari, Tismana and Pinoasa.

Due to its location, the power plant is directly fed, which is unique in Romania and offers the possibility to transform directly into energy the huge amount of coal from the pits which are included into the company ensuring a minimum transporting distance of the coal by conveyer belts.

This brings to a minimum of costs for coal transport, the power plant Rovinari being the only power plant without rail road costs.

The Power Plant Rovinari has an installed power 1320 MW, produced by four units, 330 MW each.

Boiler technical data:

- Type: Benson, tower, once-through
- Superheated steam pressure 196 bar
- Superheated steam temperature: 540 ^{o}C
- Live steam flow 1035 t/h
- Feed water temperature 260 ^{o}C
- Firewater pressure 251 bar

V.E. Balas et al. (Eds.): Soft Computing Applications, AISC 195, pp. 273–282.
springerlink.com

- Reheated steam flow at reheater inlet 974 t/h
- Reheated steam pressure at reheater inlet: 51,2 bar
- Reheated steam pressure at reheater outlet: 49,2 bar
- Reheated steam temperature at reheater inlet: 348 ^{o}C
- Reheated steam temperature at reheater outlet: 540 ^{o}C

A characteristic feature of the once-through boiler is that the feedwater pumps force the feedwater/steam through the boiler tubing, which in principle is arranged a continuous pipe. In contrast to a drum boiler there is no large internal water reservoir [3], [4], [5], [6].

The boiler process includes several steam superheating processes - most often boilers include superheaters in a number of levels often divided into parallel lines thus giving typically 4-8 high pressure superheaters and 2-4 intermediate pressure superheaters. Each of these processes serves as an energy transferring system-energy being transferred from the flue gas to the steam. Each superheater is equipped with an attemperator device (water injection at the inlet) for control of the steam outlet temperature (Fig. 1).

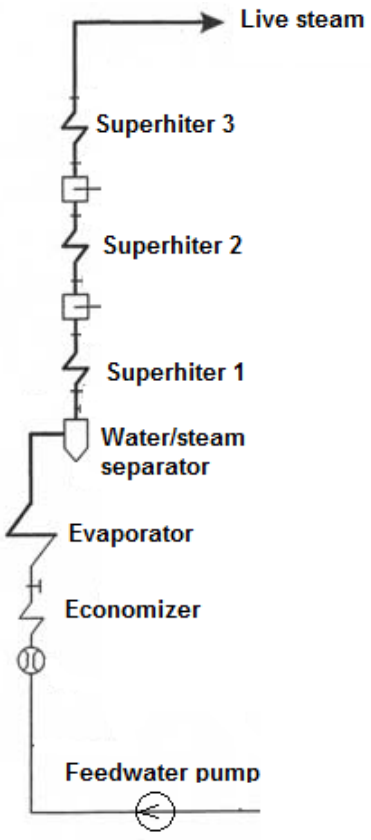

Fig. 1. Once through boiler

Economizer

Feedwater is introduced into the unit through the economizer inlet header. It flows through the economizer tube elements, and from each end of the outlet header to a common, external, unheated transfer pipe to the furnace to ensure a uniform entrance conditions into the furnace evaporator. Feeder pipes uniformly distribute subcooled feedwater to the furnace wall panel lower headers [4].

Evaporator

The furnace circuitry consists of a lower section with optimized, vertical rifled tubes that extend up to a transition header located at an elevation below the furnace nose. Above this location, vertical smooth bore tubes extend up to the furnace roof, and also form the furnace exit screen and part of the vestibule side walls [4].

Superheaters

From the in-line steam/water separators the fluid passes through the superheater circuitry which includes the furnace roof, half of the vestibule sidewalls and heat recovery area (HRA) enclosure, the primary superheater located in the outboard pass of the parallel pass HRA, the furnace platen superheaters, and the pendant finishing superheater at the furnace exit. Spray water attemperators are positioned upstream of the furnace platen superheaters, and the pendant finishing superheaters for initial rapid final main steam temperature control which is coordinated with the feedwater and firing rate controls [4].

The simplified scheme for live steam temperature control loop - 1035 t / h Benson boiler [1], [2] is shown in Fig. 2.

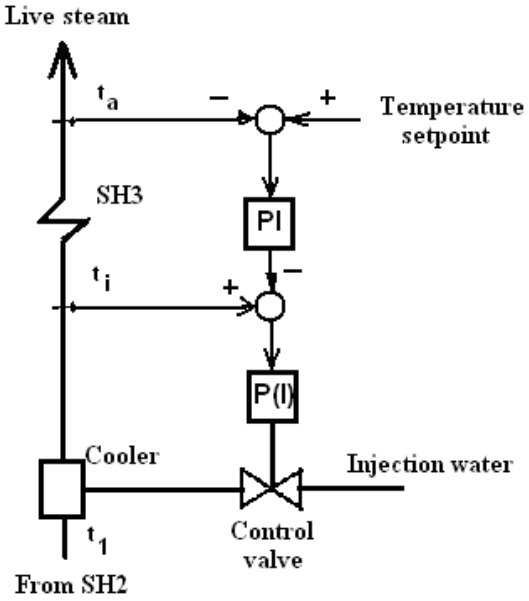

Fig. 2. The simplified scheme for live steam temperature control loop

There is a cascaded control loop where: t_1 – temperature before injection cooler (after superheater 2 – SH2); t_i – temperature after injection cooler (before superheater 3 – SH3); t_a – live steam temperature (after superheater 3) [2].

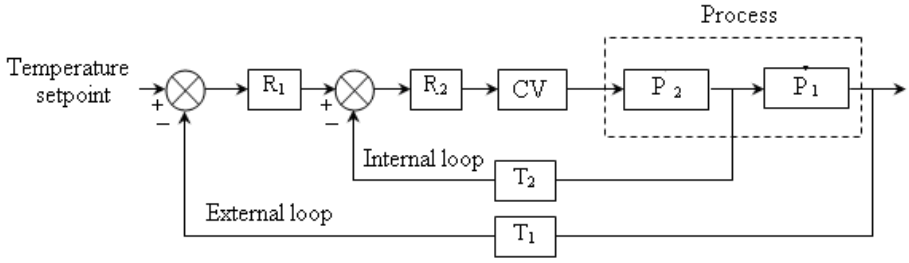

Fig. 3. Live steam temperature control loop

The cascaded control loop can be represented as in Fig. 3 were:

- R_1- main PI controller;
- R_2- cascaded PI controller;
- CV – injection water control valve;
- T_1, T_2 – temperature transmitters.

The process can be divided in two sub-processes:

- P_2 – represented by injection cooler;
- P_1 – represented by SH3.

2 Step Response Method

The dynamics of a process can be determined from the response of the process to pulses, steps, ramps, or other deterministic signals. The dynamics of a linear system is, in principle, uniquely given from such a transient response experiment. This requires, however, that the system is at rest before the input is applied, and that there are no measurement errors. In practice, however, it is difficult to ensure that the system is at rest. There will also be measurement errors, so the transient response method, in practice, is limited to the determination of simple models. Models obtained from a transient experiment are, however, often sufficient for PID controller tuning. The methods are also very simple to use. This section focuses on the step response method [2], [7], [8], [9].

The fixed part of a control loop is represented by the element that does not change behavior during operation. The fixed part is composed by the control valve, cooler and superheater – Fig. 4.

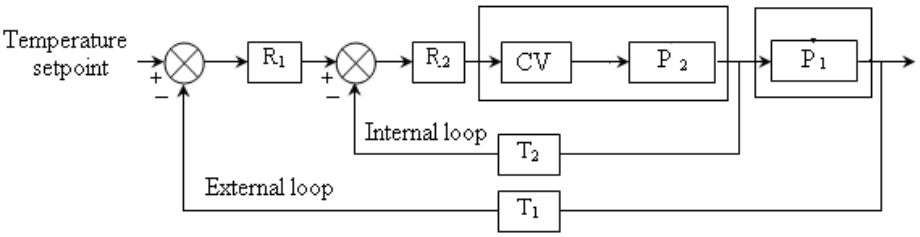

Fig. 4. The control loop with fixed part

To determine the fixed part step response, first is necessary to switch the control loop in manual mode, then to apply a step change for the opening control valve for water injection,

It is necessary to switch off all automatic systems which might influence the studied parameters, to avoid accumulation of several phenomena, because the precision of identification is affected by the existence of disturbances. So, is necessary to keep constant feedwater flow and constant fuel flow.

The test was done at 270 MW load by 2% down for the opening demand of the control valve. Applied step value was determined by the operating conditions of the unit, so not to cause significant load variations due to live steam temperature variations.

There were recorded variations for the opening value of the control valve, water injection flow rate, temperature after injection and temperature after SH3. Variation of parameters during the test is shown in Fig. 5.

The recorded values are exported to Microsoft Excel.

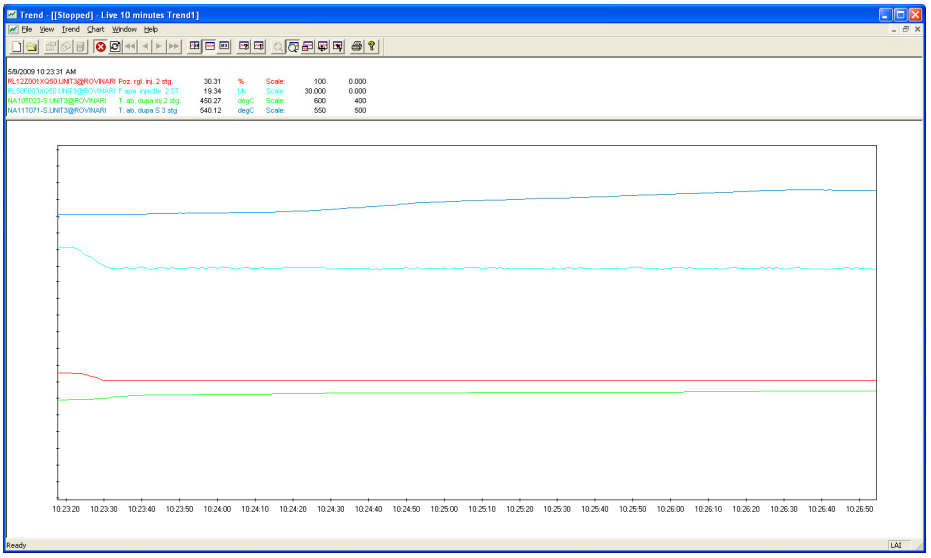

Fig. 5. Variation of the parameters during the test

For the process P_2 – represented by injection cooler – the step response is shown in Fig. 6. were: green – variation of the temperature after injection cooler, and red – variation of the control valve opening.

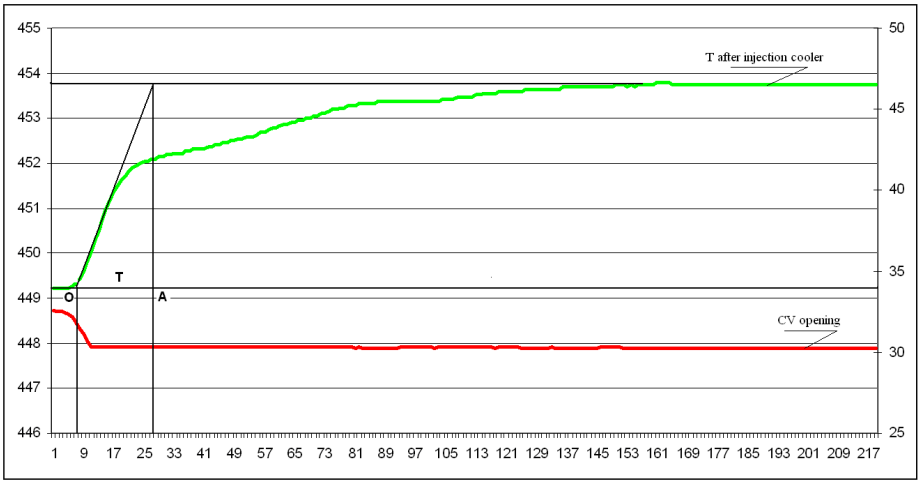

Fig. 6. Step response for process P_2

The process output is monotonically changed to a new stationary value, similar to a first order delay proportional element. The transfer function for this type of process is:

$$H(s) = \frac{K}{1 + T \cdot s}$$; K – process gain; T – time constant.

The process gain is calculated directly from the step response:

$$K = \frac{453{,}74 - 449{,}21}{30{,}31 - 32{,}56} = -2.01 \approx -2$$

The gain is negative because by closing the control valve the temperature is rising, the negative variation of the input signal determine positive variation for the output signal.

The time constant T is measured value of OA segment – figure 6.

T = 20 seconds.

The transfer function for P_2 process is:

$$H_{P2}(s) = \frac{-2}{1 + 20 \cdot s}$$

For the P_1 process is not possible to determine separately the transfer function.

In Fig. 7 is shown the temperature after SH 3 variation according to control opening variations. The step response includes both processes P_1 and P_2.

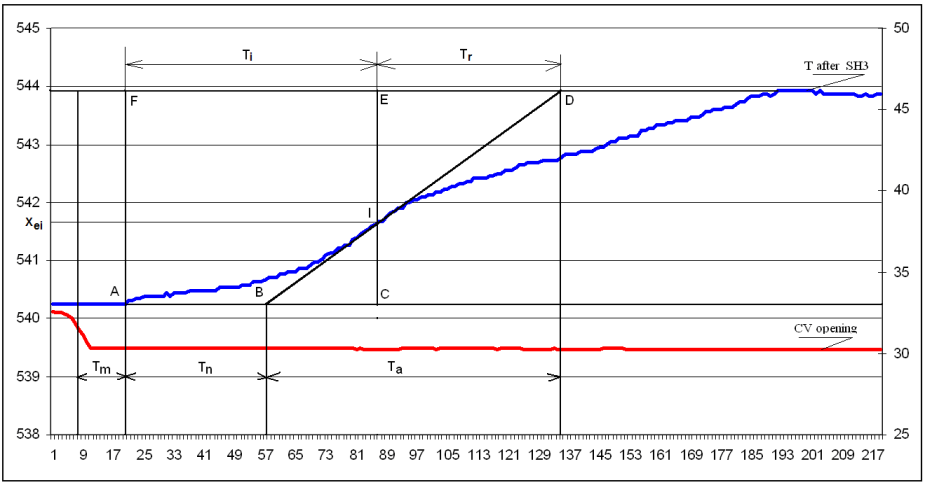

Fig. 7. Step response for process P_1+P_2

The process output is similar to an element with multiple parameters and dead time. The transfer function for this type of process is:

$H(s) = \frac{K \cdot e^{-\tau \cdot s}}{(1+T \cdot s)^n}$; K – process gain; T – time constant; τ – dead time; n–order system.

Transfer function coefficients will be determined after several graphical constructions, by the help of Table 1, where are introduced all the coefficients defined in Fig. 7 and using Strejc method.

Table 1. Transfer function coefficients

n	$\frac{T_a}{T}$	$\frac{T_n}{T}$	$\frac{T_n}{T_a}$	$\frac{T_i}{T}$	x_{ei}	$\frac{T_r}{T}$	$\frac{T_r}{T_a}$
1	1	0	0	0	0	1	1
2	2,718	0,282	0,104	1	0,264	2,000	0,736
3	3,695	0,805	0,218	2	0,323	2,500	0,677
4	4,463	1,425	0,319	3	0,353	2,888	0,647
5	5,119	2,100	0,410	4	0,371	3,219	0,629
6	5,699	2,811	0,493	5	0,384	3,510	0,616
7	6,226	3,549	0,570	6	0,394	3,775	0,606
8	6,711	4,307	0,642	7	0,401	4,018	0,599
9	7,164	5,081	0,709	8	0,407	4,245	0,593
10	7,590	5,869	0,773	9	0,413	4,458	0,587

The process gain is calculated directly from the step response:

$$K = \frac{543,92 - 540,26}{30,31 - 32,56} = -1,62$$

To determine the constants T and τ are necessary the following operations:

1. Build the tangent to the curve through the point I – segment BD.
2. Build the vertical through the point I – segment CE
3. Build the vertical through the point A (beginning of the transient process) – segment AF.
4. Measure values for T_n, T_a and, when exist, the real dead time T_m.

$T_m = 13$ seconds;
$T_n = 37$ seconds;
$T_a = 67$ seconds.

5. Determine values for T_n/T_a and T_r/T_a

$$\frac{T_n}{T_a} = \frac{37}{67} = 0,55$$

6. From table 1 choose the value below T_n/T_a. The value below 0,55 is 0,493 which corresponds to n=6.
7. For n=6 determine:

$$\frac{T_a}{T} = 5,699;\ T = \frac{T_a}{5,699} = \frac{67}{5,699} = 11,75;$$

T = 11,7 seconds.

$$\frac{T_n}{T} = 2,811;\ T = \frac{T_a}{2,811} = \frac{37}{2,811} = 13,16;$$

T = 13,1 seconds.

8. Because we have not the same value for T, proceed to calculate the dead time. Using the T value from the Table 1, proceed to calculate corrected time T_{nc}.

$$\frac{T_{nc}}{T} = \frac{T_{nc}}{11,7} = 2,811$$

$$T_{nc} = 11,7 \cdot 2,811 = 32,9;$$

$T_{nc} = 32,9$ seconds.

9. Determine correction dead time.

$$\tau' = T_n - T_{nc} = 37 - 32,9 = 4,1 \text{ seconds.}$$

The real dead time:

$$\tau = \tau' + T_m = 4,1 + 13 = 17,1 \text{ seconds.}$$

10. The transfer function:

$$H_{P1+P2}(s) = \frac{-1,62 \cdot e^{-17,1 \cdot s}}{(1+11,7 \cdot s)^6}$$

11. Considering

$$e^{-\tau \cdot s} = \frac{1}{\left(1+\frac{\tau}{n'} \cdot s\right)^{n'}},\ n' = \frac{\tau}{T} = \frac{17,1}{11,7} = 1,4\ .$$

The transfer function will be:

$$H_{P1+P2}(s) = \frac{-1,62}{(1+11,7 \cdot s)^{7,4}}$$

The combined processes can be represented like in Fig. 8.

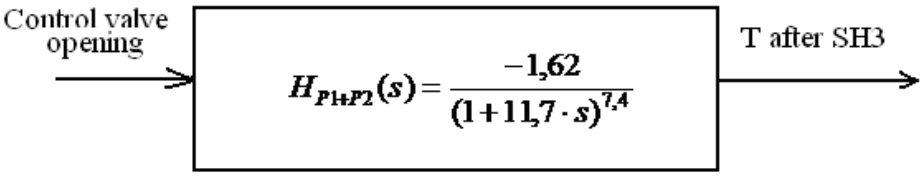

Fig. 8. The transfer function of P_1+P_2

Representing separately the processes we obtain Fig. 9.

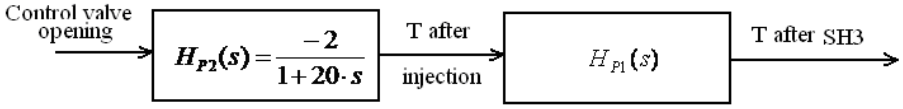

Fig. 9. Representation of P_1 and P_2 separately

The transfer function of the superheater is:

$$H_{P1}(s) = \frac{H_{P1+P2}(s)}{H_{P2}(s)}$$

$$H_{P1}(s) = \frac{-1{,}62 \cdot e^{-17{,}1 \cdot s}}{(1+11{,}7 \cdot s)^6} \cdot \frac{1+20 \cdot s}{-2} = 0{,}81 \cdot \frac{(1+20 \cdot s) \cdot e^{-17{,}1 \cdot s}}{(1+11{,}7 \cdot s)^6}.$$

$$H_{P1}(s) = 0{,}81 \cdot \frac{(1+20 \cdot s)}{(1+11{,}7 \cdot s)^{7{,}4}}$$

The transfer function of the process P_1 and P_2 is represented in Fig. 10.

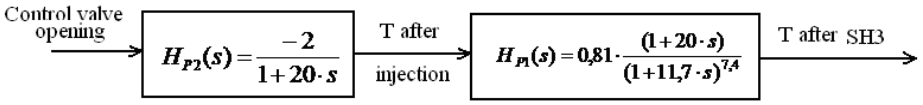

Fig. 10. The transfer functions of P_1 and P_2

3 Conclusion

This paper investigates the experimental methods to determine optimal parameters of the control loops for a complex process including the coal fired boilers.

It is presented an example using the step response method to determine the mathematical model of the live steam temperature control Benson boiler from Rovinari Power Plant.

Analytical equations and different graphic dependences of parameters were presented. Considering the live data useful recommendations for choosing parameters were formulated. Eventually the transfer functions for the processes are obtained.

References

[1] Klefenz, G.: Die Regelung von Dampkraftverken, Mannheim, Wien, Zurich (1991)
[2] Olaru, O., Bizga, M.: Structuri de reglare în centrale termoelectrice. Editura Politehnica, Timişoara (2009)
[3] Schweitzer Engineering Laboratories Inc.: Power Plant – Steam Control
[4] Foster Wheeler Power Group, Inc. - Fwpg Benson Vt Boiler Process and Operational Description
[5] Instructiuni de exploatare cazan de 1035 t/h, CTE Rovinari, Romania
[6] Moelbak, T., Mortensen, J.H.: Steam temperature control
[7] Bîzga, M.: Optimizarea SRA a cazanului dintr-o termocentrala: Sistemul de reglare automata a presiunii aerului de ardere, Diploma Thesis, AII (2006)
[8] Dumitrache, I. (ed.): Automatica. Editura Academiei, Bucharest (2009)
[9] ICEMENERG - Instrucțiuni de verificare în condiții de exploatare a performanțelor instalațiilor de automatizare din CTE

Dynamic Modeling and Computer Simulation of 3D Objects Grasping

Rim Boughdiri[1,2,*] , Hala Bezine[1], Nacer K. M'Sirdi[2],
Aziz Naamane[2], and Adel M.Alimi[1]

[1] REGIM: REsearch Group on Intelligent Machines,
University of Sfax,
National Engineering School of Sfax (ENIS),
BP 1173, Sfax, 3038, Tunisia
rimboughdiri@gmail.com
[2] LSIS, CNRS UMR 7296. Dom. Universitaire St Jérôme,
Avenue Escandrille Normandie–Niemen 13397 Marseille France

Abstract. Among the essentials functionalities of several robotic systems are grasping and manipulating of objects by multi-fingered robot hands. Therefore many researchers have studied features of the two major closely related tasks.

In this paper, we consider the problem of mathematical modeling of the robotic hand, the object and the physical interactions between the object and fingers under sliding constraints.

Development of a numerical simulator for 3-D object grasping and manipulation by multi-fingered robot hands is an active area in robotic field. By integrating the derived Lagrange's equations of motion of the fingers and object under sliding constrains in the 3D simulator HandGrasp that is designed and developed at REGIM (Laboratory of REsearch Group on Intelligent Machine), numerical simulation results of 3-D object pinching and manipulation based on the impedance control law. This simulation results show the validity of mathematical modeling and the control method

Keywords: Multi-fingered robot hand, Dynamic Modeling, Model-based control, 3D Simulation.

Nomenclature

Σ_p Task coordinate system velocity
Σ_o Object coordinate system fixed on the object
Σ_i i-th fingertip coordinate system fixed on the i-th fingertip
p_o Position vector of the origin of the object coordinate system Σ_o with respect to Σ_p
η_o Orientation vector of the origin of the object coordinate system Σ_o with respect to Σ_p
ω_o Angular velocity vector of the origin of the object coordinate system Σ_o with respect to Σ_p
q_i Joint angle vector of i-th finger

* Corresponding author.

V.E. Balas et al. (Eds.): Soft Computing Applications, AISC 195, pp. 283–293.
springerlink.com

1 Introduction

Human hands present enormous skills. They have richness architecture owing to the important degree of freedom of the fingers, the large number of muscles, the extremely sensitive sensors and the inseparable couple that forms with the brain. Therefore human hands are a great challenge and attract many researchers.

Thus the grasping task is one of the most complex functions reproduced by a robotic system because it is not so simple for a robot to hold and manipulate an object, it has to follow many steps and require many equipments and tests specifically when manipulating the object. So designing an articulated robotic hand is a difficult task with this many considerations including task requirements, mechanism complexity, and physical size and weight. However a physical prototype is often required to truly test a robot hand's ability to perform tasks, but this can be quite costly and design changes are not easy to make. What is needed is a system that would allow a user to load a hand design, to interact with it and perform grasps of objects, and to visualize and evaluate the space of forces and torques that it can apply. Therefore, the simulation has emerged as a necessary step given the opportunities it offers notably for the modeling of the hand grasping movements. Such 3D simulator allows us to render the hand in three dimensions and to move the fingers in order to grasp an object. In the last decades, many simulators of the hand, whether a human or robotic ones, has been developed [1,2,3].

In this paper we use a 3D simulator developed in our laboratory to test and validate the motion of the robot hand in specified grasping task which is described by Lagrange's equations.

First we use our methodology presented in previous work [4] to derive the dynamic equations of the grasp system hand/object. Then, to validate the developed models, we need to control the robot hand to grasp different shapes of object.

A great many control schemes have been developed in the literature to achieve stable grasp. Despite the diversity of approaches, it is possible to classify most of the design procedures as based on three major approaches: model-based controllers [5,6], adaptive controllers [7,8] and controllers based on intelligent methods [9,10]. In this paper we are interested in the model-based multi-fingered robot hand control that has been used widely for precise finger positioning because such controllers suppose the knowledge of the mathematical model parameters which describes the behavior of the system.

This article is organized as follows. In section 1, a brief literature review related to the 3D simulator and the control of grasping and manipulation by multi-fingered robots hands is presented. Then in section 2, the dynamics equations of the grasped object and the hand will be given. Section 3 describes the proposed strategy to validate the derived dynamic models. Using a 3D grasp simulator, simulation results for five-fingered hand grasping different shapes of objects is illustrated in Section 4. Finally, Section 5 concludes the paper.

2 System Modeling

Dynamic modeling is fundamental for the study of model-based controller design. In this section, we derive effective dynamic equations of an articulated robot hand grasping an object.

Consider a robotic hand with four fingers namely, index finger, middle finger, ring finger and pinky finger with three joints on each finger, the thumb with two effective joints and a wrist, manipulating a rigid object. Each joint represents one DOF, so each finger has three DOF and the thumb has two DOF. The wrist has six DOF. Fig.1 describes the hand object system with different coordinate frames. Fig.2 presents the kinematic model of the specified hand.

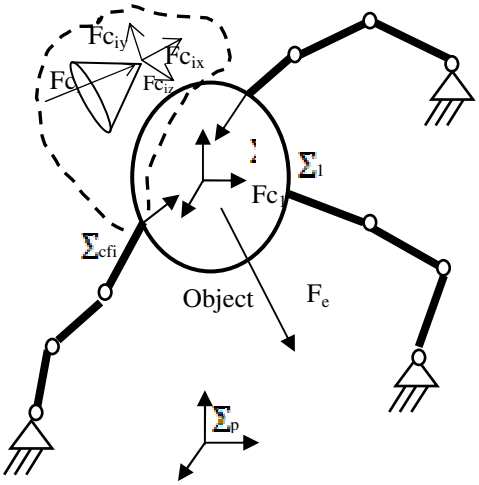

Fig. 1. Hand-Object system and coordinate frames

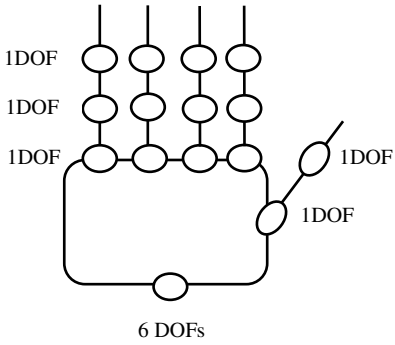

Fig. 2. Kinematic model of the specified hand

Some assumptions are made to reduce the complexity of the system and facilitate the dynamic formulation by taking into account only the important dynamic influence.

The following assumptions are:

- The hand has a modular structure. The whole hand is divided into two sections: five fingers and a supporting palm.
- The palm is considered as a rigid body with 6 DoF.
- Each finger is considered as a rigid body that has a rotational movement with the palm.
- Deformation of the fingertips is not considered.
- The contact is punctual and located in the fingertip.

We use the formalism of Lagrange to examine the general structure of the models, to emphasize the different parameters and to deduce their properties. So in order to

compute the global dynamic model we need to define the different energies and the corresponding matrices. The inertia matrixes are directly related to the expression of the kinetic energy by the following equation:

$$E_c = 1/2 \sum_{i=1}^{n} \sum_{j=1}^{n} M_{i,j} \dot{q}_i \dot{q}_j \tag{1}$$

The inertia matrix is symmetric. We have one solution to determine element of this matrix. To use certain properties used in control of mechanical systems, the matrix C must satisfy the relation: $N(q,\dot{q}) = \dot{M}(q) - 2C(q,\dot{q})$ such that matrix N is antisymmetric. A solution to determine C is to use the Christoffel symbols of the first kind [11]. This is directly implemented in symbolic computation:

$$C_{i,j} = \sum_{k=1}^{n} \left(\frac{\partial M_{i,j}}{\partial q_k} + \frac{\partial M_{i,k}}{\partial q_j} - \frac{\partial M_{i,k}}{\partial q_i} \right) \frac{q_k}{2} \tag{2}$$

The effects of gravity vector G is calculated as the gradient of the potential energy with respect to the position vector q.

$$G(q) = \nabla E_p(q) \tag{3}$$

In order to generate the dynamic model, we created a configuration file that defines the entire mechanism (frames, parameters, contacts) and we will use it in Maple software [12]. The hand nominal model is developed assuming that the contact is permanent and reduced to a single point for each fingertip.

The dynamic equations of the object and robot fingers can be described respectively by:

$$M_o(r_o)\dot{\upsilon}_o + C_o(r_o, \dot{r}_o)\upsilon_o + G_o(r_o) = F_o + F_e \tag{4}$$

$$M_{hnd}(q)\ddot{q} + C_{hnd}(q,\dot{q})\dot{q} + G_{hnd}(q) = \tau_{hnd} - J_{hnd}^T F_c \tag{5}$$

Where $M_o \in R^{6\times6}$, $C_o \in R^{6\times6}$ and $G_o \in R^{6\times1}$, denotes respectively the inertia matrix of the object, the centrifugal and Coriolis forces, and the gravitational force. $F_o \in R^{6\times1}$ is the resultant force applied to the object by the fingers and $F_e \in R^{6\times1}$ is the other possible external force applied on the object. $M_{hnd}(q) \in R^{20\times20}$ is the inertia matrix of the robot fingers, $C_{hnd}(q,\dot{q}) \in R^{20\times20}$ is the Coriolis and centrifugal matrix of the robot fingers and $G_{hnd}(q) \in R^{20\times1}$ is the gravity force term of the robot fingers. $\tau_{hnd} \in R^{20\times1}$ is the input joint torques. $J_{hnd} \in R^{6\times6}$ is the kinematic Jacobian matrix at contact point C_i.

The object velocity is given by:

$$\upsilon_o = \begin{bmatrix} \dot{p}_o^T & \omega_o^T \end{bmatrix}^T = T_o(\eta_o)\dot{r}_o \tag{6}$$

T_o is a transformation matrix between the original object velocity representation using angular velocity vector ωo and that representation using roll, pitch and yaw angle.

$$T_o(\eta_o)=\begin{bmatrix} I_3 & 0 \\ 0 & T_r \end{bmatrix}, \qquad T_r=\begin{bmatrix} 1 & 0 & \sin\theta \\ 0 & \cos\Phi & -\sin\Phi\cos\theta \\ 0 & \sin\Phi & \cos\Phi\cos\theta \end{bmatrix} \tag{7}$$

Note that in this paper we consider that $\Phi \cong 0$, so we have $T_o(\eta_o) \cong I_6$ and $\upsilon_o \cong \dot{r}_o$

Each robot finger applies a force $F_{ci} \in R^{3\times 1}$ through the contact point C_i to the object. Then the resultant force and moment, f_o, $\eta_o \in R^{3\times 1}$, applied to the object by multi-fingered hands are given by:

$$f_o = \sum_{i=1}^{5} F_{ci} \tag{8}$$

$$n_o = \sum_{i=1}^{5} (p_{oci} \times F_{ci}) \tag{9}$$

$$F_o = \begin{bmatrix} f_o^T & n_o^T \end{bmatrix}^T \tag{10}$$

$$F_o = \sum_{i=1}^{5} W_i F_{ci} \tag{11}$$

Where W_i is a grasp matrix at the contact point C_i expressed by:

$$W_i = \begin{bmatrix} I_3 \\ [p_{oci}\times] \end{bmatrix} \in \Re^{6\times 3} \tag{12}$$

Where $I_3 \in R^{3\times 3}$ is the identity matrix and $[p_{oci}\times] \in R^{3\times 3}$ is a skew-symmetric which expresses the cross product form of p.

$$F_o = W F_c \tag{13}$$

Where $W= [W_1\ W_2\ W_3\ W_4\ W_5]$ and $Fc= [F_{c1}\ F_{c2}\ F_{c3}\ F_{c4}\ F_{c5}]^T$

3 Validation Strategy

To validate the dynamic models and observe the behavior of the system, we apply a strategy of control, then we use the 3D simulator HandGrasp developed in [14]

The problem involves the determination of the required set of input joint torques such that the object tracks a defined trajectory and the contact force converge to desired value.

The following assumptions are made to design hand control law:

- The contact between the fingertips and the object is assumed to be punctual without slip or contact break. So the contact point velocity $\upsilon_c=G^T \upsilon_o$ is equal to the fingertips velocities $\upsilon_F=J_{hnd}\dot{q}$

$$\ddot{q} = J_{hnd}^{-1}\left[G^T T_o \ddot{r}_o + \left(G^T \dot{T}_o + \dot{G}^T T_o\right)\dot{r}_o - \dot{J}_{hnd}\dot{q}\right] \tag{14}$$

- $r_o=[p_o^T,\eta_o^T]^T$, υ_o, q_i , $\dot{q}_i$, F_{ci} are measurable.
- Desired trajectory of the object $r_{od}=[p_{od}^T, \eta_{od}^T]^T$, $\dot{r}_{od}$ and $\ddot{r}_{od}$ are time continuous and bounded.

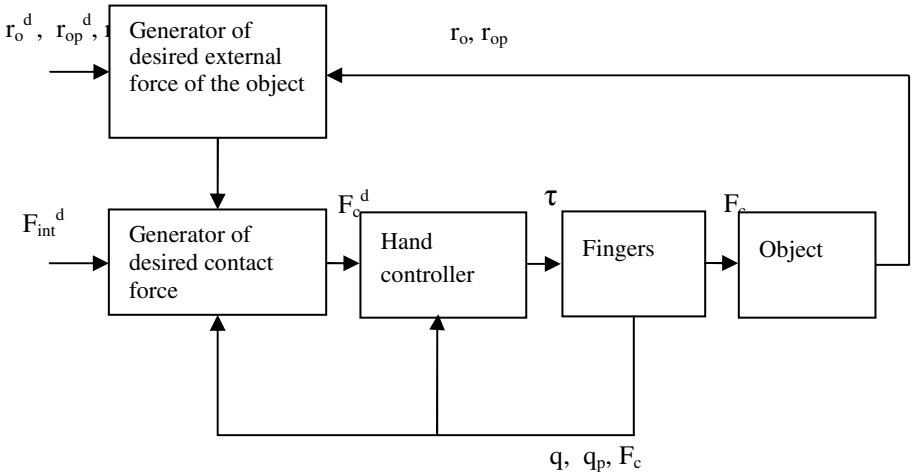

Fig. 3. Multi-fingered robot hand control architecture

Grasping is performed in two steps: hand moving and fingers closing. Therefore the conception of the Hand controller, shown in Fig.3, is based on the combination of a PD with constant gravity compensation of approach for maintaining a predefined position and orientation of the wrist and an impedance control approach for the control of the fingers.

3.1 PD Control with Constant Gravity Compensation

The proposed control is aimed at regulating the position and the orientation of the wrist to desired values. We use such controller, not only because of its simple structure and easy implementation but also its acceptable performance for trajectory tracking with the asymptotic stability if the control gains are carefully selected.

The PD control with constant gravity compensation is expressed as:

$$\begin{aligned} \tau_{wrist} &= G(\xi) - \left(k_{p1}e + k_{v1}\dot{e}\right) \\ e &= \xi - \xi_d \end{aligned} \tag{15}$$

Where ξ denotes the wrist position and orientation vector, ξ_d is the desired position and orientation vector, e is the tracking error, $\dot{e}$ denotes the derivative of the tracking error and τ_{wrist} is the applied torque. Kp_1, kv_1 are both symmetric and typically diagonal gains and $G(\xi)$ is the vector of gravitational forces.

3.2 Hybrid Position/Force Control

We derive a hybrid position/force control algorithm presented by Yoshikawa [6].

The first step in the algorithm is to linearize the nonlinear dynamics of the system by using the following linearizing control law which takes new inputs u_0 and u_1:

$$M_w T_o u_0 + J^T E u_1 + Q = \tau_{hnd} \tag{16}$$

Where:

$$M_w = M_{hnd} J^{-1} G^T + J^T G^+ T_o^{-T} M_o T_o^{-1} \tag{17}$$

$$Q = C_{hnd} + G_{hnd} + J^T G^+ T_o^{-1}(C_o + G_o) + M_{hnd} J^{-1}\left\{\left(\dot{G}^T T_o + G^T \dot{T}_o\right)\dot{r}_o - \dot{J}\dot{q}\right\} \tag{18}$$

The form of the closed loop system after applying the control law (16) is:

$$\ddot{r}_o = u_0 \tag{19}$$

$$F_{\text{int}} = u_1 \tag{20}$$

The second step is to determine the inputs u_0 and u_1:

$$u_0 = \ddot{r}_{od} - K_v(\dot{r}_o - \dot{r}_{od}) - K_p(r_o - r_{od}) \tag{21}$$

$$u_1 = F_{\text{int}}^d - K_1 \int (F_{\text{int}} - F_{\text{int}}^d) dt \tag{22}$$

Where K_v, K_p and K_1 are feedback gain matrices that must be chosen carefully to let the position and the force to converge to desired values. r_{od} and F_{int}^{d} are respectively the desired position and force trajectories.

$e_p=r_o-r_{od}$ and $e_f=F_{int}-F_{int}^{d}$ are the position and force errors which satisfy the following equation:

$$\ddot{e}_p + K_v \dot{e}_p + K_p e_p = 0, \qquad \dot{e}_f + K_1 e_f = 0 \tag{23}$$

The algorithm that determines the joint control input can be resumed in the following three steps [13]:

i. Calculate the resultant force F_o that realizes the desired object motion r_{od} by using (21) and $F_o=M_o u_o+C_o+G_o$

   Note that the desired external force applied to the object is computed based on the dynamic parameters of the object.

ii. Determine the contact force F_c that produces F_o obtained in (i) and satisfies the friction condition at the contact points and by adjusting the desired internal force parameter.

   From equation (13):

$$F_c = G^+ F_o + \left(I_{15} - G^+ G\right) F_{\text{int}}^d \tag{24}$$

Where G^+ is the pseudo-inverse of G .The first term of (24) produces the resultant external force F_o and the second term represents the internal grasping force that does not affect the object motion.

iii. Calculate the finger command torque τ_{hnd} that produces F_c obtained in (ii), using (5) and (14).

Physically, it is noticed that the computation in step (i) is for the object, that in step (ii) is for the contact points, and that in step (iii) is for the fingers.

4 3D Simulation Results and Discussions

An example of 3D simulation is performed to show the effectiveness of the proposed architecture where the dynamic parameters of the object and the robot fingers are identified by our methodology presented in previous work. The proposed control law was implemented and evaluated for two cases in which five multi-fingered hand grasp a spherical object of radius of 0.07 m and mass of 0.2kg and a square of 0,07 m . The initial values of the parameters of simulation are set to zero. We suppose that the hand is fully extended and the initial object position is located at the center of the palm.

For the control of the wrist, the parameters of the control law are set to kp_1=[1000 1000 1000 1000 1000 1000], kv_1=[100 100 100 100 100 100] to achieve the desired position and orientation.

The desired trajectory of the object is given by 5 order polynomial in time with initial $r_o^d(0)$= [0,0.1,0.14,0,1.57,0]^T(m, rad) and final $r_o^d(0.5)$=[-0.03,0.1,0.11,0,1.92,0]^T (m, rad). The magnitude of F_{int}^d is set to 1 N for the Thumb and 0.5 N for the others fingers. We assume that the desired internal force is directed along the normal to the contact surface.

Joints positions and contact forces are saved in a file data from Matlab Simulink to serve as an input for the 3D Simulator.

Initial posture Intermediate posture

Fig. 4. Simulation 3D results for the spherical object

Final posture

Fig. 4. (*continued*)

Initial posture

Intermediate posture

Final posture

Fig. 5. Simulation 3D results for the square

It is observed from the fig. 4 and fig.5 that 3D simulation results described above prove that the model-based controller can achieve high positioning performance. So the derived model is validated and it can predict the dynamic of the grasp task.

5 Conclusion

A dynamic model of a multi-fingered robot hand based on the formalism of Lagrange has been presented. Since many researchers derive the dynamic model of the hand considering the dynamic model of a manipulator three DOF each finger separately, the model derived in this paper takes into account the coupling between the fingers.

The model, because of its computational simplicity, has been easy to be integrated in a 3D simulator.

3D simulations of a grasping task for different shapes of object are quite satisfactory and show the validity of the model.

As future works, we will attempt to design controllers based on intelligent methods for the grasping task and validate the behavior of the system numerically and graphically.

Acknowledgements. The authors would like to acknowledge the financial support of this work by grants from General Direction of Scientific Research (DGRST), Tunisia, under the ARUB program.

References

[1] Miller, A., Allen, P.K.: Graspit!: A Versatile Simulator for Robotic Grasping. IEEE Robotics and Automation Magazine 11(4), 110–122 (2004)

[2] Awaad, I., Leon, B.: XPERSim: A Simulator for Robot Learning by Experimentation. In: Proceedings of the 1st International Conference on Simulation, Modeling, and Programming for Autonomous Robots, pp. 5–16 (2008)

[3] Peña-Pitarch, E., Yang, J., Abdel-Malek, K.: Virtual Human Hand: Grasping and Simulation. In: Proceedings of the 2nd International Conference on Digital Human Modeling: Held as Part of HCI International, pp. 140–149 (July 2009)

[4] Boughdiri, R., Bezine, H., M'Sirdi, N.K., Naamane, A., Alimi, A.M.: Dynamic modeling of a multi-fingered robot hand in free motion. In: International Multi-Conference on Systems, Signals & Devices, SSD 2011, pp. 1–7 (2011)

[5] Hogan, N.: Impedance control: An approach to manipulation, parts I-III. ASME Journal of Dynamic Systems, Measurement, and Control 107(1), 1–24 (1985)

[6] Yoshikawa, T., Sugie, T., Tanaka, M.: Dynamic hybrid control of robot manipulators: controller design and experiment. IEEE Journal of Robotics and Automation 4(6), 699–705 (1988)

[7] Kawasaki, H., Ueki, S., Ito, S.: Decentralized adaptive coordinated control of multiple robot arms without using a force sensor. Automatica 42, 481–488 (2006)

[8] Ueki, S., Kawasaki, H., Mouri, T.: Adaptive coordinated control of multi-fingered robot hand. Journal of Robotics and Mechatronics 21(1), 36–43 (2009)

[9] Al-Gallaf, E.: Neural network based inverse kinematics for multi-finger hand control. In: IASTED Internat. Conf. in Neural Networks, Pittsburgh, PA, pp. 82–87 (2000)
[10] Dominguez-Lopez, J.A., Vila-Rosado, D.N.: Hierarchical fuzzy control to ensure stable grasping. In: Seventh Mexican International Conference on Computer Science (ENC 2006), pp. 37–43 (2006)
[11] Canudas de Witt, C., Siciliano, B., Bastin, G.: Theory of Robot Control. Springer (1996)
[12] Beurier, G.: Modélisation, analyse et contrôle de systèmes mécaniques avec interaction avec l'environnement: Aide à la conduite d'un tunnelier pour un forage en continu., PhD Thesis, UPMC, Paris 6 (1999)
[13] Yoshikawa, T.: Multifingered Robot Hands: Control for Grasping and Manipulation (Review Paper). Annual Reviews in Control 34(2), 199–208 (2010)
[14] Walha, C., Bezine, H., M'sirdi, N.K., Naamane, A., Alimi, A.M.: HandGrasp: a new simulator for human grasping. In: Workshop on Autonomous Grasping at IEEE International Conference on Robotics and Automation, ICRA 2011 (2011)

Optimization of the Binary Adder Architectures Implemented in ASICs and FPGAs

Bojan Jovanović and Milun Jevtić

University of Niš, Faculty of Electronic Engineering,
Dept. of Electronics
A. Medvedeva 14, 1800 Niš, Serbia
{bojan,milun.jevtic}@elfak.ni.ac.rs

Abstract. In this paper both theoretical and experimental comparative performance analysis of several binary adder architectures is performed. Also, one modified carry-bypass technique for adder performance improvement is presented. When applying simple unit-gate theoretical model for area and delay estimation it has been shown that logarithmic delay architectures (carry-lookahead and prefix adders) are the fastest but the most hardware demanding. On the other hand, the implementations in modern Virtex-6 general purpose FPGAs witness that here presented carry-bypass technique is the best tradeoff for such devices in terms of area, speed and power consumption. Presented results can be considered as a valuable resource in the selection of the most appropriate adder topology that will be used to implement a given arithmetic operation in a specified technology.

Keywords: Binary adder architectures, modified carry-bypass adder, FPGA, ASIC, Power consumption.

1 Introduction

Whenever you are trying to implement any design which will process digital signals (digital filters, image analysis, neural networks, robotics and automation etc.) it is quite sure that you'll be obliged to use some arithmetic units. Furthermore, from a careful analysis of the whole processing system one can conclude that used arithmetic units are often the most responsible for the overall system performances. Bearing in mind that binary addition is the most pervasive arithmetic operation as well as the common data-path operator in hardware implementation of many other arithmetic units (multipliers, dividers etc.) the main objective of the research presented in this paper is to perform detailed performance analysis of several fast adder architectures. The purpose of such comparative analysis is to ease the selection of the most appropriate adder topology for a given target design constraints and a specified implementation technology.

The set of adder topologies covered by this research consists of the classical linear-delay adders [1], optimized carry-chain architectures [2-3] as well as logarithmic delay adders [4-5]. Besides, we propose one architectural modification intended

V.E. Balas et al. (Eds.): Soft Computing Applications, AISC 195, pp. 295–308.
springerlink.com

to close the gap between hardware wasting logarithmic-delay adders and time consuming linear-delay adders. Since the performances of a design are highly dependent on the target device it is implemented in, the main concern during the comparison of the adder topologies was to cover the area of ASICs and FPGAs – two perspective and widely used technologies. For this purpose, to evaluate the suitability of adder architectures for the cell-based ASIC implementations, unit-gate model [6] for area and delay estimation is adopted. When applying this model on a desired architecture each two-input monotonic gate (e.g. AND, OR, NAND etc.) counts as one gate (area and delay); an XOR counts as two gates both to the area and to the delay; and an *m*-bit logic cell derived from the elementary logic cells counts as $m - 1$ gates to the area and $\lceil \log_2 m \rceil$ gates to the delay. On the other hand, the adder architectures from the proposed set are described in VHDL and implemented in modern Virtex-6 family FPGA device [7]. Implementation results are then discussed from the delay, area and power consumption perspectives.

2 Related Work

Starting with mechanical addition machines in 19th century, there has been a continuous stream of research in the field of arithmetic addition. The problem of making the addition operation as efficient as possible is even today in the research focus of many authors. Processing time, circuit area and consumed power are mostly the measures of the adder quality.

While some explore the transistor level applying different CMOS logic styles and transistor structures [8-11], the others apply numerous architectural modifications and variations [12-14]. The third ones, however, try to 'tune' the transistor (by changing its size, threshold and supply voltages) so that the given architecture is most energy, area or time efficient [15].

Concerning the FPGA implementation of binary adders, in [16] it has been observed that delay models and cost analysis developed for ASIC technology are not useful in designing and implementing FPGA devices. So the authors in [16] present FPGA-specific optimization opportunities for carry-bypass and carry-select adders and show that optimized versions of these adders can be faster than the ripple-carry for large addition sizes. The trade-off study between size, latency and frequency for pipelined large-precision adders on FPGAs is presented in [17]. Some arithmetic optimizations for the mapping of carry-select/increment adders targeting the hardware carry chains of modern FPGAs are presented in [18]. The proposed architectures represent attractive alternatives to deeply pipelined ripple-carry adder schemes.

From the research conducted so far the imposing conclusion is that there is no silver bullet – the adder architecture which will exhibit the best performances (the least power, area and time consuming at the same time) regardless of the used implementation technology.

3 Adder Architectures

Let $A=a_{n-1},...,a_0$, $B=b_{n-1},...,b_0$ and c_{in} are two n-bit operands and input carry bit ($c_{in}=c_0$), respectively. The result of the addition ($A+B+c_{in}$) is the n-bit wide sum signal $S=s_{n-1},...,s_0$ as well as the overflow indicator (c_{out}).

3.1 Linear Delay Adders

In the subset of linear-delay adders two architectures are considered: the wide known ripple-carry (RC) adder composed by n cascaded full-adder cells as well as the multiplexer based carry-block (CB) adder presented in Figure 1. In both architectures, the critical path stretches from the input carry up to the output carry (c_{out}) and it is linearly proportional to the number of summands bits (n). As the full-adder outputs are expressed as:

$$s_i = a_i \oplus b_i \oplus c_i \;\; ; \;\; c_{i+1} = a_i b_i + a_i c_i + b_i c_i, \tag{1}$$

area and delay of the full-adder cell estimated by the unit-gate model are $A_{FA}=9$ and $T_{FA}=4$, respectively. Therefore, the processing time and the circuit area of the n-bit ripple-carry adder are:

$$T_{RC} = (n-1) \cdot T_{FA} + T_{XOR} = 3n-1 \tag{2}$$

$$A_{RC} = n \cdot A_{FA} = 9n \tag{3}$$

Concerning the carry-block adder from Figure 1, as the multiplexer can be characterized by $T_{MUX}=2$ and $A_{MUX}=3$, processing time and circuit area required to implement this adder are, respectively:

$$T_{CB} = (n-1) \cdot T_{MUX} + T_{XOR} = 2n \tag{4}$$

$$A_{CB} = n \cdot (2A_{XOR} + A_{MUX}) = 7n \tag{5}$$

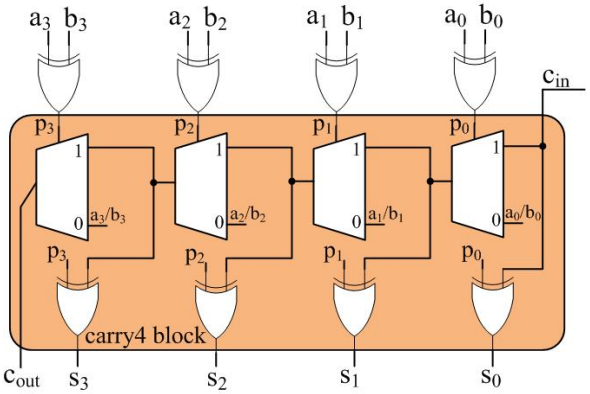

Fig. 1. Carry-block 4-bit binary adder

It is worth mentioning that the 4-bit carry-block is an integral part of the Virtex-6 FPGA slice and it is intended to decrease carry propagation time by using dedicated routes inside FPGA structure [7].

3.2 Optimized Carry Chain Architectures

The main advantage of the linear-delay adders is that they are area efficient and easy to construct. However, the fact that carry signal has to travel through every full-adder block makes them less suitable for high-speed implementations. In order to shorten the critical path of such adders (mostly by increasing the circuit area) many architectural modifications are proposed [5]. Here, we will analyze carry-select adder architecture and propose one carry-bypass technique.

Carry-select (CSL) adders speed-up the addition process by duplicating the hardware due to the fact that carry can only be either 0 or 1. Thus, an *n*-bit binary adder is divided into *n/m* blocks, where each block contains *m* bits. At each block, the hardware is replicated in order to calculate sum and carry-out bits for both possible carry-ins. Figure 2 illustrates the concept. The multiplexer at the end chooses between the carry-outs of the current stage based on the carry-out from the previous stage. In this implementation, the critical path delay comprises the carry-generate of the first block, followed by the multiplexer delays for successive blocks. Consequently, processing time of such architectures linearly depends on the number of input bits but has the significantly lower slope than in the case of previously described linear-delay adders. Circuit area is about more than duplicated.

$$T_{CSL} = T_m + \lceil (n-m)/m \rceil \cdot T_{MUX} \tag{6}$$

$$A_{CSL} = A_m + \lfloor (n-m)/m \rfloor \cdot (2A_m + (m+1)A_{MUX}), \tag{7}$$

where *Tm* and *Am* are processing time and required area of the *m*-bit adder block (see Figure 2).

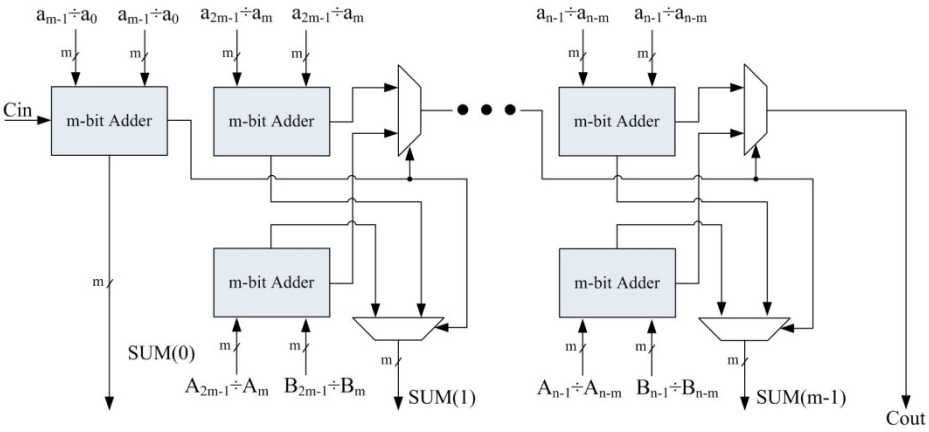

Fig. 2. Carry-select adder architecture

The blocks variable in size (m) can also yield higher performance [19]. The size of the current block is chosen so that the multiplexer inputs (carry-outs of the current block adders and carry-out signal from the previous block) arrive at the same time. For example, if the multiplexer delay is similar to the delay of full-adder, then the minimal carry delay can be achieved by adding 1 bit in the first block, 2 in the second, and so on.

3.3 Logarithmic Delay Adders

These types of adders are generally the fastest but the most area consuming. The propagation delay of such architectures is logarithmically proportional to the number of summands bits n. The logarithmic delay architecture commonly comprises three levels of logic: (1) pre-processing level where carry-generate (G) and carry-propagate (P) signals are calculated, (2) the main level containing the digital logic which calculates all the carries at once and (3) post-processing logic used to generate the carry-out and the sum bits. Two different architectures will be considered in this paper: carry-look-ahead adder and one prefix-adder structure.

Unlike the linear-delay adder implementations which impose the sequential generation of the carries, making the output carry of each stage dependent on the input carry to the stage, *carry-look-ahead* (CLA) implementation implies that the carry-out is not depending on the previous carries. Carry signals (c_i) are calculated in advance based on the carry generate and carry propagate signals obtained as:

$$G_i = a_i \cdot b_i \;;\; Pi = a_i \oplus b_i \tag{8}$$

This is illustrated in Figure 3. Having in mind (8) and the fact that carry-out signal of the current block is generated either when both summands bits (a_i and b_i) are 1 or when one of the two inputs (a_i or b_i) is 1 and the carry-in (carry-out of the previous stage) is 1, we can calculate carry outputs in parallel as:

$$\begin{aligned} &c_0 = G_0 + P_0 c_{in} \\ &c_1 = G_1 + P_1 c_0 = G_1 + P_1 G_0 + P_1 P_0 c_{in} \\ &... \\ &c_j = G_j + \sum_{i=1}^{j} G_{j-i} \prod_{k=1}^{i} P_{j-k+1} + c_{in} \prod_{p=0}^{j} P_p \end{aligned} \tag{9}$$

The sum bits are then equal to:

$$s_i = P_i \oplus c_{i-1} \tag{10}$$

Due to the parallel carry generation logic the critical path propagates from msb input (a_{n-1}/b_{n-1}) up to the msb output bit (s_{n-1}) containing two XOR and two $n+1$-input AND gates:

$$T_{CLA} = 4 + 2 \cdot \log_2 (n+1) \tag{11}$$

Based on (8), (9) and (10) circuit area required to implement this adder is:

$$A_{CLA} = \frac{1}{6} n^3 + n^2 + \frac{35}{6} n \tag{12}$$

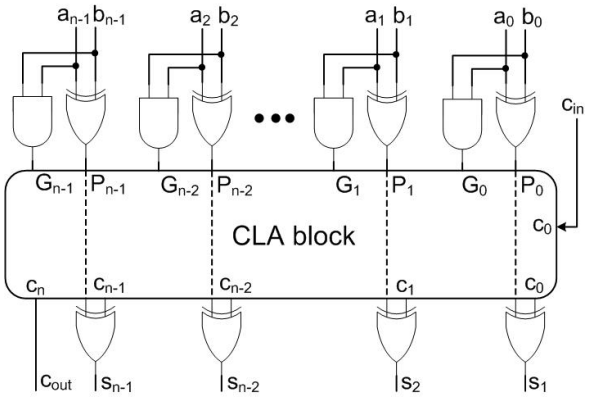

Fig. 3. Carry-look-ahead adder

The disadvantage of the CLA adders is that the carry expressions (and hence logic) become quite complex for more than 4 bits. Thus, the CLA adders are commonly used in a modular way, cascading 4-bit CLAs.

Prefix-adder architectures [4] are generally characterized by the fact that the outputs ($y_{n-1},y_{n-2},\ldots,y_0$) are computed from the n-bit inputs ($x_{n-1},x_{n-2},\ldots,x_0$) by means of an associative binary operator $*$ in a recursive form:

$$y_0 = x_0 \ ; \ y_i = x_i * y_{i-1} \ ; \ i = 1,2,\ldots,n-1 \tag{13}$$

Consequently, every output signal depends on the input signals of equal or lower weight. Due to the associative properties of this generic $*$ operator, the operations may be executed in any arbitrary order. In particular, subsets of operands can be grouped together to obtain in parallel partial solutions, giving rise to group variables $Y_{i,k}$. The variable $Y^l{}_{i,k}$ will stand for the output of the operation that takes the set of bits ($x_k,x_{k-1},\ldots,x_i$) at level l. The group variables at the last level m will comprise the entire range of the input bits, from 0 to i ($Y^m{}_{0,i}$):

$$Y^l{}_{i,k} = Y^{l-1}{}_{i,j} * Y^{l-1}{}_{j+1,k} \ , i < j < k \ ; l = 1,2,\ldots,m \tag{14a}$$

$$Y^0{}_{i,i} = x_i \ ; \ y_i = Y^m{}_{0,i} \ , \ i = 0,1,\ldots,(n-1) \tag{14b}$$

Among the several different prefix-adder architectures Sklansky topology [20] shown in Figure 4 is one of the most efficient. By adopting the tree-type model, all intermediate signals are computed in a minimal tree structure and are fed in parallel, to all higher levels that require those signals. Nevertheless, this architecture still presents some disadvantages concerned with the fan-out of the output nodes, which shows a significant increment as the number of bits of the adder increases.

Each bit (c_i) of the carry vector is computed from the signals of the last level ($G^m{}_{0,i}, P^m{}_{0,i}$). The sum bits are computed in a post-processing operation. The variables $G^l{}_{i,k}$ and $P^l{}_{i,k}$ at the intermediate levels l are computed using the blocks presented in Figure 5.

The Sklansky structure presents the following characteristics in what concerns the processing time and circuit area:

$$\begin{aligned} T_{SA} &= T^{*}{}_{\Pi} + \log_2(n)\cdot T_{\bullet} + T_{\Diamond} \\ &= 3 + 2\log_2 n + 2 = 2\log_2 n + 5 \end{aligned} \tag{15}$$

$$\begin{aligned} A_{SA} &= (n-1)\cdot A_{\Pi} + A^{*}{}_{\Pi} + (\frac{1}{2} n \log_2 n)\cdot A_{\bullet} + n\cdot A_{\Diamond} \\ &= 3(n-1) + 7 + 3(\frac{1}{2} n \log_2 n) + 2n \\ &= \frac{3}{2} n \log_2 n + 5n + 4 \end{aligned} \tag{16}$$

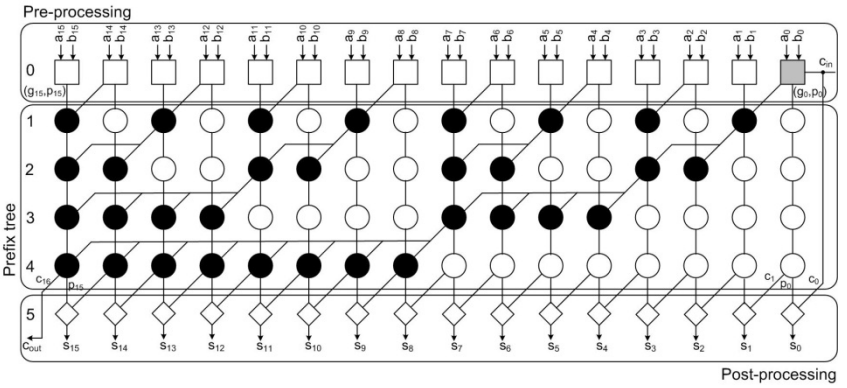

Fig. 4. Sklansky prefix-adder structure

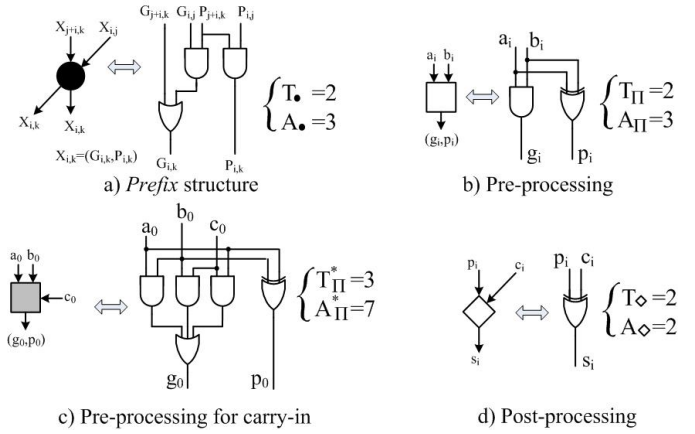

Fig. 5. Internal structure of the blocks composing the Sklansky binary adder

4 Modified Carry-Bypass Architecture for Adder Performance Improvement

Since logarithmic-delay adders suffer from the quite increased area (especially when increasing the number of summands bits (n) while linear-delay adders could be too slow for some applications, we propose a carry-bypass trade-off architecture which will close the gap.

The main idea in *carry-bypass* (bp) approach is to relocate the critical path from the carry propagation chain to the carry generation (cg) network so that the additional hardware is well traded for the decreased delay. The concept is illustrated in Figure 6. Similar to the carry-select technique, *n*-bit adder is divided into *n/m* blocks containing *m* bits. Each block also contains one D flip-flop intended to supply the block adder with the carry-in bit. Inputs to the flip-flops are provided from the carry generation network. Let c^*_i and co_i be the the carry-in and carry-out bits of the i^{th} block, respectively (c^*_i is the flip-flop input). Carry-in bit of the next block (c^*_{i+1}) will be 1 either if the sum bits as well as carry-in bit of the current block are 1 or if the carry-out of the current block is equal to 1:

$$c^*_{i+1} = (A_i \oplus B_i) \cdot c^*_i + co_i, \tag{17}$$

where A_i and B_i are *m*-bits wide summands belonging to the block *i* ($A = a_{i\cdot m-1\div(i-1)\cdot m}, B = b_{i\cdot m-1\div(i-1)\cdot m}$). Flip-flops are initially reset and then loaded with the c^*_i bits ($i \in [1, n/m]$) after being processed in the carry-generate network.

The critical path contains carry generation network, D flip-flop and *m*-bit wide adder block:

$$\begin{aligned} T_{bp} &= T_{cg} + T_{Dff} + T_m \\ &= \lceil (n-m)/m \rceil \cdot (3 + \log_2 5) + 3 + T_m, \end{aligned} \tag{18}$$

where is $T_{Dff}=3$. The area of the carry-bypass architecture is slightly increased compared to the classical linear-delay carry propagation adders:

$$\begin{aligned} A_{bp} &= A_{cg} + \lceil n/m \rceil \cdot (A_m + A_{Dff}) \\ &= \lceil (n-m)/m \rceil \cdot (3m+1) + \lceil n/m \rceil \cdot (A_m + 4), \end{aligned} \tag{19}$$

where is $A_{Dff}=4$. By changing the value of *m* as well as the type of the block adders we can influence the adder performances.

At the end of this section which gives the overview of different adder architectures it should be mentioned that parallelism and pipelining are widely used speed-up techniques which apply on given design architecture [21]. These techniques, however, are out of focus of this paper.

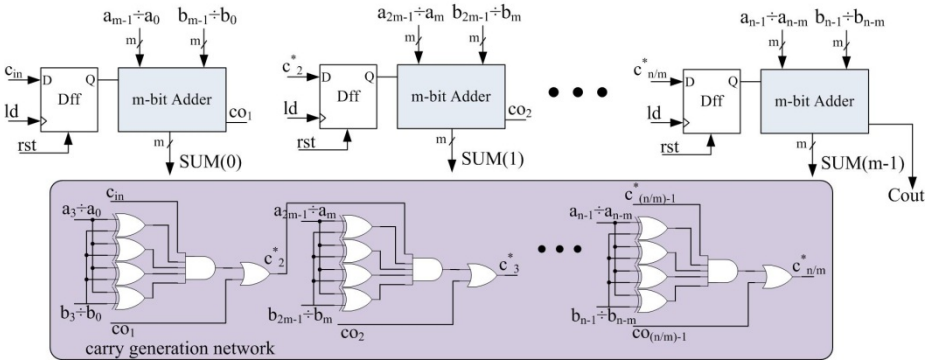

Fig. 6. Carry-bypass adder architecture

5 ASIC Implementations

The performance values of the adder architectures considered in the previous sections are summarized in Table 1. Although technology independent the unit-gate model used for architectures evaluation could be treated as a quite satisfactory reflection of the behavior of the adders implemented in ASICs.

Table 1. Performance comparison of the different adder architectures

Adder topology	Processing time	Circuit area
RC	$3n-1$	$9n$
CB	$2n$	$7n$
CSL[1]	$T_m+2\cdot\lceil(n-m)/m\rceil$	$A_m+\lfloor(n-m)/m\rfloor\cdot(2Am+3(m+1))$
bp	$\lceil(n-m)/m\rceil\cdot(3+\log_2 5)+3+T_m$	$\lceil(n-m)/m\rceil\cdot(3m+1)+\lceil n/m\rceil\cdot(A_m+4)$
CLA	$4+2\cdot\log_2(n+1)$	$1/6\,n^3+n^2+35/6\,n$
SA	$3+2\log_2 n+2=2\log_2 n+5$	$3/2\,n\log_2 n+5n+4$

The charts presented in Figures 7 and 8 illustrate the relations between the processing time and the circuit area for all considered structures in function of the number of summands bits (n). For all the modular adder architectures (consisting of n/m blocks) it was adopted that the parameter m is equal to 4. In the case of CSL adder implementation, for the m-bit adder block 4-bit carry-look-ahead realization is used. Also, two carry-bypass architectures are evaluated: one with the carry-look-ahead as a block adder (CLA_bp) and another with the carry-block 4-bit adder (CB_bp) in the place of m-bit adder.

[1] *Tm* and *Am* are the processing time and the circuit area of *m*-bit block adder, respectively.

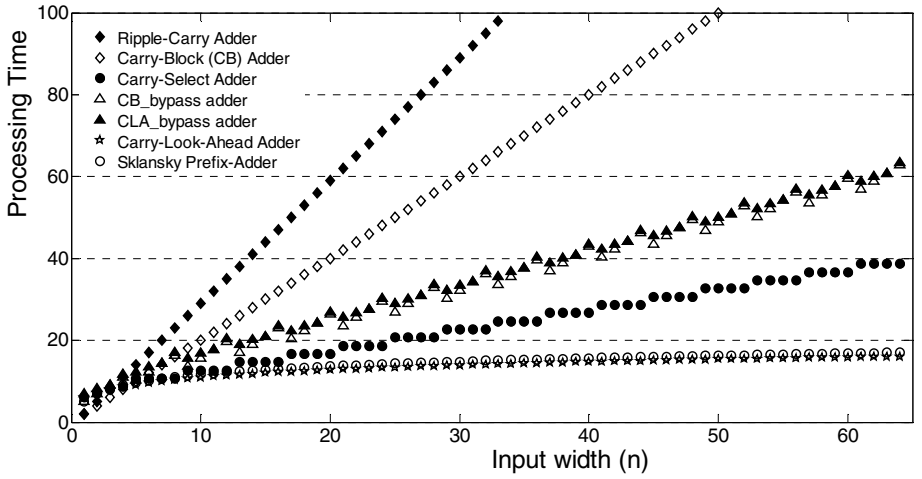

Fig. 7. Processing time of the suite of binary adder architectures

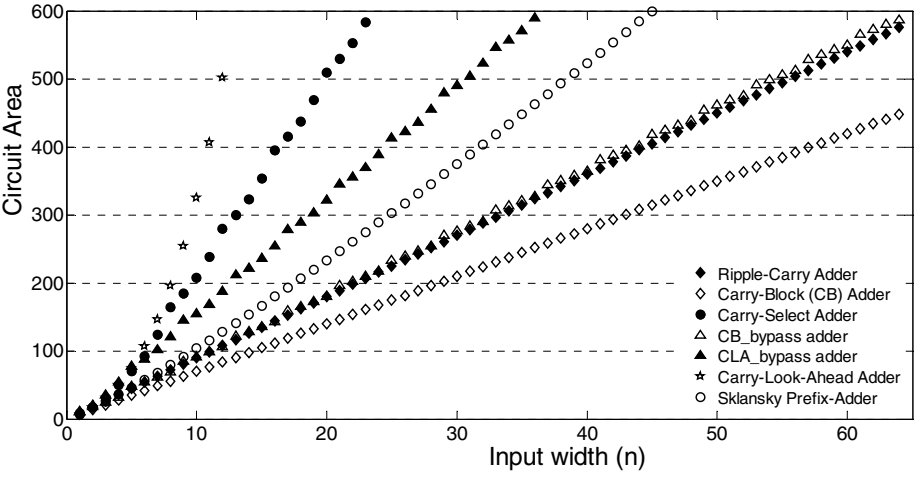

Fig. 8. Comparative analysis of the binary adder architectures implementation area

The graph corresponding to the processing time (see Figure 7) evidences the significant performance gains that can be achieved by using the fast (logarithmic-delay) adder architectures instead of the simple linear-delay adders. This gain will be even greater when the number of summands bits increases. Optimized carry-chain architectures are something in between the linear and the logarithmic delay adders. The time needed to obtain the sum bits linearly depends on the number of summands bits but with the slope which is less than in the case of linear-delay adders.

Concerning the implementation area, it is obvious that the great improvements in the speed of the logarithmic delay adders are paid with the large increase in the required circuit area. Although the slowest, linear-delay adders are the least hardware

demanding. By introducing the area-delay product as a measure of the tradeoff between the processing time and circuit area we can conclude that the Sklansky prefix-adder architecture is the most appropriate one for the ASIC implementations.

6 FPGA Implementations

All binary adder architectures introduced in sections 3 and 4 are described in VHDL and implemented in Virtex-6 family general purpose FPGA device. Carry-block adder is implemented in Virtex-6 as a cascade realization of 4-bit carry4 blocks (see Figure 1) which are the part of its slice structure [7]. XPower Analyzer tool [22] from ISE 12.4 Xilinx design suite was used to estimate the power consumption of adder architectures. Summands values were obtained by the help of MATLAB script as the vectors with 1000 elements and random (Gaussian) distribution from the range of $[0,2^n-1]$. From the XPower report we have extracted the dynamic power consumption of logic and local interconnections as a valid dynamic power consumption indicator since the power of clock distribution-tree as well as the dynamic power of global interconnections and I/Os can vary depending on the adder position inside the FPGA structure (determined during the placement and routing implementation phase).

Obtained processing times and required Virtex-6 hardware resources (expressed in the number of LUTs) are reported in Figures 9 and 10. From both speed and area perspectives can be concluded that carry-bypass techniques proposed in this paper are well suited for FPGA implementations.

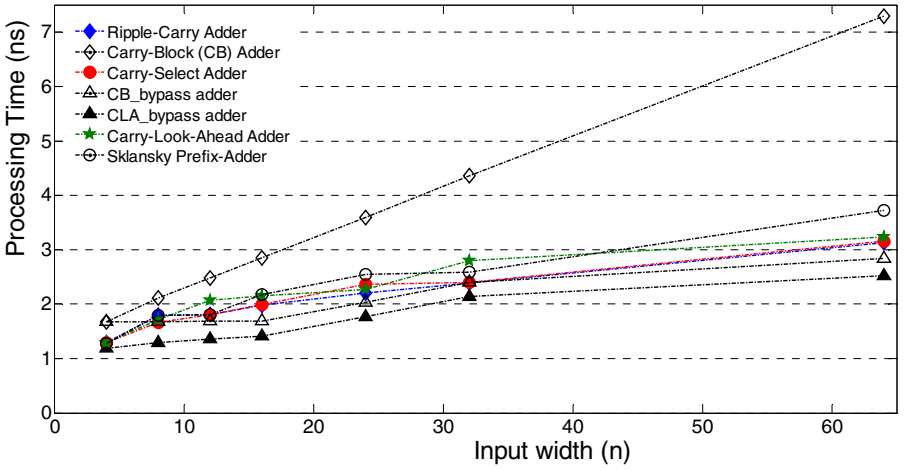

Fig. 9. Comparative speed analysis of the adder architectures when implemented in Virtex-6 FPGA device

Small number of LUTs required to implement carry-block adder is due to the fact that this kind of adder is implemented mostly of using carry4 blocks instead of LUTs. Also, although intended for fast carry propagation, carry4 blocks do not speed up the addition process when used in the chain. This is, as witnessed in Figure 9, especially true when increasing the number of chained blocks (bit width n).

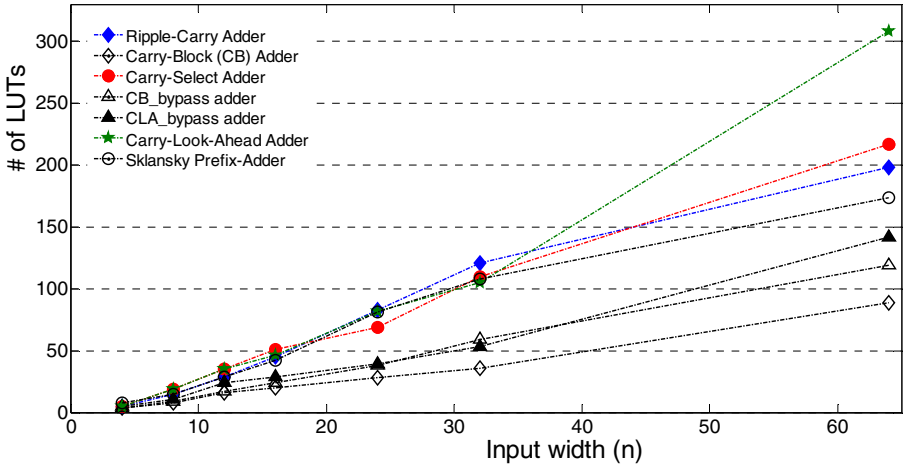

Fig. 10. Required Virtex-6 hardware resources

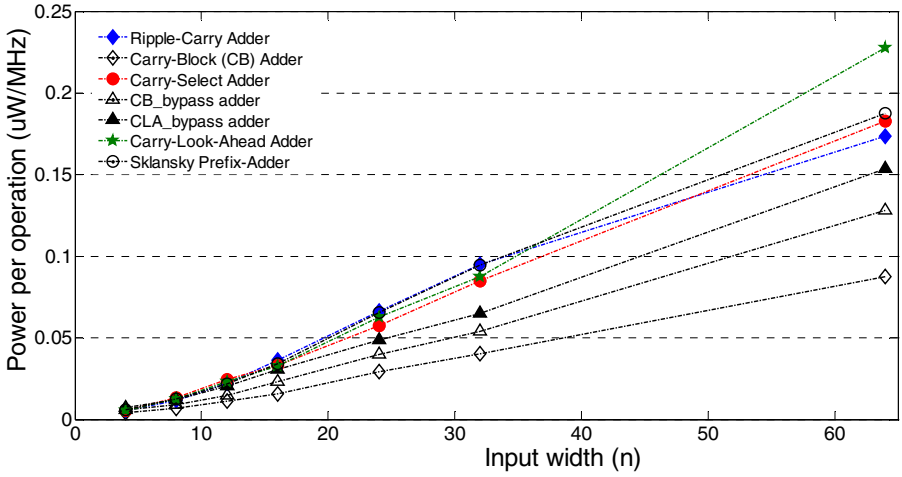

Fig. 11. Dynamic power consumed per one operation of binary addition

Average dynamic power required to perform an addition operation as well as power-delay product as the measures of energy efficiency of the adder architectures are reported in Figures 11 and 12. From the energy standpoint it is evidenced that carry-bypass architectures are also the best FPGA solution. Having implemented these architectures one assures that the power consumption the best 'translates' into the speed of operation.

Although has proven to be the most appropriate design when using ASIC technology, Sklansky prefix-adder in not the best solution in the FPGA based digital designs.

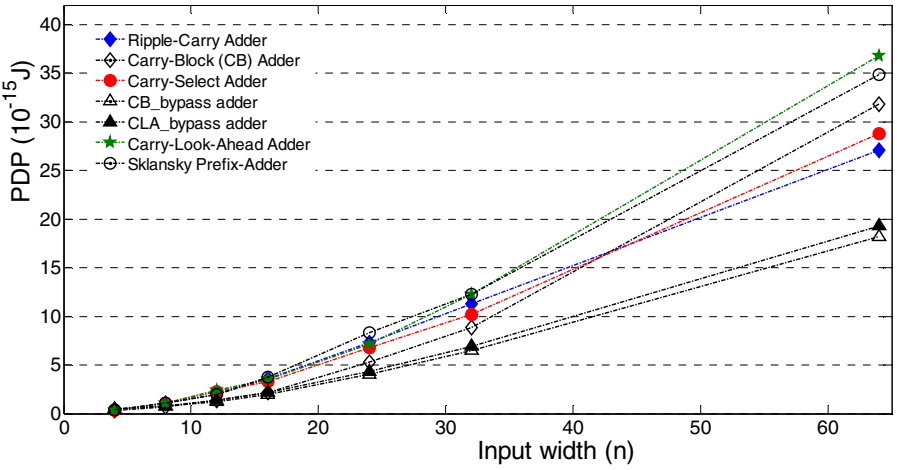

Fig. 12. Power-delay product of the suite of binary adder architectures

7 Conclusions

When determining the architecture of a digital design which ensures the best performances one can be pretty aware of the technology used for its implementation. To prove the previous statement a detailed comparative analysis of several fast adder architectures was presented in this paper. ASICs and FPGAs as two state of the art solutions are adopted to be the target implementation technologies. To evaluate adder architectures implemented in ASICs unit-gate theoretical model is applied. From the area-delay point of view logarithmic-delay Sklansky prefix-adder architecture has proven to be the best ASIC solution. On the other hand, when implemented in Virtex-6 FPGA device and evaluated in the power-delay-area space, carry-bypass architectural trade-off modification proposed in this paper exhibits the best performances.

The presented theoretical and experimental analysis could be valuable for the digital system designers when choosing the adder topology and the target implementation technology.

Acknowledgement. This work was supported in part by the Serbian Ministry of Science and Technological Development under project TR-33051.

References

1. Fang, C., Huang, C., Wang, J., Yeh, C.: Fast and compact dynamic ripple carry adder design. In: IEEE Asia-Pacific Conf. on ASIC, pp. 25–28 (2002)
2. Bedrij, O.: Carry-select adder. IRE Trans. Electron. Comput. 11, 340–346 (1962)
3. Alioto, M., Palumbo, G.: Optimized design of carry-bypass adders. In: European Conf. on Circuit Theory and Design, pp. 245–248 (2001)
4. Chen, J.: Parallel-prefix structures for binary and modulo $\{2^n-1,2^n,2^n+1\}$ adders. PhD thesis, Oklahoma State University (2008)
5. Zimmermann, R.: Binary adder architectures for cell-based VLSI and their synthesis. PhD thesis, Swiss Federal Institute of Technology (1997)
6. Tyagi, A.: A reduced area scheme for carry-select adders. IEEE Trans. Comput. 42, 1162–1170 (1993)
7. Xilinx Inc., Virtex-6 FPGA data sheet: DC and Switching Characteristics, v3.4 edition (2012)
8. Jose, B., Radhakrishnan, D.: Delay optimized redundant binary adders. In: Int. Conf. on Electronics, Circuits and Systems, pp. 514–517 (2006)
9. Shams, A., Darwish, T., Bayoumi, M.: Performance analysis of low-power 1-bit CMOS full adder cells. IEEE Trans. on VLSI Systems. 10, 20–29 (2002)
10. Chang, C., Gu, J., Zhang, M.: A Review of 0.18 /spl mu/ m full adder performances for tree structured arithmetic circuits. IEEE Trans. on VLSI Systems 13, 686–695 (2005)
11. Alioto, M., Cataldo, G.D., Palumbo, G.: Mixed full adder topologies for high-performance low-power arithmetic circuits. Microelectronics Journal 38, 130–139 (2007)
12. Amelifard, B., Fallah, F., Pedram, M.: Closing the gap between carry select adder and ripple carry adder: a new class of low-power high performance adders. In: Int. Symp. on Quality of Electronic Design, pp. 148–152 (2005)
13. Knowles, S.: A family of adders. In: 15th IEEE Symp. on Computer Arithmetic, pp. 277–281 (2001)
14. Kharbash, F.: Redundant adder architectures, PhD Thesis, University of Missouri (2011)
15. Patil, D., Azizi, O., Horowitz, M., Ho, R.: Robust energy-efficient adder Topologies. In: 18th IEEE Symp. on Computer Arithmetic, pp. 16–28 (2007)
16. Shanzen, X., Yu, W.: FPGA adders: performance evaluation and optimal design. IEEE Design&Test of Computers 15, 24–29 (1998)
17. Dinechin, F., Nguyen, H., Pasca, B.: Pipelined FPGA adders. In: Int. Conf. on Field Programmable Logic, pp. 422–427 (2010)
18. Nguyen, H., Pasca, B., Preusser, T.: FPGA-specific arithmetic optimizations of short-latency adders. In: Int. Conf. on Field Programmable Logic, pp. 232–237 (2011)
19. Oklobdzija, V., Barnes, E.: Some optimal schemes for ALU implementation in VLSI technology. In: Proc. of the 7th Symposium on Comp. Arith., pp. 2–8 (1985)
20. Sklansky, J.: Conditional sum addition logic. IRE Trans. on Electronic Computers 9, 226–231 (1960)
21. Jadhov, S.: Advanced computer arithmetic and computing. Technical Publications Pune (2009)
22. XPower Analyzer tutorial, `ftp://ftp.xilinx.com/pub/documentation/tutorials/xpowerfpgatutorial.pdf`

Memristor-Based Phase-Lead Controller Circuit Design

Tsung-Chih Lin[1], Wei-Nan Liao[1], and Valentina Emilia Balas[2]

[1] Department of Electronic Engineering, Feng-Chia University, Taichung, Taiwan
[2] Department of Automation and Applied Informatics,
Aurel Vlaicu University of Arad, Arad, Romania
{tclin,m0049793}@fcu.edu.tw, balas@drbalas.ro

Abstract. Memristor predicted and described by L. O. Chua is a new electrical element. Memristor with variable resistance which changes automatically as its voltage changing can be used as a tunable parameter in control systems. Phase-lead controller is widely used in industrial process control applications. The conventional method for adjusting phase-lead controller parameters is based on the "trial and error" procedure which leads to an inconvenient and approximated design. In the meantime, once the parameters are adjusted, they are fixed during the control system operation. In this paper, memristor-based phase-lead (M-phase-lead) controller is presented. Based on memristor constitutive relations of the memristance and memductance, the proposed M-phase-lead controller is more flexible during the design process. The theoretical description of design scheme is presented and simulation example is given to show the effectiveness of the advocated design methodology.

Keywords: Frequency-domain, Memristor, phase-lead.

1 Introduction

Memristor characterized by a relationship between the charge $q(t)$ and the flux $\phi(t)$ was predicted as the fourth circuit element and described by Leon O. Chua in 1971 [1]. In 2008, Stanley Williams and his Team at HP Information and Quantum System Laboratory announced the discovery of the missing circuit element memristor, acronym for memory resistor [4]. Recently, research on circuit based on memristor [3], [5]-[15] is becoming a focal topic for research because it will reduce power consumption to use memristors in computer by saving the time to reload data and could lead to the human-like learning.

Improvement in the response of feedback tracking control systems and disturbance rejection can be achieved in the frequency domain. The introduction of a phase-lead controller named low-frequency attenuation controller results in an increase in the resonant frequency and a reduction in the settling time of the system.

The great drawback of phase-lead controller is how to adjust parameters with many source of uncertainty in dynamic real-world environments. In industrial process control applications, the conventional method for adjusting phase-lead controller parameters is based on the "trial and error" procedure which leads to an inconvenient and approximated design. In the meantime, once the parameters are adjusted, they are fixed during the control system operation. Due to the resistance of a memristor can change

V.E. Balas et al. (Eds.): Soft Computing Applications, AISC 195, pp. 309–318.
springerlink.com

adaptively with it voltage changing, a memristor (*M*) can be used a tunable gain. In this paper, we use a memristor to replace the resistor in the phase-lead controller circuit schematic.

This paper is organized as follows. First, the circuit model of the conventional phase-lead controller is introduced in Section 2. The circuit model of the M-phased-lead controller is presented in Section 3. Simulation examples to demonstrate the performance of the proposed schemes are provided in Section 4. Section V gives the conclusion of the advocated design methodology.

2 The Circuit Model of the Conventional Phase-Lead Controller

This section presents the frequency-response characteristics by use of the cascade controller, phase-lead controller. The main objective of the controller is to reshape the frequency-response plot of the basic system by means of a controller in order to achieve the performance specifications.

In designing phase-lead controller via Bode plots, we want to change phase diagram, increasing the phase margin to reduce the percent overshoot and increasing the gain crossover to realize a faster transient response. The circuit as shown in Fig. 1 is a phase-lead controller.

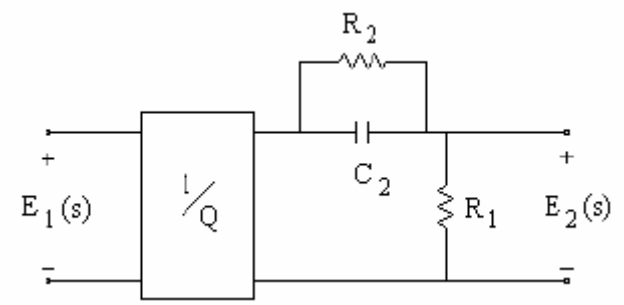

Fig. 1. Typical phase-lead controller circuit

The lead designation of this network is based on the steady-state sinusoidal response. The sinusoidal output E_2 leads the sinusoidal input E_1. The circuit transfer function is

$$\frac{E_2(s)}{E_1(s)} = \frac{1+\dfrac{s}{QT}}{1+\dfrac{s}{T}} \tag{1}$$

where $T = \dfrac{R_1 + R_2}{R_1 R_2 C_2}$, $Q = \dfrac{R_2}{R_1 + R_2} < 1$.

If the circuit elements are chosen as, $R_1 = 100\Omega$, $R_2 = 483\Omega$, $C_2 = 7*10^{-5} F$, the Bode diagram is shown in Fig. 2.

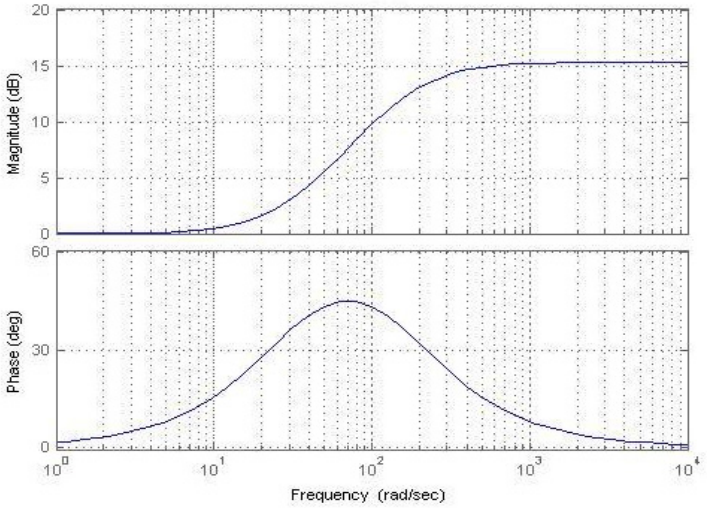

Fig. 2. Bode magnitude and phase plot for phase-lead circuit

3 The Circuit Model of the Memristor-Based Phase-Lead

The memristor is a passive two- terminal electronic device as shown in Fig. 3 [2] described by a nonlinear constitutive relation between the device terminal voltage $v(t)$ and terminal current $i(t)$.

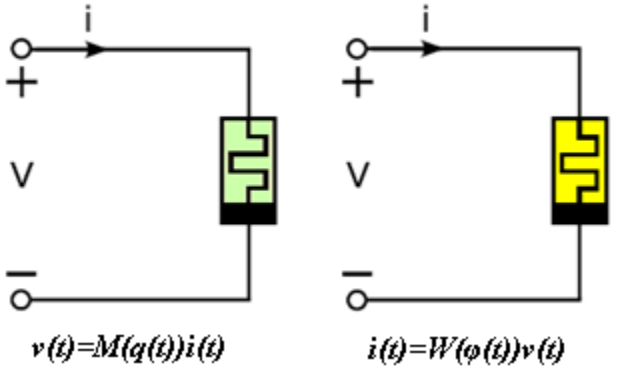

Fig. 3. Charge-controlled memristor (left) and flux-controlled memristor (right)

$$v(t) = M(q(t))i(t) \tag{2}$$

or

$$i(t) = W(\varphi(t))v(t) \tag{3}$$

where the two nonlinear functions $M(q)$ and $W(\varphi)$ called memristance and memductance, respectively, are defined as

$$M(q) \triangleq \frac{d\varphi(q)}{dq} \tag{4}$$

$$W(\varphi) \triangleq \frac{dq(\varphi)}{d\varphi} \tag{5}$$

representing the slope of a scalar function $\varphi = \varphi(q)$ and $q = q(\varphi)$, respectively, called the memristor constitutive relations.

For the charge-controlled memristor, a monotonically increasing and piecewise-linear characteristic is assumed [4]. The memristor constitutive relation as shown in Fig. 4 can be expressed as

$$\varphi(q) = bq + 0.5(a-b)(|q+1| - |q-1|) \tag{6}$$

where $a,\ b > 0$.

Therefore, the memristance can be obtained as

$$M(q) = \frac{d\varphi(q)}{dq} = \begin{cases} a, & |q| < 1 \\ b, & |q| > 1 \end{cases} \tag{7}$$

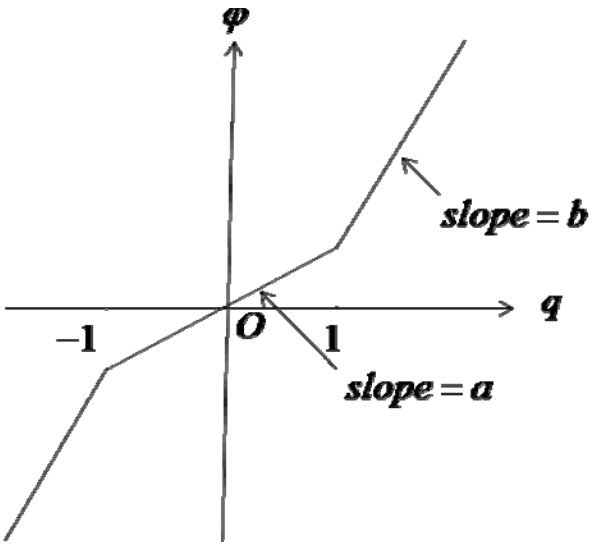

Fig. 4. The constitutive relation of the charge-controlled memristor

Similarly, for the flux-controlled memristor, a monotonically increasing and piecewise-linear characteristic is assumed [4]. The memristor constitutive relation as shown in Fig. 5 can be expressed as

$$q(\varphi) = g\varphi + 0.5(f-g)(|\varphi+1| - |\varphi-1|) \tag{8}$$

where $f,\ g > 0$.

Therefore, the memductance can be obtained as

$$W(\varphi) = \frac{dq(\varphi)}{d\varphi} = \begin{cases} f, & |\varphi| < 1 \\ g, & |\varphi| > 1 \end{cases} \tag{9}$$

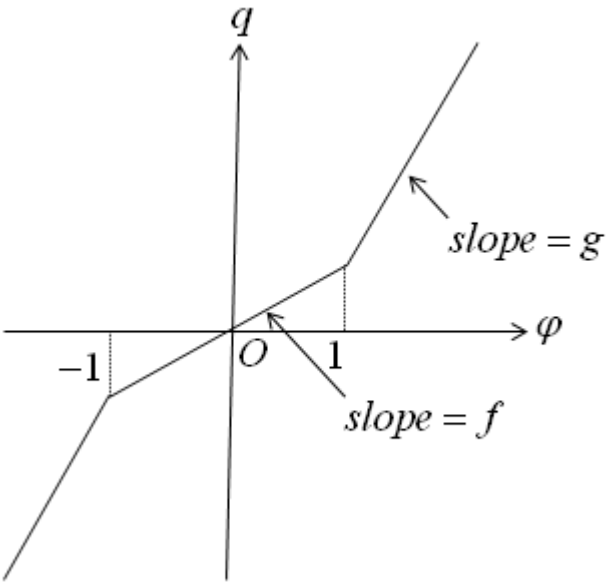

Fig. 5. The constitutive relation of the flux-controlled memristor

Because the resistance of a memristor can change adaptively with its voltage changing, the resistor from phase-lead circuit is replaced with memristor as follows.

The M-phase-lead by replacing resistor R_2 with a flux-controlled memristor whose characteristic is given by Fig. 5 is shown in Fig. 6.

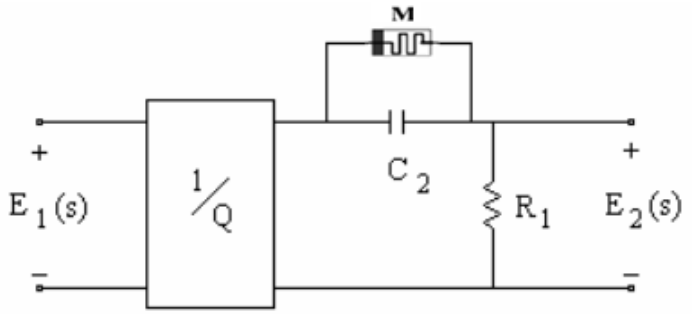

Fig. 6. The M-phase-lead circuit

The circuit transfer function (1) can be modified as

$$\frac{E_2(s)}{E_1(s)} = \frac{1+\dfrac{s}{QT}}{1+\dfrac{s}{T}} \tag{10}$$

$$\begin{cases} \dfrac{1+\dfrac{s}{(\dfrac{R_1 f}{R_1 C_2})}}{1+\dfrac{s}{(\dfrac{1+R_1 f}{R_1 C_2})}} & |\varphi|<1 \\ \dfrac{1+\dfrac{s}{(\dfrac{R_1 g}{R_1 C_2})}}{1+\dfrac{s}{(\dfrac{1+R_1 g}{R_1 C_2})}} & |\varphi|>1 \end{cases} \tag{11}$$

where $Q=\dfrac{R_1 W(\varphi)}{1+R_1 W(\varphi)}$, $T=\dfrac{1+R_1 W(\varphi)}{R_1 C_2}$.

For circuit components chosen as $R_2 = 483\Omega$, $C_2 = 7*10^{-5} F$, $f = 300$ and $g = 800$, the Bode diagram of is shown in Fig. 7.

By comparing Fig. 2 with Fig. 7, the proposed M-phase-lead controller is more flexible than the conventional phase-lead controller. During the control system operation, once the parameters are adjusted, they are fixed for conventional phase-lead

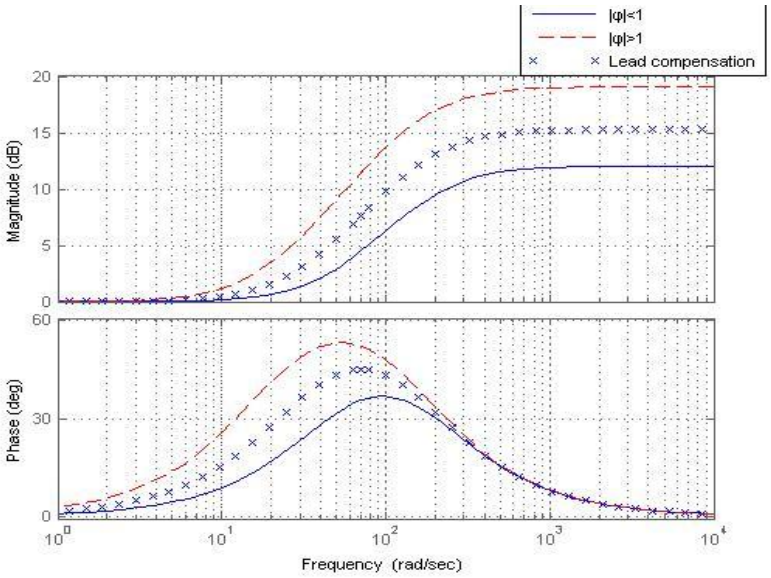

Fig. 7. Bode magnitude and phase plot for M-phase-lead circuit

controller, but there exist robust gain margin and phase margin intervals for M-phase-lead controller by adapting slopes of the constitutive relation of the charge-controlled memristor and flux-controlled memristor.

4 Simulation Example

In this section, the proposed M-phase-lead controller will be applied to an aircraft roll control system as shown in Fig. 8, where $G_M(s)$ and $G_A(s)$ are transfer functions of motor and aircraft, respectively. The torque on the aileron generates a roll rate. The resulting roll angle is then controlled to meet prescribed design specifications through a feedback system as shown. The comparisons between M-phase-lead controller and conventional phase-lead controller are given to show the proposed M-phase-lead controller is more flexible.

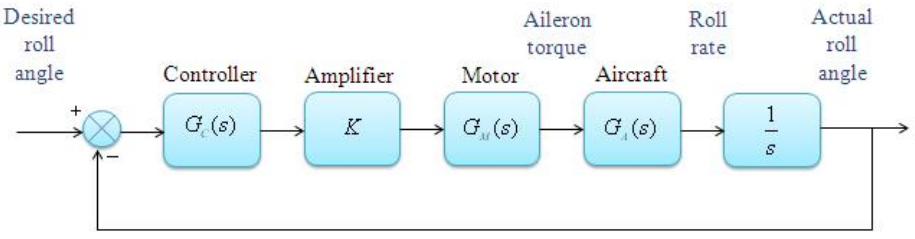

Fig. 8. The aircraft roll control system

Example: **M-Phase-Lead Controller Design**

Given the transfer functions $G_M(s)=\dfrac{1}{(s+36)}$ and $G_A(s)=\dfrac{100}{(s+100)}$, design a phase-lead controller to yield a 48° phase margin and velocity constant $k_v=40$.

First, K must be set at 1440 to meet the specification $k_v=40$, yielding the open-loop transfer function as

$$G(s)=\frac{144000}{s(s+36)(s+100)}$$

where $G(s)=\dfrac{K}{s}G_M(s)G_A(s)$. In order to meet the phase margin requirement imposed by 48°, the conventional phase-lead controller can be designed as

$$G_c(s)=\frac{2.38(s+26.07)}{(s+61.78)}$$

The circuit parameters of the phase-lead shown in Fig. 1 are chosen as $R_1=20\Omega$, $R_2=27.4\Omega$, $C_2=1.4*10^{-3}F$.

The forward transfer function of the compensated system can be obtained as

$$G_c(s)G(s)=\frac{342720(s+26.07)}{s(s+61.78)(s+36)(s+100)}$$

By replacing resistor R_2 with a flux-controlled memristor, the M-phase-lead controller can be expressed as

$$G_c(s)=\begin{cases}1.25\dfrac{s+142.9}{s+178.6}, & |\varphi|<1\\ 6\dfrac{s+7.143}{s+42.86}, & |\varphi|>1\end{cases}$$

Therefore, the compensated system's forward transfer function can be described as

$$G_c(s)G(s)=\begin{cases}\dfrac{180000(s+142.9)}{s(s+178.6)(s+36)(s+100)}, & |\varphi|<1\\ \dfrac{864000(s+7.143)}{s(s+42.86)(s+36)(s+100)}, & |\varphi|>1\end{cases}$$

Fig. 9 summarizes the design and shows the effect of the compensation of the conventional phase-lead controller and the M-phase-lead controller.

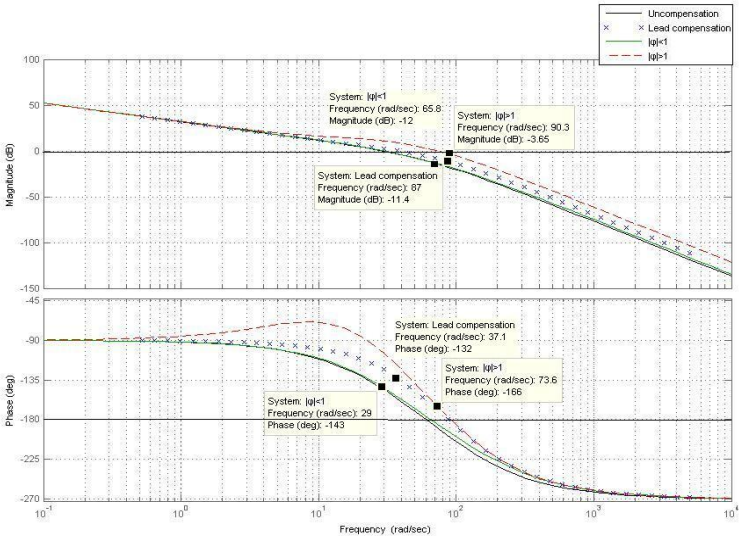

Fig. 9. Bode plots for M-phase-lead controller and conventional phase-lead controller

Final results, obtained from the simulations and the actual frequency responses are shown in Table 1.

Table 1. Characteristics of the Phase-lead and M-phase-lead compensated system

Parameter	Proposed specification	Uncompensated system	Phase-lead compensated system	M-phased-lead compensated system
k_v	40	40	40	40
Phase Margin	45°	34°	45°	14° ~ 37°
Gain-cross over frequency	----	29.4 rad/sec	37.1 rad/sec	29 rad/sec ~ 73.6 rad/sec
Closed-loop bandwidth	----	49.99 rad/sec	68.47 rad/sec	50.32 ~ 110.55 rad/sec
Gain margin	----	10.6 dB	11.4 dB	3.65 ~ 12 dB

5 Conclusion

Due to the fact that memristor with variable resistance which changes automatically as its voltage changing can be used as a tunable parameter in control systems, we have proposed a method for designing a memristor-based phase lead controller for industrial process control applications to overcome the limitation that parameters of the conventional phase-lead controller are fixed during the control system operation. An aircraft roll control system is fully illustrated to meet the prescribed specifications. The resulting M-phase-lead controller gives an adaptable specification band and it is more flexible during the design process.

References

[1] Chua, L.O.: Memristor—The missing circuit element. IEEE Trans. Circuit Theory CT-18(5), 507–519 (1971)
[2] Chua, L.O., Sung, L.O., Memristive, M.K.: Devices and systems. Proc. IEEE 64(2), 209–223 (1976)
[3] Itoh, M.: Memristor oscillators. International Journal of Bifurcation and Chaos 18(11), 3183–3206 (2008)
[4] Strukov, D.B., Snider, G.S., Stewart, D.R., Williams, R.S.: The missing memristor found. Nature 453(7191), 80–83 (2008)
[5] Itoh, M., Chua, L.O.: Memristor oscillation. Int. J. Bifurcat. Chaos Appl. Sci. Eng. 18(11), 3183–3206 (2008)
[6] Riaza, R.: Nondegeneracy conditions for active memristive circuits. IEEE Trans. Circuits Syst. II, Exp. Briefs 57(3), 223–227 (2010)
[7] Oster, G.F., Auslander, D.M.: The memristor: A new bond graph element. Trans. ASME on Dynamical Systems and Control 94, 249–252 (1973)
[8] Oster, G.F.: A note on memristors. IEEE Transactions on Circuits and Systems 21(1), 152–152 (1974)
[9] Tour, J.M., He, T.: The fourth element. Nature 453, 42–43 (2008)
[10] Sturkov, D.B., Snider, G.S., Stewart, D.R., Williams, S.R.: Switching Dynamics in titanium dioxide memristive devices. Journal of Applied Physics 106, 74508–74513 (2009)
[11] Joglekar, Y.N., Wolf, S.J.: The elusive memristor: properties of basic electrical circuits. European Journal of Physics 30(4), 661–675 (2009)
[12] Radwan, A.G., Zidan, M.A., Salma, K.N.: HP Memristor mathematical model for periodic signals and DC. In: IEEE Int. Midwest Symp. on Circuits and Systems, pp. 861–864 (2010)
[13] Mahvash, M., Parker, A.C.: A memristor SPICE modelfor designing memristor circuits. In: IEEE Int. Midwest Symp. on Circuits and Systems, pp. 989–992 (2010)
[14] Delgado, A.: The memristor as controller. In: IEEE Nanotechnology Materials and Devices Conference, pp. 376–379 (2010)
[15] Wang, X., Zhao, Y., Liao, Y.: Dynamic Performance Analysis of PID Controller with one Memristor. In: International Conference on Information Science and Technology, pp. 1234–1237 (2011)

CMOS-Integrated Temperature Relay Based on Widlar Mirror

Mircea A. Ciugudean[1] and Marius M. Bălaş[2]

[1] "Politehnica" University of Timişoara, Romania
maciugudean@yahoo.com
[2] "Aurel Vlaicu" University of Arad, Romania
marius@drbalas.ro

Abstract. One presents a new variant of temperature relay scheme for CMOS chips, based on a simple structure of voltage source with two cross-connected current mirrors (of modified-Widlar type and simple one). In this scheme the positive feedback is exploited which is designed so that, for a particular temperature the circuit toggles. In this moment his output voltage achieves a level jump, great enough to drive an interface circuit with the relay-signalisation processing part. The relay toggle condition is deduced, which clears up the relay function. The releasing temperature may be programmed in a large range through one or two resistors. The simulation results are presented for the relay conceived in 0.35µm CMOS process. The releasing-temperature process variation is reduced, by a special design procedure, to a maximum value of ±5.5°C.

Keywords: CMOS temperature relay, modified Widlar mirror.

1 Introduction

The calling attention of integrated-circuit designers about the possibility of obtaining high performances in schemes based on two cross-connected current mirrors (named as "self-biased" current sources too) was done in [1]. There, a current reference (using modified-Widlar and reverse-Widlar mirrors) is proposed which applies a very interesting I- and II-order thermal compensation technique. Leaving from this technique, others four types of "branch" and "total" reference current sources with superior performances have been elaborated [2]. In [3] the I- and II-order thermal compensation technique of [1] has been extended to four new voltage references, one of these sources achieving special performances in respect to process and supply-voltage variations.

In [4] a new idea is born, to renounce the thermal compensation of current and voltage references of [1], [2] and [3] in favour of a I- and II-order thermal sensitizing so as the used simple circuits become, by an adequate design, temperature sensors. This idea proved feasible and finally [4], [5] there were obtained more performing temperature sensors with the help of Wilson-peaking current mirrors and especially with modified-Widlar-peaking ones (fig. 1). Their main quality is that of achieving a very small process variation of the output voltage (which is a temperature function).

V.E. Balas et al. (Eds.): Soft Computing Applications, AISC 195, pp. 319–330.
springerlink.com

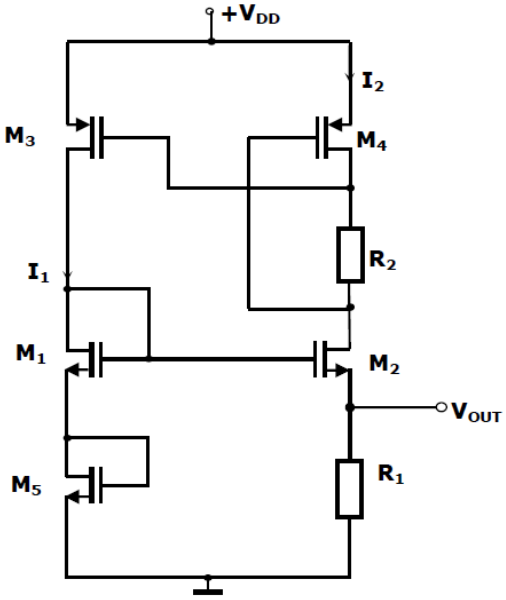

Fig. 1. Widlar-peaking temperature-sensor scheme

The performing smart temperature sensors are more and more used in VLSI modern systems. In [4] there were threaded a great number of applications which impose their use. There were presented there the numerous conditions imposed to integrated temperature sensors. One can find from the publications the temperature sensors in CMOS chips constitute an important academic and industrial research subject of the last 20 years [6]. The actuality of the research in the domain of smart temperature sensors is proved by the great number of published papers, books and PhD theses.

In this work one enunciates the idea of achieving a temperature relay whose releasing temperature can be modified by a resistor, with a simple scheme of the same category. The scheme elaboration in 0.35µm CMOS process was successful and the simulations announce promising performances. The first variant of such a relay, using a Wilson mirror, will be published separately [7]. The utility of such a temperature relay is incontestable for the protection of the CMOS chips and of embedded systems, by signalizing the reaching of a threshold temperature of ambient or industrial process/ installation.

2 Temperature-Relay Function

The used scheme is shown in fig. 2 (partially similar to temperature sensor of fig. 1, but here the superior mirror is not a peaking one) and it was adopted thanks to the possibility to ensure an enough strong positive feedback at a particular temperature and thus, a toggle output voltage V_{out}. The feedback is positive because of comprising two CS-connection amplifier stages in the loop and is amplified by the R_2 resistor in the M_4 drain.

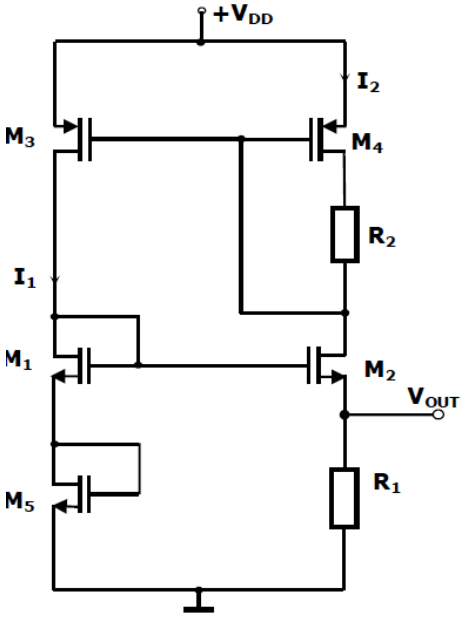

Fig. 2. Widlar-simple temperature-relay

But, essential for achieve the toggle condition is the fact that the resistor R_1 has a negative temperature coefficient (NTC) and the resistor R_2 has a positive temperature coefficient (PTC). The sub-micron CMOS process has the possibility to realize a great number of resistor types, with different temperature coefficients and even with great square resistance.

In the circuit of fig. 2 one uses a N^+ polysilicon resistor (NTC) with temperature coefficient of maximum absolute value and a N-Well resistor (PTC) with temperature coefficient of maximum value. Both resistor types present a square resistance of great value (typically1000Ω/ respectively 1080Ω/) so they do not occupy an exaggerated chip area.

The function of circuit in fig. 2 is the following. At usual temperatures all the transistors are saturated, including M_4, because the voltage drop on resistor R_2 is small. The currents in the two branches have small values (as example 0.4μA and 11μA) being practically imposed by the resistor R_1. The output voltage V_{out} has a reduced value („low logic level").

When the temperature grows and comes near the releasing value imposed by R_2, the R_1 value decreases, the current I_2 in the right branch grows, the value of resistor R_2 rises and produces a decreasing of the drain-source voltage of transistor M_4. Consequently, this transistor comes near the saturation-region limit. Also, the increasing current causes the increase of V_{GS4} voltage and of saturation-region limit voltage, V_{DSsl} of M_4, the transistor entering more quickly the linear region. The drop voltage on resistor R_1 comes greater and, because the R_1 value decreases with temperature, the I_2 current grows in addition, leading to a cumulative toggle regime.

At the middle of the output voltage jump, all transistors, excepting M_4, are still in saturation regime and the loop voltage gain is maximal. In this situation the I_1 current

on left branch increases too. The drain-source voltages of transistors M_2 and M_3 decrease, they entering the linear regime too. Thus, for a small temperature increase (0.5^oC), the I_2 current reaches an about double value in comparison with the initial value and this leads to the output-voltage toggle at „high logic level". At the toggle end, M_2, M_3 and M_4 are in deep linear regime (with small drain-source voltage and great drain current).

3 The Toggle Condition Deduction

The temperature relay function being known, a problem appears: to demonstrate theoretically the fact that, at a particular temperature – named „releasing temperature", the output-voltage toggle initiates. This study will permit to better understand the relay function and to establish the important factors determining the apparition of the toggle phenomenon that is a transition accelerated by the positive feedback with increasing gain.

One affirmed previously that the scheme presents a positive feedback, which at usual temperature do not assures a voltage gain greater than the unity which could produce the circuit toggle. But, in the new proposed scheme, at a particular temperature imposed by the resistors, the open loop attains a voltage gain greater than 1 and a cumulative process appears which makes the circuit to toggle for a temperature increase of only 0.5^oC. To this gain increase the principal role is held by the entrance of the transistor M_4 in a deeper linear regime.

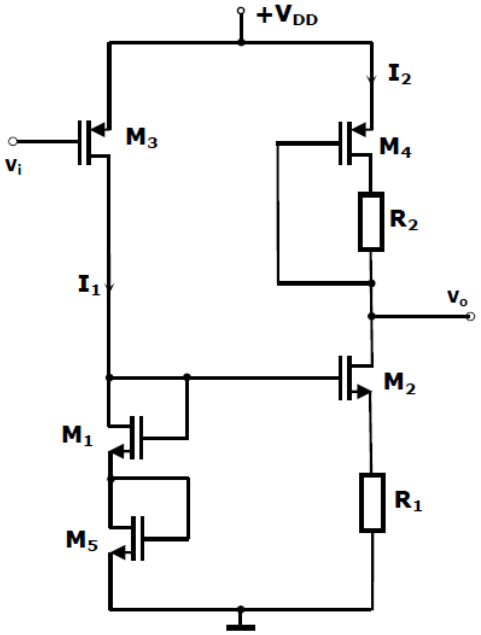

Fig. 3. The open-loop of the feedback amplifier

Therefore, the condition for the circuit to toggle is that the open-loop voltage gain's value exceeds 1. In order to ensure this gain, a feedback loop between the two branches will be opened, in the gate of transistor M_3 (fig. 2), thus obtaining the two-stage amplifier scheme of fig. 3. Here, the stage 1 is achieved by the transistor M_3, loaded by the M_1 and M_5 diodes in series. The stage 2 is realized by the transistor M_2, loaded by the „modified diode" created with transistor M_4, and has a strong local negative feedback by the resistor R_1. Because the loop comprises two CS-connection amplifier stages, between output and input one gets a total phase difference of 360^o, consequently the relay scheme feedback is a positive one.

Since the gain is estimated in a point located in the middle of current and voltage toggle jumps, whose variations being slow, it is possible to apply a low-frequency low-signal technique.

The 1-stage voltage gain is:

$$A_{v1} \cong -g_{m3}\left(r_{d1} + r_{d5}\right) \tag{1}$$

where g_{m3} is the mutual conductance of the low-frequency low-signal model of transistor M_3, r_{d1} and r_{d5} are the resistances of the M_1 and M_5 diodes:

$$r_{d1} = \frac{1}{g_{m1}} \quad , \quad r_{d5} = \frac{1}{g_{m5}} \tag{2}$$

where g_{m1} and g_{m5} are the mutual conductance of the transistors M_1 and M_5.

Now, the first-stage voltage gain may be written:

$$A_{v1} = -g_{m3}\frac{g_{m1} + g_{m5}}{g_{m1}g_{m5}} \tag{3}$$

Omitting the feedback output resistance R_{or} in the drain of Widlar-mirror transistor M_2, which is much greater in respect to the output resistance of the modified diode (composed by M_4 and R_2), the 2-stage voltage gain is:

$$A_{v2} \cong -g_{m2}\frac{R_{o4}}{1 + g_{m2}R_1} \cong -\frac{R_{o4}}{R_1}\cdot \tag{4}$$

where $g_{m2}R_1 >> 1$ and R_{o4} is the output resistance of the modified diode, seen from the drain of amplifier transistor M_2:

$$R_{o4} \cong \frac{r_{ds4} + R_2}{1 + g_{m4}r_{ds4}} \tag{5}$$

where g_{m4} and r_{ds4} are the mutual conductance respectively the drain-source resistance of the transistor M_4, working in linear regime (see APPENDIX).

So, the second-stage voltage gain may be put in the form:

$$A_{v2} \cong -\frac{1}{R_1}\cdot\frac{r_{ds4} + R_2}{1 + g_{m4}r_{ds4}} \tag{6}$$

One may write now the relay toggle condition for the open-loop gain:

$$A_{v1} \cdot A_{v2} \geq 1 \tag{7}$$

or, after the necessary replacements, this condition can be expressed:

$$g_{m3} \cdot \frac{g_{m1} + g_{m5}}{g_{m1} g_{m5}} \cdot \frac{r_{ds4} + R_2}{R_1 (1 + g_{m4} r_{ds4})} \geq 1 \tag{8}$$

The analysis of this condition leads to the following conclusions:

- here the transistor-M_2 mutual conductance g_{m2} does not intervene, what may be explained because its effect was done negligible by the strong local negative feedback,
- the resistances quicken the touching of toggle condition with temperature growth because R_2 is of PTC type while R_1 – of NTC type,
- the r_{ds4} resistance has a small value ($<< R_2$) after the toggle starts, because the M_4 transistor enters the deep linear regime, thus the R_2 effect becomes important,
- the conductance g_{m4} has a smaller and smaller value after transistor M_4 enters the linear regime, which accelerates the toggle,
- the product $g_{m4}r_{ds4}$ (see Appendix) diminishes quickly with the temperature growth when M_4 enters the deep linear regime, quickening the carrying out of condition (8) where it is the most important term,
- if one uses $M_1 \equiv M_5$, then $g_{m1}=g_{m5}$ and the condition (8) simplifies.

The numeric calculus to verify the toggle condition has considered the dependence against temperature of variables g_m and r_{ds4} (through the carrier mobility μ and the threshold voltage V_t) then of the resistances R_1 and R_2, using the temperature coefficients. For better precision it was necessary to consider the second-order temperature coefficients of the carrier mobility and resistors [2] (see Appendix). In the conductances g_{m1}, g_{m3} and g_{m5} calculus, for saturation regime, one neglected the channel-length modulation factor (λ). The values of parameters K'_n, K'_p, V_{tno} and V_{tpo} (at temperature of 0^oC) for transistors as well of temperature coefficients for mobility – $k_{\mu n}$, $k_{\mu p}$ (of I order), $k_{\mu n \mu n}$, $k_{\mu p \mu p}$ (of II order) [2], of threshold voltages – k_{Vtn} and k_{Vtp} and of resistors – k_{R1} and k_{R2} (of I order), k_{R1R1} and k_{R2R2} (of II order), were found in the model-parameter list for transistors and resistors in 0.35μm CMOS process considered.

There were used the values: $K'_n=87.35\mu A/V^2$, $K'_p=37.74\mu A/V^2$, $V_{tno}=0.759V$, $V_{tpo}=0.807V$, $k_{\mu n}= -6.17 \cdot 10^{-3}/^oC$, $k_{\mu n \mu n}= 0.0167 \cdot 10^{-3}/^oC$, $k_{\mu p}= 5.07 \cdot 10^{-3}/^oC$, $k_{\mu p \mu p}=0.0138 \cdot 10^{-3}/^oC$ [2], $k_{Vtn}=-1.97 \cdot 10^{-3}/^oC$, $k_{Vtp}= -1.86 \cdot 10^{-3}/^oC$, $k_{R1}= -2.84 \cdot 10^{-3}/^oC$, $k_{R1R1}=7.36 \cdot 10^{-6}/^oC^2$, $k_{R2}= 3.9 \cdot 10^{-3}/^oC$, $k_{R2R2}=0.01 \cdot 10^{-3}/^oC^2$. At 25^oC, the resistors have the values $R_1=0.1M\Omega$, $R_2=0.0435M\Omega$, $V_{GS1}= V_{GS5} =1.24V$, $V_{GS3}= V_{GS4}=1V$, $V_{DS4}=0.06V$.

The transistor M_4, which at toggle beginning is very close to the saturation-region limit, heaving the voltage $V_{DS4} \approx 0.1V$ while the saturation region limit voltage is $V_{DSsl} \approx 0.15V$, comes up, for a $0.25\,^oC$ temperature variation, in the deep linear region, with the voltage $V_{DS4}=0.06V$, smaller than the saturation-region-limit voltage one,

which becomes (by the increase of I_2 current and V_{GS4} voltage) V_{DSsl}= 0.4V. For this situation one verified the carrying out of the toggle condition.

The conductance and resistance values were calculated for a temperature located at the middle of voltage and current jumps measured in simulation, that is, at the releasing temperature of 115°C (for typical – TYP – parameters of scheme components). One obtained the values (see Appendix): $g_{m1}=g_{m5}=5.68\mu A/V$, $g_{m3}=15.2\mu A/V$, $g_{m4}=81.4\mu A/V$, $r_{ds4}=0.0024M\Omega$, $R_1=0.0804M\Omega$, $R_2=0.0623M\Omega$.

With these values the open-loop voltage gain resulted:

$$A_{v1} \circledcirc A_{v2}=3.6 > 1 \tag{9}$$

So, the toggle condition is fulfilled. By calculus it was possible to establish the value 1 of the open-loop voltage gain is attained for a voltage $V_{DS4}\approx 0.15V$ that is, at the beginning of the toggle, when the transistor M_4 enters the linear regime.

As it may be seen, the relay function is better described and understood after the deduction of toggle condition and after calculus. To simplify the numerical calculus were used some simulation results. But, the deduction of the releasing temperature from the toggle condition by pure analytical way is extremely complicated because all the factors implicated in this are temperature function of first or second degree and the variables g_{m4} and r_{ds4} are strongly connected with the V_{DS4} voltage in the linear region.

4 Simulation Results

The temperature relay submitted to simulation was designed for a releasing temperature of 115°C (for TYP parameters of components), closed to the maximal working temperature of numerous integrated circuits, produced at industrial scale. The characteristic dimensions of transistors in 0.35μm CMOS process were the presented in Table 1 in μm, presuming transistors of 5V. We adopted the supply voltage V_{DD}=3V.

Table 1.

M_1	M_2	M_3	M_4	M_5
1/5	30/4	8/4	120/2	1/5

The resistor's values at 25°C were $R_1=100k\Omega$, $R_2=43.5k\Omega$ and their widths were $W_{R1}=0.6\mu m$ and respectively $W_{R2}=4.15\mu m$. The occupied-on-chip area was estimated of $1280\mu m^2$.

As already shown in [3], [4], [5] and [7], to minimize the output-function variations against the process of the circuits configured by cross-connected current mirrors, one establishes particular widths of the two used resistors. Sometimes [3] the output variations against the process (which, without some special solutions, is of order of tens percents [1], [2]) is reduced to a value of only few percents, at which it begins to matter the component geometry (un-matching) errors [3]. This procedure led to surprising performances of simulated circuits and even has effect in the minimization of

standard deviation resulting in the Monte Carlo simulation [4], [5]. It is one of the special qualities of the analog circuits with cross-connected current mirrors which use two resistors.

The principal result of the simulation, presented in fig. 4, is referred to the output voltage toggle, including the process variation (tests with *typical* – TYP, *best case* – BC and *worst case* – WC – parameters), for temperature growing sense.

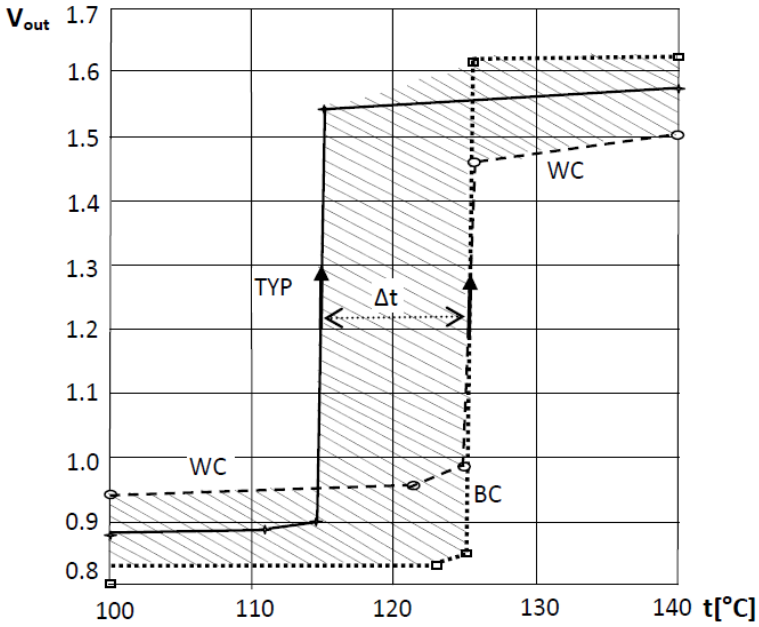

Fig. 4. Output-voltage variation with temperature and process

One can see a relative important modification of the releasing temperature occurs in the three cases (see the hatched zone). Defining this temperature at the middle of Δt difference, measured at the middle of the voltage jump for the most unfavourable curve (WC), one obtains a releasing temperature of 120.5±5.5°C. The total variation Δt = 11°C is measured at an output voltage level of 1.21V. The Δt-variation minimization was obtained by establishing suitable resistor widths, which assure the equality of output voltage levels for WC and BC cases, in the middle of the jump of the most unfavourable curve (WC) (fig. 4).

Certainly, to achieve a better precision it is necessary to provide in the manufacturing process a trimming operation; either an usual trimming of R_2 or by a special circuit digitally controlled. Thanks to the Δt-error minimization, the trimming circuit will not be so complex as the usual one included in a contemporary precision temperature sensor, with the help of which a protection temperature relay is configured in chip at the present. Namely, the trimming-control-bit quantity for trim the proposed relay will be smaller.

Even with such un-precision (fig. 4), this temperature relay can find applications because of the scheme simplicity and reduced on-chip area. The improvement of the hatched zone form, firstly by the extension of the output-voltage jump for WC parameters, is possible by increasing the transistor dimensions, especially the M_4-transistor width which is already relatively great.

The output-voltage variation against the supply voltage V_{DD} is very small, which is typical for the circuits with cross-connected current mirrors [3], [5].

The current jumps in the two branches were the following: I_1: from 0.37 to 2.2μA, I_2: from 11.24 to 19.1μA.

Fig. 5 presents the shape of the relay's characteristic, including the output-voltage variation for the temperature descending sense too, with component's TYP parameters. The hysteresis value in the zone Δt is 26°C. For BC parameters this is 16°C while for WC parameters –32°C. It is possible to reduce the hysteresis by increasing the transistor dimensions but maintaining the W/L ratio. For a releasing temperature < 90°C the ΔH value may be more reduced.

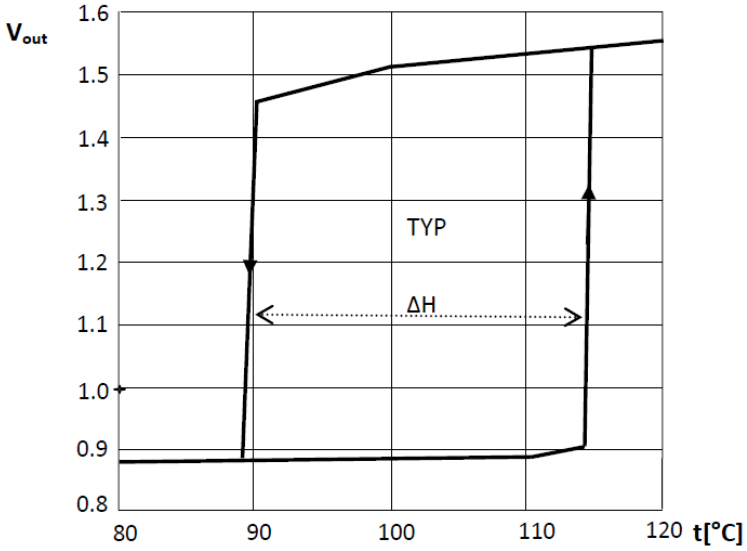

Fig. 5. Hysteresis curve for TYP parameters

Another result of the scheme simulation is referred to adjusting range of the relay releasing temperature through the R_2 resistor. One mentions, the adjusting of this temperature can be done through the R_1 resistor too but this could lead to an important modification of output-voltage logic levels. Fig.5 presents the variation ranges of the releasing temperature, considered in the middle of hatched zone (at the middle of Δt), as function of recommended R_2 -resistance value and heaving as parameter the R_1-resistance value.

In our simulation it has been established a recommended (verified) adjusting range of approximately 50-60°C for an adopted R_1-resistance value but this range may be extended by extrapolation of maximal and minimal recommended values for the resistance R_2.

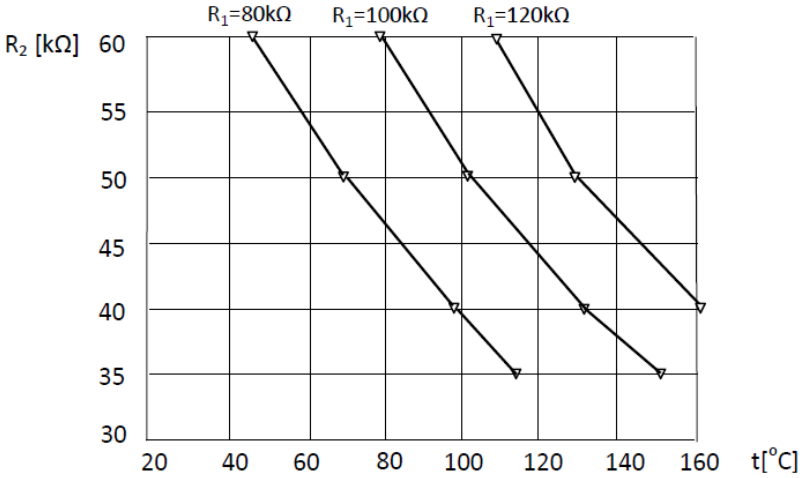

Fig. 6. Releasing-temperature adjusting ranges

5 Conclusions

At present, the function of temperature relay in chips is achieved with the help of a precise temperature sensor (with trimming) and a comparator circuit. These circuits have a relatively higher complexity and occupy greater area than our proposed temperature relay with trimming.

This work presents a second variant of temperature-relay scheme for CMOS chips, based on a simple structure of voltage source with two cross-connected current mirrors (of modified-Widlar type and simple one), corresponding designed. Similar schemes have been proposed as temperature sensors and this led to the idea of achieving a simple temperature relay. In the proposed scheme the positive feedback is exploited, which is designed to assure, at a particular temperature, an open-loop voltage gain greater than 1, such as the circuit toggles. Its output voltage exhibits a great enough level jump to drive an interface circuit with the processing part of relay signalisation.

It was established trough analytical way, by low-signal low-frequency positive-feedback analyses, the toggle condition, which more clears up the relay function. From this, by successive trial, one can determine the relay releasing temperature.

By the simulation of such a relay, conceived in 0.35µm CMOS process, were obtained the following performances:

- minimum output-voltage jump (for WC parameters) of 0.5V,
- medium releasing temperature of 120^{o}C,
- variation against process of the releasing temperature of ±5.5^{o}C,
- recommended output-voltage level to act the next circuit: 1.21V,
- hysteresis value for the most un-favourable case (for WC parameters): 32^{o}C,
- estimated on-chip area: 1280µm^{2}.

The minimum output-voltage jump can be enlarged by increasing the transistor M_4 width while the relay hysteresis can be reduced by increasing the transistor dimensions.

The releasing temperature can be programmed in a large domain by the help of one or two resistors. Its process variation is reduced by special design procedure at a maximum value of $\pm 5.5^{o}C$.

To achieve a better precision of the releasing temperature, it is necessary to provide in the manufacturing process a trimming operation. Thanks to the Δt-error minimization, the trimming circuit will not be so much complex as the usual one. Namely, the trimming-control-bit quantity for the proposed relay will be smaller.

References

1. Fiori, F., Crovetti, P.S.: A New Compact Temperature – Compesated CMOS References. IEEE Transactions on Circuits and Systems-II 52(11), 724–728 (2005)
2. Mihăescu, R.D.: Concepţia unor surse de curent de referinţă pentru circuite integrate CMOS. Doctoral thesis, "Politehnica" University of Timişoara (2008)
3. Ciugudean, M.A., Bodea, M.C., Coandă, H.G.: Simple and Performing Temperature-Compensated Voltage References. Buletinul Ştiinţific al Universităţii Politehnica, Seria Electronică şi Telecomunicaţii, Tom 56 (70), Fascicola 1, 6–11 (2011)
4. Marinca, V.B.: Concepţia şi proiectarea unor noi senzori de temperatură analogici integraţi în tehnologie CMOS. Doctoral thesis, "Politehnica" University of Timişoara (2011)
5. Marinca, V.B., Ciugudean, M.A.: CMOS Temperature sensors using peaking current source. Buletinul Ştiinţific al Universităţii Politehnica, Seria Electronică şi Telecomunicaţii, Tom 56 (70), Fascicola 1, 19–23 (2011)
6. Baker, R.J.: CMOS: Circuit Design, Layout, and Simulation, 3rd edn. Wiley - IEEE Press (2010)
7. Ciugudean, M.A.: CMOS Integrated Temperature Relay Based on Wilson Mirror (to be published)

Appendix

For the mutual conductances and resistances, as temperature functions, the following calculus relations were used:

$$g_{m1} = g_{m5} = K_n^{'} \frac{W_1}{L_1}\left(1 - 6.17 \cdot 10^{-3} t + 0.0161 \cdot 10^{-3} t^2\right)\left[V_{GS1} - V_{tno}\left(1 - 1.97 \cdot 10^{-3} t\right)\right] \quad (10)$$

$$g_{m3} = K_p^{'} \frac{W_3}{L_3}\left(1 - 5.07 \cdot 10^{-3} t + 0.0138 \cdot 10^{-3} t^2\right)\left[V_{GS3} - V_{tpo}\left(1 - 1.86 \cdot 10^{-3} t\right)\right] \quad (11)$$

$$g_{m4} = K_p^{'} \frac{W_4}{L_4}\left(1 - 5.07 \cdot 10^{-3} t + 0.0138 \cdot 10^{-3} t^2\right) V_{DS4} \quad (12)$$

$$r_{ds4} = \frac{1}{K_p^{'} \frac{W_4}{L_4}\left(1 - 5.07 \cdot 10^{-3} t + 0.0138 \cdot 10^{-3} t^2\right)\left[V_{GS4} - V_{tpo}\left(1 - 1.86 \cdot 10^{-3} t\right) - V_{DS4}\right]} = \quad (13)$$

$$= \frac{V_{DS4}}{g_{m4}\left[V_{GS4} - V_{tpo}\left(1 - 1.86 \cdot 10^{-3} t\right) - V_{DS4}\right]}$$

Thus, the product $g_{m4} \cdot r_{ds4}$ becomes:

$$g_{m4} r_{ds4} = \frac{V_{DS4}}{V_{GS4} - V_{tpo}\left(1 - 1.86 \cdot 10^{-3} t\right) - V_{DS4}} \quad (14)$$

$$R_1 = R_{1(25)}\left[1 - 2.84 \cdot 10^{-3}(t - 25) + 7.36 \cdot 10^{-6}(t - 25)^2\right] \quad (15)$$

$$R_2 = R_{2(25)}\left[1 + 3.9 \cdot 10^{-3}(t - 25) + 0.01 \cdot 10^{-3}(t - 25)^2\right] \quad (16)$$

A FPGA Floating Point Interpolator

Marius M. Băla ş[1], Marius Socaci[1], and Onisifor Olaru[2]

[1] "Aurel Vlaicu" University of Arad, Romania
marius@drbalas.ro,
mariusocaci@yahoo.com
[2] "Constantin Brancusi" University of Tîrgu Jiu, Romania
onisifor.olaru@yahoo.com

Abstract. The fuzzy-interpolative systems, a class of the Sugeno family fuzzy controllers, merge the linguistic representation of the knowledge with the effective interpolative implementations. Their application is immediate in any possible software environment, by look-up-table structures. However, their hardware implementation is not so easy. This paper is reporting a little step forward for the application of the fuzzy-interpolative systems in the field of the embedded systems: a specific FPGA block that is able to perform floating point interpolations, which can stand for a core of a future FPGA fuzzy-interpolative controller.

Keywords : fuzzy-interpolative system, floating point interpolation, FPGA.

1 Introduction

The interpolative side of the fuzzy and the neural controllers was initially mentioned by L. Zadeh [1]. In-depth studies on this matter showed that the fuzzy systems are universal approximators [2] and that they can be equalized or approximated at their turn by numerical mappings. The interpolation connection builds a bridge between the theoretical AI and Soft Computing concepts and the field control applications [3], [4]. Our approach in this matter is materialized by the *fuzzy-interpolative methodology* [5], which enables us to leave behind the comprehensive software that are commonly associated to AI and to develop fuzzy expert systems at the level of the simple programmable devices (μC, DSP) or even with analog circuitry.

The most attractive technology in the embedded systems domain is obviously the FPGA [6], [7]. Comparing FPGAs with the conventional digital computer architecture one observes that computers and the other similar binary architectures (μP, μC, DSP, etc.) are build around a central spine bone: the data/address/control bus, while FPGAs are distributed and purely parallel. That is why FPGAs are extremely fast, reliable, robust, portable, low energy consuming and cheap. If Soft Computing will be conveniently transferred into FPGAs we could expect a significant boost of the intelligent applications in all the aspects of our lives.

V.E. Balas et al. (Eds.): Soft Computing Applications, AISC 195, pp. 331–336.
springerlink.com

In a previous paper [8] our first step in this direction was done: a 8 bit interpolative controller on a FPGA Altera Cyclone II board, working with Quartus II Web Edition software. That controller was build for processing integer numbers, so the next step, presented in his paper, is the construction of an interpolation controller able to work with floating point represented numbers, in order to ensure a wide range of values and a satisfactory precision of the calculus [9].

2 A Floating Point Interpolator

Our goal is to build a VHDL block for the piecewise linear interpolation (Fig. 1).

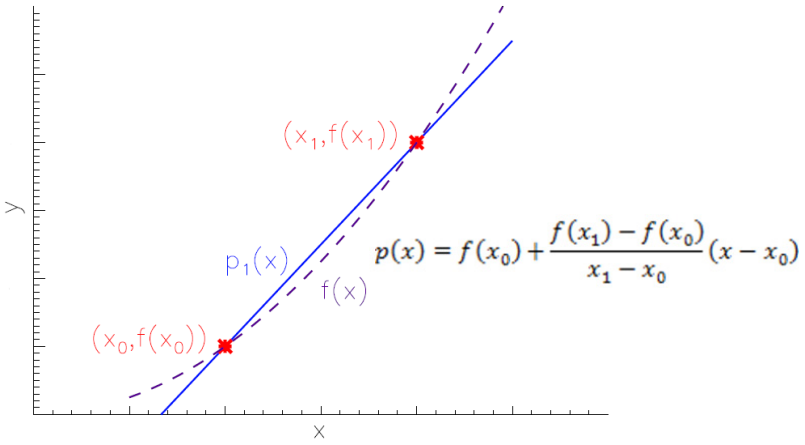

Fig. 1. The piecewise linear interpolation

The following interpolator is designed and realized using the support of the most accessible FPGA development board on the market: Digilent Spartan 3 equipped with the FPGA circuit Xilinx XC3S200-4FT256.

The Xilinx iMPACT software (included into the Xilinx ISE Design Suite 14.1 package) [10], which is the programming tool, is connected with the system by means of the board's JTAG port.

A specific software tool that is assisting the floating point units design in ISE is the Xilinx Core Generator (see Fig. 2), which overlaps the IEEE-754 standard [9].

The Fig. 3 parallel interpolator is composed by six floating point units in single precision: three subtractions, one addition, one divider and one multiplier. Its performance is shown in Fig. 4. The speed of this purely parallel architecture is obviously very good: the latency is 1.22 μs, but on the other hand this circuit is consuming all the resources of the FPGA (193 bonded IOBs) and the overmapping limit is reached.

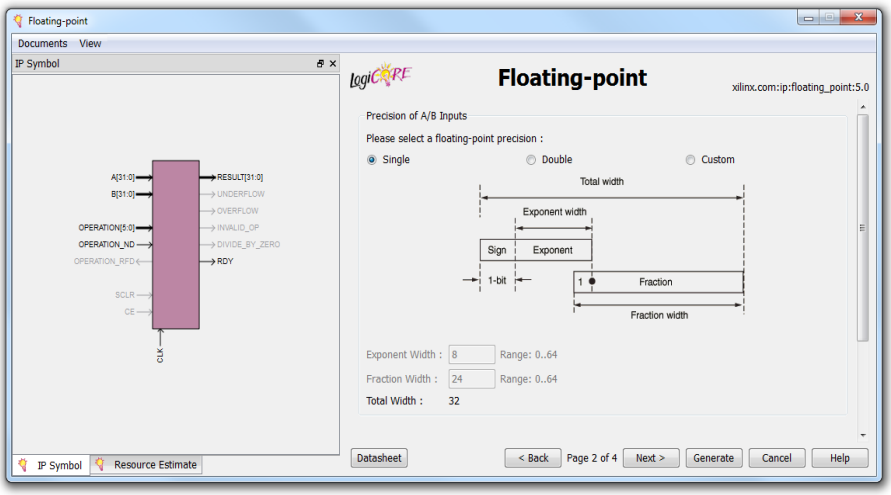

Fig. 2. The Xilinx Core Generator for the design of the floating point units

Although if using more powerful FPGAs the problem could be enshrouded, a good interpolator should be optimized simultaneously in both senses: decreasing the number of the gates (minimizing if possible) and the latency.

A possible solution to this optimization problem is to introduce pipelines techniques, but in this early stage of the research this approach would be rather costly and inadequate. We intend to fully apply the pipelining when reaching the final development stages of a complete fuzzy-interpolative controller.

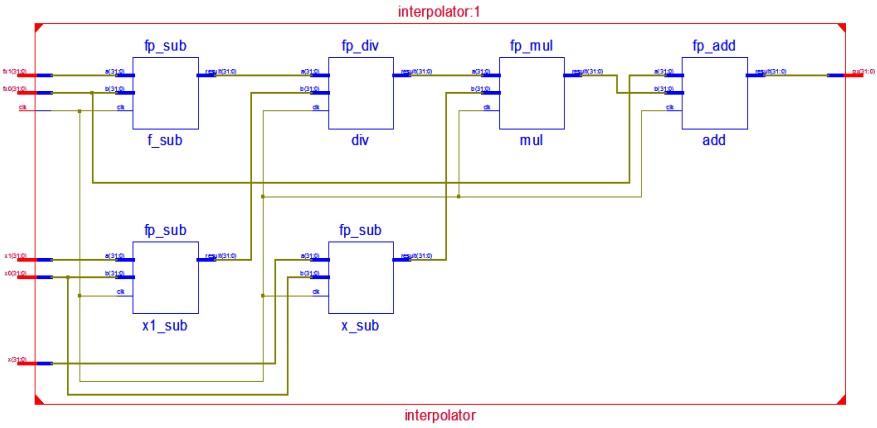

Fig. 3. The VHDL parallel interpolator

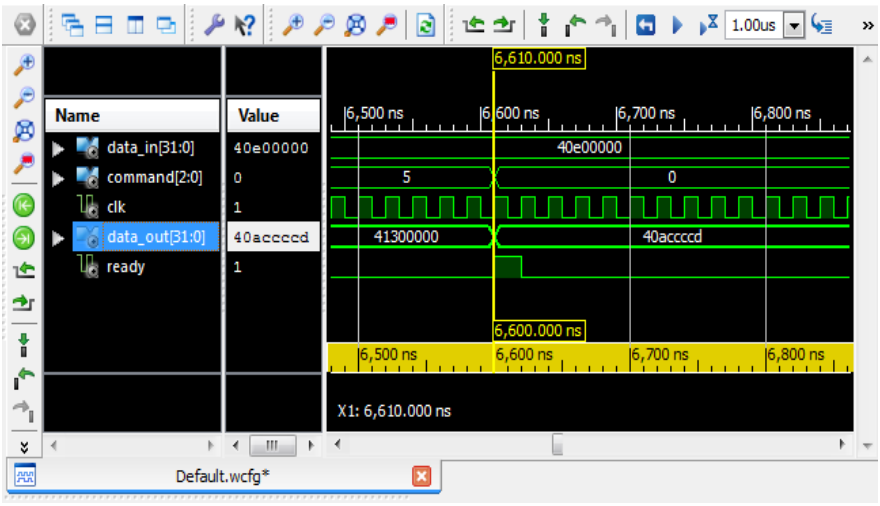

Fig. 4. The testing of the parallel VHDL interpolator

3 A Subtraction Sharing Floating Point Interpolator

A simple and effective method to reduce the interpolator's number of used gates is the resource sharing [12]. In this case we built a single floating point subtraction unit and share it for the three subtraction stages of the interpolation operation [11]. Furthermore, the subtraction unit was merged with the addition unit. A control input selects the actual operation.

The interpolation is losing its implicit parallel operation, which is turned into a sequential one, controlled by the finite-state-automation presented in Fig. 5. Due to the more flexible structure different functional optimizations can be taken into consideration. For instance, the partial results can be memorized and reused, if we need several point of the same interpolated function. The latency of this interpolator for a new set of input data is 6.6 μs. When computing a new point on a previously computed interpolated function, the latency can decrease to 0.78 μs. The number of bonded IOBs is 69.

The sequences of the interpolations are also presented in Fig. 5. The introducing of the input data can be repeated, as well as the reading of the corresponding results. The implementation of this version of the interpolator was written directly in VHDL.

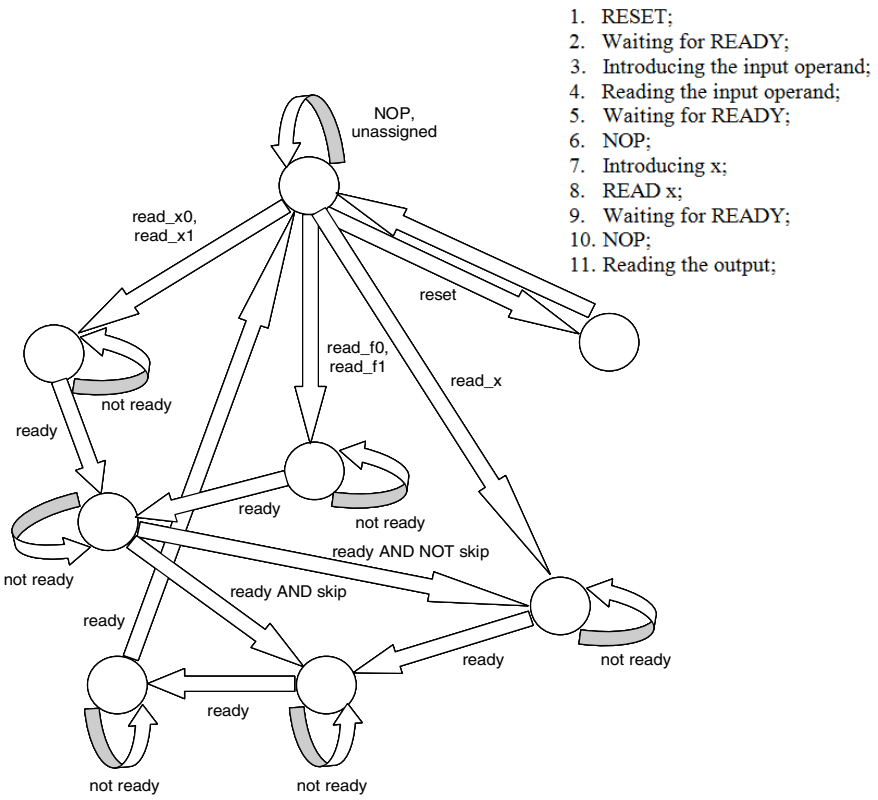

Fig. 5. The controller of the subtraction sharing floating point interpolator

4 Discussion

The paper is presenting the implementation of a floating point piecewise linear interpolation FPGA block, written in VHDL, on a Digilent Spartan 3 board. Two architectures were realized and tested:

1) A parallel interpolator containing six floating point units: three subtractions, one addition, one divider and one multiplier, which has a latency of 1.22 μs.
2) A minimized interpolator containing three floating point units: one multiplier, one divider, and one addition/subtraction merged unit, which is shared by three different stages of the interpolation algorithm, with a latency of 6.6 μs.

The final goal of this research is to implement fuzzy-interpolative applications into FPGA circuits, in other words to bring Soft Computing into the world of the field FPGA embedded systems.

References

1. Zadeh, L.A.: Interpolative reasoning as a common basis for inference in fuzzy logic, neural network theory and the calculus of fuzzy If/Then rules. Opening Talk. In: Proceedings of 2nd International Conference on Fuzzy Logic and Neural Networks, Iizuka, pp. XIII–XIV (1992)
2. Bauer, P., Klement, E.P., Moser, B., Leikermoser, A.: Modeling of Control Functions by Fuzzy Controllers. In: Nguyen, H.T., Sugeno, M., Tong, R., Yager, R. (eds.) Theoretical Aspects of Fuzzy Control, pp. 91–116. John Wiley & Sons (1995)
3. Dale, S., Dragomir, T.-L.: Interpolative-Type Control Solutions. In: Balas, V.E., Fodor, J., Várkonyi-Kóczy, A.R. (eds.) Soft Computing Based Modeling in Intelligent Systems. SCI, vol. 196, pp. 169–203. Springer, Heidelberg (2009)
4. Dale, S., Bara, A., Gabor, G.: Comparative study case for interpolative-type synthetic input controllers on a ball and beam system. In: Proceedings of the 10th WSEAS International Conference on Fuzzy Systems FS 2009, Prague, pp. 76–83 (2009)
5. Balas, M.M.: The Fuzzy-Interpolative Methodology. In: Balas, V.E., Fodor, J., Várkonyi-Kóczy, A.R. (eds.) Soft Computing Based Modeling in Intelligent Systems. SCI, vol. 196, pp. 145–167. Springer, Heidelberg (2009)
6. Rodriguez-Andina, J.J., Moure, M.J., Valdes, M.D.: Features, Design Tools, and Application Domains of FPGAs. IEEE Transactions on Industrial Electronics 54(4), 1810–1823 (2007)
7. Computer Engineering Research Group - University of Toronto: The FPGA Place-and-Route Challenge, `http://www.eecg.toronto.edu/~vaughn/challenge/fpga_arch.html`
8. Balas, M.M., Sajgo, B.A., Belean, P.: On the FPGA Implementation of the Fuzzy-Interpolative Systems. In: The 5th International Symposium on Computational Intelligence and Intelligent Informatics ISCII 2011, Floriana, Malta, September 15-17, pp. 139–142 (2011)
9. IEEE Computer Society: IEEE Std 754™ 2008. IEEE Standard for Floating Point Arithmetic. IEEE Inc., New York (2008)
10. Xilinx: ISE In-Depth Tutorial (January 18, 2012)
11. Socaci, M.: Aplicație VHDL pentru calcul în virgulă mobilă pe FPGA. Master disertation, University Aurel Vlaicu of Arad (2012)
12. Kilts, S.: Design, Architecture, Implementation and Optimization. Wiley Interscience (2007)

Achieving Semantic Integration of Medical Knowledge for Clinical Decision Support Systems

Daniel Dragu, Valentin Gomoi, and Vasile Stoicu-Tivadar

"Politehnica" University, Timişoara, Romania
{daniel.dragu,valentin.gomoi,
vasile.stoicu-tivadar}@aut.upt.ro

Abstract. Enhancing the outputs of the Clinical Decision Support systems (CDS) is a permanent concern for many research communities, which have to deal with an abundance of entities, data, structures, methods, application, tools, and so on. In the few past decades, there were theorized and standardized technologies that could help researchers to obtain better results. The paper presents a method to enrich the inputs of the CDS through a semantic integration of several medical knowledge sources, by using the Topic Maps standard, in order to obtain more refined medical recommendations. Future research directions and challenges are summarized and conclusions are issued.

1 Introduction

Large amounts of structured and unstructured pieces of medical information reside in different locations, many of them without any chance to be used afterwards. Semantic technologies could provide the solution to federate all those information constructs, seeking to obtain more refined medical recommendations at the CDS outputs. These statements come to support the idea of developing and implementing concepts like Semantic Web (SW), where "computers must have access to structured collections of information and sets of inference rules that they can use to conduct automated reasoning"[1].

Despite the large worldwide implementation of the information systems and the need to continuously improve patient safety and care quality, the evolution of CDS systems was not so rapid, even if it could. Some of the most important aspects which affect this could be the non-existence of a standardized (clinical information) informational core able to assure the functionality of any CDS, and also the compatibility between these and healthcare (clinical) information systems. In the last few decades there were made significant steps in order to achieve not only the formal interoperability between medical information, documents and applications [2.], but even the semantic interoperability [3], and consequences can be seen in the new standards that were elaborated and adopted for this cause. Virtual Medical Records (vMR) is the result of a research group from the HL7 organization; it is "a data model for representing clinical information relevant to CDS" and "encompasses data about a patient's demographics and clinical history, as well as CDS inferences about the

V.E. Balas et al. (Eds.): Soft Computing Applications, AISC 195, pp. 337–347.
springerlink.com

patient" [4]. This data model is about to be redefined within the current research activity, by using a semantic technology, trying to obtain an enhanced integration of sources.

Data, information and knowledge have to be organized and represented in such a manner that both, human and computer, to be able to understand their meaning. The Topic Maps (TM) technology is the perfect solution for this issue, being able to conceptualize and represent any subject [5] in a computer-understandable and also a human-understandable way. TM is an ISO standard, ISO/IEC 13250:2003 Topic Maps, and it was designed to give users the possibility to represent their knowledge and rapidly find information they need. It was developed "as an answer to the problem of how to automate merging of (digital) back-of-books indexes" [6].

The methods and technologies used within this approach should provide the achievement of the desired results, allowing an enhanced interoperability not only for CDS systems, but for a lot of other healthcare information systems which rely on the vMR data model to manage their own informational structures.

2 Mapping vMR to TM

2.1 Technologies - Theoretical Considerations

Finding a common data model for organizing medical knowledge was the main concern of the research activity. The requirements for that data model stated that it should be able to represent a collection of informational constructs used in Clinical Decision Support systems, and also to let this collection be updated with information from various sources. Virtual Medical Record (vMR) represents a solution provided by the HL7 organization, and even if it is not a standard yet, the probability for this model to be standardized is high [7].

The analysis of the most important semantic technologies revealed that TM standard could be eligible to represent such a model. By declaring the identity of the subjects, users have the opportunity to link the formal representation of the vMR data model to other data and knowledge sources [5]. There are other reasons that led to the decision to use TM technology:

- the flexibility, by offering an open vocabulary;
- the ability to quickly find information, by offering "very good support for full-text searching, complex queries, and also providing an excellent basis for natural language querying" [8];
- the extensibility, through the properties of merging distinct topic maps and topics;
- the ability to acquire and represent knowledge, by making computer understand it.

We can say that TM is a technology able to acquire, represent, store, manage and retrieve knowledge. Besides all these, by linking its internal constructs with external references (Fig. 1), a topic map provides an opportunity to connect it with other topic maps, and even with other representations of knowledge that use other semantic technologies. Also, it can be concluded that it offers a possibility to widely spread the contained knowledge.

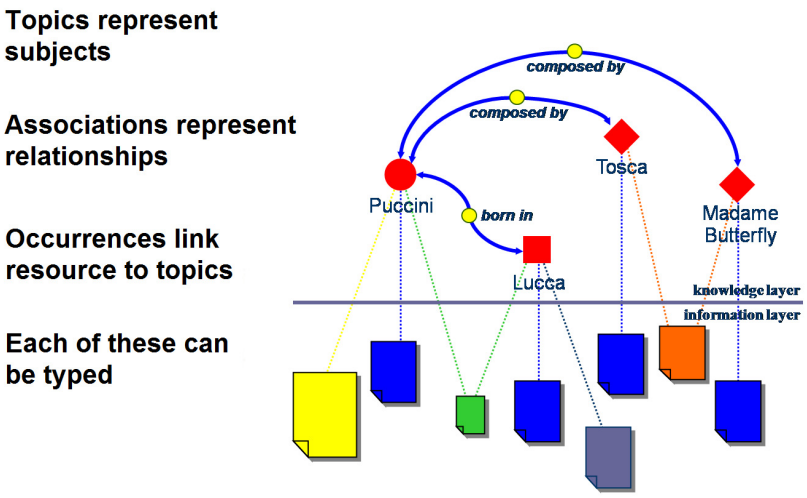

Fig. 1. The TAO[1] of Topic Maps [6]

2.2 Tools

The applicative part of the current research activity tries to implement the specifications of the technologies previously presented, seeking to obtain a high level of medical data integration. The whole system consists of two distinct applications working together: one, which has to deal with knowledge organization, and the other one, which is responsible for the conversion of the incoming informational constructs into new representations in compliance with the Topic Maps Data Model (TMDM) [5].

The tool used to represent vMR in accordance with TM specifications is *Topincs*, "a software for rapid development of web databases", which provides the possibility to represent any domain "by modeling a TM schema" (Fig. 2). It also gives developers and users opportunities "to transform, aggregate, and modify the data"[9]. Other reasons to chose *Topincs* are: "any technological jargon is hidden from the user" [9], is a solution on top of the AMP (short from Apache, MySQL, PHP) stack, is an open source, and well done documentation is provided. *Topincs* is not just a TM engine; it also gives users the possibility to control the behavior of their applications through PHP scripts. These are the most important concepts used in the programming process: *tobject* – PHP object for accessing topics, *domain classes* and *services*, *triggers* and *access filters*. The *Topincs* application includes an under development web database which will be enriched with a package of services as the support for the connection with the C# application.

[1] Short from **T**opic-**A**ssociation-**O**ccurrence.

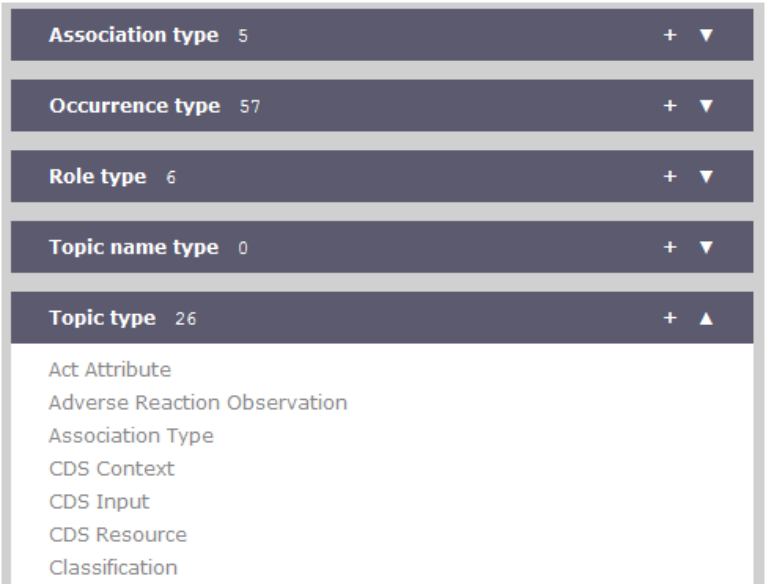

Fig. 2. TM schema for vMR data model

Topincs is an application running on top of Apache 2, MySQL and PHP 5, these being some other tools used in this project. Since PHP syntax is used to model the output of the database, it is obvious that the system lies on a server.

C# programming language under .NET platform will be used to develop the mediator, a conversion module, which has to be able to seek and identify the representations of the same subject within files written in accordance with different data models. A set of conversion algorithms is about to be developed and this work will be part of a subsequent paper. In this context, special attention is given to data validation, to ensure the correctness of the resulted TM constructs, which have to match to the data type specified in the TM schema.

2.3 Implementation

System Overview

After initial phase of the research activity, some questions regarding the implementation of this approach raised:

- what is the best way to represent vMR terms with TM?
- what algorithms will drive the conversion processes?
- what are the tools about to be used?
- is there any chance to fulfill the initial requirements?
- how many efforts the whole project will require?
- why should developers use the final product?
- is there any simple way to do the same thing?

Answering these questions we found that this research field requires knowledge from different domains and will consume a lot of human resources. Also, there are other possibilities to do the same, but this approach seems to better fit to the needs of the domain, following the current trend in information and computer technology and pushing healthcare to a step further. Afterwards, we decided to design and develop an application which relies on a web database, created and maintained with *Topincs*, and a conversion module, written in C#, that should ensure the automatic process of acquiring data from different types of sources (Fig. 3). In the next paragraphs within the current section, there will be shortly described some of the past steps, the current activity and some directions for the further development.

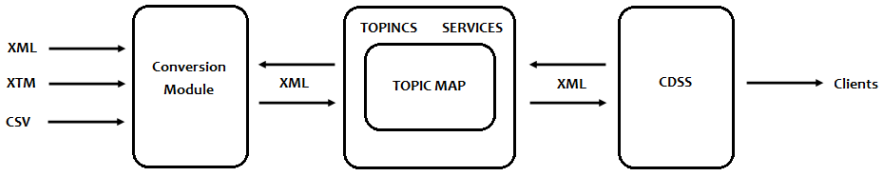

Fig. 3. System overview

The main objective of the current research is to improve the integration of medical data by using TMDM. The immediate requirement for the new data model is the easiness to be assimilated by the users familiar with the original data model, without having to know TMDM, only in case they want to change the behavior or to rewrite the data model. So, it assumes that a high level of usability is ensured for the new data model. In order to meet these objectives, a list of requirements was written:

- the result of the data translation between models can be determined;
- a common vocabulary must be developed;
- data can be translated from one model into the other and vice versa;
- the result of data translation from one model into the other and vice versa is an informational construct with the same content and semantics;
- the translation guide uses common terms of the two models;
- the limits of the translation mechanism will be specified;

We must admit that other requirements may become imperious over the research process.

Creating TM Ontology

The first step in the development of the topic map is to elaborate the TM ontology and for this purpose we used the methodology described in [10]. The most important actions were to identify the boundaries of the domain, to discover and collect the relevant documentation. The latest informative ballot regarding the data analysis model for vMR was downloaded, and there were identified the most eligible tools to be used.

The main concern for the second step, the analysis phase, was to underline the aspects involved in the process of using a common data model for CDS, and to find the

list of questions that could be addressed to the topic map. Also, there were defined the concepts within the domain and the relationships between them. One important requirement for this project was to use, for the new TM constructs, the same denomination for as many vMR terms as possible, in order to obtain a rapid integration of the new data model.

The third step was to sketch the TM ontology, by listing the new concepts and setting up the topic types, association types, occurrence types and some examples of instances for those concept types. All these concepts form a TM ontology, as it was defined in [10]. Based on this TM ontology and by using Topincs, a web database was designed and developed. To a better understanding of this part of work, a brief introduction on some of the concepts we used is presented in the subsequent two paragraphs. Also, it has to be specified that we are talking about two different activities: the design process of the TM ontology and the conception of a TM schema.

An instance of the TM technology is called topic map, and it may exists in various forms: text files, xml files, databases or even stored in human mind. For the current application we decided to manage data, information and knowledge with the help of a web database. The development process of that web database, started with the creation of a schema. This means that all topic types, association types, role types, and occurrence types were represented following the rules stated in the TMDM, and constraints were defined in accordance with The Topic Maps Constraint Language (TMCL) [11]. The result is the TM schema of the represented domain, and it controls the behavior of the whole database.

In order to achieve the requirements of the project, a package of Topincs services is intended to be written. These services are PHP parameterized scripts and they model the response of the database, allowing custom queries and further automation of the integration processes within the current project. In order to develop Topincs services, a PHP object called tobject is used to gain access to the topics. According to the TMDM specification, a topic is a conceptualization of a subject, which "can be can be anything whatsoever, regardless of whether it exists or has any other specific characteristics, about which anything whatsoever may be asserted by any means whatsoever" [5]. The tobject has a virtual programming interface, given based on the constraints within the TM schema, and the serialization names, these being formal denominations which are set by the designer of the topic map for the previously mentioned types within the TM schema. The programming interface of the tobject exposes "methods that make sense given the constraints of the topic type" [12]. New custom methods can be added to the programming interface, by the programmers, using domain classes. All these features give programmers and knowledge engineers the opportunity to rapidly develop powerful applications, based on a very flexible data model.

The next step in the development of the topic map is to refine it, and, in this case, this activity started with the creation of the first definitions and classifications, and it will last throughout whole of the implementation process. The immediate actions within the research activity are: to populate the topic map, and to design and develop the integrating algorithms that will drive the supervised and/or automatic acquisition process.

Integrating Knowledge

To ensure the automation of the data acquisition process, a mediator is under development. It has to identify and convert into TM as many pieces of information as possible from data models that use XML-based syntax (Fig. 4).

The application waits for XML files to be sent to the server and checks if their tags have any known identifiers or if they correspond to any of the predefined templates. The database has to be able to provide identifiers for all elements of the topic map ontology, and these will be further used to define and/or verify the identity of elements from the incoming messages. Identifying the subjects of representations is a process that has not only to comply with the TMDM specifications, but to ensure the automatic data fluxes between different types of information representations and the vMR-TM. Also, while the list of the subject identifiers grows, the chances to discover new information fragments about represented subjects increase, and this should conduct to a more accurate response at the requirements of the users from CDS domain.

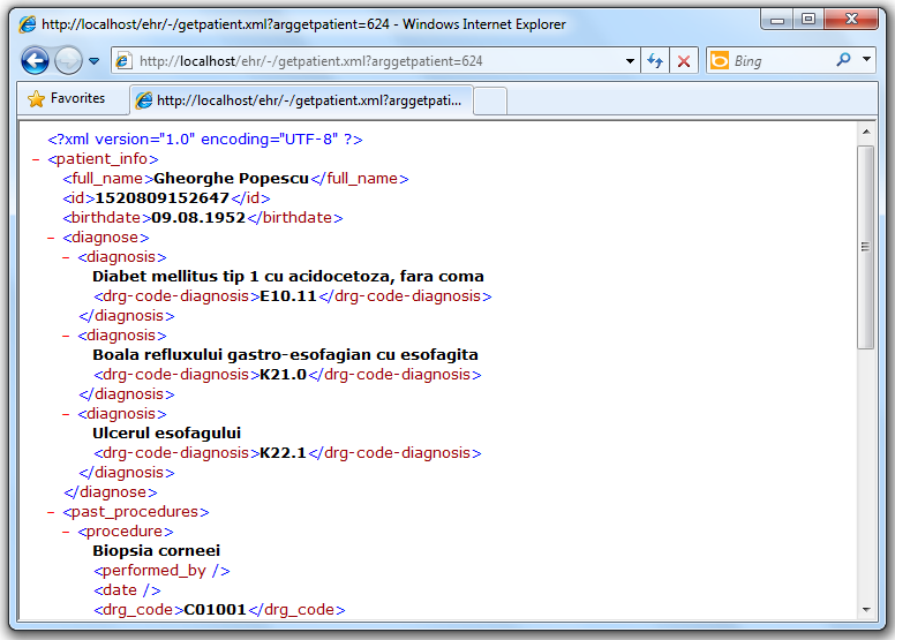

Fig. 4. Example of a potential incoming xml file

In case of any tags match to exposed identifiers, the attributes are verified to see if their subjects have an already defined topic. If topics about the same subject exist, they are updated, and else, they will be created. In case there is no matching, the user interface provides a way to supervise the identification process for unknown terms (Fig. 5). This should become deprecated as the development of the identification algorithms advances.

The identification process firstly relies on the identification methods of topic items described in TMDM, and this capability will be enhanced with other algorithms. The TMDM stipulates that "any information resource can become a subject indicator", and defines this concept as "an information resource that is referred to from a topic map in an attempt to unambiguously identify the subject represented by a topic to a human being" [5]. We can say that the subject indicator may be a web page about that subject and the subject identifier is the URI of that web page. It has to be specified that, attaching an URI to a topic as subject identifier does not imply the TM application to follow any of the contained URIs, but to compare them as a string, in order to discover and merge the distinct representations of the same subjects. According to the TMDM, the result of the merging process is a single topic, which aggregates the properties of two topics representing the same subject, and has the role to eliminate redundant informational constructs and, also, to get all data about a subject at a single location. Also, it is not a critical event in a topic map if the web page at the specified URI does not work or even does not exist. The unique identification can be done and the merging process will work fine.

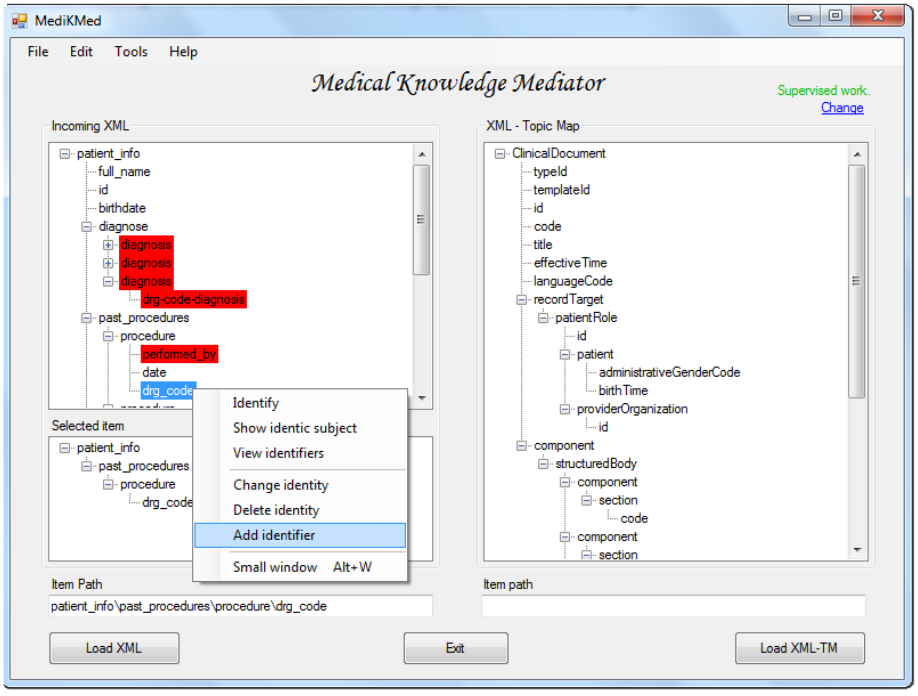

Fig. 5. Supervised identification of a tag

There are still issues with the unique identification of a subject, starting with deliberate or accidental actions that may occur over this process, and finishing with the misunderstanding of the represented domain, but these could be managed and mostly solved by following the recommendations of the Organization for the Advancement of Structured Information Standards (OASIS) about the use of the published subject (Fig. 6). The document lists the requirements, recommendations and methods used to adopt published subject indicators (PSIs) and published subject identifiers (PSIDs), providing the directions to follow in order to benefit of ”an open, scaleable, URI-based method of identifying subjects of discourse” [13].

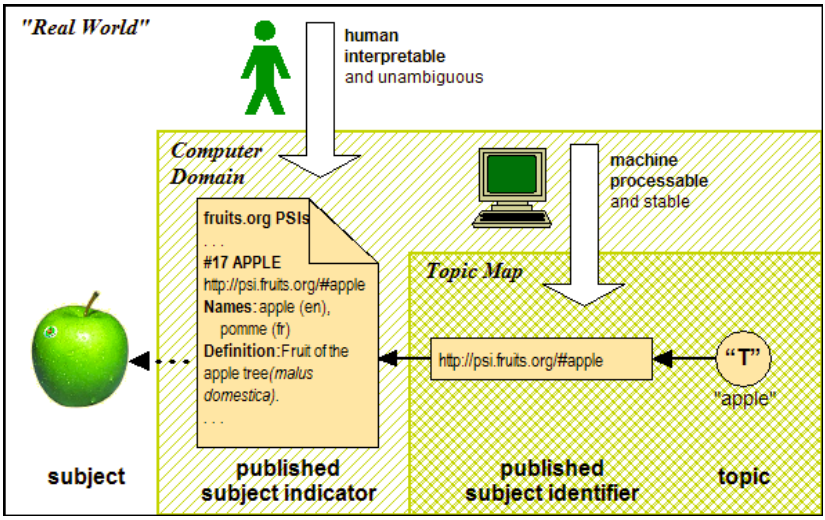

Fig. 6. Using a PSI to identify a subject [13]

3 Further Work and Expected Results

The future research focuses on the completion of TM schema, according with vMR specifications, and on the design of services, in order to meet project requirements. Based on these services and to support the automation of information acquisition, several templates will be written, expecting a better exchange of informational fluxes.

The conversion module, written in C#, is designed to identify the conceptualizations of the same subject into different data models, and represent them in accordance with TMDM, by using the new defined vocabulary and previously mentioned services. In this stage of development, the application has limits that should be considered until the completion of the identification algorithms. In this context, a new method for the subject identification process is intended to be developed, especially designed to fit on traditional RDBMS and eHR systems. This work should extend the identification features provided by TM standard with methods for supervised identification, which rely on probabilistic calculus made on some interchange formats and data models relevant for healthcare.

The expected results of the current research activity are:

- the achievement of a flexible data model which can be used to obtain accurate medical recommendations;
- the development of a set of conversion algorithms which will allow automatic acquisition and integration of medical data from TM instances and other data models;

4 Conclusions

The novelty of this approach lies in the design of a new vocabulary based on the vMR data model and according with TMDM, allowing the further integration of virtual any kind of (digital) medical data, information and knowledge. The use of the resulted topic map is as medical knowledge base, which links its content to relevant resources on the web. It allows users to navigate through a vast medical knowledge base and represent their own medical ontologies. It also can be viewed as an interface between different types of healthcare data models and the CDS systems, whose inference engines could use the content of the topic map to extract highly accurate medical recommendations.

The package of services enriches the application with some custom capabilities, and also provides a picture of how to programmatically model the response of a topic map developed with Topincs.

Comparing with other approaches, this relies on a semantic technology with an open vocabulary and n-ary associations, which translates into a high power of representing things. Some references indicate that similar technologies to TM could be: concept maps, mind maps, or RDF, but a closer look suggests that they are rather different. TM can be viewed as an envelope for almost all other knowledge representation and classification technologies, being able to represent from simple classifications, indexes, taxonomies, thesauri, folksonomies, to highly complex ontologies [15]. Because of its special characteristics, and besides the issues involved by the creation of ontological representations, TM seems to be one of the most eligible to acquire, preserve, represent, manage and disseminate knowledge. TM is a powerful data model that provides flexibility, extensibility, understandability, findability, integration and assimilation to the represented domains.

Like other knowledge representation methods, this standard has not only benefits, but issues, like how to find the most important subjects in targeted domains and how to conceptualize those subjects, or the need of human resources for hand coding and maintenance. It is also hardly recommended that any ontological assertion to be made or supported by specialists of the field represented.

Acknowledgement. "This work was partially supported by the strategic grant POSDRU 107/1.5/S/77265, inside POSDRU Romania 2007-2013 co-financed by the European Social Fund – Investing in People, and the strategic grant POSDRU/88/1.5/S/50783, Project ID50783 (2009), co-financed by the European Social Fund – Investing in People, within the Sectorial Operational Programme Human Resources Development 2007-2013."

References

1. Berners-Lee, T., Hendler, J., Lassila, O.: The Semantic Web: A new form of Web content that is meaningful to computers will unleash a revolution of new possibilities. Scientific American (2001)
2. Health Level Seven International, Inc., http://www.hl7.org
3. Foemig, F., Blobel, B.: Semantic Interoperability between Health Communication Standards through Formal Ontologies. In: Proceedings of MIE 2009 – The XXII-nd International Congress of the European Federation for Medical Informatics, pp. 200–204 (2009), doi:10.3233/978-1-60750-044-5-26
4. Kawamoto K.: Virtual Medical Record (vMR) for Clinical Decision Support– Domain Analysis Model – HL7 Project #184 Informative Ballot (2011), http://wiki.hl7.org/images/7/71/HL7vMR_vMR_Domain_Analysis_Model_Release_1.pdf (accessed May 27, 2012)
5. ISO 13250: Topic Maps, Topic Maps — Data Model, http://www.isotopicmaps.org/sam/sam-model/2008-06-03/(accessed May 29, 2012)
6. Pepper, S.: Topic Maps, 3rd edn. Encyclopedia of Library and Information Sciences (2009), doi:10.1081/E-ELIS3-120044331
7. Kawamoto, K., Del Fiol, G., Strasberg, H.R., Hulse, N., Curtis, C., Cimino, J.J., et al.: Multi-national, multi-institutional analysis of clinical decision support data needs to inform development of the HL7 Virtual Medical Record standard. In: AMIA Annu. Symp. Proc. 2010, pp. 377–381 (2010)
8. Presutti, V., Garshol, L.M., Vitali, F., Pepper, S., Gessa, N.: Towards the definition of guidelines for RDF and Topic Maps interoperability. In: Proceedings of the 5th International Workshop on Knowledge Markup and Semantic Annotation, SEMANNOT 2005, Colocated with the 4th International Semantic Web Conference, ISWC 2005, CEUR-WS Proceedings, Galway, Ireland, vol. 185, pp. 83–88 (2005)
9. Cerny, R.: Topincs: A Software for Rapid Development of Web Databases. In: Proceedings of the International Conference on Knowledge Management and Information Sharing, KMIS 2011, pp. 187–194. SciTePress (2011) ISBN 978-989-8425-81-2
10. Garshol, L.M.: Towards a Methodology for Developing Topic Maps Ontologies. In: Maicher, L., Sigel, A., Garshol, L.M. (eds.) TMRA 2006. LNCS (LNAI), vol. 4438, pp. 20–31. Springer, Heidelberg (2007)
11. ISO/IEC JTC1/SC34, Information Technology - Document Description and Processing Languages, Topic Maps Constraint Language, http://www.itscj.ipsj.or.jp/sc34/open/1053.pdf (accessed May 23, 2012)
12. Topincs manual, http://www.cerny-online.com/topincs/manual/programming (accessed May 26, 2012)
13. Pepper, S.: Published Subjects: Introduction and Basic Requirements, OASIS TC Recommendation (2003), http://www.oasis-open.org/committees/download.php/3050/pubsubj-pt1-1.02-cs.pdf (accessed May 21, 2012)
14. Park, J., Hunting, S.: XML Topic Maps: Creating and Using Topic Maps for the Web, 2nd edn., p. 25. Addison-Wesley Professional (2003) ISBN 0-201-74960-2
15. Garshol, L.M.: Metadata? Thesauri? Taxonomies? Topic Maps! Making Sense of it all. Journal of Information Science 30(4), 378–391 (2004)

Similarity Measurement of Web Sites

Doru Anastasiu Popescu and Dragos Nicolae

Faculty of Mathematics and Computer Science
University of Pitesti, Romania
National College "Radu Greceanu"
Slatina, Romania
{dopopan,dragosnicolae23}@gmail.com

Abstract. In this paper we will present a way to measure the similarity of two web sites. The web sites used are composed only of web pages created with HTML. We will present and compare two algorithms for calculating the similarity degree between two web sites. The first algorithm compares all the web pages of the web sites while the second one selects, after a certain criterion, only a part of the web pages using a relation between them. To implement the algorithms and compare the results we used Java language.

1 Introduction

Under current conditions, when we assist at an explosion of web sites, it is useful to measure their degree of similarity. This way we provide a modality of assessing the originality of web sites. In this article we use web sites that are composed of web pages created using HTML tags. Comparing them is in terms of the tags used in their creation, not in terms of the effect given by the browser (text, images, etc.).

The measurement of the similarity between two web sites will be realized using a relation between two web pages. The different modalities of defining this relation are presented in [2], [4], [6] and [8]. The version used in this paper (section 2) is also used in [2] and [6]. This relation depends on a set TG of tags.

In section 3 we present two modalities of defining the similarity degree between two web sites. The first modality is introduced for the first time in this paper while the second one was presented in [5]. The algorithms we present in section 4 use the set TG (eventually empty) with the aim of not taking in consideration the tags from TG when comparing. This is important in order to eliminate the situations when there is a huge amount of tags of the same type.

In section 5 we present the results obtained by the programs wrote in Java language for the algorithms from section 4.

We consider that respecting the restrictions referring to copyright is as current as modeling the web applications for testing and verifying. This can be also verified using applications similar to those presented in this paper.

V.E. Balas et al. (Eds.): Soft Computing Applications, AISC 195, pp. 349–356.
springerlink.com

2 Defining a Relation between Two Web Pages from Web Site

In this section we consider a web site, which has as web pages the set $P=\{p_1, p_2, ..., p_n\}$, and a set of tags TG (eventually empty). The tags from TG will be excluded from the comparison of web pages.

The relation between web pages used in this paper is described in detail in [5] and [6].

For any web page p_i from P, we write T_i the sequence of tags from p_i, which are not members of TG.

Definition 1. Let TG be a set of tags, p_i and p_j two web pages from P.

We say that T_i is in T_j as a sequence, if there exists an index in the sequence T_j from where there appears from left to right, one after the other, all the tags of T_i.

Definition 2. Let TG be a set of tags, p_i and p_j two web pages from P. We say that p_i is in relation R with p_j and we write p_i R p_j, if:

i) T_i is in T_j as a sequence;
ii) Any tag <Tg> from T_j which appears in T_i as well, if it has a closing tag <\Tg> in T_j, then <\Tg> is also in T_i.

Definition 3. The web page p_i is called *sink web page*, if the following property is fulfilled:

There does not exist p_j in P, with $i \neq j$ and p_i R p_j.

Example 1. Let us consider a web application with three web pages: $P = \{p_1, p_2, p_3\}$. p_i can be found in the file Pi.html, where $i \in \{1, 2, 3\}$.

P1.html
```
<HTML>
<HEAD> </HEAD>
<BODY> <U>Conference</U> </BODY>
<B> Day 1 </B> <BR>
<I> Day 2 </I> <BR>
</HTML>
```

P2.html
```
<HTML>
<HEAD> </HEAD>
<BODY>
<B> Day 1 </B> <BR>
<I> Day 2 </I> <BR>
</BODY>
</HTML>
```

P3.html
```
<HTML>
<HEAD> </HEAD>
```

<BODY>
<BODY> <U>Conference</U> </BODY>
<B> Day 1 </B>
</BODY>
</HTML>

Considering

TG = {<HTML>, <HEAD>, </HEAD>, <BODY>, </BODY>, </HTML>, <B>, </B>}

we obtain:

T1 = (<U>, </U>, <I>, </I>)
T2 = (<I>, </I>)
T3 = (<U>, </U>)

According to definitions 1 and 2, we obtain only two pairs of pages in relation R to each other:

p_1 R p_2 ; p_1 R p_3.

So for this web site we have only one sink web page, namely p_1. The web pages p_2 and p_3 "sink" in p_1 (excepting the tags from TG).

3 Methods of Calculating the Similarity Degree between Two Web Sites

Further we will consider two web sites S1 and S2.

Definition 4. Let p be a web page from S1 and q a web page from S2. We say that p *arises* from q, if p R q.

Using the previous notion, we will introduce the concept of similarity degree between two web sites. The first modality of defining this notion is the following:

Definition 5. We define the *similarity degree* of S1 with S2 the number a / n, where a is the number of web pages from S1 that *arise* from the web pages of S2 and n is the number of web pages from S1. We will write this number *deg1(S1, S2)*.

In [5] is defined the similarity degree of S1 with S2 using the concept of sink web page, this way:

Definition 6. We define the *similarity degree* of S1 with S2 the number b / k, where b is the number of sink web pages from S1 that *arise* from the sink web pages of S2 and k is the number of sink web pages from S1. We will write this number *deg2(S1, S2)*.

In the next section we present two algorithms that calculate the similarity degree of S1 with S2: *deg1(S1, S2)* and *deg2(S1, S2)*.

4 The Description of the Algorithms

Algorithm A1

Using the notations from the previous sections, we will present the algorithm that calculates the degree of similarity between two web sites.

Input data
the path of the file containing the set of tags TG
the path of website S1
the path of website S2

Used data structures
- tags - a string vector with the tags from TG
- *files1*, *files2* - string vectors with the paths of each website's web pages (*files1* for S1 and *files2* for S2)
- *pages1*, *pages2* - string vectors with the tags from each website's web pages, that are not included in TG (*pages1* for S1 and *pages2* for S2)

Output data
- the degree of similarity of S1 with S2
- a text file with the number of files and the number of web pages for each web site

Algorithm A1's steps
- memorizing in *tags* the tags from TG
- finding and memorizing in *files1* the paths of the web pages from S1
- finding and memorizing in *files2* the paths of the web pages from S2
- memorizing in *pages1* the tags that does not exist in *tags* from each web page of the S1
- memorizing in *pages2* the tags that does not exist in *tags* from each web page of the S2
- calculating the similarity degree between the two web sites (definition 5)

Algorithm A2
Unlike the algorithm A1, A2 algorithm determines the sink web pages and use them to calculate the similarity degree. A detailed description of this algorithm can be found in [5]. The input and output data are the same as for the algorithm A1. To the data structures from A1 are added two structures, s1 and s2, with the the indices of sink web pages from S1 and S2.

Algorithm A2's steps
- memorizing in *tags* the tags from TG
- finding and memorizing in *files1* the paths of the web pages from S1
- finding and memorizing in *files2* the paths of the web pages from S2
- memorizing in *pages1* the tags that does not exist in *tags* from each web page of the S1

- memorizing in *pages2* the tags that does not exist in *tags* from each web page of the S2
- finding the sink web pages using the concepts presented in section 2
- calculating the similarity degree between the two web sites (definition 6)

5 The Implementation and the Comparison of Results

The implementation of A1 and A2 algorithms was realized using Java language. As input data we used the path where web sites' files are. The files that did not contain tags were not taken into account. For comparing the two sequences of tags associated to the web pages, we used the pattern-matching algorithm Knuth-Morris-Pratt, [3].

To make the comparison as good as it was possible, we took into account two aspects:

- the TG set used in the composition of tags' lists associated to web pages;
- the execution time.

The creation of the following graphics (fig. 1 and fig 2.) was made the sets:

TG1=Ø
TG2={ , , <B>, </B>}
TG3={ , , <B>, </B>, , , <u>, </u>}
TG4={ , , <B>, </B>, , , <u>, </u>, <meta>, <script>, </script>,
, <pre>, </pre>, , }
TG5={ , , <B>, </B>, , , <u>, </u>, <meta>, <script>, </script>,
, <pre>, </pre>, , , <hr>, <style>, </style>}
TG6={ , , <B>, </B>, , , <u>, </u>, <meta>, <script>, </script>,
, <pre>, </pre>, , , <hr>, <style>, </style>, <img>, , }
TG7={ , , <B>, </B>, , , <u>, </u>, <meta>, <script>, </script>,
, <pre>, </pre>, , , <hr>, <style>, </style>, <img>, , , , , <small>, </small>}
TG8={ , , <B>, </B>, , , <u>, </u>, <meta>, <script>, </script>,
, <pre>, </pre>, , , <hr>, <style>, </style>, <img>, , , , , <small>, </small>, <h1>, </h1>, <h2>, </h2>, <h3>, </h3>}
TG9={ , , <B>, </B>, , , <u>, </u>, <meta>, <script>, </script>,
, <pre>, </pre>, , , <hr>, <style>, </style>, <img>, , , , , <small>, </small>, <h1>, </h1>, <h2>, </h2>, <h3>, </h3>, <h4>, </h4>, <h5>, </h5>}
TG10={ , , <B>, </B>, , , <u>, </u>, <meta>, <script>, </script>,
, <pre>, </pre>, , , <hr>, <style>, </style>, <img>, , , , , <small>, </small>, <h1>, </h1>, <h2>, </h2>, <h3>, </h3>, <h4>, </h4>, <h5>, </h5>, <h6>, </h6>}

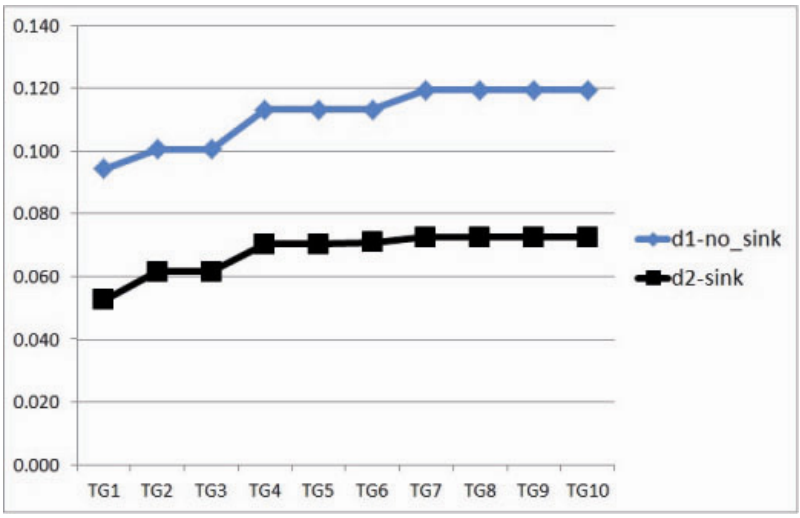

Fig. 1. Chart for comparing two web applications, the TG sets on horizontal and the value of similarity degree on vertical

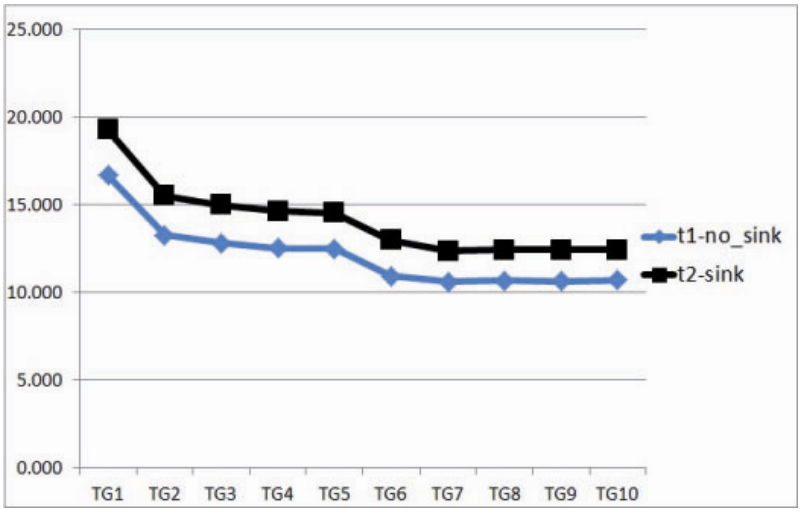

Fig. 2. Chart for comparing the execution time of algorithms A1 and A2, the TG sets on horizontal and the value of execution time on vertical.

6 Conclusion

The main purpose of this paper was to present two algorithms that calculate, using two different formulas, the similarity degree between two web sites. The obtained results showed the same graphic form in both cases for the utilized tests. We consider that there can be realized new applications to better reflect the common aspects between two web sites, using concepts presented in this paper.

Together with the ways of measuring the quality of a web site (as those presented in [9] and [10]) we believe that the aspects presented in this paper should also be taken into consideration.

Another direction we want to follow is that which treats the concept of similarity as a fuzzy concept. For this, we want to use the results obtained by Zadeh, [11].

The degree of similarity of two web sites, calculated using the formulas for *deg1* and *deg2*, can also be used as a fuzzy concept. These two formulas can be used to measure the differences between two web sites.

The results from [11], [12], [13] and [14] can be adjusted to the space of the web sites, using the measures *deg1* and *deg2*. This way, methods of fuzzy partitioning of the web site's space can be found.

References

1. Alalfi, M.H., Cordy, J.R., Dean, T.R.: Modeling Methods for Web Application Verification and Testing: State of Art. JohnWiley and Sons, Ltd. (2008)
2. Danauta, C.M., Popescu, D.A.: Method of reduction of the web pages to be verified when validating a web site. Buletin Stiintific, Universitatea din Pitesti, Seria Matematicasi Informatica, vol. (15), pp. 19–24 (2009)
3. Cormen, T.H., Leiserson, C.E., Rivest, R.L., Stein, C.: Introduction to algorithms, 2nd edn. MIT Press (1990)
4. Anastasiu, D.P., Danauta, C.M.: Validation of a Web Application by Using a Limited Number of Web Pages. BRAIN, Broad Research in Artificial Intelligence and Neuroscience 3(1), 19–23 (2012)
5. Anastasiu, D.P., Danauta, C.M.: Similarity Measurement of Web Sites Using Sink Web Pages. In: 34th International Conference on Telecommunications and Signal Processing, TSP 2011, Budapest, Hungary, August 18-20, pp. 24–26. IEEE Xplore (2011)
6. Popescu, D.A.: Sink Web Pages in Web Application. In: Schwenker, F., Trentin, E. (eds.) PSL 2011. LNCS, vol. 7081, pp. 154–158. Springer, Heidelberg (2012)
7. Popescu, D.A., Danauta, C.M., Szabo, Z.: A Method of Measuring the Complexity of a Web Application from the Point of View of Cloning. In: Proceedings of the 5th International Conference on Virtual Learning, Section Models and Methodologies, October 29-31, pp. 186–181 (2010)
8. Popescu, D.A.: A relation between web pages. In: CKS 2011 Challenges of the Knowledge Society "NicolaeTitulescu" University and "Complutense" University, Bucharest. CKS Proceedings, pp. 2026–2033 (2011)
9. Mao, C.-Y., Lu, Y.-S.: A Method for Measuring the Structure Complexity of Web Application. Wuhan University Journal of Natural Sciences 11(1) (2006)

10. Sreedhar, G., Chari, A.A., Ramana, V.V.: Measuring Qualitz of Web Site Navigation. Journal of Theoretical and Applied Information Technology 14(2) (2010)
11. Zadeh, L.A.: Toward extended fuzzy logic - A first step. Fuzzy Sets and Systems 160(21), 3175–3181 (2009)
12. Tikk, D., Gedeon, T.D., Koczy, L.T., Biro, G.: Implementation details of problems in Sugeno and Yasukawa's qualitative modeling Fuzzy Sets and Systems. Implementation details of SY qualitative modelling, RWP-IT-01-2001
13. Sugeno, M., Yasukawa, T.: A Fuzzy-Logic-Based Approach to Qualitative Modeling. IEEE Transactions on Fuzzy Systems 1, 7–31 (1993)
14. Niskanen, V.A.: Application of Zadeh's Impossibility Principle to Approximate Explanation. IFSA-EUSFLAT (2009)

Transmission of Unsolicited E-mails with Hidden Sender Identity

Ioan Virag, Antoanela Naaji*, Marius Popescu

Department of Computer Science,
"Vasile Goldis" Western University of Arad, Bd. Revolutiei nr 85-87, Romania
{ioanvirag,popescu.marius.c}@gmail.com
anaaji@uvvg.ro

Abstract. Terminal communication systems are often confronted with undesired e-mails, which reach their destination, while cloaking the real sender. Thus, in order to develop appropriate security software, it is necessary to know how to write identity-concealing software. This paper seeks to describe how the identity of undesired e-mail senders can be hidden. The final aim of the work is to detect adequate means of defense against unwanted e-mails, by generating, in the future, strong security (or filtering) algorithms and methodologies, adapted to diverse situations.

Keywords: Unsolicited e-mails, Terminal communications, Security algorithms.

1 Introduction

In the case of e-mail messages, the risk associated with the sender's impersonification is very high, since the standards used for sending e-mails are simple and have, in addition, been made public by developers. The e-mail standard is not based on any mathematical system for checking the sender's identity, but on mutual confidence among users. This disadvantage is used by malicious people to send messages from false, or even existing addresses, pretending to be the users who own those e-mail addresses. Consequently, it is practically almost impossible to identify someone who has sent such messages. The most important problem of the unwanted e-mail senders is hiding their identity. Most software variants that are used in such situations consist of using some programs to seize the administrator account of a communication terminal and install their own server onto it; after installation, a domain name is registered, with false identification data. In order to prevent such inconveniences and develop security algorithms, it is vital to know the steps that must be covered in implementing such methods for concealing identity. The simplest strategy for generating unwanted e-mails consists of using a PHP script, and then installing it on a server that provides the possibility to run it free of charge. In this case, after installation, it is no longer necessary to register a *domain name*.

* Corresponding author.

V.E. Balas et al. (Eds.): Soft Computing Applications, AISC 195, pp. 357–365.
springerlink.com

After running the software application on the server that allows it, malevolent users delete the application, with the obvious purpose of "covering their tracks".

Undesired e-mails are mostly sent for the purpose of collecting confidential information, stealing identities, sending viral programs, infecting and turning the receiving systems into zombie PCs, in order to form botnets.

In addition to e-mails, malevolent programmers also develop other routes of attack, using instant messaging (spim), weblogs, Short Messaging Services (SMS) or claiming to provide optimizing services for Internet search engines (spamdexing) or by using webshells like Pirulin, which enable direct access to the operating system on which the web and e-mail servers are installed.

2 Generating Unwanted E-mails

The method for hiding the identity of unwanted e-mail senders, analyzed in this paper, has the following main phases:

- obtaining a free e-mail account from a provider that offers such services (for example, *Gmail, Yahoo, Dcemail* etc.);
- obtaining a subdomain on a server that provides, free of charge, the possibility to run PHP code (for changing the name of the message sender);
- loading the necessary scripts on the server and running them.

Generally, the first two actions are performed from a public place (for example, an Internet café, a terminal with access to the Internet, e.g. in an airport, or a mobile device with a prepaid SIM card, that does not require one to submit personal data, etc.). Considering the fact that communication service providers record the IP (*Internet Protocol*) address from which the request was submitted, public places are preferred, as the initiator cannot be tracked [1]. However, the provider defines *Reverse DNS (PTR)* records – domain names associated to IPs – and, at the same time, it defines SPF and *SenderID* records, for domains from which the sending occurs – the records are used by servers to which messages are sent, in order to check whether the IP is authorized to perform a sending action.

It is noteworthy that the first two actions are not currently illegal at this very moment.

2.1 Obtaining a Free E-mail Account

Usually, the e-mail account is created on a server that provides this service free of charge. The services provided free of charge by the dcemail.com company are preferable, as they offer a series of advantages, such as: storage space of up to 1GB, file attachments of up to 25MB. In the scenario described by this paper, the data entered into the registration form is not real (for demonstration purposes).

2.2 Obtaining a Subdomain

The next step after having entered the data by malicious programmers is to create a subdomain (e.g. on services provided by http://www.000webhost.com/). There is a possibility to opt for a subdomain (for example, aplicatiitm.comyr.com) or to host one's own domain. The registration request is approved within no more than 24 hours by a human operator, who checks whether the data entered is false or not. Although this practice would not be illegal, ISPs such as Yahoo or Hotmail, as well as blacklists do not favor it and, consequently, it is highly likely that the domain or the IP address will be registered into a blacklist, thus resulting in a complete blockage of all messages on that IP and/or domain, or their forwarding to the Spam folder (where unwanted e-mails, sent by unknown people, are stored). Generally, the destination of e-mails is decided by their reputation (Yahoo, Gmail, Hotmail are preferred, since they use filters).

2.3 Description of the Software Application

The software application, proposed in this paper for exemplifying the algorithm that hides people's identities, is written in PHP – programming language run on the server side. A simple message formatting (without too many colors, font types, images, etc.) will keep it far from anti-spam filters. Sending messages in HTML (multipart /alternative) format includes a part of text, with the mention that the html part should not contain errors [2]. The results of running the program are interpreted by a Web browser (such as Firefox, Internet Explorer, Opera, Chrome etc. [3].

Fig. 1. The application's graphical user interface

The form generated by the *form.php* file (as it can be seen in Fig.1), will be filled with data required for communication, such as: the recipient's e-mail address, the sender's e-mail address (it can be anything, as the validity of this address is not checked), other e-mail addresses where copies of the message are sent, the subject and

content of the message. After clicking on "Send", the unwanted message will be sent to the recipients, by running the second script, entitled *send.php*. This script is designed to show whether the data were sent successfully or not (Fig.2). It can be seen that the recipient (Fig.3) received it from "initiator_mesaj@uvvg.ro", a fictitious address created by the sender.

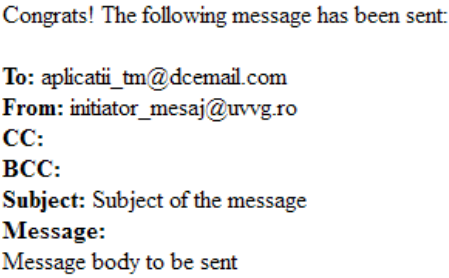
Congrats! The following message has been sent:

To: aplicatii_tm@dcemail.com
From: initiator_mesaj@uvvg.ro
CC:
BCC:
Subject: Subject of the message
Message:
Message body to be sent

Fig. 2. Explicative interface on the sent message

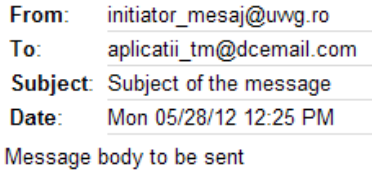
From:	initiator_mesaj@uvvg.ro
To:	aplicatii_tm@dcemail.com
Subject:	Subject of the message
Date:	Mon 05/28/12 12:25 PM

Message body to be sent

Fig. 3. Explicative interface on the falsification of the sender's identity

In order to see the real identity of the sender, one has to click on the More… button (which differs according to the service/program used for reading e-mails), which will display the extended message header (Fig.4).


Less...

Received:	from nobody by srv24.000webhost.com with local (Exim 4. 1PEhWk-0001z3-Lk for aplicatii_tm@dcemail.com; Sat, 06
Sender:	<nobody@srv24.000webhost.com>
X-AntiAbuse:	Sender Address Domain - srv24.000webhost.com
X-PHP-Script:	www.aplicatiitm.comyr.com/trimite.php for 89.35.148.34
Content-Transfer-Encoding:	7bit
Message-Id:	<E1PEhWk-0001z3-Lk@srv24.000webhost.com>
Content-type:	text/html; charset=iso-8859-1
X-Eon-Dm:	dm0218
MIME-Version:	1.0
Return-Path:	<nobody@srv24.000webhost.com>
Date:	Today 5:05 AM

Fig. 4. Explicative interface on displaying the extended message header

In the X-PHP-Script field one can see the sender's real identity (domain name and IP address). After consulting the extended header, one can contact the server's owner and inform them on the illegality that has been committed.

The application works based on the fact that users do not know how to read and interpret the extended header. Even after deactivating the account from which the undesired message has been sent, the author can still make another, without being caught (if the account is created from a public place).

The described application uses two files; the first file, named *form.php* generates an html page, stylized using CSS (Cascading Style Sheets); this file does nothing but send the data collected in the form to the next file, named *send.php*, which will call PHP's mail() function and send the message to the recipient. If the message was sent, the content of that message is shown, i.e. the e-mail addresses of the recipient and the sender, respectively.

The source code for *form.php* is:

```
<html>
<head>
<title>Form for data to be sent</title>
<style type="text/css">
body{padding:50px 0 0;
background: #827F80 url(gradient_black.png) repeat-x ;
color:#000;
font:100.01%/1.3 Verdana,Arial,sans-serif;
text-align:center;}
#div_form{width: 400px;
padding: 30px  0;
margin:0 auto;
text-align:left;
background: #9CC0FF url(gradient_blue.png) repeat-x 0 -
5px; cursor:help;}
input{width: 250px;
background: #9CC0FF url(gradient_blue.png);
margin:0 5px;
border: 2px;}
textarea{width: 250px;
height: 100px;
background: #9CC0FF url(gradient_blue.png);
margin:0 5px;
border: 2px;}
hr{width: 400px;
background: #000;
height: 2px ;}
</style>
</head>
```

```
<body>
<div id="div_form">
    <form name="theform" method="post" action="send.php">
      <table align="center">
        <tr><td>To:</td><td>
        <input type="text" name="to"></td></tr>
        <tr><td>From:</td><td>
        <input type="text" name="from"></td></tr>
        <tr><td>Cc:</td><td>
        <input type="text" name="cc"></td></tr>
        <tr><td>Bcc:</td><td>
        <input type="text" name="bcc"></td></tr>
        <tr><td>Subject:</td><td>
        <input type="text" name="subject"></td></tr>
        <tr><td valign="top">Message:</td><td>
        <textarea name="message"> Insert your message
</textarea>
        </td></tr><tr><td></td>     <td
style="float:right; padding: 30px  0;margin:0 auto; ">
        <input style="width: 100px;
          background: #827F80
url(gradient_button_black.png);
          font: Arial sans-serif;color: #FFF;"
          type="submit" value="Send" />
        <input style="width: 100px;
          background: #827F80
url(gradient_button_black.png);
          font: Arial sans-serif;color: #FFF;"
          type="reset" value="Reset" /></td></tr>
      </table>
    </form>
 </div><br /><br /><hr />
</body>
</html>
```

The source code for *send.php* is:

```
<html>
<head>
<title>Mail sent</title>
</head>
<body>
<?php
$to = $_POST["to"];
$cc = $_POST["cc"];
$bcc = $_POST["bcc"];
```

```
$from = $_POST["from"];
$subject = $_POST["subject"];
$message = stripslashes($_POST["message"]);
$headers = "From: " . $from . "\r\n";
if (!$cc == "") {
$headers .= "CC: " . $cc . "\r\n";
}
if (!$bcc == "") {
$headers .= "BCC: " . $bcc . "\r\n";
}
$headers .= "MIME-Version: 1.0\r\n";
$headers .= "Content-type: text/html; charset=utf-8\r\n";
$headers .= "Content-Transfer-Encoding: 7bit\r\n";

$mailsent = mail($to, $subject, $message, $headers);
if ($mailsent) {
echo "Congrats! The following message has been sent:
<br><br>";
echo "<b>To:</b> $to<br>";
echo "<b>From:</b> $from<br>";
echo "<b>CC:</b> $cc<br>";
echo "<b>BCC:</b> $bcc<br>";
echo "<b>Subject:</b> $subject<br>";
echo "<b>Message:</b><br>";
echo $message;
} else {
echo "There was an error...";
}
?>
</body>
</html>
```

The main threat transmitted by e-mail is due to the possibility of attaching malware. This way, unwanted messages with a viral content can be sent to spread out malware and abstract confidential data towards communication terminals. These are controversial topics in courts of justice around the world, especially as regards the right to send messages to public and private e-mail addresses.

3 Security against Undesired Messages

By even minimally securing the operating system installed on communication terminals, these messages can be treated as spam, and thus the recipient can decide whether the message will be read or not. Avoiding such undesired messages can be done by checking the sender's authenticity – using a digital signature, or ignoring messages that claim that you requested something or that you tried to send a message and a

sending error occurred, by not opening suspicious messages, or by applying heuristic rules, [3], content filters, etc.[4],[5] [6].

In order to be sure that messages get to the recipient, in the Inbox folder and not in Spam, spammers take into account the criteria according to which these filters work.

Filters can be based on a detailed analysis of several factors (keywords, sender's name/address, message title, message structure), establishing the likelihood of an e-mail message being unwanted. Thus, scanning after certain keywords is one of the criteria used by spam filters. Keyword selection is done through testing, i.e. by sending the message to e-mail addresses with anti-spam filters, and if these end up in the "Junk" folder, then changes must be made.

Likewise, software for recognizing undesired messages was developed, which analyzes e-mail messages according to the selected recognition algorithms, such as: heuristic analysis, image recognition, analysis of .RTF attachments, self-instructed text recognition algorithms etc. [7].

The script described in *send.php* file does not feature an error handling part; the only message that is received by the malevolent user is that an error occurred. This may be due to entering a wrong e-mail address, server errors etc.

In order to authenticate the sender of an e-mail message for other purposes, most of the times a public key system is used. Thus, if the sender encrypts the messages with their own private key, the data can only be decrypted by using the twin public key, therefore, anyone can verify that the message was indeed sent by the apparent sender, and not by a person claiming to be the sender (the message encrypted with a key can only be decrypted by using its twin key and it is assumed that the sender is the only one with access to their private key).

It is evidently possible to encrypt messages in parallel to authentication, so that even the sent data is encoded. For example, Outlook secures messages: by encrypting the message (preventing possible interception and ensuring confidentiality), through mechanisms implemented using the public-private key system, by adding a digital signature, by establishing security areas.

4 Conclusions

Security against undesired messages is a very important issue, as weak passwords, out-of-date software or sometimes even the recipients' lack of vigilance can enable unauthorized access for spammers, who will not hesitate to use whatever means available to send unsolicited messages.

The method for generating undesired messages, as implemented and illustrated in the application shown in paragraph 2, consists of generating a minimum number of files for running it, while also being free. Given the large number of free manuals available on the web [8], [9], describing the technical details for implementing such programs (but not for bad purposes), in the near future there will be an increasing number of script kiddies. Such unpleasant situations can be avoided by raising awareness among the target group on the existence of practices such as those described in this paper, and by developing security algorithms, based on redirecting these messages to the spam section, following the detection of such practices.

References

1. Popescu, M.C., Mastorakis, N.: New Aspect on Wireless Communication Networks. International Journal of Communications 3(1), 34–43 (2009) ISSN:1998-4480, http://www.naun.org/multimedia/NAUN/communications/19-225.pdf
2. ***, Manual de utilizare PHP, http://php.net/manual/en/function.mail.php
3. Sven, G.: Data management and query processing in semantic web databases. Springer, Heidelberg (2011)
4. Zdziarski Jonathan, A.: Ending spam: Bayesian content filtering and the art of statistical language classification. No Starch Press, San Francisco (2005)
5. Migga, K.J.: Computer network security. Springer, New York (2005)
6. Bajanescu, T.: Comunicatii prin satelit. Ed. Matrix ROM, Bucuresti (2003)
7. Resnick P.: Request for comment, http://tools.ietf.org/html/rfc5322
8. Hudson, P.: Practical PHP Programming, http://www.tuxradar.com/practicalphp
9. Achour, M., et al.: PHP Manual, http://www.php.net/manual/en/index.php

Evaluation of Experiments on Detecting Distributed Denial of Service (DDoS) Attacks in Eucalyptus Private Cloud

Alina Mădălina Lonea[1], Daniela Elena Popescu[2], Octavian Prostean[1], and Huaglory Tianfield[3]

[1] Automation and Applied Informatics Department, "Politehnica" University of Timisoara, Faculty of Automation and Computers, B-dul Vasile Parvan, nr. 2, 300223, Timisoara, Romania
madalina_lonea@yahoo.com, octavian.prostean@aut.upt.ro
[2] Computer Engineering Department, University of Oradea, Faculty of Electrical Engineering and Information Technology, Universitatii Street, nr. 1, 410087, Oradea, Romania
depopescu@uoradea.ro
[3] School of Engineering and Built Environment, Glasgow Caledonian University, Cowcaddens Road, Glasgow G4 0BA, United Kingdom
h.tianfield@gcu.ac.uk

Abstract. Denial of Service (DoS) and Distributed Denial of Service (DDoS) attacks appear to be main threats for cloud computing. The protection of cloud services against DoS and DDoS attacks is realized using Intrusion Detection Systems (IDSs).This paper aims to evaluate the experimental results of our proposed quantitative solution. The experiments are performed in a private cloud model deployed using Eucalyptus open-source, with virtual machines based IDS (VMs-based IDS) being created in three nodes and the Mysql database together with the graphical interfaces for monitoring the alerts being installed and configured in the front-end server. After a set of DDoS attacks are launched against the VMs-based IDS, we analyze all the alerts collected from the VMs-based IDS.

Keywords: attacks, cloud computing, data fusion, DDoS attacks, Dempster-Shafer Theory (DST), Eucalyptus, Intrusion Detection Systems (IDSs), Fault-Tree Analysis, Snort.

1 Introduction

Trustworthiness of cloud services become today a concern for cloud customers and providers. Denial of Service (DoS) and Distributed Denial of Service (DDoS) attacks appear to be their main threats. In the recent times, Cloud Service Providers (CSPs) had suffered security breaches and the service's availability was compromised for hours [2].

V.E. Balas et al. (Eds.): Soft Computing Applications, AISC 195, pp. 367–379.
springerlink.com

DoS and DDoS attacks are the source of the mentioned disruptions. While DoS attacks make the cloud service unavailable for authorized users by overloading the server that provides the cloud service with a large number of requests, DDoS attacks make the cloud service unavailable by overloading the victim server from distributed master locations utilizing the slave platforms [2].

The protection of cloud services against DoS and DDoS attacks is realized using Intrusion Detection Systems (IDSs) [2], [3], [4], [5], [6], [7], [8]. However, the efficiency of security provided by the IDS sensors is doubted due to the massive amounts of alerts produced by IDS, the high number of false alarm rates and the overloading problems caused by the IDS deployment strategy. These issues with IDSs were treated in our previous research work [1] by proposing an IDS Cloud Topology, for detecting Distributed Denial of Service (DDoS) attacks in cloud computing environment. We had combined the evidences obtained from Intrusion Detection Systems (IDSs) deployed in the virtual machines (VMs) of the cloud systems using a data fusion methodology in the front-end.

This paper continues our research solution proposed in [1] and aims to evaluate the experimental results of the proposed quantitative solution. Thus, the theoretical fundamentals that comprise the IDS cloud topology can refer to [1] (i.e. Dempster-Shafer theory (DST) in 3-valued logic, the fault-tree analysis, the Dempster's combination rule, the IDS in cloud computing).

Section 2 introduces a short overview of the proposed solution, together with its implementation. Section 3 describes how DDoS attacks were generated and the results and the evaluation are presented in section 4. Finally, section 5 draws the concluding remarks.

2 Implementation of the Proposed Solution

Our proposed Intrusion Detection System (IDS) Cloud topology [1] is shown in Figure 1. It presents the Eucalyptus private cloud architecture, the procedure of creating the virtual machines based IDS (VMs-based IDS) and the installation and configuration of Mysql database together with the graphical interfaces for monitoring the alerts in the Cloud Fusion Unit (CFU) of the front-end server from the Eucalyptus cloud architecture. The others two components (i.e. Basic probabilities assignment and Attacks Assessment) from the Cloud Fusion Unit (CFU) are discussed in section 4.

The IDS Cloud Topology was implemented in a Eucalyptus private cloud environment. Thus, the private cloud was built using Eucalyptus 2.0.3 open-source, which has interfaces compatible with Amazon web services. The topology used for our private cloud includes the following components: a Front-end (with Cloud Controller, Walrus, Storage Controller and Cluster Controller) and three Node Controllers. Additionally, the Eucalyptus setup uses the Managed networking mode and Xen hypervisor was used for virtualization. The deployment stage of the private cloud was based on the Eucalyptus administrator's guide [9] and the Eucalyptus user's guide [10].

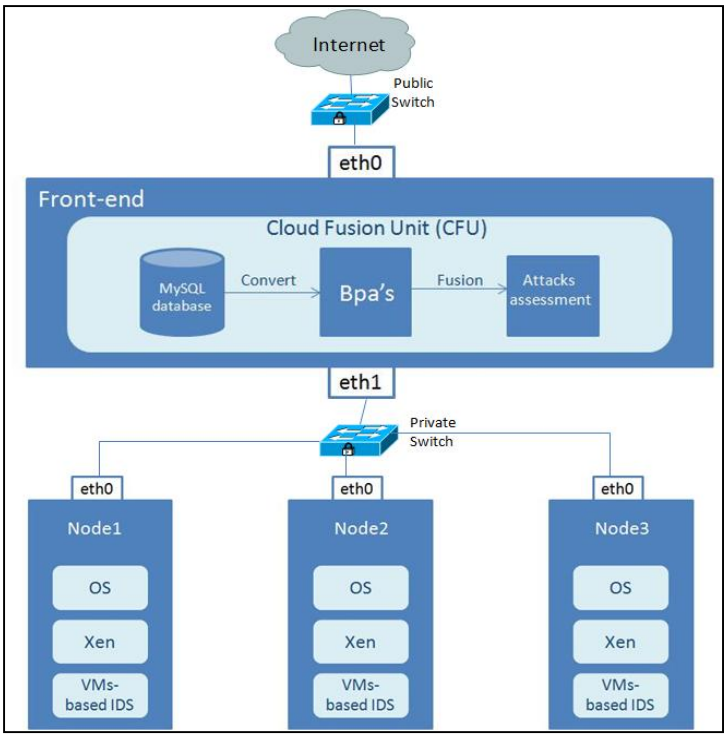

Fig. 1. IDS Cloud Topology [1]

Furthermore, the VMs-based IDS were created and Debian-based euca2ools images were utilized. The experimental results were conducted for three Debian virtual machines: one image is Debian 32-bit architecture and the other two are Debian 64-bit architectures. The operations for creating the VM-based IDS are similar for all three images and only the type of software differs based on the bit architecture (e.g. 32 or 64). The creation of the VMs-based IDS consists of the following six operations (Figure 2), using the Eucalyptus User's Guide [10], the Snort installation guides [11], [12], [13], the Snort Users Manual [14] and [15], [16]:

Step 1. Debian (e.g. 32 and 64 bit architecture) pre-packaged virtual machines were downloaded from Eucalyptus website. Afterwards, the images were bundled, uploaded and registered into our private cloud. These initial steps at the creation of the images are recorded in the image management section of Eucalyptus User's Guide [10].
Step 2. Furthermore, those images were utilized at the deployment of instances.
Step 3. Then, a Eucalyptus storage volume of 5 GB was created in order to be attached to the created instance.
Step 4. Moreover, the VMs-based IDS were deployed by installing and configuring Snort open-source Network based Intrusion Detection System (NIDS) into the VMs. The reason for selection of this NIDS is because of its characteristics: it has

packet payload; its decoded output display is user friendly and its output analysis is high performed [17]. Moreover, Snort was configured for defending against DDoS tools. In this sense the predefined DDoS rules were included in the snort configuration file. The attacks capturing procedure is made using the Barnyard tool, which stores in a binary unified file all the events with the purpose to send them to a centralized Mysql database in front-end, using a secure tunnel (i.e. stunnel) [11], [12], [13], [14], [15], [16], [18], [19]. The VMs-based IDS were configured to send all the collected data to the Mysql database using Snort together with Barnyard. Thus, the "barnyard2.conf" file on each VM-based IDS includes the following output [11], [12], [13]:

"output database: alert, mysql, user=snort password=xxxxxx dbname=snortdata host=192.168.1.50".

After the installation and configuration of the VM-based IDS was completed, the volume was un-mounted.

Step 5. In order to have a working storage volume, the Eucalyptus volume should be detached from the instance [10].

Step 6. We created backup of the above volume by deploying snapshot element [10].

After the VMs-based IDS were deployed, we started Snort and Barnyard in all three VMs-based IDS and we conducted DDoS attacks against these three VMs-based IDS using Stacheldraht tool. Snort is started with the following command: "snort -c /etc/snort/snort.conf -i eth0", while barnyard is started with: "/usr/local/bin/barnyard2 -c /etc/snort/barnyard2.conf -d /var/log/snort -f snort.log -w /etc/snort/barnyard.waldo -G /etc/snort/gen-msg.map -S /etc/snort/sid-msg.map -C /etc/snort/classification.config".

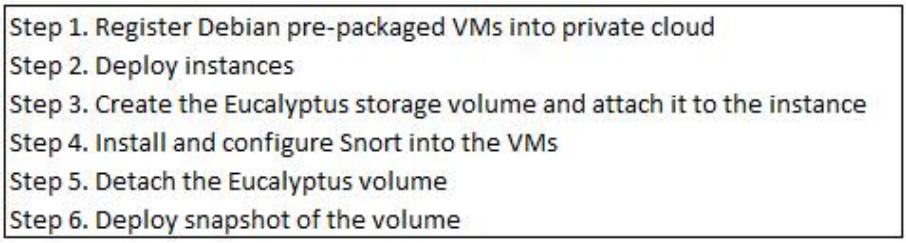

Fig. 2. VM-based IDS Deployment

The integration of IDS in Eucalyptus cloud was reported in the literature. Borisaniyia et al. (2010) presents their experimental setup of the Snort network-based intrusion detection into the Cluster Controller components of Eucalyptus private cloud and the analysis of the capture attacks transmitted every minute by IDS to the Mysql server, which is located in the Cloud Controller component of Eucalyptus. The placement of IDS in our proposed solution is into the VMs (Figure 1), which reveals a different approach comparing with the experimental setup revealed by Borisaniyia et al.

(2010). However, the centralization of the distributed sensors is recorded in a single Mysql server as in the solutions given by Borisaniyia et al. (2010), Brennan (2002), Skinner (2012).

Furthermore, the implementation of the proposed solution enhances the collaboration of the VMs-based IDS with the front-end component of the private cloud, by receiving the alerts transmitted by VMs-based IDS into Mysql server [18], [20]. The alert's transmission is secured because Stunnel is installed in the front-end (Figure 3).

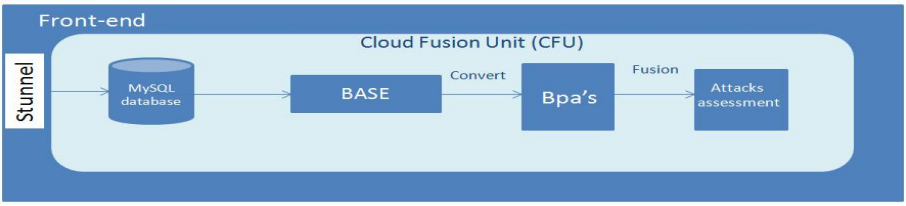

Fig. 3. Relationships of the centralization components in Cloud Fusion Unit

Figure 3 is an extended scheme of the CFU component from Figure 1. The data analysis tool (i.e. BASE - Basic Analysis and Security Engine) was introduced between the storing server (i.e. Mysql) and the Basic probabilities assignment (Bpa's) component. BASE is the successor of ACID (Analysis Control for Intrusion Detection) [16]. BASE was chosen because it is a web server analysis tool for monitoring the alerts received from the VM-based IDS sensors [15]. Additionally, its reporting strategy facilitates the procedure of obtaining the Bpa's.

3 Generating DDoS Attacks

We have simulated DDoS attacks against the VMs-based IDS using the Stacheldraht DDoS tool. Stacheldraht tool is based on the 'Client', 'Handler (s)/Master (s)', 'Agent(s)/Daemon(s)', 'Victim(s)' architecture. This three layer architecture includes the collaboration of three distributed servers (i.e. client –telnetc, master- mserv, daemon - td). Stacheldraht combines the characteristics of both Trinoo and TFN (Tribe Flood Network) DDoS attack tools and provides two additional features: an encrypted client to handler communication and the agents are automatically remotely updated [21], [22].

The types of DDoS attacks involved in this experiment are: *bandwidth depletion attacks* (i.e. ICMP- Internet Control Message Protocol flood attacks, UDP-User Datagram Protocol flood attacks) and *resource depletion attacks* (i.e. TCP SYN – Transfer Control Protocol Synchronize attacks) [23], [24].

ICMP flood attack attempts to make the victim host unavailable by sending ICMP requests to the victim using spoofed source addresses. Thus, the consumption of resources to receive back those replies from the target to the attacker is eliminated and only the victim is responsible to handle large amounts of requests and replies [22], [25].

TCP SYN flood attacks exhaust the victim by sending SYN packets to the target with invalid IP source addresses. The consequence of this action is seen in the absence of the ACK packets back to the victim, which makes the TCP connection unattainable [22], [25]. In this sense, the TCP services of the target site become unavailable for authorized users [22].

While TCP is a connection oriented protocol, UDP is connectionless. This difference between UDP and TCP makes UDP flood attack more difficult to be realized. The strategy adopted by UDP flood attack is based on sending UDP packets to dead ports from the target site. The life-threatening consequences of UDP flood attacks are produced not only against the target host and also against the hosts on the same segment [22], [25].

4 Results and Evaluation

The created Mysql database (i.e. snortdata) stores the alerts received from each VM-based IDS. Our snort database consists of the 15 tables taken from snort-mysql database and the 6 ACID (Analysis Control for Intrusion Detection) tables. We have used in our experiment 4 tables from Snort database (i.e. tcphdr, udphdr, icmphdr, sig_class) and a table from ACID database (i.e. acid_event). We created another three join tables (i.e. tcp_acid_class, udp_acid_class, icmp_acid_class) (Figure 4), with the purpose to investigate and prioritize the DDoS events based on the following three criteria: True (i.e. a DDoS attack occurs), False (i.e. a DDoS attack doesn't occur) and (True, False) case (i.e. if the type of the event is unknown).

For example, 'tcp_acid_class' table was created by matching data from 'tcphdr' table, 'acid_event' table and 'sig_class' table as follow [26]:

```
mysql> CREATE TABLE tcp_acid_class AS
(SELECT tcphdr.sid, tcphdr.cid, tcphdr.tcp_sport, tcphdr.tcp_dport, ac-
id_event.signature, acid_event.sig_class_id, acid_event.sig_priority,
sig_class.sig_class_name
FROM   tcphdr
INNER JOIN acid_event
ON tcphdr.sid=acid_event.sid and tcphdr.cid=acid_event.cid
INNER JOIN sig_class
ON acid_event.sig_class_id=sig_class.sig_class_id);
```

We have made the assumptions that DDoS attacks are detected if the priority of the event is 1 (i.e. high) or 2 (i.e. medium) and if the priority is 3 (i.e. low) or 4 (i.e. very low) an alert will be generated.

When a DDoS attack is produced, the total number of each $x \in \{$TCP SYN, UDP, ICMP$\}$ flood attack is calculated by querying the above corresponding join tables based on the 'signature', 'sig_priority' and 'sig_class_name' fields. For this situation Snort reacts with one of the following actions [14]: drop, sdrop or reject, protecting the virtual machines.

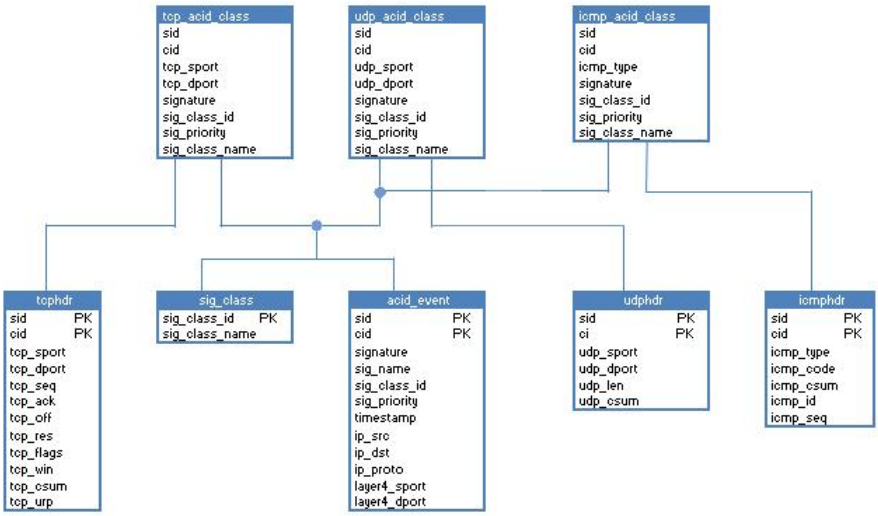

Fig. 4. Creating Join Database Tables

In the case that Snort generates alerts, we have considered two possible cases: False and (True, False). The (True, False) state is recorded when the attempts to attack the VMs-based IDS are classified as 'unknown' classtype. The attack classification of Snort rules is listed in Table 3.2 from the Snort Users Manual [14] (see Table 1) and this list appears on the 'classification.config' file of Snort installation.

The (True, False) element was introduced and modeled by Guth (1991) in the Dempter-Shafer Theory (DST) in 3-valued logic in relation with the fault-tree analysis (FTA). In this paper, a quantitative analysis of the TCP SYN flooding attacks, UDP flooding attacks and ICMP flooding attacks is carried out, in order to reduce the large amounts of false alarms rates produced by the Intrusion Detection Systems.

The creation of the above three join tables, the total number of events when a $x \in \{TCP\ SYN, UDP, ICMP\}$ flood attack occurs and the total number of events when the event is unknown, can be used to calculate the basic probability assignment for each sensor machine, according to Dempster-Shafer theory (DST).

Therefore, first the mass assignments for all three states of each sensor are defined as follows:

$$\begin{cases} m_x(T), \text{ the DDoS attack occurs} \\ m_x(F), \text{ the DDoS attack doesn't occur} \\ m_x(T, F), \text{ the "unknown" classification of the DDoS attacks.} \end{cases} \quad (1)$$

where $x \in \{TCP, UDP, ICMP\}$ flood attack in the private cloud

Table 1. Snort Default Classifications [14]

Classtype	Description	Priority
attempted-admin	Attempted Administrator Privilege Gain	high
attempted-user	Attempted User Privilege Gain	high
inappropriate-content	Inappropriate Content was Detected	high
policy-violation	Potential Corporate Privacy Violation	high
shellcode-detect	Executable code was detected	high
successful-admin	Successful Administrator Privilege Gain	high
successful-user	Successful User Privilege Gain	high
trojan-activity	A Network Trojan was detected	high
unsuccessful-user	Unsuccessful User Privilege Gain	high
web-application-attack	Web Application Attack	high
attempted-dos	Attempted Denial of Service	medium
attempted-recon	Attempted Information Leak	medium
bad-unknown	Potentially Bad Traffic	medium
default-login-attempt	Attempt to login by a default username and password	medium
denial-of-service	Detection of a Denial of Service Attack	medium
misc-attack	Misc Attack	medium
non-standard-protocol	Detection of a non-standard protocol or event	medium
rpc-portmap-decode	Decode of an RPC Query	medium
successful-dos	Denial of Service	medium
successful-recon-largescale	Large Scale Information Leak	medium
successful-recon-limited	Information Leak	medium
suspicious-filename-detect	A suspicious filename was detected	medium
suspicious-login	An attempted login using a suspicious user-name was detected	medium
system-call-detect	A system call was detected	medium
unusual-client-port-connection	A client was using an unusual port	medium
web-application-activity	Access to a potentially vulnerable web appli-cation	medium
icmp-event	Generic ICMP event	low
misc-activity	Misc activity	low
network-scan	Detection of a Network Scan	low
not-suspicious	Not Suspicious Traffic	low
protocol-command-decode	Generic Protocol Command Decode	low
string-detect	A suspicious string was detected	low
unknown	Unknown Traffic	low
tcp-connection	A TCP connection was detected	very low

Figure 5 depicts the mass assignments calculated for two VM-based IDS, which were realized by implementing the pseudocode proposed in [1]. Hence, first the detection rate ($m_x(T)$) for each flooding attack against each VM-based IDS was computed. The detection rate (i.e. $m_x(T)$) was defined the same as Yu and Frincke (2005):

$$Detection\ Rate\ (DR) = \frac{number\ of\ true\ attacks\ reported}{number\ of\ total\ observable\ attacks} \quad (2)$$

Then, the computation of the probabilities for (True, False) element was realized based on the above descriptions. $m_x(F)$ [27] will be calculated by applying DST, which says that the [sum of all masses] = 1:

$$m_x(F) = 1\text{-}m_x(T)\text{-}\ m_x(T, F) \quad (3)$$

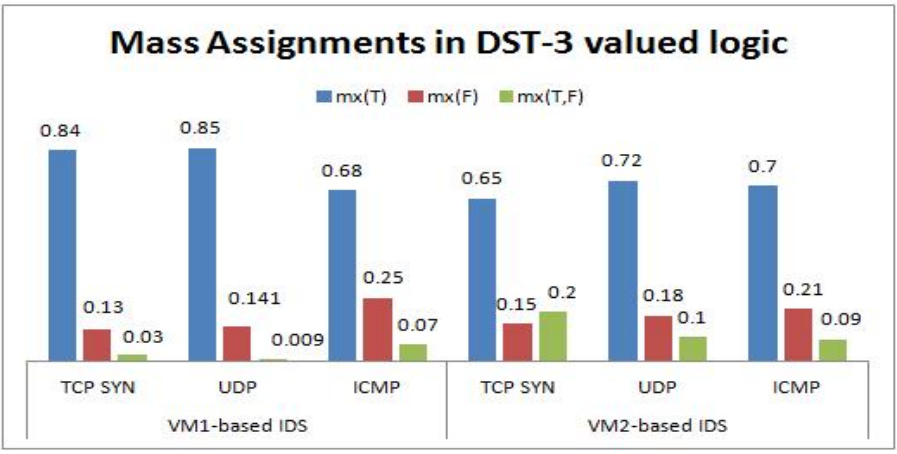

Fig. 5. Mass Assignments in DST

The results from Figure 5 reveal a high detection rate ($m_x(F) > 0.65$) and $m_x(F) \in [0.07, 0.25]$, obtained from the VM-based IDS, which were configured with proper rules and thresholds against the DDoS attackers.

Moreover, we present in depth the analysis of the obtained results by using a Fault-Tree Analysis for each VM-based IDS and combining those Bpa's results into an attacks assessment at the end using the Dempster's combination rule.

Therefore, the basic probabilities assignment will be calculated for each VM-based IDS using a Fault-Tree Analysis as described in Figure 6 and using the results in Figure 5.

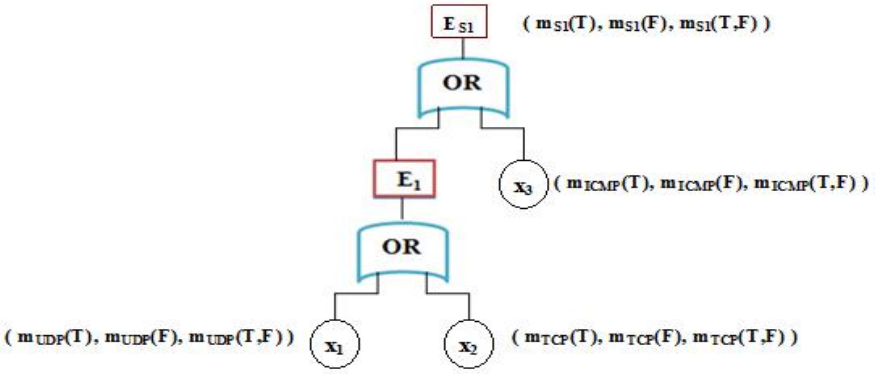

Fig. 6. Bpa's Calculation [1]

The results obtained for each VM-based IDS are described in Table 2. A high detection rate and a low false rate can be seen for both VM-based IDS. Comparing the results from Figure 5 with the results from Table 2, when a Fault-Tree Analysis is

realized, we can see the decrease in the false alarm rates (i.e. $m_y(T,F)$), together with the decrease in the true negative rate (i.e. $m_y(F)$) and the increase in the detection rate (i.e. $m_y(T)$), where y denotes one of the VM-based IDS, also called sensors (i.e. S1, S2).

Table 2. Bpa's calculation

y	$m_y(T)$	$m_y(F)$	$m_y(T,F)$
S1	0.99232	0.004583	0.003098
S2	0.9706	0.00567	0.02373

Finally, the evidences obtained from both VM-based IDS are combined using Dempster's combination rule and the results are shown in Table 3.

Table 3. Results of Dempster's combination rule

$m_{12}(T)$	$m_{12}(F)$	$m_{12}(T,F)$
0.963146	0.010227	0.026628

It can be seen that the conflict generated from the two VM-based IDS (Table 2) is irrelevant and Table 3 highlights the maximization of the detection rate, together with the minimization of the false alarm rates.

The results from Table 3 using the evaluation metrics: overall accuracy and the error rates, as described in [29] and [30] (Table 4), where:

$$\text{Overall Accuracy} = \frac{TP+TN}{TP+TN+FP+FN} \tag{4}$$

$$\text{Error Rate} = \frac{FP+FN}{TP+TN+FP+FN} \tag{5}$$

Table 4. Evaluation metrics

TP	***TN***	***False rates (FN+FP)***	***Overall Accuracy***	***Error Rate***
0.963146	0.010227	0.026628	0.9733	0.0266

TP= true positive, TN= true negative, FP=false positive, FN= false negative

5 Conclusions

While the experimental results were performed into a private cloud model deployed using Eucalyptus open-source, the IDS cloud topology could be used as well for the others cloud deployment models.

We have conducted the evaluation for two virtual machines, where Snort Network Intrusion and Detection System is installed and configured to defend against DDoS attacks. The centralization, correlation and analysis of the evidences obtained from the virtual machine based Intrusion Detection Systems (i.e. VM-based IDS) are realized in a front-end Cloud Fusion Unit.

Our experimental results show a high detection rate and a low false alarm rate using our proposed solution for detecting Distributed Denial of Service (DDoS) attacks in Eucalyptus private Cloud. Moreover, the efficiency requirements (i.e. the detection rate and the computational time) are accomplished by utilizing the Dempster-Shafer theory in 3 valued-logic.

Another advantage is the resolution of the conflict generated by the combination of the evidences produced by each VM-based IDS.

In conclusion, our experimental results comply with our theoretical formulations.

Acknowledgments. This work was partially supported by the strategic grant POSDRU/88/1.5/S/50783, Project ID50783 (2009), co-financed by the European Social Fund – Investing in People, within the Sectoral Operational Programme Human Resources Development 2007-2013.

References

1. Lonea, A.M., Popescu, D.E., Tianfield, H.: Detecting Distributed Denial of Service (DDoS) Attacks in Cloud Computing Environment. International Journal of Computers, Communications & Control, IJCCC, 1841–9836 (accepted for publication, 2012) ISSN: 1841-9836
2. Bhadauria, R., et al.: A Survey on Security Issues in Cloud Computing. CoRR (2011), http://dblp.uni-trier.de/db/journals/corr/corr1109.html#abs-1109-5388
3. Bakshi, A., Yogesh, B.: Securing Cloud from DDoS Attacks using Intrusion Detection System in Virtual Machine. In: Second International Conference on Communication Software and Networks, pp. 260–264. IEEE Computer Society, Washington, DC (2010)
4. Dhage, S.N., et al.: Intrusion Detection System in Cloud Computing Environment. In: International Conference and Workshop on Emerging Trends in Technology (ICWET 2011), pp. 235–239. TCET, Mumbai (2011)
5. Lee, J.-H., Park, M.-W., Eom, J.-H., Chung, T.-M.: Multi-level Intrusion Detection System and Log Management in Cloud Computing. In: 13th International Conference on Advanced Communication Technology, ICACT 2011, Seoul, pp. 552–555 (2011)
6. Lo, C.-C., Huang, C.-C., Ku, J.: A Cooperative Intrusion Detection System Framework for Cloud Computing Networks. In: 39th International Conference on Parallel Processing Workshops, pp. 280–284. IEEE Computer Society, Washington, DC (2010)
7. Mazzariello, C., Bifulco, R., Canonico, R.: Integrating a Network IDS into an Open Source Cloud Computing Environment. In: Sixth International Conference on Information Assurance and Security, pp. 265–270 (2010)

8. Roschke, S., Cheng, F., Meinel, C.: Intrusion Detection in the Cloud. In: Eighth IEEE International Conference on Dependable, Autonomic and Secure Computing, pp. 729–734 (2009)
9. Eucalyptus Administrator's Guide (2.0), http://open.eucalyptus.com/wiki/EucalyptusAdministratorGuide
10. Eucalyptus User's Guide (2.0), http://open.eucalyptus.com/wiki/EucalyptusUserGuide_v2.0
11. Weir, J.: Building a Debian\Snort based IDS (2012), http://www.snort.org/assets/167/IDS_deb_snort_howto.pdf
12. Moore, N.: Snort 2.9.1 CentOS 5.6 Installation Guide (2011), http://www.snort.org/assets/159/Snort_2.9.1_CentOS_5.pdf
13. Harper, P.: Snort Enterprise Install (2007), http://www.internetsecurityguru.com/documents/Snort_Base_Barnyard_CentOS_5.pdf
14. Sourcefire, Inc.: Snort Users Manual 2.9.2 (2011), http://www.snort.org/assets/166/snort_manual.pdf
15. Rehman, R. U. R.: Intrusion Detection with Snort: Advanced IDS Techniques using Snort, Apache, Mysql, PHP and ACID. Pearson Education Inc. Publishing as Prentice Hall PTR (2003)
16. Baker, A.R., Esler, J.: Snort Intrusion Detection and Prevention Toolkit. Syngress Publishing, Inc. (2007)
17. Vanathi, R., Gunasekaran, S.: Comparison of Network Intrusion Detection Systems in Cloud Computing Environment. In: 2012 International Conference on Computer Communication and Informatics (ICCCI 2012), Coimbatore, India (2012)
18. Brennan, M.P.: Using Snort for a Distributed Intrusion Detection System. SANS Institute, Version 1.3 (2002), http://www.sans.org/reading_room/whitepapers/detection/snort-distributed-intrusion-detection-system_352
19. Borisaniya, B., Patel, A., Patel, R., Patel, D.: Network-based Intrusion Detection in Eucalyptus Private Cloud. In: 2010 International Conference on Advances in Communication, Network, and Computing, India, pp. 209–212 (2010)
20. Skinner III, W.T.: Identity Management in a Public IaaS Cloud. James Madison University. Master Thesis (2012), http://www.scribd.com/doc/90183632/3/Thesis-Statement
21. Dittrich, D.: The "stacheldraht" distributed denial of service attack tool. University of Washington (1999), http://staff.washington.edu/dittrich/misc/stacheldraht.analysis.txt
22. Criscuolo, P.J.: Distributed Denial of Service Trin00, Tribe Flood Network, Tribe Flood Network 2000 and Stacheldraht. CIAC-2319. Department of Enery Computer Incident Advisory Capability, UCRL-ID-136939, Rev.1, Lawrence Livermore National Laboratory, https://e-reports-ext.llnl.gov/pdf/237595.pdf (2000)
23. Specht, S.M., Lee, R.B.: Distributed Denial of Service: Taxonomies of Attacks, Tools and Countermeasures. In: Proceedings of the 17th International Conference on Parallel and Distributed Systems, pp. 543–550 (2004)
24. Mirkovic, J., Martin, J., Reiher, P.: A Taxonomy of DDoS Attacks and DDoS Defense Mechanisms. ACM SIGCOMM Computer Communication Review 34(2), 39–53 (2004)

25. Northcutt, S., Novak, J.: Network Intrusion Detection, 3rd edn. New Riders Publishing (2002) ISBN 0-73571-265-4
26. w3schools.com, http://www.w3schools.com/sql/sql_join.asp
27. Guth, M.A.S.: A Probabilistic Foundation for Vagueness & Imprecision in Fault-Tree Analysis. IEEE Transactions on Reliability 40(5), 563–569 (1991)
28. Yu, D., Frincke, D.: Alert Confidence Fusion in Intrusion Detection Systems with Extended Dempster-Shafer Theory. In: Proceedings of the 43rd ACM Southeast Conference. ACM-SE, vol. 43, pp. 142–147 (2005)
29. Thomas, C., Balakrishnan, N.: Performance Enhancement of Intrusion Detection Systems using advances in sensor fusion. In: 11th International Conference on Information Fusion, pp. 1–7 (2008)
30. Witten, I.H., Frank, E.: Data Mining. In: Practical Machine Learning Tools and Techniques, 2nd edn. Kaufmann Press, San Francisco (2005)

Private Cloud Set Up Using Eucalyptus Open Source

Alina Mădălina Lonea

Automation and Applied Informatics Department,
"Politehnica" University of Timisoara,
Faculty of Automation and Computers,
B-dul Vasile Parvan, nr. 2, 300223, Timisoara, Romania
madalina_lonea@yahoo.com

Abstract. The evolution of Cloud Computing technology marks a long debate in terms of the changes produced in Information Technology (IT) for practitioners and academics, who acknowledge the involvement of several technologies during the years. This paper presents the experience of deploying a private cloud using Eucalyptus open source. Section 2 identifies the similarities and differences between cloud computing and other technologies. Section 3 describes the Eucalyptus private cloud deployment. Section 4 of this paper reveals the euca2ools operations. Moreover, the paper illustrates the encountered problems in our private cloud with their corresponding solutions. Finally, in section 6 the paper presents the concluding remarks.

Keywords: private cloud, Eucalyptus, euca2ools, troubleshooting, virtualization, volumes, instances, virtual machine, images.

1 Introduction

The evolution of Cloud Computing technology marks a long debate in terms of the changes produced in Information Technology (IT) for practitioners and academics, who acknowledge the involvement of several technologies.

This paper concerns only the private cloud deployment model, respectively the Infrastructure-as-a-Service (IaaS), with the purpose to emphasize my experience of working with Eucalyptus Linux-based open-source software. Eucalyptus is the acronym for Elastic Utility Computing Architecture Linking Your Programs to Useful Systems [1]. It was developed by University of California for creating private and hybrid clouds. Now, it is supported by Eucalyptus Systems, a Canonical Partner [2].

Eucalyptus provides interfaces compatible with Amazon Web Services (AWS) (e.g. Amazon Elastic Compute Cloud (EC2), Amazon Elastic Block Storage (EBS), Amazon S3 (Simple Storage Service)) [3], [4].

Further, section 2 identifies the similarities and differences between cloud computing and other technologies. Section 3 describes the Eucalyptus private cloud deployment. Section 4 of this paper reveals the euca2ools operations. Moreover, the paper illustrates the encountered problems in our private cloud with their corresponding solutions. Finally, in section 6 the paper presents the concluding remarks.

V.E. Balas et al. (Eds.): Soft Computing Applications, AISC 195, pp. 381–389.
springerlink.com

2 Cloud Computing and Related Technologies

Cloud Computing appears at the end of 2007 and it involves several enabling technologies like: virtualization, Grid Computing, cluster, Service Oriented Architecture (SOA) and web services, utility computing [5], [6].

2.1 Virtualization

At the end of the 1960s the mainframe was adapted to virtualization technology, which permits several virtual machines (VMs) to run concurrently within a physical machine [7]. Additionally, virtualization is considered the basis in cloud computing environment in order to efficiently utilize its physical resources (i.e. memory, CPU, I/O and OSs) [5], [8]. This capability provided by the virtualization layer allows multiple operating systems (OSs) to action as guest operating systems within a host operating system. One of the following software can be utilized in order to make possible this capability: an installed application into the host OS (e.g. VMware Player, Oracle VirtualBox, ACE) or a software called hypervisor or Virtual Machine Monitor (VMM), which has to be installed directly to the hardware resources (e.g. Xen, KVM – Kernel Virtual Machine) [5], [8].

Even if virtualization is an important element of cloud computing, the fact that the workload is statically allocated differentiate virtualization from cloud computing which is based on dynamic allocation the workload by using an API (Application Programming Interface) call [9].

2.2 Grid Computing

A different technology considered the basis in cloud computing is Grid Computing. At first sight Grid Computing and Cloud Computing are similar, because both of them guiding us at reducing the cost of computing, increasing reliability and flexibility by providing resources on-demand [10], [11]. But it doesn't have to overlook that Grid Computing is the backbone of Cloud Computing, with its support infrastructure. Cloud Computing followed the example of Grid Computing, which provides storage and compute resources. As a next step in technology, Cloud comes with economy aspects in delivering more abstract resources and services [10], [11]. The business model of cloud refers to delivering the services over the Internet via a pay-as-you-go formula. As compared to the cloud-based business model, the business model of grid computing is project-oriented where the organizations that adopt it are sharing the resources in a collaborative manner with other companies that are in the grid model. Grid is a virtual organization with advanced services, where distributed individuals and/or institutions share files and the most important thing: they have direct access to computers, software, data and other resources. This access is possible using condition sharing strategies that realize an organizational process, for users and providers of the resources [12], [13].

Another feature that makes difference between Grid and Cloud is that the access for a resource in Grid could be delayed, because it means that resource was allocated

first to other user and the requesting user should wait until the resource will be available again. This delayed allocation doesn't happen in the Cloud environment, users receiving the resources on-demand. Wang and von Laszewski (2008) highlight another difference between cloud computing and grid computing, related with the user-centric interfaces of cloud computing, that ensure for its users an easy to work environment compared with the Grid resources and services, which are accessed with difficulty by grid users because they are forced to learn new Grid commands and APIs.

2.3 Cluster Computing

Besides the characteristics of Grid, Cloud Computing holds also the characteristics of cluster computing, that provides for its users the resources within a single administrative domain [6]. This is justified by the fact that Cloud Computing environment is composed from high-end computers (e.g. clusters, servers) as Grid is [6].

2.4 SOA and Web Services

Service Oriented Architecture (SOA) and Web Services are utilized in cloud computing, because these services computing contribute at the automation of business processes using IT services [14]. SOA is a collection of services, which provides the interaction between distributed systems by communicating and exchanging the data [14], [15], [16], [17]. Unlike SOA which delivers Web services from applications to other programs, Cloud Computing is focused on delivering cloud services to customers. The cloud end-users access the virtual resources and computing assets, using a framework provided by SOA [16].

3 Eucalyptus Private Cloud Deployment

The private cloud was deployed using the binary packages of Eucalyptus 2.0.3 open source for CentOS operating system. The details of the Eucalyptus private cloud setup are presented in Table 1 and Figure 1. Table 2 illustrates the hardware components that constitute the physical infrastructure.

Table 1. Details of Eucalyptus private cloud

Version	Eucalyptus 2.0.3 open source
Hypervisor	Xen
Topology	One front-end (cloud controller, walrus, cluster controller, storage controller) + 3 nodes
Networking mode	Managed

Table 2. Cloud Systems Configuration

		Front-end	*Node1*	*Node2*	*Node3*
OS		CentOS 5 on 64 bits architecture	CentOS 5 on 64 bits architecture	CentOS 5 on 64 bits architecture	CentOS 5 on 32 bits architecture
Hardware	***Processor***	AMD Sempron (tm) Processor	AMD Athlon (tm) 64 Processor	AMD Athlon (tm) 64 Processor	Intel (R) Pentium (R)
	Free Memory	1024Mb	256Mb	256 Mb	128 Mb
	Disk Space	54GiB	51GiB	51GiB	162GiB
NIC		**eth0:** 192.168.1.50 **eth1:** 172.16.1.1	**eth0:** 172.16.1.10	**eth0:** 172.16.1.11	**eth0:** 172.16.1.12
Hostname		front-end	node1	node2	node3

The Eucalyptus Administrator's Guide [19] constitutes the main source guide for deploying our private cloud. Additional materials that helped us to build it are: [3], [19], [20], [21].

The cloud topology used is a front-end and three nodes (Figure 1). The front-end is the server that runs the following Eucalyptus services: cloud controller, walrus,

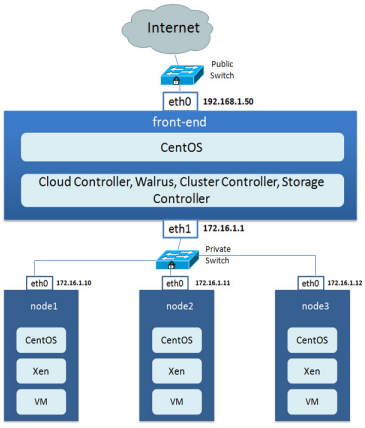

Fig. 1. Private Cloud Configuration

cluster controller and storage controller, while in nodes run the node controllers. Another important configuration in the Eucalyptus private cloud is the virtualization mode chosen, together with the networking mode.

Figure 1 describes that VMs were run in three physical machines and that each physical machines can run a single VM due to them hardware configuration.

In terms of virtualization, we chose to work with para-virtualization type, because the CPU (Central Processing Unit) of physical servers doesn't have virtualization support. In this sense, Xen hypervisor is utilized for realizing the virtualization of nodes, due to the fact that those nodes provide PAE (Physical Address Extension) support for CPU [8].

Along with the virtualization technology, in our private cloud several virtual network elements were automatically created. Figure 2 which was adapted from [8] describes the relationships between physical (i.e. eth0) and logical cards (i.e. vif0.0, vif1.0, vif2.0, vif3.0). If for example, a node has one physical interface card (eth0) and three VMs can be created inside the node (the VMs have 'eth0' for interface card), then inside the Domain 0 of the node the following virtual Ethernet interfaces will be generated: vif0.0, vif1.0, vif2.0, vif3.0. All vif's are connected to the Shared Bridge Connection (i.e. xenbr0), which behaves like a switch for all vif [8]. The Shared Bridge (xenbr0) is also called Shared Physical Network Device [22].

Xen uses the 'libvirt' virtualization API for managing the VMs [22].

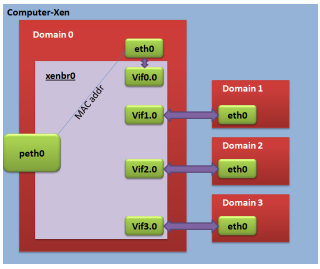

Fig. 2. Xen hypervisor configuration

Moreover, our Eucalyptus private cloud makes use of the Managed networking mode because of the feature's granularity provided (e.g. connectivity, IP control, security groups, elastic IPs, metadata service and VM isolation) [18].

Beside the installation, configuration and registration of the Eucalyptus components, several firewall rules were created, while other rules are identified as being automatically deployed by Eucalyptus. The created rules were illustrated in section 5 of this paper.

4 Euca2ools Operations

The first operations in Eucalyptus cloud environment is the registration of cloud controller, walrus, cluster controller, storage controller and nodes. After registering the

nodes, they will be available into the eucalyptus.conf file and there are 2 situations to see them, even if go the "/etc/eucalyptus/eucalyptus.conf" file is checked or the "grep NODES /etc/eucalyptus/eucalyptus.conf" command is executed [23].

Our private cloud is working properly because the 'euca-describe-availability-zones verbose' command shows our available resources [23]. Thus we can create three instances in total, from which two of them can be created using a 'medium' image type (i.e. 256 RAM + 1 CPU) and another one to be 'small' image type (i.e. 128 RAM + 1 CPU) or we can create three instances using the 'small' image type.

The euca2ools operations are focused on working with instances and volumes. The possible operations with instances are emphasized in Table 3 and the lifecycle of the states can be observed (i.e. pending, running, shutting-down and terminated) [3], [4] together with the assignment of public IP address (192.168.1.55) and private IP address (172.16.10.66) for the created instance in this case. The range of the private IP addresses was stored into "/etc/dhcp.conf" file (i.e. 172.16.10.10 -> 172.16.10.250), while the range of the public IP addresses was written into "/etc/eucalyptus/eucalyptus.conf" file (i.e. 192.168.1.55 -> 192.168.1.60) [23].

The operations accessible with storage volumes are: creation, attachment / detachment to an instance and deletion. When the volume is attached to an instance, the state of the volume will be changed from 'available' to 'in-use' [23].

Table 3. The lifecycle of a euca2ools image

euca-run-instances emi-E7EC10AA -k mykey -t m1.small	*euca-describe-instances*	*euca-describe-instances*	*euca-terminate-instances*	*euca-describe-instances*
i-375E0723 emi-E7EC10AA **0.0.0.0 0.0.0.0 pending** mykey	i-375E0723 emi-E7EC10AA **192.168.1.55 172.16.10.66 pending** mykey	i-375E0723 emi-E7EC10AA 192.168.1.55 172.16.10.66 **running** mykey	i-375E0723 emi-E7EC10AA 192.168.1.55 172.16.10.66 **shutting-down** mykey	i-375E0723 emi-E7EC10AA 192.168.1.55 172.16.10.66 **terminated** mykey

5 Problems and Solutions in the Private Cloud Setup

This section comprises several important problems that were met on the private cloud setup. These issues and the corresponding solutions were identified during the cloud operation's manipulation. Some of the issues were found in the troubleshooting Eucalyptus section of Eucalyptus Administrator's Guide, while others were discovered as problems solved by the Eucalyptus community in the Engage question and answers section [24].

Availability of cloud resources is tested with 'euca-describe-availability-zones verbose' command and it should not return '000/000'. This concern was figured out adopting the troubleshooting Eucalyptus section of Eucalyptus Administrator's Guide [18]. The solution was to de-register and register again the cluster and nodes components.

Another problem encountered in our private cloud is with the Internet access of the created instances. It was observed that at one moment the instances and the nodes didn't have Internet access. These issues were solved by adding the following three rules into the "/etc/rc.d/rc.local" file of the front-end server:

```
iptables   -I INPUT -p tcp --dport 67:68 --sport 67:68 -j ACCEPT
iptables   -I INPUT -p udp --dport 67:68 --sport 67:68 -j ACCEPT
iptables -t nat -A POSTROUTING -s 172.16.1.0/24 -o eth0 -j SNAT --to-source
192.168.1.50
```

Rule 3 allows the communication among the private addresses of the VMs (172.16.1.0/24) and the public addresses (192.168.1.50) [24].

Also, regarding the VMs usage, another problem encountered was that the installation procedure wasn't possible at a time. The approached solution was to modify the following file "/etc/apt/sources.list", by deleting the existing two lines and adding the following lines [25]:

```
deb http://archive.debian.org/debian/ lenny main contrib non-free
deb-src http://archive.debian.org/debian/ lenny main contrib non-free
deb http://archive.debian.org/debian-security lenny/updates main contrib non-free
deb-src http://archive.debian.org/debian-security lenny/updates main contrib non-free
deb http://archive.debian.org/debian-volatile lenny/volatile main contrib non-free
deb-src http://archive.debian.org/debian-volatile lenny/volatile main contrib non-free
```

Besides the mentioned problems with VMs, the private cloud has presented problems with the storage volumes. Problems with volumes could appear if there are not correctly mounted, detached and un-mounted. For mounting and un-mounting the volumes, a script "start_ebs.sh" was created inside the volume that was attached to an instance. This script was taken from [23] (i.e. install a service into an EBS volume) and it contains the mounting and un-mounting services in order to facilitate the manipulation of these mandatory services every time when we enter and get out of the instance by starting and stopping the script. However, after restarting the Eucalyptus services, the old volumes could not be attached to a new instance, due to the fact that lvm2 was inactive. The sign of this issue underlined that the state of the volumes remains 'available' instead of changing to 'in-use'. For solving this dilemma, three recovery steps discussed in [26] were followed. After processing them, the result of attaching the old volume to a new instance was obtained.

6 Conclusions

This paper presented the experience of deploying and working with Eucalyptus open-source private cloud. In the first part of the paper, cloud computing was emphasized in relation with several technologies: virtualization, Grid Computing, Cluster Computing, SOA and Web Services. Further, our test bed private cloud environment was detailed. Furthermore, the main operations which can be realized using the Command Line Interface (CLI) euca2ools, were described. The paper is also providing a useful section with the encountered and solved problems in the Eucalyptus framework, with the purpose to help the researchers who will be interested to work with Eucalyptus.

Acknowledgments. This work was partially supported by the strategic grant POSDRU/88/1.5/S/50783, Project ID50783 (2009), co-financed by the European Social Fund – Investing in People, within the Sectoral Operational Programme Human Resources Development 2007-2013.

References

1. Nurmi, D., et al.: The Eucalyptus Open-Source Cloud Computing System. In: 9th IEEE/ACM International Symposium on Cluster Computing and the Grid (CCGRID 2009), pp. 124–131 (2009)
2. Eucalyptus Systems, Inc.: Eucalyptus Open-Source Cloud Computing Infrastructure – An Overview (2009), http://www.eucalyptus.com/pdf/whitepapers/Eucalyptus_Overview.pdf
3. Johnson, D., et al.: Eucalyptus Beginner's Guide – UEC Edition. v1.0 (2010), http://cssoss.files.wordpress.com/2010/06/book_eucalyptus_beginners_guide_uec_edition1.pdf
4. Karpagam, G.R., Parkavi, J.: Setting up of an Open Source based Private Cloud. IJCSI International Journal of Computer Science Issues 8(3(1)) (2011)
5. Wang, L., von Laszewski, G.: Scientific Cloud Computing: Early Definition and Experience. In: 10th IEEE International Conference on High Performance Computing and Communications (HPCC 2008), pp. 825–830 (2008)
6. Gong, C., et al.: The Characteristics of Cloud Computing. In: 39th International Conference on Parallel Processing Workshops (ICPPW), pp. 275–279 (2010)
7. Rosenblum, M., Garfinkel, T.: Virtual machine monitors: current technology and future trends. IEEE Computer 38(5), 39–47 (2005)
8. Xen.org: Get started with Xen (2012), http://wiki.xen.org/wiki/Main_Page
9. Pemmaraju, K.: The Evolution of Clouds: Private and Hybrid Clouds (2010), http://sandhill.com/article/the-evolution-of-clouds-private-and-hybrid-clouds/
10. Foster, I., Zhao, Y., Raicu, I., Lu, S.: Cloud Computing and Grid Computing 360-Degree Compared. In: Grid Computing Environments Workshop, GCE 2008, pp. 1–10 (2008)
11. Rings, T., et al.: Grid and Cloud Computing: Opportunities for Integration with the Next Generation Network. Journal of Grid Computing 7(3), 375–393 (2009)
12. Magoulès, F., et al.: Introduction to Grid Computing. CRC Press Taylor & Francis Group, London (2009)

13. Foster, I.: What is the Grid? A Three Point Checklist. Argonne National Laboratory & University of Chicago (2002)
14. Buyya, R., et al.: Cloud Computing and emerging IT platforms: Vision, Hype and reality for delivering computing as the 5th utility. Future Generation Computer Systems 25(6), 599–616 (2009)
15. Shah, D., Patel, D.: Dynamic and Ubiquitous Security Architecture for Global SOA. In: The Second International Conference on Mobile Ubiquitous Computing, Systems, Services and Technologies, Valencia, Spain, pp. 482–487 (2008)
16. Rittinghouse, J.W., Ransome, J.F.: Cloud Computing Implementation, Management and Security. CRC Press, Boca Raton (2010)
17. Geric, S.: Security of Web Services based Service-oriented Architectures. In: Proceedings of the 33th International Convention, MIPRO 2010, Opatija, Croatia, pp. 1250–1255 (2010)
18. Eucalyptus Systems, Inc.: Eucalyptus Administrator's Guide (2.0) (2012a), http://open.eucalyptus.com/wiki/EucalyptusAdministratorGuide
19. Sharma, A.: Private cloud setup using eucalyptus and xen, http://www.akashsharma.me/private-cloud-setup-using-eucalyptus-andxen/#Cloud_(2D)_setup_private_cloud(n.d)
20. Intel: Intel Cloud Builder Guide to Cloud Design and Deployment on Intel Platforms Ubuntu Enterprise Cloud. White Paper (2011)
21. Shafer, J.: I/O Virtualization Bottlenecks in Cloud Computing Today. In: Second Workshop on I/O Virtualization (WIOV 2010), Pittsburgh, USA (2010)
22. Kamran Azeem, M.: Xen, KVM, Libvirt and IPTables (2011), http://cooker.techsnail.com/index.php/XEN,_KVM,_Libvirt_and_IPTables
23. Eucalyptus Systems, Inc.: Eucalyptus User's Guide (2.0) (2012b), http://open.eucalyptus.com/wiki/EucalyptusUserGuide_v2.0
24. Eucalyptus Systems, Inc.: Engage where you connect your needs with Eucalyptus people and knowledge (2012c), https://engage.eucalyptus.com/
25. Server Fault: Apt-get update getting 404 on debian lenny (2012), http://serverfault.com/questions/374651/apt-get-update-getting-404-on-debian-lenny
26. Canonical Ltd.: Attaching EBS volumes failed after rebooting SC host (2012), https://bugs.launchpad.net/eucalyptus/+bug/733067

Mathematical Model and Formalization for DTF Method

Emanuel Ciprian Sasu

"Politehnica" University / PhD Student, Timisoara, Romania
cipisasu@ee-software.com

Abstract. This paper defines a mathematical model for the Destination Traffic Fingerprint method (DTF). The entire process is seen as a system, composed by a certain number of subsystems. As a system, it has input and output function, depending on the time variable. Then, each component is viewed as a subsystem, with input and output functions.

Keywords: DTF Method, MAC Spoofing, Intrusion Detection.

1 Introduction

This detailed description of Destination Traffic Fingerprint method, or simply DTF, is not the purpose of this work. All the features that were developed until now, were published in other articles, like [1], [2], [3], [4]. This work focuses on the conception of a mathematical model that can describe the entire functionality.

The problem that is addressed in DTF Method is related to a network infrastructure where we have a certain number of network stations, used by a set of authorized users. A major security issue is to detect very quickly any attempt to break into the network using an unauthorized station.

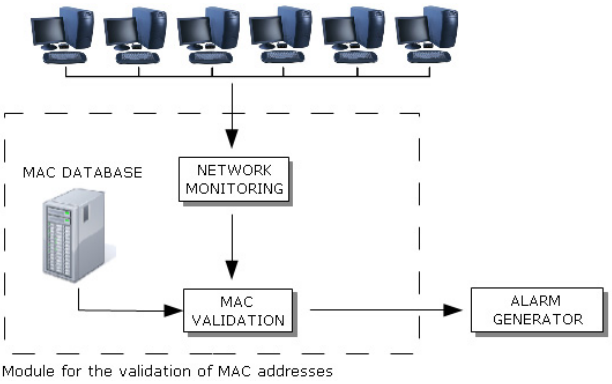

Fig. 1. Identification of authorized network stations

The solution for this threat is to monitor the entire network activity and identify each network station using a unique ID or fingerprint. Maybe the most simple method is to use the MAC address of the network interface card of each station.

V.E. Balas et al. (Eds.): Soft Computing Applications, AISC 195, pp. 391–401.
springerlink.com

As we can see in Fig. 1, the traffic generated from the network infrastructure is monitored by a software application, which extracts the MAC address of each source that originates within the network. Then, each MAC address is checked using a database and an alarm is raised for each MAC that is not found in the validation list.

This algorithm is very simple, but efficient because the MAC addresses can be easily spoofed. That is why the MAC validation process needs to be more than a simple query in a table. The module needs other functions to be applied in order to validate in an accurate manner.

Many solutions were developed to solve the MAC spoofing threat, like those described in [6] - [11]. DTF method identifies a MAC address as valid or spoofed, by creating a reference fingerprint from the network traffic in the evaluated time interval, and then comparing this reference fingerprint with the actual fingerprint extracted from the current network traffic. The reference fingerprint is composed by a set of destination IP addresses that were found to be constantly present in the traffic. The traffic is captured at the network interface card level, using Winpcap driver [5].

The fact that a network station does have a set of IP destinations that are constantly present in the traffic generated by that network station, was proved in [3], We have to keep in mind that DTF works at a minute level interval. This means that DTF is not interested to count the amount of traffic to a certain destination, but to see if we have or we don't have traffic in one minute. Then, computing this answer for every minute on the estimated time interval, DTF can decide if an IP destination can or can't be declared as “constant in traffic”, as described in [1] and [3].

For each IP destination that is recorded in the reference fingerprint, DTF stores not only the IP address, but also the percentage of presence for that IP in the traffic. Therefore, the fingerprint can be described as a set of pairs M_{REF}, like in (1):

$$M_{REF} = M\{P(IP_k, PP_k) | k = \overline{0..\mathrm{TDIP}}\} \tag{1}$$

where:

1. IP_k – represents an IP address
2. PP_k – represents the percentage of presence for IP_k,
3. TDIP – represents the total number of the IP addresses in the reference fingerprint

After the generation of the reference fingerprint, DTF method generates an actual fingerprint extracted from the real time traffic. By comparing the reference fingerprint with the actual fingerprint, DTF calculates the Overall Degree of Recognition which is a percentage value that represents how much we can be sure that the MAC address is or it is not what it claims to be.

The next chapters are organized as follows. In chapter 2, a few notations and definitions will be given, in order to make possible the mathematical and systemical description. Chapter 3 will focus on the model for generation of the reference fingerprint and chapter 4 will focus on a model for the real time validation of MAC addresses.

2 Problem Formalization and Notations

2.1 Problem Formalization

The validation process can be seen as a black box system model with an entry function *u(t)* and an exit function *y(t)*. The entry function can be defined like in (1), as a set of packets PKT_k, consisting on np_t packets for each time value *t*.

$$u(t)=M_P\{PKT_k|k=\overline{0..\mathrm{np}_t}\} \tag{2}$$

Therefore, the set of all packets that are received at the entry point in the system, will be be noted as M_P and will define the entry function.

At the exit point of the system we need to know for each MAC_k address that was found in the traffic, a degree of recognition DG_k, which tells how much we can be sure that the MAC address is what it claims to be. The MAC address together with the degree of recognition, forms a pair $P_{MAC}(MAC_k, DG_k)$. Formula (3) describes the exit function of the system, as the set that contains the pairs for all MAC addresses.

$$y(t)=M_{MAC}\{P_{MAC}(MAC_k, G_k)|G_k\in[0,100]\} \tag{3}$$

The degree of recognition was defined as a percentage value between 0% and 100%. This is the most general case. It is true that the best usability of DG is when DG can be only *true* (100%) or *false* (0%) . Still, it is quite hard to validate a MAC address in this manner. A percentage value would be much realistic.

Then, the system function can be defined as in (3). The role of the system function is to generate the set M_{MAC}, using the set M_P.

$$f: M_P \rightarrow M_{MAC} \tag{4}$$

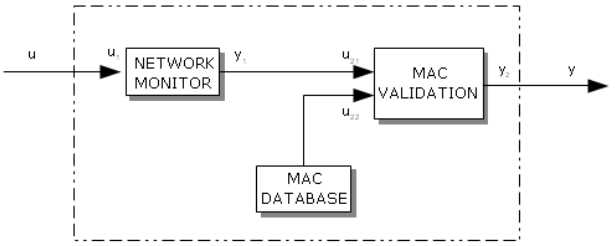

Fig. 2. MAC validation schema

2.2 Notations and Definitions

Let *NIP* be the total number of the IP addresses on he IPv4 domain and let M_{IP} be the total set of IP addresses in the IPv4 domain.

$$M_{IP}=\{IP_k, k\in[0,NIP]\} \tag{5}$$

Let *MAC* be the physical address of the network interface card of a certain network station.

Let *NP* be a network packet that is passing through the network at time *T*, and can be characterized as the following set of variables:

$$NP = \{T, IP_{src}, MAC_{src}, PORT_{src}, IP_{dest}, MAC_{dest}, PORT_{dest}\ LENGTTH, PROTOCOL\ \} \quad (6)$$

where *src* refers to the source and *dest* to the destination.

Let PP_k be the percentage of presence for IP_k destination.

Let *LP* be the minimum limit for the percentage of presence, in order to accept an IP destination in the reference fingerprint.

Let S_{INTERV} be the number of equal divisions used to divide the entire evaluation interval for a DTF fingerprint, and let *NSI* be the number of divisions where traffic is directed to the evaluated IP destination. Also let *MININTERV* be the minimum number of divisions with traffic, required to accept an IP address in the fingerprint.

3 Model for the Generation of Reference Fingerprint

3.1 The Process Seen as a Black Box System

The generation process of the reference fingerprint can be seen as a black box system, with an input signal *u(t)* and an output signal *y(t)*. The input of the system is the traffic captured at a certain point in the network. The output signal is the reference fingerprint. The function of the system is responsable to take the input signal and to generate the output signal from the input.

Based on these considerations, the input signal can be defined as the set of all network packets NP_k, captured from the network at time *t*.

$$u(t) = M_{NP}\{NP_k(t)\}. \quad (6)$$

The output signal can be defined as in (1), which is the set M_{REF}, composed by all the pairs $P(IP_k, PP_k)$, where IP_k refers to a destination IP address and PP_k is the corresponding percentage of presence in traffic for IP_k destination.

$$y(t) = M_{REF} = M\{P(IP_k, PP_k) | k = \overline{0..TDIP}\} \quad (7)$$

As we can see in Fig. 3, the generation process of the reference fingerprint consists in three major steps:

- The extraction of all IP destinations from the traffic, that belongs to a certain MAC address.
- Determine which of these IP destinations have a constant traffic.
- Fingerprint generation using the filtered IP destinations.

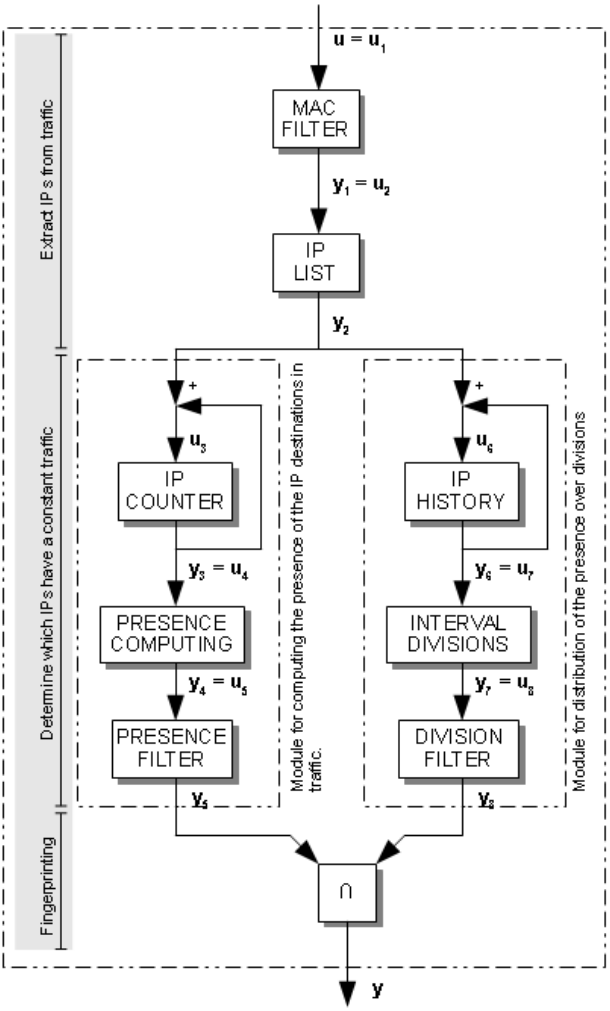

Fig. 3. Reference fingerprint generation process

3.2 Extraction of IP Destinations from the Traffic

The first step required in order to generate the reference fingerprint is to extract the set of IP destinations associated to a certain MAC address, at a minute level time interval *t*. It is not important for DTF method to calculate any quantity of traffic, but only to know what IP destinations are found every minute in the traffic that originates from a certain MAC address.

The first subsystem is the „MAC Filter" which filters all the packets found in the network traffic and lets to the output only the packets that originates from a certain MAC address.

$$u_1(t) = u(t) \tag{8}$$

$$y_1(t) = M_{NPM}\{NP_k(t) | MAC_k = MAC\}, M_{NPM} \subset M_{NP} \quad (9)$$

This means that the input of „MAC Filter" subsystem is the system input *u(t)*. From all the captured network packets NP_k, the subsystem will output only those that have a MAC address equal with the MAC address that is evaluated, as defined in (9).

The second step is to extract from the packets only the IP addresses, and create a list with them. This is done by the „IP List" subsystem, which receives at the input, the output $y_1(t)$ of the „MAC Filter" subsystem, and outputs the set of IP destinations M_2, as defined in (11).

$$u_2(t) = y_1(t). \quad (10)$$

$$y_2(t) = M_2\{IP_k | \forall NP_k \in M_{NPM}\} \quad (11)$$

The resulting $y_2(t)$ signal, composed by the set of IP destinations, has to be checked in order to find those IP destinations that are constantly found in the traffic.

3.3 Determining the IP Addresses with Constant Traffic

This part of the process is the most important. It has to filter the IP list received from the previous subsystem and output only those that can be part of the reference fingerprint.

Here we have a few modules that are connected in a parallel design. The input is the same for all the modules, and each module filters the IP list in a certain way and outputs a subset of the input, which is considered to have a constant traffic. For the moment, the system has only two modules in this parallel connection, but as a future work, it is very possible to add others too.

The first module receives the IP list, calculates the percentage of presence for each IP and filters the list according to certains predefined settings.

The process starts with the „IP counter" subsystem which counts the apparitions of each IP, generating a set of pairs M_3, where each IP destination IP_k is associated with its number of apparitions a_k. This number of apparitions is in fact the total number of minutes when it was traffic to that IP destination.

$$u_3(t) = y_2(t) \quad (12)$$

$$y_3(t) = y_2(t-1) + u_3(t) = M_3\{P(IP_k, a_k)\} \quad (13)$$

The output $y_3(t)$ becomes input for the „Presence Computing" subsystem which calculates the percentage of presence for each IP destination. The output is given as a set of pairs, where each IP_k destination is associated with its percentage of presence PP_k.

$$u_4(t) = y_3(t) \quad (14)$$

$$y_4(t) = M_4\{P(IP_k, PP_k) | PP_k = \frac{a_k}{t}\} \quad (15)$$

This set of pairs is transferred to the input of „Presence Filter", which checks the pairs from (15) and outputs only those that have a percentage of presence at least equal to a treshold value *LP*.

$$u_5(t) = y_4(t) \tag{16}$$

$$y_5(t) = M_5\{P(IP_k, PP_k) | PP_k \geq LP\} \tag{17}$$

But, as discussed in previous articles, the percentage of presence parameter is not enough to distinguish between constant and non constant traffic. That is why, other modules are required in order to be sure that the traffic to a certain IP destination can be declared as constant.

The second module receives also the same list of IP destinations, as the first module. The purpose of this module is to check if the percentage of presence is distributed over the whole interval or not. To do so, the module divides the time interval in four divisions, equal in size and seeks to find traffic to the IP destination in all of them.

The process starts with the „IP History" subsystem, which keeps a record of all IP destination in every minute. In fact, the output is a set of pairs, where each IP_k address is associated with the time *t*.

$$u_6(t) = y_2(t) \tag{18}$$

$$y_6(t) = M_6\{P(IP_k, t)\} \tag{19}$$

The output is directed to the „Interval Divisions" Module, which divides the whole interval into four equal divisions and checks to see how many of those divisions have traffic to the evaluated IP destination. In fact, the output is a set of pairs where each IP_k destination is associated with the number of divisions NSI_k, with traffic to IP_k.

$$u_7(t) = y_6(t) \tag{20}$$

$$y_7(t) = M_7\{P(IP_k, NSI_k)\} \tag{21}$$

The last subsystems in the module is "Division Filter", which receives at the input all the pairs in M_7, and sends to the output only those that have NSI_k value greater or equal to *MININTERV* parameter.

$$u_8(t) = y_7(t) \tag{22}$$

$$y_8(t) = M_8\{P(IP_k, NSI_k) | NSI_k \in M_7, NSI_k \geq MIN_{INTERV}\} \tag{23}$$

The last subsystem receives at the input, the outputs from all modules. It applies a function of interesection on the sets received at the input. The output is a new set, composed by pairs. Each pair contains an IP address, associated with its percentage of presence. The intersection determines to output only the pairs that are containing IP addresses found in all inputs.

$$u_9(t) = y_5(t) \, with \, y_8(t) \tag{24}$$

$$y_9(t) = y_5(t) \cap y_8(t) = M_{DTF}\{P(IP_k, PP_k) | IP_k \in M_5 \, si \, IP_k \in M_8\} \tag{25}$$

As it was said before, the output of this subsystem is the output of the entire system, like in the formula below:

$$y(t) = y_9(t) \tag{26}$$

In conclusion, lets review the input and output of the system:

$$u(t) = M_P\{PKT_k | k = \overline{1..\mathrm{np}_t}\} \tag{27}$$

$$y(t) = M_{REF}\{P(IP_{kREF}, PP_{kREF}) | kREF = \overline{1..\mathrm{TDIP}_{REF}}\} \tag{28}$$

4 Model for the Validation of Mac Addresses in the Real Time Network Traffic

4.1 General Considerations

After the generation of the reference fingerprints for all the MAC addresses in the network, the system will use those fingerprints in the real time traffic, to distinguish between true or spoofed MAC addresses. Fig. 4 shows this process as a system with an entry *u(t)* and an output *y(t)*.

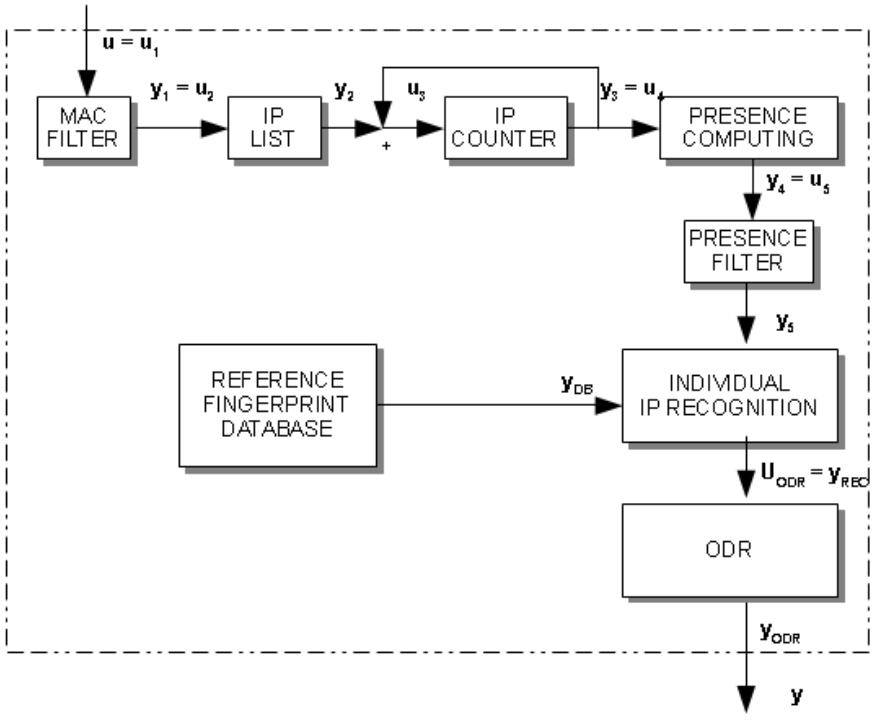

Fig. 4. Real Time validation for MAC addresses

The input *u(t)* can be defined as in (2), like a set of network packets that are captured from the traffic at time *t*:

$$u(t)=M_P\{PKT_k|k=\overline{1..\mathrm{np}_t}\} \tag{29}$$

The output is a percentage value, marked as *ODR*, which represents how much can we trust that the MAC address is or is not what it claims to be.

The first five interconnected subsystems are the same as in the previous chapter. They have the purpose to generate the components of the actual fingerprint, extracted from the real traffic. So, $y_5(t)$ is defined as in (28):

$$y_5(t)=M_{ACT}\{P(IP_{kACT},PP_{kACT})|kACT=\overline{1..\mathrm{TDIP}_{ACT}}\} \tag{30}$$

The Reference Fingerprint Database subsystem will output the previously recorded reference fingerprint as in (28):

$$y_{DB}(t)=M_{REF} \tag{31}$$

In this way, there are two signals of the same kind, M_{ACT} and M_{REF}, which have to be compared in order to generate the Overall Degree of Recognition. They become entries for the Individual IP Recognition subsystem. In here, the percentage of presence value *PP* for each *IP* in M_{REF}, is compared with the correspondent percentage of presence value of the same *IP* in M_{ACT}.

The comparison between the two values can be done in a non ponderated fashion or in a ponderated fashion, as described below. The first one is very simple, but the recognition process is highly influenced by the temporary absence of an IP. The second recognition method improves the performances by considering how important is each IP address in the reference fingerprint.

4.2 Unweighted Recognition

In this case, the output y_{REC} is defined as a set of values RD_i, each of them representing the recognition of one IP address from the reference fingerprint. The RD_i value is calculated as a percentage value, by dividing the percentage of presence of the actual fingerprint with the corresponding value in the reference fingerprint, if the percentage of presence in the actual fingerprint is less or equal with the corresponding value in the reference fingerprint. If not, the RD_i value is considered as 100%. The reason behind this is the fact that DTF Method seeks to find if an IP exists or not. This is why, if the percentage of presence in the actual fingerprint is higher than the one in the reference fingerprint, RD_i value is considered 100%.

$$y_{REC}(t)=M_{REC}\{RD_k,k=\overline{1..\mathrm{TDIP}_{REF}}\} \tag{32}$$

$$RD_k=\begin{Bmatrix}\dfrac{PP_{kACT}}{PP_{kREF}},if\ PP_{kACT}<PP_{kREF}\\ 100,if\ PP_{kACT}\geq PP_{kREF}\end{Bmatrix} \tag{33}$$

The Overall Degree of Recognition is computed as in (34):

$$ODR = \frac{\sum_{i=1}^{TDIP_{REF}} RD_i}{TDIP_{REF}} \tag{34}$$

This ODR value is very simple to obtain, but small variations or even temporary absences, will bring to big variations of the ODR value. As a consequence, the recognition process can be affected and false alarms could be raised.

4.3 Weighted Recognition

In this case, the performances are improved by considering the importance of every IP destination in the reference fingerprint. Each component of the fingerprint is accopained by a different percentage of presence. If a destination with a high level of presence is absent, is worst than the case when the percentage is small. That is why, the weighted version of the recognition calculates a level of importance for each IP destination and then generates the Overall Degree of Recognition.

$$WVAL_k = \frac{\sum_{i=1}^{TDIP_{REF}} PP_{iREF}}{TDIP_{REF}} * PP_k, k = \overline{1..\mathrm{TDIP}_{REF}} \tag{35}$$

$$WRD_k = WVAL_k * RD_k \tag{36}$$

$$y_{REC}(t) = M_{REC}\{WRD_k, k = \overline{1..\mathrm{TDIP}_{REF}}\} \tag{37}$$

The Overall Degree of Recognition is computed as in (38):

$$ODR = \frac{\sum_{i=1}^{TDIP_{REF}} WRD_i}{TDIP_{REF}} \tag{38}$$

5 Conclusions

As final conclusions, this paper represents a mathematical and systemic view of DTF Method. Implementing the method in this way, allows a detailed study and understanding of the main features.

The entire functionality of DTF Method was described as a black box system, composed by a set of subsystem, each of them having an entry and an output. The entries and outputs are explained using mathematical formulas. Every detail can be easily described and comprehended. From the initial set of network packets, the data is filtered and processed step by step, leaving at the end only the IP addresses that can be part of the reference fingerprint. Each IP address is accompanied by the percentage of presence in the traffic.

The identification in real time is based in the first place on the database containing all the reference fingerprints that were generated, and in the second place, based on the actual fingerprints taken from the actual traffic. The modeling of the process shows how the Overall Degree of Recognition is calculated.

All future work in this area can be adapted to develop the mechanisms described in this paper. Each new facility will add new subsystems in the main scheme and will adjust and improve the performances of DTF Method.

References

1. Sasu, E.C., Prostean, O.: Using Constant Traffic to Specific IP Destinations for Detecting Spoofed MAC Addresses in Local Area Networks. In: IEEE International Joint Conferences on Computational Cybernetics and Technical Informatics, Timisoara, Romania, pp. 677–681 (2010)
2. Sasu, E.C., Prostean, O., Groza, V.: Proving the Efficiency of DTF Method in a Local Area Network. In: IEEE International Joint Conferences on Computational Cybernetics and Technical Informatics, Timisoara, Romania, pp. 683–687 (2010)
3. Sasu, E.C., Prostean, O.: Testing DTF Method for Applicability in a Real Environment. In: 7th IEEE International Symposium on Applied Computational Intelligence and Informatics, Timisoara, Romania, pp. 285–289 (2012)
4. Sasu, E.C., Prostean, O.: Network Simulation for MAC Spoofing Detection, using DTF Method. In: 7th IEEE International Symposium on Applied Computational Intelligence and Informatics, Timisoara, Romania, pp. 291–296 (2012)
5. WinPcap driver, `http://www.winpcap.org/`
6. Bratus, S., Cornelius, C., Kotz, D., Peebles, D.: Active Behavioral Fingerprinting of Wireless Devices. In: WiSec 2008, Alexandria, Virginia, USA, pp. 56–61 (2008)
7. Wang, H., Jin, C., Shin, K.G.: Defense Against Spoofed IP Traffic Using Hop-Count Filtering. IEEE/ACM Transactions on Networking 15(1), 40–53 (2006)
8. Loh, D.C.C., Cho, C.Y., Tan, C.P., Lee, R.S.: Identifying Unique Devices through Wireless Fingerprinting. In: WiSec 2008, Alexandria, Virginia, USA, pp. 104–115 (2008)
9. Jana, S., Kasera, S.K.: On Fast and Accurate Detection of Unauthorized Wireless Access Points Using Clock Skews. In: MobiCom 2008, San Francisco, California, USA, pp. 46–55 (2008)
10. Wei, W., Suh, K., Wang, B., Gu, Y., Kurose, J., Towsley, D.: Passive Online Rogue Access Point Detection Using Sequential Hypothesis Testing with TCP ACK-Pairs. In: IMC 2007, San Diego, California, USA, pp. 365–378 (2007)
11. Brik, V., Banerjee, S., Gruteser, M., Oh, S.: Wireless Device Identification with Radiometric Signatures. In: MobiCom 2008, San Francisco, California, USA, pp. 46–55 (2008)

Contribution to Watermarking Techniques

Crina Rațiu[1], Dominic Bucerzan[2], and Mihaela Crăciun[2]

[1] Daramec SRL, Arad, România, Sofronea FN
ratiu__anina@yahoo.com
[2] "Aurel Vlaicu" University of Arad, Faculty of Exact Sciences,
Department of Mathematics-Informatics, România, 310330 Arad, 2 Elena Drăgoi
dominic@bbcomputer.ro, qbt@rdslink.ro

Abstract. The development of computers technology and the Internet has helped the expansion of various methods for creation and distribution of digital media content. Information in transit through the Internet is vulnerable, so the importance of reducing the chance of the information being stolen during the transmission is being a real issue. Data can be accessed, altered and deleted without proper authentication and authorization. There are various security technologies that enhance the security of digital media. This paper provides a comprehensive idea about the technology most widely used to prevent illegal copy or reproduction of digital content, namely watermarking.

Keywords: digital watermarking, hash function, cryptography.

1 Introduction

The development of nowadays communication technologies is a result from the increasing use of the Internet and e-Commerce. Despite this, we still cannot have 100% copyright protection and authentication of digital content. Digital information surrounds us leading to the development of several techniques for protecting digital content. Among these methods we can find encryption and watermarking. The target of encryption schemes is to protect digital data during their transition through the network. Marking techniques may complement encryption by placing a signal in the original data to ensure their origin. The fallowing characteristics should define an effective mark: imperceptible, robust, universal, unambiguous, complex, associated key, detection, detection of trust and statistical invisibility.

In this paper we intend to make up a comprehensive idea about this technology and its usage.

2 Marking Techniques – Literature Review

Marking techniques can be divided into two main categories: perceptible and imperceptible watermarking. The imperceptible marking techniques can be classified in: fragile and robust watermarking. The robust watermarking category includes: public

V.E. Balas et al. (Eds.): Soft Computing Applications, AISC 195, pp. 403–410.
springerlink.com

watermarking, private watermarking, "in the field spatial/temporal" watermarking and "in the field transform" watermarking [7].

Perceptible markings create noticeable changes in the original data, when they are incorporated, but it does not prevent them to communicate the original message. Imperceptible watermarks, depending on the application, can be fragile or robust. A weak watermark embedded in an electronic dataset means that any processing will result in unwanted alteration of the data.

In contrast to fragile watermarks, robust watermarks embedded to a dataset are difficult to remove. In the robust marking techniques, there are defined two types of marking systems, namely public and private. Public marking systems for detecting and extracting the watermark are using the marked electronic dataset and a marking key and do not need the original dataset. These systems are less robust in estimating the marking, but the volume of calculation is much lower. Scored dataset and the original dataset are both used in private marking systems for detection and extraction of marking. These systems, although they are more robust, are not suitable in applications that require speed and efficiency.

2.1 Robust, Space Algorithm Proposed by A. Tefas and I. Pitas

This algorithm works in space. This means that costly processing (time for calculations) is not needed for the inclusion of the watermark. Brightness values (L (x, y) ϵ {1, ..., L}) or the red, green and blue (r (x, y), g (x, y), b (x, y) - Red Green Blue) are directly manipulated [4]. Watermark W is a ternary image with pixel value {0, 1 or 2}. These values are generated using digital key K. Watermark insertion is made by modifying the pixel value of the original image:

$$P'(x,y) = \begin{cases} P(x,y), if\ W(x,y) = 0 \\ E1\big(P(x,y), IN(x,y)\big), if\ W(x,y) = 1 \\ E2\big(P(x,y), IN(x,y)\big), if\ W(x,y) = 2 \end{cases} \quad (1)$$

Where: P - original image (grayscale), (x, y)-location of a pixel, P '- image with watermark, IN - image neighborhood, E1 and E2 - functions for the inclusion of a watermark defined as follows:

$$\begin{aligned} \text{E1 (P,IN)} &= (1-\text{a1}) \bullet \text{IN(x,y)} + \text{a1} \bullet \text{P(x,y)} \\ \text{E2 (P,IN)} &= (1-\text{a1}) \bullet \text{IN(x,y)} + \text{a2} \bullet \text{P(x,y)} \end{aligned} \quad (2)$$

Where: a1 > 0, a2 < 0, scaling constant.

The multiplying by (1 - a1) in scaling IN's value is used to ensure that the value P' of the image with watermark will not overcome the maximum value for a representation of the image, 8 bits, corresponding to a white pixel. The value of a neighborhood pixel is calculated as the arithmetic mean of its neighboring pixel values in the original image, for a given value of neighborhood radius r. For ex-ample, if r = 1, then the value is calculated as follows:

$$IN(x,y) = \frac{P(x+1,y)+P(x+1,y+1)+P(x,y+1)}{3} \quad (3)$$

2.2 Other Algorithms

The watermark algorithm proposed by G.C. Langelaar consists of a bit string. The algorithm manipulates the pixel brightness, in blocks of 8 x 8 pixels. Thus we get XY/64 possible locations (XY is the number of pixels in the image). No qualitative selection is made among the possible locations which are randomly selected. It creates a binary model, pseudorandom size 8 x 8 pixels, which will be used for each insertion.

This algorithm proposed by Ingemar J. Cox, is considered a classic between the watermarking algorithms and was first introduced in 1997 [1]. The image is divided into two parts: the background and the object of interest of the owner. A watermark is then generated by a key. It consists of a series of random real numbers, which are distributed according to a Gaussian curve. Based on the reference image, the selected object is transformed into frequency domain using discrete cosine transformation.

Although watermarking techniques are developing constantly and become more complex, the attacks methods are also increasing. Below we present the main types of attacks that target the watermarking algorithms.

3 Attacks on Watermark

Attackers try to reduce the security of marking system. More precisely they try to reduce the probability of extraction / detection of the original watermark, i.e. to increase the likelihood of extraction / detection of a watermark inserted in a signal that was not marked (false extraction).

3.1 Attacks on the Watermark's Robustness

These attacks change the image pixel values and can be classified into two categories: attacks based on signal processing algorithms and attacks with algorithmic characteristics [6].

The first category includes attacks that use conventional methods of image processing: compression, filtering or scanning. Attacks using methods of video processing to modify images by adding noise are meant to weaken the strength of the watermark. There are currently several software programs that demonstrate the strength of attacks. One of them is UnZig. Image degradation in this case is reasonable, concluding that this attack is particularly effective.

Compression - the most common category of unintentional attack. This method removes insignificant items from a multimedia signal from the perceptual point of view. Thus, by compression, perceptually similar signals come to be identical. Filtering - marks the signal like an additive noise, which is a reasonable assumption for transparent marking spread spectrum type. Removing the marking is equivalent to a problem of disposal of a noise from an image, resulting in an estimation of the original image.

Random Noise - introduces imperceptible distortions even at high signal per noise of 20 dB, but the impact on the detection of the watermark is insignificant.

Attacks on cryptographic security - cryptographic security refers to the integrity of the semantics marking and to the authentication to ensure confidentiality to robust marking. Attacks on cryptographic security are illegal attacks. The second category includes algorithmic attacks witch speculate the weaknesses of insertion or detection algorithms. Attacks, such as cryptographic attacks, have as target the cryptographic components from the transparent marking system. They use standard methods of cryptanalysis to attack the system: brute force search for the inserted message or key search.

Estimation attacks - in these cases, watermark or the host signal is estimated without knowing the secret key, but with information about the statistical of the watermark, and of the host signal. These attacks are applicable when the marking has been inserted into a redundant way, or when there are more marked copies available [5].

The re-modulation attack - with an estimated watermark an attacker can re-modulate the image: the estimated watermark (negative modulation) is extracted from the marked image. In the case of a correlation detector, this action cancels the positive correlation, provided the watermark is similar to the original. On the other hand, by extracting an amplified version of the estimated watermark, the detector using the correlation will fail to find the watermark in the marked image.

Attacks using multiple marked copies (multiple-copy) - occur when the host signal is the same, and the marking is different. Essentially, these attacks are collision attacks [3]. There are two main approaches: signal processing and information encoding. In a collision attack, a coalition of pirates who have different versions of multimedia products, examine different copies in the hope of creating a new signal that is not tied to any one of them. There are several types of collision. One method consists in synchronizing the marked copies differently and mediating them, which is a simple example of linear collision. Another collision attack is called "copy-and-paste", in which attackers assemble parts cut from their copies, resulting in a new signal.

3.2 Attacks on Watermark's shape

The attacks on the presentation differ from the previous. The purpose is not to eliminate the watermark, but to change it so that a detector cannot find it. Examples of such attacks are: rotation, minimize, maximize, affine transformations in general [6].

The mosaic attack - divides the signal as if it is displayed as an entity, but marker detection is not possible. This is called a Stirmark attack. An example of such an attack was given by Petitcolas (Cambridge University Computer Laboratory). The attack is to divide an image into smaller parts. These parts will be assembled on a Web page using HTML. An intelligent agent responsible for searching the network for watermarked images will find only blocks of images which are too small to constitute a watermark. The attack does not cause a degradation of image quality because the pixel values are preserved.

Geometric attacks – try to desynchronize the detector in such a way that the detector cannot find the watermark. Examples of geometric attacks: translation, rotation, resizing (scaling) and their combinations; nonlinear image curving.

3.3 Attacks on the Interpretation of the Watermark's Presence

This attack consists in the creation of another watermark by the cyber attacker and the insertion of that watermark into the image. The newly created Watermark will have the same intensity and shape with that of the owner. In this situation, a correct decision cannot be taken regarding the property of that image [6].

Attack of ambiguity or inversion / reversion - The attacker extracts its own watermark from the watermark signal, resulting in a pseudohost signal, which when used in informational detection, will allow detection of the attacker's watermark. So we are faced with the uncertainty regarding the identity of the copyright owner. To protect copyright, the markings must not be reversible. In other words, an attacker should not be able to extract a watermark from the original multimedia signal. A solution to this problem is to make the watermark addicted to the original signal by means of one-way function (no inverting).

Copy Attack - estimates the marking from a marked signal and inserts it into another signal, called the target signal. This type of attack can be applied if the target signal can be produced without knowing a valid marking system for marking or key. Again, the marking signal depending on the original signal may be resistant to copy attack.

Attack of the multiple marking - the marked image will be marked again with another watermark algorithm. The question that rises is: which was the first watermark? A possible solution would be to generate time-stamped watermarks. Possible solutions against these types of attacks are the establishment of some rules for the construction of the marking system, to combat the known ones, such as using noninvertible marks in the case of ambiguity attack.

3.4 Attacks by Law

These types of attacks are of a completely different nature than those described above. Attacks by law may involve existing or future laws of copyright and ownership of digital images, data interpretations of laws, the owner and the credibility of the attacker, attacker's ability to spread doubts about a scheme of watermark in a courtroom and so on. One should also consider other factors such as financial strength of the owner or the attacker that the experts brought in as witnesses, the competence of judges involved in such trials.

Nowadays it is more popular to use compression with loses in the preparation of digital images via electronic data transmission. JPEG is most commonly used, but the wavelet methods are to replace TCD methods in the near future [6].

4 Contribution to Watermarking Techniques

To increase the security of electronic data against deleting or replacing, we drew some conclusions comparing the invisible watermarking algorithm proposed by A.Tefas and I. Pitas implemented in Delphi environment by A.Benczik and D. Bucerzan in [7] and the solution presented by C.Ratiu and D.Bucerzan at SICOMAP2010 which proposes a digital watermark completed by a hash function implemented in JAVA [6].

In order to reduce the threats that aim digital information and to increase the security of transactions of electronic data, C. Ratiu and D. Bucerzan have designed an application which marks an image through a watermark technique which is secured by a hash function which uses the MD5 algorithm. In order to reach the above mentioned goals, JAVA has been chosen as the environment programming language, because it has been designed for a complex environment like the internet.

Fig. 1. The loaded image – marked with double intensity watermark and the digest code obtained after having applied the hash algorithm

As seen in Figure 1, after loading an image, the hash cod is processed. The user can select which watermark to use from the main menu of the program. In the next step the image is marked with the selected watermark. Finally the hash code for the watermarked image is processed. It can be observed that a different digest code is obtained.

To implement the Pitas algorithm, the Borland Delphi programming environment was chosen. Delphi is a software development environment based on components, facilitating rapid development of highly efficient applications based on Microsoft Windows and requires only minimal code writing. Delphi class library is a solution for the traditional Windows programming requirements, sparing us of complicated and often repetitive programming [2].

As seen in Figure 2, taking advantage of the opportunities offered by the Delphi environment, we will use the application to see an image selected by the user. In the next step the user chooses a key needed to mark the image. To show that the two images are not identical, we create the difference image.

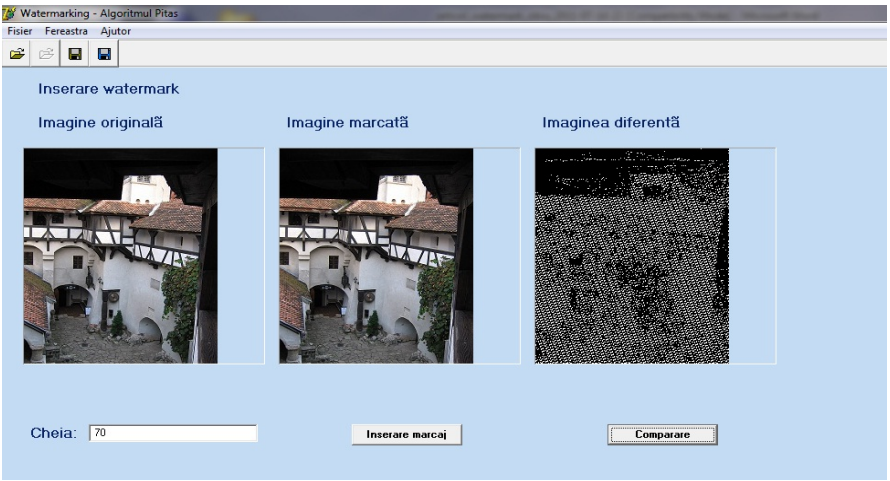

Fig. 2. Pitas algorithm implemented in Delphi

5 Conclusions

The watermarking technique is a complex one and it must take into consideration a series of elements and concepts from other fields such as cryptography, authentication, steganography, human perception, data fusion, and communication through unsecure channels.

Many studies of research, reviewed analysis and publications are needed in the future in the field of watermarking because it has a positive impact on ensuring the authenticity and originality of shared information into computer networks.

The main advantage of our solution implemented in Java (presented in the rows above) is the cancelation of the keys issue, issue that is present in the Pitas algorithm. This is solved by applying a HASH cryptographic function to the marked image. This process increases the degree of protection of image by ensuring its authenticity.

After comparing the results obtained from the presented applications we can say that the Pitas algorithm implemented in Delphi is faster than the visible marking algorithm proposed in Java. This is due to the facilities of mending the images in Delphi environment such as the drawing canvas and its pixels property. The main disadvantage of the application made in Delphi is that it can process only files of BMP type; the application implemented in Java can process different types of images. A disadvantage of Java solution is the fact that it has a longer execution time than the Pitas algorithm. In the future work we intend to apply steganography techniques to encompass the hash code into the image file.

By using these techniques of perceptible or imperceptible marking, many cases in which the copyright is either violated or doubtful, can be clarified or even avoided. This technique proves to be useful if the multimedia document is used in medical applications, commercial transactions, evidence in court, etc. The electronic data must be first of all authenticated, and then a test will be made upon its integrity. Watermark can authenticate the electronic data.

Acknowledgments. This paper would not have been written without the help of several colleagues who offered their knowledge and unconditional support. Also special thanks to the family and best friends who have always been there for us.

References

1. Cox, I.J., Killian, J., Leighton, F.T., Shamoon, T.: Secure Spread Spectrum Watermarking for Multimedia. IEEE Transactions on Image Processing 6(12), 1673–1687 (1997)
2. Delphi User's Guide, Delphi for Windows, Borland International (1995), http://zeus.nyf.hu/~bajalinov/my_special/SW/Delphi%20eBooks/Delphi/Delphi%20-%20Delphi%20User%27s%20Guide%20-%20Delphi%20for%20Windows.pdf
3. Naforniță, C.: Creşterea securității rețelelor de comunicații de date prinautentificarebazatăpe watermarking. Research report, UniversitateaPolitehnica, Timişoara (2006), http://shannon.etc.upt.ro/corina/TR-corina-06.pdf
4. Tefas, A., Pitas, I.: Robust Spatial Image Watermarking Using Progressive Detection. In: Proceedings of the IEEE International Conference on Acoustics, Speech, and Signal Processing, CD-ROM, Salt Lake City, Utah, USA, vol. 3, pp. 1973–1976 (May 2001)
5. Bucerzan, D., Benczik, A.: Protecția dreptului de autorasupra produselor multimedia. Tehnici de Watermarking, Dissertation Report, Universitatea Aurel Vlaicu, Arad (2008)
6. Bucerzan, D., Ratiu, C.: Attacks on the Watermark Techniques. In: The Second Symposium on Business Informatics in Central and Eastern Europe, Cluj Napoca, pp. 235–245 (2011)
7. Solachidis, V., Pitas, I.: Optimal Detector for Multiplicative Watermarks Embedded in the DFT Domain of Non-White Signals. EURASIP Journal on Applied Signal Processing, 2522–2532 (2004)

Android Personal Digital Life Software Agent

F. Khan and A. Altaf

Department of Software Engineering,
University of Engineering and Technology Taxila, Pakistan
fahad.khan@uettaxila.edu.pk, amnaaltaf66@yahoo.com

Abstract. Evolution in mobile technology has entailed development of thousands of application every week. Android being one of the dominant mobile platforms provides vast number of efficient, fast, user friendly apps. This paper has reviewed and analyzed an android application which aims at all the android users and /or web users who are paving their way to digitize their life style. Considering the eminence and importance of the Android Operating System, we planned to device Digital life software agent that provides you with the opportunity to capture ideas, experiences and inspirations. In addition to making it easy to remember things; it lets you perform day-to-day activities, big and small using your computer, phone, tablet and the web by note taking. It is mainly developed for the Android OS installed smart phones and is accessible from website too. There are many applications that offer features similar to the Digital life application like Catch Notes, Tap Note and Personal Assistance but this is a complete feature-packed application that supports additional feature for better functionality that helps users to organize their daily life applications, setting remainders, alarms and memos.

Keywords: Digital Life software agent, Android, synchronization.

1 Introduction

Android market is full of attractive android applications that lets the user take notes and manipulate them according to customized needs. However, they lack the diversity as they limit the users to digitizing their typed notes only. With Digital Life software agent, you can store all your memories in computer, phone and device you use. Here "note" can be a piece of formatted text, a webpage copied excerpt, a photograph, a voice memo, or an audio clip.

"Digital Life" is a life-organizer which provides users with an ability to digitize almost everything and watch it as it instantly synchronizes from your Android device to Web. It allows content posting and management only by authenticated users (Members). All of your notes, audio clips, files and images are made available on every device (phone or tablet) and computer you use via web. Notes can be added, edited, deleted or searched as part of E-Notes, E-Music and E-Photo Gallery. In addition, the suite contains a "Digital Secretary" that helps you organize your daily life applications, setting reminders, alarms and memos. This stack enables you to keep all itineraries, travel schedule, and meeting plans along everywhere, so you'll have them when you need. Currently, "Digital Life" supports android and Web operating

V. E. Balas et al. (Eds.): Soft Computing Applications, AISC 195, pp. 411–420.
springerlink.com

system and also offers online synchronization and backup. This android based application is aimed to be designed efficiently both in terms of user interface (UI) and source code.

Different technologies are used in applications like REST(Representational state transfer), SQLite and XML(Extensible Markup Language), Google Map direction API, and Android framework etc. Services that utilize Web services standards, e.g., Universal Description Discovery and Integration registry (UDDI), Web Services Description Language (WSDL) and Simple Object Access Protocol (SOAP) are the most popular type of services available today. We preferred using SOAP(Simple Object Access Protocol) web services for our application [1]. In order to understand the processes involved in creating and consuming web services we went through the book "Professional ASP.NET Web Services". It involves the case studies that helped us to get the concept of web services application and the core standards to Web Services architecture that are integrated into ASP.NET [2].

Also, we reviewed the IBM research report which thoroughly introduces the basic understanding of Web services, discuss the levels of service integration, and also focus on the technical problems that may arise for the developer of webservices in the future [3].

Research has been carried out and purpose of this review was to critically ana- lyze the existing android applications and compare their different aspects with the "Digital life" application. Android has been in the limelight among the developers across the globe. Android is a Linux-based platform; consisting of the operating system, middle-ware, and user interface and application software [4]. Considering the tremendous growth of the platform, we market survey for the need of various applications among the users and planned on developing "Digital Life" application.

Research has revealed many applications (free and restricted both) that helps user generate and manage notes [5]. But unlike these applications (AK Notepad, Evernote, ColorNote, SpringPad Catch Notes, GDocs, GooMemo, OI Notepad) [6] it embeds many rich functionalities together that lets the user to take notes (text /voice), capture photos, record memos, set reminders and alerts, and makes these notes completely searchable .Our product is specially designed for those people who want to keep themselves organized, save ideas and improve productivity. Some challenges like data consistency are also addressed using webservices [7].

The information relevant to the development of android applications was reviewed and analyzed using secondary data sources like the book "Hello, Android: Introducing Google's Mobile Development Platform" progresses from less advanced to the more advanced topics giving us the key concept of android basics to Sqlite database and web services [8], [9].

And the online help through the site The Developer's Guide - Android Develop- ers which holds the extensive documentation on android platform provides various useful tutorials and lets you to discuss your topic with other developers on android forum [10].

2 System Description

This section briefly describes the detailed design of the components that are assembled to make Digital Life's architecture. The complete structure of the application is graphically shown in Fig. 1. Our application consists of mainly three parts:

1. A host website that maintains user data on web by managing database server.
2. An android application that stores and retrieves user data in Digital Life's database which is a local SQlite database on android device for each user.
3. Finally a middle ware that keeps the data on local database (i.e. phone) consistent with the web data for specific user account by using SOAP (Simple Object Access Protocol).

In this paper we discuss different phases for Digital Life's architecture. The first phase Registration via website for an account in Digital Life returning a unique username and a password activated via automatic email delivery of the user specified account. Second phase is of database management on the Server and managing individual user database on android device. Third phase includes interface designing for the website and Android OS. Fourth phase is data synchronization between android and web databases. Finally, fifth phase comprise of the distinct features of Digital Life software agent.

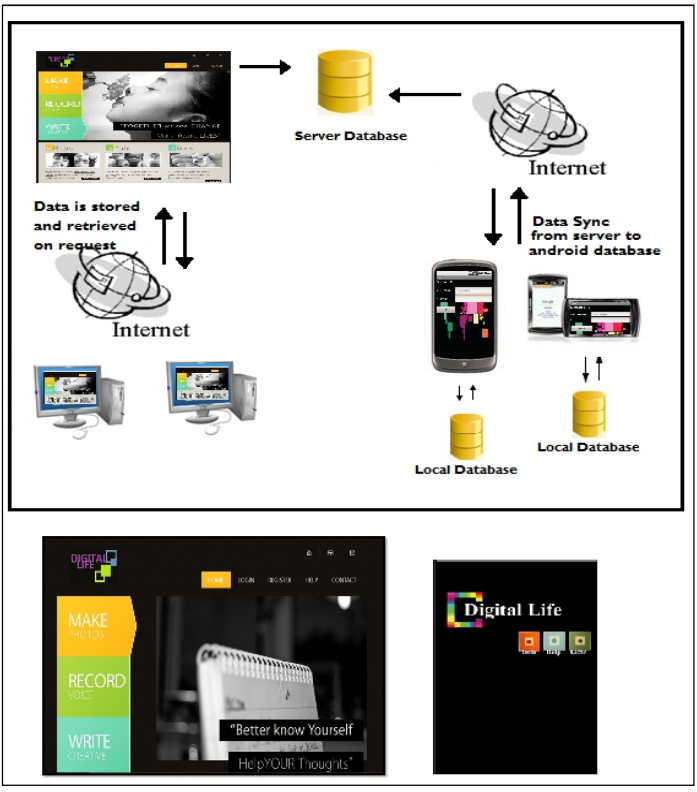

Fig. 1. System Layout

2.1 Database Management

Information of each user is handled on the server. The database manages information of all the registered users of Digital Life. The database has secure access through server login and password and can be updated as and when requested by the user. For each user the record of all the Text, Audio and Photo notes is maintained. The database resides on the Server only and its information is shared by the clients in the network on user request. Another database of the same design is kept on the each android device that has registered for Digital Life.

2.2 Data Synchronization

Digital Life software agent consists of two application one running for web users and other for android users. Digital Life enables user to create account, for the consistency at any time one can sync data from web account to their android devices by providing username and password. Digital Life software agent will verify username and password from the server and sync data from database on the server to user's local database using SOAP (Simple Object Access Protocol). SOAP Web Services are used in lots of enterprise software; for example, Google implements their Web Services using SOAP, with the exception of Blogger, which uses XML-RPC, an early and simpler pre-standard of SOAP [11].

For the data sync a middle layer is established that uses SOAP(Simple Object Access) for data transfer. SOAP(Simple Object Access) is a protocol for transferring messages which has been accepted as the default message protocol in SOA(Service Oriented Architecture) [12]. Messages are created in SOAP by wrapping appli- cation specific XML (EXtensible Markup Language) messages within a standard XML(EXtensible Markup Language) based envelope structure [13]. The result is an extendable message structure which can be transported through most underlying network transports like SMTP (Simple Mail Transfer Protocol) and HTTP [14].

2.3 Implementation

In the implementation se, we describe how different phases within Digital Life software agent are mapped from design to actual application. In this paper we describe each module's basic working via flow charts. And finally, present a few interfaces for illustration of the system.

2.3.1 Registration

A user requests an account on website; he is presented with a registration form. User fills in the entries. The system check the authenticity of each field and validates that user name is unique for each of the user. System must not allow a user with invalid or missing details to continue. Therefore in case of error he is shifted to error page. Registration phase is graphically demonstrated in Fig. 2.

2.3.2 Login

The user types in the correct username and password to log into his account.If there is any mismatch of username and password he will be shifted to error page. Fig. 3 shows the flow chart and interfaces of this phase.

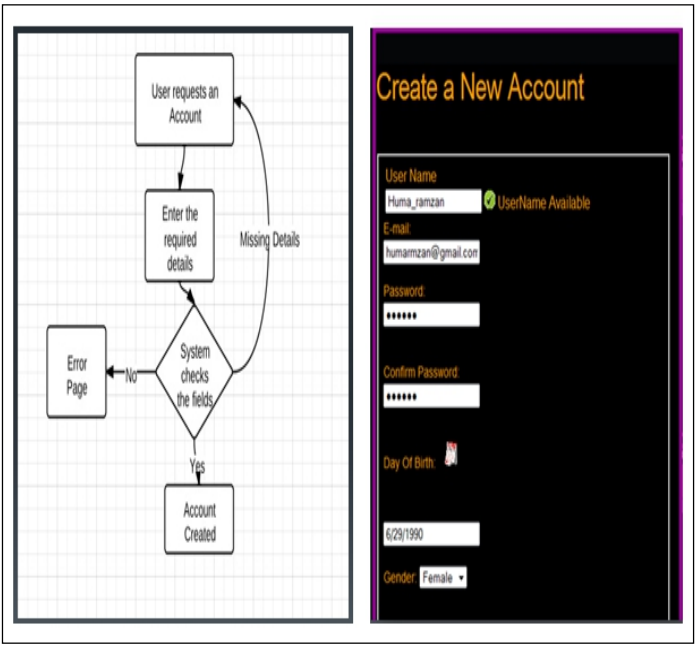

Fig. 2. Digital Life account registration: Flowchart and Interface

2.3.3 eTextNote Module

The user can add a new note by typing in the note name and the note body. He can than open the same date for editing or can delete it if he wants to. The implementation of module is expressed graphically in Fig. 4.

2.3.4 ePhoto

The user can add a new Photo Album by typing in the Album name. He can than open the same Album for adding the photos. After saving the changes he can open the Album in order to delete the individual photos or to edit the caption. He can delete a full Album and all of its pictures together by deleting the Photo Album itself. Module is graphically demonstrated in Fig 5.

2.3.5 eMusic

The user can add a new song to his play list or can create and manage a new play list.as he wants to. Fig. 6 Shows the implementation of module EMusic.

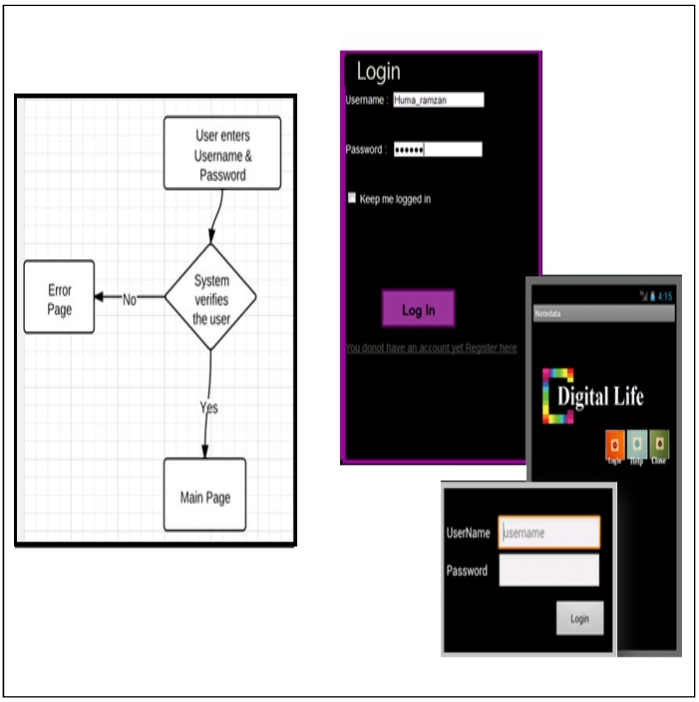

Fig. 3. Login Activity: Flowchart and Interface

2.4 Unique Features

2.4.1 Speech Recognition

Digital Life also integrates the unique feature of text to speech conversion. The working of speech engine in the application is described with the help of flow chart in Fig. 7.

2.4.2 Decision Making Application

Decision making is the study of identifying and choosing alternatives based on the values and preferences of the decision maker. Making a decision implies that there are alternatives based on the values and preferences of the decision maker. Making decision implies that there are alternative choices to be considered, and in such a case we not only want to identify as many of these alternatives as possible but to choose the one that best fits with our goals, objectives, desires, values, and so on.. [15]

The application is present in the e-secretary module of Digital Life, android application. It allows users to choose from the available decision making option that are carefully designed on the basis of generic scenarios like Which Laptop/Cellular Phone/Car one should buy? Or where to hang out this vacations? Or Which Candidate to hire for the job? Also the application allows adequate level of customizability so user can help their thoughts. Fig. 8 shows a flow chart of decision making application.

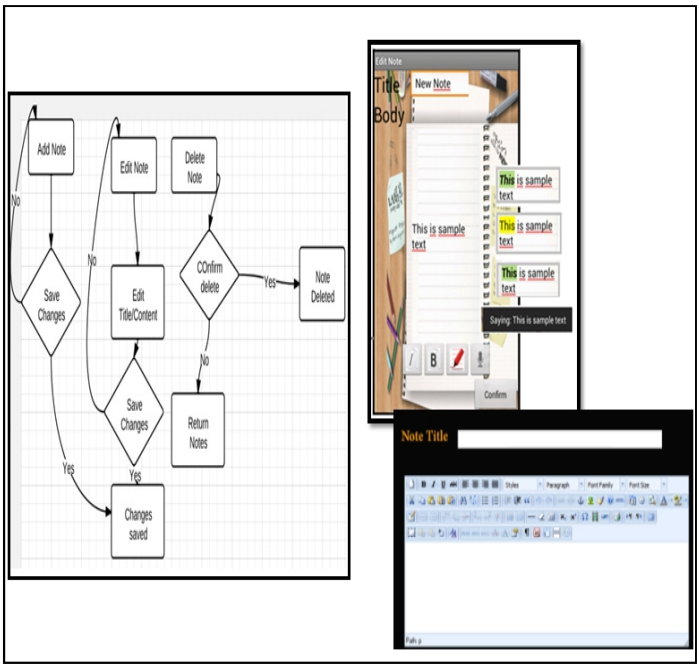

Fig. 4. TextNotes: Flowchart and Interface

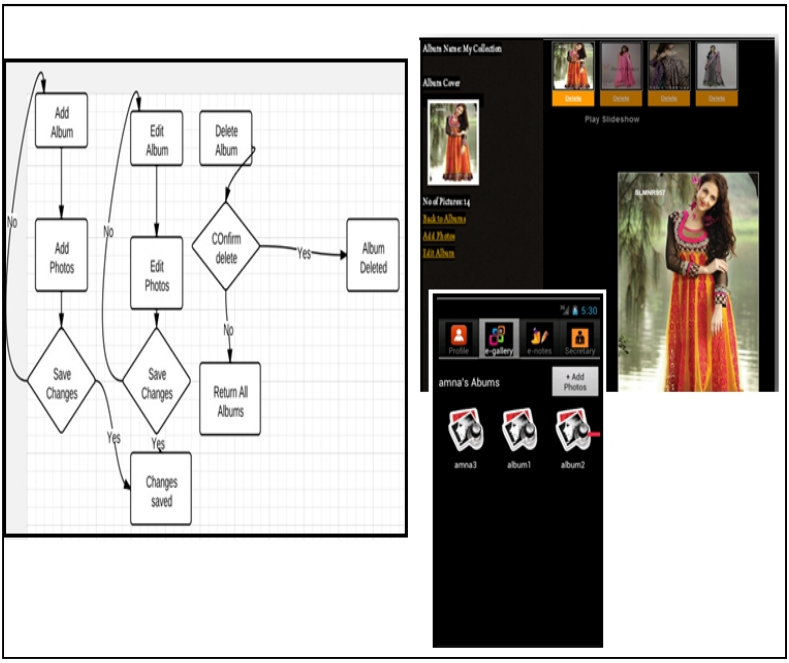

Fig. 5. PhotoGallery: Flowchart and Interfaces

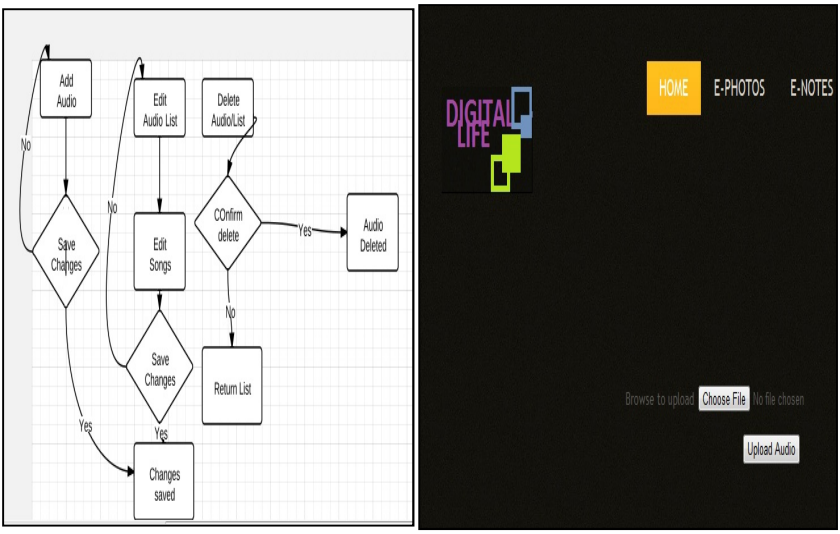

Fig. 6. AudioGallery: Flowchart and Interface

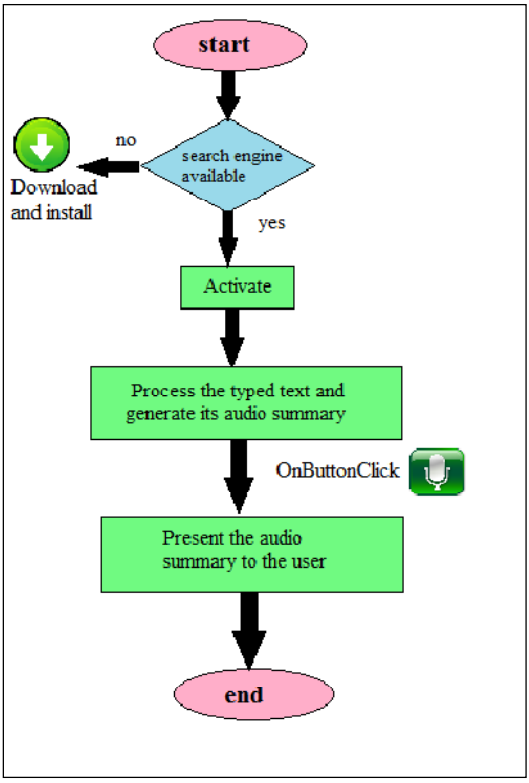

Fig. 7. Flowchart for Speech Recognition Feature of software Agent

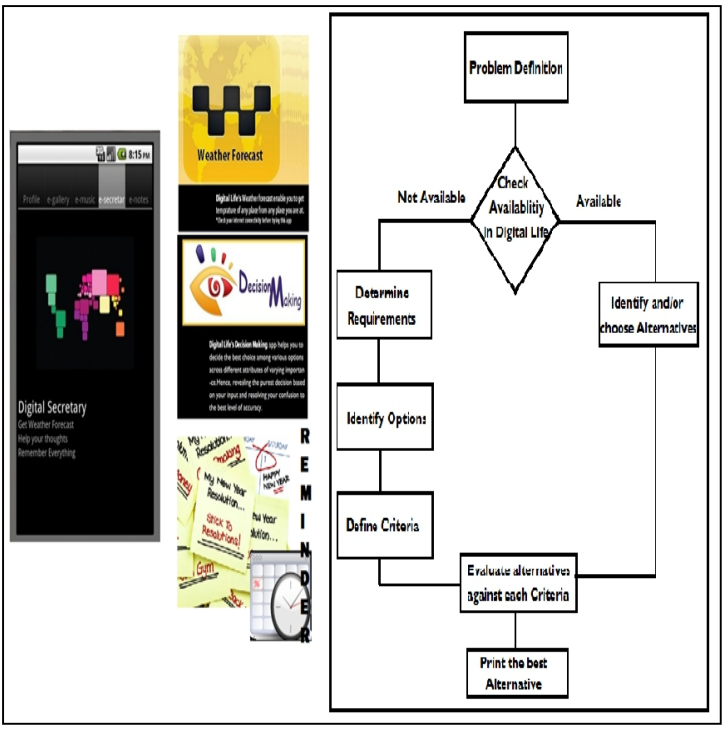

Fig. 8. Digital Secretary and Decision Making app

Currently, Digital Life supports decision making for Multiple Criteria, Multiple Alternative Problems using decision making metric. In future, we are planning to add solutions for the Cost Benefit Analysis problems.

3 Conclusion and Future Work

Digital life App provides users with an ability to digitize everything and watch it as it instantly synchronizes from your Android device to Web. We are keeping the User interface of this application simple as require for conveying functionality and usability of the application.

We are focusing on achieving high modularity of the application since this application is being developed primarily for smart phone that are memory constrained memory requirement and thus optimize application as well as assure better understanding of the code.

References

1. Papazoglou, M.P., van den Heuvel, W.: Service oriented architectures: approaches, technologies and research issues. VLDB Journal 16, 389–415 (2007)
2. Eide, A., Miller, C., Sempf, B., Sivakumar, S., Batongbacal, M., Reynolds, M., Clark, M., Loesgen, B., Eisenberg, R., Bohling, B., Basiura, R., Lee, D.: Professional ASP.NET Web Services. Publishers Wrox Press (2001) ISBN-13: 978-1861005458
3. Arsanjani, A., Hailpern, B., Martin, J., Tarr, P.L.: Web services: Promises and compromises. IBM Research Report (2002)
4. Wu, Y., Luo, J., Luo, L.: Porting mobile web application engine to the android platform. In: Proc. of the 10th IEEE International Conference on Computer and Information Technology (CIT), Bradford (2010)
5. Best note taking apps for android (December 2011), `http://androidapplications.com/apps/lists/best-note-taking-apps-for-android`
6. Android note taking apps review (September 2011), `http://www.ilikespam.com/android-note-taking-apps-review`
7. Leymann, W.F., Roller, D., Schmidt, M.T.: Web services and business process management. IBM Systems Journal 41(2), 198–211 (2002)
8. The developer's guide - android developers (May 2012), `http://developer.android.com/guide/index.html`
9. Hoffer, J.A., Prescott, M., Topi, H.: Modern Database Management, 9th edn. Publishers Prentice Hall (2008) ISBN-13: 978-0136003915
10. Burnette, E.: Hello, Android, Introducing Google's Mobile Development Platform, 2nd edn. Publishers Pragmatic Bookshelf (2009) ISBN-13: 978-1934356494
11. Castillo, P.A., Garcia-Sanchez, P., Arenas, M.G., Bernier, J.L., Merelo, J.J.: Distributed evolutionary computation using soap and rest web services. In: First International Symposium on Distributed Evolutionary Computation in Informal Environments, pp. 1–20 (2011)
12. Erl, T.: SOA Principles of Service Design. Publishers Prentice Hall (2007) ISBN-13: 978-0132344821
13. Kanneganti, R., Chodavarapu, P.: Soa security in action. Manning Publications Co., Greenwich (2007)
14. Knutsen, J.: Web service clients on mobile android devices. Master thesis Norwegian University of Science and Technology (2009)
15. Fulop, J.: Introduction to decision making methods. laboratory of operations research and decision systems. Computer and Automation Institute, Hungarian Academy of Sciences (2005)

Characterization of Temperature-Dependent Echo-Shifts and Backscattered Energy Induced by Thermal Ultrasound

Maria Graça Ruano[1], César A. Teixeira[2], and Javid J. Rahmati[3]

[1] CISUC, University of Coimbra and University of Algarve, Portugal
mruano@ualg.pt
[2] CISUC, University of Coimbra
cteixei@dei.uc. pt
[3] University of Algarve, Portugal
rjavid@csi.fct.ualg.pt

Abstract. Existence of accurate temporal-spatial temperature models, which would enable non-invasive estimates, will promote ultrasound-based thermal therapy applications. These models should reflect the tissue temperature with a maximum absolute error of 0.5 ºC within 1 cm^3.

In-vitro experiments have been developed to evaluate the temperature variations induced by standard ultrasound therapeutic device emitting continuously on gel-based phantom and on pork meat tissue using three different emitting intensities (1, 1.5 and 2 W/cm^3). Temperature estimates were performed based on raw RF data collected using a second ultrasound transducer (imaging transducer). This second transducer worked in pulse-echo mode, and was placed perpendicularly to the therapeutic transducer. In order to access the quality of the estimates, temperatures were acquired by five and by two thermocouples placed in the gel-based phantom and on the porcine sample, respectively. At every 10 seconds the temperature and one RF-line is stored in a PC for future processing.

The possibility to estimate temperature was assessed by considering two RF-line features: temporal echo-shifts produced by changes in speed-of-sound and medium expansion/contraction and by changes on the backscattered energy originated by medium inhomogeneities.

On one hand, results prove that echo-shifts correlated with temperature in both types of medium (phantom and ex-vivo porcine muscle). On the other hand, analyzing the backscattered energies one may conclude that this measures correlates with temperature in the porcine sample and not on the phantom. This led us to conclude that the developed phantom is not appropriate for studying changes on backscattered energy with temperature. Energy analysis of the porcine sample confirms the non-uniform temperature variation due to the existence of a heterogeneous media with different sound propagation velocities.

Keywords: tissue temperature estimation, ultrasound echo-shifts, ultrasound backscattered energy, thermal therapy.

V.E. Balas et al. (Eds.): Soft Computing Applications, AISC 195, pp. 421–431.
springerlink.com

1 Introduction

Ultrasound has a long history of diagnostic applications and more recently has been applied as a therapeutic procedure, namely in physiotherapy, hyperthermia, and surgery. The ultrasound non-ionizing nature together with inexpensive and easy-to-use characteristics makes it a very promising modality for non-invasive therapy treatments. Despite the demonstrated capabilities, its extensive usage in thermal therapies still requires detailed studies on spatial-temporal mapping of the ultrasound-induced temperature variations within 0.5ºC in $1cm^3$ volumes [1].

Since the 90's, several works have been published describing non-invasive temperature estimation methods envisaging uniform heating of tumors at therapeutic levels. Suggested methods have as a base: electrical impedance tomography [2], microwave radiometry [3], magnetic resonance imaging (MRI) [4] and backscattered ultrasound (BSU) [5]. From the proposed technologies only the MRI one achieves the desired spatial resolution, being penalized by its cost and the difficulty to use in some therapies [1]. In contrast, the application of BSU presents some advantages: low-cost procedure, good spatial and temporal localization and ease of use. Typical methods of using BSU as non-invasive thermometer include: those who track the echo-shifts produced by changes in sound velocity and medium expansion/compression, the ones which are based on the measurement of the attenuation coefficient, and those that measure the change on backscattered energy [1]. The temperature dependence of the attenuation coefficient is only sufficiently noticeable for temperatures above 50ºC [6] which is not the case of this study.

The study hereby described follows the authors' research in non-invasive temperature estimation (NITE). Previous works were concerned with temporal echo-shifts analysis, employed as inputs of radial-basis-functions neural-networks (RBFNNs), optimized by a multi-objective genetic algorithm. We started testing the NITE model in homogeneous gel-based phantom [7] investigating several operating conditions. Then we developed multilayered phantoms and investigated the performance of the proposed NITE model on the estimation of temperature inside each layer and at their interfaces [8-10]. More recently the temperature has been estimated through analysis of the ultrasound images [11]. Except for this later work, where a bovine muscle sample was employed, all other experiments included gel-based phantoms.

Present work report the temperature evaluations of gel-based phantoms and pork loin samples when these two different tissue mimicking phantoms are subject to ultrasound heating at hyperthermia values. The aim of this study is to compare the performance of two non-invasive thermometer categories, echo-shifts data and changes in backscattered energy, for potential inclusion on the tissue temperature estimation RBFNNs model above referred.

2 Methodology

When tissues are heated, changes in the velocity of propagation of sound in media occur. These changes in association with changes in the attenuation levels induce shifts on the apparent position of the scattering regions and changes on the signal strength [1].

The gel-based phantom experimental setup employed to collect the RF data and compute the echo-shifts and changes of backscattered energy is presented in Fig. 1.

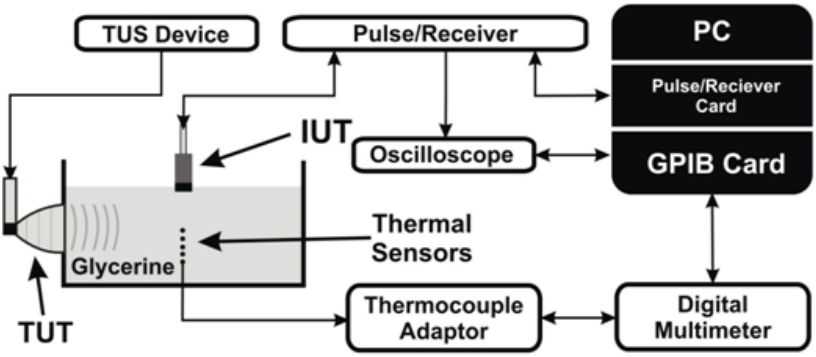

Fig. 1. Experimental setup

The gel-based phantom was emerged in a degassed water tank, in order to discard abrupt room temperature changes and to improve the coupling between the transducers and the medium. The phantom was prepared by mixing (in % weight): 86.5% of degassed water, 11% of glycerin, and 2.5% of agar-agar. The medium was heated by a commercial circular piston ultrasound transducer (Ibramed, Sonopulse generation 2000), used for diathermia purpose. The TUS transducer has an effective radiation area of 3.5 cm^2, and worked in continuous mode at 1 MHz. Three different intensities were applied: 1.0 W/cm^2, 1.5 W/cm^2, and 2.0 W/cm^2. The RF-lines were collected using an imaging ultrasound (IUS) transducer (Panametrics-NDT, V310SU), which worked in pulse-echo mode, driven by a pulser/receiver (Panametrics-NDT, 5800PR). The pulser/receiver sent the analog RF-lines to an oscilloscope (Tektronix, TDS2024) which digitalized it at 50 MHz, and each one is composed by 2500 points. The oscilloscope sent the digitalized RF-lines to a personal computer (PC) via a GPIB bus. In order to measure the temperature five thermocouples were placed 5 cm spaced from the TUS transducer face, as shown in Fig. 2.

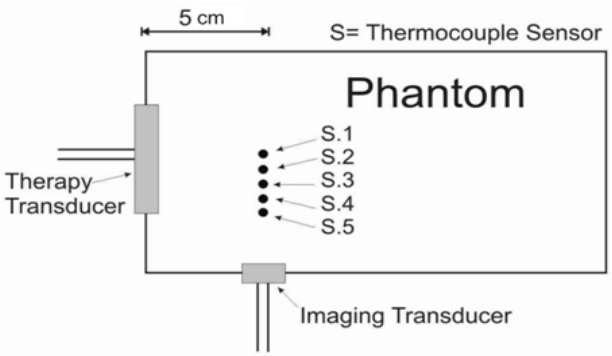

Fig. 2. Thermocouples disposition in relation to the therapeutic and imaging transducers

The thermocouples were 5 mm spaced across the radial line of the TUS transducer. The ultrasound beams were placed perpendicular between each other in order to reduce interference. The thermocouples were connected to a digital multimeter (Keithley, 2700/7700) which had an integrated multiplexer with cold junction compensation (CJC) terminals. As well as the RF-lines, the temperature values were transferred to the PC via the GPIB bus. At each 10 s a RF-line was collected, as well as the five temperature values. The medium was heated only in the first 15 min, then the medium was allowed to cool down to water temperature during more 15 min.

When the pork loin sample was employed, the same general setup was used, except that the ex-vivo sample was allocated inside a plastic box as shown in Fig. 3 and two thermocouples, spaced by 10mm, were placed 42 mm apart from the TUS transducer face.

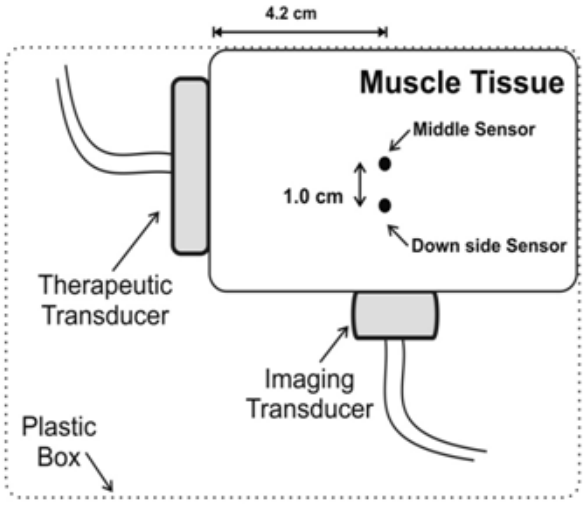

Fig. 3. Location of pork loin sample on plastic box and thermocouples disposition in relation to the therapeutic and the imaging transducers

3 Results and Discussion

As stated earlier, the application of backscattered ultrasound for temperature estimation depends on the extraction of temperature-dependent features from the RF-lines. In this study the echoes originated by the thermocouples were isolated and the temporal echo-shifts (TES) were computed for each spatial point along each experiment trial. The computation of TES was performed following the strategy proposed by [12]. This algorithm estimates continuous time delays from sample data by applying a spline interpolation to a reference signal (in our case the echoes in the first BSU arranged in separated files, according to the related intensity and signal in each experiment trial).

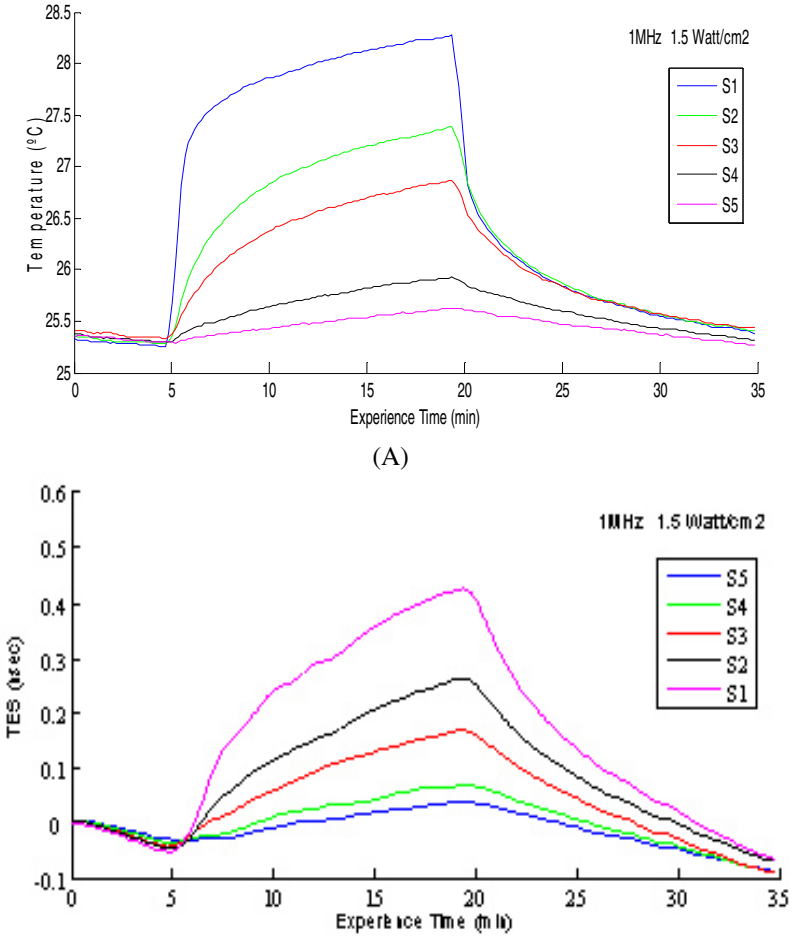

Fig. 4. Example of (A) temperature changes signals and correspondent (B) temporal echo-shifts from gel-based phantom at different locations (See S1, S2, S3, S4 and S5 in Fig. 2)

Fig. 4 enables a comparison between the evolutions of temperature (Fig. 4 (A)) and the temporal echo-shifts (Fig. 4 (B)) calculated at different spatial points. These results were obtained for the gel-based phantom when the TUS was settled to a frequency of 1MHz and a power intensity of 1.5 Watts/cm^2. The first five minutes of the experiment time were record to allow a reference for the rest of the experience, so, in this example one can see that the initial phantom's temperature was 25.35ºC (in S1, the thermocouple closest to the heating source) and at the end of the heating stage (20 minutes after starting) the same sensor had achieved a temperature of 28.28ºC. After 15 minutes of cooling, this point of the phantom presented a temperature of 25.45ºC. From Fig. 4 (B) one can see that the computed echo-shifts show a clear but nonlinear relation with the temperature where the curve increases and decreases with the temperature.

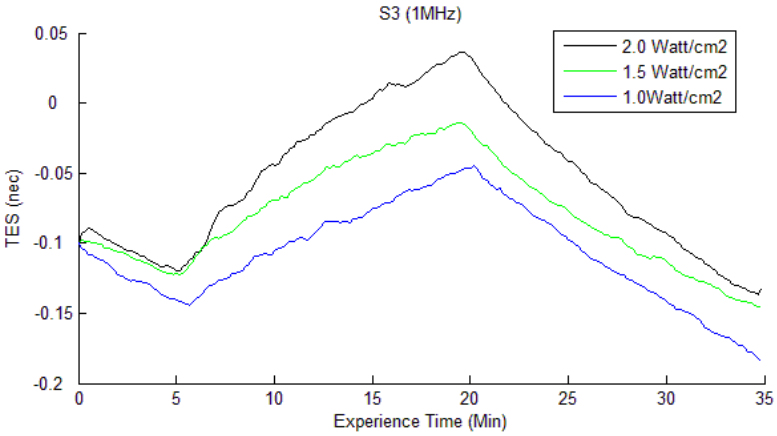

Fig. 5. Comparison of temporal echo-shifts for spatial position of S3 in the gel-based phantom when different power intensities are applied

If we now compare the behavior of the phantom's location of thermocouple 3, identified as S3 in figures) when different power intensities are applied, we obtain the temporal echo-shifts expressed on Fig. 5. From this figure we can see that higher power intensities produce greater temporal echo-shifts as a consequence of correspondent increased temperatures at that position of the phantom. This result is theoretically supported.

In fact if we compare, for different power intensities, the increase in temperature observed for each spatial location during the experiment (see Fig. 6) one can conclude that increased intensities produce higher temperature increases. One can also clearly see that far locations (like S5) are more smoothly influenced by the therapeutic heating than the region close to the heating source (S1). Recall that S5 is just located 20mm distant from S1, the latter located in the axial line at 50mm from the face of the heating transducer. The variation of temperature observed for S5 is less than the temperature resolution internationally recognized as a gold standard for non-invasive temperature estimation. On the other hand, S1 verified a temperature increase of nearly 3ºC in 15minutes of heating. Another interesting conclusion from this figure is that the temperature increase is directly proportional to the power intensity applied.

Similar results were obtained for the pork loin sample. As can be seen in Fig. 7 a nonlinear increase in temperature is observed during heating (from 5 to 35minutes of the experiment time). In this case the effects of tissue heating remained after allowing the tissue to naturally cool during the same amount of time as it has been heated (procedure similar to the one followed with the gel-based phantoms experience). In fact, after 30 minutes of cooling the tissue was still with approximately 1ºC above the initial temperature.

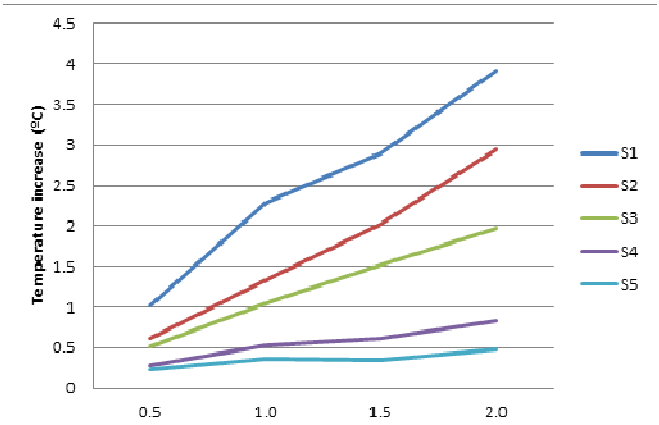

Fig. 6. Temperatures increases measured on the gel-based phantom at each spatial position (S1, S2, S3, S4 and S5 in Fig. 2) as function of power intensities applied

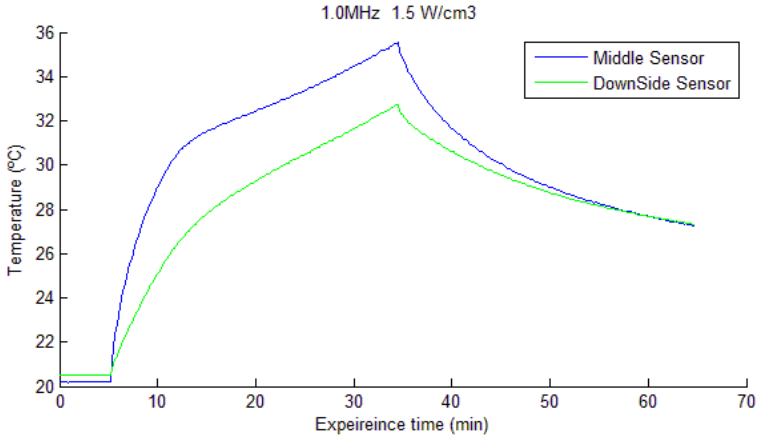

Fig. 7. Temperature changes for signals from pork loin sample at two spatial locations (See Down Sensor and Middle Sensor in Fig. 3)

Fig. 8 shows the comparative behavior of the temperature variation with different power intensities applied to the spatial point located at the axial line of the heating transducer (Middle sensor on Fig. 3). One can conclude that the strength of the effects of heating the tissue is a function of the power intensity applied.

If we observe the temporal echo-shits for the same experimental conditions, (Fig. 9) one can associate the rough curve behavior with the tissue characteristics. The ex-vivo sample employed is generally constituted by muscle fibers, fatness tissue and water-like liquids. These components present different sound velocity propagations and different attenuation factors therefore leading to a combined influence on the collected echo-shifts data.

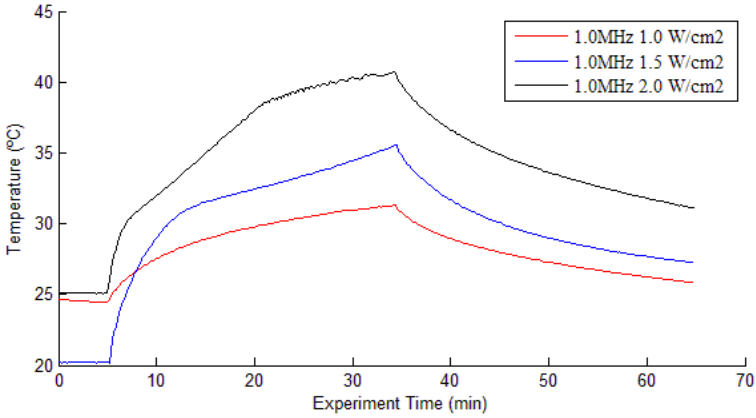

Fig. 8. Comparison of temperatures measured at Middle Sensor (see Fig. 3) when different power intensities are applied to the pork loin sample

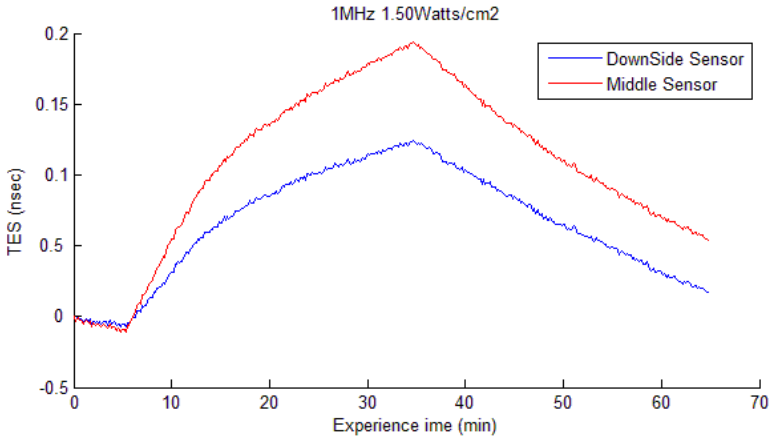

Fig. 9. Comparison of temporal echo-shifts (TES) for both sensors of the pork loin sample

In what concerns the backscattered energy computed from the RF data, one can see from Fig. 10 (A) that the gel-based phantom did not produce results capable of processing the backscattered energy to estimate temperature relationships. However, the pork loin sample example (Fig. 10 (B)) does reflect the heating and cooling phases of the experiment being as so suitable for use on temperature estimation models.

If we in detail the relationship between the backscattered energy and temperature for the pork loin sample example represented in Fig. 11 one can confirm the existence of interference of several tissue characteristics by observing the variability on the localization of the relational points.

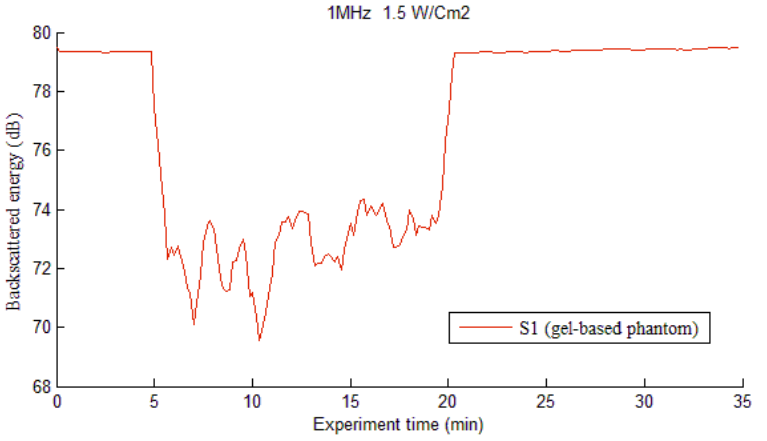

(A)

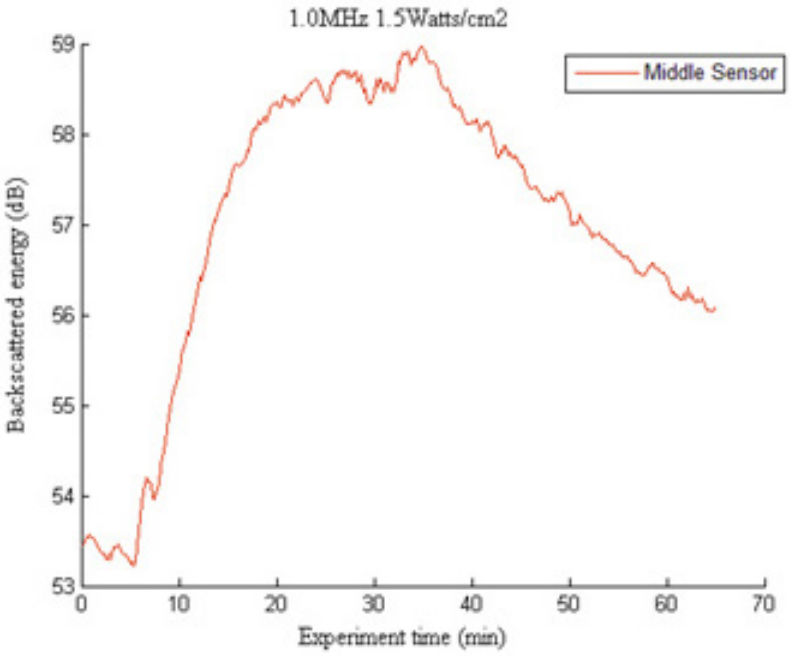

(B)

Fig. 10. Backscattered energy computed from (A) gel-based phantom and (B) pork loin sample at the axial line of the therapeutic transducer (Middle Sensor of Fig. 3), when 1.5 Watts/cm^2 using a 1MHz frequency is applied.

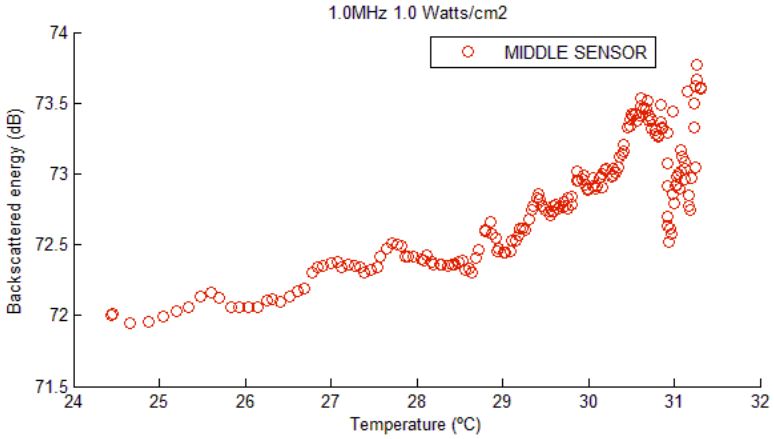

Fig. 11. Relationship between backscattered energy and temperature at middle sensor (see Fig. 3) in the pork loin sample

4 Conclusions and Future Work

The work hereby presented compares the behavior of two categories of methods of non-invasively estimating ultrasound-induced temperature on tissues: the analysis of temporal echo-shifts and the changes in backscattered energy. These methods were tested on two different media, a gel-based phantom and a sample of pork loin subject to different therapeutic ultrasound device operating conditions.

Analyzing the results we may conclude that the estimated temperatures computed from the echo-shifts collected from both the gel-based phantoms and the pork loin samples reflected the increase in temperature induced by the therapeutic transducer. In both media, the echo-shifts presented nonlinear curves as theoretically expected. In the case of the gel-based phantom, a tissue region distanced by 20mm far from the axial line is almost insensitive to 0.5Watts/cm^2 heating intensities. On the other hand, the use of ex-vivo sample of pork loin to mimic human tissues enables us to conclude that the effects of heating remains active on the tissue for longer than the heating period, being more evident as higher power intensities are applied. In what concerns the temperature estimation based on the backscattered energy calculations on the pork loin sample lead to appropriate relations with temperature. The same did not happened with the gel-based phantom were the backscattered energy shown to be insensitive to temperature changes. These backscattered energy results should be considered for inclusion on a future RBFNN-based temperature estimation model.

References

1. Arthur, R.M., Straube, W.L., Trobaugh, J.W., Moros, E.G.: Noninvasive temperature estimation of hyperthermia temperatures with ultrasound. Int. J. Hyperthermia 21, 589–600 (2005)

2. Paulsen, K.D., Moskowitz, M.J., Ryan, T.P., Mitchell, S.E., Hoopes, P.J.: Initial in vivo experience with eit as a thermal estimator during hyperthermia. Int. J. Hyperthermia 12, 573–591 (1996)
3. Meaney, P.M., Paulsen, K.D.: Microwave imaging for tissue assessment: initial evaluation in multitarget tissue equivalent phantoms. IEEE Trans. Biomed. Eng. 43, 878–890 (1996)
4. Hynynen, K., Chung, A., Fjield, T., Buchanan, M., Daum, D., Colucci, V., Lopath, P., Jolesz, F.: Feasibility of using ultrasound phased arrays for mri monitored noninvasive surgery. IEEE Trans. Ultrason. Ferroelectr. Freq. Control 43, 1043–1052 (1996)
5. Simon, C., VanBaren, P., Ebbini, E.S.: Two-dimensional temperature estimation using diagnostic ultrasound. IEEE Trans. Ultrason. Ferroelectr. Freq. Control 45, 1088–1099 (1998)
6. Damianou, C.A., Sanghvi, N.T., Fry, F.J., MaassMoreno, R.: Dependence of ultra-sonic attenuation and absorption in dog soft tissues on temperature and thermal dose. Journal of the Acoustical Society of America 102, 628–634 (1997)
7. Teixeira, C.A., Graça Ruano, M., Ruano, A.E., Pereira, W.C.A.: Non-invasive tissue temperature evaluation during application of therapeutic ultrasound: precise time-spatial nonlinear modelling. In: Kim, S.I., Suh Seoul, T.S. (eds.) IFMBE Proceedings –WC 2006 World Congress on Medical Physics and Biomedical Engineering, Seoul, Korea, August 27- September 1, pp. 70–73 (2006)
8. Teixeira, C.A., Pereira, W.C.A., Ruano, A.E., Graça Ruano, M.: NARX structures for non-invasive temperature estimation in non-homogeneous media. In: Proceedings of the IEEE International Symposium on Intelligent Signal Processing, Alcalá de Henares, Spain, October 3-5, pp. 169–174 (2007)
9. Teixeira, C.A., Graça Ruano, M., Ruano, A.E., Pereira, W.C.A.: A soft-computing methodology for non-invasive time-spatial temperature estimation. IEEE Transactions on Biomedical Engineering 55(2), 572–580 (2008)
10. Teixeira, C.A., Pereira, W.C.A., Ruano, A.E., Graça Ruano, M.: On non-invasive multilayer temperature estimation using soft-computing methods. Ultrasonics 50(1), 32–43 (2010)
11. Alvarenga, A.V., Teixeira, C.A., Graça Ruano, M., Pereira, W.C.A.: Influence of temperature variations on the entropy and correlation of the gray-level co-occurence matrix from B-Mode images. Ultrasonics 50, 2 (2010)
12. Viola, F., Walker, W.F.: A spline-based algorithm for continuous time-delay estimation using sampled data. IEEE Trans. Ultrasonics, Ferroelectrics, Frequency Control 52(1), 80–89 (2005)

On the Use of Artificial Neural Networks for Biomedical Applications

Maria Graça Ruano[1] and António E. Ruano[2]

[1] CISUC, University of Coimbra, and the University of Algarve, Portugal
mruano@ualg.pt
[2] Centre for Intelligent Systems,
IDMEC, IST and the University of Algarve, Portugal
aruano@ualg.pt

Abstract. Artificial Neural Networks (ANN) are being extensively used in many application areas due to their ability to learn and generalize from data, similarly to a human reaction. This paper reports the use of ANN as a classifier, dynamic model, and diagnosis tool. The examples presented include blood flow emboli classification based on transcranial ultrasound signals, tissue temperature modeling based on imaging transducer's raw data and identification of ischemic cerebral vascular accident areas based on computer tomography images. In all case studies the performance of ANN proves to produce very accurate results, encouraging the more frequent use of these computational intelligent techniques on medical applications.

Keywords: biomedical applications, artificial neural networks.

1 Introduction

In this paper we report the use of ANN in practical biomedical applications. ANNs date back to 1940 and since then they have been used in many research and development applications. Since biomedical engineering involves interdisciplinary areas, the development of clinical applications requires the use of state-of-art technology such as the artificial neural networks (ANNs).

The efficiency of ANNs depends on the matching of the type of network and the addressed problem and the suitability of the ANNs parameters as representative of the target goal.

As examples of successful combinations between ANNs types and medical applications we expose the following case-studies: blood flow emboli classification based on transcranial ultrasound signals, tissue temperature modeling based on imaging transducer's raw data and identification of ischemic cerebral vascular accident areas based on computer tomography images.

Short description of the problems to be solved, calling attention to particularities of each case-study is presented in the next section. Summary versions of the NN's employed are included and finally the results are presented.

V.E. Balas et al. (Eds.): Soft Computing Applications, AISC 195, pp. 433–451.
springerlink.com

2 Case-Studies

We focus on three types of problems: classification of different type of emboli within blood flow signals, a diagnostic tool based on CT images and tissue temperature non-invasive estimation.

Transcranial Doppler (TCD) ultrasound is an established method for detecting emboli in the cerebral circulation. The differentiation between gaseous and particulate emboli in cerebral blood flow is clinically relevant because different therapeutics should be administrated. The application of TCD in clinical practice relies on human expertise to detect and classify events in the generated signals, constituting a fastidious and time consuming task. The existence of alternative and preferably software-based automatic detection led to the investigation of the applicability of ANN in emboli classification.

At the time this research was held, several signal processing methods had been proposed in literature, essentially based on signal processing methodologies. To be mentioned, the application of the Wigner distribution [1] where the separation between types of emboli was based on measurements of the sample volume length (given by the product of embolic duration and velocity) against the physical length over which the signal could be detected. Blood velocity measurements are by themselves difficult to obtain with accuracy due to flow velocity dependence on many parameters inducing as so a non-stationary nature. Alternatively researchers applied time-frequency and time-scale based matched-filters like the Wavelet Transform (WT) [2-3] proving that WT were better suited for processing this type of signals. To be also referred that Kemény et al. [4] reported the detection and classification of cerebral embolic signals from TCD systems using ANNs after pre-processing the signals with the help of Fourier Transforms. Since the embolic signals present a similar shape to the Morlet wavelet (see Fig. 1), a wavelet neural seemed appropriate for identifying emboli within the blood flow signal and then we tested the classification of the type of emboli using a Multi-Layer Perceptron (MLP) NN [5].

Later a radial basis function (RBF) ANN was also assessed to distinguish among solid emboli, liquid emboli, or artifacts, using as indicators a ratio between signal powers and emboli duration [6].

In what considers the diagnosis tool application one should recall that the ischemic cerebral vascular accident (ICVA) is one of the major causes of death in the developed countries. The early diagnosis of this pathology is fundamental to minimize the consequences of this disease. ICVA is typically diagnosed through Computerized Tomography (CT) by identification of hemorrhages (characterized by a high density (white) image and usually occupying a round-spaced area), or an infarct (characterized as a low density (dark) image and occupying a vascular territory with some swelling) [7]. CT provides images from inside the human body with anatomic detail, being able of generating images of the human body in different planes [8] through image processing workstations. This facility has the disadvantage of producing a large increase in the number of images to be analyzed in terms of their content on anatomic information, besides the fact that each patient exhibits several individual images to be examined. Detailed examinations of each image become a very time consuming task for the radiologists therefore the existence of a computational facility capable of

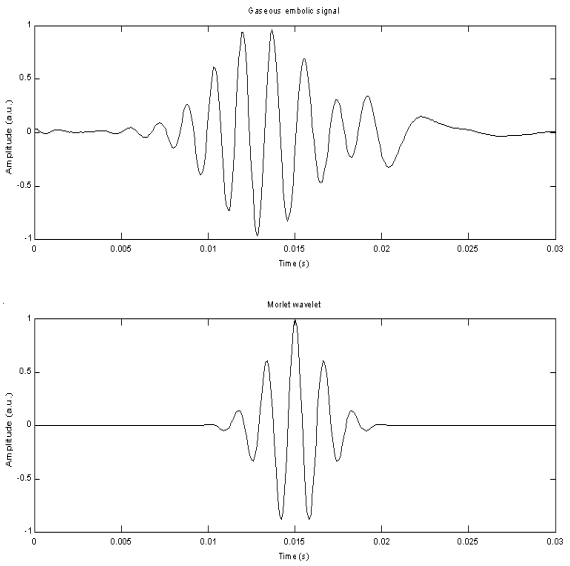

Fig. 1. The shape of an embolic signal (a)) is similar to a Morlet wavelet (b)) (a. u. = arbitrary units)

assisting the clinician on the task of ICVAs identification would be of great help. In this sense Radial Basis Function Neural Networks (RBFNN) were applied in images of encephalon acquired by CT scan to research their ability to identify ICVA areas.

The last case-study to be reported in this paper is concerned with tissue temperature estimation. Ultrasound is daily used in medicine for diagnosis and its applicability in therapy has been increasing within the last two decades. Ultrasound thermal therapies are being deeply researched towards the controlled spatial and temporal application of heat to delimited regions aiming at cancer tissue treatment [9]. Precise control of ultrasound instrumentation requires knowledge of accurate models capable of determining non-invasively the temperature of the tissues under treatment in both space and time variables [10]. Since *in-loco* determination of temperature in real patients is not desirable, several experiments using tissue mimicking materials, the so called phantoms, have been performed. The phantoms vary according to their chemical composition, mimicking single type of tissue or, the more complex and realistic ones, mimicking structures composed of different tissues [11]. Tissue reaction to heat depends on several variables, namely the velocity of propagation of sound on that particular tissue, the tissue rate of absorption and attenuation, the way the ultrasound waves are reflected and refracted when crossing two different media. So, realistic models of ultrasound induced temperature are expected to be nonlinear due to the combination of so many variables. The gold standard error for temperature estimation on tissues is considered to be 0.5ºC/cm^3 [10], value obtained by magnetic resonance imaging. Typical methods of non-invasive thermometer make use of backscattered ultrasound signals in different approaches: those who track the echo-shifts produced by changes in sound velocity and medium expansion/compression, the ones which are

based on the measurement of the attenuation coefficient, and those measuring the change on backscattered energy [10].

Among the ultrasound temperature dependent features pointed out for estimation under hyperthermia range, we concentrate on temporal echo-shifts. We started to analyze the behavior of temperature induced by ultrasound in homogenous medium phantoms and then we developed to heterogeneous phantoms. Radial basis functions NN were tested in comparison with autoregressive with exogenous inputs (ARX) models [12]. The NN promising results lead to the application of RBFNNs with best fitted NN parameters selected by a Multi-Objective Genetic Algorithm (MOGA) to increasingly complex data models [13-15].

3 Methods

To enable the reader with a more clear understanding of the particularities of each case-study in relation with the type of ANN methodology employed, each method will be independently presented.

3.1 WNN for Emboli Classification

The gaseous embolic signals present great dynamic range while solid emboli are normally of lower amplitude. When these signals are recorded from TCD systems with two channels (as the case of signals employed in this study) the channels are set to have 40dB attenuation between them to accommodate these differences. Solid and gaseous emboli are collected from the first and second channels respectively. In our study we employed 200 files (both channels), each containing 30000 samples of 2.4s of Doppler signal. A group of experts classified the signals so we were sure that each signal contained at least one event (solid or gaseous emboli). Manual analysis of the events enabled selection and recording of 1000 sample signals correspondent to 80ms of Doppler signals, including 137 gaseous emboli, 119 solid emboli and 150 normal flow events.

Primarily all signals from the sample data set were approximated using a wavelet NN (WNN) whose network nodes used a Morlet wavelet. The WNN was composed of a number of wavelet nodes (10), each described by three parameters: the dilation of the wavelet function (d), the translation (t) and the linear weight (w). The output of such a network is given by [16]

$$g(x) = \sum_{i=1}^{10} w_i \cdot \psi\left(d_i\left(x - t_i\right)\right) \tag{1}$$

where x represents time and ψ is the wavelet function used in the WNN, defined by:

$$\psi(x) = \cos(2\pi x) \cdot \exp\left(-x^2/2\right) \tag{2}$$

The WNN required an initialization phase where the desired resolution levels (dilations) are selected using a regular wavelet lattice. Then, from this data, the desired number of wavelets was selected using the algorithm of stepwise selection by orthogonalization [17].

The training of the WNN is based on a set of input/output pairs $\{x, f(x)\}$ where $f(x)$ is the function to be approximated. After the initialization, the network was trained by a Gauss-Newton procedure [17]. To perform this approximation, the normalized square root of the mean square error (NSRMSE), given by (3), was used to verify the quality of the approximation.

$$NSRMSE = \sqrt{mse} \Big/ \sigma_y \tag{3}$$

In (3) above, $mse = \sum_{n=1}^{N} (y - g)^2 \Big/ N$ is the mean square error of the approximation, with y the value of the function, g the approximation, N the dimension of y, and σ_y the standard deviation of y.

Then two NNs were trained with the parameters obtained from the approximation part. One network learned to distinguish between normal flow signals and embolic signals while the other learned to separate gaseous from solid embolic signals. Supervised learning with the same learning algorithm was used in both networks: a Multi-Layer Perceptron (MLP) implemented in Matlab and trained by a version of the Levenberg-Marquardt algorithm, which explicitly separates the role of the linear and nonlinear network parameters [18].

3.2 RBFNN for Emboli Classification

For the same type of embolic data another ANN approach has been tried, the RBFNN [19]. A RBFNN consists of three fully connected layers. The first is the input layer connecting the source nodes to the hidden layer of the network. The second is a hidden layer of sufficient dimension for the problem at hand which applies a non-linear transformation to the input space generating a (usually) higher-dimensional hidden-units space. The third and last layer applies a linear transformation from the hidden-units space to the output space.

The topology of a RBF neural network is shown in figure 1. Its output is given by

$$f(\mathbf{x}) = \alpha_0 + \sum_{i=1}^{n} \omega_i \varphi_i (\mathbf{x}, \mathbf{c}_i, \sigma_i), \tag{4}$$

where n is the number of neurons, α_0 is a bias term and ω_i are weights for the output linear combiner. The function used in the RBF hidden layer cells is usually a Gaussian function of the form:

$$\varphi(\mathbf{x}, \mathbf{c}_i, \sigma_i) = e^{-\frac{\|\mathbf{x}-\mathbf{c}_i\|^2}{2\sigma_i^2}} \tag{5}$$

$\mathbf{c_i}$ and σ_i are, respectively, the centre locations and spreads of the Gaussian function φ_i and $\mathbf{x}$ is the input pattern.

TCD exams have also been used. In this particular study six files of TCD exams (each file with 1880000 points) were preprocessed before used in the training and testing phases.

Primarily data was divided into 128 points segments using a Hanning window and 50% overlap was employed during spectrograms' calculations. Then, computation of clinically relevant characteristic, the embolic power by segment (EPS) and the embolic temporal duration [20], this is, the time interval where the embolic signal amplitude is 10dB above the scattered blood flow signals, were performed. These data information was used to calculate the ANN target output. To reflect the subjective nature of the specialists' decisions emboli duration and EPS were classified according to the range of values specified in Table 1.

Table 1. Emboli classification used in creation of the target output of the RBFNN approach

Parameters	Solid emboli	Gaseous emboli
Duration	(5.76 to 27.52)ms	(39.12 to 65.04)ms
EPS	(16.3 to 24.9)dB	(34.5 to 39.4)dB

The convention used in the assignment of values to the target output was the following:

- If EPS and Embolic Duration do not lie in the intervals presented in Tab. 1 then the target output should be 0, and the signal is classified as an artifact.
- If EPS $\in$ [16*:*3*dB;* 24*:*9*dB*] and Duration $\in$ [5*:*76*ms;* 27*:*52*ms*] then the signal is classified as a solid emboli, and the target output is assigned with the value 1.
- If EPS $\in$ [34*:*5*dB;* 39*:*4*dB*] and Duration $\in$ [39*:*12*ms;* 65*:*04*ms*] then the signal is classified as a gaseous emboli, and the target output is assigned with the value 2.

After these calculi the data sets to be used in the training and test phases were created as a concatenation of the signal characteristics and the target outputs to avoid patient's dependency. To optimize the training of the RBFNN and reduce the training time the concatenated data was normalized, shuffled and non-relevant data was eliminated to optimize the RBFNN's training. With this procedure the 60000 patterns available at the beginning of this study were reduced to 134 patterns, where 90 patterns were used during training and 44 patterns were left for the testing phase.

The training of the NNs was performed by the Levenberg-Marquardt (LM) algorithm using preprocessed data. The LM is a completely supervised learning algorithm. This means that given the initial values of the parameters, the training algorithm iteratively, having as objective the minimization of a cost function, can determine the "optimum" value of the network parameters (linear weights, centers, and spreads). In this paper the initial values of the parameters were determined using the optimal k-means algorithm (OAKM) [21].

Using the referred algorithm, 19 networks were trained using a different number of neurons in the hidden layer. The number of neurons varied between 2 and 20, and it was imposed 3 as the number of correct digits in the objective function. With this accuracy an acceptable quality for the trained networks was achieved, without originating sub-modulated networks.

3.3 ICVA Diagnosis Tool

A RBFNN model has also been employed in this case-study. The training method [22] employed consisted of two steps: primarily, an unsupervised procedure known as the *optimal adaptive k-means clustering* (OAKM) algorithm [21] was used to compute the initial centre locations, and a simple method [23] is adopted to determine the initial spreads. The second step uses a supervised training method that employs the Levenberg-Maquardt (LM) [24] algorithm to further optimize the non-linear parameters ($\mathbf{c}_i$, σ_i - see equations 4 and 5) of the network. In each training iteration the output linear weights, α_i , are computed as a least-squares solution. The method reflects the non-linear/linear topology of the RBF neural network. The termination criterion used to stop the training procedure is commonly used in non-linear optimization problems. It depends on one parameter related to the number of correct figures in the objective function and uses also the gradient and parameter vectors to assess convergence of the parameter values [22]. When all the stopping conditions are met the training stage is ended and the parameters of the network are stored for latter usage.

A group of images from 25 encephalon exams with previous ICVA diagnosis were used. The images employed were all acquired by means of the same CT equipment, respecting the protocol for encephalon study (5/5-10/10mm), and archived in DICOM format. In the laboratory they were converted into the Portable Network Graphics (PNG) format with 256 tones of grey, respecting the original image size (512x512). HUV values for each series of the study had been respected, to ease the process of analysis of the NN. All the points of interest were automatically masked in order to remove the white parts corresponding to bone or other regions not meant to be classified. Some small regions of interest were manually labeled as 1 when ischemic and 0 when normal. From each image and the pixels within the chosen regions, a set of features was extracted. The features were chosen to reflect the image statistics and those related to the context of the pixels of interest, the presence of structures having sharp edges and the position within the image. Altogether, these features form one possible data set suitable to train a RBFNN pixel classifier.

3.4 Dynamic Model for Tissue Temperature Estimation

Our research in temperature modeling of human tissue subjected to ultrasound for therapeutic purposes was based on data collected from artificial tissues, the so called phantoms. Homogeneous and heterogeneous phantoms under different ultrasound devices operating conditions have been tested. The laboratorial experimental setup is based on a typical structure shown in Fig. 2.

The phantom is heated by a therapeutic transducer while immersed in a degassed water tank in order to discard abrupt room temperature changes and to improve the coupling between the transducers and the medium. The medium is heated by a commercial therapeutic ultrasound transducer (TUS). The TUS transducer has an effective radiation area of 3.5 cm^2, and works in continuous mode at 1or 3 MHz. Different intensities are available at user's definition. The RF-lines are collected using an imaging ultrasound (IUS) transducer working in pulse-echo mode, driven by a pulser/receiver. The pulser/receiver sends the analog RF-lines to an oscilloscope which

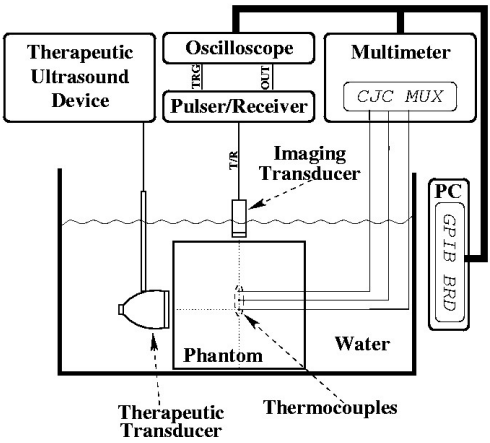

Fig. 2. Basic ultrasound experimental setup

digitalizes them at 50 MHz. The digitalized RF-lines are then sent to a personal computer (PC) via a GPIB bus. The effective temperature of the medium is measured by a certain number of thermocouples placed at a specific distance from the TUS transducer face in its radial line and aligned with the IUS. In the case of figure 2, three thermocouples are shown. The thermocouples are connected to a digital multimeter. The temperature values are transferred to the PC via the GPIB bus. At each 10s a RF-line is collected, as well as the thermocouples' temperature values. The medium is heated for a pre-defined period of time, and typically allowed to cool for an equal period.

The study of the temperature evolution is to be performed independently at the points defined by each thermocouple location, then each echo was isolated using a rectangular window, and the echo-shifts computed for each one. The echo-shifts were computed using an algorithm that directly evaluates continuous time echo shift (TES) from sample data. This method constructs a splinebased, piecewise continuous representation of a reference signal (in this case the echoes in the first RF-line), then finds the minimum of the sum of the squared errors between the reference and the delayed signals to determine their relative time-shift [25]. Also past temperatures of the medium were considered as important information on the estimation procedure.

Considering the huge amount of data available the selection of the appropriate number of neurons that produces the smallest NN error, the identification of the most relevant input variables to fit the model, the important lags of those variables are decisions difficult to be taken. To help on this task the best fitted RBF structures were selected by MOGA [26]. The MOGA is an evolutionary computing approach based on the natural evolution, and designed to minimize (or maximize) a number of problem-dependent objectives. Having in mind the attainment of good and also feasible solutions for a given application the objectives are defined as goals to meet. Each goal can have an associated priority which describes the relative importance of the related goal for the problem solution. At the end of a MOGA run a set of preferable individuals (solutions) are attained which are the ones that fulfill or almost fulfill the a-priory defined goals.

In almost all our case studies the MOGA search space was delimited by defining the possible number of neurons in the hidden layer, the possible number of inputs, and the maximum lag for TES and the changes in temperature signals (ΔT). The number of neurons and the maximum number of inputs was, in general, defined as a number in the interval [8, 20] and 25, respectively. These values were selected after several runs considering other parameter's arrangements.

Several models have been implemented, considering variations in experimental conditions. We started by estimating temperature in a single spatial location of a glycerine (homogeneous medium) tank, testing three TUS intensities (1 Watt/cm^2, 1.5 Watt/ cm^2, and 2 Watt/ cm^2)[12]. Experiences took 110 minutes where the first 60min correspond to medium heating and in the remaining 50min data was also collected to observe the cooling stage of the experiment. The RBFNN input variables in this preliminary study considered the fundamental component of the intensity spectrum and the measured temperature. The number of model inputs was allowed in the interval [2,30], while the possible number of neurons was accepted to be in the interval [2,15].

The RBFNN single point temperature estimation was then compared with the results of an ARX model defined by the equation

$$y[t] + a_1 y[t-1] + \cdots + a_{na} y[t-na] = b_1 u[t-nk] + \cdots + b_{nb} u[t-nk-nb+1] \quad (6)$$

Where the actual output y[t] is related with a finite number of values of the output y[t-k] and of the input x[t-k]. The structure of the model is defined by the number of poles (na), the number of zeros (nb-1) and the time delay of the system (nk). The model coefficients $\{a_i\}_{i=1}^{na}$and $\{b_i\}_{j=1}^{nb}$were determined using the least squares strategy.

Later we increased to three the spatial points where temperature was to be estimated as seen in Fig. 3. In terms of the model, the position along the axis was considered as another input. The phantom, still a homogeneous medium, was prepared to mimic human muscle by mixing (in % weight): 86.5% of degassed water, 11% of glycerin, and 2.5% of agar-agar. Data has been collected during 35minutes where the first 5 minutes enabled representation of resting conditions of the medium, the next 15min correspond to heating phase and the remaining time is representative of the cooling stage. The computed echo-shifts and the measured temperature values were filtered and normalized to values between -0.5 and 0.5. The filtration was performed to reduce the computational and measurement noise, and the normalization was computed to discard the difference in scale between the echo-shifts signals and the measured temperature signals. Afterwards the normalized and filtered *TES* and ΔT were arranged in separated files, according to the related intensity and spatial point (P1, P2, or P3 in Fig. 3), and applied in the RBFNN construction [13].

The neural network parameters were found using the Levenberg Marquardt (LM) algorithm and the least-squares strategy. At each MOGA iteration the performance of each NN is accessed in order to extract the problem-dependent objectives under minimization, this is, the model errors, validity tests, linear weight norm, and computational complexity.

Aiming at a more detailed analysis, the number of spatial points inside the tissue phantom have then been increased to five (with relative positions as in Fig. 3 but spaced among them by 5mm) and a new TUS intensity (0.5W/cm^2) was tested [14].

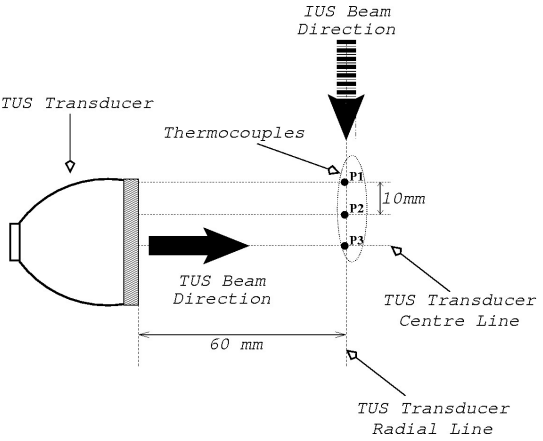

Fig. 3. Thermocouples disposition in relation to the therapeutic (TUS) and imaging (IUS) transducers denoting spatial point locations for temperature estimation

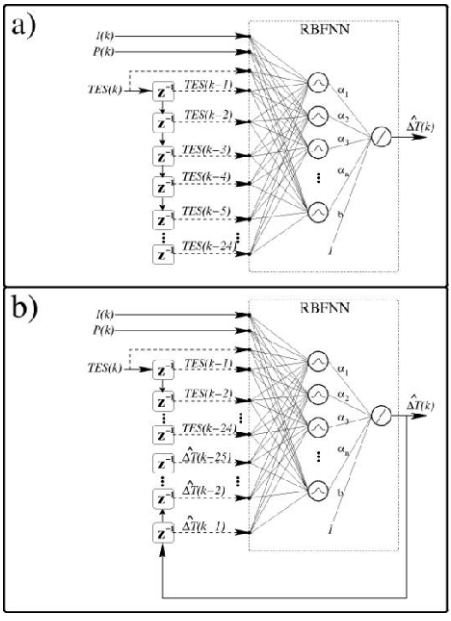

Fig. 4. Generic RBFNN structures applied. (a) non-regressive and (b) regressive.

Also the temperature of the degassed water tank containing the phantom was maintained at approximately 22 ºC, by using a 75-W aquarium heater. The NN input variables considered up to 25 past lags of ΔT and *TES*. With these data two three-layered RBFNN structures were tested: a generic non-regressive structure considering only the past lags of *TES* as inputs, as presented in Fig. 4a; and, a regressive structure where both the ΔT and the *TES* past values were considered, as shown in

Fig. 4b. In both structures two additional inputs were considered to discriminate the intensity and spatial point under estimation. Four MOGA runs of 200 generations were performed for both structure types. To test the spatial generalization capacity of the best obtained models, training and structure selection considered only estimations in three of the five spatial points (extremes and middle points). Then, at the final step, the validation set contained data from all the five points, implementing a real generalization assessment procedure.

Maintaining the recursive RBFNN structure (Fig. 4 (b)) the research developed to estimate temperature on a three-layered non homogeneous phantom (Fig. 5) with attenuation and speed-of-sound similar to in vivo muscle [15]. Besides using a more complex phantom, the number of intensity levels applied was increased (0.3, 0.5, 0.7, 1.0, 1.3, 1.5, 1.7, and 2.0W/cm^2). Since the influence of the ultrasound operating conditions were to be tested in this study, the division of the available data set considered for training and testing data sub-sets where only four intensity levels were considered (0.5, 1.0, 1.5, and 2.0W/cm^2). Validation was performed on all range of intensities evaluated experimentally.

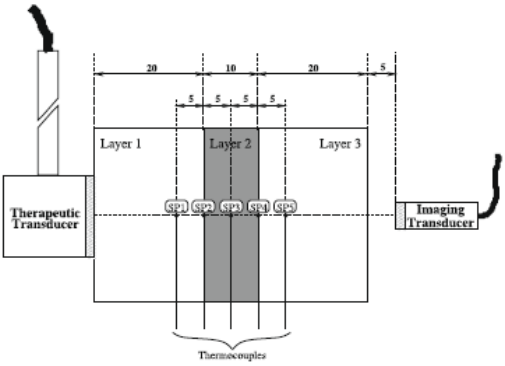

Fig. 5. Transducers (located face to face) and thermocouples location inside the heterogeneous phantom (all length units are in mm)

4 Experimental Data and Results

Following the same policy as in the previous section, the experimental data available, how it was used as input to the NNs and the correspondent results will be exposed separately for each case study.

4.1 Classification of Emboli

As previously stated in this case-study, from the 200 data files recorded from a TCD system, where each file contained at least one gaseous or solid embolic event (already classified by a group of experts) were manually selected and recorded as 1000-sample signals (corresponding to 80 ms blood flow signals). For each signal, the network parameters were adapted for 10 epochs to minimize the error between the original

signal and the output of the WNN, using the Gauss-Newton method. The wavelet parameters that best fitted each signal were saved to be used during the classification stage. The performance of the approximation of the Gauss-Newton procedure was assessed by the normalized square root of the mean square error (NSRMSE) whose values ranged from 0.07 to 0.73 to accomplish the fact that the surrounding signal presented amplitudes of the order of the event itself.

Next the MLP was implemented with 30 inputs, one hidden layer with 3 nodes and one output layer with 2 nodes.

The first NN was trained to classify signals as normal flow or embolic. This target and the training set (composed of the 170 examples of embolic signals, gaseous and solid, plus the 100 examples of normal flow signals) were presented to the NN. Training was repeated 100 times with different initial conditions and the best results chosen.

The results obtained for this first NN, as percentages of correctly classified signals, are shown in Table 2.

Table 2. Classification results for embolic and normal signals

	Training phase	Test phase
Embolic signals	98.8	91.9
Normal signals	97.0	96.0

The second NN was trained to classify embolic signals in gaseous or solid emboli. Training of this network (also 100 times repeated under different initial conditions) was done with 170 example signals in the training set and 86 in the test set. Table 3 shows the percentages of correct classifications obtained.

Table 3. Classification results of wnn for gaseous and solid emboli

	Training phase	Test phase
Gaseous emboli	91.1	91.5
Solid emboli	98.8	97.7

When the embolic data was assessed by the RBFNN, all networks were evaluated having in mind the decision levels described in Table 1. Table 4 shows the performance of a network with 2, 6 and 18 neurons. The network employing 6 neurons was the best performing one, presenting approximately 88% of success.

Table 4. RBFNN performance

Neurons	Training success	Testing success
2	71.7	62.5
6	100	87.5
18	100	12.5

Comparing these results with the WNN methodology and considering the success of RBFNN networks on other applications one should conclude that, besides the very good performance obtained there is still room for exploring other methods of pre-processing the data to be used in training and testing phases and to investigate the incorporation of more entries in the network.

4.2 ICVA Diagnosis Tool

When computing the features, only the points lying within the mask are considered. The left image in Fig. 6 shows an example of a masked exam. Bone areas and other artifacts are all shown in black. The right image shows the complete exam.

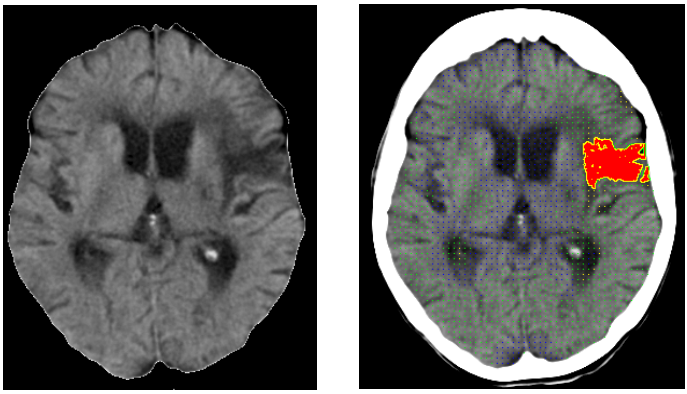

Fig. 6. Image from patient P06, exam 01. Left: masked image submitted to the network; right: Output from the classifier.

From a set of 25, exams were randomly collected from 2 patients (P03, P06). P06 contributed with 10 points to the training set, while 2 points were taken from PO3 (see Table 5).

Table 5. Points used to train the RBF neural network

	Image 02		Image 03		Image 05		total
	Positive	Negative	Positive	Negative	Positive	Negative	
P06	2	4	1	1	2	-	10
P03	-	-	-	-	1	1	2

A first experiment considered NNs trained with 3 parameters. Different number of trials were run varying the number of neurons in the NN and performances were recorded. The performance was evaluated by the error measured between the desired classification and the network output. For the best neural network achieved, all images from the patients sample were submitted to the classifier and the results were analyzed and compared to the radiologist report.

In operation, to avoid so heavy computation burden, instead of feeding all the pixels to the network, only those in a sub-sample grid were submitted. When one of these was reported as corresponding to pathology, all its neighbors were also submitted to the network. The process is repeated in a recursive way until no neighbor pixels are reported as pathological. The whole process was repeated by removing or adding features to the network input and by varying the number of neurons for each input configuration. After a number of trials the results were significantly improved by a 5 neurons neural network having 6 features.

The output images of the classifier are marked with different colors depending on the neural network output for each tested pixel. The following color code was used regarding the network output:

- [0.0, 0.2[– clear absence of pathology (blue);
- [0.2, 0.5[– absence of pathology (green);
- [0.5, 0.75[– marginal positive (yellow);
- [0.75, 1.0] – pathology (red).

As it can be seen in the right image of Fig. 6 the NN located the ischemic areas and marked them as described in medical report. In Fig. 6 it can be seen that the NN delimits the ischemic injury, marking the border of the injury (in yellow) with satisfactory accuracy. In possible areas of error such as sharp ridges and hypertrophic ventricles, the NN accuracy is confirmed by the mapping of colors.

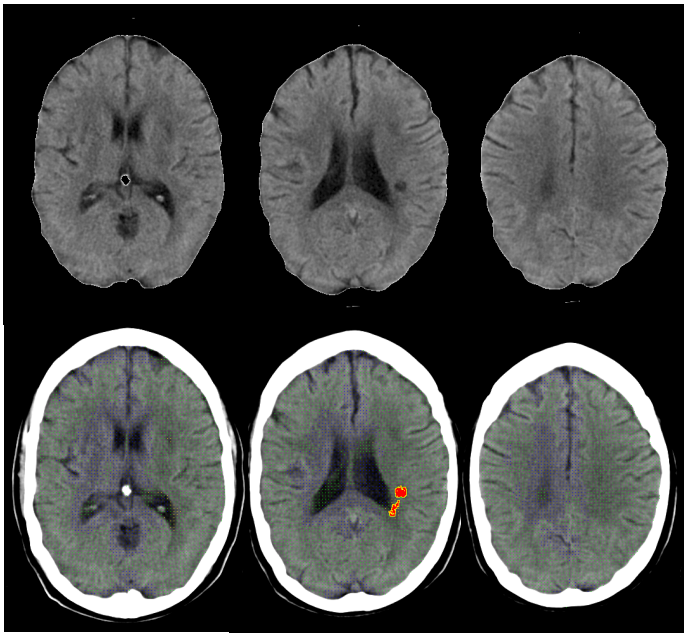

Fig. 7. Images from patient P19. Top: input images; bottom: output from the classifier.

Fig. 7 presents results regarding patient P19. In these images a small lacuna infarct is visible and correctly marked by the NN. This type of injury, usually visible only in one cut because of the reduced dimensions (perhaps in two according to the thickness of the cut), was also detected by the NN. The classifier demonstrated capacity of generalization when marking this zone of ischemia, considering that none of the training images included a similar injury. On the other hand a small error in the posterior horn of the left lateral ventricle is present, when the results of the NN are compared to the radiologist report.

The results obtained with this study [27-28] achieved around eighty percent of success. Besides the need for more tuning of the methods one can conclude that the neural network approaches can offer to the area of image based medical diagnose a great value, minimizing the time to report and therefore providing a faster treatment.

4.3 Dynamic Model for Tissue Temperature Estimation

Our preliminary NN temperature modeling considered 11 models (identified by MOGA) with different combinations of fundamental components of the spectrum and ΔT lags. The best ARX structure was computed considering a scanning of 48 lags (na = 1,...,48, nb = 1,...,48) for each variable, and a null delay for the inputs (nk =0). The ARX model presented a RMSE in the validation set of 0.0253, and a maximum absolute error of 2.1 ºC while the best fitted RBFNN model presented a maximum absolute error of less than 0.2ºC encouraging research of RBFNNs for temperature estimation. A graphical representation of the comparative behavior of these methods can be observed in Fig. 8.

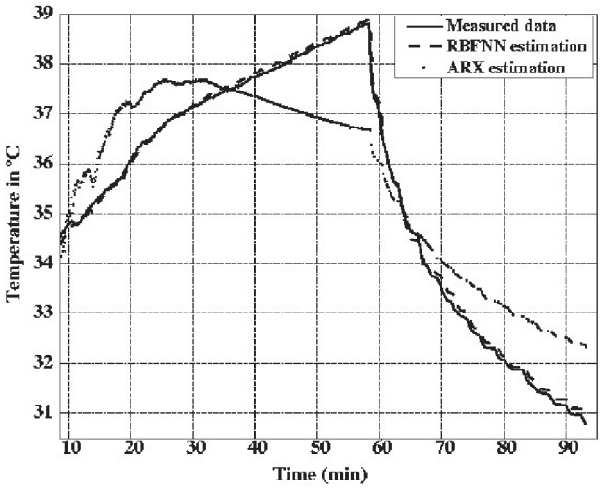

Fig. 8. Estimated outputs of RBFNN and ARX models in comparison with a measured output when a homogeneous phantom is employed

When we improved the tissue mimicking properties of the phantom in use (although still as a homogeneous medium) and investigated the behavior of three different TUS intensities, the best RBFNN presented a maximum absolute error of 0.45 ºC, which was inferior to the value required for hyperthermia/diathermia purposes. This best model was validated for all the possible situations, i.e. at all the intensities and points (positions) studied. The estimated temperature curves followed the curves of the measured temperature both at heating and the cooling phases of the experiment denoting a high generalization capacity of the model.

The regressive and non- regressive RBFNN structures, tested for five spatial points and four TUS intensities proved that the regressive approach presented less temperature estimation errors (see Fig. 9). In fact, considering the trained (extreme and middle spatial points) and untrained (other two points) and all the best models, a maximum absolute error of 0.5ºC and 4.4ºC was respectively obtained for the non-regressive structure. The best model (18 neurons and 9 inputs, reaching a number of 199 parameters) attained a mean maximum error of 0.8ºC. On the other hand, the best performed regressive RBFNN structure presented a maximum absolute error of 0.4ºC for the trained spatial points and 0.5ºC for the untrained ones. This regressive model

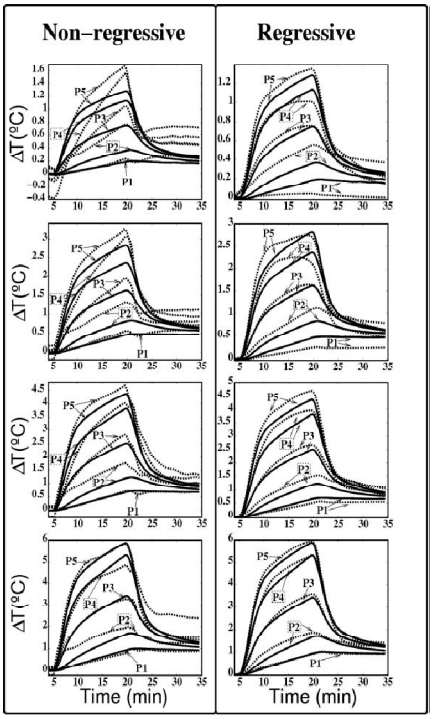

Fig. 9. Estimated versus measured temperature waveforms by the best regressive and non-regressive RBFNN estimators

presented 10 neurons and 13 inputs reaching a number of 151 parameters. It is worth mentioning that the advantage of using the non- regressive model would not to need to know the initial temperature of the medium, which might be considered a valuable issue in terms of clinical application of these estimators.

When a three-layered media phantom was experimented under eight TUS intensities, the best achieved model respected the gold standard 0.5ºC maximum error, independently of the intensity and the spatial position considered, which was a novel achievement. During this study models were trained and selected to estimate temperature at four intensities, then during the validation phase, the best fitted models were analyzed in data collected at the eight intensities. Therefore, once more the generalization ability of RBFNN was proved. More detailed description of RBFNN modeling of tissue temperature estimation could be find in [29-33].

5 Conclusions

This paper reports several biomedical cases and how they have been dealt to achieve parameters' estimation using NNs in particular RBFNNs. From classification of emboli based on transcranial Doppler ultrasound blood flow signals, to the design of a diagnostic tool for ICVA identification, and finally the temperature estimation on ultrasound induced hyperthermia making use of simple to more realistic phantoms, we described the methods employed and detailed how data was used as inputs of the NNs. In all cases, very high performance was achieved proving that ANN should be used more frequently and included on medical applications.

References

1. Fan, L., Evans, D.H.: Extracting instantaneous mean frequency information from Doppler signals using the Wigner distribution function. Ultrasound Med. Biology 20, 429–443 (1994)
2. Devuyst, G., Vesin, J.-M., Despland, P.-A., Bogousslavsky, J.: The matching pursuit: a new method of characterizing microembolic signals? Ultrasound Med. Biology 26, 1051–1056 (2000)
3. Matos, S., Leiria, A.I., Ruano, M.G.: Blood flow parameters evaluation using wavelet transforms. World Congress on Medical Physics and Biomedical Engineering, 4235-52803.pdf, CD-ROM, Chicago, USA (2000)
4. Kemény, V., Droste, D.W., Hermes, S., Nabavi, D.G., Schulte-Altedorneburg, G., Siebler, M., Ringelstein, B.: Automatic embolus detection by a neural network. Stroke 30, 807–810 (1999)
5. Sérgio Matos, A.E., Ruano, M., Ruano, G., Evans, D.H.: Neural network classification of cerebral embolic signals. In: 23rd Annual International Conference of the IEEE Engineering in Medicine and Biology Society, paper 1123, track 4.3, CDROM, Instambul, Turkey (2001)
6. Teixeira, C.A., Graça Ruano, M., Ruano, A.E.: Emboli classification using RBF neural networks. In: Proceedings of CONTROLO 2004, Faro, Portugal, June 7-9, pp. 630–635 (2004)

7. Wardlaw, J.: Radiology of Stroke. J. Neurol Neurosurg Psychiatry 70(suppl. I), i7–i11 (2001)
8. Robb, W.: Perspective on the First 10 Years of the CT Scanner Industry. Academic Radiology 10(7), 756–760 (2003)
9. Arthur, R.M., Straube, W.L., Trobaugh, J.W., Moros, E.G.: Noninvasive temperature estimation of hyperthermia temperatures with ultrasound. Int. J. Hyperthermia 21, 589–600 (2005)
10. Arthur, R.M., Straube, W.L., Starman, J.D., Moros, E.G.: Noninvasive temperature estimation based on the energy of backscattered ultrasound. Medical Physics 30, 1021–1029 (2005)
11. Zell, K., Sperl, J.I., Vogel, M.W., Niessner, R., Haisch, C.: Acoustical Properties of Selected Tissue Phantom Materials for Ultrasound Imaging. Physics in Medicine and Biology 52, 475–484 (2007)
12. Teixeira, C.A., Cortela, G., Gomez, H., Ruano, M.G., Ruano, A.E., Negreira, C., Pereira, W.C.A.: Temperature models of a homogeneous medium under therapeutic ultrasound. Brazilian Journal of Biomedical Engineering 20(2-3), 97–101 (2004)
13. Teixeira, C.A., Ruano, A.E., Ruano, M.G., Pereira, W.C.A., Negreira, C.: Non-invasive Temperature prediction of in-vitro therapeutic ultrasound signals using neural networks. Medical and Biological Engineering and Computing 44(1-2), 111–116 (2006)
14. Teixeira, C.A., Graça Ruano, M., Ruano, A.E., Pereira, W.C.A.: A soft-computing methodology for non-invasive time-spatial temperature estimation. IEEE Transactions on Biomedical Engineering 55(2), 572–580 (2008)
15. Teixeira, C.A., Pereira, W.C.A., Ruano, A.E., Graça Ruano, M.: On non-invasive multilayer temperature estimation using soft-computing methods. Ultrasonics 50(1), 32–43 (2010)
16. Zhang, Q., Benveniste, A.: Wavelet Networks. IEEE Trans. Neural Networks 3, 889–898 (1992)
17. Zhang, Q.: Using wavelet network in nonparametric estimation. IEEE Trans. Neural Networks 8, 227–236 (1997)
18. Ruano, A.E., Jones, D.I., Fleming, P.J.: A new formulation of the learning problem for a neural network controller. In: IEEE Conference on Decision and Control, Brighton, U.K., pp. 865–866 (1991)
19. Ferreira, P.M., Faria, E.A., Ruano, A.E.: Neural network models in greenhouse air temperature prediction. Neurocomputing 43(1-4), 51–75 (2002)
20. Matos, S., Ruano, M.G., Ruano, A.E.: Embolic signals characterization using wavelet neural networks. In: Proc. of the BioEng 2001, paper 41. University of Algarve (2001)
21. Chinrungrueng, C., Séquin, C.H.: Optimal adaptive k-means algorithm with dynamic adjustment of learning rate. IEEE Transactions on Neural Networks 6(1), 157–169 (1995)
22. Ruano, A.E., Ferreira, P.M., et al.: An Overview of Nonlinear Identification and Control with Neural Networks. In: Ruano, A.E. (ed.) Intelligent Control Using Intelligent Computational Techniques. IEE Control Series (2005)
23. Haykin, S.: Learning In Neural Networks. A Comprehensive Foundation. Prentice-Hall (1998)
24. Levenberg, K.: A Method for the Solution of Certain Problems in Least Squares. Quarterly Applied Mathematics 2, 164–168 (1944)
25. Viola, F., Walker, W.F.: A spline-based algorithm for continuous time-delay estimation using sampled data. IEEE Trans. Ultrasonics &Ferroelectric Freq. Control 52, 80–93 (2005)

26. Ferreira, P.M., Ruano, A.E., Fonseca, C.M.: Genetic assisted selection of RBF model structures for greenhouse inside air temperature prediction. In: Proc. IEEE Conference on Control Applications, Istambul, Turkey, vol. 1, 2, pp. 576–581 (2003)
27. Ribeiro, L., Ruano, A.E., Graça Ruano, M., Pedro, M.: Neural networks as-sisted diagnosis of ischemic CVA's through CT scan. In: Proceedings of the IEEE International Symposium on Intelligent Signal Processing, Spain, pp. 223–227 (2007)
28. Ribeiro, L., Ruano, A.E.B., Ruano, M.G., Ferreira, P., Várkonyi-Kóczy, A.R.: Improving the Diagnosis of Ischemic CVA's through CT Scan with Neural Networks. In: Proceedings of the 2nd IEEE International Workshop on Soft Computing Applications, Hungary, Romania (2007)
29. Teixeira, C.A., Graça Ruano, M., Pereira, W.C.A., Ruano, A.E.: Temperature modelling of an homogeneous medium using genetically selected RBF(LIC). In: Proceedings of the 16th IFAC World Congress, paper no 2387 DVD, July 4-8. Elsevier, Prague (2005)
30. Teixeira, C.A., Ruano, A.E., Graça Ruano, M., Pereira, W.C.A.: Generalization assessment of non-invasive data-driven temperature estimators from therapeutic ultrasound. Brazilian Journal of Biomedical Engineering 23(2), 143–151 (2007)
31. Teixeira, C.A., Graça Ruano, M., Ruano, A.E., Pereira, W.C.A.: Multilayered non-invasive temperature estimation from backscattered ultrasound. In: Proceedings of the Acoustics 2008, France (2008)
32. Teixeira, C.A., Pereira, W.C.A., Ruano, A.E., Graça Ruano, M.: NARX structures for non-invasive temperature estimation in non-homogeneous media. In: Proceedings of the IEEE International Symposium on Intelligent Signal Processing (WISP 2007), Spain, pp. 169–174 (2007)
33. Teixeira, C.A., Graça Ruano, M., Ruano, A.E., Pereira, W.C.A.: Neuro-genetic non-invasive temperature estimation: intensity and spatial prediction. Artificial Intelligence in Medicine 43(2), 127–139 (2008)

Optic Disc Localization in Retinal Images

Florin Rotaru, Silviu Ioan Bejinariu, Cristina Diana Niță, and Mihaela Costin

Institute of Computer Science, Romanian Academy, Iasi Branch, Romania
{florin.rotaru,silviu.bejinariu,cristina.nita,
mihaela.costin}@iit.academiaromana-is.ro

Abstract. The paper proposes an optic disc localisation method in color retinal images. It is a first step of a retinal image analysis project which will be completed later with other tasks as fovea detection and measurement of retinal vessels. The final goal is to detect in early stages signs of ophthalmic pathologies as diabetic retinopathy or glaucoma, by successive analysis of ophthalmoscopy images. The proposed method first detects in the green component of RGB image the optic disc area and then on the segmented area extracts the optic disc edges and obtains a circular optic disc boundary approximation by a Hough transform.

Keywords: optic disc, retinal images, vessel segmentation, Hough transforms.

1 Introduction

The traditional assessment way of ophthalmic pathologies signs is prone to the presence of specially trained examiners. More than that sophisticated measurements on the fundus images are not possible by direct visualization. Since the early detection of these diseases is crucial for a reasonable treatment and the traditional ways do not cope with this complex task, automatic analysis is required to assist the specialists. Even in the last decade many automatic methods were proposed the problem is not yet fully solved, mainly due to the large variations between individuals and uneven quality and diversity of the acquired retinal images.

However, some important results were achieved. Part of the proposed techniques, so called bottom-up methods, first locates the optic disc and then starting from that area track the retinal vessels and do the required measurements. The analysis of optic disc area is essential for diagnosis of different aspects caused by diabetic retinopathy. Also, optic disc segmentation can be useful for detection of some other eye condition as glaucoma, which can be diagnosed by identifying the changes in the optic disc area. Another important argument for optic disc recognition is that once the disc is located, the fovea localization, otherwise difficult to compute, becomes an easier task due the relatively constant distance between the fovea and optic disc.

A second group of techniques, top-down approaches, first track the retinal vessels and get the optic disc as the root of the vessels tree. There are arguments pro and contra for one or another approach. The presence of exudates makes very difficult the optic disc direct segmentation. In some other circumstances, as in the case of

V.E. Balas et al. (Eds.): Soft Computing Applications, AISC 195, pp. 453–463.
springerlink.com

peripapillary atrophy, bright areas in the very vicinity of the optic disc might distort its round shape. In these circumstances the direct localization of the disc becomes a quite challenging task. On the other hand vessels tracking might be a very difficult task if there are discontinuities in the vessel structure. We mention just two top-down approaches, [4] and [5]. While in [4] the retinal vessels convergence point is detected by employing a voting-type algorithm named fuzzy convergence, in [5] first there are identified the four main vessels in the image. Then the four branches are modeled by two parabolas whose common vertex is identified as optic disc centre.

A very known now bottom-up technique was proposed in [3]. The optic disc area localization is performed by employing a principal component analysis method. This implies a previous training step. Then a modified active shape model is proposed to identify the disc boundary.

Another important work is the one presented in [1]. Part of this methodology was also implemented in our system to process retinal images. First the optic disc area is located using a voting procedure. There were implemented three methods for a rough identification of optic disc area. The green channel of the RGB input image is used. The first method starts by filtering the green image using a 21 x 21 median filter. For each pixel in the filtered image is computed the difference between the maximum and minimum grey levels in a 21x21 window centered on the current pixel. As optic centre is chosen the pixel with the maximum difference. Second approach to approximate optic disc detection calculates the statistical variance for every pixel using a 71x71 window. Also, applying the Otsu technique the blue channel image is binarized. The pixel presenting the maximum statistical variance and having at least 10 white pixels in a 101x101 area centered on it but in the blue binarized channel is declared disc centre. Finally, the third voting method applies a Fourier transform to the input image. A Gaussian low-pass filter is applied in the frequency domain and the result image is transformed back in the spatial domain. The brightest pixel in the new image is taken as the third optic disc centre candidate. The voting procedure establishes the estimated disc centre in the following way: 1) if all three candidates are close to their centre this one is proposed as an approximate disc centre; 2) if only two from three candidates are close to the centre the average point of these two is chosen; 3) if all candidates are far apart from their centre the candidate proposed by the second method, the most reliable considered by the authors, is chosen.

Then a 400x400 window is centered on the estimated disc centre, and extracted from original green and red channels. A morphological filter is employed from [6] to erase the vessels in the new window. A Prewitt edge detector is then applied and by the same Otsu technique the image is binarised. The result is cleaned by morphological erosion and finally a Hough transform is applied to get the final optic disc boundary. Finally, the boundary with the best fitting from the two channels is chosen. The authors report for 1200 retinal images a score of 100% for approximated localisation and a score of 86% for final optic disc localization.

A mixed approached, independently detecting the optic disc centre and retinal vessels, is proposed in [2]. The vessels are segmented in the green channel of RGB retinal image using several image processing techniques. A first pre-processing step to smooth the homogenous regions of image without blurring vessel boundaries is done

applying a contrast limited adaptive histogram equalization followed by an edge-preserving anisotropic diffusion filter. Then the blood vessels are segmented using in a first stage a filtering technique based on eigenvalue analysis of the Hessian matrix. The result image is binarized by an iterative thresholding method. A skeletonization is applied on the vessel network. After processing the skeleton image to eliminate spurious branches, the vessel medians are superimposed on the original image. Starting from specific median points measurements of the vessel width are performed. Independently, several Mean Shift processes are equidistantly seeded in the green channel image. Using a circular kernel each process migrates to a local grey intensity maximum. The processes reaching low intensity values are disregarded and the centre with the maximum dark pixels around is chosen. To estimate the disc boundary the method proposed in [7] is then applied.

2 Optic Disc Recognition

In order to exactly locate the optic disc first we started following a similar methodology as the one proposed in [1]. Tests were done on 720x576 RGB retinal images, some of them of patients strongly affected by eye disorder. From the three methods of the voting procedure presented in [1] good optic disc area localization we obtained only with the Low-Pass Filter Method, the third method of the voting procedure in [1]. Our implementation it is a common one: to smooth out the little white patches which can perturb the right disc localization the green channel of the input image is transformed in frequency domain. As in [1] on the image of the magnitude of the FFT transform a Gaussian low-pass filter was applied:

$$H(u,v) = \exp\left(-\frac{D^2(u,v)}{2D_0^2}\right) \tag{1}$$

where $D(u,v)$ is the Euclidean distance from point (u,v) to the origin of frequency domain and D_0 is the cutoff frequency, of 25 Hz. The filtered result is transformed back to the spatial domain and the brightest pixel of the result image is chosen as an optic disc area centre candidate.

Good results were obtained also with another approach derived from the Maximum Difference Method proposed in [1]. As in [1] a 21x21 median filter is first applied on the green channel of the input image to eliminate isolated peaks. Then for each (i, j) pixel of the filtered green channel I (x, y) is calculated the difference between the maximum gray value and minimum gray value of the pixels inside a 21 x 21 window centered on the current (i, j) pixel:

$$Diff(i,j) = I_W^{max}(i,j) - I_W^{min}(i,j) \tag{2}$$

There are retained four pixels with the greatest values $Diff\ (i, j)$. Then, starting from texture operators:

$$\begin{aligned} L5 &= \begin{bmatrix} 1 & 4 & 6 & 4 & 1 \end{bmatrix} \\ E5 &= \begin{bmatrix} -1 & -2 & 0 & 2 & 1 \end{bmatrix} \\ S5 &= \begin{bmatrix} -1 & 0 & 2 & 0 & -1 \end{bmatrix} \end{aligned} \tag{3}$$

where:

L5 - mask to asses the gray level average;
E5 - edge mask;
S5 - corner mask.

the following masks, as in [8], are synthesized:

$$\begin{aligned} L5^{t}xE5 &= \begin{bmatrix} -1 & -2 & 0 & 2 & 1 \\ -4 & -8 & 0 & 8 & 4 \\ -6 & -12 & 0 & 12 & 6 \\ -4 & -8 & 0 & 8 & 4 \\ -1 & -2 & 0 & 2 & 1 \end{bmatrix} \quad L5^{t}xS5 = \begin{bmatrix} -1 & 0 & 2 & 0 & 1 \\ -4 & 0 & 8 & 0 & 4 \\ -6 & 0 & 12 & 0 & 6 \\ -4 & 0 & 8 & 0 & 4 \\ -1 & 0 & 2 & 0 & 1 \end{bmatrix} \\ E5^{t}xL5 &= \begin{bmatrix} -1 & -4 & -6 & -4 & -1 \\ -2 & -8 & -12 & -8 & -2 \\ 0 & 0 & 0 & 0 & 0 \\ 2 & 8 & 12 & 8 & 2 \\ 1 & 4 & 6 & 4 & 1 \end{bmatrix} \quad S5^{t}xL5 = \begin{bmatrix} -1 & -4 & -6 & -4 & -1 \\ 0 & 0 & 0 & 0 & 0 \\ 2 & 8 & 12 & 8 & 2 \\ 0 & 0 & 0 & 0 & 0 \\ -1 & -4 & -6 & -4 & -1 \end{bmatrix} \end{aligned} \tag{4}$$

For each pixel of the filtered green channel I(x,y) the texture parameter $f(i,j)$ is computed:

$$f(i,j) = \sqrt{(f_{L5^{t}xE5}(i,j))^2 + (f_{L5^{t}xS5}(i,j))^2 + (f_{E5^{t}xL5}(i,j))^2 + (f_{S5^{t}xL5}(i,j))^2} \tag{5}$$

The value $f(i,j)$ is normalized:

$$F(i,j) = \frac{f(i,j) - f_{\min}}{f_{\max} - f_{miin}} \tag{6}$$

where $f_{\max} = \max\{f(i,j)\}, f_{\min} = \min\{f(i,j)\}, 0 \le i \le H-1, \ 0 \le j \le W-1$. H is the image height and W is the image width.

From the four pixels with the greatest values $Diff(i,j)$ selected in the first stage is retained the one with the largest average of $F(i,j)$ computed on the 21x21 window centered on the processed pixel.

From our tests we conclude that on the retinal images of healthy patients or in the early stages of affection this second voting method provides a closer point to the real optic disc centre than the first one. However, on the retinal images strongly affected it fails. Finally, if the two methods to approximate the optic disc centre provide close centers is chosen the one computed by the second method. Otherwise the centre

computed by the first method is chosen. The results obtained with the two procedures are illustrated by figure 1, where the little cross is the point found out by maximum difference method and the big cross is the point provided by the second algorithm.

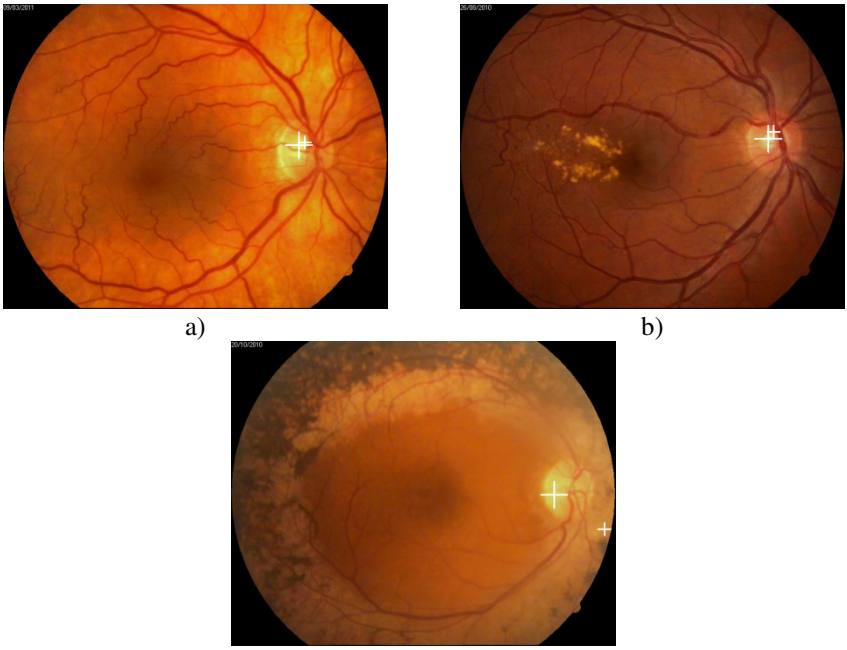

Fig. 1. Results of detecting approximate optic centre position by two voting procedures. Point marked with little cross is provided by the first method and the one indicated by large cross is computed by second voting algorithm. When the two points are far apart, as in the c) image, the centre computed by the first method is chosen.

Once the preliminary optic disc centre is established by voting procedure, as in [1], the further work was done on a window, 300x300 in our case, centered on the optic centre. The tests were done on green channel of 86retinal images. Following the same technique employed from [6] in the established window the blood vessels were eliminated. Next we shall describe shortly this method. The grayscale erosion on a image I by a structuring element B, as in [6], is the minimum grey value of the pixels in the vicinity defined by structuring element and centered on pixel (x,y):

$$[\varepsilon_B(I)](x,y) = \min_{(a,b)\in B} I(x+a, y+b) \tag{7}$$

For the same structuring element B the dilation is defined as the maximum grey value of the pixels:

$$[\delta_B(I)](x,y) = \min_{(a,b)\in B} I(x+a, y+b) \tag{8}$$

The opening $\gamma_B(I)$ of an image I by the structuring element B is:

$$\gamma_B(I) = \delta_B(\varepsilon_B(I)) \tag{9}$$

The closing $\varphi_B(I)$ of an image I by the structuring element B is:

$$\varphi_B(I) = \varepsilon_B(\delta_B(I)) \tag{10}$$

Considering as in [1] a line of 27 pixels length and 1 pixel width as the structuring element, for each of 12 different orientation of the line was performed an opening of the original 300x300 selected window. Noting the current image (300x300 window) with I , the clean image, without vessels, is:

$$I_B = \min_{i=1,\ldots 12}\left(\gamma_{B_i}(I)\right) \tag{11}$$

This means that each pixel of the result image has the minimum value from the set of 12 values of the same coordinate pixel in each of the 12 openings of I .

Results of the vessels erasing operation are illustrated by figure 2.

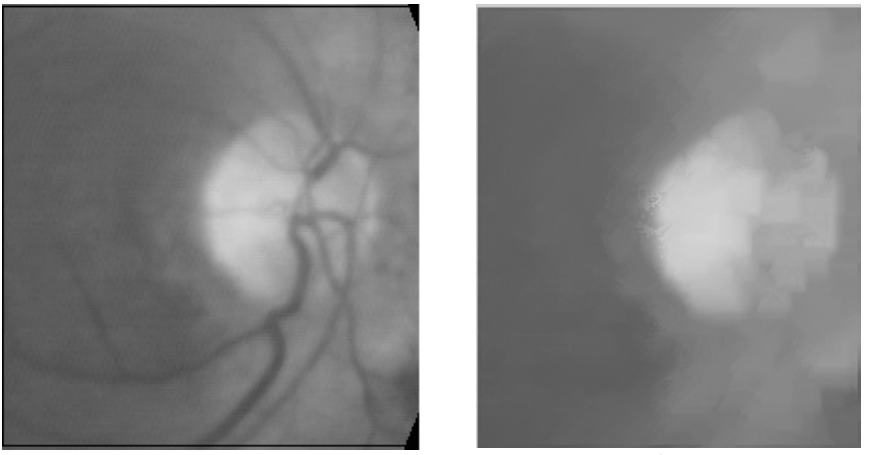

a) b)

Fig. 2. a) The 300x300 working window of image 1.c, also illustrated by figure 3.a. b) The result of vessels erasing

Tests have been made with different lengths of structuring element but no smoother images were obtained.

Eventually for further development, to measure the vessels width in certain point of interest, similar vessels segmentation technique as the one proposed in [6] will be tested. For instance in [6] from the initial image is obtained, in a similar way as image I_B , a cleaner image than the original one: $I_C = \max_{i=1,\ldots 12}\left(\gamma_{B_i}(I)\right)$. If the image I is used as a mask image and the image I_C as a marker image applying a reconstruction,

as defined in [6], a much cleaner image I_D is obtained: $I_D = R_I(I_C)$. The image with very clear segments of the vessels, suitable for measurements, is: $I_V = I_D - I_B$.

Coming back to our disc segmentation approach the next operation on image I_B is a Canny filtering followed by binarization to obtain the disc edges, in order to perform a final circle fitting. Let us note with I_{Canny} the binary image containing the Canny edges.

Due the great variability of pathology and image primary sources a fixed threshold for Canny filter is not desirable. We propose an iterative approach:

1. Compute a binarization threshold using Otsu method, [9], on image I_B, without performing the binarization.
2. Choose a value close to Otsu threshold as a primary threshold for Canny filtering.
3. Perform Canny filtering.
4. For an interval $[r_{\min}, r_{\max}]$ of circle radius compute a circle fitting by Hough transform applied on the whole window.
5. Choose the centre radius with the best fitting score and best distribution of fitting points.
6. If the fitting score is not desirable or there are few points to perform the fitting decrease the Canny threshold by a certain amount (constant in our implementation). Not more than a predefined number of iterations resume the process from step 3.
7. Even the fitting score and the distribution fitting points are acceptable run at least one more time all the cycle (steps 3-5) with a new Canny decreased threshold.
8. If the detected circles have comparable fitting scores and fitting point distributions choose the circle with the longest radius.

Results of the proposed approach are illustrated by figure 3 where are depicted: a) the original image from figure 1.c; b) the Canny edge extraction results for the starting threshold; c) Canny edges for adapted threshold; d) final circle.

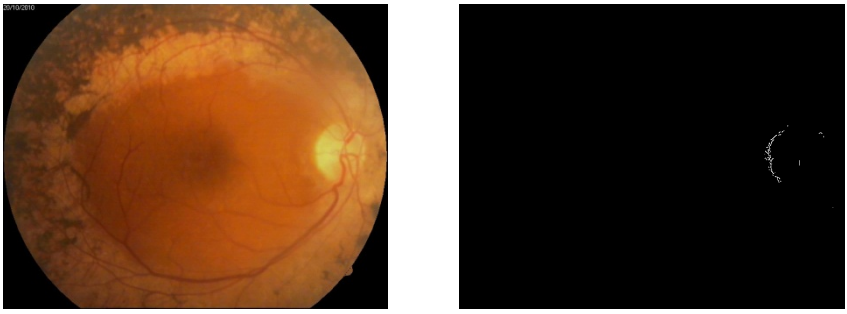

a) b)

Fig. 3. a) the input RGB image, in this case the same as in figure 1.c; b) the Canny edge extraction results for the starting threshold; c) Canny edges for adapted threshold; d) final circle.

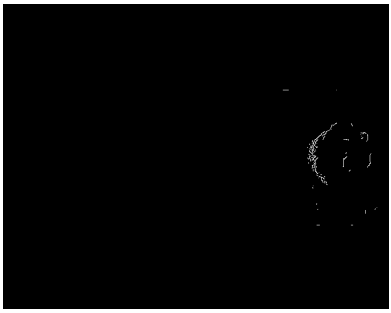

c)

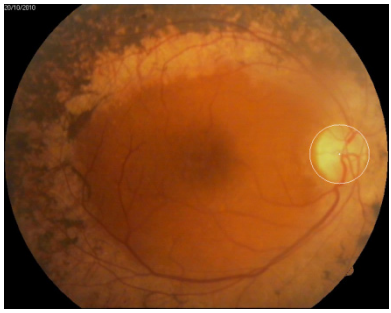

d)

Fig. 3. (*continued*)

While Canny filtering was performed using the OpenCV function for Hough transform we implemented our own method:

1 Create image accumulator I_{acc}.

2 For each radius integer r in the interval $[r_{\min}, r_{\max}]$ do:

2.1 Clean I_{acc}.

2.2 For each pixel $p(x_c, y_c)$ of I_{Canny} image do:

2.2.1 For $x = x_c - \frac{r}{2}$ to $x_c + \frac{r}{2}$ do:

2.2.1.1 $y_{frac} = \sqrt{r^2 - (r-x)^2}$

2.2.1.2 If there are pixels "1" in a 3x3 neighborhood of $I_{Canny}(x, y_c + y_{frac})$

then $I_{acc}(x_c, y_c) = I_{acc}(x_c, y_c) + 1$

2.2.1.3 If there are pixels "1" in a 3x3 neighborhood of $I_{Canny}(x, y_c - y_{frac})$

then $I_{acc}(x_c, y_c) = I_{acc}(x_c, y_c) + 1$

2.2.2 For $y = y_c - \frac{r}{2}$ to $y_c + \frac{r}{2}$ do:

2.2.2.1 $x_{frac} = \sqrt{r^2 - (r-y)^2}$

2.2.2.2 If there are pixels "1" in a 3x3 neighborhood of $I_{Canny}(x + x_{frac}, y)$

then $I_{acc}(x_c, y_c) = I_{acc}(x_c, y_c) + 1$

2.2.2.3 If there are pixels "1" in a 3x3 neighborhood of $I_{Canny}(x - x_{frac}, y)$

then $I_{acc}(x_c, y_c) = I_{acc}(x_c, y_c) + 1$

2.3 Choose the current centre the pixel $p(x_c, y_c)$ for which $I_{acc}(x_c, y_c) = \max_{x=1,n;\, y=1,m} I_{acc}(x, y)$.

2.4 Keep track of the best fitting circle considering the number of fitting points and the distance between the current circle centre and the mass centre of the fitting points.

We opted for our own Hough transform implementation in order to get more control on the distribution of the fitting points. This way some configurations can be rejected even there are generated by an acceptable number of fitting points if the points are not equally distributed around circle center.

3 Results and Conclusions

Tests have been done on 86 RGB retinal images of 720x576 resolution. The rough optic disc localization has been successful on whole the image set. The final circle fitting failed on two images strongly affected. Figure 4 illustrates some final circle localization results. The further tests will be done to validate and eventually to improve our optic disc detection approach.

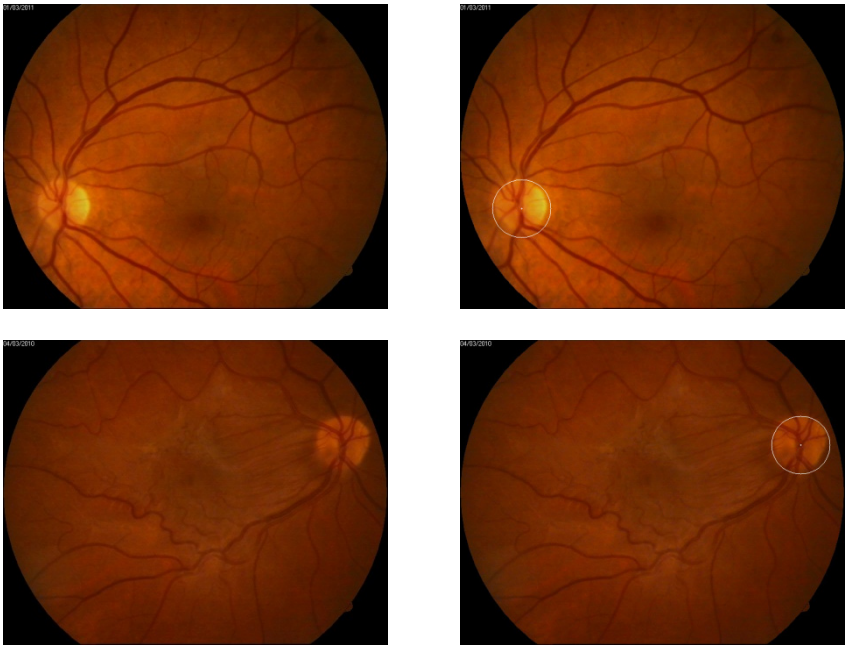

Fig. 4. On the left column: original retinal images. On the right: the final optic disc localization results.

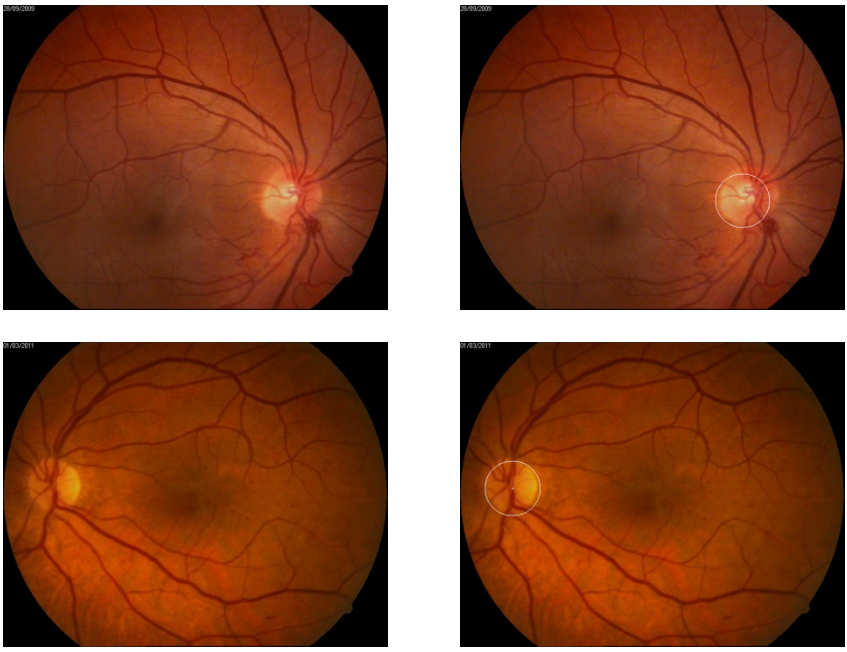

Fig. 4. (*continued*)

The reported work is a first stage of a larger project that will be completed later on with other tasks as fovea detection and measurement of retinal vessels. The final goal is to detect in early stages signs of ophthalmic pathologies as diabetic retinopathy or glaucoma.

The optic disk localization procedure was implemented and tested in an image processing framework developed by authors. It is implemented as a Windows application, in C++ using Microsoft Visual Studio. For image manipulation and some processing functions, the OpenCV library is used.

Acknowledgments. The work was done as part of a research contract with University of Medicine and Pharmacy „Gr.Popa" Iasi to analyze retinal images for early prevention of ophthalmic diseases. The authors would like to tank Dr. Traian Mihaescu for his assistance.

References

1. Aquino, A., Gegundez-Arias, M.E., Marin, D.: Detecting the Optic Disc Boundary in Digital Fundus Images Using Morphological, Edge Detection, and Feature Extraction Techniques. IEEE Transactions on Medical Imaging 29(11), 1860–(1869)
2. Manikis, G.C., Sakkalis, V., Zabulis, X., Karamaounas, P., Triantafyllow, A., Douma, S., Zamboulis, C., Marias, K.: An Image Analysis Framework for the Early Assesement of Hypertensive Retinopathy Signs. In: Proceedings of the 3rd IEEE International Conference on E-Health and Bioengineering - EHB 2011, Iaşi, Romania, November 24-26, pp. 413–418 (2011)

3. Li, H., Chutatape, O.: Automated Feature Extraction in Color Retinal Images by a Model Based Approach. IEEE Transactions on Biomedical Engineering 51(2), 246–254 (2004)
4. Hoover, A., Goldbaum, M.: Locating the optic nerve in a retinal image using the fuzzy convergence of the blood vessels. IEEE Trans. Med. Imag. 22(8), 951–958 (2003)
5. Foracchia, M., Grisan, E., Ruggeri, A.: Detection of optic disc in retinal images by means of a geometrical model of vessel structure. IEEE Trans. Med. Imag. 23(10), 1189–1195 (2004)
6. Heneghan, C., Flynn, J., O'Keefe, M., Cahill, M.: Characterization of changes in blood vessel width and tortuosity in retinopathy of prematurity using image analysis. Med. Image Anal. 6, 407–429 (2002)
7. Lindeberg, T.: Detecting salient blob-like image structures and their scales with a scale-space primal sketch: A method for focus-of attention. International Journal of Computer Vision 11, 283–318 (1993)
8. Guo, Y.: Computer-Aided Detection of Breast Cancer Using Ultrasound Images. PhD Thesis, Utah State University (2010)
9. Otsu, N.: A Threshold Selection Method from Gray-Level Histograms. IEEE Transactions on Systems, Man, and Cybernetics 9(1), 62–66 (1979)

Parallel Multiclass Support Vector Interpretation of Haemodynamic Parameters for Manifestation of Aortic and Arterial Occlusive Diseases

S.H. Karamchandani[1], V.K. Madan[2], P.M. Kelkar[3], S.N. Merchant[1], and U.B. Desai[4]

[1] Indian Institute of Technology – Bombay, Mumbai 400076, India
[2] Kalasalingam University, Krishnankoil, Virudhunagar Dt (TN) 626126, India
[3] Sneha Health Care Centre, Mumbai 400602, India
[4] Indian Institute of Technology – Hyderabad, Hyderabad 502205, India
karamchandani@iitb.ac.in, KLvkmadan@gmail.com, drprasannakelkar@yahoo.com, merchant@ee.iitb.ac.in, ubdesai@iith.ac.in

Abstract. Aortic and arterial occlusive diseases are congenital conditions manifested in impedance plethysmography and are difficult to interpret. A parallel multiclass support vector classification of haemodynamic parameters computed from plethysmographic observations is proposed for diagnosis of aortoarteritis, atherosclerotic narrowing and coarctation of aorta. The proposed support vector algorithm was able to detect more precisely the presence of thrombotic occlusions at proximal and distal arteries. The proposed method provided better accuracy and sensitivity of 97.46% and 98.3% compared to principal component analysis (PCA) based backpropagation and non-weighted support vector architectures respectively. The results of the genotype were ably supported by receiver operating characteristics (ROC) curves which depict a ratio of true positive rate and false positive rate of over 0.9 for all classes as compared with ratios varying from 0.7 to 0.9 for majority of classes as observed in case of non weighted architecture. A reduction of over 60% in negative likelihood ratio with a 5% increase in negative predictive value was observed as compared to Elman and PCA based backpropagation architectures. The results were validated from angiographic findings at Grant Medical College, J.J. Hospital, and Bhabha Atomic Research Centre (BARC) all in Mumbai. The proposed method also distinguished cases with nephritic syndrome, lymphangitis, and venous disorders against those with arterial occlusive diseases. Application of the proposed method has potential to enhance performance of impedance plethysmography.

Keywords: Impedance Cardiovasography, Aortic Occlusive Diseases, Arterial Occlusive Diseases, Parallel Multiclass support vector machines.

V.E. Balas et al. (Eds.): Soft Computing Applications, AISC 195, pp. 465–486.
springerlink.com

1 Introduction

Vascular obstruction to blood flow at young age are very low (~0.01%). However they become significant above 40 years of age (~1%) and above 60 years of age (~20 to 30%) [1]. Different non invasive techniques such as photo plethysmography and Doppler exist for tracking vascular obstructions. The photo plethysmography is useful on fingers, toes and ear lobes, but not on limbs [2]. The conventional Doppler is useful for superficial blood vessels, and the performance is and operator dependent. The color Doppler is an expensive technique and demands expertise. Moreover its performance degrades significantly for collateral circulation and distal runoff. Impedance cardiovasography (ICVG) based on the principle of impedance plethysmography is a non invasive procedure for diagnosis of aortic occlusive diseases such as coarctation of aorta, aortoarteritis, atherosclerotic narrowing and Leriche's syndrome [3-4]. Calin et al. have designed an equilibrated bridge which uses an external signal generator for measuring haemodynamic parameters on the plethysmographic wave [5]. However the procedure discussed for normal subjects does not portray the variations in the plethysmographic waves for diseased cases [6]. A color relation analyzer (CRA) classifier detects plethysmographic signals for lower limb peripheral vascular occlusive disease (PVOD) assessment [7], and signals are measured at the toes to arrive at disease prognosis. It does not provide analysis of haemodynamic parameters. Hull et al restrict the use of impedance plethysmography for detection of deep vein thrombosis [8]. Forearm impedance plethysmography introduced for monitoring the cardiac pumping function [9] was not useful for determining absolute stroke volume.

It is proposed to enhance diagnostic capabilities of impedance plethysmography through measurement of hemodynamic parameters of amplitude and time for diagnosis of occlusive diseases such as aortoarteritis, atherosclerotic narrowing and coarctation of aorta. For the study of peripheral circulation, impedance cardiograph was recorded from the neck, and at four locations in the lower extremities of thigh, knee, calf and ankle using ICVG [10]. The mentioned measurements were used as pattern recognition parameters and a real time technique classifier was developed using an assortment of multiclass parallel support vector machine (pSVM) algorithms.

The paper describes below the acquisition of the plethysmographic data, estimation of the haemodynamic parameters and their relevant significance, interpretation of the parameters for diagnosis of aortic and arterial occlusive diseases, the proposed multiclass pSVM, experimental results, conclusion, and a possible direction for further work.

2 Data Acquisition

Impedance plethysmography gives an indirect assessment of blood volume changes in any part of the body segment as a function of time [11-14]. The impedance plethysmography relates volume of blood (ΔV) entering a body segment during entire systole to the total change in impedance (ΔZ) occurring during the period [15] as Eq. 1

$$\Delta V = \rho_b \frac{L^2}{z_o^2} \Delta Z \tag{1}$$

where ρ_b is the resistivity of blood, L is the length of the limb segment, and z_o is the basal impedance of the body segment. This change in impedance is measured for locations of thigh, knee, calf and ankle in the supine and elevated postures (45°).

About 200 subjects with severe joint pains, oedema in legs, pain in calf muscles, and swelling in the ankle were subjected to plethysmographic observations for disease characterization. ECG electrodes, E1 and E2 were applied in the lead II configuration. The sensing electrodes were applied around the segment of interest with the patient in the supine, while current electrodes were applied as far away as possible from sensing electrodes on the limb. The magnitude of current flowing through the body was 2 mA. The waveforms were recorded from each of the extremity for about 300 sec followed by ensemble averaging to enhance signal to noise ratio. A typical impedance waveform is shown in Fig. 1(e) courtesy ref. (1).

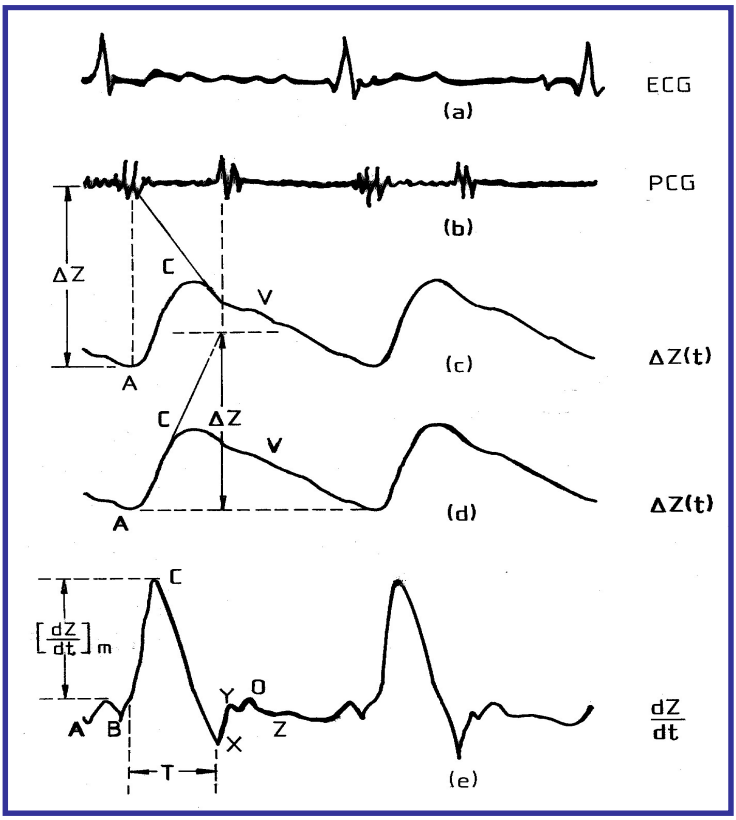

Fig. 1. Impedance cardiovasographic ΔZ (t) and dZ/dt waveforms in relation to electrocardiogram and phonocardiogram

Haemodynamic parameters used were z_o, ΔZ (t), dZ/dt, and the time elapsed between the R-wave and various phase reversal points in the impedance waveform [16]. An ICVG system provides normalized rate of change of impedance (NdZ/dt) [17-18].

3 Computation of Haemodynamic Parameters from Impedance Waveform

Parametric measurements of amplitude and time are useful for computing haemodynamic parameters from the impedance waveform. The maximum rate of change of impedance is calculated as a measure of the peripheral blood flow while the relative time measurements are performed in terms of differential pulse arrival time (DPAT).

3.1 Peripheral Blood Flow

Change in impedance, ΔZ, is obtained as the product of the maximum rate of change of impedance with systolic time interval T_s. Modifying Eq. 1, we get,

$$dV = \rho_b \frac{L^2}{Z_o^2} (dZ/dt)_m T_s \tag{2}$$

where $(dZ/dt)_m$ is the maximum amplitude of the normalized impedance waveform
Resistivity is related to other parameters as

$$\rho_b L^2 = Z_o V \tag{3}$$

From (2) and (3)

$$dV = V \frac{(dZ/dt)_m T_s}{z_o} \tag{4}$$

Blood Flow in ml per 1000 cc of body tissue per cardiac cycle is defined as

$$dV = 1000 \frac{(\frac{dZ}{dt})_m}{z_o} T_s \tag{5}$$

The product $(dZ/dt)_m T_s$ represents the total change in the impedance during the systolic period. BCX in Fig. 2(b) depicts systolic wave, and T_s was computed by measuring the distance RX-RB in the figure. T_s represents the left ventricular ejection time (LVET) and it remains fairly constant in a person [19]. Maximum amplitude of dZ/dt waveform was computed by measuring BC. The Eq 5 is rewritten as

$$dV = 1000 \frac{(BC)}{z_o} (RX - RB) \tag{6}$$

The normalized dZ/dt waveform measures the ratio $(BC)/z_o$. From Eq. 6 we get parameter Blood Flow Index (BFI) representing maximum amplitude of $\frac{dZ}{dt}$ for arterial blood flow.

$$\text{Blood flow Index} = k \frac{(BC)}{z_o} \tag{7}$$

3.2 Differential Pulse Arrival Time

As shown in Fig. 2 courtesy ref. (1), RC represents the time taken by the blood to reach a particular location measured with respect to the R-wave of the ECG, and is designated as pulse arrival time (PAT). Differential pulse arrival time (DPAT) between two locations was obtained from PAT by subtracting RC of proximal location from RC of distal location.

Table 1. Ideal DPAT conditions at measured anatomical locations

Segment	DPAT (ms)
Neck to upper arm	30 ± 2.5
Upper arm to elbow	20 ± 2.5
Elbow to wrist	25 ± 2.5
Neck to upper thigh	75 ± 5.0
Upper thigh to knee	35 ± 5.0
Knee to ankle	40 ± 5.0

Data from Clinical Investigation on Normal Subjects at J.J.Hospital, Mumbai

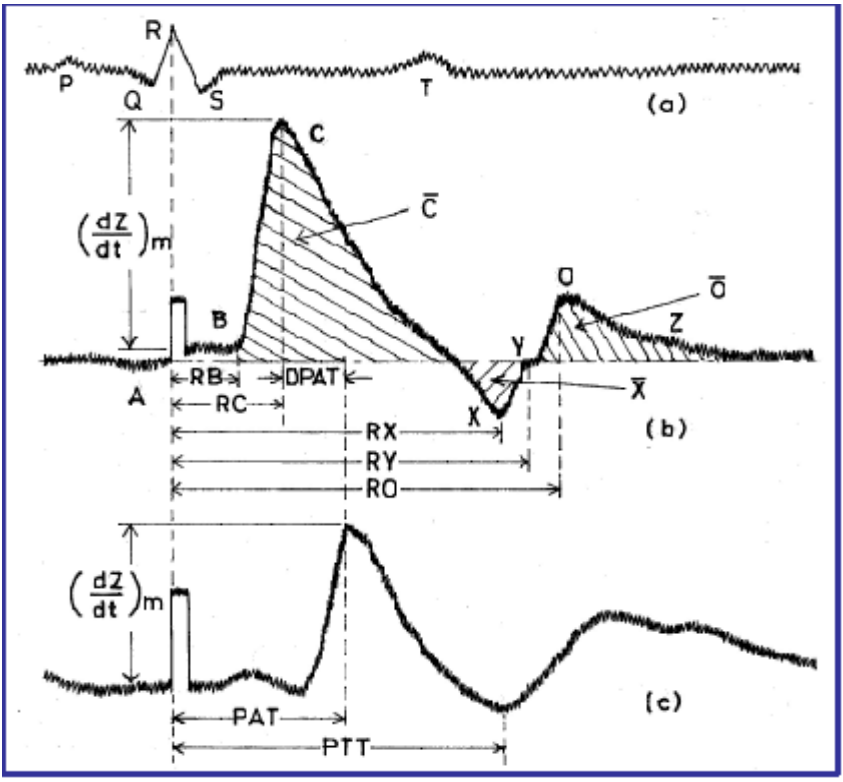

Fig. 2. Impedance waveforms at proximal and distal locations

.A: Atrial Systole; B: Aortic valve opening; C: Instant of Maximum Ejection Rate of Left Ventricle; X: Aortic valve closure; Y: Pulmonary valve closure; O: Mitral Valve Opening; Z: End of Rapid Filling Phase.

It is observed from the Table 1 that the DPAT may increase, remain unchanged or decrease depending upon whether the occlusion is complete, partial or has generalized narrowing of the blood vessels. Protective role of collaterals on myocardial electrophysiology was suggested in [20-21]. In case of complete occlusion, blood reaches the distal segment through the collaterals developed biologically and therefore traverses more distance taking more time to reach the distal segment, and hence causing an increase in the value of DPAT. In case of partial occlusion, change in the value of DPAT may not be significant. In case of generalized narrowing of blood vessels the blood may reach the distal segment faster as the blood velocity increases due to decreased lumen of blood vessel and its compliance. This causes a decrease in the value of DPAT.

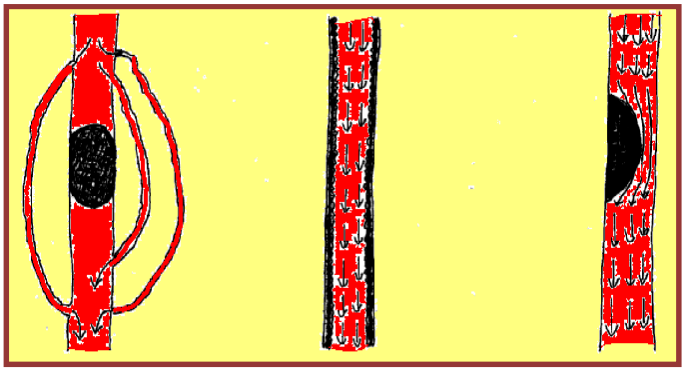

Fig. 3. (a) Complete Occlusion (b) Generalized Narrowing of the Arteries (c) Partial Occlusion

4 Interpretation of Haemodynamic Parameters in Diagnosis of Aortic and Arterial Occlusive Diseases

From the ICVG waveforms depicted in Fig. 4 courtesy ref. (2), the parameters BFI and DPAT were extracted at four locations; thigh, knee, calf and ankle from both the right and the left limbs. It provides feature vectors for multiclass pSVM for diagnosis and disease characterization.

ICVG waveform recorded from subject with aortoarteritis. Polyphasic C wave at thigh level can be observed which is specific to aortoarteritis.

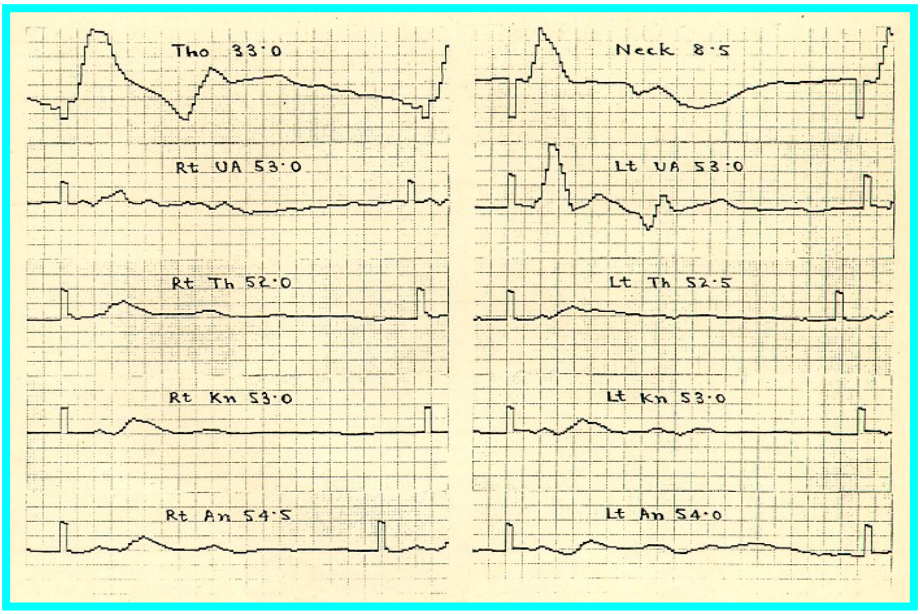

Fig. 4. ICVG waveforms recorded from subject with aortoarteritis

Table 2. ICVG parameters extracted from subject

	Right Leg		Left Leg	
Location	BFI	DPAT	BFI	DPAT
Upper Arm	0.98	20	0.93	20
Thigh	0.75	60	0.79	40
Knee	0.85	50	0.93	50
Calf	0.66	-	0.82	-
Ankle	0.80	20	0.61	50

Interpretation of the BFI and DPAT for arriving at the exact diagnosis is tabulated in Table 3.

ICVG data recorded from a 48 years old male with lymphangitis in the left lower extremity. The amplitude of the waveform does not show any variation on elevation of the limb. Table 4 depicts z_o, observed in the left extremity with lower impedance values.

Table 3. Interpretation of haemodynamic parameters for assessment of physiological functionality

Physiological functionality	Interpretation of Haemodynamic Parameters
Aorto Arteritis	Decreased BFI with marginal increase in DPAT in both legs. Systolic wave at the thigh level, which is caused by either multiple occlusions or narrowing in the aorta.
Atherosclerotic narrowing of the aorta	Significant decrease in the value of DPAT at thigh level in both the extremities with marginal decrease in the value of BFI. The morphology of the dZ/dt waveform is different in these cases due to contribution from change in the resistivity of blood moving with higher velocity. These changes are evident at knee and ankle locations due to higher bone to muscle ratio. The amplitude of the systolic wave is either normal or increased in contrast to other conditions and is not representative of the value of blood flow
Occlusions at aorto-iliac bifurcation	Characterized by marked decrease in blood flow at thigh level with a marked increase in DPAT at the knee location. If such changes are observed in one extremity, other remaining normal, such a subject is diagnosed as hemi-Leriche's syndrome.
Co-arctation of the aorta	Blood flow in both the lower extremities at the thigh location is significantly reduced with increase in the value of DPAT.
Nephrotic syndrome, Lymphangitis Deep vein thrombosis	There is a marked decrease in blood flow without any abnormalities in value of DPAT. However oedema due to these diseases causes a marked decrease in the value of basal impedance z_o, which is a clear indication for the clinicians to classify the subject to have oedema of extra vascular nature. The diagnosis of arterial occlusive diseases if present is not possible in such cases by impedance cardiovasography. A case of lymphangitis is reported in Table 4.

Table 4. ICVG parameters for subject with lymphangitis

Location	Right Leg			Left Leg		
	BFI	DPAT	z_o	BFI	DPAT	z_o
Thigh	0.88	70	25.51	0.48	70	16.14
Knee (s)	1.41	20	54.21	0.63	20	31.99
Calf (s)	1.64	-	48.73	0.81	-	32.69
Ankle(s)	1.57	20	69.15	0.79	20	27.49
Ankle(e)	1.66	-	71.03	0.89	-	34.44

5 Proposed Architecture of Multiclass Parallel Support Vector Machine (pSVM)

Based on the construes in Section IV, a taxonomical classification of the cardiovasographic data into seven different classes was proposed and depicted in Table 5.

Table 5. Classification of the cardiovasographic data

Assigned Class	Anatomical Condition
I	Normal
II	Narrowing
III	Block
IV	Good Collaterals
V	Moderate Collaterals
VI	Poor Collaterals
VII	Further Block

The status at each of the considered locations is established according to the flow chart shown in Fig. 5.

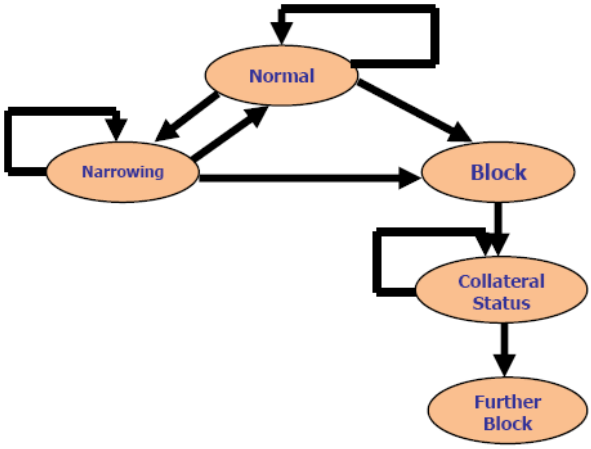

Fig. 5. Flow chart for identification of block and status of collateral circulation using extracted BFI and DPAT parameters based on the depicted anatomical conditions

A multiclass pSVM is proposed. It helps in determining location of anatomical block, and in predicting the status of collateral circulation leading to the diagnoses of aortic and arterial occlusive diseases. The pSVM is useful for multiclass classification using either the one versus all (OVA) or one versus one technique (OVO). The performance of OVA classification is quite comparable to OVO method [22-23].

The latter has its lesser training time due to a smaller training data set for each classifier [24]. Due to existence of seven different classes, the multiclass pSVM designed consisted of 7 choose 2, meaning 21 possible combinations, and hence separate SVMs to execute the OVA architecture. As depicted in Fig. 6, SVM 1 learns from outputs of class I and class II, SVM 2 from class I and class III, thus SVM 21 will compare the outputs of class VI and class VII.

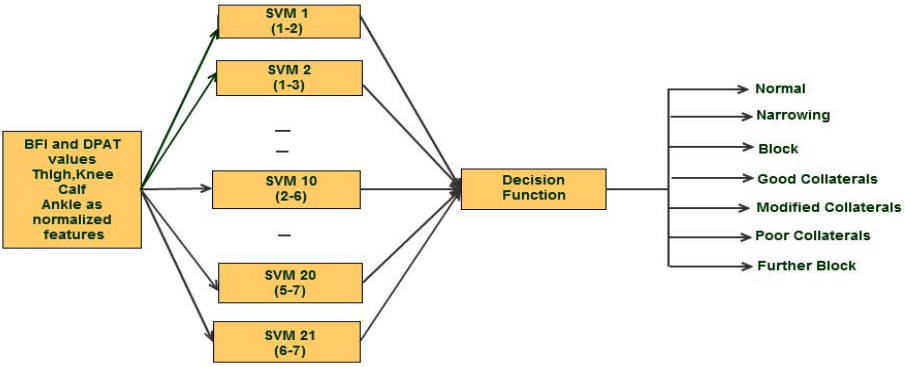

Fig. 6. Proposed pSVM architecture for multiclass classification

The pSVM was implemented in weighted and non weighted architectures. Weighted multiclass SVM assigned a different value of penalty parameter for each training sample thus compensating for the undesirable effects caused by the uneven size of the eight training classes [25]. This is incorporated in the proposed algorithm by applying equal weights to the training sample belonging to same class, and setting weights for different classes with an inverse proportion to the training class size. The weights assigned to the individual classes are given as

$$w(i) = \frac{n - n_i}{n} \tag{8}$$

where w(i) represents the weight assigned to the i^{th} class, n is the total number of training samples and n_i represents the number of training samples in the i^{th} class. The demographics of the individual seven classes and their calculated weights are shown in Table 6.

Table 6. Demographics of the training classes for pSVM architecture

Classes	I	II	III	IV	V	VI	VII
No of Training set	272	166	92	51	46	32	21
weights for each class	0.6	0.75588	0.8647	0. 925	0.9324	0.9529	0.9691

For the training vectors (x_i, y_i), i = 1, 2, 3…n, each of the twenty one SVMs solve a binary classification problem which is implemented as a soft margin classifier in Eq. 9. $x_i \in \mathbb{R}^n$ represents feature vectors and $y_i \in \{-1, +1\}$ as the complementary outputs of binary classifier.

$$\min_{w^{ij}, b^{ij}, \xi^{ij}} 1/2\ (w^{ij})^T w^{ij} + C \sum_t \xi_t^{ij}$$

With

$$(w^{ij})^T \phi(x_t) + b^{ij} \geq 1 - \xi_t^{ij}\ \text{, if } x_t \text{ in the } i^{th} \text{ class}$$
$$(w^{ij})^T \phi(x_t) + b^{ij} \geq -1 - \xi_t^{ij}\ \text{, if } x_t \text{ in the } j^{th} \text{ class}$$
$$\xi_t^{ij} \geq 0 \tag{9}$$

The feature vectors are mapped to a higher dimension using a radial basis kernel ϕ as implemented in Eq. 10

$$\phi(x_i, x_j) = \exp\left(-\gamma \left\|x_i - x_j\right\|^2\right) \tag{10}$$

$C > 0$ is a penalty parameter on the training error and ξ_i is a positive slack variable. Keerthi et al [26] indicated that if complete model selection (dynamic changes in C and γ) using the radial basis kernel were conducted, there was no need to consider linear SVM. The sigmoid kernel with scaling parameter 'a' and shifting parameter 'γ' was used as in Eq. 11 where negative values of γ are preferred to control the threshold of mapping in pSVM.

$$\phi(x_i, x_j) = \tanh(a x_i^t x_j + \gamma) \tag{11}$$

However, the kernel matrix using sigmoid may not be positive definite, has a higher number of parameters than RBF and suggests lower accuracy than RBF [27] kernels. Twenty one hyperplanes were created in the feature space $\emptyset$. The weight $w \in \emptyset$ denotes a dot product space and $\boldsymbol{b}$ represents the shift of the hyper plane in that space. The support vector algorithm was based on maximizing the hyper plane between any two classes of data in a higher dimension feature space $\emptyset$. $C(\sum_{j=1}^{j=l}(\xi_j^i)_t$ term indicates that two data sets are not linearly separable. The optimum values of required parameters, C and γ, were determined by maximizing the cross validation prediction. Each SVM solved a dual quadratic optimization problem given as

$$\max_{\alpha \in \mathbb{R}^n} W(\alpha) = \sum_{i=1}^n \alpha_i - \frac{1}{2} \sum_{i=1}^n \sum_{j=1}^n \alpha_i \alpha_j y_i y_j \phi(x_i, x_j)$$

provided

$$\sum_{i=1}^m \alpha_i y_i = 0 \tag{12}$$

where $0 \leq \alpha_i \leq C$ denotes the Lagrangian multiplier. Support vectors of the pSVM correspond to data points for which the α values are nonzero. The Hessian matrix formed by $y_i y_j \emptyset(x_i x_j)$ of order (n x n), has a computational complexity of $O(n^2)$. The computational load for OVO ($O(2\frac{(k-1)n^2}{k})$) is lesser than that of OVA technique with ($O(k\,n^2)$, where k represents the number of classes with n data points. The i^{th} SVM is trained with all examples in the i^{th} class with positive labels and all other examples with negative labels. For each class j the SVM is trained in class j as positive and rest of the instances as negative.

A leave 20% out cross-validation is performed on the training data set. Optimum accuracy for the overall algorithm was obtained by finding the optimum values of C and γ using a grid search procedure [28-29]. These optimum values of C and γ were fixed and used for prediction. Given a new input x, its class by was predicted by evaluation of the decision function given as

$$d = \mathrm{sgn}\left(\sum_{k=1}^{n} y_n \alpha_k^{ij} \phi(x, x_k) + b^{ij}\right) \tag{13}$$

for

$$\alpha_k \geq 0.1 \tag{14}$$

Based on the above decision function, the algorithm discriminated between every pair of classes, and in selection of classes using a majority voting rule [30], meaning it selects a class with most winning two class decisions as given below.

$$\delta_p = \sum_i (\arg\max_j \sum I_{(d_{ij} > d_{ji})}) \tag{15}$$

where δ_p is a label predicting the i^{th} class while the indicator function I represents a unity value if $d_{ij} > d_{ji}$. An SVM with larger margin and/or a smaller number of support vectors is expected to have better generalization performance [31].

6 Experimental Results

Data acquired from 164 subjects were used. Out of the 164 subjects (excluding those with nephortic syndrome, lymphangitis or deep vein thrombosis) undergoing ICVG, 79 subjects with various aortic and arterial disorders were considered for testing. The plot for cross validation accuracy against the penalty parameter C is plotted for different values of γ in Fig. 7.

The value of the parameters C (276) and γ (0.2) are obtained by maximizing the cross validation prediction. The above values of C and γ provide the highest cross validation accuracies. The corresponding test accuracies obtained are shown in Table 7.

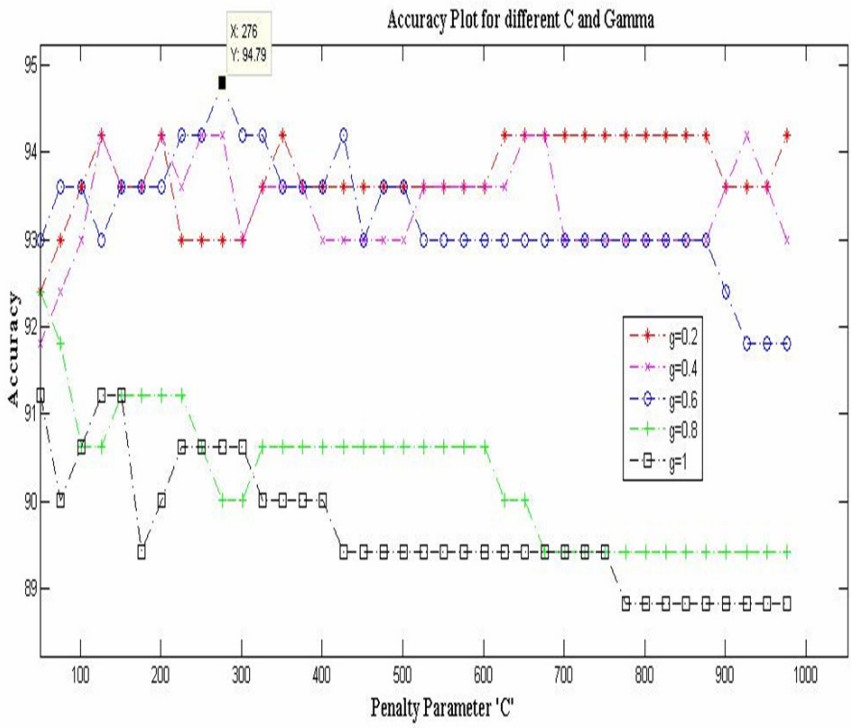

Fig. 7. Cross validation prediction

Table 7. Cross validation and classification accuracy for pSVM and weighted pSVM architectures

Parameters	pSVM	Weighted pSVM
Cross validation accuracy (%)	94	94.79
Classification (Test) accuracy (%)	96.2	97.46

Fig. 8 courtesy ref. (2), illustrates the ICVG waveform of subject with diseases of the calf vessels. The required BFI and DPAT parameters at the four locations are extracted using impedance cardiovasograph. Table 8 illustrates these parameters which represent the input to the pSVM architectures. The predicted output of the weighted pSVM is observed in Table 9.

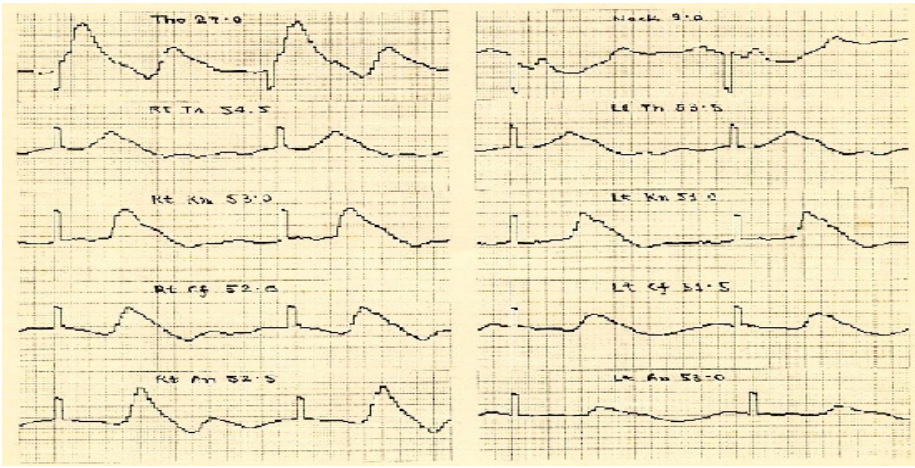

Fig. 8. ICVG waveform recorded from a patient with disease of calf vessels

Table 8. Extracted parameters from subject SJB-30-M

Location	Right Leg		Left Leg	
	BFI	DPAT	BFI	DPAT
Thigh	1.25	80	1.23	80
Knee	1.56	50	1.29	40
Calf	1.47	-	1.10	-
Ankle	1.61	20	0.70	50

Table 9. Weighted pSVM prediction

Location	Right Leg	Left Leg
Thigh	I	I
Knee	I	I
Calf	I	III
Ankle	I	V

Table 9 gives the diagnosis for subject based on the weighted pSVM algorithm. Though there is a slight reduction in DPAT value of the ankle in the right leg, the same is ignored in the view of normal and consistent BFI values. There is a marginal decrease in the value of BFI at the calf and a further decrease in its value at the ankle in the left leg with a marginal increase in DPAT indicating presence of an occlusion at the calf in the left leg.

Table 10 shows the performance results of the weighted pSVM on a set of 79 subjects with different combinations of aortic, femoral and distal blocks.

Table 10. Performance of proposed weighted support vector algorithm (pSVM)

Diagnosis with proposed weighted pSVM	No. of Subjects	Angiographic Results
Normal subjects correctly classified.	8	TN 16
Normal subject Aroposed algorithm predicts a distal artery block in the right limb	1	TN 1 FP 1
Normal subject Algorithm predicts a block at the thigh level in the right limb	1	TN 1 FP 1
Femoral artery occlusion in both limbs with varying collateral status at calf and ankle.	7	TP 14
Femoral artery occlusion in left leg with collateral status at calf and ankle. Right Leg gives normal diagnosis.	6	TP 6 TN 6
Femoral block with collateral conditions at calf and a further block at ankle in both limbs.	2	TP 4
Femoral block in one limb with a further block above the ankle. Normal diagnosis in the other limb.	4	TP 4 TN 4
Femoral block in the affected limb with collateral circulation. Atherosclerotic affection of aorta in the other limb	6	TP 12
Atherosclerotic affection of arteries. However, for one patient, our algorithm predicts normal for both limbs.	5	TP 8 FN 2
Narrowing of the aorta which persists throughout. Block above ankle in other limb. Arteriographic findings revealed a slight narrowing in one patient.	5	TP 10
Block above ankle in one limb. Normal diagnosis of the other limb.	3	TP 3 TN 3
Block above the ankle in both the limbs.	2	TP 4
Co-arctation of aorta with collateral condition at knee, calf and ankle.	3	TP 6
Hemi Leriche's syndrome Diagnosis of the other limb is Normal.	5	TP 5 TN 5
Occlusion at aortic-iliac bifurcation.	5	TP 10
Hemi Leriche's syndrome with collateral status at distal locations Narrowing detected in the other limb.	3	TP 6
Hemi Leriche's syndrome with a Further Block at ankle. Normal diagnosis of the other limb	2	TP 2 TN 2

TP: True Positive TN: True Negative FP: False Positive FN: False Negative

Fig. 9 depicts the angiographic correlation which agrees with the experimental results.

Arteriogram of the left leg reveals external iliac, common femoral, superficial and deep femoral arteries to be normal. The trifurcation of popliteal artery and proximal portions of anterior and posterior tibial and the common peroneal arteries are seen to be normal. Posterior tibial is seen up to the distal calf region and not seen at ankle or below ankle region. The anterior tibial and common peroneal are not seen below mid calf region. These observations validate the ICVG diagnosis in this patient.

Fig. 9. Angiographic correlation (Courtesy, J.J Hospital)

Tables 11 - 13 show examples of false positive and false negative diagnosis of the weighted pSVM.

Table 11. False positive diagnosis by the weighted pSVM

Location	Right Leg		Left Leg	
	BFI	DPAT	BFI	DPAT
Thigh	0.86	80	0.95	60
Knee	1.26	30	0.58	30
Calf	1.25	00	1.47	00
Ankle	1.27	30	1.46	50

The case detected as false positive is of a 56 year female as analyzed in Table 11. The support vector algorithm predicts a 'block' at the thigh level followed by 'good collaterals' at the knee, calf and ankle locations for the left limb while providing diagnosis for the other as 'normal'. Angiogram of the patient however shows normal blood circulation in both the limbs. There is an inconsistency in the data of the left leg which was not recognized by the algorithm.

Table 12. False positive diagnosis by the weighted pSVM

Location	Right Leg		Left Leg	
	BFI	DPAT	BFI	DPAT
Thigh	0.75	70	0.73	70
Knee	1.37	30	1.21	50
Calf	1.23	-	1.33	-
Ankle	1.22	50	1.26	30

The case is of 25 year old male. Angiogram of the patient shows no significant arterial occlusion in the right limb. Our algorithm predicts a 'block' at the distal location in the right leg and a normal prediction for the left.

Table 13. False negative diagnosis by weighted pSVM

Location	Right Leg		Left Leg	
	BFI	DPAT	BFI	DPAT
Thigh	1.03	50	0.98	60
Knee	1.09	30	0.83	30
Calf	1.03	-	1.07	-
Ankle	0.85	30	0.82	30

The above is a case of 60 year old male with pain in the right leg and an inability to walk for a long time. Digital angiogram in the patient shows tapered narrowing of both the subclavian arteries; however the algorithm predicts 'normal' diagnoses in both the limbs. Table 14 shows the confusion matrix for the weighted pSVM architecture.

Table 14. Confusion matrix for the weighted pSVM architecture

I	244 38.6%	0 0.0%	2 0.3%	1 0.2%	2 0.3%	1 0.2%	0 0.0%	97.6% 2.4%
II	7 1.1%	153 24.2%	0 0.0%	0 0.0%	0 0.0%	0 0.0%	0 0.0%	95.6% 4.4%
III	0 0.0%	0 0.0%	78 12.3%	0 0.0%	0 0.0%	0 0.0%	0 0.0%	100% 0%
IV	0 0.0%	0 0.0%	0 0.0%	40 6.3%	2 0.2%	0 0.0%	0 0.0%	95.2% 4.8%
V	0 0.0%	0 0.0%	0 0.0%	0 0.0%	42 6.6%	0 0.0%	0 0.0%	100% 0%
VI	0 0.0%	0 0.0%	0 0.0%	0 0.0%	1 0.0%	43 6.8%	4 0.6%	97.7% 2.3%
VII	0 0.0%	0 0.0%	0 0.0%	0 0.0%	0 0.0%	0 0.0%	16 2.5%	100% 0%
TP FN	97.2% 2.8%	100% 0%	97.5% 2.5%	97.6% 2.4%	89.4% 10.6%	97.7% 2.3%	100% 0%	97.5% 2.5%
Class	I	II	III	IV	V	VI	VII	TN FP

Output Class

Target Class

The coefficient of confusion is calculated as

$$c = \frac{\text{Number of misclassifications}}{\text{Total number of classifications}} = 0.0253 \quad (16)$$

Table 15performs the ROC analysis for the weighted pSVM.

Table 15. ROC analysis of weighted multiclass pSVM

Disease					
Test	Present	n	Absent	n	Total
Positive	True Positive (TP)	116 *(a)*	False Positive (FP)	2 *(c)*	118 *(a + c)*
Negative	False Negative (FN)	2 *(b)*	True Negative (TN)	38 *(d)*	40 *(b + d)*
Total	--	118 *(a + b)*	--	*40 (c + d)*	158

The ROC curves for non-weighted and weighted pSVM are as shown in Fig. 10 (A) and 10 (B) respectively.

The performance of the multiclass weighted pSVM is compared against the Elman and PCA based backpropagation architectures in shown in Table 16. Backpropagation and PCA based backpropagation algorithms were implemented by the authors in [32] with the same plethysmographic data set.

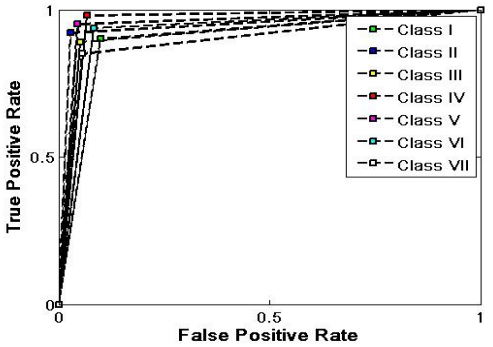

Fig. 10. (A). ROC-non-weighted pSVMs

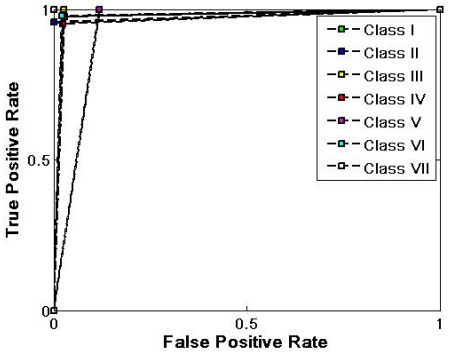

Fig. 10. (B). ROC-weighted pSVMs

Using the confusion matrices, benchmark parameters were evaluated for the non-weighted and the weighted support vector multiclass pSVMs. While the other parameters have standard definitions, the F- score is defined as the harmonic mean between specificity and positive predictive value, and Matthews Correlation Coefficient (MCC) is defined as

$$\mathrm{MCC} = \frac{\mathrm{TP}*\mathrm{TN}-\mathrm{FP}*\mathrm{FN}}{\sqrt{(\mathrm{TP}+\mathrm{FN})(\mathrm{TN}+\mathrm{FP})(\mathrm{TP}+\mathrm{FP})(\mathrm{TN}+\mathrm{FN})}} \tag{17}$$

Table 16. Performance comparison of proposed and existing architectures

Confusion Parameters	Backpropagation	PCA based backpropagation	Non-weighted pSVM	Weighted pSVM
Accuracy (%)	91.4	96.09	96.2	97.46
Precision (%)	94.19	98.85	98.29	98.3
Sensitivity (%)	93.1	95.5	96.63	98.3
Specificity (%)	87.8	97.36	94.8	95
F-score (%)	93.69	97.46	96.51	96.62
Negative Predictive Value (%)	85.71	90.24	90.24	95
Positive Likelihood Ratio	7.6311	36.31	18.58	19.66
Negative Likelihood Ratio	7.858	4.622	3.55	1.78
MCC	0.804	0.9098	0.90	0.933

Proposed weighted pSVM performs better than PCA based backpropagation and non-weighted pSVMs. A reduction of about 2% in the specificity (ability to identify the negative results) was compensated well by a 5% increase in the negative predictive value. The positive likelihood ratio greater than 10 significantly increases the likelihood that the subject is suffering from the disease if the diagnosis is positive as predicted by PCA based backpropagation and weighted and non-weighted pSVMs. However 60% reduction in the negative likelihood ratio due to a higher number of true negatives (subject is not affected with the disease when diagnosis is negative) as compared with other mentioned architectures is a significant contribution of the weighted pSVMs in the diagnosis of arterial occlusive diseases. In addition the highest MCC, a noteworthy parameter for multiclass comparison, exhibited by weighted pSVM substantiates this claim.

7 Conclusion

ICVG is used for diagnosis and early recognition of arteriosclerosis, chronic and/or acute arterial vascular diseases, and functional circulatory disturbances. It helps in estimating impact of pharmaceuticals on a vascular system. With the aid of an improved machine learning algorithms it enhances its utility to guide a clinician and aids a doctor in diagnostics.

A weighted pSVM architecture based method was proposed. The proposed method provides higher accuracy and sensitivity than PCA based backpropagation and non weighted pSVM architectures. Although the architectures suggest nearly equal values of precision, a 2% reduction is observed in the specificity of the weighted pSVM. The significant contribution of the weighted pSVM method, however, is the reduction of the negative likelihood ratio by over 60% and increase in the negative predictive value by more than 5% as compared with the above mentioned architectures. A positive likelihood ratio of over 10 provided a large and conclusive increase in the likelihood of a disease, and it was supported with multiclass performance characteristic with Matthews correlation coefficient of 0.933.

The machine interpretation of the haemodynamic parameters, as proposed, may aid in proliferation of medical access to more individuals.

References

1. Jindal, G.D., Ananthakrishnan, T.S., Kataria, S.K.: An introduction to impedance cardiovasography. In: Proc. Symposium on Biomedical Engineering and Nuclear Medicine (SBME-NM). Bhabha Atomic Research Centre, Mumbai E /003 (2001)
2. Jindal, G.D., Ananthakrishnan, T.S., Kataria, S.K.: Electrical impedance and photo plethysmography for medical applications. In: Proc. Symposium on Biomedical Engineering and Nuclear Medicine (SBME-NM), Bhabha Atomic Research Centre, Mumbai, E /025, Microfiche 2005/60371 (Q), pp. 134–138 (2005)
3. Golden, J.C., Miles, D.S.: Assessment of Peripheral Haemodynamic using Impedance Plethysmography. Physical Therapy 66(10), 1544–1547 (1986)

4. Mohapatra, S.N., Helena, A.M.: Measurement of peripheral blood flow by electrical Impedance technique. Journal of Med. Engg. & Tech. 3(3), 132–137 (1979)
5. Corciova, C., Ciorap, R., Zaharia, D., Matei, D.: On using impedance plethysmography for estimation of blood flow. In: 2011 IEEE International Workshop on Medical Measurements and Applications Proceedings (MeMeA), pp. 84–87 (2011)
6. Corciova, C., Ciorap, R., Zaharia, D., Matei, D.: Hemodynamic monitoring using peripheral impedance plethysmography. In: 7th International Symposium on Advanced Topics in Electrical Engineering (ATEE), pp. 1–4 (May 2011)
7. Lin, C.H.: Assessment of bilateral photoplethysmography for lower limb peripheral vascular occlusive disease using color relation analysis classifier. Comput. Methods Prog. Biomed. 103(3), 121–131 (2011)
8. Hull, R.D., Raskob, G.E., Carter, C.J.: Serial impedance plethysmography in pregnant patients with clinically suspected deep-vein thrombosis, clinical validity of negative findings. Annals of Internal Medicine 112(9), 663–667 (1990)
9. Wang, J.J., Hu, W.C., Kao, T., Peng Liu, C., Lin, S.-K.: Development of forearm impedance plethysmography for the minimally invasive monitoring of cardiac pumping function. Journal of Biomedical Science and Engineering 4(6), 122–129 (2011)
10. Peripheral Pulse Analyzer, Internet, `http://www.larsentoubro.com/lntcorporate/uploads/product/Nivomon.pdf` (last accessed June 2012)
11. Webster, J., Shankar, R., Yong, S.S.: The Contribution of Vessel Volume Change and Blood Resistivity Change to the Electrical Impedance Pulse. IEEE Transactions on Biomedical Engineering 32(3), 192–198 (1985)
12. Brown, B.H., Pryce, W.H., Clarke, R.G.: Impedance Plethysmography: Can it measure Changes in limb blood flow. Medical & Biological Engg. 13, 674–681 (1975)
13. Kubicek, W.G., Kottke, E.J., Ramos, F.J., Patterson, R.P., Witsoe, D.A., Labree, J.W., Remole, W.: The Minnesota impedance cardiograph theory and applications. Biomedical Engg. 9, 410–416 (1974)
14. Ananthakrishnan, T.S., Jindal, G.D., Sinha, V., Jain, R.K., Kataria, S.K., Deshpande, A.K.: Clinical validation of software for a versatile variability analyzer: Assessment of autonomic function. Journal of Medical Physics 32(3), 97–102 (2007)
15. Jindal, G.D., Babu, J.P.: Calibration of dZ/dt in Impedance Plethysmography. Med. & Bio. Engg. & Comput. 23, 279–280 (1985)
16. Bhuta, A.C., Babu, J.P., Parulkar, G.B.: Technical aspects of impedance plethysmography. Journal of Post Graduate Medicine 36, 264–270 (1990)
17. Jindal, G.D., Babu, J.P., Nerurkar, S.N., Kelkar, M.D., Deshpande, A.K.: Corrected formula for estimating peripheral blood flow by impedance plethysmography. Med. Bio.Engg. Comput. 32, 625–631 (1994)
18. Karamchandani, S.K., Desai, U.B., Merchant, S.N., Jindal, G.D.: Principal Component Analysis Based Backpropagation Algorithm for Diagnosis of Peripheral Arterial Occlusive Diseases. In: 22nd Canadian Conference on Electrical and Computer Engineering (CCECE), Newfoundland, Canada, May 3-6, pp. 482–485. IEEE (2009)
19. Babu, J.P., Ananthakrishnan, T.S., Jindal, G.D.: PC based impedance cardio-vasography, SBME-NM, BARC (2000)
20. Ozcan, O., Mustafa, S., Duran, D.A., Bilal, G., Omer, A., Gokhan, C., Serkan, T., Dursun, A., Yucel, B., Hatice, S.: Do collaterals affect heart rate variability in patients with acute myocardial infarction? Coronary Artery Disease 15(7), 405–411 (2004)
21. Hill, R.D., Smith, R.B.: Examination of the extremities: Pulses, Bruits, and Phlebitis. Clinical Methods, 148–153 (1990)

22. Chang, C.C., Lin, C.J.: LIBSVM: a library for support vector machines (2001)
23. Ivanciuc, O.: Applications of support vector machines in chemistry. Reviews in Computational Chemistry 23, 291–400 (2007)
24. Hsu, C., Lin, C.: A comparison of methods for multi-class support vector machines. IEEE Transactions on Neural Networks 13, 415–425 (2002)
25. Huang, Y.-M., Du, S.-X.: Weighted support vector machine for classification with uneven training class sizes. In: Proceedings of the Fourth International Conference on Machine Learning and Cybernetics, Guangzhou, pp. 4365–4369 (2005)
26. Keerthi, S.S., Lin, C.J.: Asymptotic behaviors of support vector machines with Gaussian kernel. Neural Computation 15(7), 1667–1689 (2003)
27. Lin, H.T., Lin, C.J.: A Study on Sigmoid Kernels for SVM and the Training of non-PSD Kernels by SMO-type Methods. [Technical Report]. Department of Computer Science and Information Engineering, National Taiwan University, pp. 3–4 (2003)
28. Chamasemani, F.F., Singh, Y.P.: Multiclass Support Vector Machine (SVM) classifiers - An application in hypothyroid detection and classification. In: Sixth International Conference on IEEE Bio-Inspired Computing Theories and Applications (BIC-TA), pp. 351–356 (2011)
29. Hsu, C., Chang, C., Lin, C.: A practical guide to support vector classification, [Technical Report]. Department of Computer Science and Information Engineering, National Taiwan University, pp. 3–4 (2003)
30. Wu, T.F., Lin, C.J., Weng, R.C.: Probability Estimates for Multi-class Classification by Pairwise Coupling. Journal of Machine Learning Research 5, 975–1005 (2004)
31. Liu, Y., You, Z., Cao, L.: A novel and quick SVM-based multiclass classifier. Pattern Recognition 39, 2258–2264 (2006)
32. Karamchandani, S.K., Desai, U.B., Merchant, S.N., Jindal, G.D.: Principal Component Analysis Based Backpropagation Algorithm for Diagnosis of Peripheral Arterial Occlusive Diseases. In: 22nd Canadian Conference on Electrical and Computer Engineering (CCECE), Newfoundland, Canada, pp. 482–485. IEEE (2009)

Linguistic Hedges Fuzzy Feature Selection for Differential Diagnosis of Erythemato-Squamous Diseases

Ahmad Taher Azar[1], Shaimaa A. El-Said[2],
Valentina Emilia Balas[3], and Teodora Olariu[4]

[1] Misr University for Science & Technology (MUST), 6th of October City, Egypt.
[2] Faculty of Engineering, Zagazig University, Zagazig, Sharkia, Egypt
[3] Aurel Vlaicu University of Arad, Romania
[4] Vasile Goldis Western University of Arad, Romania
Ahmad_t_azar@ieee.org, eng.sahmed@windowslive.com,
balas@drbalas.ro, olariu_teodora@yahoo.com

Abstract. The differential diagnosis of erythemato-squamous diseases is a real challenge in dermatology. In diagnosing of these diseases, a biopsy is vital. However, unfortunately these diseases share many histopathological features, as well. Another difficulty for the differential diagnosis is that one disease may show the features of another disease at the beginning stage and may have the characteristic features at the following stages. In this paper, a new Feature Selection based on Linguistic Hedges Neural-Fuzzy classifier is presented for the diagnosis of erythemato-squamous diseases. The performance evaluation of this system is estimated by using four training-test partition models: 50–50%, 60–40%, 70–30% and 80–20%. The highest classification accuracy of 95.7746% was achieved for 80–20% training-test partition using 3 clusters and 18 fuzzy rules, 93.820% for 50–50% training-test partition using 3 clusters and 18 fuzzy rules, 92.5234% for 70–30% training-test partition using 5 clusters and 30 fuzzy rules, and 91.6084% for 60–40% training-test partition using 6 clusters and 36 fuzzy rules. Therefore, 80–20% training-test partition using 3 clusters and 18 fuzzy rules are the best classification accuracy with RMSE of 6.5139e-013. This research demonstrated that the proposed method can be used for reducing the dimension of feature space and can be used to obtain fast automatic diagnostic systems for other diseases.

Keywords: Erythemato-Squamous Diseases, Soft Computing, Takagi-Sugeno-Kang (TSK) fuzzy inference system, Linguistic Hedge (LH), Feature selection (FS).

1 Introduction

Decision support systems helping physicians play an important role in medical decision making particularly in those situations where decision must be made effectively and reliably. The differential diagnosis of erythemato-squamous diseases is a difficult

V.E. Balas et al. (Eds.): Soft Computing Applications, AISC 195, pp. 487–500.
springerlink.com

problem in dermatology (Barati et al. 2011). There are six classes of erythemato-squamous diseases. They are psoriasis (C_1), seboreic dermatitis (C_2), lichen planus (C_3), pityriasis rosea (C_4), chronic dermatitis (C_5) and pityriasis rubra pilaris (C_6). Usually a biopsy is necessary for the correct and definite diagnosis but unfortunately these diseases share many histopathological features (Govenir and Emeksiz 2000). Another problem for the differential diagnosis is that a disease may show the features of another disease at the beginning stage and may have the characteristic features at the following stages. Patients were first evaluated clinically with 12 features. Afterwards, skin samples were taken for the evaluation of 22 histopathological features. The values of these histopathological features are determined by an analysis of the samples under a microscope (Guvenir et al. 1998). Therefore, various new methods have been used for diagnosis of Erythemato-Squamous diseases like Artificial Neural Network (ANN) (Kabari and Bakpo 2009; Übeyli 2009; Karabatak and Ince 2009), Support Vector Machines (SVM) (Abdi and Giveki 2012; Xie and Wang 2011; Xie et al. 2010, 2012; Ubeyli 2008; Nanni 2006), Fuzzy expert systems and neuro-fuzzy classification (Luukka 2011a, b; Lekkas and Mikhailov 2010; Parthiban and Subramanian 2009; Polat and Günes 2006; Ubeyli and Güler 2005), nearest neighbor classifier (NNC) (Polat and Günes 2006; Govenir and Emeksiz 2000), Instance-based classifiers (Gagliardi 2011), rough sets (Revett et al. 2009), decision trees classifiers (DTC) (Ozcift and Gulten 2012; Polat and Gunes 2009; Polat and Günes 2006; Guvenir et al. 1998).

Feature selection methods have been successfully used in many areas especially in medical diagnosis to reduce the size of features collected during the clinical testing and experiments (Chrysostomou 2008). The process of feature selection is very important because it reduces the dimensionality of the data and enables learning algorithms to operate faster (reduction of the computation time), more efficiently and therefore increases the accuracy of the resulting model (Guyon et al. 2006). Therefore, this paper presents a fuzzy feature selection (FS) method based on the linguistic hedges (LH) concept (Cetişli 2010a, b) for Erythemato-Squamous diseases classification. The proposed method is used to achieve a very fast, simple and efficient computer aided diagnosis (CAD) system. It helps to reduce the dimensionality of the used data set, to speed up the computation time of a learning algorithm and therefore simplifies the classification task.

The rest of this paper is organized as follows: in Section 2, a review of the classifiers that are considered in Erythemato-Squamous diseases diagnosis. Section 3 provides subjects and methods that are used in this study. In Section 4, a detailed description of the proposed feature selection method that is considered in Erythemato-Squamous diseases diagnosis is presented. Section 5 reports the results of experimental evaluations of the adaptive neural-fuzzy classifier and finally, in Section 6, conclusion and directions for future research are presented.

2 Related Works

Güvernir et al. (1998) developed a classification algorithm VFI5 called ''Voting Feature Intervals'' and it was applied for the differential diagnosis of erythemato-squamous diseases. Genetic algorithm for learning the feature weights was used with

the Nearest Neighbor classification algorithm and was applied to determine the weights of the features to be used with the VFI5 algorithm which achieved 96.2% accuracy on the Dermatology dataset. Govenir and Emeksiz (2000) presented an expert system for differential diagnosis erythemato-squamous diseases incorporating decisions made by three classification algorithm: nearest neighbor classifier, naive Bayesian classifier and voting feature intervals-5. The features are assigned weights such that the irrelevant features have lower weights while the strongly relevant features are given higher weights. Govenir and Emeksiz (2000) used a genetic algorithm to learn the feature weights to be used with the classification algorithm. Further research by Übeyli and Güler (2005) showed a new approach based on adaptive neuro-fuzzy inference system (ANFIS) for the detection of erythemato-squamous diseases, the ANFIS model was assessed in terms of training performance and classification accuracies and showed to perform well in detecting erythemato-squamous diseases, the model achieved a total classification accuracy of 95.5% which is concluded to be good in comparison to the one of 85.5% achieved with the stand-alone neural network. Nanni (2006) investigated an ensemble of support vector machines (SVM) classifier based on random subspace (RS) and feature selection for the diagnosis of erythemato-squamous diseases, and tested it on a real-world dataset. The results improved the average predictive accuracy obtained by a ''stand-alone'' SVM or by a RS ensemble of SVM (Nani 2006). Polat and Günes (2006) developed a novel method for differential diagnosis of erythemato-squamous disease. Their method was based on fuzzy weighted pre-processing, k-NN (nearest neighbor) based weighted pre-processing and decision tree classifier. Luukka and Leppälampi (2006) presented a new approach based on similarity classifier with generalized mean and applied it for medical data. The presented method was managed to detect erythemato-squamous diseases with a good mean classification accuracy of 97.02%. In recent published study by Luukka (2011a), fuzzy entropy measures were used in feature selection. This method successfully managed to discard the non-important features in the datasets; this has positively facilitated the classification task which was done by using the similarity based on Lukasiewicz structure where a mean accuracy of 98.28% was achieved. In Luukka (2011b) study, a new nonlinear fuzzy robust principal component analysis (NFRPCA) algorithm was developed to get data into more feasible form. This new nonlinear fuzzy robust principal component analysis algorithm achieved a classification accuracy of 97.09 % accuracy with dermatology data. Ozcift and Gulten (2012) proposed a new multi-class feature selection method based on Rotation Forest meta- learner algorithm and was tested on Erythemato-Squamous diseases dataset. The Rotation Forest selection based features achieved accuracies between 98% and 99% in various classifiers. Xie et al. (2012) proposed hybrid feature selection algorithms based on generalized F-score (GF) and SVM. The new hybrid feature selection algorithms combined the strengths of filters and wrappers to uncover the optimal feature subset with the best diagnostic efficiency. Experimental results showed that the proposed hybrid methods construct efficient diagnosis classifiers with high average accuracy when compared with traditional algorithms.

3 Subjects and Methods

The dataset was taken from UCI (University of California, Irvine) machine learning repository (UCI 2012). There are 366 records in this database and each record has 34 attributes; 33 of which are linear (continuous) valued and one of them is nominal (discrete). After the 9 instances are removed from the dataset due to 8 missing values

Table 1. Erythemato-squamous diseases class distribution

Class Number	Class Name	No. of instances
1	Psoriasi	110
2	Seboreic dermatitis	60
3	Lichen planus	71
4	Pityriasis rosea	48
5	Cronic dermatitis	48
6	Pityarisis rubra pilaris	20
Total		357

Table 2. Description of Erythemato-squamous diseases attributes

Clinical Attributes	Histopathological Attributes
Att.1: erythema Att.2: scaling Att.3: definite borders Att.4: itching Att.5: koebner phenomenon Att.6: polygonal papules Att.7: follicular papules Att.8: oral mucosal involvement Att.9: knee and elbow involvement Att.10: scalp involvement Att.11: family history Att.34: age	Att.12: melanin incontinence Att.13: eosinophils in infiltrate Att.14: PNL infiltrate Att.15: brosis of the papillary dermis Att.16: exocytosis Att.17: acanthosis Att.18: hyperkeratosis Att.19: parakeratosis Att.20: clubbing of the rete ridges Att.21: elongation of the rete ridges Att.22: thinning of the suprapapillary epidermis Att.23: pongiform pustule Att.24: munro microabscess Att.25: focal hypergranulosis Att.26: disappearance of the granular layer Att.27: vascularization and damage of basal layer Att.28: spongiosis Att.29: saw-tooth appearance of retes Att.30: follicular horn plug Att.31: perifollicular parakeratosis Att.32: inflammatory mononuclear infiltrate Att. 33: band-like infiltrate

and one zero value of age, there are 357 instances. Distribution according to class variable of this dataset is given in Table 1. Each record contains 12 clinical features and 22 histopathological features (see Table 2). The family history feature in the dataset has the value 1 if any of these diseases has been observed in the family and 0 otherwise. The age feature simply represents the age of the patient. Every other feature (clinical and histopathological) was given a degree in the range of 0–3. Here, 0 indicates that the feature was not present; a 3 indicates the largest amount possible and 1, 2 indicate the relative intermediate values.

4 Adaptive Neuro-Fuzzy Classifiers

The usage of ANFIS (Jang 1993; Jang and Sun 1995, Jang et al. 1997) for classifications is unfavorable. For example, if there are three classes labeled as 1, 2 and 3. The ANFIS outputs are not integer. For that reason the ANFIS outputs are rounded, and determined the class labels. But, sometimes, ANFIS can give 0 or 4 class labels. These situations are not accepted. As a result ANFIS is not suitable for classification problems. In this section, adaptive neuro-fuzzy classifier is discussed in details. In these models, k-means algorithm is used to initialize the fuzzy rules. Also, Gaussian membership function is only used for fuzzy set descriptions, because of its simple derivative expressions.

4.1 Adaptive Neuro-Fuzzy Classifier with Linguistic Hedges (ANFCLH)

Adaptive neuro-fuzzy classifier (ANFC) with Linguistic hedges (Cetişli 2010a, b) is based on fuzzy rules. Linguistic hedges are applied to the fuzzy sets of rules, and are adapted by Scaled Conjugate Gradient (SCG) algorithm. By this way, some distinctive features are emphasized by power values, and some irrelevant features are damped with power values. The power effects in any feature are generally different for different classes. The using of linguistic hedges increases the recognition rates. A fuzzy classification rule that has two inputs$\{x_1, x_2\}$ and one output y is defined with LHs as IF x_1 is A_1 with p_1 hedge AND x_2 is A_2 with p_2 hedge THEN y is C_1 class, where A_1 and A_2 denote linguistic terms that are defined on X_1 and X_2 feature space; p_1 and p_2 denote linguistic hedges, respectively; C_1 denotes the class label of the output y. Fig. 1 shows the ANFCLH architecture.

The feature space with two inputs $\{x_1, x_2\}$ is partitioned into three classes $\{C_1, C_2, C_3\}$, in the Figure. The feature space $X_1 \times X_2$ is separated into fuzzy regions (Jang et al. 1997). This technique is based on zero-order Sugeno fuzzy model (Takagi and Sugeno 1985). The crisp outputs of fuzzy rules are determined by weighted average operator (Jang et al. 1997). In this classifier, the nodes in the same layer have the same type of node functions. The layers and their properties are given as follows:

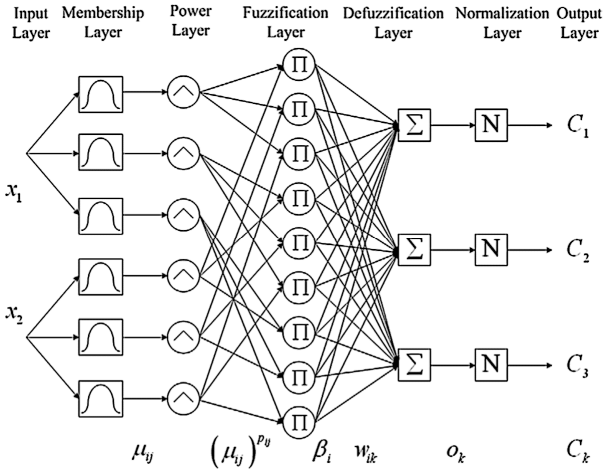

Fig. 1. A neuro-fuzzy classifier with LHs (Cetişli 2010a)

Layer 1: In this layer, the membership grade of each input to specified fuzzy region is measured. Gaussian function is employed as MF due to smooth partial derivatives of its parameters, and has less parameter. The Gaussian MF is given as follows (Cetişli 2010a):

$$\mu_{ij}(x_{sj}) = \exp\left(-0.5\frac{(x_{sj}-c_{ij})^2}{\sigma_{ij}^2}\right) \tag{1}$$

where $\mu_{ij}(x_{sj})$ represents the membership grade of the *i*th rule and the *j*th feature; x_{sj} denotes the *s*th sample and the *j*th feature of input matrix $X\{X \epsilon R^{NxD}\}$; c_{ij} and σ_{ij} are the center and the width of Gaussian function, respectively.

Layer 2: In this layer, the secondary meanings of fuzzy sets are calculated with their LHs as in Eq. (2) (Cetişli 2010a):

$$\alpha_{ijs} = [\mu_{ij}(x_{sj})]^{p_{ij}} \tag{2}$$

where α_{ijs} denotes the modified membership grades of μ_{ij} (x_{sj}); p_{ij} denotes the LH value of the *i*th rule and the *j*th feature.

Layer 3: The degree of fulfillment of the fuzzy rule for x s sample is determined in this layer. It is also called as the firing strength of rule. So, the B_{is} firing strength of the *i*th rule for D number of features is defined as in Eq. (3) (Cetişli 2010a):

$$\mathrm{B}_{is} = \prod_{j=1}^{D} \alpha_{ijs} \tag{3}$$

Layer 4: In this layer, the weighted outputs are calculated as in Eq. (4) (Cetişli 2010a), and every rule can affect each class according to their weights. However, if a rule controls a specific class region, the weight between this rule output and the

specific class is to be bigger than the other class weights. Otherwise, the class weights are fairly small:

$$O_{sk} = \sum_{i=1}^{U} \beta_{is} w_{ik} \tag{4}$$

where w_{ik} represents the degree of belonging to the kth class that is controlled with the ith rule; O_{sk} denotes the weighted output for the sth sample that belongs to the kth class, and U is the number of rules.

Layer 5: If the summation of weights is bigger than 1, the outputs of the network should be normalized in the last layer as follows (Cetişli 2010a):

$$h_{sk} = \frac{O_{sk}}{\sum_{l=1}^{k} O_{sl}} = \frac{O_{sk}}{\delta_s}, \delta_s = \sum_{l=1}^{k} O_{sl} \tag{5}$$

Where h_{sk} represents the normalized degree of the sth sample that belongs to the kth class; and K is the number of classes. After then, the class label (C_s) of sth sample is determined by the maximum h_{sk} value as in Eq. (6) (Cetişli 2010a):

$$C_s = \max_{k=1,2,...,k} \{h_{sk}\} \tag{6}$$

The antecedent parameters of the network $\{c, \sigma, p\}$ could be adapted by any optimization method. In this study, scaled conjugate gradient (SCG) method is used to adapt the network parameters (Moller 1993). The cost function that is used in the SCG method is determined from the least mean squares of the difference target and the calculated class value (Jang et al. 1997; Sun and Jang 1993). According to the above definition, the cost function E is defined as in Eq. (7) (Cetişli 2010a):

$$E = \frac{1}{N} \sum_{s=1}^{N} E_s, \; E_s = \frac{1}{2} \sum_{k=1}^{K} (t_{sk} - h_{sk})^2 \tag{7}$$

4.2 Linguistic Hedges Neural-Fuzzy Classifier with Selected Features (LHNFCSF)

Cetişli (2010a, b) presented a fuzzy feature selection (FS) method based on the LH concept. It uses the powers of fuzzy sets for feature selection. The values of LHs can be used to show the importance degree of fuzzy sets. When this property is used for classification problems, and every class is defined by a fuzzy classification rule, the LHs of every fuzzy set denote the importance degree of input features. If the LHs values of features are close to concentration values, these features are more important or relevant, and can be selected. On the contrary, if the LH values of features are close to dilation values, these features are not important, and can be eliminated. According to the LHs value of features, the redundant, noisily features can be eliminated, and significant features can be selected. In this technique (Cetişli 2010b), if linguistic hedge values of classes in any feature are bigger than 0.5 and close to 1, this feature is

relevant, otherwise it is irrelevant. The program creates a feature selection and a rejection criterion by using power values of features. There are two selection criteria, one is the selection of features that have the biggest hedge value for any class and the other is the selection of features that have a bigger hedge value for every class, because any feature cannot be selective for every class. For that reason, a selective function should be described from the hedge values of any feature as in Eq. (8) (Cetişli 2010b):

$$p_j = \prod_{i=1}^{k} p_{ij} \tag{8}$$

where P_j denotes the selection value of the jth feature, and K is the number of classes. The Feature selection and classification algorithms were discussed in detail in Cetişli (2010b).

5 Results and Discussions

In this section, the performance analysis is presented. The simulations were performed by using an Intel (R) Core (TM) i3 CPU 530-2.93 GHz personal computer and a Microsoft Windows 7 64-bit operating system. The core of the NFC calculations was implemented by using the MATLAB software package.

5.1 Training and Testing Phases of Classifier

The collection of well-distributed, sufficient, and accurately measured input data is the basic requirement in order to obtain an accurate model. The classification process starts by obtaining a data set (input-output data pairs) and dividing it into a training set and testing data set. The training data set is used to train the NFC, whereas the test data set is used to verify the accuracy and effectiveness of the trained NFC. Once the model structure and parameters have been identified, it is necessary to validate the quality of the resulting model. In principle, the model validation should not only validate the accuracy of the model, but also verify whether the model can be easily interpreted to give a better understanding of the modeled process. It is therefore important to combine data-driven validation, aiming at checking the accuracy and robustness of the model, with more subjective validation, concerning the interpretability of the model. There will usually be a challenge between flexibility and interpretability, the outcome of which will depend on their relative importance for a given application. While, it is evident that numerous cross-validation methods exist, the choice of the suitable cross-validation method to be employed in the NFC is based on a trade-off between maximizing method accuracy and stability and minimizing the operation time. To avoid overfitting problems during modeling process, the data set were randomly split into four training-test partition model sets: 50–50%, 60–40%, 70–30% and 80–20%. The number of training and test data for each of classes is given in Table 3.

Table 3. The number of training and test data for each of class

Erythemato-Squamous Class	50-50%	60-40%	70-30%	80-20%
Class-1: Psoriasi	51-59	61-49	75-35	86-24
Class-2: Seboreic dermatitis	41-19	49-11	53-7	58-2
Class-3: Lichen planus	37-34	47-24	53-18	58-13
Class-4: Pityriasis rosea	18-30	19-29	22-26	34-14
Class-5: Cronic dermatitis	23-25	28-20	35-13	35-13
Class-6: Pityarisis rubra pilaris	9-11	10-10	12-8	15-5
Total	179-178	214-143	250-107	286-71

In feature reduction stage of the ANFCLH for diagnosis of erythemato-squamous diseases, the feature extraction and the feature reduction processes are performed. The number of fuzzy rules is determined according to the number of classes. According to the feature selection algorithm, features 1-18 are common relevant features for each class while features from 19-34 are irrelevant for each class. The LHNFCSF classification results during training and testing phases of erythemato-squamous diseases are shown in Table 4 and also represented graphically in Fig. 2.

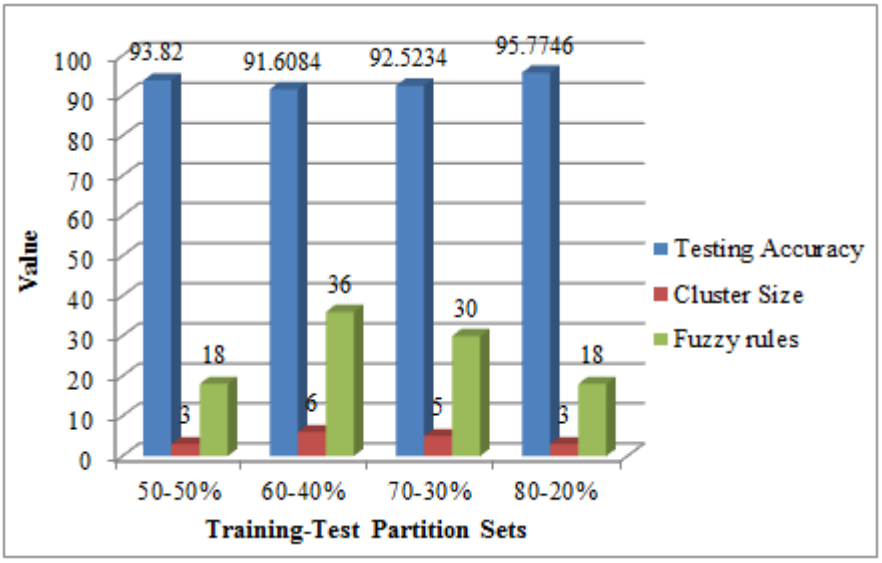

Fig. 2. LHNFCSF Classification results of erythemato-squamous diseases based on feature selection, fuzzy rules and cluster size for each class using for 80–20% training-test partition

Although the number of selected features is reduced to 18 from 34 features, the classification is still successful as seen in Table 4. The number of cluster size was opted between 1 and 6 to check the optimum topology for each model. With this assumption, different trials were performed to find the best Neural-fuzzy in each method using different cluster sizes with different fuzzy rules.

Table 4. The LHNFCSF classification results of erythemato-squamous diseases dataset

training-test partition sets	Features	Cluster size for each class	Training accuracy	Testing Accuracy	RMSE	No. of Rules	Epoch
50-50%	1-18	1	98.8827	91.0112	0.0259	6	75
		2	100	89.8876	4.8452e-013	12	325
		3	**100**	**93.820**	**5.5845e-013**	**18**	**300**
		4	100	92.6966	1.4583e-011	24	150
		5	100	91.0112	7.0032e-013	30	175
		6	100	91.573	5.9842e-013	36	175
60-40%	1-18	1	95.3271	90.2098	0.0755192	6	75
		2	100	88.1119	6.7298e-013	12	425
		3	99.065	90.9091	0.0198467	18	125
		4	100	90.9091	1.5839e-011	24	250
		5	100	88.8112	8.3029e-013	30	375
		6	**100**	**91.6084**	**0.000382048**	**36**	**75**
70-30%	1-18	1	98.8	86.9159	0.0241916	6	100
		2	100	90.6542	1.6108e-011	12	325
		3	100	92.5234	6.4936e-013	18	275
		4	100	91.5888	6.1730e-013	24	300
		5	**100**	**92.5234**	**9.2392e-013**	**30**	**275**
		6	100	89.7196	7.7009e-013	36	150
80-20%	1-18	1	98.951	92.9577	0.0289586	6	125
		2	99.6503	94.3662	0.00669146	12	825
		3	**100**	**95.7746**	**1.3057e-005**	**18**	**675**
		4	99.6503	94.3662	0.00657387	24	425
		5	100	91.5493	7.4613e-013	30	250
		6	100	92.9577	1.1043e-006	36	400

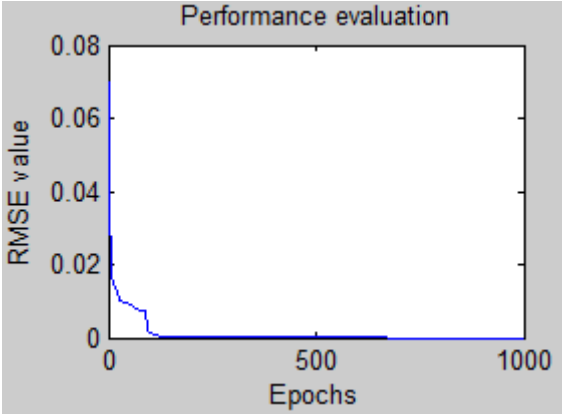

Fig. 3. Performance Evaluation of LHNFCSF after selection of relevant features using three clusters for 80–20% training-test partition

Among the four training-test partition sets, the highest classification accuracy of 95.7746% was achieved for 80–20% training-test partition using 3 clusters and 18 fuzzy rules, 93.820% for 50–50% training-test partition using 3 clusters and 18 fuzzy rules, 92.5234% for 70–30% training-test partition using 5 clusters and 30 fuzzy rules, and 91.6084% for 60–40% training-test partition using 6 clusters and 36 fuzzy rules. Therefore, 80–20% training-test partition using 3 clusters and 18 fuzzy rules are the best classification accuracy with RMSE of 6.5139e-013 as shown in Fig. 3.

It's noted from Table 4 also that the selected features according to four different partitions were always the same. The results indicated that, the selected features increase the recognition rate for test set. It means that some overlapping classes can be easily distinguished by selected features. The LH values of erythemato-squamous diseases for 6 features only as example are given in Table 5. After the classification step, it can be seen that some of the hedge values are bigger than 1, because the hedge values are not constrained in the classification step. Each class for ANFCLH is intuitively defined with 18 fuzzy rules. The neural fuzzy classifier surface of feature 1 and feature 2 using 80–20% training-test partition is shown in Fig. 4

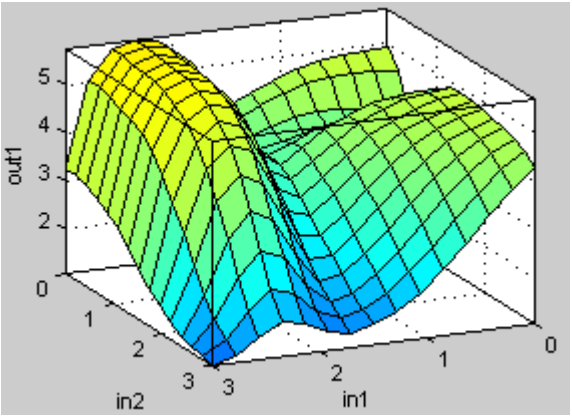

Fig. 4. Neural Fuzzy classifier surface using three clusters for 80–20% training-test partition

Table 5. The LH values of erythemato-squamous for every class after selection of relevant features (values for only 6 from 18 relevant features)

Class	F1	F2	F3	F4	F5	F6
C1	1.004206	1.021716	1.042981	1.011113	1.031387	1.000265
C2	1.027196	0.9907	0.984645	1.039615	1.011038	1.000047
C3	0.981362	0.992032	0.984563	0.984836	0.998278	0.955953
C4	1.02159	1.038587	1.006401	1.013554	1.042992	1.0066
C5	0.969889	0.993738	0.990568	0.991844	1.009644	1.003435
C6	1.03143	1.005849	1.001836	1.008994	1.00656	1

6 Conclusion

In this study, the proposed Feature Selection based on Linguistic Hedges Neural-Fuzzy classifier managed to discard redundant and irrelevant features in erythemato-squamous disease dataset. The computation time was reduced and this has positively impacted to achieve highest classification accuracy of 95.7746% for 80–20% training-test partition using 3 clusters and 18 fuzzy rules. Experimental results showed that when the linguistic hedge value of the fuzzy classification set in any feature is close to 1, this feature is relevant for that class, otherwise it may be irrelevant. The results demonstrate that using of Linguistic Hedges in daptive neural-fuzzy classifier improves the success of the classifier. Also, when the ANFCLH is compared with the other methods, it can be noted that this classifier uses less parameter than the others with the best recognition rates. The results strongly suggest that the proposed method not only help to reduce the dimensionality of large data sets but also to speed up the computation time of a learning algorithm and therefore simplify the classification task. It can aid in the diagnosis of erythemato-squamous diseases and can be very helpful to the physicians for their final decision on their patients. The future investigation will pay much attention to evaluate Neural-Fuzzy classifier with Linguistic Hedges in other medical diagnosis problems like micro array gene selection, internet, and other data mining problems. Therefore, the impressive results may be obtained with the proposed method and improving the performance of NFCs using high-performance computing techniques. In addition, the combination of the approaches mentioned above will yield an efficient fuzzy classifier for a lot of applications.

References

1. Abdi, M.J., Giveki, D.: Automatic detection of erythemato-squamous diseases using PSO–SVM based on association rules. Eng. Appl. Artif. Intel. (2012), doi:10.1016/j.engappai.2012.01.017
2. Barati, E., Saraee, M., Mohammadi, A., et al.: A Survey on Utilization of Data Mining Approaches for Dermatological (Skin) Diseases Prediction. Cyber Journals: Multidisciplinary Journals in Science and Technology, Journal of Selected Areas in Health Informatics (JSHI): March Edition, 1–11 (2011)
3. Cetişli, B.: Development of an adaptive neuro-fuzzy classifier using linguistic hedges: Part 1. Expert Systems with Applications 37(8), 6093–6101 (2010a)
4. Cetişli, B.: The effect of linguistic hedges on feature selection: Part 2. Expert Systems with Applications 37(8), 6102–6108 (2010b)
5. Chrysostomou, K.A.: The Role of Classifiers in Feature selection Selection: Number vs Nature, PhD dissertation, School of Information Systems. Computing and mathematics, Brunel University (2008)
6. Diamantidis, N.A., Karlis, D., Giakoumakis, E.A.: Unsupervised stratification of cross-validation for accuracy estimation. Artif. Intell. 116(1-2), 1–16 (2000)
7. Francois, D., Rossi, F., Wertz, V.: Verleysen M Resampling methods for parameter-free and robust feature selection with mutual information. Neurocomputing 70, 1276–1288 (2007)

8. Gagliardi, F.: Instance-based classifiers applied to medical databases: diagnosis and knowledge extraction. Artif. Intell. Med. 52(3), 123–139 (2011)
9. Govenir, H.A., Emeksiz, N.: An expert system for the differential diagnosis of erythemato-squamous diseases. Expert Syst. Appl. 18(1), 43–49 (2000)
10. Güvenir, H.A., Demiroz, G., Ilter, N.: Learning differential diagnosis of erythemato-squamous diseases using voting feature intervals. Artif. Intell. Med. 13(3), 147–165 (1998)
11. Guyon, I., Steve, G., Nikravesh, M., Zadeh, L.A.: Feature Extraction: Foundations and Applications. Springer, Heidelberg (2006)
12. Jang, J.S.R.: ANFIS: Adaptive-Network-Based Fuzzy Inference System. IEEE Transactions on Systems, Man, and Cybernetics 23(3), 665–685 (1993)
13. Jang, J.S.R., Sun, C.T.: Neuro-fuzzy modeling and control. Proceedings of the IEEE 83(3), 378–406 (1995)
14. Jang, J.S.R., Sun, C.T., Mizutani, E.: Neuro-Fuzzy and soft computing. Prentice-Hall, Englewood Cliffs (1997)
15. Kabari, L.G., Bakpo, F.S.: Diagnosing skin diseases using an artificial neural network. In: Proceeding of 2nd International Conference on Adaptive Science & Technology (ICAST 2009), pp. 187–191. IEEE Press, New York (2009)
16. Karabatak, M., Ince, M.C.: A new feature selection method based on association rules for diagnosis of erythemato-squamous diseases. Expert Syst. Appl. 36(10), 12500–12505 (2009)
17. Lekkas, S., Mikhailov, L.: Evolving fuzzy medical diagnosis of Pima Indians diabetes and of dermatological diseases. Artif. Intell. Med. 50(2), 117–126 (2010)
18. Luukka, P.: Feature selection using fuzzy entropy measures with similarity classifier. Expert Syst. Appl. 38(4), 4600–4607 (2011a)
19. Luukka, P.: A New Nonlinear Fuzzy Robust PCA Algorithm and Similarity Classifier in Classification of Medical Data Sets. International Journal of Fuzzy Systems 13(3), 153–162 (2011b)
20. Luukka, P., Leppälampi, T.: Similarity classifier with generalized mean applied to medical data. Comput. Biol. Med. 36(9), 1026–1040 (2006)
21. Moller, M.F.: A scaled conjugate gradient algorithm for fast supervised learning. Neural Networks 6, 525–533 (1993)
22. Nanni, L.: An ensemble of classifiers for the diagnosis of erythemato-squamous diseases. Neurocomputing 69(7-9), 842–845 (2006)
23. Ozcift, A., Gulten, A.: A Robust Multi-Class Feature Selection Strategy Based on Rotation Forest Ensemble Algorithm for Diagnosis of Erythemato-Squamous Diseases. J. Med. Syst. 36(2), 941–949 (2012)
24. Parthiban, L., Subramanian, R.: An intelligent agent for detection of erythemato-squamous diseases using Co-active Neuro-Fuzzy Inference System and genetic algorithm. In: International Conference on Intelligent Agent & Multi-Agent Systems, IAMA, pp. 1–6. IEEE Press, New York (2009)
25. Polat, K., Gunes, S.: A novel hybrid intelligent method based on C4.5 decision tree classifier and one-against-all approach for multi-class classification problems. Expert Systems with Applications 36(2), 1587–1592 (2009)
26. Polat, K., Günes, S.: The effect to diagnostic accuracy of decision tree classifier of fuzzy and k-NN based weighted pre-processing methods to diagnosis of erythema-to-squamous diseases. Digital Signal Processing 16(6), 922–930 (2006)
27. Revett, K., Gorunescu, F., Salem, A.B., El-Dahshan, E.S.: Evaluation of the feature space of an erythematosquamous dataset using rough sets. Ann. Univers. Craiova, Romania, Math. Comput. Sci. Ser. 36(2), 123–130 (2009)

28. Salzberg, S.L.: On comparing classifiers: Pitfalls to avoid and a recommended approach. Data Mining and Knowledge Discovery 1, 317–327 (1997)
29. Sun, C.T., Jang, J.S.R.: A neuro-fuzzy classifier and its application. In: Proc. of IEEE Int. Conf. on Fuzzy Systems, vol. 1, pp. 94–98. IEEE Press, San Francisco (1993)
30. Takagi, T., Sugeno, M.: Fuzzy identification of systems and its applications to modeling and control. IEEE Trans. Syst. Man. Cybern. 15(1), 116–132 (1985)
31. Xie, J., Lei, J., Xie, W., Gao, X., Shi, Y., Liu, X.: Novel Hybrid Feature Selection Algorithms for Diagnosing Erythemato-Squamous Diseases. In: He, J., Liu, X., Krupinski, E.A., Xu, G. (eds.) HIS 2012. LNCS, vol. 7231, pp. 173–185. Springer, Heidelberg (2012)
32. Xie, J., Wang, C.: Using support vector machines with a novel hybrid feature selection method for diagnosis of erythemato-squamous diseases. Expert Syst. Appl. 38(5), 5809–5815 (2011)
33. Xie, J.Y., Xie, W.X., Wang, C.X., et al.: A novel hybrid feature selection method based on IFSFFS and SVM for the diagnosis of erythemato-squamous diseases. In: JMLR Workshop and Conference Proceedings. Workshop on Applications of Pattern Analysis, vol. 11, pp. 142–151. MIT Press, Windsor (2010)
34. UCI, Machine Learning Repository, `http://archive.ics.uci.edu/ml/index.html` (accessed on July 12, 2012)
35. Übeyli, E.D.: Combined neural networks for diagnosis of erythemato-squamous diseases. Expert Syst. Appl. 36(3), 5107–5112 (2009)
36. Ubeyli, E.D.: Multiclass support vector machines for diagnosis of erythemato-squamous diseases. Expert Syst. Appl. 35(4), 1733–1740 (2008)
37. Ubeyli, E.D., Güler, I.: Automatic detection of erythemato-squamous diseases using adaptive neuro-fuzzy inference systems. Computers in Biology and Medicine 35(5), 147–165 (2005)

Automated Sleep Staging Using Detrended Fluctuation Analysis of Sleep EEG

Amr F. Farag[1,2,*], Shereen M. El-Metwally[1], and Ahmed Abdel Aal Morsy[1]

[1] Department of Systems and Biomedical Engineering,
Cairo University, Giza, Egypt
[2] Department of Biomedical Engineering,
Shorouk Higher institute of Engineering, EL-Shorouk, Egypt
bme_amr_fawzy@yahoo.com,
shereen.elmetwally@k-space.org,
amorsy@iee.org

Abstract. An accurate sleep staging is crucial for the treatment of sleep disorders. Recently some studies demonstrated that the long range correlations of many physiological signals measured during sleep show some variations during the different sleep stages. In this study, detrended fluctuation analysis (DFA) is used to study the electroencephalogram (EEG) signal autocorrelation during different sleep stages. A classification of these stages is then made by introducing the calculated DFA power law exponents to a K-Nearest Neighbor classifier. Our study reveals that a 2-D feature space composed of the DFA power law exponents of both the filtered THETA and BETA brain waves resulted in a classification accuracy of 94.44%, 91.66% and 83.33% for the wake, non-rapid eye movement and rapid eye movement stages, respectively. We conclude that it might be possible to build an automated sleep assessment system based on DFA analysis of the sleep EEG signal.

Keywords: Electroencephalogram (EEG), Detrended fluctuation analysis (DFA), sleep, K-Nearest Neighbor (KNN).

1 Introduction

Sleep is not just a constant state controlled by metabolic needs for the body being at rest. Instead, sleep consists of different well-defined sleep stages, namely, wake (WK), rapid eye movement (REM) and non-REM sleep. In a normal restorative sleep, these stages follow a well-structured temporal order [1].

For more than 40 years, visual assessment of wakefulness and sleep in clinical sleep studies has been based on standard manual of Rechtschaffen and Kales (R&K) [2]. Although this manual is considered the gold standard inside sleep research community, a considerable amount of research has been carried to define methods that would give a more detailed and accurate sleep description of sleep macrostructure and overcome the known limitations of the R & K manual [3-5].

* Corresponding author.

V.E. Balas et al. (Eds.): Soft Computing Applications, AISC 195, pp. 501–510.
springerlink.com

During recent decades, multitude methods aiming at objective, continuous-scale quantification of sleep depth have been presented [4, 6, 7]. Most of the important early findings of clinical sleep medicine were based on period analysis, which makes it possible to carry out time–frequency analysis even visually for properly band-pass filtered data [4]. Hjorth parameters were introduced to characterize amplitude, time scale and complexity of the EEG through time-domain operations and were exemplified to be applicable in the analysis of objective sleep depth [8]. More recently, more studies on sleep staging have been conducted including: at least stochastic complexity measures [9], relations of certain spectral bands [10-12], models on EEG micro-continuity [13], Hidden Markov Models [14], segmentation approaches [15], k-means clustering based feature weighting combined with K-Nearest Neighbor and decision tree classifier [16], and Fuzzy logic combined with genetic algorithm [17].

The electrophysiological activities on the cortex reflected by EEG vary with the electrophysiological activities of the nerve cell in a special part of brain. When people are performing some mental tasks, the EEG signal shows highly non-stationary and non-linear characteristics. The detection of the mental EEG properties was studied using detrended fluctuation analysis (DFA) [18]. DFA is a new method recently introduced for analyzing power-law long-range correlations in a variety of non-stationary time series. DFA was used to characterize long-rang correlations between nucleotide sequences [19]. The advantage of the DFA method is that it systematically eliminates trends of various order caused by imperfect measurement [20].

Recently researchers applied the DFA for the analysis of the physiological time series as the heart rate variability (HRV) [21, 22] and breathing rate variability (BRV) intervals during sleep [23]. These studies revealed that both the HRV and BRV show high autocorrelation exponents during both WK and REM stages while they lose autocorrelation during NREM sleep stage.

In this paper, we used DFA to study the correlation properties of the EEG signal and its filtered components (Alpha, Beta, Delta and Theta) during various sleep stages. Our aim was to gain better understanding of the relative importance of the DFA-derived features for automated sleep staging. The DFA power-law exponents derived from a single EEG signal were then used to design a K-Nearest Neighbor- based classifier for sleep stages detection with a high degree of accuracy.

2 Subjects and Methods

2.1 Subjects and Sleep Recording

Twelve subjects aged 20-32 underwent one overnight polysomnographic recording which comprised EEG signal acquisition (4 channels, Ag/AgCl electrodes placed according to the 10-20 International System referred to linked earlobes: C3, C4, F3, F4). Recordings were carried out using Alice Polysomnogramic System (Respironics, Inc.). The signals were sampled at 100 Hz using 12-bit A/D precision and stored on hard disk for further analysis.

2.2 Sleep Scoring

Sleep stages were initially scored and labeled using the automated scoring algorithm of Alice Sleepware software then the scored signals were reviewed by a specialist for correction according to standard criteria (R&K) on 30-second epochs. For subsequent analysis, the labeled sleep stages were grouped into three classes: "NREM sleep", "REM sleep" and "wakefulness". Nine minutes for each sleep stage were extracted from each patient EEG record to be investigated. The first and last epochs of each sleep stage is excluded from our analysis in order to avoid the effect of transitions between sleep stages. Thus, the whole dataset is composed of 108 min/sleep stage or 324 min representing all the stages.

2.3 EEG Signal Analysis

The raw EEG signal was introduced to a filter bank as shown in Fig. 1 to separate known brain waves: Delta, Theta, Alpha and Beta waves. The filtered signals are shown in Fig 2. Each wave was then segmented by 1 minute long window and studied separately during each sleep stage using DFA to reveal the variations in the autocorrelation properties of each of these waves during various sleep stages.

2.4 Detrended Fluctuation Analysis(DFA)

DFA is a technique used to characterize the correlation structure of non-stationary time series. DFA reveals the properties of non-stationary time series by calculating the scaling exponents which index the long-range power-law correlations. The DFA procedure [19, 20] consists of four steps.

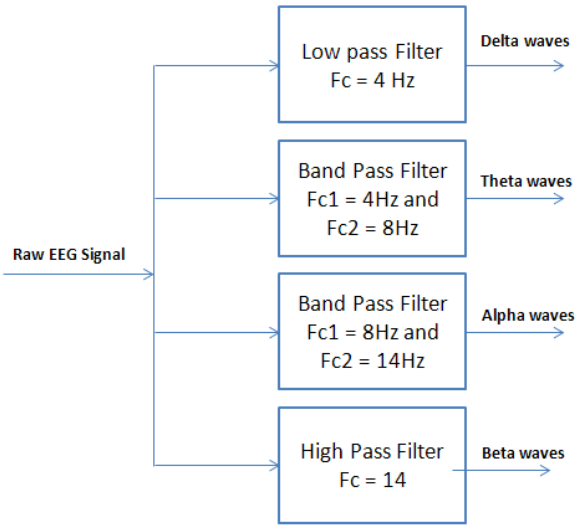

Fig. 1. Block diagram of the filter bank system

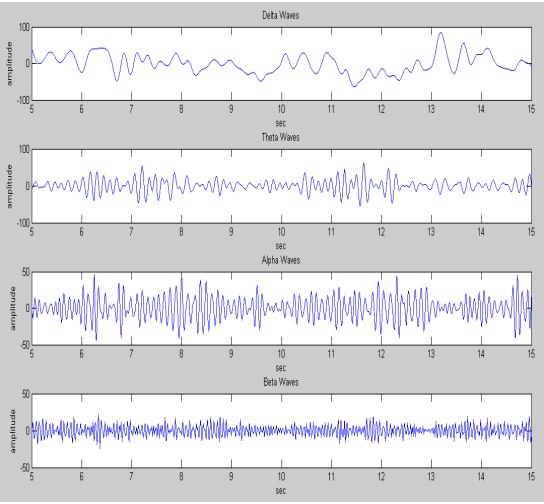

Fig. 2. The filtered EEG signals: Delta, Theta, Alpha, and Beta

- Step 1: Determine the "profile"

$$Y(i) = \sum_{k=1}^{i} \left(\tau_k - \langle \tau \rangle\right), \quad i = 1,.....,N \tag{1}$$

of the data series τ_k of length N and a mean $\langle \tau \rangle$.

- Step 2: we divide $Y(i)$ into N_t = int(N / t) non-overlapping segments of equal length t. Since the length N of the series is often not a multiple of the considered time scale t, a short part at the end of the profile may remain. In order not to disregard this part of the series, the same procedure is repeated starting from the opposite end. Thereby, $2N_t$ segments are obtained altogether.
- Step 3: Calculate the local trend for each of the segments by a least-square fit of the data. Then determine the variance

$$F_t^2(\upsilon) \equiv \frac{1}{t} \sum_{i=1}^{t} \left[Y\left((\upsilon - 1)t + i\right) - p_\upsilon(i)\right]^2 \tag{2}$$

for each segment υ, υ = 1,……, N_t . Here, $p_\upsilon(i)$ is the fitting polynomial in segment υ. Linear, quadratic, cubic, or higher order polynomials can be used in the fitting procedure (conventionally called DFA1, DFA2, DFA3,…..) .

- Step 4: Average over all segments and take the square root to obtain the fluctuations function

$$F(t) \equiv \left[\frac{1}{2N_t} \sum_{\upsilon=1}^{2N_t} F_t^2(\upsilon)\right]^{\frac{1}{2}} \tag{3}$$

The logarithm of $F(t)$ is then plotted as a function of the logarithm of the time scale t. The slope, α, of the plot of $\mathrm{Log}_2(F(n))$ versus $\mathrm{Log}_2(n)$ is called the scaling or self-similarity exponent. If the time series shows self-similarity, this plot will display a linear scaling region and slope $\alpha > 0.5$. This exponent is 0.5 for white noise, where the values of the time series are completely uncorrelated. When the exponent is $\alpha < 0.5$, power-law anti-correlation is present, such that large values in the time series are more likely to be followed by small values and vice versa. When $\alpha > 0.5$, correlations exist but cease to follow a power-law form.

In order to determine how $F(t)$ depends on the time scale t, steps 2 to 4 were repeated 30 times with different time scales between $t = 4$ and 6000. The long range auto-correlation properties of the raw sleep EEG signal and the filtered brain waves of each sleep stage were investigated separately using DFA2 as shown in Fig. 3. The mean and standard deviation of the computed DFA2 parameters for the different sleep stages are given in Table 1.

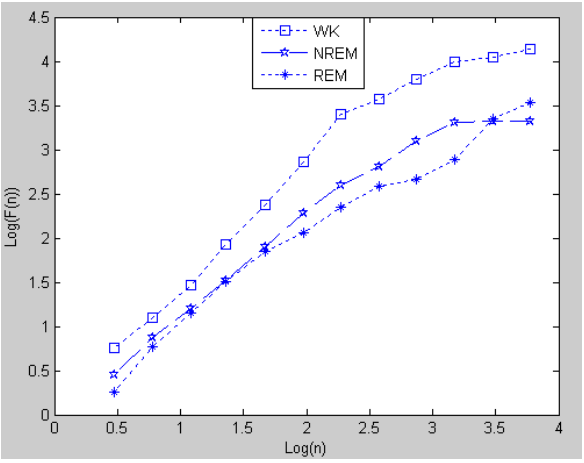

Fig. 3. DFA analysis of a 1-min long EEG record of a single subject corresponding to the WK, NREM and REM sleep stages

Table 1. The DFA characteristic values for each sleep stage

Sleep Stage	Raw EEG	Delta	Theta	Alpha	Beta
WK	0.858 ± 0.1003	1.0665 ± 0.0908	0.2853 ± 0.0203	0.1582 ± 0.013	0.0437 ± 0.0108
NREM	0.4099 ± 0.1675	0.9626 ± 0.0926	0.3021 ± 0.007	0.1566 ± 0.0095	0.0616 ± 0.0078
REM	0.8628 ± 0.0835	1.0128 ± 0.0809	0.2937 ± 0.0118	0.1597 ± 0.01	0.0551 ± 0.0095

Table 2. The significane levels for the group differences between sleep STAGES USING Bonferroni test. each line lists the results for the comparison of the stages named in coloumn 1 and 2

Stage 1	Stage 2	Raw EEG	Delta	Theta	Alpha	Beta
WK	NREM	P < 0.001	P < 0.001	P < 0.001	n.s	P < 0.001
WK	REM	n.s	P < 0.001	P < 0.001	n.s	P < 0.001
NREM	REM	P < 0.001	P < 0.001	P < 0.001	P < 0.05	P < 0.001

2.5 Statistical Analysis

In order to check the difference between individual groups, Bonferroni test was applied to DFA data sets. Statistical significance was stated for $p < 0.05$. The statistical test was performed by SPSS version 10 (SPSS Inc, Chicago, IL).

The results of the Bonferroni test are listed in Table 2. It can be seen that the Alpha waves showed no significance on comparing both the WK versus REM stages and the WK versus NREM stages. For this reason, the DFA2 parameters of the Alpha waves are excluded from the features vector construction to be used in sleep stages classification.

2.6 K-Nearest Neighbor Classifier (KNN)

The Nearest Neighbor Classification is the most straightforward in machine learning where examples are classified based on the class of their nearest neighbor. It is often useful to take more than one neighbor into account so a modified technique commonly referred to as K- Nearest Neighbor (KNN) classification uses the K nearest neighbors in determining the class of the unknown example [24]. Fig. 4 depicts the basic idea of a 5-Nearest Neighbor classifier applied for a two class problem in a two dimensional feature space.

In general, the distance d between q and x_i is calculated as :

$$d(q, x_i) = \sum_{f \in F} \omega_f \, \delta(q_f, x_{if}) \tag{4}$$

where q is unknown example, F is the training set, x_i is i-dimensional feature vector, ω_f is the class label and $\delta(q_f, x_{if})$ is defined as follows:

$$\delta(q_f, x_{if}) = \begin{cases} 0 & f \text{ discrete and } q_f = x_{if} \\ 1 & f \text{ discrete and } q_f \neq x_{if} \\ |q_f - x_{if}| & f \text{ continuous} \end{cases} \tag{5}$$

Hence, q is classified according to the majority class of the N-nearest neighbors.

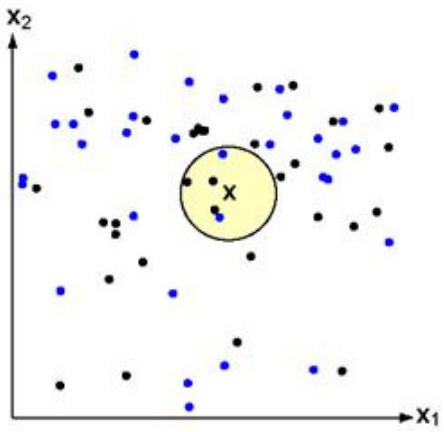

Fig. 4. A simple example of 3-Nearest Neigbour classification

In this study, the classification of the different sleep stages is done and compared using the DFA2 parameters of the raw EEG signal on one hand and the filtered signals on the other hand. The raw EEG parameters were used to construct a 1-D feature space. The parameters of the Delta, Theta and Beta waves were used to construct three sets of 2-D features spaces. Fig. 5 shows the 2-D feature space derived from the Theta and Beta waves. Also, a one 3-D features space is derived from the three filtered signals together as illustrated in Fig. 6. The whole dataset size composed of 324 stages is divided into a training set of 216 stages and a testing set of 108 stages.

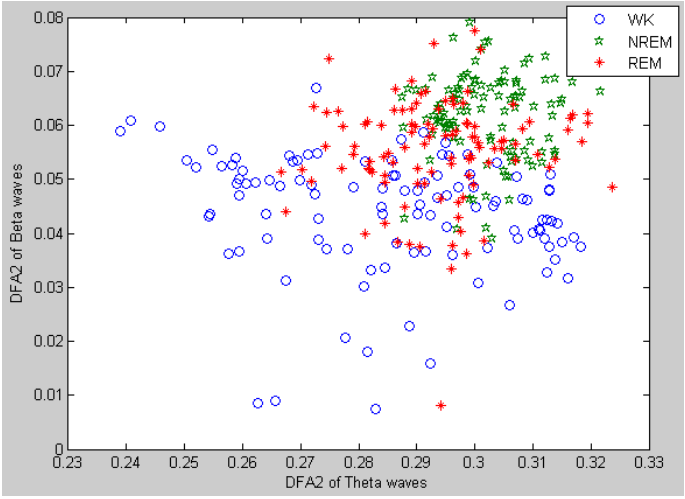

Fig. 5. The 2-D features space constructed from the DFA2 parameters of Theta waves versus BETA waves

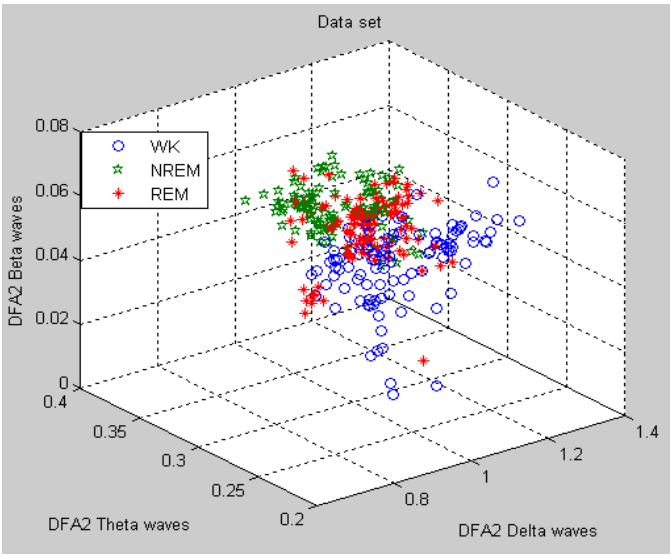

Fig. 6. The 3-D feature space constructed from the DFA2 parameters of Theta, Beta and Delta waves

Table 3. The accuracy of KNN classifier to classify varous sleep stages based on three different sets of 2-D feature spaces

Sleep Stage	Delta vs Beta		Delta vs Theta		Beta vs Theta	
	K	accuracy	K	accuracy	K	accuracy
WK	7	72.22%	5	55.55%	7	94.44%
NREM		50.00%		75.00%		92.66%
REM		55.55%		50.00%		83.33%

3 Results

The KNN classification using the raw EEG parameters resulted in an accuracy of 61.11%, 83.33% and 44.44% at K=7 for the WK, NREM and REM sleep stages, respectively. The 3-D feature space showed an accuracy of 55.55%, 58.33% and 55.55% at K=7 to separate the WK, NREM and REM sleep stages, respectively.

The introduced three sets of 2-D feature spaces to the KNN classifier showed the classification accuracies listed in Table 3. It can be seen that Beta versus Theta features showed the highest accuracy in differentiating between the different sleep stages.

4 Discussion

In our knowledge, this paper presents the first study which systematically investigates the autocorrelation properties of the sleep EEG signal and its extracted waves: Alpha, Beta, Theta, and Delta, using DFA. The study reveals that the EEG signal is almost

uncorrelated during NREM ($\alpha \approx 0.5$) while long-range correlations ($\alpha > 0.5$) exist during the WK and REM stages. These results are consistent with the DFA analysis results for both the heart rate variability and the breathing rate variability during sleep [21, 22, 23]. The mechanism underlying such fluctuations may be related primarily to the different autonomic regulations during REM and NREM sleep stages. The extracted components, Theta, Beta, and Alpha, however, show anti-power-law correlation properties ($0 < \alpha < 0.5$) which indicates the high roughness inherent in these waves during the different sleep stages.

An attempt of separating the sleep stages using KNN classifier based on the feature space derived from the power-law exponents of the EEG signals and its filtered components is done. Results revealed that the Beta versus Theta features had superior ability to separate sleep stages than the other features.

The small number of subjects is considered as a limitation in our study as we think the accuracy of the classifier could be enhanced with increasing the training data set as the KNN classifier are considered as *Lazy* classifiers.

Our results do indicate that it might be possible to build a sleep assessment system based on EEG signal only to reduce the large number of electrodes that is mounted on the subject with a conventional polysomnogram method which obviously affects the comfort ability of the subject and may interfere with the accuracy of his sleep assessment.

Acknowledgments. The authors would like to thank A. Hassan for his great help in recording the data and Dr. A.EL Bialy for the statistical advice. The data was recorded at Dr Shahira Loza private clinic for sleep disorders.

References

[1] Carskadon, M.A., Dement, W.C.: Normal human sleep: An overview. In: Kryger, M.H., Roth, T., Dement, W.C. (eds.) Principles and Practice of Sleep Medicine, vol. 3. Saunders, Philadephia (2000)

[2] Rechtschaffen, A., Kales, A.: A manual of standardized technology, techniques, and scoring system for sleep stages of human subjects. US Public Health Service. U.S. Govt. Printing Office, Washington, DC (1968)

[3] Himanen, S.L., Hasan, J.: Limitations of Rechtscaffen and Kales. Sleep Med. Rev. 4(2), 149–167 (2000)

[4] Hasan, J.: Past and future of computer-assisted sleep analysis and drowsiness assessment. J. Clin. Neurophysiol. 13(4), 295–313 (1996)

[5] Penzel, T., Conradt, R.: Computer based sleep recording and analysis. Sleep Med. Rev. 4(2), 131–148 (2000)

[6] Penzel, T., Stephan, K., Kubicki, S., Herrmann, W.M.: Integrated sleep analysis, with em-phasis on automatic methods. In: Degen, R., Rodin, E.A. (eds.) Epilepsy, Sleep and Sleep Deprivation, 2nd edn. Epilepsy Res. suppl. 2, pp. 177–200. Elsevier Science Publishers B.V. (1991)

[7] Kemp, B.: A proposal for computer-based sleep/wake analysis. J. Sleep Res. 2, 179–185 (1993)

[8] Hjorth, B.: EEG analysis based on time domain properties. Electroencephalogr. Clin. Neurophysiol. 29, 306–310 (1970)
[9] Rezek, I., Roberts, S.: Stochastic complexity measures for physiological signal analysis. IEEE Trans. Biomed. Eng. 45(9), 1186–1191 (1998)
[10] Jobert, M., Schulz, H., Jähnig, P., Tismer, C., Bes, F., Escola, H.: A computerized method for detecting episodes of wakefulness during sleep based on the alpha slow-wave index (ASI). Sleep 17(1), 37–46 (1994)
[11] Dimpfel, W., Hofmann, H.C., Schober, F., Todorova, A.: Validation of an EEG-derived spectral frequency index (SFx) for continuous monitoring of sleep depth in humans. Eur. J. Med. Res. 3, 453–460 (1998)
[12] Hammer, N., Todorova, A., Hofmann, H.C., Schober, F., Vonderheid-Guth, B., Dimpfel, W.: Description of healthy and disturbed sleep by means of the spectral frequency index (SFx)—a retrospective analysis. Eur. J. Med. Res. 6, 333–344 (2001)
[13] Mourtazaev, M.S., Kemp, B., Zwinderman, A.H., Kamphuisen, H.A.C.: Age and gender affect different characteristics of slow waves in the sleep EEG. Sleep 18(7), 557–564 (1995)
[14] Flexer, A., Gruber, G., Dorffner, G.: A reliable probabilistic sleep stager based on a single EEG signal. Artif. Intell. Med. 33(3), 199–207 (2005)
[15] Kaplan, A., Röschke, J., Darkhovsky, B., Fell, J.: Macrostructural EEG characterization based on nonparametric change point segmentation: application to sleep analysis. J. Neurosci. Meth. 106, 81–90 (2001)
[16] Gunes, S., Polat, K., Yosunkaya, S.: Efficient sleep stage recognition system based on EEG signal using k-means clustering based feature weighting. ELSEVIER, Expert Systems with Applications 37, 7922–7928 (2010)
[17] Jo, H.G., Park, J.Y., Lee, C.K., An, S.K., Yoo, S.K.: Genetic fuzzy classifier for sleep stage identification. ELSEVIER, Computers in Biology and Medicine 40, 629–634 (2010)
[18] Jiang, Z., Ning, Y., An, B., Li, A., Feng, H.: Detecting mental EEG properties using detrended fluctuation analysis. In: 27th Annual Conference on Engineering in Medicine and Biology, Shanghai, China (2005)
[19] Peng, C.K., Buldyrev, S.V., Goldberger, A.L., Havlin, S., Sciortino, F., Simons, M.: Fractal landscape analysis of DNA walks. Physica A (1992)
[20] Kantelhardt, J.W., Koscielny-Bunde, E., Rego, H.H.A., Havlin, S., Bunde, A.: Detecting long-range correlations with detrended fluctuation analysis. Physica A 295, 441–454 (2001)
[21] Penzel, T., Kantelhardt, J.W., Grote, L., Bunde, A.: Comparison of detrended fluctuation analysis and spectral analysis for heart rate variability in sleep and sleep apnea. IEEE Trans. Biomed. Eng. 50(10), 1143–1151 (2003)
[22] Peng, C.K., Havlin, S., Stabley, H.E., Goldberg, A.L.: Quantification of scaling exponents and crossover exponents phenomena in non-stationary heartbeat time series. Chaos 5(1), 82–87 (1995)
[23] Kantelhardt, J.W., Penzel, T., Sven R., Becker, H., Havlin, S.: ArminBun Breathing during REM and non-REM sleep: correlated versus uncorrelated behavior. Physica A 319 (2003)
[24] Alpaydın, E.: Introduction to machine learning, 2nd edn. MIT Press, Cambridge (2008)

An Expert System to Improve the Energy Efficiency of the Reaction Zone of a Petrochemical Plant

Iñigo Monedero, Félix Biscarri, Carlos León, and Juan Ignacio Guerrero

School of Computer Science and Engineering, Electronic Technology Department,
Av. Reina Mercedes S/N, 41012 Seville, Spain
imonedero@us.es

Abstract. Energy is the most important cost factor in the petrochemical industry. Thus, energy efficiency improvement is an important way to reduce these costs and to increase predictable earnings, especially in times of high energy price volatility. This work describes the development of an expert system for the improvement of this efficiency of the reaction zone of a petrochemical plant. This system has been developed after a data mining process of the variables registered in the plant. Besides, a kernel of neural networks has been embedded in the expert system. A graphical environment integrating the proposed system was developed in order to test the system. With the application of the expert system, the energy saving on the applied zone would have been about 20%.

Keywords: Energy efficiency, petrochemical plant, data mining, expert system.

1 Introduction

Expert systems are being successfully applied for the realization of diverse tasks (interpretation, prediction, diagnosis, design, planning, instruction, control, etc.) in multiple fields such as medicine, geology, chemistry, engineering, etc. Such applications are very affective in situations when the domain expert is not readily available [1]. There are diverse problems which need to be solved in the real world and they are difficult to solve by the expert at the moment of carrying out his work. Thus, the expert systems, and specifically the decision systems, become prolific in many fields [2]. On the other hand, data mining (or the analysis step of the knowledge discovery in databases) [3] is a discipline intimately related to expert system and which makes it possible to extract the necessary knowledge for them.

The energy efficiency of plants is an important issue in any type of business but particularly in the chemical industry. Not only is it important in order to reduce costs, but also it is necessary even more as a means of reducing the amount of fuel that gets wasted, thereby improving productivity, ensuring better product quality, and generally increasing profits. At the same time, and as an added advantage of this optimization, keeping energy efficiency in petrochemical plants helps to reduce climate change.

Besides, in chemical industry, one of the complex problems for the control of which a computational intelligent approach has sense, is a crude oil distillation unit.

V.E. Balas et al. (Eds.): Soft Computing Applications, AISC 195, pp. 511–520.
springerlink.com

In a crude distillation process, the first objective is to perform an entire process optimization including high production rate with a required product quality by searching an optimal operating condition of the operating variables. In the previous decade, there was considerable research concerning the optimization of crude distillation process. In [4], the optimal feed location on both the main column and stabilizer is obtained by solving rigorous "a priori" models and mixed integer nonlinear programming. The sensitivity to small variations in feed composition is studied in [5]. Julka et al. propose in a two-part article [6][7] a unified framework for modeling, monitoring and management of supply chain from crude selection and purchase to crude refining. In addition to analytical non-linear models, computational intelligence techniques such as neural networks [8] and genetic algorithms [9] are used for the same purpose. In particular, neural networks have been used for modeling and estimation of processes in petrochemical and refineries [10][11][12]. ´

There is a part of the crude oil distillation called the platforming unit. The objective of present study is focused with this part. This zone is constituted of two subunits: the catalytic reforming or reaction unit and the distillation unit or train distillation. The expert system is focused on optimizing the production rate of the reaction unit.

2 The Petrochemical Plant

Refineries are composed of several operating units that are used to separate fractions, improve the quality of these fractions and increase the production of higher valued products like gasoline, jet fuel, diesel oil and home heating oil. The function of the refinery is to separate the crude oil into many kinds of petroleum products. This work pays special attention to Platforming Unit. This unit is constituted of two basic units: The catalytic reforming or reaction unit and the distillation unit or train distillation.

The catalytic reforming of naphtha is an important refining process that seeks to improve the octane number of gasoline due to a conversion to paraffins and naphthenes in aromatics. The feed to the naphtha reformer is a crude oil fraction from the refinery crude unit with a boiling range between 100°C and 180°C. This process is adiabatically carried out at high temperatures, building up gasoline with a high octane number, LPG, in three reformers: hydrogen, fuel gas and coke. The coke deposits on the spent catalyst surface causing its deactivation. To recover its activation, the catalyst with coke is regenerated after certain running time.

In the first reactor, the major reactions such as dehydrogenation of naphthenes are endothermic and very fast, causing a very sharp temperature drop. For this reason, this process is designed using a set of multiple reactors. Heaters between the reactors allow an adequate reaction temperature level to maintain the catalyst operation.

This process is performed in three different distillation columns (Fig. 1). The separator liquid and a stream, called aromatic LPG from the external platforming unit, feed off the first column, the debutanizer column. This column fractionates the input into two basic products: butane, to the top of the column and a high hydrocarbon flow, also called platformer, to the bottom of the column. Platformer feeds off the

debenzenizer, the second distillation unit. Its goal is to obtain a light aromatic flow to the top free to the high hydrocarbon. This stream is fed off the third distillation column that produces benzene and toluene. Benzene and toluene are the important products to the plant. The products are sent to the Morphylane Unit and, the bottom product to the second column and the top product to the third column, are stored up or sent to the other units of the refinery.

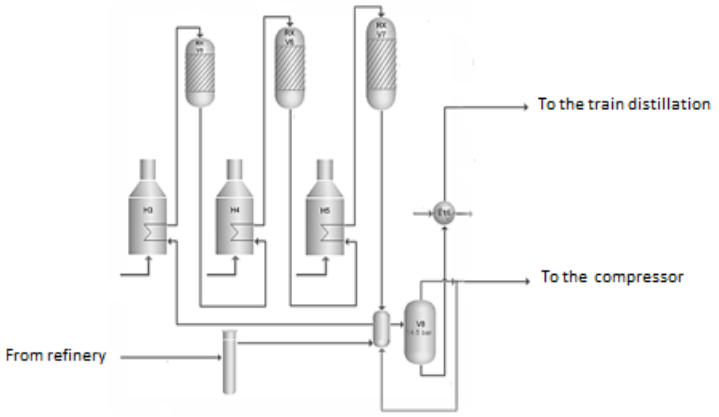

Fig. 1. Flow diagram of the catalytic reforming plant

As the platforming unit is one of the critical and important unit operations for the petroleum industry, the goal is to achieve a well-controlled and stable system, high production rate and product quality as well as low operating cost for the economic consideration. For this reason, the attention has been paid to this unit to improve product rate, efficiency and quality assurance in petroleum industry in recent years. Our work of improving of the energy efficiency is focused in the first zone of the platforming unit: the reaction zone.

3 Data Mining Process

First of all, in order to design of the expert system we carried out a data mining process of the variables registered in the reaction zone of the petrochemical plant. Thus, this type of processes requires, first of all, a selection of the sample set and, later, a preprocessing where the data are analyzed, filtered, and formatted [13][14]. The frequency of registering of the plant was hourly, but the quality of the product is analyzed only once a day. The time interval of the samples of data that we had was from January 2009 to May 2010. So, the total sample contained 12149 records corresponding to the set of variables of the plant in hourly register. The parameters of the reaction zone of the plant, which we used as inputs for our expert system, are described in Table 1.

Table 1. Main variables of the reaction zone of the plant

Variable name	Meaning
WAIPTF (C)	The variable that measure the catalysts Deterioration
TPRIN PPPV7 (C)	The input PPV7 reactor's temperature.
TPROUT PPV6 (C)	The output PPV6 reactor's temperature.
TPROUT PPV5 (C)	The output PPV5 reactor's temperature.
TPRIN PPV7 (C)	The input PPV7 reactor's temperature.
TPRIN PPV6 (C)	The input PPV6 reactor's temperature.
TPRIN PPV5 (C)	The input PPV5 reactor's temperature.
CSMFGPPH3 (m3/h)	The fuel gas PPH3 heater's consumption.
CSMFGPPH4 (m3/h)	The fuel gas PPH4 heater's consumption.
CSMFGPPH3 (m3/h)	The fuel gas PPH5 heater's consumption.
PTFINFLOW (m3/h)	The platforming input flow.
P PPV8 (bar)	The PPV8 product separator pressure.
TPROOM (C)	The room temperature.
DENRECGAS (Kg/(N*m3))	The recycle gas density. This variable manitain the PPPV8 brought under control.
TPRPPV567 (C)	The temperature increase between the three reactors.

In the first step of preprocessing, 120 outliers corresponding to the days where the plant did not have a usual operation were filtered and deleted from the training sample. Besides, the resulting sample was filtered on the basis of a quality requirement (Concretely that the limit of the level of impurities in the distillate satisfies a determining conditions). Thus, 2747 registers were filtered. Thus, after the selection and preprocessing processes, the resulting sample had 9282 records.

In order to quantify the objective of our mining, in the phase of transformation we added to each register of the sample an indicator of the energy efficient of the reaction zone:

$$EEI_{REACTION} = \frac{\sum_{i=3}^{5} CSMFGPPH_i}{PTFINFLOW} \quad (1)$$

As a first algorithm in the data mining modeling, we applied a discriminant analysis [13][14] to the set sample. This type of analysis is used for classification and prediction. Thus, this model tries to predict, on the basis of one or more predictor, or independent variables, whether an individual or any other subject can be placed in a particular category of a categorical-dependent variable. Our aim with this analysis was to study the influence of the variables of the zone in the EEI parameter as well as the grade of importance of each of these variables.

Thus, the result of this analysis was a discretization and separation of the five classes of *EEI_Reaction* through a linear combination of the input parameters. The model evaluation was performed first using ten-fold cross validation in the training sample. Later, a new validation by means of the testing sample was done. This kind of

evaluation was selected to train the algorithms using the entire testing data set and obtain a more precise model.

The result of the discriminant analysis was two canonical functions (named *Function1* and *Function2*). *Function1* covered 96.8% of the variance, and *Function2* covered only an additional 1.5%. So, and in view of this difference in percentage, we use only *Function1* as a guide of *EEI_Reaction*.

Using the normalized variables, the discriminant analysis offers a structure matrix that allows building the discriminant functions from discriminating variables, without using the canonical form. From now on, the N prefix indicates a normalized attribute. Variables are ordered by the absolute size of correlation within functions. Using the normalized variables, and by weighing up the high percentage of variance covered by *Function1*, the plant energy efficiency will be improved by means of the new attribute defined in (2).

$$F = 0.28 * N\_CSMFGPPH5 + 0.27 * N\_CSMFGPPH3 - 0.27 * N\_PTFINFLOW - 0.213 * N\_P\_PPV8 + 0.009 * N\_DENRECGAS + 0.160 * N\_CSMFGPPH4 + 0.160 * N\_TPROOM + 0.013 * N\_TPRPPV567 \quad (2)$$

Thus, this function marks the way that follows the operating points registered for the plant. As observed in Fig. 2, low values of F (specifically below -0.6) guarantee, in a high percentage, low consumption (an *EEI_Reaction* that is between 15 and 36) with regard to the platforming input flow. This resulting function F would be used as a guide and an input parameter in the optimization algorithm based on neural networks [13][14].

4 Expert System Based on Neural Networks

In order to carry out a system for the optimization of the energy efficiency of the operation points in the plant, an expert system based on a neural network kernel was developed. The system combines an algorithm based on the historical data of working environment of the plant, and an artificial neural network module for additional interpolations of new work environments. Therefore, in order to take decisions this solution uses a combination of the known conditions given in the past in the plant and the capacity of the neural network to generate new interpolated conditions when it is necessary.

We developed an application programmed in C++ to work on Microsoft Windows, where we integrated our expert system. This application makes it possible to test the system and to visualize its results. In this section of the work, we will show screenshots of various windows to explain the system and to show its results. The environment includes the following working areas:

- The value of different parameters for the operating point to optimize (distinguishing between controllable and not controllable variables, depending if they are variables whose value is adjustable by the operator of the plant or not). Besides, editable values beside each variable indicate the percent value of each variable that can be moved by the operator in each iteration.

- A plot in which you can observe, for each of the various operating point of the historic, its *EEI_Reaction* and *F*.
- The configuration of the ratio of improvement that the neural networks applied to the operation point (the X-axis corresponds to *F* offset and the Y-axis corresponds to *EEI_Reaction* and a ratio by which these values are multiplied).
- A historic text showing the evolution of different variables along the process of iterations of the algorithm to optimize the energy efficiency.
- A set of buttons to carry out the execution and test the hybrid model for a particular operating point.

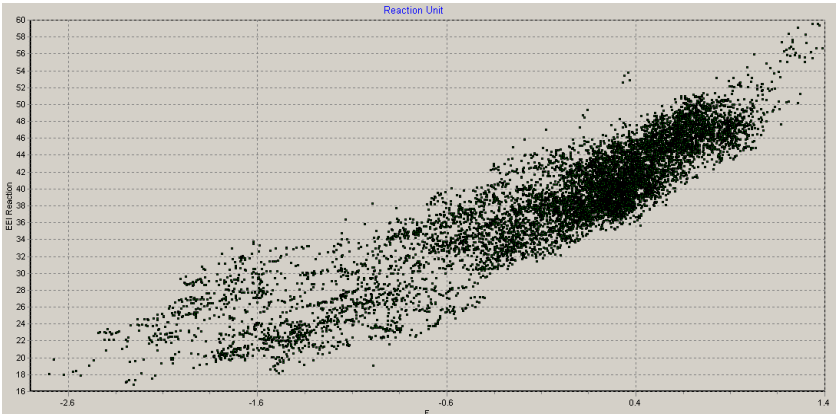

Fig. 2. Representation of the operations points with respect to *EEI_Reaction* and *F*

On the other hand, the algorithm of the expert system works in the following way once that is selected the operation point that is necessary to optimize:

1. First of all, it is filtered the sample by the environmental conditions in the actions of the operator of the plant (Selecting those registers whose values are out of a maximum percentage in which the values of the variables can be moved in each one of the iterations). In this respect, we distinguished between the conditions of the not controllable variables (those conditions for the starting point of work you want to optimize and which shall not be violated throughout the optimization process from that point) and the conditions set for the controllable variables (valid for the point which is currently being processed). The result of this filtering process is shown in Fig. 3.

2. With the *Start* button is activated the optimization process. This process consists of a loop which in each iteration is searched for a point (from the set of points of the historical) which meets the environmental conditions marked (described in the point 3 of the algorithm) that has the lowest energy. Thus, each one of these iterations improves the energy conditions since the previous point and shows the operator of the plant how carry out that improvement.

3. When it is not possible to improve the energy index of the current point using the historical register of the plant and meeting the conditions of iteration, the previous

loop stops. At this point a neural network module is fired in order to improve the energy index. This module generates, by means an interpolation process, a new working point, fulfilling the conditions set for improving the energy index variables that point. (This improvement consists of a shift of both the energy index as the function F -described in section 3-).

4. In this state, you can shoot again the optimization process to search, from this new point generated by interpolation, historical points that improve the *EEI_Reaction* to meet the conditions for the variables configured. Thus, once a new interpolated point is generated, the steps 2 and 3 can be executed by the user iteratively, until that operator of the plan reaches the desired improvement in the *EEI_Reaction*. The objective is to get the operation point with less *EEI_Reaction* of the resulting of the step 1 (as it is shown in Fig. 4).

The scheme of neural networks used for our system is shown in Fig. 5. It consists of a sequential structure of networks. Each network has got as inputs the not controllable variables (*N_PTFINFLOW, N_DENRECGAS, N_TPROOM, N_TPRPPV567*) as well as the two parameters that guide the energy efficiency (*F* and *EEI_Reaction*). The neural network 1 generates a value for the most important controllable variable (*N_P_PPV8*). The generated output is taken additionally as input by the neural network 2 and so on. The order of importance of the variables generated is given by the weight in equation (2). With this scheme, we get a less error in the adjustment for the most important variables.

The configuration of the neural networks was a Backpropagation network and they had a single hidden layer with 6 neurons for the case of the first network and 8 in the other networks. For the training process of these networks we used the 80% of the points of historical work as training patterns and 20% as validation patterns. The results reached in the adjustments of the neural networks were respectively 96.58%, 96.33%, 99.75% and 99.74%.

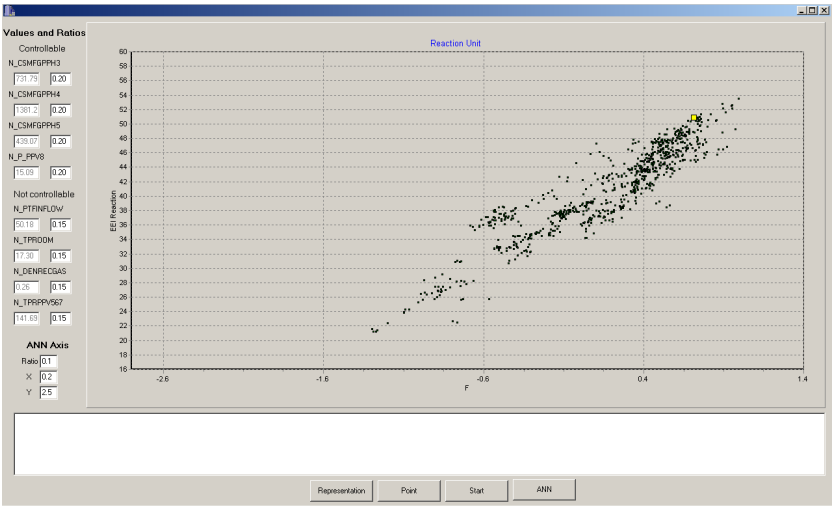

Fig. 3. Representation of the operation points for the current work conditions

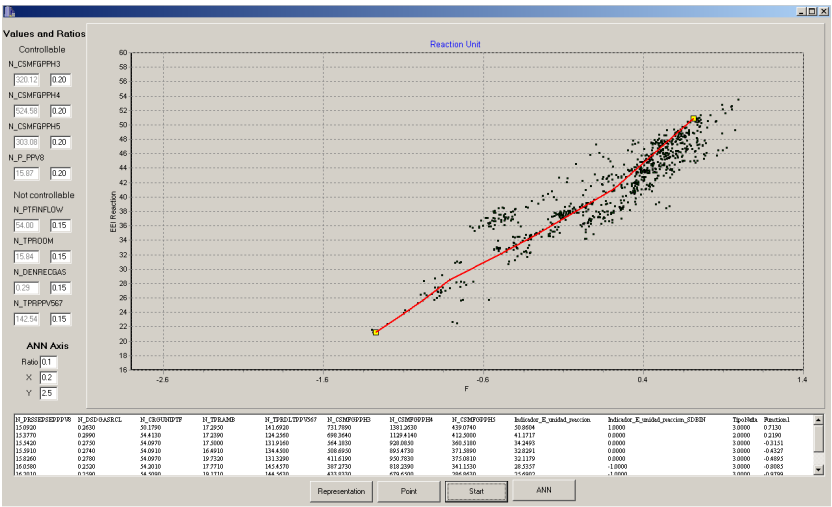

Fig. 4. Result after the optimization process carried out by the system

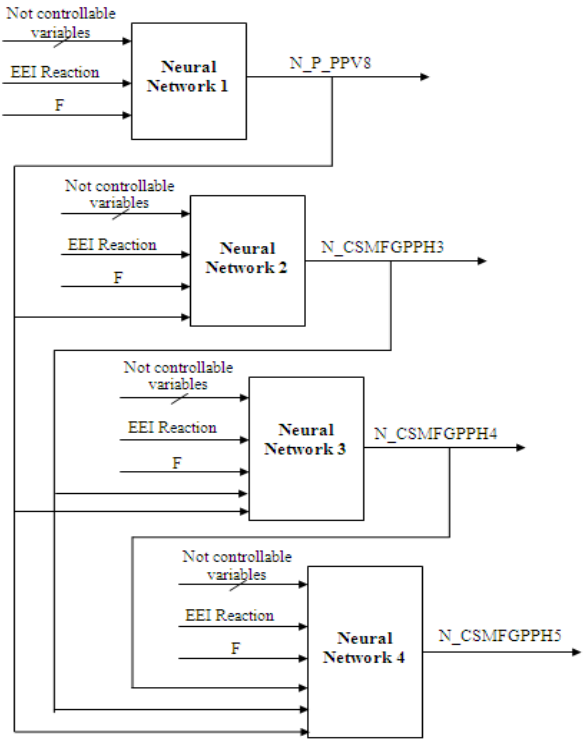

Fig. 5. Scheme of neural networks of the expert system

5 Results and Conclusions

For the quantification of the results, we generated a methodology in order to carry out a measurement of the overall improvement that would have been reached with our system for the total number of registers occurred in the past. Thus, the objective of the methodology was to apply our expert system to all the points of the sample set calculating the improvement percentage for each point and to calculate the mean improvement for the entire sample. Thus, if the expert system becomes applied on the operation points registered in the past, the energy efficiency of the zone (*EEI_Reaction*) would have improved 18.52%. This result is very good taking into account that a lot of operating points were in the range of [15,40] in their *EEI_Reaction* value and therefore, the scope of improvement was less. Thus, in an analysis of the results, we can observe as the improvement was 26.12% for those operating points with *EEI_Reaction* higher that 45 (some operating points reached an improvement of 40%).

As a conclusion of this work, it is necessary to emphasize that we have developed a tested expert system based on a module of neural networks for the optimization of the consumption of a part of a petrochemical plant. The energy efficiency is an important task that at the same time that it improves the consumption of the plant, it helps to reduce climate change. The expert system has been developed after a data mining process. It is integrated by an algorithm which uses the information relative to the parameters registered for the plant, and other hand, a scheme of neural networks for optimizing additional future operation points. Thus, this algorithm makes it possible for the operator to guide its work with a security in energy efficiency issues. This methodology for the optimization, which is the main contribution of our work, has got two advantages:

- The system is working on real conditions of operation. Thus, the use of an interpolation algorithm as neural networks is only for linking the operation point in the present with operation points that had already happened in the past. This fact ensures results that are not only theoretical but also eminently practical.
- The system can be constantly improved by means of the use of the operation points occurred in the future which can be used to adjust the neural networks.

Currently, we are working to apply the expert system to the whole plant. Besides, our objective is to integrate the expert system in the SCADA monitoring system.

Acknowledgements. This work has been supported by the Consejería de Innovación, Ciencia y Empresa, Junta de Andalucía, Spain, through the excellence project eSAPIENS (reference number TIC-5705).

References

1. Shiau, W.L.: A profile of information systems research published in expert systems with applications from 1995 to 2008. Expert Systems with Applications 38(4), 3999–4005 (2011)

2. Liao, S.H.: Expert system methodologies and applications–a decade review from 1995 to 2004. Expert Systems with Applications 28(1), 93–103 (2005)
3. Köksala, G., Batmazb, I., Testikc, M.C.: A review of data mining applications for quality improvement in manufacturing industry. Expert Systems with Applications 38(10), 13448–13467 (2011)
4. Seo, J.W., Oh, M., Lee, T.H.: Design optimization of a crude oil distillation process. Chemical Engineering & Technology 23(2), 157–164 (2000)
5. Dave, D.J., Dabhiya, M.Z., Satyadev, S.V.K., Ganguly, S., Saraf, D.N.: Online tuning of a steady state crude distillation unit model for real time applications. Journal of Process Control 13(3), 267–282 (2003)
6. Julka, N., Srinivasan, R., Karimi, I.: Agent-based supply chain management1: framework. Computers & Chemical Engineering 26(12), 1755–1769 (2002)
7. Julka, N., Karimi, I., Srinivasan, R.: Agent-based supply chain management2: a refinery application. Computers & Chemical Engineering 26(12), 1771–1781 (2002)
8. Liau, L.C., Yang, T.C., Tsai, M.T.: Expert system of a crude oil distillation unit for process optimization using neural networks. Expert Systems with Applications 26(2), 247–255 (2004)
9. Motlaghi, S., Jalali, F., Ahmadabadi, M.N.: An expert system design for a crude oil distillation column with the neural networks model and the process optimization using genetic algorithm framework. Expert Systems with Applications 35(4), 1540–1545 (2008)
10. Shirvani, Y., Zahedi, G., Bashiri, M.: Estimation of Sour Natural Gas Water Content. Journal of Petroleum Science and Engineering 73, 156–160 (2010)
11. Zahedi, G., Parvizian, F., Rahimi, M.R.: An Expert Model for Estimation of Distillation Sieve Tray Efficiency Based on Artificial Neural Network Approach. Journal of Applied Sciences 10(12), 1076–1082 (2010)
12. Falla, F., Larini, C., Leroux, G., Quina, F., Moro, L., Nascimento, C.: Characterization of crude petroleum by NIR. Journal of Petroleum Science and Engineering 51(1-2), 127–137 (2006)
13. Maimon, O., Rokach, L.: Data Mining and Knowledge Discovery Hand-book, 2nd edn. Springer US (2010)
14. Han, J., Kamber, M.: Data Mining. Concepts and Techniques, 1st edn. Morgan Kaufmann (2001)

Estimation Aspects of Signal Spectral Components Using Neural Networks

Viorel Nicolau and Mihaela Andrei

Department of Electronics and Telecommunications,
"Dunarea de Jos" University of Galati 47 Domneasca St.,
Galati 800008, Galati, Romania
{viorel.nicolau,mihaela.andrei}@ugal.ro

Abstract. Many neural network models have been mathematically demonstrated to be universal approximators. For accurate function approximation, the number of samples in the training data set must be high enough to cover the entire input data space. But this number increases exponentially with the dimension of the input space, increasing the space- and time-complexity of the learning process. Hence, the neural function approximation is a complex task for problems with high dimension of the input space, like those based on signal spectral analysis. In this paper, some aspects of neural estimation of signal spectral components are discussed. The goal is to find a feed-forward neural network (FFNN) model for estimating spectral components of a signal, with computational complexity comparable with Fast Fourier Transform (FFT) algorithm, but easier to implement in hardware. Different FFNN architectures, with different data sets and training conditions, are analyzed. A butterfly-like FFNN (BFFNN) was proposed, which has much less weight connections and better performance than FFNN.

Keywords: Feed-forward neural networks, neural estimator, spectral components, signal processing, FFT algorithm.

1 Introduction

Considering the approximation problem with neural networks (NN), the main design objective is to find a neural network which is a good approximator to some desired input-output mapping. Many neural network models have been mathematically demonstrated to be universal approximators.

The related results include proofs for the conventional multilayer perceptron [5], the radial basis function (RBF) NN [16], the rational function NN [13].

The feed-forward neural networks (FFNN), with a variety of activation functions, can be used as universal approximators [4], [5], [12], [8]. For accurate function approximation and good generalization, many aspects must be taken into account, regarding neural network topology [2], [18], training data set selection, and learning algorithm [3], [6].

For problems with small dimension of the input space, the main learning concern is related to over-training, which can lead to poor generalization capability of the

V.E. Balas et al. (Eds.): Soft Computing Applications, AISC 195, pp. 521–530.
springerlink.com

network and this fact must be considered when the neural network is designed and trained. In addition, the network size must be bounded, much less than the number of training samples. Otherwise, the network just memorizes the training samples, resulting in poor generalization [6].

If the dimension of the input space is big, the time complexity of the learning process increases, and good approximation capability is hard to be reached for the entire domain of interest in the input space [1]. The role of input dimension on function approximation is studied in [10], for various norms, and target sets using linear combinations of adjustable computational units. It results that for good approximation, input upper bounds must decrease, as the input space dimension increases, which means that the smoothness of function being approximated would have to be increased.

The theory of function approximation by neural networks is the basis to many neural applications such as pattern recognition, data compression, time series prediction, process state estimation, adaptive control, etc.

In signal processing, there are many ANN applications combined with spectral analysis, using Fast Fourier Transform (FFT) algorithm. Frequently, the problems have small dimension of the input space, and frequency spectra are used as input data for ANN. In this case, neural networks are used as classifiers of signal spectral components computed with FFT [14], [15].

If the input space dimension is high, ANN applications focus on few spectral components, like in power industry, where FFNN are widely used for harmonics analysis and prediction [20], [11]. FFT computation using cellular neural networks (CNN) was studied in [17], [19], where cell neighborhood is defined from functional rather than topological point of view. In CNN, each cell is connected only to its n-nearest neighborhood cells.

In this paper, some aspects of neural estimation of signal spectral components are discussed. The goal is to find a FFNN model to estimate several spectral components, with computational complexity comparable with FFT algorithms. Such FFNN spectral estimator has advantages over FFT algorithm, even if the model is implemented on sequential machines. It is easier to implement than FFT algorithm, which requires specialized processors with bit-reversed addressing mode.

Different FFNN architectures, with different data sets and training conditions, are analyzed. A new FFNN was proposed, with local connections of the inputs to the hidden layers, forming input butterflies like in radix-2 FFT algorithm.

The paper is organized as follows. In section 2 some elements of signal spectral analysis are discussed. In section 3, aspects of neural approximation and generalization, along with neural prediction techniques are presented. Section 4 describes some simulation results based on different neural architectures, training data sets and noise conditions. Conclusions are presented in section 5.

2 Elements of Signal Spectral Analysis

A physical signal $x(t)$ has finite energy, and it is referred as a finite energy process. If all process characteristics are time invariant, then the process is called stationary. If a

stationary process has its mean values equals with corresponding temporal mean values across of a representative process instance, then the process is called ergodic. Signal types as ergodic processes are studied in this paper.

Let $x_k(t)$ be a representative instance of an ergodic process $x(t)$ into finite time interval T, as shown in Fig. 1.

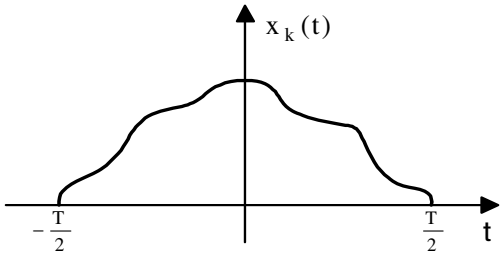

Fig. 1. Representative instance $x_k(t)$ of the ergodic process $x(t)$

The energy of $x_k(t)$ instance is:

$$E = \int_{-\infty}^{\infty} x_k^2(t)\,dt = \frac{1}{2\pi}\int_{-\infty}^{\infty} \left|X_k(j\omega)\right|^2 d\omega, \tag{1}$$

where $X_k(j\omega)$ is the continuous-time Fourier transform of $x_k(t)$. If the process energy is finite, then the integrals in (1) are bounded.

In signal spectral analysis, frequency spectra are desired, along with spectral component characteristics, such as magnitude of spectral components, and signal energy or power distribution into the spectrum. Frequency spectra are computed, according to input signal type, continuous- or discrete-time signal. For continuous-time signals $x(t)$, integral transforms, like continuous-time Fourier transform (CTFT), are used to compute frequency spectra, which are complex continuous functions in the frequency domain. CTFT analytical expression is:

$$X(j\omega) = \int_{-\infty}^{\infty} x(t)\cdot e^{-j\omega t}\,dt \tag{2}$$

Digital signal processing is based on discrete-time signals $x(n)$, as measurements of physical continuous-time signals $x(t)$, at discrete moments of time, $t = nT_S$, where T_S = sampling period, and n = sampling time index (integer). The samples are obtained with the sampling frequency $f_S = 1/T_S$. In this case, frequency spectra are computed with discrete transforms, like discrete-time Fourier transform (DTFT), which are also complex continuous functions in the frequency domain. DTFT analytical expression is obtained by changing integral symbol into infinite series with discrete moments of time:

$$X(j\omega) = \sum_{n=-\infty}^{\infty} T_S \cdot x(nT_S)\cdot e^{-j\omega\cdot nT_S} = \sum_{n=-\infty}^{\infty} x[n]\cdot e^{-j\omega\cdot n} \tag{3}$$

DTFT is a continuous periodic function, with a period of $\omega_S = 2\pi f_S = 2\pi/T_S$. This can be easily verified in (3), by changing variable ω with $\omega + \omega_S$. In general, DTFT provides an approximation of CTFT, being applied on infinite input data series. If $f_S \to \infty$, then $T_S \to dt$ and DTFT $\to$ CTFT. But in practical applications it is impossible doing computations on infinite series. Even for finite series with very long sequences of input data, the computations are very difficult.

Discrete Fourier Transform (DFT) is a discrete transform for spectral analysis of finite-domain of discrete-time functions. It is a particular type of DTFT, applied on a time-window with a finite number (N) of input samples of a longer input data sequence. As a result, DFT computes only N different frequency components, denoted X_k, equally spaced into a finite frequency range, corresponding to the first period of DTFT frequency domain, [0, ω_S]. DFT is an approximation of DTFT on this frequency domain, which gets better as the number N increases.

DFT analytical expression is obtained by sampling DTFT in frequency domain, for the finite input sequence, denoted x_n, n = 0 … N-1:

$$X_k = \sum_{n=0}^{N-1} x_n \cdot e^{-j2\pi \cdot \frac{k}{N} \cdot n}, \quad k = 0 \ldots N-1 \tag{4}$$

Fast Fourier Transform (FFT) is an efficient class of algorithms to compute DFT and its inverse (it is not another discrete transform). FFT computes more quickly the frequency components of the discrete spectrum than DFT expressed in (4). Considering a finite input sequence of N samples, the computing complexity of DFT is $O(N^2)$, which means that the number of operations needed to obtain the result is proportional with N^2. By contrast, FFT algorithms have $O(N \cdot log_2 N)$. The difference in speed is important, especially for big values of N, when computational time can be reduced by several orders of magnitude (e.g. if $N = 1024 = 2^{10}$, then $O(N^2) = 1048576$, while $O(N \cdot log_2 N) = 10240$).

There are many forms of FFT algorithms, with decimation-in-time and decimation-in-frequency. Radix-2 FFT algorithms need the length of input sequence (N) to be a power of 2. Other FFT algorithms need N to be equal to the product of mutual prime numbers (e.g. 9·7·5 = 315 or 5·16 = 80). In addition, FFT algorithms for real input data are about 60% effort of the same sized complex data FFT.

In general, a radix-n FFT algorithm recursively breaks down the DFT of composite size $N = n \cdot m$ into n smaller DFTs of size m, where n is the radix number. By far the most commonly used radix-2 FFT is the Cooley–Tukey algorithm, which successively breaks a DFT of size N into 2 smaller DFTs of size N/2. In this case, the shape of the data-flow diagram is called butterfly diagram. At its basis, the butterfly diagram takes 2 inputs (x_1, x_0) and generates 2 outputs (y_1, y_0).

A decimation-in-time FFT algorithm with the length of input sequence $N = 2^p$, based on primitive N-th root of unity $\omega = exp(-j \cdot 2\pi / N)$ uses butterfly forms:

$$\begin{cases} y_0 = x_0 + x_1 \cdot \omega^k \\ y_1 = x_0 - x_1 \cdot \omega^k \end{cases}, \tag{5}$$

where k = 0 … N-1 and it depends on the part of the transform to be computed.

3 Aspects of Neural Estimation Using FFNNs

Neural network models are specified by the net topology, node characteristics, and training or learning rules. Static neural network (SNN) models, like FFNN, are characterized by neuron equations without memory, meaning that their outputs are functions only of the current inputs. SNNs implement nonlinear transformations of the form $\mathbf{y} = G(\mathbf{x})$, with input vectors $\mathbf{x} \in \Re^n$, and output vectors $\mathbf{y} \in \Re^m$, where n and m represent the vector dimensions of $\mathbf{x}$ and $\mathbf{y}$, respectively [7]. In this paper, FFNN models are used for neural estimation of signal spectral components.

There are many aspects which must be solved when using FFNNs, regarding the optimal network topology, learning algorithms to deal with local minima, the conditions to achieve good generalization, and efficacy in scaling to larger problems [7]. The most practical concerns are: the network size, time complexity of learning and network ability to generalize.

The network size is important, but in general it is not known for a given problem. If the network is too small, it will not be able to give a good model of the problem. If the network is too big, it will give more solutions which are consistent with training data set, but they are all poor approximations of the problem [2].

The training process consists in finding the correct set of network parameters (weights and biases), which produces the desired mapping for the training data set. Time complexity of learning is directly connected with the complexity of the problem. If the dimension of the input space is very large, then it is unlikely to determine if the correct set of weights and biases can be found in a reasonable amount of time [3]. This is the case when trying to approximate a function like FFT, with a huge dimension of the input space.

One way to reduce the number of network weights is to use local connections of the inputs to the hidden layers, so that individual neurons in the hidden layers to process local regions of the input space [7].

Neural estimation of several spectral components of a signal is a case of approximation problem, with big dimension of the input space. The inputs are N consecutive signal samples of finite input sequence, denoted x_n, n = 0 … N-1, and the outputs represent estimated amplitude of the desired spectral components. Unlike neural approximation of FFT, which tries to find an approximation into the entire input space, spectral estimation takes into account a much smaller input region, for signals with bounded variations in frequency and amplitude.

At every k moment of time, the time-window contains a finite number (N) of time-delayed samples, which form the input sequence of FFNN, as illustrated in Fig.2. The input sequence x_n was denoted according with time moment considered: $x_0 = x(k-N+1)$, …, $x_{N-1} = x(k)$.

It can generally be assumed that any real data will have some degree of uncertainty, generated by systematic or random errors. The estimates take into account the uncertainty in the target data or the uncertainty in the input data. Therefore, it is necessary for any learning system to be able to cope with such uncertainty, producing valid estimates based on real data sets. In this paper it is assumed that there is noise on the input data sets, generated by measurement system.

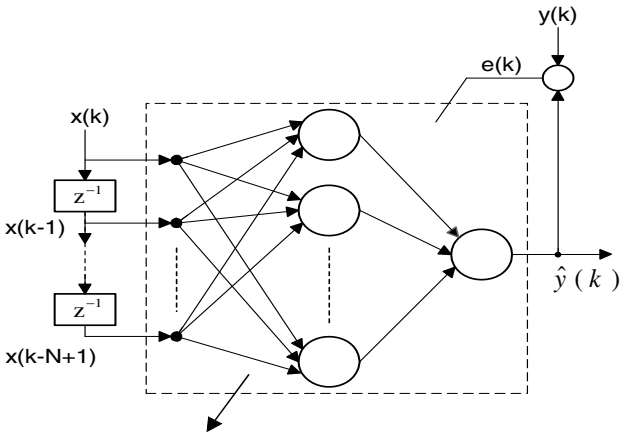

Fig. 2. Spectral component estimation using feed-forward neural networks

For every step k, the estimation error $e(k)$ is computed based on the computed and estimated values of spectral component amplitudes.

The performance goal has to be small enough to assure good estimation performance, but not too small to avoid loss of generalization. The mean squared error *mse* was chosen as performance function:

$$mse = E[e^2(k)] = \frac{\sum_{i=1}^{M} e^2(k)}{M}, \tag{6}$$

where M is the number of vectors in data sets.

4 Experimental Results

For simulations, signal data sets are generated, as sequences of samples from noisy signals with different narrow frequency bandwidth. In spectral analysis, time-windows with $N = 32$ samples are used, as inputs to FFNN and also to FFT algorithm, which computes the desired frequency spectra. The sampling frequency was chosen as f_S = 3200 Hz, resulting a frequency resolution of deltaf = 100 Hz.

Using FFT algorithm, the computed frequency spectra have 32 spectral components, of which only 16 are used, into the frequency domain [0, 1500] Hz. They form the desired frequency spectra in supervised learning process.

Due to large dimension of the input space, $\Re^N$, approximation of the entire FFT function is a very complex task. Hence, a smaller region of interest into the input space has to be selected, taking signals with narrow frequency bandwidth and bounded variations of magnitude. In this case, noisy signals in 2 narrow frequency intervals (3 components) are generated, I_1 = [100, 300], and I_2 = [700, 900] Hz.

The signals are series of sinusoidal functions, with variable number of spectral components, N_{rsc} = 1, 2 or 3, with discrete frequencies randomly selected in intervals. Also, the amplitudes and phases are bounded and randomly selected between the limits: $A_j \in [1, 3]$ and $[-\pi/2, \pi/2]$, respectively. The signal analytical expression is:

$$x(t) = \sum_{j=1}^{N_{rsc}} A_j \cdot \sin(2\pi \cdot f_j t + \varphi_j) \tag{7}$$

The signal parameters are: N_{rsc}, A_j, f_j, and φ_j, $j = 1 \ldots N_{rsc}$. For every parameter set with chosen N_{rsc}, a data sequence is generated. Time horizon includes $N_{tw} = 10$ distinct time-windows. Hence, each data sequence contains $N \cdot N_{tw} = 320$ samples.

In addition, signals can be affected by different types of noise (measurement, conversion, digital processing), which in general is considered as additive noise *z(t)*, resulting a noisy signal: *xz(t) = x(t) + z(t)*. In this paper, additive noise is considered with limited variations and uniform distribution. The signal-noise ratio is *SNR* = 20. An example of data set, with- and without noise, is shown in Fig. 3.

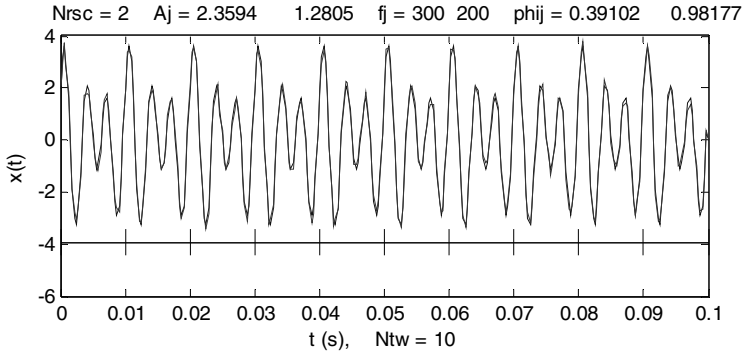

Fig. 3. Data sequence generated with 2 spectral components, f_{j1} = 300 Hz and f_{j2} = 200 Hz

For FFNN training and testing, each input data sequence is organized as a matrix of type *[N, N_{tw}]*, where each column contains *N* samples of time-windows. For example, the samples of first time-window of data sequence, presented in Fig. 3, are illustrated on the left side in Fig. 4. The noisy samples are illustrated with continuous line and the noiseless values are drawn with dotted line. On the right side, spectral components are represented with circle and diamonds marks, respectively.

For every frequency interval, I_1 and I_2, 2 training sets, with N_{rsc} = 1 and 2, respectively, and 3 testing sets, with N_{rsc} = 1, 2 and 3 are generated. The training sets contains a number of N_{lds} = 50 data sequences, with N_{tw} = 10 time-windows each. So, each training set contains a number of learning vectors N_{lv} = 500. Similarly, the testing sets contains a number of N_{tds} = 5 data sequences, with a total number of testing vectors N_{tv} = 50.

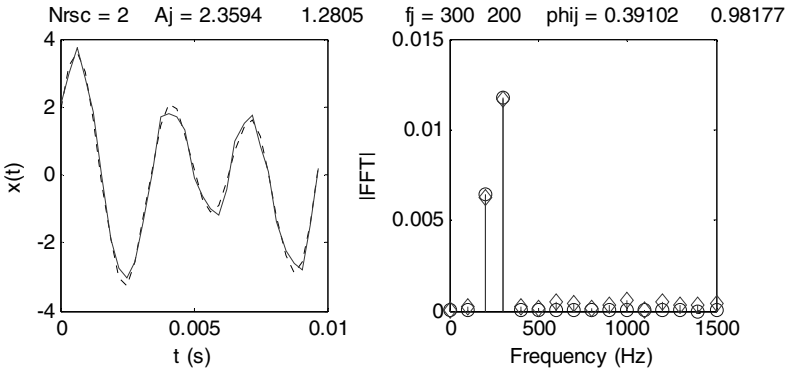

Fig. 4. Samples of first time-window, along with its computed FFT magnitude

All neural networks were trained using Levenberg-Marquardt back-propagation algorithm. During network learning and testing, the same performance criterion was used, the mean squared error (*mse*) of spectral component estimation related to initial noisy frequency spectrum, denoted *msel* and *mset*, respectively.

Two different FFNN architectures were tested. The first type of FFNN architecture is a standard FFNN with one N-dimensional input, one hidden layer with N_{hn} neurons, and one N/2-dimensional output, as illustrated in Fig. 5. The neurons in hidden layer have tansig transfer functions, and output neurons have poslin transfer functions, so that only positive values to be generated for spectral component amplitudes. Two feed-forward neural networks were generated with different number of neurons in hidden layer, N_{hn} = 32, and 64, respectively.

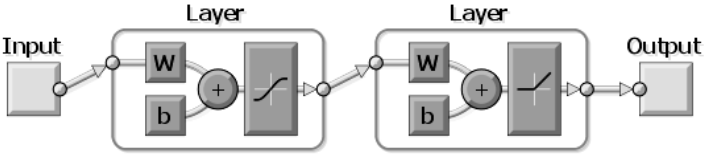

Fig. 5. First type of FFNN architecture, with one N-dimensional input

The second type of FFNN architecture is a butterfly-like FFNN (BFFNN) with two N/2-dimensional inputs, two hidden layers with $N_{hn1} = N_{hn2} = N/2$ neurons, connected separately with the inputs, and one N/2-dimensional output, as illustrated in Fig. 6. The neurons in hidden layers have linear transfer functions, and output neurons have poslin transfer functions.

The N input data samples are separated in two N/2-dimensional inputs, in the same manner as in radix-2 FFT algorithm to form butterfly diagram. The samples with even index are grouped into the first neural input, and the odd index samples form the second neural input. In this way, better performance than FFNN is obtained with less effort (much less weight connections).

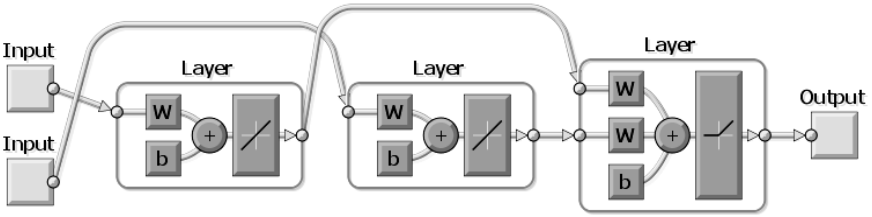

Fig. 6. Butterfly-like FFNN architecture, with two N/2-dimensional inputs

The training and testing results for 3 NNs are represented in Table 1. The parameter *mset1* represents the testing performance for testing data sets with N_{rsc} = 1, while *mset2* is for testing data sets with N_{rsc} = 2. It can be observed that butterfly-like FFNN has much better performance than FFNN, and *mse* has similar values in both frequency ranges.

Table 1. Network Performance for Different Neural Predictors

Freq. Range	Nrsc	FFNN with Nhn = 32			FFNN with Nhn = 64			Butterfly-like FFNN		
		msel $\cdot 10^{-6}$	mset1 $\cdot 10^{-6}$	mset2 $\cdot 10^{-6}$	msel $\cdot 10^{-6}$	mset1 $\cdot 10^{-6}$	mset2 $\cdot 10^{-6}$	msel $\cdot 10^{-6}$	mset1 $\cdot 10^{-6}$	mset2 $\cdot 10^{-6}$
I_1	1	5.89	6.244	3.246	5.93	6.215	5.81	0.331	0.369	7.494
	2	3.29	6.461	3.342	3.02	6.31	3.01	1.38	2.218	0.845
I_2	1	5.99	6.310	3.560	6.12	6.227	9.665	0.331	0.379	7.108
	2	3.81	6.799	3.483	3.28	6.477	3.345	1.32	0.378	0.768

5 Conclusions

In this paper, some aspects of neural estimation of signal spectral components are discussed. Different FFNN architectures, with different data sets and training conditions, are analyzed. A butterfly-like FFNN (BFFNN) was proposed, which has much less weight connections and better performance than FFNN.

References

[1] Barron, A.R.: Approximation and estimation bounds for artificial neural networks. Mach. Learn. 14(1), 115–133 (1994)
[2] Baum, B., Haussler, D.: What size net gives valid generalization? Neural Computation 1, 151–160 (1989)
[3] Blum, A., Rivest, R.L.: Training a 3-node neural network is NP-complete. In: Proc. of Computational Learning Theory Conference (COLT), pp. 9–18 (1988)
[4] Hornik, K., Stinchcombe, K.M., White, H.: Multilayer feedforward networks are universal approximators. Neural Networks 2, 359–366 (1989)
[5] Hornik, K.: Approximation capabilities of multilayer feedforward networks. Neural Networks 4, 251–257 (1991)

[6] Huang, S.C., Huang, Y.F.: Bounds on the number of hidden neurons in multilayer perceptrons. IEEE Transactions on Neural Networks 2(1), 47–55 (1991)
[7] Hush, D.R., Horne, B.G.: Progress in Supervised Neural Networks. IEEE Signal processing Magazine 10(1), 8–39 (1993), doi:10.1109/79.180705
[8] Ilin, R., Kozma, R., Wetbos, P.J.: Beyond Feedforward Models Trained by Backpropagation: A Practical Training Tool for a More Efficient Universal Approximator. IEEE Trans. on Neural Networks 19(6), 929–937 (2008)
[9] Lippmann, R.P.: An Introduction to Computing with Neural Nets. IEEE ASSP Magazine 4, 4–22 (1987), doi:10.1109/MASSP.1987.1165576
[10] Kainen, P.C., Kurkova, V., Sanguineti, M.: Dependence of Computational Models on Input Dimension: Tractability of Approximation and Optimization Tasks. IEEE Trans. on Information Theory 58(2), 1203–1214 (2012)
[11] Keerthipala, W.W.L.: Low Tah Chong, and Tham Chong Leong Artificial neural network model for analysis of power system harmonics. In: Proc. of IEEE Int. Conf. on Neural Networks, vol. 2, pp. 905–910 (1995)
[12] Leshno, M., Lin, V.Y., Pinkus, A., Schocken, S.: Multilayer feedforward networks with a nonpolynomial activation function can approximate any function. Neural Networks 6, 861–867 (1993)
[13] Leung, H., Haykin, S.: Rational function neural network. Neural Comput. 5, 928–938 (1993)
[14] Nakayama, K., Kaneda, Y., Hirano, A.: A Brain Computer Interface Based on FFT and Multilayer Neural Network. Feature Extraction and Generalization. In: Proc. of Int. Symp. on Intelligent Signal Processing and Comm. Systems (ISPACS 2007), pp. 826–829 (2007)
[15] Onishi, S., Tanaka, A., Hasegawa, H., Kinoshita, K., Kishida, S.: Construction of Individual Identification System using Voice in 3-lyered Neural Networks. In: Proc. of Int. Symp. on Intelligent Signal Processing and Comm. Systems (ISPACS 2009), pp. 635–637 (2009)
[16] Park, J., Sandberg, I.W.: Universal approximation using radial-basis-function networks. Neural Comput. 3, 246–257 (1991)
[17] Perko, M., Fajfar, I., Tuma, T., Puhan, J.: Fast Fourier Transform Computation using a Digital CNN Simulator. In: 5th IEEE Int. Workshop on Cellular Neural Networks Abd Their Applications, pp. 230–235 (1998)
[18] Segee, B.E.: Using spectral techniques for improved performance in ANN. In: Proc. of IEEE Int. Conf. on Neural Networks, pp. 500–505 (1993), doi:10.1109/ICNN.1993.298608
[19] Tamayo, O.M., Pineda, J.G.: Filtering and spectral processing of 1-D signals using cellular neural networks. In: Int. Symp. on Circuits and Systems (ISCAS 1996), vol. 3, pp. 76–79 (1996)
[20] Wu, X., He, W., Zhang, Z., Deng, J., Li, B.: The harmonics analysis of power system based on Artificial Neural Network. In: World Automation Congress (WAC 2008), pp. 1–4 (2008)

On-Line Operation of an Intelligent Seismic Detector

Guilherme Madureira[1], António E. Ruano[2], and Maria Graça Ruano[3]

[1] Institute of Meteorology, Geophysical Center of S. Teotónio, Portugal
guilherme.madureira@meteo.pt
[2] Centre for Intelligent Systems, IDMEC,
IST and the University of Algarve, Portugal
aruano@ualg.pt
[3] CISUC, University of Coimbra, and the University of Algarve, Portugal
mruano@ualg.pt

Abstract. This study describes the on-line operation of a seismic detection system to act at the level of a seismic station providing similar role to that of a STA / LTA ratio- based detection algorithms. The intelligent detector is a Support Vector Machine (SVM), trained with data consisting of 2903 patterns extracted from records of the PVAQ station, one of the seismographic network's stations of the Institute of Meteorology of Portugal (IM). Records' spectral variations in time and characteristics were reflected in the SVM input patterns, as a set of values of power spectral density at selected frequencies. To ensure that all patterns of the sample data were within the range of variation of the training set, we used an algorithm to separate the universe of data by hyper-convex polyhedrons, determining in this manner a set of patterns that have a mandatory part of the training set. Additionally, an active learning strategy was conducted, by iteratively incorporating poorly classified cases in the training set. After having been trained, the proposed system was experimented in continuous operation for unseen (out of sample) data, and the SVM detector obtained 97.7% and 98.7% of sensitivity and selectivity, respectively. The same type of ANN presented 88.4 % and 99.4% of sensitivity and selectivity when applied to data of a different seismic station of IM.

Keywords: Seismic detection, neural networks, support vector machines, spectrogram.

1 Introduction

In the past decade, Computational Intelligence (CI) techniques have been applied in the area of seismology for several classes of problems: earthquake prediction [1,2], control and monitoring of civil engineering structures [3,4], discrimination between event types (earthquakes, explosions, volcanic, underwater) [5,6], phase determination [7-9] and seismic image [10].

Although a significant amount of research has been devoted to automatic seismic detection algorithms, the majority of the systems employed in seismic centers are

V.E. Balas et al. (Eds.): Soft Computing Applications, AISC 195, pp. 531–542.
springerlink.com

based on the Short Time Average (STA) / Long-Time Average (LTA) ratio and its variants [11]. These algorithms produce a significant number of false alarms and missing detections, therefore needing human supervision at all times. Thus, continuous research efforts are required aiming at highly efficient real time seismic event detectors to be applicable on continuous seismic data.

CI techniques were also applied to the detection of seismic events. Dai and co-workers [12] developed a MultiLayer Perceptron to identify the the P and S arrivals. Compared with manual detection, the systems correctly identified between 76.6% and 82.3% of the P arrivals, and between 60.5% and 62.6% of the S arrivals. In [13], two types of Artificial Neural Networks (ANNs) were trained with different types of inputs. Experiments have shown that these systems performed better than those algorithms based on a threshold of the STA/LTA ratio.

The authors, in a previous work [14], used SVMs to design a seismic detector, to be applied at station level, which obtained, offline, an almost perfect classification. Section 2 describes briefly this past work. Section 3 describes the results obtained with this detector in continuous, on-line operation, for data originated from the same seismic station. Section 4 illustrates the performance of the same detector for data originated from a different station. Conclusions and future work are expressed in section 5.

2 Offline Operation

2.1 Training Data

The data used was collected from a seismic station, located in the south/center of Portugal: PVAQ, located in Vaqueiros, Algarve (37º24.22'N, 07º43.04'W). In this work, the spectrogram is used as the first stage of earthquake detection.

The Power Spectrum Density (PSD) is estimated using periodogram averaging. Only positive frequencies are taken into account (the so-called one-sided PSD). PSD values are slightly smoothed by taking the average of PSD values in a constant relative bandwidth of 1/10 of a decade. The procedure to achieve that smoothness was as follows: Let $P(f)$ be the PSD values in some set of discrete frequencies F. Starting with the lowest frequency of F, (f_{min}), we created a sequence of frequencies separated by 1/10 of a decade,

$$f_k = f_{\min} 10^{\frac{k-1}{10}}, \quad k = 1, 2, \ldots \tag{1}$$

We then split F into disjoint subsets D_k,

$$D_k = \{f\} : f_k \le f \le f_{k+1}, f \in F, k = 1, 2, \ldots \tag{2}$$

each set D_k is associated with a frequency f_k as defined above. The smoothed PSD, $Ps(f_k)$, is given by,

$$P_S(f_k) = \frac{\sum_{f \in D_k} P(f)}{\#D_k} \tag{3}$$

We have divided segments of 120 seconds into 5 non-overlapping intervals. For each one of them we computed the PSD. This is done with standard Matlab functions. We then picked the power spectrum at 6 frequencies 1, 2, 4, 8, 10 and 15 Hz. This means that 30 different features (5 frequencies for each of the 5 intervals) will be used for the classifier. This was a constraint that we imposed, in order to limit the classifiers complexity. Fig. 1 illustrates a seismic-record and the spectral content for each of the 5 intervals considered, presented with the selected frequencies highlighted.

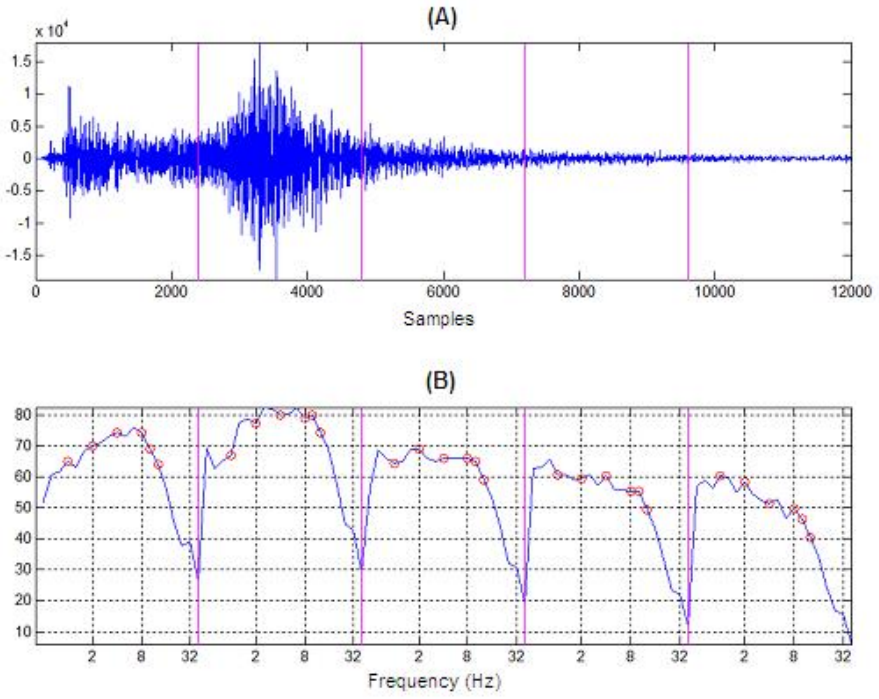

Fig. 1. (A) 120 seconds of seismic record; (B) Spectrogram

Seismic data from the IM PVAQ seismic station, and previously classified by seismologists of the National Data Center (NDC), was collected. The seismic detector used at a station level (like PVAQ) is a standard STA/LTA ratio based detector. Fig. 2 outlines the operation of such a detector.

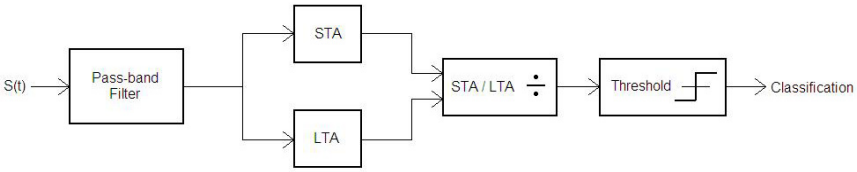

Fig. 2. Block diagram of a typical STA/LTA detector

The input data is band-pass filtered to maximise sensitivity within a specific frequency band of interest, and to reject noise outside this band. Averages of the modulus of signal amplitude are computed over two user-defined time periods, a short time average (STA) and a long time average (LTA), and the ratio of the two, (STA/LTA), at each sample point is computed. If this ratio exceeds a user-defined threshold, then a trigger is declared, and the system remains in a triggered state until the ratio falls below the defined threshold.

From the year of 2007, 2903 examples were collected, 502 representing Class 1 (classified as seismic event by the seismologists at NDC, and where seismic phases were identified in the PVAQ records), and the other 2401 classified as non-seism. For the positive case, the station detection system miss-classified 50% of the events. In the non-seism class, 50% of the examples were randomly selected representing events that triggered the detection system, but that were not classified as seismic by the NDC, while the rest of the examples were selected randomly, neither coinciding with events detected by the system nor classified as earthquakes by the NDC. This way, the station automatic detection system achieved values of 50% of sensitivity, or Recall (R) and Specificity (S) in the data collected.

$$R = \frac{TP}{TP + FN} \tag{4}$$

$$S = \frac{TN}{FP + TN} \tag{5}$$

where TP, TN, FP and FN denote the number of True Positives, True Negatives, False Positives and False Negatives, respectively.

2.2 Training Methods

SVMs, trained with the algorithm described in [15] were used as classifiers. The first experiment was conducted by assigning randomly 60% of the data to the training set, 40% to the validation set. It was only ensured that a similar percentage of positive cases were assigned to each data set. The training set consisted of 1744 examples, with 307 positive cases; the test set had 582 examples, with 99 positive cases; the validation set consisted of 577 events, with 96 positive cases.

Subsequently, another set of experiences regarding different partitioning of data between the training and validation sets was conducted. First of all, an approximate convex hull of the input data has been obtained, and the examples that lie in the hull were integrated in the training set. In order to maintain an approximate distribution of 60% and 40% of the data to the two sets, examples of the original training set were moved to the validation set. Then, a naïve form of active learning was applied. The examples badly classified in the validation set were incorporated in the training set, and randomly removed the same number of examples of the validation set, provided they were not in the approximate convex hull previously determined. This procedure was repeated three times. The results are presented in Table 1.

Table 1. SVM performance with active learning

SVs	R	S	R(All)	S(All)
583	100.00	100.00	99.62	99.35
609	100.00	100.00	99.72	99.66
626	100.00	100.00	99.76	99.72
640	100.00	100.00	100.00	99.93

The first column in Table 1 denotes the number of support vector. The second and third denote the Recall and Specificity values, for the training set, while the two last columns show these values for the whole data.

The first row shows the values obtained without active learning, while the other lines illustrate the results obtained, for each active learning iteration.
Further off-line results, for SVMs and MLPs, can be seen in [14].

3 Continuous Operation

The SVM classifier, due to its superior performance, was chosen as the seismic detector. Subsequently, it was applied in continuous operation, for the seismic record corresponding to the year of 2008. The 120 sec. window slides within the whole seismic record, in intervals of 50 samples (0.5 sec). Each window of 120 sec. is applied to the classifier, and its output compared with the seismic catalogue, resulting in a label of TP, FP, TN or FP for that segment.

The neural network classifier was applied to the first 256 days of 2008. As the station was not working correctly in the Julian days 3, 200 and 201, these days were not considered.

During the period of 253 days, 1545 seismic events were found in the Portuguese Catalogue, corresponding to this seismic station. From these, 964 were considered as local, and 581 as regional events. The number of tectonic events was 638. and the remaining -907- were classified as explosions. Figure 3 illustrates the histogram of magnitudes of the seismic events, within the period considered. The minimum magnitude is 0.1, and the maximum is 4.7.

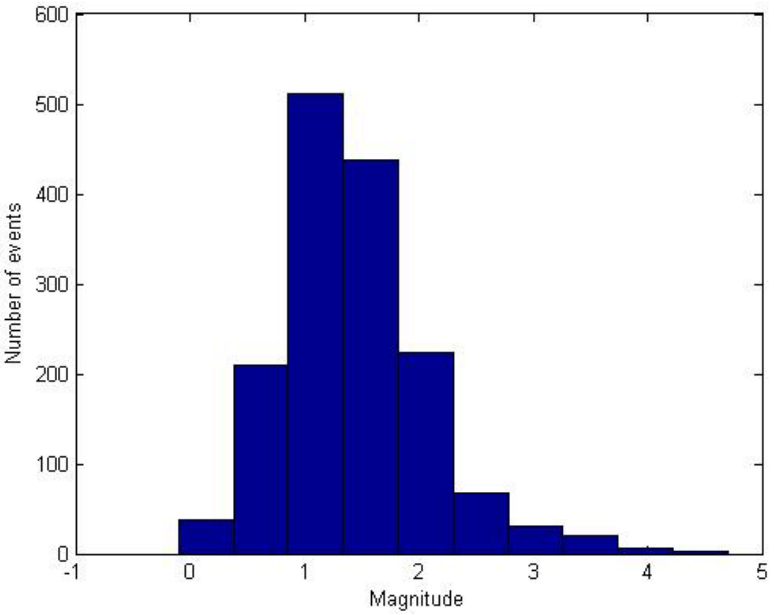

Fig. 3. Histogram of the seismic magnitudes for PVAQ

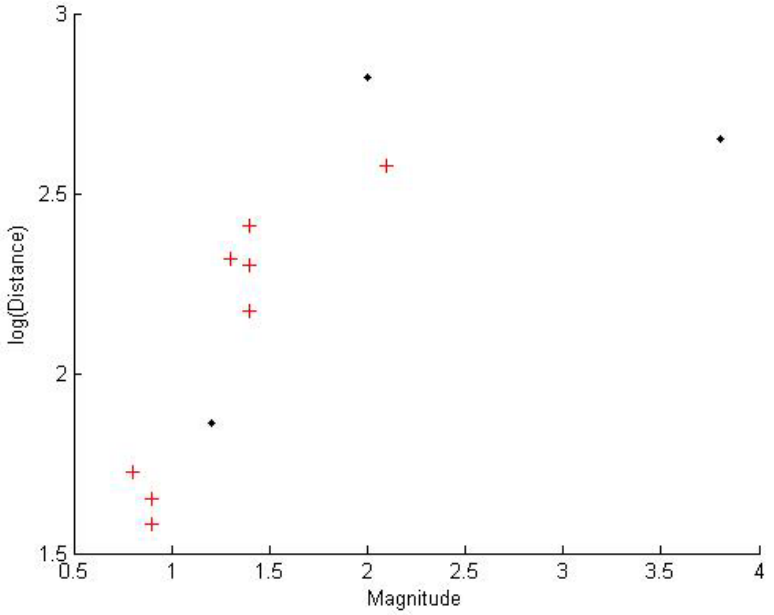

Fig. 4. Magnitude vs. decimal logarithm of the distance, for events non-detected in PVAQ

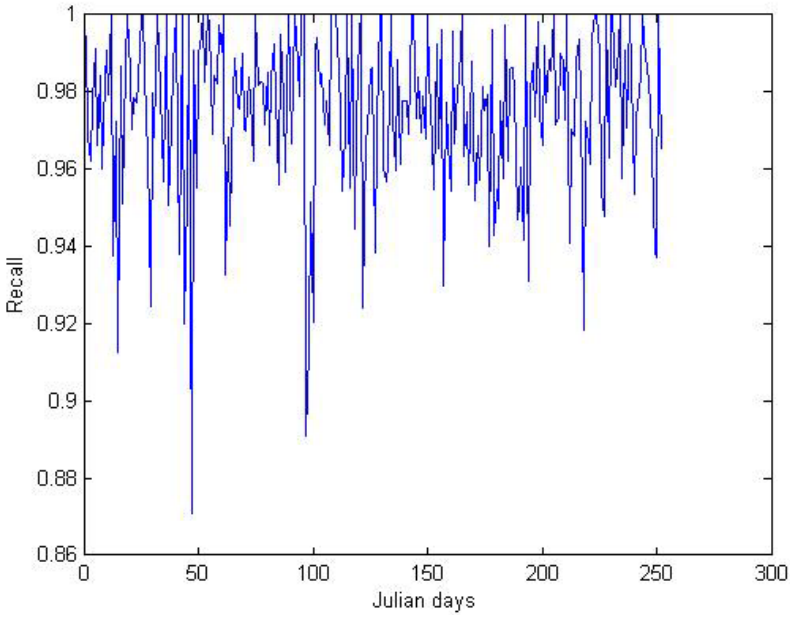

Fig. 5. Values of Recall for PVAQ

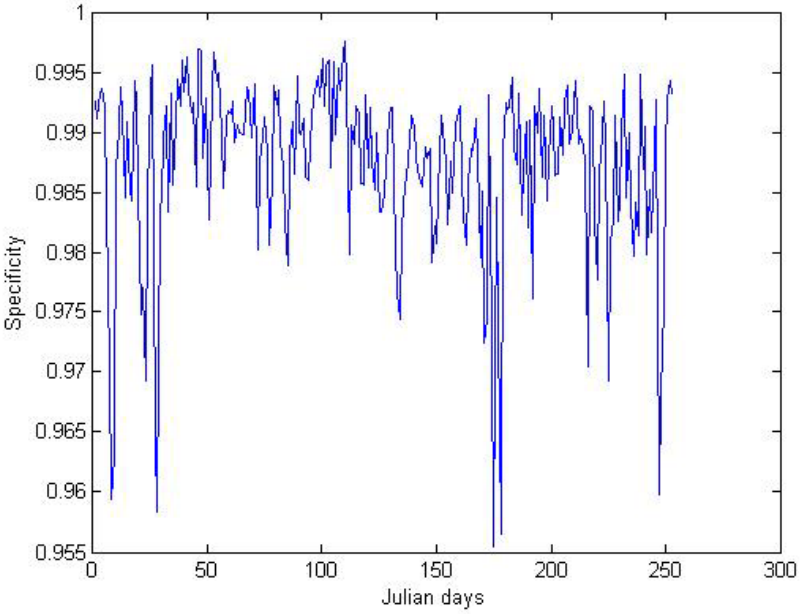

Fig. 6. Values of Specificity for PVAQ

Out of the 1545 events, the classifier did not detect 11 events. Figure 4 shows, for those events, the magnitude versus the decimal logarithm of the distance (in Kms) to the hypocenter. The symbol '+', in red, denotes explosions, while the black dot denotes earthquakes. As it can be seen, events with large magnitude that were not detected have hypocenters with a large distance from the station.

Figures 5 and 6 show the Recall (R) and Specificity (S) computed for each day, within the 253 days considered. In the Julian day 125 no seismic events did occur and no false negatives were obtained. For this reason, this day is not considered in figure 6.

Computing the R and S values for the whole period considered, 97.7% and 98.7% were obtained, respectively.

4 Continuous Operation for Estremoz Station

The SVM classifier, trained with the 2007 year data from PVAQ station, was applied in continuous operation, for the first 185 days of 2008, of another station within the Portuguese seismic network, Estremoz – PESTR, located in Central Alentejo (38º52.03'N 07º35.41'W).

Figure 7 shows the histogram of the magnitudes of the seismic events for the period considered. The minimum magnitude was 0.5, and the maximum 4.7.

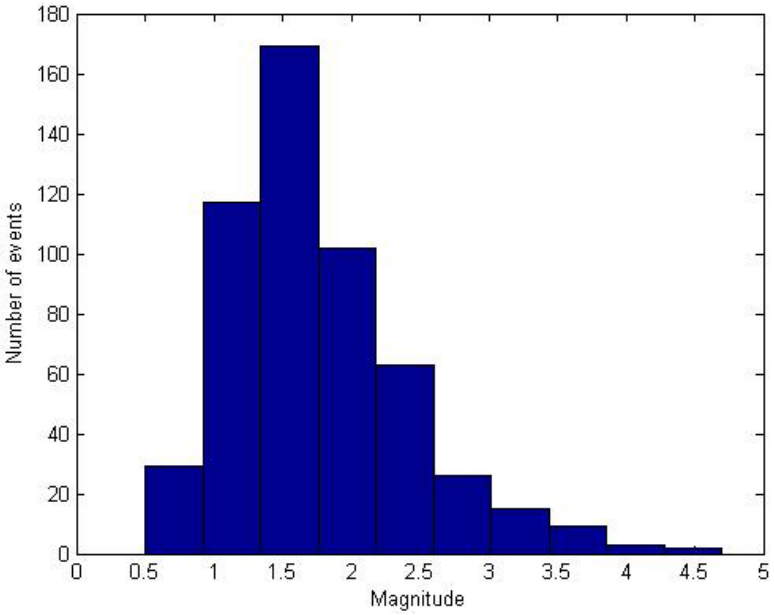

Fig. 7. Histogram of the seismic magnitudes for PESTR

During the period considered, there were 535 events, 272 being considered local events, and 263 regional events. From these, 226 were earthquakes, and 309 were explosions. The SVM classifier was not able to detect 71, out of the 535 events.

Figure 8 shows the Recall values, computed for each day. For Julian days 3, 7, 14, 17, 20, 26, 43, 47, 48, 76, 96, 118, 122, 125, 132, 181, there were no seismic events recorded, nor classifier false negatives. For Julian days 50, 89, 155 and 159 there were no seismic events recorded. For this reason, these days are not represented in the graph.

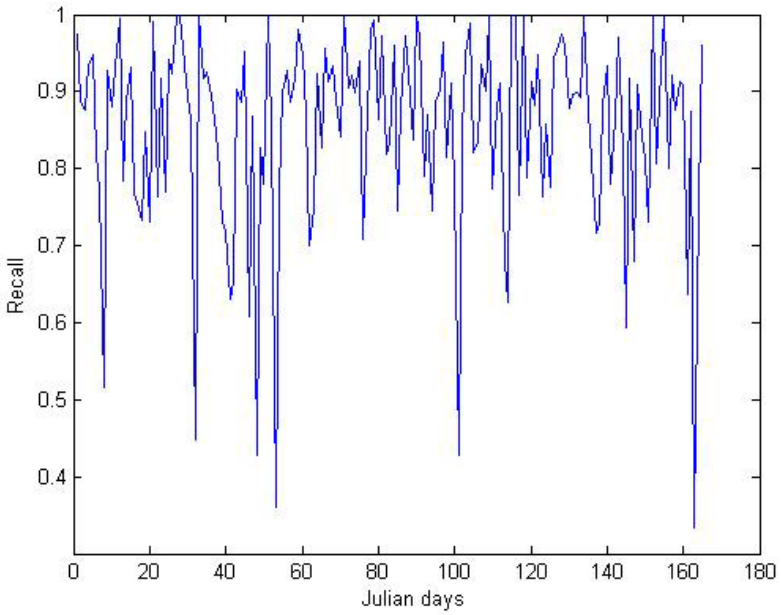

Fig. 8. Recall values for PESTR

Figure 9 illustrates the Specificity values, computed for each day.

Figure 10 illustrates the characteristics of the events not detected by the classifier. The same conventions of figure 4 were used.

The R and S values, for the whole period considered, are 88.4% and 99.4%. Considering the S values (nearly perfect) for the two stations, it can be concluded that the SVM classifier learnt how to separate seismic events from background noise. In terms of the R values, it is no surprise a worse value for PESTR, as the classifier was trained with positive examples for PVAQ. In terms of the geophysical properties of the soil of the two stations, they should be very different as PVAQ is near the seaside and PESTR in the interior. The distance between the 2 stations is nearly 200 kms.

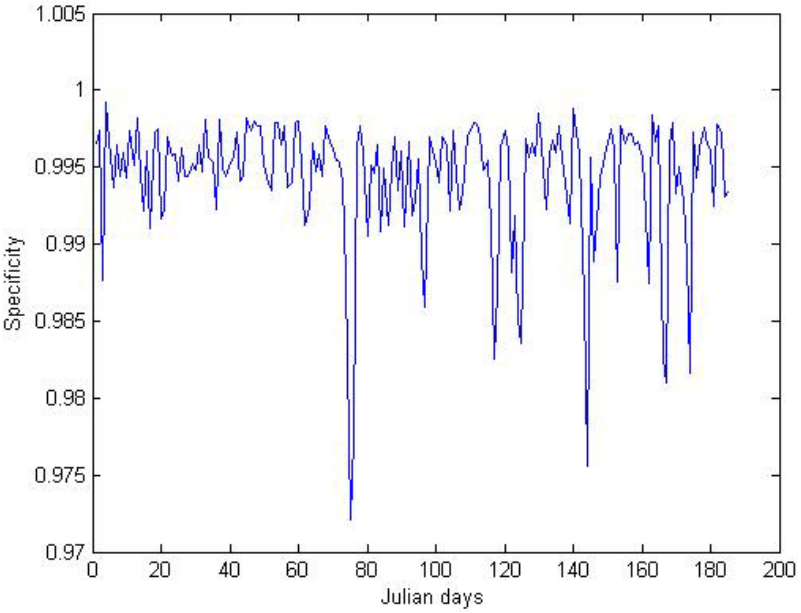

Fig. 9. Specificity values for PESTR

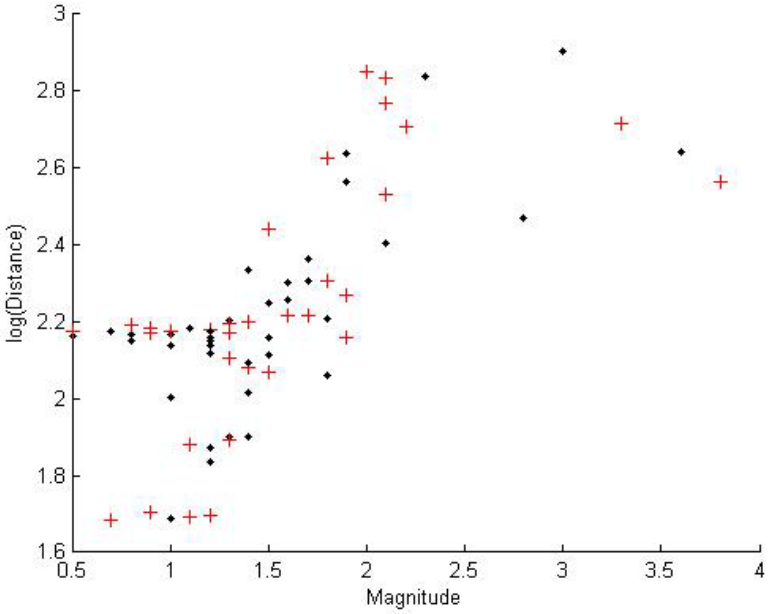

Fig. 10. Magnitude vs decimal logarithm of the distance, for events non-detected in PESTR

5 Conclusions

With the same data that produced 50% Sensitivity and Selectivity values in an existing detection system, based on the LTA/STA ratio, we were able to obtain, with a SVM classifier, almost perfect classification.

The SVM classifier, in continuous operation, achieved Recall and Sensitivity values of 97.7% and 98.7%, for 253 days of unseen data, from PVAQ, and 88.4 % and 99.4 %, for 185 days of PESTR. Taking into account that seismic events of magnitude as small as 0.1 were considered, and that the results for PESTR were obtained with a classifier trained with PVAQ data, these results can be seen as excellent.

In the future we aim to derive classifiers for all seismic stations in the South and South/Center of Portugal. This will enable an automatic detection system that can monitor, very accurately, the seismic activity in the South of Portugal. Another issue that will be looked at is the time taken to detect an event. The classifier was trained with 120 sec. segments, where, for the positive cases, the P phase was in the beginning of the segment. In continuous operation, we should expect the classifier to have the same behavior, i.e., a pick-up time of 120 sec should be expected. Analyzing the continuous operation, the average time is actually 84 sec. But, if only events with magnitude greater than 3.0 are considered, the delay time decreases to 16 sec. It can be expected that, by training the classifier with segments where the P phase is not necessarily in the beginning of the segment, the pick-up time can be significantly reduced.

References

1. Adeli, H., Panakkat, A.: A probabilistic neural network for earthquake magnitude prediction. Neural Networks 22, 1018–1024 (2009)
2. Suratgar, A., Setoudeh, F., Salemi, A.H., Negarestani, A.: Magnitude of Earthquake Prediction Using Neural Network. In: Fourth International Conference on Natural Computation, ICNC 2008, Los Alamitos, vol. 2, pp. 448–452 (2008)
3. Andreadis, I., Tsiftzis, I., Elenas, A.: Intelligent seismic acceleration signal processing for damage classification in buildings. IEEE Transactions on Instrumentation and Measurement 56, 1555–1564 (2007)
4. Furuta, H., Frangopol, D.M., Nakatsu, K.: Life-cycle cost of civil infrastructure with emphasis on balancing structural performance and seismic risk of road network. Structure and Infrastructure Engineering 7, 65–74 (2011)
5. Orlic, N., Loncaric, S.: Earthquake-explosion discrimination using genetic algorithm-based boosting approach. Computers & Geosciences 36, 179–185 (2010)
6. Scarpetta, S., et al.: Automatic classification of seismic signals at Mt. Vesuvius volcano, Italy, using neural networks. Bulletin of the Seismological Society of America 95, 185–196 (2005)
7. Gentili, S., Michelini, A.: Automatic picking of P and S phases using a neural tree. Journal of Seismology 10, 39–63 (2006)
8. Lancieri, M., Zollo, A.: A Bayesian approach to the real-time estimation of magnitude from the early P and S wave displacement peaks. Journal of Geophysical Research-Solid Earth 113, 17 (2008)

9. Tasic, I., Runovc, F.: Automatic S-phase arrival identification for local earthquakes. Acta Geotechnica Slovenica 6, 46–55 (2009)
10. Valet, L., Mauris, G., Bolon, P., Keskes, N.: A fuzzy linguistic-based software tool for seismic image interpretation. IEEE Transactions on Instrumentation and Measurement 52, 675–680 (2003)
11. Sharma, B.K., Kumar, A., Murthy, V.M.: Evaluation of seismic events detection algorithms. Journal of the Geological Society of India 75, 533–538 (2010)
12. Dai, H.C., MacBeth, C.: The application of back-propagation neural network to automatic picking seismic arrivals from single-component recordings. Journal of Geophysical Research-Solid Earth 102, 15105–15113 (1997)
13. Wang, J., Teng, T.L.: Artificial neural-network-based seismic detector. Bulletin of the Seismological Society of America 85, 308–319 (1995)
14. Madureira, G., Ruano, A.E.: A Neural Network Seismic Detector. In: 2nd IFAC International Conference on Intelligent Control Systems and Signal Processing (ICONS 2009), Istambul, Turkey (2009)
15. Frieß, T., Cristianini, N., Campbel, C.: The Kernel Adatron Algorithm: A Fast and Simple Learning Procedure for Support Vector Machines. In: 15th Intl. Conf. Machine Learning. Morgan Kaufmann Publishers (1998)

Exploiting the Functional Training Approach in Takagi-Sugeno Neuro-fuzzy Systems

Cristiano L. Cabrita[1], António E. Ruano[2,*], Pedro M. Ferreira[3], and László T. Kóczy[4]

[1] University of Algarve, Portugal
ccabrita@ualg.pt
[2] Centre for Intelligent Systems, IDMEC, IST and the University of Algarve, Portugal
aruano@ualg.pt
[3] Algarve STP – Algarve Science & Technology Park, Portugal
pfrazao@ualg.pt
[4] Faculty of Engineering Sciences, Széchenyi István University, Győr, Hungary
koczy@sze.hu

Abstract. When used for function approximation purposes, neural networks and neuro-fuzzy systems belong to a class of models whose parameters can be separated into linear and nonlinear, according to their influence in the model output. This concept of parameter separability can also be applied when the training problem is formulated as the minimization of the integral of the (functional) squared error, over the input domain. Using this approach, the computation of the derivatives involves terms that are dependent only on the model and the input domain, and terms which are the projection of the target function on the basis functions and on their derivatives with respect to the nonlinear parameters, over the input domain. These later terms can be numerically computed with the data.

The use of the functional approach is introduced here for Takagi-Sugeno models. An example shows that this approach obtains better results than the standard, discrete technique, as the performance surface employed is more similar to the one obtained with the function underlying the data. In some cases, as shown in the example, a complete analytical solution can be found.

Keywords: Takagi-Sugeno models, Functional training, Parameter separability.

1 Introduction

One of the crucial problems of fuzzy rule based modelling is how to find an optimal or at least a quasi-optimal rule base for a certain system. If there is a human expert who can tell the rules explicitly or if there is a linguistic description of the modelled

* The second author would like to acknowledge the support of FCT grant SFRH/BSAB/1229/2012.

V.E. Balas et al. (Eds.): Soft Computing Applications, AISC 195, pp. 543–559.
springerlink.com

system available then the fuzzy rule base can be easily constructed. However, in most applications, none is available. In this case some automatic method to determine the fuzzy rule base must be employed. Some of these methods were inspired by the evolutionary processes can be found in nature. Apart from the evolutionary methods, in the area of neural networks there are training algorithms known and these can be applied to fuzzy systems as well. These are useful when there are only numerical data about the problem.

Provided some assumptions are met in the rule base and in the membership functions, a fuzzy system, and in particular, a Takagi-Sugeno (TS) fuzzy system, can be seen as a system whose parameters can be separated, according to their influence on the output, as linear and nonlinear. This is shown in Section 2.

Having in mind that the ultimate goal of modelling is to obtain a "good" approximation of the function behind the data, and not to the data in itself, the modelling problem can be formulated as the minimization of the integral of the (functional) squared error, along the input domain, and not as the usual sum of the square of the errors. This new formulation, denoted as functional approach, is discussed in Section 3.

Section 4 applies this new formulation, employing the separability property, to TS systems. This is achieved using a simple example. In the functional approach, the training algorithms employ two types of terms. i) terms dependent only on the model and the input domain, and independent on the target function, and ii) other terms which are dependent on the model, the target function and the input domain. As the latter are integrals, which have to be approximated, in Section 5 we compare the performance of different numerical integration techniques. Conclusions and future work directions are drawn in Section 6.

2 TS Fuzzy Systems

It is assumed that the model consists of a rule base:

$$R = \{R^{(i)}\} \tag{1}$$

where, for the SISO case:

$$R^{(i)} ::= \text{if}\,(x \text{ is } X^{(i)}) \text{ then } \mathrm{y}^{(i)} = u_0^{(i)} + u_1^{(i)} x; \quad i = 1,\ldots,r \tag{2}$$

r being the number of rules.

Given a crisp input datum x, assuming that for implementing logic connectives such as the conjunction and implication, the *t-norm* used is the algebraic product, the output, y, of this model is:

$$y = \frac{\sum_{i=1}^{r} \mu_{X^{(i)}}(x) y^{(i)}}{\sum_{i=1}^{r} \mu_{X^{(i)}}(x)}, \tag{3}$$

where $\mu_{X^{(i)}}$ is the membership function for the input linguistic term $X^{(i)}$. Assuming that the membership functions form a Ruspini partition, the denominator of (3) is unitary. Therefore, (3) can be written as $y = \boldsymbol{\varphi}^T \mathbf{u}$, with

$$\boldsymbol{\varphi}^T = \begin{bmatrix} \mu_{X^{(1)}}(x) & \mu_{X^{(2)}}(x) & \dots & \mu_{X^{(r)}}(x) & \mu_{X^{(1)}}(x)x & \mu_{X^{(2)}}(x)x & \dots & \mu_{X^{(r)}}(x)x \end{bmatrix} \quad (4)$$

and

$$\mathbf{u}^T = \begin{bmatrix} u_0^{(1)} & u_0^{(2)} & \dots & u_0^{(r)} & u_1^{(1)} & u_1^{(2)} & \dots & u_1^{(r)} \end{bmatrix} \quad (5)$$

The generalisation for the multi-input, single output case is straightforward. Assuming k inputs, n_i linguistic terms for the i^{th} input, and denoting by

$$\mathbf{u}_{(i)} = \begin{bmatrix} u_i^{(1)} & u_i^{(2)} & \dots & u_i^{(r)} \end{bmatrix} \quad (6)$$

and by

$$\boldsymbol{\mu}(\mathbf{x}) = \begin{bmatrix} \mu_{X^{(1)}}(\mathbf{x}) & \mu_{X^{(1)}}(\mathbf{x}) & \dots & \mu_{X^{\left(\prod_{i=1}^{k} n_i\right)}}(\mathbf{x}) \end{bmatrix}, \quad (7)$$

eqs (4) and (5) can be transformed to:

$$\boldsymbol{\varphi}^T = \begin{bmatrix} \boldsymbol{\mu}(\mathbf{x}) & \boldsymbol{\mu}(\mathbf{x})\mathbf{I}\mathbf{x}_1 & \dots & \boldsymbol{\mu}(\mathbf{x})\mathbf{I}\mathbf{x}_k \end{bmatrix} \quad (8)$$

and

$$\mathbf{u}^T = \begin{bmatrix} \mathbf{u}_{(0)} & \mathbf{u}_{(1)} & \dots & \mathbf{u}_{(k)} \end{bmatrix} \quad (9)$$

In this work trapezoidal membership functions will be used. The j^{th} (out of p_i) interval on the i^{th} input is defined as:

$$I_{i,j} = \begin{cases} [\lambda_{i,j-1}\ \lambda_{i,j}[& j = 1, \dots, p_i - 1 \\ [\lambda_{i,j-1}\ \lambda_{i,j}] & j = p_i \end{cases} \quad (10)$$

The j^{th} membership in the i^{th} dimension is defined as:

$$\mu_{i,j}(x_i) = \begin{cases} 1, & x_i \in I_{i,2j-1} \\ \dfrac{x_i - \lambda_{i,2j-3}}{\lambda_{i,2j-2} - \lambda_{i,2j-3}}, & x_i \in I_{i,2j-2} \\ \dfrac{\lambda_{i,2j} - x_i}{\lambda_{i,2j} - \lambda_{i,2j-1}}, & x_i \in I_{i,2j} \\ 0, & otherwise \end{cases} \quad (11)$$

As it can be seen, from the previous equations, the *u* parameters appear linearly in the output, and the λ parameters nonlinearly.

In this work, the model parameters are estimated with data, a process known in the neural network jargon as training. Considering m patterns, $\mathbf{y}$ is the output of the model, a vector with m elements, and $\mathbf{X}$ is the input matrix, with dimensions *m*n* (*n* is the number of inputs). It is assumed that the model has n_u linear parameters and n_v nonlinear parameters[1]. $\mathbf{\Gamma}$ is the matrix of the basis functions (dimensions $m * n_u$), so that the output can be seen as:

$$\mathbf{y}(\mathbf{X},\mathbf{v},\mathbf{u}) = \mathbf{\Gamma}(\mathbf{X},\mathbf{v})\mathbf{u} \tag{12}$$

The training criterion normally employed is

$$\Omega_d(\mathbf{X},\mathbf{v},\mathbf{u},\mathbf{t}) = \frac{\left\|\mathbf{t}-\mathbf{\Gamma}(\mathbf{X},\mathbf{v})\mathbf{u}\right\|_2^2}{2} = \frac{\left\|\mathbf{e}(\mathbf{X},\mathbf{v},\mathbf{u},\mathbf{t})\right\|_2^2}{2}, \tag{13}$$

where $\mathbf{t}$ is the target vector, $\mathbf{e}$ is the error vector and $\|\ \|_2$ is the Euclidean norm. As the model parameters can be decomposed into linear and nonlinear ones, we can determine the optimal value of the linear parameters with respect to (wrt) the nonlinear ones:

$$\hat{\mathbf{u}}_d(\mathbf{X},\mathbf{v},\mathbf{t}) = \left(\mathbf{\Gamma}^T\mathbf{\Gamma}\right)^{-1}\mathbf{\Gamma}^T\mathbf{t} = \mathbf{\Gamma}^+\mathbf{t} \tag{14}$$

where the symbol '+' denotes a pseudo-inverse. We can incorporate this value in the usual criterion and introduce a new criterion (independent on the linear parameters):

$$\Psi_d(\mathbf{X},\mathbf{v},\mathbf{t}) = \frac{\left\|\mathbf{t}-\mathbf{\Gamma}\hat{\mathbf{u}}_d\right\|_2^2}{2} = \frac{\left\|\mathbf{t}-\mathbf{\Gamma}\mathbf{\Gamma}^+\mathbf{t}\right\|_2^2}{2} = \frac{\left\|\mathbf{P}_{\Gamma_\perp}\mathbf{t}\right\|_2^2}{2} \tag{15}$$

Where $\mathbf{P}_{\Gamma(\mathbf{x},\mathbf{v})_\perp} = \mathbf{I}-\mathbf{\Gamma}\mathbf{\Gamma}^+$ is the projector on the orthogonal complement of the space spanned by the basis functions.

The concept of separability of parameters in general nonlinear least-squares problems has been introduced in [1]. A good review on the applications of this concept can be found in [2]. In the context of neural networks, it has been introduced in [3], for Multilayer Perceptrons, in [4] for Radial Basis Functions and in [5] for B-splines and neuro-fuzzy systems.

3 The Functional Approach

Let us assume that the function to approximate was known, and let it be denoted by $t(x)$. In this case, (12) and (13) can be replaced by:

[1] From now on, we shall denote, for compatibility with previous works, the nonlinear parameters as v.

$$\mathrm{y}(\mathrm{x},\mathbf{v},\mathbf{u})=\boldsymbol{\varphi}^{\mathrm{T}}(\mathrm{x},\mathbf{v})\mathbf{u} \tag{16}$$

and

$$\Omega_f(\mathrm{x}_{\min},\mathrm{x}_{MAX},t,\mathbf{u},\mathbf{v})=\frac{\int_{\mathrm{x}_{\min}}^{\mathrm{x}_{MAX}}\left(t(\mathrm{x})-\boldsymbol{\varphi}^T(\mathrm{x},\mathbf{v})\mathbf{u}\right)^2 d\mathrm{x}}{2}=$$
$$\frac{\int_{x_{\min}}^{\mathrm{x}_{MAX}}\left(t-\mathbf{u}^T\boldsymbol{\varphi}\right)^2 dx}{2}=\frac{\int_{\mathrm{x}_{\min}}^{\mathrm{x}_{MAX}}e^2(\mathrm{x},t,\mathbf{v},\mathbf{u})d\mathrm{x}}{2} \tag{17}$$

Notice that in (16) x is now a multi-dimensional real variable:

$$\mathrm{x}=x_1,\ldots,x_{i,}\ldots,x_n \tag{18}$$

and that in (17)

$$\int_{\mathrm{x}_{\min}}^{\mathrm{x}_{MAX}} f(\mathrm{x},.)d\mathrm{x}=\int_{x_{1\min}}^{x_{1MAX}}\cdots\int_{x_{k\min}}^{x_{kMAX}}\cdots\int_{x_{n\min}}^{x_{nMAX}} f(x_1,\ldots,x_k,\ldots,x_n,.)dx_1\ldots dx_k,\ldots,dx_n \tag{19}$$

t and e are also real functions. $\boldsymbol{\varphi}$ is a vector of basis functions, and not a matrix as in the discrete case. The Jacobian is given as:

$$\mathbf{j}(\mathrm{x},\mathbf{v},\mathbf{u})=\frac{\partial\mathbf{y}(\mathrm{x},\mathbf{v},\mathbf{u})}{\partial\left[\mathbf{u}^T \mid \mathbf{v}^T\right]}=\left[\mathbf{j}_{\mathbf{u}}(\mathrm{x},\mathbf{v}) \mid \mathbf{j}_{\mathbf{v}}(\mathrm{x},\mathbf{v},\mathbf{u})\right]=$$
$$=\left[\boldsymbol{\varphi}^T(\mathrm{x},\mathbf{v}) \mid \left[\frac{\partial\boldsymbol{\varphi}(\mathrm{x},\mathbf{v})}{\partial\mathbf{v}^T}\right]^T\mathbf{u}\right] \tag{20}$$

and the gradient as:

$$\mathbf{g}_{\Omega_{f_{\mathbf{u}}}}(\mathrm{x}_{\min},\mathrm{x}_{MAX},t,\mathbf{v})=\frac{\partial\Omega_f}{\partial\mathbf{u}^T}=-\int_{x_{\min}}^{x_{MAX}}\mathbf{j}_{\mathbf{u}}^T e d\mathrm{x}$$
$$\mathbf{g}_{\Omega_{f_{\mathbf{v}}}}(t,\mathbf{v},\mathrm{x}_{\min},\mathrm{x}_{MAX})=\frac{\partial\Omega_f}{\partial\mathbf{v}^T}=-\int_{\mathrm{x}_{\min}}^{\mathrm{x}_{MAX}}\mathbf{j}_{\mathbf{v}}^T e d\mathrm{x} \tag{21}$$

Equating the first eq.of (21) to $\mathbf{0}$, we have:

$$-\int_{\mathrm{x}_{\min}}^{\mathrm{x}_{MAX}}\boldsymbol{\varphi}\left(t-\boldsymbol{\varphi}^T\mathbf{u}_f\right)d\mathrm{x}=0\Leftrightarrow\left[\int_{\mathrm{x}_{\min}}^{\mathrm{x}_{MAX}}\boldsymbol{\varphi}\boldsymbol{\varphi}^T d\mathrm{x}\right]\hat{\mathbf{u}}_f=\int_{\mathrm{x}_{\min}}^{\mathrm{x}_{MAX}}\boldsymbol{\varphi}t d\mathrm{x}\Leftrightarrow$$
$$\Leftrightarrow\hat{\mathbf{u}}_f(t,\mathbf{v},\mathrm{x}_{\min},\mathrm{x}_{MAX})=\left[\int_{\mathrm{x}_{\min}}^{\mathrm{x}_{MAX}}\boldsymbol{\varphi}\boldsymbol{\varphi}^T d\mathrm{x}\right]^{-1}\int_{\mathrm{x}_{\min}}^{\mathrm{x}_{MAX}}\boldsymbol{\varphi}t d\mathrm{x} \tag{22}$$

As in the discrete case, we can incorporate this value in criterion (17), and have a new criterion, independent of the linear parameters:

$$\Psi_f\left(\mathrm{x},\mathbf{v},\mathrm{x}_{\min},\mathrm{x}_{MAX}\right)=\frac{\int_{\mathrm{x}_{\min}}^{\mathrm{x}_{MAX}}\left(t-\boldsymbol{\varphi}^T\left[\int_{\mathrm{x}_{\min}}^{\mathrm{x}_{MAX}}\boldsymbol{\varphi}\boldsymbol{\varphi}^T d\mathrm{x}\right]^{-1}\int_{\mathrm{x}_{\min}}^{\mathrm{x}_{MAX}}\boldsymbol{\varphi}t d\mathrm{x}\right)^2 d\mathrm{x}}{2} \tag{23}$$

3.1 Training Algorithms

If we want to apply the Back-Propagation (BP) algorithm [6] to train the model:

$$\begin{aligned}\mathbf{v}[k+1]&=\mathbf{v}[k]+\mathbf{s}[k]\\ \mathbf{s}[k]&=-\eta\mathbf{g}_{\Psi_f}[k]\end{aligned}, \tag{24}$$

We need to compute the gradient of criterion (23). It can be proved (please see [7] for details) that it can be obtained as:

$$\mathbf{g}_{\Psi_f}=-\int_{\mathrm{x}_{\min}}^{\mathrm{x}_{MAX}} t\frac{\partial\boldsymbol{\varphi}^T}{\partial\mathbf{v}^T}d\mathrm{x}\hat{\mathbf{u}}_f+\hat{\mathbf{u}}_f^T\frac{\partial\int_{\mathrm{x}_{\min}}^{\mathrm{x}_{MAX}}\boldsymbol{\varphi}\boldsymbol{\varphi}^T d\mathrm{x}}{2\partial\mathbf{v}^T}\hat{\mathbf{u}}_f \tag{25}$$

Therefore, to use this methodology, we need to have available:

$$\left[\int_{\mathrm{x}_{\min}}^{\mathrm{x}_{MAX}}\boldsymbol{\varphi}\boldsymbol{\varphi}^T d\mathrm{x}\right]^{-1} \tag{26}$$

$$\left[\int_{\mathrm{x}_{\min}}^{\mathrm{x}_{MAX}}\boldsymbol{\varphi}\boldsymbol{\varphi}^T d\mathrm{x}\right]^{-1}\frac{\partial\int_{\mathrm{x}_{\min}}^{\mathrm{x}_{MAX}}\boldsymbol{\varphi}\boldsymbol{\varphi}^T d\mathrm{x}}{2\partial\mathbf{v}^T}\left[\int_{\mathrm{x}_{\min}}^{\mathrm{x}_{MAX}}\boldsymbol{\varphi}\boldsymbol{\varphi}^T d\mathrm{x}\right]^{-1} \tag{27}$$

which are independent on the function to approximate, and can be obtained analytically for the model at hand.

The only terms involving the function to approximate are:

$$\int_{\mathrm{x}_{\min}}^{\mathrm{x}_{MAX}}\boldsymbol{\varphi}t d\mathrm{x} \tag{28}$$

$$\int_{\mathrm{x}_{\min}}^{\mathrm{x}_{MAX}} t\frac{\partial\boldsymbol{\varphi}^T}{\partial\mathbf{v}^T}d\mathrm{x} \tag{29}$$

In a practical application the underlying function is not known (otherwise it should be used). The integrals (28) and (29) can be numerically approximated using the training data.

4 An Example

We are going to use a very simple example to illustrate how the functional approach can be applied to TS systems. Our aim will be to approximate the function $t(x)=\frac{Sin(10x)}{x}$, over the domain $x\in[-1,1]$ with a TS system, with only 2 rules.

For this domain, $\int_{x_{\min}}^{x_{MAX}} \boldsymbol{\varphi}\boldsymbol{\varphi}^T dx$ can be given as:

$$\begin{bmatrix} \frac{3+2\lambda_1+\lambda_2}{3} & \frac{\lambda_2-\lambda_1}{6} & \frac{-6+3\lambda_1^2+2\lambda_1\lambda_2+\lambda_2^2}{12} & \frac{\lambda_2^2-\lambda_1^2}{12} \\ & \frac{3-\lambda_1-2\lambda_2}{3} & \frac{\lambda_2^2-\lambda_1^2}{12} & \frac{6-\lambda_1^2-2\lambda_1\lambda_2-3\lambda_2^2}{12} \\ & & \frac{10+4\lambda_1^3+3\lambda_1^2\lambda_2+2\lambda_1\lambda_2^2+\lambda_2^3}{30} & \frac{-3\lambda_1^3-\lambda_1^2\lambda_2+\lambda_1\lambda_2^2+3\lambda_2^3}{60} \\ & & & \frac{10-\lambda_1^3-2\lambda_1^2\lambda_2-3\lambda_1\lambda_2^2-4\lambda_2^3}{30} \end{bmatrix} \tag{30}$$

Notice that, as the matrix is symmetric, only the upper-diagonal elements are shown. Notice also that, due to lack of space, we could not shown (26), the inverse of (30).

For the same reason, we can not show (27). Instead, we will illustrate $\frac{\partial \int_{x_{\min}}^{x_{MAX}} \boldsymbol{\varphi}\boldsymbol{\varphi}^T dx}{\partial \mathbf{v}^T}$.

$$\frac{\partial \int_{x_{\min}}^{x_{MAX}} \boldsymbol{\varphi}\boldsymbol{\varphi}^T dx}{\partial \lambda_1} = \begin{bmatrix} \frac{2}{3} & -\frac{1}{6} & \frac{3\lambda_1+\lambda_2}{6} & -\frac{\lambda_1}{6} \\ & -\frac{1}{3} & -\frac{\lambda_1}{6} & -\frac{\lambda_1+\lambda_2}{6} \\ & & \frac{6\lambda_1^2-3\lambda_1\lambda_2+\lambda_2^2}{15} & \frac{-9\lambda_1^2-2\lambda_1\lambda_2+\lambda_2^2}{60} \\ & & & \frac{-3\lambda_1^2-4\lambda_1\lambda_2-3\lambda_2^2}{30} \end{bmatrix} \tag{31}$$

$$\frac{\partial \int_{x_{\min}}^{x_{MAX}} \boldsymbol{\varphi}\boldsymbol{\varphi}^T dx}{\partial \lambda_2} = \begin{bmatrix} \frac{1}{3} & \frac{1}{6} & \frac{\lambda_1+\lambda_2}{6} & \frac{\lambda_2}{6} \\ & -\frac{2}{3} & \frac{\lambda_2}{6} & -\frac{\lambda_1+3\lambda_2}{6} \\ & & \frac{3\lambda_1^2+4\lambda_1\lambda_2+3\lambda_2^2}{30} & \frac{-\lambda_1^2+2\lambda_1\lambda_2+9\lambda_2^2}{60} \\ & & & \frac{-\lambda_1^2-3\lambda_1\lambda_2-6\lambda_2^2}{15} \end{bmatrix} \tag{32}$$

We can train the TS model analytically. Equation (24) will be used, with $\eta=0.02$, for 5 different starting points. The training will be stopped whether when a maximum number of 200 iterations is reached, or when the following criteria are simultaneously satisfied:

$$\begin{aligned} &\Psi[k-1]-\Psi[k]<\beta[k] \\ &\left\|\mathbf{v}[k-1]-\mathbf{v}[k]\right\|_2<\sqrt{\tau}\left(1+\left\|\mathbf{v}[k]\right\|_2\right), \\ &\left\|\mathbf{g}[k]\right\|_2\le\sqrt[3]{\tau}\left(1+\left|\Psi[k]\right|\right) \end{aligned} \tag{33}$$

where

$$\beta[k]=\tau\left(1+\left|\Psi[k]\right|\right) \tag{34}$$

and τ is a measure of the desired number of correct digits in the objective function. This is a criterion typically used in unconstrained optimization [8]. In all examples, $\tau=10^{-6}$ is used.

As an order relation must be preserved for the nonlinear parameters (i.e. $\lambda_2>\lambda_1$), the standard BP algorithm needs to be modified. In order to maintain the same search direction, the update vector ($s[k]=-\eta\mathbf{g}[k]$), when a violation is detected ($\boldsymbol{\lambda}_{i+1}[k]<\boldsymbol{\lambda}_i[k]$), is reduced of a factor g so that the position of the $(i+1)^{\text{th}}$ knot is located half-way between the previous distance of the two corresponding knots:

$$g=\frac{\boldsymbol{\lambda}_{i+1}[k-1]-\boldsymbol{\lambda}_i[k-1]}{2\left(\mathbf{s}_{i+1}[k]-\mathbf{s}_i[k]\right)} \tag{35}$$

Therefore, when there is a violation of the order relation, the learning rate for the BP algorithm is updated at that iteration.

Figure 1 shows the analytical performance surface, together with the results of five different trainings.

As it can be seen, even with a very simple example, several local minima exist. The surface is symmetric, and there are two global minima, located at [-0.357,-0.116] and [0.116, 0.357], with a value of 4.4.for criterion (23).

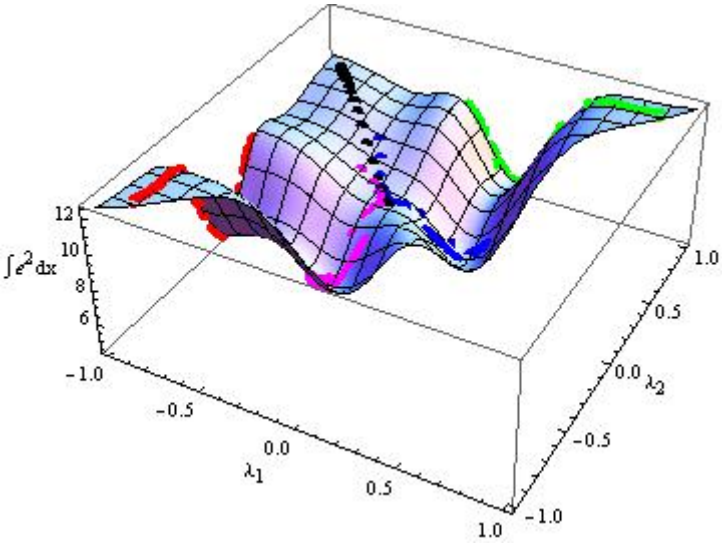

Fig. 1. Analytical performance surface

The flowing table illustrates the different trainings.

Table 1. Analytical trainings

$\mathbf{v}_a[1]$	[-0.90,-0.85]	[-0.90,0.90]	[0.85,0.90]	[-0.5,0.6]	[-0.5,0.4]
n	55	26	55	200	200
$\Psi_a[n]$	5.22	7.01	5.22	4.82	6.15
$\mathbf{V}_a[n]$	[-1.0,-0.087]	[-0.28,0.28]	[0.088,1.0]	[0.182,0.395]	[-0.28,0.06]

The first line shows the starting points, and *n* is the number of iterations taken by the training. Notice that no training attains the global minima. This is due to the setting of the maximum number of iterations (200). The two last evolutions would attain the global minima with a few more iterations.

If the function is not known, but only data is available, a same methodology can be employed, this time approximating the integrals (28) and (29). In a first case, we shall use a Gaussian quadrature algorithm. In this technique, the integral is approximated as:

$$\int_{x_{\min}}^{x_{\max}} f(x)dx \approx \sum_{i=1}^{m} f(x_i) w_i \tag{36}$$

Notice that the abscissas x_i are chosen by the method. The following figure and table illustrate the results obtained with m=25.

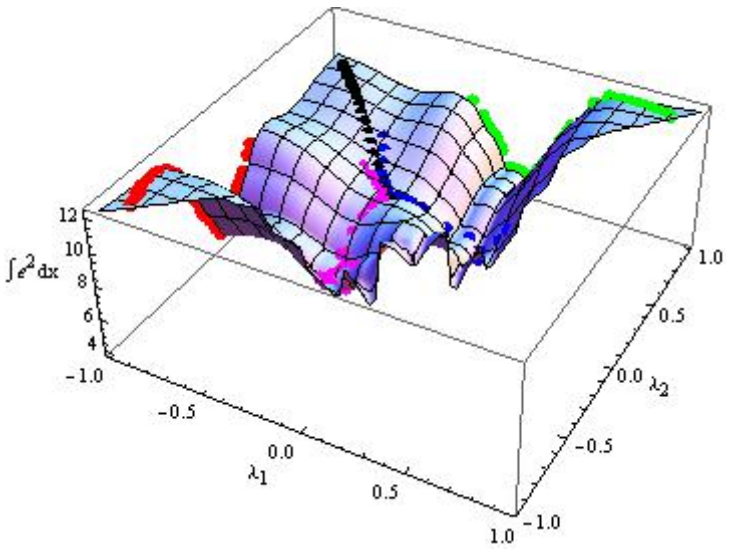

Fig. 2. Gaussian quadrature performance surface

The performance surface is very similar with the analytical one. The different evolutions go to the same minima, as it can be also seen in Table 2.

Table 2. Gaussian quadrature trainings

$v_G[1]$	[-0.90,-0.85]	[-0.90,0.90]	[0.85,0.90]	[-0.5,0.6]	[-0.5,0.4]
n	102	39	55	29	32
$\Psi_G[n]$	5.02	7.01	4.99	4.27	4.15
$v_G[n]$	[-1.0,-0.118]	[-0.29,0.29]	[0.121,1.0]	[0.12,0.41]	[-0.31,-0.16]
$\Psi_a\|_{v_a[n]}$	5.34	7.01	5.36	4.49	4.49

The last line in the table shows the value of the analytical criterion, evaluated for the last parameters values obtained by the training performed with the data, using Gaussian quadrature. As it can be seen, comparing with Table 1, similar values were obtained.

4.1 Different Integration Techniques

As pointed above, although the last training was performed with data, the training inputs were obtained with Gaussian quadrature. In practice, we do not usually have control over the training data. For this reason, we conducted afterwards a series of trainings, where the input data was randomly generated. Different integration techniques were also compared. In all experiments, 25 input patterns were used, In order to compare the different methods, we fixed the extrema to -1 and +1. Therefore, only 23 of the 25 values were randomly generated.

Besides comparing the different integration techniques, we also compared the functional approach with the standard, discrete training, minimizing (15). The following figure and table show the results obtained.

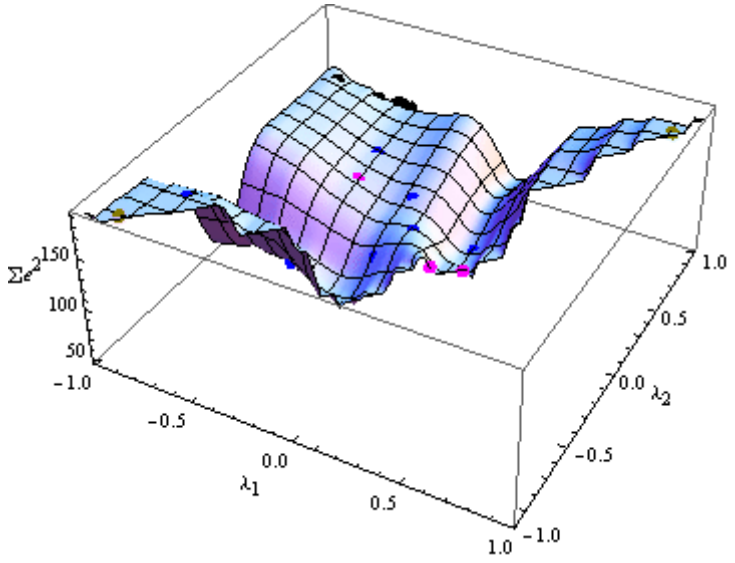

Fig. 3. Discrete performance surface

Table 3. Discrete trainings

$v_d[1]$	[-0.90,-0.85]	[-0.90,0.90]	[0.85,0.90]	[-0.5,0.6]	[-0.5,0.4]
n	2	200	2	3	4
$\Psi_d[n]$	181.31	112-81	172.82	63.43	72.54
$v_d[n]$	[-0.90,-0.85]	[-0.58,1]	[0.85,0.90]	[0.12,0.39]	[0.17,0.18]
$\Psi_a\big\vert_{v_G[n]}$	12.21	9.00	12.21	4.65	5.35

Comparing these results with the analytical results, and the Gaussian quadrature ones, we can conclude that for 3 of the 5 initial points, very different (worse) results were obtained.

Subsequently, with the same random data, the functional methodology was experimented, with different integration techniques.

The first one used was the forward integration. The integral is approximated as:

$$\int_{x_{\min}}^{x_{\max}} f(x)dx \approx \sum_{i=1}^{m-1} f(x_i)(x_{i+1} - x_i) \tag{37}$$

The results obtained are shown in the fig. and table below.

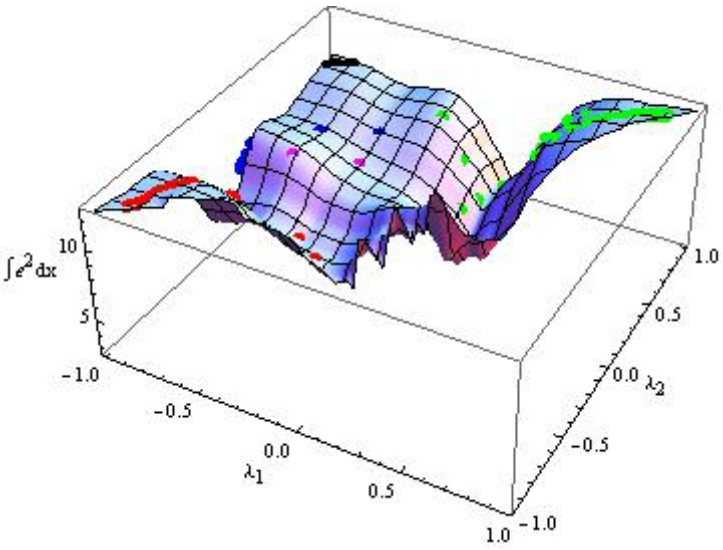

Fig. 4. Forward integration

Table 4. Forward integration trainings

$v_f[1]$	[-0.90,-0.85]	[-0.90,0.90]	[0.85,0.90]	[-0.5,0.6]	[-0.5,0.4]
n	15	7	42	46	3
$\Psi_f[n]$	4.82	9.54	4.69	7.02	5.21
v_f [n]	[-0.43,-0.14]	[-0.85,0.95]	[0.08,0.81]	[-0.99,0.12]	[-0.87,-0.04]
$\Psi_a\big\vert_{v_f[n]}$	4.70	9.75	5.71	7.85	5.67

The results obtained are better than the discrete training for 2 out of the 5 initial points. The 2nd and the 5th trainings are similar and only in the 4th evolution the discrete version is clearly better.

The next integration method tested was the backward approximation:

$$\int_{x_{\min}}^{x_{\max}} f(x)dx \approx \sum_{i=1}^{m-1} f(x_{i+1})(x_{i+1} - x_i) \tag{38}$$

The results obtained are summarized in Fig. 5 and Table 5.

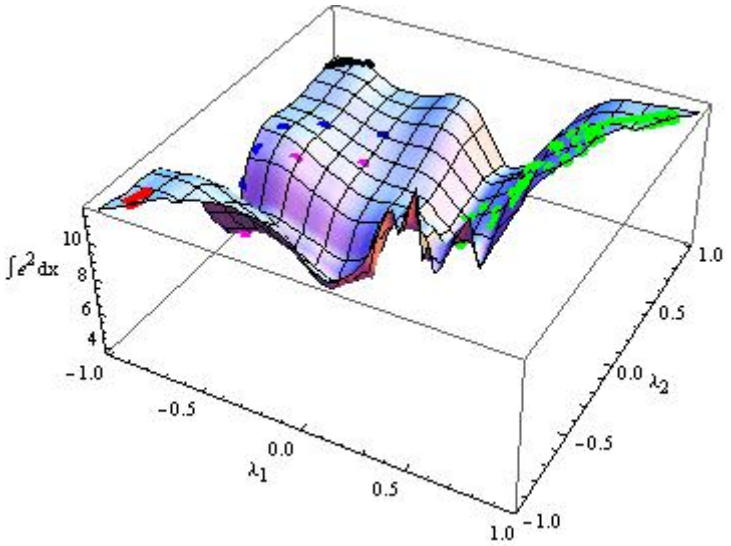

Fig. 5. Backward integration

Table 5. Backward integration trainings

$v_b[1]$	[-0.90,-0.85]	[-0.90,0.90]	[0.85,0.90]	[-0.5,0.6]	[-0.5,0.4]
n	7	9	59	7	3
$\Psi_b[n]$	11.60	9.16	5.14	4.70	5.09
v_b [n]	[-0.88,-0.75]	[-0.80,0.98]	[0.08,0.32]	[-0.99,-0.05]	[-0.87,-0.09]
$\Psi_a\big\vert_{v_b[n]}$	12.16	9.64	4.58	5.32	5.51

Subsquently, a trapezoidal technique was experimented. In the trapezoidal, or Tustin method, the approximation employed is:

$$\int_{x_{\min}}^{x_{\max}} f(x)dx \approx \frac{1}{2}\sum_{i=1}^{m-1}\left(f(x_{i+1})+f(x_i)\right)(x_{i+1}-x_i) \tag{39}$$

The results obtained are summarized below.

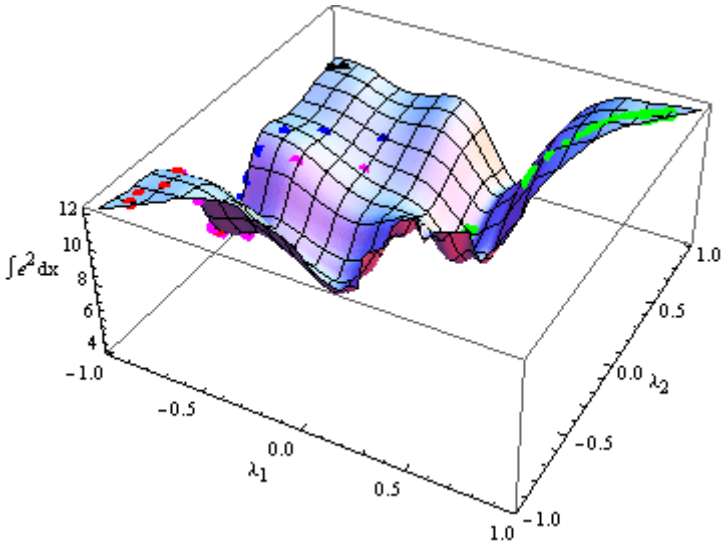

Fig. 6. Trapezoidal integration

Table 6. Trapzoidal integration trainings

$v_t[1]$	[-0.90,-0.85]	[-0.90,0.90]	[0.85,0.90]	[-0.5,0.6]	[-0.5,0.4]
n	6	2	24	22	12
$\Psi_t[n]$	5.59	9.43	4.74	5.11	5.80
$v_t[n]$	[-0.98,-0.16]	[-0.95,0.86]	[0.03,0.49]	[-0.99,-0.02]	[-0.99,0.18]
$\Psi_{a\|_{v_t[n]}}$	5.81	9.77	5.08	5.60	6.06

The results are more consistent across the different initial points. The last training technique experimented was a polynomial interpolation algorithm, available in Mathematica©. The order 3 was experimented.

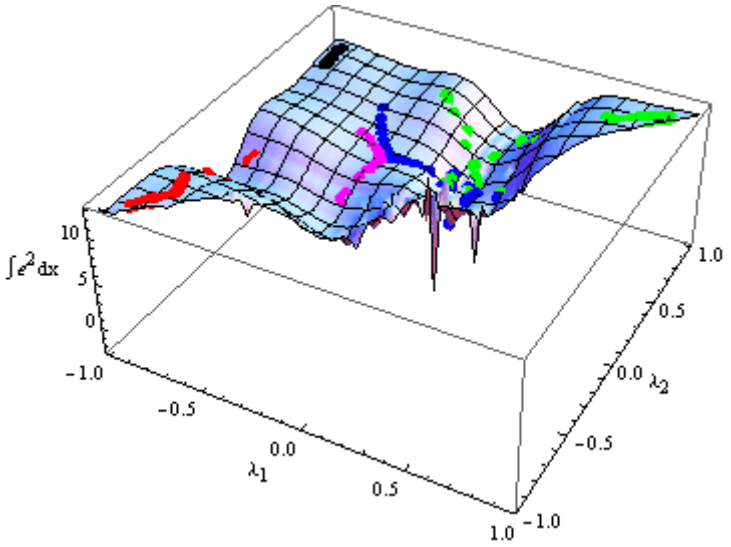

Fig. 7. 3rd order polynomial integration

Table 7. 3rd order polynomial integration trainings

$v_p[1]$	[-0.90,-0.85]	[-0.90,0.90]	[0.85,0.90]	[-0.5,0.6]	[-0.5,0.4]
n	35	12	45	35	15
$\Psi_p[n]$	6.46	9.77	4.31	3.88	5.66
$v_p[n]$	[-0.91,0.03]	[-0.91,0.74]	[0.071,0.36]	[0.08,0.19]	[-0.39,0.03]
$\Psi_{a\|_{v_p[n]}}$	6.34	9.51	4.65	5.59	5.32

Finally, Table 8 compares the different methods tested, together with the analytical and the discrete methods.

On bold we highlight the best results obtained with the random data. The discrete technique obtains the best values, for 3 out of the 5 starting points. In the other 2 points very bad results were obtained, compared with the other functional approaches

In a final test, 20 experiments were performed for each method, for each one of the 5 starting points. The results are presented in terms of mean (μ) and standard deviation (σ). Table 9 presents these statistics for the optimal values of the criteria optimized, and Table 10 shows the same statistics, but translated to the analytical criterion, evaluated at the final points for each different optimization.

Table 8. Comparison of different methods

	[-0.90,-0.85]	[-0.90,0.90]	[0.85,0.90]	[-0.5,0.6]	[-0.5,0.4]
$\Psi_a[n]$	5.22	7.01	5.22	4.82	6.15
$\Psi_a\big\vert_{v_G[n]}$	5.34	7.01	5.36	4.49	4.49
$\Psi_a\big\vert_{v_d[n]}$	12.21	**9.00**	12.21	**4.65**	**5.35**
$\Psi_a\big\vert_{v_f[n]}$	**4.70**	9.75	5.71	7.85	5.67
$\Psi_a\big\vert_{v_b[n]}$	12.16	9.64	**4.58**	5.32	5.51
$\Psi_a\big\vert_{v_t[n]}$	5.81	9.77	5.08	5.60	6.06
$\Psi_a\big\vert_{v_f[n]}$	6.34	9.51	4.65	5.59	5.32

Table 9. Mean and standard deviation of the criteria optimized

	[-0.90,-0.85]	[-0.90,0.90]	[0.85,0.90]	[-0.5,0.6]	[-0.5,0.4]
$\mu_d \pm \sigma_d$	119±56	71±28	136±37	56±13	54±14
$\mu_f \pm \sigma_f$	5.6±2.6	9.5±1.5	7.8±4.3	5.2±2.1	4.2±1.9
$\mu_b \pm \sigma_b$	9.7±3.0	7.7±3.7	3.5±2.4	4.1±3.1	4.0±2.5
$\mu_t \pm \sigma_t$	10.9±3.2	9.0±1.5	4.4±1.1	5.0±1.1	4.9±1.5
$\mu_p \pm \sigma_p$	10.2±3.5	7.5±2.7	9.1±3.3	3.1±2.3	3.2±2.5

Table 10. Mean and standard deviation of the analytical criteria, for the optima found for each criterion

	[-0.90,-0.85]	[-0.90,0.90]	[0.85,0.90]	[-0.5,0.6]	[-0.5,0.4]
$\mu_a \pm \sigma_a\big\vert_{v_d[n]}$	11.8±1.7	**7.5±2.2**	12.2±0.03	5.7±1.3	5.5±0.84
$\mu_a \pm \sigma_a\big\vert_{v_f[n]}$	**6.0±2.1**	9.3±1.0	8.3±3.3	6.0±1.2	5.4±0.2
$\mu_a \pm \sigma_a\big\vert_{v_b[n]}$	11.6±1.2	9.7±0.1	5.4±0.5	5.9±1.1	5.8±0.6
$\mu_a \pm \sigma_a\big\vert_{v_t[n]}$	11.5±2.1	9.7±0.1	**4.9±0.4**	5.8±0.9	5.4±0.2
$\mu_a \pm \sigma_a\big\vert_{v_p[n]}$	9.4±3.5	7.7±2.4	8.8±3.5	**5.3±1.0**	**5.2±1.6**

The discrete criterion obtains the better results only for 1 out of the 5 initial points, and even for this case, with results very similar to the polynomial version of the functional approach. Comparing the different integration schemes, we can conclude that, for this particular example, the polynomial integration technique is the best method, as it obtains 2 best results overall, and 3 out of 5, comparing only the functional approaches.

5 Conclusions

In this paper we have shown how to apply the functional methodology for TS fuzzy models, with trapezoidal membership functions, that form a Ruspini partition of the input space.

The functional approach offers important advantages over the standard, discrete approach. We have not mentioned that it achieves important savings in computational time, if the training data is large (for results please see [9]). We have shown, previously and in this paper that, in most of the cases, it obtains a better approximation over the whole input domain than the discrete training algorithms. This is due to the fact that the functional performance surface is closer to the analytical performance surface than the discrete one. Another important point of this methodology is that it allows determining the local minima and the performance of a specified model, if the function generating the data is known.

As the performance of the functional approach is strongly related with the numerical integral approximation used, we have compared different alternatives and concluded that, for the example considered, a polynomial interpolation algorithm of order 3 should be chosen. The results, however, are not conclusive and further work on this topic should be done, and extended for the multi-dimensional case.

References

1. Golub, G.H., Pereyra, V.: Differentiation of pseudo-inverses and nonlinear least-squares problems whose varables separate. Siam Journal on Numerical Analysis 10(2), 413–432 (1973)
2. Golub, G., Pereyra, V.: Separable nonlinear least squares: the variable projection method and its applications. Inverse Problems 19(2), R1–R26 (2003)
3. Ruano, A.E.B., Jones, D.I., Fleming, P.J.: A New Formulation of the Learning Problem for a Neural Network Controller. In: 30th IEEE Conference on Decision and Control, Brighton, UK, December 11-13, pp. 865–866 (1991)
4. Ferreira, P.M., Ruano, A.E.: Exploiting the separability of linear and nonlinear parameters in radial basis function networks. In: Adaptive Systems for Signal Processing, Communications, and Control Symposium (AS-SPCC), Lake Louise, Canada, pp. 321–326 (October 2000)
5. Ruano, A.E., Cabrita, C., Oliveira, J.V., Koczy, L.T.: Supervised training algorithms for B-Spline neural networks and neuro-fuzzy systems. Int. J. Syst. Sci. 33(8), 689–711 (2002), doi:10.1080/00207720210155062

6. Werbos, P.: Beyond Regression: New Tools for Prediction and Analysis in the Behavioral Sciences. PhD, Harvard University (1974)
7. Ruano, A.E., Cabrita, C.L., Ferreira, P.M.: Towards a More Analytical Training of Neural Networks and Neuro-Fuzzy Systems. In: IEEE 7th International Symposium on Intelligent Signal Processing (WISP 2011), Floriana, Malta, September 19-21 (2011)
8. Gill, P.E., Murray, W., Wright, M.H.: Practical Optimization. Academic Press, Inc. (1981)
9. Cabrita, C.L., Ruano, A.E., Ferreira, P.M., Koczy, L.T.: Extending the functional training approach for B-Splines. In: 2012 IEEE International Joint Conference on Neural Networks (IJCNN), Brisbane, Australia, June 10-15, pp. 2702–2709. IEEE (2012)

Reconstruction of Binary Images Represented on Equilateral Triangular Grid Using Evolutionary Algorithms

Elisa Valentina Moisi[1], Vladimir Ioan Cretu[2], and Benedek Nagy[3]

[1] Department of Computer Science and Information Technology,
Faculty of Electrical Engineering and Information Technology, University of Oradea,
1, University Street, 410087, Oradea, Romania
emoisi@uoradea.ro
[2] Department of Computer and Software Engineering, "Politehnica" University of Timisoara,
2, V. Parvan Blvd., 300223, Timisoara, Romania
vladimir.cretu@cs.upt.ro
[3] Department of Computer Science, Faculty of Informatics, University of Debrecen,
26, Kassai Street, H-4028, Debrecen, Hungary,
nbenedek@inf.unideb.hu

Abstract. In this paper we study the problem of reconstructing a binary hexagonal image represented on an equilateral triangular grid from its projections. We propose an evolutionary algorithm for reconstructing this images from its projections in three directions. We will consider three projections as the points in the grid are triangles and by the symmetry of the grid there are three natural directions. Genetic operators, e.g., crossover and mutation operators are defined, as well as an operator based on the switch operator from discrete tomography. We use a compactness operator to eliminate the isolated points of an image and improve the quality of the image. The initial population and the children images are generated using the network flow algorithm with some restrictions due to the equilateral triangular grid and point shape and type. Some artificial binary images were used to test the efficiency of the algorithm.

Keywords: discrete tomography, triangular grid, genetic algorithm, memetic algorithm.

1 Introduction

An equilateral triangular grid can be represented by a set of unit triangles (Fig.1). A projection of the triangular grid in a direction is a function which gives the number of points on each line which is parallel to that direction. Actually the directions orthogonal to the axes can be used for this purpose. Therefore we call projections, X projections if their direction is orthogonal to axis x, Y projections if their direction is orthogonal to axis y and Z projections if their direction is orthogonal to axis z, see Fig. 2. The problem of reconstructing an image from projections is important in the field of image processing. Many authors have studied the problem of reconstructing images from its projections where the image is represented on a square grid [2].

V.E. Balas et al. (Eds.): Soft Computing Applications, AISC 195, pp. 561–571.
springerlink.com

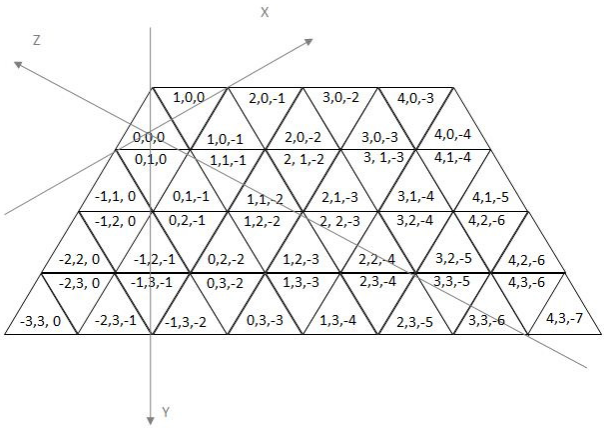

Fig. 1. Triangular grid

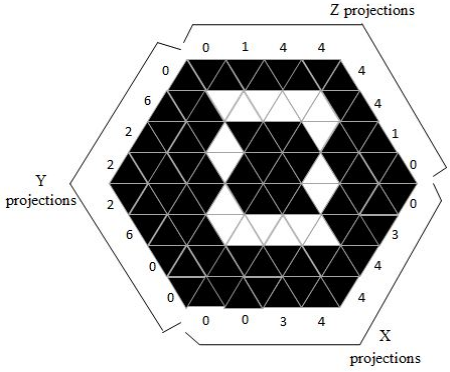

Fig. 2. Projection directions

In this paper, we study the reconstruction of binary images from their projections considering three directions as the points in the grid are triangles and by the symmetry of the grid there are three natural directions [12],[13].

The basic problem is to determine the binary hexagonal image which projections are (X,Y,Z), $X,Y,Z \in \mathbb{N}^n$. We consider reconstruction of a binary hexagonal image through a memetic algorithm and three projections. Our work is based on paper [9]. In this paper we show some further development of our algorithm such as the generation of the initial population using network flow algorithm with three combinations of the projections X-Y, Y-Z and X-Z, to which we add the third coordinate of a point. This procedure assures a better diversity of the initial population. Also some new operators are introduced, a crossover and a mutation operator. Based on the guided mutation operator and on the elementary switch operator we construct two operators which apply the guided mutation and the elementary switch as long as they help improving the image. The population evolves to a solution by using evolutionary algorithm

operators: selection, crossover, mutation and by applying two operators, one based on the switch operator and one based on a guided mutation operator, and a compactness operator. In real images the isolated points usually come from noise, and they are not significant parts of the objects presented in the image. The compactness operator will eliminate these isolated points to improve the image quality.

The paper is structured as follows: Section 2 presents some notations that are used for the definition of the algorithm; Section 3 presents the evolutionary algorithm presenting the mutation, crossover, compactness and two operators: one based on the switch operator and one based on a guided mutation operator; Section 4 shows some results of our experiments taking into account some artificial binary hexagonal images; finally Section 5 presents some conclusions and future works.

2 Basic Notations

We will represent a binary hexagonal image as a set of n x n x n pixels, $A = \{a_{\mathrm{xyz}}\}$, $x, y, z \in \mathbb{Z}$, where the elements equal to 0 if the corresponding pixel is black and 1 if the pixel is white. We consider addressing to the triangular grid using three axes of symmetry of the triangle, where the third axis z can have two values $z = -x - y$ or $z = 1 - x - y$, depending on the orientation of the triangle pixel. If the coordinate sum of a point is 0 the point has even parity, else (if the coordinate sum is 1) its parity is odd (Fig.1) [10], [12].

The number of projections used is three, on the three directions orthogonal to the coordinate axes x, y, z. Fixing a coordinate value, e.g., $x = 3$ the set of the triangles sharing this value, e.g., $(3, y, z)$ build a lane [11]. Counting the values (i.e., the 1's) of the picture by lanes we obtain its projections. We denote with $p_{\mathrm{k}}^{\mathrm{v}}$ the number of 1's along v. In this case the projection is $P_{\mathrm{v}} = (p_1^{\mathrm{v}}, p_2^{\mathrm{v}}, \dots, p_{\mathrm{n}}^{\mathrm{v}})$ where $p_{\mathrm{k}}^{\mathrm{v}} = \sum_{a_{\mathrm{xyz}} \in \mathcal{L}_{\mathrm{k}}^{\mathrm{v}}(\mathrm{A})} a_{\mathrm{xyz}}$, and $\mathcal{L}_{\mathrm{k}}^{\mathrm{v}}(\mathrm{A}), k = 1, \dots, n$ represents one ofthe projection lines parallel to a direction v.

3 The Proposed Algorithm

The proposed evolutionary algorithm is a genetic algorithm extended with a local search, i.e., a memetic algorithm. The memetic algorithm uses fitness function to evaluate the individuals, optimization operators to improve the individuals and selection process to lead the population towards the optimum solution. In the next paragraphs we will define new optimization operators: a crossover and a mutation operator as well as a hill climb operator based on the switching operator from discrete tomography. Another optimization operator used to improve the quality of the image is the compactness operator, which assures the elimination of the isolated points. After applying the optimization, children images are generated via operators crossover and mutation. The algorithm generates a number of children images. From the current population and the children images a new population is generated selecting the best individuals from the reunion of the current population and the children images. The selection process of the new population uses the tournament selection [7], [14].

The fitness function calculates the difference between the input projections and the projections of the created image, see equation (1) [6]. The goal of the algorithm is the minimization of the fitness function. (In this way the fitness function does not compute the 'fitness' in traditional sense, but it is an error measure giving about the same amount of information about the binary hexagonal image.)

$$\mathcal{F}(A) = \sum_{i=1}^{3} l_1\left(P_{\mathrm{v_i}}, \mathcal{P}_{\mathrm{v_i}}\right). \tag{1}$$

$$l_1\left(P_{\mathrm{v_i}}, \mathcal{P}_{\mathrm{v_i}}\right) = \sum_{k=1}^{n} |p_{\mathrm{k}}^{\mathrm{v}} - \hat{p}_{\mathrm{k}}^{\mathrm{v}}|, \tag{2}$$

where $\mathcal{P}_{\mathrm{v_i}}$ is the input projection and $P_{\mathrm{v_i}}$ is the projection of an individual.

The initial population is generated using the network flow algorithm as seen in Fig. 3. In this paper we consider the network flow algorithm for all the three directions X, Y and Z, being assured much more diversity in the initial population (than in [9] where only two directions were used). In this way, for the generation of the flow $B = \{b_{\mathrm{ij}}\}$, we will consider pairs Y-X, X-Z and Y-Z. After generating the flow, the initial population is generated taking into consideration the values of the flow and the values of the third projection: the generation of the initial images takes into consideration parity of the triangle pixels. We know that in an image represented on the triangular grid we have two types of triangle pixels, even and odd, depending on the sum of the coordinates of the pixel points.

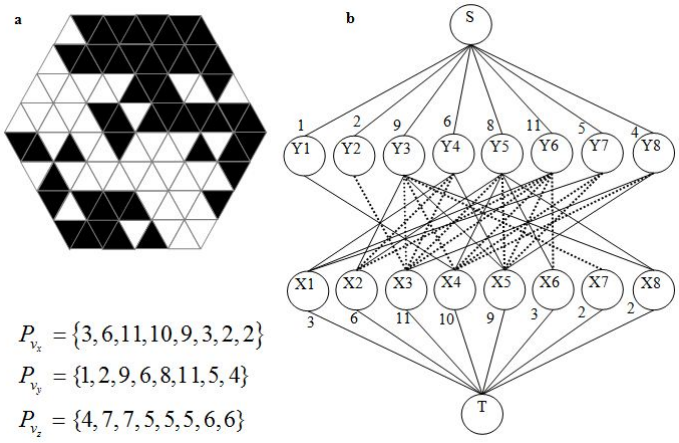

Fig. 3. (a) Example of binary image represented on triangular grid. (b) Network representation for directions Y and X

The first step is the use of the network flow algorithm on two directions which are included in the graph G with a source S and a sink T and two layers of edges between S and T. Each arc of G has a capacity:

$$c_{\mathrm{SY_i}} = \hat{p}_{\mathrm{i}}^{\mathrm{v}^1}, c_{\mathrm{Y_iX_j}} = 2, c_{\mathrm{X_jT}} = \hat{p}_{\mathrm{j}}^{\mathrm{v}^2}. \tag{3}$$

and flow:

$$f_{\mathrm{SY_i}} = \hat{p}_{\mathrm{i}}^{\mathrm{v}^1}, f_{\mathrm{Y_iX_j}} = b_{\mathrm{ij}}, f_{\mathrm{X_jT}} = \hat{p}_{\mathrm{j}}^{\mathrm{v}^2}. \tag{4}$$

where $i = 1, \dots, n$ and $j = 1, \dots, n$.

Moreover, we assign a cost $cost_{\mathrm{ij}} = -m_{\mathrm{ij}}$ to every arc $(\mathrm{Y_i}, \mathrm{X_j})$. Here $M = (m_{\mathrm{ij}})$ represents a random binary matrix which is generated for each individual of the population. For generating the flows we used MCF solver [4], [5]. The dotted arcs in Fig. 3.b represent a flow of weight 2 and the solid arcs represent a flow of weight 1. Where we have no arks we consider that the flow is 0.

3.1 Operators

In the following paragraphs we will present the crossover and the mutation operators introduced on the triangular grid. The generated child image has some features from both parents. Another operators that are introduced have as input a parent image and applies a series of elementary switch or guided mutation operators. For each parent we apply a compactness operator which aim is to eliminate the isolated pixels.

Crossover operator. The input of the crossover operator consists of two parent images. The output is a child image which has some features from both parents.

The first step in generating the child image is the computation of a crossover mask [2] $C_{\mathrm{mask}} = (cm_{\mathrm{xyz}}) \in \{0,1\}$. This mask determines every pixel from which parent is inherited. In this way assigning cell (x, y, z) to the first parent means setting $cm_{\mathrm{xyz}} = 0$ and assigning cell (x, y, z) to the second parent means setting $cm_{\mathrm{xyz}} = 1$. Then for the construction of the crossover mask we use the concept of neighbor cells of a cell (x, y, z). For this we use the concept of the neighbors of a pixel [10], [11]. Each triangle pixel has three 1-neighbors, nine 2-neighbors including the 1-neighbors and six more 2-neighbors, and twelve 3-neighbors: nine 2-neighbors and three more 3-neighbors as shown in Fig. 4. For the algorithm we consider various neighborhoods: each time when the crossover operator is applied one of the three neighborhoods of a pixel is chosen randomly. To each neighborhood type a selection probability is associated and the neighborhood type used for the crossover mask is selected randomly, depending on the associated selection probability. The construction of the neighbor cells of a given pixel depends on the parity of the pixel.

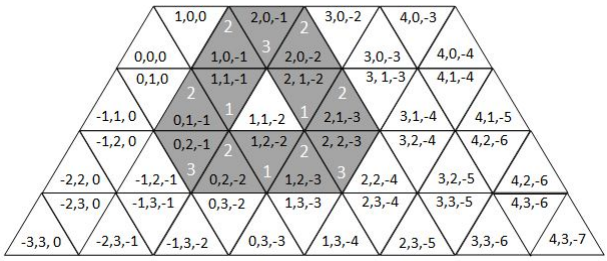

Fig. 4. Neighbor cells of cell $(1, 1, -2)$ are marked with gray, their type are also indicated

Our new crossover operator will assign areas of the two parents at the child. For this we will consider the division of the image in six parts as shown in Fig.5. We select one random pixel in each of the six parts of the image. Three of the randomly chosen pixels are assigned to the first parent and three to the second parent. The six pixels are marked as the border cells. Next the algorithm randomly selects a border pixel (x, y, z), marks all unassigned neighbor pixels of the selected border pixel, as a border pixel; assigns these pixels to the same parent as (x, y, z); removes the border status of (x, y, z) [2]. These steps are repeated until there are no border pixels left.

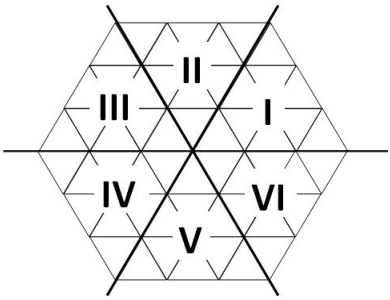

Fig. 5. Division of the image to six parts

After computing the crossover mask, a model image $M = \{m_{\text{xyz}}\}$ is created using the two parent images $R = \{r_{\text{xyz}}\}$ and $Q = \{q_{\text{xyz}} right\}$ as follows [2]:

$$m_{\text{xyz}} = \begin{cases} r_{\text{xyz}}, & \text{if } cm_{\text{xyz}} = 0, \\ q_{\text{xyz}}, & \text{if } cm_{\text{xyz}} = 1. \end{cases} \tag{5}$$

The child image is constructed by applying the flow algorithm using as a cost function the mask M.

Mutation operator. The mutation operator modifies a part of the image but it still keeps the prescribed projections. As an input for the mutation operator we have an image and the operator generates a child using a similar algorithm to the crossover algorithm. In this case a mutation mask $M_{\text{mask}} = (mm_{\text{xyz}}) \in \{0,1\}$ [2] is computed as

follows: first a random number $k \in [k_{\min}, k_{\max}]$ and a random pixel (x, y, z), are selected.

Then to mm_{xyz} is assigned the value 1 and (x, y, z), is marked as border pixel. Then the steps as in the case of the crossover operator are executed k times. The neighbors of the (x, y, z) pixel are computed using either the 1-neighbors, 2-neighbors and 3-neighbors. All unassigned pixels after the loop terminates are assigned the value 0. After computing the mutation mask, a model image $M = \{m_{\text{xyz}}\}$ is created using the parent image $R = \{r_{\text{xyz}}\}$ as follows:

$$m_{\text{xyz}} = \begin{cases} r_{\text{xyz}}, & \text{if } mm_{\text{xyz}} = 0, \\ rand(0,1), & \text{if } mm_{\text{xyz}} = 1. \end{cases} \tag{6}$$

The child image is constructed by applying the flow algorithm using as a cost function the mask M.

Compactness operator. The compactness operator uses the concept of isolated pixels. An isolated pixel is a pixel which is surrounded by 12 pixels with different color (Fig.6). The operator randomly locates the same number of black and white isolated pixels and sets them to the same value as their neighbors [9].

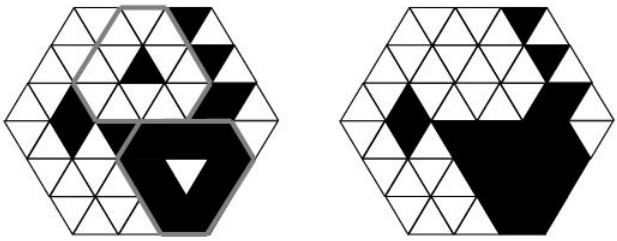

Fig. 6. Application of compactness operator

Elementary switch based operator. Being given an image A, the elementary switch means switching the pixel a_{xyz} with $a_{\text{x}_1\text{yz}_1}$ and the pixel $a_{\text{x(y+1)z}}$ with $a_{\text{x}_1\text{(y+1)z}_1}$ (Fig.7) where z, z_1 and x_1 satisfy (7) [9].

$$\begin{aligned} z &= -x - y \\ z_1 &= -x_1 - y \\ x_1 &= \begin{cases} 0, \dots, -\dfrac{n}{2} - y, & \text{if } y < \dfrac{n}{2} \\ -y + \dfrac{n}{2}, \dots, -n + 1, & \text{if } y \geq \dfrac{n}{2}. \end{cases} \end{aligned} \tag{7}$$

The pixels a_{xyz}, $a_{\text{x}_1\text{yz}_1}$, $a_{\text{xy}_1\text{z}}$ and $a_{\text{x}_1\text{y+1z}_1}$ have to satisfy the following conditions:

$$\begin{cases} a_{\text{xyz}} = 1 \\ a_{\text{x(y+1)z}} = 0 \end{cases} \qquad \begin{cases} a_{\text{x}_1\text{yz}_1} = 0 \\ a_{\text{x}_1\text{(y+1)z}_1} = 1. \end{cases} \tag{8}$$

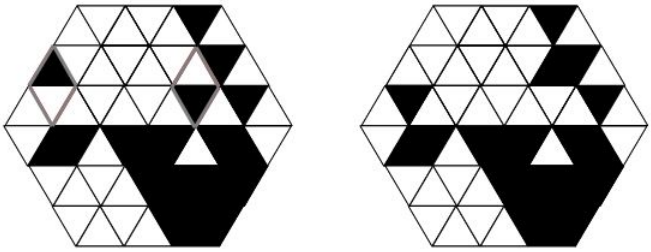

Fig. 7. An elementary switch operator

The elementary switch based operator applies a sequence of small modifications which increase the evaluation function until local optimum is reached [2]. This operator randomly selects a switch operator that improves the evaluation and applies this operator. These steps are repeated as long as switching operator that improves the evaluation exists. Each time one switch is applied, if the image is improved, the parent image is replaced with the child image and the operator is deleted from the list of operators, deleting all the other operators that contain the pixels from the current operator.

Guided Mutation Based Operator. The guided mutation selects a pair of points having two axes with the same value and the third axes differs with one unit as shown in Fig.8. The selected pairs should satisfy condition (8), i.e., the color of the two selected pixels must be different. The guided mutation is considered on each of the three directions [9].

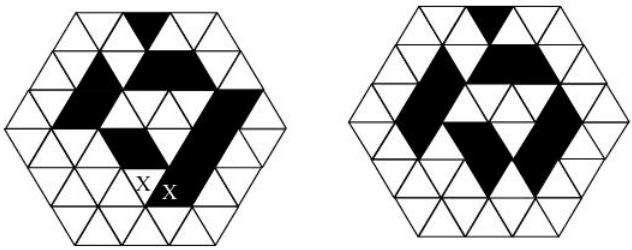

Fig. 8. Possible pixels for the guided mutation

The guided mutation based operator follows the same steps as the elementary switch operator using this time as a modification the guided mutation.

4 Results

The algorithm is tested on artificial images (see Fig.9 for some examples). The evolutionary algorithm generates a child image by selecting either the crossover operator or the mutation operator. For adjusting the selection probability of the crossover operator versus mutation operator after each generation the algorithm keeps track of the

number of children generated from crossover (a_c) and the number of children generated from mutation (a_m) after a generation. After selecting the new population the number of children from crossover (b_c) and mutation (b_m) are counted [2].

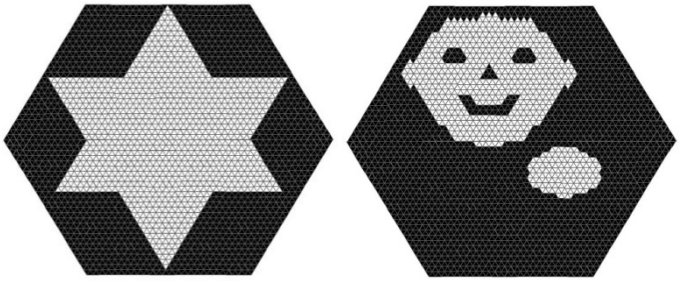

Fig. 9. Images used for tests

Using these information the average crossover yield is $y_c = b_c/(a_c + 1)$ and the number of mutation yield is $y_m = b_m/(a_m + 1)$. Then the probability that a child will be generated from crossover in the next generation becomes $y_c/(y_c + y_m)$. If the value of y_c is not between 0.1 and 0.9, then its value is adjusted by selecting a random number between 0.1 and 0.9 as in [2] and [3].

As presented in the above paragraph, the mutation operator uses a random number k which is between the bounds $k_{min} = n^2/64$ and $k_{max} = 5n^2/64$.

Table 1. Image reconstruction results

Image	Generation	Population	Reconstruction result of an example run (%)	Runtime (seconds)
1	10	30	79.45	1453
		50	79.88	2312
		75	80.21	3018
	20	30	79.33	2325
		50	79.88	3179
		75	80.21	4700
	25	30	79.00	2720
		50	79.33	3776
		75	80.10	5387
2	10	30	84.50	1100
		50	85.26	5120
		75	85.65	2814
	20	30	85.25	2000
		50	85.65	3768
		75	86.62	5083
	25	30	85.10	2520
		50	85.10	4084
		75	85.65	6015

The algorithm uses tournament selection for the selection of the new population, with tournament size 3.

Table 1 shows the results obtained by running the algorithm for each image represented in Fig. 9. The images from Fig. 9 have 4056 pixels (6 x$(n/2)$ x $(n/2)$) where n is 52. Table 1 presents the results obtained in the case when we use at the generation of the crossover and mutation mask the 1-neighborhood with probability 0.4, 2-neighborhood with the probability 0.2 and 3-neighborhood with probability 0.3.

Our experiments were run on a computer with processor Intel(R) Core(TM) i5-2430M CPU @ 2.40GHz with 4.00 GB memory. For the tests we considered different values for the population size and for the maximum generation.

5 Conclusions and Future Works

Reconstruction binary images represented on the triangular grid is presented, using an evolutionary algorithm, memetic algorithm, for reconstructing images from three natural directions of projections in this grid. New crossover, mutation and operators based on switch were used. Our plan is to find a better algorithm for reconstructing images on triangular grid. Future work could imply creating and applying other switch operator and creating new crossover and mutation operators to improve the quality of the reconstructed image. Another option could be to use six projections as in [8], where simulated annealing is used for image reconstruction.

Acknowledgements. The work is partly supported by the TÁMOP 4.2.1/B-09/1/KONV-2010-0007 project. The project is implemented through the New Hungary Development Plan, co-financed by the European Social Fund and the European Regional Development Fund.

References

1. Balázs, P., Balogh, E., Kuba, A.: Reconstruction of 8-connected but not 4-connected hv-convex discrete sets. Discrete Applied Mathematics 147, 149–168 (2005)
2. Batenburg, K.J.: Network Flow Algorithms for Discrete Tomography. PhD thesis (2006)
3. Batenburg, K.J.: An evolutionary algorithm for discrete tomography. Discrete Applied Mathematics 151, 36–54 (2005)
4. Bertsekas, D., Tseng, P.: RELAX-IV: a faster version of the RELAX code for solving minimum cost flow problems. LIDS Technical Report LIDS-P-2276, MIT (1994)
5. Bertsekas, D., Frangioni, A., Gentile, C.: Relax IV, The MCF Class Project (2004), `http://www.di.unipi.it/di/groups/optimize/Software/MCF.html`
6. Di Gesù, V., Lo Bosco, G., Millonzi, F., Valenti, C.: A Memetic Algorithm for Binary Image Reconstruction. In: Brimkov, V.E., Barneva, R.P., Hauptman, H.A. (eds.) IWCIA 2008. LNCS, vol. 4958, pp. 384–395. Springer, Heidelberg (2008)
7. Goldberg, D.E.: Genetic Algorithms in Search Optimization and Machine Learning. Addison Wesley (1989)

8. Lukic, T., Nagy, B.: Energy-minimization based Discrete Tomography Reconstruction Method for Images on Triangular Grid. In: 15th International Workshop on Combinatorial Image Analysis, IWCIA 2012 (accepted for publication, 2012)
9. Moisi, E., Nagy, B.: Discrete Tomography on the Triangular Grid: a Memetic Approach. In: 7th International Symposium on Image and Signal Processing and Analysis (ISPA 2011), Dubrovnik, Croatia, pp. 579–584 (2011)
10. Nagy, B.: Finding Shortest Path with Neighborhood Sequences in Triangular Grids. In: 2nd IEEE R8-EURASIP International Symposium on Image and Signal Processing and Analysis (ITI-ISPA 2001), Pula, Croatia, pp. 55–60 (2001)
11. Nagy, B.: Shortest Path in Triangular Grids with Neighbourhood Sequences. Journal of Computing and Information Technology 11, 111–122 (2003)
12. Nagy, B.: Generalised triangular grids in digital geometry. Acta Mathematica Academiae Paedagogicae Nyíregyháziensis 20, 63–78 (2004)
13. Nagy, B.: Distances with Neighbourhood Sequences in Cubic and Triangular Grids. Pattern Recognition Letters 28, 99–109 (2007)
14. Spears, W.M.: Evolutionary Algorithms: The Role of the Mutation and recombination. Springer (2000)

Morphological Wavelets for Panchromatic and Multispectral Image Fusion

Silviu Ioan Bejinariu, Florin Rotaru, Cristina Diana Niță, and Mihaela Costin

Institute of Computer Science, Romanian Academy, Iasi Branch
{silviu.bejinariu,florin.rotaru,cristina.nita,
mihaela.costin}@iit.academiaromana-is.ro

Abstract. Image fusion is the combining process of relevant information from one or more images to create a single image with more informational content. In remote sensing applications, the spatial resolution of the multispectral images is enhanced using detail information from the panchromatic images which have a higher resolution. This process is known as pansharpening. One of the most used pansharpening method is based on wavelet decomposition. The edge information from the panchromatic image is injected in the wavelet decomposition of the multispectral image. In this paper a fusion method based on morphological wavelets is proposed. The main advantage of morphological wavelets is the computing complexity, because only integer operations are used.

Keywords: image fusion, multispectral image, morphological wavelet transform.

1 Introduction

Image Fusion is the combining process of combining the relevant information from one, two or more images to create a single image that is more complete than any of the initial images in order to facilitate the analysis by a human operator or a computer vision system.

The remote sensing systems, panchromatic and multispectral images are combined for an accurate analysis of the studied area. Panchromatic images have a finer spatial resolution and can be used for texture analysis and edges / boundaries detection. On the other hand, multispectral images have a better spectral resolution and offer the possibility to discriminate the different types of soil, land cover types, wetlands or other features which are not perceptible by the human eye.

The most used spectral bands are: blue (wavelength 450-520 nm) – atmospheric and water images; green (520-600nm) – vegetation and water images; red (600-690nm) – man-made objects, soil, vegetation and water; near-infrared (750-900nm) – for vegetation images; mid-infrared (1550-1750nm) – for vegetation, soil humidity; mid-infrared (2080-2350nm) – for soil humidity, geological features, fire and thermal-infrared (10400-12500nm) – for night images. In case of thermal-infrared band, the image is created by the emitted radiation.

V.E. Balas et al. (Eds.): Soft Computing Applications, AISC 195, pp. 573–583.
springerlink.com

In practice, different combinations of spectral bands are used: True-Color is the combination of Red / Green / Blue channels in the visible spectrum, Green / Red / Infrared is used for images representing vegetation or camouflages (military applications), Blue / Near-Infrared / Mid-Infrared to analyze the vegetation soil humidity, water.

The panchromatic image is represented as a single band where the pixel intensity is proportional to the reflection of the ambient light. Usually, the panchromatic images have a greater resolution offering more detailed information about edges and region boundaries.

The resolution of multispectral and panchromatic images depends on the used acquisition devices. The IKONOS satellite offers images having 0.82-1.00m resolution in panchromatic and 3.2-4.0m in multispectral, for QuickBird satellite images the resolution is 0.61-0,72m in panchromatic and 2.44-2.88m in multispectral and the LANDSAT7 images resolution is 30m [14].

The combining process of multispectral (MS) and panchromatic (PC) images is known in literature as pansharpening. A wide variety of pansharpening methods were studied. Principal Component Analysis based methods use PCA to select the principal image representation [13], [15] between PC and MS images using the assumption that the component of higher variance is the ideal choice for higher spatial details injection. The Gram-Schmidt pansharpening methods use the GS transform to enhance the spatial resolution of MS images [1]. Multiresolution methods, based on the wavelet transform, offer better performances. The decimated wavelet approaches requires an upsampling step to be applied for different resolution problem solving. The non-decimated approaches seem to give better results [2].

2 Multiresolution Based Pansharpening

Multiresolution based pansharpening methods were developed keeping in consideration that PC and MS images have different spatial resolution. The most common technique is the component substitution method. It is applied for MS images that contain at least 3 spectral bands. In this case, the panchromatic image substitute a component of the transformed MS image and finally the inverse transform is applied to obtain the fused image. If MS image contains 3 spectral bands, these bands may be considered as RGB channels of a color image and the used transform is RGB to IHS (Intensity-Hue-Saturation). Because both, I component of the transformed image and the PC image are signal intensities, the I component is substituted by the PC image.

When the MS image contains more than 3 spectral bands, more elaborated (generalized) transforms are used, depending on the different types of followed analysis / processing. Some fusion methods are based on PCA (principal Component Analysis) and the substitution / insertion of higher spatial resolution is made in the first principal component with greater variance. Other methods use GA (Genetic Algorithms) to compute the weights of the spectral components, by minimizing the inserted distortions.

Modulation based fusion is not used for spatial resolution enhancement but to modulate the spatial details in the MS image by multiplying it as in eq. 1, by a ratio of PC image to a synthetic image. Usually, the synthetic image is a lower resolution of the PC image.

$$F^k_{(i,j)} = MS^k_{(i,j)} \frac{PC(i,j)}{syn(i,j)} \tag{1}$$

where $F^k_{(i,j)}$ is the pixel (i, j) in band k of the MS fused image, $MS^k_{(i,j)}$ is the pixel (i, j) in the original band k of the MS image, $PC(i, j)$ is the (i, j) pixel in the PC image and $syn(i, j)$ is the (i, j) pixel in the synthetic image.

The synthetic image may be computed as the average of RGB channels (Brovey transform), a low pass filtered image (Smoothing Filter Based Intensity Modulation). Another method uses a high pass filtered version of the PC image which is added pixel by pixel to the MS image.

The fusion schemes based on IHS transforms or modulation are considered traditional [5] because are easy to implement. The main advantage is that these methods are efficient from the computing time point of view. The main disadvantage is that the input images must be exactly registered and also some distortions are inserted in the fused spectral image.

The multiresolution based methods use the wavelet decomposition or Laplacian pyramids for MS and PC image fusion. The processing steps are the same: the transform is applied to both images, the scaled signal from the PC image transformed space is replaced by the scaled signal from the MS image transform and then the inverse transform is applied [7].

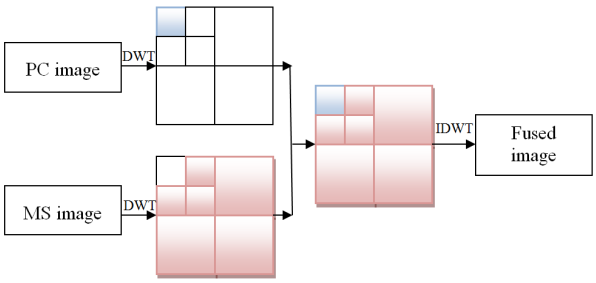

Fig. 1. General scheme of wavelet multiresolution based pansharpening

MS and PC images have different spatial resolutions, so, most pansharpening approaches perform an upsampling step in which the MS bands are scaled to match the PC image resolution, using bi-cubic or B-spline interpolations. Once both sources have the same resolution, different strategies may be applied to create the fused image. The first approach combine each MS band with the PC image and finally the results are combined to obtain the MS fused image. Another approach already discussed use the RGB-HIS transform. Because the I image is similar to the PS image,

this channel is fused with the PC image and the result, jointly with the original H and S components are transformed back into the RGB color space.

In the fusion step, the wavelet decomposition with the same number of levels is applied to both MS and PC images. The detail components LH_{PC}, HH_{PC} and HL_{PC} of the PC decomposition on the last level, are combined to the scaled component LL_{MS} on the last level of MS image decomposition in order to obtain the wavelet decomposition of the fused image.

Another step that must be performed before the I channel and PC image fusion is the histogram matching. Using a nonlinear histogram matching which is more accurate or a simple linear transformation, the PC image histogram is aligned to the I component histogram [3].

Using the fact that the ratio of the PC image resolution to the MS image resolution is a power of 2, in [10] is proposed a method to solve the spatial resolution problem inside the wavelet Multiresolution analysis step. In case of Lidar MS images used in the experiment presented in the next section, the spatial resolution is 15m for the PC image, 30m for most of the MS bands and 60m for the thermal-infrared bands.

In this case the upsampling step applied before the wavelet decomposition can be eliminated. Then the wavelet decomposition depth will be different for PC image and I channel to match the spatial resolutions.

The procedure of image fusion between a PC image and a single channel MS image is presented below:

Input:
PC image,
MS image,
n – depth of the wavelet decomposition to be applied on PC image.

1. computes depth of the two wavelet decompositions:
   - $n_{PC} = n$,
   - $n_{MS} = n - log_2 \frac{res(PC)}{res(MS)}$
2. Histogram matching. The PC image histogram is aligned to the MS image histogram;
3. Apply n_{PC} levels of wavelet decomposition to PC image;
4. Apply n_{MS} levels of wavelet decomposition to MS image;
5. The $LL_{PC}^{n_{PC}}$ component is replaced by the $LL_{MS}^{n_{MS}}$ component from the MS image decomposition;
6. The inverse wavelet transform is applied to rebuild the fused MS image.

For a three channel MS image, the fusion procedure is similar, excepting that the MS image is first transformed into the HIS space and the I component is fused with the PC image. Because the two input images have different resolutions, the H and S

components have to be scaled by a $n_{PC} - n_{MS}$ factor. This scaling may be accomplished by applying an inverse wavelet transform in which the H and S components are considered a scaled signal and the detail signal is 0. In figure 2 is presented the general structure of the pansharpening procedure using decimated wavelets without scaling.

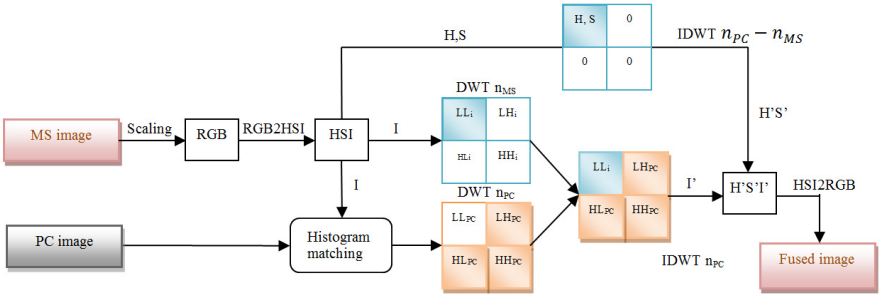

Fig. 2. Pansharpening procedure using decimated wavelets without scaling [10]

Our proposal is to substitute the classical wavelet transform by morphological wavelets which wave the great advantage of reduced computing time.

3 Morphological Wavelets in Image Fusion

Morphological wavelets were introduced by Heijmans and Goutsias [8], [9] in 2000, as the morphological version of the linear Haar wavelet transform, using the morphological dilation and erosion operators. De and Chanda [4] proposed in 2006 a morphological decomposition scheme based only on operations with integer numbers.

The analysis $\left(\psi^{\uparrow}, \omega^{\uparrow}\right)$ and synthesis $\left(\psi^{\downarrow}, \omega^{\downarrow}\right)$ operators are defined by the following relations:

$$\psi^{\uparrow}(X)(B) = M = \max\{X(r,c),\ X(r,c+1),\ X(r+1,c),\ X(r+1,c+1)\} \tag{2}$$

$$\omega^{\uparrow}(X)(B) = (y_v, y_h, y_d), \tag{3}$$

where y_v, y_h, y_d are the vertical, horizontal and diagonal signal details:

$$y_v = \begin{cases} M - X(r,c+1) & if \quad M - X(r,c+1) > 0 \\ X(r,c+1) - M & otherwise \end{cases} \tag{4}$$

$$y_h = \begin{cases} M - X(r+1,c) & if \quad M - X(r+1,c) > 0 \\ X(r+1,c) - M & otherwise \end{cases} \tag{5}$$

$$y_d = \begin{cases} M - X(r+1,c+1) & if \quad M - X(r+1,c+1) > 0 \\ X(r+1,c+1) - M & otherwise \end{cases} \tag{6}$$

The signal reconstruction is made using the synthesis operator:

$$\begin{aligned} &X'(u,v) = \hat{X}(u,v) \dot{+} \hat{Y}(u,v) \\ &(u,v) \in \{(r,c),(r,c+1),(r+1,c),(r+1,c+1)\} \end{aligned} \tag{7}$$

The $\dot{+}$ operator is the usual additive operator and

$$\hat{X}(r,c) = \hat{X}(r,c+1) = \hat{X}(r+1,c) = \hat{X}(r+1,c+1) = M \tag{8}$$

$$\begin{aligned} \hat{Y}(r,c) &= \min(y_v, y_h, y_d, 0) \\ \hat{Y}(r,c+1) &= \min(-y_v, 0) \\ \hat{Y}(r+1,c) &= \min(-y_h, 0) \\ \hat{Y}(r+1,c+1) &= \min(-y_d, 0) \end{aligned} \tag{9}$$

Nobuhara and Hirota defined [11] the wavelet analysis operators as:

$$\psi^{\uparrow}(X)(B) = m = min\{X(r,c),\ X(r,c+1),\ X(r+1,c),\ X(r+1,c+1)\} \tag{10}$$

$$\omega^{\uparrow}(X)(B) = (y_v, y_h, y_d), \tag{11}$$

$$\begin{aligned} y_v &= (X(r,c) - X(r,c+1) + X(r+1,c) - X(r+1,c+1))/2 \\ y_h &= (X(r,c) + X(r,c+1) - X(r+1,c) - X(r+1,c+1))/2 \\ y_d &= (X(r,c) - X(r,c+1) - X(r+1,c) - X(r+1,c+1))/2 \end{aligned} \tag{12}$$

and synthesis operators as:

$$X'(u,v) = \hat{X}(u,v) \dot{+} \hat{Y}(u,v), \tag{13}$$

$$\hat{X}(r,c) = \hat{X}(r,c+1) = \hat{X}(r+1,c) = \hat{X}(r+1,c+1) = m, \tag{14}$$

$$\begin{aligned} \hat{Y}(r,c) &= \max(y_v + y_h, y_h + y_d, y_d + y_v, 0) \\ \hat{Y}(r,c+1) &= \max(-y_v + y_h, y_h - y_d, -y_d - y_v, 0) \\ \hat{Y}(r+1,c) &= \max(y_v - y_h, -y_h - y_d, -y_d + y_v, 0) \\ \hat{Y}(r+1,c+1) &= \max(-y_v - y_h, -y_h + y_d, y_d - y_v, 0) \end{aligned} \tag{15}$$

The morphological operators introduced by Nobuhara and Hirota were implemented in the pansharpening procedure to insert in the MS images edge information which is richer in the PC images. The morphological wavelet operates with integer numbers only, reducing in this way the processing time.

4 Experiments and Conclusions

The pansharpening procedure was implemented and tested in an image processing framework developed by authors. It is implemented as a Windows application, in C++ using Microsoft Visual Studio. For image manipulation and some processing functions, the OpenCV library is used [12].

The procedure was tested on different multispectral sets of images available on internet.

The first dataset, freely downloaded from Landsat.org [17] contains collections of 8 multispectral images (MS) and one panchromatic image (PC) already registered. The multispectral bands, with 30 meter resolution are: visible blue-green, visible green, visible red, near infrared and two bands in the middle infrared interval. It contains also two bands in the thermal-infrared interval with 60 meter resolution. The resolution of the panchromatic image is 15m per pixel. Because these images are enough large, our tests were made on smaller cropped images.

In the following experiment, the pansharpening procedure was applied for the 15m resolution panchromatic image (fig. 3.a) and a 60m resolution thermal-infrared band (fig. 3.c). The MS image was directly injected (fig. 3.d) in the second level wavelet decomposition of the PC image (fig. 3.b), using the fact that the dimensions ratio is 2^2. The wavelet transform uses the morphological operators proposed by Nobuhara and Hirota and the original images were used (without histogram alignment). The results are presented in the figure 3.

The fused image is presented in fig 3.e as it was reconstructed from the wavelet decomposition and fig. 3.f, after histogram equalization was applied.

The second test was performed on images with a smaller edges density, where the fusion result is more visible. The multispectral data collection available in „Multispectral Image Database" [16] was used. Each collection contains images in the visible spectrum, wavelength between 400 and 700 nm in steps of 10 nm. All 31 images are in '.png' format, 16-bit gray levels. Figure 4 illustrates the original scene illuminated with a neutral light in full color format.

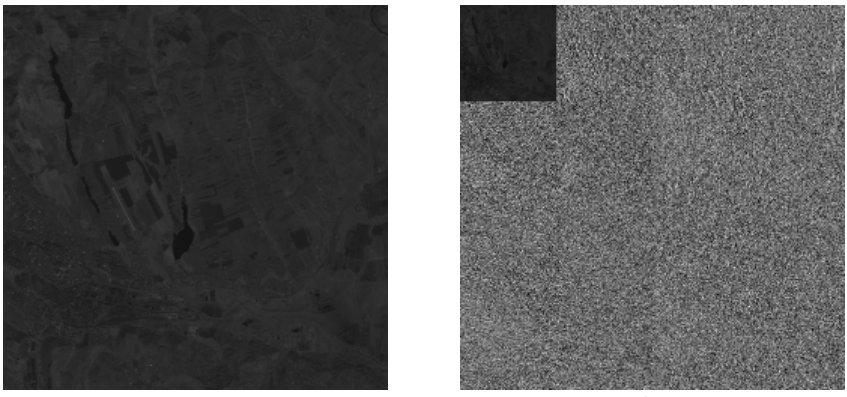

a. b.

Fig. 3. Steps of the morphological wavelet based pansharpening procedure using Landsat images [17]

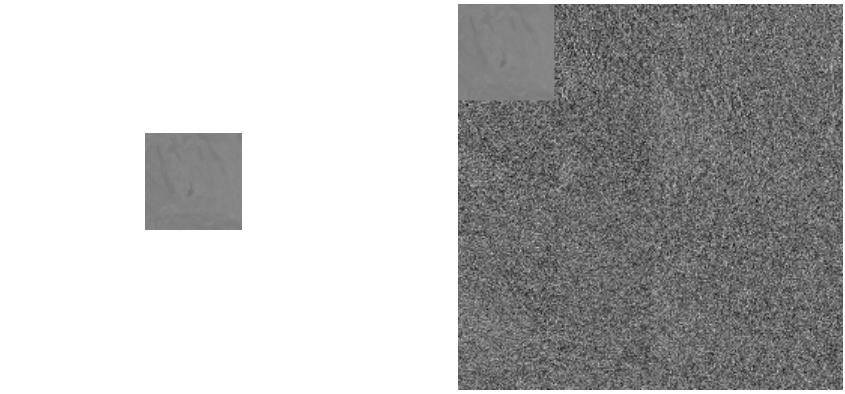

c. d.

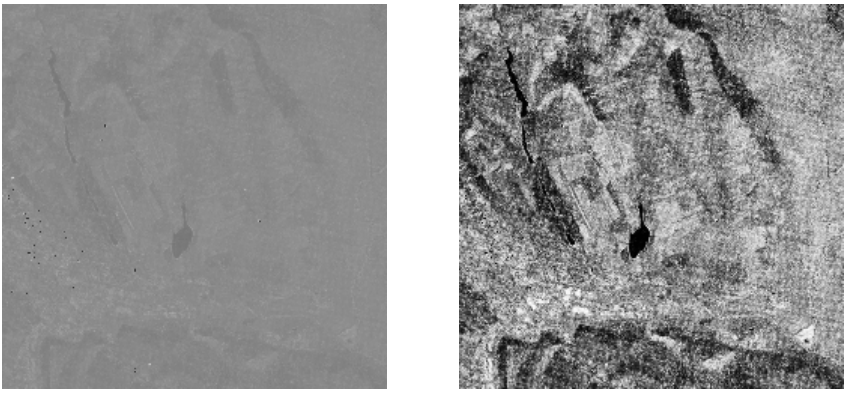

e. f.

Fig. 3. (*continued*)

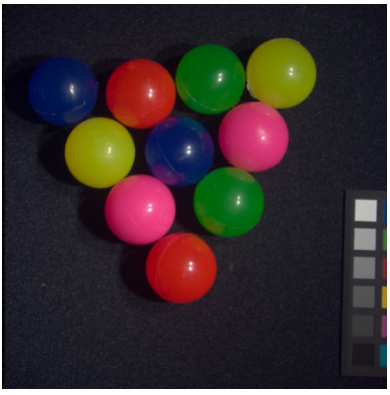

Fig. 4. Original image, full color [16]

Because all images have the same resolution, in the following test, we used as panchromatic image the original color image (fig.4) converted to 256 gray levels (fig.5.a) and as multispectral image the 540nm band rescaled to half of its resolution (fig.5.c). Because the dimension of the PC image is twice the dimension of the MS image, two-level morphological wavelet decomposition was applied to the PC image (fig. 5.b) and a single level decomposition to the MS image (fig. 5.d). The transformed images are fused by injecting the scaled image from the MS transform in the PC transform (fig.5.e) and the fused image is reconstructed by applying the inverse morphological wavelet transform (fig.5.f).

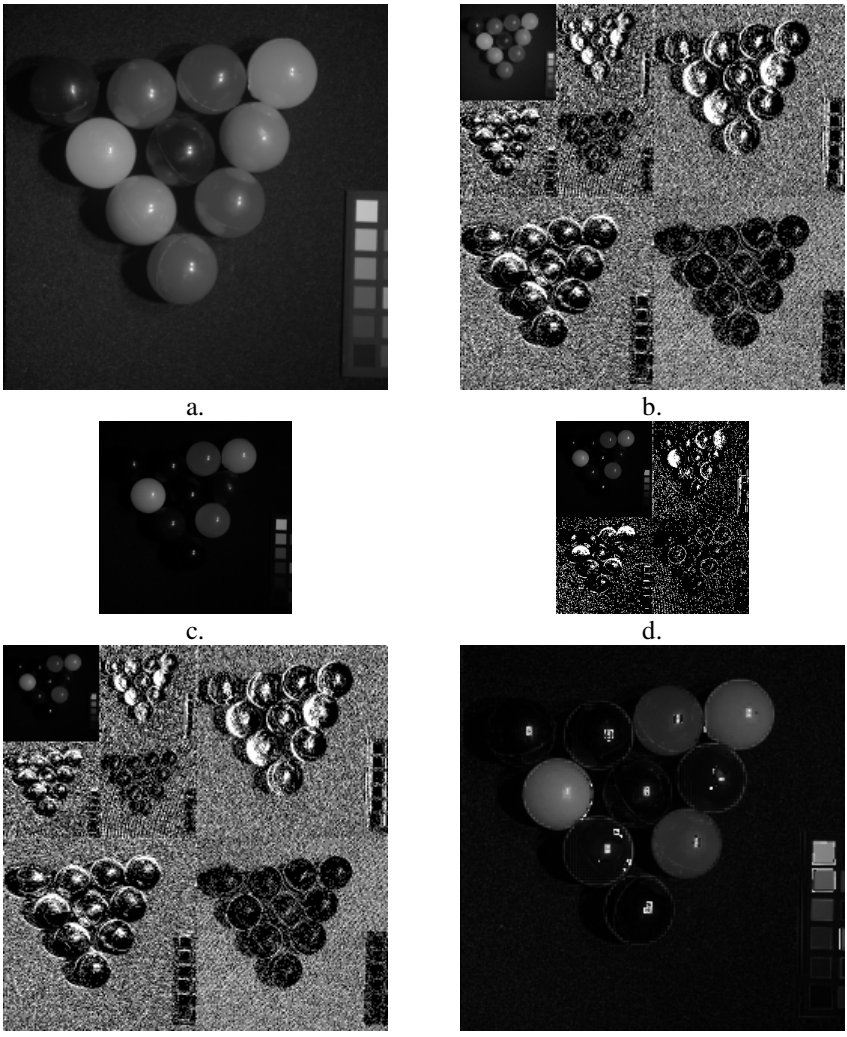

Fig. 5. Steps of the morphological wavelet based pansharpening procedure using the test images from Columbia database

In the fused image (fig.5.f) the edges of the dark balls become visible, excepting for the ball in the top left corner which has a gray level similar to the background.

In this paper, the morphological wavelet decomposition was applied for multispectral and panchromatic image fusion. Its main advantage is that is faster than the Haar wavelets. In our tests, the morphological wavelet based pansharpening was about 10 times faster than the classical wavelet based fusion. The method will be developed by adding objective quality evaluations of the fusion process and testing using higher resolution multispectral images, with lower edges density.

References

1. Aiazzi, B., Baronti, S., Selva, M.: Improving component substitution pansharpening through multivariate regression of MS+PAN data. IEEE Transactions on Geoscience and Remote Sensing 45(10), 98–102 (2007)
2. Alparone, L., et al.: Comparison of Pansharpening Algorithms: Outcome of the 2006 GRS-S Data-Fusion Contest. IEEE Transactions on Geoscience and Remote Sensing 45(10), 3012–3021 (2007)
3. Coltuc, D., Bolon, P., Chassery, J.-M.: Exact histogram specification. IEEE Transactions on Image Processing 15(5), 1143–1152 (2006)
4. De, I., Chanda, B.: A simple and efficient algorithm for multifocus image fusion using morphological wavelets. Signal Processing 86(5), 924–936 (2006)
5. Dong, J., Zhuang, D., Huang, Y., Fu, J.: Survey of Multispectral Image Fusion Techniques in Remote Sensing Applications. Image Fusion and Its Applications, Intech., 1–22 (2011)
6. Gomez, R.B., Jazaeri, A., Kafatos, M.: Wavelet-based hyperspectral and multispectral image fusion. In: Proc. SPIE. Geo-Spatial Image and Data Exploitation II, vol. 4383, pp. 36–42
7. González-Audícana, M., Saleta, J.L., Catalán, R.G., García, R.: Fusion of Multispectral and Panchromatic Images Using Improved IHS and PCA Mergers Based on Wavelet Decomposition. IEEE Transactions on Geoscience and Remote Sensing 42(6), 1291–1299 (2004)
8. Goutsias, J., Heijmans, H.J.: Nonlinear multiresolution signal decomposition schemes, Part 1: morphological pyramids. IEEE Trans. Image Processing 9, 1862–1876 (2000)
9. Heijmans, H.J., Goutsias, J.: Nonlinear multiresolution signal decomposition schemes, Part 2: morphological wavelets. IEEE Trans. Image Processing 9, 1897–1913 (2000)
10. Mitianoudis, N., Tzimiropoulos, G., Stathaki, T.: Fast Wavelet-based Pansharpening of Multi-Spectral Images. In: Proc. of 2010 IEEE International Conference on Imaging Systems and Techniques (IST), pp. 11–16 (2010)
11. Nobuhara, H., Hirota, K.: A Fuzzification of MorphologicalWavelets Based on Fuzzy Relational Calculus and its Application to Image Compression/Reconstruction. Journal of Advanced Computational Intelligence and Intelligent Informatics 8(4), 373–378 (2004)
12. Open Source Computer Vision Library, Reference Manual, Copyright 1999-2001 Intel Corporation
13. Shah, V.P., Younan, N.H., King, R.L.: An Efficient Pan-Sharpening Method via a Combined Adaptive PCA Approach and Contourlets. IEEE Transactions on Geoscience and Remote Sensing 46(5), 1323–1335 (2008)
14. SATELLITE IMAGING CORPORATION, `http://www.satimagingcorp.com/satellite-sensors`

15. Yang, S., Wang, M., Jiao, L.: 'Fusion of multispectral and panchromatic images based on support value transform and adaptive principal component analysis. Information Fusion 13(3), 177–184 (2012)
16. Multispectral Image Database, http://www1.cs.columbia.edu/CAVE/databases/multispectral/
17. Global Observatory for Ecosystem Services, Michigan State University, http://landsat.org

Image Categorization Based on Computationally Economic LAB Colour Features

Adrian Ciobanu, Mihaela Costin, and Tudor Barbu

Institute of Computer Science of the Romanian Academy
{adrian.ciobanu,mihaela.costin,
tudor.barbu}@iit.academiaromana-is.ro

Abstract. An easy to compute and small colour feature vector is introduced in this paper, as a tool to be used in the process of retrieval or classification of similarly coloured digital images from very large databases. A particular set of „ab" planes from the LAB colour system is used, along with a specific configuration of colour regions within them. The colour feature vector is low dimensional (only 96 components), computationally economic and performs very well on a carefully selected database of rose images, publicly available.

Keywords: image retrieval, feature vector, colour similarity, colour classification, agglomerative hierarchical algorithm.

1 Introduction

In this paper we introduce a computationally economic colour feature vector extracted from digital images that are previously converted in the CIELAB colour space format (called simply LAB from here on). This kind of feature vector can be easily used for retrieving images from large databases based on their colour content, as well as for classifying/indexing these images.

The LAB colour space can be seen as a stack of „***ab***" planes, each one containing all the possible colours for a given luminance ***L*** [2]. The perpendicular ***L*** axis is going through the centre of these "***ab***" planes from low luminance values to high luminance values. The conversion of a digital image from the RGB format (with parameter values ranging from 0 to 255 for each red, green and blue colour channel) into the LAB format, results in real numbers for the luminance ***L***, and ***a*** and ***b*** parameters, but these values can be conveniently transformed again into the range from 0 to 255, as it is automatically done, for instance, in Matlab.

We can see the uniform distribution of colours in the "***ab***" planes of a LAB color space in Fig. 1, with colours varying from green to red along the "***a***" axis and from blue to yellow along the "***b***" axis. A particular color is defined by a certain point (a_i, b_i) in the "***ab***" plane of the corresponding luminance L_i. Moving gradually away from this point in the same plane results in going through uniformly changed similar colours. The LAB color space was specially designed with the purpose of the human eye to perceive this gradual change of colour as a uniform one.

V.E. Balas et al. (Eds.): Soft Computing Applications, AISC 195, pp. 585–593.
springerlink.com

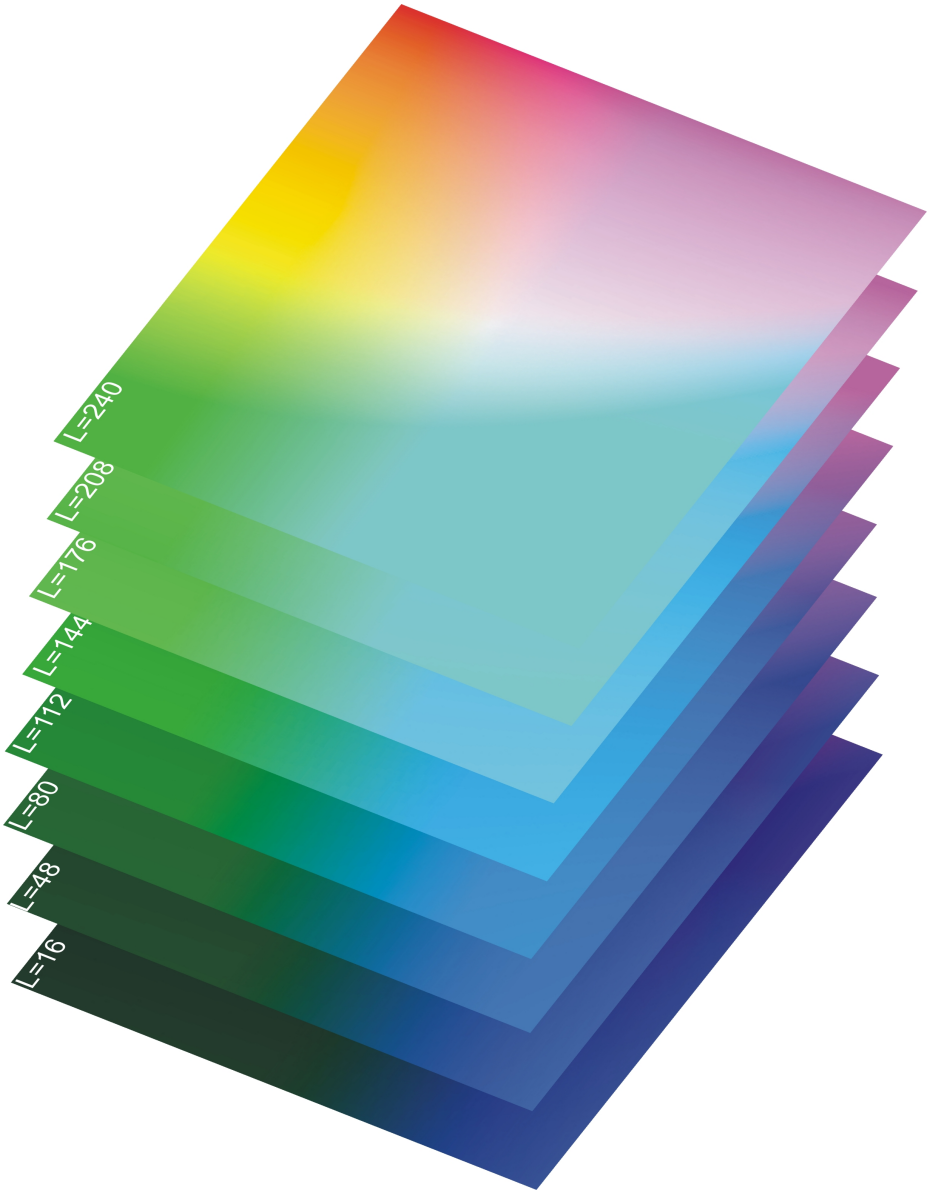

Fig. 1. The distribution of colours in the LAB colour space

2 Simple LAB Colour Feature Vector

It is usual to reduce the number of possible colours before extracting a feature vector. This is better to have as few components as possible if it is devised for large databases of images. Within the LAB colour space, we can obtain this reduction just by cutting

the number of the "***ab***" planes from a total of 256 to just 8. The following central ***L*** values were taken into consideration by us: 16, 48, 80, 112, 144, 176, 208 and 240. The reduction was implemented simply by browsing all the pixels in the image and replacing the values of ***L*** with the nearest value in this set. The image is not significantly changed after this procedure from the point of view of colour content, while there is some loss in texture.

In our previous works [3][4][5] we used to create a 256×256 bins histogram for each of the 8 "***ab***" planes. However, we noticed that the bins of such histograms are mostly empty, as only a few of the (***a***,***b***) possible pairs correspond to pixels in images. Moreover, it was hard to extract only a small number of features from these histograms. So, in this paper we are taking another approach that simply divides each "***ab***" plane in 12 particular regions and constructs a histogram with only 12 bins for each plane (see Fig. 2). This is resulting in only 96 bins for the LAB histograms of an image, taking in consideration all the 8 considered "***ab***" planes.

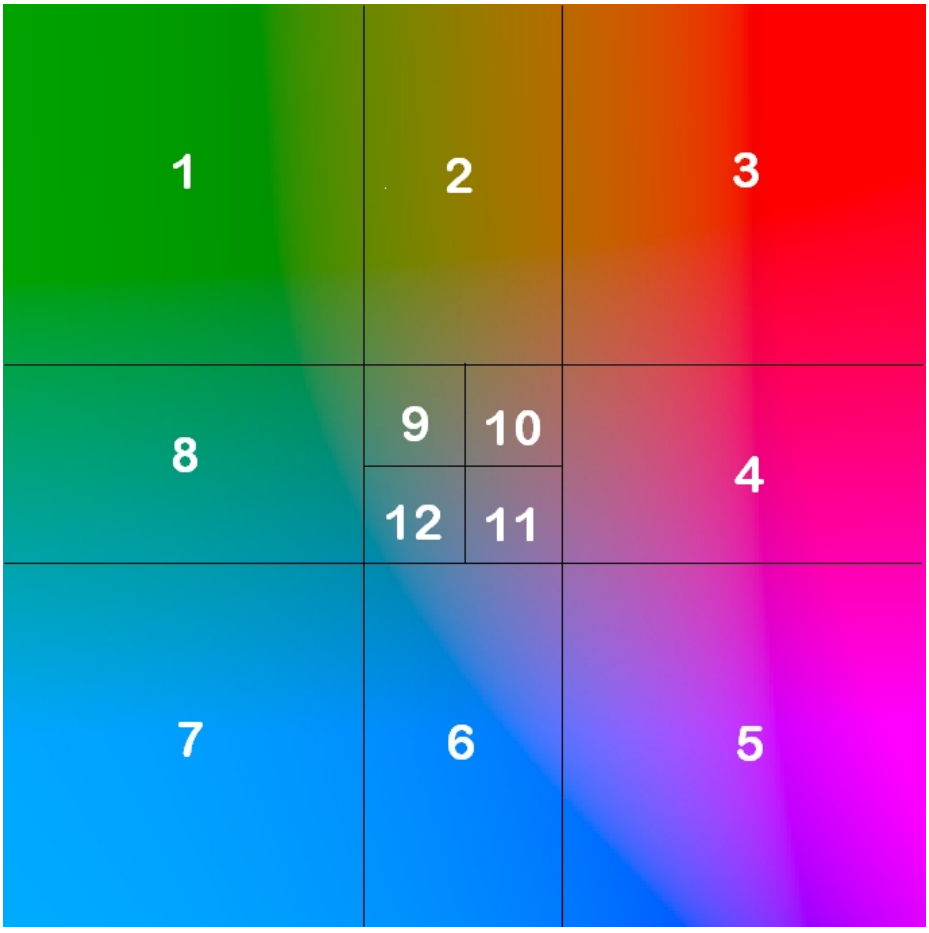

Fig. 2. The choice for splitting an „ab" plane into 12 regions

This particular choice of the set of regions resulted from our extensive tests concerning possible colour feature vectors within the LAB colour system. Regions 1, 3, 5 and 7 are somehow uniform in colour. However, in everyday pictures taken outside, a few numbers of colours correspond to these regions. Most of them are found in areas of the regions nearing the center of an "ab" plane. More colours in digital images fall in the 2, 4, 6 and 8 regions, as here we have colours that combine red and green (for instance yellow at high luminance values), red and violet, violet and blue, and blue and green. We found still more colours in the centre of the "***ab***" planes, as here is the region for black (at low luminance values), white (at high luminance values) and all sort of gray and brownish tones that are very much present in everyday pictures. In our experiments we found a lot of hits in the regions 9, 10, 11 and 12 and this is the reason why we have devised such small regions in the center of the "***ab***" planes.

To compute the histogram based on the 8 "***ab***" planes and the 12 regions for each plane, we simply browse all the pixels of an LAB converted image and for each pixel we add one unit to the corresponding bin. First we find the ***L*** value and select the corresponding "***ab***" plane and then we find the corresponding colour region in that plane by testing the ***a*** and ***b*** values of each pixel. So, extracting the feature vector is just a problem of counting, without any computation that could induce long processing times for high resolution images. The feature vector with 96 components is then constructed by putting the 12 values for each plane in the order indicated in Fig. 2 and then by concatenating the values for each plane in the order of their specific ***L*** value, from low values (16) to high values (240). For an image ***I***, the colour feature vector can be expressed as:

$$F(I) = \left(n_1, n_2, ..., n_{12}, n_{13}, ..., n_{24}, n_{25}, ..., n_{96}\right) \tag{1}$$

where n_i, $i = 1,\ldots,96$, are the number of pixels counted as corresponding to each colour region in the above described configuration. In order to compare the feature vectors computed for two images I^1 and I^2, we used as a distance the sum of the absolute differences of these feature vectors:

$$d(I^1, I^2) = d(F^1, F^2) = \sum_{i=1}^{96} \left| n_i^1 - n_i^2 \right| \tag{2}$$

A small value of the distance ***d*** means images I^1 and I^2 are similarly close to each other from their colour composition point of view.

3 Experimental Results

In order to assess the performances of our colour feature vector, we performed extensive trials on the known reduced Corel database that consists of 1,000 colour images, grouped in 10 classes of 100 images of the same dimension: 384×256 pixels or 256×384 pixels, with 24 bits allocated for each RGB coded pixel. The images are conveniently numbered from 0 to 999. While each class of images has a specific theme, from the colour point of view they are not so homogenous. With this simple colour feature vector we have obtained better results in retrieving similar images than those obtained with our previous colour feature vectors. However, running tests on

the whole Corel database is not as significant as running tests on some images where the colour content matter the most. And for this purpose we selected the class of images depicting roses, numbered from 600 to 699. Normally each image presents only one rose in the center of the image on some dark background. There are also some images with several roses and the backgrounds may differ from one image to another. So, we make the colour of roses even more important by taking into account only the center of each image, an area of 144×96 pixels, or 96×144 pixels, depending on the initial orientation of the image.

With this arrangement of 100 centers of the original images as input image files, we extracted the feature vectors and computed the distance between all the possible pairs of images and then, for each image, we have retrieved the five closer images. Figure 3 shows several examples of retrieved images and we can see that the computed distance between images, based on our simple colour feature vector, works very well in finding similarly coloured images.

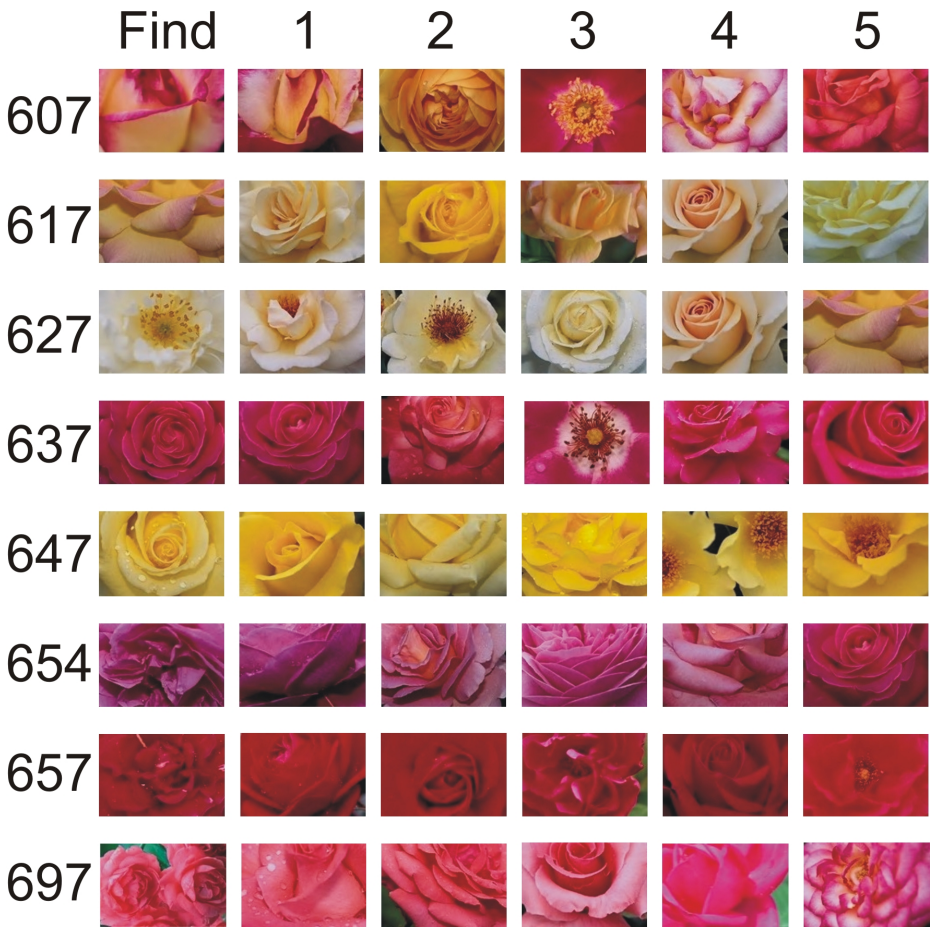

Fig. 3. Examples of images retrieval

Moreover, we wanted to see how this colour similarity distance performs in the case of a classification task. We used an agglomerative hierarchical algorithm [6] to classify the 100 images ($\boldsymbol{I^1}$, $\boldsymbol{I^2}$, …, $\boldsymbol{I^{100}}$) of roses based on our colour feature vector and its associated sum of absolute differences distance. Image $\boldsymbol{I^1}$ corresponded to image file 600 in the Corel database, image $\boldsymbol{I^2}$ to image file 601 and so on up to $\boldsymbol{I^{100}}$ that corresponded to image file 699. The following steps were taken:

1. Initially, we had $\boldsymbol{m}$ = 100 clusters, which were represented by the colour feature vector of each rose image

$$C_1 = \{ F(I^1)\},..., C_{100} = \{ F(I^{100})\} \tag{3}$$

2. The overall minimum distance $\boldsymbol{d_{min}}$ between the 100 initial clusters is then found by inspecting the table with all the distances between the rose images. Then the two initial clusters C_i and C_j ($i < j$) that correspond to that minimum distance are merged into cluster C_i and the cluster C_j is emptied, so that we remain with only $\boldsymbol{m}$ = 99 clusters.

$$dist(C_i, C_j) = d_{min} \Rightarrow C_i = C_i \cup C_j, C_j = \phi \tag{4}$$

3. Now, we recomputed the distances between the remaining clusters with the following formula:

$$dist(C_i, C_j) = \frac{\sum_{x \in C_i} \sum_{y \in C_j} d(x, y)}{card(C_i) \cdot card(C_j)} \tag{5}$$

where $\boldsymbol{x}$ and $\boldsymbol{y}$ are colour feature vectors for the images in clusters $\boldsymbol{C_i}$ and $\boldsymbol{C_j}$, $\boldsymbol{d}$ is computed according to (2), and $\boldsymbol{card(C_i)}$ represents the cardinality of the cluster $\boldsymbol{C_i}$, i.e. the number of colour feature vectors in that cluster at a given iteration. The minimum distance is again computed with:

$$d_{min} = \min_{i \neq j \in [1,m]} dist(C_i, C_j) \tag{6}$$

and the move (4) is again applied, reducing the number of remaining clusters to $\boldsymbol{m}$ - 1.

The step 3 can be repeated several times, for instance until a specific number of clusters is reached. However, we were very much interested how the clusters are developing and we followed the algorithm step by step. Figure 4 shows the situation when 34 clusters were reached.

11	600	636	628	605	614	649	615	633	666	619	631	0	0	0
6	601	610	657	667	616	678	0	0	0	0	0	0	0	0
14	602	621	691	653	603	630	608	626	639	643	634	669	673	696
3	604	627	642	0	0	0	0	0	0	0	0	0	0	0
1	606	0	0	0	0	0	0	0	0	0	0	0	0	0
2	607	655	0	0	0	0	0	0	0	0	0	0	0	0
7	609	623	647	670	658	644	641	0	0	0	0	0	0	0
2	611	617	0	0	0	0	0	0	0	0	0	0	0	0
1	612	0	0	0	0	0	0	0	0	0	0	0	0	0
6	613	645	674	665	693	695	0	0	0	0	0	0	0	0
6	618	624	629	659	620	650	0	0	0	0	0	0	0	0
5	622	660	664	668	661	0	0	0	0	0	0	0	0	0
2	625	685	0	0	0	0	0	0	0	0	0	0	0	0
2	632	638	0	0	0	0	0	0	0	0	0	0	0	0
1	635	0	0	0	0	0	0	0	0	0	0	0	0	0
2	637	663	0	0	0	0	0	0	0	0	0	0	0	0
2	640	654	0	0	0	0	0	0	0	0	0	0	0	0
3	646	648	697	0	0	0	0	0	0	0	0	0	0	0
2	651	689	0	0	0	0	0	0	0	0	0	0	0	0
3	652	677	690	0	0	0	0	0	0	0	0	0	0	0
1	656	0	0	0	0	0	0	0	0	0	0	0	0	0
1	662	0	0	0	0	0	0	0	0	0	0	0	0	0
2	671	684	0	0	0	0	0	0	0	0	0	0	0	0
2	672	681	0	0	0	0	0	0	0	0	0	0	0	0
1	675	0	0	0	0	0	0	0	0	0	0	0	0	0
2	676	680	0	0	0	0	0	0	0	0	0	0	0	0
1	679	0	0	0	0	0	0	0	0	0	0	0	0	0
2	682	687	0	0	0	0	0	0	0	0	0	0	0	0
2	683	694	0	0	0	0	0	0	0	0	0	0	0	0
1	686	0	0	0	0	0	0	0	0	0	0	0	0	0
1	688	0	0	0	0	0	0	0	0	0	0	0	0	0
1	692	0	0	0	0	0	0	0	0	0	0	0	0	0
1	698	0	0	0	0	0	0	0	0	0	0	0	0	0
1	699	0	0	0	0	0	0	0	0	0	0	0	0	0

Fig. 4. The formation of clusters when only 34 were reached (first column gives the number of images in one cluster and then the file names of the images contained in each cluster are listed)

We stopped the iterations when 17 clusters remained because we considered the result sufficiently good to demonstrate the capabilities of classification for our simple colour feature vector (see Figure 5)

11	600	636	628	605	614	649	615	633	666	619	631	0	0	0
14	601	610	657	667	616	678	688	618	624	629	659	620	650	662
14	602	621	691	653	603	630	608	626	639	643	634	669	673	696
6	604	627	642	625	685	656	0	0	0	0	0	0	0	0
10	606	646	648	697	613	645	674	665	693	695	0	0	0	0
4	607	655	612	635	0	0	0	0	0	0	0	0	0	0
7	609	623	647	670	658	644	641	0	0	0	0	0	0	0
4	611	617	692	698	0	0	0	0	0	0	0	0	0	0
12	622	660	664	668	661	640	654	637	663	652	677	690	0	0
2	632	638	0	0	0	0	0	0	0	0	0	0	0	0
4	651	689	683	694	0	0	0	0	0	0	0	0	0	0
2	671	684	0	0	0	0	0	0	0	0	0	0	0	0
2	672	681	0	0	0	0	0	0	0	0	0	0	0	0
2	675	679	0	0	0	0	0	0	0	0	0	0	0	0
2	676	680	0	0	0	0	0	0	0	0	0	0	0	0
3	682	687	699	0	0	0	0	0	0	0	0	0	0	0
1	686	0	0	0	0	0	0	0	0	0	0	0	0	0

Fig. 5. The formation of clusters when we stopped the iterations and 17 clusters were formed

The obtained classification is presented in Figure 6, where we concatenated the image files that correspond to file numbers in Figure 5. Here we show the entire rose images, although overlapped, but one must keep in mind that the features were taken only for their central part, as mentioned above.

Fig. 6. Example of rose categorization

We can see that we obtained 5 large classes, two of them with 14 images (nuances of red roses), and three of them with 12, 11 (nuances of pink roses) and, respectively 10 images (nuances of orange roses). There are two other relevant clusters with 7 and 6 images for white and, respectively, yellow roses. And there are some small clusters, which would probably attach to one of the big clusters if we would not have stopped the iterations. There is only one image that didn't cluster at all, and it is very different from the others, which is a good result, too. Notice that the clusterization is done only by colour, different petal types of roses getting together in the same class because of their similar colour. Probably, a supplementary stage of texture classification would give good results in identifying the same species of roses.

4 Conclusion

We introduced in this paper a simple colour feature vector based on processing images in the LAB colour format. After converting images from the usual RGB format in the CIELAB format, the features are obtained just by counting the number of pixels in the images belonging to some specific ranges of colour, so the computation burden is low. Also, the relatively reduced number of components, only 96, make this colour feature vector feasible to be used with very large databases of images. We presented some interesting experimental results showing the good capabilities of this colour feature vector when used for the tasks of retrieving similarly coloured images or even classifying them on the base of their colour content.

Further research will be done for preprocessing images in the LAB format and make a selection of the most important colour pixels to be counted, in order to obtain an even more characteristic feature vector.

References

[1] Jain, A.K.: Fundamentals of Digital Image Processing. Prentice-Hall International, Inc. (1989)
[2] Fairchild, M.D.: Color and Image Appearance Models. Color Appearance Models, pp. 340–385. John Wiley and Sons (2005)
[3] Ciobanu, A., Costin, M., Barbu, T.: Extraction of main colors from a digital color image. In: Proceedings of the International Multidisciplinary Scientific Geo-Conference SGEM 2010, Albena, Bulgaria, June 20-25, vol. 1, pp. 1069–1076 (2010)
[4] Ciobanu, A., Costin, M.: Improved Color Analysis and Feature Extraction Method for Digital Images. In: 6th European Conference on Intelligent Systems and Technologies, ECIT 2010, Iasi, Romania (October 2010)
[5] Barbu, T., Ciobanu, A., Costin, M.: Unsupervised Color-Based Image Recognition using a LAB Feature Extraction Technique, Buletinul Institutului Politehnic Iaşi, Universitatea Tehnică "Gheorghe Asachi", Tom LVII (LXI), Fasc. 3, Secţia Automatică şi Calculatoare (2011)
[6] Kanungo, T., Mount, D.M., Netanyahu, N.S., Piatko, C.D., Silverman, R., Wu, A.Y.: An Efficient K-Means Clustering Algorithm: Analysis and Implementation. IEEE Trans. on Pattern Analysis and Machine Intelligence 24(7), 881–892 (2002)
[7] Sonka, M., Hlavac, V., Boyle, R.: Image Processing, Analysis, and Machine Vision. International Student Edition, Thomson (2008)
[8] Schettini, R., Ciocca, G., Zuffi, S.: Indexing and Retrieval in Colour Image Databases. In: Lindsay, W., RonnierLuo, M. (eds.) Indexing and Retrieval in Colour Image Databases. ch. 10, pp. 183–213. John Wiley & Sons, England (2002)

Some Results on Ultrasonic Image Generation with Biomimetic Sonar Head and Focused Narrow Beams

Dorel Aiordachioaie and Laurentiu Frangu

"Dunarea de Jos" University of Galati, Galati, Romania
Electronics and Telecommunications Department, Domneasca-47, Galati-800008
Dorel.Aiordachioaie@ugal.ro

Abstract. Airborne ultrasonic images are not often used in practice, mainly because of the poor propagation properties (high absorption) of ultrasonic waves and necessary high computation resources. The paper presents preliminary results of ultrasonic image generation and processing system by a biomimetic sonar head and narrow beams focused on target. The images are generated by a discrete and uniform exploring approach, i.e. the environment is uniformly scanned. Experiments were conducted for 11 cases, based on the combination of 3 main objects, and various image resolutions, 20x20 and 40x40. The objective of the experiments was to estimate the complexity of the ultrasonic image generation method, provided the final purpose, i.e. the recognition of the objects in the image. The results are encouraging and suggest optimization of the proposed method.

Keywords: ultrasonic signals, image, detection, signal processing, pattern recognition, sonar.

1 Introduction

Ultrasonic imaging means 2D or 3D representation of the environment, based on ultrasound waves. An element of the image (which could be assimilated as pixel) has an intensity proportional to the amplitude of the received signals, which is in turn reflected by the surface of the objects from the explored environment.

The modern way to generate ultrasonic images is to use array of ultrasound sensors, as described, e.g. by [1] to [4]. This solution requires high power signal processors, is expensive, and quite complex. Solutions based on discrete sensors are more suitable from the cost point of view and for simple applications. The approach of obtaining ultrasonic images by discrete composition (i.e. pixel by pixel) is not new. The major drawback is the necessary processing time to obtain the ultrasonic signals, considering that an echo is associated with a pixel. More, the missing of high spatial selective (narrow beam) ultrasonic transducers generates uncertainty in the exact localization of the reflecting surface, and thus uncertainty in ultrasonic images. Details and solutions can be found in [5] or [6].

The generation of airborne ultrasonic images is a challenge, the scientific literature and practical experiments are almost missing. This paper uses a simple method for

V.E. Balas et al. (Eds.): Soft Computing Applications, AISC 195, pp. 595–604.
springerlink.com

obtaining ultrasonic sonar images (in air), under the objective of object (target) detection and classification.

This is a third paper, which considers ultrasonic images, and uses a biomimetic sonar head (described in [7]). Paper [8] presents the results of ultrasonic images using ordinary sensors, with wide beam of directivity. Paper [16] explores the case of narrow beam for ultrasound transducers, when these are oriented on the same direction as the transmitter. On the contrary, the solution adopted in this work uses beams focused on the target. The rationale of this is on expectation of higher details of target's surface and higher amplitude of the received signals, comparing with the two previous works.

The bio-mimetic sonar head (ROVIBAT-01, which stands for **RO**manian **VI**rtual **BAT**) works on fixed frequency (40 kHz) with discrete ultrasonic sensors. Literature of robotics and target recognition based on sonar present some biomimetic sonar heads, similar to this one, e.g. [9], [10] and [11], but none of them uses a specialized signal processing module, part of the sonar head, neither do they aim at image generation and processing.

This work presents preliminary results from sonar ultrasonic image processing system working on fixed frequency and a biomimetic structure of the sonar head with one emitter and two receivers. The receivers' directivity is narrow and the receivers' beams are focused on the target. Section 2 describes the experiments, section 3 introduces the identification algorithm of the transmitted ultrasonic signal, and section 4 presents the proposed method for ultrasonic image generation. Finally, the results are compared and main conclusions are drawn.

2 Description of the Experiments

The biomimetic structure of the sonar head was considered and used in experiments for ultrasonic image generation. The bio-mimetism is referring to the structure (one transmitter plus two independent receivers) and behavior (the degrees of freedom at the level of receiving transducers and sonar head).

The structure of the sonar system has: (1) the sonar electro-mechanic head, which is a mechanical structure composed of bearings and servomotors; (2) a position control module (board), performing the synthesis of the driving signals necessary to reach the imposed orientations; (3) the signal processing module (board), performing the initial signal processing functions, i.e. filtering, sampling, synchronous (parallel) conversions, and synthesis of the emitted signal for various tasks (exploration, detection, recognition, navigation, etc.). The signal acquisition board performs simultaneous acquisition of four signals at a rate of maximum 2 MSPS and 12 bit resolution. The sonar head is connected to a standard computer for coordination and supervised control. More details are presented in [7].

Horizontal reflectors are attached to ultrasound receivers and have a special shape (parabolic like), which allow a narrower width of the main lobe in the directivity pattern, approx. 7 degrees at –3dB. More details on design, measuring and performances of the selective shapes (pinnae) are presented in [12] and [13].

In the paper we suppose that an obstacle was already detected, and then the range and direction were estimated, in a separate process (task), using the sonar head and one of the multiple methods available, as described e.g. in [14] or [15]. The task described in the paper concerns the generation of an image of that particular obstacle, for recognition purposes. Fig. 1 shows a diagram presenting the wide beam of the transmitter (T) related to the narrow beams of the two receivers (R_1– left and R_2– right). The receivers are focused on the target, then the sonar head explores the directions around the target, in order to build an image, detailed as possible.

The objective of the experiments was to evaluate the complexity of ultrasonic images generation process using a set of three different objects (targets) as: (1) a ball of 18 cm diameter; (2) - a rectangular box (cube); (3) – a polyhedron. The objects are presented in Fig. 2. It should be mentioned that they are difficult objects in any recognizing process. Table 1 presents the configuration of the 11 experimental cases for image generation.

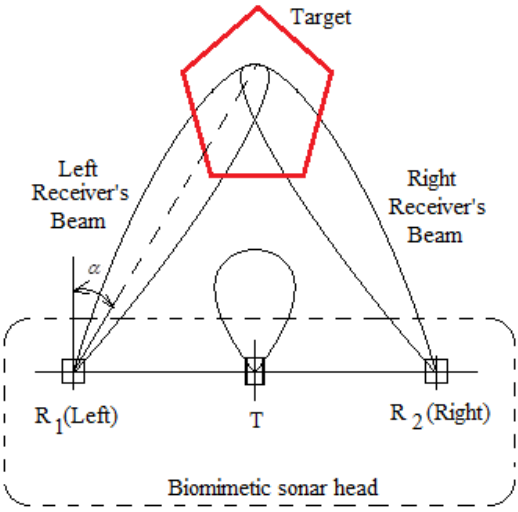

Fig. 1. Schematic on directivity of ultrasonic transducers

Fig. 2. Objects under study: polyhedron, ball, and box

Table 1. Details of the experiments

Case	Target	Image size *nxn* [pixel]	Obs.
1.	Ball	20 x 20	18 cm diameter
2.	Edge box	20 x 20	19.5 cm edge
3.	Front box	20 x 20	19.5 cm edge
4.	Ball	40 x 40	18 cm diameter
5.	Edge box	40 x 40	19.5 cm edge
6.	Front box	40 x 40	19.5 cm edge
7.	Ball + edge box	40 x 40	Same plane
8.	Ball + front box	40 x 40	Same plane
9.	Big size polyhedron	20x20	Hexagonal faces; edge of 11 cm
10.	Big size polyhedron	40x40	
11.	Small size polyhedron	20x20	Hexagonal faces; edge of 6 cm
12.	Small size polyhedron	40x40	

The sampling frequency was 1 MHz and the distance to targets was 0.85 m. The 3D data has $N = 8192$ frames (corresponding to the N samples of the received signal), each frame with n lines and n columns (corresponding to the nxn directions of the exploration). Five experiments considered 20x20 pixels, the others used a 40x40 pixel resolution. The exploring time window is 18.2 ms, which corresponds to a maximum range of R=3.1 m. The exploring parameters for a single image range as follows: azimuth $\pm 20^0$ and elevation $\pm 40^0$, both centered on target's direction.

3 Identification of Transmitted Signals

Time delay estimation and image generation processes need the transmitted signal (the pressure signal at the output of the ultrasonic transmitter), which can be obtained from measured or simulated data. Because measurement data are not always available, a simple identification procedure was used for the transmitted signal. The model for signal identification (modeling+ parameter estimation) is presented in Fig.3. At the transmitter stage, TR, the input is a voltage signal composed of pulses, *i(t)*, and the output is the ultrasonic signal pressure, *x(t)*. The (measurement) channel is free of obstacles and has a very short length, e.g. 1-2 cm. Thus, the effects of the channel on the measurement chain can be neglected.

Both transducers, at the transmitter and receiver stages, have a resonant behavior modeled by a transfer function

$$H(s) = \frac{K \cdot s}{T^2 s^2 + 2T\xi \cdot s + 1} \tag{1}$$

where the parameters are T=0.025/2/pi [ms] (corresponding to a free oscillation frequency of 40 kHz), the attenuation constant ξ=0.02, and K=0.5e-6 is a conversion factor from the derivative of the voltage to the acoustic pressure.

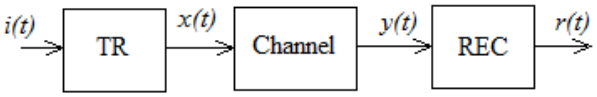

Fig. 3. The structure for signal identification

The model (1) was converted to discrete-time, by using Tustin method and a sampling frequency of Fs=1 MHz, and next simulated. The used discrete-time model is

$$H(z^{-1}) = \frac{0.1579 \cdot 10^{-7} \cdot (1 - z^{-2})}{1 - 2z^{-1} + z^{-2}} \tag{2}$$

As an example, Fig. 4 presents a set of the involved signals. The simulated signal *x(t)* (left) and a measured signal *r(t)* (right) are displayed. Simulation proves to be close to the measured signal.

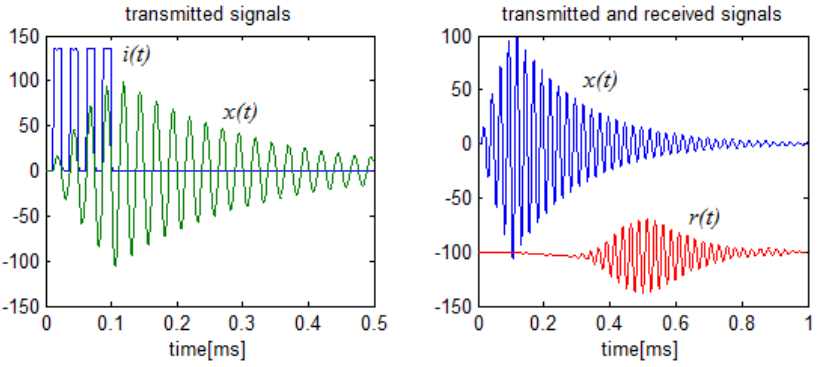

Fig. 4. Example of the involved (transmitted and received) signals

4 Ultrasonic Image Generation

Image generation is made element-by-element technique, uniformly exploring the environment around the direction where the obstacle is located. Exploring means pulse transmission plus waiting and storage of received echoes during a fixed time

window. The intensity of each pixel is associated with the amplitude of the echo received from the corresponding direction.

The set of resulted frames can be described by a 3D function

$$I = I(r, \theta, \varphi) \tag{3}$$

where r is the range to target, θ and φ are angular coordinates (azimuth and elevation), and I means the intensity. Knowing that the distance D to the obstacle was already estimated, only a small set of frames are useful for the recognition task, i.e. values of r around the distance D.

Fig. 5 presents the main computation blocks of the used method to obtain the ultrasonic images. Each explored direction is described by the pair of coordinates x and y (corresponding to desired azimuth and elevation), each from the set of {1, 2,…, 20} or {1, 2,…, 40}. The computation of the proper values for x and y and the correct positioning of the transducers are the tasks of the position controller and electrical drives of the sonar head. The orientation of each receiver, as described in figure 2, is computed as follows:

$$\alpha = \tan^{-1}\left(d/2D\right) \qquad \text{[rad]} \tag{4}$$

where d is the distance between the receivers.

A small number of impulses start the acquisition process. The number of pulses depends on the distance to the target and it is chosen prior to the experiment, to avoid a small energy of the transmitted signals (as effect, a low amplitude echo signal) or – in the opposite case – the saturation of the final linear amplifiers. The received signals, $L_{xy}(t)$ and $R_{xy}(t)$, are band pass filtered and amplified (signal conditioning). For each signal a set of N=8192 samples are recorded.

By software implementation, the cross correlation between transmitted, $s(t)$, and received signal, $r(t)$, is estimated and, next, envelope detection is performed by using the Hilbert transform:

$$R_{rs}(\tau) = E\{r(t) \cdot s(t+\tau)\} \tag{5}$$

$$s_h(t) = Hilbert\{R_{rs}(\tau)\} \tag{6}$$

$$ENV(t) = |s_h(t)| \tag{7}$$

where the envelope signal is considered for all points of the explored grid defined by θ and φ. The total number of envelopes is imposed by the resolution of the grid, i.e. *lines* x *columns*.

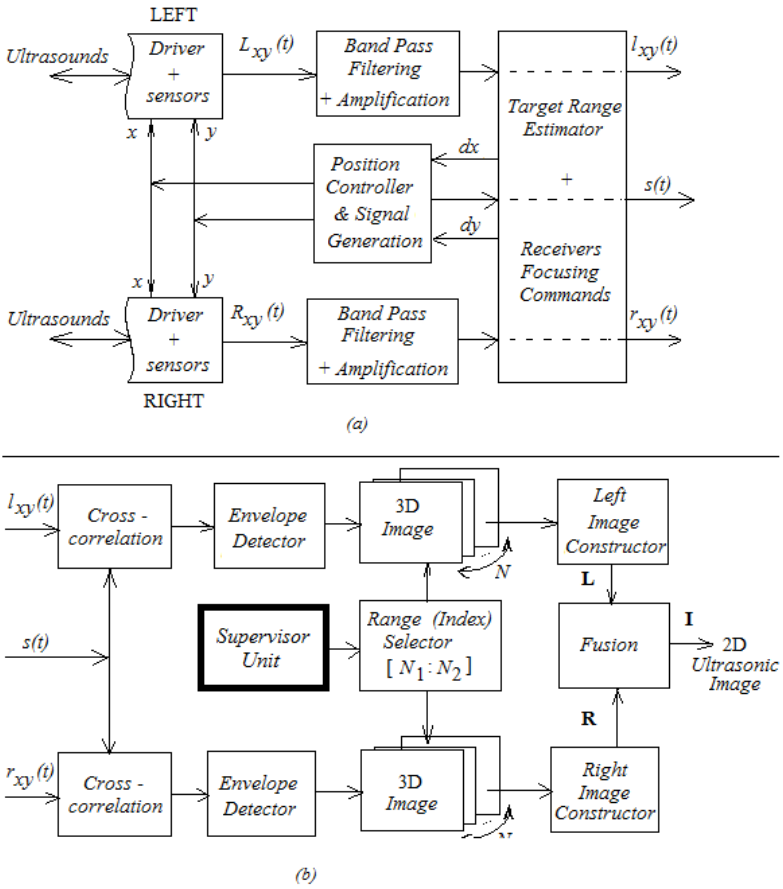

Fig. 5. The structure of the ultrasonic image generation process: (a) acquisition and (b) processing

The signal processing sequence may continue with two sets of algorithms, according to the objective of the sonar sensing: detection or recognition. The supervisory unit decides which one is active. If the objective is the detection of the obstacles, the processing algorithm explores the 3D image, detects the large values of the intensity, measures the distances to the obstacles and estimates their sizes. This variant is not considered here.

If the objective is the recognition of the obstacles, we suppose that distance D is known and the orientation of the receivers, during the exploration, was maintained to the value of eq. (4). The system has to build a single 2D image of the environment, around the distance D. In this respect, the two images (left and right), are the outputs of an image constructor block, which starts from the envelopes introduced by eq. (7). It searches and retains the local maximum value of envelopes on each direction, among the frames with indexes from N_1 to N_2:

$$\mathbf{I}_{nxn} = \left\{ I(i,j), i, j = \overline{1,n} \right\} = \max \left\{ ENV(i,j,k), k = \overline{N_1, N_2} \right\} \quad (8)$$

assuming the index of the frame corresponding to the distance D is placed between N_1 and N_2. The final ultrasonic image is obtained by fusion from the set of two available images, i.e. left and right. This final image has the same size as the left and right and gray levels with eight bpp (bit per pixel). At this stage of the method, the fusion block performs image registration only (shifting and weighted averaging).

Some results from the set of ultrasonic images are presented in Fig. 6. For each case, three images are presented: left, right and the final image obtained by fusion.

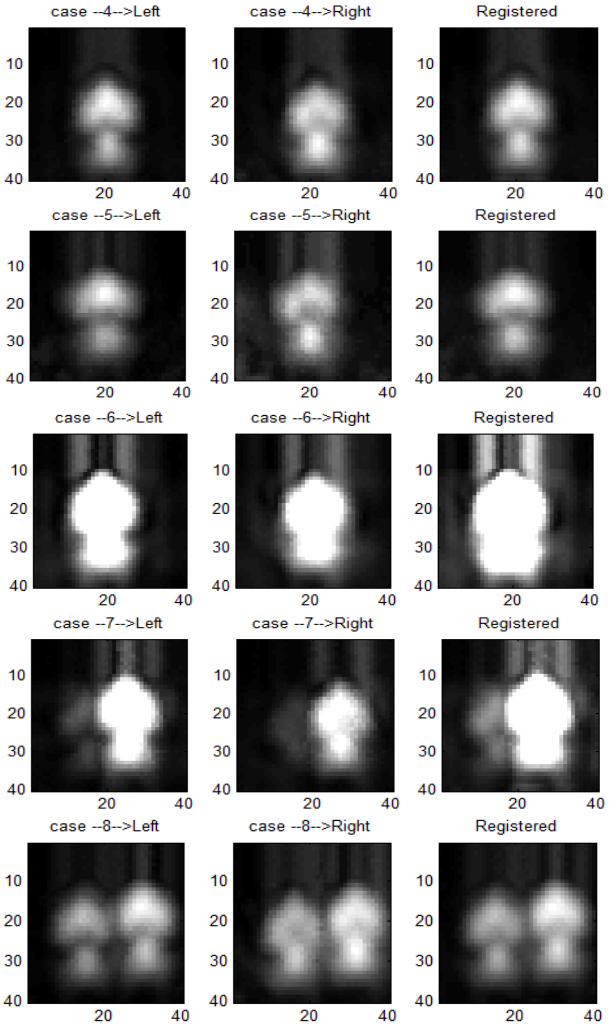

Fig. 6. Examples of the processed ultrasonic images (with reference to Table 1)

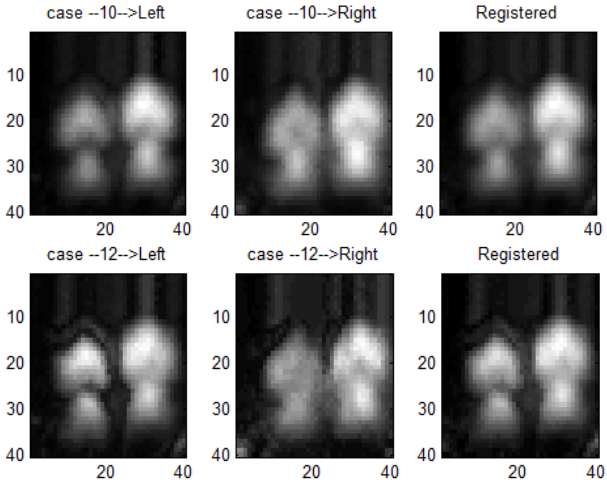

Fig. 6. (*continued*)

The images are not very close to the shape of real objects. This is an expected result because the explored objects are quite similar and the images are the first step of processing: raw generation. The next is related to image processing, e.g. filtering, enhancement.

The obtained set of images imposes the use of complex algorithm for classification. It could use the intensity of the image and the distribution of the intensity on image (i.e. the gradient). For example, the image associated to the ball (case 4) has a high gradient in the area of pixels with high values comparing with the image associated with a frontal box (case 6).

All images have artifacts, a "shadow" like at the bottom of each image. This is an effect of the directivity on the vertical plane, which have two asymmetric main lobes. Further steps of image processing can compensate the effect.

5 Conclusions

Preliminary results of airborne ultrasound image processing were presented and discussed. The objective of the study was to evaluate the discrete methodology for generation of low-resolution ultrasonic images (with fixed working frequency) able to be used for simple target classification algorithms. The obtained images are not very close to the shape of explored objects, but provide enough information for object detection and classification.

The proposed method is general, simple, and close to the used structures in sonar, but has (particular) features, e.g. fusion of left and right images. This is the first step, the raw image generation. The second step, which is not considered here, is called image processing and will contain methods to improve the quality of images.

An important cross point for target and texture recognition based on ultrasonic images, and which will be considered in the next immediate future, will be the

elaboration and the fusion of the ultrasonic images obtained with different working frequencies, e.g. 40, 100, and 150 kHz. More effort must be oriented to the optimization of the image generation process, by considering random exploration and generation, in direction of decreasing of the computation time.

References

[1] South, H.M., et al.: Technologies for sonar processing. John Hopkins APL Technical Digest 19(4), 459–469 (1998)
[2] Jensen, J.A., et al.: Synthetic aperture ultrasound imaging. Ultrasonics 44, e5–e15 (2006)
[3] Jensen, J.: Ultrasound Imaging and its Modelling. In: Fink, et al. (eds.) Imaging of Complex Media with Acoustic and Seismic Waves, vol. 84, pp. 135–165. Springer (2002)
[4] Ossant, F., Poisson, G., Tran-Huu-Hue, L.P., Roncin, A., Lethiecq, M.: Airborne ultrasonic imaging system for parallelepipedic object localization. IEEE Trans. on Instrumentation and Measurement 45(1), 107–111 (1996)
[5] Smith, R.C., Cheesemna, P.: On the representation and estimation of spatial uncertainity. The International Journal of Robotics Research 5(4), 56–68 (1986)
[6] Ribo, M., Pinz, A.: A comparison of three uncertainity calculi for building sonar-based occupancy grids. Robotics and Autonomous Systems 35, 201–209 (2001)
[7] Mazarel, M., Epure, S., Chiculita, C., Miholca, C., Aiordachioaie, D.: On biomimetic sonar head. Hardware description and analysis. In: The 6th IEEE Int. Symp. for Design and Technology in Electronic Packaging (SIITME 2010), Pitesti, Romania, September 23-26 (2010)
[8] Aiordachioaie, D., Frangu, L.: Some results on low resolution airborne ultrasonic image generation and processing. In: The IEEE International Symp. on Signal Processing and Information Technology (ISSPIT 2011), Bilbao, Spain, December 14-17, pp. 434–439 (2011)
[9] Peremans, H.: CIRCE project, Univ. of Antwerp, Belgium (2005), http://www.ua.ac.be/main.aspx?c=.APL&n=40656
[10] Hallam, J.: ChiROPing project, University of Southern Denmark (2012), http://www.chiroping.org/
[11] Muller, R., Kuc, R.: Biosonar-inspired technology: goals, challenges and insights. Bioinspiration & Biomimetics 2, 146–161 (2007)
[12] Carmena, J.M., Kampchen, N., Kim, D., Hallam, J.C.T.: Artificial ears for a biomimetic sonar head: From multiple reflectors to surfaces. Artificial Life 7(2), 147–169 (2001)
[13] Epure, S., Aiordachioaie, D.: On pinnae design and fabrication technology. In: The 17th IEEE Int. Symp. for Design and Technology in Electronic Packaging (SIITME 2011), Timisoara, Romania, October 20-23, pp. 133–136 (2011)
[14] Azaria, M., Herts, D.: Time delay estimation by generalized cross correlation methods. IEEE Trans. on ASSP 32(2), 280–284 (1984)
[15] Quazi, A.H.: Overview on the time delay estimate in active and passive systems for target localization. IEEE Trans. on ASSP 29(3), 527–533 (1981)
[16] Aiordachioaie, D., Frangu, L.: On Ultrasonic Image Generation with Biomimetic Sonar Head and Narrow Beam. In: The 9th International Conference on Communications (COMM 2012), Bucharest, Romania, June 21-23, pp. 91–94 (2012)

Using License Plates Recognition for Automate Cruise Control

Marius M. Balas, Nicolae A. Chira, Sergiu A. Matisan, and Flavius M. Suciu

"Aurel Vlaicu" University of Arad, Romania
marius@drbalas.ro

Abstract. This paper is presenting an experimental assemblage that is proving the principle of following cars by using in a new way a license plate recognition system. Once the license plate of the followed car is focused by a monoscopic CCD camera, its image is recognized and measured by pixel counting. The image's dimension is converted into a measure of the distance between the cars, while its position measures the direction. A simple model car, provided with a CCD camera, is wireless controlled by means of a laptop computer, which is running the Image acquisition Toolbox and the Video and Image Processing Blockset of Matlab Simulink. We draw some preliminary conclusions, project the final algorithm that is to be tested and discuss the future implementation of this method.

Keywords: CCD camera, automate cruise control, license plate recognition.

1 Introduction

The Automate Cruise Control ACC is a concept that aims to improve the driving performances and to reduce the crash risks [1], [2]. Besides the simple presetting of the speed when the traffic allows, one major ACC issue is to automatically follow a car that is driving in a convenient manner. Several cars running in the following mode may form large platoons. A following car must reproduce the trajectory of the followed vehicle, maintaining in the same time a desired distance between them [3]. A key problem in this issue is the online measurement and control of the distance gap between cars. A basic ACC principle is to avoid the use of any external assistance (satellite, roadside infrastructure or cooperative support from other vehicles). Hence ACC implies exclusively on-board sensors, which basically means laser or radar sensors [4]. In a previous paper (2004) it was proposed an alternative solution for the distance measurement: the use of CCD cameras, monoscopic or stereoscopic [5], afterwards discussed also in ref. [6]. This vision-based approach has obvious advantages in what concerns the costs and the clarity, but it is not reliable by itself in bad weather conditions. Here we can invoke the modern trend of the sensor and information fusion [7]. Adding a complementary vision based sensor to the existing echolocation laser or radar ones can only improve the performance and the safety of the vehicles.

V.E. Balas et al. (Eds.): Soft Computing Applications, AISC 195, pp. 605–609.
springerlink.com

New facts are encouraging this research. Since 2004 CCD and CMOS cameras have emerged in many applicative fields, and the transportation industry assimilated the *license plate recognition* LPR especially in the traffic monitoring [8].

Besides conventional LPR systems that are generally installed on highways and in traffic nodes, more and more video cameras are present on board of vehicles (targeting the front and rear sides of automobiles and also its inside). They fulfill different tasks such as obstacle and lane recognition, night vision, parking assistance or monitoring drivers and passengers.

Our intention is simply to use the information provided by the front camera for a supplementary function: the recognition and the positioning of the license plate of the followed car. Contrarily to LPR, whose prior goal is to recognize the inscriptions of the license plates, we only need to find their shapes and dimensions.

2 The Experimental Assemblage

The model car provided with a wireless control system and a monoscopic CCD camera is presented in Fig. 1.

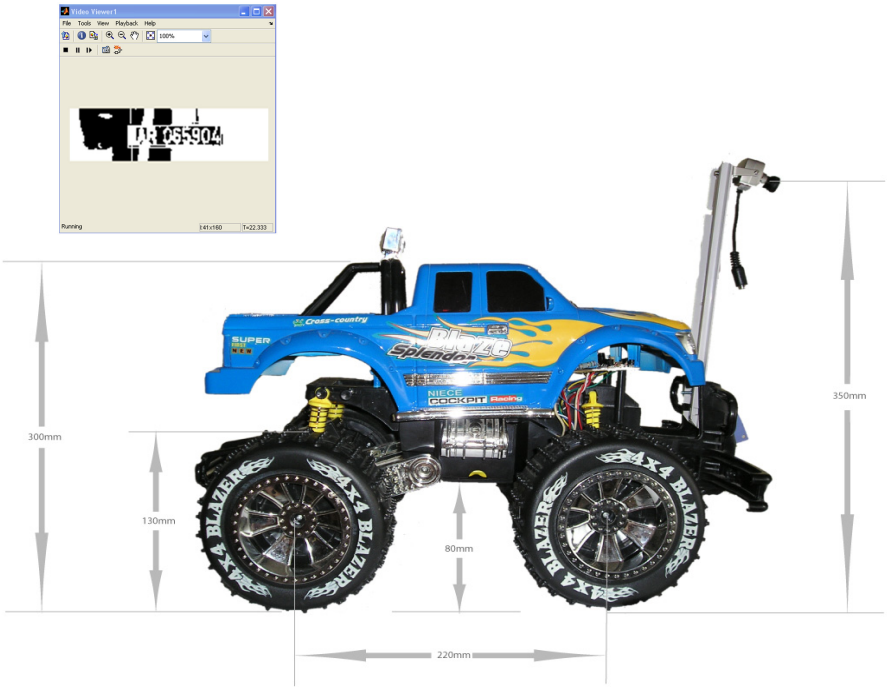

Fig. 1. The model car provided with a monoscopic CCD camera

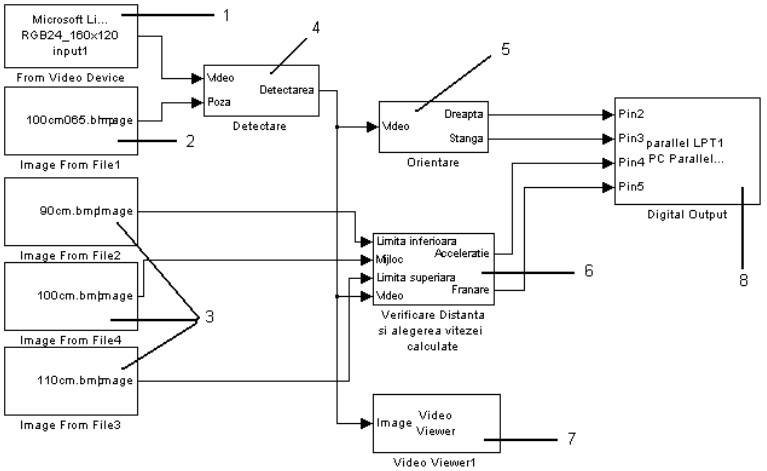

Fig. 2. The Simulink cruise control system with monoscopic CCD camera

The Simulink cruise control system is presented in Fig. 2. The main blocks of this system are the following:

1) *From Video Device* – this block is processing the signal of the video camera;
2) *Image From File 1* – the comparison image of a license plate (recognition);
3) *Image From File* 2, 3, 4 – images of the license plates from three different distances 90/100/110 cm (used for the measurement of the distance gap);
4) *Detectare* – the recognition block;
5) *Orientare* – the tracking controler;
6) *Verificare Distanta* – the distance gap controller;
7) *Video Viewer*;
8) *Digital Output* – the interface with the model car.

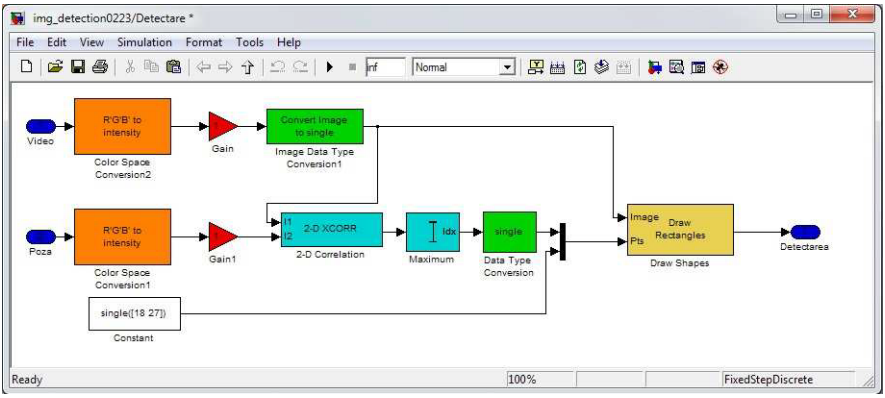

Fig. 3. The license plate recognition block

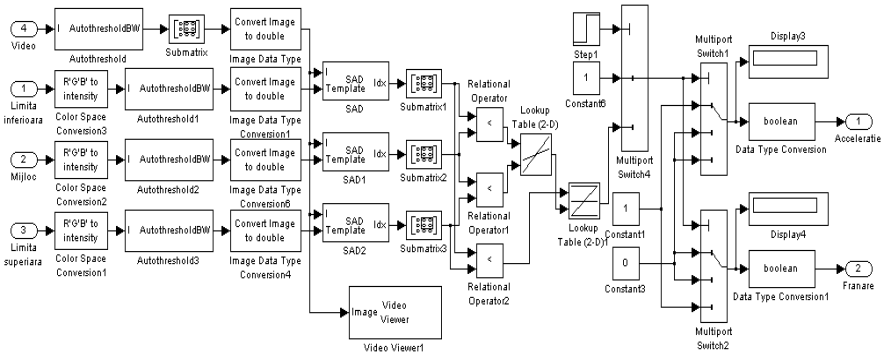

Fig. 4. The distance gap controller

3 Future Work

The key development of this work must replace the relay type controller by a fuzzy-interpolative one, using a particular speed adaptation planning. This planning connects an optimized imposed distance gap between cars $\mathbf{d_i}$ with the following car's velocity $\mathbf{v}$. A precise method for building optimized $\mathbf{d_i}(\mathbf{v})$ functional mappings may be found in ref. [9]. This mapping will be associated with the detailed curves that are capturing the image dimension vs. distance gap, which were introduced in ref. [6].

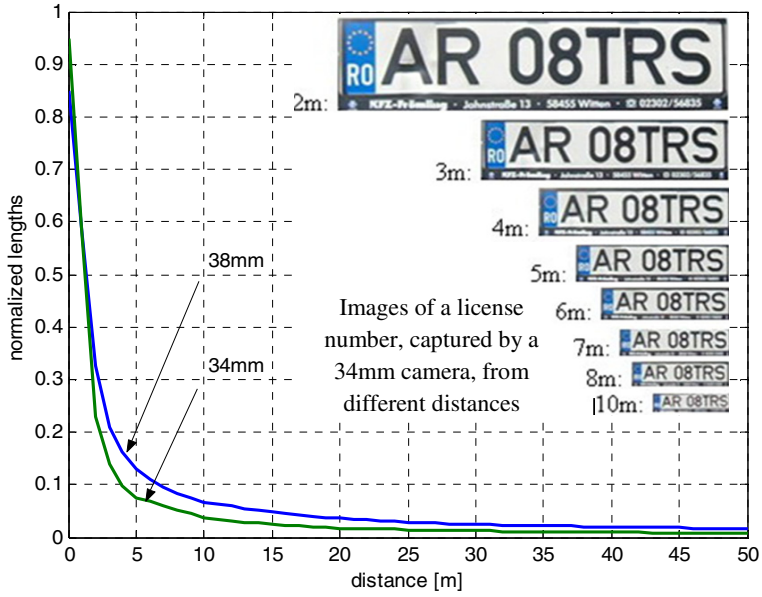

Fig. 5. The normalized graphs of the license plate image's dimensions vs. distance gap function, for two focal lengths of the CCD camera

4 Conclusions

The previous described experimental arrangement allowed us to test a generic cruise control structure that uses a single monoscopic CCD camera as distance and tracking sensor. The first positive result of such a structure, implemented in Matlab-Simulink, needs further improvements in what concerns the refinement of the algorithms and the optimization of the architecture, in order to increase the reliability and the speed of the performance (the time delays are exceeding one second for the time being).

So far the image recognition stage is performed for a single license plate, using only implicit Simulink resources (Image acquisition Toolbox and Video and Image Processing Blockset) although the recognition of the characters is not necessary for our method, which is one of the causes for the great time delay.

For the moment the system is working by imposing a constant distance gap **d** of 100 cm between cars, using a simple relay distance controller. The hysteresis of the relay's characteristics is set between 90 and 110 cm.

The choice of Matlab Simulink for the algorithm development stage is natural; even its rather slow operation is advantageous because it is helping us to estimate easier the time delays introduced by the diverse components of the algorithms. We envisage a final FPGA implementation.

References

1. Girard, A.R., Borges de Sousa, J., Misener, J.A., Hendrick, J.K.: A Control Architecture for Integrated Cooperative Cruise Control and Collision Warning Systems. Berkeley University of California, http://path.berkeley.edu/~anouck/papers/cdc01inv3102.pdf
2. Minderhoud, M.M., Hoogendoorn, S.P.: Extended Time-to-Collision Safety Measures for ADAS Safety Assessment. Delft University of Technology, http://www.Delft2001.tudelft.nl/paper%20files/paper1145.doc
3. Zhang, Y., Kosmatopoulos, E.B., Ioannou, P.A., Chien, C.C.: Autonomous Intelligent Cruise Control Using Front and Back Information for Tight Vehicle Following Maneuvers. IEEE Transactions on Vehicular Technology 48(1), 319–328 (1999)
4. Widmann, G.R., Daniels, M.K., Hamilton, L., Humm, L., Riley, B., Schiffmann, J.K., Schnelker, D.E., Wishon, W.H.: Comparison of Lidar-Based and Radar-Based Adaptive Cruise Control Systems. In: Delphi Automotive Systems Wishon. SAE World Congress, March 6-9 (2000)
5. Balas, M.M., Barna, C.: Using CCD cameras for the car following algorithms. In: Proc. of IEEE International Symposium on Industrial Electronics, ISIE 2005, Dubrovnik, pp. 57–62 (2004)
6. Balas, M.M., Balas, V.E.: Monoscopic CCD Cameras as Distance Sensors. In: Proceedings of the 1st International Conference on Bio-Inspired Computational Methods Used for Difficult Problems Solving: Development of Intelligent and Complex Systems. AIP Conference Proceedings, vol. 1117, pp. 67–73 (2009)
7. Murphy, R.: Sensor and Information fusion for Improved Vision-Based Vehicle Guidance. IEEE Intelligent Systems (November 1998)
8. Jiao, J., Ye, Q., Huang, Q.: A configurable method for multi-style license plate recognition. Pattern Recognition (42), 358–369 (2009).
9. Balas, M.M., Balas, V.E., Duplaix, J.: In: Proceedings of IEEE International Symposium on Industrial Electronics, ISIE 2007, Vigo, pp. 304–309 (June 2007)

Automatic Classification of Liver Diseases from Ultrasound Images Using GLRLM Texture Features

Raghesh Krishnan K.[1] and R. Sudhakar[2]

[1] Department of Information Technology, Amrita Vishwa Vidyapeetham,
Amrita Nagar – Coimbatore 641 112 – Tamilnadu – India
raghesh82@yahoo.com
[2] Department of Electronics and Communication Engineering,
Dr. Mahalingam College of Engineering and Technology,
Udumalai Road, Pollachi 642 003 – Tamilnadu – India
sudha_radha2000@yahoo.co.in

Abstract. Ultrasound imaging is considered to be one of the most cost-effective and non-invasive techniques for conclusive diagnosis in some cases and preliminary diagnosis in others. Automatic liver tissue characterization and classification from ultrasonic scans have been for long, the concern of many researchers, and has been made possible today by the availability of the most powerful and cost effective computing facilities. Automatic diagnosis and classification systems are used both for quick and accurate diagnosis and as a second opinion tool for clarifications. This paper analyzes the effect of various linear, non linear and diffusion filters in improving the quality of the liver ultrasound images before proceeding to the subsequent phases of feature extraction and classification using Gray Level Run Length Matrix Features and Support Vector Machines respectively.

Keywords: Filters, Texture, Gray Level Run Length Matrix, Classification, Support Vector Machine.

1 Introduction

The growth, accumulation and transfer of knowledge in the field of image processing in the past decade, has had tremendous impact across various disciplines. In the field of biomedical image analysis, images form the basis for identifying various pathological conditions depending upon which the medication is administered.

The advancement in physics has made possible a wide variety of medical imaging modalities such as ultrasound, x-ray, computed tomography and magnetic resonance imaging, each one having its own utility based on the pathological condition and the organ under study. Ultrasound imaging is the most common modality, widely used for the diagnosis of diseases, due to its preliminary, non-invasive, cost-effective and accurate characteristics. Automatic Classification and diagnostic systems if accurate, aid as an excellent decision support and second opinion tool for radiologists.

The critical steps for developing any classification system include pre-processing, segmentation, feature extraction and classification. The poor quality of ultrasound

V.E. Balas et al. (Eds.): Soft Computing Applications, AISC 195, pp. 611–624.
springerlink.com

image is of major concern as it is often affected by speckle noise. This paper analyzes a series of linear, non-linear and anisotropic diffusion filters to select the one that produces the best classification without any loss of useful texture and vital diagnostic information. Pre-processing is followed by feature extraction. Gray level run length matrix (GLRLM) forms the basis for feature extraction following which classification is attempted using Support Vector Machines (SVM) using the extracted features.

The paper is organized as follows. Section 2 deals with related work. Section 3 gives an overview of the proposed method and section 4 deals with filtering techniques. In Section 5, feature extraction is discussed. Section 6 deals with classification and Section 7 presents the experimental results and performance analysis. Section 8 provides the conclusions and scope for future work.

2 Related Work

Biomedical image analysis, diagnosis and classification is an area of intense research and automatic classification of liver diseases from ultrasound images is under exploration by many researchers. Ultrasound image analysis finds its most usefulness in classifying chronic liver diseases as discussed in [22]. Abou zaid Sayed Abou zaid, Mohamed Waleed Fakhr, Ahmed Farag Ali Mohamed in [2] propose an automatic liver disease diagnostic system for early detection of liver diseases. A classification is performed between normal liver, bright liver, cirrhosis and carcinoma based on ROI selected using gray level statistics. A series of feature extraction techniques and classification techniques are proposed in the literature [27].

Various combinations of noise removal, segmentation, features and classification techniques give varied results and these have been analyzed by various researches to find the best model. A combination of Gabor features, Bayes classifier, multiple ROI voting and Adaboost based learning are attempted in detecting cirrhosis in [30]. As a subset of this vast problem, the application of various filters in [5, 20, 24, 31], feature extraction in [16, 28] and classification techniques in [28] are analyzed for their utility in automatic classification of diseases from ultrasound images in the literature. This work analyzes the combination of various such techniques in classifying five types of commonly occurring liver diseases.

3 Proposed Method

The overall system architecture is divided into 5 phases as depicted in fig.1. The first phase consists of image acquisition. This phase involves acquiring images from various sources. The images used in the work were obtained from SonoScan Ultrasonic Scan Center, Sunitha Scan and Diagnostic Center and the internet. This work concentrates on five types of commonly occurring diseases such as carcinoma, cirrhosis, fatty livers, hepatitis and cystic livers for which the images are easily available. The acquired images are de-speckled and partitioned. From the partitioned image, the GLRM features are extracted and presented to the SVM for classification.

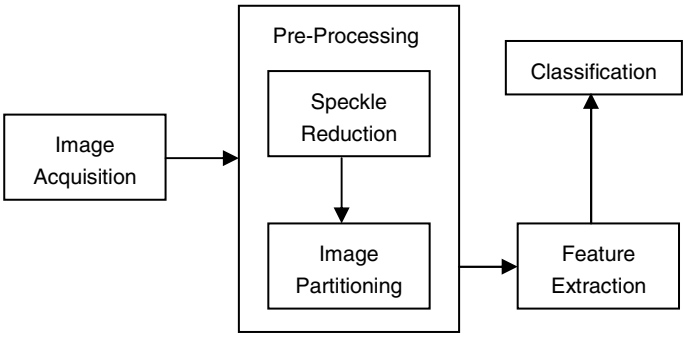

Fig. 1. System Architecture

4 Filtering Techniques

In medical imaging, the ultrasound images are obtained with the help of a probe, which introduces a granular appearance called speckle noise. Speckle noise is a multiplicative noise formed due to diffuse scattering that reduces the resolution and contrast of the image there by degrading the diagnostic accuracy of the ultrasound image. Speckle occurs when an ultrasound pulse randomly interferes with the soft organs such as liver and kidney whose underlying structures are too small to be resolved by the large ultrasound wavelength.

The speckle noise model may be approximated as multiplicative and is given by

$$f_{i,j} = g_{i,j} u_{i,j} + \alpha_{i,j} \tag{1}$$

Where $f_{i,j}$ is the noisy pixel $g_{i,j}$ represents the noise free pixel, $u_{i,j}$ and $\alpha_{i,j}$ represent the multiplicative and additive noise respectively and *i, j* are indices of the spatial locations.

De-speckling or speckle suppression is a pre-processing step for many ultrasound image processing problems. A wide variety of filters exist in the literature [1,18,19,30].This work analyzes the effect of applying select filters such as Box, Gaussian in linear filters, Min, Max, Midpoint, Median in Non Linear Order statistics filters,), Wiener Filter (Adaptive), Homomorphic Filter and Speckle Reduction Anisotropic Diffusion filters[5,6,31] on liver ultrasound images for the removal of speckle noise. The performance of these filters is measured using various statistical parameters such as Noise Mean Value (NMV), Noise Standard Deviation (NSD), and Effective Number of Looks (ENL) and also by visual quality of the images.

5 Feature Extraction

Feature Extraction is an integral part of any classification problem. The objective is to collect the measurements of various characteristics from the various portions of the

image and employ them in the subsequent phase of recognition or classification. Image textures are prominent features in ultrasound images which give information about the spatial arrangement of color or intensities in an image or selected region of an image. Generally, the texture of an image can be analyzed using two approaches namely structured approach and statistical approach [21].

Structured approach sees an image texture as a set of primitive texels in some regular or repeated pattern. This works well when analyzing for objects especially in artificial textures. Statistical approach sees an image texture as a quantitative measure of the arrangement of intensities in a region. In general this approach is easier to compute and is more widely used in analyzing ultrasound images [7, 28], since natural textures are made of patterns of irregular sub elements. Statistical approach is implemented in a number of ways. The current work makes use of local relative texture features extracted from the ultrasound medical images using the Gray Level Run Length Matrix (GLRLM) based global features proposed by Abu Sayeed Md. Sohail et.al [3]. Three - level partitioning of the image helps in capturing the local features in terms of global image properties. The absolute difference of global features of each lower layer partition sub-block and that of its corresponding upper layer partition block gives the local relative features.

Prior to the process of calculating the GLRLM, the ultrasound image is partitioned into 4^k blocks, where k is taken as 1. k is a non negative integer carefully chosen such that $k<\log_2 \min(M,N) - 1$. The partitioning continues to a next level, where $4^k/4$ blocks are formed by overlapping the every four first level blocks, adjacent to each other. The condition to form the second level blocks is that the area of the first and second levels must be equal to and also residing at the centre of intersection of first level blocks. Next level, the third level, is just the sub-partition of all the blocks formed earlier. Every block intersects horizontally and vertically at the centre such that each partition has four sub-partitions. Therefore, a three level hierarchy of partitioning applying above conditions leads to extraction of local relative feature set. Fig. 2 illustrates First and second level partitioning of an image when k=1 and third level of partitioning of an image for the block 1. After subdividing an image into several partitions, the GLRLM is computed for each of the partitions and is used in the calculation of 11 statistical features (discussed in the results) which represent the run-length features of the image.

The range of intensities in the image is sliced into 64 gray levels and run length is the maximum value among the rows and columns. Local relative difference is a measure derived from the partitions, represents the local relativity to obtain the local features set. The difference is calculated from third level partitioned sub-blocks and its next level partitioned blocks i.e. $\alpha_1(X_i)$, $\alpha_2(X_i)$, … , $\alpha_{11}(X_i)$ are features of blocks of first and second levels and $\beta_1(X_{ij})$, $\beta_2(X_{ij})$, … , $\beta_{11}(X_{ij})$ are the features of sub-blocks. Then, Local relative difference for each sub-block is

$$LRD_k^{\theta}(X_{ij}) = |\beta_k(X_{ij}) - \alpha_k(X_i)| \tag{2}$$

Here, θ takes 0,45,90,135 for run lengths, k =1,2,3,…,11, the number of features, i = 1,2,3,…,5 are the partitioned blocks of first and second levels and j = 1,2,3,…,4 are the sub-blocks of third level. Hence, 5 x 4 x 4 x 11 = 880 features are extracted for an image.

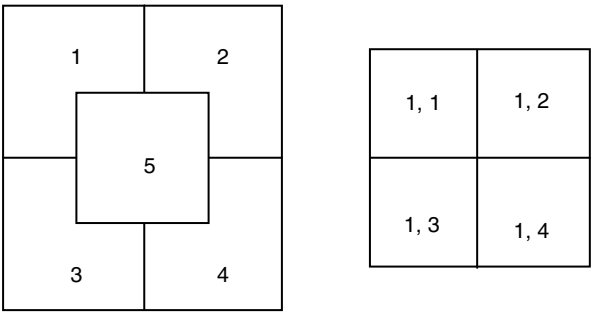

Fig. 2. Illustration of First and Second Level Partitioning

6 Classification

The classification of liver diseases is attempted using Support Vector Machine (SVM). The local relative features extracted from the GLRLM of the training dataset are used to create feature vectors which are subsequently used to train the SVM. During the testing phase for every test image, after calculating of feature vector, the feature vector is presented to the SVM for classification. If the image is normal, the diagnosis ends there. If otherwise, the feature vector is passed on to the next binary SVM classifier which differentiates between Cirrhosis and other diseases. If the classification turns out to be other disease, the feature vector is presented to the next SVM classifier which decides if the disease is hepatitis or any other disease other than cirrhosis. The process continues until the vector is classified into any one of the disease categories. Fig. 3 illustrates the training and testing phases.

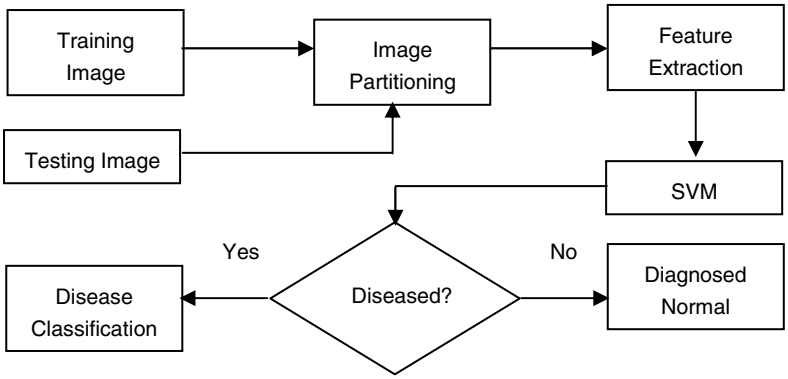

Fig. 3. Outline of Classification Stage

7 Experimental Results

The work concentrates on five commonly occurring liver diseases such as cirrhosis, carcinoma, fatty liver, haemangioma and cyst. The images have been collected from various scan centers and the internet. The dataset comprises of 100 images with 20 images in each category.

7.1 Noise Removal

Various linear and non-linear filters discussed above are applied to the image dataset and the results of speckle reduction are analyzed using statistical measures such as Noise Mean Variance, Noise Standard Deviation, and Effective Number of Looks. The definition for each measure is given below.

- *Noise Standard Deviation (NSD):* This determines the quantity of the speckle in the image. If the quantity of speckle is less, then NSD will be less. Mathematically NSD is represented as

$$NSD = \sqrt{\frac{\sum_{i=1}^{R}\sum_{j=1}^{C}(I_{d(i,j)} - NMV)^2}{R * C}} \tag{3}$$

$$NMV = \frac{\sum_{i=1}^{R}\sum_{j=1}^{C} I_{d(i,j)}}{R * C} \tag{4}$$

Where I_d is the de-speckled image and R is the row size and C is the column size of the image.

- *Equivalent Numbers of Looks (ENL):* To estimate the speckle noise level another assessment parameter known as ENL over a uniform region is used. A larger value of ENL shows a better quantitative performance. Mathematically ENL is given as

$$ENL = NMV^2 / NSD^2 \tag{5}$$

The statistical measures computed for the original and De-Noised images are given in table 1.

Some important inferences made in the study are discussed below:

- Filtering techniques such as min, max, midpoint, Gaussian, box filters are not suitable for ultrasound images because they introduce severe blurring and loss of diagnostically significant information. Min, Max and Mid-point filters distort the texture information of the liver image. Fig. 4 illustrates the effects of applying some non-linear filters on the image visually.

Table 1. Statistical measures showing filter performance

Disease	Metrics	NMV		NSD		ENL	
	Range	Min	Max	Min	Max	Min	Max
Cirrhosis	Original	55.1	65.7	9.6	9.9	31.7	43.8
	SRAD	55.1	65.7	9.6	10.3	31.7	44.1
	Homomorphic	41.9	49.8	9.6	9.8	18.7	25.9
	Wiener	55.1	65.7	9.6	10.4	31.7	43.9
	Median	55.0	65.5	9.6	10.4	31.6	43.8
Liver Cyst	Original	37.5	80.7	9.0	9.7	17.5	69.7
	SRAD	37.6	80.8	9.0	9.7	17.6	69.6
	Homomorphic	30.1	61.4	8.8	9.5	11.8	42.2
	Wiener	37.5	80.7	9.0	9.7	17.5	69.3
	Median	37.3	79.9	9.0	10.0	17.0	67.0
Carcinoma	Original	30.0	55.8	8.9	10.9	10.7	26.3
	SRAD	30.0	55.9	8.9	11.0	10.5	26.0
	Homomorphic	23.9	42.7	8.5	10.7	7.2	16.0
	Wiener	30.0	55.8	8.9	10.9	10.6	26.1
	Median	29.7	55.7	8.9	10.9	10.4	26.1
Haemangioma	Original	14.5	42.2	7.2	9.2	4.0	21.2
	SRAD	14.6	48.2	7.0	9.2	4.4	31.2
	Homomorphic	12.5	32.9	6.8	9.0	3.3	13.3
	Wiener	14.5	48.1	7.2	9.2	4.1	31.0
	Median	14.0	47.9	7.1	8.6	3.8	31.0
Fatty Liver	Original	23.8	46.5	7.3	10.3	8.7	20.2
	SRAD	23.9	46.5	7.1	10.3	8.8	20.4
	Homomorphic	19.8	36.0	6.7	10.1	5.9	12.7
	Wiener	23.8	46.5	7.2	10.4	8.7	20.0
	Median	22.9	46.2	7.4	10.4	8.4	19.8

- SRAD filter suppresses speckle in terms of lower NSD values and slightly higher ENL values from the table 1. When number of iterations exceeds 10, SRAD introduces serious blurring in the images. When the number of iterations is less than 8, there is no noticeable difference when compared to other filters. Hence the optimal number of iterations for better de-speckling is fixed to be between 8 and 10 iterations.
- Homomorphic filter flattens the speckle variance since it has low NMV and NSD values. Also the ENL values are found to be low from table 1.
- NSD values obtained for Wiener filter remain the same as that of the noisy image as observed from table 1 which indicates that it has little effect on speckle suppression. Also blurring is introduced in the image which results in loss of vital image information.

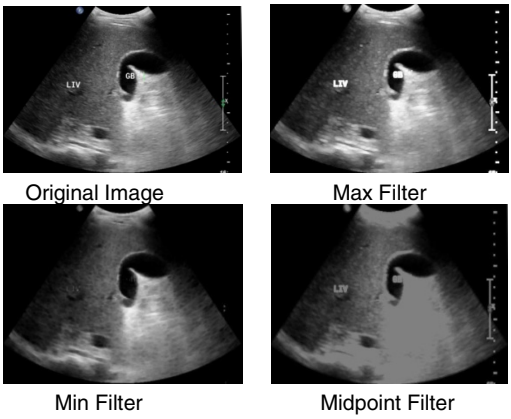

Fig. 4. Samples of Original and Non-Linear Filtered Images

Of the various filters analyzed on the ultrasound images, from the measures and visual quality of the images, SRAD was found to give better results in noise suppression.

7.2 Feature Extraction and Classification

The usage of GLRLM statistical parameters avoids image segmentation and subsequently, Region of Interest selection which is the case in conventional image processing. 880 GLRLM features are extracted from the original image and the various parameters tabulated in the table 2 are calculated. These features are then used for training the SVM. This feature extraction can be applied on segmented images to obtain a deeper understanding of the diseased portion.

Table 3 shows the 11 extracted features from the image after performing the first level of partitioning with k=1. Subsequent to classification by SVM using the feature vector set, the classification efficiency is computed by finding the number and percentage of outcomes in the form of true positives (t_p), false positives (f_p),true negatives (t_n) and false negatives (f_n). Table 4 illustrates outcome of this analysis and it is represented graphically in Fig. 5.

The overall accuracy for the whole system was calculated as the average of the accuracies measured for each disease category. Table 5 shows the overall accuracy which was found to be 92.91% approximately.

Various classification parameters such as sensitivity, specificity and accuracy were computed for the system and this is depicted graphically in Fig. 6.

Misclassification results obtained for HCC are shown in Fig. 7. Misclassification is due to the lack of proper texture content in the image, due to the dominant overlap of dark (black) regions on portions of the liver. Similarly, misclassifications of fatty liver are shown in fourth image in fig. 7. The misclassification is due to "heterogeneity" in the texture. Fig.8. shows diagnosis screen implemented using Matlab.

Table 2. GLRLM Features

S. No	Feature	Formula
1	Short Run Emphasis	$SRE = \sum_{i=1}^{G}\sum_{j=1}^{R} \frac{p(i,j\mid\theta)}{j^2} \Big/ \sum_{i=1}^{G}\sum_{j=1}^{R} p(i,j\mid\theta)$
2	Long Run Emphasis	$LRE = \sum_{i=1}^{G}\sum_{j=1}^{R} j^2 p(i,j\mid\theta) \Big/ \sum_{i=1}^{G}\sum_{j=1}^{R} p(i,j\mid\theta)$
3	Gray Level Non-uniformity	$GLN = \sum_{i=1}^{G}\left(\sum_{j=1}^{R} p(i,j\mid\theta)\right)^2 \Big/ \sum_{i=1}^{G}\sum_{j=1}^{R} p(i,j\mid\theta)$
4	Run-length Non Uniformity	$RLN = \sum_{i=1}^{R}\left(\sum_{j=1}^{G} p(i,j\mid\theta)\right)^2 \Big/ \sum_{i=1}^{G}\sum_{j=1}^{R} p(i,j\mid\theta)$
5	Run Percentage	$RP = \frac{1}{N}\sum_{i=1}^{G}\sum_{j=1}^{R} p(i,j\mid\theta)$
6	Low Gray Level Run Emphasis	$LGLRE = \sum_{i=1}^{G}\sum_{j=1}^{R} \frac{p(i,j\mid\theta)}{i^2} \Big/ \sum_{i=1}^{G}\sum_{j=1}^{R} p(i,j\mid\theta)$
7	High Gray Level Run Emphasis	$HGLRE = \sum_{i=1}^{G}\sum_{j=1}^{R} i^2 p(i,j\mid\theta) \Big/ \sum_{i=1}^{G}\sum_{j=1}^{R} p(i,j\mid\theta)$
8	Short Run Low Gray Level Emphasis	$SRLGLE = \sum_{i=1}^{G}\sum_{j=1}^{R} \frac{p(i,j\mid\theta)}{i^2 j^2} \Big/ \sum_{i=1}^{G}\sum_{j=1}^{R} p(i,j\mid\theta)$
9	Short Run High Gray Level Emphasis	$SRHGLE = \sum_{i=1}^{G}\sum_{j=1}^{R} \frac{i^2 p(i,j\mid\theta)}{j^2} \Big/ \sum_{i=1}^{G}\sum_{j=1}^{R} p(i,j\mid\theta)$
10	Long Run Low Gray Level Emphasis	$LRLGLE = \sum_{i=1}^{G}\sum_{j=1}^{R} \frac{j^2 p(i,j\mid\theta)}{i^2} \Big/ \sum_{i=1}^{G}\sum_{j=1}^{R} p(i,j\mid\theta)$
11	Long Run High Gray Level Emphasis	$LRHGLE = \sum_{i=1}^{G}\sum_{j=1}^{R} i^2 j^2 p(i,j\mid\theta) \Big/ \sum_{i=1}^{G}\sum_{j=1}^{R} p(i,j\mid\theta)$

Table 3. Features Extracted After First Level of Partitioning

Features	Block 1	Block2	Block 3	Block 4
SRE	0.3728	0.5273	0.4730	0.5257
LRE	710.7345	507.4113	583.5598	517.8796
GLN	172.7372	138.6842	158.9043	148.4437
RLN	50.8445	133.2612	87.8564	130.9881
RP	0.0485	0.0989	0.0806	0.0978
LGRE	0.6885	0.5301	0.5788	0.5477
HGRE	2891.4423	1103.9220	1740.6937	1155.7514
SRLGE	0.1129	0.1028	0.1087	0.1090
SRHGE	2889.9062	1103.0548	1739.0225	1154.7231
LRLGE	710.1630	499.4453	550.6866	513.2663
LRHGE	3605.0294	1641.1695	2498.9234	1691.0216

Table 4. Experimental Results for Possible Outcomes

Type	t_p	t_n	f_p	f_n
Cirrhosis	15	33	0	5
Cyst	16	42	0	0
HCC	6	42	3	0
Hepatitis	6	43	0	0
Fatty	5	33	3	1

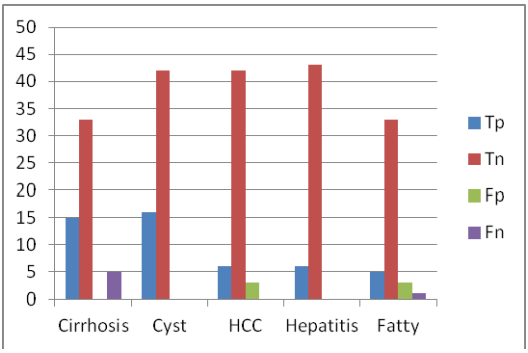

Fig. 5. Graph showing the possible outcomes for five liver diseases

Table 5. Overall accuracy of the classifier

Disease	Total Test images	Correctly classified	Sensitivity	Specificity	Accuracy (in %)	Overall Accuracy
Cirrhosis	20	15	0.75	0.894	84.17	92.91%
Fatty	17	16	0.94	0.92	92.50	
Hcc	10	6	0.60	0.937	87.88	
Cyst	6	6	1.00	1.00	100	
Hepatitis	5	5	1.00	1.00	100	

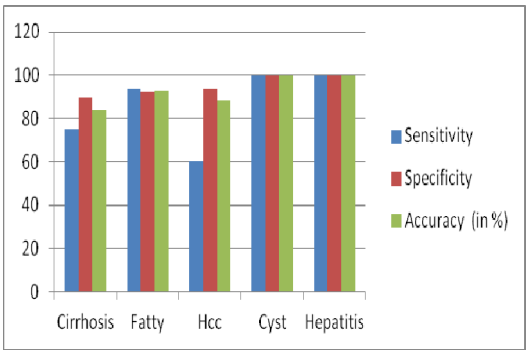

Fig. 6. Performance Analysis Graph

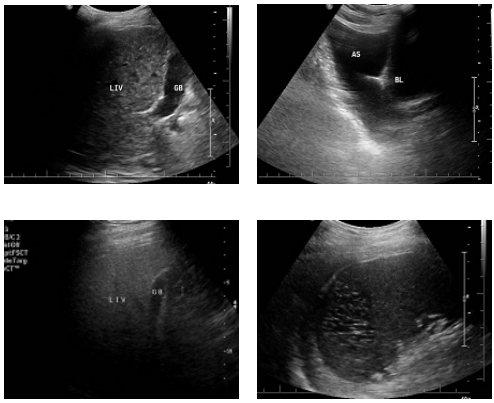

Fig. 7. Instances of false results due to misclassification

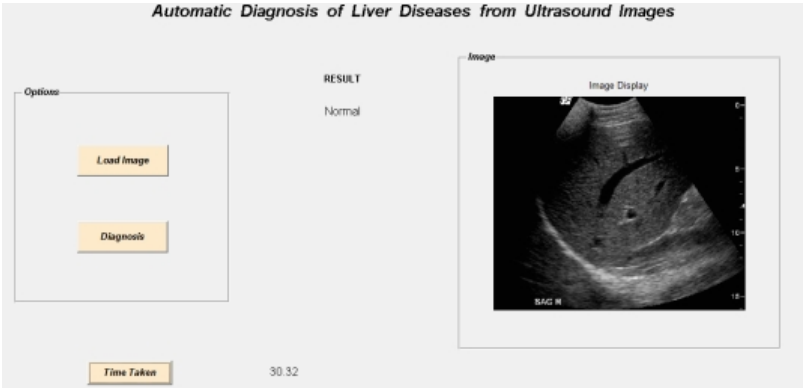

Fig. 8. Implementation screen shot

8 Conclusions and Scope for Future Work

This work concentrates on classifying five types of liver diseases based on texture features. Statistical properties have been applied to extracted features which have been subsequently used for classification. Future work is to concentrate on more number of diseases with a different set of features extracted from the image dataset. Also shape based detection can be attempted for further enhancement of results. Segmentation followed by intelligent region of interest selection algorithms can be attempted to select the ROIs. Likewise Neural Networks and other soft computing techniques can be attempted to further enhance the classification accuracy.

Acknowledgments. We would like to extend our heartfelt thanks to SonoScan Ultrasonic Scan Center, Coimbatore and Sunitha Scan and Diagnostic Center, Guntur for providing the images and the necessary support. We would also like to thank Ms.Padmavathi S, Assistant Professor, Department of Information Technology, Amrita Vishwa Vidyapeetham, Mr. Santan, Ms. Gouthami R, Mr. Dilip Kumar A and Ms. Aswini M for extending their valuable help and support in bringing out this work successfully.

References

[1] Aboshosha, A., Hassan, M., Ashour, M., El Mashade, M.: Image denoising based on spatial filters, an analytical study. In: Proc. International Conference on Computer Engineering & Systems, ICCES, pp. 245–250 (2009), doi:10.1109/ICCES.2009.5384036

[2] Zaid, A.Z.S.A., Fakhr, M.W., Mohamed, A.F.A.: Automatic Diagnosis of Liver Diseases from Ultrasound Images. In: Proc. International Conferenceon Computer Engineering and Systems, pp. 313–319 (2006), doi: 10.1109/ICCES.2006.320467

[3] Md. Sohail, A.S., Bhattacharya, P., Mudur, S.P., Krishnamurthy, S.: Local Relative GLRLM-Based Texture Feature Extraction for Classifying Ultrasound Medical Images. In: Proc. 24th Canadian Conference on Electrical and Computer Engineering (CCECE), pp. 001092–001095 (2011), doi:10.1109/CCECE.2011.6030630

[4] Materka, A., Strzelecki, M.: Texture Analysis Methods – A Review. Technical University of Lodz, Institute of Electronics, COST B11 Report, Brussels (1998)

[5] Yoo, B., Nishimura, T.: A Study of Ultrasound Images Enhancement using Adaptive Speckle Reducing Anisotropic Diffusion. In: Proc. IEEE International Symposium on Industrial Electronics, pp. 581–585. Seoul Olympic Parktel, Seoul (2009), doi:10.1109/ISIE.2009.5213936

[6] Christos, P., Loizou, C.S.: Pattichis Despeckle Filtering Algorithms and Software for Ultrasound Imaging. Morgan & Claypool (2008)

[7] Umarani, C., Ganesan, L., Radhakrishnan, S.: Combined Statistical and Structural Approach for Unsupervised Texture Classification. International Journal of Imaging Science and Engineering (IJISE) 2(1), 162–165 (2008) ISSN: 1934-9955

[8] Balasubramanian, D., Srinivasan, P., Gurupatham, R.: Automatic Classification of Focal Lesions in Ultrasound Liver Images using Principal Component Analysis and Neural Networks. In: Proc.29th Annual International Conference of the IEEE EMBS Cité Internationale, Lyon, France, pp. 2134–2137 (2007)

[9] Kyriacou, E., Pavlopoulos, S.: Computer Assisted Characterization of Liver tissue using Image Texture analysis techniques on B-scan images. In: Proc. of the 19th Annual International Conference of the IEEE Engineering in Medicine and Biology Society, pp. 806–809 (1997), doi:10.1109/IEMBS.1997.757766
[10] Gonzalez Rafael, C., Woods Richard, E.: Digital Image Processing. Prentice-Hall, India (2008)
[11] Gonzalez Rafael, C., Woods Richard, E., Eddins Steven, L.: Digital Image Processing Using MATLAB Pearson Education (2004)
[12] Jayaraman, S., Esakkirajan, S., Veerakumar, T.: Digital Image Processing. Tata McGraw Hill Education, New Delhi (2010)
[13] Abd-Elmoniem, K.Z., Youssef, A.-B.M., Kadah, Y.M.: Real-Time Speckle Reduction and Coherence Enhancement in Ultrasound imaging via nonlinear anisotropic diffusion. Proc. IEEE Trans. on Biomedical Engineering 49(9), 997–1014 (2002), doi:10.1109/TBME.2002.1028423
[14] Thangavel, K., Manavalan, R., Laurence Aroquiaraj, I.: Removal of Speckle Noise from Ultrasound Medical Image based on Special Filters: Comparative Study. ICGST-GVIP Journal 9(III), 25–32 (2009)
[15] Tuceryan, M.: Texture Analysis.The Handbook of Pattern Recognition and Computer Vision, 2nd edn. World Scientific Publishing Co. (1998)
[16] Galloway, M.M.: Texture Analysis Using Gray Level Run Lengths. Computer Graphics Image Processing 4, 172–179 (1975), doi:10.1016/S0146-664X(75)80008-6
[17] Sharma, M., Singh, S.: Texture Analysis Experiments with Meastex and Vistex Benchmarks. In: Proc. International Conference on Advances in Pattern Recognition, pp. 417–424 (2001), doi:10.1.1.18.5374
[18] Motwani, M.C., Gadiya, M.C., Motwani, R.C., Harris Jr., F.C.: Survey of image denoising techniques, doi:10.1.1.107.1823
[19] Kaur, N., Chadda, S., Thakur, R.: A Survey of Image De-noising Filters. IJCST 3(1), 505–507 (2012) ISSN 0976-8491(Online), 2229-4333 (Print)
[20] Maini, R., Aggarwal, H.: Performance Evaluation of Various Speckle Noise Reduction Filters on Medical Images. International Journal of Recent Trends in Engineering 2(4), 22–25 (2009)
[21] Hawlick, R.M.: Statistical and Structural Approaches to Texture. Proceedings of the IEEE 67(5), 786–804 (1979), doi:10.1109/PROC.1979.11328
[22] Ribeiro, R., Marinho, R.T., Velosa, J., Ramalho, F., Miguel Sanches, J., Suri, J.S.: The Usefulness of Ultrasound in the Classification of Chronic Liver Disease. In: Proc. 33rd Annual International Conference of the IEEE EMBS, Boston, pp. 5132–5135 (2011), doi:10.1109/IEMBS.2011.6091271
[23] Ribeiro, R., Marinho, R., Velosa, J., Ramalho, F., Miguel Sanches, J.: Chronic liver disease staging classification based on ultrasound, clinical and laboratorial data. In: Proc. International Symposium on Biomedical Imaging: From Nano to Macro, pp. 707–710. IEEE (2011), doi:10.1109/ISBI.2011.5872504
[24] Sivakumar, R., Gayathri, M.K., Nedumaran, D.: Speckle Filtering Of Ultrasound B-Scan Images - A Comparative Study between Spatial And Diffusion Filters. In: Proc. IEEE Conference on Open Systems (ICOS), pp. 80–85 (2010), doi:10.1109/ICOS.2010.5720068
[25] Vanithamani, R., Umamaheshwari, G., Ezhilarasi, M.: Modified Hybrid Median Filter for Effective Speckle Reduction in Ultrasound Images. In: Proc. of the 12th International Conference on Networking, VLSI and Signal Processing, ICNVS 2010, pp. 166–171 (2010)

[26] Kalaivani Narayanan, S., Wahidabanu, R.S.D.: A view on Despeckling in Ultrasound Imaging. International Journal of Signal Processing, Image Processing and Pattern Recognition 2(3), 85–98 (2009)
[27] Zhou, S., Wan, J.: A Survey of Algorithms for the Analysis of Diffused Liver Disease from B-mode Ultrasound Images. In: Proc. The Ninth International Conference on Electronic Measurement & Instruments ICEMI 2009, pp. 576–582. IEEE (2009), doi:10.1109/ICEMI.2009.5274499
[28] Vasconcelos, V., Silva, J.S., Marques, L., Barroso, J.: Statistical Textural Features for Classification of Lung Emphysema in CT Images:A comparative study. In: Proc. 5th Iberian Conference on Information Systems and Technologies (CISTI), pp. 1–5 (2010)
[29] Nailon, W.H.: Texture Analysis Methods for Medical Image Characterisation. Biomedical Imaging InTech, 75–100 (2010), doi:10.5772/8912
[30] Fujita, Y., Hamamoto, Y., Segawa, M., Terai, S., Sakaida, I.: An Improved Method for Cirrhosis Detection using Liver's Ultrasound images. In: International Conference on Pattern Recognition, pp. 2294–2297 (2010), doi:10.1109/ICPR.2010.561
[31] Yu, Y., Acton, S.T.: Speckle Reducing Anisotropic Diffusion. IEEE Transactions on Image Processing 11(11), 1260–1270 (2002), doi:10.1109/TIP.2002.804276
[32] Wu, Y.-H., Huang, J.-Y., Cheng, S.-C., Yang, C.-K., Lin, C.-L.: Evolutionary Feature Construction for Ultrasound Image Processing and Its Application to Automatic Liver Disease Diagnosis. In: Proc. International Conference on Complex, Intelligent, and Software Intensive Systems, pp. 565–570 (2011), doi:10.1109/CISIS.2011.93

Analysis of the Bankruptcy Prediction Model in the Present Economic Situation

Crina Rațiu[1], Dominic Bucerzan[2], and Mihaela Crăciun[2]

[1] Daramec SRL, Arad, România, Sofronea FN
ratiu__anina@yahoo.com
[2] "Aurel Vlaicu" University of Arad, Faculty of Exact Sciences,
Department of Mathematics-Informatics, România, 310330 Arad, 2 Elena Drăgoi
dominic@bbcomputer.ro, qbt@rdslink.ro

Abstract. One of the research topics that garnered worldwide attention in the last decades is the prediction of bankruptcy risk. This led to the development and the diversification of methods and techniques used to quantifying this kind of risk. In this paper we analyzed the existing tools for predicting the risk of bankruptcy that are available to the decision maker, with a clear and concise study comprising a total of 60 companies in the Romanian economy.

Keywords: analysis and prediction, discriminant analysis, bankruptcy prediction, Altman model, Anghel model.

1 Introduction

Bankruptcy may be defined as a function of three variables: individual capability of the owners and management, industry characteristics, economic environment in which they operate. Even though the term bankruptcy is usually used to describe companies in difficulty, it should be taken into consideration that bankruptcy is a process that begins financially and it ends legally. This study provides a comprehensive comparative analysis of existing tools for predicting the risk of bankruptcy, based on real data sets, collected from the actual Romanian economy.

2 Multiple Discriminant Analysis (MDA) Applied in Economic Field

Multiple discriminant analysis (MDA) is a statistical technique used to classify an a-priory observation in two or more groups based on observable individual characteristics. This technique is used mainly to classify or to make predictions in case of dependent variables which appear in a qualitative form (bankruptcy (B) / non-bankruptcy (N-B)). From a technical standpoint, the following steps should be taken: establishing explicitly the classified groups (equal or greater than 2); collecting data for the objects analyzed by groups.

V.E. Balas et al. (Eds.): Soft Computing Applications, AISC 195, pp. 625–635.
springerlink.com

MDA technique tries to establish a linear combination of features that best separates the groups. For example, if a business has the financial ratios and features that can be quantified for all the analyzed companies, the statistical technique determines a set of coefficients of discrimination. Thus, MDA considers all of the common characteristics for the surveyed companies and the interactions of these characteristics. The role of the discriminant function is to convert the value of the variables into a single discriminant value Z, feature that allows the classification of objects (firms) in groups initially set (bankrupt / non-bankruptcy).

Discriminant function syntax is:

$$Z = a_1X_1 + a_2X_2 + \cdots + a_nX_n \quad (1)$$

where:

- a_i - is the weighting coefficients,
- X_i - represent the variables (financial ratios).
- MDA is correct only under the hypothesis of the following restrictions [1]:
- discriminant variables of the identified groups must have a normal multivariate distribution,
- the matrix of group dispersion to be equal across all groups (common variance - covariance matrix),
- discriminant analysis requires that a priori probability of occurrence of each group and the cost of classification to be specified.

Financial ratios represent the traditional way of analysis of company's financial position. Analysis based on rates represents the calculation and interpretation of the relationship between two comparable sizes from economic and logic point of view. Most classifications retain four categories of financial ratios: activity rates, liquidity rates, rates of indebtedness and equilibrium long term and rates of return. Financial analysis is based on an integrated use of rates and not a divided one, even if the interests of users is different (banks which grant loans are primarily interested in current liquidity and cash flow the short term, while private shareholders are interested in the return of the invested capital in business). Relevance and redundancy of financial ratios were approached in recent decades, so, in 1975 Pinches examined a total of 48 rates for which he highlighted seven key points (each of them having two representative financial ratios) [2].

Corporate bankruptcy causes economic damages for management, investors, creditors and employees together along with social cost. For these reasons bankruptcy predict, credit scoring is an important issue in finance. Survival analysis will be a new credit scoring model [13].

2.1 Approaches and Developments of Score Functions

There were several methods to detect financial difficulties of the company. Altman and Anghel Models are based on the starting rates method for detecting financial difficulties of the enterprise. One of the important reasons in using the rates method is

linked to the theoretical and practical developments that found connections between analysis using financial ratios and statistical techniques [3]. With financial ratios, we can compare the profitability of different sized companies from different branches [2]. Risk of bankruptcy can be determined by the so-called method of scoring. This is based on statistical techniques of discriminant analysis (DA).

The score, as final of discriminant analysis, represents a method of diagnosis that consists in measuring and interpreting the future economic risks for the company. The method uses a group of significant financial ratios, resulting mainly from the annual financial statements. In the following we present two models for prediction of bankruptcy.

2.2 The Altman Model

Altman is a reference name cited in studies concerning the prediction of bankruptcy. The model proposed by Altman considers a number of 22 potential variables (based on annual financial statements) grouped into five categories: liquidity, profitability, debt, solvency and activity.

Altman describes how he uses statistical techniques and discriminant analysis (DA) to develop a model of financial indicators that provide enterprise bankruptcy. In the model development, he has selected a group of 33 companies with financial problems; the sample included industrial (manufacturing) companies. Healthy business group companies were selected by the principle of similarity, to each of the bankrupt companies (size, industry, etc.) corresponded a healthy firm. From the initial list of 22 indicators, the author chooses the five most significant. Between the years 1969-1990, he develops three score function models, named: Z, Z' and Z''. The first model built by Altman includes five variables, each having attached weights [11].

$$Z = 1.2X_1 + 1.4X_2 + 3.3X_3 + 0.6X_4 + 1.0X_5 \quad (2)$$

where:

- X_1 - working capital/total assets,
- X_2 - retained earnings/total assets,
- X_3 - earnings before interest and taxes/total assets,
- X_4 - market value equity/book value of total liabilities,
- X_5 - sales/total assets, and Z - overall Index or Score.

To make the model operational, the two groups of companies were analyzed and classified by Z score size, setting the two limits and the uncertainty. Altman's model works based on the following decision rules:

- If $Z \leq 1.8$ then imminent bankruptcy situation, the company is likely headed towards bankruptcy,
- If $1.8 < Z < 2.99$ then uncertainty,
- If $Z \geq 2.99$ then good financial situation.

It should be noted that the first four coefficients (X_1-X_4) of the score function are as a percentage while the last one, X_5, has a decimal form [5]. Later, Altman refined the model. The aim was to reflect the economic reality of the companies, through the financial information. He modified the variable X_4 substituting the market value with the book values of equity [4]. The following score function was obtained [11]:

$$Z' = 0.717X_1 + 0.847X_2 + 3.107X_3 + 0.420X_4 + 0.998X_5 \quad (3)$$

The decision rules changed as follows:

- If Z' ≤ 1.23 then imminent bankruptcy situation
- If 1.23 < Z'< 2.90 then uncertainty
- If Z' ≥ 2.90 then good financial situation.

Finally, from its previous models, which include a variable sensitive to the type of industry (X_5 = sales/total assets), Altman reviews the score function, retaining only four variables [11]:

$$Z'' = 6.56X_1 + 3.26X_2 + 6.72X_3 + 1.05X_4 \quad (4)$$

The decision rule becomes:

- If Z'' ≤ 1.10 then imminent bankruptcy situation,
- If 1.10 < Z'' < 2.60 then uncertainty,
- If Z'' ≥ 2.60 then good financial situation.

We note that in the three score function models Z, Z' and Z'', Altman obtained three different areas of ignorance, as follows:

- 1.8 < Z < 2.99,
- 1.23 < Z'< 2.90,
- 1.10 < Z'' < 2.60.

The intervals of ignorance have the following lengths: 1.19 for Z, 1.67 for Z' and 1.50 for Z''.

2.3 The Anghel Model

The "Anghel Model" is the recent model developed by the Romanian School and it consists in building the function score model for the Romanian economy on multiple discriminant analysis (MDA). The score function consists of four variables, four parameters and one constant [12].
To obtain the score function Anghel took the following steps:

- Choosing the sample of companies divided in two groups: N-B group – companies without financial problems and B group – failed companies. His study is based on a sample of 276 companies from 12 branches of national economy. The companies were selected randomly. The information for each enterprise was taken from the annual financial statements for the period 1994-1998.

- A comparison is made over time period based on a set of significant indicators for the two groups of companies. Anghel analysis 20 financial indicators to see which of them covers a particular interest for the companies and divides them in: rates of activity, rates of liquidity, rate debt, rates of return and other economic and financial data's.
- Selecting indicators that make the best discrimination. Following the selection phase he chooses the following four financial variables: revenue performance, coverage of debt to cash flow, leverage the asset and period for payment of obligations:

    - X_1 - earning after taxes / incomes;
    - X_2 - Cash Flow / total assets;
    - X_3 - liability / total assets;
    - X_4 - liability/ sales * 360

- Development through discriminant analysis technique of A linear combinations of relevant indicators Xi. In case of the two groups of previous assumptions there is a function representing the best discrimination B versus N-B. Based on economic and financial information since 1998 for a total of 276 Romanian companies it was build the A score function [11]:

$$A = 5.676 + 6.3718X_1 + 5.3932X_2 - 5.1427X_3 - 0.0105X_4 \quad (5)$$

- Choosing a point (or points) of inflection which makes predictive classification of companies in the two groups. Computing the A score for each enterprise from the sample and sorting ascending the information obtained for the A score results a situation for all companies.
- A-priori analysis of the success rate of A score by comparing the predictive classification with the known situation of companies in the sample. The assessment is based on the following classification:

    - If $A \leq 0$ then imminent bankruptcy situation
    - If $0 < A < 2.05$ then uncertainty
    - If $A \geq 2.05$ then good financial situation

- A-posteriori analysis of the success rate of the function A by analyzing the degree of relevance for another sample of companies.

A sample of companies was considered, separated in the two groups B and N-B, and the subject of analysis was the prediction accuracy that the function A performs. The sample used to validate the proposed model includes 55 companies, 28 from the N-B and the other 27 from group B. Companies in the test sample were similar in size and industry sectors with the initial sample.

In these conditions the prediction success rate, reported by the author, is similar to a-priori prediction, namely 97.8%. This allowed the assessment that the score A was

effective and could be applied to companies in the Romanian economy (retaining the limits in order to built the model) [11].

Observing the prediction models mentioned above, we can see that there exists a constant in the scoring function from the Anghel model, while it is missing from the scoring function from the Altman model. This difference is because in the Anghel prediction model the number of N-B companies (166) is different from the number of B companies (110), while in the Altman model the number of N-B companies is equal to the number of B companies (33).

3 Current Views on the Use of Quantitative Techniques Data to Estimate the Bankruptcy Risk

Using financial ratios in bankruptcy prediction is based on the assumption that the bankruptcy process is characterized by a systematic deterioration of the value of financial ratios. Diagnostic models for the bankruptcy risk developed based on disccriminant analysis such as Altman model can be slightly misleading, as Heffernan notes, because models are based on historical data [6]. Even if they were reasonably accurate, when these models were developed, if no action is taken to update the variables considered and / or recalibration of the models, their accuracy decreases in time. Consider that the analyzed financial rates may change over time, even on the market on which the company is operating. It is necessary to test the discriminant analysis models with a sufficiently high frequency and to regularly update the risk models used in practice [6].

A disadvantage of using quantitative data techniques to estimate the risk of bankruptcy is that the result obtained by using the model is a binary one: bankrupt or non-bankrupt company. In practice, there are several possible scenarios. The used discriminant analysis models used may not include the state of solvency, insolvency and restructuring simultaneously [7].

Everyone in finance is familiar with the Altman Z-Score and many analysts use it. In 2001 Shumway shows that half of the variables included in Altman-Z are no longer predictive of bankruptcy–ouch. He also identifies a model that trumps the Altman-Z in out of sample tests–double ouch [8]. Also in 2004, Chavez and Jarrow have checked with extensive data that Altman model is not as good as the Shumway model [9]. Analysts say the 2009 Z-scores, based on 2008 balance sheets, are far lower than in previous years as companies absorb the strain of the downturn in their accounts.

Graham Secker, Morgan Stanley strategy analyst says there's been a lot of change between 2007 and 2008 [accounting years], tightening of credit and a vast deterioration in corporate balance sheets and 2009 is expected [Z-scores] to be much worse. Also analysis of the Financial Times and Capital IQ, corroborates that the 2009 scores have been badly affected by the crisis [10].

3.1 Analysis of Altman and Anghel Bankruptcy Prediction Models

In our study we demonstrated that discriminant analysis methods are no longer valid in period of crisis. For this we constructed a statistic which was based on a sample of 60 companies in the Romanian economy.

The 60 companies were chosen randomly from a population of 200 companies. Note that when the companies were selected, the number of firms bankrupted is equal to the number of firms non-bankrupted, fact noticed in the Altman's model.

As mentioned above, we grouped the firms into two categories: group 1 - business bankrupted – B, group 2 - business non-bankrupted - N-B. The study was conducted over a period of five years (2005-2009).

Applying the two bankruptcy prediction models, Altman's model respectively Anghel's model, we obtained the percentage of correct predictions, reported in years and reported to the company.

Also the study revealed the average of the percentage of correct predictions reported at years both for the Altman's model and for the Anghel's model.

As it may be seen in Figure 1, we obtained a graph of the correct percentage of predictions in the models studied.

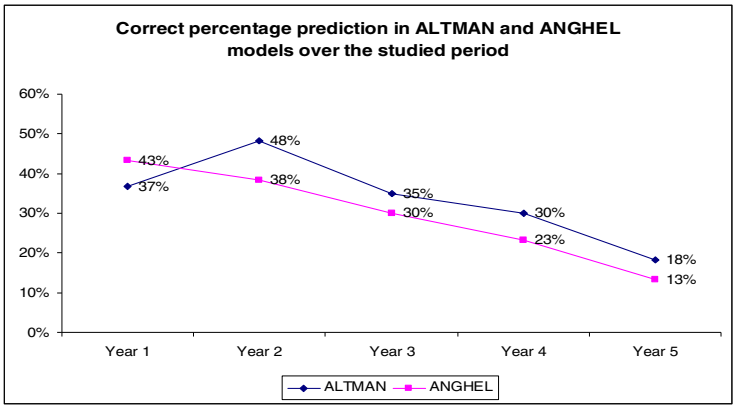

Fig. 1. The Altman and Anghel - percentage of correct predictions / year

The table below, Table 1, contains statistical data that we obtained in the study. The meaning of the heading and footer table is the following:

- COM – Company
- CS - The current situation
- CPP/C - Correct percentage prediction / company
- CPP/Y - Correct percentage prediction / year
- APCP/Y - Average percentage of correct predictions / years
- APCP/C - Average percentage of correct predictions / company

Table 1. Accurate predictions of bankruptcy reported both years and the company, obtained with Anghel's and Altman's predictive models

		ALTMAN						ANGHEL					
COM	**CS**	**Year 1**	**Year 2**	**Year 3**	**Year 4**	**Year 5**	**CPP/C**	**Year 1**	**Year 2**	**Year 3**	**Year 4**	**Year 5**	**CPP/C**
1	N-B	B	U				0%	B	B				0%
2	N-B	U	U	U	U	U	0%	B	U	B	U	U	0%
3	N-B	U	B	U	U	B	0%	B	B	U	B	B	0%
4	N-B	B	B	B	B	B	0%		B	B	B	B	0%
5	N-B	B					0%	B					0%
6	N-B	B	B	B	B		0%	B	B				0%
7	N-B	B	B	B	B		0%	B	B	B	B		0%
8	N-B	N-B	N-B	N-B	U		75%	N-B	B	B	B		25%
9	N-B	U					0%	B					0%
10	N-B	B	B	B	B		0%	B	B	B	B		0%
11	N-B	B	B				0%	B	B				0%
12	N-B	N-B	N-B	N-B	N-B		100%	N-B	N-B	B	N-B		75%
13	N-B	U	U	U	B	B	0%	U	B	B	B	B	0%
14	N-B	B	B	B	B		0%	B	B	B	B		0%
15	N-B	B	B	B	B		0%	B	B	B	B		0%
16	N-B	B	B	B	B		0%	B	B	B	B		0%
17	N-B	U	B	B			0%	B	B	B			0%
18	N-B	B	B				0%	B					0%
19	N-B	B	N-B				50%	B	U				0%
20	N-B	B	U	B	B	B	0%	B	B	B	B	B	0%
21	N-B	B	U	B	B		0%	B	B	B	B		0%
22	N-B	B	B	B			0%	B					0%
23	N-B	N-B	N-B	N-B	N-B		100%	N-B					100%
24	N-B	N-B	N-B				100%	N-B	N-B				100%
25	N-B	U	U	B			0%	N-B	N-B				100%
26	N-B	N-B	N-B	U	U	B	40%	B	B	B	B	B	0%
27	N-B	N-B	U				50%	N-B	N-B				100%
28	N-B	N-B	N-B	U	U	U	40%	N-B	N-B	B	B	B	40%
29	N-B	B	B	B			0%	B	B	B			0%
30	N-B	B					0%	B					0%
31	B	B	B	N-B			67%	B	B	N-B			67%
32	B	U	B	B			67%	B	B	B			100%
33	B	B	B	B	B	B	100%				B		100%
34	B	N-B	N-B	N-B	N-B	B	20%	B	B	B	B	B	100%

Table 1. (*continued*)

		ALTMAN						ANGHEL					
COM	**CS**	**Year 1**	**Year 2**	**Year 3**	**Year 4**	**Year 5**	**CPP/C**	**Year 1**	**Year 2**	**Year 3**	**Year 4**	**Year 5**	**CPP/C**
35	B	U	N-B	B			33%	B	U	B			67%
36	B	B	B	B	B		100%	B	B	B	B		100%
37	B	N-B	B	B	B	B	80%	N-B			B		50%
38	B	B	B	U	B	U	60%	B	B	B	B	B	100%
39	B	B	B	B	B	B	100%	B	B	B	B	B	100%
40	B	B	B	B			100%	B	B	B			100%
41	B	B	B	B	B	B	100%	B					100%
42	B	N-B	B	B	B	B	80%	B	B	B	B	B	100%
43	B	N-B	B				50%	N-B	B				50%
44	B	B	B	N-B	B		75%	B	B	B	B		100%
45	B	U	B	B			67%	N-B	U	B			33%
46	B	U	B	U	B		50%	B	B	B	B		100%
47	B	N-B	N-B	N-B	N-B	B	20%	N-B	B	B	U	B	60%
48	B	U	B	B			67%	U	U				0%
49	B	B	U	B	B		75%	B	B	B	B		100%
50	B	B	B				100%	B	B				100%
51	B	N-B	N-B	N-B	N-B	B	20%	N-B	N-B	N-B	N-B	B	20%
52	B	B	B	B	B	B	100%	B	B	B			100%
53	B	B	N-B	B	B	U	60%		N-B		B	U	33%
54	B	N-B	N-B	B	B		50%	N-B	N-B	B			33%
55	B	B	B	B	B	B	100%	B	B	B	B	B	100%
56	B	B	B	B	B		100%	B					100%
57	B	B	B	B			100%	B	B	B			100%
58	B	N-B	U	U	U	B	20%	N-B	N-B	U	U	B	20%
59	B	N-B	B	N-B	B		50%	B	B	U	B		75%
60	B	N-B	B				50%	N-B	N-B	B			33%
CPP/Y		**37%**	**48%**	**35%**	**30%**	**18%**	**APCP/C**	**43%**	**38%**	**30%**	**23%**	**13%**	**APCP/C**
APCP/Y		**34%**					**44%**	**30%**					**46%**

4 Conclusions

We can conclude that the percentage of correct predictions / years in the Altman model is between 18% and 48% while in the Anghel model the range is between 13% - 43%. The Anghel model has a decreasing linear behavior. In the Altman model, at first a growth is observed, followed by a linear decrease. What is common to the two methods is that prediction is not over 50%, a success rate well below the forecast given by the two authors. Anghel's model report a success rate greater than 97%, while in the Altman's model the success rates were: 93.9% for N-B companies and 97% for B companies. This result proves that the two methods are not valid. Also the average percentage of correct predictions / year highlights this fact. In Altman model 44% and 46% in Anghel model, both values are below 50%. Taking this study into consideration, we may conclude that the use of the Altman and Anghel bankruptcy prediction models is no longer valid in today's economic environment.

Such studies were also approached by other researchers and the results were not far from those obtained by us. In this paper we present a concise and complex study, which comprises 60 companies and demonstrates that the existing analysis tools for predicting bankruptcy risk are no longer valid in today's economic conditions. As a future research direction stands out the development of an adequate analysis method for the current period that include the bankruptcy risk prediction, the analysis and prediction of the stage of incapacity of payment, and to determine the appropriate timing for commencement of insolvency proceedings.

Acknowledgments. This paper would not have been written without the help of several colleagues who offered their knowledge and unconditional support. Also special thanks to the family and best friends who have always been there for us.

References

1. Kareks, G., Prakash, A.: Multivariat Normality and Forecasting of Business Bankruptcy. Journal of Business & Bankruptcy, 573–593 (1987)
2. Pinches, G., Eubank, A., Mingo, K., Caruthers, K.: The Hierarchical Classification of Financial Ratios. Journal of Business Research, 309–310 (October 1975)
3. Altman, E.I.: Financial Ratios, Discriminant Analysis and the Prediction of Corporate Bankruptcy. Journal of Finance, 589–609 (September 1968)
4. Altman, E., Haldemon, R., Narayama, P.: Zeta Analysis. Journal of Banking and Finance, 89–108 (June 1977)
5. Altman, E.I., Lafleur, J.K.: Managing a return to financial health. Journal of Business Strategy, 31–38 (June 1981)
6. Heffernan, S.: Modern Banking, 2nd edn. John Wiley & Sons, Ltd. (2005) ISBN 10: 0470095008, 13: 978-0470095003
7. Armeanu, Ş.D., Vintilă, G., Moscalu, M., Filipescu, M.-O., Lazăr, P.: Using Quantitative Data Analysis Techniques for Bankruptcy Risk Estimation for Corporations. Theoretical and Applied Economics XIX(1), (566), 97–112 (2012)
8. Shumway, T.: Forecasting bankruptcy more accurately: a simple hazard model. Journal of Business 74, 22–23 (2001)

9. Chava, S., Jarrow, R.A.: Bankruptcy prediction with industry effects. Review of Finance 8(4), 537–569 (2004)
10. New study rewrites the A-Z of value investing – Financial Times, http://www.ft.com/intl/cms/s/2/7ca640a8-88f4-11de-b50f-00144feabdc0.html#axzz1zC2OGQgD (August 14, 2009)
11. Crăciun, M., Rațiu, C., Bucerzan, D., Manolescu, A.: On the Applicability of the Anghel and Altman Bankruptcy Prediction Models in the Actual Crisis Conditions. Presented at Workshop on Intelligent Decision Support Systems for Crisis Management, Oradea (2012)
12. Anghel, I.: Falimentul – Radiografie si Predictie, pp. 135–150. Editura Economica, Bucuresti (2002)
13. Lee, M.-C.: Enterprise Credit Risk Evaluation models: A Review of Current Research Trends. International Journal of Computer Applications (0975 – 8887) 44(11), 37–44 (2012)

Monitoring Help Desk Process Using KPI

Diana Betina Mirsu

"Politehnica" University of Timisoara, Faculty of Management in Production and Transportation
betinaiovan@yahoo.com

Abstract. The paper presents an originally way of setting and calculating key performance indicators for a Help Desk problem based on Fishbone analysis - a six sigma technique. The paper focuses on analyzing the process data collected during two months. The process is modeled using BPMN language and an original process enhancement in three steps is applied. The first month is allocated to observing the process behavior and establishing improvement methods. During the second month the impact of the improvements is measured. The results of the research show process improvement as a result of organizational decision that has a positive and visible impact on kpi. The originally manner that kpi was developed can be easily customized to other business process types.

Keywords: key performance indicators, fishbone diagram, BPMN, process monitoring.

1 Introduction

For staying competitive in a dynamic market, organizations constantly improve their functionality by identifying new process improvement strategies customized to their specific needs. According to Tony Riches, one of the top 10 business priorities for 2011 is improving business process. [1]

One of business process improvement methods is monitoring it with key performance indicators. [2]

When establishing key performance indicators the strategy of the organization plays an important role. From the strategy, the objectives of the organization, that need to be monitored, are defined. It is important to establish the correct and relevant kpi's for the organization.

In the first instance the paper presents Help Desk process modeled with BPMN language. The process inefficiency causes will be determined with Fishbone analyze [3] and customized kpi will be developed as improvement method and also as process control method. The quality of the process needs to be improved through applying improvement measures for: - reducing process complains, reducing rework time, respecting SLA (service legal agreement) for level 1 and level 2 activities of Help Desk process.

V.E. Balas et al. (Eds.): Soft Computing Applications, AISC 195, pp. 637–647.
springerlink.com

2 Help-Desk Software Service Process Description

The process starts when the customer of the software service signals an incident (error) in the flow of the process. The customer calls level 1 support and sends an e-mail with the problem description. At level 1 support a person responsible with receiving incidents filters the problem in two categories: software problems that can be solved by phone assistance and hardware problems that require movement of an intervention team.

A. If the incident can be solved by phone, the following steps will be followed: the incident is saved in an .xls sheet, a solution to the incident will be found and a feedback request will be sent to the customer. The customer will give a short feedback regarding the incident: a) if the feedback is negative, level 1 support will receive the feedback and the incident resolution procedure is restarted till the solution for the problem is found. b) if the feedback is positive, level 1 support closes the ticket and sends a message to the customer that ticket is closed.
B. If the incident requires movement of an intervention team to the place of the incident the next steps will be followed: the ticket is saved to level 2 support and a message with ticket number is sent to the customer. The intervention is planned. The team moves to the place of the incident and a direct feedback regarding the resolution is received from the operational equipment and from the customer. The ticket closes and after intervention finishes a message to the customer is sent confirming the ticket closure. The process ends.

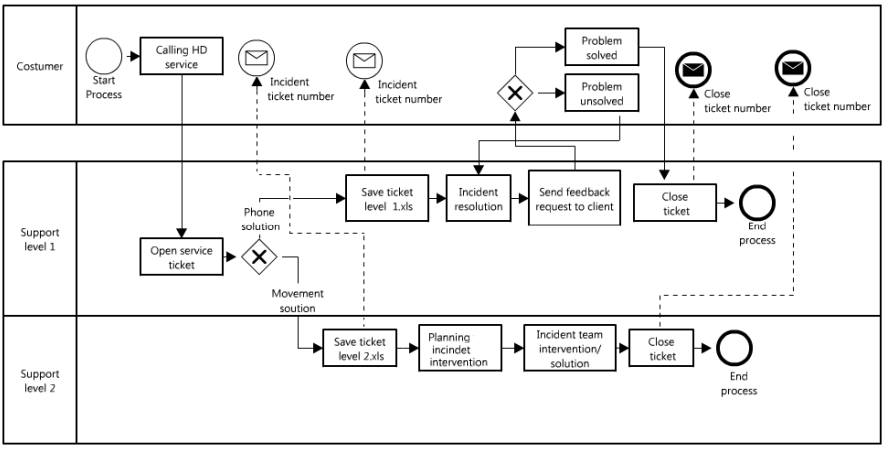

Fig. 1. Help Desk process map

3 Cause- Effect Diagram for Process Problems

The cause-effect diagram was created by Kauro Ishikawa in the late ´60. [3]. This diagram is a Six Sigma technique widely used in identification of the causes that determine the appearance. of a problem. It is also known as the Ishikawa diagram or Fishbone diagram.

The diagram develops as a fishbone. The spine of the fishbone is a right or left sided arrow with the problem written at the end of it. From spine develops arrows for each main cause of the problem. For each main problem causes there may be: one, two or more factors according to the detail level of the analyzed problem.

In determining the main causes of the problem there is predefine variation of fishbone structure. Some of these methods are: 4M -methods, man, machines, materials;4P -policy, procedure, people or plant/equipment; 5S -surroundings, suppliers, systems, skill, and safety; 6M –machine, method, material, manpower, measurement, milieu/mother nature; 7P- product, price, place, promotion people/personnel, process, physical evidence.

A big advantage of this diagram is that it can be customized to the problem that needs to be solved, and is easy to assemble and understand [4]. In the analyzed case study a customized diagram is created, to answer the HD process needs.

Fig.2 shows the problems that appear in HD process. For each category of causes (equipment, people, data and quality) there are few related factors.

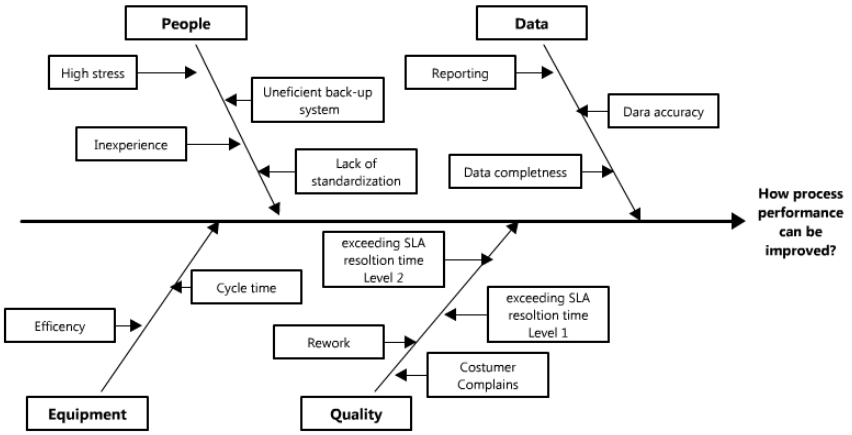

Fig. 2. Fishbone analyze for HD process

This case study will focus only on quality process improvement with the following related factors: customer complaints, rework, exceeding SLA resolution time for level 1 support, and level 2 support. For each of these factors key performance indicators (KPI) will be developed and the process will be monitored.

4 HD Process Improving Analyze

In order to enhance the process, an original improving cycle (fig. 3) in three steps will be performed for each of the unsatisfactory quality factors.

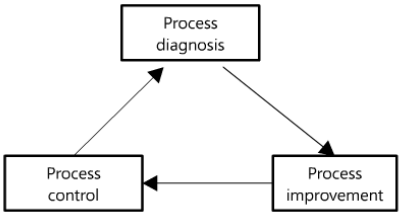

Fig. 3. Enhancement cycle

1. Process diagnosis- the process performance is measured in order to know the process status.
2. Process improvement: in this step corrective action will be developed and implemented at a detail level of the process.
3. Process control- in this step the results of the process will be evaluated in order to measure the improvements impact.

Process diagnosis (step 1) will be performed again for continuous process improvement. The most important objective of the control stage is to reduce process resources consumption by removing mistakes and to assure that the process mistakes doesn't reach the customers.

4.1 Developing the KPI for HD Process

When developing KPI for a process the organizational objectives have to be taken into consideration [5]. The process objectives had to be aligned with the organizational strategy. The SMART strategy has to be considered for developing efficient kpi's. When defining right KPIs for the process, the organizational goals and objectives are easier to achieve. KPIs enables the organization to measure organizational aspects against an established target. [6]

Table 1 shows how the HD process key performance indicators are set. The below key performance indicators are developed only for quality, one of the main causes of process inefficiency.

Measuring the Process Improvement with KPI Level 1 Incidents
At this level the incidents are solved by phone assistance. These types of incidents appear due to a software malfunction.

Process Level 1diagnose: The level has exhibited difficulties regarding time overdue for solving incidents and difficulties in monitoring open tickets. The roots of these difficulties are problems solving inefficiency (due to new personnel with low experience in solving the issues); inefficient back-up system and problems monitoring the opened tickets.

Improvement Measures:-personnel training for each type of level 1incidents; -establishing an appropriate backup system;-improve ticket monitoring system with and established codes incidents.

Table 1. Developing KPI for quality aspect of the process

	Key performance indicator	**Definition**	**Source of information**	**Measurment/ Procent**
1	Time resolution for level 1 support	It is measured from the time that the request is received till the resolution confirmation is sent to customer via e-mail	Customer database	< 48 h (100%) < 60 h (50 %) > 60 h (0 %)
2	Time resolution for level 2 support	It is measured from the time that the request is received till the resolution confirmation is sent to customer via e-mail	Customer database	< 3 days (100%) < 4 days (50 %) > 4 days (0%)
3	Complains	It is considered any notification from constumer regarding the noncompliance of service quality offered.	Customer relashionship database	0 = 100% 0 – 40 = 80% 40 – 100 = 10% >100 = 0%
4	Rework	It is considered the work done for an incident that was solved partially or totally incorrect the first time.	Customer database	Quantitative measurements in a predefined time frame

Table 2. Monitoring kpi for Level 1 incidents

	Before			**After**		
	Incidents resolution time			Incidents resolution time		
Resolution Time	<48 h	< 60 h	> 60 h	<48 h	< 60 h	> 60 h
Weight	**0,9**	**0,1**	**0**	**0,9**	**0,1**	**0**
Week 1	310	45	20	590	16	0
Week 2	308	46	18	508	16	1
Week 3	290	33	25	589	6	0
Week 4	358	21	15	513	0	0
Total	**1266**	**145**	**78**	**2200**	**38**	**1**

Table 2 shows level 1 incidents before and after improvement methods were applied.

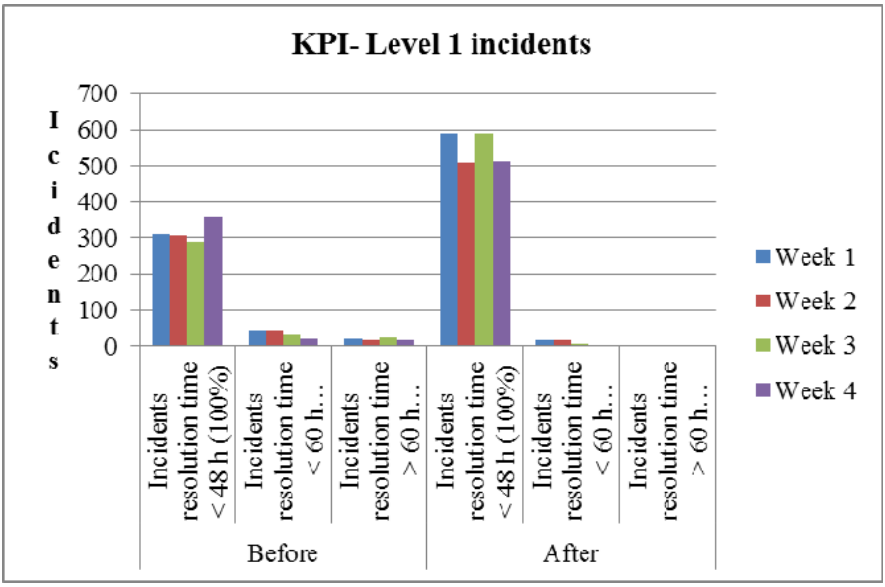

Fig. 4. Monitoring Level 1 incidents with kpi

Figure 4 shows level 1 incidents before and after improvement.

Process Control: Before any improvements were implemented at the 1 level the process recorded 1266 incidents solution in SLA time, 145 incidents with time overdue solution (kpi accuracy of 50%) and 78 incidents that required a time overdue bigger than 60 hours. After improvements were applied the number of incidents, solved in the SLA time, rose with 934, due to improvement measures and also because of the rising workload, the incidents solved in a time frame smaller than 60 hours decrease with 107 incidents, and incidents that were solved in a time frame bigger than 60 hours reduce to 1.

To calculate the overall improvement at level 1 the below formula (1) will be used:

$$(a*0,\ 9+b*0,\ 1+c*0)\ /3, \text{ where:} \quad (1)$$

a= incidents solved in SLA time
b= incidents solved between 48 and 60 hours
c= incidents solved after 60 hours

After calculating the process incidents weights for level 1 resulted an incident resolution improvement with 171,92 % *[(661,26/384,63) *100]*

Measuring the Process Improvement with KPI Level 2 Incidents

At this level the incident is solved at the customer place, due to nonconformity of hardware functionality.

Process Level 2 Diagnose: Similar to level 1 of Help Desk process, level 2 exhibit difficulties in meeting the SLA time. The main causes are: -poor staff trainings regarding intervention procedure,-low efficiency planning of team intervention; -problems with hardware quality components.

Improvement Measures:- staff training for acknowledging the intervention procedure; -establishing a standard intervention procedure; - quality hardware components.

Table 3. Monitoring kpi for Level 2 incidents

	Before			**After**		
	Incidents resolution time			Incidents resolution time		
Resolution Time	< 3days	< 4days	> 4 days	< 3 days	< 4 days	> 4 days
Weight	**0,8**	**0,2**	**0**	**0,8**	**0,2**	**0**
Week 1	320	35	16	371	0	0
Week 2	330	37	12	329	0	0
Week 3	340	39	19	358	0	0
Week 4	326	29	19	374	0	0
Total	**1316**	**140**	**66**	**1432**	**0**	**0**

Table 3 shows level 2 incidents before and after improvement methods were applied.

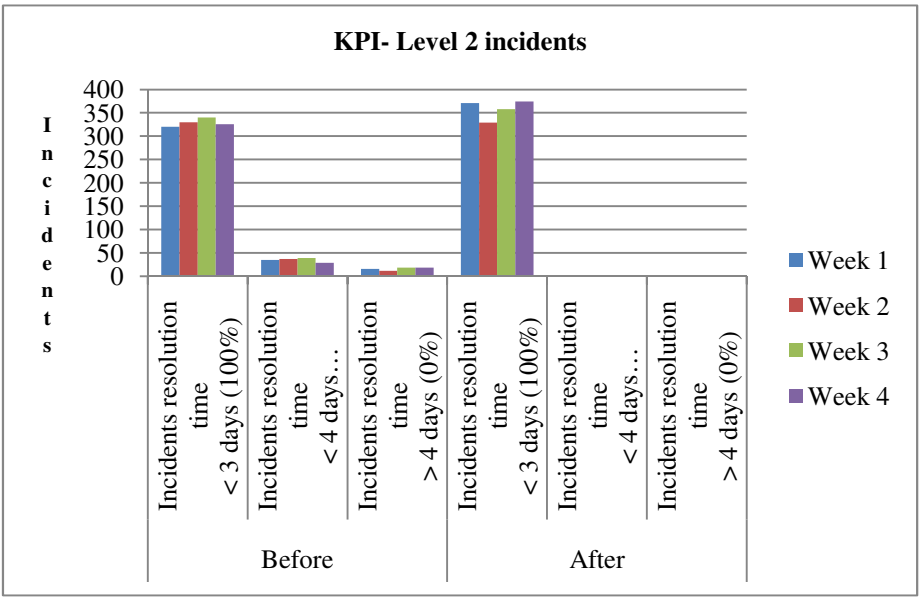

Fig. 5. Monitoring Level 2 incidents with kpi

Fig.5 shows the level 2 process before and after the above improvements were implemented.

Process Control: before applying any improvement the process recorded 1316 incidents resolved in the SLA time frame, 140 incidents solved in less than 4 days and 66 incidents solved in more than 4 days. After the improvements were applied the incidents solved in less or more than 4 day ware reduced to 0.The incidents solved in the SLA time has increased with 116 incidents. This rising number is due to new project start.

Overall, after applying equation 1, the level 2 process has exhibited a resolution improvement of 105, 99 *% [(381,86 / 360,26)*100]*

Measuring Process Improvement by Monitoring Process Free Complaints

This kpi measures the process accuracy; as fewer complaints are as more accurate the process is.

Customer Complaints Diagnose: the main cause of customer complain is the time overdue for solving incidents issues. Quality issues that produce customer complaints are detailed at level 1 and level 2.

Improvement Measures: All the improvement actions detailed at level 1 and level 2 will produce also a positive impact upon complaints reduction.

Table 4. Customer Complaints

		Before				After			
KPI- Complaints	**Complaints free**	**Week 1**	**Week 2**	**Week 3**	**Week 4**	**Week 1**	**Week 2**	**Week 3**	**Week 4**
0 Complaints	100%	0	0	0	0	0	0	0	0
0 – 40 Complaints	80%	32	0	35	0	16	17	6	0
40 – 100 Complaints	10%	0	63	0	70	0	0	0	0
>100 Complaints	0%	0	0	0	0	0	0	0	0

Table 4 shows customer complaints before and after improvement methods were applied.

Process Control: The improvement will be measured by applying the below formula:

$$\begin{cases} 100 - 20 * \frac{C}{40}, C \in (0 \div 40) \\ 80 - 70 * \frac{C-40}{60}, C \in [40 \div 100) \\ 10 - 10 * \frac{C-100}{50}, C \in [100 \div 150) \end{cases} \quad (2)$$

, where C is the number of customer complaints.

The equation (2) is applied on table 4 and the results are reflected in table 5. A gross reduction from 200 complaints to 39 is observed.

Table 5. Linear interpolation of process complains

	Week 1	Week 2	Week 3	Week 4	Average process complaints free
Before	84	53,16	82,5	45	**66,165**
After	92	95	97	100	**96**

Before the improvement measures were applied the process exhibits a process complaints accuracy of 66.165 %. After applying the improvements, the process complaints accuracy rise to 96% (rising with 29,69%).

Measuring Process Rework Hours

The rework hours refer to the time that exceeds the SLA and is necessary for solving an incident. It addresses only to level 1 because only this level exhibits feedback via mail from the customer. Level 2, because the movement at the place of the incident it receives direct feedback. (operational feedback from equipment and customer feedback.)

Rework Diagnose: the rework hours are process waste of resources, and the aim of the organizational team is to eliminate it. The main cause of rework is wrong resolution.

Improvement Measures: to eliminate the waste of rework, personal training will be performed at all levels of the process. Another direction in waste elimination is raising the quality of hardware components.

Process Control: After improvement were implemented an average reduction of 6 hours and half in the second month was recorded (tab.6, fig.6)

Table 6. Rework hours before and after improvement

	Before	After	Average / improvement
Week 1	4	1	2,5
Week 2	2	0,5	1,25
Week 3	3	1	2
Week 4	1	0,5	0,75
Total	**10**	**3**	**6,5**

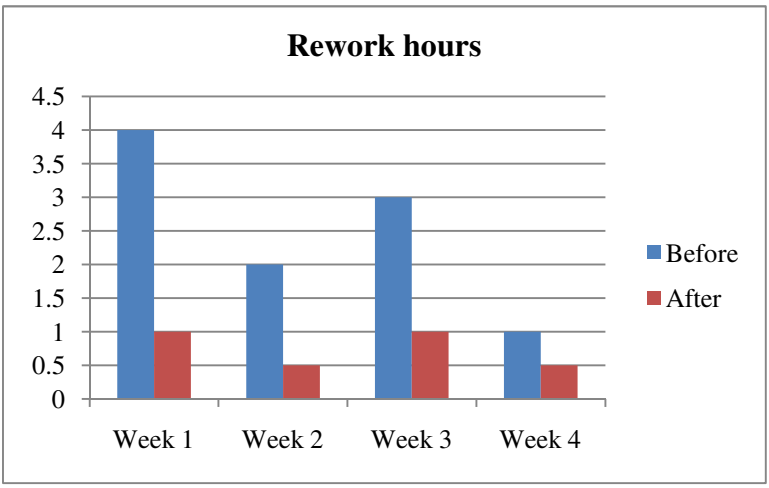

Fig. 6. Rework hours before and after improvement

Fig.6 shows rework hours before and after the above improvements were implemented.

5 Conclusion

Monitoring process with kpi helps the organizations to achieve ambitious goals in the dynamic business environment.

The paper aim was to improve a Help Desk process that presented numerous problems regarding: people, data, equipment and quality. Each of this cause presented its own factors that became visible with Fishbone analyze. The paper presents a solution for one cause of the process inefficiency – quality. The factors of quality problems were: incidents resolution, time overdue, customer complaints and rework hours. For each of these factors customized kpi were developed and measurement methods were set. After improvements were implemented the process performance raised: at level 1 with 171,92%, at level 2 with 105,99%, process accuracy (customer complaints free) with 29,69% and average rework hours ware reduce with 6 hours and a half.

One novelty of the research paper is the original 3 step process enhancement and also the flexibility of adapting the kpi development to different types of processes from diverse industry areas.

The paper has the limitation that it focuses only on the quality part of the process, other causes of process inefficiency presented in the fishbone analyze are overlooked, but it represents a strong base for future work.

Acknowledgment. This work was partially supported by the strategic grant POSDRU 107/1.5/S/77265 (2010) of the Ministry of Labour, Family and Social Protection, Romania, co-financed by the European Social Fund – Investing in people.

References

1. Riches, T.: Top 10 Business Priorities for 2011, BPTrends (January 2011)
2. Amyot, A.P.D., Weiss, P.C.M., Forster, A.J.: Business Process Monitoring and Alignment: An Approach Based on the User Requirements Notation and Business Intelligence Tools-2007/5. In: Proceedings of the 10th Workshop of Requirement Engineering (WERE 2007), Toronto, pp. 80–91 (2007)
3. Ishikawa, K.: Introduction to Quality Control. Productivity Press (1990), ISBN 10: 490622461X, 13: 9784906224616
4. Six Sigma ONLINE Aveta Business Institute, http://www.sixsigmaonline.org/
5. Kaufman, R.: - Preparing Useful Performance Indicators. Train. Dev. J. 42(9), 80 (1988)
6. Taylor, C.: Fitz-Gibbon-Performance Indicators 1990 Number 2, Multilingual Matters Ltd., Clevedon (1990), ISBN 10: 1853590924, 13: 978185359092

Optimizing E-Business Using Learning-Based Systems

Irina-Steliana Stan and Ion-Sorin Stroe

Department of Economic Informatics, Faculty of Cybernetics,
Statisics and Economic Informatics, Academy of Economic Studies, Bucharest, Romania
stan_irinasteliana@yahoo.com, soso@soso.ro

Abstract. The main element of profit-bringing in the business, so in the e-business too, is the client; therefore increasing the financial efficiency can be achieved by optimizing the components that stimulate him to allocate more money for the business products and services. This article aims to propose a technical frame, an orientation and a development analysis in terms of learning-based systems. Using ontology, learning-based system will have as purpose understanding user preferences and correctly predicting them by starting from a minimal knowledge accumulation, so that the interest rate reached by this information to be larger. Learning-based system will work with web platform, so that the generated decisions to be implemented dynamically, rapidly and automatically.

Keywords: Learning-based Systems, E-Business, Ontology, Optimize.

1 Introduction

The purpose of any physical or legal entity is to have performance, meaning long-term profitability. Profitability is the most important defining element. There are no economic arguments for a business to continue operations when, constantly, costs are higher than income. This main element is not exclusive, meaning that it should be taken into consideration the idea of finding a competitive model to comply with all applicable rules and possibly anticipate them.

Growing and maintaining profitability is achieved through continuous optimization of the factors that make the business. Thus, the online component used to improve performance, whether applies in parallel with a traditional business, whether is seen as a self-contained element.

Comparing the two businesses, the classical and the online one, the latter may have a higher success rate, due to how it can be extended: a large number of potential customers readily available at low cost, high financial returns which leads to performance for customers and automatically, for business.

Among the most profitable companies in the world, made by Fortune magazine in 2011 [1], Google (activity carried out exclusively online) is positioned in 19th place. This shows that the environment is an optimal climate for business development. Moreover, there is international support in this regard: attention in this area (there is a strong tendency to support consistent online environment by all the major internation-

V.E. Balas et al. (Eds.): Soft Computing Applications, AISC 195, pp. 649–657.
springerlink.com

al companies), the incentive legislative base, context for research, special funds (including European Union funds [2]).

Optimization can take place only if it is known the state of the online business, meaning if an internal audit is made in order to classify the system and to find vulnerabilities (those elements that can be improved). Knowledge will be dynamic because the business has dynamic elements that require repetitive analysis, knowledge cycles on a certain period of time.

Current economic environment revealed that only business entities which had a very well structured internal system could maintain a positive rate of return so as not to leave the market.

Dynamic and important continuous changes in society presented interest in conducting analyzes on specific situations related to development and business continuity in various fields. So, a question to be asked would be what is the logic behind the fact that two businesses having the same profile, same development opportunities and recognition, influenced by the same factors have different returns? The answer comes after a detailed study on every internal process and on the correlation between different processes within the business.

The current economic environment highlighted the non-consistency of business and the fact that many of them could not cope with the economic environment, while others had a considerable profit.

Analyzing the internal processes of the successful companies of today revealed features that distinguish them in the competition:

- Automation of internal processes;
- Using an evolving knowledge base [3];
- Implementation of decisions in a short period;
- Decision analysis in multiple phases in order to detect non-profitable decisions before they cause major adverse effects;
- Use a predictive system to provide to the customers an environment that he expects to have involuntarily, but is not aware of that.

This article aims to propose methods that increase efficiency by optimizing components regarding the interaction with the users. Thus, we propose an ontology structure and directions for developing a learning-based system algorithm, in order to achieve an environment in which online business operates so that the degree of satisfaction on users to be maximal. This is done only by advanced knowledge on the customers, such as their preferences in time, the learning-based system being responsible on the predictive proposals.

2 Ontology and Learning-Based Systems

The word ontology was introduced in computer science as a way to assign meaning to certain things, in order to support intelligent systems in perceiving knowledge similar to how humans do it. It expands the acceptance mainly used in philosophy, namely "the study of Being or Existence" [4].

Given the high amount and complexity of data, ontology helps on the homogenization and almost total elimination of chaotic and dispersed nature of the data [5]. Multiple sources make difficult to understand and link data so, using this concept, it can be grouped, prioritized and give the possibility to create between it bonds of sense, form and understanding. So, looking at the logic behind this concept, we can admit that ontology is one of the most efficient ways to represent complex and detailed knowledge [6].

The existence of large amounts of data affects the final result in the creation of ontology. As more details are, the senses will be more complex, but the end result will have a higher level of completeness.

The difference between ontology and learning-based systems is on complexity. If ontology groups certain knowledge and defines relations between them by giving a human understanding on information, the learning-based system includes that feature that completes ontology with the ability to make decisions with reduced involvement of individuals and to engage dynamic data set.

Introducing the learning-based system concept shows that there is a continuous effort to achieve systems that improve their performance through experience, so-called "learning" activity performed by a learning agent being similar to the learning done by the human subject.

Some systems based on the technology of learning-based systems tend to eliminate the need for human intuition in the analysis of data, while others adopt a collaborative approach between man and machine. Human intuition cannot be completely removed since the system designer must specify the logic on the representation of the data and what mechanism will be used for their search. Learning systems resemble with an attempt to automate parts of a scientific method.

The learning-based systems refers to changes in systems that perform various tasks related to artificial intelligence, tasks involving recognition, diagnosis, planning, forecasting, which cannot be completely defined only through examples, but by specifying input data and expected results. Results are derived on the assumption that there is some input, without having a well defined input-output function, but only by approximating implicit relations. Often, correlations and connections are "hidden" behind the huge quantities of data, but using the learning-based systems technology this information can be extracted.

Often, systems are designed not to function effectively in the environment that they are used because some features of the working model could not be clearly defined at the time of their creation, but the learning-based systems methods are used on supporting them. Information diversifies and generates new knowledge flows, which would require replication of artificial intelligence systems, but since this is not a practical solution, it is expected that the learning-based systems technology would successfully cope with these situations.

Automatic learning presumes identifying and implementing more efficient ways to represent information in order to facilitate search, reorganization, change and awarding a plurality of multidirectional relationships. Choosing how to qualify such knowledge refers on the general conception of how to solve the problem and on the data features which are used to work.

Learning should lead on getting enough "rules" so as to allow solving problems in a wider area than under which the learning was done. That learning must improve the performance of a system not only by resolving the same set of problems, but also by solving some new problems.
The possibility of implementing a learning algorithm and generally using learning for designing intelligent systems implies generalization of the solving methods obtained to cover a large number of possible instances and at the same time maintaining a sufficient specialization so as to correctly identify the accepted courts.

3 Analysis on Building a Learning-Based System

Specialized learning systems contain a minimal basis and, in addition, they have features closely related to the domain to be used. Learning systems in electronic business will include the features that define the knowledge used routinely in online business. In this regard, we classify all the information that a business can have as follows:

- Management knowledge, related to internal mechanisms;
- Knowledge about knowledge related to working with certain types of information;
- Knowledge about customers;
- Knowledge of different.

The purpose of this article is to show a way to increase e-business efficiency by optimizing the component related to the client.

E-business, as well as classic business, is built around customers, as they are the ones that give directions for development. The client can be any person or entity. Potential customers of e-business are generically called visitors so we will refer to them in terms of specifics they have.

The bridge of interaction with the clients is the technical platform. It receives and provides information, dependent or not. This dependence is given by the complexity of the technical platform meaning all of its subcomponents. As the system's ability to process information coming from the client is greater, the yield - from all points of view - may increase. Thus, an efficient system is one that is dynamic and makes use of the advantage received by the visitor (user) in order to obtain from him a higher income on the long run.

Having a pragmatic approach, we can say that optimizing the component that keeps the user interaction can be achieved by implementing a learning system and providing ontology for aggregating knowledge from different sources.

Learning-based systems should provide two minimal functions:

- Automatically find relevant business information: e-business works with a huge number of information, as part of internal processes or as part of output for clients. Reducing this information is imperative and the result is to provide to the visitors personalized content, meaning potential income bringing content. The chances of a visitor to become a customer decrease with the amount of irrelevant business information provided.

- Prediction: preferential positioning over the competition is made by obtaining exclusive knowledge with a high degree of accuracy and detail. The result of knowledge processing will be providing functionalities in accordance with future needs.

The proposed ontology will structure the knowledge with what an e-business is working with, oriented on the consumer. So, the goal would be identifying and predicting the customer's needs in order to get at the end his satisfaction [7]. Top-level element will be the user and from him will be created sub levels containing user-specific elements of detail in order to obtain meanings.

The learning system will use structured knowledge based on the defined ontology, will process and issue options that will be dynamically integrated or will be subject to supervision and human decisions.

This paper aims not to research on how to obtain the data coming from different databases, libraries or other sources [8], but to show the processing and use logic, starting from the idea that knowledge is available in specific databases - owned or external, complete or incomplete and will be managed using specific technologies of extraction.

A very important aspect to note on the ontology to be created is that all data, regardless of the usefulness in time, will be saved for future processing. Data will be chronologically ordered, having an historical character.

Ontology will group and use the following data types, aggregated in classes:

1. Personal Data Class

Positioned on the topmost level, the data in this category should be as relevant and accurate so as to uniquely identify a particular consumer. This condition is not mandatory but is a goal, the ideal situation.

Class components will include: Identification number, Name, Physical address, E-mail address, Telephone number, Income and other information useful to describe in a more complex way the user.

Also in this class we will include personal preferences and occupations related to the user such as Occupation, Styles and Hobbies - items included in subclass Preferences.

Within this class will be stored Person-to-Person relationships that could help identify the person and increase the level of detail. In other words, based on the relationships, we will be able to identify a user, indirectly, even if we will not have data on it.

2. Data on Online Accessing Activity

We will monitor the online activities developed around the customer [9], that type of interaction between them and the entities present in the web. We will want to know all aspects related to Web browsing, and that part of a web page that had the highest activity or what was the time spent on a page related to the content offered (content classification can indicate the level of interest on the visitor reported on the assumed interest calculated level - for each content offered will calculate an index that shows which should be the time spent on the page so as to conclude the level of interest).

Class components will include: Unified Resource Locator - URL, Date, File, Technical details (connection type, time spent, operating system, location).

3. Data on Commercial Activity

If there was an e-commerce activity that the user has made in online environment, the details of this should highlight any issue that may be taken into account in the learning system.

Class components include details obtained from accessing class and in addition: Purchased Product, Amount, Date, Price, Method of payment.

4. Data on Used Services

Certain online products do not have an interface accessible using a Web browser, so identifying how the client interacts with such services will be part of a distinct category.

Class components will include: Technical Details, Product Details, Reports - its frequency of use in relation to other services, Used Technologies.

5. Data for Offline Activity

This category will include all knowledge about the user from traditional media and beyond: mobile phones (position, specific information - call, messages), physical locations accessed.

This class will have a large number of components, depending on the number and homogeneity of data. Among all types of data described above we will define a multi-directional relationship in order to provide meaning to knowledge, so that all these classes together with the links between them to form a homogeneous entity, specific to ontology with the ability to improve and self develop.

Having defined ontology and data structure, the next step is to analyze and get those specifications and directions needed to integrate the knowledge presented in the learning system. This article aims to propose an interim methodology, as part of the final objective - creating a complex algorithm, generally used, based on which the learning system will operate in optimal conditions, meaning to attend all business decisions within e-business; this will bring a significant efficiency increase.

Fundamentals of the proposed methodology are based on principles supported by the following statements: "No information will be thrown" and "All data is valuable at one moment in time ". Data contained in the defined classes will be grouped according to their relevance and importance in the algorithm. It will be processed and, according to the results obtained, will be used by the application in generating solutions. Whether after multiple iterations we can or cannot get a trend or a rule to be used and combined with other types of data, it will still be stored so that the possible future links found to be integrated.

In Fig. 1 it is shown the way data is processed, organized, grouped, how the classes are populated and the relationships between them – the ontology.

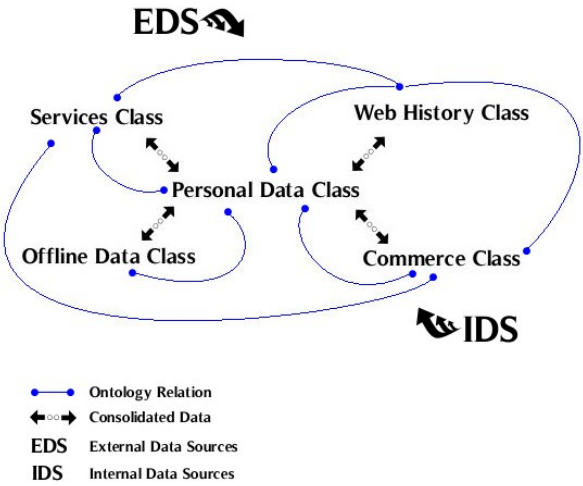

Fig. 1. Proposed Ontology Structure

For a successful integration of data from the ontology in the learning system features it should be taken into account the following aspects:

Process 1. Will be processed the data and relationships contained in Personal Data class. The purpose of this process is to position and identify the user as completely and accurately as possible, so, the learning potential in this category is relatively reduced. The nature of this class allows the learning system to validate information and attach knowledge from other unused classes until that point. Incomplete data which cannot be attached to a feature from Personal Data class will be stored and later trained to obtain additional knowledge.

That class includes subclass Preferences and the result will get the complete user profile and will lead to preferences classification according to their importance.

Process 2. In this process, we will aggregate all the knowledge and existing relationships in order to provide optimal user interface, by taking into account not only technical aspects but also elements of content.

For each web entity accessed it will be extracted some defining elements such as content offered, its quality relative to other similar environments and will be included in an algorithm, which in turn will issue elements that characterize the client profile. The engineering of the algorithm will result in more analytical details about the connection between time spent on a site, the user's interest rate, real quality and perceived quality of content, accessing period [10].

Commercial information from Acquisitions class processed by the learning system will result in products and types of services framed in a certain margin based on quantity purchased and other specific interest result of this class. It will be taken into account the user income and certain exceptions that he was willing to do because of his high interest on that product.

The outcome will result in multiple filters applied to the content offered by e-business having as objective consolidating user profile and online preferences, so as to provide him services having a conversion into acquisitions rate above medium.

As information is more attractive and relevant to the specific user profile, profitability rate is even higher. Providing useless data exponentially lowers interest and perception of the user that this e-business may satisfy his needs. The goal is not to only offer elements that give interest to it, but also to propose new solutions that could be considered by him interesting. The system features based on learning must therefore imperatively include predictions. The user capacity is limited in saying what he might be interested in for the future, but can be eased by offering possibilities. Learning-based system will process all information received and will propose solutions, with a high converting rate - the user to become customer.

Process 3. Profile will be completed using knowledge from ontology that is related to the offline environment. It will be watched the physical activity of the user and we will try structuring it. Given the heterogeneous nature of this data, it will be used for refining and detailing optional prior information.

The described processes will be integrated in a cycle that hould be followed in the algorithm. The logc is presented in Fig. 2.

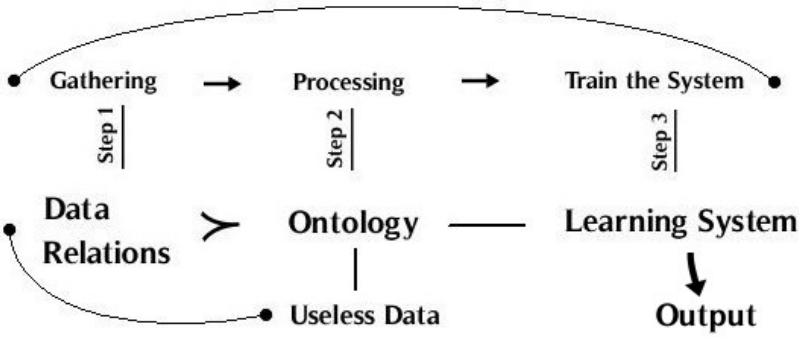

Fig. 2. The Logic of The Platform Based on Learning Systems and Ontology

4 Conclusions

Learning-based systems can complete the meaning of the ontology by optimizing existing relationships and establishing new ones; the result can contain some new meanings, revolutionary ones, which will contribute on making visible progress of the business in question.

The amount of existing and then structured information in the ontology is essential in obtaining more refined, detailed and realistic results. Training sets which will apply the learning system algorithm will process and generate solutions to complex and qualitative data in direct proportion to the data quality. The result is in most cases accomplished by taking decisions so the more the solution is customer oriented and

offers him guidance on what he wants and helps him to find certain needs, the more e-business will be successful.

The Web platform of the business must be constantly synchronized with the learning system because certain decisions need to be taken instantly, automatically, by using results directly from the system.

Analyzing the significant progress on the learning systems, on the methods of intelligent data collection and on the technologies that allow collecting, storing, processing and using a huge amount of data, it can be concluded that the tendency is to maximize information role on the decision-making in any type of business, especially within the e-businesses.

Acknowledgments. This work was cofinaced from the European Social Fund through Sectoral Operational Programme Human Resources Development 2007-2013, project number POSDRU/107/1.5/S/77213 „Ph.D. for a career in interdisciplinary economic research at the European standards".

References

[1] Magazine, Fortune. Fortune 500 2011: Top Performers. CNNMoney. Cable News Network (January 1, 2012), http://money.cnn.com/magazines/fortune/fortune500/2011/performers/companies/profits/ (Web. June 27, 2012)

[2] Union, European. Europe's Digital Competitiveness Report 2010. Europe's Digital Competitiveness Report 2010 (January 1, 2011), http://ec.europa.eu/information_society/digital-agenda/documents/edcr.pdf (Web. March 1, 2012)

[3] Hsu, G., Lin, Y., Wei, Z.: Competition Policy for Technological Innovation in an Era of Knowledge-based Economy. Knowledge-Based Systems 21(8), 826–832 (2008)

[4] Simperl, E.: Reusing Ontologies on the Semantic Web: A Feasibility Study. Data & Knowledge Engineering 68(10), 905–925 (2009)

[5] García-Castro, R., Gómez-Pérez, A.: Interoperability Results for Semantic Web Technologies Using OWL as the Interchange Language. Web Seman-tics: Science, Services and Agents on the World Wide Web 8(4), 278–291 (2010)

[6] Park, J., Cho, W., Rho, S.: Evaluating Ontology Extraction Tools Using a Comprehensive Evaluation Framework. Data & Knowledge Engineering 69(10), 1043–1061 (2010)

[7] Liu, X., Zhang, W.J., Tu, Y.L., Jiang, R.: An Analytical Approach to Customer Requirement Satisfaction in Design Specification Development. IEEE Transactions on Engineering Management 55(1), 94–102 (2008)

[8] D'Aquin, M., Noy, N.F.: Where to Publish and Find Ontologies? A Survey of Ontology Libraries. Web Semantics: Science, Services and Agents on the World Wide Web 11, 96–111 (2012)

[9] Liu, Y., Xue, Y., Xu, D., Cen, R., Zhang, M., Ma, S., Ru, L.: Constructing a Reliable Web Graph with Information on Browsing Behavior. Decision Support Systems (accepted, 2012)

[10] Zhou, Q., Ye, H., Ding, Z.: Performance Analysis of Web Applications Based on User Navigation. Physics Procedia 24, Part B, 1319–1328 (2012)

The Efficiency in Time and Financial Resources Management of an Individual by Developing an Informatics Support

Serban Popa and Gabriela Prostean

Politehnica University, Management Department, Timisoara, Romania
popaserban@yahoo.com, gabriela.prostean@mpt.upt.ro

Abstract. This article presents a solution for managing the monthly and/or yearly payments of an individual, either a person, either a company. In the future terminology in this article an individual will also be called an user. The solution is based on an online platform which manages all the users expenses. The time spent for the payments is zero and the indirect costs for these payments are low. The rent, home, car and personal assurance, the utilities: electricity, gas, mobile and fix telephony, internet, TV, water and local taxes are some of the payments that are managed by our service.

Keywords: utilities payment, utilities management, optimize time, efficiency in payments, electricity payment, gas payments, online solution, domestic payments management.

1 Introduction

Persons have a large number of invoices to pay during a certain period of time. These invoices are send via post, mailed or given in a copy or original to the final user. The user (basically the consumer) has to receive all invoices, have to review them, track the deadlines and finally pay them. As users receive a larger quantity of invoices the payment process become more and more elaborated and harder to be managed. More time is spent by the user if he must contact the originator of the invoice, the supplier, if a problem appears in the invoice (the sum to be paid is not the correct one, the deadline is not correct or any other dispute). In all situations there is a need for time, effort and resources to be invested in the process that could be fully automated. Due to these facts many persons are having delays in paying their expenses, fact proven by the study that can be seen in the figure 1 [1].

Several ways for managing the users payments have been developed. In [2] a method is presented that involves receiving identification (ID) for a payer payment from a card reader e.g. credit card inquiring apparatus and detecting applicant and history corresponding to the ID for the received payment. The use is for utility bill payment method. In [3] a transaction barcode is read to collect the supplier identification information and verify the client information of the corresponding supplier upon receipt

V.E. Balas et al. (Eds.): Soft Computing Applications, AISC 195, pp. 659–667.
springerlink.com

of a transaction request made by the customer. It is used for paying educational fee, insurance bill, utility bill, rental fee. The disadvantage is that it requires human resources during the process and it is not fully automated. In [4] a novel AMR system based on IEEE 802.15.4 compliant wireless networks is proposed. A star or peer to peer topology is used for the data collection. The advantage of the peer-to-peer solution is its increased flexibility and robustness. The automated collection of data from the energy meters, described in [5], would save time for the payer. Data is collected by the mobile devices that pass near the meters and the payer must not declare each month this data. The domestic utilities payment can be paid by using a mobile phone. This solution, described in [6], is more efficient in time than the classic payment solutions but has higher costs.

Our solution is configured as an online service that can be accessed anywhere at any moment with a minimum of hardware and software: a computer (desktop or laptop), tablet or phone using a web browser. The service manages all the utilities payments, rent, assurance and local taxes of a user. It provides different automated mechanisms for handling the monthly sums to be paid, different priority mechanisms that allow invoices with most appropriate maturity dates to be paid first if the users budget is limited.

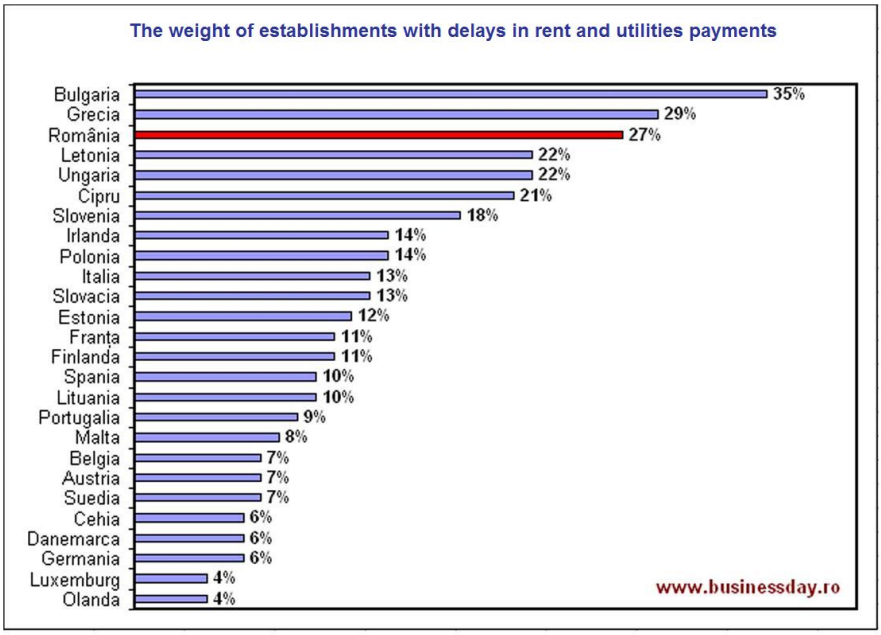

Fig. 1. The weight of establishments with delays in payments

2 The Proposed Service

2.1 Development and Implementation

The application has three modules: the website, the client module and the administration module. The user interacts with two of these modules: the website and the client module. The first interface for the user is the website where he has to register and login. After the login, the user will be redirected to the client module interface where he can access all the information related to the invoices, statistics, payments or maturity dates. The client module is implemented using Google Guice, Apache PDFBox, Hibernate, JPA, Java Mail and Log4J. It retrieves from the invoice storage the user invoices and displays them in the user account. This process can be found in figure 2. Apache PDFBox is licensed with Apache License Version 2.0 that means it can be used in commercial applications. The library is used for extracting text from the pdf files. Hibernate is an open source object relational mapping tool for Java platform. It is used to store and retrieve Java domain objects via Object Relational Mapping. It also provides powerful query service for Java. Hibernate allows the development of persistent classes using association, inheritance, polymorphism, composition and the Java collections framework. The HQL (Hibernate Query Language) is designed as a object-oriented extension to SQL and allows the developer to write queries using native SQL or Java-based Criteria and Example queries. Java Mail API is a framework that provides classes which model a mail system (e.g. reading and sending emails). The package javax.mail defines classes common to all mail systems. The package javax.mail.internet defines classes specific to the mail systems based on internet standards like POP3, SMTP or IMAP. It is platform independent and protocol independent. Java Mail works in any web browser that supports the required JDK version. If it does not support it, then a Java plug-in must be installed.

Figure 3 presents the flow of the client module. All the invoices of the suppliers for all users are arriving in one mailbox. There is a detector that has the role of detecting and extracting each invoice from each mail. An analyzer analyzes each invoice and detects the user from that invoice. All the invoices of a user are moved to the user application account where they can be accessed. Each supplier invoice of the detected user is analysed. Information from the invoice is extracted and using this data a payment notification for each user summing all the billing entities invoices is sent to the user. After the payment notification is paid and the software mechanisms from our solution detects the incomes, the money are redirected to each supplier. The process is finalized at this moment and will be reiterated at the next time period, usually the next month.

Figure 4 presents the database schema. All the mails that arrive in the application mailbox have attachments. If the attachment is a supplier invoice then it is moved into the invoice_in table, else it is moved into the failed_mails table. All the documents from the failed_mails table are managed manually by an operator. If the document is still an invoice it is moved to invoice_in else it is deleted. The java application gets the invoices from invoice_in and moves them to invoice_out for each user. All the

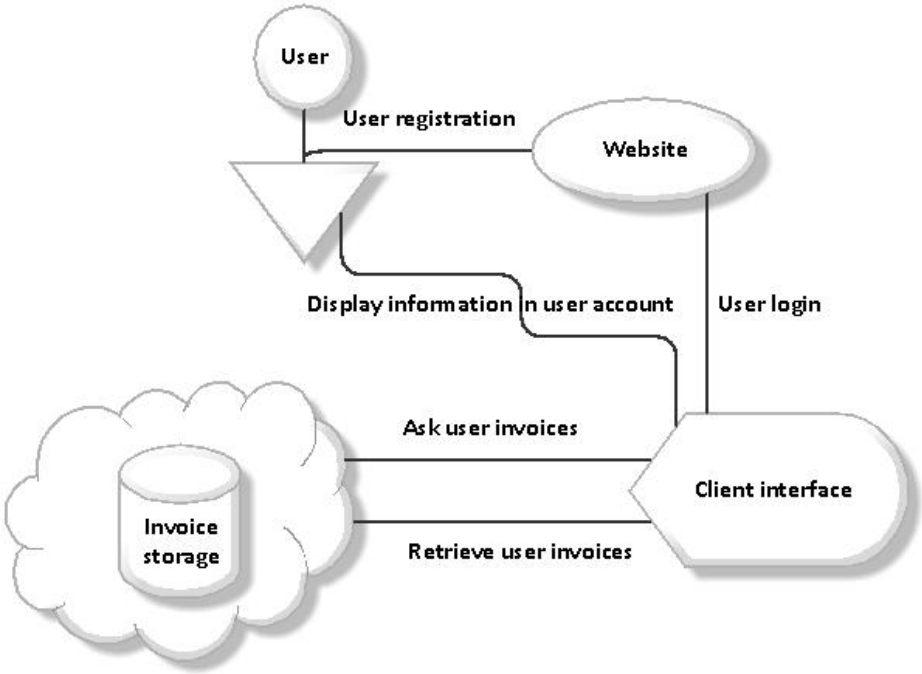

Fig. 2. Flow of information

invoices from invoice_out of a user are used to build the notification payment (usually monthly notification payment). Besides these invoices the notification payment has also the application invoice for the monthly commission. When the user logs into his account he can see a list with all the supplier invoices and their states. This state is stored into the invoices_states. All the suppliers are saved into the providers table. The services are saved into the categories table and the mapping between the suppliers and the services is done in services table. The users are saved into the clients table and the users subscribers are kept into the people table. Each user has a credentials to log into the client module, credentials saved into the client_service_credentials. Client_services table stores the relations between the client and the services, basically which services did choose each client. The service_quits table stores all the supplier services that a user deactivated. These services are not deleted by the application but they are hidden and not use for computing the notification payment. The client_document table stores all the legal documents that a user has to sign when he registers using the website and the client module. Bank_exports table contains all the payment orders issued by the application when it redirects the money to each supplier. This can happen only after the notification payment is paid. Bank_imports table contains all the bank account statements where using the relation with client_bank_imports table the users who paid the notification payment are identified.

Between the payments that are managed by the application there are also the local taxes. These taxes represent car taxes, house taxes, etc. Basically these are taxes on a user goods. These goods are kept into the goods table and the payments related to these goods are in the payments table.

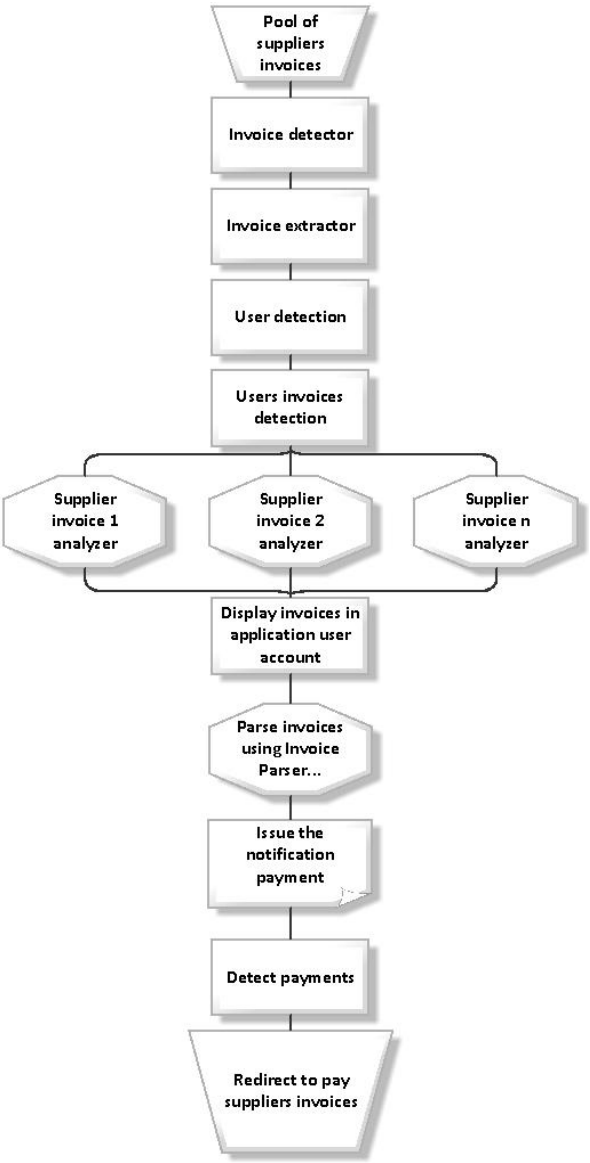

Fig. 3. The flow in the client module

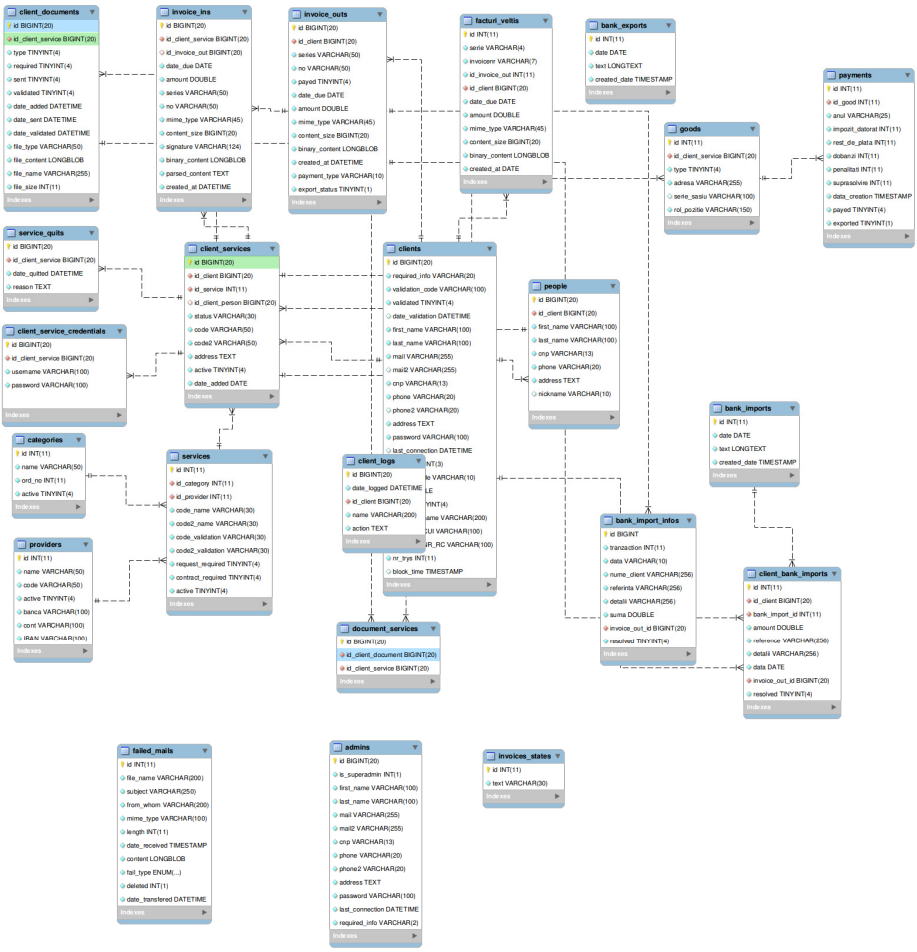

Fig. 4. The database schema of the application

Google Guice is used in the implementation of our solution. Google Guice is an open source software framework for the Java platform released by Google under an Apache license. It is a Dependency Injection Framework that can be used by applications where Relation-ship/Dependency between business objects have to be maintained manually in the application code. As an example of how it is used, I propose the code below. To create a Guice persistence module, we have to create a class Persistence Module and configure the bindings inside of configure method.

```
public class PersistenceModule extends AbstractModule {
 @Override
 protected void configure() {
  install(new JpaPersistModule("demo-jpa-test"));
  bind(JPAInitializer.class).asEagerSingleton();
```

```
 bind(new  TypeLiteral<GenericDAO<User, Long>>() {
 }).to(new  TypeLiteral<UserDAO>() {
 });
 bind(new  TypeLiteral<GenericDAO<Role, Long>>() {
 }).to(new  TypeLiteral<RoleDAO>() {
 });
 }
}
```

The second step is to create a class called JPAInitializer in order to initialize the persistence service when is necessary and to create the connection with the database:

```
public  class  JPAInitializer
{
 @Inject
 public  JPAInitializer(final  PersistService service)
 {
  service.start();
 }
}
```

2.2 **Testing**

Testing is very important and our implementation allows to easy create an object UserDAOTest by injecting the GenericDAO.

```
public  class  UserDAOTest {
 @Inject
 GenericDAO<User, Long> dao;
 @Before
 public  void  setUp() throws  Exception
 {
  Injector injector = Guice.createInjector(new  PersistenceModule());
  injector.injectMembers(this);
  dao.getEntityManager().getTransaction().begin();
 }
 @After
 public  void  tearDown() throws  Exception
 {
  dao.getEntityManager().getTransaction().rollback();
 }
```

The tests allow an efficient management of the database for rollbacks. There is no need to implement transaction. begin() and transaction.commit() methods because the transactions management is done by the framework. Let's consider a method M1() that has a transaction and calls a method M2() which also has a transaction. If the

transaction form M2() fails then the transaction form M1() can be continued and the code does not have to throw an exception.

```
@Test
 public  void  testFindsetUsername("user1");
  user.setPassword("password");
  user.setStatus(Boolean.TRUE);
  Long id = dao.insert(user);
  assertNotNull(dao.find(id));
 }
 }
```

2.3 Security Issues

MD5 encryption is the base for the security. MD5 algorithm calculates a checksum string corresponding to a string that will always return the same checksum. Any change in the string, even a tiny change, leads to major changes for the MD5 checksum.

Obtaining a SSL (short from Secure Sockets Layer) certificate is the next step. The SSL certificate is a certificate for a web interface that assures the security of the on-line transactions. It allows the secure transactions to be made on 256 bits. The two keys to encrypt data used by the cryptographic system of the SSL are a private key known only by the receiver of the message and a public key known by everyone. SSL works by following the next steps:

- A secure page is requested by a browser (usually https://).
- The public key is send by the web server together with its certificate.
- The browser checks that the certificate was issued by a trusted party (usually a trusted root CA), that the certificate is still valid and that the certificate is related to the site contacted.
- The browser then uses the public key, to encrypt a random symmetric encryption key and sends it to the server with the encrypted URL required as well as other encrypted http data.
- The web server decrypts the symmetric encryption key using its private key and uses the symmetric key to decrypt the URL and http data.
- The web server sends back the requested html document and http data encrypted with the symmetric key.
- The http data and html document is decrypted by the browser using the symmetric key and displays the information.

2.4 Risks

The risks associated with our solution can be enumerated below:

- Risks associated with development, implementation and human resources. Refers to the possible erroneous choice of the project manager in selecting proper software developers and architects.

- Risks associated with the competition. There are several applications that have a similar use but they all have downsides, either in costs, either in time effort.
- Risks associated to the financial part. The finance must be split in different budgets for all the operational activities. The ROI (Return of Investment) is hard to be estimated but we expect a positive ROI after minimum 3 years.
- Risks associated with perception. The public perception is vital for the success of the solution. To minimize these type of risks we must invest a lot in communication and associate our name with different suppliers and banks.
- Risks associated with the technology. The technologies evolve very quickly and we must always implement the latest ones for a fast use of the application. The software model must be object oriented and must be adjusted for all new features.
- Risks associated to the management. These risks refer to the management of the relations with the suppliers and the users and to a good planning of the activities and of the development sprints.

3 Conclusions

The paper described a novel and original solution for managing the utilities payments of an individual or a company. It is an informatics solution, online, and it requires no time involved for the users and has the minimum cost possible comparing to all the other existing payment solutions.

References

1. Economie si Finante, http://www.businessday.ro
2. Wi, J., Joon, S.W.: Utility bill payment method, involves receiving identification for payer payment from card reader, and detecting applicant and demand history corresponding to identification for received payer payment. Patent number KR 1014368-B1 (2011)
3. Wee, J., Wee. J.S.: Payment service for paying e.g. educational fee, insurance bill, utility bill, rental fee, involves requesting approval of transaction made by purchaser for merchant to finance company corresponding to financial institution card. Patent Number JP 2009521764-W (2009)
4. Zhu, J., Pecen, R.: A Novel Automatic Utility Data Collection System using IEEE 802.15.4-Compliant Wireless Mesh Networks. In: Proc. of the 2008 IAJC-IJME International Conference, Nashville, Tennessee, November 17-19 (2008)
5. Popa, M.: Data Collecting from Smart Meters in an Advanced Metering Infrastructure. In: Proceedings of INES 2011, The 15th International Conference on Intelligent Engineering Systems, pp. 137–142 (2011) ISBN 978-1-4244-8955
6. Ahmad, F., Nasr, M.: A proposed e-government framework utilities payment: a case study for electricity utility. Ubiquitous Computing and Communication Journal (2011) ISSN 1992-8424

Planning Business Process Management Implementation by a Human Resources Development Support Initiative

Cristian Olariu[1], Alexandru Canda[1], Anca Draghici[1], and Tomislav Rozman[2]

[1] "Politehnica" University of Timisoara, Romania
{cristian83,alexandru.canda}@yahoo.com, adraghici@eng.upt.ro
[2] BICERO d.o.o Maribor, Slovenia
tomislav.rozman@bicero.com

Abstract. Through this article we intent to demonstrate how a qualification and certification program, as CertiBPM, developed and implemented with the support of European Certification and Qualification Association (ECQA), can be use for the Human Resources Development in the field of Business Process Management. The described initiative has been tested, validated and successfully implemented on Romanian market (especially in West and Bucharest Regions). After a brief description of the proposed training and certification program, there will be shown the training needs (marketing research results) collected from employees from Romanian companies from different industrial sectors. In the third part, there will be describe the e-learning facilities correlated with the design skill card and the ECQA guidelines for training and certification. Finally, some conclusions and lessons learned will complete the article. The presented paper is linked with the research activities of the project: CertiBPM - Certified Business Process Manager LLP-LdV/TOI/10/RO/010, founded with support from the European Commission. This paper and its communication reflect the views only of the authors, and the Commission cannot be held responsible for any use, which may be made of the information contained therein.

Keywords: Business Process Management (BPM), Marketing Survey, Training, Certification, Human Resources, e-Learning.

1 Introduction

In the complex environment of actual businesses, with ever-changing variables and conditions, the needs for continuous improvement and agile approach emerged are natural and viable consequence. In order to react and manage these changes and, furthermore, in order generate changes in the business environment (by forecasting, business simulation techniques and high focus on innovation), organizations have to be aligned around the future and for a further success [5] through responsible and capable human resources management (teams, leadership). Thus, the business units / enterprise must develop a business architecture that will facilitate the speed of change [15], architecture that is linked not only to business strategies and methods or new

V.E. Balas et al. (Eds.): Soft Computing Applications, AISC 195, pp. 669–680.
springerlink.com

working paradigms, but also (and more important) to create the appropriate mindset and attitude towards the business environmental change – external and internal. In this context, the role of human resources management is determinant.

Every action or event that takes place inside a particular business is most of the times generated, monitored, analyzed and influenced by the person / employee or a team work that is part of human resources management in an organization. Furthermore, in order to have a proper response to these changes there have to be change the way people / employee / human resources behave inside the organization, and from here to forecast, predict and influence the external environment context and/or conditions [7].

There is recognized that best results and appropriate responses come from people that are professional in their field of specialization, but also who are well support, motivated and enthusiast. One of the roles of the business's core management team is to design jobs that challenge employees to maximize their potential [14]. Throughout these, people must also see not only the impact that their work is generation on the immediate environment, but also "the big picture" of their business; by this there will be created a team with a social responsible behavior [6]. At the core of these approaches, attitudes and paradigms, we have the knowledge that is share and spread in and by the company. In order to have a knowledge-based approach that will further support the agile paradigm, there have been proposed the following five levels of role perspectives [16] inside a business unit/enterprise (Figure 1).

Fig. 1. The Five Levels of the Role Perspective on Intellectual Capital Governance vs. Knowledge Management Activities (adapted from [16])

Above all the human resources and working teams/groups are the managers and leaders that must not only expect positive attitudes towards the agile approaches, but, they must generate, create an Agile-Oriented Culture (AOC) as an evaluate organizational culture characterize by specific dimensions of the organizational behavior. Simultaneously, managers have to develop themselves to be agile leaders – they must learn to lead [3] under the agile principles. These are important and mandatory aspect of the agile paradigm implementation strategy. The current leaders learning to be agile will be the company's future teachers and trainers for their teams. The agile leaders must not only overview and focus on the work results, but also the human resources activities of all categories, including the communication processes inside the working groups/teams. The teams, the leaders and the communication are three important and necessary aspects of an efficient and successful agile implementation [17].

From this brief overview of the agile paradigm, phenomenon that modern organization are confronted with, there have to be underlie the important role of human resources management (individual expertise and competencies, core competence of the organization and intellectual capital extended overview) in the process of organizational changes and/or adaptation. In the same context, there have to be analyze the external vs. internal environment challenges by taking into consideration the variety of the business processes, correlated with the systemic approach of the organization. Modern organizations have to developed and sustained progressively complex business processes that faced the external environment opportunities and/or threats. Enterprises processes improvements are achieved goals if an ongoing process improvement program is followed but also, refinement and up-date by considering the new turbulent global market conditions. Extensive experience and expertise in achieving institutionalization of process improvements are desirable pre-condition to gain/generate a positive impact in any organization that want to become agile in the nearest future [1].

Sometime, organizations built-up specific improvement capabilities to better optimize their business process. Such capability is linked with issues as: process assessment, process design and deployment, process knowledge management, quality management, systems and software quantitative solutions etc. When growing their businesses, organizations should not only put effort into developing and executing their business strategies, but also into managing and improving their internal processes and aligning them with business growth strategies, but everything in a strong relation with the human resources development strategy. It is only in this way they may confirm that their businesses grow in a healthy and sustainable way [11], [13].

In organizations that operate with a Business Process Management (BPM) system as an integral part of their mission and objectives, it becomes clear that they are focused on targets for process improvement convergent to agile principles implementation. From the empirical perspective, it has been found that continuous improvement activities can be key source of environmental improvement [4] by taking into consideration the social responsibility framework, too.

BPM represents a holistic management approach (or a modern management system) based on continuous improvement processes, change management theories, and

support by modern information and communication technologies/systems. This approach aim to attend an optimal balance between organization's external environment dynamics and its internal processes functionalities based on innovation, flexibility and agility [1]. In additional, BPM represent and it is also associated with a complex project related to continuous improvement and adaptation of the organizations relations from the perspective of the internal and external environment.

The present articles objective is to present the effects generated by the CertiBPM - Certified Business Process Manager (LLP-LdV/TOI/10/RO/010) - CertiBPM training program in Romania [2]. That initiative was designed to support the human resources development (qualification and certification) in the field of implementing and using/exploitation of BPM systems in Romanian organizations (of all types – small and medium size, big companies, multinational, public and private that belong to different economic sectors). The described initiative has been tested, validated and successfully implemented on Romanian market (especially in West and Bucharest Regions). After a brief description of the proposed training and certification program, there will be shown the training needs (marketing research results) collected from employees from Romanian companies from different industrial sectors. In the third part, there will be describe the e-learning facilities correlated with the design skill card and the ECQA guidelines for training and certification [8], [9]. Finally, some conclusions and lessons learned will complete the article.

2 The Romanian Market Need For BPM - An Offer and Demand Analyze

2.1 CertiBPM Training and Certification Program

The motivation for the CertiBPM project lies on the Romanian market training needs satisfaction in the field of BPM. These needs were capture and characterized during the second semester of 2009 when a series of focus groups interviews were conducted with representatives from companies located in West and Bucharest Regions of Romania (the most economic developed Regions that were proposed for the CertiBPM project implementation). In 2009 the CertiBPM project proposal was developed. The following ideas have arisen from the preliminary marketing research:

1. Representatives of different companies agree on an important need regarding the training and certification in the field of BPM, because of numerous problems and incidents in the specific management systems exploitation and for better supporting the business processes (with the main target of organizations resources optimization);
2. Managers of different level agree on coupling the human resources development strategies with the future CertiBPM initiative;
3. The competencies improving processes for the employees / human resources of Romanian companies will have a positive impact upon their results and also, upon the BPM implementation initiatives. The CertiBPM Training/Qualification Program – Learning Units and Elements are shown in Table 1.

Table 1. The CertiBPM Training/Qualification Program – Learning Units and Elements

Units and Elements Code	Learning Units and Elements Title	No. of Performance Criteria
BPM.U0	**Informative package**	5
BPM.U0.E0	Introduction	2
BPM.U0.E1	ECQA and certification information (demonstration on www.ecqa.org and the Learning Portal)	2
BPM.U0.E2	Conclusions and References data base	1
BPM.U1	**Process Oriented Management**	24
BPM.U1.E1	Management System (ISO 9001:2008)	5
BPM.U1.E2	Managing BPM projects	5
BPM.U1.E3	BPM and Modeling	5
BPM.U1.E4	Documenting Business Process	4
BPM.U1.E5	Process Simulation and Analysis basics, tools and techniques	5
BPM.U2	**BPM and Information Technologies (IT)**	16
BPM.U2.E1	Choosing your BPM tool/platform	5
BPM.U2.E2	BPM tools/platform	7
BPM.U2.E3	BPM and Enterprise architecture	2
BPM.U2.E4	BPM systems and IT integration	2
BPM.U3	**BPM human aspects. Frameworks and Standards**	12
BPM.U3.E1	Human factors in BPM	4
BPM.U3.E2	Motivating people for process change	3
BPM.U3.E3	BPM models, frameworks and standards	5
BPM.U4	**BPM Specializations**	-
BPM.U4.E1	BP manager for IT processes	-
BPM.U4.E2	BP manager for core sales & marketing processes	-

CertiBPM initiative is related to the transfer of innovation process from Slovenia and Austria to Romania. It consists of: Transfer of Education, Training and Certification concept of ECQA into the university and manufacturing domain in Romania. Aspects of the project impact are related to: CertiBPM will build on BPM knowledge and competencies in different industrial sectors, which are represented by the consortium members due to their activities with national and international enterprises; transfer of the ECQA concept and platform into Romanian market; implementing the CertiBPM job-role and examination committees for certifying training bodies and exam tools in multilingual environment; the important knowledge of CertiBPM and

the important system of an uniform European certification will be very useful for Romanian manufacturing industry, especially for automotive and telecommunication industries [2]. The core of the results envisaged is a skill set which clearly fit the competencies required for becoming a BPM specialist (basic level and advanced level). For all the skill elements training material will be provided in several languages (English, Slovenian, and Romanian) and will be upload on an e-learning system. A pool of test questions will be defined, which provides the basis for the trainees' certification process.

The CertiBPM qualification and certification addresses itself to employees from companies departments related to: Quality management (as TQM), CRM (Customer Relationship Management), ERP (Enterprise Resource Planning), SCM (Supply Chain Management), and enterprise information system's specialists etc., who want to complement and/or certify their advanced BPM skills. The target group typically has abilities for self-development and self-learning, creativity, innovative initiatives etc. One of the biggest challenges is to conceive a training program that covers the complete skills set that better satisfy the target group specific needs. The original training program and materials have been developed trough creative, synergetic energy of the project members' interactions (during face-to-face project meetings, and virtual meeting using Skype conference facilities, from December 2010 till December 2011). Training Material version 2012 (Table 1) was developed within the international consortium of the project.

The CertiBPM training materials content and structure were elaborated with respect and according to the guidelines and requirements of the European Certification and Qualification Association (ECQA, www.ecqa.org). According to these requirements, issues that are mandatory for defining a new profession are: the skill set description, the learning units and elements, and the performance criteria for each learning element (this is a typical tree structure of the training program). This basic structure shown in Table 1 was elaborated after the methodology described in [10].

The structure is well define and the units and elements are well described and consistent in relation with the performance criteria, the profession is recognized by the ECQA (the Job Role Committee – usually representatives from a Leonardo da Vinci (that assure the financial support for this development) project partners - that join together specialists and personalities in the specific professional field is also recognized by ECQA as a valid body) and they could support the examination process in order to generate ECQA certificates for the corresponding profession (the Job Role Committee can start prepare the examination question pool that is related to the corresponding performance criteria, in accordance with the ECQA Examination Guide) [12].

2.2 BPM Training Needs Identification – Marketing Research Results

The study surveyed companies located in the West and Bucharest Regions of Romania, from different industries (Table 2 shows the sample structure). Small and medium size enterprises and big companies (public and private) were considered for the research sample. Companies were selected randomly and for each of them one executive (CEO, CIO or quality manager etc.) was interviewed together with other

middle and low-level managers. 44 organizations were interviewed but 64 questionnaires fill-up were received and process (sample size n=102, answer rate 0.627). The telephone, e-mail and face-to-face structured interview method were adopted to obtain responses to the study's survey instrument. Although it was a resource intensive option, it was chosen over the standard methods of administrating paper or online surveys for various reasons:

- To be able to clarify respondents' queries;
- To avoid the situation whereby a busy executive or senior manager delegated the task of fill-up the survey to a secretary; and
- To ensure that most of the responses collected were complete and usable for data analysis.

The research was developed from March to end of May 2012 and it has generated mature research results, because the sample consists of managers, representatives from companies that were involved in the CertiBPM training program (in-class training).

Table 2. The Research Sample Structure

Field of economic sector or industry	No of companies	%	No. of respondents	%
1. Automotive	10	22.73	18	28.13
2. Telecommunications, Electronics, Energetic	6	13.64	7	10.94
3. Manufacturing Machinery	11	25.00	13	20.31
4. IT and software developers	5	11.36	7	10.94
5. Logistics Distributions	5	11.36	7	10.94
6. Tourism and Financial Service Industries	5	11.36	5	7.80
7. University professors and students	2	4.54	7	10.94
TOTAL	44	100	64	100

For the structured interview method approach a questionnaire has been developed. The questionnaire structure follows the CertiBPM skill set/card. In the beginning of the questionnaire, the research aims and a brief introduction in BPM (based on references) have been explained. The questions considered for the CertiBPM training needs identification and collection were detailed in accordance with the charters of the training program (Table 1) and the respondents have to answer the following question: Do you consider an opportunity for your organization to be involved in a training program related to U/E?

All questions on BPM training needs identification were measured on a six point Likert scale (1="fully disagree" – 6="fully agree"). In the final part of the questionnaire, there were collected data for the respondent characterization (company, position, age, sex, and contact data) for better described the research sample.

Table 3. The Skill Matrix with Gap Indicators

Sector*/ Questions	1	2	3	4	5	6	7	Total score	Specific needs %
BPM.U0.E0	X	X	X	X	X	X	X	7	100
BPM.U0.E1	X	X	X	X	X	X	X	7	100
BPM.U0.E2	X	X	X	X	X	X	X	7	100
BPM.U1.E1	X	X	X	X	X	X	X	7	100
BPM.U1.E2	X	X	X	X	X	X	X	7	100
BPM.U1.E3	X	X	X	X	X	X	X	7	100
BPM.U1.E4	X	X	X	X	X	X	X	7	100
BPM.U1.E5	X	X	X	X	X	X	X	7	100
BPM.U2.E1	X	-	-	X	-	-	-	2	29
BPM.U2.E2	X	-	-	X	-	-	-	2	29
BPM.U2.E3	X	-	-	X	-	-	-	2	29
BPM.U2.E4	X	-	-	X	-	-	-	2	29
BPM.U3.E1	X	X	X	X	X	X	X	7	100
BPM.U3.E2	X	X	-	X	X	X	X	6	86
BPM.U3.E3	X	-	-	X	-	X	X	4	57
BPM.U4.E1	X	-	-	X	-	-	X	3	43
BPM.U4.E2	X	-	-	X	-	-	X	3	43
Total score	17	10	9	17	10	11	13		
Specific needs %	100	59	53	100	59	65	76		

*) As shown in Table 1.

The research methodology allows a depth analysis of the skills needed to be trained in a BPM training program (skills analysis method). Table 2 is the skill matrix build as a quick and effective way of identifying the BPM training needs. For the results' presentation there have been consider the respondent structure by their industry/economic field as shown in Table 2.

The Excel software was used for the results visualization of the data process (responds obtained through questionnaires, absolute values). The skills matrix (Table 3) was built by cumulating the responds per each economic sector (the vertical columns data). As it can be seen, companies from manufacturing and IT sectors (total score 17) expressed their total need for the BPM training program. In addition, representatives of IT and software developers companies, from universities, from tourism and financial services industries and from the automotive industry expressed their training need about all units and elements of CertiBPM (maximum score related to the acceptance of all units and elements, 17).

In the same time, the skills matrix offered information about the training needs related to each units/elements. In this context, BPM.U0.E0, BPM.U0.E1, BPM.U0.E2, BPM.U1.E1, BPM.U1.E2, BPM.U1.E3, BPM.U1.E4, BPM.U1.E5 and BPM.U3.E1 are the preferred for all industries in the sample. In addition, representatives declare that also BPM.U4.E1 and BPM.U4.E2 should be taken into consideration for the CertiBPM training program.

3 CertiBPM e-Learning and Certification Facilities

The examination questions (for the on-line examination procedure by login on the www.ecqa.org, section: Certification and Examination – Exam Registration) are developed as multiple choice one (maximum 4 types of answers). The examination process has to be very well understood for the participant with respect to the ECQA procedure [8], [9]. The start and end time of the exam is set by the exam organization (after the agreement of the members of the Job Role Committee that have contributed to the development of the training materials and that were involved in the organization of some training sessions). All the participants at an examination process have to be registered on the web portal.

The user can attend the exam at any time after the examination period has started and before it will end. During the exam, the participant can log in and log out from the system. The answers are stored in the database. If an internet connection break occurs (the wireless connection drops, the internet does not work etc.), a warning message will be displayed. The user has to log out. After the connection has been re-established, the user can log in and has to re-check if his/her last answers have been correctly saved. In case any problems occur, the person supervising the exam should be informed.

The results of the exam are displayed after the exam is closed by the exam organization. If the user finishes the test earlier, he/she will not be able to view the results. The results are calculated and displayed per learning element. To pass a learning element, at least 66% coverage of the respective learning element is required. 10 random questions are selected out of each learning element. Each question has at least one correct answer. If the participant selects a wrong answer, the question is scored zero (0%). All questions are equally weighted; the results are calculated with the average algorithm (total scores of all questions per element / number of questions per element).

What do the trainees have to do to pass the CertiBPM course and certified themselves? Trainees have to prepare a case study, pass the exam (but they have the opportunity to self assess their knowledge and decide the right moment for the final examination).

For this purpose, trainees should start: studying learning materials (multimedia or handouts), participating in discussions, preparing an exercise, case study, installing and get familiar with the tools, define their business process according to the CertiBPM knowledge pool, methods and tools.

The attendee will receive a course certificate if he/she prepares a case study (see link) or exercise. If the participants attend the ECQA Examination for the Certified BPM he receives upon success the ECQA certificate. The whole training and certification process is presented in Figures 2 and 3. There are two levels of CertiBPM training/examination/certification; the details are shown in Table 4.

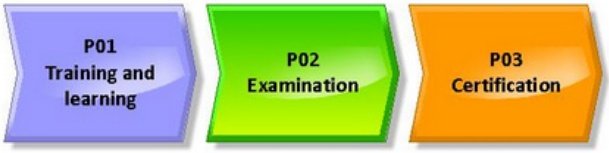

Fig. 2. The CertiBPM Certification Process (P0)

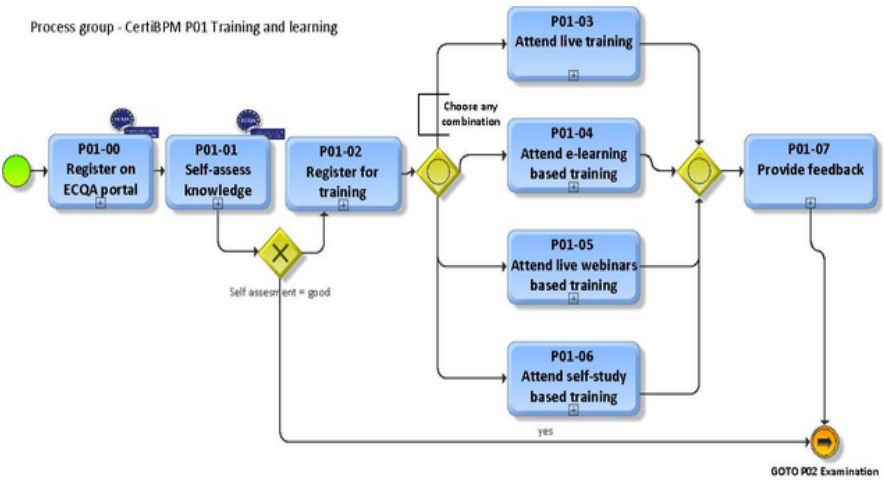

Fig. 3. The CertiBPM Certification Process Detailed (P03)

Table 4. Levels of CertiBPM Training/Examination/Certification

Unit/Element	Basic level	Advanced level	Content specificity
U1			Management
U1 E1	X		
U1 E2	X		
U1 E3	X		
U1 E4	X		
U1 E5		X	
U2			Technology
U2 E1	X		
U2 E2		X	
U2 E3		X	
U3			Psychology and Standards
U3 E1	X		
U3 E2	X		
U3 E3		X	
U4		X	Specializations

4 Conclusions and Lessons Learned

Through this article we intent to demonstrate how a qualification and certification program, like CertiBPM, developed and implemented with the support of ECQA, have been successful implemented on Romanian market (needed and valorized by Romanian companies).

The research results about the training needs identification show a mature level of understanding the need for BPM (collected through representatives and employees responds). In addition, the marketing research has confirmed that the CertiBPM training/examination/certification solution is well designed and accepted on the Romanian market (also, validated through the face-to-face training session developed in March 2012 - May 2012). In the final part of the paper the CertiBPM e-learning training/examination/certification was presented to demonstrate the facilities created to accomplish the CertiBPM project objectives.

Through the CertiBPM initiative there have been several lessons learned: an international partnership can facilitate the transfer of innovation in the field of training, examination and certification and can easy facilitate the implementation of the wisdom gain (e.g. from Slovenia to Romania using the facilities developed in Austria); the similarities and differences characteristics of the trainees that belong to different markets (culture or subculture) can be easy identified and the training program can be easy adapt to the target market specificities; the CertiBPM training and certification program implementation in Romania has benefit from the existing knowledge gain in other market (e.g. Slovenia) and also, from the e-learning facilities that were already created and has to be adapt to the new training program.

In the future, the CertiBPM e-learning portal will be completed (training materials in multimedia format and the examination pool questions will be ready to use) till the end of July and then it will be tested and used with Romanian trainees.

The CertiBPM project is financially supported by the European Commission in the Leonardo da Vinci part of the Lifelong Learning Programme under the project number LLP-LdV/TOI/10/RO/010. This paper and communication reflects the views only of the authors, and the Commission cannot be held responsible for any use, which may be made of the information contained therein.

References

1. Brocke, J., Rosemann, M.: Handbook on Business Process Management: Strategic Alignment, Governance, People and Culture. In: International Handbooks on Information Systems, vol. 1, Springer, Berlin (2010)
2. CertiBPM project: Certified Business Process Manager, contract no. LLP-LdV/TOI/10/RO/010 (2009)
3. Clarke-Epstein, C.: 78 Important Questions Every Leader Should Ask and Answer. AMACOM, New York (2002)
4. Hanna, M.D., Newman, W.R., Johnson, P.: Linking Operational and Environmental Improvement Through Employee Involvement. International Journal of Operations & Production Management 20(2), 148–165 (2000)

5. Johnston Jr., R.E., Bate, J.D.: The Power of Strategy Innovation: a New Way of Linking Creativity and Strategic Planning to Discover Great Business Opportunities. AMACOM, New York (2003)
6. Kaen, F.R.: A Blueprint for Corporate Governance. AMACOM, New York (2003)
7. Kirschenbaum, A.: Chaos Organization and Disaster Management. Marcel Dekker, Inc., New York (2004)
8. Messnarz, R., Richardson, I., Runeson, P.: Software Process Improvement – EuroSPI 2006 Conference. In: Richardson, I., Runeson, P., Messnarz, R. (eds.) EuroSPI 2006. LNCS, vol. 4257, pp. 1–4. Springer, Heidelberg (2006)
9. Messnarz, R., et al.: The EQN Guide. Graz, Austria (2008)
10. Riel, A.: EU Certificates and Knowledge Communities in Europe: An unbeatable Symbiosis. In: Keynote at EQN Founding and Dissemination Conference, Krems, Austria, CD-ROM edition (2006)
11. Caballero, E., Calvo-Manzano, J.A., Cuevas, G., Feliu, T.S.: Implementation of Software Process Improvement through TSPi in Very Small Enterprises. In: Riel, A., O'Connor, R., Tichkiewitch, S., Messnarz, R. (eds.) EuroSPI 2010. CCIS, vol. 99, pp. 280–289. Springer, Heidelberg (2010)
12. Korsaa, M., Biro, M., Messnarz, R., Johansen, J., Vohwinkel, D., Nevalainen, R., Schweigert, T.: The SPI Manifesto and the ECQA SPI Manager Certification Scheme. Journal of Software Maintenance and Evolution: Research and Practice (2010)
13. Pries-Heje, J., Johansen, J.: SPI Manifesto. Version A.1.2.2010 (2010), http://www.iscn.com/Images/SPI_Manifesto_A.1.2.pdf
14. Vinal, K.A.: The Extracted MBA: A topical reference for the contemporary MBA. Universal Publishers, Parkland (2000)
15. Wagter, R., Berg, M., Luijpers, J., Steenbergen, M.: Dynamic Enterprise Architecture: How to Make It Work. John Wiley & Sons, Inc., Hoboken (2005)
16. Wiig, K.: People Focused Knowledge Management. Elsevier Butterworth-Heinemann, New York (2004)
17. Wolf, C., Harmon, P.: The State of Business Process Management, BPTrends Report, http://www.bptrends.com/surveys_landing.cfm (retrieved from 2010)

Incidents Management Process Improvement of IT Systems

Gabriela Prostean, Diana Betina Mirsu, and Anca Draghici

"Politehnica" University of Timisoara, Faculty of Management in Production and Transportation
gabriela.prostean@mpt.upt.ro, betinaiovan@yahoo.com, adraghici@eng.upt.com

Abstract. The main objective of incidents management in IT system is to provide high performance IT services crowned by full satisfaction of the customers. This can be achieved by continuous process improvement with innovative ideas of service diversification that enables a positive impact on process performance indicators. The paper presents an improvement solution of a Help-Desk (HD) software service by integrating a knowledge database in the selection of service procedure influencing the decreasing resolution time of process incidents.

Keywords: incident management, process, knowledge database.

1 Introduction

In the last years there has been an increasing interest for business process management (BPM) in all fields of industries [1],[2].Incident management in IT systems represents [3] the process of coordinating all resources in order to return solutions to faulty services, in the shortest time possible.

The process is based on symptom identification, with primer focus on speed answer to incident, capital assurance and continuity in work process.

The application presented in the paper describes a Help-Desk (HD) software service for a program that has a web interface. The HD service receives requests over the phone from customers, which in this case are the users of the program. The customers request solutions for two types of problems: simple problems that can be solved remotely over the phone; hardware related problems that require mobility. The hardware solutions refer to repairing malfunctions, installation and maintenance.

Customer requests are received and solved in a priority based system: -priority type 0, urgency that must be resolved within a 24 hour timespan. This type of priority refers to software problems that can be solved remotely; -priority type 1- urgency with 48 hour time available for resolution. This type of priority refers to hardware problems that need movement to the problem site.

V.E. Balas et al. (Eds.): Soft Computing Applications, AISC 195, pp. 681–689.
springerlink.com

In the proposed process, the following types of problems [4] can be identified:

1. Time overdue for ticket resolution – requires level 1 support. (timing service)
2. Wrong ticket assignment (level 2 instead of level 1 support)
3. Customer ticket forwarded to board of administration for failure in respecting SLA (service legal agreement) regarding the resolution time.
4. Other customer complains.

In addition to the process problems, a workload increase of 20% is expected. The estimations for the next period are rising from 750 incidents/ week to 900 incidents/ week.

Incident management integrates business process modeling standardization, possible improvement detection, workflow efficiency, rising productivity and complex process problem analysis.

2 Help-Desk Software Service Process Description

The HD process (fig. 1) starts when the software user signals an incident during the run-time of the program. The user requests level 1 support of the HD service. This level receives the request and makes a description [5] of it in a document; next, the problem is classified as described below: (A) problem known – level 1 support is responsible for finding a solution; (B) problem unknown – in this case it is the level 2-support that must find a solution to the problem.

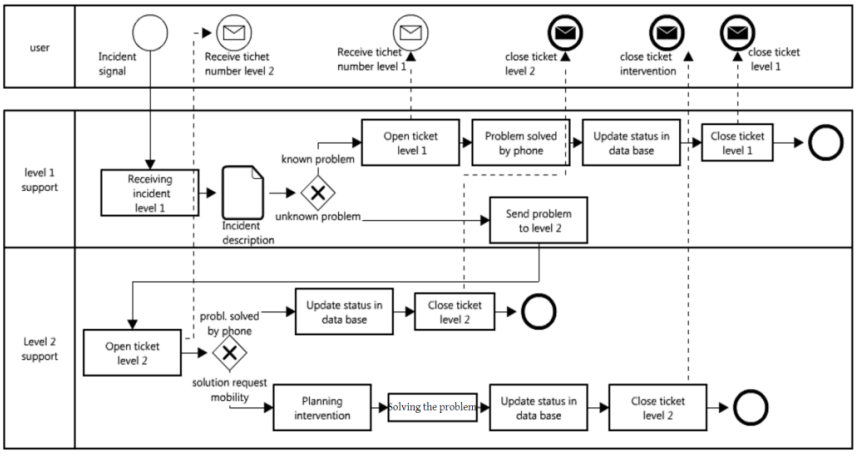

Fig. 1. Help Desk process map

A. Problem known - for this type of problem level 1 support opens a ticket and sends the number of the ticket to customer via e-mail. These types of incidents are solved by phone assistance. Once problem is solved it is saved in the knowledge database and the ticket is closed by the level 1 support. An e-mail is send to customer for confirming the ticket closure. The process ends.

B. Problem unknown - the problem is send from level 1 support to level 2.

The personnel from level 2-support open a ticket for it and send the ticket number to customer via e-mail. Level 2 support decides if: (1) the incident is a software problem and can be solved via phone but requires high expertise; (2) or if the incident is a technical problem and requires mobility of an intervention team to the site of the incident.

1. If the problem can be solved via phone the database is updated with the problem solution, the ticket is closed and an e-mail with the ticket closure number is sent to the customer. The process ends.
2. If the problem is technical and requires movement of an intervention team, a planning of the intervention is made. The movement of the team is done according to plan and a solution for the incident is found. The database is updated with the solution. The ticket is closed and an e-mail is send to customer with the ticket closure number. The process ends.

3 Knowledge Database Functions and Automation

To increase process efficiency a knowledge database is introduced in the form of a structured table. The knowledge database procedures are a set of conditions and actions, which are memorized in a collection named rules database. The knowledge database procedure enhancement follows next rule: each time a phone assistance problem from level 2-support is solved; a process procedure for these type of problem is created, enabling these way the knowledge transfer from level 2 –support to level 1 –support. After training level 1 support with the new process procedure for the new type of problem, the responsibility will be transferred.

The control of knowledge database is represented by decision rules [6] that regard the action sequence in the process of solutions finding. The control action of the knowledge database: provides procedures rules that specify the sequence of procedure in solving a problem and enables transfer of knowledge from level 2 to level 1 support.

By introducing knowledge database automation HD software service process benefit from automat incident prioritization, automat e-mail sending to customer with ticket number and incident status, automat visualization of available mobile-intervention team calendar.

4 Help-Desk Software Service Process Description After Knowledge Database Introduction

The process improved starts when the level 1-support receives a message from customer regarding an error in the usage of software platform (fig.2). Level 1-support receives the request and opens a ticket and that describes briefly the problem. The ticket is saved in knowledge database. Next the incident is filtered by knowledge database [7] in one of three types of problem –'problem known': this type of problem address to level 1, who will be in charge for finding a solution. – 'problem unknown'

and 'problem that requires mobility': both types of problems address to level 2 and it will be in charge for finding solutions.

A. If the problem is known: the solution is standardized and requires a small amount of experience. For finding solutions level one goes through the following steps: opens a ticket for the problem, sends a message to user with the ticket number and offers phone solution. After the problem is solved the status of the problem is updated in database and the ticket is closed. Last step is sending a message to user with the message that the ticket is closed.

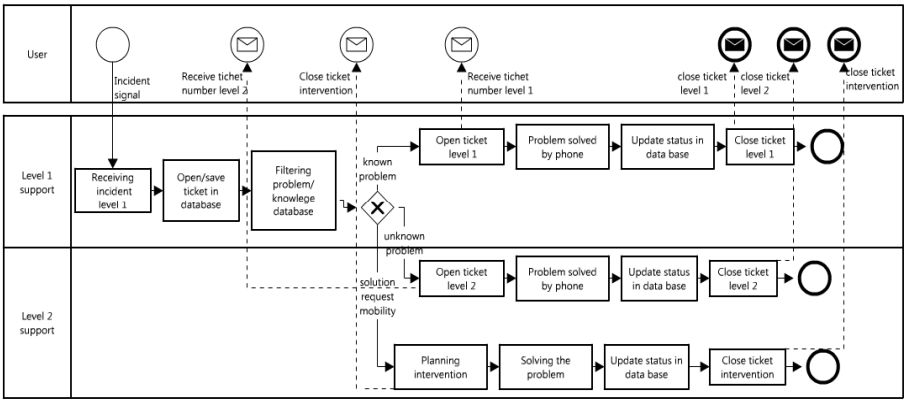

Fig. 2. Help Desk process map- with knowledge database introduction

B. If the problem is unknown: it means that these problems could not been found in the knowledge database and the solution for these problems are a customized one. For solving these types of problems level 2 follows the next steps: opens the ticket, solves the problem through phone, updates the database information with the status of the problem and sends a message to users with the number of the ticket that has been closed.

C. If the problem requires mobility next steps will be followed: planning the intervention, sending the number of the intervention ticket to the customer, solving the problem at the place of the incident, updating problem status in database, closing the intervention ticket and sending a message to users with the number of the ticket that has been closed.

5 Non Value Added Analysis for HD Process

For measuring the impact of knowledge database automation in HD process non-value added analysis is performed [8]. The activities of the process will be evaluated by the below criteria:

1. VAA- Value Adding Activities- are those activities that are required by customer and the customer is willing to pay for them.
2. NVA- Non Value Adding Activities – are those activities that support value adding activities and can suffer improvement or can be done differently.
3. NVAN -Non Value Adding Activities that are Not Necessary- are those activities that can be eliminated without impacting the quality of customer service.

Table 1. HD process timing before improvement

Help Desk Process steps before improvement	**Maxim duration**		
	VAA	NVA	NVAN
Call help desk		1 min	
Get incident basic information		4 min	
Incident description	15 min		
Evaluate severity of incident	5 min		
A. Open ticket level 1 (known problem)		1min	
Send e-mail regarding ticket number to customer			3 min
Solving problem by phone	5-60 min		
Update status in database		3 min	
Close ticket		1 min	
Send e-mail regarding ticket number to user			3 min
B. Send problem level 2 (unknown problem)			5 min
Open ticket level 2		1 min	
Send e-mail customer regarding ticket number			3 min
Prioritizing problem		5 min	
1 Solving problem by phone	5-60 min		
Update problem status in database		3 min	
Close ticket action		1 min	
Send e-mail customer regarding close ticket number			3 min
2. Problem request mobility/ Planning the team intervention calendar		20 min	
Solving the problem	0-48 h (0-2880 min)		
Update status in database		20 min	
Send e-mail customer regarding ticket number			3 min
Close ticket		1 min	
TOTAL TIME	3120 min	61 min	54 min

Table 2. HD process timing after introduction of knowledge database and removing NVAN

Help Desk Process steps after improvement	**Maxim duration**		
	VAA	NVA	NVAN
Call help desk		1 min	
Get incident basic information		4min	
Incident description	15 min		
Open/ save ticket in database	2 min		
Filtering problem with knowledge database	3 min		
A. Open ticket level 1 (known problem)		1min	
Send e-mail regarding ticket number to customer (automation knowledge database)		0 min	
Solving problem by phone	5-60 min		
Update status in database (automation knowledge database)		0 min	
Close ticket		1 min	
Send e-mail regarding ticket number to user (automation knowledge database)		0 min	
B. Open ticket level 2 (unknown problem)		1 min	
Send e-mail customer regarding ticket number (automation knowledge database)		0 min	
Solving problem by phone	5-60 min		
Update problem status in database (automation knowledge database)		0 min	
Close ticket action		1 min	
Send e-mail customer regarding close ticket number (automation knowledge database)		0 min	
C. Problem request mobility/ Planning the team intervention calendar		20 min	
Solving the problem	0-48 h (0-2880 min)		
Update status in database (automation knowledge database)		10 min	
Close ticket		1 min	
Send e-mail customer regarding ticket number (automation knowledge database)		0 min	
TOTAL TIME	3020 min	40 min	0 min

Table 3. NVA HD analysis overview

Help Desk Process	VAA	NVA	NVAN
Before improvement	3120 min	61 min	54 min
After improvement	3020 min	40 min	0 min

Table 3 shows a decrease of VAA, NVA and NVAN times with 100 min, 21 min and 54 min respectively. This increase is due to automation.

Table 4. Improvement time for process types of problem

Type of problem	Time before	Time after	Total Improvement	Time improvement percent
Known problem (level 1 support)	96 min	87 min	9 min	9,3%
Unknown problem (level 2 support)	106 min	87 min	19 min	18%
Problem request mobility (level 2 support)	2963 min	2936 min	27 min	1%

Table 4 shows improvement times for each main problem presented in HD process. The higher percent of improvement is represented by 'unknown problem' that comes in the level 2-support responsibility. The explanation is the introduction of knowledge database automation which removes unneeded steps of problem analyze and problem transfer form level 1 to level 2.

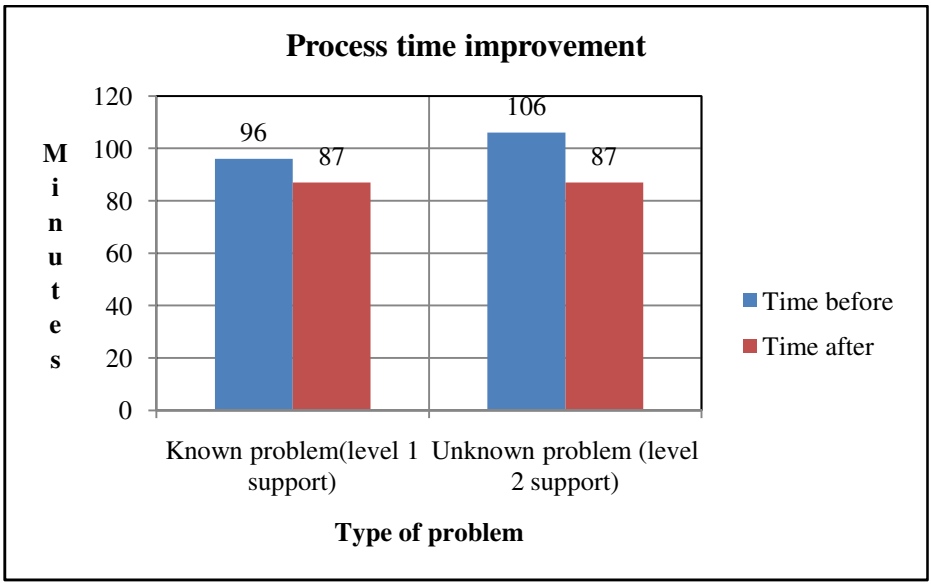

Fig. 3. Process time improvement for phone assistance problems

Fig.3 and fig.4 show the reduction the times allocated for the tasks completion.

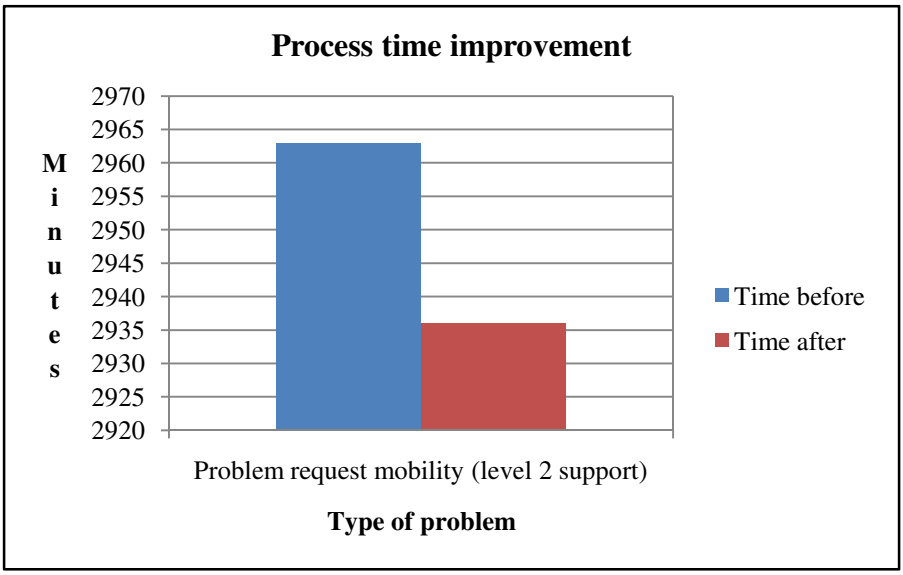

Fig. 4. Process time improvement for problems that require intervention team movement

Besides automation and quality process improvement for each of the organizational problem presented at the beginning of the paper the following solutions (table 5) should be taken into consideration for:

Table 5. Process problems- Solutions

Nr	Process problems	Solutions
1	Time overdue for ticket resolution level 1 support	-ticket tracking and prioritizing (introduction of knowledge data-base) -HD personnel training- to create a backup system
2	Wrong ticket assignment (level 2 in-stead of level 1 support)	-knowledge database automation -HD personnel training
3	Customer ticket escalation to board of administration for failure in respecting SLA (service legal agreement) regard-ing the resolution time.	-HD personnel training
4	Different customer complains	-respecting SLA (service legal agreement) -monitoring customer satisfaction through feedback
5	Future workload increase estimation	Comply ticket time resolution through above actions

6 Conclusion

Incident management aims to reestablish and maintain the service to its normal parameters in accordance with the time frame set in SLA (service legal agreement) with customer. The paper presents an incidents management process improvement of IT systems. The solution consists in implementation of a knowledge database which includes steps in solution finding with a minimum difficulty level and a written procedure.

Knowledge database of a HD software service generates a selection and sequences of service procedure, which are initially provided by level 2 of HD process and witch, can be easily processed by competent persons form level 1of HD process. The usage advantage of knowledge database is automat procedure prioritization of tasks, automat e-mail sending and automat visualization of available intervention team. The total improvement time for each step of the process is: for known problem (level 1 support) 9 min (9, 3 % time improvement); for unknown problem (level 2 support) 19 min (18% time improvements); for problem that request mobility (level 2 support) 27 min (1% time improvement).

Secondary by reducing incident solving time an available time frame is created which offers the opportunity of rising workload.

Future enhancement of the process is the transfer of all incident standardize solutions, that do not require mobility from level 2-support to level 1-support. In the future process level 2-support will be responsible only for problems that require movement to the place of the incident. Knowledge database introduction enables this future improvement.

Acknowledgment. This work was partially supported by the strategic grant POSDRU 107/1.5/S/77265 (2010) of the Ministry of Labour, Family and Social Protection, Romania, co-financed by the European Social Fund – Investing in people.

References

1. Vom Brocke, J., Rosemann, M., vom Brocke, J.: Handbook on Business Process Management 1: Introduction, Methods, and Information Systems. Springer (2010) ISBN 10: 3642004156,13: 9783642004155
2. Weske, M.: Business Process Management Methodology, 2nd edn. Springer (2012) ISBN 978-3-642-28615-5, 978-3-642-28616-2
3. Palmberg: Experience in implementing process management: a multiple case study. Afaceri Process Management Journal 16(1), 93–113 (2010)
4. Sun, S.X., Leon Zhao, J., Nunamaker, J.F., Liu Sheng, O.R.: Formulating the Data-Flow Perspective for Business Process Management. ISR (Information Systems Research)
5. Prostean, G.: Tehnici de inteligenta artificiala in management, Orizonturi Universitare, p. 89 (2007) ISBN 978-973-638-299-4
6. Leung, N.: Encyclopaedia of Knowledge Management. In: Cap 131 A Re-Distributed Knowledge Management Framework in Help Desk, 2nd edn., vol. 2, IGI Global (2010) ISBN 10:1599049317, 13:9781599049311
7. Kannan, N.: `http://www.isixsigma.com/operations/human-resources/improving-help-desk-functions-using-lean-six-sigma/` (found on June 13, 2012)

Models for Sharing Resources in Agile Project Management

Adrian Adam and Gabriela Prostean

Politehnica University of Timisoara, Management Department
Romania, 300222 Timisoara, Bd. Mihai Viteazul no.1
mihaela.adrian.adam@gmail.com, gabriela.prostean@mpt.upt.ro

Abstract. This paper attempts to identify the role and the importance of the transfer of knowledge in managing a project. Information is the lifeblood of change and adaptation. Interactions between project agents involve the exchange of information, social communication and transfer of lessons learned previously. Virtually, the work is a model of combining Agile Scrum method with Kanban, in order to manage the common resources within two projects. This process is represented by ARIS program of business process modelling (BPM).

Keywords: Key words: agile project management, scrum, kanban, shared resources.

1 Introduction

Traditional project management based on rigid procedures and planning, hierarchical organizational structures and low involvement of the owner (client) has shown its limits especially in software development projects. Thus, Agile methodologies appeared, proposing the fast delivery of the product, flexible approach in management and cost reduction. The main advantages of using the Agile methodologies are:

- the priority features of the business are delivered first;
- simple rules and a transparent process for the owner;
- the project may also start with incomplete requirements;
- requirements may be changed during the project whenever needed;
- high degree of self-organization, adaptability and continuous innovation. [1]

The project-based organizations differ significantly from the functional organizations in terms of structure, viewpoint on time, processes, people and geographical location.

Traditional management theory assumes that:

- rigid rules can regulate the change;
- order can be established through hierarchical organizational structures and processes;
- more control generates more order;

V.E. Balas et al. (Eds.): Soft Computing Applications, AISC 195, pp. 691–697.
springerlink.com

- organizations must be static hierarchies;
- employees are interchangeable in the organization;
- risks and problems can be solved mostly by using reductionist task breakdown and allocation;
- projects and tasks can be predictably managed through complex up-front planning [2].

Using agile methodologies, the manager becomes an adaptive leader: setting the direction, establishing the simple, generative rules of the system and encouraging constant feedback, adaptation and collaboration. This management framework provides teams implementing agile methodologies with:

- an intrinsic ability to deal with change;
- a perspective on the organizations as flexible, adaptive systems based on intelligent living beings;
- a recognition of the limits of external control in establishing order and of the importance of intelligent control that employs self-organization as a main tool of establishing order;
- an overall problem solving approach that is humanistic in that:
  - it treats employees as capable and important stakeholders in the team-management
  - it relies on the collective ability of autonomous teams as the main problem solving mechanism
  - it limits up-front planning to minimum based on an assumption of unpredictability and instead, lays stress on adaptability to changing conditions [2].

2 Outcomes and Discussions

2.1 What Is SCRUM Project Management

Any project has as starting point a vision, an idea and some requirements to be met or solutions to be found. In technical projects and especially in information technology, the client requires the settlement of a specific problem, therefore they refer to specialists.

They put together project teams, to whom the owner (sponsor) presents their vision, experiences and wishes of the clients and prepares a list of features (Product Backlog) (Fig. 1) that the final product must meet. Some of them are selected from this list in turn (Selected Product Backlog) with requirements to be addressed in a defined time interval (sprint).

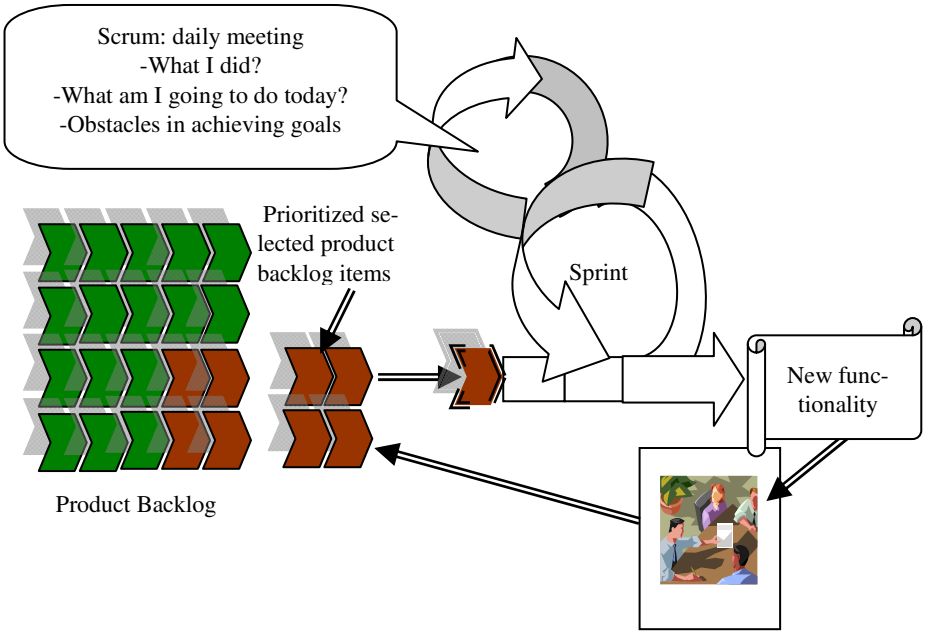

Fig. 1. Scrum Method

Activity itself begins with the initial team meeting (Sprint Planning) [4]. Here there are set the priority functionalities of the Product Backlog and the Sprint Backlog is created, namely the requirements to be met in a sprint. The team that will work in a "sprint" (Scrum Team) is created and led by a Scrum Master. This is a project manager who must ensure that all activities take place in the best way and in time. In Scrum there is no chief in the hierarchical meaning of the word.

A "sprint" usually takes place over 2-4 weeks, and the daily meetings of the team members (Daily Scrum) are crucial for the success of the project, during which there is analyzed what was done yesterday, what is going to be done today and if there are any problems or difficulties that could jeopardize the undertaken objective. At the end of the "sprint" a meeting is held (Sprint Reviews) in order to review the features completed or not, usually in the form of a practical demonstration. Some teams also participate in an internal retrospective of that sprint (Sprint Retrospective).

During the performance of a "sprint" it was found that an activity progress chart may be useful (Burndown Chart). Initially the total quantity of work is represented, decreasing with every sprint (sprint segment).

Once a "sprint" is finalized, the process resumes by drafting a new Sprint Backlog until all Product Backlog requirements are met.

For efficient approach and expressive presentation of the process based on Agile Scrum method, in the phase of architectural design, the process of developing the product may be designed with ARIS program (Architecture of Integrated Information System) used for business process modeling (BPM). The efficiency of modeling with

ARIS program is materialized by specifying, visualizing, constructing and documenting processes, providing process analysis methods, as well as holistic approach to the design process, by tracking the information processing flow, respectively transfer of knowledge within project management. In this regard, for understanding, communication, measurement, namely process management based on Agile Scrum methodology, fig. 2. shows the modeling of the process with ARIS program [6], [7].

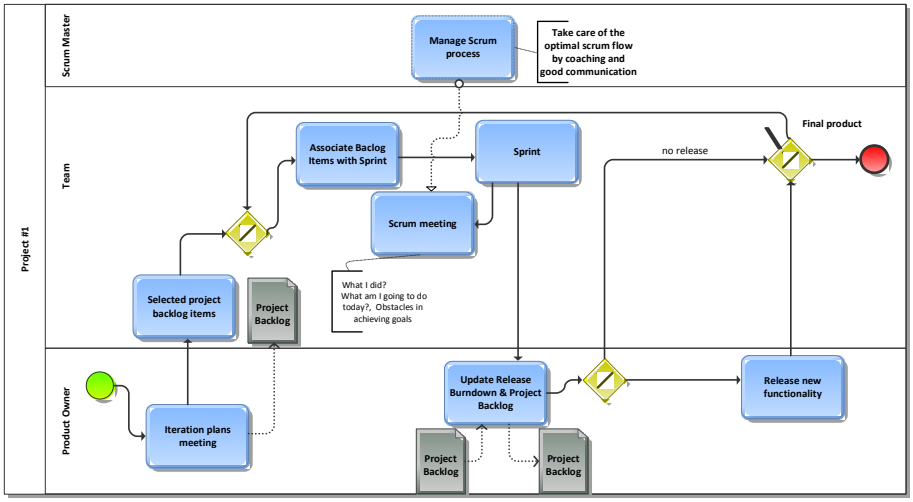

Fig. 2. Scrum Process modeled within ARIS program

2.2 About Kanban Method

Kanban is another methodology based on "Agile" project management. Unlike Scrum, which has a declarative feature, Kanban is a smooth method:

- no sprints performed. Development is based on a flow of objectives translated by the project team.
- the work flow is viewed. A special panel that shows the current status of the project, on three columns: list of requirements (Backlog), in progress (In Progress) and Done (Done).
- the number of requests in progress is limited in each stage. This approach helps detect the constraints and "bottlenecks", which thus may be immediately restored.
- time saving is achieved. There are no estimates, as there is no need. The work flow does not stop at the end of the iteration, which ensures permanent work flow for the project team.
- no roles defined. The project team and the client may specify any roles necessary for the successful running of the project.
- it enables the adding of any rules and practices of other methods, such as SCRUM, XP, etc.

Kanban methodology is suitable for development projects where requirements change constantly, and the iterations may not be clearly defined, and also for projects in stages of ensuring support [3]. Kanban requires thorough understanding of software development processes and greater involvement of the owner (client).

2.3 "Shared Resources" Management in Agile

In practice, situations often occur where two or several teams work simultaneously within the same project with SCRUM method, but resources may not be assigned equally and simultaneously to everybody [5]. For example, if there is only one database developer within a project, he/she may work only within one team, the other teams having to wait for the assignment of this "common resource".

Obviously, the major problem arising in this situation is to set the priorities within the project in order to use this resource in several "sprints" simultaneously, and especially to set the site and the tasks this "resource" performs every moment. A "to do list" is necessary.

Here is where the Kanban method becomes useful. Their owners may meet and continue following their requirement list (Backlog) and may feed the project thereon in a smooth way. How may these things be synchronized? The answer is to organize some "common resources" assignment meetings before the daily "spring meetings" of SCRUM teams, so that each owner (client) may consider at a certain moment the use of the "common resource" when setting the "sprint" plan for that day. Only the owners (clients) and the "common resource" participate in this meeting.

How does Kanban panel change? As the "common resource" is unique, only one requirement shall be recorded under "In work", also keeping the team that resource was assigned to. The panel has to be installed in a common place for all teams so that it may be visible for all involved in order to be aware of the "common resource" assignment anytime.

The main benefits of this procedure are owners' satisfaction, knowing exactly where the "resource" they share is, as well as the additional motivation offered to the "common resource" person, enjoying visibility and high accountability, the advantages for the subsequent evolution in their professional career.

Obviously, the method of the "common resources" is not easy to implement as it requires a lot of organizational talent and power of negotiation in order to meet the requirements of all the persons involved in the project.

In order to obtain a flexible model that shall be adaptive to the information processing flow, respectively transfer of knowledge within project management, the work presents in fig.3. the solution for the distribution of the common resource between projects. The process model represented with ARIS program suggests the proper information processing flow using the common resource, considering that the same process image corresponds both to the first and second project setting identical connections with "Not started" and "In progress" Kanban panels.

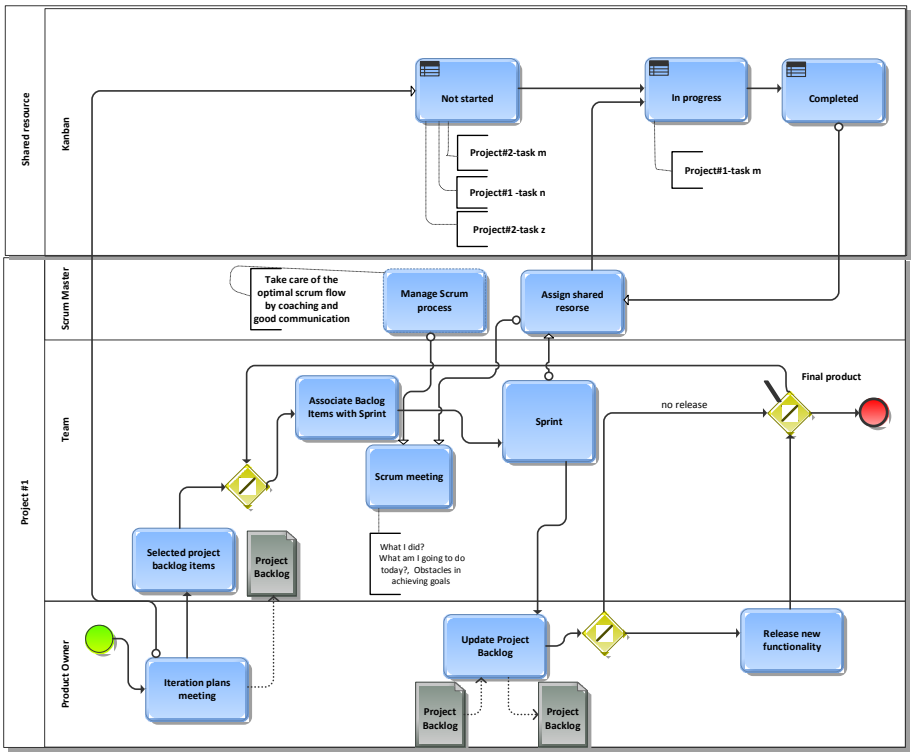

Fig. 3. Scrum process modeling, respectively common resource management in Kanban

3 Conclusions

In spite of some early success with agile methodologies, a number of factors are preventing their widespread adoption, even in the software industry. Agile methodology advocates often find it difficult to obtain management support for implementing what seem like dramatic changes in a project-based organization. That new approach requires developers, managers and users to change in the same time the way they act and think. The proposed models may provide the systematic control of the configuration change and the maintenance of the integrity and traceability of the configuration throughout the life cycle of the system. The advantage of Agile Scrum and Kanban process modeling is the facilitation of understanding the sequence of activities, harmonizing the common resource management process, respectively reducing the level of risk by creating explicit structures.

Acknowledgement. This work was partially supported by the strategic grant POSDRU 107/1.5/S/77265 (2010) of the Ministry of Labor, Family and Social Protection, Romania, co-financed by the European Social Fund – Investing in people.

References

[1] Wiewiora, A., Trigunarsyah, B., Murphy, G., Gable, G., Liang, C.: The Impact of Unique Characteristics of Projects and Project-Based Organizations on Knowledge Transfer. In: 10th European Conference on Knowledge Management, September 3-4, Università Degli Studi Di Padova, Vicenza (2009)
[2] *** "Agile Project Management", http://www.ccpace.com
[3] Anderson, D.: Agile Management for Software Engineering: Applying the Theory of Constraints for Business Results. Prentice Hall (2003) ISBN 0-13-142460-2
[4] Sutherland, J.: Agile Development: Lessons learned from the first Scrum (2004), http://www.scrumalliance.org/resources/35
[5] Taipale, M.: Managing shared resources in agile way (2009), http://huitale.blogspot.ro/2009/08/managing-shared-resources-in-agile-way.html
[6] Stein, S.: A BPM view on SCRUM (2010), http://www.ariscommunity.com
[7] BICERO, Business Informatics Center Rozman Ltd., Slovenia, ECQA Certified Business Process Manager-Training Material version (2011), http://www.bicero.com

A Multicriteria Approach in the Selection of a SAP UI Technology

Adela D. Berdie[1], Mihaela Osaci[1], and Nicolae Budişan[2]

[1] Department of Electrical Engineering and Industrial Informatics, Faculty of Engineering Hunedoara, Politehnica University of Timisoara, Hunedoara, Romania
{adela.berdie,mihaela.osaci}@fih.upt.ro
[2] Faculty of Automation and Computers, Politehnica University of Timişoara, Romania
nicolae.budisan@aut.upt.ro

Abstract. The selection of a web technology in realizing a project is a complex and important decision for small and medium enterprises. The purpose of this paper is to develop an efficient model, using the AHP (Analytic Hierarchy Process) method as a basis and applying the SuperDecisions software, which makes it possible to evaluate the performance of web applications implemented in three SAP UI (user interfaces) technologies: WD (Web Dynpro) ABAP (Advanced Business Application Programming), FPM (Floorplan Manager) and CRM (Customer Relationship Manager) WebClient UI and then make a selection between these technologies. The results found in this research make possible the evaluation between these SAP UI technologies in terms of response time, database request time and CPU time. The application platform where the study is realized is SAP NetWeaver 7.02.

Keywords: web technologies, integrated system SAP, multicriteria decision making, SuperDecision software.

1 Introduction

Nowadays, most of enterprises have been facing difficulties regarding the technologies selection for implementing new projects. These difficulties come from the complexity of the analyzed problems before a decision making.

This study, focuses both on the assessment of an SAP UI technology, as well as on decision making. The evaluation of an web technology is performed on the SAP NetWeaver platform. This platform provides the integration of business information and processes, collaboration, industry-specific functionality, and scalability [1].

The SAP NetWeaver User Interface Technology enables SAP application developers and customers to efficiently build, extend and maintain user-centric infrastructure for Business Applications and enriches SAP business applications with value-adding UI services for collaboration, personalization and content creation [2]. At the same time the platform, enables harmonized, multi-channel access through the client.

V.E. Balas et al. (Eds.): Soft Computing Applications, AISC 195, pp. 699–706.
springerlink.com

For ABAP developers, SAP technologies and tools include Web Dynpro ABAP, Floorplan Manager and WebClient UI Framework. WebClient UI Framework is used for development of applications that complement SAP CRM.

For the decision making, the proposed model used the AHP method as a basis and applying the SuperDecisions software, which makes it possible the evaluation.

2 Objectives of the Study

The objectives of the study include:

- implementing the same web application in all three technologies (WD ABAP, FPM and CRM WebClient UI)
- measuring the system parameters: response time, CPU (central process unit) time and database request time with the transaction STAD (Business Transaction Analisys)
- applying the decision model SuperDecision for evaluation and selection

For the implementation of web applications will be adopted different methods, depending on the technology chosen. With Web Dynpro technology, through the method of componentization, the implemented interfaces will transport the data in the database tables of the SAP system. With Floorplan Manager and CRM WebClient UI technologies, for achieving the interfaces, will be choose UI Building Blocks.

The parameters: response time, CPU time and database request time are measured for each web business application, with transaction STAD for the same query in the database system.

For evaluation and selection between the three technologies is used the SuperDecision model that implement the AHP. The AHP methodology was introduced by Saaty (1980) and provides a means of decomposing the problem into a hierarchy of sub-problems which can more easily be comprehended and subjectively evaluated. The AHP has four major features [3]:

- It decomposes a complex problem into its constituent elements and orders them into a “hierarchy”, or classification system;
- it uses pairwise comparisons to establish priorities among elements in each level of the hierarchy;
- it provides a measurement theory to estimate the relative weights of the elements;
- it aggregates the relative weights to derive a single overall rating for each decision alternative.

The SuperDecisions is a hierarchical decision model that has a goal, criteria and alternatives, make judgments (paired comparisons), and compute the results to find the best alternative.

3 Results and Interpretations

Implementing the same web application in all the three technologies and testing using transaction STAD, the results for the parameters response time, CPU time and database request time are translated in the Table 1.[4]

Table 1. Values of measured parameters

UI Technology/ STAD Parameters (ms)	Web Dynpro ABAP	Floorplan Manager	CRM WebClient UI
Response Time	859	887	5068
CPU Time	644	644	4319
DB Request Time	263	300	1331

From these measurements results that, the WD ABAP technology is the best in terms of the measured parameters, because the obtained values are the smallest.

Making a decision model using the software SuperDecision involves the creating a hierarchy that has a goal, criteria and alternatives, make judgments (paired comparisons), and compute the results to find the best alternative. Criteria are evaluated for their importance to the goal, and alternatives are evaluated for how preferred they are with respect to each criterion. [5]

In the hierarchical structure shown in Fig. 1, each comparison set is made up of a parent node and the nodes it connects to in the cluster below.

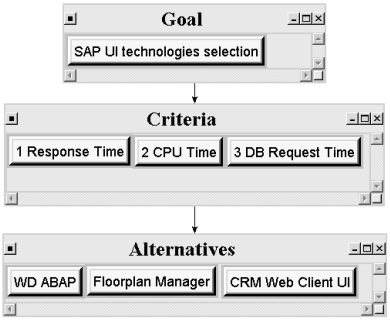

Fig. 1. SuperDecisions Hierarchical Model

Table 2. Saaty's intensity scale

1 Equal
2 Between Equal and Moderate
3 Moderate
4 Between Moderate and Strong
5 Strong
6 Between Strong and Very Strong
7 Very Strong
8 Between Very Strong and Extreme
9 Extreme

The main criteria of the structure are weighted by using AHP. The intensity scale from Saaty represented in Table 2 is used to make pair wise comparisons between the criteria with respect to the goal and/or between the alternatives with respect to the each criteria. The pair wise comparison is the process of comparing the relative importance of two elements with respect to another element in the level above to establish priorities for the elements being compared.[6]

For this hierarchical model exists three sets of pair wise comparisons. They are the alternatives with respect to each of the criteria. The dates come from measurements put in the SuperDecision give the result which is shown in the figures 2, 3 and 4. These values will be directly introduced in the model will be converted to priorities by summing and dividing each entry by the total. Then the matrix will be generated automatically.

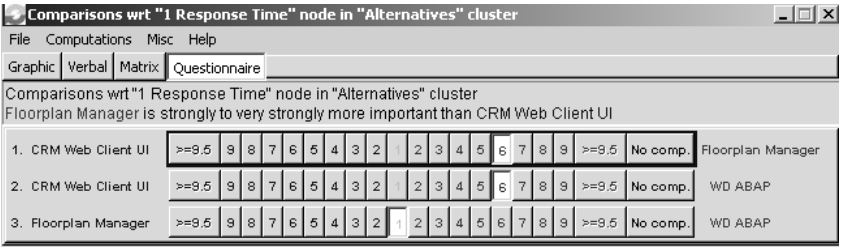

Fig. 2. The Comparison Screen for the Alternatives with respect to the Response Time

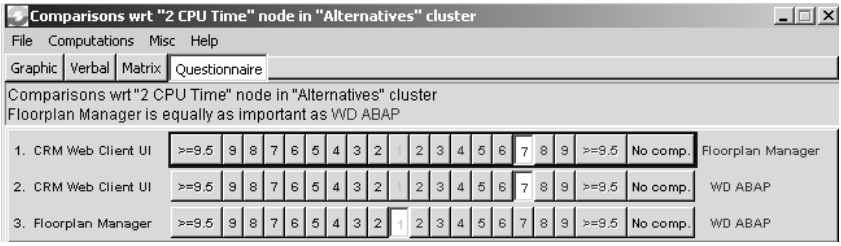

Fig. 3. The Comparison Screen for the Alternatives with respect to the CPU Time

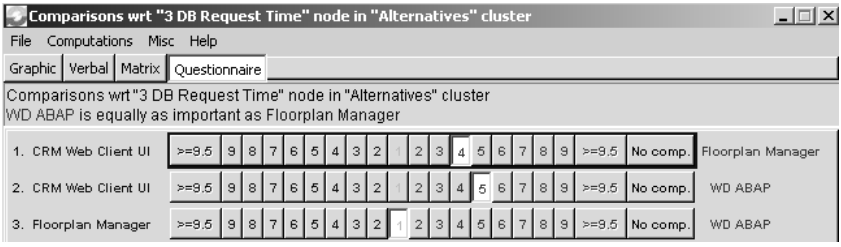

Fig. 4. The Comparison Screen for the Alternatives with respect to the DB Request Time

Numerical judgements are made in matrix (Figures 5a, 6a and 7a) using the Saaty's intensity scale that represents how many times one element is more important than another. The dominant element is represented from the arrow at the left of the entry points.

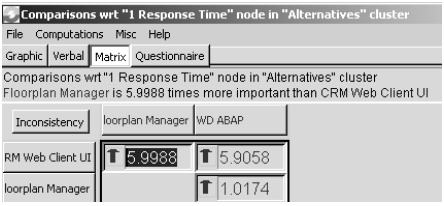

Fig. 5a. Matrix mode for Response Time

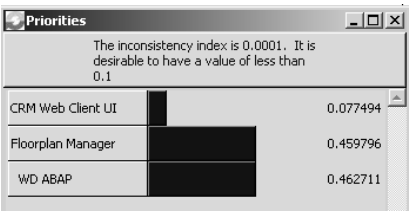

Fig. 5b. The Priorities Screens for Request time

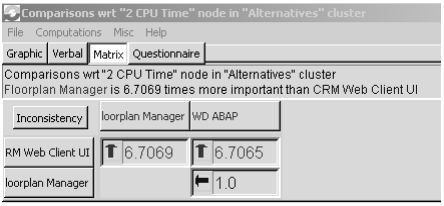

Fig. 6a. Matrix mode for CPU Time

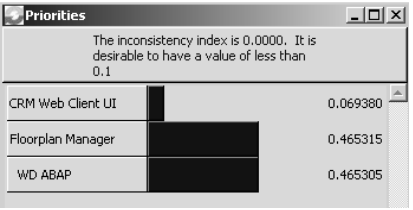

Fig. 6b. The Priorities Screen for CPU time

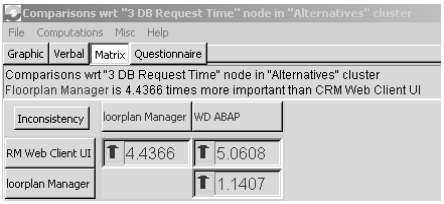

Fig. 7a. Matrix mode for DB Request Time

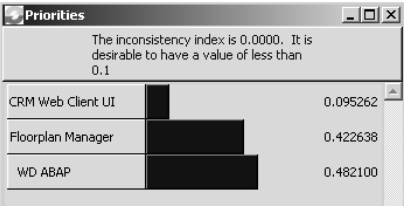

Fig. 7b. The Priorities Screen for DB request time

The results of these pairwise comparisons and the inconsistency index are shown in figures 5b, 6b and 7b. The inconsistency indexes in all three cases are less then 0.1, so no correction of judgments is needed.

The results for the alternatives are obtained in the Main Model View through synthesis. The final results are shown in Fig. 8.

The Normals column presents the results in the form of priorities. The Ideals column is obtained from the Normals column by dividing each of its entries by the largest value in the column and the Raw column is read directly from the Limit Supermatrix.[3]

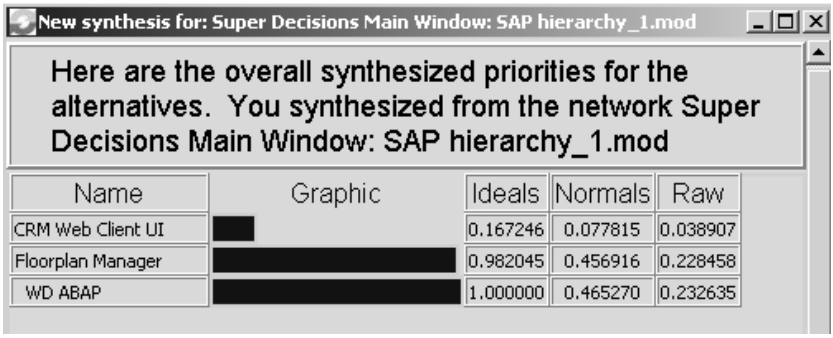

Fig. 8. Priorities of proposed model created in SuperDecision software

These results show that the Web Dynpro ABAP would be the best choice for this decision maker. The Ideals column shows the results divided by the largest value so that the best choice has a priority of 1.0. The others are in the same proportion as in Normals and are interpreted this way: CRM WebClient UI is 16.7 % as good as Web Dynpro ABAP and Floorplan Manager is 98.2% as good as Web Dynpro ABAP.

For the sensitivity analysis are set the independent variable and the graph shown as in Fig. 9, one line for each alternative.

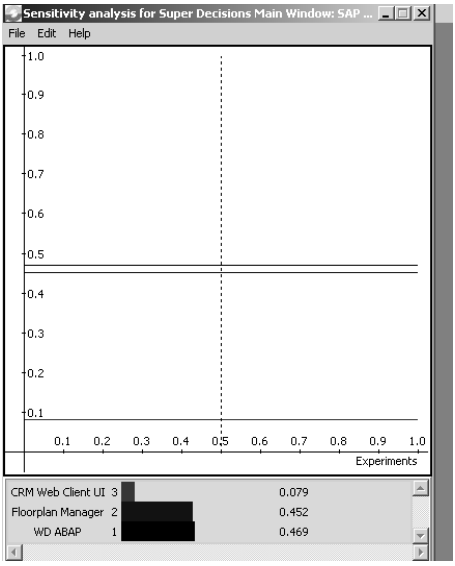

Fig. 9. Sensitivity analysis

The priorities that were derived in the comparison process appear in the Unweighted Super Matrix shown in Fig. 10. The Weighted Supermatrix is the same as the Unweighted Super Matrix but the clusters are not weighted. Raising the Weighted Super Matrix to powers yields the Limit Matrix from which the final answers are extracted. The final priorities for the Alternatives are in the column under the Goal. [7]

The final Super Matrix (Fig. 11) is the limit matrix and will display the intermediate priorities under every node in the model.

Super Decisions Main Window: SAP hierarchy_1.mod: Unweighted Super Matrix

Cluster Node Labels		Alternatives			Criteria			Goal
		CRM Web Client UI	Floorplan Manager	WD ABAP	1 Response Time	2 CPU Time	3 DB Request Time	SAP UI technologies selection
Alternatives	CRM Web Client UI	0.000000	0.000000	0.000000	0.079276	0.069380	0.095262	0.000000
	Floorplan Manager	0.000000	0.000000	0.000000	0.452988	0.465315	0.422638	0.000000
	WD ABAP	0.000000	0.000000	0.000000	0.467736	0.465306	0.482100	0.000000
Criteria	1 Response Time	0.000000	0.000000	0.000000	0.000000	0.000000	0.000000	0.700975
	2 CPU Time	0.000000	0.000000	0.000000	0.000000	0.000000	0.000000	0.192880
	3 DB Request Time	0.000000	0.000000	0.000000	0.000000	0.000000	0.000000	0.106145
Goal	SAP UI technologies selection	0.000000	0.000000	0.000000	0.000000	0.000000	0.000000	0.000000

Done

Fig. 10. The Unweighted Super Matrix

Super Decisions Main Window: SAP hierarchy_1.mod: Limit Matrix

Cluster Node Labels		Alternatives			Criteria			Goal
		CRM Web Client UI	Floorplan Manager	WD ABAP	1 Response Time	2 CPU Time	3 DB Request Time	SAP UI technologies selection
Alternatives	CRM Web Client UI	0.000000	0.000000	0.000000	0.079276	0.069380	0.095262	0.039532
	Floorplan Manager	0.000000	0.000000	0.000000	0.452988	0.465315	0.422638	0.226072
	WD ABAP	0.000000	0.000000	0.000000	0.467736	0.465306	0.482100	0.234396
Criteria	1 Response Time	0.000000	0.000000	0.000000	0.000000	0.000000	0.000000	0.350488
	2 CPU Time	0.000000	0.000000	0.000000	0.000000	0.000000	0.000000	0.096440
	3 DB Request Time	0.000000	0.000000	0.000000	0.000000	0.000000	0.000000	0.053072
Goal	SAP UI technologies selection	0.000000	0.000000	0.000000	0.000000	0.000000	0.000000	0.000000

Priorities for each Criterion

Fig. 11. The Limit Matrix

4 Conclusions

The main conclusion of this article is the proposed evaluation model by this study demonstrates the sensitivity and efficiency in evaluating UI technologies selection.

It is important that one or more comparison judgment within considering problem can be changed in the SuperDecision software and the new ranking immediately can be seen according that. This makes the program ideal for applying as a tool in decision making problems.

We can say that this paper is focused, on practical issues and a quickly implementation. Further studies with respect to combination of other decision models, would be very interesting to analyze.

References

[1] SAP Portal, http://sap.com
[2] SAP Community Network, http://scn.sap.com
[3] Saaty, T.L.: Decision making with the analytic hierarchy process. Int. J. Services Sciences 1(1) (2008)
[4] Berdie, A.D., Osaci, M., Prostean, G., Cristea, A.D.: Web Programming features on integrated system SAP. In: 6th IEEE International Symposium on Applied Computational Intelligence and Informatics (SACI), Timisoara, Romania, pp. 227–230 (2011)
[5] Saaty, R.W.: Decision making in complex environments, http://www.superdecisions.com/Tutorial2003.doc
[6] Osman, K., Bojčetić, N., Marjanović, D.: Multicriteria decision making in Product platform development an evaluation. In: International Design Conference - Design 2010, Dubrovnik - Croatia, May 17-20, pp. 1623–1632 (2010)
[7] William, J.L.: Adams and Rozann Saaty, Super Decisions Software Guide (2011) http://www.ii.spb.ru/admin/docs/SuperDecisionHelp2011.pdf

Studies on Efficiency of the Data Access by ABAP Programming

Mihaela Osaci[1], Adela Diana Berdie[1], and Ana Daniela Hammes[2]

[1] Department of Electrical Engineering and Industrial IT, Faculty of Engineering Hunedoara, Politehnica University of Timisoara, Hunedoara, Romania
{mihaela.osaci,adela.berdie}@fih.upt.ro
[2] Cellent AG Stuttgart, Germany
anadaniela05@yahoo.com

Abstract. Currently, the implementation of the integrated information systems in companies represents a sine qua non condition for providing higher and more reliable accessibility to the information resources. One of the most used integrated platform is SAP Netweaver, a multilingual & multitasking system based on the three-tier client-server technology. The development environment is the Application Server ABAP and/or Java. This paper provides a series of studies performed to optimise the processing codes of the data found in the related tables in SAP Netweaver Application Server ABAP. To access the data from the persistence level tables, we use, in the ABAP codes, the Open SQL instructions, which represent a subset of the standard SQL instructions.

Keywords: software integrated system, business application programming.

1 Introduction

The SAP NetWeaver Application Server is the core of SAP software stack which enables the development of ABAP and/or Java applications for data storage and processing [1], [2], [3]. It completely supports the J2EE (Java 2 Enterprise Edition Platform) standard. The SAP NetWeaver Application Server is also developed for Web applications. The SAP NetWeaver Application Server has a three-tier architecture [1], [2], [3]: the presentation level, application level and persistence level. The three levels communicate through appropriate interfaces: Internet Communication Manager (ICM), which makes the connection to the Internet, the Remote Call Function (RCF), connection through which the external software applications can have access, or another SAP NetWeaver AS system, the Database Interface for communication with the persistence level (databases). The native programming language of the system is the ABAP language, a 4GL language. In the Application Server environment there are created and organized, besides the programs, all the development objects needed by an application.

V.E. Balas et al. (Eds.): Soft Computing Applications, AISC 195, pp. 707–713.
springerlink.com

2 Objectives of the Study

For reading data from the related tables in the level of persistence, we can use several techniques [4], [5], [6], i.e. *select...endselect* instructions nested with the *where* clause, *select* instructions with join in the *from* clause, and the *select* instruction, the data source being a database view. In the last two cases, we can also use the *array fetch* technique. The internal table, in which we bring data in the application level, can be defined based on a local or global mixed structure, or based on the view [6]. Accessing data from the internal tables for processing and displaying them in the presentation level can be done in several ways: through a workarea data object, through a data reference variable or through a field symbol [6]. To determine which combination of these techniques is more efficient in terms of time and memory occupied, we will use an integrated system testing tool, called ABAP Runtime Analysis [7].

The database of this case study retains information about the payroll of employees in a company. We will work on related tables. We also propose to read data from the 3 tables related according to the selection criteria introduced through a selection screen with two parameters, and to display the data after processing in a classic SAP GUI (SAP Graphic User Interface) list. These case study programs are called according to Fig. 1.

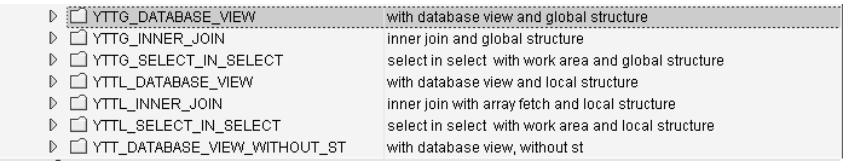

Fig. 1. The case study programs

In the program group YTTL_* , the internal table in which we bring data from the persistence level in the applications level is defined based on a local structure.

To read the data, we use nested select cycles – the program YTTL_SELECT_IN_SELECT, select with the *inner join* clause in the program YTTL_INNER_JOIN, and select with database view as data source in the program YTTL_DATABASE_VIEW.

In the program group YTTG_*, the internal table in which we bring data from the persistence level in the application level is defined based on a global structure. In case of working with view, we will define the internal table based also on the view.

We carry out the study depending on the number of records in the tables ytb_angajat_ma and ytb_statpl_ma.

3 Results and Interpretations

The number of records in the tables varies (10, 40, 70 and 100 records). The data are read from the three related tables, through three techniques: nested select ... endselect cycles, select with inner join at the from clause, allowing also array fetch, and array

fetch having, as database, a database view. The internal table in which we bring the data is defined based on a global structure (groups of yttg codes), local structure (the yttl code group), or based on the view (ytt).

We work with or without the buffering property set for the database tables.

The set buffering property [6] allows the use of an intermediate memory zone - buffer – in the application server, where the first reading records are moved, so that, at a new reading from the table, the records will not be taken from the table, but from that memory zone, called buffer. The results without the set buffering property, for those two groups of programs, are graphically shown in Figs. 2-7.

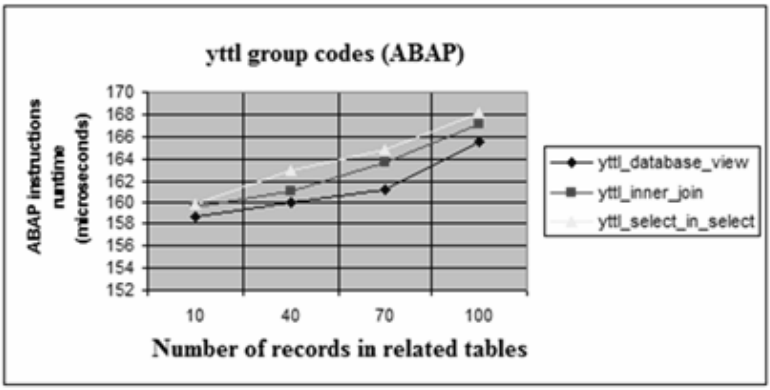

Fig. 2. Time required to execute the ABAP instructions, depending on the number of records in the tables for the YTTL program group

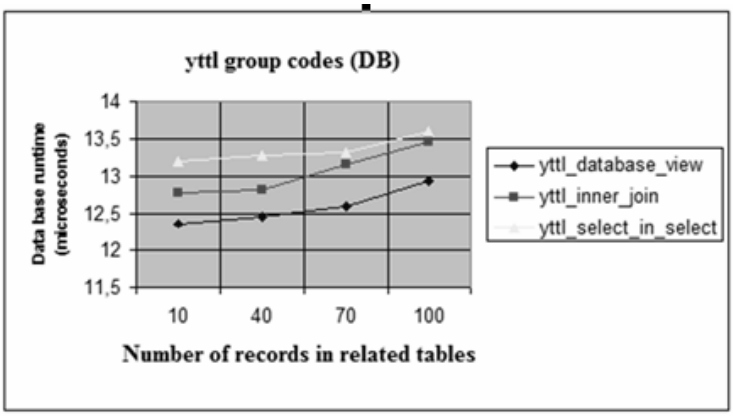

Fig. 3. Time required to work with the database, depending on the number of records in the tables, for the YTTL program group

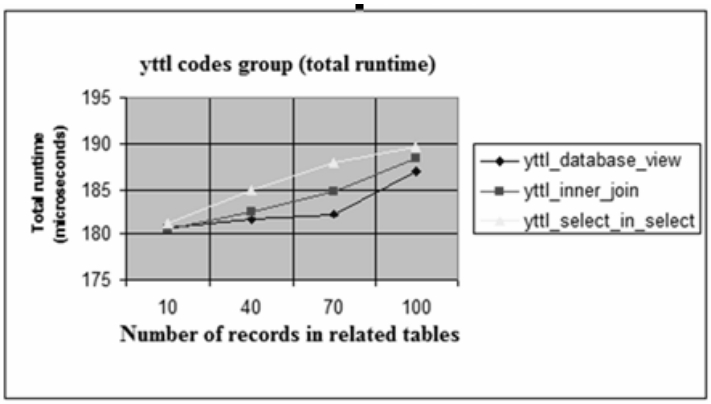

Fig. 4. Total runtime, depending on the number of records in the tables, for the YTTL program group

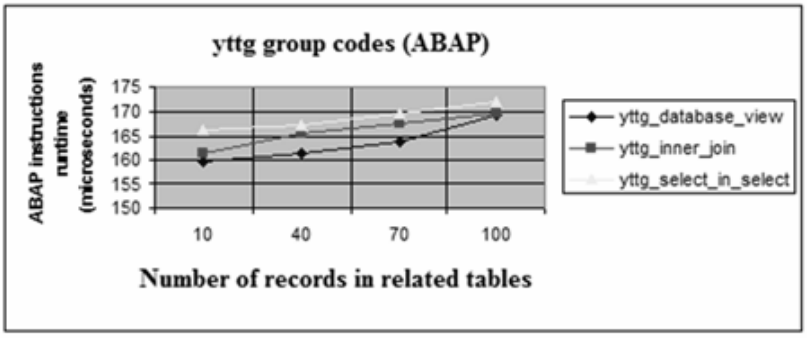

Fig. 5. Time required to execute the ABAP instructions, depending on the number of records in the tables, for the YTTG program group

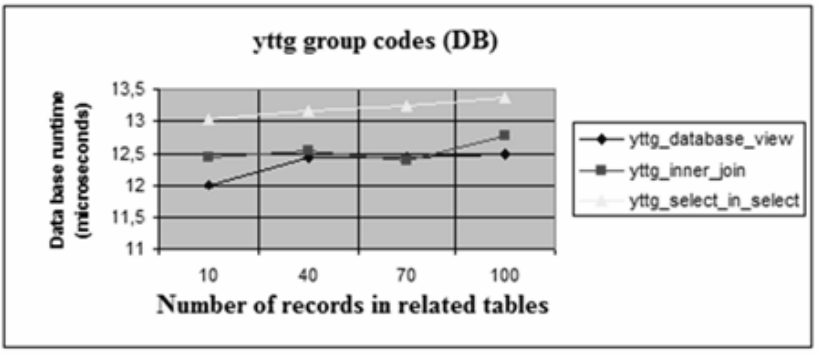

Fig. 6. Time required to work with the database, depending on the number of records in the tables, for the YTTG program group

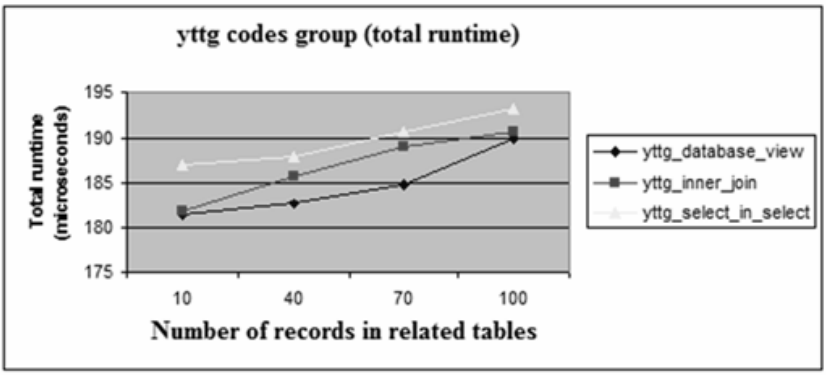

Fig. 7. Total runtime, depending on the number of records in the tables, for the YTTG program group

In Fig. 2-7, we can see that either when using a type of global structure or a local one for defining the internal table, the most efficient solution is the array fetch, having the database view as data source, followed by the array fetch with inner join at the *from* clause, and the most inefficient solution remains the one based on nested select ... endselect cycles. In all the examined cases, the processing time and the time of working with the database increased, depending on the number of records in the tables.

Then, we study how the modality of defining the internal table in which we bring the data influences the total processing time. We obtain the results shown in Figs. 8-10.

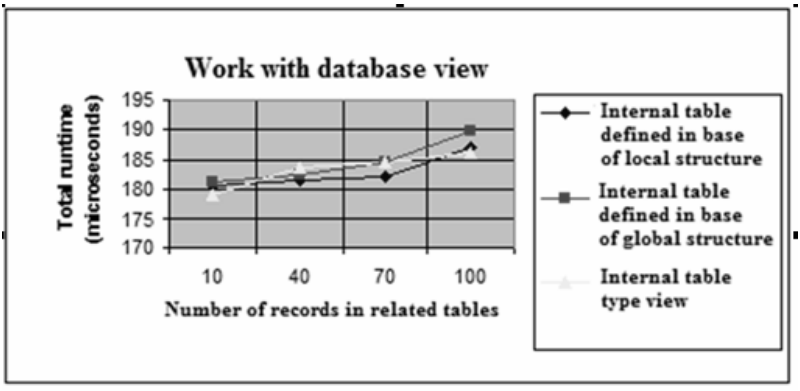

Fig. 8. Total runtime, depending on the number of records in the tables in case of working with the database view

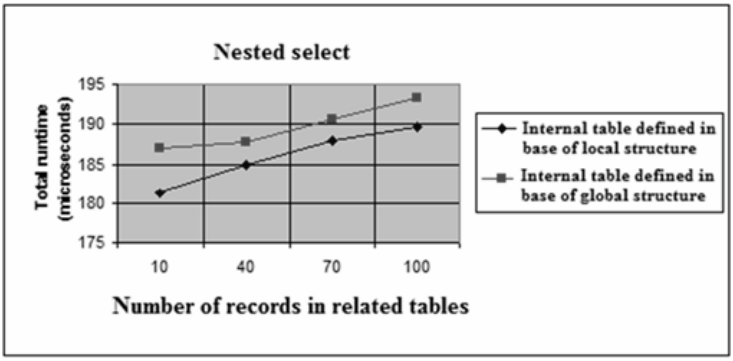

Fig. 9. Total runtime, depending on the number of records in the tables in case of working with nested select cycles

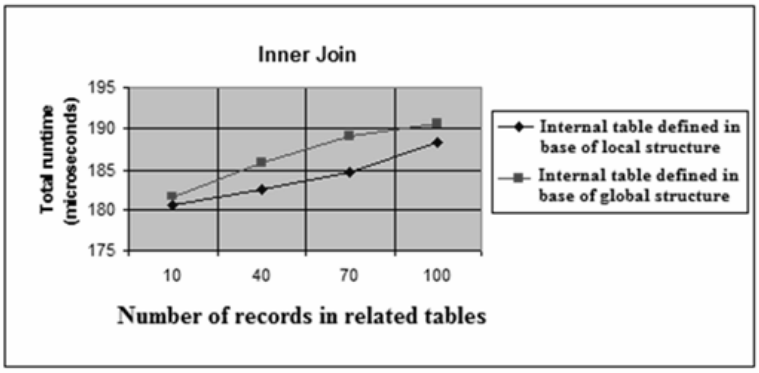

Fig. 10. Total runtime, depending on the number of records in the tables in case of working with select with the inner join clause

In case of using other techniques (array fetch with inner join at the *from* clause and nested select ... endselect cycles, it is more efficient to work with local type structure.

To study how the technical setting of buffering influences the processing time, we use the yttg code groups. The test results are shown in Table 1.

Table 1. Influence of the buffering setting on the time of working with the database

Code	Time of working with the database (micro-seconds)	
	Without buffering	With buffering
yttg_database_view	12.497	12.259
Yttg_inner_join	12.778	12.410
Yttg_select_in_select	13.364	12.567

It can be seen that, when using the buffering property for related tables, the time of working with the database decreases. In case of working with the buffering property, we must remember that the table updates made in the meantime are not known anymore.

4 Conclusions

This paper provides a series of studies related to the methods used to optimise the processing codes of the data found in the related tables, from the level of persistence, on the system SAP Netweaver 2004s Application Server ABAP. To monitor the performances relative to the runtime, we used the ABAP Runtime Analysis utility. The most effective technique for reading data proves to be the array fetch. It appears that the array fetch technique is more efficient when working with database view as data source. We also found that the set buffering property decreases the working time with the database. It is recommended to work with buffering if we do not update the table in this time.

All these studies are very useful for an efficient coding on this integrated system, which is also a ERP (Enterprise Resource Planning) system, especially when the number of records in the database tables is very high.

References

[1] SAP Help Portal, `http://help.sap.com`
[2] SAP Developer Network, `http://sdn.sap.com`
[3] Cristea, A.D., Proştean, O., Muschalik, T., Tirian, O.: The advantages of using SAP NetWeaver platform to implement a multidisciplinary project. In: IEEE Conference on ICCC-CONTI, Timişoara Romania, pp. 383–386 (2010)
[4] Cristea, A.D., Berdie, A.D., Osaci, M.: Working with ABAP Persistent Data. In: The International Symposium Interdiscipliny Regional Research, Hunedoara (2009)
[5] Cristea, A.D.: ABAP Dictionary used in Web Dynpro application. Journal of Engineering, Annals of the Faculty of Engineering Hunedoara, Tome VI, Fascicle 3, 222–227 (2008)
[6] Keller, H., Krüger, S.: ABAP Objects. SAP Press, Bonn (2007)
[7] Osaci, M., Berdie, A.D., Cristea, A.D.: Control Tools For Optimizing ABAP Codes. Acta Technica Corviniensis - Bulletin of Engineering, Tome V, Fascicle 2, 107–110 (2012)

The Comparative Analysis of the Innovation Level for the Entrepreneurial Education

Matei Tămăşilă and Ilie Mihai Tăucean

"Politehnica" University of Timisoara
matei.tamasila@mpt.upt.ro, ilie.taucean@mpt.upt.ro

Abstract. The paper makes a comparative analysis, regarding the offer of facilitators for entrepreneurship education in a region of Central and Eastern Europe (Romania, Bulgaria, Hungary, Serbia), using a model that is starting from Kano's model of satisfaction, the five levels of inventiveness proposed by Altshuller, and the activities and product/services degree of ideality, a methodology for the assessment of the innovation level, in general, and of the entrepreneurship education in particular. In order to sustain the practicability of the proposed methodology, the research includes a case study about innovation level for the activities of the main facilitators for entrepreneurship education in Romania, and a comparative analysis between Romania and Bulgaria, Hungary and Serbia.

Keywords: Education, Entrepreneurship, Innovation.

1 Introduction

This paper sustains that the entrepreneurship facilitators and their offer in the field of entrepreneurship education must to respond to the new economic context arising starting from few years ago because of the subsequent global recession and financial crisis. This new context has profound implications to the psychological, social, economic, cultural and also educational level because it changes the influences and in the same time challenges the intellectual assumptions of entrepreneurship [2].

The entrepreneurship education is influenced by economic and market driven changes, learners' expectations, government policy, changing technology, ethic and cultural changes etc. (see the Figure 1[9]).

These structural and attitudinal changes calling for better entrepreneurial skills and abilities for dealing with an uncertain future and current challenges, therefore educational institutions including universities have to reconsider their role as promoters of entrepreneurship.

In this new era the role of education is to shape ideas of what it means to be an entrepreneur, not to promote an ideology of entrepreneurship, and to create critical awareness that contributes to the accountability of the entrepreneurs to society.

In the same time the special challenge of entrepreneurship education is in the facilitation of learning to support the entrepreneurial process [2].

V.E. Balas et al. (Eds.): Soft Computing Applications, AISC 195, pp. 715–723.
springerlink.com

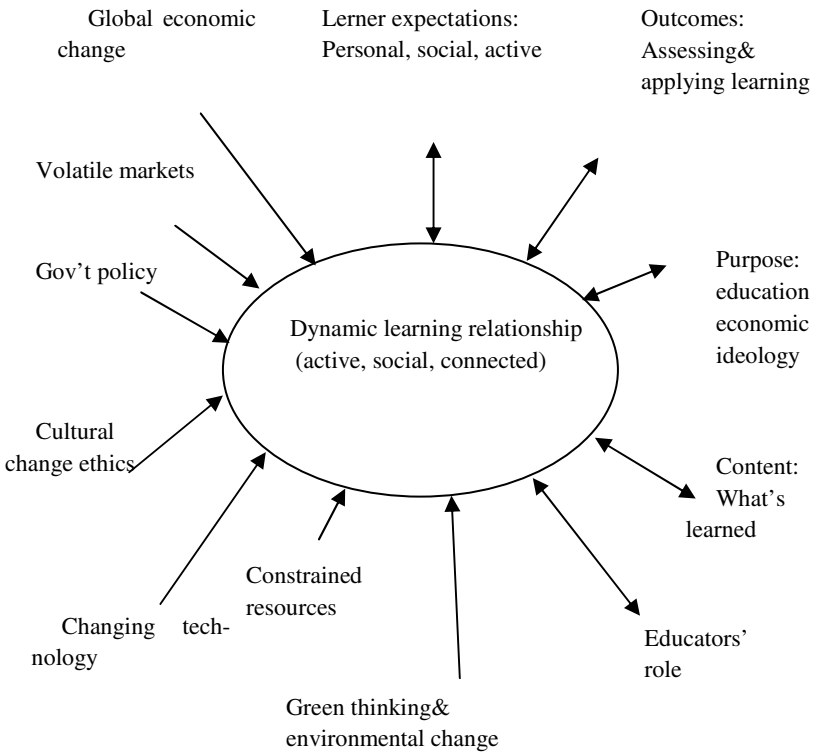

Fig. 1. Entrepreneurial education in the new era

In this context more than never entrepreneurship education is necessary, because the role of educators is major in defining the new entrepreneurship. But of course we are looking for a new learning and teaching methods, able to be interactive, creative and innovative.

Starting from these premises, follow-up we propose a methodology able to identify the innovation level of the entrepreneurship facilitators offer in the field of education in a region of Central and Eastern Europe (Romania, Bulgaria, Hungary, Serbia), based on a global innovation indicator, II, achieved through the level-headed summing up of three indicators: the indicator of the entrepreneurial education satisfaction IES, corresponding to the exciting characteristics from Kano's model [5], the indicator of inventiveness IIN, associated to Altshuller's five levels of inventiveness [1], and the indicator of ideality, IID to reflect the level of ideality for products and services.

2 Methodology

Starting from these premises, in order to determine the value for the global innovation indicator - II , in the field of education for Romania, it is necessary to use the following relation:

$$I_I = I_{SS} \cdot p_{ES} + I_{IN} \cdot p_{IN} + I_{ID} \cdot p_{ID} = I_{ES} \cdot p_{ES} + I_{IN} \cdot p_{IN} + \left(\sum_{k=1}^{9} i_k \cdot q_k \right) \cdot p_{ID} \quad (1)$$

where p_{ES}, p_{IN} and p_{ID} represent the weights corresponding to the three indicators, i_1, i_2, …, i_9 are the indicators of the degree of ideality, and q_1, q_2 …, q_9 are the weights of the indicators of ideality. The sum of the weights from each category is equal to 1, i.e. $p_{ES} + p_{IN} + p_{ID} = 1$ and $q_1 + q_2 + \ldots + q_9 = 1$. Some weights can be null, as function of the field where the methodology is applied.

Generally, the characteristics of a product or a service, according to Noriaki Kano's model [5], from the point of view of customers' satisfaction, are as follows: non-satisfying characteristics, satisfying characteristics, and charming characteristics.

Unsatisfactory features in the sense of dissatisfaction are the features of a product or service that causes customer dissatisfaction when they are missing or are done at a low level, and indifference, when they exist and also are built to a high level. Unsatisfactory features are "expected quality".

Satisfactory characteristics are those characteristics of a product or service that customers know them want and asking about, when buy the products or services. When they not find them on the product/service, they are dissatisfied customers, and if these characteristics are done they are satisfied.

In Kano's model [5] horizontal axis indicates the level of product performance or accomplishment of each of these three categories of features, and the vertical axis shows the degree or level of customer satisfaction as determined by the three categories of characteristics.

In the proposed methodology, we have considered that, in this case, it is necessary that the indicator of the entrepreneurial education satisfaction, I_{ES}, refer only to the unsatisfactory characteristics from Kano's model, because, their elimination implies an innovation effort from the part of the supplier, and also they represent, most often, the decisive element for the failure of a product or service in the market. A possible scale for the customer (student) satisfaction it is presented in the table 1.

Table 1. Scale for entrepreneurial education "satisfaction" level

Grades	1	2	3	4	5	6	7	8	9	10
Characteristics	≥ 5		4		3		2		1	

For the assessment purposes, there has been proposed that I_{ES} indicator be attributed grades on a scale from 1 to 10, as function of the number of exciting characteristics (see table 1).

In order to take into account the degree of inventiveness, there has been proposed in the paper to make an adjustment on the basis of the five levels of the inventiveness solutions and of the required inspirations sources established by Altshuller, with the grades corresponding to the inventiveness indicator, I_{IN} as follows:

Level one activities – which do not imply any invention, can be achieved by routine improvements of some existing products/services through well-known methods in the field and that inspiration comes from inside (grade 2).

Level two activities – which imply minor improvements of some existing products/services; the inspiration source comes from the scientific field where the specialists work (grade 4).

Level three activities – which imply fundamental improvements of some existing products or services through known methods; the solutions shall be looked for in related fields or in other fields (grade 6).

Level four activities – which imply new products/services or new generation products and services for which there are used new principles, and the solutions come from the clearing up of some phenomena from various fields (grade 8).

Level five activities – which imply rare scientific discoveries, whole new products or services, whose solutions can be found by exceeding the borders of the scientific knowledge known at a certain moment (grade 10).

The ideality indicator, I_{ID}, takes into account the ideality of the product through nine indicators. These indicators are as follows:

- indicator of the system dimensionality degree (i_1), highlights the levels of system;
- indicator of the aggregation status (i_2), takes account of system to increase its flexibility, regarding the entrance in the system, the rules etc.;
- indicator of the type, nature, and frequency of the actions applied to the system (i_3), take into account the frequency with which the system operates and the nature of actions ;
- indicator of the degree of the system ”porosity” (i_4), highlights the increased flexibility of the system through its evolution from a closed to an open system, decentralized ;
- indicator of degree of the system dynamic capability (i_5) ;
- indicator of the degree of human involvement (i_6), is focused on human involvement with the evolution of the system ;
- indicator of the degree of the system multiplicity (i_7);
- indicator of the nature, type and dimensionality of the system functions and features (i_8);
- indicator of the degree of the system convolution (i_9), is estimated by the convolution coefficient (Cc) which is defined as the ratio between the number of fields and total number of elements of the system or between the number of functions and the total number of elements involved in the achievement of function, having values in the range (0, 1).

These indicators and associated notes of their levels of achievement are presented in the table 2.

Table 2. Scale for ideality level

Grades	1	2	3	4	5	6	7	8	9	10
i_1		0		1		2		3		≥4
i_2		0		1		2		3		≥4
i_3	≥4			3		2		1		0
i_5	annual		biannual		quarterly		monthly		bi-monthly	
i_6			reduced			medium			big	intense
i_7		1		2		3		4		5
i_8		1		2		3		4		5
i_9	0-0.25		0.25-0.45		0.45-0.65		0.65-0.85		0.85-1	

3 Case Study – Romania

In order to highlight the use of the developed researches, here we will present below the application of the proposed methodology for the very assessment of the level of innovation in the specific case of the entrepreneurship facilitators and their offer in the field of entrepreneurship education in Romania.

3.1 Determining the Indicator of the Entrepreneurial Education Satisfaction (I_{ES})

It has been considered that there are at least 4 unsatisfactory characteristics, such as:

- the promotion and implementation of learning by doing (e.g. projects, a virtual business, possibilities to use the theoretical knowledge in practice) unfortunately still remain in the Romanian schools to the stage of challenge. For example, in terms of practical work that students must perform annually, the vast majority of universities (whether they are public or private) have adopted to run that activity merged at the end of the school year, before summer holidays, or this work remains solely the responsibility of students during summer holidays. In both variants, we believe that it meets just a formality or marked an event, but there is a long way since achieve the European objectives declared who claim that genuine entrepreneurial skills should be initiated, developed and enhanced especially at the higher education level.
- the involvement of entrepreneurs and local companies in designing and implementing entrepreneurial courses and activities in order to develop the entrepreneurial skills it is only in the documents. For example, considering only a development region of Romania (West, region of development 5), there is a recorded activity: a

nearly ten business incubators (Business Incubator Software Timişoara- UBIT, The business incubator and center for technological transfer, integrated in the Industrial and Technological Park Timisoara- PITT, The cross-border business incubator, Business Incubator Jimbolia, Timis, Business incubator for retired military personnel, Timis, Business and Technology Incubator Deva -ITA-BMTECH, Business Incubator Pecica, Arad, Business Incubator ITA, Arad, Business and Technology Incubator UAV-IT Arad), chamber of commerce, regional development agency, other programs (The Entrepreneurship Program – a career alternative for the West Region). Unfortunately eight of the nine business incubators are concentrated on the area of Timis and Arad counties, so there is a total uneven distribution and inversely proportional to the level of economic development. Also collaboration between universities and local successfully multinational companies (Alcatel, Siemens, Continental, etc.) is more difficult in the last period of time, perhaps because of financial crisis, so their involvement in the design, implementation and development of curricula became extremely meteoric, inconstant and inconsistent with very few exceptions;

- the level of the teachers motivation (financial but not only) it is very low by comparison with another countries which really have entrepreneurial education and as a consequence the best chose to leave the system.
- lack of correlation and coordination of entrepreneurial education promoters to ensure continuity, efficiency and effectiveness in a context where there isn't a partnership (public - private) very clearly regulated. Thus there are often overlaps that lead to wasted effort and resources, or uncovered areas, specifically: poorly managed and questionable projects implemented companies that are hiding behind the wall of privacy, programs of study more or less theoretical, not dynamic, not innovative and not entrepreneurial.

According to the grades scale, the indicator I_{ES} is given grade 3.

3.2 Determining the Inventiveness Indicator (I_{IN})

The literature suggests that the possible "targets" for entrepreneurship education should be derived from the entrepreneurial process goals, which in the broadest meaning, refers: 1- to increase the level of entrepreneurial knowledge; 2 - to develop the entrepreneurial skills of individuals and 3 - to initiate new business [3].

For this case study, to the indicator IIN it was given grade 8, because the entrepreneurial education imply more than fundamental improvements of some existing products or processes. Starting from multidimensional model for entrepreneurship approach [4], which highlights the entrepreneurship as a complex and multidimensional framework that emphasizes the individual, the environment, the organization and venture process, it is obviously that outcomes of entrepreneurial education imply new products/services or new generation products and services for which there are used new principles, and the solutions come from the clearing up of some phenomena from various fields.

3.3 Determining the Ideality Indicator (I_{ID})

This indicator reflects the degree of ideality. In order to determine the level of ideality, in this case, there have been taken into account only the indicators i1, i2, i3 , i5, i6, i7 ,i8 and i9 because it has been considered that only these ones are relevant for our analysis. Thus, indicator i1, which gives the system degree of dimensionality, it was given grade 7, according to the presented classification, because the entrepreneurial education runs almost consistently in the high school and universities and sometimes in special projects. Indicator i2, estimates the aggregation status of the system, takes account of system to increase its flexibility, regarding the entrance in the system it was given grade 6, because in our case study entrepreneurial education is available only through participation in master programs of study or short-term trainings in the framework of projects. Indicator i3 analyze the type, nature, and frequency of the actions applied to the system it was given grade 2, because in Romania in general lately, meaning the last twenty years, the educational system was subjected to a considerable number of legal amendments and beyond, without the benefit of a clear strategy, including long-term entrepreneurial education perspective. Indicator i5, which shows the degree of flexibility, of the system dynamic capability, it was given grade 1 according to the presented scale because the dynamic of the educational system is very low, for example curriculum for a program of studies it is possible to be changed every 3 or 5 years in order that permits the authorization or accreditation. The most common changes are being able to attend the annual level syllabus / discipline.

Indicator i6, namely the degree of human involvement, has been given grade 10, because represents the most important resources for entrepreneurial phenomenon and the necessary level of involvement is at least big.

The degree of the system multiplicity, taken into account through indicator i7, it was given grade 5, because in accordance with literature the most detailed approach of the entrepreneurship highlights four major dimensions: individual, environmental, organizational and process [7].

Indicator i8, which estimates the dimensionality, it was given grade 6, because the "functions" of entrepreneurial education can be derived from the entrepreneurial goals that are three: 1-to increase the level of entrepreneurial knowledge, 2 – to develop the entrepreneurial skills of individuals and 3 - to initiate new business. The indicator of the degree of the system convolution (i9), it was given grade 4, because the ratio between the number of action plans of entrepreneurial education (which is 3 as you can observe to the previous indicator) and the number of entrepreneurial individual dimensions approach (which is 8: need for achievement, locus of control, risk-taking propensity, job satisfaction, previous work experience, entrepreneurial parents, age and education) is 0,37.

The eight indicators taken into account there given the following weights: q1=0.05; q2=q5=q6=q8=q9= 0.15; q3= q7 = 0.10. The weight for the eliminated indicator has been considered to be null.

3.4 Calculation of the Global Indicator of the Innovation Level Indicator (I_I)

In order to calculate the global indicator, there have been established the following weights associated to the three indicators: the weight of the indicator of the enterprise's satisfaction pES = 0.30, the weight of the indicator of inventiveness pIN = 0.40 and the weight of the indicator of ideality pID = 0.30.

4 Comparative Analysis

Regarding the comparative analysis between the mentioned four country of Central and Eastern Europe, we present in the following (see table 3) the results (grades) of the analysis, taken in consideration several studies regarding innovation level of the entrepreneurship facilitators offer in the field of education [10] [11] [8] [12] [6].

Table 3. Comparative results

Indicators / Countries	I_{ES}	I_{IN}	I_{ID}								I_{ID}	I_I
			I_1	I_2	I_3	I_5	I_6	I_7	I_8	I_9		
Weights	0.3	0.4	0.05	0.15	0.10	0.15	0.15	0.10	0.15	0.15	0.3	1
Romania	4	7	7	6	2	1	9	5	6	4	4.95	5.49
Bulgaria	4	7	7	6	6	1	9	5	6	4	5.35	5.61
Hungary	7	8	8	5	6	1	8	7	6	4	5.30	6.89
Serbia	5	8	5	6	6	1	7	6	6	4	5.05	6.22
Average	5	7.5	6.75	5.75	5	1	8.25	5.75	6	4	5.16	6.05

In the table you can see some similarities between countries and some differences of values. Similarities are regarding indicators IIN and indicator IID for I2, I5, I8, I9. Main differences are for IES and for IID for I1, I6 and I7.

Through the use of relation presented (1), the global indicator of innovation level of methodology proposed in this paper came to be equal to 5.49 for Romania, which represent a little under the average of the region analyzed (6.05). As we can see also Bulgaria is below average, very close to Romania, but Hungary and Serbia are over the average (with the higher score for Hungary – 6.89).

5 Conclusions

The innovation level of the entrepreneurial education for Romania, in accordance by the proposed evaluation model is modest in this moment (scored 5.49 out of 10), but is modest for all region analysed (with a maximum of 6.89).

In our opinion the result, for the analysed period of time, is a consequence of: a low level of implementation for learning by doing (e.g. projects, a virtual business,

and possibilities to use the theoretical knowledge in practice); a theoretical involvement of entrepreneurs and local companies more than practical in designing and implementing entrepreneurial courses and activities in order to develop the entrepreneurial skills; a low level of the teachers motivation (especially financial but not only); a lack of correlation and coordination of entrepreneurial education promoters to ensure continuity, efficiency and effectiveness in a context where there is a relative inflexible educational system but in the same time too dynamic system regarding: structure, the principles or legal amendments.

In our opinion, the solution to improve the situation in the near future involve: legislative stability, educational strategy clearly defined and more intense use of resources and European experience.

Acknowledgment. This paper received financial support through the project" Post-Doctoral Studies in Economics: long learning program for elite researchers - SPODE ", financing contract no: POSDRU/89/1.5/S/61755, project founded from European Social Fund through Human Resources Development Operational Program 2007-2013.

References

[1] Altshuller, G.: The Innovation Algorithm: TRIZ, Systematic Innovation and Technical Creativity. Technical Innovation Ctr, Worcester (1999)

[2] Heinonen, J., Poikkijoki, S.A.: An entrepreneurial-directed approach to entrepreneurship education: mission impossible. Journal of Management Development 25(1), 80–94 (2006)

[3] Hytti, U., Stenholm, P., Heinonen, J.: Perceived learning outcomes in entrepreneurship education. Education + Training 52(8/9), 587–606 (2010)

[4] Johnson, B.R.: Toward a Multidimensional Model of Entrepreneurship: The case of Achievement Motivation and the Entrepreneur. Entrepreneurship: Theory and Practice (spring), 39–54 (1990)

[5] Kano, N.: Attractive quality and must-be quality. Journal of the Japanese Society for Quality Control, 39–48 (April 1984)

[6] Kelley, D.J., et al.: GEM 2011 Global Report. Babson College, Universidad del Desarrollo (2012)

[7] Kuratko, D.F., Hodgetts, R.M.: Entrepreneurship: theory, process, practice. Thomson South – Western, Manson-Ohio (2004)

[8] Pavlov, D., Tamasila, M.: Methodological approach for questionnaires development in Bulgarian-Romanian scientific project. In: Annual Scientific Conference of Ruse University, vol. 50, book 5.2, pp. 34–41 (2011)

[9] Rae, D.: Universities and enterprise education: responding to the challenges of the new era. Journal of Small Business and Enterprise Development 7(4), 591–606 (2010)

[10] Ruset, V., et al.: Training opportunities in Central and Eastern Europe – Summary results of the HELP training needs analysis. Publishing House Politehnica, Timisoara (2010)

[11] Tamasila, M., Foltean, F.S.: The analysis of the innovation level for the entrepreneurial education in the west region of Romania. In: 8th International Conference MTC-Management of Technological Changes, Alexandroupolis, vol. 2, pp. 445–448 (2011)

[12] Todorova, M.S., Ruskova, S., Gedinach, V., Buciuman, C., Taucean, I.: Willingness and readiness of students to become entrepreneurs. In: Annual Scientific Conference of Rousse University, vol. 50, book 5.1, pp. 150–155 (2011)

Author Index